BRITISH JOURNAL OF
APPLIED PHYSICS

EDITOR

H. R. LANG

A.R.C.S., PH.D., F.INST.P.

Secretary of The Institute of Physics

VOLUME 6

including

Supplement No. 4

LONDON

THE INSTITUTE OF PHYSICS

BRITISH JOURNAL OF APPLIED PHYSICS

ADVISORY COMMITTEE, 1954–55

T. E. ALLIBONE, PH.D., D.SC., M.I.E.E., F.INST.P., F.R.S., *Chairman*

C. B. ALLSOPP, PH.D., D.SC., F.INST.P., *Representing the British Institute of Radiology*

H. BARRELL, A.R.C.S., D.SC., F.INST.P.

W. BETTERIDGE, B.SC., PH.D., F.INST.P.

R. L. BROWN, M.A., F.INST.P.

W. H. J. CHILDS, PH.D., D.SC., F.R.S.E., F.INST.P., *Representing the Scottish Branch*

SIR JOHN COCKCROFT, K.C.B., C.B.E., PH.D., D.SC., F.INST.P., F.R.S., *President, The Institute of Physics*

B. M. CROWTHER, M.A., PH.D., F.INST.P.

T. J. DILLON, M.SC., F.INST.P., *Representing the Education Group*

B. P. DUDDING, M.B.E., A.R.C.S., PH.D., F.INST.P., *Honorary Secretary, The Institute of Physics*

E. K. FRANKL, M.A., *Representing the Stress Analysis Group*

M. R. GAVIN, D.SC., F.INST.P., *Representing the Midland Branch*

A. G. GAYDON, A.R.C.S., PH.D., D.SC., A.INST.P., *Representing the Physical Society*

M. E. HAINE, M.SC., F.INST.P., *Representing the Electron Microscopy Group*

S. T. HENDERSON, M.A., PH.D., F.INST.P.

H. KOLSKY, A.R.C.S., PH.D., F.INST.P., *Representing the Physical Society*

F. LLEWELLYN JONES, M.A., D.PHIL., F.INST.P., *Representing the South Wales Branch*

R. MEREDITH, D.SC., F.INST.P., *Representing the Manchester and District Branch*

W. J. MEREDITH, M.SC., F.INST.P.

G. D. ROBINSON, B.SC., PH.D., F.INST.P., *Representing the Royal Meteorological Society*

L. A. SAYCE, M.SC., PH.D., F.INST.P.

W. E. SCHALL, B.SC., F.INST.P., *Representing the Non-destructive Testing Group*

R. W. SILLARS, B.A., D.PHIL., A.M.I.E.E., F.INST.P.

E. G. STEWARD, B.SC., PH.D., A.INST.P., *Representing the X-ray Analysis Group*

E. C. STONER, B.A., PH.D., SC.D., F.INST.P., F.R.S.

A. M. TAYLOR, M.A., PH.D., F.INST.P., *Representing the London and Home Counties Branch*

R. S. TEBBLE, B.SC., PH.D., F.INST.P., *Representing the Yorkshire Branch*

N. THORLEY, B.SC., PH.D., F.INST.P., *Representing the North Eastern Branch*

E. VAN SOMEREN, B.SC., F.INST.P., *Representing the Industrial Spectroscopy Group*

S. WHITEHEAD, PH.D., D.SC., M.I.E.E., F.INST.P., *Honorary Treasurer, The Institute of Physics*

R. G. WOOD, M.SC., A.M.I.E.E., F.INST.P.

D. A. WRIGHT, D.SC., F.INST.P., *Representing the Electronics Group*

CONTENTS OF VOLUME 6

JANUARY 1955

SPECIAL ARTICLE — PAGE

Some researches into the electrical conduction and breakdown of liquid dielectrics. By K. A. MACFADYEN . 1

ORIGINAL CONTRIBUTIONS

Thulium 170 for industrial radiography. By R. HALMSHAW . 8
A direct method of phase measurement on the cathode-ray tube. By D. KARO . 10
The calculation of voltage surges in a Van de Graaff generator. By B. MILLAR . 13
The calculation of heat flow through disks and its application to conductivity measurements. By J. C. JAEGER and A. BECK . 15
A method of identifying double-flash exposures. By N. DOMBROWSKI . 17
Heat transfer through oxide-cathode materials. By A. E. PENGELLY . 18
The rubber membrane and the solution of Laplace's equation. By W. FULOP . 21
The preparation of uniform plastic films. By R. S. M. REVELL and A. W. AGAR . 23
On the representation of rheological results with special reference to creep and relaxation. By P. FELTHAM . 26
Comparison of radioactivities by the use of X-ray film. By A. N. DAVENPORT and G. W. W. STEVENS . 31
The laminar flow of suspensions in tubes. By T. V. STARKEY . 34

NOTES AND NEWS

New books . 38

Notes and comments . 40

FEBRUARY 1955

ORIGINAL CONTRIBUTIONS

Some dynamic mechanical properties of polyisobutylene over a wide temperature range. By D. A. THOMAS and D. W. ROBINSON . 41
Some properties of a simple omegatron-type mass spectrometer. By A. G. EDWARDS . 44
The physical and computing significance of an electrical analogue of creep and recovery. By A. J. KENNEDY . 49
The field due to an infinite dielectric cylinder between two parallel conducting planes. By C. MACK . 59
Growth of the barium orthosilicate interface of oxide-coated cathodes. By M. G. HARWOOD and N. FRY . 62
Phase and amplitude balance methods for permittivity measurements between 4 and 50 cm. By T. J. BUCHANAN and E. H. GRANT . 64

NOTES AND NEWS

Correspondence:

Probe impedance in the electrolytic tank. From J. C. BURFOOT . 67
Electrical dehydration of tar emulsions. From H. A. HOWE and C. A. R. PEARCE . 68

New books . 70

Notes and comments . 72

MARCH 1955

ORIGINAL CONTRIBUTIONS — PAGE

The measurement by ionization methods of the peak kilovoltage across X-ray tubes. By J. R. GREENING . 73
Elastic work involved in rolling a sphere on another surface. By D. TABOR . 79
Role of partition coefficient in permeability of surface layers with low diffusion coefficient. By G. R. LESTER . 82
Studies of the viscosity and sedimentation of suspensions. Part 3.—The sedimentation of isometric and compact particles. By S. GUREL, S. G. WARD and R. L. WHITMORE . 83
The resistance of an elliptic plate. By E. E. JONES . 88
The estimation of the specific surface of a soil from mechanical analysis data. By J. R. H. COUTTS . 90
Formulae for the transformation of indices in twinned crystals. By K. W. ANDREWS and W. JOHNSON . 92
Ionic bombardment heating of magnetron cathodes. By A. E. BARRINGTON . 96
Single exposure photography of a high speed event. By K. R. TUSON . 99
A method of measuring the intensity distributions of radio-frequency electric and magnetic fields in resonant cavities. By J. G. LINHART and T. H. B. BAKER . 100
Some lithium iodide phosphors for slow neutron detection. By K. P. NICHOLSON and G. F. SNELLING . 104

NOTES AND NEWS

Correspondence:

Electric breakdown at very low gas pressures. From J. W. LEECH . 107
A method of making silicon junction diodes. From J. W. GRANVILLE . 109

New books . 110

Notes and comments . 112

APRIL 1955

ORIGINAL CONTRIBUTIONS

The electrical conductivity and permittivity of mixtures, with special reference to emulsions of water in fuel oil. By C. A. R. PEARCE . 113
Effect of low temperature on the stability of permanent magnets. By A. G. CLEGG . 120
The cracking of layers of brittle material by differential strains. By D. J. MILLARD . 124
High-frequency plasma-electron oscillations. By K. G. EMELEUS and R. A. BAILEY . 127
The solution of transient heat flow and heat transfer problems by relaxation. By G. LIEBMANN . 129
Measurement of mass transfer by an electrical conductivity method. By E. W. GAYLORD and W. FORSTALL . 135
Low-frequency dynamic response of photosensitive neon discharge tubes. By T. J. DILLON . 138

NOTES AND NEWS

Correspondence:

A rubber-membrane model for axially-symmetric electric fields. From B. J. MAYO . 141

New books . 142

Notes and comments . 144

PAGE

MAY 1955

ORIGINAL CONTRIBUTIONS

The solution of plane stress problems by an electrical analogue method. By G. LIEBMANN . . . 145
The resistivity of thin metallic films. By D. E. CLARK . 158
Desorption of gas in the cold cathode ionization gauge. By E. BROWN and J. H. LECK 161
The rheology of Portland cement pastes. By G. H. TATTERSALL 165
X-ray emission spectroscopy with electron excitation covering elements $_4Be$–$_{92}U$. By G. L. MACDONALD and M. G. HARWOOD 168
A two-state light activated circuit element using germanium. By J. W. GRANVILLE 172
An analogue study of the temperature distribution in cooled gas-turbine blades. By C. F. KETTLEBOROUGH 174
The orientation of fibres in an electric field. By J. O. ISARD 176

NOTES AND NEWS

Correspondence:

The study of semiconductor crystal perfection by X-ray diffraction methods. From P. J. HOLMES . . . 180
A simple and rapid method of measuring the complex permittivity of a liquid. From E. H. GRANT . . 181
The thermal conductivity of some technical materials at low temperatures. From R. BERMAN, E. L. FOSTER and H. M. ROSENBERG 181

New books 183

Notes and comments 184

JUNE 1955

SPECIAL ARTICLE

Electronic fluctuations in semiconductors. By R. E. BURGESS 185

ORIGINAL CONTRIBUTIONS

A replica technique for "reflexion" electron microscopy. By D. E. BRADLEY 191
Conditions for aperiodicity in linear systems. By A. T. FULLER 195
Rheological behaviour of continuously sheared polythene. By W. F. O. POLLETT 199
Forming procedures for silicon point-contact transistors. By J. W. GRANVILLE, W. BARDSLEY and A. F. GIBSON . 206
Measurement of the statistical time lag of breakdown in gases and liquids. By R. F. SAXE and T. J. LEWIS . 211
Indium antimonide as a fluxmeter material. By E. W. SAKER, F. A. CUNNELL and J. T. EDMOND . . . 217
The disturbance of stress in an infinite plate by a lemniscate-shaped hole. By W. SNOWDON 220

NOTES AND NEWS

Correspondence:

Motion of water droplets of an emulsion in a non-uniform field. From C. BEZEMER and G. A. CROES; C. A. R. PEARCE 224

Notes and comments 226

JULY 1955

SPECIAL ARTICLE

Čerenkov radiation and its applications. By J. V. JELLEY 227

PAGE

ORIGINAL CONTRIBUTIONS

Time-lag data for spark discharges in uniform field gaps. By A. AKED, F. M. BRUCE and D. J. TEDFORD . . . 233
The resistance of the oxide-coated cathode at ultra high frequences. By L. J. HERBST and J. E. HOULDIN . 236
The sedimentation of suspensions of spheres. By R. L. WHITMORE 239
A general mathematical treatment applicable to certain electrode systems. By G. POWER 245
Electrode shapes for a cylindrical electron beam. By P. N. DAYKIN 248
A germanium point-contact transistor to operate at high ambient temperatures. By A. F. GIBSON, J. W. GRANVILLE and W. BARDSLEY 251
The determination of the dynamic properties of crystal diodes. By G. STUART-MONTEITH 254
Measurement of the pressure distribution between rollers in contact. By G. J. PARISH 256

NOTES AND NEWS

Correspondence:

Thulium 170 for industrial radiography. From K. LIDÉN and N. STARFELT: R. HALMSHAW 262
Radiation from a hollow cylinder. From M. G. ROSSMANN 262

New books 264

AUGUST 1955

SPECIAL ARTICLE

Mass transfer theories of fuel bed combustion. By R. S. SILVER and R. W. MACKAY 267

ORIGINAL CONTRIBUTIONS

Changes in the structure of oxide cathodes at high temperatures. By H. P. ROOKSBY 272
Identification of materials by electron diffraction in the electron microscope. By H. I. MATTHEWS and H. WILMAN 277
The flexural vibrations of an end-loaded vertical strip. By R. F. S. HEARMON and E. H. ADAMS 280
Phenomenological approach to "current noise." By D. A. BELL 284
Electron liberation by low energy ions at metal surfaces and in gases. By H. FETZ 288
The square wave response method of analysing process control systems. By L. MANDEL 291

NOTES AND NEWS

New books 297

Notes and comments 300

SEPTEMBER 1955

SPECIAL ARTICLE

Alloys for use at high temperatures. By W. BETTERIDGE 301

ORIGINAL CONTRIBUTIONS

An attempt to simplify coding for the Manchester electronic computer. By R. A. BROOKER 307
Instability of photomultipliers. By L. P. DE VALENCÉ . 311
A polarized light study of glass fibre laminates. By G. A. HORRIDGE 314
The appearance of some oscillating discharges. By T. K. ALLEN, R. A. BAILEY and K. G. EMELEUS . . . 320

PAGE

The measurement of elastic wave velocity in small cylindrical specimens. By N. B. TERRY and H. J. WOODS . 322
Thermal constants of pyrophyllite and their change on heating. By A. E. CARTE 326
Discontinuities in the saturation curves of vacuum photocells. By J. S. PRESTON and G. W. GORDON-SMITH . 329
Photoelectric recording of reflected echelon fringes. By T. A. LITTLEFIELD 333
Millimicrosecond exposures by image tubes. By R. F. SAXE and R. A. CHIPPENDALE 336

NOTES AND NEWS

New books 339

Notes and comments 342

OCTOBER 1955

ORIGINAL CONTRIBUTIONS

The diffuse reflexion of silver atoms at a metallic target at high temperature. By S. CHOMET and J. YARWOOD . 343
Air circulations about a vibrating plate. By M. D. WALLER 347
Plastic flow in coal. By P. C. NEWMAN 348
The determination of the order of interference in white light. By R. C. FAUST and H. J. MARRINAN . . 351
The use of electronic analogue computers with resistance network analogues. By W. J. KARPLUS 356
The permittivity of two phase mixtures. By C. A. R. PEARCE 358
Transient heat conduction in multiphase media. By J. H. WEINER 361
Measurement of metallurgical equilibria by thermal conductivity gas analysis. By J. W. EVANS . . . 364
An X-ray method for studying radial current distributions in electron beams. By J. S. THORP 366
A thermally triggered spark gap. By T. E. BROADBENT and J. K. WOOD 368
Initiation of hot-cathode discharges. By N. R. DALY and K. G. EMELEUS 370

NOTES AND NEWS

New books 373

Notes and comments 375

NOVEMBER 1955

CONFERENCE REPORT

Summarized proceedings of a conference on the structures and textures of metals—London, October, 1954. By K. ROBINSON and E. G. STEWARD 377

ORIGINAL CONTRIBUTIONS

Reduction of noise in photoconductive cells. By R. E. BURGESS 385
Determination of the velocity of ultrasonic vibrations in molten salts. By N. E. RICHARDS, E. J. BRAUNER and J. O'M. BOCKRIS 387
The scanning electron microscope and its fields of application. By K. C. A. SMITH and C. W. OATLEY . . . 391
Stability criteria for an electrical or mechanical system with distributed parameters. By A. S. GLADWIN . . 400
Creep and static friction. By R. T. SPURR 402

PAGE

The capacity and field of a cylindrical trough with a plane conductor in the axial plane of symmetry. By H. J. PEAKE and N. DAVY 404

NOTES AND NEWS

New books 409

Notes and comments 412

DECEMBER 1955

SPECIAL ARTICLE

Industrial applications of ultrasonics. By E. G. RICHARDSON 413

ORIGINAL CONTRIBUTIONS

The thermal conductivity of liquid and gaseous oxygen. By H. ZIEBLAND and J. T. A. BURTON 416
Propagation of transient fields from dipoles near the ground. By H. PORITSKY 421
Technical properties of iron powder magnets. By E. H. CARMAN 426
A simple adaptation of the carbon replica technique for the examination of selected areas in the electron microscope. By D. E. BRADLEY 430
The influence of cathode standing waves on valve stability. By W. W. H. CLARKE 433
The deposition of thin films of gold on cylindrical specimens by sputtering. By F. R. LIPSETT . . . 442
The γ-ray spectrum of fission products from slow neutron irradiation of uranium 235. By D. H. PEIRSON . . 444

NOTES AND NEWS

Correspondence:

Conditions for aperiodicity in linear systems. From R. H. MACMILLAN; A. T. FULLER 450
The flexural vibrations of an end-loaded vertical strip. From J. P. ELLINGTON 451
The orientation of fibres in an electric field. From S. WHITEHEAD; P. LAROSE; J. O. ISARD 452

New books 453

Notes and comments 454

SUPPLEMENT No. 4

LUMINESCENCE

Paper *Page*

The development of luminescence since the 1938 Oxford Conference. By S. T. HENDERSON . . . . S 1
Some unsolved problems in luminescence. By J. W. STRANGE . . . . . S 4
1. Applied cathodoluminescence. By C. G. A. HILL . S 6
2. Preparation and characteristics of calcium halophosphates. By M. DOHERTY and W. HARRISON . . S 11
3. The investigation of new phosphors, with particular reference to the pyrophosphates. By P. W. RANBY, D. H. MASH and S. T. HENDERSON . . . . S 18
4. The luminescent properties and crystal structure of some new phosphor systems. By A. H. MCKEAG and E. G. STEWARD . . . . . S 26

Paper	*Page*
5. Some unusual phosphors. By S. ROTHSCHILD	S 32
6. Electroluminescence of zinc sulphide phosphors. By K. H. BUTLER and J. F. WAYMOUTH	S 33
7. The mechanism of electroluminescence of zinc sulphide. By W. W. PIPER and F. E. WILLIAMS	S 39
8. Brightness waveforms in electroluminescence. By Prof. G. DESTRIAU	S 49
9. Electroluminescence of organic compounds. By A. BERNANOSE	S 54
10. Some experimental results on electroluminescence. By A. LUYCKX and A. J. STOKKINK	S 57
11. The physical chemistry of sulphide phosphors. By F. A. KROGER	S 58
12. Physical measurement and the nature of the luminescent centre. By J. H. SCHULMAN	S 64
13. Energy transfers in the calcium halophosphate phosphors. By G. R. FONDA	S 69
14. Divalent manganese as a luminescent centre. By C. C. KLICK	S 74
15. Atomic configurations in luminescent centres. By W. A. RUNCIMAN	S 78
16. Absorption, emission and storage of energy in phosphors. By G. F. J. GARLICK	S 85
17. Luminescence and electrical conductivity of crystal phosphors. By I. BROSER and R. BROSER-WARMINSKY	S 90
18. Use of radioactive isotopes for research on inorganic phosphors. By E. GRILLOT and M. BANCIE-GRILLOT	S 95
19. Theory of activator systems in luminescent solids. By F. E. WILLIAMS	S 97
20. Excitation of phosphors by electrons. By G. F. J. GARLICK	S 103
21. Nonlinearity in photoconducting phosphors. By C. A. DUBOC	S 107
SUBJECT INDEX TO LUMINESCENCE	S 112
NAME INDEX TO LUMINESCENCE	S 117
SUBJECT INDEX TO VOLUME 6	
AUTHOR INDEX TO VOLUME 6	

INDEX TO VOLUME 6

SUBJECT INDEX

Acoustical terms, Glossary of 412
Alloys for use at high temperatures 301
Amplitude balance methods, Phase and, for permittivity measurements between 4 and 50 cm 64
Analogue
computers, electronic, The use of, with resistance network analogues 356
, electrical, The physical and computing significance of an, of creep and recovery 49
, electrical, The solution of plane stress problems by an, method 145
study of the temperature distribution in cooled gas-turbine blades, An 174
Aperiodicity in linear systems, Conditions for 195, 450
Atomic energy, peaceful uses of, Proceedings of the Geneva conference on the 375
Atoms, silver, The diffuse reflexion of, at a metallic target at high temperature 343
Availability of places for students in universities and technical colleges, The 375

Barium orthosilicate interface of oxide-coated cathodes, Growth of the 62
Beam, cylindrical electron, Electrode shapes for a 248
Beams, electron, An X-ray method for studying radial current distributions in 366
Blades, cooled gas-turbine, An analogue study of the temperature distribution in 174
Bombardment heating, Ionic, of magnetron cathodes 96
Books, New
Abstracts of the literature on semiconducting and luminescent materials and their applications 453
Advances in electronics and electron physics, Vol. 6 297
An advance treatise on physical chemistry, Vol. 5, *Molecular spectra and structure dielectrics and dipole moments* 143
Analytical chemistry—the working tools (Vols. 1 and 2) 411
Applied geophysics in the search for minerals 143
Applied mass spectrometry 265
Applied X-rays 373
Atlas of typical expansion chamber photographs, An 70
Atomic energy research at Harwell 340
Behaviour of metals under impulsive loads 298
Beta- and gamma-spectroscopy 409
Design and analysis of industrial experiments, The 265
Dielectric materials and applications 297
Dynamical theory of crystal lattices 264
Einführung in die Quantenelektrodynamik 410
Electrical characteristics of overhead lines 339
Electroacoustics—the analysis of transduction, and its historical background 266
Elektronische Halbleiter 341
Engineering dynamics, Vol. 1, *Theory of elasticity: analytical and experimental methods* 299
Vol. 3, *Steam turbines* 71
Vol. 4, *Internal-combustion engines* 374
Errors of observation and their treatment 453
Fatigue tests on rolled alloy steels made in electric openhearth furnaces 266
Ferromagnetic domains 39
Fluorescence analysis in ultra-violet light 39
Fundamentals of radiobiology 340
Gyroscope applied, The 299
Books, New (*continued*)
Handbook on electrical characteristics of overhead lines 339
Heat and Cold, Part II, *Descriptive catalogue of exhibits in the Science Museum* 143
Higher transcendental functions, Vol. 3 409
Humidity 453
Hydraulic systems and equipment 70
Insulation of electrical equipment, The 39
International Scientific Radio Union (*URSI*): Special Report No. 4. *The distribution of radio brightness on the solar disk*. Special Report No. 5. *Interstellar hydrogen* 111
Introduction to atomic and nuclear physics 373
Introduction to nuclear engineering 374
Inventor of the valve, The 297
Laplace transforms for electrical engineers 39
Linear feedback analysis 453
Linearized theory of steady high-speed flow 298
Magnetic cooling 142
Mass spectrometry 142
Massbalancing of aircraft control surfaces 183
Mathematics of engineering systems 111
Metallurgy of the rarer metals, Vol. 3, *Manganese* 410
Molecular theory of gases and liquids 110
Noise and stochastic processes 111
Notes on applied science, No. 6, *Volumetric glassware* 71
No. 8, *Audio frequency power measurements* 183
No. 9, *Measurements of pressure with the mercury barometer* 265
Nuclear physics 298
Occasional Notes, No. 16, *Radio astronomy* 71
Optical properties of thin solid films 299
Optics: lectures in theoretical physics (Vol. 4) 183
Physical meteorology 38
Physics of experimental method, The 143
Physics of fibres 453
Physics of the ionosphere, The, 1954 410
Principles of modern acoustics 183
Proceedings of the Eleventh General Assembly of the International Scientific Radio Union, Part 1, "*On radio measurements and standards*" 409
Proceedings of the third meeting of the joint commission on radiometeorology 299
Progress in biophysics and biophysical chemistry, Vol. 5 339
Progress in low temperature physics 298
Progress in metal physics, Vol. 5 110
Progress in nuclear physics, Vol. 4 341
Progress in photography, Vol. 2 374
Protective wrappings 374
Quantum mechanics 70
Quantum theory of solids 410
Radio, Vol. 2 111
Radiobiology symposium, 1954 340
Radioisotope conference, 1954 110, 142
Rohrhydraulik 71
Selected meteorological papers of Sir Napier Shaw, F.R.S. 453
Sensations of tone 71
Sensitometry 339
Solar system, The, Vol. 2, *The earth as a planet* 411
Some aspects of the crystallization of high polymers 410
Sonics. Techniques for the use of sound and ultrasound in engineering and science 339

For *Luminescence* and cognate subjects *see also* separate index to the supplement

Books, New (*continued*)
Strömung durch Rohre, Umströmung von Körpern bei zweidimensionaler Strömung, Umströmung von Körpern bei raumlicher Strömung 373
Structure Reports for 1950 (Vol. 13) 38
Temperature measurement and control, Part 11, *Descriptive catalogue of exhibits in the Science Museum* 409
Text-book of radar, A 38
Theoretical structural metallurgy 409
Theory of cohesion, The 142
Theory of lenses 110
Transistoren 38
Transistors, theory and applications 266
Wool, its chemistry and physics 70
Wool research 1918–1954, Vol. 3, *Testing and Control* 266
X-ray diffraction of polycrystalline materials 183
X-ray diffraction procedures for polycrystalline and amorphous materials 264
Breakdown
, electric, at very low gas pressures 107
in liquids and gases, Measurement of the statistical time lag of 211
of liquid dielectrics, Some researches into the electrical conduction and 1
British
Nuclear Energy Conference 300
Standards Institution 454
Brittle material, cracking of layers of, by differential strains, The 124

Capacity and field of a cylindrical trough with a plane conductor in the axial plane of symmetry 404
Carbon replica technique, A simple adaptation of the, for the examination of selected areas in the electron microscope 430
Cathode
, cold, ionization gauge, Desorption of gas in the 161
, oxide-coated, The resistance of the, at ultra high frequencies 236
, oxide-, materials, Heat transfer through 18
-ray tube, A direct method of phase measurement on the 10
standing waves, The influence of, on valve stability 433
Cathodes,
magnetron, Ionic bombardment heating of 96
oxide, Changes in the structure of, at high temperatures 272
oxide-coated, Growth of the barium orthosilicate interface of 62
Cavities, resonant, A method of measuring the intensity distributions of radio-frequency electric and magnetic fields in 100
Cells, photoconductive, Reduction of noise in 385
Cement pastes, Portland, The rheology of 165
Čerenkov radiation and its applications 227
Circuit element, A two-state light activated, using germanium 172
Circulations, Air, about a vibrating plate 347
Coal, Plastic flow in 348
Coding, An attempt to simplify, for the Manchester electronic computer 307
Combustion
fuel bed, Mass transfer theories of 267
, Joint conference on 112
Computer, Manchester electronic, An attempt to simplify coding for the 307
Computers, analogue, electronic, The use of, with resistance network analogues 356
Computing significance, The physical and, of an electrical analogue of creep and recovery 49
Conduction,
electrical, and breakdown of liquid dielectrics, Some researches into the 1
Transient heat, in multiphase media 361
Conductivity
, electrical, and permittivity of mixtures, with special reference to emulsions of water in fuel oil, The 113
, electrical, Measurement of mass transfer by an, method 135
measurements, The calculation of heat flow through disks and its application to 15
, thermal, gas analysis, Measurement of metallurgical equilibria by 364
, thermal, of liquid and gaseous oxygen, The 416
, thermal, of some technical materials at low temperatures, The 181
Conference
, British Nuclear Energy 300
on combustion, Joint 112
on illumination and wear 376
on mass spectrometry 72
on plant and process dynamic characteristics 412
on the peaceful uses of atomic energy, Proceedings of the Geneva 375
on the production and utilization of electromagnetically enriched isotopes 144
on the structures and textures of metals—London, October 1954, Summarized proceedings of a 377
Control systems, process, The square wave response method of analysing 291
Convention, Plastics exhibition and 184
Cracking of layers of brittle material by differential strains 124
Creep and
recovery, The physical and computing significance of an electrical analogue of 49
relaxation, On the representation of rheological results with special reference to 26
static friction 402
Crystal
diodes, The determination of the dynamic properties of 254
perfection, Semiconductor, by X-ray diffraction methods, The study of 180
Crystals, twinned, Formulae for the transformation of indices in 92
"Current noise," Phenomenological approach to 284
Cylinder,
hollow, Radiation from a 262
infinite dielectric, between two parallel conducting planes, The field due to an 59
Cylindrical specimens, small, The measurement of elastic wave velocity in 322

Data, mechanical analysis, The estimation of the specific surface of a soil from 90
Dehydration, Electrical, of tar emulsions 68
Deposition of thin films of gold on cylindrical specimens by sputtering, The 442
Desorption of gas in the cold cathode ionization gauge 161
Dielectric cylinder, infinite, between two parallel conducting planes, The field due to an 59
Dielectrics, liquid, Some researches into the electrical conduction and breakdown of 1
Diffraction, electron, Identification of materials by, in the electron microscope 277
Diodes,
crystal, The determination of the dynamic properties of 254
silicon junction, A method of making 112
Dipoles near the ground, Propagation of transient fields from 421
Discharges,
hot-cathode, Initiation of 370
oscillating, The appearance of some 320
spark, Time-lag data for, in uniform field gaps 233
Discontinuities in the saturation curves of vacuum photocells 329
Disks, The calculation of heat flow through, and its application to conductivity measurements 15

For *Luminescence* and cognate subjects *see also* separate index to the supplement

Droplets, water, of an emulsion in a non-uniform field, Motion of 224
Duddell Medal, Award of the 144
Dynamic
characteristics, Conference on plant and process 412
properties of crystal diodes, The determination of the 254

Elastic
wave velocity in small cylindrical specimens, The measurement of 322
work involved in rolling a sphere on another surface 79
Electric
breakdown at very low gas pressures 107
field, The orientation of fibres in an 452
fields, A rubber-membrane model for axially-symmetric 141
Electrical or mechanical system with distributed parameters, Stability criteria for an 400
Electrode
shapes for a cylindrical electron beam 248
systems, A general mathematical treatment applicable to certain 245
Electrolytic tank, Probe impedance in the 67
Electron
beam, cylindrical, Electrode shapes for a 248
beams, An X-ray method for studying radial current distributions in 366
diffraction in the electron microscope, Identification of materials by 277
excitation covering elements $_4$Be-$_{92}$U, X-ray emission spectroscopy with 168
liberation by low energy ions at metal surfaces and in gases 288
microscope and its fields of application, The scanning 391
microscope, A simple adaptation of the carbon replica technique for the examination of selected areas in the 430
microscope, Identification of materials by electron diffraction in the 277
microscopy, "reflexion," A replica technique for 191
Electronic
analogue computers, The use of, with resistance network analogues 356
components for use in telecommunications, Review of 342
computer, Manchester, An attempt to simplify coding for the 307
Electronics exhibition 184
Elliptic plate, The resistance of an 88
Emulsion, Motion of water droplets of an, in a non-uniform field 224
Emulsions
of water in fuel oil, The electrical conductivity and permittivity of mixtures, with special reference to 113
, tar, Electrical dehydration of 68
End-loaded vertical strip, The flexural vibrations of an 280, 451
Equilibria, metallurgical, Measurement of, by thermal conductivity gas analysis 364
Exhibition
and convention, Plastics 184
, Electronics 184
of electrical standards and metering 342
of instruments and apparatus, The Physical Society's annual 40
of X-ray photography 375
, The Physical Society's 112
Excitation, electron, covering elements $_4$Be-$_{92}$U, X-ray emission spectroscopy with 168
Exposure photography, Single, of a high speed event 99
Exposures,
double-flash, A method of identifying 17, 144
Millimicrosecond, by image tubes 336

Fibre laminates, glass, A polarized light study of 314
Fibres in an electric field, The orientation of 176, 452
Field
due to an infinite dielectric cylinder between two parallel conducting planes, The 59
, electric, orientation of fibres in an, The 176
gaps, uniform, Time-lag data for spark discharges in 233
, non-uniform, Motion of water droplets of an emulsion in a 224
, The capacity and, of a cylindrical trough with a plane conductor in the axial plane of symmetry 404
Fields
in resonant cavities, A method of measuring the intensity distributions of radio-frequency electric and magnetic 100
, electric, axially-symmetric, A rubber-membrane model for 141
, Propagation of transient, from dipoles near the ground 421
Film, X-ray, Comparison of radioactivities by the use of 31
Films
of gold, The deposition of thin, on cylindrical specimens by sputtering 442
, thin metallic, The resistivity of 158
, uniform plastic, The preparation of 23
Fission products from slow neutron irradiation of uranium 235, The γ-ray spectrum of 444
Flash, double-, exposures, A method of identifying 17, 144
Flexural vibrations of an end-loaded vertical strip, The 280, 451
Flow,
laminar, of suspensions in tubes, The 34
Plastic, in coal 348
Fluctuations, Electronic, in semiconductors 185
Fluxmeter material, Indium antimonide as a 217
Friction, static, Creep and 402
Fringes, reflected echelon, Photoelectric recording of 333
Fuel oil, emulsions of water in, The electrical conductivity and permittivity of mixtures, with special reference to 113

Gamma-ray spectrum of fission products from slow neutron irradiation of uranium 235, The 444
Gas
analysis, Measurement of metallurgical equilibria by thermal conductivity 364
, Desorption of, in the cold cathode ionization gauge 161
-turbine blades, cooled, An analogue study of the temperature distribution in 174
Gases
and liquids, Measurement of the statistical time lag of breakdown in 211
, electrical discharges in, International symposium on 72
, Electron liberation by low energy ions at metal surfaces and in 288
Gauge, ionization, Desorption of gas in the cold cathode 161
Generator, Van de Graaff, The calculation of voltage surges in a 13
Geneva conference on the peaceful uses of atomic energy, Proceedings of the 375
Germanium
, A two-state light activated circuit element using 172
point-contact transistor to operate at high ambient temperatures, A 251
Glass fibre laminates, A polarized light study of 314
Gold, deposition of thin films of, on cylindrical specimens by sputtering, The 442

Heat
conduction, Transient, in multiphase media 361
flow through discs and its application to conductivity measurements, The calculation of 15
flow, transient, and heat transfer problems, The solution of, by relaxation 129
transfer through oxide-cathode materials 18
Heating, change on, Thermal properties of pyrophyllite and their 326

For *Luminescence* and cognate subjects *see also* separate index to the supplement

High
-frequency plasma-electron oscillations 127
temperature, The diffuse reflexion of silver atoms at a metallic target at 343
temperatures, Alloys for use at 301
Hole, lemniscate-shaped, The disturbance of stress in an infinite plate by a 220
Hot-cathode discharges, Initiation of 370

Image tubes, Millimicrosecond exposures by 336
Impedance, Probe, in the electrolytic tank 67
Indium antimonide as a fluxmeter material 217
Industrial radiography, Thulium 170 for 8
Instability of photomultipliers 311
Institute of Physics, The 226
Elections to 72, 144, 226, 412, 454
Instrument technology, Post-graduate courses in 184
Instruments, scientific, Safe transport of 376
Interface, barium orthosilicate, of oxide-coated cathodes, Growth of the 62
Interference in white light, The determination of the order of 351
Ionization
gauge, Desorption of gas in the cold cathode 161
methods, The measurement by, of the peak kilovoltage across X-ray tubes 73
Ions, low energy, Electron liberation by, at metal surfaces and in gases 288
Isotope School, Harwell 72
Isotopes, electromagnetically enriched, Conference on the production and utilization of 144

Journal of Electronics 375
Journal of Scientific Instruments, Prizes for original contributions published in the 300
Journal of Nuclear Energy 40
Journal of the Institution of Telecommunication Engineers 342

Kilovoltage, peak, The measurement by ionization methods of the, across X-ray tubes 73

Laminates, glass fibre, A polarized light study of 314
Laplace's equation, The rubber membrane and the solution of 21
Layers
of brittle material, Cracking of, by differential strains, The 124
, surface, with low diffusion coefficient, Role of partition coefficient in permeability of 82
Light-activated circuit element, two-state, using germanium, A 172
Light, white, The determination of the order of interference in 351
Linear systems, Conditions for aperiodicity in 195, 450
Liquid
, complex permittivity of a, A simple and rapid method of measuring the 181
dielectrics, Some researches into the electrical conduction and breakdown of 1
Liquids, gases and, Measurement of the statistical time lag of breakdown in 211
Lithium iodide phosphors for slow neutron detection, Some 104
Low temperature, Effect of, on the stability of permanent magnets 120
Low temperatures, thermal conductivity of some technical materials at, The 181
Lubrication and wear, Conference on 376

Magnetic materials, Symposium on 342
Magnets, iron powder, Technical properties of 426
Magnetron cathodes, Ionic bombardment heating of 96
Magnets, permanent, Effect of low temperature on the stability of 113
Manufacturers, British, Register of 40
Mass
spectrometer, Some properties of a simple omegatron-type 44
spectrometry, Conference on 72
transfer, Measurement of, by an electrical conductivity method 135
transfer theories of fuel bed combustion 267
Mathematical treatment, A general, applicable to certain electrode systems 245
Mechanical system with distributed parameters, Stability criteria for an electrical or 400
Membrane, rubber,
and the solution of Laplace's equation, The 21
model for axially-symmetric electric fields, A 141
Metal surfaces and in gases, Electron liberation by low energy ions at 288
Metallic target, at high temperature, The diffuse reflexion of silver atoms at a 343
Metals, Summarized proceedings of a conference on the structure and texture of—London, October 1954 377
Meteorological Office Annual Report for 1953–4 112
Metering, Exhibition of electrical standards and 342
Microscope, electron, *see* Electron microscope
Mixtures, two phase, The permittivity of 358
Multiphase media, Transient heat conduction in 361

Neon discharge tubes, photosensitive, Low-frequency dynamic response of 138
Neutron
detection, slow, Some lithium iodide phosphors for 104
irradiation of uranium 235, The γ-ray spectrum of fission products from slow 444
Noise Control 184
"Noise, current," Phenomenological approach to 284
Noise in photoconductive cells, Reduction of 385
Notes for prospective authors 454
Nuclear Energy Conference, British 300
Nuclear Energy, Journal of 40

Omegatron-type mass spectrometer, Some properties of a simple 44
Optics, physical, frontiers in, Symposium on 454
Orientation of fibres in an electric field, The 176, 452
Oscillating discharges, The appearance of some 320
Oscillations, High-frequency plasma-electron 127
Oxide
-cathode materials, Heat transfer through 18
cathodes, Changes in the structure of, at high temperatures 272
-coated cathode, The resistance of the, at ultra high frequencies 236
-coated cathodes, Growth of the barium orthosilicate interface of 62
Oxygen, liquid and gaseous, The thermal conductivity of 416

Papers for publication, Length of 375
Particle size analysis, The physics of (*errata*) 112
Particles, isometric and compact, The sedimentation of 83
Partition coefficient in permeability of surface layers with low diffusion coefficient, Role of 82
Pastes, Portland cement, The rheology of 165
Peak kilovoltage across X-ray tubes, The measurement by ionization methods of the 73
Permeability of surface layers with low diffusion coefficient, Role of partition coefficient in 82
Permittivity
, complex, of a liquid, A simple and rapid method of measuring the 181

For *Luminescence* and cognate subjects *see also* separate index to the supplement

Permittivity (*continued*)
measurements between 4 and 50 cm, Phase and amplitude balance methods for 64
of mixtures, The electrical conductivity and, with special reference to emulsions of water in fuel oil 113
of two phase mixtures, The 358
Phase and amplitude balance methods for permittivity measurements between 4 and 50 cm 64
Physical Society's annual exhibition of instruments and apparatus, The 40, 112
Physics students in universities and technical colleges, The availability of places for 375
Phosphors, Some lithium iodide, for slow neutron detection 104
Photocells, vacuum, Discontinuities in the saturation curves of 329
Photoconductive cells, Reduction of noise in 385
Photoelectric recording of reflected echelon fringes 333
Photography,
Single exposure, of a high speed event 99
X-ray, Exhibition of 375
Photomultipliers, Instability of 311
Photosensitive neon discharge tubes, Low-frequency dynamic response of 138
Places for physics students in universities and technical colleges, The availability of 375
Planes, parallel conducting, The field due to an infinite dielectric cylinder between two 59
Plant and process dynamic characteristics, Conference on 412
Plasma-electron oscillations, High-frequency 127
Plastic
films, uniform, The preparation of 23
flow in coal 348
Plastics exhibition and convention 184
Plate,
elliptic, The resistance of an 88
infinite, The disturbance of stress in an, by a lemniscate-shaped hole 220
vibrating, Air circulations about a 347
Polarized light study of glass fibre laminates, A 314
Polyisobutylene, Some dynamic mechanical properties of, over a wide temperature range 41
Polythene, continuously sheared, Rheological behaviour of 199
Portland cement pastes, The rheology of 165
Post-graduate courses in instrument technology 184
Powder magnets, iron, Technical properties of 426
Pressure distribution between rollers in contact, Measurement of the 256
Prizes for original contributions published in the *Journal of Scientific Instruments* 300
Process
control systems, The square wave response method of analysing 291
dynamic characteristics, Conference on plant and 412
Propagation of transient fields from dipoles near the ground 421
Protection, Radiological 300
Publication, Length of papers for 375
Pyrophyllite, Thermal constants of, and their change on heating 326

Radiation
, Čerenkov, and its applications 227
from a hollow cylinder 262
Radioactivities, Comparison of, by the use of X-ray film 31
Radio-frequency electric and magnetic fields in resonant cavities, A method of measuring the intensity distributions of 100
Radiography, industrial, Thulium 170 for 8, 262
Radiological protection 300
Radiology, Glossary of terms used in 342
Recording, Photoelectric, of reflected echelon fringes 333
Recovery, creep and, The physical and computing significance of an electrical analogue of 49
"Reflexion" electron microscopy, A replica technique for 191
Reflexion of silver atoms at a metallic target at high temperature, The diffuse 343
Relaxation,
creep and, On the representation of rheological results with special reference to 26
The solution of transient heat flow and heat transfer problems by 129
Resistance
network analogues, The use of electronic analogue computers with 356
of an elliptic plate, The 88
of the oxide-coated cathode at ultra high frequencies, The 236
Resistivity of thin metallic films, The 158
Rheological
behaviour of continuously sheared polythene 199
results, On the representation of, with special reference to creep and relaxation 26
Rheology of Portland cement pastes, The 165
Rollers in contact, Measurement of the pressure distribution between 256
Rolling a sphere on another surface, Elastic work involved in 79
Rubber membrane
and the solution of Laplace's equation, The 21
model for axially-symmetric electric fields, A 141

Saturation curves of vacuum photocells, Discontinuities in the 329
Scanning electron microscope and its fields of application, The 391
Sedimentation
of isometric and compact particles, The 83
of suspensions of spheres, The 239
Semiconducting materials and transistors—a bibliography 184
Semiconductor
crystal perfection by X-ray diffraction methods, The study of 180
symposium 375
Semiconductors, Electronic fluctuations in 185
Silicon
junction diodes, A method of making 112
point-contact transistors, Forming procedures for 206
Silver atoms, The diffuse reflexion of, at a metallic target at high temperature 343
Soil, The estimation of the specific suface of a, from mechanical analysis data 90
Spark
discharges in uniform gaps, Time-lag data for 233
gap, A thermally triggered 368
Spectroscopy, X-ray emission, with electron excitation covering elements $_4$Be-$_{92}$U 168
Sphere, Elastic work involved in rolling a, on another surface 79
Spheres, suspensions of, The sedimentation of 239
Sputtering, The deposition of thin films of gold on cylindrical specimens by 442
Square wave response method of analysing process control systems, The 291
Stability criteria for an electrical or mechanical system with distributed parameters 400
Standards, electrical, and metering, Exhibition of electrical 342
Static friction, Creep and 402
Strains, differential, The cracking of layers of brittle material by 124
Stress
, disturbance of, in an infinite plate by a lemniscate-shaped hole, The 220
problems, plane, The solution of, by an electrical analogue method 145

For *Luminescence* and cognate subjects *see also* separate index to the supplement

Strip, end-loaded vertical, The flexural vibrations of an 280, 451
Structure of oxide cathodes at high temperatures, Changes in the 272
Surface
, Elastic work involved in rolling a sphere on another 79
layers with low diffusion coefficient, Role of partition coefficient in permeability of 82
, specific, The estimation of, of a soil, from mechanical analysis data 90
Surfaces, metal, and in gases, Electron liberation by low energy ions at 288
Surges, voltage, in a Van de Graaff generator, The calculation of 13
Suspensions
in tubes, The laminar flow of 34
of spheres, The sedimentation of 239
, Studies of the viscosity and sedimentation of 83
Symposium
on electrical discharges in gases, International 72
on magnetic materials 342
, Semiconductor 375

Tar emulsions, Electrical dehydration of 68
Technical colleges, universities and, The availability of places for physics students in 375
Telecommunications, Review of electronic components for use in 342
Temperature distribution in cooled gas-turbine blades, An analogue study of the 174
Theories, Mass transfer of fuel bed combustion 267
Thermal
conductivity gas analysis, Measurement of metallurgical equilibria by 364
conductivity of liquid and gaseous oxygen, The 416
conductivity of some technical materials at low temperatures, The 181
constants of pyrophyllite and their change on heating 326
Thermally triggered spark gap, A 368
Thulium 170 for industrial radiography 8, 262
Time-lag
data for spark discharges in uniform field gaps 233
, statistical, Measurement of the, of breakdown in gases and liquids 211
Transfer,
heat, problems, transient heat flow and, The solution of, by relaxation 129
mass, Measurement of, by an electrical conductivity method 135
Transient fields, Propagation of, from dipoles near the ground 421
Transistor, germanium point-contact, to operate at high ambient temperatures, A 251
Transistors 184
, silicon point-contact, Forming procedures for 206
Transport, safe, of scientific instruments 376
Tube, cathode-ray, A direct method of phase measurement on the 10
Tubes,
image, Millimicrosecond exposures by 336
laminar flow of suspensions in, The 34

Ultrasonic vibrations in molten salts, Determination of the velocity of 387
Ultrasonics, Industrial applications of 413
Universities and technical colleges, The availability of places for students in 375
Uranium 235, The γ-ray spectrum of fission products from slow neutron irradiation, of 444

Vacuum photocells, Discontinuities in the saturation curves of 329
Valve stability, The influence of cathode standing waves on 433
Van de Graaff generator, The calculation of voltage surges in a 13
Velocity of ultrasonic vibrations in molten salts, Determination of the 387
Vibrations, flexural, of an end-loaded vertical strip, The 280, 451

Water
droplets of an emulsion in a non-uniform field, Motion of 224
, emulsions of, in fuel oil, The electrical conductivity and permittivity of mixtures, with special reference to 113
Wave velocity, elastic, in small cylindrical specimens, The measurement of 322
Waves, cathode standing, The influence of, on valve stability 433
Wear, lubrication and, Conference on 376
Vibrating plate, Air circulations about a 347

X-ray
diffraction methods, The study of semiconductor crystal perfection by 180
emission spectroscopy with electron excitation covering elements $_4$Be-$_{92}$U 168
film, Comparison of radioactivities by the use of 31
method for studying radial current distributions in electron beams, An 366
photography, Exhibition of 375
tubes, The measurement by ionization methods of the peak kilovoltage across 73

AUTHOR INDEX

Adams, E. H., *see under* Hearmon, R. F. S.
Agar, A. W., *see under* Revell, R. S. M.
Aked, A., F. M. Bruce and D. J. Tedford, Time-lag data for spark discharges in uniform field gaps 233
Allen, T. K., R. A. Bailey and K. G. Emeleus, The appearance of some oscillating discharges 320
Andrews, K. W., and W. Johnson, Formulae for the transformation of indices in twinned crystals 92

Bailey, R. A., *see under* Allen, T. K.
Bailey, R. A., *see under* Emeleus, K. G.
Baker, T. H. B., *see under* Linhart, J. G.
Bardsley, W., *see under* Gibson, A. F.
Bardsley, W., *see under* Granville, J. W.
Barrington, A. E., Ionic bombardment heating of magnetron cathodes 96
Beck, A., *see under* Jaeger, J. C.
Bell, D. A., Phenomenological approach to "current noise" 284
Berman, R., E. L. Foster and H. M. Rosenberg, The thermal conductivity of some technical materials at low temperatures 181
Betteridge, W., Alloys for use at high temperatures 301
Bezemer, C., and G. A. Croes, Motion of water droplets of an emulsion in a non-uniform field 224
Bockris, J. O'M., *see under* Richards, N. E.

For *Luminescence* and cognate subjects *see also* separate index to the supplement

Bradley, D. E., A replica technique for "reflexion" electron microscopy 191
A simple adaptation of the carbon replica technique for the examination of selected areas in the electron microscope 430
Brauner, E. J., *see under* Richards, N. E.
Broadbent, T. E., and J. K. Wood, A thermally triggered spark gap 368
Brooker, R. A., An attempt to simplify coding for the Manchester electronic computer 307
Brown, E., and J. H. Leck, Desorption of gas in the cold cathode ionization gauge 161
Bruce, F. M., *see under* Aked, A.
Buchanan, T. J., and E. H. Grant, Phase and amplitude balance methods for permittivity measurements between 4 and 50 cm 64
Burfoot, J. C., Probe impedance in the electrolytic tank 67
Burgess, R. E., Electronic fluctuations in semiconductors 185
Reduction of noise in photoconductive cells 385
Burton, J. T. A., *see under* Zeibland, H.

Carman, E. H., Technical properties of iron powder magnets 426
Carte, A. E., Thermal constants of pyrophyllite and their change on heating 326
Chippendale, R. A., *see under* Saxe, R. F.
Chomet, S., and J. Yarwood, The diffuse reflexion of silver atoms at a metallic target at high temperature 343
Clarke, D. E., The resistivity of thin metallic films 158
Clarke, W. W. H., The influence of cathode standing waves on valve stability 433
Clegg, A. G., Effect of low temperature on the stability of permanent magnets 120
Coutts, J. R. H., The estimation of the specific surface of a soil from mechanical analysis data 90
Croes, G. A., *see under* Bezemer, C.
Cunnell, F. A., *see under* Saker, E. W.

Daly, N. R., and K. G. Emeleus, Initiation of hot-cathode discharges 370
Davenport, A. N., and G. W. W. Stevens, Comparison of radioacitivities by the use of X-ray film 31
Davy, N., *see under* Peake, H. J.
Daykin, P. N., Electrode shapes for a cylindrical electron beam 248
Dillon, T. J., Low-frequency dynamic response of photosensitive neon discharge tubes 138
Dombrowski, N., A method of identifying double-flash exposures 17

Edmond, J. T., *see under* Saker, E. W.
Edwards, A. G., Some properties of a simple omegatron-type mass spectrometer 44
Ellington, J. P., The flexural vibrations of an end-loaded vertical strip 451
Emeleus, K. G., and R. A. Bailey, High-frequency plasma-electron oscillations 127
Emeleus, K. G., *see under* Allen, T. K.
Emeleus, K. G., *see under* Daly, N. R.
Evans, J. W., Measurement of metallurgical equilibria by thermal conductivity gas analysis 364

Faust, R. C., and H. J. Marrinan, The determination of the order of interference in white light 351
Feltham, P., On the representation of rheological results with special reference to creep and relaxation 26
Fetz, H., Electron liberation by low energy ions at metal surfaces and in gases 288
Forstall, W., *see under* Gaylord, E. W.
Foster, E. L., *see under* Berman, R.
Fry, N., *see under* Harwood, M. G.
Fuller, A. T., Conditions for aperiodicity in linear systems 195, 450
Fulop, W., The rubber membrane and the solution of Laplace's equation 21

Gaylord, E. W., and F. Forstall, Measurement of mass transfer by an electrical conductivity method 135
Gibson, A. F., J. W. Granville and W. Bardsley, A germanium point-contact transistor to operate at high ambient temperatures 251
Gibson, A. F., *see under* Granville, J. W.
Gladwin, A. S., Stability criteria for an electrical or mechanical system with distributed parameters 400
Gordon-Smith, G. W., *see under* Preston, J. S.
Grant, E. H., A simple and rapid method of measuring the complex permittivity of a liquid 181
Grant, E. H., *see under* Buchanan, T. J.
Granville, J. W., A method of making silicon junction diodes 109
A two-state light activated circuit element using germanium 172
Granville, J. W., W. Bardsley and A. F. Gibson, Forming procedures for silicon-point contact transistors 206
Granville, J. W., *see under* Gibson, A. F.
Greening, J. R., The measurement by ionization methods of the peak kilovoltage across X-ray tubes 73
Gurel, S., S. G. Ward and R. L. Whitmore, Studies of the viscosity and sedimentation of suspensions. Part 3.—The sedimentation of isometric compact particles 83

Halmshaw, R., Thulium 170 for industrial radiography 8, 262
Harwood, M. G., and N. Fry, Growth of the barium orthosilicate interface of oxide-coated cathodes 62
Harwood, M. G., *see under* Macdonald, G. L.
Hearmon, R. F. S., and Adams, E. H., The flexural vibrations of an end-loaded vertical strip 280
Herbst, L. J., and J. E. Houldin, The resistance of the oxide-coated cathode at ultra high frequencies 236
Holmes, P. J., The study of semiconductor crystal perfection by X-ray diffraction methods 180
Horridge, G. A., A polarized light study of glass fibre laminates 314
Houldin, J. E., *see under* Herbst, L. J.
Howe, H. A., and C. A. R. Pearce, Electrical dehydration of tar emulsions 68

Isard, J. O., The orientation of fibres in an electric field 176, 452

Jaeger, J. C., and A. Beck, The calculation of heat flow through disks and its application to conductivity measurements 15
Jelley, J. V., Čerenkov radiation and its applications 227
Johnson, W., *see under* Andrews, K. W.
Jones, E. E., The resistance of an elliptic plate 88

Karo, D., A direct method of phase measurement on the cathode-ray tube 10
Karplus, W. J., The use of electronic analogue computers with resistance network analogues 356
Kennedy, A. J., The physical and computing significance of an electrical analogue of creep and recovery 49
Kettelborough, C. F., An analogue study of the temperature distribution in cooled gas-turbine blades 174

Larose, P., The orientation of fibres in an electric field 452
Leck, J. H., *see under* Brown, E.
Leech, J. W., Electric breakdown at very low gas pressures 107

For *Luminescence* and cognate subjects *see also* separate index to the supplement

Lester, G. R., Role of partition coefficient in permeability of surface layers with low diffusion coefficient 82
Lewis, T. J., *see under* Saxe, R. F.
Lidén, K., and N. Starfelt, Thulium 170 for industrial radiography 262
Liebman, G., The solution of plane stress problems by an electrical analogue method 145
The solution of transient heat flow and heat transfer problems by relaxation 129
Linhart, J. G., and T. H. B. Baker, A method of measuring the intensity distributions of radio-frequency electric and magnetic fields in resonant cavities 100
Lipsett, F. R., The deposition of thin films of gold on cylindrical specimens by sputtering 442
Littlefield, T. A., Photoelectric recording of reflected echelon fringes 333

Macdonald, G. L., and Harwood, M. G., X-ray emission spectroscopy with electron excitation covering elements $_4$Be-$_{92}$U 168
Macfadyen, K. A., Some researches into the electrical conduction and breakdown of liquid dielectrics 1
Mack, C., The field due to an infinite dielectric cylinder between two parallel conducting planes 59
Mackay, R. W., *see under* Silver, R. S.
Macmillan, R. H., Conditions for aperiodicity in linear systems 450
Mandel, L., The square wave response method of analysing process control systems 291
Marrinan, H. J., *see under* Faust, R. C.
Matthews, H. I., and H. Wilman, Identification of materials by electron diffraction in the electron microscope 277
Mayo, B. J., A rubber-membrane model for axially-symmetric electric fields 141
Millar, B., The calculation of voltage surges in a Van de Graaff generator 13
Millard, D. J., The cracking of layers of brittle material by differential strains 124

Newman, P. C., Plastic flow in coal 348
Nicholson, K. P., and G. F. Snelling, Some lithium iodide phosphors for slow neutron detection 104

Oatley, C. W., *see under* Smith, K. C. A.

Parish, G. J., Measurement of the pressure distribution between rollers in contact 256
Peake, H. J., and N. Davy, The capacity and field of a cylindrical trough with a plane conductor in the axial plane of symmetry 404
Pearce, C. A. R., Motion of water droplets of an emulsion in a non-uniform field 224
The electrical conductivity and permittivity of mixtures with special reference to emulsions of water in fuel oil 113
The permittivity of two phase mixtures 358
Peirson, D. H., The γ-ray spectrum of fission products from slow neutron irradiation of uranium 235 444
Pengelly, A. E., Heat transfer through oxide-cathode materials 18
Pollett, W. F. O., Rheological behaviour of continuously sheared polythene 199
Poritsky, H., Propagation of transient fields from dipoles near the ground 421
Power, G., A general mathematical treatment applicable to certain electrode systems 245
Preston, J. S., and G. W. Gordon-Smith, Discontinuities in the saturation curves of vacuum photocells 329
Revell, R. S. M., and A. W. Agar, The preparation of uniform plastic films 23
Richards, N. E., E. J. Brauner and J. O'M. Bockris, Determination of the velocity of ultrasonic vibrations in molten salts 387
Richardson, E. G., Industrial applications of ultrasonics 413
Robinson, D. W., *see under* Thomas, D. A.
Robinson, K., and E. G. Steward, Summarized proceedings of a conference on the structures and textures of metals—London, October 1954 377
Rooksby, H. P., Changes in the structure of oxide cathodes at high temperatures 272
Rosenberg, H. M., *see under* Berman, R.
Rossmann, M. G., Radiation from a hollow cylinder 262

Saker, E. W., F. A. Cunnell and J. T. Edmond, Indium antimonide as a fluxmeter meterial 217
Saxe, R. F., and R. A. Chippendale, Millimicrosecond exposures by image tubes 336
Saxe, R. F., and T. J. Lewis, Measurement of the statistical time lag of breakdown in gases and liquids 211
Silver, R. S., and R. W. Mackay, Mass transfer theories of fuel bed combustion 267
Smith, K. C. A., and C. W. Oatley, The scanning electron microscope and its fields of application 391
Snelling, G. F., *see under* Nicholson, K. P.
Snowdon, W., The disturbance of stress in an infinite plate by a lemniscate-shaped hole 220
Spurr, R. T., Creep and static friction 402
Starfelt, N., *see under* Lidén, K.
Starkey, T. V., The laminar flow of suspensions in tubes 34
Stevens, G. W. W., *see under* Davenport, A. N.
Steward, E. G., *see under* Robinson, K.
Stuart-Monteith, G., The determination of the dynamic properties of crystal diodes 254

Tabor, D., Elastic work involved in rolling a sphere on another surface 79
Tattersall, G. H., The rheology of Portland cement pastes 165
Tedford, D. J., *see under* Aked, A.
Terry, N. B., and H. J. Woods, The measurement of elastic wave velocity in small cylindrical specimens 322
Thomas, D. A., and D. W. Robinson, Some dynamic mechanical properties of polyisobutylene over a wide temperature range 41
Thorp, J. S., An X-ray method for studying radial current distributions in electron beams 366
Tuson, K. R., Single exposure photography of a high speed event 99

de Valencé, L. P., Instability of photomultipliers 311

Waller, M. D., Air circulation about a vibrating plate 347
Ward, S. G., *see under* Gurel, S.
Weiner, J. H., Transient heat conduction in multiphase media 361
Whitehead, S., The orientation of fibres in an electric field 452
Whitmore, R. L., The sedimentation of suspensions of spheres 239
Whitmore, R. L., *see under* Gurel, S.
Wilman, H., *see under* Matthews, H. I.
Wood, J. K., *see under* Broadbent, T. E.
Woods, H. J., *see under* Terry, N. B.

Yarwood, J., *see under* Chomet, S.

Zeibland, H., and J. T. A. Burton, The Thermal conductivity of liquid and gaseous oxygen 416

For *Luminescence* and cognate subjects *see also* separate index to the supplement

PRINTED IN GREAT BRITAIN BY UNWIN BROTHERS LIMITED, WOKING AND LONDON

SPECIAL ARTICLE

Some researches into the electrical conduction and breakdown of liquid dielectrics*

By K. A. MACFADYEN, M.Sc., F.Inst.P., Department of Physics, University of Birmingham

A résumé of work on the subject up to 1946 is given followed by a brief account of researches in the Department of Physics, University of Birmingham. A discussion of some related contemporary work is included.

1. INTRODUCTION

The chief aim of this paper is to present a short account of the work with which the author has been connected at Birmingham, but in order to allow readers to see how this fits into the general state of knowledge on this subject a review of previous and contemporary work will be included.

Insulating liquids, particularly oils, have received a considerable measure of attention during the present century on account of their technical importance in electrical engineering. A review[1] of the earlier part of this period is quite unsuggestive of any basic mechanism of electrical breakdown; this appears to arise from the fact that experimenters in the main kept closely to the conditions prevailing in electrical equipment and were thus concerned with the rupture initiated by dust particles, water and other impurities rather than by the physical properties of the liquid itself.

More recently attention has been directed to liquids of simple molecular constitution under the best laboratory conditions obtainable with the aim of determining an "intrinsic" dielectric strength which could be related to molecular structure. We shall see that although some progress has been made towards this goal the idea of the intrinsic strength of a liquid may perhaps be illusory. The material and surface state of the electrodes appears to play a part.

2. THEORIES OF CONDUCTION

In spite of the suggestion from earlier work that there was no connexion between conduction and breakdown in insulating liquids the author and his colleagues felt that, under conditions sufficiently approaching the ideal, the explanation of breakdown must be bound up with the mechanism of conduction. An examination of the literature available in 1946 showed that studies of conduction between metal electrodes immersed in simple organic liquids could be divided into the following classes:

(1) Conduction induced by radioactivity.[2-4]
(2) Natural conduction.
  (*a*) at low field strengths (a few kV/cm)
  (*b*) at high field strengths (above about 100 kV/cm).

The interest of the first class is that the use of a source of ionization provided valuable information, as early as the first decade of this century, about the properties of organic liquid ions; in particular, the mobilities and recombination coefficients were ascertained. The more recently-discovered properties of liquid argon are not typical of most liquid dielectrics and will not be considered here.

Even in the absence of a source of radiation organic liquids exhibited slight conduction which was attributed to ionic impurities, residual radioactivity and cosmic rays. In many cases ions were certainly present without radiation; organic substances with dipolar groups in their molecules either dissociate spontaneously to a sufficient degree to give conduction, or promote, by virtue of their high permittivity, the dissociation of impurities from the air and other sources. With field strengths limited to a few kilovolts per centimetre this type of conduction behaves in a manner which can be fairly completely understood, though complications are introduced by the formation of large ions which are apparently not readily discharged at the electrodes.[5] The resulting field-distortion has been demonstrated with the help of the electro-optical Kerr effect.[6, 7] A great deal of work has been published on this type of conduction, which, however, lies outside the scope of the present paper.

When the field is intensified to a hundred or more kilovolts per centimetre, samples of non-dissociating liquids such as the lower paraffins (hexane, etc.) show a behaviour quite unlike that already described. Far from exhibiting saturation as would be expected if stray radiation or impurities were the cause of conduction, the current increases sharply for comparatively small increments of field strength. Some fairly recent measurements on iso-octane by Pao[8] are reproduced in Fig. 1. This phenomenon has been explained in a great

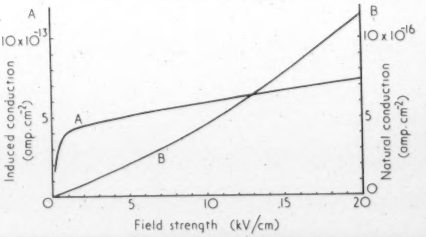

Fig. 1. Curves illustrating natural conduction (*B*) and conduction induced by γ-radiation (*A*) in pure iso-octane (after C.-S. Pao)

variety of ways and it may seem surprising that the evidence at present available is insufficient to settle the matter beyond doubt. The reason for this uncertainty is that the experimental data are far from consistent, perhaps because of apparently minor differences in experimental technique. The same situation exists in the field of breakdown measurements, hence, as might be expected, few attempts have been made to evolve a theory to cover both conduction and breakdown.

One of the earliest interpretations of the experimental facts of high-field conduction was made by a group at Munich following the accepted ideas of discharges in gases. Thus Nikuradse[9] in 1931 put forward evidence for the view that

* Based on a lecture given to the Electronics Group of The Institute of Physics on 18 December, 1953.

for a constant field strength the conduction current I could be expressed as

$$I = I_c \exp(\alpha l) \quad (1)$$

where l is the electrode separation and α is a constant for the liquid and the particular field strength in use. The physical picture suggested by this equation is the Townsend *régime* of collision ionization: a current (I_c) of electrons leaves the cathode and each electron produces α ion-pairs per centimetre of travel in a direction parallel to the field.

This view of the situation was the basis of much work during the period 1930–1940 and although experimental confirmation was not always entirely satisfactory, the hypothesis was retained. It was attacked, curiously enough, by a member of the same group of workers. K. H. Reiss,[10] in 1937, repudiated the idea of collision ionization and substituted a theory of field-assisted spontaneous ionic dissociation of molecular impurities, rather on the lines of Onsager's treatment of the non-Ohmic behaviour of weak electrolytes. The author, however, later withdrew this interpretation of his results.[11]

Independently of this attack on the collision ionization theory an entirely new view of high-field conduction came at about the same time from Baker and Boltz,[12] who published results suggesting that the current was in fact thermionic emission from the cathode, the work function having been reduced by the presence of the liquid (toluene) sufficiently to make this possible at room temperature. The possibility of collision ionization was rejected. Their experiments were repeated, with some improvements in technique and interpretation, by LePage and DuBridge,[13] and by Dornte,[14] but the idea that conduction current was identical with cathode emission remained. Unfortunately none of these experimenters used apparatus in which the electrode separation could be varied whilst keeping other things constant, so the question of the existence of collision ionization and of the consequent possible amplification of the emission currents by ionization remained undecided.

This view of high-field conduction was in turn attacked by Plumley[15] who cast doubt on the purity of the liquids used. As a result of his own experiments,[16] which were characterized by extreme rigour in cleansing and de-gassing, he advanced a theory of field-assisted ionic dissociation, but, unlike Reiss, he postulated that the molecules of the liquid itself (not those of an impurity) were dissociated. In view, however, of the high energy (about 10 eV) required to produce an ion-pair in this way it is hard to account for the observed currents at low field-strengths even though the rate of rise of current with field strength can be approximately explained on this theory. Although different electrode-separations were used the measurements exhibit such a large scatter that they cannot be regarded as evidence either for or against the collision-ionization theory. Incidentally, large scatter seems to be associated with extremely rigorous cleansing, as we shall see later in breakdown experiments. It is possible that the crystallization of the electrode surfaces resulting from intense heating in a vacuum may be responsible.

Plumley's theory received nominal support from Pao,[8] though an examination of his paper shows a number of points of divergence from the theory. The range of field strength covered by Pao was hardly adequate for a comparison with earlier work.

In 1943 Ruhle[17] published some results in Germany reaffirming Nikuradse's theory of collision ionization, though it is strange that in this paper he makes no reference either to Reiss or to the pre-war adherents of the emission theory.

The foregoing sketch conveys an idea of the state of knowledge of high-field conduction when work was begun at Birmingham. It was then felt that the collision theory had been rejected largely on the grounds

(i) that free electrons would not exist in the liquid but would be combined as negative ions, and

(ii) that even if free electrons existed they would not have sufficient free path to acquire the ionization energy (about 10 V; with fields near the breakdown intensity a path of 10^{-5} cm would be needed).

Whilst clause (i) is almost certainly true for all ordinary liquids the "solvated" electrons are bound to their molecules by energies of less than 1 V, and a small fraction will at any instant be free as a result of thermal agitation. Clause (ii) is based on the assumption that collisions between free electrons and molecules are inelastic. The retention and accumulation of energy through numerous collisions with molecules having perhaps 10^5 times the electronic mass seems, however, quite possible. Molecular excitation will, of course, drain away much of the acquired energy but there seems no reason to reject *a priori* the possibility of an occasional ionizing collision. The existence of energetic electrons during high-field conduction is confirmed by the appearance of a wax-like substance, apparently a polymer formed from the liquid, on the anode. Since it requires about 4 eV to break a C–H bond the existence of 10 V electrons does not seem improbable.

At a time when developments in the writer's laboratory were suggesting a return to the hypothesis of collision ionization a paper by Young[18] appeared which dealt with conduction and breakdown in carbon dioxide in both the gaseous and liquid forms. As well as showing the continuity of the phenomena in the two phases, Young was able to explain his results on the hypotheses of field emission from the cathode and ionization by collision in the body of the liquid. In short, he combined the theories of two of the contending schools of thought, though it should be mentioned that earlier work[19, 20] had focused interest on the metal-liquid interface as the source of ionization.

3. THE ELECTRICAL BREAKDOWN OF LIQUIDS

The task of explaining breakdown under technological conditions is a very difficult one owing to the paradoxical nature of the experimental evidence. A further difficulty is that many factors, such as the presence of minute solid particles and of dissolved water and air, either facilitate the more basic processes of rupture (by locally concentrating the electric field) or introduce entirely new kinds of breakdown, perhaps by bubble-formation or the building of conducting bridges across the inter-electrode gap. Some recent work on the influence of pressure on breakdown[21] has suggested that some form of cavitation may in certain cases be operative. This possibility draws attention to the hydrostatic pressure

$$p = \left(\frac{\epsilon - 1}{8\pi}\right) E^2$$

existing in a liquid of dielectric constant ϵ when exposed to a field of intensity E. With fields approaching breakdown this pressure may reach 1 atmosphere.

Even when we leave the field of technological breakdown for experiments of a more fundamental character we unfortunately do not find that reproducibility of result which improved conditions would lead us to expect. Thus as late

as 1939 results as different as 190 and 1150 kV/cm were recorded by Dornte[26] for benzene according to the cleaning technique used. One is obliged to conclude that treatment of the electrodes with acid or intense heat leaves the surface in a condition unsuitable for this work.

One of the most potent causes of error in experiments of this kind is the presence of minute solid particles. Naeher[22] in 1928 showed that tests conducted with pulses of voltage of rectangular waveform showed very great increases of strength as the pulse duration was reduced. He attributed this to the absence of sufficient time for the movement of particles into the regions of strong field. In passing, it is interesting to notice that Naeher used the technique of discharging overhead power transmission lines (temporarily out of service) through appropriate resistors in order to obtain rectangular pulses. The advantages of using pulses, however, have not been always recognized, though Inge and Walther[23] employed this method. They rejected the collision-ionization theory (at that time generally held) and tentatively suggested that field emission from the electrodes might play some part.

The experimental researches then and for the next five years were characterized by the most scrupulous cleanliness in the apparatus, but the reproducibility of the results was disappointing.[24–26] It is noteworthy that pulsed fields were not used and that rigorous de-gassing of electrode surfaces was preferred to a mirror-like polish.

During these years no theory of liquid breakdown comparable with those in the domain of the rupture of solids[27] was advanced, though it is noteworthy that Attwood and Bixby,[28] who used pulse methods, did in fact put forward a theory to account for the time-lag which their method of measurement revealed. Their arguments rested, perhaps rather artificially, on Fröhlich's[27] theory of breakdown in crystalline solids, but their view of the breakdown process involved the idea of collision ionization and the migration of ions, a view to which the present writer was later led by different considerations.

Komelkov,[29] by photographing discharges in liquids, was led to believe that ionization was an essential part of breakdown, though he unfortunately did not exclude the possibility that his discharges were in vapour and not in the liquid itself.

4. WORK OF THE AUTHOR AND HIS COLLEAGUES

The reader is now in a position to appreciate the situation in 1946 when the work at Birmingham was begun. Perhaps matters did not at that time appear quite as clear-cut as the foregoing review suggests, but it was decided that the most promising experimental line of attack was to employ rectangular pulses of adjustable duration, to keep the gap under careful observation by microscope in order to detect solid particles, to use a fresh area of electrode surface and a fresh sample of liquid for each determination and to maintain a high degree of cleanliness in both liquid and electrodes, but not to do anything to destroy the mirror-like polish of the electrodes.

The earlier forms of apparatus as described by Edwards[30] consisted of an all-glass distilling and filtering system which supplied liquid to a glass vessel containing a removable electrode assembly, the central feature of which was a pair of polished metal spheres $\frac{3}{8}$ in. in diameter forming the electrodes. The gap between the balls was so small that in the absence of conduction the field would be uniform. By means of rods passing through rotatable ground cone joints the balls could be turned to present fresh surfaces to each other at the gap; also the separation could be adjusted from outside the vessel. The spheres were removed for polishing, which was done with the finest grade of jeweller's rouge. Coarser media led to scatter in results. Electrolytic polishing has been successfully employed. A small pad of carefully-cleaned cotton wool was sometimes arranged to rest against each ball on the side away from the gap so that adhering particles could be removed if necessary by turning the ball. This device is particularly desirable when the spheres are placed one above the other.[30]

Some early results are shown in Fig. 2.[31] It will be seen that as the pulse duration is reduced below a certain value

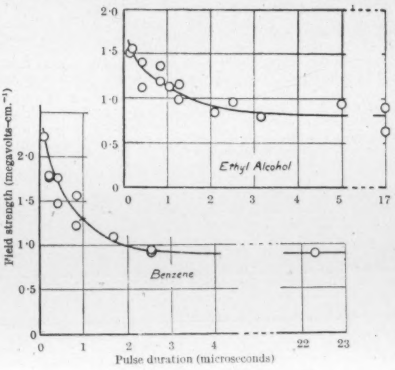

[Reproduced from *Nature*]

Fig. 2. Early measurements showing rise in dielectric strength of pure liquids as pulse-duration is reduced below a critical value (after Macfadyen and Edwards)

called the "limiting breakdown time" the dielectric strength of the liquid rises above the value for sufficiently long pulses. Edwards[30] also showed that the wider the gap between the electrodes the longer was this limiting breakdown time, τ_0. With gaps narrower than a certain value the whole curve of Fig. 2 moves upwards to higher values of breakdown field strength F^*. A set of curves of this kind plotted from experiments by Goodwin[32] is given in Fig. 3 on which the symbols

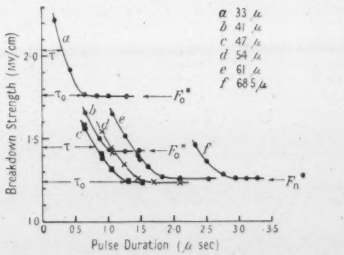

[Reproduced from *Proceedings of the Physical Society*]

Fig. 3. Variation in dielectric strength of *n*-hexane with pulse-duration and gap breadth (after Goodwin and Macfadyen)

used here have been inserted. It will be seen that for long enough gaps and pulses a fairly constant value of F^* which may be called the "normal breakdown strength" F_n^* for the liquid-electrode system is shown. It may be mentioned in passing that the reproducibility of measurement exhibited in Fig. 3 was in part due to very careful polishing of the electrodes followed by rigorous de-greasing. The use of γ-radiation to provide electrons to initiate breakdown was found to be unnecessary.

The general picture just outlined was given considerable significance when Goodwin[32] observed that there was a proportionality between the limiting breakdown time τ_0 and the time required for a positive ion to cross the gap, as calculated from the field strength and the published values of ionic mobility. This relationship is shown in Fig. 4 in which different liquids, temperatures and gap lengths were responsible for the variations in τ_0.

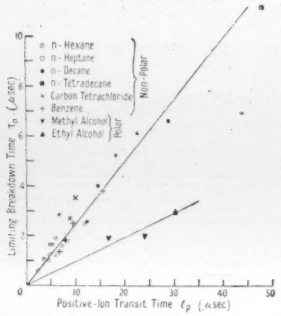

[Reproduced from *Proceedings of the Physical Society*]

Fig. 4. Relationship between the limiting breakdown time τ_0 and the positive-ion transit time t_p for various liquids. Phosphor-bronze electrodes were used (after Goodwin and Macfadyen)

At first it was puzzling that the ratio of these times was such that breakdown occurred when an ion had apparently traversed only about one-quarter of the gap, but it must be remembered that the published mobilities were measured at field strengths of only a few kilovolts per centimetre. With the high field strengths prevailing in breakdown experiments the actual mobilities may well be less owing to the removal of attached molecules by the high velocity through the liquid.

Further experiments[32] revealed considerable variations of normal breakdown strength F_n^* with cathode metal. Metals with high work function, as judged from the published values, gave higher values of F_n^* than metals with low work function. The former type of cathode tended also to give longer delay-times.

Fig. 5 shows a set of determinations of F_n^* for different members of the paraffin series over a range of temperatures. It will be seen that while the strength increases with the number of carbon atoms in the chain it decreases with rising temperature.

These and other experimental results suggested an examination of the high-field conduction of the liquids used. Briefly, it was found that they behaved much as Nikuradse and, later, Ruhle had described. The logarithms of the currents plotted against electrode separations at constant field strength yielded a set of curves (Fig. 6) which, extrapolated to zero separation, gave the (hypothetical) cathode emission current. On the simple Townsend theory these curves should have been straight lines, but a number of possible processes might account for the curvature. Subsequent experiments showed that in the present case space charge was not the cause.[40]

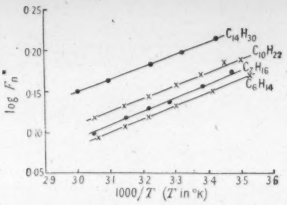

[Reproduced from *Proceedings of the Physical Society*]

Fig. 5. Variation of normal breakdown strength F^* of four paraffins with temperatures (F^* in MV/cm) (after Goodwin and Macfadyen)

It was found that the cathode emission could be represented by the Fowler–Nordheim equation for field emission. The constants of the equation, if the emission is regarded as uniform, correspond to a very low work function. This is in agreement with the work of Llewellyn Jones and his colleagues[33, 34] who have found similar behaviour in the

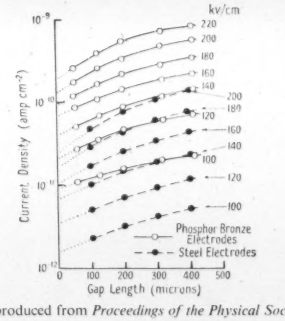

[Reproduced from *Proceedings of the Physical Society*]

Fig. 6. Conduction in *n*-hexane plotted in accordance with equation (1), showing the effect of cathode metal (after Goodwin and Macfadyen)

emission from tarnished and oxidized metal surfaces in air. It is thus convenient to regard the cathode emission into a liquid as field emission though this is not essential to the theory of breakdown to be considered in the next section.

5. THEORY OF BREAKDOWN

On the basis of the experimental work which has been briefly sketched in the preceding section a theory of breakdown was given in the original publication.[32] It will be re-stated here in a somewhat different form which reveals the magnitudes of the physical quantities involved. It will be

shown that conduction by collision ionization gives rise, at high field strengths, to an intensification of the field at the cathode. This, in conjunction with the dependence of cathode emission on field strength, produces a state of instability leading to breakdown when the applied voltage is sufficient.

Two plane parallel electrodes are assumed to be immersed in a liquid of dielectric constant ϵ. They are separated by a distance l. An electron current of density i_c e.s.u. per cm^2 leaves the cathode. Although captured by molecules of the liquid, these electrons travel towards the anode with occasional thermal liberations resulting in the production of ion-pairs. If the average ion-pair production is α per centimetre in the x-direction (normal to the electrodes) it can be shown[35] that the field strength E at a distance x from the cathode is given by

$$\epsilon \frac{d}{dx}(E^2) = -8\pi i_c \left(\frac{e^{\alpha l} - e^{\alpha x}}{k_p} - \frac{e^{\alpha x}}{k_n} \right) \qquad (2)$$

where k_p and k_n are respectively the mobilities of positive and negative ions.

Equation (1) must be integrated subject to the boundary condition that

$$\int_0^l E dx = Fl$$

where F is the mean applied field strength, i.e. V/l, V being the applied potential difference. This condition presents difficulties unless the simplifying assumption is made that the field strength is disturbed from its mean value F to a relatively small extent. With this and another simplification justified by the magnitude of the quantity αl a simple expression for E_c, the field strength at the cathode, may be found:

$$E_c = F + \frac{2\pi e^{\alpha l} l}{\epsilon k_p F} i_c \text{ e.s.u.} \qquad (3)$$

or, if practical electrical units are used,

$$E_c = F + \frac{2\pi . 9 . 10^{11} e^{\alpha l} l}{\epsilon k_p F} i_c \text{ volts. cm}^{-1} \qquad (3a)$$

Thus the field strength at the cathode exceeds the average value by an amount ΔE_c represented by the second term, which is proportional to i_c, the cathode emission density. This suggests the following graphical method of representing the steady state corresponding to any particular applied field strength F:

Let the curve $OABCD$ (Fig. 7) represent cathode emission density i_c plotted against cathode field strength E_c. The actual curve has been produced by extrapolation from Fig. 9 of the original paper[32] which shows cathode emission plotted in accordance with the Fowler–Nordheim equation. The values of emission were deduced from Fig. 6 by producing the graphs to cut the axis $l = 0$. The slopes of these curves give the values of α.

When a mean field strength F is applied to the electrodes the equilibrium state is found by combining this relationship between i_c and E_c with that represented by equation (3a). Accordingly a straight line having reciprocal slope equal to

$$\frac{\Delta E_c}{i_c} = \left(\frac{2\pi . 9 . 10^{11} l}{\epsilon k_p} \right) \frac{e^{\alpha l}}{F} \text{ ohms} \qquad (4)$$

is drawn through the point on the E_c axis (Fig. 7) representing the applied field strength F. The intersection of this line and the emission curve represents the steady state of conduction, e.g. the point A corresponds to the conduction at an applied field strength of 1·1 MV per cm.

If now F is increased the reciprocal slope increases (points B, C, etc.) mainly by virtue of the increase in the exponential factor $e^{\alpha l}$ [equation (4)], and at a certain value of F (1·28 MV per cm) the line fails to intersect the emission curve; steady conduction is then no longer possible and breakdown ensues. Clearly the value of F^* so found would be that given by a d.c. or a long-pulse test.

Fig. 7 has been plotted for a 0·1 mm gap between phosphor bronze electrodes in hexane. The values of α and i_c have necessarily been obtained by a very large extrapolation and it is thus to a great extent fortuitous that the breakdown strength so found agrees well with the measured value shown in Fig. 3. Measurements of emission and of α at field strengths close to breakdown would be required in order to test the theory accurately. Again, the assumption of uniform emission from the cathode is almost certainly an over-simplification since field emission is known to occur in spots.[36] However, the work of Dornte[37] suggests that close to breakdown the spots may become so numerous as to furnish a nearly uniform emission.

In favour of the theory, it may be claimed that it explains the dependence of breakdown strength on cathode material or surface condition, for if this is a poor emitter of electrons the emission curve $OABCD$ (Fig. 7) is depressed at all points and a higher value of F must be applied in order to secure non-intersection of the straight line with the curve. A further feature of the theory is that it appears to be capable of explaining the increase in dielectric strength at small breadths of gap, since this quantity occurs in the power of the exponential. In a general way the enhanced strength resulting from the admixture of chloro and fluorocarbons (e.g. CCl_4) with hydrocarbons[38] can be explained as due to the reduction in α, an effect which is known to occur in gases.[39] Although information is not available on the effect of temperature on α, a positive temperature coefficient, resulting in a negative one for breakdown (compare Fig. 5), would be in general accordance with the physical picture underlying the theory.

As is to be expected from the experimental basis of the theory, time-lag seems capable of a simple explanation in terms of the time required for the space-charge to be built up. The mathematical treatment is unfortunately rather complicated.

6. A CONFIRMATORY EXPERIMENT

One of the predictions of the theory given in the preceding section is that with an applied field approaching the breakdown value the field strength at the cathode should exceed the mean field strength, as is easily seen from Fig. 7 in which the abscissa of C represents the cathode field strength resulting from an applied field of 1·25 MV/cm. This can be checked experimentally by means of the Kerr electro-optical effect. The experiment was carried out by Goodwin[40] and although experiments of a similar kind had been done before[6, 7] under conditions of steady fields and impure liquids, the task in this case was far more exacting since pulsed fields very close to the breakdown intensity, liquids of high purity and electrode gaps of a small fraction of a millimetre had to be used. Unfortunately the simple liquids employed in the preceding researches had far too small a Kerr coefficient for the present purpose so chlorobenzene, a liquid combining moderately high Kerr coefficient with good electrical properties, was used. The optical arrangement was basically similar to Dantscher's, whereby an interference-fringe superimposed on the image of the electrodes (vertical planes) became displaced vertically by

an amount proportional to the square of the field strength at each point on a line normal to the electrodes. The fringe thus constituted a graph of E^2 against x. Insuperable experimental difficulties prevented a direct correlation with the

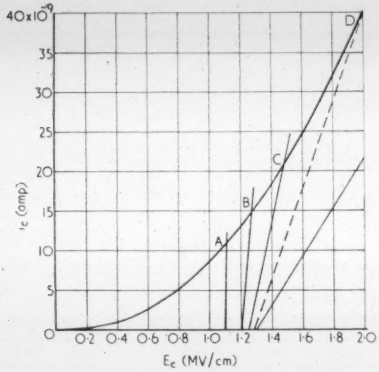

Fig. 7. Breakdown condition for *n*-hexane between phosphor-bronze electrodes. The curve represents the cathode emission and the straight lines represent field-distortion due to ionization

theory but at field strengths near breakdown a definite tilt of the fringe, indicating the predicted intensification of field at the cathode, was recorded photographically.

7. OTHER RECENT WORK

The publications which have appeared whilst the work described in the last three sections was in progress show interesting relationships with it although there are important divergences. A selection of points from these papers will now be given.

Salvage[41] has carried out breakdown experiments with pulsed and steady fields but most of his conclusions are drawn from the latter type of test. His results are generally similar to those of Goodwin and the writer,[32] though the actual values of normal breakdown stress F_n^* are lower. After a preliminary examination of the effects of filter pore-size Salvage shows, amongst other things, a correlation between F_n^* for normal hexane and the work function of the electrode metal. A negative temperature coefficient of F_n^* between 0 and 60° C is recorded. A progressive increase in F_n^* through the range of normal paraffins from pentane to nonane is also found (compare Fig. 5).

Using various refinements, including a thyratron device to cut off the applied voltage within a fraction of a microsecond of the instant of breakdown, Lewis[42] has been able to reduce the wear resulting from repeated use of the same pair of electrodes. The coefficient of variation of the results is greatly reduced and higher values of F_n^* are recorded than in earlier measurements. The increased strength for narrow gaps is reproduced and new data are presented for the effects of temperature and number of carbon atoms in the paraffin molecule. Although these are in general agreement with results already described the form of the temperature-dependence curves is appreciably different.

Dependence on cathode material is found to be somewhat uncertain; this has been explained in a later paper[43] in which experiments using point-and-plane electrodes are described. Only when the cathode is the plane is there a significant dependence on cathode metal; it is then in the direction to be expected from the work function.

Lewis, in discussing his results, employs the concepts of ionization by collision and field emission from the cathode. When the pointed electrode is the cathode there is a copious supply of electrons but rupture does not occur until the field strength in the body of the liquid reaches a high enough value to turn a simple conduction into a catastrophic discharge. Cathode dependence is not shown in this case. When, on the other hand, the plane electrode is the cathode the field strength must be raised until field emission occurs. The liquid near the pointed anode is already "over-stressed" and breakdown ensues. The breakdown voltage will then depend on the cathode material. This view of breakdown, although not specifically employing the notion of field distortion by space charge, contains the assumption that breakdown is contingent upon the simultaneous presence in the liquid of a high enough current density and a strong enough field. It thus has much in common with the theory given in Section 5.

The hypothesis that the body of the liquid requires to be exposed to a certain field strength to cause rupture is also inherent in a recent paper by Bragg, Sharbaugh and Crowe,[44] though in this case current density enters only in an indirect way. Electron emission from the cathode is assumed and, as a result of the finite mobility of electrons in the liquid, a negative space charge accumulates, intensifying the field near the *anode* until a hypothetical "breakdown intensity" is reached. If cathode emission is low this condition may be reached without field distortion. It will be noticed that ionization is not invoked, so we may regard this view as a development of the ideas of the American "emission" school.[12–14]

The authors develop the theory in some detail and obtain experimental confirmation from breakdown measurements employing an aqueous solution of an ionic salt, the concentration of which can be varied at will so that the emission (of negative ions) is under control. Breakdown under these conditions is obviously a specialized phenomenon and can hardly be compared with rupture in more usual circumstances.

In another paper,[45] however, the same authors report investigations into the dielectric strengths of the paraffins using a mercury cathode. Corrections are applied for the movement of the cathode under the influence of the (pulsed) electric field. It is found that the dielectric strengths so measured are closely proportional to the densities of the liquids, which range from pentane to heavy oil. This proportionality is treated as a generalization of Paschen's law for gaseous breakdown. The changes in density envisaged in Paschen's law are brought about by changing the concentration of molecules of a constant type by varying the pressure; the underlying variable, namely, the mean free path of an electron, at once provides a simple explanation of the law. In a range of hydrocarbons, however, the variations of density are due to a quite different cause and the simple explanation is no longer valid. Dimensional arguments are put forward in the paper to give significance to the proportionality. Temperature dependence is also explained as a by-product of density change, though the evidence on this point is slender.

Since these measurements were carried out with a constant pulse length of 1·8 μs it would seem that much of the increase with number of carbon atoms is due to time-lag effect (Fig. 3). In a private communication, however, Bragg states that the relatively long time lags shown in Fig. 3 are not found in the methods used by himself and his collaborators.

Edwards,[46] using techniques which are essentially developments of those used in his earlier work,[30] has reported exceedingly high values of dielectric strength for carbon tetrachloride and other liquids. He attributes this to a high degree of freedom from solid particles.

8. CONCLUSION

The present situation appears to be that improved techniques during the last twenty years have enabled different experimenters to reach some measure of unanimity as to general trends of the dependence of breakdown strength on a number of variables, though exceptions exist and agreement upon absolute values is not satisfactory. Views on high-field conduction, which have suffered many vicissitudes, are still in a state of flux though the evidence available does not seem to rule out ionization by collision as a basic ingredient of the process. Workers in this field are understandably unwilling to commit themselves to a definite view of conduction, having regard to the history of the subject, and this reacts upon the prospects of an ultimate explanation of breakdown. Progress along these lines is undoubtedly hampered by the fact that our information about atomic and molecular processes occurring in liquids is so much less complete than our knowledge of the corresponding processes in gases and solids. A greater range and diversity of experimental researches on liquids, rather than further specialized investigation into conduction and breakdown, seems to be necessary. It may be that even at the present stage a closer collaboration between the rather scattered groups of workers on conduction and breakdown in liquids might bring about a significant advance in our understanding of the subject.

ACKNOWLEDGEMENTS

In connexion with the researches carried out at Birmingham the author desires to express his gratitude to Prof. P. B. Moon and the Department of Scientific and Industrial Research for the facilities and funds placed at his disposal.

REFERENCES

(1) WHITEHEAD, S. *Dielectric Phenomena*, Vol. 2. *Electrical Discharges in Liquids* (London: E. Benn, Ltd., 1928).
(2) CURIE, P. *C.R. Acad. Sci.* [*Paris*], **134**, p. 420 (1902).
(3) JAFFÉ, G. *Ann. Phys.* [*Leipzig*], **32**, p. 149 (1910).
(4) VAN DER BIJL, H. J. *Ann. Phys.* [*Leipzig*], **39**, p. 170 (1912).
(5) ECK, J.-L. *J. Phys. Radium*, **4**, p. 12 (1949).
(6) DANTSCHER, J. *Ann. Phys.* [*Leipzig*], **9**, p. 179 (1931).
(7) VADIADIS, G. *Ann. Phys.* [*Leipzig*], **35**, p.23 (1939).
(8) PAO, C.-S. *Phys. Rev.*, **64**, p. 60 (1943).
(9) NIKURADSE, A. *Naturwiss.*, **19**, p. 233 (1931).
(10) REISS, K. H. *Ann. Phys.* [*Leipzig*], **28**, p. 325 (1937).
(11) REISS, K. H. *Ann. Phys.* [*Leipzig*], **30**, p. 34 (1937).
(12) BAKER, E. B., and BOLTZ, H. A. *Phys. Rev.*, **51**, p. 275 (1937).
(13) LEPAGE, W. R., and DUBRIDGE, L. A. *Phys. Rev.*, **58**, p. 61 (1940).
(14) DORNTE, R. W. *Industr. Engng Chem.*, **32**, p. 1529 (1940).
(15) PLUMLEY, H. J. *Phys. Rev.*, **52**, p. 140 (1937).
(16) PLUMLEY, H. J. *Phys. Rev.*, **59**, p. 200 (1941).
(17) RUHLE, F. *Phys. Z.*, **44**, p. 89 (1943).
(18) YOUNG, D. R. *J. Appl. Phys.*, **21**, p. 222 (1950).
(19) NIKURADSE, A. *Phys. Z.*, **32**, p. 945 (1931).
(20) EDLER, H., and ZEIER, O. *Z. Phys.*, **84**, p. 356 (1933).
(21) WATSON, P. K., and HIGHAM, J. B. *Proc. Instn Elect. Engrs*, **100** (IIA), p. 168 (1953).
(22) NAEHER, R. *Arch. Elektrot.*, **21**, p. 169 (1928).
(23) INGE, L., and WALTHER, A. *Tech. Phys. U.S.S.R.*, **1**, p. 539 (1935).
(24) BÄHRE, W. *Arch. Elektrot.*, **31**, p. 141 (1937).
(25) BREDNER, R. *Arch. Elektrot.*, **31**, p. 351 (1937).
(26) DORNTE, R. W. *J. Appl. Phys.*, **10**, p. 514 (1939).
(27) FRÖHLICH, H. *Proc. Roy. Soc. A*, **160**, p. 230 (1937).
(28) ATTWOOD, S. S., and BIXBY, W. H. *J. Franklin Inst.*, **235**, p. 259 (1943).
(29) KOMELKOV, V. S. *C.R. Acad. Sci., U.S.S.R.*, **47**, p. 268 (1945).
(30) EDWARDS, W. D. *Canad. J. Phys.*, **29**, p. 310 (1951).
(31) MACFADYEN, K. A., and EDWARDS, W. D. *Nature* [*London*], **163**, p. 171 (1949).
(32) GOODWIN, D. W., and MACFADYEN, K. A. *Proc. Phys. Soc.* [*London*], *B*, **66**, p. 85 (1953).
(33) JONES, F. LLEWELLYN, and DE LA PERRELLE, E. T. *Proc. Roy. Soc. A*, **216**, p. 267 (1953).
(34) MORGAN, C. GREY, and HARCOMBE, D. *Proc. Phys. Soc.* [*London*], *B*, **66**, p. 665 (1953).
(35) LOEB, L. B. *Fundamental Processes of Electrical Discharges in Gases*, p. 387 (New York: John Wiley and Sons, Inc., 1939).
(36) WEHNELT, A., and SCHILLING, W. *Z. Phys.*, **98**, p. 286 (1935–36).
(37) DORNTE, R. W. *Industr. Engng Chem.*, **32**, p. 1529 (1940).
(38) RUHLE, F. *Arch. Elektrot.*, **35**, p. 490 (1941).
(39) WARREN, J. W., HOPWOOD, W., and CRAGGS, J. D. *Proc. Phys. Soc.* [*London*], *B*, **63**, p. 180 (1950).
(40) GOODWIN, D. W. To be published.
(41) SALVAGE, B. *Proc. Instn Elect. Engrs*, **98**, Pt IV, p. 15 (1951).
(42) LEWIS, T. J. *Proc. Instn Elect. Engrs*, **100**, Pt IIA, p. 141 (1953).
(43) LEWIS, T. J. *Proc. Phys. Soc. B*, **66**, p. 425 (1953).
(44) BRAGG, J. K., SHARBAUGH, A. H., and CROWE, R. W. *J. Appl. Phys.*, **25**, p. 382 (1954).
(45) CROWE, R. W., BRAGG, J. K., and SHARBAUGH, A. H. *J. Appl. Phys.*, **25**, p. 392 (1954).
(46) EDWARDS, W. D. *J. Chem. Phys.*, **20**, p. 753 (1952).

Thulium 170 for industrial radiography

By R. HALMSHAW, B.Sc., A.R.C.S., A.Inst.P., Armament Research Establishment, Woolwich, London

[*Paper first received* 7 *May, and in final form* 4 *August*, 1954]

The use of ^{170}Tm for industrial radiography has been investigated. The exact nature of the γ-ray spectrum does not appear to be agreed and the absorption curves which have been obtained suggest the presence of some high energy radiation, probably due to *Bremsstrahlung*. Exposure curves for steel and aluminum are given and a sensitivity-curve for step penetrameters is derived. The values calculated are compared with experimental values using step and wire penetrameters and with radiographs taken with ^{192}Ir and X-rays. The suitability of intensifying screens is discussed and some possible applications of ^{170}Tm, taking into account the low activity of present sources, are suggested.

Early in 1953 the Atomic Energy Research Establishment, Harwell, made available a radioisotope, ^{170}Tm, which was stated[1] to have low-energy, γ-ray components and to be suitable for the radiography of light alloys. An investigation has been made of some of its properties and its suitability for industrial radiography, particularly of thin steel specimens, has been examined.

GENERAL PROPERTIES

The source used had physical dimensions of 2×2 mm and an initial strength of 450 mc. The half-life is stated to be 127 days, and the γ-radiation output 45×10^{-4} rhm/c.[2]

The decay is by β-ray emission, the spectrum consisting of two components of energies 968 and 884 keV, the second component leading to an excited state of ^{170}Yb which emits a γ-ray in decaying to the ground state.[10]

There appears to be considerable difference of opinion on the energy and relative intensities of the γ-ray spectrum. There is general agreement on the presence of a spectrum line of energy 0·084 MeV, but whereas Fraser[3] and Cork[4] state that no other γ-rays were found, Grant and Richmond[5] identified two high-energy lines. Their figures are:

Table 1. *Gamma-ray spectrum*

Energy (keV)	*Relative intensity*
82·6 ± 0·5	100·0 ± 20
205·0 ± 10·0	13·5 ± 1·2
430·0 ± 20·0 (complex)	2·4 ± 0·4

Graham and Tomlin[6] suggest that there is one γ-ray line at 0·083 MeV, and no others with intensities greater than 1% of the disintegration rate, but that there is a weak component of higher energy of 400–500 keV, due to *Bremsstrahlung* from the β-rays. The energy and relative intensity of these rays were found to vary with the absorber. Grant,[7] in a later report, gives some evidence for γ-ray lines at 198, 360 and 550 keV.

There are also internal conversion X-radiations of low energy, and as much of the energy of decay is emitted as β-radiation, only a small proportion of the energy is emitted as γ-rays, hence the very low output in roentgens/millicurie.

EXPERIMENTAL

(*a*) *Exposure curves.* Exposure curves were made in the conventional manner for steel and for aluminium, and are shown in Fig. 1. The results are shown converted to a source strength of 500 mc, at a source-film distance of 10 in. This value of source-film distance has been chosen because of the long exposures needed with present ^{170}Tm sources, and the likelihood that they will only be applied to relatively thin specimens. For the same reason, Ilford Industrial B film has been used, although better quality radiographs could be obtained on slower, fine-grain films. Conversion factors

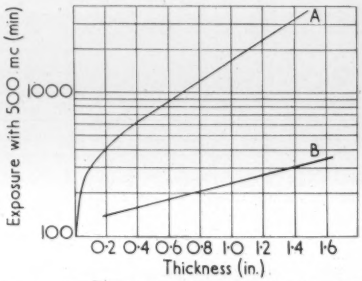

Fig. 1. Exposure chart for steel and aluminium with a 500 mc thulium 170 source

Curve *A*, steel; Curve *B*, aluminium.
Ilford Industrial B film with lead screens 0·002 in. front and 0·020 in. back. Source-film distance 10 in. Film density 1·5.

can be used for other films and other film-densities. The curve for steel is characterized by a very long "toe," so that the effective absorption coefficient is changing rapidly with increase in the thickness of the specimen up to at least $\frac{3}{8}$ in. steel. Exposure data for aluminium was not obtained for thicknesses below $\frac{1}{4}$ in. On the approximately straight portion of the exposure curves, the effective linear absorption coefficients are:

steel = 1·65 in.$^{-1}$: half-value thickness = 0·42 in.
aluminium = 0·67 in.$^{-1}$: half-value thickness = 1·03 in.

By comparison with the slopes of X-ray exposure curves for steel determined under similar conditions, these values suggest that the radiation, after this initial filtration, is equivalent in energy to X-rays generated at about 600 kV. The exposure curve for aluminium confirms this figure, but the change in absorption coefficient at this voltage is very slow and great accuracy is not possible. These figures confirm the results of Graham[6] and Grant[5] in that there is some very high energy radiation, which with thick specimens becomes predominant.

(*b*) *Screens.* The thickness of lead foil screens required to

give the maximum intensification factor was also investigated, and it was found that a front screen of about 0·001 in. would be the most satisfactory, and that if this screen is thicker than 0·0025 in. the effect of filtration is greater than the intensification. The thickness of the lead back screen was found to be uncritical, so that the recommended lead screen thicknesses are 0·001–0·002 in. front, and 0·010–0·020 in. back.

Because of the long exposures necessary with metal foil screens, the use of tungstate intensifying screens was investigated. With a steel specimen 0·2 in. thick it was found possible to give about one-fortieth of the exposure required with lead screens and Ilford Industrial B film, and obtain a correctly exposed radiograph, using fast calcium tungstate screens and Kodak Industrex S film.

The result, however, was very inferior to the radiographs taken with lead screens; there was a loss in contrast and a very considerable loss in definition. A fine crack in a weld 0·2 in. thick was not recognizable as a crack on the salt-screen radiograph due to excessive blurring, although it could be seen that some defect was present. The results were compared with X-radiographs of the same specimen on lead and salt screens taken at 100 and 65 kV respectively and it was found that the deterioration of the image due to the use of salt screens was very much greater with ^{170}Tm than with X-rays.

The same degradation of image detail was observed in the radiograph of a specimen ½ in. thick: using tungstate screens small fine cracks were lost completely and only the grosser details of the image could be discerned. It is concluded therefore that although the shortening of exposure times obtained is considerable, the use of tungstate intensifying screens with ^{170}Tm is very undesirable. It will be shown later that with specimens thicker than ½ in. steel, the use of ^{192}Ir with metal screens and the appropriate films is very much preferable to ^{170}Tm in conjunction with tungstate screens.

(*c*) *Sensitivity*. By producing exposure curves with "broad" and "narrow" beams of radiation, the ratio of scattered to direct radiation, I_S/I_D, can be obtained, and the attainable step-penetrameter sensitivity calculated in terms of the minimum visible density-difference on the film (taken as 0·006), and the film gradient. Fig. 2 shows sensitivity curves, calculated for a value of the film gradient corresponding to a film density of about 2·0 on Ilford Industrial B film. It will be seen that the sensitivity improves with increasing thickness of steel, and that the sensitivity is still better than 1% for thicknesses of steel down to about ⅛ in. This relatively gradual fall-off in sensitivity on thin sections, much slower than with ^{192}Ir,[9] makes ^{170}Tm more suitable for the radiography of very thin sections than any other isotope at present available. The penetrameter-sensitivity curve for ^{192}Ir radiation, also shown on Fig. 2, indicates that on a ¼ in. steel specimen there is an improvement in sensitivity of 45% with ^{170}Tm against ^{192}Ir.

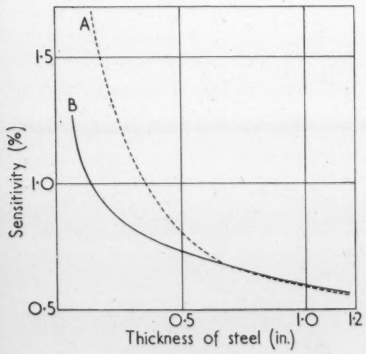

Fig. 2. Step penetrameter sensitivity curve for thulium 170 and iridium 192

Curve *A*, iridium 192; Curve *B*, thulium 170.

Direct measurement of penetrameter sensitivities on such thin sections is not very practical, owing to the small thicknesses of metal involved, but some data has been obtained to confirm the values of Fig. 2.

Table 2. *Feeler-gauge penetrameters (steel)*

Steel thickness (*in.*)	*Film*	*Film density*	*Source film distance* (*in.*)	*Thinnest visible step* (%)	*Calculated sensitivity* (%)
0·1	B	1·4	15	1·5	1·9
0·2	B	1·07	15	1·0	1·3
0·4	B	1·6	9	0·9	1·1
0·5	B	1·5	9	1·2	1·2

Some sensitivity measurements have also been made with tungsten wire penetrameters and the results obtained are listed below together with the same wires used for X-ray exposures. These percentage figures are much lower than the penetrameter sensitivities normally obtained with wire penetrameters, because of the use of tungsten wire, but they do serve as a comparison between radiographs taken with ^{170}Tm and with X-rays. They indicate that over this range of thickness, the sensitivity attainable with ^{170}Tm is generally inferior to that attainable with X-rays of the appropriate voltage, but that the differences are not very great.

Table 3. *Wire penetrameters (tungsten wires)*

Steel thickness (*in.*)	*Film*	*Film density*	*Source-film distance* (*in.*)	*Diameter of thinnest visible wire* (*in.*)	(%)
0·25	B	1·0	10	0·002	0·8
0·5	B	1·0	10	0·003	0·6
1·0	B	1·0	10	0·003	0·3
0·5	B	—	5	0·0025	0·5
0·2	B	1·1	15	0·002	1·0
0·2	B	1·8	22	0·002	1·0
0·4	B	1·5	22	0·0025	0·6
0·5	B	1·33	22	0·0025	0·5
		X-rays			
			kV		
0·25	B	1·5	100	0·001	0·4
0·5	B	1·2	125	0·0015	0·3
0·75	B	1·2	150	0·003	0·4
1·0	B	1·7	175	0·003	0·3

SCOPE OF APPLICATION

It appears unlikely that ^{170}Tm sources of strength greater than 500 mc will be available in the immediate future, so that it is clear from the exposure curves of Fig. 1 that long exposure times will be required. Such methods as the use of fast film rather than slow, fine-grain emulsions, and the use of prolonged development[8] with certain films can be applied to

enable shorter exposure times to be employed, but even then it will often be necessary to employ shorter than usual source-film distances if the exposure time is to be kept reasonably short. Some exposures have therefore been made to compare the effects of different distances. A weld 0·2 in. thick with considerable porosity and some fine cracks was radiographed with ^{170}Tm at different source-film distances between 2 and 24 in. The cracks were clearly visible in all the radiographs, and it is therefore concluded that the use of source-film distances of the order of 4–6 in. is quite feasible with such thin sections.

Secondly, a circumferential weld in a pipe of 3 in. bore and $\frac{3}{16}$ in. wall was radiographed with the ^{170}Tm source at the centre of the weld, with an exposure time of about 1 h, and the result compared with an X-ray exposure through a single wall with the film inside the pipe. The ^{170}Tm radiograph is noticeably more blurred, and has slightly less sensitivity, but two small cracks in the weld are still recognizable as such and would not be overlooked. With small pipe welds, therefore, it appears feasible to use a ^{170}Tm source at the centre of pipe, and with film wrapped round the outside, obtain a radiograph of the whole weld in one exposure.

CONCLUSIONS

On steel sections less than $\frac{1}{2}$ in. thick, ^{170}Tm can be used to obtain better quality radiographs than with any other isotope source at present available. For thicknesses greater than $\frac{1}{2}$ in. the sensitivity obtainable becomes closely comparable to that obtained with ^{192}Ir, and as small-dimensioned, high-intensity sources of the latter are available with which short exposures can be used, it would be used in preference to ^{170}Tm.

With thicknesses below $\frac{1}{2}$ in. steel the radiographs obtained with ^{170}Tm have poorer sensitivity than those obtained with X-rays, but the differences are not large. Exposures are, however, very prolonged and it is probable that the principal use of ^{170}Tm will be for locations where the use of X-rays is completely unpractical, and for specimens less than $\frac{1}{2}$ in. thick where a short source-film distance can be used.

ACKNOWLEDGEMENT

Acknowledgement is made to the Chief Scientist, Ministry of Supply, for permission to publish this paper. Crown copyright reserved. Reproduced with the permission of the Controller, H.M. Stationery Office.

REFERENCES

(1) Data sheet for thulium 170. A.E.R.E. Harwell (1953).
(2) West, R. *Nucleonics*, **11**, No. 2 (20 Feb., 1953).
(3) Fraser, J. S. *Phys. Rev.*, **76**, p. 1540 (1949).
(4) Cork, J., and others. *Phys. Rev.*, **76**, p. 986 (1949).
(5) Grant, J., and Richmond, R. *Proc. Phys. Soc.* [*London*], **62A**, pp. 573–575 (1949).
(6) Graham, R., and Tomlin, D. *Nature* [*London*], **164**, p. 278 (1949).
(7) Grant, J. *Nature* [*London*], **165**, p. 108 (1950).
(8) Durant, R. L. *Brit. J. Appl. Phys.*, **2**, pp. 42–45 (1951).
(9) Halmshaw, R. *Brit. J. Appl. Phys.*, **5**, pp. 238–243 (1954).
(10) Graham, R. *Canad. J. Phys.*, **30**, p. 459 (1952).

A direct method of phase measurement on the cathode-ray tube

By D. Karo, Dr.Ing., Dipl.Eng., A.M.I.E.E., Electrical Engineering Department, Northampton Polytechnic, London

The paper describes a direct method of phase measurement on the cathode-ray oscillograph. The circuit is the same as that used in the "roulette" method of measuring frequency.

Two voltages of equal frequencies trace circles on the cathode-ray oscillograph, the resultant trace being either a circle or a line, according to the connexions. The diameter of the circle varies with the phase difference between the voltages, the spot describing a spiral; in these circumstances it is possible, modulating the grid of the cathode-ray oscillograph by means of a short pulse, to determine the phase difference between the voltages by means of concentric circles, as well as radial lines, on a graticule placed before the screen. Since the position on the screen of the modulating pulse will be on the intersection of a circle and a radial line, no measurement of length on the graticule is necessary.

When a line is being traced and the phase difference between the voltages varies, the line will rotate; here again it is possible to measure the phase difference between the voltages by locating the position of a pulse which modulates the grid of the cathode-ray oscillograph. Frequency can be measured by the speed of rotation of the line or by the frequency of alteration of the circle.

It is well known that methods of direct measurement of phase difference on the cathode-ray oscillograph are not very accurate. The method of tracing an ellipse on the screen of the cathode-ray oscillograph and the method of tracing, simultaneously, the two voltages the phase difference between which has to be determined, are both based on measuring lengths on a graticule placed in front of the screen. The accuracy is therefore only of the order of 5° to 10°.

A recently described method,* based on the relation between the semiminor and the length of the side of a square, in which the ellipse is described, claims an accuracy of ±1°. In this method no measurement of length on a graticule is required.

The method in which one voltage traces a circle on the screen whilst the other voltage modulates the grid of the cathode-ray oscillograph through a limiter circuit, so that only a semicircle appears on the screen, is more accurate. The displacement of the ends of the semicircle from a reference diameter gives the phase difference between the two voltages. The reason for the increased accuracy (about 2°) is that the phase difference is determined by the position of the ends of the semicircle relative to radial lines issuing from the centre of the graticule.

It is evident that the accuracy would be still further increased if the ends of the semicircle, or the position of a short pulse modulating the grid, could, for any phase difference, be determined relative to radial lines as well as concentric circles centred on the centre of the graticule.

In the method described the same circuit is used as in the well-known "roulette" method, this has, however, hitherto been used only for comparison of different frequencies and not for phase measurement or even for comparison of nearly

* Wischmeyer, Carl R., and Pfeiffer, Paul E. *Rev. Sci. Instrum.*, **25**, p. 41 (1954).

equal frequencies. In the circuit used, two voltages are connected through two phase-splitting circuits to the deflecting plates of the cathode-ray oscillograph; each of the voltages traces a circle on the screen, the resultant trace being a circle or a line according to the connexions. If the voltages are equal and of the same frequency, the diameter of the resultant circle will vary with the phase difference between the voltages from a maximum to a point. If the resultant trace is a line, the position of the line will vary with the phase difference. If the voltages are unequal, but of the same frequency, the diameter of the resultant circle will vary with the phase difference from a maximum to a minimum. If the frequencies are not equal, yet near enough to one another not to distort the circle appreciably, or if the phase difference between the two voltages varies continuously with time, the spot will describe a spiral. In the case of the resultant trace being a line, the line will rotate around its centre the spot describing a spiral.

Thus, if the frequencies are equal and the grid is modulated by a short pulse, the phase difference between the two voltages will be determined by the position on the screen of the pulse relative to radial lines and concentric circles traced on a graticule. The grid can, of course, be modulated by a sine wave through a limiter circuit.

CIRCUIT ARRANGEMENT AND PRINCIPLE OF THE METHOD

Circuit arrangement. The circuit is shown in Fig. 1. The plates of the two pairs of deflecting plates x_1, x_2, y_1, y_2 are connected separately as shown. One source of voltage V_1 and frequency f_1 is connected through the phase splitting

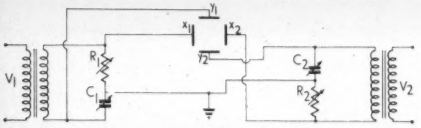

Fig. 1. Circuit arrangement for phase measurement on the cathode-ray tube

circuit R_1 and C_1, to x_1 and y_1; another source of voltage V_2 and frequency f_2 is connected through R_2 and C_2 to x_2 and y_2. V_2 being disconnected, V_1, R_1 and C_1 are set so that a circle of required diameter appears on the screen; next V_1 is disconnected and V_2, R_2 and C_2 are set so that another circle of required diameter appears. When V_1 and V_2 are connected as in Fig. 1, the resultant trace will be a circle.

Case of equal voltages, the trace being a circle. Let x_1, x_2, y_1 and y_2 represent the deviations of the spot from the centre of the screen due to the voltages on the respective plates; let $V_1 = V_2 = V$ and $f_1 = f_2 = f$, then,

$$\left.\begin{aligned} x_1 &= KV\sin\omega t; \quad & x_2 &= KV\sin(\omega t+\phi)\\ y_1 &= KV\cos\omega t; \quad & y_2 &= KV\cos(\omega t+\phi), \end{aligned}\right\} \tag{1}$$

where K is a constant, $\omega = 2\pi f$ is the angular frequency and ϕ is the phase angle between the two voltages.

With the connexions as in Fig. 1, the total deviations are,

$$\left.\begin{aligned} x &= x_1 + x_2 = 2KV\cos\tfrac{1}{2}\phi\,\sin(\omega t+\tfrac{1}{2}\phi)\\ y &= y_1 + y_2 = 2KV\cos\tfrac{1}{2}\phi\,\cos(\omega t+\tfrac{1}{2}\phi) \end{aligned}\right\} \tag{2}$$

The radius of the resulting circle is,

$$r = 2KV\cos\tfrac{1}{2}\phi. \tag{3}$$

The radius of the resulting circle will therefore vary with ϕ, being equal to $r_{max} = 2KV$ when $\phi = 0°$ and $r = 0$ when $\phi = 180°$. Furthermore there is an additional rotation of the spot when ϕ changes and the spot describes a spiral. If a short pulse modulates the grid of the cathode-ray oscillograph and ϕ varies, then the locus of the pulse appearing on the screen will be a circle of radius equal to half the radius of the resulting circle.

Fig. 2 shows the resultant maximum circle of radius $r_{max} = 2KV$ traced out by two equal voltages of equal frequencies and the circle a that would be traced out by a modulating pulse for a variation of ϕ between 0° and 360°.

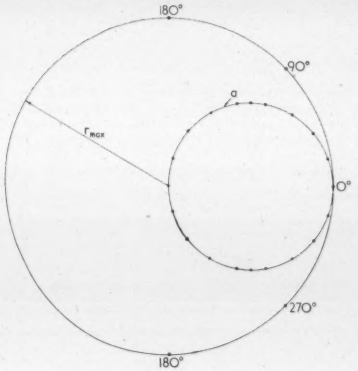

Fig. 2. Locus of a modulating pulse when the voltages tracing the circle are of equal magnitude

It is therefore possible to determine the phase difference between the two voltages tracing the resultant circle, by the position on the screen of a modulating pulse, relative to radial lines, concentric circles and circles such as a in Fig. 2. If the angular frequencies of V_1 and V_2 are respectively ω_1 and ω_2, ω_1 being near enough to ω_2 so as not to distort the circle, then with $V_1 = V_2 = V$ and writing $\omega_2 - \omega = \Delta\omega$, we have,

$$\left.\begin{aligned} x_1 &= KV\sin\omega t; \quad & x_2 &= KV\sin(\omega_1+\Delta\omega)t\\ y_1 &= KV\cos\omega t; \quad & y_2 &= KV\cos(\omega_1+\Delta\omega)t. \end{aligned}\right\} \tag{4}$$

Writing $\Delta\omega t = \phi$, we have

$$r = 2KV\cos\tfrac{1}{2}\phi. \tag{5}$$

The angle ϕ will vary with time; if therefore the grid is modulated by a short pulse the circle of Fig. 2 should be obtained on the screen.

Case of unequal voltages, the trace being a circle. Let the voltages tracing the circle be V_1 and V_2 and the angular frequency of both ω, then,

$$\left.\begin{aligned} x_1 &= KV_1\sin\omega t; \quad & x_2 &= KV_2\sin(\omega t+\phi)\\ y_1 &= KV_1\cos\omega t; \quad & y_2 &= KV_2\cos(\omega t+\phi). \end{aligned}\right\} \tag{6}$$

The total deviations of the spot are,

$$\left.\begin{aligned} x = x_1 + x_2 &= \sqrt{[(KV_1)^2 + (KV_2)^2 + 2K^2V_1V_2\cos\phi]}\,\sin(\omega t+\theta)\\ y = y_1 + y_2 &= \sqrt{[(KV_1)^2 + (KV_2)^2 + 2K^2V_1V_2\cos\phi]}\,\cos(\omega t+\theta) \end{aligned}\right\} \tag{7}$$

where

$$\tan\theta = \frac{V_2\sin\phi}{V_1 + V_2\cos\phi}. \tag{8}$$

The radius of the circle will be

$$r = \sqrt{[(KV_1)^2 + (KV_2)^2 + 2K^2V_1V_2\cos\phi]} \qquad (9)$$

and this radius will vary from $r_{max} = [\sqrt{K^2(V_1 + V_2)^2}]$ when $\phi = 0°$, to $r_{min} = \sqrt{[K^2(V_1 - V_2)^2]}$ when $\phi = 180°$.

The phase difference between the two voltages can again be determined by the position of a modulating pulse relative to concentric circles, radial lines and the locus of the pulse. Fig. 3 shows the resulting circles b and b_1 of maximum and

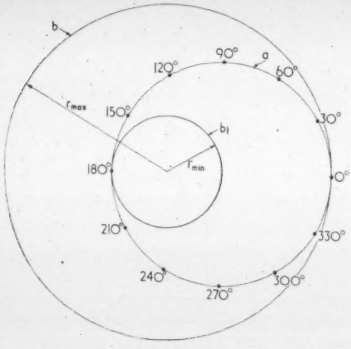

Fig. 3. Locus of a modulating pulse when the voltages tracing the circle are of unequal magnitude

minimum radius respectively, in the case of $V_1 = 2V_2$ and the locus of a modulating pulse (circle a) for a variation of ϕ between 0° and 360°.

Practical manipulation. When the voltages V_1 and V_2, the phase difference between which has to be measured, are equal, the manipulation is very simple. A thin graticule d, Fig. 4,

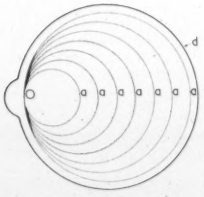

Fig. 4. Special graticule

on which circles such as a in Fig. 2 are drawn, is attached to an ordinary graticule containing radial lines and concentric circles; graticule d can be moved around the centre 0.

The magnitudes of the voltages $V_1 = V_2$ are measured by means of a voltmeter and the resultant circle is first traced on the screen by the voltage V_1 and a voltage V_{21} equal in magnitude to V_1 and in phase with it (voltage V_{21} is normally taken from the source V_1); the resultant circle will have a maximum radius equal to $2KV$. The grid is now modulated by a short pulse obtained from and in phase with V_1, the pulse will appear on the circumference of the resultant circle and graticule d is turned till the position of the pulse coincides with the end of a diameter of one of the circles a. When the voltages V_1 and V_2 are next applied, as shown in Fig. 1, the position of the pulse on the circle a will show the phase difference between V_1 and V_2. When the voltages V_1 and V_2 are not equal, the manipulation is slightly more complicated. The magnitudes V_1 and V_2 are measured by means of a voltmeter and the resultant circle of minimum radius is first traded by means of the voltage V_1 and a voltage V_{21} equal to V_1 but in phase opposition with V_1; secondly, V_{21} is reversed so that it is in phase with V_1, the resultant circle will then be of maximum radius.

The grid is now modulated by a short pulse and this pulse will appear on the circumference of the circle of maximum radius, the position of the pulse being at 0° in Fig. 3. The circle a is therefore determined so that if V_1 and V_2 trace the resultant circles their phase difference will be given by the position of the pulse on the circle a.

Case of the resultant trace being a line. By reversing the positions of R_1 and C_1 (or R_2 and C_2) in the circuit of Fig. 1, a line will appear on the screen if $V_1 = V_2$.

In the case of $f_1 = f_2 = f$ the deviations of the spot from the screen centre and due to the voltages on the respective plates are,

$$\left.\begin{aligned} x_1 &= -KV\cos\omega t; \quad x_2 = KV\sin(\omega t + \phi) \\ y_1 &= -KV\sin\omega t; \quad y_2 = KV\cos(\omega t + \phi) \end{aligned}\right\} \qquad (10)$$

The total deviations will be

$$\left.\begin{aligned} x &= x_1 + x_2 = KV\sqrt{[2(1 - \sin\phi)]}\sin(\omega t - \theta) \\ y &= y_1 + y_2 = -KV\sqrt{[2(1 + \sin\phi)]}\sin(\omega t - \theta) \end{aligned}\right\} \qquad (11)$$

where $$\tan\theta = (1 - \sin\phi)/\cos\phi \qquad (12)$$

The inclination of the line will vary with ϕ, the line will be vertical when $\phi = 0°$ and horizontal when $\phi = 180°$.

If the phase difference varies continuously, or if the frequencies of V_1 and V_2 are different, yet near enough not to distort the line, the spot will trace out a spiral, whilst the line will rotate around its axis.

It is therefore possible, as in the case of the circle, to determine the phase difference between the voltages tracing the line by means of a short pulse modulating the grid. The position of the pulse relative to radial lines and concentric circles traced on the graticule will determine the phase difference between the voltages.

The locus of a modulating pulse for a variation of ϕ from 0° to 360° will be a circle of radius equal to half the length of the traced line.

Practical manipulation. The manipulation is the same as in the case of a circle. The voltages V_1 and V_2 which have to be equal are measured by means of a voltmeter. A line is first produced by means of V_1 and V_{21} equal in magnitude to V_1 and in phase with it; the modulating pulse and the end of one of the circles a of the graticule shown in Fig. 4 are made to coincide with the end of the line.

The voltages V_1 and V_2 are now applied and the phase difference between them will be given by the position of the pulse on the circle a.

MEASUREMENT OF FREQUENCY

The circuit of Fig. 1 is very suitable for the comparison of the frequencies of V_1 and V_2.

In the case of $V_1 = V_2$, the frequencies being respectively f_1 and f_2, the circle will contract and expand passing from maximum radius to zero in 1 sec for a 1 c/s difference between f_1 and f_2; the frequencies can therefore be compared very conveniently and very accurately to a small fraction of a cycle. The method is preferable to a Lissajous figure since observation of a contracting circle is easier and less likely to induce an error.

In the case of a line being traced, the line will rotate through 180° in 1 sec for a 1 c/s difference between f_1 and f_2; again, the frequencies can be compared accurately and conveniently.

The calculation of voltage surges in a Van de Graaff generator

By B. MILLAR, B.A., Research Laboratory, Associated Electrical Industries Ltd., Aldermaston, Berks.

[*Paper first received* 19 *November*, 1952, *and in final form* 5 *August*, 1954]

Calculations have been made on the transient voltage changes occurring in the stack of a Van de Graaff electrostatic generator under spark-over conditions, and it is shown that these changes are strongly influenced by the capacitances from the stack plates to the tank. Breakdown between two adjacent stack plates may lead to the breakdown of the whole generator. Radial breakdown can cause the potential between adjacent stack plates to be reversed in polarity and increased in magnitude to several times its normal value. The insertion of resistors between accelerator tube electrodes and the adjacent stack plates can protect the accelerator tube from damage in the event of axial breakdown of the generator stack.

1. INTRODUCTION

The accelerator tubes in Van de Graaff accelerators tend to be damaged by surges in the generator, even though protective spark gaps are used and the voltage normally existing between electrodes is much less than that needed to produce breakdown.* A possible explanation is that the time lags of breakdown in vacuum are generally less than those of breakdown in high-pressure gas. Then, if voltage surges of large amplitude and short rise time occur in the generator, breakdown might occur in the accelerator tube rather than across the spark gaps, even though the latter are subjected to the greater overvoltage. It is clear that if a spark occurs anywhere in the generator, then surge voltages will be produced at other points of the generator, but the magnitudes of these surges have not hitherto been known. This paper describes some calculations on the subject, and shows that large amplitude surges of short rise time can occur.

2. EQUIVALENT CIRCUIT

The investigation neglected the effects of time lags, estimated to be of the order of 10^{-8} s, in the propagation of voltages through the machine due to distributed inductance effects.

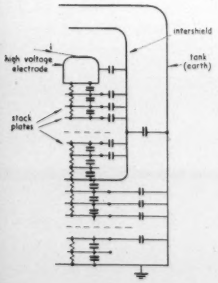

Fig. 1. Equivalent circuit of generator

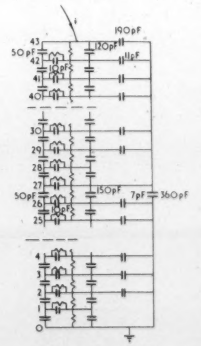

Fig. 2. Equivalent circuit of generator with resistors between plates and spinnings

With this simplification, the machine may be considered as a network of the stack resistors and a large number of capacitances fed from a high impedance source (the belt). Fig. 1 is an equivalent circuit for a machine with one intershield, and shows the capacities considered to be of the greatest importance. The intershield completely separates the inner and outer portions of the generator, so that the two sections may be considered separately. Since the configuration of the circuit elements in the two sections is identical, an analysis developed for one may be applied, merely by changing numerical values, to the other, or to a portion of another generator, no matter what number of intershields it may have.

A breakdown between any two points in the generator is considered to be equivalent to the closing of a switch between them. The potential differences in the generator shortly after a breakdown are equal to those existing before the breakdown, plus those produced in the equivalent circuit, initially uncharged, by the application between the points of breakdown of a voltage equal and opposite to that existing between those points of the generator before the breakdown.

The potentials existing before breakdown (i.e. under steady conditions) are determined by the stack resistors only. Since distributed inductance and series resistance have been neglected, the potential changes at breakdown may be considered to be instantaneous, and their magnitudes depend only on the capacities between the electrodes. The subsequent return to the normal state is determined by the time constants of the circuits; but these are large (0·1 s and upwards), and hence the changes in potential when a spark occurs may be calculated from an equivalent circuit consisting only of the capacities of the generator, and this will hold with sufficient accuracy in the period 0·1 μs to 1 ms after the assumed breakdown. This covers the period in which further breakdowns, as a consequence of the first, are most likely to occur.

3. CALCULATION OF SURGES

Numerical values relating to the outer section of the 4 MV generator at Aldermaston will be used. This has twenty-six intermediate stack plates, the intershield being connected to the twenty-seventh, so that there are twenty-seven plate-to-plate gaps which normally all have equal voltages, say E, across them. The capacity between the adjacent plates has been measured and found to be 200 pF, including the capacity between accelerator tube electrodes. The capacity from each plate to the tank was estimated to be 7 pF, and that from the intershield to the tank to be 360 pF. In making calculations, portions of the stack were regarded as infinite ladder attenuators, whenever this simplification appeared to be justified. The results of some of these calculations are given in Table 1.

If breakdown occurs between two adjacent plates somewhere in the middle of the stack (e.g. plate 12 to plate 13) the greatest increase in voltage resulting is about 9%, and it occurs across the two immediately adjacent plate-to-plate gaps. If the gaps stand this voltage without breakdown, all

* MIRANDA, F. J., and CHICK, D. R. *J. Sci. Instrum.*, **29**, p. 340 (1952).

the voltages in the generator return slowly to normal. If, however, another gap breaks down, the magnitudes of the surge voltages throughout the generator are increased, and this may lead by cumulative effects to the breakdown of the whole generator. If the initial breakdown is between two plates either just below the intershield or near the bottom of the stack, the results are similar, but the magnitudes of the surge voltages are raised by a factor of between 1 and 2, so that cumulative breakdowns are more likely.

Table 1. *Surge voltages caused by inter-electrode breakdown*

Breakdown assumed plate numbers	*Inter-electrode gap considered*	*(Voltage across gap)/E*
12 to 13	13 to 14	1·09
	or 11 to 12	
	14 to 15	1·07
	or 10 to 11	
12 to 13 and 13 to 14	14 to 15	1·17
	or 11 to 12	
All pairs of adjacent plates from 8 to 18 (i.e. 10 pairs)	7 to 8	1·85
	or 18 to 19	
Intershield to tank	26 to 27	−3·60
	25 to 26	−2·82
Intershield to tank and 26 to 27	25 to 26	−3·43

The bottom stack plate is No. 1, and the intershield is connected to plate 27.

The case of breakdown from intershield to tank is of particular interest, for the voltages across the plate-to-plate gaps just below the intershield are reversed in polarity and increased in magnitude by a factor of up to 3·6. Thus this breakdown also is likely to cause further breakdown, but in this case the magnitude of the greatest surge voltage existing after successive breakdowns becomes progressively less.

The effect of the capacitances from the stack plates to the tank is important for, without them, the transient equivalent circuit would reduce to a large number of capacitances in series. The effect of a breakdown between two adjacent plates in the stack would then be to raise the voltage between every other pair of adjacent plates by about 4%, while the effect of breakdown from intershield to tank would be to reduce the voltage between any two stack plates to zero.

4. THE INTRODUCTION OF RESISTORS

Resistors may be connected between the stack plates and the adjacent accelerator tube electrodes of a Van de Graaff generator, with the object of reducing the energy dissipated in sparks in the accelerator tube by separating the capacitances between accelerator tube electrodes from the relatively large capacitances between generator stack plates. The equivalent circuit then becomes more complicated, as shown in Fig. 2. The transient equivalent circuit is again obtained by omitting the resistors. Calculations on this circuit similar to those described in Section 3 would be exceedingly laborious. However it was noticed that the response of a capacitance network to a step function drive is the same as the response to d.c. of a similar network in which each capacitance is replaced by a conductance proportional to it. A resistance network was made on this basis as the analogue of the capacitance network and gave the changes in potential due to a surge in the generator. Its validity was subject to exactly the same considerations as were discussed with regard to the capacitance equivalent circuit (Section 2).

To represent any gap in the generator which had broken down, a potential was applied between the corresponding points of the analogue network of a magnitude corresponding to the potential previously existing across the gap in the generator, but of opposite sign. The resulting potential between any two points of the model then represented the change in potential between the corresponding points of the generator. This, added to the potential initially existing between the same two points, gave the resultant potential in the generator. The method could readily be extended to give the potential changes resulting from several breakdowns in quick succession.

Some results obtained from the use of the analogue network are shown in Table 2.

Table 2. *Surge voltages in generator with additional resistors*

Breakdown assumed	*Inter-electrode gap considered*	*(Gap voltage)/F*
P12–P13	P13 to P14	1·11
	S12 to S13	0·85
	S13 to S14	0·93
	S18 to S19	1·02
	P13 to S13	0·42
S12 to S13	S13 to S14	1·16
	P12 to P13	0·96
	S13 to P13	0·31
Intershield to tank	P26 to intershield	−3·97
	S24 to S25	−1·49
	P27 to S27	4·12

Pn denotes the *n*th plate from the bottom of the generator stack.

Sn denotes the *n*th accelerator tube electrode from the bottom of the generator stack.

If a breakdown occurs between two stack plates, the voltages between nearby accelerator tube electrodes are reduced. The voltages between accelerator tube electrodes further away are raised, but only very slightly. If the insulation between points on the accelerator tube and points on the generator stack normally at the same potential is sufficiently good (able to stand about 1·3 *E*) it is possible for a cumulative breakdown of the whole generator stack to take place without any large surge voltages between accelerator tube electrodes ever being produced, so that the tube is fully protected against damage caused by a breakdown of this type.

In the cases of a breakdown between accelerator tube electrodes or from intershield to tank, this arrangement does not appear to have any significant advantage or disadvantage as compared to the simpler one.

5. CONCLUSIONS

It has been shown that the transient voltage disturbances under spark-over conditions in a Van de Graaff electrostatic generator are very strongly affected by the capacitances from the stack plates to the tank.

In particular, in the case of radial breakdown of a section of the generator (e.g. intershield to tank), the potential between adjacent stack plates near the top of that section is reversed in polarity and increased in magnitude, up to 3·6 times in a particular case. This potential reversal may be important in considering the design of accelerator tubes.

Axial breakdown between two adjacent stack plates or accelerator tube electrodes cannot cause potential reversals, but it does cause increases in the potentials across adjacent

gaps which can lead by cumulative effect to the breakdown of the whole of that section of the generator. Further, it has been shown that the connexion of resistors between accelerator tube electrodes and the adjacent stack plates can protect the tube from damage initiated by axial breakdown of the generator stack, but not from the effects of breakdown from intershield to tank.

ACKNOWLEDGEMENTS

This work was undertaken as part of an investigation into the behaviour of the ion accelerator tube in the Aldermaston generator. The author is indebted to Mr. D. R. Chick and Dr. F. J. Miranda for helpful discussions during the work, and to Dr. T. E. Allibone for permission to publish the results.

The calculation of heat flow through disks and its application to conductivity measurements

By PROF. J. C. JAEGER, D.Sc., F.Inst.P., and A. BECK, B.Sc., Grad.Inst.P., Australian National University, Canberra

[*Paper received* 29 *June*, 1954]

A method for numerical calculation of steady flow of heat in an axial direction through a cylinder or a number of cylinders of different diameters is described. It is applied to determine a correction for errors in the diameter of disks used in the divided bar method of determining the thermal conductivity of rocks.

1. INTRODUCTION

The study of the steady flow of heat or electricity into cylindrical bodies through restricted areas of their surfaces dates back to Weber.[1] In this note a fairly general method, related to his, will be described for the solution of problems on axial flow through one or more disks. It was developed in order to obtain a theoretical correction for small errors in the diameter of the disks used in the divided bar method of measuring thermal conductivity which, following Benfield,[2] has been widely used for measurement of the conductivities of rocks. In this method a disk of the rock is introduced between two metal rods as in Fig. 1(*a*) and the conductivity of the rock is determined in terms of that of the rods by means of temperature measurements in the rods. The effect of the contact resistance between the rods and the rock is eliminated by making measurements with three or more disks of different thicknesses.

It frequently happens that the conductivity of a large number of samples from a drill core has to be measured; these usually vary in diameter by amounts of up to 5% so that either they must be machined to the diameter of the rods of the apparatus or a correction must be applied for the error in diameter. In the present instance a large number of samples of approximately 21 mm in diameter has had to be measured and an apparatus with rods of this diameter has been constructed.[3]

If the diameter of the disk is greater than that of the rods the situation will be that shown in Fig. 1(*b*), and the apparent conductivity of the sample will be high because of refraction of the lines of flow into the outer ring of the sample. Similarly, if the diameter of the disk is smaller than that of the rods, the apparent conductivity will be low. The general problem with rods and disks of different conductivities is a complicated one which may be discussed accurately by the methods of Section 4. The simplest idealizations of it which enable the effect of refraction of the lines of flow to be estimated are obtained by considering a disk of thickness l and diameter b, with either (i) constant temperature $\pm V$ over circles of radius a in its plane faces, in which case the total flow between these circles is calculated, or (ii) constant flux $\pm F$ over these circles, in which case the average temperature over the circles can be calculated [Fig. 1(*c*)]. These two problems may be regarded as having equal status as first approximations to the physical problem, and the second of them is the more valuable since, in this case, a simple exact solution is obtainable which is given in Section 2, while for the first problem the methods of Section 4 must be used. Numerical calculations have shown that the difference between the results of the two problems is negligible in the present context. In Section 3 it will be shown that the calculated results agree adequately with observations.

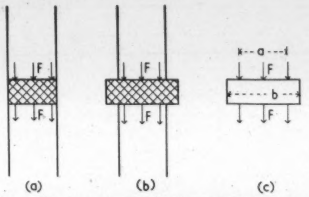

Fig. 1. The divided bar apparatus

The edge corrections of Section 2 are, of course, directly applicable both to the corresponding electrical problem and to the important case of the measurement of the permeability of a porous rock.

In Section 4 a general method for the solution of more complicated problems will be indicated.

2. EXAMPLE

Consider the problem of steady flow of heat in a disk of radius b and thickness l to which heat is supplied at a constant rate F per unit time per unit area over a concentric circle of radius a ($< b$) on one face and from which it is removed in the same manner from the opposite face. Assume that there is no loss of heat from the remainder of the surface of the disk. The temperature at any point may be calculated by the methods indicated in Section 4. From the present point of view the interesting quantity is v_a, the average temperature difference between the circles of radius a over which heat is supplied and removed. This is given by

$$v_a = \frac{Fl}{k}\left\{1 - \frac{16}{\pi^2}\sum \frac{I_1(n\pi a/l)}{n^2 I_1(n\pi b/l)} \times \left[I_1\left(\frac{n\pi b}{l}\right)K_1\left(\frac{n\pi a}{l}\right) - K_1\left(\frac{n\pi b}{l}\right)I_1\left(\frac{n\pi a}{l}\right)\right]\right\} \quad (1)$$

where k is the thermal conductivity of the disk, I_1 and K_1 are

the modified Bessel functions of order unity, and the summation is over the odd values 1, 3, 5 . . . of n.

The quantity

$$k_a = \frac{Fl}{v_a} \tag{2}$$

may be regarded as the apparent conductivity which is observed. In Fig. 2 the percentage error $100(k_a - k)/k$ in k is plotted against the percentage error $100(b - a)/a$ in

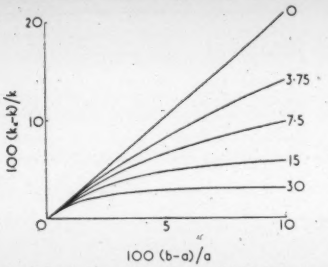

Fig. 2. Percentage error in conductivity plotted against percentage error in diameter. The numbers on the curves are values of $\pi a/l$

diameter b for the values 30, 15, 7·5 and 3·75 of $\pi a/l$ which correspond approximately to the sizes of the disks used in the apparatus under consideration.

For the case in which the disk is a long cylinder, equation (1) reduces to

$$v_a = \frac{Fla^2}{kb^2} \tag{3}$$

This gives the curve $\pi a/l = 0$ of Fig. 2 and corresponds to the case in which the diameter of the disk is smaller than that of the rods in the divided bar apparatus.

3. COMPARISON WITH EXPERIMENT

To check these theoretical results and to determine an experimental calibration for the apparatus, a number of disks was cut with varying diameters and all of thickness 4 mm. It was assumed in all cases that the contact resistance had the value determined in the normal way with a set of disks of varying thicknesses and of diameters equal to those of the rods. The results of a number of such experiments are shown in Fig. 3 with the theoretical curve for comparison. Since measured conductivities of contiguous rock samples may vary by as much as 2 or 3%, it appears that the correction of Fig. 2 may be applied without fear of exceeding this limit.

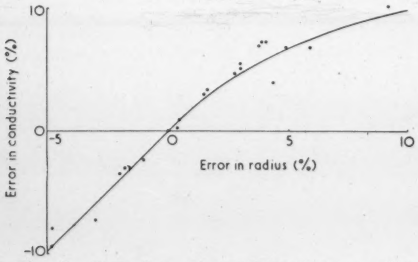

Fig. 3. Comparison of experimental values with calculated results for the case $\pi a/l = 15$

4. GENERAL THEORY

The problem of steady flow of heat in a stack of cylinders with different diameters as in Fig. 1(*b*) is one of considerable difficulty. It can, of course, be solved numerically in particular cases by relaxation methods, but we shall indicate here an alternative numerical method which is useful in problems of this type.

The fundamental result is the following: suppose that heat is supplied to the finite circular cylinder, $0 < r < b$, $0 < z < l$, at a constant rate (unity) per unit time per unit area over the ring $r' < r < r''$, $z = l$ and is removed at the same rate over the ring $r' < r < r''$, $z = 0$, there being no flow of heat over the remainder of the surface, then the average temperature $v(r_1, r_2; r', r'')$ over the region $r_1 < r < r_2$, $z = l$ of the surface is given by

$$v(r_1, r_2; r', r'') = \frac{8l}{k\pi^2(r_2^2 - r_1^2)} \sum_{n=1,3,5,\ldots} \frac{1}{n^2} \frac{[r_2 I_1(n\pi r_2/l) - r_1 I_1(n\pi r_1/l)]}{I_1(n\pi b/l)} \times \left\{ \begin{array}{l} I_1\left(\frac{n\pi b}{l}\right)\left[r' K_1\left(\frac{n\pi r'}{l}\right) - r'' K_1\left(\frac{n\pi r''}{l}\right)\right] \\ + K_1\left(\frac{n\pi b}{l}\right)\left[r'' I_1\left(\frac{n\pi r''}{l}\right) - r' I_1\left(\frac{n\pi r'}{l}\right)\right] \end{array} \right\} \tag{4}$$

for the case $r_1 < r_2 \leqslant r' < r''$ with similar results for other cases. This result may be derived by the methods of Gray and Matthews[4] or Carslaw and Jaeger.[5] The series (4) is rapidly convergent and easily evaluated.

Putting $r_1 = 0$, $r_2 = r' = a$, $r'' = b$ and subtracting the result from Fl/k (corresponding to supply of heat over the whole circle) gives equation (1). Now suppose that the range $0 < r < b$ is divided into N equal parts ϵ so that $b = N\epsilon$, and that all the quantities $v[m\epsilon, (m+1)\epsilon; m'\epsilon, (m'+1)\epsilon]$ giving the average temperature over one ring of width ϵ due to unit flux over another ring are calculated. Then, if $F_{m'}$, $m' = 0, \ldots, N-1$, is the rate of heat supply over the m'th ring, the average temperature over the mth ring is

$$\sum_{m'=0}^{N-1} F_{m'} v[m\epsilon, (m+1)\epsilon; m'\epsilon, (m'+1)\epsilon]$$

The boundary conditions which are linear relations between the temperature and the flux of heat then lead to a set of algebraic equations for the determination of $F_{m'}$. These equations are strongly diagonal and easily solved by iteration. As remarked in Section 1, a first application of this method has been made to the case of a disk with circular areas on its plane surfaces maintained at constant temperature; the calculated results being very little different from those of Fig. 2.

REFERENCES

(1) Weber, H. *J. Reine Angew. Math.*, **75**, p. 75 (1873).
(2) Benfield, A. E. *Proc. Roy. Soc., A*, **173**, p. 428 (1939).
(3) Newstead, G., and Beck, A. *Austral. J. Phys.*, **6**, p. 480 (1953).
(4) Gray, A., and Matthews, G. B. *Treatise on Bessel Functions*, Chap. 12 (London: Macmillan and Co. Ltd., 1922).
(5) Carslaw, H. S., and Jaeger, J. C. *Conduction of Heat in Solids*, Sections 153, 142 (London: Oxford University Press, 1947).

A method of identifying double-flash exposures

By N. Dombrowski, Ph.D., High Speed Fluid Kinetics Laboratory, Imperial College of Science and Technology, London, S.W.7

[*Paper first received* 23 *August, and in final form* 9 *September*, 1954]

A method is described of identifying two exposures taken in rapid succession on one photographic plate. It employs two light sources of differing spectral constitution with two plates, face to face, of suitable colour sensitivities. By this means a reference negative containing one image is obtained, in addition to the usual double-flash photograph.

The phenomena occurring in high-speed fluid flow have been studied by a number of workers by means of high-speed cinematography. Where the event is continuous in character, it has been found more convenient to take two exposures in rapid succession on the same negative. A few pairs of such exposures taken at random can then be used to determine both the velocity and history of an event. This method is particularly advantageous when detailed investigations are made of phenomena requiring high image/object ratios and, hence, large negative sizes.

The method has been used in this laboratory to study such phenomena as the manner of disintegration of liquid sprays, and the stream velocities of gases and liquids. The latter are usually derived from measurements of distances between successive images of suspended light reflecting particles such as aluminium powder. In order to attain a high degree of accuracy, the distance between the two images, and thus the delay between the two flashes, should be as large as possible. This cannot be easily achieved since it becomes difficult to select the correct pairs of images. A further complication arises when both the magnitude and direction of velocity are varying.

Attempts have been made to solve this problem by employing flashes of different light intensity so that one image is lighter than the other. This has not proved completely successful, since in the case of suspended aluminium particles,

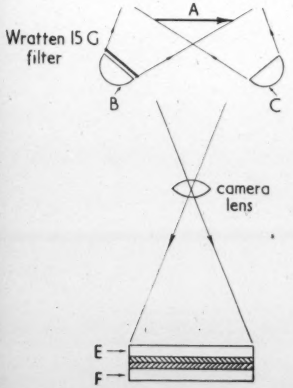

Fig. 1. Optical system

the light reflected also depends upon the inclination of their surfaces to the camera lens. Thus, in some instances, one image may be lost, or it may be brighter than the other, irrespective of the flash intensity. In addition, the loss in detail produced by the weaker flash may impair a true interpretation of the result.

This note describes a simple technique by which the two exposures may be identified. It consists of illuminating the object with two flashes of differing spectral constitution and exposing two plates of suitable sensitivities. Two images are obtained on one plate to provide the double exposure, and one image is obtained on the other plate to provide a reference negative.

2. Optical System

Fig. 1 illustrates the optical system. The object *A* is illuminated by high-pressure xenon flash lamps *B* and *C*, which can be triggered with delays varying from 5 μs to 10 ms.* The light emitted by *B* is filtered through a Wratten 15G filter so that only wavelengths between 5200 and 6500 Å illuminate the object. The light from lamp *C* is unfiltered so

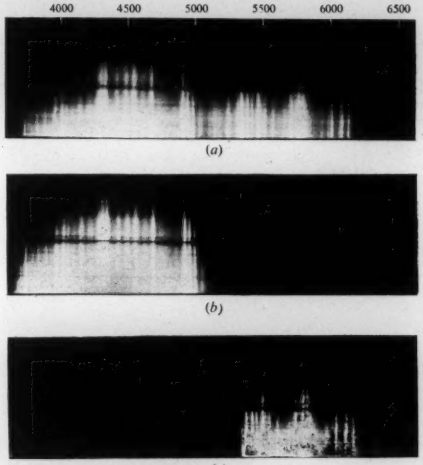

Fig. 2. Wedge spectra of plates and filter to light from high pressure xenon flash tubes

(*a*) P300 emulsion (light emitted by lamp *C*); (*b*) scientific 00 emulsion; (*c*) Wratten 15G filter (light emitted by lamp *C*).

that the total emission from 3500–6500 Å is effective. The light from the two flashes is then received by the camera on two plates *E* and *F* held face to face in a plate holder. Thus the light exposes plate *E* through the glass plate before it reaches plate *F*. Plate *E* is unbacked panchromatic, sensitive to the light of all wavelengths between 3400 and 6500 Å,

* Dombrowski, N., Fraser, R. P., and Peck, G. T. *J. Sci. Instrum.* To be published.

whilst plate *F* is backed non-colour-sensitized, sensitive only to wavelengths between 3500 and 5200 Å.

Fig. 2 illustrates the wedge spectra of the two materials and filter taken with light emitted by the two flash lamps. It can be seen that the light from lamp *C* will expose both plates whilst that from lamp *B* will only expose the panchromatic plate, since the filter absorbs light below 5200 Å to which the non-colour-sensitized plate is sensitive. Thus, two images will be exposed on the panchromatic plate whilst one image will be exposed on the non-colour-sensitized plate.

Experiments have shown that a suitable combination of plates is the fast Kodak Scientific 00 non-colour-sensitized (*F*) and the medium speed Kodak P300 panchromatic (*E*). A higher speed is required for the non-colour-sensitized plate because much of the light is absorbed by the sensitive layer of the other plate. Flash lamp *B* was placed nearer the object than lamp *C* in order to obtain equal densities for the double image on plate *E*.

As the rear of plate *E* occupies the plane on which images are normally focused, the ground glass focusing screen on the camera is reversed in order to coincide with the new plane of the two sensitive layers.

3. AN APPLICATION TO THE STUDY OF DROP FORMATION

Fig. 3 shows an example of this technique applied to the study of the disintegration of liquid sprays. It illustrates the breakdown of a sheet of liquid into drops, and their subsequent paths. Fig. 3(*a*) shows the double-exposure photograph obtained with the P300 plate. Fig. 3(*b*) shows the reference exposure obtained with the scientific 00 plate. In this example, flash lamp *B* has been triggered first so that Fig. 3(*b*) represents the first flash. The expansion of the perforations in the sheet and the production and behaviour of drops can now be interpreted.

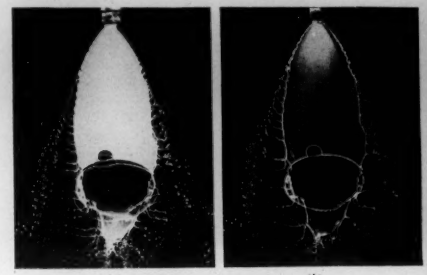

(*a*) (*b*)

Fig. 3. Drop formation from spray sheet
(*a*) Double exposure; (*b*) reference exposure.

The technique could be further extended by employing negative colour film with corresponding tricolour filters. This would enable both exposures, as well as the composite image, to be individually printed.

ACKNOWLEDGEMENTS

The author wishes to express his thanks to the Agricultural Research Council for the provision of a research grant, to Mr. R. P. Fraser for his advice and interest, to Dr. A. G. Gaydon for his help in obtaining the wedge spectra, and to colleagues of the High Speed Fluid Kinetics Laboratory.

Heat transfer through oxide-cathode materials

By A. E. Pengelly, B.Sc., Research Laboratories, The General Electric Co. Ltd., Wembley, Middlesex.

[*Paper first received* 20 *May, and in final form* 28 *June*, 1954]

A method of measuring the thermal conductivity and opacity of poorly conducting translucent materials has been developed and used to measure the conductivities at about 150° C of polycrystalline barium oxide, strontium oxide and an equimolecular mixture of the two with and without 2½% zirconium oxide or 5% zirconium added. These oxides were in the form used for typical oxide-cathode coating. The sum of the absorption and scattering coefficients has in each case been estimated from the results.

EXPERIMENTAL APPARATUS

The object of this work was to study the thermal conductivity and obtain incidentally some information about opacity for the barium–strontium oxide material as used in valve and lamp cathode manufacture. The oxides are unstable in air and are therefore applied to their metal base as carbonates which are decomposed in vacuum. The barium–strontium carbonates consist of particles of diameter about 2 μ prepared by precipitation from the double nitrate solution using sodium carbonate. The single carbonates were barium carbonate and strontium carbonate of particle size 2–3 μ, both precipitated from ammonium carbonate.

The method used was a modification of Lees disk apparatus for poor conductors. Fig. 1 is a diagram of the experimental vacuum tube. Two pure nickel disks 15 mm in diameter and 5 mm thick were turned hollow to have 1 mm walls and fitted with molybdenum–tungsten heaters insulated with alumina and rated to give 45 W each at 30 V and 900° C. A pure nickel disk 1 mm thick was pressed into the open end of each block as shown in section in Fig. 1. Both assemblies were thoroughly outgassed by heating in a vacuum at 1050° C for 1 h as were all the metal parts used in the vacuum tube. The two blocks were sprayed on their plane face with the carbonates of the materials to be examined, the surfaces of which were then faced in a lathe to a thickness of 0·45 mm and pressed together.

The blocks were held together by three ceramic tubes 2 mm outside diameter and 15 mm long seated in recesses spaced symmetrically in each lid and in nickel pressure plates at the far ends. The pressure was maintained at about 500 g by two steel springs shown in Fig. 1. 0·05 mm Chromel and Alumel thermocouple wires were spot welded to each disk and the whole assembly was mounted in a glass bulb and evacuated to a vacuum better than 10^{-6} mm of mercury. The tube was then baked for 6 h at 400° C and further outgassing of the pressure plates accomplished by eddy current heating at 900° C. The disks were outgassed and the carbonates decomposed to oxides by lighting the heaters.

This was done by increasing the temperature in stages from 500 to 1040° C to allow the carbon dioxide and binder breakdown products to escape through the interstices of the material. When the temperature had reached 1040° C it was held for 6 h. Subsequent examination of the material showed that the coating was even, of proper colour, and well bonded to the nickel disks. The two layers fused completely in all cases. The thermocouples were calibrated in the range 650–1100° C with an optical pyrometer and in one case the wires were brought through the pinch. It was found in this way that errors due to heating of the cold junctions could be accurately corrected in terms of the total watts dissipated in the tube and temperatures measured to within 1%.

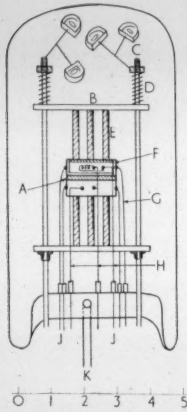

Fig. 1. Details of experimental vaccum tube

A, specimen material;
B, pressure plate;
C, getters;
D, springs;
E, 2 mm ceramic tubes;
F, section of upper disk;
G, thermocouple wires;
H, heater leads;
J, leads;
K, pumping stem.

EXPERIMENTAL METHOD

The experiment to measure heat transfer per unit temperature difference was made in two distinct parts.

1. The power dissipated in each of the blocks was measured when they were held in equilibrium at various equal temperatures. Since the system is symmetrical about the plane of the coating the power in each should have been, and was, to 1%, the same. The temperature of the glass envelope was kept below 60° C by a forced-air draught, thereby reducing to negligible quantities the errors in heat loss caused by varying ambient temperatures.

2. Using one heater only one block was held at a predetermined temperature and the equilibrium temperature of the other was measured. From the temperature of the second block the amount of heat dissipated was determined from the results of the first part of the experiment and since this must all have passed through the oxide the effective conductivity K' was calculated from the equation:

$$H = K' \frac{A}{l}(T_1 - T_2) \qquad (1)$$

H = total heat dissipated per second (W)
K' = apparent conductivity (W. cm^{-1}. °C^{-1})
T_1 = higher temperature (°K)
T_2 = lower temperature (°K)
A = area of coating (cm)
l = thickness of coating (cm)

This experiment was repeated for a series of different temperatures T_1, between 150 and 750° C and a graph of K' against the mean temperature $\bar{T}$ was drawn (Fig. 2). Table 2 shows a typical series of results for barium oxide. It will be noted that at low temperatures the curves are asymptotic to finite values of K' and these are taken to be the values of K_0, the true conductivity. In the cases of barium oxide and the pure mixture, measurements were made on two tubes and excellent agreement was obtained in each case between the independent results.

An anode in the form of a nickel ring was placed concentric with the blocks and the thermionic emission from the exposed side edge of coating was measured at several temperatures. These emissions were found to be slightly low but not greatly different from normally accepted values, e.g. D. A. Wright.[1] (For barium oxide $\phi = 1{\cdot}5$, for the pure mixture $\phi = 1{\cdot}3$.)

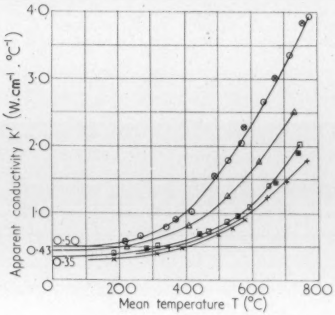

Fig. 2. Showing relation between mean temperature and apparent conductivity

○ tube no. 3 BaO.
⊗ tube no. 5 BaO.
△ tube no. 2 SrO.
⊡ tube no. 7 BaSrO.
⊞ tube no. 9 BaSrO.
+ tube no. 4 BaSrO + 2½% ZrO.
× tube no. 6 BaSrO + 5% Zr.

An attempt was made to measure the heat transfer with a constant small temperature difference, $(T_1 - T_2)$ by heating both disks and subtracting the input to that at lower temperature from the heat which it dissipated. This was, however, found to be impracticable with the present power supply and measurement system.

Probable error in K_0. The values of K_0, the true conductivity quoted in Table 1, are derived directly from the graphs and are subject only to errors in measurement of the quantities in equation (1). It should be noted that these values apply to the polycrystalline material and are probably several times lower than those for single crystals.

Computation of the probable error from equation (1) gives a maximum of about 10% and this is the basis for the limits set in Table 1 on K_0.

The absorption and scattering coefficient (ϵ). The values of ϵ (cm) can be estimated as follows:

As a first approximation to the heat transfer equation we may take:

$$H\frac{l}{A} = K_0(T_1 - T_2) + B(T_1^4 - T_2^4)\sigma \qquad (2)$$

where l, A, H, T_1, T_2, K_0 have meanings as above, σ = Stefan's constant = 5·75 joules cm^{-2}. s^{-1}. °K^{-4} and

B = constant of dimensions (cm) which arises because of absorption and scattering in the medium.

This equation assumes that the temperature gradient is constant and that black-body conditions prevail within the medium. The actual variation of the temperature gradient is not important since at low temperatures it is minimum and at high temperatures the first term in equation (2) is small compared with the second. Since equation (2) assumes black-body condition and since this implies that $T_1 \gg (T_1 - T_2)$ we may write the expression in the differential form:

$$\left(\frac{l}{A}\right)\left(\frac{\Delta H}{\Delta T}\right) = K' = K_0 + 4B\sigma T_1^3 \qquad (3)$$

Now van der Held[2] gives the equation below for the apparent conductivity when black-body conditions apply, i.e. under the same restrictions.

$$K' = K_0 + (16n^2/3\epsilon)\sigma T_1^3 \qquad (4)$$

where n = optical refractive index, ϵ = sum of absorption and scattering coefficients and both n and ϵ are assumed independent of wavelength.

Thus we identify B with $4n^2/3\epsilon$ and rewrite equation (2):

$$Hl/A = K_0(T_1 - T_2) + (T_1^4 - T_2^4)\sigma(4n^2/3\epsilon) \qquad (5)$$

This expression is, however, still true only when black-body conditions hold and the emissivities of the metal faces are effectively unity.

O. A. Saunders[3] gives the expression:

$$H/A = \sigma(T_1^4 - T_2^4)e^2/(2e - e^2) \qquad (6)$$

for the heat transfer between two plane parallel surfaces of total emissivity e, separated by a non-absorbing medium.

Thus, a better approximation to the heat flow equation in the present work is obtained by introducing the factor $\rho = e^2/(2e - e^2)$ to account for the error when $T_1 \not\gg (T_1 - T_2)$ Thus

$$Hl/A = K_0(T_1 - T_2) + (4n^2/3\epsilon)\rho(T_1^4 - T_2^4)\sigma \qquad (7)$$

where $$\rho = e^2/(2e - e^2)$$

Evidently if we know both e and n^2 we can derive estimates of ϵ.

The values of e and n². The values of n^2 for pure barium oxide and strontium oxide crystals are accurately known,[4] and the values for a polycrystalline mass may be calculated[5] from the equation;

$$\frac{(K_m - 1)}{(K_m + 2)} = V_2\frac{(K_2 - 1)}{(K_2 + 2)} \qquad (8)$$

where V_2 = fraction of volume occupied by crystals, K_2 = optical dielectric constant = n^2 for single crystal, K_m = optical dielectric constant of polycrystalline mass.

The values calculated for $K_m(=n^2)$ for polycrystalline barium, strontium and barium–strontium oxides are given in Table 1 and the zirconium and zirconium oxide additions are assumed to have negligible effect.

The value of e, the total emissivity of the nickel-coating interfaces, was estimated by comparing them visually with similar surfaces of known emissivity, e.g. nickel oxide and carbon black, and a value of 0·8 decided upon. The value of ρ to be taken is thus 0·65 and the probable maximum error is $\pm 0{\cdot}15$.

Computation of ϵ from the equation (7) using the figures for e and n^2 discussed above gives the values shown in Table 1 but it is to be stressed that they are estimates only. The nearly constant values of $B\rho$ shown in Table 2 indicate that equation (7) is quite a good approximation.

Table 1. *Summary of results*

Material	$B\rho$ *at 600° C* (*cm*)	ϵ (cm^{-1})	K_m *from known values*	K_0 *W. cm⁻¹. °C⁻¹*
BaO	0·019	94	1·33	$(0{\cdot}50 \pm 0{\cdot}05) \times 10^{-4}$
SrO	0·009	192	1·29	$(0{\cdot}43 \pm 0{\cdot}04)$
BaSrO	0·0022	794	1·31	$(0{\cdot}35 \pm 0{\cdot}03)$
BaSrO and ZrO_2	0·0019	920	1·31	$(0{\cdot}35 \pm 0{\cdot}04)$
BaSrO and and Zr	0·0015	1160	1·31	$(0{\cdot}35 \pm 0{\cdot}05)$

Table 2. *Barium oxide detailed results*

W. cm⁻¹. s⁻¹ *K'*	*°C⁴* $\Delta(T)^4$	*°C* ΔT	*W/s* *H*	*°C* $\bar{T}$	*cm* $B\rho$
4·07	$1{\cdot}62 \times 10^{-12}$	289	2·976	839	0·012
3·93	1·194	251	2·432	778	0·012
3·35	0·891	226	1·909	7·7	0·013
2·64	0·614	202	1·349	639	0·012
2·06	0·448	183	0·951	571	0·011
1·79	0·331	171	0·776	530	0·012
1·00	0·206	154	0·390	420	0·012
0·78	0·112	121	0·239	341	0·005
0·66	0·051	84	0·139	262	0·005

From this table K by graph $= 0{\cdot}50 \times 10^{-4}$ (W. cm^{-1}. $°C^{-1}$).
Area = 1·76 (5) (cm^2). Thickness = 0·07 (cm).

SUMMARY AND CONCLUSIONS

The values of thermal conductivity have been measured and the sum of absorption and scattering coefficients estimated for samples of typical oxide cathode materials in a condition approximating to that normally acceptable. The value of K_0, the true conductivity, was found not to vary greatly among the materials studied and was about $0{\cdot}4 \times 10^{-4}$ (W. cm^{-1}. $°C^{-1}$). The estimates of absorption coefficients, while not claimed to be individually accurate, should relatively be reliable. The values are different for the two single oxides but both are less than 200. The much higher values for the double oxides may be due in part to the different structures of the coating comparing ammonium precipitated single carbonates with sodium precipitated double carbonates. The magnitude of the difference between the values for the two single oxides makes it safe, however, to assume that this is not the only factor.

An absorption and scattering coefficient ϵ (cm^{-1}) implies that in a distance $1/\epsilon$ cm the intensity of radiation is reduced by a factor $1/e = 0{\cdot}37$. Thus for a normal oxide-cathode coating of thickness about 0·1 mm the fraction of the radiation leaving the base metal and passing straight through the coating would be for barium oxide about one-third, for strontium oxide about one-ninth and for the mixtures a very small fraction.

REFERENCES

(1) WRIGHT, D. A. *Proc. Instn Elect. Engrs*, **100** (III), p. 125 (1953).
(2) VAN DER HELD, E. F. M. *Appl. Sci. Res.*, **A3**, p. 237 (1952).
(3) SAUNDERS, O. A. *Proc. Phys. Soc.*, **41**, p. 569 (1928–29).
(4) HAASE, M. *Z. Krist*, **55**, p. 509 (1927).
(5) ROBERTS, S. *J. Opt. Soc. Amer.*, **42**, p. 850 (1952).

The rubber membrane and the solution of Laplace's equation

By W. Fulop, B.Sc., A.Inst.P., Department of Physics and Mathematics, College of Technology, Birmingham

[*Paper first received* 11 *May, and in final form* 22 *June*, 1954]

Previous theory of the rubber membrane predicted Laplace's equation to hold only for small inclinations of the membrane to its horizontal undisplaced position. In practice the equation has, however, been found to hold for quite large inclinations. In addition, it has been observed that the motion of any point in the membrane is purely vertical for vertical displacements of the "electrodes." This suggested that it is the horizontal component of the tension which remains constant and equal to the tension in the undisplaced position. On this assumption it is found that Laplace's equation holds without restriction. It is interesting to note that this assumption is equivalent to assuming that vertical displacements satisfy Hooke's law, which experiments have shown to hold for quite large inclinations.

The equation governing the vertical displacement of a uniformly stretched rubber membrane from its initial position in the horizontal XY plane is

$$(\partial^2 h/\partial x^2) + (\partial^2 h/\partial y^2) = 0 \qquad (1)$$

under equilibrium conditions, where h equals vertical displacement, the pressure being the same on both sides of the membrane. This is Laplace's equation in two dimensions and this property of the membrane has made it valuable in the experimental study of potential distribution and electron paths where the effect of space charge can be neglected. The method seems originally to have been suggested by Oliphant and Moon.[1] It has been discussed in detail by Kleynen[2] and Walker[3] and used by Zworykin and Rajchman[4] in the development of an electron-multiplier.

The theory used in deriving equation (1) assumed the tension to be constant throughout the membrane and was valid only for small inclinations of the membrane to its undisplaced position in the horizontal plane. Experiments have, however, shown the membrane to satisfy equation (1) for quite large inclinations. In this paper a modification to the theory is suggested using less restrictive assumptions.

PREVIOUS THEORY

Consider the equilibrium of an element $ABCD$ of the membrane (Fig. 1) with its edges parallel to the co-ordinate planes. The membrane is assumed to be perfectly flexible and the pressure is the same on both sides, so that only surface forces need be considered.

Let the forces perpendicular to the edges AD and BC, due to the rest of the membrane, be F_1 and F_2 respectively. If the tension is uniform and equal to T then

$$F_1 = T\delta s \text{ and } F_2 = T\delta s'$$

If the inclination to the y-axis is small then

$$\delta s \simeq \delta s' \simeq \delta y \text{ and } F_1 \simeq F_2 \simeq T\delta y$$

Let θ be the inclination of the membrane to the x-axis at the point $A(x, y)$. The net vertical force due to F_1 and F_2 will then approximately equal

$$F_2 \sin \bar{\theta}_{BC} - F_1 \sin \bar{\theta}_{AD} = T\delta y (\sin \bar{\theta}_{BC} - \sin \bar{\theta}_{AD}) \qquad (2)$$

where $\bar{\theta}$ is the mean value of θ along the appropriate edge. So long, however, as θ is small

$$\sin \theta \simeq \tan \theta = \partial h/\partial x$$

and equation (2) therefore yields

$$T\delta y[(\overline{\partial h/\partial x})_{BC} - (\overline{\partial h/\partial x})_{AD}]$$

where $\overline{(\partial n/\partial x)}$ is the mean value of $(\partial h/\partial x)$ along the appropriate edge.

But

$$[(\overline{\partial h/\partial x})_{BC} - (\overline{\partial h/\partial x})_{AD}] \simeq (\partial^2 h/\partial x^2)\delta x$$

The resultant vertical force for edges AD and BC is therefore

$$T(\partial^2 h/\partial x^2)\delta y \delta x$$

Similar arguments hold for the net vertical force for edges AB and CD and if the element is in equilibrium

$$T[(\partial^2 h/\partial x^2) + (\partial^2 h/\partial y^2)]\delta x \delta y = 0$$

and thus equation (1) holds.

So far, it should be noted, the assumptions have been, apart from perfect flexibility, that:

(*a*) the resultant tension in the membrane is constant for all values of x and y;

(*b*) the inclination of the membrane to either of the axes is small.

Another way of regarding the equilibrium position of the membrane[3,4] is to examine the conditions of minimum surface potential energy which leads, with assumptions (*a*) and (*b*), again to equation (1).

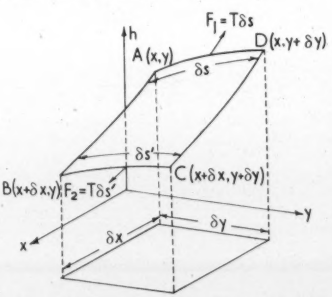

Fig. 1. Element of rubber membrane in equilibrium

ALTERNATIVE THEORY

On using the rubber membrane for the investigation of potential distribution it is observed that if the boundaries representing the electrodes are displaced vertically and if horizontal slip of the membrane across the electrodes is prevented, the motion of any point in the membrane is also purely vertical. This is seen to hold in regions where $(\partial h/\partial x)$ and $(\partial h/\partial y)$ are appreciable. So long as this observation is valid, then whatever the final configuration of the membrane, the horizontally resolved distance between any two points in

the membrane must remain constant and equal to their distance apart in the horizontal undisplaced position.

This observation suggested the assumption that, rather than the resultant tension T being constant throughout the membrane, it is the horizontally resolved tension T_0 that is constant, T_0 being defined as the horizontal force per unit length in the XY plane (and equal to the tension in the undisplaced position).

The horizontal forces acting on edges AD and BC (Fig. 1) in opposite directions are then accurately given by

$$T_0\delta y = F_1 \cos\overline{\theta}_{AD} = F_2 \cos\overline{\theta}_{BC}$$

If this is the case the approximation

$$\sin\theta \simeq \tan\theta$$

is no longer necessary and the resultant vertical force for edges AD and BC is given by

$$T_0\delta y[\overline{(\partial h/\partial x)}_{BC} - \overline{(\partial h/\partial x)}_{AD}]$$

leading, as before, to

$$T_0(\partial^2 h/\partial x^2)\delta x\delta y$$

and hence to Laplace's equation. So long as the above assumption is correct the rubber membrane should obey Laplace's equation in two dimensions for all values of $(\partial h/\partial x)$ and $(\partial h/\partial y)$.

DISCUSSION

Fig. 2 shows a section of the membrane displaced by an electrode. The capacitance of this electrode can be evaluated as follows.[5]

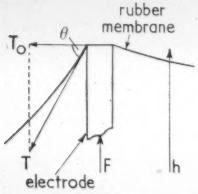

Fig. 2. Force F acting on "electrode" and displacing rubber membrane through height h

Let θ be the inclination of the membrane at a boundary and F the force required to displace the electrode; then for equilibrium,

$$T_0 \oint \tan\theta\, ds = F$$

where T_0 is defined as before, and the integration is round the boundary of the electrode.

According to the rubber membrane analogue, $\tan\theta$ is equivalent to the electrostatic field intensity E and therefore

$$F/T_0 = \oint Eds = 4\pi q$$

where q is the charge residing on unit vertical length of the electrode. Since h, the vertical displacement of the electrode is equivalent to its potential, the capacitance C per unit vertical length is given by

$$C = q/h = KF/T_0h$$

where K is a constant.

If the membrane accurately simulates the electrostatic field, then C must be independent of the voltage, i.e. of h, and therefore

$$F \propto T_0h$$

for a given configuration.

Since T_0 is assumed constant and independent of h it follows that

$$F \propto h$$

i.e. the membrane obeys Hooke's law for vertical displacements. The argument can be extended by considering the equilibrium along any line of constant h.

EXPERIMENTS TESTING VALIDITY OF HOOKE'S LAW

The rubber membrane used was of unstretched thickness 0·046 cm and had a 30% stretch on a rectangular frame, the dimensions of which were large compared with the "electrode" system. It was alined in the horizontal plane by means of spirit levels, and two circular boundaries of radii 1 cm and 13·5 cm respectively formed the "electrode" system of coaxial cylinders. The outer "cylinder" was fixed below the membrane and loads were applied to the inner cylinder. Deflexions were measured by means of a micrometer screw with twenty turns to the inch.

The results obtained are shown in Fig. 3 which indicate that Hooke's law is fairly well obeyed up to a deflexion of

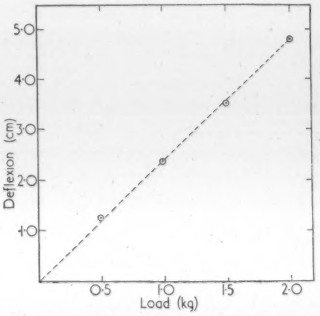

Fig. 3. Relation between the load applied to and the deflexion of the inner cylinder. The values of θ, the inclination of the membrane to the horizontal at the inner cylinder, were approximately 25°, 50° and 60° for deflexions of 1·0, 3·0 and 4·0 cm respectively

about 4·0 cm. Under these conditions the contour of the membrane was found to satisfy Laplace's equation to within 5%, even though the inclination of the membrane at the inner cylinder was as large as 60° with 4 cm deflexion.

The experiment was repeated with the inner "cylinder" placed asymmetrically and linearity was confirmed over the same range of deflexions.

CONCLUSIONS

To account for the fact that the rubber membrane follows Laplace's equation fairly well for large inclinations, it is suggested that T_0, the horizontal force per unit horizontal length of the membrane, is constant throughout the membrane and equal to the tension in the undisplaced position. This assumption was suggested by the observation that any point in the membrane moves only vertically on vertical displacement of the electrodes. It is shown that if the assumption is true the membrane not only satisfies Laplace's equation but also Hooke's law for vertical displacements.

Experiments confirmed Hooke's law for coaxial cylinders and also for an asymmetrical position of the inner cylinder for a range of deflexions corresponding to an inclination of the membrane to the horizontal of approximately 60°. It is also known that Laplace's equation holds for the coaxial system under similar conditions.

ACKNOWLEDGEMENTS

The author wishes to acknowledge with thanks the advice given by Dr. M. R. Gavin and Dr. J. E. Houldin in the preparation of this paper. In addition the author wishes to thank Mr. Hill and Mr. Orwin for the use of their apparatus and for access to some unpublished results obtained by them.

REFERENCES

(1) OLIPHANT, M. L., and MOON, P. B. *Proc. Cambridge Phil. Soc.*, **25**, p. 461 (1929).
(2) KLEYNEN, P. H. J. A. *Philips Tech. Rev.*, **2**, p. 338 (1937).
(3) WALKER, G. B. *Proc. Instn Elect. Engrs*, **96**, p. 319 (1949).
(4) ZWORYKIN, V. K., and RAJCHMAN, J. A. *Proc. Instn Radio Engrs*, **27**, p. 558 (1939).
(5) FREMLIN, J. H., and WALKER, J. *J. Sci. Instrum.*, **24**, p. 50 (1947).

The preparation of uniform plastic films

By R. S. M. REVELL, B.Sc., A.Inst.P., and A. W. AGAR, B.Sc., A.M.I.E.E., A.Inst.P.,* Research Department, Metropolitan-Vickers Electrical Co. Ltd., Manchester

[*Paper received* 3 *September*, 1954]

A simple method has been devised for casting thin uniform films of Formvar on flat solid surfaces. The film thickness appears to be proportional to the concentration of the plastic in the original solution, and can readily be controlled over a range from 150 to 1300 Å.

Thin Formvar films are extensively used in electron microscopy as supports for many types of specimens and as replica films for the study of surfaces. The films are usually prepared by pouring a solution of plastic over a microscope slide or a specimen surface, which is then held in a vertical or inclined position to dry. This process not infrequently gives rise to films of irregular thickness (local variations of up to 100% have frequently been observed) and successive films from the same solution may be of quite different average thickness. In some experiments carried out in this laboratory it was necessary to have substantially uniform replica films and a new preparation technique was required. The description which follows refers to the preparation of replica films; for the formation of support films, a glass microscope slide is substituted for the specimen surface and the method is otherwise similar.

PREPARATION OF UNIFORM FILMS

Factors affecting film thickness. The variable thickness encountered between successive films prepared by the normal method is due to differing amounts of solution applied to the surface and to varying conditions of draining and drying. Local thickness variations are caused by streaming of excess liquid down the surface upon which the film is being cast and variation in the gross amount of liquid adhering to different parts of the surface.

Method of preparation. Some control of film thickness can be obtained by immersing the specimen to be examined in a solution of Formvar in chloroform and withdrawing it slowly at a uniform rate with the surface held vertical. The slower the rate of withdrawal, the thinner the resultant film (due to increased drainage of film solution from the specimen surface into the meniscus). Local variations in film thickness are also reduced in this way.

The first apparatus used to simplify this process was a cylindrical shaped evaporating funnel containing the film solution. The surface on which the film was to be cast was immersed vertically in the solution, which was then allowed to drain away through the tap. The rate of fall of liquid level down the length of the specimen is approximately constant if the specimen is relatively short compared with the head of liquid, and results in a fairly uniform film. Various film thicknesses were obtained by changing the concentration of the film solution.

The liquid drained from the funnel in only 7 sec. The rapid flow gave rise to turbulence at the specimen/liquid boundary and also accentuated the end effects described below. This resulted in variations (up to $\pm 25\%$) in the thickness of films produced from a given solution. It therefore seemed probable that if the flow time were increased the films obtained would be more uniform.

The apparatus finally adopted was as shown in Fig. 1. The tubing below the ground glass tap of an evaporating funnel was replaced by a length of capillary tubing, which made the flow rate very much smaller. The top of the funnel had a loose fitting metal plate which reduced the atmospheric disturbance around the surface upon which the film is drying and also reduced the rate of evaporation of solvent. The cover plate was fitted with a simple spring clip which gripped the sides of the specimen and held the surface on which the film was to be cast vertically in the solution. Alternative top plates with clips suitable for different specimen sizes were made. The whole of the funnel and capillary was enclosed by a constant temperature jacket (not shown) in order that the effect of temperature could be studied.

The initial level of the film solution in the funnel was arranged to be well above the top of the specimen so that steady flow conditions had been achieved before the meniscus reached the specimen. The films were always allowed to dry *in situ*, after which the specimen was removed and the apparatus was washed through with two rinses of chloroform to remove any traces of plastic which might gradually alter the solution concentrations or block the capillary.

Dimensions of the apparatus. The thickness of a film produced in the apparatus will be dependent on the concentration of the solution, its viscosity, the rate of fall of the liquid meniscus and perhaps to some extent on the surface tension at the liquid/specimen boundary and on the vapour pressure of the solvent vapour around the drying film.

* Now at Associated Electrical Industries, Ltd., Aldermaston, Berks.

The rate of fall of the liquid meniscus is governed by the dimensions of the apparatus for a given solution. In considering the requirements of the apparatus it is convenient to refer to the simplified model shown in Fig. 2.

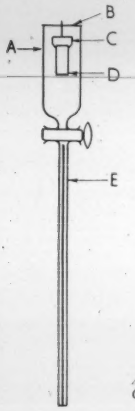

Fig. 1

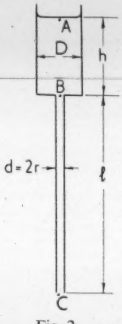

Fig. 2

Fig. 1. Film casting apparatus

A, evaporating funnel; *B*, brass plate; *C*, clip for specimen; *D*, specimen; *E*, capillary tube.

Fig. 2. Simplified model of the film casting apparatus

Assuming streamline conditions, the liquid flow from the funnel can be expressed approximately by Poiseuille's equation for flow of liquids through capillary tubes, a term being added to allow for the gravitational pull on the liquid in the capillary itself. Thus, quantity of liquid discharged in unit time, Q, is

$$Q = \frac{\pi r^4}{8\eta}\left(\frac{P_B - P_C}{l} + \rho g\right) \qquad (1)$$

where η is the viscosity of the solution, P_B and P_C are the pressures at B and C respectively, and ρ is the density of the solution. Since $P_A = P_C$, $P_B - P_C = h\rho g$ and

$$Q = \frac{\pi r^4}{8\eta} \cdot \rho g\left(1 + \frac{h}{l}\right) \qquad (2)$$

This neglects the effect of the kinetic energy of the liquid leaving the capillary, which introduces a small correction to the effective head $(h + l)$ of liquid causing the flow. Equation (2) shows that l should be large compared with h if the flow rate is not to alter appreciably during the time the liquid is flowing out of the funnel. In practice, since the largest specimens which can be accommodated in the funnel must not extend beyond the cylindrical portion of the funnel and must be well immersed in the solution, the change of head across even a large specimen is hardly more than half the height h and is frequently much less.

The dimensions of the apparatus used were

$h = 8$ cm $\qquad d = 0{\cdot}15$ cm

$l = 22{\cdot}5$ cm $\qquad D = 3{\cdot}2$ cm

Using this apparatus, the change in flow rate between top and bottom of a large specimen was found to be about 6% and no resulting change in film thickness was detected.

Although this indicated that the apparatus dimensions were suitable for our purpose, it would be more convenient to choose the funnel length so that it would accommodate a standard microscope slide for the preparation of support films. As the speed of liquid flow through the capillary at the lowest concentrations of Formvar in chloroform is approaching the critical value at which turbulent flow sets in, a slight reduction in capillary bore would be advisable if the best results are to be obtained for very thin films. This would reduce the rate of fall of liquid level in the funnel and produce films rather thinner for a given solution concentration than those obtained in the experiments described here.

The dimensions of the specimen seem to be immaterial provided that the solution level can clear the top edge and that the lower edge does not extend into the region where the funnel narrows towards the tap. The necessity to clip the specimen by its sides will in general ensure that it is far enough from the funnel walls to avoid any undesirable boundary effects.

End effects. On account of the collection of the film solution at the top edge of the specimen, the film thickness in the first 1–2 mm of surface is greater (20%–50%) than that over the rest of the surface. However, the disturbance is restricted to this small area by the slow rate of fall of level and the consequent opportunity for surplus liquid to drain into the meniscus. There is likewise a slightly wider patch of thicker film at the bottom end of the specimen. These effects could, of course, be reduced by using a capillary of smaller bore.

It was found that the method was unsatisfactory with metal specimens mounted in Bakelite or other plastic. The junction between the metal and the mounting secretes a quantity of the film solution, which flows down over the metal surface after the liquid meniscus has retreated. This gives rise to flow lines over the surface, across which the film thickness varies widely. There does not seem to be any difficulty with unmounted metal specimens of any shape so far encountered.

RESULTS OBTAINED

Measurements of film thickness. Three films were cast on to glass slides from each of nine solutions of Formvar in chloroform in the concentration range 0·5 to 5% (wt/vol). The films were cut longitudinally and the film thickness at the cut edge measured by Tolansky's multiple beam interference method[1] over selected lengths of about 3 mm. Because of the end effects, approximately 3 mm at each end of the film was avoided. Between twenty-five and forty measurements were made on each film whenever possible. A further two films from each of eight solutions were prepared, and measurements were made at a number of random points along the cut edges of the films using Dyson's interference microscope.[2] Dyson's method is simpler to apply because the cut edge of the film is frequently jagged and unsuitable for an accurate determination of fringe shifts by Tolansky's method. It is also less dependent on the cleanliness of the slide for its accuracy. However, the results obtained with both methods of measurement were in good agreement. These films were cast on glass slides to simplify the preparation and measurement, but a few films cast on to metal gave results in agreement with those recorded below.

The spread of individual thickness measurements for any given film was within a range of ±10% of the average value, and for several of the films was within ±5%. The average film thicknesses so determined were consistent within ±3% for different films from a given solution for thicknesses greater

than about 600 Å. The variation in the average value for thinner films was up to ±7%. This was probably due to the decreased accuracy of measurement in this range.

When the average of all thickness measurements for all films from a given solution had been calculated, it was found that more than 90% of these measurements lay within ±10% of this average. This overall average film thickness is plotted against the concentration of the film solution in Fig. 3 and shows a linear relationship.

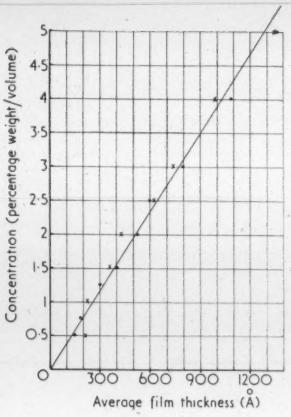

Fig. 3. Relation between solution concentration and resultant film thickness

• Tolansky's method. × Dyson's method.

Films cast from a 2·5% solution at a range of temperatures between 0 and 30° C were found to be of constant thickness within the ±10% variation found above. It was concluded that normal variations in ambient temperature would cause insignificant changes in average film thickness from solutions of this concentration (the one to be used in our future experiments) and no special jacketing arrangements were necessary.

Viscosity of film solutions. Since the viscosity of the film solutions increased markedly with increase in concentration of the Formvar, the time taken for a given volume of film solution to drain out of the funnel was noticeably affected by the concentration (see the table).

Effect of concentration of Formvar on the flow time of a given volume of film solution

Concentration of Formvar in chloroform (%)	*Flow time from funnel* (s)
0	22·5
0·5	24
1	30
1·5	40
2	57
3	107
4	200
5	355

Thus, by timing the flow for the various solutions, a sensitive indication of any change in concentration, which would affect the film thickness produced, is obtained. In practice, it was found that a very large number of films could be cast from a solution before the average thickness increased significantly. It is, of course, necessary to expose the solutions to the atmosphere as little as possible and to store them in well-stoppered bottles.

It was also found advisable to check the flow time for the chloroform rinse from time to time, as this quickly indicated the presence of any obstruction in the capillary.

Film thickness and interference colours. It was very interesting to note the interference colours of the various films when floated on a water surface. The mounting films normally prepared are colourless, and have generally been supposed to be 100–200 Å in thickness. The measurements now made show that colourless films may be up to 400 Å in thickness and that in fact 150 Å films are so thin and fragile that it is unlikely that many films used for electron microscope supports are of this order of thickness. The results for plastic replica films (usually assumed to be 400–500 Å thick) are equally surprising. The "thin film" plastic replicas usually prepared in this laboratory (requiring a thick backing film for safe removal from the specimen surface) usually exhibit a straw or blue coloration on a water surface. Such films were found to lie in the thickness range 750–1000 Å. Films removed by dry stripping methods must be considerably thicker than this. Some further detailed measurements on replica films are to be published shortly elsewhere.

CONCLUSIONS

A simple apparatus has been devised in which Formvar plastic replica films of uniform and predictable thickness can be prepared. The resulting films appear to be much cleaner than those prepared by the standard methods. The method can therefore be used with advantage for preparing support films for other specimens for the electron microscope. Once the apparatus has been calibrated, films of any desired thickness may be prepared without further measurement.

The accuracy of ±10% in film thickness was adequate for the work envisaged, and further refinements were not attempted. This degree of variation may well be due to microscopical particles on the surface which are extremely difficult to remove.

It seems very probable that the method could be used for preparing thin uniform films of other liquid-soluble plastics for other applications.

ACKNOWLEDGEMENTS

The authors are pleased to acknowledge the assistance of Miss I. Walsh in the earlier part of this work and of Mr. R. M. Elliott, who made many of the measurements. We also wish to thank Dr. Willis Jackson, Director of Research and Education, and Mr. B. G. Churcher, Manager of the Research Department, Metropolitan-Vickers Electrical Co. Ltd., for permission to publish this paper.

REFERENCES

(1) TOLANSKY, S. *Multiple Beam Interferometry of Surfaces and Films* (Oxford: The Clarendon Press, 1948).

(2) DYSON, J. *Nature* [*London*], **171**, p. 743 (1953).

On the representation of rheological results with special reference to creep and relaxation

By P. Feltham, M.Sc., Ph.D., F.Inst.P., Department of Metallurgy, The University, Leeds

[*Paper received* 21 *July*, 1954]

The remarkable qualitative similarity in the response of solids of widely different structures to applied stresses, particularly in creep and relaxation, is ascribed to relaxation centres all of which, in a given solid, have approximately the same heat of activation, but, on account of variations in their geometry such as shape and size, have different entropies of activation. A normal distribution of entropies of activation is shown to lead to a log-normal spectrum of relaxation times of the type originally proposed by Wiechert on heuristic grounds. Boltzmann's superposition principle and the relation between creep and relaxation derived by Zener are used to show that this distribution yields a form of stress relaxation curve common to many solids, as well as Andrade's $t^{\frac{1}{3}}$-creep law. Experimental data, given in the literature, on the creep and relaxation in pure polycrystalline aluminium, rubber, polymethylmethacrylate and ceramics are shown to be in good agreement with the theory. The significance of Nutting's law of deformation is discussed.

Stress relaxation curves of solids of vastly different structures, as for example polycrystalline aluminium of high purity,[1] polymethylmethacrylate,[2] ceramics,[3] and an abundance of others show a pronounced similarity. Parallel observations, relating to the similarities in the character of creep curves, are best exemplified by the $t^{\frac{1}{3}}$-creep law, sometimes known as Andrade's[4] β-flow, which is obeyed by many polycrystalline metals at high temperatures,[1,5] by concrete,[6] rubber,[7] celluloid,[8] and many other diverse materials to a high degree of accuracy.

The striking similarities in the laws of deformation of materials of widely differing structure and chemical composition have frequently attracted attention and have been discussed by Scott Blair[9] and co-workers, and more recently by Umstätter.[10] In these discussions the emphasis was upon stress relaxation under constant strain, while in the case of creep under constant stress Kennedy[11] reached the conclusion that an aggregate possessing very simple properties may provide, statistically, a creep law of the Andrade $t^{\frac{1}{3}}$ type. The view that the $t^{\frac{1}{3}}$-law, as observed in many metals, represents the statistical expression of a transition from the unstressed state of static equilibrium to a state of dynamic equilibrium characterized by the stage of steady, constant creep rate was also expressed by Feltham.[12]

In the particular case of pure metals Mott[13] was in effect able to deduce the $t^{\frac{1}{3}}$-law on the basis of the assumption of random stress fluctuations on a submicroscopic scale, and some of the implications of the theory were found to be in agreement with data on the creep of a number of metals and alloys published in the literature.[5]

The principal purpose of this paper is to show that it is in effect possible to account for the characteristic similarities in the stress relaxation and creep behaviour of materials on the basis of a generalized statistical model.

THE STATISTICAL MODEL

The assumption is made that in a hypothetical, stable solid, the physical properties of which are not further specified, there exists a distribution of relaxation centres. In view of the well-known sensitivity to temperature changes generally manifest in creep and relaxation, each centre is associated with a temperature-dependent Maxwellian relaxation time, i.e. the relaxation time of a centre characterized by the subscript l is given by

$$\tau_l = (1/\nu) \exp (\Delta F_l/kT) \qquad (1)$$

where ν is a vibrational frequency and

$$\Delta F_l = \Delta H_l - \Delta S_l T$$

where ΔH_l and ΔS_l are the heat and entropy of activation respectively.

Now, from Kê's[1] results on the stress relaxation and slow creep in 99·991% polycrystalline aluminium the heat of activation appears to have a single value which is close, or equal, to that of self-diffusion. In the case of the viscosity of long-chain paraffins Flory[14] has also established that the entropy but not the heat of activation depended upon the chain length. Since the heat of activation of relaxation processes and of viscous flow should be approximately equal in the absence of crosslinks,[15] it can be inferred that the heat of activation will be approximately the same for every relaxation centre. This invariance of the heat of activation in organic long-chain compounds was explained by Eyring and Kauzmann[16] by the help of the conception that the chains do not move as rigid wholes but piecemeal, the elementary displacement being due to a relatively small number of links.

The assumption will therefore be made that in the hypothetical solid under consideration, which may be representative of an annealed metal or other homogeneous material, ΔH_l will have the same value ΔH irrespective of l, while ΔS_l will depend upon geometrical features, such as the entanglement in the case of long-chain molecules, i.e. upon the shape and dimensions of the relaxing centre. Now for a given, arbitrarily chosen l, say l_0, a probability p_0 is defined by Boltzmann's relation

$$\Delta S_{l_0} = k \ln p_0$$

and we assume that to a first approximation

$$\Delta S_l = k \ln p_0^{l/l_0} \qquad (2)$$

If, reverting to the above example, l_0 were to refer to the length of a characteristic molecular segment capable of surmounting the energy barrier ΔH, then equation (2) implies no coupling between the l/l_0 segments of the chain or relaxing unit of length l. In view of the large number of degrees of freedom of most polymer chains, this approximation is not likely to introduce large errors particularly if, as would generally be the case, the range of l/l_0 is comparatively small.

Using equation (2), equation (1) can then be written:

$$\ln \tau_l + \ln \nu = \Delta H/kT - (l/l_0) \ln p_0$$

or

$$\ln [\tau_l \nu \exp (-\Delta H/kT)] = \alpha l \qquad (3)$$

where

$$\alpha = \ln (1/p^{1/l_0}) = \text{const.}$$

Further, equation (3) implies that a normal distribution in l will correspond to a log-normal distribution in $\tau_l \nu \exp (-\Delta H/kT)$, or, since ΔH is assumed independent of l, and $\nu \exp (-\Delta H/kT)$ is therefore a constant factor associated

with all relaxation times in that distribution, to a log-normal distribution of Maxwellian relaxation times. Such a distribution was first proposed by Wiechert[17] on heuristic grounds, and appears to be of very wide occurrence.

Thus Jenckel and Klein[2] experimentally established the existence of a log-normal distribution of Maxwellian relaxation times in polymethylmethacrylate, Jenckel and Fuehles[18] in Buna-*S*, Tobolsky and co-workers[19, 20] in other rubbers and polymers. The relaxation spectrum for some ceramics, expressed by Macey[3] for mathematical convenience by a modified Hankel function of the second kind, can at least as well be represented by a log-normal distribution which, as will be shown, is also implied by the creep and relaxation experiments carried out by Kê[1] on pure polycrystalline aluminium; it would probably be found to account also for the relaxation curves of iron,[21] steel,[22] and other metals.

THE GENERALIZED RELAXATION FUNCTION

Let σ_0 be the initial stress applied to a specimen of a solid, which is subsequently maintained at the initial strain, and let $\sigma = \sigma(t)$ be the stress as measured after time t. For a given Maxwell element of Newtonian viscosity η and shear modulus G, stress relaxation under constant strain obeys the law

$$\sigma/\sigma_0 = \exp(-t/\tau), \quad \tau = \eta/G$$

The normalized log-normal distribution $F[\ln(\tau/\tau^*)]$ is defined by

$$dF[\ln(\tau/\tau^*)] = \psi[\ln(\tau/\tau^*)]d\ln\tau = (b/\sqrt{\pi})\exp\left\{-b^2[\ln(\tau/\tau^*)]^2\right\}d\ln\tau \quad (4)$$

where τ^* is the relaxation time corresponding to the maximum, $b/\sqrt{\pi}$, in the distribution curve $\psi[\ln(\tau/\tau^*)]$.

The stress relaxation resulting from the linear superposition of a log-normal distribution [equation (4)] of Maxwellian relaxation times is then

$$\frac{\sigma}{\sigma_0} = \frac{b}{\sqrt{\pi}}\int_{-\infty}^{\infty}\exp\left(-\frac{t}{\tau}\right)\exp\left[-b^2\left(\ln\frac{\tau}{\tau^*}\right)^2\right]d\ln\tau \quad (5)$$

The model represented by this integral consists of an array of Maxwell elements connected in parallel, but not otherwise coupled. The justification of the use of this model is to be found in the theorem[23] that the stress relaxation of any assembly of parallel and series connected systems of Maxwell elements can be represented by the relaxation of an equivalent system of such elements connected in parallel. The relaxation times of the individual elements of the equivalent distribution will be related to the relaxation times of the actual submicroscopic processes occurring in the solid in a manner analogous to the relation between the frequencies of oscillations and the normal modes of a system of coupled Hookean oscillators. Thus the detailed physical interpretation of the significance of the relaxation times as used in equation (5) will in general be a matter of considerable difficulty, as was also pointed out by Roesler and Pearson[24] in their recent work on the determination of relaxation spectra, though some attempts at interpreting them have been made, i.e. in the case of rubbers,[25] and metals.[26]

Now, the integral in equation (5) cannot be solved in closed form. A simple, approximate solution in terms of the tabulated error function can, however, be obtained by writing instead of equation (5):

$$\frac{\sigma}{\sigma_0} = \frac{b}{\sqrt{\pi}}\int_{\ln\tau}^{\infty}\exp\left[-b^2\left(\ln\frac{\tau}{\tau^*}\right)^2\right]d\ln\tau \quad (6)$$

obtained from the integral in equation (5) by replacing $\exp(-t/\tau)$ by a cut-off function which is zero for $\log\tau < \log t$, and unity where $\log\tau \geqslant \log t$. An indication of the approximation involved can be obtained from Fig. 1 in which $\exp(-t/\tau)$ as well as the step function are plotted against $\log_{10}(t/\tau)$. The error introduced by using equation (6) instead of equation (5) will depend to some extent upon the

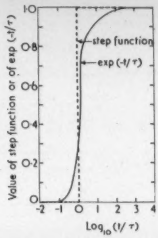

Fig. 1. Approximation to the relaxation term $\exp(-t/\tau)$ by a step function

value of b, but with values of b such as occur most frequently in practice it will be unimportant, at least over the major part of the spectrum, and a more detailed examination of its nature will not here be attempted. Physically, the replacement of the exponential term by the step function implies that the behaviour of individual relaxing centres is not truly Maxwellian, but that a centre to which a relaxation time τ is ascribed (at a given temperature) remains unrelaxed up to the time $t = \tau$, at which instant complete relaxation occurs. It is possible that in some materials, such as metals,[13] the latter mechanism would in any case present a better description of the actual process of relaxation than the one implied by equation (5).

The solution of equation (6) is:

$$\frac{\sigma}{\sigma_0} = \frac{1}{2}\left[1 + \operatorname{erf}\left(b\ln\frac{\tau^*}{t}\right)\right] \quad (7)$$

with the convention that if $t \geqslant \tau^*$ then

$$\operatorname{erf}[b\ln(\tau^*/t)] = -\operatorname{erf}[b\ln(t/\tau^*)]$$

The stress relaxation curve under constant strain is therefore determined by the parameters b and τ^*, which also determine the log-normal spectrum [equation (4)], with $\sigma/\sigma_0 = \frac{1}{2}$ when $t = \tau^*$.

STRESS RELAXATION IN POLYMERS

Jenckel and Klein,[2] and Tobolsky and co-workers,[19, 20] studied stress relaxation in a number of linear and cross-linked polymers, and deduced a log-normal distribution of relaxation times empirically from the curves of stress relaxation under constant strain by graphical methods. In particular, complete data on the stress relaxation of a polysulphide rubber (*H.11*) were available, and these were used to examine the applicability of equation (7) in this particular case. As can be seen from Fig. 2, there is good agreement between the curves of Tobolsky and Stern,[19] shown as full lines, and the circles calculated by means of equation (7), with values of b shown in the legend. These were found to increase linearly with the temperature over the whole range employed (40–100° C), implying a progressive increase in the peak and a corresponding narrowing of the relaxation spectrum. The displacement of τ^* with temperature, along the time axis, is shown by Tobolsky and Stern to result from a heat of activation $\Delta H = 22{\cdot}9$ kcal/g.mole.

It should be noted that the value of b increases, and the

spectrum thus becomes narrower, as the temperature is increased. The curves of stress relaxation (Fig. 2) cannot therefore be superimposed by displacements parallel to the time axis. However, in stable solids it is implied by equation (3), and by the constancy of the parameter α, that the shape of the spectrum, and consequently also the shape of the relaxation curve, should not depend upon the temperature, and this, as will be seen, is found to be the case in metals.

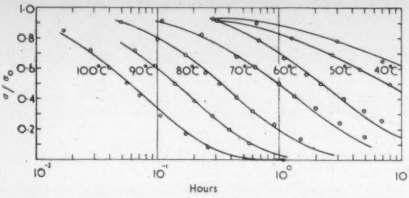

Fig. 2. Stress relaxation at constant strain in polysulphide rubber (*H.11*). Full lines represent experimental results;[19] circles from equation (7) with the following values of b:

°C	40	50	60	70	80	90	100
b	0·28	0·33	0·41	0·43	0·50	0·56	0·60

The anomaly observed in rubbers, and also in other polymers, is to be expected in view of the changes in polymerization equilibria, i.e. the average chain-length decreases on account of the partial breakdown at elevated temperatures. These phenomena are reflected in the high positive temperature coefficient of the specific heat, and in the associated changes in the total entropy.

While none of the considerations leading to the equations of stress relaxation would be invalidated in systems subject to such structural changes, the parameter α [equation (3)] would have to be assumed to vary with the temperature. The functional form of the distribution function of relaxation times need not be affected.

STRESS RELAXATION AND CREEP IN METALS

Creep under constant stress and stress relaxation at constant strain in annealed polycrystalline aluminium wire of 99·991% purity was measured by Kê[1] in the temperature range 150–375° C by means of a simple technique utilizing the principle of a moving coil galvanometer. Since the experiments were conducted only at a low level of stress, the current passing through the galvanometer gave a direct measure of the shear stress acting on the test wire which formed the suspension; the deflexion $d = d(t)$ of the galvanometer gave a measure of the deformation. The creep strain $\epsilon = \epsilon(t)$ and the deflexion are then related by

$$\epsilon \propto (d/d_0) - 1 \tag{8}$$

where d_0 is the immediate initial deflexion.

The full curve in Fig. 3 represents the stress relaxation curve as measured by Kê; σ and σ_0 here denoting the instantaneous and initial values of the shear stress respectively. The circles were obtained from the equation

$$\frac{\sigma - \sigma_y}{\sigma_0 - \sigma_y} = \frac{1}{2}\left[1 + \operatorname{erf}\left(b \ln \frac{\tau^*}{t}\right)\right] \tag{9}$$

with $b = 0{\cdot}227$ and $\tau^* = 53$ seconds at 200° C. The stress σ_y may be regarded as a yield stress below which stress relaxation no longer occurs. Zener[27] has shown that in the case in which shear stresses are relaxed by a mechanism involving grain boundary slip

$$\sigma_y/\sigma_0 = 2(7 + 5\theta)/5(7 - 4\theta)$$

where θ is Poisson's ratio. With $\theta = 0{\cdot}355$, obtained by Birch[28] for polycrystalline aluminium of commercial purity at 30° C, $\sigma_y/\sigma_0 = 0{\cdot}636$, in good agreement with the value of 0·65 adopted in applying equation (9) to Kê's data. Poisson's ratio thus appears to be a significant parameter in both creep and relaxation, a fact which does not seem to have been utilized to any appreciable extent in the study of the non-Hookean behaviour of solids. (See, however, Cherkasov,[29] and Liotsau and Rovinskii.[30])

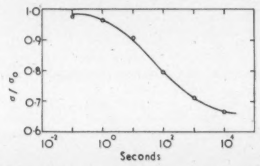

Fig. 3. Composite curve of shear stress relaxation in 99·991% polycrystalline aluminium. Full line represents experimental results;[1] circles from equation (9).

Temperature, °C	150	175	200	225
Multiply time scale by	0·014	0·133	1·00	6·20

Kê further observed that the relation between creep under constant stress as defined by the creep function d/d_0 [equation (8)], and the stress relaxation function σ/σ_0,

$$(d/d_0)(\sigma/\sigma_0) = 1 \tag{10}$$

derived by Zener,[31] correlated his experimental results on creep and stress relaxation in aluminium to a high degree of accuracy. The standard deviation between experimental values of the creep function and corresponding ones calculated from stress relaxation data by means of equation (10), based on about ten points per curve, amounts to less than 0·01. In Fig. 4 a constant multiple of $(d/d_0) - 1$ [equation

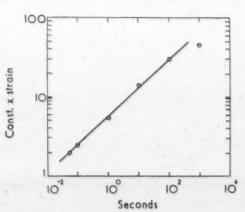

Fig. 4. Composite creep curve of 99·991% polycrystalline aluminium. Circles represent experimental results;[1] the full line corresponds to Andrade's $t^{\frac{1}{3}}$-creep law, equation (11).

Temperature, °C	150	175	200	225	250
Multiply time scale by	0·014	0·133	1·00	6·10	31·0

(8)] is plotted against time on log-log co-ordinates. The circles represent both the direct experimental data on creep and the creep data deduced from the stress relaxation curve (Fig. 3) by means of Zener's relation [equation (10)] by Kê. The equation of the full line drawn through the points is

$$\epsilon = \beta t^{0{\cdot}333} \tag{11}$$

where β is a constant at any given temperature at the invariant, constant stress used. Equation (11), which represents Andrade's β-flow, thus appears as a direct consequence of a mode of stress relaxation derived from the superposition of a distribution of relaxation times of the type postulated. Since equations (7) and (9) can be regarded as functions of t/τ^*, where $\tau^* = \tau_0^* \exp(\Delta H/kT)$, and τ_0^* is a constant, equation (11) can be written in the form

$$\epsilon = \beta_0[t \exp(-\Delta H/kT)]^{\frac{1}{3}}$$

a result derived by Mott[13] for the transient creep of pure metals by a different method.

NUTTING'S LAW OF DEFORMATION

In a paper entitled "A new general law of deformation" Nutting[32] first showed that the empirical relation between the time, the stress and the strain or, more generally, between the time and the corresponding components of the deviators of the tensors of stress and strain, of the form

$$\phi = \epsilon^{-1}\sigma^n t^k \tag{12}$$

lent itself very well to the description of the deformation in many materials. In that equation n, k and ϕ are constants which may, and generally do, vary with temperature. With different values of the exponents n and k various types of behaviour can be described, some special cases being the Hookean solid ($n = 1$, $k = 0$), the Newtonian fluid ($n = 1$, $k = 1$), or the visco-elastic body capable of non-Newtonian flow and of stress relaxation ($n = 1$, $1 > k > 0$).

One obtains from the equation a power law for stress relaxation under a constant strain:

$$\sigma/\sigma_0 = (t/t_c)^{-m}, \quad m = k/n > 0 \tag{13}$$

where t_c is a constant the significance of which becomes obvious on comparing equations (12) and (13). If the material has a yield point, the left-hand side of equation (13) must be modified and expressed as in equation (9).

Owing to its mathematical simplicity Nutting's equation as such, or the power laws of creep and relaxation consistent with it, have frequently been used for the interpretation of experimental data obtained in the study of the deformation of materials. Scott Blair[9] and co-workers, who examined the applicability of Nutting's equation to about forty organic materials, including polymers, bitumens, rubbers, etc., by experiments on creep and on stress relaxation, came to the conclusion that equation (12), but particularly the power law of stress relaxation which it implies, described the experimental data in most cases with reasonable accuracy only for limited periods, e.g. from a few seconds to a few hours. Buchdahl and Nielsen,[33] who used Nutting's equation for the representation of their data on the deformation of polystyrene, confirmed this view. Similar limitations were observed in the power law of the stress dependence of the creep rate, characterized by the exponent n in equation (12). The stress dependence of the creep rate of several types of steel was shown by McVetty[34] to obey the power law only over a limited range of values of σ.

Nutting's equation, though of considerable practical value for the presentation of rheological data, is therefore of comparatively little value for predicting the long-time creep or relaxation behaviour of materials by extrapolation from short-time tests, unless the nature of its limitations are understood. Its wide applicability suggests that it may embody an approximation to more general laws of deformation, and that the observed restrictions upon the ranges of the variables within which it applies in any particular application arise as a consequence. This will be shown to be the case by examining the nature of the power laws of stress relaxation and creep which can separately be derived from it.

THE POWER LAW OF STRESS RELAXATION

Let $\psi_m[\ln(\tau/\tau^*)]$ represent that spectrum, of Maxwellian relaxation times, on a logarithmic base, which will yield a power law of stress relaxation [equation (13)] by linear superposition. Then

$$t^{-m} \times \text{const.} = \int_{-\infty}^{\infty} \exp(-t/\tau) \quad \psi_m\left(\ln \frac{\tau}{\tau^*}\right) d \ln \tau$$

or

$$t^{-m} \times \text{const.} = \int_{0}^{\infty} \exp(-t/\tau) \quad \psi_m\left(\ln \frac{\tau}{\tau^*}\right) \frac{d\tau}{\tau}$$

which, by the use of the transformation $\tau = 1/u$ and subsequent Laplace inversion, yields

$$\psi_m\left(\ln \frac{\tau}{\tau^*}\right) = c\left(\frac{\tau}{\tau^*}\right)^{-m} = c \exp\left(-m \ln \frac{\tau}{\tau^*}\right) \tag{14}$$

where c is a normalizing constant. If τ_0 is the smallest relaxation time in this spectrum, then the integral of the distribution function

$$F_m\left(\ln \frac{\tau}{\tau^*}\right) = \int_{\tau_0}^{\tau} \psi_m\left(\ln \frac{\tau}{\tau^*}\right) d \ln \tau$$

yields, after substitution for $\psi_m[\ln(\tau/\tau^*)]$ from equation (14), integration and normalization:

$$F_m\left(\ln \frac{\tau}{\tau^*}\right) = 1 - \left(\frac{\tau_0}{\tau}\right)^m \tag{15}$$

From equation (15) it then follows that

$$d \ln \left[1 - F_m\left(\ln \frac{\tau}{\tau^*}\right)\right] \Big/ d \ln \tau = -m \tag{16}$$

so that a log-log plot of $1 - F_m[\ln(\tau/\tau^*)]$ against τ should give a straight line of slope $-m$. A comparison of $1 - F_m[\ln(\tau/\tau^*)]$ with $1 - F[\ln(\tau/\tau^*)]$, where $F[\ln(\tau/\tau^*)]$ refers to the log-normal distribution [equation (4)], is shown in Fig. 5. The points represented by circles in that figure were obtained from the log-normal spectrum of Maxwellian relaxation times as determined by the dropping-sphere method in polymethylmethacrylate at 80° C by Jenckel and Klein.[2] The full, straight line is derived from a corresponding section of the spectrum leading to a power law of stress relaxation [equations (15) and (16)]. The absolute value of its slope is

$$m = 0{\cdot}14 \tag{17}$$

and this is approximately equal to the average slope of Jenckel and Klein's curve in the restricted interval extending from about 0·1 to 100 sec. Outside this interval no agreement exists.

Nevertheless, if measurements of the stress relaxation are confined to the interval extending from about 1 to 100 sec, the contribution to the relaxation by Maxwell elements having relaxation times of less than 0·1 sec or more than a few hundred seconds will be small, so that the lack of agreement between the two spectra outside these limits will not have an appreciable effect on the mode of relaxation over the interval to which observations are assumed to be confined. Also, it must be borne in mind that on a linear τ-scale

the log-normal spectrum would cease to be symmetrical, the section of the log τ-range extending from $-\infty$ to the origin condensing into the interval $0 \leqslant \tau \leqslant 1$. The fact that the log-normal distribution has a maximum whereas the distribution corresponding to Nutting's law [equation (14)] has no maximum may also remain of no significance in stress relaxation experiments in which, for example, the peak of the log-normal spectrum lies in a range of relaxation times far below the resolution of the method of time measurement employed. In fact, experiments carried out by Feltham[35] on the stress relaxation of ordinary, untreated polymethylmethacrylate maintained at 80° C by means of an electrically heated oil bath built into a Hounsfield Tensometer, gave a good straight line for the $\log(\sigma/\sigma_0)/\log t$ plot for stress relaxation under constant strain, over the entire range investigated, i.e. from a few seconds to about a hundred seconds. The absolute value of the slope, $m = 0{\cdot}12$ was in reasonable agreement with the value $m = 0{\cdot}14$ [equation (17)] obtained by the straight line approximation to Jenckel and Klein's results, shown in Fig. 5.

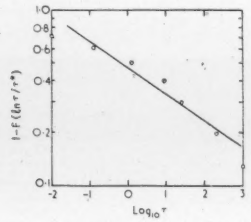

Fig. 5. The relation between $F[\ln(\tau/\tau^*)]$, the integral of the log-normal distribution function [equation (4)] as measured in polymethylmethacrylate at 80° C by Jenckel and Klein,[2] and the integral of the distribution function corresponding to a power law distribution of Maxwellian relaxation times. Full line from equations (15) and (16). (τ expressed in seconds)

The power law of stress relaxation [equation (13)] will therefore be found suitable for the representation of experimental results if the true distribution of relaxation times approximates with reasonable accuracy to a power law distribution [equation (14)] over a range of $\log\tau$ which is approximately commensurate with the range of $\log t$ in which measurements are actually made.

STRESS DEPENDENCE OF THE STRAIN RATE IN NUTTING'S EQUATION

For creep rates such as are generally observed in practice the value of the exponent n of the stress [equation (12)] takes values which lie most frequently in the range 1–2 in the case of polymers and other organic materials tested at room temperature.[9] In ice Nye[36] finds $n = 3$ to 4, while in magnesium Roberts[37] obtains $n = 4{\cdot}0$.

Now it was pointed out by McVetty[34] that the stress dependence of the creep of several steels can be described with greater accuracy if $(\sigma/\sigma_c)^n$ is replaced by $\sinh(\sigma/\sigma_c)$, where σ_c is a temperature-dependent constant characteristic of the particular metal. In fact, in a number of cases of creep at elevated temperatures McVetty determined the errors introduced by using the commonly employed power law instead of the "sinh"-law, and constructed nomograms for the evaluation of σ_c from conventional representations of creep data. The "sinh"-law is in fact to be expected to apply on the basis of the applicability of the theory of rate processes to creep in metals[5, 26, 38] and other materials. A reconciliation with the power law would require that

$$d\log[\sinh(\sigma/\sigma_c)]/d\log(\sigma/\sigma_c) = n$$

over wide, experimentally often encountered, ranges of σ/σ_c. It is easily seen from a log-log plot of $\sinh(\sigma/\sigma_c)$ against σ/σ_c that this is the case. Although there is a certain arbitrariness involved in fitting straight lines to a curve of steadily increasing slope, a good fit is obtained by lines with slopes $n = 1{\cdot}0$, $1{\cdot}7$ and $4{\cdot}0$ over the ranges $0 \leqslant \sigma/\sigma_c \leqslant 1$, $1 \leqslant \sigma/\sigma_c \leqslant 2{\cdot}6$, and $2{\cdot}6 \leqslant \sigma/\sigma_c \leqslant 5{\cdot}5$ respectively. These values of n are characteristic of the magnitudes of this index most frequently reported.

CONCLUSIONS

The principal conclusions which can be arrived at from the present research are as follows:

(1) The mode of stress relaxation under constant strain of materials of vastly differing structures and chemical compositions can be accounted for with considerable accuracy on the basis of an assumed log-normal distribution of relaxation times.

(2) The creep law derivable from such stress relaxation curves by Zener's method can be identified as the Andrade $t^{\frac{1}{3}}$-law which is known to be of wide occurrence.

(3) A log-normal distribution of relaxation times can be derived on the assumption, justified experimentally for a number of materials, that the relaxing centres in the solid have the same, or almost the same, heat of activation, with the further hypothesis that the configurational entropies of activation which are to be ascribed to the relaxation centres are normally distributed.

(4) The relation of the relaxation times of the log-normal distribution to the relaxation times of the actual molecular or atomic processes is complex.

(5) Nutting's law of deformation represents an approximation to more general laws over ranges of the variables which, though restricted, are nevertheless sufficiently wide to permit its use, or the use of the power laws of stress relaxation at constant strain and of creep under constant stress implied by it, in many practical applications for the presentation of rheological results.

REFERENCES

(1) Kê, T. S. *Phys. Rev.*, **71**, p. 533 (1947).
(2) Jenckel, E., and Klein, E. *Z. Naturforsch.*, **7a**, p. 619 (1952).
(3) Macey, H. H. *J. Sci. Instrum.*, **25**, p. 251 (1948).
(4) Andrade, E. N. da C. *Proc. Roy. Soc., A*, **84**, p. 1 (1910); **90**, p. 329 (1914).
(5) Feltham, P. *Phil. Mag.*, **45**, p. 9 (1954).
(6) Glanville, W. H. *Struct. Engng*, pp. 11, 54 and 143 (1931).
(7) Braun, M. L. *Physics*, **8**, p. 129 (1937).
(8) Jessop, H. T., and Filon, L. N. G. *Phil. Trans Roy. Soc., A*, **223**, p. 89 (1923).
(9) Scott Blair, G. W., Veinoglou, G. C., and Caffyn, J. E. *Proc. Roy. Soc., A*, **189**, p. 69 (1947).
(10) Umstätter, H. *Schweiz. Arch. angew. Wiss. Tech.*, **19**, p. 194 (1953).
(11) Kennedy, A. J. *J. Mech. Phys. Solids*, **1**, p. 172 (1953).
(12) Feltham, P. *Proceedings of the Second International Congress on Rheology*, p. 266 (London: Butterworths Scientific Publications Ltd., 1953).

(13) MOTT, N. F. *Phil. Mag.*, **44**, p. 742 (1953).
(14) FLORY, P. J. *J. Amer. Chem. Soc.*, **62**, p. 1057 (1940).
(15) FERRY, J. D., and FITZGERALD, E. R. *Proceedings of the Second International Congress on Rheology*, p. 140 (London: Butterworths Scientific Publications Ltd., 1953).
(16) EYRING, H., and KAUZMANN, W. *J. Amer. Chem. Soc.*, **62**, p. 3113 (1940).
(17) WIECHERT, E. *Ann. Phys. Chem.*, **50**, pp. 335, 546 (1893).
(18) JENCKEL, E., and FUEHLES, J. *J. Makromol. Chem.*, **1**, p. 203 (1943).
(19) TOBOLSKY, A. V., and STERN, M. D. *J. Chem. Phys.*, **14**, p. 93 (1946).
(20) TOBOLSKY, A. V., BISCHOFF, J., and CATSIFF, E. *J. Amer. Chem. Soc.*, **74**, p. 3378 (1952).
(21) WEST, W. A. *Trans Amer. Inst. Min. Met. Eng.*, **167**, p. 192 (1946).
(22) NÁDAI, A., and BOYD, J. *Proceedings of the Fifth International Congress on Applied Mechanics*, p. 245 (Massachusetts Institute of Technology, 1938).
(23) KUHN, W. *Helv. Chim. Acta*, **30**, p. 487 (1947).
(24) ROESLER, F. C., and PEARSON, J. R. A. *Proc. Phys. Soc.* [*London*], *B*, **67**, p. 339 (1954).
(25) KUHN, W., KUENZLE, O., and PREISSMANN, A. *Helv. Chim. Acta*, **30**, p. 307 (1947).
(26) FELTHAM, P. *Symposium on Creep and Fracture of Metal at High Temperatures*, Discussion of Papers 1–7 (London: H.M. Stationery Office, to be published).
(27) ZENER, C. M. *Phys. Rev.*, **60**, p. 906 (1941).
(28) BIRCH, F. *J. Appl. Phys.*, **8**, p. 129 (1937).
(29) CHERKASOV, I. I. *Zh. Tekh. Fiziki*, **22**, p. 1834 (1952).
(30) LIOTSAU, V. G., and ROVINSKII, B. M. *Izv. Ak. Nauk, SSSR (O.T.N.)*, **10**, p. 1471 (1953).
(31) ZENER, C. M. *Elasticity and Anelasticity of Metals*, Ch. 5 (Chicago: University of Chicago Press, 1948).
(32) NUTTING, P. G. *J. Franklin Inst.*, **191**, p. 679 (1921).
(33) BUCHDAHL, R., and NIELSEN, L. E. *J. Appl. Phys.*, **22**, p. 1344 (1951).
(34) MCVETTY, P. G. *Trans Amer. Soc. Mech. Engrs*, **65**, p. 761 (1943).
(35) FELTHAM, P. *Bull. Brit. Soc. Rheol.*, No. 39, p. 4 (1953).
(36) NYE, N. F. *Proc. Roy. Soc., A*, **219**, p. 477 (1953).
(37) ROBERTS, C. S. *J. Metals*, **5**, p. 1121 (1953).
(38) NOVICK, A. S., and MACHLIN, E. S. *J. Appl. Phys.*, **18**, p. 79 (1947).

Comparison of radioactivities by the use of X-ray film*

By A. N. DAVENPORT, Ph.D., and G. W. W. STEVENS, Ph.D., F.R.P.S., Kodak Research Laboratories, Wealdstone, Harrow, Middlesex

[*Paper first received* 1 *June, and in final form* 15 *July*, 1954]

A direct comparison has been made of the use of a counter and of autoradiography as alternative methods for measuring relative radioactivity. The silver contents of a number of uniform photographic images were determined analytically, and portions of these images were quantitatively converted to silver iodide in the presence of ^{131}I. The resultant sources were compared both with a counter and by autoradiography, the sources being placed against different areas of a sheet of X-ray film for a series of times. When the activities were assessed by measuring the densities of the processed film, the results agreed with the analytical data as well as did those obtained with the counter. Even visual density matching afforded accuracy adequate for many tracer experiments. Circumstances in which autoradiography may be preferable to the use of a counter are also discussed.

Although the initial discovery of radioactivity resulted from its action on a photographic plate, electronic instruments have to-day become accepted as the first choice for detecting and, more particularly, for measuring radioactivity. It has, however, been shown that photographic emulsions can, with suitable methods for internal calibration, be used to give reasonably accurate comparisons. Zuber[1] obtained an overall accuracy of 20% when using autoradiography for comparing radioactivities, and Dudley and Dobyns[2] assessed the relative activities of different parts of a histological section by measuring the photographic densities of an autoradiograph with a microdensitometer and calibrating the results with densities produced by exposure to sources of known activity. In addition it has recently been confirmed that the response of photographic emulsions to β-particle exposures obeys the reciprocity law,[3] and data obtained during that investigation suggested that comparisons made by autoradiography may be almost as accurate as comparisons made with a counter.

The experiment, already reported in outline,[4] was designed to test this suggestion more fully, and was planned in the following way. A photographic step-wedge image was tested for uniformity, and then cut into halves. On one half the silver contents of all the steps were determined by direct chemical analysis, and on the other, the images were quantitatively bleached to silver iodide in the presence of the radioisotope ^{131}I. It has already been shown that measurement with a counter of samples treated in this way permits the relative silver contents to be estimated with a precision of 1%.[5] The bleached strips were assessed both by the counter and by autoradiography. The tests thus permitted not only direct comparison of results obtained with the counter and autoradiography, but also allowed either method to be directly compared with the results given by chemical analysis.

EXPERIMENTAL

Pairs of 12 × 9 mm samples were cut from the two halves of a photographic step-wedge image on film. When the optical densities of the pairs of specimens were measured, the readings were equal up to a density of 1·0, and did not differ by more than 0·01 up to a density of 2·0.

One set of samples was used for a chemical determination of the silver contents of the images. The silver in the second set of samples was bleached to silver bromide, with a ferri-

* Kodak Communication No. 1658H.

cyanide-bromide solution, which was then converted into silver iodide in a solution of potassium iodide containing radioactive ^{131}I ions.[5]

In order to reduce the time required for the autoradiographic exposures and thereby eliminate the need for applying decay corrections, the iodide used for the conversion was adjusted to the rather high specific activity of 12·5 mc/g. Such a high activity was, however, in no way essential and was merely used for convenience in the present experiments. To simplify handling the small specimens, they were mounted together on a glass plate coated with an adherent layer of Kodaflat, from which they were removed after conversion, washing and drying.

Assessment with a counter.

The relative radioactivities of the specimens were compared with a Geiger counter, each specimen being covered with a 3 mm thick brass mask, so that effectively only the radiation passing through a 6 mm diameter window could reach the counter tube.[5] A minimum of 5000 counts was recorded for each specimen, so that a probable error of 1% was to be expected, and the figures were corrected for the resolution time of the counter.

Assessment by autoradiography.

The radioactive specimens were remounted on a glass plate and a series of autoradiographs was then made by pressing the array of samples against different areas of a sheet of a high-speed, non-screen, X-ray film for periods of 3½, 5, 7, 10, 14, 20, 28, 40, 56, 80 and 114 min. This range of times ensured that the maximum density produced by the weakest sample was greater than the minimum density produced by the strongest, so that the results could be evaluated by finding the times required by the specimens to produce a common density.

The exposed film was developed in Kodak D.19b developer in a deep tank with intermittent agitation for 10 min at 20° C, this full development being chosen to reduce errors due to uneven development. A typical autoradiograph made using nine different exposure times is shown in Fig. 1.

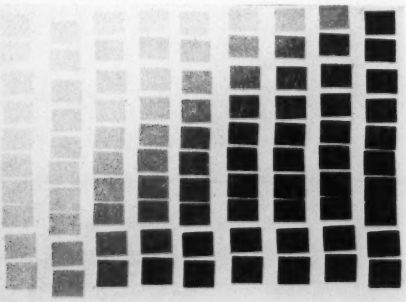

Fig. 1. Autoradiographs produced by array of samples (activity increasing down vertical columns) pressed against X-ray film for times increasing from left to right

Assessment of the autoradiographs.

The autoradiographs were assessed firstly by density measurement, and secondly by visual judgment. The results of the first method should therefore indicate the accuracy obtainable when a photometer is available, whilst those of the second show what can be achieved with the absolute minimum of equipment.

1. *By density measurement.* The densities given by the series of exposure times with each specimen were plotted against the log (exposure time) on a large scale. This gave a series of characteristic curves of similar shape, the position of each curve relative to the log (exposure time) axis being governed by the activity of the sample (Fig. 2). Hence the

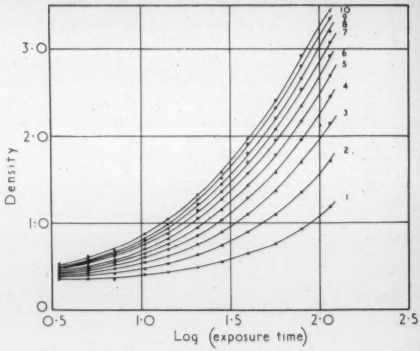

Fig. 2. Characteristic curves obtained by measuring the densities of the autoradiograph (see Fig. 1). Silver contents increasing from curve 1 to curve 10

activity of each sample relative to that of the strongest could be determined from the displacement between the corresponding curves. Average values for these displacements were obtained by taking the mean of measurements made on the graphs at density intervals of 0·2.

2. *Visual density matching.* The log (exposure time) required for each specimen to produce an arbitrarily chosen density was estimated visually without instrumental aid. Comparison pieces for this purpose were made by exposing X-ray film to light, through a mask having an aperture of the same shape and size as the specimens. Comparison densities were within the range common to all the specimens, but knowledge of their actual values was quite unnecessary. The comparison pieces were used by laying them in turn against the series of densities produced by one specimen until a match was obtained. When the comparison density obviously resulted from an intermediate exposure, an interpolated value for the log (exposure time) was estimated by using the assumption that the density/log (exposure time) dependence was linear over a small interval. With a little practice, it was found that ten specimens could be assessed carefully in 15 min. Judgment of the samples in this way was carried out by two operators, each using two comparison densities.

RESULTS

The values for relative silver contents obtained by chemical analysis, with the counter, and from autoradiographs, are shown in the table.

The numerical presentation of the data was complicated by the fact that the analytical method used for determining

silver on small areas of film was believed only to give a precision of about 1%, similar to that expected from the counter measurements and, possibly, from the autoradiography. It was therefore decided that the mean of all three determinations provided the best basis for testing the accuracy of each. The results were treated in the following manner.

The lower readings obtained by each method (including visual assessment of autoradiographs) were first expressed as percentages of the greatest. The percentage values in each set of data were then multiplied by the factor required to make their sum equal to the average sum for the three instrumental methods before adjustment. The figures so derived are given in the table. The best estimate for the relative silver content of any specimen was now taken as the mean of the three values tabulated for analysis, the counter, and autoradiography, and these averages are quoted in the first column of the table.

constant ratio between successive times. Thus in the present experiment the times used ($3\frac{1}{2}$, 5, 7, 10, . . . min) form a geometric series in which each member is approximately $\sqrt{2}$ times its predecessor. As already stated, the range of exposure times should be sufficient to ensure that the maximum density produced by the weakest sample is greater than the minimum density produced by the strongest. In cases where the specimens fall into groups of widely differing activities, it might be advantageous to give separate series of exposures designed so that each group produced a similar range of densities.

For accurate visual density matching, the densities must be placed side by side, so that there is at least a short line along which the areas to be compared just touch. Under these conditions, and if the image colour and graininess are similar, a density difference as small as 0·01, corresponding to an intensity difference of 2% at a gamma value of 1·0, can just

Comparison of silver determinations by different methods

Relative masses of silver per unit area scaled to equalize the mean values

Average values from columns 2–4	*Chemical analysis*	*Silver converted to radioactive silver iodide—activities measured by:*					
		Geiger counter	*Autoradiography*				
			Densities measured	*Densities judged visually*			
				Observer 1		*Observer 2*	
				Comparison density A	B	A	B
15·0	16·1	14·1	15·0	16	17	18	20
27·1	26·9	26·7	27·8	27	31	28	30
38·4	38·5	37·5	39·1	40	43	39	38
49·1	49·6	48·1	49·6	50	54	50	49
59·0	58·6	59·5	58·8	58	57	53	61
68·4	70·2	67·2	67·8	69	65	62	68
77·2	77·2	77·3	77·0	79	75	78	74
84·5	83·3	85·8	84·5	85	80	87	78
92·3	91·0	93·5	92·4	89	90	87	86
100·0	99·7	101·4	99·0	98	99	110	108
Standard deviation of differences from average values	1·0	1·0	0·5	2	4	5	5

In order to obtain a measure of the variability of the results from a given method, the corresponding average values were subtracted from them and the standard deviation of the resultant differences was calculated. The standard deviations so derived (see table) suggest that in favourable circumstances autoradiography should not be less precise than the use, with average care, of a counter and that neither of these methods is appreciably less precise than the technique used for silver analyses. The visual estimations showed substantially larger standard errors, but even so were sufficiently accurate for a fair proportion of tracer experiments.

DISCUSSION

Apart from the usual sources of error introduced by the use of photographic methods, the accuracy obtainable by autoradiography depends on the gap to be bridged by graphical or visual interpolation; it should thus be improved by an increase in the number of exposures. It is obviously desirable to choose exposure times which give equal accuracy at all parts of the scale, and this requirement is satisfied by using a

be discerned. If the density patches on the autoradiograph are of such a shape that accurate juxtaposition of the comparison piece is not possible, the images can still be viewed side by side by standing a polished cube of glass or Perspex on one edge between them, so that they appear to meet in a sharp line.

Whilst the autoradiographic method is likely to be of most interest to workers who do not have convenient access to a counter, it has certain other advantages. Autoradiographs constitute permanent records of relative activities, on which the actual measurements can be made whenever convenient. In the sense that one sheet of film can be exposed simultaneously to a large number of specimens, an autoradiographic exposure is equivalent to the use of a whole battery of counters. This feature simplifies, or makes unnecessary, corrections for decay, facilitates more accurate assessment of isotopes having short half-lives, and makes practicable comparisons of many weak sources which would each require to be left for a long time in a counter.

Unless a microdensitometer is available, densities can only be compared with reasonable accuracy if patches having

substantially uniform density over an area of several square millimetres can be obtained. In this connexion it is important to note a difference in the "geometry" of radiation measurement by a counter and autoradiography. The volume of the ionizable gas in a Geiger–Müller tube and the distance between the tube and the sample ensure that the counting rate is proportional to the total radioactivity integrated over the whole area of the sample. On the other hand, the thin sensitive layer and close contact normally used for autoradiography mean that the film records the point-to-point distribution of radioactivity over the area of the specimen. Straightforward autoradiography will, therefore, only give the desired uniformity of density when the specimen itself is uniform. More uniform density from uneven specimens could, however, be obtained by increasing the distance between the film and the source. If a number of sources were measured simultaneously in this way it might be necessary to place a metal plate with suitably positioned apertures between the specimens and the film, to reduce the extent to which the density opposite one source is influenced by "cross-fire" from adjacent sources.

REFERENCES

(1) Zuber, K. *Helv. Phys. Acta*, **21**, p. 365 (1948).
(2) Dudley, R. A., and Dobyns, B. M. *Science*, **109**, pp. 327, 342 (1949).
(3) Ray, R. C., and Stevens, G. W. W. *Brit. J. Radiol.*, **26**, p. 362 (1953).
(4) Davenport, A. N., and Stevens, G. W. W. *Nature [London]*, **174**, p. 178 (1954).
(5) Ballard, A. E., Zuehlke, C. W., and Stevens, G. W. W. *Radioisotopes Techniques, Vol. II*, p. 105 (London: H.M. Stationery Office, 1951).

The laminar flow of suspensions in tubes

By T. V. Starkey, B.Sc., Ph.D., F.Inst.P., The Technical College of Monmouthshire, Crumlin, Mon.

[*Paper received* 10 *May*, 1954]

The conception of viscosity as action per unit volume is used in the analysis of the flow of a suspension or macromolecular solution in a tube. The flow mechanism adduced involves the postulation of molecular vortices of which the suspended particles or molecules form the nuclei. This mechanism is used as a basis for the derivation of a relationship between the specific viscosity of the suspension and the linear dimensions of the vortices. The laws of Einstein, Staudinger, Huggins and their co-workers are derived simply and as special cases of this relationship. The law relating viscosity with concentration is also derived with reference to the same mechanism. This law assumes the form $\eta_{isp} = an + bn^2$ where a and b are constants and η_{isp} and n are respectively the specific viscosity and molecular concentration of the solution. It is shown to be in good agreement with typical experimental results. The effect of the aspect ratio of the suspended particles or molecules is also considered and it is shown that the longest particle dimension rotates in a plane normal to the vortex axis. Although no quantitative relationship between viscosity and velocity gradient has been derived the mechanism is observed to lead to results in qualitative agreement with the experimental data.

1. Introduction

The very extensive use of capillary viscometers in investigations into the physical characteristics of suspensions, and particularly in the indirect determination of macromolecular weights, calls for a closer study of the mechanics of flow for fluids of this kind than has apparently been attempted hitherto. Although an enormous number of so-called viscosity measurements have been made on such fluids there seem to have been but few attempts to interpret these in terms of any clearly-conceived flow model. Many empirical relationships have been devised but these have in the main yielded no significant ideas relevant to the processes involved.

The well-known equations of Einstein, Staudinger and Huggins[1, 2, 3] represent perhaps the most successful attempts so far to investigate theoretically the relation between the apparent viscosity of a solution and the physical constants of the solvent and of the particles of solute dispersed in it. Although these laws show good agreement with experiment in certain cases, they have limited applicability and provide no satisfactory basis for correlating viscosity and concentration where the relation between these is known to be non-linear.

In the present paper an attempt is made to analyse the mechanical processes of flow of suspensions and macromolecular solutions of non-electrolytes through tubes. The evidence derived from this analysis is employed in the construction of a flow mechanism and this is in turn used in the derivation of fundamental viscosity relationships. These are compared with the corresponding experimental relationships.

2. The nature of viscosity in suspensions

Consideration of the dimensions of viscosity, as defined by Newton's equation, shows it to be a measure of the action per unit volume within a fluid. In the case of a homogeneous fluid moving through a tube under laminar flow conditions the action results from the relative motion in translation of adjacent parts of the fluid. In these circumstances a fluid can be regarded as having a continuous structure, and, for the purposes of analysis, can be imagined as being made up of elementary cylinders of liquid each subject to viscous forces resulting from the translational motion relative to it of neighbouring elements. The integration of the equation representing the dynamic equilibrium of such an elementary cylinder under the opposing actions of the force due to the applied pressure and the viscous resisting force leads to the familiar expression for the velocity along a streamline and thence to Poisseuille's formula. This approach, however,

breaks down in the case of an inhomogeneous fluid, for here the action arises not only through the relative motion in translation of adjacent parts of the continuous phase, but also to the motion of the solute molecules, or the particles, within it.

It has been shown that, in general, the motion of a viscous liquid cannot be irrotational,[4] and consideration of the variation of velocity gradient within a tube, and hence of the forces acting on a suspended particle, suggests that under these circumstances rotation of the particle certainly occurs.

The total action involved in the flow of an inhomogeneous fluid is thus seen to consist in general of three components. These are respectively, the action arising through the relative motion in translation of adjacent parts of the continuous phase, that due to the rotation within it of the macromolecules or other inhomogeneities and the action resulting from the translation of these suspended particles relative to the continuous phase. This last component, as will be shown later, is small compared with the other two except at fairly high concentrations.

3. FLOW MECHANISM

The observations made in the last section lead directly to the conception of the flow mechanism in the cases under consideration as involving the translation of the solvent and the simultaneous translation and rotation of the particles of solute within it.

The suggested rotation of solute particles will obviously involve the movement with them of some entrained solvent and for this reason the proposed flow mechanism must be modified slightly so as to involve the translation through the tube of what may be called "macromolecular vortices" rather than of isolated particles.

Let us now consider some of the implications of this proposed flow mechanism, and, in the first instance, let us consider the flow of a suspension involving only a single solute particle.

If η_s denotes the coefficient of apparent viscosity of the solution (that is, the volume-average action per unit volume) and η the coefficient of viscosity of the solvent, the total action, A_1, within the tube due to the single vortex is given by:

$$A_1 = \pi R^2 l(\eta_s - \eta) \tag{1}$$

where R and l are respectively the radius and length of the tube. It should be noted that, since action per unit volume varies from point to point, it is necessary to deal with the total action within the tube and the total internal volume of the tube as a means of arriving at any relation between measured values of viscosity and the constants of the solute and solvent.

Regarding the vortex as an "ideal" vortex of radius a and length h, two extreme cases can readily be distinguished, e.g. one in which a is negligible compared with h,—a rod-like vortex,—and the other in which a is large compared with h,—a disk-like vortex.

(i) *h much greater than a.* In this case the total action due to the rotation of the vortex will arise almost wholly as a result of the viscous forces on its curved surface and the resisting couple G acting on it will be given by:

$$G = 4\pi\eta h a^2 \omega \text{ (see Ref. 5)} \tag{2}$$

where ω is its angular velocity.

As an isolated vortex no forces tending to produce translation relative to the solvent will act on it.

Hence $$A_1 = 4\pi\eta h a^2 \omega^2 l^2/v^2 \tag{3}$$

where v is the linear velocity of the solvent on the streamline along which the vortex moves.

The factors appearing on the right-hand side of equation (3) can be grouped and equation (3) rewritten as

$$A_1 = k_1 \eta F \tag{4}$$

where k_1 is a "flow" factor and F a "form" factor of the vortex, i.e. $F = 4\pi h a^2$. (F is the viscous resisting couple per unit angular velocity in a fluid of unit viscosity.)

Assuming that Poisseuille's law holds in this case $v = P(R^2 - r^2)/4\eta l$ and hence, in accordance with the requirement of least action, $\omega = dv/dr$, i.e. $\omega = Pr/2\eta l$, where r is the radius of the streamline, P being the applied pressure difference.

Therefore, $$k_1 = 4l^2 r^2/(R^2 - r^2)^2$$

Again, for least action A_1 must have its least value and therefore the vortex must flow along a streamline adjacent to the tube axis. Assuming a fixed value of r, k_1 is seen to be constant.

For very dilute solutions in which it can be assumed that the motion of any one vortex is unaffected by neighbouring vortices, the total action within a tube A, when the number of particles per unit volume in the solution is n, is $n\pi R^2 l$ times as great, assuming all vortices to be identical.

i.e. $$A = nA_1 \pi R^2 l \tag{5}$$

(In view of the "normal" particle size distribution usually assumed, the present analysis can only be regarded as applicable to "average" particles.) Now $\eta_s - \eta = A/\pi R^2 l$ in the present case.

Therefore $$\eta_s - \eta = k_1 n \eta F \tag{6}$$

from equation (4).

In words, the specific viscosity of a very dilute suspension (that is, the fractional change in the viscosity of the solvent due to the suspension in it of the solute) is directly proportional to the number of suspended particles per unit volume provided that the "form" factor of the molecular vortices remains constant.

(ii) *a much greater than h.* In this case the total action due to the rotation of the vortex arises almost wholly as a result of the viscous forces acting on the plane vortex surfaces. Here $G = (32/3)\eta a^3 \omega$,[6] and the "form" factor is in this case given by $F = (32/3)a^3$.

Subject only to the different value of F in this case equation (6) can be shown, as previously, to hold.

(iii) *h and a of the same order of magnitude.* Subject again only to a further different value of the form factor, equation (6) can be shown similarly to hold in this case also.

4. THE LAWS OF EINSTEIN, STAUDINGER AND HUGGINS

Empirical equations based on the analyses of Einstein, Staudinger and others are commonly used in the determination of molecular weights from viscosity measurements. It is of interest, therefore, to consider the significance of such equations in the light of the flow mechanism postulated in the last section.

Previous workers have made no hypothesis in regard to the existence of molecular vortices but have dealt with the suspended particles themselves and have variously assumed that they are spherical (Einstein),[1] cylindrical (Staudinger and Hever)[2] or rod-like (Huggins).[3]

By replacing the molecular vortices assumed in the present analysis by particles having the shapes referred to, these laws can be derived very simply.

Thus, assuming the particles to be spherical

$$G = 8\pi\eta a^3\omega \text{ (see Ref. 7)}$$

and therefore, $F = 8\pi a^3$.

Now the total volume of the spheres in unit of volume of the suspension, ϕ, is given by $\phi = n(4/3)\pi a^3$, and therefore, from equation (6),

$$\eta_s - \eta = k_2\phi\eta \tag{7}$$

where k_2 is a constant.

The specific viscosity is therefore directly proportional to the volume-concentration as shown by Einstein.

Next, let us assume that the particles are cylindrical with lengths great compared with their radii, and rotate about their cylindrical axes. Here, as in Section 3(*i*), F has the value $4\pi a^2 h$ where a is now the radius of the cylindrical particle and h its length.

For particles of constant section the mass M of the particle is proportional to h.

The mass-concentration, c, of the solution is nM and, from equation (6), therefore

$$\eta_s - \eta = k_3\eta c \tag{8}$$

where k_3 is a constant.

That is, the specific viscosity is directly proportional to the mass-concentration and independent of the particle size, as shown by Staudinger and Hever for solutions of monosaccharides and disaccharides.

Finally, let us assume that the particles are rod-like and rotate about axes normal to their lengths. Here, the molecules, together with the entrained solvent must be regarded as comprising disk-like particles. The molecular weight is therefore proportional to the diameter of the disk.

As in Section 3(ii), $F = (32/3)a^3$.

But $a^3 = k_4 M^3$, where M is the molecular weight and k_4 a constant. Therefore $F = k_5 M^3$, k_5 being constant.

If c is the mass-concentration of the solution, from equation (6), we have

$$\eta_s - \eta = k_6\eta c M^2 \tag{9}$$

k_6 being constant.

This agrees with the results of Huggins and other workers, who showed that the intrinsic viscosity (that is, the limiting value as the concentration approaches zero of the specific viscosity per unit concentration) is proportional to the square of the molecular weight.

The applicability of equations (8) and (9) in certain limited cases has led to the general adoption of an empirical molecular weight equation of the form $\eta_{Int} = kM^\alpha$ where η_{Int} is the intrinsic viscosity and k and α are constants. In the light of equation (6) it would appear that α is a shape factor for the suspended particles. Its value, as seen from the two extreme cases cited in Sections 3(i) and 3(ii), lies somewhere between 0 and 2.

5. THE VISCOSITY-CONCENTRATION LAW

The mechanisms considered to date all lead to a linear relationship between viscosity and concentration. This relationship rests on the assumption that individual molecular vortices or the individual particles themselves are independent of their neighbours; it must therefore be regarded as only an approximation and an approximation moreover which becomes progressively less valid as concentration is increased. Departure from such a linear relationship is, furthermore, clearly indicated by the relevant experimental data; this confirms the validity of the straight-line law only as an approximation in the case of very dilute solutions.

In view of this limitation of current theory it becomes important to consider whether the proposed molecular vortex theory can be extended so as to take account of the conditions existing in more concentrated solutions.

The flow mechanism outlined in Section 3 leads, in accordance with the principle of least action, to the conclusion that an individual particle flowing through a tube would follow a path adjacent to the tube axis. The stability of the vortices associated with a succession of such particles, however, requires the formation about the tube axis of a "Kármán vortex street."[8] Let us then consider some of the main implications of this requirement in the present case.

According to the theory of vortex streets each vortex has a translational velocity, U, impressed on it as a result of the combined action of all other vortices, where

$$U = K/2\sqrt{(2)}L \tag{10}$$

K being the vortex strength and L the distance measured in the direction of flow between the vortices in either "lane."[9] By definition the vortex strength, K, is given by the equation

$$K = 2\pi a^2\omega \tag{11}$$

where a is the radius of the "ideal" vortex and ω its angular velocity.

Since, in the present case, a and ω are both small the molecular vortices postulated must in general be "weak" vortices. Even at moderate concentrations of the solutions, then, U will be small, but will increase as concentration increases under given external conditions.

An approximate equation relating specific viscosity and concentration, applicable at moderate and even fairly high concentrations, can now be derived.

Let n be the number of solute molecules per unit volume of solution. The number emerging from both lanes in the vortex street per second is therefore $2(v + U)/L$.

Therefore,

$$n = 2(v + U)/LV \tag{12}$$

where V is the volume of solution discharged per second from the tube. Neglecting U compared with v, and making use of the approximate constancy of v/V, we have,

$$n = k_7/L \tag{13}$$

or, from equation (10),

$$n = k_8 U \tag{14}$$

In words, the relative velocity of the solute with respect to the solvent increases approximately linearly with concentration. The action, A_T, involved as a result of this relative translation, since the resisting force is proportional to ηU, is given by

$$A_T = k_9\eta n^2 \tag{15}$$

Since the action A_R, due to rotation, as previously shown, is given by

$$A_R = k_{10}\eta n \tag{16}$$

the total action, A, is

$$A = \eta(k_{10}n + k_9 n^2) \tag{17}$$

k_9 and k_{10} being constants.

That is, the specific viscosity of a solution is related parabolically with its concentration.

As a means of testing equation (17) by experiment the typical results of Kendall and Monroe[10] have been used. In the first and third columns of the table the corresponding values obtained by them for the molecular concentration

and the viscosity of a solution of naphthalene in benzene at 25° C are quoted. The values of (concentration)^2 and specific viscosity given respectively in the second and fourth columns were calculated directly from these. Using the co-ordinates of two points on the specific viscosity-concentration graph the constants k_9 and k_{10} of equation (17) were evaluated. The specific viscosity-concentration law in the present case was hence found to be

$$\eta_{sp} = 1{\cdot}60.10^{-2}n + 1{\cdot}08.10^{-4}n^2 \qquad (18)$$

The values of the specific viscosity obtained by substituting the values of n and n^2, given in the first two columns, in equation (18), are recorded in the fifth column, the percentage discrepancies between these calculated values and the experimental values of column four being shown in the last column.

Corresponding experimental and theoretical values of specific viscosity at various concentrations

n	n^2	γ_{sp}	*Experimental* γ_{sp}	*Calculated* γ_{sp}	*Discrepancy* %
0·00	0·0	0·6048	0·000	0·000	0·0
5·10	26·0	0·6565	0·085	0·085	0·0
11·21	125·7	0·7261	0·200	0·193	3·5
15·38	237·2	0·7707	0·274	0·272	0·7
19·29	372·5	0·8263	0·366	0·349	4·6
23·98	576·0	0·8764	0·449	0·446	0·6
26·93	723·6	0·9178	0·517	0·508	1·7

6. EFFECT OF ASPECT RATIO

In the derivation of equation (6) in Section 3 two extreme cases were distinguished, namely (i) that of the rod-like vortex in which the length is big compared with the radius and (ii) that of the disk-like vortex in which the radius is large compared with the length. Equation (6) was shown to be equally applicable to both, though it was noted that the "form" factor differed in the two cases.

In view of the considerable use made of viscosity measurements in the study of high polymers it is of interest to consider whether macromolecules in which one dimension is large compared with the others would lead under the flow conditions under discussion to the formation of rod-like or disk-like vortices. That is, would macromolecules of large aspect ratio κ/d, κ being the longest and d the shortest dimension, orientate themselves so that κ is parallel to or perpendicular to the vortex axis?

Making the assumption that under the circumstances visualized entraining of the solvent by the solute molecules occurs only to a limited extent, the dimensions κ and d can be identified approximately and respectively with h and $2a$ in the former case and with $2a$ and h in the latter.

The ratios of the actions involved in the two cases is the same as the ratio of the form factors and therefore equal to $3\pi h/8a$. Since κ is much greater than d, the action involved when the molecule is orientated parallel to the axis of rotation is big compared with that for perpendicular rotation. In accordance with the principle of least action, therefore, the molecule will rotate so that its longest dimension is normal to the axis of rotation, the molecular vortex consequently being disk-like.

This conclusion is consistent with the observations of Binder.[11] He investigated the relationship between the orientations of sections of human hair and their aspect ratios and found that for very large values of the latter the specimens orientated themselves in the perpendicular position.

In the light of the above it becomes apparent that the direct association of specific or intrinsic viscosity with molecular weight, M, in the manner suggested by the equations of Staudinger and Huggins and their co-workers may be misleading.

The index of M in an empirical formula of the type $\eta_{Int} = kM^{\alpha}$ must clearly depend upon the form factor of the vortices and hence on the aspect ratio of the molecules themselves. The index would, however, appear to provide an indirect measure of the shape, degree of branching, etc., of molecules of given molecular weight.

7. GENERAL OBSERVATIONS

The mechanism outlined in the previous sections involves the motion of vortices along streamlines adjacent to the tube axis, as shown in Section 3. The action per unit volume is hence greatest in those regions where the velocity gradient is least; that is, the coefficient of viscosity decreases with increasing velocity gradient. This qualitative result is consistent with the variation found experimentally and investigated quantitatively by Tyler and Richardson,[12] and hence, indirectly, with the well-established fact that the volume of solution discharged per second increases with applied pressure to a value in excess of that to which simple proportionality would lead.

Further work is necessary to reduce to quantitative terms these and other qualitative relationships suggested by the analysis.

8. CONCLUSIONS

The flow mechanism described follows directly from the conception of viscosity as action per unit volume. It leads simply to the laws of Einstein, Staudinger and Huggins and their co-workers as special cases of a general law which is derived. The quadratic law connecting specific viscosity with concentration, which is also derived, is shown to be in good agreement with typical experimental results. The mechanism is observed to be qualitatively consistent with other experimental data.

ACKNOWLEDGEMENTS

I am grateful for the interest shown in this work by members of the science department staff of the Technical College of Monmouthshire, and of the research staff of British Nylon Spinners Ltd., Pontypool.

REFERENCES

(1) EINSTEIN. *Ann. Phys.* [*Leipzig*], **19,** p. 289 (1906).
(2) STAUDINGER and HEVER. *Ber. Deuts. Chem. Ges.*, **63,** p. 222 (1930).
(3) HUGGINS. *J. Phys. Chem.*, **42,** p. 911 (1938).
(4) SUPINO. *Atti. Accad. Naz. Lincei*, **6,** pp. 615 and 708 (1949).
(5) MERRINGTON. *Viscometry*, p. 31 (London: E. Arnold and Co., 1951).
(6) MERRINGTON. *Viscometry*, p. 38 (London: E. Arnold and Co., 1951).
(7) MERRINGTON. *Viscometry*, p. 38 (London: E. Arnold and Co., 1951).
(8) KÁRMÁN and RUBACH. *Phys. Z.*, **13,** p. 49 (1912).
(9) RICHARDSON. *Dynamics of Real Fluids*, p. 18 (London: E. Arnold and Co., 1950).
(10) KENDALL and MONROE. *J. Amer. Chem. Soc.*, **39,** p. 1802 (1917).
(11) BINDER. *J. Appl. Phys.*, **10,** p. 711 (1939).
(12) TYLER and RICHARDSON. *Proc. Phys. Soc.* [*London*], **45,** p. 142 (1933).

New books

A text-book of radar. 2nd Edition. Edited by E. G. BOWEN. (London: Cambridge University Press, 1954.) Pp. xiii + 617. Price 45*s*.

Very wisely, this book has been made a collective effort by a number of authors in the Radiophysics Laboratory, C.S.I.R.O., Australia. A wide field had to be covered but with the chapter subdivisions chosen and careful editing the reading flows smoothly and without noticeable repetition. It is well to regard the work as a general text-book concerned more with overall principles rather than with detail: it would be very suitable for engineering students.

The volume under review is the second edition, the first having been published in 1947 and the editor states that only small corrections and some minor alterations of sense have been made to the first sixteen chapters of the book: these deal with fundamentals and discussions of all the component parts from transmitter to aerial and back *via* receiver to display. The last three chapters, dealing with applications of radar, have been completely rewritten, but they are very condensed and more could, perhaps, have been made of them. However, it is strange to find in a treatise on radar (defined in line 1 of the book) sections dealing with linear accelerators and microwave spectroscopy (presumably because pulses of r.f. energy are employed).

It is a pity that this second edition could not have been brought rather more up-to-date. Though published in April 1954, the preface indicates that it was completed in March 1952. Little change has occurred in the major part of the book, and most of the references are to work published in 1946, with a few in 1948; only for such subjects as radio astronomy are references given as late as 1951.

Printing (by the photo-offset process), diagrams and general clarity of the layout are excellent.

A. J. MADDOCK

Physical meteorology. By JOHN C. JOHNSON. (Published jointly by the Technology Press of the Massachusetts Institute of Technology and John Wiley and Sons, Inc.; London: Chapman and Hall, Ltd., 1954.) Pp. xii + 393. Price 60*s*.

Physical meteorology is not a clearly defined section of atmospheric studies, so that Johnson's selection of topics is necessarily somewhat arbitrary. The first six chapters are concerned with the interactions between radiation and the atmosphere, and include such topics as refraction, scattering, the thermal effects of solar and terrestrial radiation and atmospheric optics. Chapters 7 and 8 treat the rapidly advancing subjects of cloud and rain formation. Chapter 9 is devoted to atmospheric electricity and Chapters 10 and 11 to the upper atmosphere. The book is designed for the third or fourth year undergraduate who intends to specialize in meteorology.

The general layout, the good printing and production, the many excellent illustrations and the numerical examples at the end of each chapter provide a framework for a most useful contribution to the literature. However, the student must be warned of the many blemishes revealed by a detailed examination of the text. The explanation is often very confusing, and sometimes the treatment is too superficial for the student to have any chance of understanding it. There are too many inaccuracies and some misconceptions, which at times extend to the fundamental physical ideas where they should have been avoided at all costs.

The following are just a few examples of errors or confusions in fundamental matters: the statement that the Lorentz line shape is similar to the Doppler shape (p. 136); the definition of a *lumen* which can be constructed from table 3.5 and the definition of *visibility* on pp. 68 and 69; the discussion of *temperature* on pp. 375 and 376 the mixing up of Fourier's law of heat conduction and Newton's law of cooling on p. 153; the discussion of elliptical polarization and Rayleigh scattering in Chapter 2, which seems to be at variance with the idea of a diagonal scattering matrix.

R. M. GOODY

Transistoren. By M. J. O. STRUTT. (Zürich: S. Hirzel Verlag, 1954.) Pp. 166. Price Swiss frs. 21.

The book attempts to give a brief account of the state of transistor applications current at the time of writing. To do this in 166 pages on a rapidly expanding new subject is a very difficult task which, on the whole, the author has performed very well. The book opens with a chapter on fundamental concepts and comparison with vacuum tube triodes. This is followed by a discussion of the principal bulk properties and contact properties of semiconductors. Chapter 4 discusses the point contact transistors, Chapter 5 the large area contact transistors (junction and field effect). The following four chapters are devoted to duality of transistors and triodes, applications of transistors to amplifier input and output stages and in oscillators. There are a few pages outlining the principles of measurements of semiconductor and transistor parameters. There is a list of 148 references. In the physics section the drawing of Fermi levels is highly confusing. Limitations of space did not allow the inclusion of detailed examples of circuit applications, similarly the discussion of such topics as high frequency behaviour of transistors is very limited.

The book may be recommended as an introductory text to a new subject on which only one other comprehensive book is known to the reviewer.

A. K. JONSCHER

Structure Reports for 1950 (Vol. 13). General editor: A. J. C. WILSON. Section editors: N. C. BAENZIGER, J. M. BIJVOET and J. M. ROBERTSON. (Holland: N. V. A. Oosthoek's Uitgevers Mij., 1954.) Pp. viii + 643. Price 151*s*.

The production of *Structure Reports*, which take the place of *Strukturbericht*, is one of the major successes of the International Union of Crystallography and the appearance of Volume 13, dealing with work published in 1950, is important for all concerned with structural studies. As in the earlier volumes, the editors present very complete accounts of the structural aspects of the researches reviewed. Moreover, the value of the reports is often enhanced by the addition of critical editorial comments, by the recasting of the original results into a more convenient form, or by reference to other related researches not strictly eligible for inclusion in the 1950 volume. It is virtually impossible, in a work of this kind, to ensure complete absence of errors; but if those noticed by the reviewer in scrutinizing a few pages taken at random are typical, no great harm has been done by the editors' failure to detect them—thus, for example, p. (iv), the Copyright notice; middle of p. 281 *reasons* for *reason*; bottom of p. 372, title of paper quoted incorrectly; and bottom of p. 373 *andularia* for *adularia*.

While admiring the excellence of the production, and

appreciating the immense amount of work which has gone into the preparation and editing of the reports contained in the four volumes now available, the reviewer feels bound to stress the need for increased speed. We now have Volumes 11 (for 1947–48), 12 (for 1949), 10 (for 1945–46) and 13 (for 1950) which have appeared in 1951, 1952, 1953 and 1954. Can we expect that in the near future the editors will be able not only to close the gap since Volume 7 (for 1939) of *Strukturbericht* by producing Volumes 8 and 9, but also to reduce to one year or less the present serious time-lag of 3½ years before the publications of a given year are reported in the appropriate volume? All who need structural information for their researches will hope that this may be possible.

W. H. TAYLOR

The insulation of electrical equipment. Edited by WILLIS JACKSON, D.Sc., D.Phil., M.I.E.E., F.Inst.P., F.R.S. (London: Chapman and Hall Ltd., 1954.) Pp. ix + 340. Price 42*s*.

As explained in the foreword, this book is a compilation of a series of lectures delivered by a group of experts in the insulation field at a post-graduate vacation school held in the Electrical Engineering Department of Imperial College, London, in September 1952.

The first chapter is an historical survey of insulation development, and the rest of the book may be broadly divided into two parts; four chapters devoted to insulation properties in terms of composition and structure, and six chapters on the application of insulator materials in various branches of electrical engineering. The treatment is generally non-mathematical, and in spite of the condensation necessary to give an adequate survey of such a complex subject in a relatively small space, most of the book makes easy reading. There is a useful bibliography at the end of each chapter.

Since the approach throughout is of an "engineering" nature it is unlikely to appeal to physicists as a text-book on insulation, but it could be read with profit by those whose work brings them into contact with insulation problems.

R. D. NIXON

Ferromagnetic domains. By K. H. STEWART, M.A., Ph.D. (Cambridge monographs on physics). (London: Cambridge University Press, 1954). Pp. viii + 176. Price 25*s*.

At the present time considerable interest is being taken in the development of the concept of the ferromagnetic domain. We now have much beautiful experimental work by American, English and Japanese workers which has made visible in a most striking fashion the existence of domain structures in single crystal and even to a limited extent, in polycrystalline specimens of ferromagnetic metals. We also have a substantial body of theoretical work on these domains, and particularly on the behaviour of the walls between them, which we may hope will eventually assist us in explaining many of the complicated phenomena of ferromagnetism. The author of this pleasing little treatise has himself made some interesting contributions to their study, and in his book he has given in a convenient form accounts of the more outstanding results up to 1952, without great attention to experimental details. The treatment is sound and the book can be recommended to the general reader, although the latter would probably like some references to work on the ΔE effect. Incidentally, the reviewer does not approve of Fig. 47, or of certain remarks about complicated domain structures on p. 88.

L. F. BATES

Laplace transforms for electrical engineers. By B. J. STARKEY, Dipl.Ing., A.M.I.E.E. (London: Iliffe and Sons Ltd., 1954) Pp. 279. Price 30*s*.

With so many books on Laplace transforms in existence any new book on the subject requires some justification. The author's aim is to introduce the subject from ideas familiar to the electrical engineer. He is concerned to remove any difficulties in the fundamentals, usually glossed over, by elaborating the first chapters with more special notation than is usual. The significance of the complex p-plane is illustrated as an "animated" vector field. The subject is covered up to contour integration and higher functions. The book is published for the *Wireless Engineer* which seems a new departure in this type of literature. The printing space has been used economically and one misses heavier printing of the subtitles, but otherwise the printing is clear and there are many figures. Some familiar with the subject might find it slightly harder to find their way in this book than in one of those already existing but some new to the subject might like it. There are many applications and worked out examples.

H. PELZER

Fluorescence analysis in ultra-violet light. 4th edition. By J. A. RADLEY, M.Sc., F.R.I.C., and J. GRANT, Ph.D., M.Sc., F.R.I.C. (London: Chapman and Hall Ltd., 1954.) Pp. xvi + 560. Price 52*s*. 6*d*.

This fourth edition of a well-known text has been considerably enlarged and revised, account being taken of the many papers on fluorescence analysis which have appeared during the fifteen years since the publication of the third edition. The authors have themselves checked much of this new work.

Part I of the book deals with the apparatus and technique of fluorescence analysis. Despite the authors' claim that in preparing this edition much "dead wood" has been cut out, this section of the book is still far from satisfactory. The accuracy of some of the statements is open to question, whilst information which one could reasonably expect to find, regarding the radiant power output of lamps at various wavelengths or the spectral transmission characteristics of commercial filters, is not included. In a later chapter, dealing with measurement of ultra-violet intensity, the impression is given that a method described in a medical journal some thirty years ago represents current practice in photo-electric photometry!

Part II of the book, amounting to about four fifths of the volume is devoted to applications and here the authors appear to be on more familiar ground. The subject matter is divided into some twenty chapters, each dealing with a special field of work such as bacteriology, museum work, textiles, minerals and gems, etc. Each of these chapters is a most useful review, some containing several hundred references to original publications. However, this degree of annotation does, in places, detract from ease of reading.

At the end of the book nearly fifty excellently reproduced photographs illustrate various applications of the technique. A little extra care in describing some of these would make it absolutely clear whether they illustrate fluorescence phenomena or merely differences in ultra-violet reflexion characteristics.

Even with its present shortcomings this book contains a very great deal of useful reference material not readily found elsewhere. The reviewer suggests that a physicist familiar with the subject should be consulted about Part I before the book is again revised.

B. S. COOPER

Notes and comments

The Physical Society's annual exhibition of instruments and apparatus

The Physical Society announces that its 39th annual exhibition will be held in the New Hall of the Royal Horticultural Society in Westminster from 25 to 28 April, 1955, inclusive. Continued growth has necessitated moving the exhibition from the Imperial College in South Kensington, where it has previously been held, to this larger hall which will, in many ways, be more convenient. The Council of the Society has instructed its Exhibition Committee to use its best endeavours to keep the style and spirit of the exhibition unchanged, namely to provide an opportunity, of a non-commercial nature, for showing new instruments and apparatus to scientists and technicians. About 140 offers to exhibit have been accepted compared with 103 exhibitors last year. The handbook issued in connexion with the exhibition will be produced as usual a few weeks in advance.

Details regarding tickets for admission (for which there is no charge) will be announced in due course.

Journal of Nuclear Energy

The first issue has just appeared of a new quarterly to be devoted primarily to the publication of technical articles from the staff of European nuclear energy projects and their associated industrial groups. In his foreword, Sir John Cockcroft says that it is hoped that its establishment will "promote that interchange of ideas which is the basis of scientific and technological development in peace." The issue before us is one of 92 pages measuring $6\frac{3}{4} \times 10$ in. and is well printed and produced. It contains ten contributions, seven of which are from Harwell, covering a wide range of subjects. Papers will be accepted in English, French or German, but English abstracts accompany all the papers. There is a strong International Editorial Advisory Board; the Editors are Dr. J. V. Dunworth (Editor-in-Chief) of Harwell, Dr. J. Guéron of the French Atomic Energy Commission, and Dr. G. Randers of the Joint Establishment for Nuclear Energy Research, Norway. We wish them and their journal success.

The publishers are the Pergamon Press Ltd. of Maxwell House, Marylebone Road, London, N.W.1, and the annual subscription price is £4 10*s*. (U.S.A. $12.60), or for individual subscribers certifying that the journal is for their personal use, £3 10*s*. (U.S.A. $9.80).

Register of British manufacturers

The 1955 edition of the register of British manufacturers who are members of the Federation of British Industries is even larger than the 1954 edition. It has 1115 pages and contains a new section entitled Language glossaries in which every heading used in the buyers' guide is translated into French, German and Spanish. The remainder of the book is divided into the following sections: Products and services; Advertisements; Addresses; Trade associations; Brands and trade names; Trade marks.

The register is published by Kelly's Directories Ltd., and Iliffe and Sons Ltd., Dorset House, Stamford Street, London, S.E.1. The price is 42*s*. (including postage).

Journal of Scientific Instruments

Contents of the January issue

ORIGINAL CONTRIBUTIONS

Papers

A recording volumeter for small gas evolutions. By W. E. Hoare.
An apparatus for the measurement of dynamic mechanical properties of polymers over a wide temperature range. By D. W. Robinson.
An optical interferometer method of calibrating a crystal gauge for the measurement of sound wave transients. By G. J. Barber.
A machine for the measurement of rolling friction. By J. Halling.
Infra-red filters using evaporated layers of lead sulphide, lead selenide and lead telluride. By J. G. N. Braithwaite.
The production of accurate linear scales by means of the Merton nut. By L. A. Sayce.
The processing and some characteristics of coaxial cylinder, corona stabilizer tubes. By A. J. L. Collinson and D. W. Hill.
A measuring apparatus employing a reference line of variable brightness. By C. S. Lees.
A combined strain and curvature gauge for use in testing concrete beams. By J. M. Prentis.
An apparatus giving an α-particle microbeam for the irradiation of living cells. By H. A. B. Simons.
On the preparation of precision resolving-power test objects. By G. D. Dew.
Analysis of ortho- and para-hydrogen mixtures by the thermal conductivity method. By A. T. Stewart and G. L. Squires.
The necessary torque requirements for a servo-motor. By J. C. West and J. L. Leonard.

Laboratory and workshop notes

An adjustable bilateral slit for use with a photomultiplier in a soft X-ray spectrometer. By P. Fisher.
An automatic thermostat warming-up device. By M. W. Jervis.
An effective method of gripping short specimens of wire strand for tensile tests. By F. D. Hills.
A method of estimating distortion in cloud chamber tracks. By N. Cusack and P. Stott.
The preparation of unbacked gold films of known thickness. By W. E. Spear.
A multi-range laboratory flowmeter. By K. H. Todhunter and B. Wolstenholme.

NOTES AND NEWS

Correspondence

A trap-current controlled emission regulator for a mass spectrometer ion-source. From D. Greenhalgh and P. M. Jeffery.
Photographic enlargement and reduction in one dimension only. From R. N. Bracewell.

New instruments, materials and tools

Electronic motor controller. Pipette control. Germanium junction photocells and power rectifiers. Pulse height analyser. Stylus oscillograph. Precision potentiometers. Precision vernier potentiometer.

Notes and comments

British Journal of Applied Physics

Original contributions accepted for publication in future issues of this Journal

Role of partition coefficient in permeability of surface layers with low diffusion coefficient. By G. R. Lester.
Conditions for aperiodicity in linear systems. By A. T. Fuller.
An analogue study of the temperature distribution in cooled gas-turbine blades. By C. F. Kettleborough.
A rubber-membrane model for investigating axially-symmetric systems in electron optics. By B. J. Mayo.
Measurement of the statistical time lag of breakdown in gases and liquids. By R. F. Saxe and T. J. Lewis.
The cracking of layers of brittle material by differential strains. By D. J. Millard.
The electrical conductivity and permittivity of mixtures, with special reference to emulsions of water in fuel oil. By C. A. R. Pearce.

THIS JOURNAL is produced monthly by The Institute of Physics, in London. It deals with all branches of applied physics (including theory and technique). All rights reserved. Responsibility for the statements contained herein attaches only to the writers.

EDITORIAL MATTER. Communications concerning editorial matter should be addressed to the Editor, The Institute of Physics, 47 Belgrave Square, London, S.W.1. (*Telephone:* Sloane 9806.) Prospective authors are invited to prepare their scripts in accordance with the *Notes on the preparation of contributions*. (Price 2*s*. 6*d*. including postage.)

REPRODUCTION. The Institute of Physics is a signatory to The Royal Society's Fair Copying Declaration. Details may be obtained upon application from The Royal Society, London, W.1.

ADVERTISEMENTS. Communications concerning advertisements should be addressed to the agents, Messrs. Walter Judd Ltd., 47 Gresham Street, London, E.C.2. (*Telephone:* Monarch 7644.)

CLAIMS FOR MISSING JOURNALS. Claims from regular subscribers to this *Journal* for missing numbers will only be considered if received within 60 days of the date of mailing plus normal outward time of transit and time for lodging the claim. Losses attributable to failure to notify a change of address or to similar omissions will not be considered.

SUBSCRIPTION RATES. A new volume commences each January. The charge is £4 per volume ($11.50 U.S.A.), including index (post paid), payable in advance. Single parts, so far as available, may be purchased at 8*s*. each ($1.15 U.S.A.), post paid, cash with order. Orders should be sent to The Institute of Physics, 47 Belgrave Square, London, S.W.1, or to any bookseller.

Some dynamic mechanical properties of polyisobutylene over a wide temperature range

By D. A. Thomas, B.Sc., and D. W. Robinson, B.Sc., D.Phil., Imperial Chemical Industries Ltd., Plastics Division, Welwyn Garden City, Herts.

[*Paper first received* 10 *August, and in final form* 11 *October*, 1954]

A cantilever resonance method has been used to measure the complex Young's modulus of polyisobutylene from 90 to 560° K at a number of points in the frequency range 30–300 c/s. Using the method of reduced variables, the results have been expressed as a function of frequency at constant temperature and compared with other published data on this material over comparable reduced frequency ranges. Agreement is quite good over a limited reduced frequency range, but the present results predict a higher value for the real part of the modulus at infinitely high frequencies, and show the small dispersion peak in the imaginary modulus curve displaced to a higher reduced frequency. The validity of extrapolating the frequency shift factor to high and low temperatures is questioned, and suggested as a possible explanation for the discrepancies. A comparatively large value of the temperature coefficient of the modulus at 90° K suggests that an appreciable configurational entropy term is still contributing to the free energy of the polymer at these low temperatures.

A detailed investigation of the viscoelastic properties of high polymers involves a number of different experimental techniques, there being as yet no single method which yields information over a sufficiently wide frequency and temperature range on a given specimen. In general, no one laboratory is equipped with a range of techniques so that it is often necessary to utilize the data from a number of workers at different laboratories. Inaccuracies can then arise due to accidental and inherent experimental errors in the equipment, and results are often difficult to compare, owing to the uncertainties involved in the preparation of a reproducible species of a given material. In 1949 the National Bureau of Standards, Washington, in an attempt to overcome these difficulties, initiated a co-operative testing programme on a standardized batch of polyisobutylene, the interim results of which have already been reported.[1]

The experiments reported here have been undertaken as part of this programme. The important feature of this work is the very wide temperature range over which measurements of the complex dynamic Young's modulus ($E = E' + iE''$) have been made. Transverse resonance vibrations of small strain amplitude ($\sim 10^{-3}$) are excited in a cantilever specimen of the polymer and, from the resonant frequency and band width of the resonance curve, the real part E' of the complex Young's modulus and the ratio of the imaginary to the real part E''/E' can be calculated. The temperature range extends from 90 to 560° K and the frequencies of the various resonances lie in the range 30–300 c/s. The apparatus and experimental procedure have been described in detail elsewhere.[2]

THE EXPERIMENTS

The molecular weight of the standard sample $M_n = 1{\cdot}35 \times 10^6$ was determined from intrinsic viscosity experiments. The material was moulded into a template (giving a reed approximately $6 \times 0{\cdot}15 \times 0{\cdot}10$ cm) at 408° K under a pressure of 1 t/in.^{2} for 45 min, this pressure being maintained while the temperature was reduced to 290° K. Owing to the very soft nature of the polymer, it was not possible to clamp the specimen between small steel jaws in the usual way, and still ensure rigidity of mounting over a wide temperature range. Some pieces of polymer were therefore dissolved in chloroform to produce a viscous cement, and this was used to stick the end of the specimen on to a flat-ended steel pin which was itself clamped to the transducer. This procedure was very satisfactory, the specimen remaining firmly fixed throughout the whole experiment. Measurements were made from room temperature down to 90° K with a 4·0 cm length specimen (thickness 0·104 cm) and from room temperature to 560° K with a 1 cm specimen of the same thickness. The large change in the modulus of the material with temperature necessitated the use of two specimens of different lengths in order to bring the resonant frequency of the cantilever within the useful working range of the equipment.

RESULTS

The table summarizes the results on both specimens. In Figs. 1 and 2 the real and imaginary parts of the complex

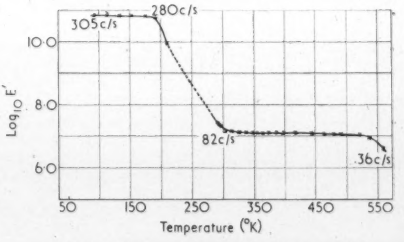

Fig. 1. Real modulus—temperature graph

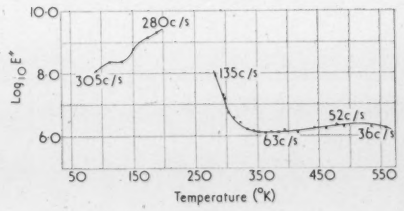

Fig. 2. Imaginary modulus—temperature graph

Young's modulus derived from measurements on the fundamental mode of vibration are plotted against temperature and the frequency of the measurement is indicated at various points. The real part of the modulus E' is calculated from the expression:

$$E' = \frac{4\pi^2 \rho f_0^2 l^4}{m^4 (t^2/12)}$$

where ρ = density of the specimen, l = length of the specimen, t = thickness, f_0 = resonant frequency (Estimated at the appropriate temperature of measurement using expansion coefficient data given in Ref. (1)).

m = parameter appropriate to the particular mode of vibration and = 1·875 for the fundamental resonance.

The imaginary modulus E'' is calculated from the expression $\tan\delta = \frac{E''}{E'} \simeq \frac{\Delta f}{f_0}$, Δf being the bandwidth of the resonance curve measured at $1/\sqrt{2}$ of the maximum amplitude, and f_0 the resonant frequency. This approximation holds within 1% for $\tan\delta > 0{\cdot}2$ and is therefore less accurate in the vicinity of a large loss peak such as occurs with polyisobutylene at about 230° K.

In Figs. 3 and 4 our results, converted to shear moduli by assuming Poisson's ratio = 0·5, are presented as a function

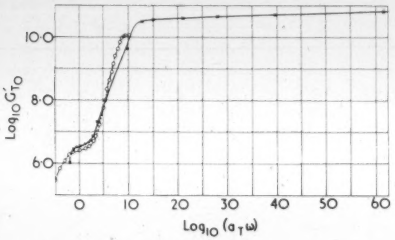

Fig. 3. Reduced real modulus—frequency graph

× = present experiments; ○ = results of other participants.

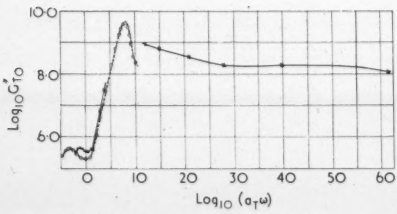

Fig. 4. Reduced imaginary modulus—frequency graph

× = present experiments; ○ = results of other participants.

of angular frequency at a standard temperature of 298° K by use of the Ferry reduction scheme.[3] For comparison the composite reduced curve deduced by Marvin[1] is also plotted. Ferry's reduction method interrelates the frequency and temperature dependence of the viscoelastic behaviour of the material according to the expression:

$$(\rho_0 T_0/\rho T) G_T(\omega) = G_{T_0}(\omega a_T) \qquad (1)$$

Where $G_T(\omega)$ is a dynamic modulus measured at a temperature T, and angular frequency ω, and $G_{T_0}(\omega a_T)$ the modulus characterizing the same viscoelastic response but at a new reference temperature T_0 and frequency $a_T\omega$, a_T being a function of temperature. ρ_0, ρ_T refer to the polymer density at T_0 and T respectively. In carrying out this reduction, the expression for the shift factor a_T has been calculated from an equation given by Leaderman and Smith,[4] to describe their results over the temperature range 223 to 303° K.

$$\log_{10} a_T = 5{\cdot}04 \times 10^5 \left(\frac{1}{T^2} - \frac{1}{298^2}\right) + \log_{10}\frac{298}{T} + \log_{10}\frac{\rho_0}{\rho} \qquad (2)$$

In this equation the last two terms are neglected, and the resulting linear relationship between $\log_{10} a_T$ and $1/T^2$ has been extrapolated down to 90° K and to temperatures beyond 300° K.

The validity of such an extrapolation may be questioned on the grounds that a $1/T^2$ function gives a misleading representation of the low temperature behaviour of the shift factor a_T, and furthermore, may be in error at higher temperatures. However, in the absence of further experimental data we have used the extrapolated form of equation (2) and treated the results at very high and low reduced frequencies with some reserve. The density ratios occurring in equation (1) have been computed from the relationship

$$\rho_0/\rho = [1 + 0{\cdot}585 \times 10^{-3}(T - T_0)]$$

given by Marvin,[1] and where necessary extrapolated to high and low temperatures.

DISCUSSION

Figs. 1 and 2 show the two main processes known to be present in polyisobutylene. In the region from 200 to 270° K, a very large loss peak (beyond the measuring range of the apparatus) characterizes the transition from the "rubbery" to the "glassy" state, and at much higher temperatures a somewhat smaller loss peak, associated with flow of the polymer, is found. The dynamic Young's modulus changes by more than three decades in the temperature range 200–300° K. No loss processes have been observed below the rubber-glass transition temperature, and it therefore appears that unless any further changes occur below 90° K, the modulus has reached a value of $7{\cdot}20 \times 10^{10}$ dyn/cm^2.

An estimate of the temperature coefficient of the modulus gives a value of about 10^7 dyn/cm^2 degree at 90° K, and a simple calculation of the theoretical temperature coefficient based on the assumption that only the thermal vibration of the atoms in the polymer can contribute to its free energy, gives a value of about 10^4 dyn/cm^2 degree at 90° K. Since the observed value is very much higher, additional terms must be contributing to the free energy at this temperature, the most probable factor being a configurational entropy term arising from the flexible nature of the polymer chains.

Comparing the values of $\log_{10} G'(\omega a_T)$ and $\log_{10} G''(\omega a_T)$ deduced from the present work with those computed by Marvin (Figs. 3 and 4), there is seen to be quite reasonable agreement for values of $\log_{10}(\omega a_T)$ between 0 and 5. Disagreement exists in the vicinity of the large transition and at

the highest and lower frequencies, the present results rising to a value of $\log_{10} G' = 10{\cdot}85$ at an equivalent frequency of $\log_{10}(\omega a_T) = 60$. The lack of agreement in the actual transition may be due to uncertainties in measuring the precise temperature of the material in a region where cyclic heating is important, and as the modulus is changing very rapidly with temperature, a 1 degree change could give rise to a 5% change in $\log_{10} E'$. However, a more probable explanation is suggested by the fact that the discrepancies are appreciable outside the reduced frequency range $\log_{10}(a_T\omega) = 0$ to at infinite frequencies as being probably too low. It is usual to identify the high-frequency modulus G_∞ with the zero point modulus G_0 (i.e. the modulus at $T = 0°$ K). Assuming this to be true for polyisobutylene, we note that our highest measured value of Young's modulus leads to a value of $\log_{10} G' = 10{\cdot}34$, which is higher than the $\log G'_\infty$ value quoted above, and is computed without any reference to the reduction principle. With the high value of the temperature coefficient at 90° K the modulus figure will almost certainly rise still further.

Dynamic mechanical data for polyisobutylene

Temperature (° K)	*Frequency* (c/s)	*Real part of dynamic Young's modulus E'* (dyn/cm²)	$\text{Log}_{10} E'$	*Imaginary part of dynamic Young's modulus E''* (dyn/cm²)	$\text{Log}_{10} E''$	$\text{Log}_{10} G'_{T_0}$	$\text{Log}_{10} G''_{T_0}$	$\text{Log}_{10}(a_T\omega)$
		Length of specimen = 1·0 *cm. Thickness* = 0·104 *cm*						
281·4	135·0	$5{\cdot}87 \times 10^7$	7·769	$8{\cdot}12 \times 10^7$	7·910	7·314	7·453	+ 3·69
294·5	82·0	2·16	7·334	1·93	7·286	6·861	6·811	+ 2·87
296·7	79·5	2·05	7·312	1·57	7·196	6·836	6·723	+ 2·70
303·2	68·5	1·52	7·182	$5{\cdot}71 \times 10^6$	6·757	6·699	6·274	+ 2·43
312·5	66·1	1·42	7·152	3·88	6·589	6·658	6·093	+ 2·10
323·2	65·4	1·38	7·140	2·71	6·433	6·633	5·927	+ 1·72
335·0	63·9	1·33	7·124	1·57	6·196	6·606	5·679	+ 1·34
345·2	63·7	1·32	7·121	1·42	6·152	6·591	5·622	+ 1·08
353·1	63·6	1·31	7·117	1·33	6·124	6·539	5·587	+ 0·92
363·2	63·7	1·32	7·121	1·29	6·111	6·535	5·565	+ 0·65
372·6	63·3	1·31	7·117	1·36	6·134	6·560	5·580	+ 0·48
385·0	63·2	1·31	7·117	1·33	6·124	6·551	5·559	+ 0·23
393·9	63·5	1·33	7·124	1·47	6·167	6·548	5·593	+ 0·01
416·4	63·0	1·31	7·117	1·33	6·124	6·522	5·530	− 0·33
443·3	62·9	1·31	7·117	1·63	6·212	6·502	5·597	− 0·70
463·1	61·9	1·27	7·104	1·72	6·236	6·476	5·605	− 0·92
479·2	61·3	1·26	7·100	2·09	6·320	6·459	5·679	− 1·10
490·9	60·6	1·23	7·090	1·94	6·288	6·442	5·641	− 1·22
520·3	56·5	1·07	7·029	2·46	6·391	6·364	5·723	− 1·52
536·6	52·8	$9{\cdot}36 \times 10^6$	6·971	1·97	6·294	6·294	5·621	− 1·67
559·3	35·65	4·34	6·637	1·64	6·215	5·947	5·524	− 2·00
566·1	—	specimen mechanically unstable			—	—	—	—
		Length of specimen = 4·0 *cm. Thickness* = 0·104 *cm*						
206·3	113·0	$1{\cdot}00 \times 10^{10}$	10·000	—	—	9·659	—	+ 9·56
188·1	280·5	6·22	10·794	$2{\cdot}00 \times 10^9$	9·301	10·489	8·946	+12·01
172·1	291·5	6·70	10·826	1·15	9·061	10·556	8·792	+14·82
148·7	296·5	6·85	10·836	$5{\cdot}78 \times 10^8$	8·762	10·619	8·548	+20·88
130·1	300·0	7·04	10·848	2·34	8·369	10·684	8·283	+27·84
110·4	302·5	7·10	10·851	2·36	8·373	10·756	8·276	+39·71
89·1	305·2	7·20	10·857	1·18	8·072	10·849	8·064	+61·68

+5. Reference to the table shows that these frequency limits roughly correspond to the temperature range over which the reduction factor a_T has been experimentally determined, and this again raises the question of the validity of a linear $\log_{10} a_T - (1/T^2)$ extrapolation to higher and lower temperatures. In support of this objection, we note that the magnitude and shape of the low frequency absorption peaks (Fig. 4) correspond quite well.

The interesting feature of our results is the fact that the real part of the reduced modulus G'_∞ tends to a higher value than that suggested by Marvin ($\log_{10} G'_\infty = 10{\cdot}08$). By virtue of the low temperatures at which our measurements were carried out, it has been possible to extend the reduced frequency range considerably beyond $\log_{10}(\omega a_T) = 10$ and we are inclined to regard the Marvin value of $\log_{10} G' = 10{\cdot}08$

ACKNOWLEDGEMENTS

Thanks are due to Dr. R. S. Marvin, of the National Bureau of Standards, Washington, who kindly supplied the standard sample of polyisobutylene used in our experiments.

REFERENCES

(1) MARVIN, R. S. *Proceedings of Second International Congress on Rheology*, Edited by V. G. W. Harrison, p. 156 (London: Butterworths Scientific Publications, 1954).
(2) ROBINSON, D. W. *J. Sci. Instrum.*, **32**, p. 2 (1955).
(3) FERRY, J. D. *J. Amer. Chem. Soc.*, **72**, p. 3746 (1950).
(4) LEADERMAN, H., and SMITH, R. G. *Phys. Rev.*, **81**, p. 303 (1951).

Some properties of a simple omegatron-type mass spectrometer

By A. G. EDWARDS, M.Sc., Ph.D., Research Laboratories, Associated Electrical Industries Ltd., Aldermaston, Berks.

[*Paper first received* 20 *July and in final form* 2 *September*, 1954]

An experimental investigation is described, designed to show the effect of changing tube parameters on the resolution, sensitivity and resonant frequency for the N_2 peak recorded by an omegatron-type mass spectrometer. Various departures from simple operation are reported, some of which are attributed to space charge, but it is shown that, under suitable operating conditions, the omegatron may readily be used for analysing simple mixtures of the lighter gases. For the apparatus described, the partial pressure detection limit at low total pressures is about 10^{-11} mm of mercury.

The omegatron is the name given by Sommer, Thomas and Hipple[1] in 1951 to a device in which, of various ions generated simultaneously in a region of uniform magnetic field, those of a single-charge mass ratio are accelerated in spiral orbits of increasing energy by a crossed, spatially uniform, electric field alternating at the cyclotron frequency. If the strength of the magnetic field or the frequency of the electric field is varied, ions of different mass/charge ratios are accelerated in turn, and the detection of these resonant effects enables the identity of the ions present to be established. The instrument thus used constitutes a mass spectrometer which holds promise of being both simple and sensitive. This was pointed out in the original paper, and more recently Morgan, Jernakoff and Lanneau[2] have described the use of a similar instrument for the analysis of organic vapours, Berry[3] has presented a theoretical treatment of the ion trajectories, while Alpert and Buritz[4] have reported its use when adjusted to have high sensitivity, the associated resolution being low.

The present paper discusses experimentally measured omegatron characteristics. Many details of performance are not predicted by the theoretical treatment, so that such information is desirable in assessing the suitability of the omegatron for specific analytical tasks. This investigation has been primarily concerned with establishing its use for low-pressure gas analysis, in connexion with investigations of high-vacuum processes and techniques.

PRINCIPLE OF OPERATION

Fig. 1 is a schematic diagram of the omegatron electrode assembly. The electron beam is fired along the magnetic field, across the centre of the ionization chamber to an electron collector on the opposite side. Ions are formed within the beam by electron collision with molecules of the residual gas, and their thermal and dissociation energies cause them to spiral round the lines of force with angular velocity $\omega = eH/M$ radians/s (e = particle charge, M = particle mass, H = magnetic field strength). The radius of these spiral orbits is, in general, so small that only a small fraction of the ions generated within the electron beam can escape from it radially as a direct result of their initial energies.

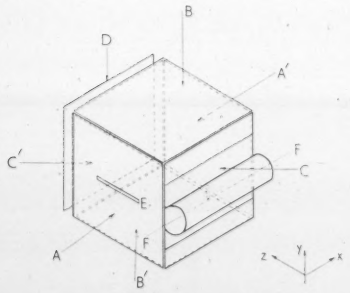

Fig. 1. The omegatron assembly

AA' = side electrodes; BB' = condenser plates; C = anode; C' = secondary electron suppressor; D = electron collector; E = slot for ion collector; F = filament.

If a weak electric field in the y-direction alternates with the angular frequency eH/M_a, ions of charge/mass ratio e/M_a are continuously accelerated and spiral away from the electron beam to an ion collector parallel to it, and at a distance r_0 cm.

The resonating ions drift parallel to the magnetic field with the axial component of their initial velocities, and this drift, if unrestrained, would bring the majority of them into collision with the omegatron electrodes before they were accelerated to the ion collector. To prevent this, d.c. trapping potentials are applied and the shape and strength of the electric field thus established have considerable influence on omegatron characteristics.

Sommer, Thomas and Hipple[1] have discussed the simple theory, and have derived expressions for collection energy, resolution, time of flight, and path length. These are given in the table, together with numerical values in typical cases.

APPARATUS

The design of omegatron used in the present investigation is similar to that of both Sommer and Alpert. Basically, the assembly consists of a box which is square in a plane perpendicular to the magnetic field, while its length in the direction of the field is somewhat less. The electron gun consists of a sprung 0·004 in. tungsten filament held axially in a metal tube by ceramic bushes. This tube is fixed to one side of the ionization box, and a slot is cut perpendicular to the filament in the wall through which the electrons pass in a beam strongly focused by the magnetic field. This beam passes through an aperture in the opposite wall to an electron collector biased positively with respect to it so that secondary electron emission is suppressed in the usual way. The condenser plates, between which the alternating voltage is applied, form the top and bottom of the ionization chamber.

The electrodes are made from a non-magnetic copper–nickel alloy and are held together by nuts and bolts with ceramic and mica insulation. The design is such that the assembly in its glass envelope will fit into a magnet gap 1¼ in. wide.

Tubes have been constructed in which guard rings were inserted between the condenser plates to ensure spatial uniformity of the alternating electric field, but this additional complexity was not always found necessary. If guard rings were not used, the remaining two sides of the omegatron

Some properties of a simple omegatron-type mass spectrometer

Algebraic expressions and typical numerical values for principal characteristics of omegatron-type mass spectrometer

Quantity	*Symbol*	*Relationship*	*Case 1*		*Case 2*	
			M/e = 2	*M/e* = 28	*M/e* = 2	*M/e* = 28
Resonant angular frequency (rad/s)	ω_0	$\omega_0 = \frac{eH}{M}$	$1{\cdot}1 \times 10^7$	$7{\cdot}9 \times 10^5$	$2{\cdot}16 \times 10^7$	$1{\cdot}54 \times 10^6$
Collection energy in volts	V	$V = \frac{H^2 r_0^2 e}{2M}$	62	4·4	240	17
Resolution*	R	$R = \frac{er_0H^2}{2E_0M}$	190	13·5	360	26
Path lengths (ignoring movement in z-direction), cm	L	$L = 2Rr_0$	270	19	500	36
Time of flight to ion collector at resonance (μs)	T_0	$T_0 = \frac{2Hr_0}{E_0}$	69		67	

Case 1
$H = 2{\cdot}3$ kG, $r_0 = 0{\cdot}7$ cm.
Applied r.f. voltage is 0·5 V r.m.s. between plates 1·5 cm apart.

Case 2
$H = 4{\cdot}5$ kG, $r_0 = 0{\cdot}7$ cm.
Applied r.f. voltage = 1·0 V r.m.s. between plates 1·5 cm apart.

* The theory assumes 100% collection efficiency and hence predicts parallel-sided peaks. Resolution is then defined as $\frac{\text{mid-peak frequency}}{\text{peak width}}$

assembly were filled with solid sheet or mesh electrodes. In both cases, the ion collector was supported directly from the glass envelope of the tube. In the former case it was positioned between two guard rings and projected slightly into the interior of the box, while in the latter it projected into the box through a slot milled in one of the side electrodes.

The omegatron is pumped on an all-glass system by a mercury diffusion pump backed with an oil-filled rotary pump. Provision is made for baking the tube and the liquid air traps in separate ovens so that vigorous vacuum processing can be applied and the background pressure reduced to a low value.

If magnetic field non-uniformity is not to limit resolution, the maximum fractional departure of field strength from the average value must be small compared with the reciprocal of the highest required resolution. In the present case, a permanent magnet, weight about 30 lb, is used to give a field strength of 2·3 kG, while for more intense fields, this is replaced by an electromagnet with associated stabilized power pack. In both cases, shimming of the polepieces results in a magnetic field uniform to about two parts per thousand over the volume in which acceleration of ions takes place. The low current measuring unit is of vibrating reed type (see, for example, Kandiah and Brown[5]) and has a noise level less than 10^{-15} A. The radio-frequency voltage is obtained direct from a standard signal generator, and the omegatron power supplies from accumulators and high-tension batteries, though latterly a mains driven electron beam current stabilizer has come into operation.

CHARACTERISTICS

General. At 2·3 kG, the spectrum obtained by varying the frequency when the magnetic field is fixed depends markedly on operating conditions. In order to discuss these effects, four tube parameters and three peak characteristics may be distinguished. The four tube parameters are (*a*) strength of the varying electric field, (*b*) magnitude and shape of the trapping field, (*c*) magnitude of the electron beam current, and (*d*) pressure of the gas. The three peak characteristics are (*a*) the frequency corresponding to peak maximum, from which is inferred the e/m ratio of the resonating ion, (*b*) peak height which determines the sensitivity, and (*c*) peak width at half height which is a measure of the resolution. A study has here been made of the dependence of peak characteristics on tube parameters for the molecular ion of nitrogen taken as typical of those of interest in high vacuum investigations.

Trapping potential. Although the mean thermal energies of molecules at room temperature correspond to a few hundredths of an electron volt, it is found that trapping potentials of order 1 volt can be used with advantage to increase the peak height obtained under fixed conditions. One method of trapping is to maintain the two condenser plates at d.c. earth potential, while applying a positive bias to the remaining electrodes enclosing the ionizing region, and the characteristics given here apply to trapping of this type when guard rings are not used.

In Fig. 2(*a*), peak height pressure curves are drawn for three values of trapping bias; also, the frequency corresponding to peak maximum and the widths of the peaks at half height. An experimental value for resolution may then be defined as the ratio of resonant frequency to the width at half height. For the conditions quoted it is seen that a trapping bias of 0·6 V is to be preferred to 1·0 V and 0·3 V on the scores both of sensitivity and linearity of response.

Strength of alternating electric field. Theory predicts that a reduction of the alternating electric field strength will increase the resolution by decreasing the energy increment per cycle of the resonating particle. The increased time of flight would be expected to give larger ion losses and hence diminished peak height.

So far as resolution is concerned, experimental results fall in line with the predictions of theory. Fig. 2(*b*) shows, however, that with 0·1 μA of electron beam current, under the conditions quoted, a radio-frequency voltage of 0·8 V r.m.s. gives a greater sensitivity than either 0·6 V or 1·0 V. This figure also shows a departure from linearity at higher pressures, a feature which is always present, though the pressure at which it occurs depends on the value of the other parameters, particularly the electron beam current. With an

electron beam of 1 μA, and lower pressures, a radio-frequency voltage of 0·6 V r.m.s. was found to be the optimum and gave resonance at a frequency about 1½ kc/s lower than did 1·0 V r.m.s.

Effect of electron beam current. If the efficiency of ion collection is constant, the peak height will be proportional to the rate of ionization, that is to the product of gas pressure and electron beam current. Experimentally, this is found to be approximately true for low rates of ionization. Fig. 2(*c*) shows a plot of log peak height against log pressure for several values of electron beam current plotted for the pressure range before marked non-linearity sets in. The gradient of these curves is approximately unity, except for the 2·8 μA characteristic for which peak height is less than proportional to pressure. The separation of the curves shows that peak height, at fixed pressure, is approximately proportional to electron beam current.

At this magnetic field strength, electron beam current has a marked effect on both resonant frequency and peak width. A change from 2·8 to 0·1 μA produces a frequency shift of 11½% or more than 3 mass numbers in this region of the spectrum, while resolution for a beam of 2·8 μA is more than three times as great as for a beam of 0·3 μA.

Harmonic effects. "Mass harmonics" will be recorded as a result of two processes. The first is the acceleration of an ion by a harmonic in the output of the oscillator providing the alternating electric field. In a standard variable frequency signal generator, second harmonic distortion may be appreciable, and then, for example, mass 28 ions are recorded to a diminished extent, in the mass 56 position as well. Mass harmonic acceleration will also occur as a result of spatial non-uniformity of the alternating electric field. In the idealized cyclotron, the dee system gives a particular form of spatial non-uniformity, for which a given mass is accelerated by the fundamental frequency f and also by higher frequencies, $3f$, $5f$, etc. In the omegatron, similar effects can result from spatial non-uniformity of the field, the particular harmonics excited depending on the type of non-uniformity present.

Stability. Barnard[6] has described some experiments on the charging up of the surface of nominally conducting electrodes when subjected to bombardment by charged particles, and has shown that this effect is most pronounced for low-velocity particles at grazing incidence. The sensitivity of the omegatron is markedly dependent on the relative potentials of the six walls of the ionization chamber, and these are bombarded under just those conditions which lead to maximum charge build-up effects, so that constancy of characteristics is difficult to obtain. Surface smoothness and cleanliness of electrodes helps to minimize such effects and gold plating is of some value.

This difficulty is more serious in work on hydrocarbons than in many high-vacuum studies where approximate analyses are adequate, and gases present are few and simple. Morgan, Jernakoff and Lanneau,[2] who have worked extensively with hydrocarbons in an omegatron-type instrument, report good stability for the cracking pattern of normal butane.

Typical spectra. Fig. 3(*a*) represents the result of scanning the residual gases in a sealed-off ionization gauge which, after evacuation both on the plant and by electrical clean-up,

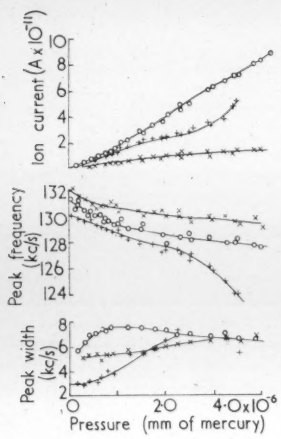

Fig. 2(*a*). Effect of trapping potential on omegatron characteristics

High-tension voltage = 72 V; H = 2·3 kG; electron beam current = 1 μA; radio frequency voltage = 0·6 V r.m.s.

○ Trapping potential 0·6 V.
+ Trapping potential 1·0 V.
× Trapping potential 0·3 V.

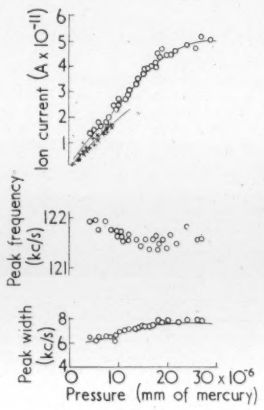

Fig. 2(*b*). Effect of alternating electric field strength on omegatron characteristics

High-tension voltage = 72 V; H = 2·3 kG; electron beam current = 0·1 μA; trapping potential = 0·75 V.

× Radio-frequency voltage 1·0 V r.m.s.
○ Radio-frequency voltage 0·8 V r.m.s.
+ Radio-frequency voltage 0·6 V r.m.s.

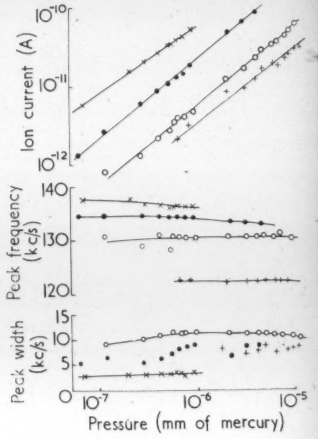

Fig. 2(*c*). Effect of electron beam current on omegatron characteristics

High-tension voltage = 72 V; H = 2·3 kG; radio-frequency voltage = 1·0 V r.m.s.; trapping potential = 0·75 V.

× Electron beam current 2·8 μA.
● Electron beam current 1·0 μA.
○ Electron beam current 0·3 μA.
+ Electron beam current 0·1 μA.

was left with the ionization gauge turned off for 5 weeks. Spot readings of the gross pressure before and after the experiment gave 3×10^{-7} (mm of mercury) nitrogen equivalent. The large mass 4 peak resulted from the penetration of the glass envelope by helium from the atmosphere, as discussed by Alpert and Buritz,[4] while the remaining peaks indicated the presence of carbon monoxide and probably nitrogen. The effect of running the ionization gauge for 3 days was to diminish the helium partial pressure both absolutely and also relative to the other components.

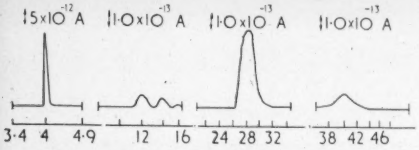

Fig. 3(*a*). Spectrum of residual gases in sealed-off ionization gauge

High-tension voltage = 72 V; H = 2·3 kG; beam = 2·8 μA; gross pressure = 3×10^{-7} mm of mercury; trapping potential 0·4 V on anode and secondary electron suppressor only (system 2).

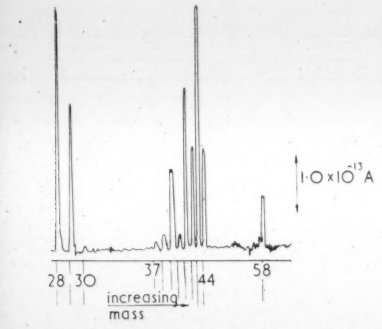

Fig. 3(*b*). Spectrum of impure form of butane

High-tension voltage = 72 V; beam current = 0·5 μA; d.c. potential on guard rings = 0·2 V; pressure = 1·4 × 10^{-6} mm of mercury; H = 3·8 kG.

Fig. 3(*b*) is the result of running an organic mixture consisting largely of normal butane. A guard-ring system was used to give a spatially uniform electric field, and the conditions adjusted to give good resolution rather than high sensitivity. The peaks round mass 43 were then completely resolved, but this was not true of the peaks near mass 58.

DISCUSSION

Trapping field. The initial requirement of the trapping field is that it should restrict the free movement of ions along the magnetic field, and thus minimize loss of resonating particles as a result of the z components of their initial velocities.

In Fig. 1, the radio-frequency voltage is applied between B and B', and the electron beam is normal to C and C'. If B and B' are maintained at d.c. earth potential, and the other four electrodes are raised to the same positive potential, it is found that there is an optimum value of this potential, usually less than 1 volt, to give maximum peak height. In Fig. 4(*a*), the lines of force are shown which minimize escape of positive ions in the z direction, and in Fig. 4(*b*) is shown the complementary set in a plane at right angles. The dotted

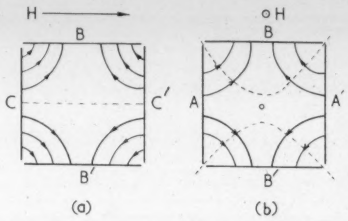

Fig. 4(*a*). Lines of force in a plane parallel to the electron beam

Fig. 4(*b*). Lines of force in a plane perpendicular to the electron beam

lines show the equipotentials along which charged particles can move in trochoidal paths at a net speed E/H. It is apparent qualitatively from these diagrams that a positive potential on C and C' will produce a trapping effect, while a potential on A and A' will increase an ion's ability to escape to the walls across the field.

If we compare operation when AA' is joined electrically to CC' (bias system 1) with that obtained when AA' is joined electrically to BB' (bias system 2), we observe that relative to system 1, system 2 frequently gives (*a*) an increase of that background component of ion current which is largely independent of the frequency of the radio-frequency voltage, (*b*) a general increase of peak height accompanied by peak splitting and the appearance of spurious broad peaks, and (*c*) the occurrence of appreciable peak heights at small radio-frequency voltages, though not with the full predicted increase in resolution. The overall spectrum complication is such that operation under these conditions is only advantageous if the maximum possible sensitivity is essential.

If the potential of A is mid-way between that of B and C, the sensitivity of system 2 can be combined in some measure with the spectrum purity associated with trapping system 1. The background current to the probe can also be reduced in other ways, for example by making large apertures in C and C', placing behind them additional negatively biased electrodes, through which small holes are drilled for passage of the electron beam.

An ideal trapping system is selective in that it operates exclusively on the resonating particles. A trapping field which is weakest on the central axis of the tube is selective in this sense to a certain extent, but it may prove possible to obtain better results with a time varying trapping field, and this is being investigated.

Potential depression in the electron beam. A calculation of the potential barrier which an ion generated in a 1 μA electron beam must overcome to escape to a distance of, say, $\frac{1}{2}$ mm from it, gives a value comparable with the thermal energy of the ion. This suggests the possibility that an appreciable proportion of the ions produced in the beam are unable to escape from it, since the frequency for resonant acceleration near the beam, where the space charge field is

high, is appreciably different from that elsewhere. Experimental evidence supporting this idea is as follows:

(1) a plot of background current to the collector against electron beam current gives an inverted parabolic-type curve;

(2) a plot of peak height against beam gives a similar type of curve, though the maximum occurs at much smaller beam currents. A particular example is shown in Fig. 5;

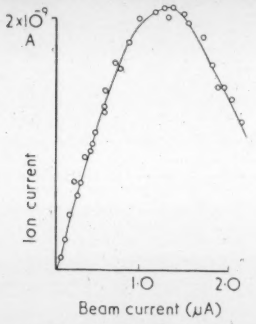

Fig. 5. Variation of peak height with beam current at fixed pressure

High-tension voltage = 72 V; H = 4·7 kG; pressure = $1{\cdot}2 \times 10^{-5}$ mm of mercury; radio-frequency voltage = 100 mV r.m.s.; trapping potential: CC' = 1·5 V; AA' = 0·3 V; $CO^+ = N_2^+$.

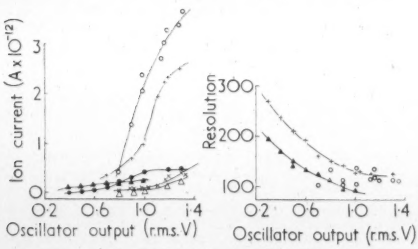

Fig. 6. Variation of peak height with alternating electric field strength at fixed pressure

High-tension voltage = 72 V; H = 3·2 kG; guard ring d.c. potential zero; resonant ion N_2^+.
Electron beam current:
× 3 μA
○ 1 μA
+ 0·3 μA
} Pressure = $2{\cdot}4 \times 10^{-6}$ mm of mercury.
△ 3 μA
● 1 μA
▲ 0·3 μA
} Pressure = $2{\cdot}4 \times 10^{-7}$ mm of mercury.

(3) plots of peak height against radio-frequency voltage for different beam currents (see Fig. 6) show that with a weak alternating electric field, a small beam gives a bigger peak height than a large one. The implication is that the radio-frequency field is instrumental in extracting ions from the beam, largely by a non-resonant process;

(4) the frequency at which maximum peak height is obtained is found experimentally to depend not only on trapping potential but also on beam, current, radio-frequency voltage and, to a small extent, on pressure.

Sommer, Thomas and Hipple pointed out that, in the presence of a weak radial electric field, the angular frequency at resonance ω is given by:

$$\omega = \omega_0 - E_r/Hr$$

where $\omega_0 = eH/M$, E_r = radial field at radius r. The radial electric field arises from both the trapping potential applied and the disposition of space charge, and it is through this latter term that radio-frequency voltage, beam and pressure are able to affect the frequency of resonance. An important contribution to this correction term comes from the negative charge in the electron beam, and since the resonant frequency of an ion varies with position unless E_r/r is constant, the electron beam current can also affect resolution.

If E_r is fixed, the correction term becomes relatively less important as the square of the magnetic field and the inverse of the mass number. Thus, the relative frequency shift of one part in 5000 per volt trapping potential reported by Sommer, Thomas and Hipple for mass 1 is equivalent to about 2% per volt for mass 28 at half the magnetic field, a value in reasonable agreement with that observed in the present case.

CONCLUSION

The electrical discharge taking place in the omegatron is similar to other types of discharge in magnetic fields in that the processes are difficult to understand and describe in detail. Provided, however, that operating conditions are kept within certain empirically established limits, the omegatron can readily be used as an ionization gauge able to measure partial pressures of the various components in a mixture of the lighter gases. For this work, it has the advantage that it can be degassed both by pre-processing and by baking on the plant.

With a relatively simple apparatus, the detection limit corresponds to a partial pressure of about 10^{-11} mm of mercury, and the resolution is adequate to separate adjoining masses up to the A^+ and CO_2^{++} region of the spectrum.

ACKNOWLEDGEMENTS

The author is indebted to Dr. G. Liebmann of this Laboratory for calculating the optimum shim dimensions for the magnet polepieces used and the uniformity of field they produce.

The author would also like to acknowledge the help he has received from discussions with Mr. M. E. Haine, and to thank Dr. T. E. Allibone, the Director of the Laboratory, for permission to publish this paper.

REFERENCES

(1) Sommer, H., Thomas, H. A., and Hipple, J. A. *Phys. Rev.*, **82**, p. 697 (1951).

(2) Morgan, W. A., Jernakoff, G., and Lanneau, K. P. American Chemical Society, Symposium on Process Instrumentation, Chicago, September 1953.

(3) Berry, C. E. *J. Appl. Phys.*, **25**, p. 28 (1954).

(4) Alpert, D., and Buritz, R. S. *J. Appl. Phys.*, **25**, p. 202 (1954).

(5) Kandiah, K., and Brown, D. E. *Proc. Instn Elect. Engrs*, **99**, II, p. 314 (1952).

(6) Barnard, G. P. *Modern Mass Spectrometry*, p. 67, 1st ed. (London: The Institute of Physics, 1953).

The physical and computing significance of an electrical analogue of creep and recovery

By A. J. KENNEDY, Ph.D., A.M.I.E.E., F.Inst.P.,* The Royal Institution, London, W.1

[*Paper first received* 30 *August, and in final form* 22 *October*, 1954]

The instrument described is basically a simple non-inductive transmission line, made up of identical sections, with the capacitance divided into recoverable and irrecoverable elements, in series, by the use of rectifiers. A voltage programme can be set up and applied automatically to simulate the stressing, and the charge taken by the network, with time, is integrated and recorded as the creep strain analogue. The simple power-type creep curve exhibited by solids (in particular the cubic type) is accurately reproduced. The time-functions which relate the character of the creep in metals with the times of stress and off-stress are very similar to those obtained with the analogue. Creep recovery, permanent flow and creep under changed stress (including reversed stress) can all be satisfactorily handled. The character of transient creep and recovery does not, therefore, demand special models involving arbitrary distributions of relaxation times. Problems must be set up on the machine using data obtained from short-term tests: calculations of prolonged intermittent creep can then be quickly completed. No account can at present be taken of temperature changes. On this basis, a comprehensive analogue creep computer, of a much higher operating speed, appears possible. This would be complex and expensive, but no more so than many analogue machines now in use for other purposes, and the cost and delay of extensive long-term testing would be much reduced.

Models which exhibit exponential characteristics have been widely used to express the stress and strain behaviour of solids. A variety of systems have been built up using Maxwell and Voigt elements with a view to simulating the response of biological fibres,[1] rubber[2] and a number of other solids.[3] The whole subject has been comprehensively reviewed by Zener.[4] The exact quantitative behaviour of any particular solid clearly depends upon the distribution function of the relaxation times, and considerable attention has been given to this aspect of the problem in recent years, leading to attempts to correlate such properties as creep, relaxation and internal friction.[5]

At the same time other work, notably that in the field of metal physics, has been concerned with the nature of certain discontinuous and largely irreversible processes, such as the motion of dislocations.[6] A considerable advance has been made in the last few years in interpreting a number of deformation phenomena in terms of the motion and interaction of such dislocations[7] yet we still have no certain theory for either creep or recovery. As far as creep is concerned, the question is why a law of the general form $\epsilon = \beta t^p$ should be exhibited, where β and p are constants (and p a fraction), and ϵ the creep strain at a time t after the application of the stress. In particular, why is p very near to the Andrade value $\frac{1}{3}$ over a large range of conditions for a variety of metallic and non-metallic materials?[8] One explanation of this fact, based on the behaviour of dislocations, has been put forward by Mott.[9]

Recently, a number of experiments on the creep and recovery behaviour of materials have revealed certain very significant features.[10, 11, 12] In general, these experiments demonstrate the great importance of the stress history on the creep response of metals: large errors can arise if attempts are made to compute the actual creep strain attained under discontinuous stress on the basis of the continuous stress characteristics. While the behaviour of a metal in a simple discontinuous test (such as one in which the stress is removed for one or two periods) is relatively easy to express analytically, the behaviour when the stress is varied irregularly over extended periods is far too complex to treat rigorously. Approximations have been made[10] to cover certain cases, such as those of regular stress pulses, but some means of quickly computing the more general (and possibly more practical) problem is clearly desirable.

For this reason, an electrical analogue computer has been developed which simulates the behaviour of metals under a variety of test conditions. Besides being a useful tool in creep design, the circuits necessary to reproduce the mechanical properties of solids themselves suggest how these phenomena may arise and interact. This paper describes the electrical functioning of the computer, compares its performance in detail with the behaviour of solids, and suggests how it may be developed to handle even more complex conditions.

THE BASIC ANALOGUE METHOD

The use of exponential functions in various combinations is a familiar computing technique.[24] The principle has been applied, for example, to computers used in the analysis of earthquake records,[13] to problems in heat transfer,[14] oil reservoir behaviour,[15] the performance of jet engines,[16] cable temperatures[17] and magnetic circuits.[18] Networks can readily be devised to reproduce a typical creep curve; although it is often asserted by those concerned with the subject that the creep curve cannot be made up out of exponential functions and must be considered as a true power law. There would be little point in developing some special complex network which, by judicious adjustment, happened to provide the type of curve characteristic of creep. The question is whether some simple, regular network can exhibit the required features. In fact, can the apparently arbitrary nature of the distribution function of relaxation times be eliminated, and the distribution follow as a natural consequence of the network itself, that is, of the way in which such elements are interconnected? The electrical analogy usually adopted is that of replacing strain by voltage, and stress by current, with the elastic and the viscous elements replaced by resistance and capacitance respectively.[19] In the machine to be described, the basic network is a non-inductive transmission line in which are included certain irreversible elements (rectifiers); this behaves analogously to a metal if the voltage applied and the total charge taken by the network are considered as the electrical analogies of stress and strain. Such a system is essentially a chain of equal repeated sections, but the effective relaxation times are

* Now at The British Iron and Steel Research Association, London, S.W.11.

not equal, and differ for charge and discharge conditions, depending upon the position of the element in the chain.

The elementary unmodified non-inductive transmission line is shown in the inset to Fig. 2, the voltage being applied at the input terminals on the left. This simple type of network can indeed reproduce a creep curve (charge against time) of the required form, and a variety of such curves is possible, depending on the relative capacitive and resistive values. In order to demonstrate this general qualitative similarity, curves obtained using the simple network are reproduced in Fig. 1

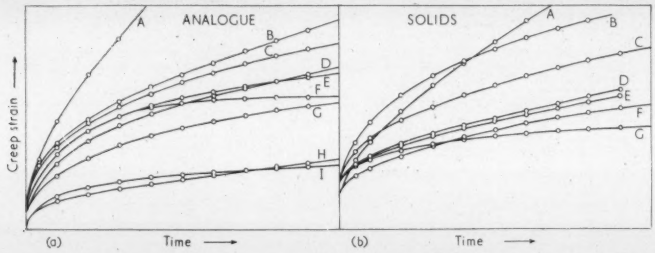

Fig. 1. Demonstrating the general qualitative similarity between (*a*) the charging behaviour of a simple *RC* transmission line and (*b*) the creep behaviour of a variety of solids. Details are given in the table, the creep results being taken from previously published curves[8]

together with some creep curves for various materials, taken from the literature. The time and strain scales are, of course, quite arbitrary. The analogue cannot, with its present type of output recorder, reproduce an instantaneous extension (this will be evident when the whole machine is described in detail), but the close correspondence between the charging properties of the network and the creep properties of solids appeared to justify an examination of the possibilities of this main principle.

Details of the curves drawn in Fig. 1

	(a)				(b)
Curve	*C*	*R*	R_T	R_P	
A	10 μF	2 MΩ	17 MΩ	finite	Aluminium
B	10 μF	2 MΩ	17 MΩ	∞	Mortar
C	10 μF	2 MΩ	27 MΩ	∞	Concrete
D	10 μF	2 MΩ	17 MΩ	∞	Steel
E	10 μF	2 MΩ	37 MΩ	∞	Lead
F	10 μF	2 MΩ		∞	Nylon
G	10 μF	4 MΩ	47 MΩ	∞	Rubber
H	*	220 kΩ	2·2 MΩ	∞	
I	10 μF	220 kΩ		∞	

[* *C*-values are non-uniform, being 10, 10, 8, 8, 2 and 2 μF reading from the input.]

The conditions which an analogue network has to fulfil are extremely rigorous, and the development of the device proceeded by successive trials and modifications until the following set of solid characteristics were all simulated by a single network (simulation of one only is quite simple).

(*a*) The form of the creep curve: that is strain = β(time)^p where β is a constant and p fractional (near to $\frac{1}{3}$).

(*b*) The form of the creep curve after a stress interruption.

(*c*) The dependence of the creep behaviour, after a stress interruption, on the prior creep time for a constant period of interruption (recovery).

(*d*) The dependence of the creep behaviour, after a stress interruption, on the duration of that interruption (recovery) for a constant prior creep time.

(*e*) The creep behaviour when stress is changed for a period during a constant stress test.

(*f*) The form of the creep recovery curve.

This search for the simplest possible network involved hundreds of tests before the final system was achieved. Many of these results are of considerable interest in a negative sense, in that they demonstrate very strikingly the falsity of certain types of network: this point will be taken up again in the subsequent discussion.

The analysis of the simple transmission line under steady-state conditions is straightforward, but the response to repeated transients is extremely complex. The value of the current flowing into the network at the instant t after the application of the voltage is

$$I = \frac{E}{mR} + \frac{E}{mR}\exp(-4t/RC) + \frac{2E}{mR}\sum_{s=1}^{m-1}\exp\left[-2t\left(1-\cos\frac{s\pi}{m}\right)\Big/RC\right] \quad (1)$$

where m is the number of sections in the network, and $s = 1, 2, 3 \ldots$ The solution of the general problem of repeated impulses, of various duration and spacing, for more complex networks containing non-linear elements, such as rectifiers, is an impossibly difficult task by analytical methods. This is particularly true if the influence of changing the values of components or the effect of non-uniformity of the sections, is to be investigated. It is significant that a similar difficulty was encountered in attempting to express the behaviour of solids under discontinuous conditions in an analytical form.[10]

The instrument developed, then, enables such an investigation of the influence of the test and circuit parameters to be reasonably undertaken.

THE DEVELOPMENT OF THE BASIC NETWORK ELEMENT

The general qualitative results of the type reproduced in Fig. 1 were, then, promising. In more detail, one such creep curve is reproduced in Fig. 2, with the same curve also plotted again (time)$^{\frac{1}{3}}$. The linearity of this relationship is striking. The creep curve of a solid, when plotted in this way, cuts the

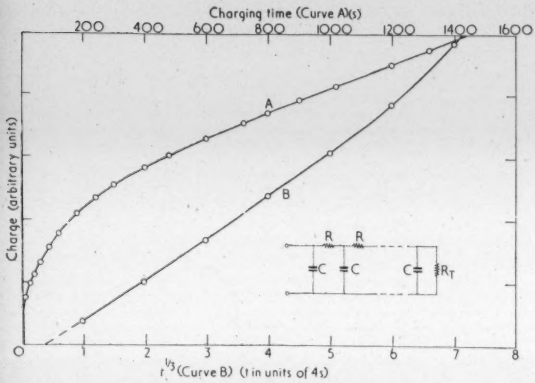

Fig. 2. Charging behaviour of simple *RC* transmission line

$C = 10\ \mu F$; $R = 2\ M\Omega$; $R_T = 17\ M\Omega$. Curve *B* is simply Curve *A* plotted against $(\text{time})^{1/3}$. The straight line section of Curve *B* has been extended by the dotted line: the curve itself must pass through the origin, of course

ordinate above zero, at a point taken to represent the instantaneous extension. It has already been noted that the method of recording the strain analogue cannot respond to instantaneous changes, because the speed of the output motor must be finite, and consequently the type of result shown in Fig. 2 is observed. It is an interesting fact that some workers, in attempting to fit a cubic equation to their results, have derived, in certain cases, an "initial specimen length" less than that measured. This could clearly arise if the instantaneous extension were insufficient to compensate for the effect shown in Fig. 2.

It would be tedious and pointless to enumerate all the stages in the development of the analogue circuits. The final network is substantially that shown in the inset to Fig. 4, to which is added some terminating resistance. Results on metals clearly demonstrate the operation of an irreversible element of some kind: complete recovery (softening) does not necessarily occur (even after an infinite time) if the temperature is not sufficiently high. It is essential, therefore, to introduce some form of irreversible element, and this has been achieved by the use of rectifiers. Before describing the analogue in more detail, it is worth while considering one essential property of any such system. This property may be termed "overtake" and in terms of the network it may be expressed as follows. It must be possible (if only just possible), by removing the applied voltage for a certain selected period (or periods), to obtain a greater total charge than that which would have been obtained by maintaining the same voltage constant for the same total test period. In

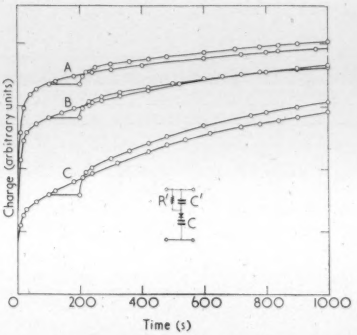

Fig. 3. The behaviour of single-element, open-ended networks of the type shown when the voltage is reduced to zero for 100 s during the test, compared with the behaviour under a continuous voltage. All exhibit the essential "overtake" characteristic

Curve	$C'(\mu F)$	$C(\mu F)$	$R'(M\Omega)$
A	18	10	100
B	10	10	100
C	2	10	100

Fig. 4. The behaviour of a six-element, open-ended network ($R_T = \infty$) under continuous voltage Curve *A*, and interrupted for 25 s every 50 s Curve *B*. A continuous curve has been drawn through the Curve *B* points for simplicity, although in detail the curve is obviously a series of small steps. This network is the essential transient element in the full analogue machine, and clearly exhibits the characteristic of overtake

$R' = 100\ M\Omega$; $R = 2\ M\Omega$; $C' = 2\ \mu F$; $C = 10\ \mu F$

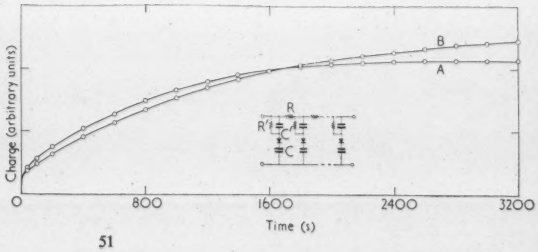

the solid case, experiments have demonstrated[10, 11] that a greater creep strain may be achieved in some chosen time by actually removing the stress at intervals rather than leaving it imposed the whole time.

It is necessary, then, that this property should be exhibited and in Fig. 3 the overtake is shown occurring, in a single-section network, for three different sets of component values. The ordinate scale is the same for all three tests. Overtake clearly occurs after only one interruption in a network such as this (the curves are not, of course, cubic). The point is further demonstrated by Fig. 4, which shows the result of interrupting the voltage for 25 s in a 50 s cycle, the network being of six sections and open-ended. At any selected time on the axis, then, the network under curve *B* conditions has been subjected to voltage for only one-half the scale time, and yet, eventually, it overtakes curve *A*.

Another important feature of the transmission line type of network is that a permanent flow component arises naturally by virtue of the direct current path through the terminating resistance.

In the next section the full machine is described and the results of experiments with this type of basic circuit presented.

THE ANALOGUE MACHINE

The full circuit diagram of the apparatus is given in Fig. 5. The original six-section non-inductive transmission line contains variable resistance and capacitance (R_1, R_2,... and C_1, C_2,...) with jacks included in the sections enabling additional components to be plugged in, or section current to be read and integrated. The modifications required to reproduce the network drawn in Fig. 4 are shown at the top of the diagram. Each plug, P_1 to P_6, is connected in to the corresponding jack, J_1 to J_6. A number of shorting switches have been omitted for simplicity: these are used to examine the influence of short-circuiting the rectifiers, and to discharge

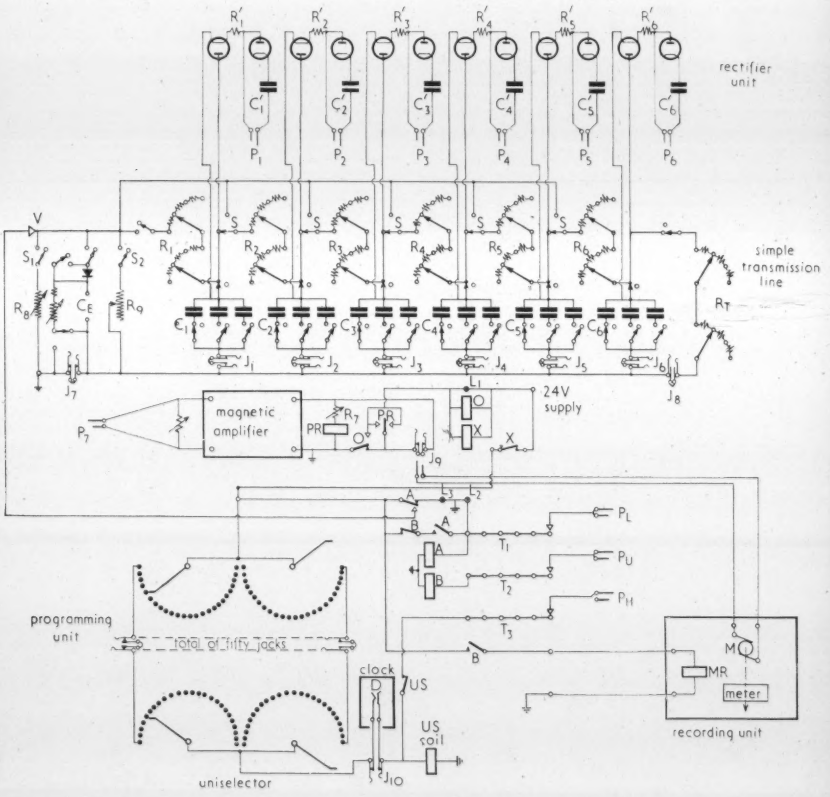

Fig. 5. Circuit diagram of the analogue

the condensers rapidly after a test. Other switches S enable the sections to be connected in parallel, rather than in series, if desired, and rectifiers can also be connected in series with the R' resistors.

The d.c. voltage (24 V) is applied at V. In the tests reported in this paper, the total current flowing into the network has been integrated by plugging P_7 into J_7. This current is amplified by a magnetic amplifier and the output voltage applied to an integrating motor M which drives a five-digit counter through continuous gearing. A protection circuit is interposed between the output and the motor, the value of the cut-out voltage (irrespective of sign) being set by R_7. If the relay PR operates, the fault lamp L_1 is illuminated, and voltage is taken off the motor, the transmission line and the programming unit. The circuits remain held open through the hold contact of relay O until manually released.

At the input end of the transmission line a number of additional special facilities are incorporated. Creep recovery (that is, creep in a reverse direction on stress removal) can be simulated by closing S_1. A discharge path through R_8 now exists if the section rectifiers are short-circuited. The switch S_2 and the variable resistance R_9 constitute the permanent flow component control: a constant current through R_9 is simply integrated and added to the transient component. It should be remembered that the main network itself also has a permanent component. There is provision at C_E for the connexion of an external condenser, as required, for simulating instantaneous extension. This possibility has not been examined here, because of the unsuitability of the recording device. The switches associated with condenser C_E control the circuits through which condenser C_E may discharge during the recovery periods, and whether or not these instantaneous changes appear in creep recovery.

The programming, or control, unit enables the loading (voltage) programme to be set up in a relatively simple manner. It operates in the following way. A uniselector is driven by clock pulses at half-second intervals, derived from D, or from any external pulse source plugged in to J_{10}. Four banks of the uniselector are used, the wiper arms being so cut and connected that four banks of twenty-five contacts each are effectively converted into two banks of fifty contacts each. These two effective banks are wired as shown to fifty jacks; only the first and last jacks are shown wired in Fig. 5, the rest being omitted for simplicity. The centre spring contacts of all the jacks are short-circuited, so that if a jack is unplugged, the uniselector coil US has a through contact to the 24 V supply when the clock contact closes. It therefore simply pulses the uniselector wipers on to the next set of tags. If it is required to apply voltage at any particular jack or jacks (that is, "load"), then a plug (or plugs) connected as shown by P_L to a row of commoned terminals T_1 is plugged in at the relevant jack. When the wiper arms reach the tags connected to this jack, the relay A operates and holds, the "load" lamp L_2 is illuminated and voltage is applied to the network. The uniselector continues stepping until the wipers encounter tags connected through the jack to a plug of the P_U type. When this occurs, relay B operates, relay A is released, power is transferred from the load lamp L_2 to the unload lamp L_3, and voltage is cut off from the network. This process occurs repeatedly, as desired, with the limitation that after fifty steps the whole sequence is repeated. To increase the facilities offered by the programmer, a further set of commoned terminals, and their associated plugs, enable the recycling period to be reduced. As an example, suppose the loading cycle required is one of six intervals (say three on and three off). Eight such cycles can be fitted into the fifty positions, with two positions spare. If these two positions are connected to T_3 through P_H type plugs, then the uniselector will drive itself over these positions through its own break contact US, the clock path being broken. These positions, then, are effectively discarded. The number of cycles of loading is recorded by the message register MR.

To sum up, the instrument integrates the charge flowing into a transmission line type of network when this network is subjected to a voltage interrupted automatically according to some chosen programme. The charge is recorded on motor-driven dials, the loading cycles by a counter, and the time by a stopwatch.

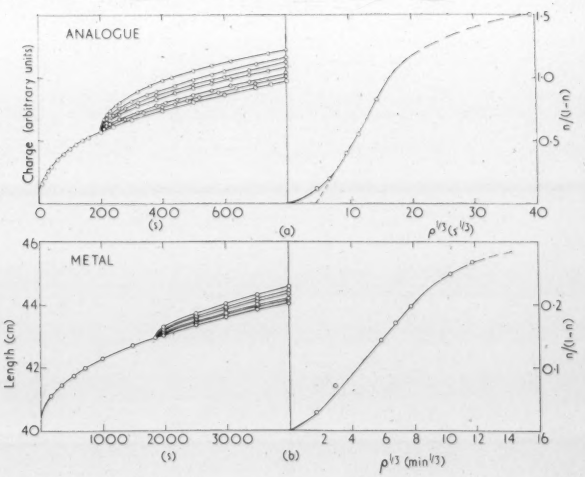

Fig. 6. (*a*) The behaviour of the analogue when interrupted for different times (ρ) after a pre-creep of 200 s. The ρ-values are: 60 420, 3000, 1500, 900, 300 and 100 s

(*b*) The behaviour of lead under similar conditions taken from published work[10]

THE BEHAVIOUR OF THE MACHINE COMPARED WITH THE BEHAVIOUR OF METALS

(*a*) *Single interruption.* The behaviour of the machine when subjected to a single interruption is represented by the results given in Figs. 6 and 7. There are two general cases. In the first, the time of recovery ρ is varied for a constant previous creep time τ: in the second, τ is varied for a constant ρ-value. It has already been demonstrated for metals[10] that the form of the creep curve on reloading is fairly accurately represented by assuming that a fraction n of the material has recovered in full its transient creep properties. The remainder of the material is assumed to behave as if unloading had not occurred. The quantity n thus provides an index of the extent of the recovery, taking values between zero and unity. Figs. 6 and 7 demonstrate the general similarity of behaviour not only of the form of the curves on reloading, but also the form of the n–τ and n–ρ relationships. It has been possible to show, for metals, that the quantities n, τ and ρ for an isothermal test are related by the expression

$$(1 - n)/n = A(\tau/\rho)^{\frac{1}{3}} \qquad (2)$$

if the continuous stress creep curve is of cubic form. A is a constant descriptive of the recovery properties of the material: for a number of metals, at temperatures about half the melting point absolute, the value of A is approximately 10. The quantity $n/(1 - n)$ should therefore be linear with $\rho^{\frac{1}{3}}$ over the range of ρ-values for which equation (2) applies. In Fig. 6(*b*) the results of tests on lead[10] are shown, and a reasonable initial linearity is observed up to a value for $\rho^{\frac{1}{3}}$ of about 10, above which the curve flattens—that is, recovery is less than that predicted by the relationship. This has been commented upon in the original publication.[10] The analogue provides the results shown in Fig. 6(*a*), a region of good linearity is exhibited, but there is a curvature near the origin, as well as the flattening out at higher $\rho^{\frac{1}{3}}$-values. The general form of these $n/(1 - n)$ against $\rho^{\frac{1}{3}}$ curves is, however, very similar. The value of A deduced from the initial slope of the curve is 10, while for the middle linear region A falls to 4. The results in Fig. 6(*b*) for lead at room temperature give $A = 16$.

In Fig. 7 the behaviour for a constant ρ and variable τ are compared. If equation (2) is valid, n^{-1} should be linear with $\tau^{\frac{1}{3}}$: there is excellent agreement in this, and the A-values deduced from the slopes of the straight lines in the inset graphs are in reasonable agreement with those deduced from Fig. 6. The line drawn in Fig. 7(*a*) gives $A = 12$, while for the metal the slope gives $A = 18$.

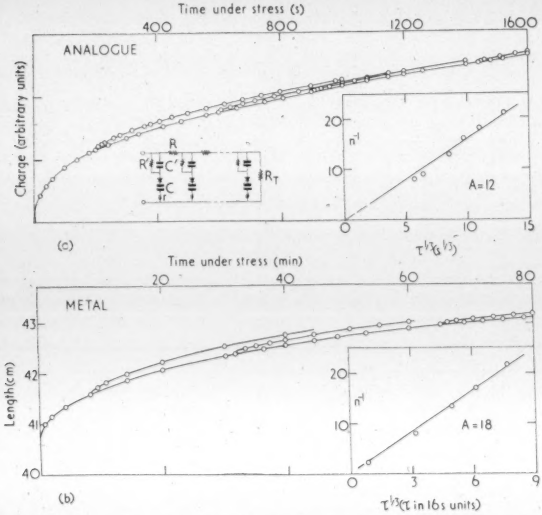

Fig. 7. (*a*) The behaviour of the electrical network when the voltage is removed for a fixed period (ρ) of 300 s at different points on the curve (different τ-values). In the inset the straight line through the origin (as drawn) gives $A = 12$. The best straight line through the points gives $A = 15$

(*b*) The behaviour of lead when subjected to similar interrupted creep tests at 30° C, taken from previously published work.[10] The value of ρ in these experiments is 53 min. The character of the dependence of the quantity n^{-1} is strikingly similar in the two cases

The analogue network, then, behaves in a very similar way to a metal. It must be emphasized that the actual rate of recovery (as represented, say, by the A-value) can be varied by means of the R' resistors. A difference between the analogue and the metal, as far as the exact A-values are concerned, is not important here, although the actual value obtained should be consistent in all the tests. (It must be remembered that in principle A can assume any value between zero and infinity, so that the numerical agreement is, in fact, very reasonable.) It may be added here that any type of network which recovers by sharing charge between its sections (a network, say, with no rectifiers in at all) would lead to quite the wrong kind of curve on reloading. It is essential that all recovery processes should occur solely within the individual sections.

(*b*) *Waveform effect under repeated pulsing.* It has been shown by work on lead[10] and copper[11] that if a material is subjected to square-wave stress pulses repeatedly then the creep strain achieved after some chosen time depends upon the waveform of these pulses: that is, it depends on the values of τ and ρ, in a series of tests where $\tau + \rho = \lambda$, the wavelength of the cycle. The full analysis, which was in any case necessarily approximate for these repeated pulsing problems,

need not be reproduced here. The type of result obtained with metals is demonstrated in Fig. 8(*b*), which is taken from experiments on copper.[11] In the inset, the creep strain achieved at the end of the intermittent creep test is plotted against r, the ratio τ/λ. (Thus the point $r = 1$ represents the continuous stressing case.) These points lie close to the

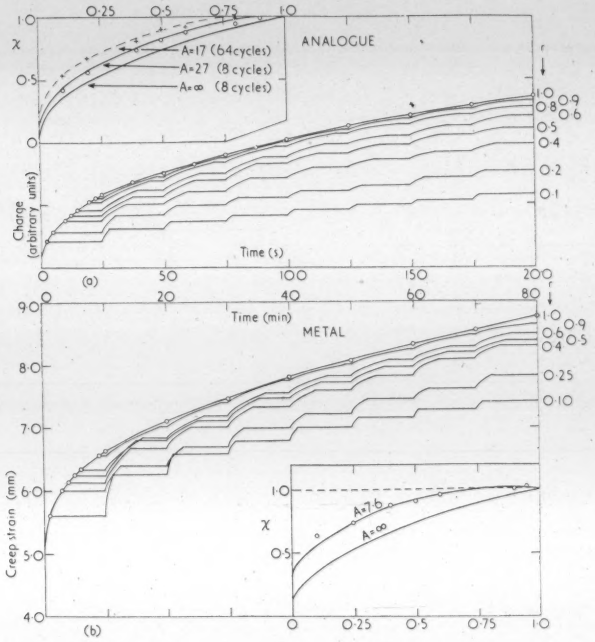

Fig. 8. The waveform effect in (*a*) the analogue and (*b*) copper. In the insets, the creep strain reached at the end of the test is plotted (circles) against r, the ratio $\tau/(\tau + \rho)$, and the continuous curves are calculated for the A-values shown. In the inset to (*a*), the crosses indicate the results after extending the test to 64 cycles, compared with the calculated, dashed, curve for $A = 17$

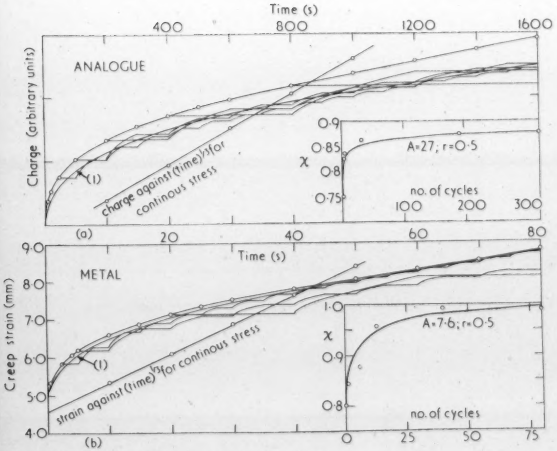

Fig. 9. The frequency effect in (*a*) the analogue, (*b*) copper, for the case $r = 0{\cdot}5$. The curve marked (1) in (*a*) is for a loading cycle of 5 s (2·5 s on, 2·5 s off), and that marked (1) in (*b*) is for a loading cycle of 1 min (30 s on, 30 s off). Both these curves are, of course, stepped, but for simplicity they have been drawn as continuous

theoretical curve drawn for the case $A = 7{\cdot}6$. The curve for the case $A = \infty$ is also drawn for comparison: this is the result which would be obtained if no recovery occurred during the off-stress periods. Fig. 8(*a*) demonstrates the behaviour of the analogue; the points plotted in the inset, for eight cycles, lie close to the curve for $A = 27$. After sixty-four such cycles, the points plotted as crosses were obtained, and these lie near to the curve (shown dashed) for $A = 17$.

(*c*) *Frequency effect under repeated pulsing.* Previous analysis on metals has led to the conclusion that if the waveform is kept constant, then the creep achieved, after some selected time, is independent of frequency provided a sufficient number of cycles is taken, and provided the value of ρ is not so large that it lies in the upper curved region of the characteristics drawn in Fig. 6. Again, the analysis will not be reproduced here. The results for copper are shown in Fig. 9(*b*), with the calculated and experimental points in the inset. Fig. 9(*a*) shows the behaviour of the analogue, with the points lying close to the calculated curve for the case $A = 27$. For copper, the curve $A = 7{\cdot}6$ (the same value as that derived from the Fig. 8 results) is in good agreement with the observations.

(*d*) *Change of stress during a creep test.* In metals, the variation of the constant β in the transient creep equation noted above, namely $\epsilon = \beta t^{\frac{1}{3}}$, is not linear with stress, but varies in a sigmoid manner, with a critical stress below which β is negligible.[20] Clearly the present analogue will give a response which is linearly related to voltage, that is, β is linear with the stress σ. It would be possible to devise a limiter-type network which would reproduce the form of the β–σ relationship, and some such development must be the next step in this type of analogue. However, considering a small region of stress-variation where β and σ are reasonably linear in their relation, what sort of qualitative comparison is possible? The results of such tests are shown in Fig. 10. Both analogue and metal show the same type of behaviour, but in the case of the metal the response is altogether more critical with stress. This is to be expected from the differences noted in the β–σ relations. However, the flattening in the inset curves in the region near $\sigma = \sigma_0$ is reasonably distinctive, and it is easy to see how Fig. 10(*a*) will approach more nearly to Fig. 10(*b*) as the σ-scale is compressed. In particular, there is an exact reproduction of the observation that if the stress on a metal is reduced slightly (but sufficiently) creep ceases for some incubation period until the internal stress relaxes enough and creep recommences.[12] This can be shown up much more distinctively than has been done in Fig. 10.

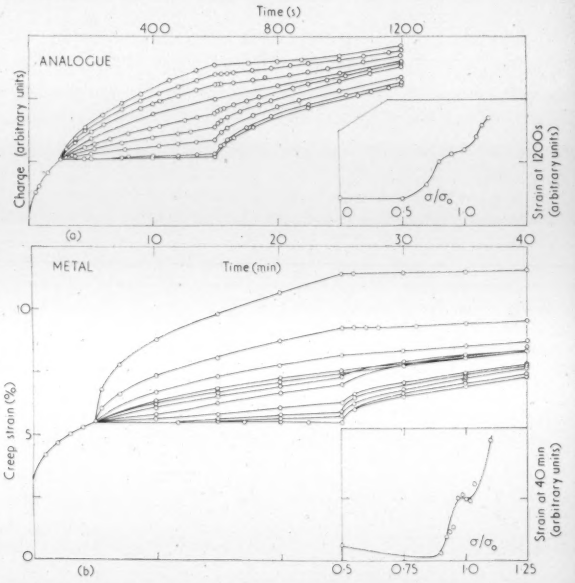

Fig. 10. The behaviour of (*a*) the analogue and (*b*) lead, when the creep stress is changed for some period during an otherwise constant stress (σ_0) creep test. In the insets, the strain achieved after some period of subsequent creep is plotted against σ/σ_0, where σ is the intermediate stage stress. Each of the curves branching from the common initial curve represents a different value of σ

(*e*) *Creep recovery and creep under reversed stress.* The amount of creep recovery in the analogue depends upon two main factors: the value of R_8 (in Fig. 5) and the extent to which the charge entering the network is rendered irreversible by rectifiers. If all the rectifiers of Fig. 5 are in circuit, there will be no creep recovery at all. For the purposes of comparison with published data, a fully reversible network has been used, and this may very well correspond with the micro-creep conditions under comparison. Fig. 11 shows creep and creep recovery in cadmium,[21] where the maximum strain reached is only 0·02%, compared with the analogue behaviour. In the analogue results, the instantaneous extension and instantaneous recovery have been added arbitrarily merely to aid comparison. A number of experiments have been made with the analogue on the dependence

of this creep recovery behaviour upon the test conditions, such as pre-creep time. These results cannot be detailed here, but they fit in with Henderson's treatment of the problem, from whose publication[21] the cadmium results are taken.

Creep under reversed stressing has received little physical attention, partly because of experimental difficulty in cases other than those of shear stressing. Again, the behaviour of the analogue depends upon the extent to which rectification is introduced into the network. Some results for varying degrees of reversibility are reproduced in Fig. 12(*a*), and they may be compared with published curves for lead and cadmium.[22] It should be noted that the analogue in these cases had no added permanent flow component. Such a component, on the analogue model, would appear equally in the reversed creep, and would lead to a much more linear creep behaviour, more like that exhibited by the curve *D*. Another difference between Figs. 12(*a*) and (*b*) is that in Fig. 12(*b*) the stress is reversed until zero strain is achieved, when it is reversed again, whereas in Fig. 12(*a*) the stress is reversed in regular cycles. With some degree of reversibility, intermediate between that of curves *A* and *B*, it is easy to see how a curve similar to type *C* could arise. As this reversed stressing type of experiment is a special case of the general class of changed stress experiments, it appears pointless to develop these arguments until the β-against-σ behaviour of the analogue is developed to be comparable with that of metals. This point has already been noted under item (*d*) above.

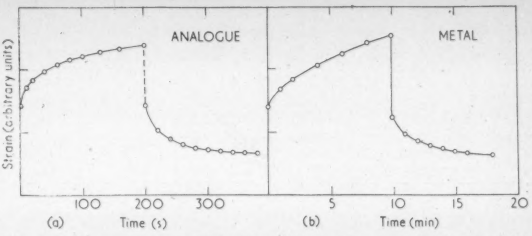

Fig. 11. Creep recovery exhibited by (*a*) the analogue and (*b*) cadmium.[21] The maximum strain in (*b*) is less than 2×10^{-4}

Qualitatively the curves are in excellent agreement, but the middle linear region provides too high a recovery rate ($A \simeq 4$). This may be a genuine analogy with solid behaviour which requires further investigation, or it may arise (for instance) from the failure of the analogue to reproduce instantaneous extensions with consequent errors in the derivation of n.

This type of network also necessarily gives rise to a permanent creep component. It is significant that even where apparently perfect simple cubic creep curves are exhibited (as in 0·05% tellurium lead at room temperature), the creep rate does not fall off continuously. A permanent component of some form can always be detected if the experiment is extended sufficiently. The temperature dependence of these two components constitutes an important clue to any further developments in machines of this type. The present system, then, could compute fairly successfully the constant temperature creep behaviour of a metal over some complex history of stress and recovery (the recovery being under zero stress). All that is required is the constant A for the metal and the power of time in the transient creep equation. The form of the creep curve is set by varying R and R_T, and A is set by varying C' and R'. The best way of setting up such problems still requires further research. The machine cannot at present take account of (*a*) the effect of recovery on tertiary creep—this is probably insignificant, just as it is with permanent creep, or (*b*) temperature changes or (*c*) generalized stress changes. What has been developed, however, is an essential basis for any such machine, and it probably embodies the most difficult analogue problems. The solution of the problem of generalized stress changes appears reasonably possible at this stage; the question of temperature changes is certainly much more difficult. Some preliminary experiments suggest that temperature change might be considered as

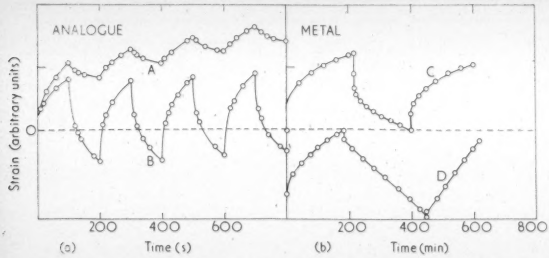

Fig. 12. Creep under stress reversals in (*a*) the analogue and (*b*) metals.[22] In (*a*), Curve *B* is for the completely reversible network, and Curve *A* for the partially reversible network. In (*b*), Curve *C* shows the behaviour of cadmium under shear, and Curve *D* the behaviour of lead under similar conditions: in both cases there is no strain reversal, the stress being restored to a forward direction when the net strain reaches zero. This is in contrast with (*a*), where the stress is reversed in regular cycles

THE LIMITATIONS AND POSSIBLE DEVELOPMENTS OF THE MACHINE

The analogue has been shown to reproduce a number of features of transient creep and recovery in solids. It has been suggested previously that the creep behaviour of metals under discontinuous stress conditions may be expressed in terms of a particular index (the constant A), and this is largely substantiated by the analogue. The values of A obtained for the same network, from different experiments, were: 10, 12, 27, 27 and 17. Considering that A may in principle have any value from zero to infinity, and remembering that certain approximations are involved, this is a good consistency. For lead at room temperature, $A \simeq 16$, and for copper at 260° C $A \simeq 8$, so that the order of this constant is certainly correct. The greatest anomaly lies in the behaviour reproduced in Fig. 6(*a*), in contrast with that of Fig. 6(*b*).

altering the ratio between the two capacitances C (recoverable) and C' (irrecoverable) together with a uniform change in all the resistors. This is purely conjectural. The general deduction to be drawn from these results is that a comprehensive computer, capable of calculating the creep response of solids under complex discontinuous conditions is within the range of possibility. The present pilot system has used fairly long time constants of the order of hundreds of seconds, with corresponding recording and switching devices. Once the validity of the method is established for more general conditions, there is no reason why the speed of operation should not be increased by a factor of a thousand or more using wholly electronic control. Creep over a period of years, which can already be reduced to a scale of hours, may then be reproduced in a few seconds. The full machine will be complex and fairly expensive, but may in the long run be more economical than the execution of prolonged creep tests, under a variety of complex user conditions. In any case, such a machine would be no more complex than other analogues, such as power-line computers,[23] now in commercial use. Short term tests will, of course, always be necessary in order to derive the data for setting up the metal on the machine. It is certain that this setting up will be impossible in any other way, although with increased knowledge the amount of preliminary testing required may be made quite small.

CONCLUSIONS

The creep and recovery behaviour of solids can be adequately reproduced by relaxation-type networks, containing rectifiers, connected as a transmission line. As far as the empirical measurements are concerned, these processes can arise from elements which have basically exponential characteristics, and it is unnecessary to invoke special models to simulate the observations. The analogue is quantitatively accurate enough to enable computations of creep under discontinuous stress to be made, and could in principle be developed to handle more general stress and temperature conditions, and to operate more accurately at much higher speeds. This development would, however, be complex and expensive.

The use of long-term data in making analogue comparisons would have improved the force of the arguments developed above, but unfortunately the type of data required (waveform and frequency effects) is not available. Very little work has been done over long times, although what does exist confirms the main features of the behaviour. It is hoped that such data will be forthcoming eventually, and it will be of the utmost importance to see if it fits in with the present work.

ACKNOWLEDGEMENTS

The machine has been developed during the tenure of the Fellowship awarded by The Royal Society and The Armourers and Braziers' Company: to both these bodies I extend my warm thanks. I should also like to thank The Royal Institution for the facilities accorded to me in The Davy Faraday Laboratory. In particular, it gives me pleasure to acknowledge the skilful assistance of Mr. J. R. Johnson of this Laboratory who has been personally responsible for much of the construction.

REFERENCES

(1) JORDAN, H. J. *First Report on Viscosity and Plasticity*, p. 215 (Amsterdam: N. V. Noord-Hollandsche Uitgevers Maatschappij, 1939).
LEVIN, A., and WYMANN, J. *Proc. Roy. Soc. B*, **101**, p. 218 (1927).
WINTON, F. R. *J. Physiol.*, **69**, p. 693 (1930).
GASSER, H. S., and HILL, A. V. *Proc. Roy. Soc. B*, **96**, p. 398 (1924).
(2) KUHN, W., KÜNZLE, O., and PREISSMANN, A. *Helv. Chim. Acta*, **30**, p. 307 (1947).
KUHN, W., KÜNZLE, O., and PREISSMANN, A. *Helv. Chim. Acta*, **30**, p. 464 (1947).
(3) POOLE, H. J. *Trans Faraday Soc.*, **21**, p. 114 (1925).
SHORTER, S. A. *J. Textile Inst.*, **15**, p. 215 (1924).
TROUTON, F. T., and RANKINE, A. O. *Phil. Mag.*, **8**, p. 555 (1904).
(4) ZENER, C. *Elasticity and Anelasticity of Metals* (Chicago: University of Chicago Press, 1948).
(5) GROSS, B. *J. Appl. Phys.*, **18**, p. 212 (1947).
KÊ, T.-S. *Phys. Rev.*, **71**, p. 533 (1947).
RANDALL, R. H., ROSE, F. C., and ZENER, C. *Phys. Rev.*, **56**, p. 343 (1939).
(6) NABARRO, F. R. N. *Advances in Phys.*, **1**, p. 271 (1952).
READ, W. T. *Dislocations in Crystals* (London: McGraw-Hill Publishing Co. Ltd., 1953).
COTTRELL, A. H. *Dislocations and Plastic Flow in Crystals* (London: Oxford University Press, 1953).
(7) COTTRELL, A. H. *Report of a Conference on the Strength of Solids*, p. 30 (London: Physical Society, 1948).
MOTT, N. F., and NABARRO, F. R. N. *Report of a Conference on the Strength of Solids* (London: Physical Society, 1948).
MOTT, N. F. *Phil. Mag.*, **43**, p. 1151 (1952).
SEITZ, F. *Advances in Phys.*, **1**, p. 43 (1952).
(8) KENNEDY, A. J. *J. Mech. Phys. Solids*, **1**, p. 172 (1953).
(9) MOTT, N. F. *Phil. Mag.*, **44**, p. 742 (1953).
(10) KENNEDY, A. J. *Proc. Roy. Soc. A*, **213**, p. 492 (1952).
(11) KENNEDY, A. J. *Nature* [*London*], **171**, p. 927 (1953).
KENNEDY, A. J. *International Congress on Rheology, Oxford* (London: Butterworths Scientific Publications, 1954).
(12) KENNEDY, A. J. *Brit. J. Appl. Phys.*, **4**, p. 225 (1953).
(13) HOUSNER, G. W., and MCCANN, G. D. *Bull. Seismol. Soc. Amer.*, **34**, p. 47 (1949).
(14) PASCHKIS, V., and BAKER, H. D. *Trans Amer. Soc. Mech. Engrs*, **64**, p. 105 (1942).
PASCHKIS, V. *Trans Amer. Inst. Elect. Engrs*, Pt I, **68**, p. 70 (1949).
MALAVARD, L., and MIROUX, J. *Proceedings of the Fourth International Congress on Industrial Heating*, Paper No. 82 (Paris: 1952).
(15) BRUCE, W. A. *Trans Amer. Inst. Min. Metall. Engrs*, **151**, p. 112 (1943).
(16) See, for instance, *Electronics*, **20**, p. 188 (1947).
(17) NEHER, J. H. *Elect. Engng*, **70**, p. 870 (1951).
(18) KOENIG, E. C. *Electronics*, **23**, p. 124 (1950).
(19) BURGERS, J. M. *First Report on Viscosity and Plasticity*, p. 5 (Amsterdam: N. V. Noord-Hollandsche Uitgevers Maatschappij, 1939).
(20) ANDRADE, E. N. DA C. *Proc. Roy. Soc. A*, **84**, p. 1 (1910).
ANDRADE, E. N. DA C. *Proc. Roy. Soc. A*, **90**, p. 329 (1914).
ANDRADE, E. N. DA C., and KENNEDY, A. J. *Proc. Phys. Soc.* [*London*] *B*, **64**, p. 363 (1951).
(21) HENDERSON, C. *Proc. Roy. Soc. A*, **206**, p. 72 (1951).
(22) ANDRADE, E. N. DA C., and JOLLIFFE, K. H. *Proc. Roy. Soc. A*, **213**, p. 3 (1952).
(23) LYON, G. *Proc. Instn Elect. Engrs*, **97**, Pt II, p. 697 (1950).
(24) LIEBMANN, G. *Brit. J. Appl. Phys.*, **4**, p. 193 (1953).

The field due to an infinite dielectric cylinder between two parallel conducting planes

By C. Mack, M.A., The British Cotton Industry Research Association, Shirley Institute, Manchester

[*Paper received* 31 *May*, 1954]

This paper shows that, whatever the distance of the cylinder from the planes, this field can be calculated by first solving an infinite set of linear equations with comparatively simple coefficients. By neglecting all except the first few unknowns, a good approximation to the correct solution is obtained. The simplest approximation is sufficient for most practical purposes, and it is shown that the increase in capacity between the planes due to the presence of the cylinder is nearly proportional to the cylinder radius squared times a simple function of its dielectric constant, provided that this radius is small compared with the distance between the planes.

1. Introduction

The change in capacity resulting from the insertion of a cylindrical thread of textile material between the plates of a condenser is already used to measure departure from uniformity in the thread[1] and such methods may be applicable in wider fields.

It is the purpose of this paper to solve the theoretical problem which enables such changes in capacity to be evaluated. The problem is idealized to that given in the title which is a reasonable approximation to the cases which are likely to arise in practice. No account is taken here of the fact that the plates of a condenser are not infinite and that there may be variations in diameter of that portion of the material between the plates at any one time. Another source of error may arise when applying results of a purely electrostatic theory to changes in capacity which, owing to their small magnitude, are measured by high frequency techniques (e.g. at 500 kc/s).

Bearing these limitations in mind, it can be seen from the results of this paper that, if the cylinder radius b is sufficiently small compared with other dimensions of the condenser, the change in capacity can be made proportional to $(K-1)b^2/(K+1)$ where K is the cylinder dielectric constant; and hence, if, say, K is constant, changes in b^2 can be measured quantitatively. (The case of a conducting cylinder is dealt with by making $K=\infty$.)

Besides this special case, the general method described here enables the field to be calculated at any point between the planes whatever the position, radius and dielectric constant of the cylinder. Previously the author has dealt with the particular case when the cylinder is midway between the planes,[2,3] but by combining results from the theory of meromorphic functions (Titchmarsh,[4] p. 110) with the method of circular harmonics (Smythe,[5] p. 62) the slowly-convergent series arising from a direct application of the author's previous method, can be summed. Thus an infinite set of linear equations for the coefficients of the circular harmonics is simply obtained. If b is small we can solve these approximately and thus obtain the formulae of Section 2. For a more accurate solution we neglect all harmonic coefficients above, say, the Nth and solve the resulting N simultaneous linear equations. Numerical tests show that as N increases the method appears always to converge. This method is described in detail in Section 3.

The mathematical proofs of all the formulae, etc., used are collected together in Section 4, thus enabling the important results to be given without their becoming involved with the detailed mathematical reasoning.

2. Approximate formula

Fig. 1 shows a cross-section of the cylinder and the planes. P_0 is the centre of the cylinder and is at a distance T from the plane LM, the two planes being a distance D apart. We assume that, before the cylinder is inserted there is a field of strength E between the planes, which are therefore at a potential difference ED, and we further assume that this potential difference is kept constant when the cylinder is inserted, thus causing the induced charge on the planes to increase.

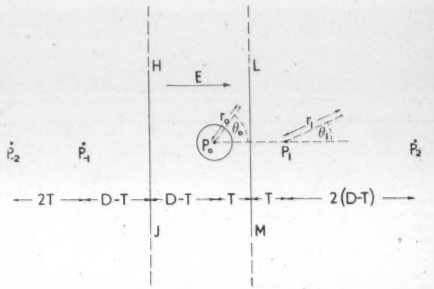

Fig. 1.

We shall write $(K-1)/(K+1) \equiv k$ and $z \equiv r_0 \exp(i\theta_0)$ where r_0 and θ_0 are polar co-ordinates measured from P_0 as shown in Fig. 1. Now the potential between the planes before the insertion of the cylinder is

$$\mathscr{R}(Ez) \tag{1}$$

where $\mathscr{R}$ means "real part of". After the insertion and provided b is small compared with T and $D-T$, the potential becomes, to a good approximation [see Section 4, Part (i)]

$$\mathscr{R}\left\{Ez + \frac{\pi A_1}{2D}\left[\cot\left(\frac{\pi z}{2D}\right) + \cot\left(\frac{\pi(z-2T)}{2D}\right)\right]\right\} \tag{2}$$

where

$$A_1 = -kEb^2/\left\{1 - k[\pi b/(2D)]^2[\operatorname{cosec}^2(\pi T/D) + \tfrac{1}{3}] + 0(b^6)\right\}$$

The charge on the planes due to the field (2) is of considerable interest. Now, as shown by Smythe[5] (p. 73), the charge on, say, LM, is $1/(4\pi)$ times the change in the imaginary part of the expression in square brackets in (2) in going from L to M. (The change in the imaginary part of Ez gives the charge on LM due to the original field, the change in the remainder of (2) gives the charge induced by the insertion of the cylinder.)

The following result will facilitate calculation of this induced charge:

$$\cot(X+iY) \equiv (\sin 2X - i\sinh 2Y)/(\cosh 2Y - \cos 2X) \quad (3)$$

Dividing the induced extra charge by ED (the potential difference between the planes) gives the resulting increase in capacity. It is to be noted, however, that, if the cylinder is not midway between the planes, corresponding lengths of the planes will have different induced charges. This difference is small, however, if these lengths are of the order of D and project appreciably on either side of the cylinder and the mean induced charge may safely be used in calculating capacity. These conditions will also ensure that these charges are not affected to the first order of approximation by small changes in T.

Hence, provided $k[\pi b/(2D)]^2[\mathrm{cosec}^2(\pi T/D) + \frac{1}{3}]$ is small compared with unity, A_1 is proportional to kb^2 and since the induced charge is proportional to A_1 the change in capacity will then be proportional to kb^2. This fact enables changes in b^2 to be detected and to be measured quantitatively.

To complete this section we give a good approximate formula for the case in which b is comparable with T. Formula (2) still holds but with A_1, this time [see Section 4, Part (ii)] given by

$$A_1 = -kEb^2\beta/[1 - \pi^2kb^2\beta/(6D^2) + 0(b^2T^2/D^4)] \quad (5)$$

where $$\beta = 1 + kb^2/(2T)^2 + k^2b^4/[(2T)^2 - b^2]^2 + \ldots \quad (6)$$

The general term of equation (6) is given in Section 4, Part (ii). It may appear at first sight that A_1 departs significantly from proportionality to b^2. If, however, $b = T$ (as would be the case were the cylinder to touch the plane LM in Fig. 1), then

$$\beta = 1 + k/(2)^2 + k^2/(3)^2 + \ldots \quad (7)$$

In this case β is independent of b and, provided b/D is small enough, A_1 is proportional to kb^2. Since the coefficient of b^2 in the denominator of equation (5) is somewhat smaller than the corresponding coefficient in expression (2), since $\beta < 2$ and $\mathrm{cosec}\,(\pi T/D) \geqslant 1$, this position of the cylinder may be considered slightly more favourable than the midway position ($T = D/2$), as A_1 is then more nearly proportional to kb^2.

3. THE GENERAL SOLUTION

It is proved in Section 4, Part (i) that, writing $\pi z/(2D) \equiv Z$ and $\pi T/D \equiv Z_0$, the potential V_0 outside the cylinder is of the form

$$\begin{aligned} V_0 = \mathscr{R}\{ & Ez + (\tfrac{1}{2}\pi/D)A_1[\cot Z + \cot(Z - Z_0)] \\ & + (\tfrac{1}{2}\pi/D)^2A_2[\mathrm{cot}_1 Z - \mathrm{cot}_1(Z - Z_0)] \\ & + (\tfrac{1}{2}\pi/D)^3A_3[\mathrm{cot}_2(Z) + \mathrm{cot}_2(Z - Z_0)] \\ & + (\tfrac{1}{2}\pi/D)^4A_4[\mathrm{cot}_3 Z - \mathrm{cot}_3(Z - Z_0)] + \ldots\} \end{aligned} \quad (8)$$

where $\mathrm{cot}_m(Z) \equiv [(-1)^m/(m!)]d^m \cot Z/dZ^m$.

The values of the A_i may be calculated from the infinite set of simultaneous equations

$$\begin{aligned} & A_1/(kb^2) + E = A_1(C_2 + U_2) + 2A_2C_3 + 3A_3(C_4 + U_4) \\ & \quad + 4A_4C_5 + \ldots \\ & 2!A_2/(kb^4) = 1.2\,A_1C_3 + 2.3\,A_2(C_4 - U_4) \\ & \quad + 3.4\,A_3C_5 + 4.5\,A_4(C_6 - U_6) + \ldots \\ & 3!A_3/(kb^6) = 1.2.3\,A_1(C_4 + U_4) + 2.3\,A_2C_5 \\ & \quad + 3.4.5\,A_3(C_6 + U_6) + \ldots \\ & 4!\,A_4/(kb^8) = 1.2.3.4.\,A_1C_5 + 2.3.4.5.\,A_2(C_6 - U_6) + \ldots, \text{ etc.} \end{aligned}$$

where $U_q = [2/(2D)^q][\sum_1^\infty 1/r^q]$, $C_q = [\frac{1}{2}\pi/D]^q \cot_{q-1}(\pi T/D)$ (9)

Tables of $\Sigma 1/r^q$ are available[6-8], while the following results enable C_q to be found easily:

Writing $S = \sin Z$, $C = \cos Z$,

$$\begin{aligned} & \cot_1 = 1/S^2,\ \cot_2 = C/S^2,\ \cot_3 = 1/S^4 - 2/(3S^2), \\ & \cot_4 = C[1/S^5 - 1/(3S^3)], \\ & \cot_5 = 1/S^6 - 1/S^4 + 2/(15S^2), \\ & \cot_6 = C[1/S^7 - 2/(3S^5) + 2/(45S^3)], \\ & \cot_7 = 1/S^8 - 4/(3S^6) + 2/(5S^4) - 4/(315S^2) \end{aligned} \quad (10)$$

The charge on a length of the plane is again (Smythe,[5] p. 73) $1/(4\pi)$ times the change in the imaginary part of equation (8). In calculating this change the following results will be found to be useful:

$$\begin{aligned} & \cot_1(X + iY) = 2[1 - \cos 2X\cosh 2Y \\ & \quad - i\sin 2X\sinh 2Y]/(\cosh 2Y - \cos 2X)^2, \\ & (\cosh 2Y - \cos 2X)^3\cot_2(X + iY) \\ & \quad = (\sin 2X)[3 - 2\cos 2X\cosh 2Y - \cosh 4Y] \\ & \quad + i(\sinh 2Y)[2\cos 2X\cosh 2Y + \cos 4X - 3] \end{aligned} \quad (11)$$

If we solve for the A_i by expansions in powers of b we obtain

$$\begin{aligned} & A_1 = -kb^2E/[1 - kb^2(C_2 + U_2) - 2k^2b^6C_3^2 + \ldots], \\ & A_2 = kb^4A_1C_3/[1 - 3kb^4(C_4 - U_4) + \ldots], \text{ etc.} \end{aligned} \quad (12)$$

Neglecting terms of the order b^6 we obtain the first approximation (2), A_2, A_3, etc., being negligible.

Alternatively we may neglect A_i for $i > N$ and thus reduce expression (9) to a finite set of linear equations. This method has been tested numerically to see if it converged as N increased. As the following table (in which the cases are all stringent) shows, convergence is marked, except perhaps in the last case, but this is approaching the limiting case $b/T = 1$, $T/D = 0{\cdot}5$ and $K = \infty$ when there is no solution as it corresponds to a conducting cylinder touching *both* planes.

Table of approximations to $-A_1/(Eb^2)$

b/T	T/D	K	$N=1$	$N=2$	$N=3$	$N=4$	Value given by expression (12)	True value given by expression (5)
1	$\to 0$	∞	1·333	1·405	1·456	1·487	1·465	1·645
1	$\to 0$	4	0·706	0·717	0·722	—	0·719	0·728
1	0·25	∞	1·562	1·656	1·710	1·743	1·674	—
1	0·5	7/3	0·298	0·303	0·304	—	0·302	—
1	0·5	9	1·169	1·356	1·419	—	1·304	—

4. MATHEMATICAL PROOFS

(i) *Proof of the general method.*

We assume that, arising at each of the P_n (the image points of P_0 obtained by repeated reflexion in the planes LM, HJ, as shown in Fig. 1), is a potential of the form

$$v_n = \frac{A_1 \cos\theta_n}{r_n} \pm \frac{A_2 \cos 2\theta_n}{r_n^2} + \frac{A_3 \cos 3\theta_n}{r_n^3} \pm \frac{A_4 \cos 4\theta_n}{r_n^4} + \dots \tag{13}$$

where r_n, θ_n are polar co-ordinates measured from P_n. The A_i are *independent* of n and when n is odd the alternate signs in expression (13) are negative, but all are positive when n is even. Now on LM, v_0 and v_1 cancel since $r_0 = r_1$, but $\theta_0 = \pi - \theta_1$. Similarly v_{-1} and v_2, v_{-2} and v_3, etc., cancel on LM; while, on HJ, v_0 and v_{-1}, v_1 and v_{-2}, etc., cancel. Now $z_1 = z_0 - 2T$, $z_{-1} = z_0 + 2D - 2T$, $z_2 = z_0 - 2D$, $z_{-2} = z_0 + 2D$, etc. So, since $(\cos m\theta_n)/r_n^m = \mathscr{R}(1/z_n^m)$, and

$$\begin{aligned}\sum_{n=-\infty}^{\infty} v_n = \mathscr{R}\Bigg[&\frac{A_1}{z_0} + \frac{A_2}{z_0^2} + \frac{A_3}{z_0^3} + \dots + \frac{A_1}{z_0 - 2T} \\ &- \frac{A_2}{(z_0 - 2T)^2} + \dots + \frac{A_1}{z_0 + 2D - 2T} \\ &- \frac{A_2}{(z_0 + 2D - 2T)^2} + \dots\Bigg] \\ = \mathscr{R}&\left(\frac{A_1}{z_0} + \frac{A_2}{z_0^2} + \dots + F_0 + F_1 z_0 + F_2 z_0^2 + \dots\right), \text{(say)} \\ = F,& \text{ (say)} \end{aligned} \tag{14}$$

Now since

$$G^m/(z+G)^m = 1 - mz/G + m(m+1)z^2/(2!\,G^2) - \dots$$

provided $|z| < G$, (and hence in our case, if $|z_0| < 2T$ we can use this formula) we find that

$$\begin{aligned} -F_1 &= A_1(C_2 + U_2) + 2A_2C_3 + \dots, \\ -2!F_2 &= 1.2\,A_1C_3 + \dots, \\ -3!F_3 &= 1.2.3\,A_1(C_4 + U_4) + \dots, \text{ etc.} \end{aligned} \tag{15}$$

where the right hand sides are identical in form with those of expression (9), though as far as we have gone at the moment all we know is that

$$\begin{aligned} U_q &\equiv 2/(2D)^q + 2/(4D)^q + 2/(6D)^q + \dots, \\ C_q &\equiv 1/(2T)^q + 1/(2T-2D)^q + 1/(2T+2D)^q \\ &\quad + 1/(2T-4D)^q + 1/(2T+4D)^q + 1/(2T-6D)^q + \dots \end{aligned}$$

The formula given for U_q in expression (9) may be deduced immediately. Now Titchmarsh[4] (p. 113) shows that

$$\lim_{N\to\infty} \sum_{n=-N}^{N} \frac{1}{Z - \pi n} = \cot Z$$

hence, differentiating m times with respect to Z

$$\sum_{n=-\infty}^{\infty} \frac{1}{(Z-n)^{m+1}} = \frac{(-1)^m}{m!}\frac{d^m \cot Z}{dZ^m} \equiv \cot_m(Z)$$

and the formula for C_q in expression (9) can now be deduced.

The potential V_1 external to the cylinder is simply

$$V_1 = Er_0 \cos\theta_0 + F \tag{16}$$

and suppose the internal potential V_0 given by a series

$$V_0 = B_0 + B_1 r_0 \cos\theta_0 + B_2 r_0^2 \cos 2\theta_0 + \dots \tag{17}$$

No negative powers of r_0 appear since V_0 is finite when $r_0 = 0$.

We now consider conditions on the boundary of the cylinder ($r_0 = b$). These boundary conditions (Smythe,[5] p. 65) are

$$V_0 = V_1 \text{ and } K\frac{\partial V_0}{\partial r_0} = \frac{\partial V_1}{\partial r_0}$$

Substituting from equations (14), (16) and (17) and equating coefficients of $r_0^m \cos m\theta$ we find that

$$\begin{aligned} (K-1)(F_1 + E)b^2 + (K+1)A_1 &= 0, \\ (K-1)F_m b^{2m} + (K+1)A_m &= 0, \\ (K-1)B_m &= -2A_m/b^{2m}. \end{aligned}$$

Substitution for the F_i in equation (15) completes the proof of expression (9). Again, the functions $\cot_m(Z)$ sum the series appearing in equation (14) very nicely, and thus prove equation (8).

(ii) *Case when the cylinder is close to a plane.*

We shall assume that b is of the order of T and both are small compared with D. If the cylinder were in the field E alone a two dimensional dipole of strength μ would be induced at P_0 where

$$\mu = \tfrac{1}{2}kEb^2$$

and this would give the correct field external to the cylinder. The presence of the plane LM means that an image dipole μ will appear at P_1 (see Fig. 2) to ensure that the potential on

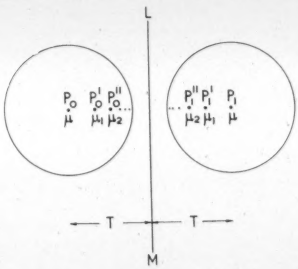

Fig. 2.

LM is unaltered. To restore conditions on the cylinder boundary a dipole μ_1 at P_0' is required where

$$\text{where} \qquad \mu_1 = k\mu b^2/(2T)^2 \text{ and } P_0P_0' = b^2/(2T)$$

This may be deduced from the results given by Smythe[5] (p. 68). Now, to restore the potential on LM an image dipole μ_1 at P_1' is required, and, hence a further dipole μ_2 at P_0'' where

$$\mu_2 = k\mu_1 b^2/[2T - b^2/(2T)]^2, \quad P_0P_0'' = b^2[2T - b^2/(2T)]$$

Hence we get a series of dipoles μ_n with their images, where

$$\mu_n = k^n b^{2m}/(w_n)^2 \text{ and}$$

$$w_n = \left\{[T + (T^2 - b^2)^{\frac{1}{2}}]^{n+1} - [T - (T^2 - b^2)^{\frac{1}{2}}]^{n+1}\right\}/[2(T^2 - b^2)^{\frac{1}{2}}]$$

If we allow for the fact that the field E should be modified to include the effect of images in the other plane HJ we arrive at the result (5). The fact that the dipoles are not all centred on P_0 or P_1 will not seriously affect our result as it is assumed that b is much smaller than T, D or the length LM, HJ.

REFERENCES

(1) BOYD, G. N. *J. Text. Inst. Manchr.* (*Trans*), **40**, p. 407 (1949).
(2) MACK, C. *Phil. Mag.*, (7), **42**, p. 428 (1951).
(3) MACK, C. *Shirley Institute Memoirs*, **25**, p. 191 (1951).
(4) TITCHMARSH, E. C. *Theory of Functions*, 2nd edition (London: Oxford University Press, 1939).
(5) SMYTHE, W. R. *Static and Dynamic Electricity* (New York: McGraw-Hill Book Co. Inc., 1939).
(6) DALE, J. B. *Five-Figure Tables of Mathematical Functions*, p. 92 (London: Edward Arnold and Co., 1943).
(7) DAVIS, H. T. *Tables of Higher Mathematical Functions*, Vol. II, p. 243 (Indiana, U.S.A.: Principia Press, 1935).
(8) BROMWICH, T. J. I'A. *Introduction to the Theory of Infinite Series*, 2nd edition, pp. 297, 298 (London: Macmillan and Co. Ltd., 1942).

Growth of the barium orthosilicate interface of oxide-coated cathodes

By M. G. HARWOOD, B.Sc., A.Inst.P., and NORA FRY, B.Sc. Ph.D., Philips Electrical Ltd., Mitcham Junction, Surrey

[*Paper received* 30 *June*, 1954]

The core-coating interface of oxide cathodes with nickel alloy cores containing 0·048 and 0·17% silicon has been examined. In addition to barium orthosilicate a layer of nearly pure strontium oxide was found. The growth of the barium orthosilicate layer with time of heating the cathodes was examined. In the case of the first alloy, growth continued until all the available silicon was used, but this was not so for the alloy of higher silicon content, where other factors, possibly diffusion of silicon through barium orthosilicate, appeared to limit the growth.

The existence of a grey layer between the silicon-nickel alloy core (2 or 5% silicon) and the alkaline earth oxide coating of oxide cathodes was demonstrated by Fineman and Eisenstein,[1] and the layer was identified as barium orthosilicate by Rooksby[2] working with an 0·4% silicon-nickel alloy core. These alloys have a higher silicon content than those normally used for commercial cathodes, but since Rooksby's identification, the presence of barium orthosilicate at the core-coating interface of cathodes with nickel cores containing 0·05% silicon has been reported by Wright,[3] quoting unpublished work by Rooksby, and on cathodes with 0·1% silicon-nickel cores by Waymouth,[4] and by Eisenstein.[5] When barium oxide is a constituent of the alkaline earth oxide coating only barium orthosilicate has been reported as the interface compound, but Eisenstein,[5] working with a pure strontium oxide coating, has found strontium orthosilicate.

It is now widely assumed, and has been amply confirmed in this Laboratory, that the barium orthosilicate interface appears on most commercial cathodes unless special silicon-free core materials are used. Little, however, is known regarding its growth during the life of the cathode. Eisenstein[5–7] found that with a 5 or 4% silicon-nickel alloy the interface thickness grew to 2×10^{-3} cm in 100 h at 1125 or 1150° K, whereas with an 0·1% silicon-nickel core, it was approximately 10^{-4} cm after 5000 h at normal temperature. For 0·10% magnesium, 0·05% silicon–nickel Wright[3] has quoted the thickness of an interface including barium orthosilicate and magnesium oxide as 10^{-4} cm, and for 0·4% silicon–nickel the interface thickness as 10^{-3} cm, but the heating period and conditions were not specified.

In this paper results are presented on the growth of the barium orthosilicate interface with cathode life on two cathode nickel core materials of different silicon content, similar to two commercial cathode nickel alloys.

PREPARATION AND OPERATION OF TEST VALVES

The two nickel core materials used in this investigation gave the following analyses:

	Alloying constituent (weight) %							
Type	*Co*	*Fe*	*Si*	*Mg*	*Mn*	*Al*	*Cu*	*Zn*
I	0·21	0·083	0·048	0·22	0·053	0·008	0·014	0·005
II	0·64	0·098	0·17	0·011	0·013	0·009	0·005	0·005

The materials were received in the shape of cathodes 1·1 mm diameter, and coated with barium strontium carbonate (approximate molecular composition 50 barium: 50 strontium) to a length of 2 cm. The coated cathodes were mounted in diodes which were continuously pumped to a pressure of approximately 10^{-4} mm of mercury. After baking for 1 h at 380° C, the cathode coating was decomposed at a brightness temperature of 1080° C for 1 min, and after degassing the nickel anode and guard rings, firing the barium getter, and sealing the valve, the cathodes were activated at 950° C for 30 min and further at 845° C for 30 min. An emission current of approximately 15 mA/cm² was drawn during activation. Temperatures were measured with an optical pyrometer focused near the centre of the cathode.

Of the valves thus prepared a small number were immediately opened and the interface layer examined. The others were operated for varying periods at normal filament voltages (6·3 V) corresponding to a brightness temperature of 765° C, drawing anode current of approximately 15 mA/cm².

MEASUREMENT OF INTERFACE THICKNESS

Before measuring the interface thickness, the barium strontium oxide coating was dissolved away in dry ethyl alcohol. This method is slow, but the barium orthosilicate is not attacked. Only a thin oxide film remained attached to the coating after the treatment and was examined with the orthosilicate layer.

Comparative thickness measurements were made by the following X-ray diffraction technique. The specimen was mounted in a Debye–Scherrer camera and irradiated with Kα radiation from a copper target filtered through 19 μ nickel. The diffraction patterns given by the barium orthosilicate, the thin superposed carbonate film (formed by exposure of the oxide to air), and the nickel core were recorded, generally photographically on Ilford Industrial G film and in a few cases with a Geiger–Müller counter. The intensities of the (112) plane of the barium orthosilicate, giving the strongest reflexions, and of the (111) plane of nickel were compared; these are only a small Bragg angle apart. On account of the very low intensities of the barium orthosilicate lines, it was necessary to use para-focusing conditions.[8] The

cathodes were therefore flattened to provide a smooth surface; this incidentally cold-worked the nickel sufficiently to render continuous the reflexions which were otherwise spotty. The flat sample was oscillated in the centre of the camera so that the angle subtended between the face and the beam varied between 9° and 19°. On account of the high intensity differences between the reflexions from the (112) barium orthosilicate and (111) nickel planes (ratios as low as 1 : 2000 occurred), the latter were selectively filtered so that an intensity ratio near unity was obtained. The exposure was controlled to give a density of about unity, thus employing the most sensitive part of the characteristic curve of the film. Density comparisons were made by eye. The results obtained by this method did not differ by more than 10% from those obtained with a Geiger–Müller counter.

To calibrate the intensity ratios thus obtained in terms of mass of barium orthosilicate per unit area, bare nickel strips were weighed on a chemical micro-balance, coated with artificially prepared barium orthosilicate, reweighed, and the X-ray diffraction patterns recorded.

The barium orthosilicate was prepared by mixing barium carbonate and silica in the ratio 2 : 1, pressing the mixture into a pellet, and firing this in a continuously pumped vacuum system until the pressure fell to 10^{-4} mm of mercury. After this treatment no unreacted components could be detected by X-ray diffraction.

To calculate the layer thickness from the mass of barium orthosilicate per unit area, a visual estimation of the packing density had to be made. The X-ray density of barium orthosilicate, according to O'Daniel and Tscheischwili[9] is 5·42 g/cm³. Since the layer appeared densely packed, a value of 5 was assumed for its density. The results reported later are given both as mass per unit area and as layer thickness of barium orthosilicate. Optical microscopic methods of arriving at the thickness directly were considered but discarded, since they would only have been applicable to the thicker coatings and the labour involved in averaging over a reasonable area was considered too large.

The reproducibility of individual thickness results was $\pm 0{\cdot}1\ \mu$, but since a number of readings were taken on each cathode, the error in the mean result should be considerably less than this. All measurements were made in a region not more than 0·5 cm from the centre of the cathode where temperature variations during heating did not exceed 10° C and no variation in thickness from place to place was found.

EXPERIMENTAL RESULTS

The only interface compound, containing constituents of the core, observed on any of the cathodes examined was barium orthosilicate. In addition to the barium orthosilicate, however, a layer of barium strontium carbonate was sometimes observed containing a considerably smaller proportion of barium than the bulk of the coating. It was not possible to determine the relative positions of the barium orthosilicate and strontium-rich layers with certainty, i.e. whether they were intermixed or parallel, but there is evidence which points to the fact that the carbonate layer was superposed on the orthosilicate.

The growth of the barium orthosilicate interface thickness with time of heating the cathodes is shown in the figure. Each point is an average of between two and five results at the same period; in particular, the points at 2000 hours are averages of three values in close agreement. With Type 1 nickel no interface was observed immediately after activating the cathode, but with Type 2 nickel which contained more than three times as much silicon, a thin layer of barium orthosilicate could be detected even at this early stage. The maximum layer thickness to be expected on the basis of the silicon content, weight and dimensions of the core was $0{\cdot}5\ \mu$ for Type 1 and $1{\cdot}7\ \mu$ for Type 2. This thickness is reached with Type 1 nickel after about 1000 h when no further

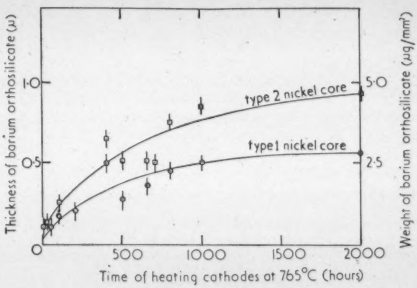

Variation of thickness of barium orthosilicate interface with time of heating at 765° C

(Accuracy of measurement indicated by length of lines.)

growth occurs (the value $0{\cdot}55\ \mu$ for 2000 h is within experimental error of the theoretical value $0{\cdot}5\ \mu$). With Type 2 nickel, the interface has reached only about one-half its maximum possible thickness after 2000 h, but the rate of growth at this stage is low, and one may assume that the maximum possible interface thickness would not normally be reached within the useful life of the cathode.

A subsidiary experiment to determine the variation with temperature of the extent of interface formation showed that with Type 2 nickel core cathodes heated for 330 h to brightness temperatures of 830, 775 or 720° C the barium orthosilicate thicknesses were in the ratio of 2·5 : 1·1 : 0·6. Although temperature variations along that part of the cathode where thickness measurements were made did not exceed 10° on one cathode, the high sensitivity to temperature may in part explain the comparatively large scatter of the results.

DISCUSSION AND CONCLUSIONS

The results reported above deal with the chemical nature and thickness of the interface formed between two types of nickel alloy core and the barium strontium oxide coating of oxide cathodes. No attempt has been made to relate these results to the electrical characteristics of the interface. Though the electrical properties are the result of chemical composition, the relation is complicated by the fact that we are dealing with semiconductors whose electrical properties are largely determined by the deviations from stoichiometric composition and by impurities incorporated in them. Thus Eisenstein[6] has found widely differing electrical properties with barium orthosilicate interfaces of similar thickness, and the experience in this Laboratory has been similar.

The presence of strontium-rich oxide next to the interface does not appear to have been reported previously. This must be taken into account when considering the physical properties of the interface; for the electrical properties, in particular, of

strontium oxide can differ appreciably from those of approximately equimolar barium strontium oxide.

The order of magnitude of the interface thickness obtained is in agreement with Eisenstein's results. For accurate comparison of the results of different authors it would be necessary to know not only the percentage of silicon in the nickel, but also the mass of silicon available per unit area of core surface, since at least in some cases it appears that growth proceeds until all the silicon is used. The general shape of the curve with Type 2 nickel is compatible with limitation of growth by diffusion of silicon in barium orthosilicate, but other explanations cannot be excluded on the basis of these experiments alone. When the barium orthosilicate interface has reached its maximum thickness, silicon is no longer available for activating the alkaline earth oxide coating. Other reducing elements in the core metal may still be available for this purpose; and if they cannot directly reach the alkaline earth oxide coating they may produce free barium in the interface which, in turn, may diffuse or distil into the coating and activate it.

ACKNOWLEDGEMENTS

We wish to thank Mr. J. A. M. van Moll and the Directors of Philips Electrical Ltd., for permission to publish this paper.

REFERENCES

(1) FINEMAN, A., and EISENSTEIN, A. *J. Appl. Phys.*, **17**, p. 663 (1946).
(2) ROOKSBY, H. P. *Nature* [*London*], **159**, p. 609 (1947).
(3) WRIGHT, D. A. *Proc. Phys. Soc.* [*London*] *B*, **62**, p. 188 (1949).
(4) WAYMOUTH, J. F. *J. Appl. Phys.*, **22**, p. 80 (1951).
(5) EISENSTEIN, A. *J. Appl. Phys.*, **22**, p. 138 (1951).
(6) EISENSTEIN, A. *J. Appl. Phys.*, **20**, p. 776 (1949).
(7) EISENSTEIN, A. *Advances in Electronics*, Vol. I, 1st Ed., p. 27 (New York: Academic Press Inc., 1948).
(8) BRENTANO, G. *Proc. Phys. Soc.* [*London*], **47**, p. 932 (1935).
(9) O'DANIEL, H., and TSCHEISCHWILI, L. *Z. Krist.*, **104**, p. 351 (1942).

Phase and amplitude balance methods for permittivity measurements between 4 and 50 cm

By T. J. BUCHANAN, M.A., Ph.D., A.Inst.P., and E. H. GRANT, B.Sc., Department of Physics Applied to Medicine, The Middlesex Hospital Medical School, London, W.1

[*Paper first received* 2 *September, and in final form* 12 *October*, 1954]

Coaxial-line equipment has been constructed to measure a wide range of permittivities of liquids in the wavelength range 4 to 50 cm. Several alternative ways of using the apparatus are given, and two types of liquid cell are described. The apparatus has been used mainly for medium-loss but also for high-loss liquids. For very low-loss liquids the accuracy is low and cavity methods are essential.

1. GENERAL DESCRIPTION OF APPARATUS AND METHODS

The apparatus is arranged in bridge form (Fig. 1), one arm containing the cell, the phase changer, mixer 1 and valve V_1, the other arm containing the cut-off attenuator, mixer 2 and valve V_2. The valves V_1 and V_2 feed into a common anode load. This arrangement greatly reduces interaction between the arms of the bridge. The phase changer controls the phase of the vector at the grid of V_1 without altering its amplitude; the cut-off attenuator controls the amplitude at the grid of V_2 without affecting the phase. These two vectors can thereby be adjusted to cancel in the common anode load of V_1 and V_2. The vector derived from the cut-off attenuator can be regarded as a reference vector of fixed phase and variable amplitude. The vector from the liquid cell can then be balanced against this reference vector and, if this is done for two positions of the probe in the liquid cell, the ratio of the vectors at these two probe positions can be found from the increments in the readings of the phase changer and cut-off attenuator.

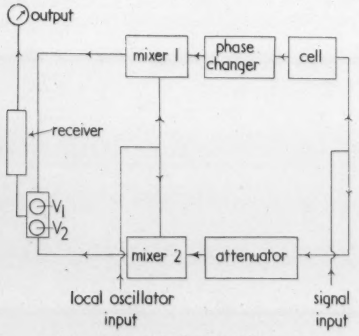

Fig. 1. Schematic diagram of apparatus

The first cell (Fig. 2) consists of a short-circuited length of coaxial line with a movable tubular inner conductor. The output cable passes down inside the tubular inner conductor and terminates in a thin probe which projects into the cell through a small hole in the inner conductor. When the inner conductor is moved it carries the probe with it and the probe thus samples the vector at various points along the cell axis. If a null balance has been found at two positions of the probe in the manner described above, then the vector ratio corresponding to these positions can be found. From this vector ratio and a knowledge of the distances of the probe from the short circuit it is, in particular cases, possible to derive the propagation coefficient of the liquid. The probe position is accurately measured by a micrometer. The cell temperature is thermostatically controlled. The diameter of the inner conductor is about 0·36 cm and the internal diameter of the outer conductor is about 1·60 cm. The length of the column of liquid is about 14 cm.

For measurements on high-loss liquids a second cell of

different design was constructed (Fig. 3) and was used in connexion with the travelling-wave method to be described later. In this cell the liquid column is contained between two interfaces; a fixed one at the bottom of the cell and a movable one, formed by the lower end of a sliding coaxial line, the

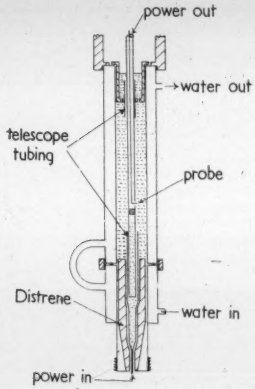

Fig. 2. Cell for low- and medium-loss liquids

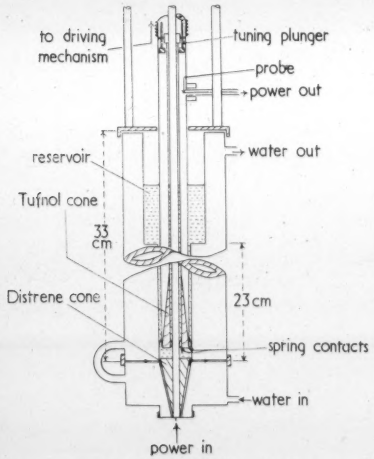

Fig. 3. Cell for high-loss liquids

position of which can be varied by the drive mechanism at the top of the cell. This sliding coaxial line fits closely inside the main fixed coaxial line and serves the dual purpose of varying the depth of the liquid column and collecting the energy which has traversed this liquid column. The diameter of the fixed inner conductor is about 0·5 cm and the internal diameter of the fixed outer conductor is approximately 2·5 cm. The depth of the liquid column can be varied from zero to about 20 cm. When the column is long enough for any residual reflexion to be neglected the phase and amplitude of the output from the cell is controlled by the length of the liquid column and the propagation coefficient is readily determined.

The cut-off attenuator for the longer wavelengths is made from 1 × 0·5 in. precision rectangular waveguide and for the lower wavelengths an attenuator of similar design with a cross-section 1·12 × 0·5 cm is used. The coaxial line phase changer is made from thin telescopic tubing and is fitted at each end with tapered resistive attenuators. The receiver output should remain constant when the phase changer is altered while the other arm of the bridge is disconnected; this indicates that the phase change is unaccompanied by amplitude change. By careful tuning of the mixer it is possible to reduce the reflected voltage in the phase changer to less than 1%.

2. THEORY AND EXPERIMENTAL PROCEDURE

2.1. *Determination of* β. When the cell is filled with liquid the first step (with mixer 2 disconnected) is to move the probe along the cell to investigate the amplitude variation. With low-loss liquids the minima will be sharp, but with high-loss liquids they may be undetectable. With low- and medium-loss liquids an accurate measurement of the phase constant β can be made as follows. If γ be the propagation constant of the liquid the electric field x cm from the short circuit may be written

$$E = E_0(e^{\gamma x} - e^{-\gamma x}) \tag{1}$$

If $\alpha^2 \ll \beta^2$ a close approximation to the positions of the minima is given by

$$x = \frac{n\lambda_m}{2}\left(1 - \frac{\alpha^2}{\beta^2}\right) \tag{2}$$

n an integer, and from this a close approximation to β can be found. For water at 25° C and a wavelength of 50 cm the error in β due to ignoring α^2/β^2 is approximately 0·03%.

When α is large enough, or the cell long enough, for reflected waves to be ignored, then any two points one wavelength apart must differ in phase by 2π radians. The procedure for finding β is then to establish a null balance at a suitable point in the cell; a second point is then found where the null balance can be restored by readjustment of the cut-off attenuator alone. When this is achieved the points are one wavelength apart and β is obtained.

2.2. *Determination of* α *and* β *by the double-distance method.* The ratio of the vectors at two points P and Q on the axis of the cell is given by

$$re^{j\theta} = \frac{e^{\gamma x_1} - e^{-\gamma x_1}}{e^{\gamma x_2} - e^{-\gamma x_2}} \tag{3}$$

where x_1 and x_2 are the distances of P and Q from the short circuit; r and θ are experimentally determined by the cut-off attenuator and phase changer respectively. If now $x_1 = 2x_2$ equation (3) can be solved for α and β to give

$$\cosh \alpha x_1 = r^2/4 + [(1 - r^2/4)^2 + r^2 \sin^2 \theta]^{\frac{1}{2}} \tag{4}$$

$$\cos \beta x_1 = r^2/4 - [(1 - r^2/4)^2 + r^2 \sin^2 \theta]^{\frac{1}{2}} \tag{5}$$

These equations are exact and the method can be used for any liquid.

For low- and medium-loss liquids it can be shown that, for optimum accuracy, P should be chosen near a minimum an odd number of half-wavelengths from the short circuit.

Q will then be at a maximum. For high-loss liquids the conditions for optimum accuracy are less exacting and it is sufficient to choose x_1 as large as possible. For a medium-loss liquid α could be obtained within $\pm 2\%$ and β within $\pm 0{\cdot}1\%$.

If we put $\theta = \pi/2$ in equations (4) and (5) we obtain

$$\sinh \alpha x_1 = r/2 \tag{6}$$

$$\cos \beta x_1 = -1 \tag{7}$$

Equation (7) shows that P must then be at a point $(2n + 1)$ half-wavelengths from the short circuit. This leads to an accurate determination of α, since it is only necessary to go back half-way to the short circuit from any one of the above points and measure the amplitude ratio; α can be immediately determined from equation (8). The above points can be readily found by a knowledge of β and the position of the short circuit as described in Section 2.1. This modified method is independent of the phase changer.

2.3. *Determination of α from the ratio of minimum to maximum.* From equation (1) it can be shown that the amplitude at a distance x cm from the short circuit is

$$E = E_0[2(\cosh 2\alpha x - \cos 2\beta x)]^{\frac{1}{2}} \tag{8}$$

From equation (8) we can derive the approximation

$$E_{min}/E_{max} = r \simeq \frac{\sinh \alpha x_1}{\cosh \alpha x_2} \simeq \sinh \alpha x_1 \tag{9}$$

where x_1 and x_2 are the distances of the minimum and the maximum respectively from the short circuit. This is a good approximation in liquids when $\alpha^2 \ll \beta^2$ and when $\cosh \alpha x_2 \simeq 1$. When this latter condition is not satisfied successive approximations must be used.

The best estimate of the error in α is given in practice by the scatter in the results obtained by working out all the determinations given by the various possible combinations of the different maxima and minima.

The phase changer is not used in this method and the accuracy of the results depends mainly on the cut-off attenuator.

2.4. *Phase method of measuring α for low- and medium-loss liquids.* If P and Q are two points on the axis of the cell where the amplitudes of the electric vectors are equal, it can be shown that

$$j \tan (\theta/2) = \tanh \gamma\xi / \tanh \gamma d \tag{10}$$

where $2d = x_1 + x_2$ and $2\xi = x_2 - x_1$; x_1 and x_2 are the distances of P and Q from the short circuit and θ is the phase difference between the vectors. Since θ, d and ξ can be measured experimentally then γ can, in theory, be determined from equation (10). If now P and Q are on opposite sides of and close to a minimum, then $2d \simeq n\lambda_m$ and ξ is small. In this case equation (10) reduces to the approximation

$$\tanh \alpha d \simeq \tan \beta\xi / \tan (\theta/2) \tag{11}$$

θ and ξ are determined experimentally and β is found as described in Section 2.1. This method applies to any liquid which has a detectable minimum in the standing-wave pattern.

The experimental procedure for this method is straightforward. With the signal through the attenuator reduced to zero the probe is set to a point to one side of a minimum. The signal through the attenuator is then increased and the phase changer is adjusted until a null balance is obtained. The cut-off attenuator is then fixed in position, the probe is moved through the minimum to a position roughly equidistant on the other side and the phase changer and probe are then alternately adjusted until a second null balance is obtained. Since the attenuator has not been altered for this second null balance the vector amplitudes are unaltered and the conditions for the application of equation (11) are satisfied. This procedure can be repeated at the different minima.

2.5. *Determination of α and β by the travelling wave method.* When α is large enough for the effects of the reflected wave to be ignored then conditions at the input of the cell (Fig. 2) correspond to the propagation of a pure travelling wave. The electric vectors E_1 and E_2 at distances d and $d + \lambda_m$ from the input end of cell are 2π radians out of phase and

$$E_1/E_2 = e^{\alpha\lambda_m} \tag{12}$$

If a null balance is obtained at each point and l cm is the difference in the readings of the cut-off attenuator then, if α_l is the attenuator constant, we have

$$E_1/E_2 = e^{\alpha\lambda_m} = e^{\alpha_l l} \tag{13}$$

Therefore

$$\alpha = \alpha_l l/\lambda_m \tag{14}$$

This method is rapid and capable of very high accuracy, and because of this the cell of Fig. 3 was constructed. This new cell was used successfully for measurements on water at wavelengths of 10 and 17 cm, but at 50 cm for water the value of α was too low to attenuate the reflected waves sufficiently. With this modified form of cell it is easy to measure β to $\pm 0{\cdot}1\%$ and the accuracy of the determination of α is limited mainly by the accuracy with which the attenuation constant of the cut-off attenuator is known.

3. ERRORS

The above methods have all been discussed on the assumption of a perfect short circuit and a non-reflecting probe. In practice these conditions do not exist so an investigation has been made of the effects of a dissipative short circuit and a reflecting probe.

If the method described in Section 2.3 is used then equation (9) must be modified to

$$r \simeq \frac{\sinh \alpha x_1}{\cosh \alpha x_2}\left[1 + \frac{1}{2}\delta\left(\frac{e^{-\alpha x_1}}{\sinh \alpha x_1} + \frac{e^{-\alpha x_2}}{\cosh \alpha x_2}\right)\right] \tag{15}$$

where $\delta = 1 + \rho_2$ and is assumed to be real, ρ_2 is the reflexion coefficient of the short circuit.

Similarly if the probe has a complex reflexion coefficient $\rho_1 = |\rho_1|e^{j\phi}$ then

$$r \simeq \frac{\sinh \alpha x_1}{\cosh \alpha x_2}[1 - |\rho_1| \cos \phi(e^{-\alpha x_1} + e^{-\alpha x_2})] \tag{16}$$

where ρ_1^2 is small.

Both effects could, in theory, be detected by the calculated values of α being larger for positions near the short circuit than for positions further away, but in the apparatus described neither effect was noticed.

The correction to β is negligible.

ACKNOWLEDGEMENTS

Thanks are due to Professor J. E. Roberts for the facilities provided and the workshop staff for help in the design and construction of equipment. One of the authors (E. H. G.) is indebted to the Medical Research Council for a research grant.

REFERENCES

(1) Buchanan, T. J. *Proc. Instn Elect. Engrs*, **99**, p. 61 (1952).

(2) Branin, F. H. *J. Appl. Phys.*, **23**, p. 9 (1952).

Correspondence

Probe impedance in the electrolytic tank

Since high probe impedances necessitate circuit elaborations,[1,2] probe design is important. The impedance is usually ascribed to capacity or polarization effects, but in many cases the simple ionic conduction mechanism will give a useful estimate, so that the optimum size and shape may be calculated.

Consider a submerged probe tip, represented by a closed conducting surface (ignore the insulated connexion[3]) in an electrolyte of specific resistance s. Let the probe be small enough to assume the surrounding field initially uniform (of strength E), and suppose it takes up a potential V relative to the original electrolyte potential (r.m.s.) at its electrical centre. Since V is not zero the current lines near the probe are distorted unsymmetrically, and it is to be shown that this results in an effective probe impedance depending only on the probe geometry (represented by parameters p) and s, and independent of E and of the probe position and orientation (parameters o).

Let parameter q represent the co-ordinates of a general point relative to the probe (not to the direction of E), and let e represent the electrical parameters E, V, s, and i (difference between ionic probe currents ingoing and outgoing). The potential distribution $\phi(o, p, q, e)$ may be regarded as the superposition of: (i) that due to the conductor, at zero potential, in the field E; and (ii) that due to the conductor, at potential V, in a zero field. The current flow due to distribution (i) is symmetric, so that net current is zero. It is therefore sufficient to consider distribution (ii), and it is immediately apparent that no expression derived from such consideration can involve E or o. This establishes the necessary independence, and it remains to show that i is proportional to V.

Now $\phi(p, q, e)$ is determined by these conditions: it must be finite and continuous; it must vanish at infinity [which would not be true of distribution (i)]; it must satisfy Laplace's equation; and it must take a constant value over the surface. The function thus defined is unique but for an arbitrary multiplying factor (fixed by the value of V). Apart from the factor, therefore, this function depends only on the geometrical parameters p, q and is independent of the electrical parameters e. The multiplying factor g must be a function of e. So $\phi = g(i, V, s) f(p, q)$. The function f must be independent of q on the surface $[f(p, q) \to f_0(p)]$ where $\phi = V$. Thus $\phi(p, q, e) = [V/f_0(p)] f(p, q)$. The function f must also take the form $F(p)/r$ at large distances; in fact we must have

$$\phi \to is/4\pi r \tag{1}$$

at large distances, so that

$$(V/i)/s = f_0(p)/4\pi F(p) \tag{2}$$

i.e. (probe "impedance")/(electrolyte resistivity) is a function of the probe shape and size.

[In unrationalized units, the right-hand sides of equations (1)–(5) must be multiplied by 4π. Equation (6) is unchanged.]

Expressions for f are better known in the analogous electrostatic problems concerning total charge Q on the surface, and dielectric constant ϵ of the surrounding material ($i \to Q$, $s \to 1/\epsilon$). In these terms, the above is a demonstration that the capacity of the conductor does not depend on the orientation or magnitude of a uniform field established in the dielectric.

For an ellipsoid with semi-axes $a > b > c$, it is known that distribution (ii)* is $\phi = CI_\xi$,

where $$I_\xi \equiv \int_\xi^\infty \frac{d\xi}{\sqrt{[(\xi + a^2)(\xi + b^2)(\xi + c^2)]}}$$

the suffix indicating the lower limit. ξ is the ellipsoidal co-ordinate such that the surface $\xi = 0$ coincides with the conducting surface. But at large distances, I_ξ becomes $2/r$,

while $$\phi \to is/4\pi r \tag{3}$$

so that we have at any point [compare Ref. (4), p. 208 (7)]

$$\phi = (is/8\pi) I_\xi \tag{4}$$

On the surface ϕ equals V and I_ξ becomes I_0, so using

$$1/\text{probe impedance} = i/V \tag{5}$$

we have finally

$$\text{probe impedance}/s = I_0/8\pi \tag{6}$$

By taking the new variable $v = (-1/k)(\xi - \beta)/(\xi - \alpha)$ where

$$\alpha \equiv -c^2 - R \qquad \lambda_1 \equiv -a^2 - b^2 + 2c^2 + 2R$$
$$\beta \equiv -c^2 + R \quad \text{with} \quad \lambda_2 \equiv -a^2 - b^2 + 2c^2 - 2R$$
$$k^2 \equiv \lambda_1/\lambda_2 \qquad R \equiv \sqrt{[(a^2 - c^2)(b^2 - c^2)]}$$

I_0 becomes

$$\frac{2}{\sqrt{-\lambda_2}} \int_{\beta/\alpha}^1 \frac{dv}{\sqrt{[(1 - v^2)(1 - k^2 v^2)]}}$$
$$= \frac{2}{\sqrt{-\lambda_2}} [\bar{K}(k) - K(k, \sin^{-1} \beta/\alpha)]$$

K is the standard elliptic integral of the first kind, and $\bar{K}$ is the corresponding "complete integral."

Notice that the inverse of the impedance varies with the linear dimension of the probe tip, in order of magnitude, while the inverses of the electrolyte "arms" vary with its square.

If the volume of the probe tip is fixed ($abc = 1$), the probe impedance expression varies with shape as shown in the figure [part (a)]. Thus rod-like shapes give a lower impedance than disk-like shapes of the same thickness, especially when the thickness is small. The sphere seems the worst choice from this point of view.[3] On the other hand, it seems possible that the rod will be the shape to cause the worst disturbance, in a non-uniform field, when its orientation happens to be unfortunate (longest dimension parallel to field).

Expressions for the special cases $a = b$ and $b = c$ may be found in Stratton,[4] p. 209 [see figure, part (b)]. The impedance of a cylinder will lie between that of inscribed and

* See for example Ref. (4) p. 208. I am indebted to Dr. C. Strachan for pointing out that it is not necessary to use the more complicated expression given by Stratton as equation (26).

exscribed ellipsoids. For long cylinders the former is larger[5] by $\sqrt{2}$, and may be taken as an upper limit.

The limits of validity of the conduction mechanism are unknown. A few simple measurements with an available probe show quantitative agreement within the limits of the experiment. Twenty-six gauge platinum wire projects vertically from an insulating holder in a 1000 c/s horizontal uniform field in tap water, about 1 V/cm. The circuit is a null potentiometer with oscilloscope detector (resistance R_g). (*a*) The depth of immersion is varied from 1 to 13 mm at various fixed positions and with R_g fixed at values between 4 kΩ and ½ MΩ. Plots of (1/signal) against theoretical

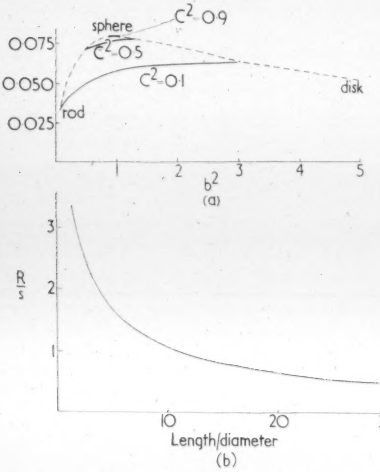

Resistance of ellipsoidal probe tips

(*a*) constant volume ($abc = 1$);
(*b*) prolate ellipsoids ($b = c = 0{\cdot}2286$ mm).

impedance values are straight lines, confirming the *form* of the relation "impedance *versus* geometry" in the rod-like case. The intercept agrees with the known R_g values. (*b*) With the 13 mm length of probe tip completely submerged (and also at several fixed partial immersions), R_g is varied, and (1/signal) against $1/R_g$ are straight lines, the intercept giving probe impedance values in quantitative agreement with the theory. Apparent downward trends in the value appear (i) very near balance position; (ii) near the main electrodes; (iii) with the field strength halved; and (iv) at frequency 4 kc/s. Careful experiments would be needed to show whether these trends are significant. The values are fairly low, of order 10 kΩ. Capacitative probe coupling was noticed only at very small immersions.

Department of Natural Philosophy, University of Aberdeen.

J. C. Burfoot

REFERENCES

(1) Einstein, P. A. *J. Sci. Instrum.*, **27**, p. 27 (1950).
(2) Sander, K. F., and Yates, J. G. *Proc. Instn Elect. Engrs*, **100**, II, p. 167 (1953).
(3) Softky, S., and Jungerman, J. *Rev. Sci. Instrum.*, **23**, p. 306 (1952).
(4) Stratton, J. A. *Electromagnetic Theory* (New York: McGraw-Hill Book Co. Inc., 1941).
(5) Weber, E. *Electromagnetic Fields*, Vol. I, p. 110 (New York: J. Wiley and Sons Inc., 1950).

Electrical dehydration of tar emulsions

In a recent paper[1] it was shown that when emulsions of water in fuel oil and many other suspensions are placed in a direct or alternating electric field the droplets or particles line up into chains in the direction of the field and in the case of emulsions the droplets may coalesce and the phases separate. Emulsions of water in tar occur in gas making plant and are a source of operating difficulties. Electrical dehydration is one of the methods employed to resolve such emulsions but is well known to be ineffective with certain tars. The authors recently had an opportunity of studying the process and although insufficient work has been done to establish a complete theory some of the results obtained are of interest.

When the effect of electric fields on emulsions of water in tar was examined in the concentric cell and in the manner already described,[1] the action observed was of two main types. The first is illustrated in Fig. 1 which refers to a low temperature tar produced in a Gray–King assay[2] and shows an action similar to that already noted in emulsions of water in fuel oil. Fig. 2 refers, however, to a commercial tar and illustrates a quite different effect. Unlike the first, this tar is seen to contain in addition to the water droplets, solid particles, presumably carbon, which under the action of the field form a network of chains in which the droplets are held separate one from another. In this way contact between droplets and consequent coalescence is prevented.

It will be observed that whereas the voltage applied to the cell in the case of the low temperature tar was 350 V, that for the coke oven tar was 1000 V. This difference is not significant, however, as the values were chosen to provide demonstrations of the two types of action in reasonable times. The rates at which the chains form are dependent on a number of factors in addition to the value of the applied voltage, the most important of them being the viscosity of the tar. Low temperature tar is less viscous than that from coke ovens and the chains of droplets thus form in it at a lower electric field strength.

The characteristics of tar have rendered impossible the complete range of experiments that was carried out with fuel oil emulsions but the foregoing indicates one factor hindering the electrical dehydration of certain types of tar.

This note appears by permission of the Director of Fuel Research and the illustrations which are Crown copyright are reproduced by permission of the Controller, H.M. Stationery Office.

Fuel Research Station,
Greenwich,
London, S.E.10.

H. A. Howe
C. A. R. Pearce

REFERENCES

(1) Pearce, C. A. R. *Brit. J. Appl. Phys.*, **5**, p. 136 (1954).
(2) King, J. G., Tasker, C., and Edgcombe, L. J. *The Assay of Coal for Carbonisation Purposes. Part II.* Fuel Research Technical Paper No. 21 (London: H.M. Stationery Office, 1929).

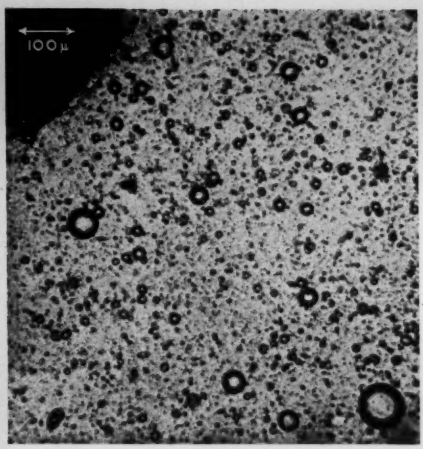

(*a*) Untreated material. The silhouette in the top left-hand corner is the central electrode.

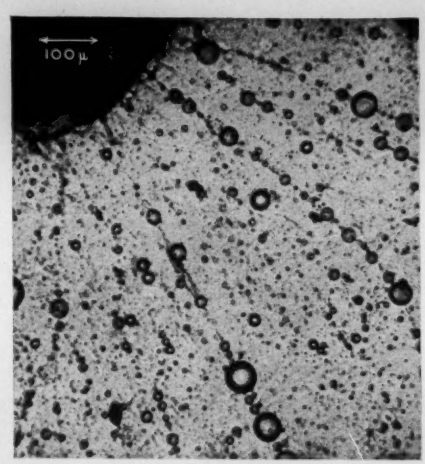

(*b*) After the application of an alternating voltage (350 V) to the cell. The droplets have started to form chains and some coalescence has occurred.

Fig. 1. Photomicrographs of an emulsion of low temperature tar produced by the Gray–King assay

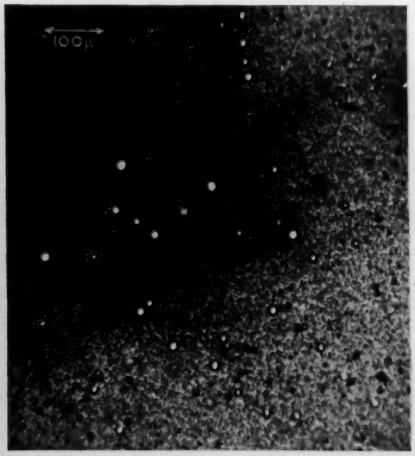

(*a*) Untreated material. The white circles are droplets and the black specks are particles of carbon. The dark mass in the top left-hand corner is a thicker layer of tar surrounding the electrode.

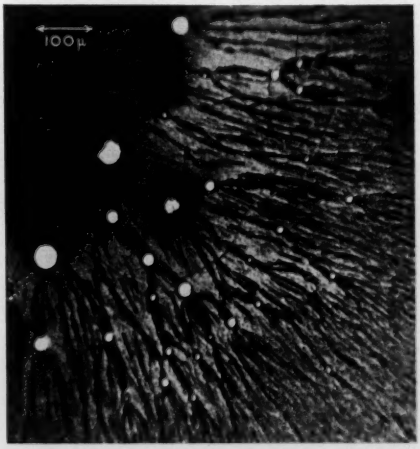

(*b*) After the application of an alternating voltage (1000 V) to the cell. The carbon particles have formed chains and although there has been some coalescence of the droplets, no further action can occur because of the carbon chains.

Fig. 2. Photomicrographs of an emulsion of coke oven tar

New books

Wool, its chemistry and physics. By PETER ALEXANDER and ROBERT HUDSON. (London: Chapman and Hall, Ltd., 1954). Pp. viii + 404. Price 45*s*.

"Even physical theories . . . were first studied and developed by scientists working on wool fibres before being extended to other systems."

This quotation from the preface is a good guide to the contents of the book: it uses physics to gain a better understanding of the structure and chemistry of wool. The important thermal and water repellent properties of wool are not mentioned, and the chapter on mechanical properties gives no indication of the value of any elastic moduli; sorption, swelling and diffusion are fully discussed.

Research workers concerned with the application of physical methods to polymers, and particularly to proteins, will find the book most stimulating. The controversy of multi-molecular absorption *versus* solution theory is carefully presented, and might well inspire those conversant with statistical thermodynamics to attempt, at least mathematically, to bridge the gap between them. There is, too, much of interest to the physicist in the acid-base characteristics of wool, whilst the Donnan and Gilbert and Rideal theories of dyeing might well be tidied up. All these, and many more polymer problems, together with the usual chemistry of wool, are carefully described in a book that is easy to read and excellently produced. A. B. D. CASSIE

An atlas of typical expansion chamber photographs. By W. GENTNER, H. MAIER-LEIBNITZ and W. BOTHE. (London: Pergamon Press Ltd., 1954.) Pp. x + 199. Price 105*s*.

Some fourteen years ago the authors of this volume published the *Atlas typischer Nebelkammerbilder*, a collection of pictures showing the application of the cloud chamber to nuclear physics and cosmic rays. This book went out of print during the war and when, five years ago, a new edition was being considered, it was decided to republish as a series of three volumes covering the two principal pictorial techniques of atomic physics, the cloud chamber and the photographic emulsion. The first volume, entitled *Cloud chamber photographs of the cosmic radiation*, appeared in 1952, the present volume is the second, and the third, *Emulsion method photographs*, is ready and will appear shortly. The aim of the series is to present photographs of historical importance and typical examples of many of the main phenomena of atomic physics so that physicists, and perhaps others also, can get a clear picture of sub-atomic processes.

The present volume, which is dedicated to the inventor of the cloud chamber, C. T. R. Wilson, includes natural and artificial radioactivity, the radiations from radioactive substances, nuclear transmutations and cosmic rays. Like its predecessor it is a collection of beautiful photographs, excellently reproduced. Technical details are printed in small type, while in the main text there is given the accepted description of the phenomena which the photograph illustrates. Legends are in three languages, English, German and French. The impression gained by reading these legends and studying the pictures is that the original aim has been fully achieved. The descriptions are simpler and easier to read than those in the first volume where the element of critical interpretation was stressed and rather more emphasis was placed on technical details.

The reviewer makes only two critical comments, the first concerning the absence of a list of plates or an index, surely a serious omission in a volume intended to be an encyclopaedia of cloud chamber photographs, and the second the high price, which will unfortunately limit the extent to which the book will be used. Since the high standard of reproduction of the photographs is quite essential, it would seem that the only way of achieving a reduction in price would have been by limiting the scope, perhaps by devoting the book to nuclear physics only. G. D. ROCHESTER

Hydraulic systems and equipment. By R. HADEKEL. (London: Cambridge University Press, 1954.) Pp. viii + 224. Price 18*s*.

This book is concerned exclusively with hydraulic machinery as used to control the transmission of force and motion to solid bodies. Thus the hydraulics of civil engineering is not dealt with, nor are other fluid handling problems such as engine fuel systems or lubrication systems. By specifically limiting his scope in this way, Mr. Hadekel has been able to give a concise and systematic account of the type of machinery involved in presses, machine tools, lifting jacks, brakes, etc. The main emphasis is on hydraulic circuitry, and particularly on those aspects which are analogous to switching and relay techniques in electrical engineering. Feedback control systems are barely touched on, though the bibliography is strong in this respect.

The author maintains a high standard of lucidity considering that some hundreds of intricate mechanisms are discussed. This is partly due to the use of exceptionally clear diagrams, which dispense with the need for the heavy verbiage often found in machine literature. The treatment is essentially descriptive, mathematics being confined to a few basic design formulae. Performance figures are seldom quoted.

There is a dearth of objective literature on this increasingly important branch of modern technology, and Mr. Hadekel's book is a welcome contribution. A. T. FULLER

Quantum mechanics. By F. MANDL, M.A., D.Phil. (London: Butterworths Scientific Publications, 1954; New York: Academic Press Inc.) Pp. viii + 233. Price 35*s*.

This book concentrates specially on those points which are not adequately covered or not discussed in enough detail in other existing textbooks. It should be very welcome, therefore, to a conscientious student whom the other books may have left dissatisfied about several items. On the other hand, the author sometimes, rather than duplicate them, frankly refers the reader to the books of, for example, Sommerfeld or Schiff, even for important mathematical details which are very fully discussed in standard textbooks. Thus it is doubtful whether the book can be considered as a self-contained introduction, but reference to other textbooks is made whenever appropriate, and in compensation the book gives a sound and quite modern treatment (including, for example, the operator $\exp(-iHt/\hbar)$ rarely found in other introductions) which covers non-relativistic quantum theory including spin, perturbation theory, collision processes, and an introduction to group theoretical ideas. Not many examples are worked out in the text, but thirty pages are devoted to hints for solving the exercises at the end of each chapter. The book developed originally from a course of lectures to experimentalists. The aim "to give them a thorough grasp of quantum mechanics enabling them to perform quantum mechanical calculations and to read the theoretical literature

without demanding a previous high standard of mathematics," as stated on the dust cover, and the author's contention that, in spite of its lack of mathematical rigour, the book should serve the theoretical student as an introduction to more advanced work, are admirably realized. H. PELZER

Occasional Notes, No. 16: Radio astronomy. (London: Royal Astronomical Society, 1954.) Pp. 49. Price 6*s*.

The custom of the Royal Astronomical Society, of understating the intellectual weight of their publications by calling them "notes," is exemplified in this highly informative and scholarly monograph; it summarizes the history, principles and methods of radio astronomy, with accounts of recent results in some of its more striking fields. The authors are from Professor Lovell's group at the Jodrell Bank Institute associated with the Physics Department of the University of Manchester, but the other workers from Cambridge, Sydney and Leyden are given due prominence, and the whole vast subject is outlined from a basis of clearly indicated first principles. Experimental physicists in other fields may be especially interested in the chapters on technique; but if they are not mere technologists they will also share with the astronomers and cosmologists a keen enjoyment of the chapters on solar, galactic, interstellar and extra-galactic sources of radio emission. The little book expresses excellently the advance made possible by extending optical into radio frequencies for exploring the sky.

MARTIN JOHNSON

Engineering dynamics, Vol. 3, Steam turbines. By Professor C. B. BIEZENO and Professor R. GRAMMEL. (London and Glasgow: Blackie and Son Ltd., 1954.) Pp. 264. Price 40*s*.

Of recent years the increase of both power and speed of machinery has beset the engineer with many new problems and few texts are available to guide him in his investigations. Admittedly there are numerous specialist papers scattered throughout the literature of the world, but little has been done to collect this information. The present volume is the third of four which set out to give the postgraduate mechanical engineer a comprehensive text on the solution of the dynamical problems encountered in steam turbines and internal combustion engines.

This volume goes very fully into the problems of the strength, modes of vibration and deflexions of rotating disks of various forms and of turbine blades, and gives a very thorough discussion of the critical speeds of shafts. The mathematics is unavoidably somewhat heavy, for the subject is not one which admits of superficial treatment, but the authors have shown the application of their theory to practical problems and have indicated in many cases graphical methods of evaluation.

It is perhaps to be regretted that volumes 1 and 2 have not yet reached publication for they are scheduled to contain the basic elastic and mechanical theories and methods which are largely used in this volume, and to which continual reference is made. Nevertheless, the text is admirably clear, and if the other volumes are of the same character the advanced engineer will certainly be in the debt of Professors Biezeno and Grammel.

Incidentally the translators, E. F. Winter and H. A. Havemann, are to be congratulated in that the book shows no sign of having been translated from another language.

H. T. JESSOP
B. J. LLOYD EVANS

Rohrhydraulik. By H. RICHTER, Dr.Ing. (Berlin: Springer-Verlag, 1954.) Pp. xi + 328. Price D.M. 34·50.

The first edition of this book was published in 1933. For this second edition the text has been revised to take account of the recent developments in the subject, but the arrangement and scope of the book remains unaltered. The first half of the book consists of a review of the present state of knowledge of the fluid mechanics of pipe flow. Little previous knowledge of the subject is assumed, and the material is presented clearly, with excellent diagrams. In the remainder of the book this information is put into a form suitable for practical calculations on flow through piping systems. Various charts and nomograms are given as aids to rapid calculation, and there are a number of worked examples.

Pipe friction data for turbulent flow are in this edition presented in the now widely accepted form of $f \sim Re$ diagrams based on the Colebrook–White function. Bend losses are dealt with quite fully, but more could have been said about the losses in valves and fittings, since these can in certain systems be the most serious source of loss.

Although much of the latter part of the book will be of limited value in this country owing to the use of metric units, the excellent survey of theoretical and experimental work given in the first half of the book is of general interest.

H. C. WILKINSON

Sensations of tone. By HERMANN L. F. HELMHOLTZ. (New York: Dover Publications, Inc., 1954.) Pp. xix + 576. Price $4.95.

This famous classic of acoustics, source book for all writers on the subject, has just been re-issued as an exact reprint of the English edition of 1885, translated by Alexander J. Ellis from the 4th German edition of 1877. The translator's additional notes "especially adapted to the use of musical students" are also given in full. Professor Henry Margenau of Yale University provides a short biography of Helmholtz by way of introduction, together with a bibliography of his scientific publications.

Despite all the recent revolutionary applications of electronics in the acoustical field, most of the problems discussed by Helmholtz are still vital to-day—indeed, on sounds considered in isolation, he has probably dealt with all the relevant phenomena and leads us to the point where the musician and psychologist take over their task of considering the melodic and harmonic relations of sounds.

H. LOWERY

Notes on applied science No. 6. Volumetric glassware. (London: Her Majesty's Stationery Office, 1954.) Pp. v + 45. Price 1*s*. 6*d*.

The purpose of this useful monograph, which has been prepared by the National Physical Laboratory, is to present the basic scientific information which must be taken into account in the preparation of standards for volumetric glassware, and to set out the main features of standardization which apply in both rationalization and verification. Certain features which apply only to particular instruments are also dealt with and, for those vessels intended to deliver (not to contain) a specified volume, examples showing the need for close control of the conditions of delivery are given. The notes are supplementary to any test pamphlets issued by the N.P.L. and British Standards issued by the British Standards Institution. They do not, however, discuss techniques of manufacture, or the uses of the apparatus.

Notes and comments

Elections to The Institute of Physics

The following elections have been made by the Board of The Institute of Physics:

Fellows: F. I. Hurley, A. J. Kennedy, J. D. McGee, M. E. Pillow, A. Radcliffe, H. C. von Bertele.

Associates: M. E. Baird, G. A. Bassett, S. S. Baxter, W. R. Blevin, J. S. M. Botterill, D. S. Briggs, E. S. Brown, W. F. Caplehorn, G. K. Eaton, R. W. M. Fane, G. G. Fowlie, R. Gill, D. Greene, S. Griffiths, W. D. Hardy, A. K. Head, J. F. Hills, K. R. Hodgson, S. B. Hudson, I. H. Jenkins, Y. Klinger, J. E. Laby, D. H. Le Croissette, S. N. A. Margerson, R. H. Norman, P. G. Parish, W. D. Parkinson, N. J. C. Peres, A. G. Pulford, J. M. Rooke, H. B. Sarjeant, G. R. Sharp, S. E. F. Smallwood, F. Smith, J. A. S. Smith, A. M. A. Swindells, K. E. Timmel, R. Vollprecht, B. R. H. Warrell, C. G. Webb, F. J. Weinberg, R. E. Weston, W. S. Whitlock.

Forty-six Graduates, eighteen Students and seven Subscribers were also elected.

International symposium on electrical discharges in gases

An international symposium on electrical discharges in gases will be held at the Technical University of Delft, Netherlands, from 25–30 April, 1955, with the support of U.N.E.S.C.O. (through the intermediary of the International Union of Pure and Applied Physics), the Fund of the Technical University of Delft and the Philips' Works, Eindhoven.

The following main subjects will be discussed:

1. Fundamental processes and new views on the mechanism of gas discharges.
2. Instabilities and conditions of stability, oscillations and noise phenomena in gas discharges.
3. Breakdown potential as a function of potential difference and frequency.
4. (*a*) New methods of measurement applied to the investigation of gas discharges.
   (*b*) Gas discharges applied to other physical problems as a method of measurement.
5. Arc discharges.
6. Spark discharges.
7. Miscellaneous.

The languages to be used are English, French and German; with a preference for English in the discussions. A programme for ladies visiting Delft but not attending the symposium will be arranged.

Enquiries concerning the symposium should be addressed to the Secretary of the Symposium Committee, Ir A.W. van Wagensveld, Mijnbouwplein 11, Delft, Netherlands.

Conference on mass spectrometry

The Third Annual Conference on Mass Spectrometry under the sponsorship of American Society for Testing Materials will be held from 23 to 27 May, 1955, at the Mark Hopkins Hotel in San Francisco, California. The programme will consist of papers covering all aspects of the theory and application of mass spectrometry. Papers are invited and titles should be submitted by 15 February, 1955, to Mr. William Priestley, Jr., Standard Oil Development Co., Box 121, Linden, New Jersey, U.S.A.

An exhibition of mass spectrometry equipment will also be arranged and prospective exhibitors may obtain information from Dr. J. G. Hutton, General Electric Co., 1 River Road, Schenectady, New York, U.S.A.

Harwell Isotope School

The Harwell Isotope School, which since it was founded in 1951 has had 329 students from 24 different countries, is now preparing its programme for the next twelve months. Training is given at this school in the applications of radioactive materials in research and industry and in the techniques of producing, measuring and handling such materials. The courses, which last for four weeks, include both lectures and practical work in the laboratory. Students should be graduates of a university. The courses for early 1955 are already fully booked, but there are at present vacancies on the courses commencing on 25 April and 27 June, 1955. Details of the course fee and further information can be obtained on application to The Isotope School, Atomic Energy Research Establishment, Harwell, Berks.

Journal of Scientific Instruments

Contents of the February issue

ORIGINAL CONTRIBUTIONS

Papers

A logarithmic photocell circuit. By V. H. Attree.
Errors of friction wheel integrators. By J. G. L. Michel.
An instrument for the formation of visual images of ionizing radiations. By W. V. Mayneord, H. D. Evans and S. P. Newbery.
An automatic pressure recorder for the study of gas phase kinetics. By D. Patterson and R. C. Seymour.
Piezoelectrically-activated low-frequency mechanical resonators. By J. F. W. Bell.
A servo-controlled microdensitometer for X-ray diffraction photographs. By J. R. Brown, H. K. Moneypenny and R. J. Wakelin.
An instrument for the accurate measurement of low optical densities. By A. S. Cross.
A simple ratio-recording spectrometer. By N. H. E. Ahlers and H. P. Freedman.
The stability of the calibration of liquid sample Geiger–Müller counter tubes. By N. Veall, A. E. Lowe and R. E. Whyard.
A tuned detector-amplifier for power-frequency measurements. By W. K. Clothier and W. E. Smith.
A rotational viscometer for surface films. By S. C. Ellis, A. F. Lanham and K. G. A. Pankhurst.

Laboratory and workshop notes

Liquid developers for xerography. By K. A. Metcalfe.
A compact high voltage static electrification eliminator. By D. T. R. Dighton.
A device for preparing gas mixtures. By N. R. Hansen.
Apparatus for the production of a desired periodic flow in fluids. By V. R. Peterson.
Coaxial cable termination vacuum seal. By E. E. Pesterfield and P. A. Einstein.
A method for the simultaneous rotation of two polarizing prisms. By H. G. Jerrard.
Balance with approximately logarithmic scale. By O. Kantorowicz.
Adaptation of a standard X-ray powder camera for work at low temperatures. By J. Thewlis and A. R. Davey.

NOTES AND NEWS

New instruments, materials and tools
New books
Notes and comments

THIS JOURNAL is produced monthly by The Institute of Physics, in London. It deals with all branches of applied physics (including theory and technique).

All rights reserved. Responsibility for the statements contained herein attaches only to the writers.

EDITORIAL MATTER. Communications concerning editorial matter should be addressed to the Editor, The Institute of Physics, 47 Belgrave Square, London, S.W.1. (*Telephone:* Sloane 9806.) Prospective authors are invited to prepare their scripts in accordance with the *Notes on the preparation of contributions.* (Price 2*s.* 6*d.* including postage.)

REPRODUCTION. The Institute of Physics is a signatory to The Royal Society's Fair Copying Declaration. Details may be obtained upon application from The Royal Society, London, W.1.

ADVERTISEMENTS. Communications concerning advertisements should be addressed to the agents, Messrs. Walter Judd Ltd., 47 Gresham Street, London, E.C.2. (*Telephone:* Monarch 7644.)

CLAIMS FOR MISSING JOURNALS. Claims from regular subscribers to this *Journal* for missing numbers will only be considered if received within 60 days of the date of mailing plus normal outward time of transit and time for lodging the claim. Losses attributable to failure to notify a change of address or to similar omissions will not be considered.

SUBSCRIPTION RATES. A new volume commences each January. The charge is £4 per volume ($11.50 U.S.A.), including index (post paid), payable in advance. Single parts, so far as available, may be purchased at 8*s.* each ($1.15 U.S.A.), post paid, cash with order. Orders should be sent to The Institute of Physics, 47 Belgrave Square, London, S.W.1, or to any bookseller.

The measurement by ionization methods of the peak kilovoltage across X-ray tubes

By J. R. GREENING, B.Sc., Ph.D., A.Inst.P., St. George's Hospital, London, S.W.1

[*Paper received* 24 *August*, 1954]

The difficulties of measuring the kilovoltage across modern X-ray tubes immersed in oil within earthed shields are pointed out, and the need for a method of measurement applicable when the apparatus is installed ready for use is emphasized. Methods are developed based on observing the threshold of phenomena associated with the absorption of X-rays from the apparatus by the K-shells of various irradiated materials. These phenomena are (i) the emission of characteristic radiation, (ii) the emission of photo- and Auger electrons, and (iii) the additional absorption of the X-ray beam. A method employing a combination of effects (i) and (iii) is finally adopted, and several examples are given for X-ray machines operated at both high and low milliamperages. A simpler technique is described suitable for measuring the voltage drop under various loads.

The kilovoltage across an X-ray tube is generally indicated on the control panel of the generator by means of a voltmeter in the low tension circuit of the high tension transformer, or by means of numbered stud settings on the controlling autotransformer. Both these indicators have to be calibrated, and the variety of methods used is perhaps an indication that none of them is thought to be entirely satisfactory. Firstly, the open circuit kilovoltage from the transformer, or, better, the kilovoltage across the X-ray tube at a low tube current, may be measured by the sphere gap method. The voltage drop at higher tube currents is then allowed for, either theoretically or by means of a "radiographic calibration." (This technique is discussed in the final section of this paper.) A powerful argument in favour of this latter method is that with tubes used for medical radiography, it is a "photographically effective" rather than a "physically exact" kilovoltage that is required. Secondly, the kilovoltage across the X-ray tube may be measured by a sphere gap at all tube currents. As the permissible exposure times at the higher currents are severely limited the sphere gap has to be set by trial before the exposure is made, with the risk that surge voltages will be measured rather than the true peak voltage. Thirdly, in order to overcome this last criticism, several tubes may be connected in parallel across the transformer so that the current through any one tube is reduced with a consequent increase in the permissible exposure time. The sphere gap may then be adjusted during the exposure. A criticism of this method is that the voltage is not measured with the actual tube which is to be used with the transformer.

All these methods may be used in the factory for an initial calibration, but after final installation the apparatus will probably be operating from mains of different resistance (allowance is usually made for this) and with cables of another length. For these reasons a check of the voltage is desirable, and in any case a subsequent measurement may be required after repair or modification of the apparatus. The method employing X-ray tubes in parallel is hardly applicable as the apparatus can only be transported with difficulty. If a sphere gap is to be connected directly across an X-ray tube after its installation, special adaptors will be required to allow the conductors to pass through the earthed shielding of the tube head or cables. There would, therefore, appear to be a need for a method of voltage measurement which could be employed with equal facility in factory or hospital, and which involved no disturbance of the apparatus in any way.

In the present paper, it is shown that the peak kilovoltage across an X-ray tube may be determined by observing the threshold of some phenomenon associated with the absorption of the X-rays by the K-shells of various irradiated materials.

K-SHELL ABSORPTION PHENOMENA

There are three phenomena associated with photoelectric absorption which might be used to determine the reading of the kilovoltage indicator at which this absorption first occurs. These are (i) the emission of characteristic radiation, (ii) the emission of photo- and Auger electrons, and (iii) additional absorption of the primary beam. These methods are not applicable at voltages above 116·3 kV which corresponds to the K-edge of uranium but the normal kilovoltage range used in medical radiography can be covered.

(i) *Emission of characteristic radiation.* An ionization chamber *A* placed as shown in Fig. 1 within a thick lead

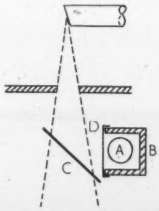

Fig. 1. Experimental arrangement for detection of characteristic radiation

screen *B* will be exposed to secondary radiation coming from the irradiated sheet *C*, but will receive very little direct radiation from the X-ray tube. The secondary radiation will be composed of scattered radiation, both coherent and incoherent, together with radiation characteristic of the material *C*. When the peak voltage across the X-ray tube exceeds the voltage corresponding to the K-absorption edge

of C, K-characteristic radiation will also be produced. Since the K-radiation will be of shorter wavelength than most of the scattered radiation, and of all other characteristic radiation, the proportion of the total radiation reaching the chamber which is K-radiation will be increased if a suitable differential absorber D is placed in the path of the secondary radiation. A suitable material for this differential filter is that of which the secondary radiator C is made, as any material has a low absorption coefficient for its own K-radiation, and a higher absorption coefficient for radiation of longer wavelength. Nevertheless a material of atomic number higher than that of the secondary radiator is also effective.

In Fig. 2 are shown the results of measurements made on a line focus, stationary anode tube in a two-valve half-wave

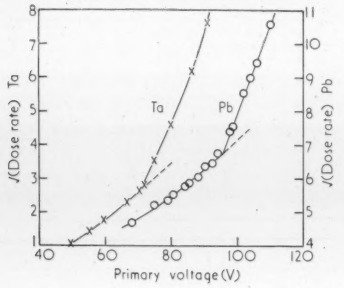

Fig. 2. Tantalum and lead K-radiation thresholds for a two-valve, half-wave, line focus, stationary anode unit

circuit. The readings of a voltmeter connected across the primary of the h.t. transformer are plotted against the square root of the ionization current in a 500 cm^3 chamber. The irradiated materials were tantalum (K-edge at 67·6 kV) and lead (K-edge at 88·2 kV), the differential filters being 0·1 mm lead and 0·5 mm lead respectively.

Fig. 3 shows similar results for a hooded anode self-rectified therapy tube. It will be seen that the square root of the ionization current is almost a linear function of the voltage, the slope changing as K-radiation is produced.

The value of the method depends on the accuracy with which the point at which the slope changes may be determined, and this accuracy increases as the angle between the two straight lines increases. Any improvement of accuracy would seem to depend on reducing the "background" of scattered radiation reaching the measuring instrument, and this is most readily done by increasing the thickness of the differential absorber. However, if this absorber is made too thick the quantity of K-radiation reaching the detector becomes too small for accurate measurement. It is possible that a Geiger counter, with its increased sensitivity over the ionization chamber, would allow of the use of a thicker differential absorber, with a consequent sharper change of slope.

(ii) *Emission of photo- and Auger electrons.* The ionization in a chamber of very small electrode spacing irradiated by monochromatic X-rays should show a sudden increase as the X-ray wavelength is changed from one just on the long wavelength side of the K-absorption edge of the wall material of the chamber to one just on the short wavelength side, as there will be an increase of the photoelectron (and associated Auger electron) emission from the walls. In a practical case with a heterogeneous X-ray beam, the sudden increase would be masked (*a*) by the ionization produced by the X-rays of wavelength longer than the K-absorption edge, and (*b*) by the ionization produced by electrons liberated in the air of the chamber rather than in the chamber walls themselves. For the effect to be apparent, therefore, the X-ray beam should be very heavily filtered and the ionization chamber should have the smallest practical electrode spacing.

Even with these precautions it is unlikely that it would be possible to detect a change in slope of the ionization *versus* kilovoltage curve, and consequently, in applying this method to the measurement of kilovoltage, the *ratio* of the ionizations in two chambers lined with materials of about the same atomic number has been measured. Both chambers then show approximately the same variation of ionization with X-ray wavelength for all radiation except that lying between the K-absorption edges of the chamber lining materials. Furthermore, the *ratio* of the ionizations in two chambers may be measured with great accuracy using a Kemp comparator.[1,2]

Some results of measurements made on a hooded anode self-rectified therapy tube using two chambers lined with

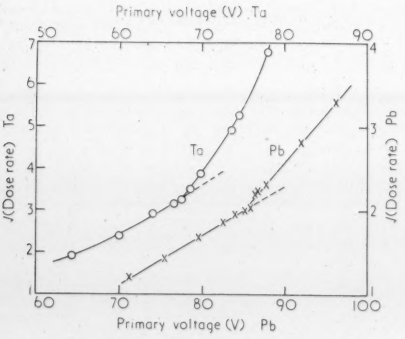

Fig. 3. Tantalum and lead K-radiation thresholds for a self-rectified, hooded anode, therapy unit

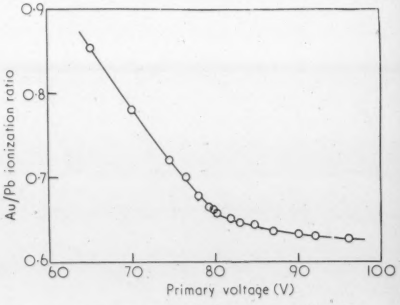

Fig. 4. Gold, photo- and Auger electron threshold for a self-rectified, hooded anode, therapy unit

gold leaf and lead foil respectively and a primary filter of 0·5 mm lead are shown in Fig. 4. The absorption in the gold leaf was negligible, but to overcome any difference in wavelength response of the chambers due to absorption in the rather thicker (0·1 mm) lead foil lining one chamber, the other chamber had a similar thickness of lead foil wrapped round it.

The change of slope shown in Fig. 4 is not as sharp as might be desired, and in fact, although there is a sudden increase in absorption as the K-edge of the chamber material is crossed, all this energy does not appear as kinetic energy of electrons, and for the wavelength of the K-edge the photoelectrons have no kinetic energy, only just escaping from the atom whose K-shell they have vacated. It is possible, therefore, that no *sharp* change of slope should be expected.

(iii) *Additional absorption of primary beam as K-edge is crossed.* A graph of ionization current *versus* kilovoltage for a chamber irradiated through a thick filter should show a change in slope as the kilovoltage corresponding to the K-absorption edge of the filter is reached. However, as in the previous section, the change of slope would be masked by the presence of radiation other than that at the short wavelength limit of the spectrum, and by the rapid variation of ionization with kilovoltage. Similar methods can be adopted to overcome these masking effects, namely to measure the *ratio* of the ionizations in two chambers, the radiation reaching which has been absorbed by one of two different materials of approximately the same atomic number, and furthermore has been heavily absorbed so that only radiation near the short wavelength limit remains in the beam.

Results showing the variation with kilovoltage of the ratio of the ionizations in two 6 cm³ chambers are given in Fig. 5.

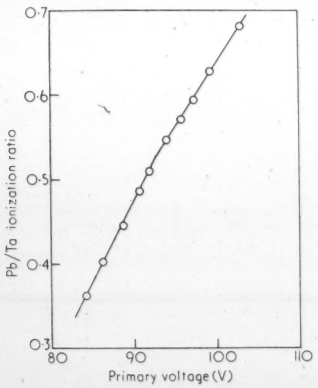

Fig. 5. Detection of lead K-absorption edge

The radiation reaching one chamber had been filtered by approximately 0·4 mm of tantalum and that reaching the other had passed through 0·5 mm of lead. The change in slope corresponding to the lead K-edge is very small, but could probably be increased by more careful matching of the absorber thicknesses and attention to other detail. This method has not been pursued further because of the success of the method described in the next section.

IMPROVED METHOD OF DETECTING THRESHOLD OF K-RADIATION EMISSION

Of the methods so far described for detecting a phenomenon associated with the K-absorption edge of a secondary absorber or emitter, that which attempts to detect the threshold of the emission of characteristic radiation is the most promising. An attempt has been made to improve this method by (*a*) monitoring the radiation output, (*b*) using a null method of measurement with consequent increased sensitivity, and (*c*) combining the emission of K-radiation with the additional absorption on the short wavelength side of the K-edge.

The experimental arrangement is the same as that shown in Fig. 1 with the addition of a 6 cm³ chamber placed just below the irradiated sheet *C*. This chamber measures the radiation transmitted by *C* while the larger (500 cm³) chamber at *A* measures the scattered and characteristic radiation. The ratio of the ionizations in the 6 and 500 cm³ chambers is determined using a modification[3] of the previously-mentioned Kemp comparator. As the kilovoltage is increased, this ionization ratio increases, due to the increasing penetration of the irradiated sheet, until the kilovoltage of the irradiated material's K-edge is reached. The characteristic radiation, which on further increase of kilovoltage reaches the 500 cm³ chamber, reverses the trend in the ionization ratio, as may be seen in Figs. 6, 7 and 8.

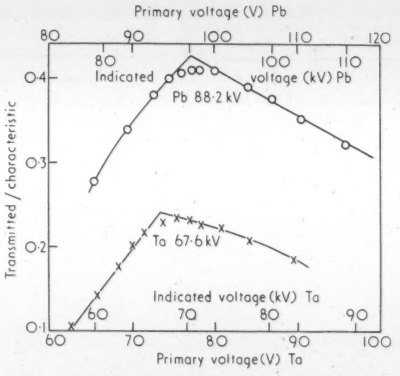

Fig. 6. Tantalum and lead K-radiation thresholds for a two-valve, half-wave line focus stationary anode unit (improved method)

In calibrating these three different types of X-ray unit, the K-radiation of cerium, tantalum or lead was excited. The tantalum and lead secondary radiators were sheets of the pure metal 0·4 mm and 1 mm thick respectively. The cerium radiator consisted of a layer of the pure oxide spread at approximately 0·1 gm/cm² on a $\frac{1}{16}$ in. sheet of perspex and retained by a sheet of Cellophane. The differential filter was 0·1 mm of lead.

The kilovoltage of the unit of Fig. 6 was normally adjustable only in steps of 10 kV. For purposes of calibration smaller increments were obtained, but the ratio of transmitted to characteristic radiation had to be plotted against the voltage fed to the primary of the high tension transformer rather than against the nominal kilovoltage, although this has been

shown at the 10 kV intervals for which it was known. The calibration showed that the 70 kV stud indicated correctly, while at the 90 kV stud setting the true voltage was 88 kV. While this may be regarded as satisfactory, the unit of Fig. 7 indicated 5 kV higher than true kilovoltage at the lead point (88·2 kV) and that of Fig. 8 will be seen to read 6½ kV high at the tantalum point (67·6 kV).

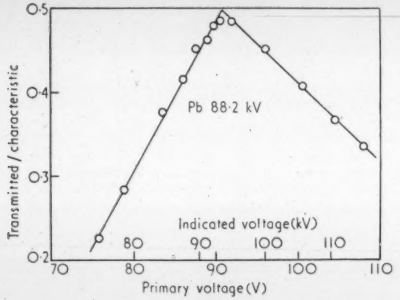

Fig. 7. Lead K-radiation threshold for a self-rectified, hooded anode, therapy unit (improved method)

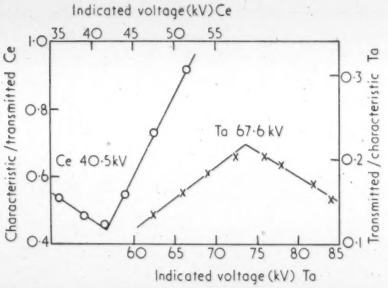

Fig. 8. Cerium and tantalum K-radiation thresholds for a four-valve, full-wave, line focus rotating anode unit

The results obtained on the line-focus stationary anode tube (Fig. 6) show a smoother transition as the K-edge is passed through than those of any other machine yet examined and this has been apparent in the results obtained by other methods on this machine. This may be an indication that the voltage waveform is peaky and the current waveform flat-topped, with the result that the radiation which is produced at peak voltage is a small proportion of the whole. The converse would be the case if the voltage waveform was flat-topped and the current waveform was peaky. It would be inferred that a constant potential generator should give a sharper transition than a half- or full-wave generator, and the results which have been obtained on a constant potential generator (Fig. 9) certainly show very sharp transitions. (At the two points calibrated the indicated kilovoltage is about 2 kV less than the true voltage.) In general it would be expected that the transition would be sharp for an X-ray beam having a steep rise in its spectral distribution curve at the short wavelength limit, since it is the radiation corresponding to the shaded area of Fig. 10 that can produce characteristic radiation, this area being roughly proportional to $(\lambda_k - \lambda_0)^2$ for small values of $\lambda_k - \lambda_0$ and the constant of proportionality depending on the slope of the portion $\lambda_0 A$ of the spectral distribution curve.

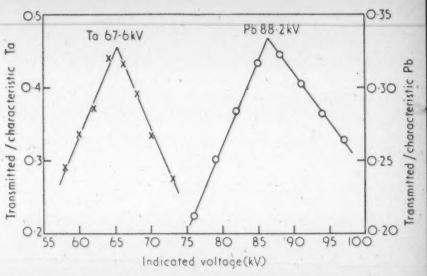

Fig. 9. Tantalum and lead K-radiation thresholds for a constant potential, line focus, rotating anode unit

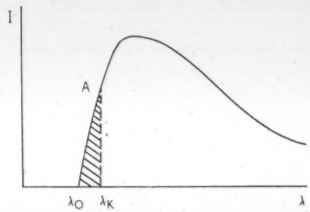

Fig. 10. Illustrating factors affecting the sharpness of transitions near K-absorption edges

An additional advantage of this method over that relying solely on the detection of K-radiation is that readings need only be taken over about 10 kV (or even less) on either side of the particular kilovoltage being calibrated, whereas the latter method requires measurements over 15 to 20 kV on either side of the K-edge. The former method, therefore, not only reduces the measurements required but makes possible the checking of the voltage at points within 5 to 10 kV of the upper and lower limits of kilovoltage at which a machine may be operated.

CALIBRATION POINTS AVAILABLE

In theory, calibration points are available from the kilovoltage corresponding to the K-edge of the latest transuranic element downwards. In practice, limitations are imposed by the rarity of some elements and the unsuitable form of others. A list of elements which might be of practical use either as element, salt or oxide is given in the table. It may be seen that there is a considerable gap between elements 73 and 58 (kilovoltages of 67·6 and 40·5). All the elements 59 to 71 are rare earths which are difficult to obtain uncontaminated by others of neighbouring atomic numbers.

However, cerium is readily obtainable as the pure oxide and provides a convenient calibration point towards the lower end of the scale for machines which can be operated down to 30 or 35 kV. While tantalum is suitable for checking an intermediate voltage, the kilovoltage of the lead K-edge (88·2) is unfortunately a little too high for many existing diagnostic X-ray generators (but not those likely to be installed in the future) since it is necessary to take readings up to about 10 kV above the point being checked.

List of elements of possible use for kilovoltage calibrations

At. No.	*Element*	*Kilovoltage of K-edge*
92	Uranium	116·3
90	Thorium	110·0
83	Bismuth	90·7
82	Lead	88·2
81	Thallium	86·0
80	Mercury	83·2
79	Gold	80·9
78	Platinum	78·6
77	Iridium	76·5
74	Tungsten	69·6
73	Tantalum	67·6
58	Cerium	40·5
56	Barium	37·5
52	Tellurium	31·9
50	Tin	29·3
47	Silver	25·6
46	Palladium	24·4
42	Molybdenum	20·0

THE MEASUREMENT OF KILOVOLTAGE AT HIGH TUBE CURRENTS

The measurement of kilovoltage by normal methods at high tube currents presents additional difficulties because of the short exposure times which can be permitted. However, none of the techniques previously described are fundamentally affected by the use of high tube currents. In practice, it may be difficult to keep the ionization chambers working under saturation conditions, but any variation in the degree of saturation as the kilovoltage is increased should not obscure the transition being observed. Fig. 11 shows the calibration of the tantalum point (67·6 kV) for a full-wave rectified unit at 6, 200 and 400 mA. It will be seen that the indicated kilovoltage is 1½ kV high at 6 mA and 6½ kV low at 400 mA, an overall change of 8 kV with milliamperage, showing that the unit has been appreciably overcompensated for voltage drop under load.

Unfortunately, all these methods involve several measurements in the determination of any one kilovoltage. It is very desirable in the complete voltage calibration of an X-ray apparatus at several milliamperages, that the peak kilovoltage at any nominal kilovoltage and milliamperage should be determinable from a single measurement. Once the kilovoltage calibration has been established at one particular milliamperage it is possible to calibrate some function of kilovoltage, such as the percentage of X-rays transmitted by an absorber, against kilovoltage at this milliamperage, and subsequently to use the percentage X-ray transmission as a measure of kilovoltage at other milliamperages. This principle has been applied in deriving the results shown in Fig. 12. The ratio of the ionizations in two chambers, one of which was covered with 0·1 mm copper, has been plotted against the

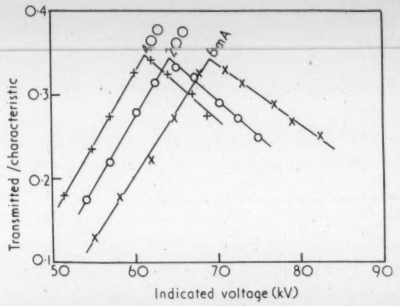

Fig. 11. Calibration of tantalum point (67·6 kV) at 400, 200 and 6 mA on a four-valve, full-wave, line focus, rotating anode unit

nominal kilovoltage for tube currents of 6, 200 and 400 mA. If the voltage drops at the various currents had been correctly compensated and there were no waveform changes, the curves for the three tube currents would have been coincident. In fact, the voltage drop at the high currents had been overcompensated, and for the same true kilovoltage, i.e. the same ionization ratio, the nominal kilovoltage at 400 mA had to be 7½ kV less than that at 6 mA in the region of 60–70 kV, in good agreement with the value of 8 kV (see Fig. 11) found by the more direct method.

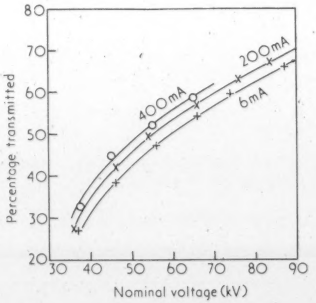

Fig. 12. Variation of transmission through 0·1 mm copper with nominal kilovoltage at 400, 200 and 6 mA on a four-valve, full-wave, line focus, rotating anode unit

It must be emphasized that this method, using a copper absorber, is really a measure of X-ray quality rather than a measure of true peak kilovoltage, and exact agreement with the method measuring kilovoltage can only be expected if

there are no waveform changes when the tube current is varied. In another case examined in detail it was found that the nominal kilovoltage was 6 kV high at 3 mA and 2 kV low at 300 mA, when using the true kilovoltage method. Thus while an 8 kV difference in nominal kilovoltage was required to give the same true peak value, it was found that a difference of only 4 kV was needed to give the same "quality" reading, i.e. percentage transmission through a copper absorber.

Some of the practical points involved in the copper absorber method of measuring kilovoltage warrant discussion. Fig. 12 shows that over the greater part of the kilovoltage range the percentage transmitted varies by about 0·7 per kV. The ratio, therefore, needs to be accurately measured if the kilovoltage is to be determined closely. The comparator described by Kemp[1,2] has been of great value for this purpose.

The ionization chambers used must be of sufficient volume to collect an adequate charge during an exposure of 5 to 10 sec when using screening currents at 40 kV, but at the same time must remain saturated when using 400 mA, say, at the maximum allowable kilovoltage. The dose rates to be dealt with thus cover a range of a few hundreds to one, and to achieve saturation with reasonable polarizing voltages at the maximum dose rates, chambers with plane parallel electrodes are necessary. The chambers used are illustrated in Fig. 13.

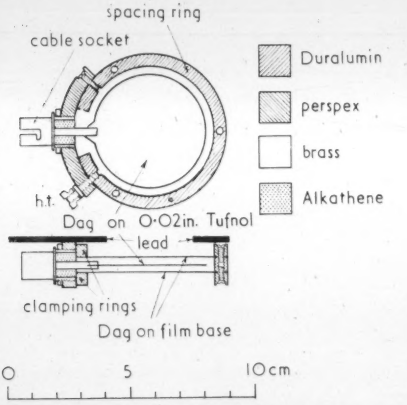

Fig. 13. Type of ionization chamber used for measurements at high dose rates and short exposures

The absorber used should have a large variation of absorption coefficient in the kilovoltage range to be investigated but should not have an absorption edge in this range. The thickness of absorber should be the maximum that will keep the ionization ratio within the range of the measuring instrument for all kilovoltages to be measured. This thickness will increase as the filtration of the X-ray beam is increased. A suitable absorber has been found to be 0·05 mm of copper for unfiltered beams in the 35 to 85 kV range, or 0·1 mm of copper for beams filtered by 2 mm aluminium, which is the filter normally inserted into machines used for radiography at this hospital.

COMPARISON WITH TECHNIQUE OF "RADIOGRAPHIC CALIBRATION"

A method commonly adopted at present for determining the voltage drop occurring at a high tube current is to make a series of exposures all with the same milliampere-seconds of an aluminium step wedge placed on a film or film-screen combination. The first exposure is made at the required kilovoltage using a low tube current where the kilovoltage is known or assumed to be correct. The others (probably three in number) are made at the high tube current and a series of nominal kilovoltages within the range of which the true kilovoltage is thought to lie. After development of the film the nominal kilovoltage required at the high milliamperage to produce the same blackening as for the low milliamperage may be assessed (using a densitometer if necessary) if this kilovoltage lies within the range for which exposures were made at the high milliamperage.

This technique has the advantage that with the exception of the densitometer the apparatus required is extremely simple. As a photographic method of measurement is used to assess the conditions required in practice to produce a given photographic effect, there is automatic compensation for any reciprocity law failure that may occur when using screen-film combinations.

(Morgan[4] has examined reciprocity law failure for four X-ray films exposed with fluorescent screens. For exposures between 0·1 and 1·0 sec the speed varied, on the average, by only $\pm 5\%$, and reducing the exposure to 0·02 sec increased the variation in only one of the four cases. Between exposures of 1 and 10 sec the speed fell by about 30%. Since in modern medical radiography exposures of 1 sec are rarely appreciably exceeded, it is concluded that reciprocity law failure is of little practical significance in the great majority of cases, and it is for this majority that the kilovoltage calibration should cater. With non-screen exposures there is no reciprocity law failure.[5])

There is also compensation for any lack of proportionality between tube output and milliamperes. The disadvantage of the method is that it is tedious and time-consuming, necessitating many tube exposures and using an appreciable quantity of film. It is not known until after the films have been developed whether the correct kilovoltage setting has been included in the range over which exposures were made. Furthermore, the milliampere-seconds have to be accurately controlled.

In contrast, the ionization chamber method described in the last section gives a direct reading of the kilovoltage once the ionization ratio has been plotted against kilovoltage at a low milliamperage, as would be done in an extended calibration. The method is therefore quick, few tube exposures are required, there are no extra expenses and the results are known immediately. Furthermore, since an ionization *ratio* is being measured it is not necessary to measure the exposures or control them accurately. The disadvantages of the method are that it requires more complex apparatus than the photographic method, and does not allow for any lack of proportionality between tube output and milliamperes.

REFERENCES

(1) Kemp, L. A. W. *Brit. J. Radiol.*, **18**, p. 107 (1945).
(2) Kemp, L. A. W. *Brit. J. Radiol.*, **19**, p. 233 (1946).
(3) Greening, J. R. *Brit. J. Radiol.*, **26**, p. 53 (1953).
(4) Morgan, R. H. *Radiology*, **42**, p. 471 (1944).
(5) Greening, J. R. *Proc. Phys. Soc.* [*London*] *B*, **64**, p. 977 (1951).

Elastic work involved in rolling a sphere on another surface

By D. Tabor, Ph.D., The Laboratory for the Physics and Chemistry of Surfaces, University of Cambridge

[*Paper first received* 25 *May, and in final form* 14 *August*, 1954]

A theoretical calculation is made of the elastic work involved in rolling a ball over another surface. The analysis is based on Hertz's equation for the static deformation of spherical surfaces since it is assumed that the additional stresses produced by rolling are small compared with those produced by the normal load. The results show that the work involved in rolling a sphere on a flat surface is substantially the same as that involved in rolling a sphere in a groove of almost the same curvature as the sphere. This conclusion is in line with certain previous work by the author on the rolling friction of steel spheres on rubber.

In the course of an investigation of the mechanism of rolling friction in the elastic range[1] it was found that differential slip between the rolling surfaces[2, 3] could account for only a very small fraction of the rolling resistance. It seemed that a major part of the resistance to rolling arose from elastic hysteresis losses and it was therefore necessary to calculate the total amount of elastic energy involved in rolling. Calculations for cylindrical surfaces are not easy, but for spherical surfaces the Hertzian equations may be directly applied and a relatively simple result is obtained.

In the treatment here we assume that the tangential forces generated between the rolling surfaces are very small compared with the normal forces. This is generally true. This means that we may assume the stresses and strains to be substantially the same as those taking place under conditions of static loading. The problem then simply becomes one of calculating from Hertz's equations the elastic work done when one surface rolls over the other surface through unit distance.

1. Ball Rolling on a Flat

Suppose the ball has a radius r_1, Young's modulus E_1 and Poisson's ratio σ_1, and the flat surface has a Young's modulus E_2 and Poisson's ratio σ_2. Under a normal load W_0 a circle of contact of diameter $2a_0$ is formed. The elastic work done in forming such a circle of contact has already been described[4] and has the value

$$\frac{3}{10}\frac{W_0^2}{a_0}f(E)$$

where $$f(E) = \left(\frac{1-\sigma_1^2}{E_1} + \frac{1-\sigma_2^2}{E_2}\right)$$

Consider in the first instance a line of contiguous-stepped impressions of the ball. There are $1/(2a_0)$ such impressions per centimetre of track [Fig. 1(*a*)]. Then the elastic work of rolling per centimetre is simply

$$\phi = \frac{3}{20}\frac{W_0^2}{a_0^2}f(E) \qquad (1)$$

This is clearly an underestimate since between each individual indentation there are undeformed patches. Further, both the amount of deformation and the normal pressure distribution in each indentation fall off from the centre to the edge, whereas in rolling, every portion of the surface is ultimately subjected to the deformation and stress occurring across the central band [Fig. 1(*b*)]. It is indeed evident that the work done on the central band as it rolls out its path is the true measure of the elastic work of rolling. We calculate the energy involved in forming the central band of any individual indentation in the following way. From Hertz's equations we determine the load supported by the central band at some intermediate value W of the applied load and then consider the incremental distance the surfaces sink together over this band as the load is increased by ΔW. The integral of the work done in this process up to the full load W_0 gives the total elastic work expended in forming the central band of the full indentation.

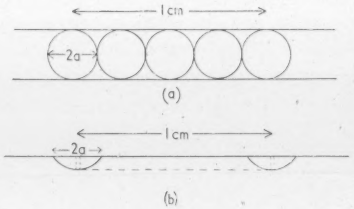

Fig. 1. Rolling of a sphere over a flat surface producing an elastically deformed groove of width $2a$

(*a*) Crude model assuming grooved track is composed of a series of contiguous circular impressions.

(*b*) Model showing that every portion of the surface is ultimately subjected to the deformation across the central band.

Load. Suppose when the applied load is W the circle of contact has radius a, the rolling direction being along the x-axis. Take the centre of the circle as the origin [Fig. 2(*a*)]. According to the Hertzian pressure distribution the normal pressure at any point Q on the y-axis is given by

$$P = P_0\left(1 - \frac{y^2}{a^2}\right)^{\frac{1}{2}} \qquad (2)$$

where P_0 is the maximum pressure at the centre. For this pressure distribution P_0 is $\frac{3}{2}\times$ (the mean pressure) so that $P_0 = 3W/2\pi a^2$.

Hence $$P = \frac{3}{2}\frac{W}{\pi a^2}\left(1 - \frac{y^2}{a^2}\right)^{\frac{1}{2}} \qquad (3)$$

The total load w supported by this band of width dx is simply

$$w = \int_{-a}^{a} P\,dx\,dy = \frac{3}{4}\frac{W}{a}dx \qquad (4)$$

Distance of approach. We must now consider what happens when W is increased by dW. On the one hand the circle of contact grows by da and the band as a whole sinks in. Fortunately, the incremental distance by which the surfaces approach is everywhere constant. This follows because the common interface of contact is a sphere of constant radius whatever the load. It may be shown analytically in the following way.

For a sphere resting on a flat, the element P originally on the flat [Fig. 2(*b*)] is depressed by a distance[5]

$$\Sigma_1 = \frac{3}{4}\frac{W}{a^3}\frac{1-\sigma_2^2}{E_2}\left(a^2 - \frac{e^2}{2}\right) \tag{5}$$

The ball is compressed by a similar term Σ_2, so that the load over the point P has descended a total distance

$$\eta = \Sigma_1 + \Sigma_2$$
$$= \frac{3}{4}\frac{W}{a^3}f(E)\left(a^2 - \frac{e^2}{2}\right)$$

Since in the elastic deformation of spherical surfaces the circle of contact always has a radius proportional to $W^{\frac{1}{3}}$ we

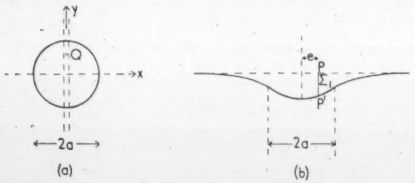

Fig. 2. (*a*) Figure to illustrate calculation of load supported across the central band of the circle of contact. (*b*) Elevation showing depression of a flat surface by a spherical surface

may replace W/a^3 by W_0/a_0^3, the final values of these quantities. Hence

$$\eta = \frac{3}{4}\frac{W_0}{a_0^3}f(E)\left(a^2 - \frac{e^2}{2}\right) \tag{6}$$

If now W is increased by dW, we have

$$d\eta = \frac{3}{2}\frac{W_0}{a_0^3}f(E)ada \tag{7}$$

Thus $d\eta$ is independent of e and is constant everywhere.

Work done. The work done on the central band as the total load increases from 0 to W_0 is then obtained from equations (4) and (7) and is given by

$$\int_{a=0}^{a=a_0} w\,d\eta = \frac{9}{32}\frac{W_0^2}{a_0^5}f(E)dx$$

This work is the elastic energy over the width dx of the band. Consequently if every element is subjected to this deformation and stress the elastic work done per centimetre of rolling is simply

$$\phi = \frac{9}{32}\frac{W_0^2}{a_0^5}f(E) \tag{9}$$

This is nearly twice as great as the value given by the crude estimate in equation (1).

2. SPHERE ROLLING IN A GROOVE

Suppose a sphere of radius r_b rolls in a straight groove of radius of curvature r_t. An ellipse of contact is formed, the shape of which remains constant whatever the load.

For reasons similar to those discussed above, every element of the ellipse of contact sinks in by the same increment when the load is increased by a small amount. If at load W the major and minor axes are a and b respectively the overall distance by which the surfaces approach at the *centre* of the ellipse of contact is given by[6]

$$\eta = \frac{3}{2}\frac{W}{a}\frac{K}{\pi}f(E) \tag{10}$$

where K is an elliptic integral depending only on the ratio a/b. If the final load W_0 produces an ellipse of semi-major axis a_0 we again have

$$W_0/a_0^3 = W/a^3 \tag{11}$$

so that W/a in equation (10) may be replaced by $(W_0/a_0^3).a^2$. Hence for an increment in load dW producing an increment da in a, the incremental depth sunk at the centre and at all other points on the ellipse of contact is

$$d\eta = \frac{3W_0}{a_0^3}\frac{K}{\pi}f(E)ada \tag{12}$$

Once again, therefore, we may calculate the elastic work done on a narrow band of width dx running across the central major axis of the ellipse.

According to Hertz the pressure distribution across the axis is the same as in equation (2) except that now $P_0 = 3W/2\pi ab$.

The load w supported on this band, corresponding to equation (4), is

$$w = \frac{3}{4}\frac{W}{b}dx = \frac{3}{4}\frac{W_0}{a_0^3}\frac{a^3}{b}dx \tag{13}$$

We use the identity $a/b = a_0/b_0$ to eliminate b. This gives

$$w = \frac{3}{4}\frac{W_0}{a_0^3}\frac{a_0}{b_0}a^2dx \tag{13a}$$

The elastic work done on this strip as the total load increases from 0 to W_0, i.e. as the semi-major axis increases from 0 to a_0 is

$$\int_{a=0}^{a=a_0} w\,d\eta = \frac{9}{16}\frac{W_0^2}{a_0^5}\frac{a_0}{b_0}\frac{K}{\pi}f(E)dx$$

Hence again, if every element during rolling is subjected to the deformation process occurring across the central band, the elastic work done per centimetre of rolling is

$$\phi = \frac{9}{16}\frac{W_0^2}{a_0^5}\frac{1}{\pi}f(E)K\frac{a_0}{b_0} \tag{14}$$

Note that for a circular instead of elliptical contact $a_0/b_0 = 1$ and $K = \pi/2$, so that this equation reduces to equation (9).

The value of K depends only on the ratio a_0/b_0 itself and this in turn depends only on the ratio of the groove or track radius r_t to the ball radius r_b. Consequently the value of Ka_0/b_0 may be expressed solely in terms of the ratio r_t/r_b. Some approximate values of these parameters and of the quantity m (see below) have been calculated and plotted in nomogram form in Fig. 3.

3. DEPENDENCE OF ϕ ON THE RATIO r_t/r_b

It should be borne in mind that for any given materials, a_0 will also vary with the ratio r_t/r_b and it is of considerable

interest to see how the resultant value of ϕ varies for different values of this ratio. For convenience we shall therefore compare the work ϕ_0 involved in rolling a ball on a flat ($r_t/r_b = \infty$) with the work ϕ_1 involved in rolling the same ball under the same load in a groove.

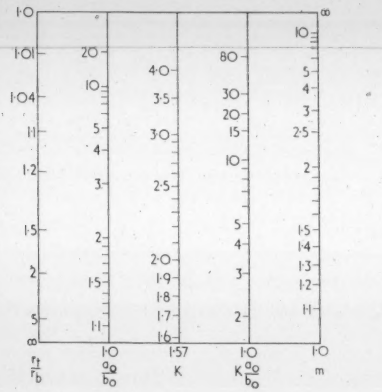

Fig. 3. Approximate values of various parameters tabulated in scalar form. For any point on the r_t/r_b scale the corresponding values of the other parameters are obtained by drawing a horizontal line through the given point

We first calculate ϕ_1. For a sphere of radius r_b resting in a groove of radius r_t, the semi-major axis a_0 of the ellipse of contact is given by the relation

$$a_0 = m\left[\frac{3}{2}W_0 f(E)\left(\frac{2}{r_b} - \frac{1}{r_t}\right)^{-1}\right]^{\frac{1}{3}} \qquad (15)$$

where m is determined solely by the ratio r_t/r_b. Inserting in equation (14) we have

$$\phi_1 = \frac{9}{16}\frac{W_0^{4/3}[f(E)]^{\frac{1}{3}}K\left(\frac{a_0}{b_0}\right)}{m^2\left(\frac{3}{2}\right)^{\frac{1}{3}}\pi}\left(\frac{2}{r_b} - \frac{1}{r_t}\right)^{\frac{1}{3}} \qquad (16)$$

We may at once use this to determine ϕ_0 by noting that for a ball rolling on a flat $r_t = \infty$, $Ka_0/b_0 = \pi/2$ and $m = 1$

$$\phi_0 = \frac{9}{16}\frac{W_0^{4/3}[f(E)]^{\frac{1}{3}}}{2\left(\frac{3}{2}\right)^{\frac{1}{3}}}\left(\frac{2}{r_b}\right)^{\frac{1}{3}} \qquad (17)$$

Then

$$\frac{\phi_1}{\phi_0} = \frac{2}{\pi m^2}K\left(\frac{a_0}{b_0}\right)\left[\left(\frac{r_t}{r_b} - \frac{1}{2}\right)\Big/\left(\frac{r_t}{r_b}\right)\right]^{\frac{1}{3}} \qquad (18)$$

It is seen that m and Ka_0/b_0 depend only on the ratio r_t/r_b (see Fig. 3) so that ϕ_1/ϕ_0 also depends only on this ratio. Detailed calculation shows that for r_t/r_b ranging from 1·04 to ∞, the ratio ϕ_1/ϕ_0 ranges from 0·96 to 1·0. This means that the elastic work of rolling is almost the same whether the sphere rolls on a flat or in a groove of almost the same curvature.

The physical reason for this striking result is clear in terms of the rough picture described above. When a ball rolls in a groove of almost its own curvature the ellipse of contact is an extremely narrow one. The elastic work done in forming any individual ellipse of contact is small but the number of ellipses per centimetre of path is large. In contrast, a sphere resting on a flat makes a circle of contact. The elastic work done in forming such an impression is relatively large but a small number of circles is required per centimetre of path. As a result the work done in both cases is substantially the same. We may therefore use equation (17) to calculate the work of rolling a sphere of radius r_b over a surface without specifying in detail the shape of the groove involved. The result is

$$\phi = 0{\cdot}34W_0^{4/3}[f(E)/r_b^2]^{\frac{1}{3}} \qquad (19)^*$$

This relation has been examined for steel spheres rolling on rubber surfaces. Cyclic loading and unloading experiments show that the hysteresis losses in the rubber are independent of the magnitude of the deformation but dependent on the speed of deformation. For constant speeds of deformation the losses in the rubber during rolling, according to equation (19), should therefore be proportional to $W^{4/3}$. If we assume losses in the steel to be negligible it follows that the rolling force should be proportional to $W^{4/3}$. Experiments with steel spheres rolling on flat rubber surfaces showed that this is indeed so.(1) Similar experiments for balls rolling in grooves machined in the rubber surface gave substantially the same results, except for very deep grooves where there was evidence of a slip component similar to that originally suggested by Heathcote.(3) Finally, the rolling experiments were carried out on two types of rubber of the same Young's modulus but of widely differing hysteresis losses.(1) The observed frictional values agree with the calculated elastic energy values [equation (19)] if hysteresis loss factors of 12% for one rubber and 1·3% for the other are assumed. Direct determination of the hysteresis losses under cyclic normal loading gave values of 11% and 1·4% respectively. The agreement is very satisfactory. A recent investigation shows that similar considerations apply in the rolling of spheres on metal surfaces. This will be discussed in greater detail elsewhere.(7)

REFERENCES

(1) TABOR, D. *Phil. Mag.*, **43**, p. 1055 (1952).
(2) REYNOLDS, O. *Phil. Trans*, **166**, p. 1 (1875).
(3) HEATHCOTE, H. L. *Proc. Inst. Aut. Eng.*, **15**, p. 569 (1921).
(4) TABOR, D. *The Hardness of Metals*, p. 119 (Oxford: Clarendon Press, 1951).
(5) PRESCOTT, J. *Applied Elasticity*, p. 631 (London: Longmans, Green and Co. Ltd., 1927).
(6) ALLAN, R. K. *Roller Bearings*, p. 107 (London: Sir Isaac Pitman and Sons Ltd., 1945).
(7) ELDREDGE, K. R., and TABOR, D. *Proc. Roy. Soc.* To be published (1955); ELDREDGE, K. R. *Ph.D. Dissertation* (University of Cambridge, 1952).

* The fraction of this work involved in deforming the ball is $\frac{(1-\sigma_1^2)}{E_1}\cdot f(E)$ and the fraction involved in deforming the other surface is $\frac{1-\sigma_2^2}{E_2}\cdot f(E)$.

Role of partition coefficient in permeability of surface layers with low diffusion coefficient

By G. R. Lester, Ph.D., A.Inst.P., Imperial Chemical Industries Ltd., Blackley, Manchester

[*Paper received* 2 *November*, 1954]

Diffusion through a surface film into an underlying layer is examined using Laplace transformation. An important characteristic of the process is the rate at which equilibrium concentrations are attained, and in certain cases this is simply related to the diffusion coefficient of the film and the partition coefficient at the interface.

For a number of technical applications it is required to specify the rate of diffusion of matter through a surface film into an underlying receiving layer. The effective permeability of the combination will clearly depend on the thicknesses of the layers, their diffusion coefficients and the partition coefficient at the interface; general formulae in the form of infinite series are derived relating the varying concentrations to these properties of the layers. As a particular case it may be supposed that the diffusion coefficient in the receiving layer is many times greater than that of the surface film, the concentration of diffusing substance levelling up virtually instantaneously after penetrating the film. The main purpose of this paper is to draw attention to the particular significance for this case of the partition coefficient at the interface between the layers, since the rate of attainment of equilibrium is then found to be equally dependent on this factor and on the diffusion coefficient in the film. The formulae obtained suggest that the ratio of these quantities is the appropriate physical variable to specify the effective permeability, where this is measured with regard to the rate of attaining equilibrium.

The mathematical derivation of the required relationship follows the standard procedure for discussing the diffusion equation, consequently only outlines of the derivation will be given here. (See especially Carslaw and Jaeger† where some related problems in heat conduction are discussed in detail.) In the present case the boundary conditions are as follows:

(1) no flow across a plane at $x = 0$ (i.e. impermeable substrate);

(2) flow continuous at $x = a$, the interface between the diffusing layers;

(3) the ratio of concentration at $x = a^-$ to the concentration at $x = a^+$ is a constant R, the partition coefficient;

(4) concentration at $x = a + b$ is constant and determined by that in the reservoir;

(5) initially, concentrations are everywhere zero in the diffusing layers.

In the receiving layer and the surface film the diffusion coefficients will be denoted by D^* and D respectively where $D^* \gg D$, and the diffusion process will be regarded as one-dimensional. Then, if θ denotes concentration of solute,

$$D(\partial^2\theta/\partial x^2) = \partial\theta/\partial t$$

By standard methods, the Laplace transforms for the respective layers have the following forms

$$\bar{\theta}_1 = A\cosh\sqrt{(s/D^*)}x \quad (0 \leqslant x \leqslant a)$$

$$\bar{\theta}_2 = B\cosh\sqrt{(s/D)}x + C\sinh\sqrt{(s/D)}x, \ (a \leqslant x \leqslant a + b)$$

and the boundary conditions are expressed as follows:

$$kA\sinh\sqrt{(s/D^*)}a = B\sinh\sqrt{(s/D)}a + C\cosh\sqrt{(s/D)}a$$

$$A\cosh\sqrt{(s/D^*)}a = R[B\cosh\sqrt{(s/D)}a + C\sinh\sqrt{(s/D)}a]$$

$$\phi/s = B\cosh\sqrt{(s/D)}(a + b) + C\sinh\sqrt{(s/D)}(a + b)$$

where $k = \sqrt{(D^*/D)}$ and ϕ is the fixed concentration in the film at $x = a + b$.

By the inversion theorem

$$\theta = \frac{1}{2\pi i}\int_{\sigma - i\infty}^{\sigma + i\infty} \exp(st)\bar{\theta}.ds$$

and the poles of the integrand are at $s = 0$ and where $\Delta(s) = 0$, $\Delta(s)$ being the determinant formed by the coefficients of A, B, C in the set of simultaneous equations.

It then follows that

$$\theta_1 = R\phi\left\{1 - 4\sum_{\alpha_n}\frac{\exp(-D\alpha_n^2 t/b^2).\cos(q\alpha_n x/a)}{\alpha_n\{(1 + kR)(1 + q)\sin[\alpha_n(1 + q)] + (1 - kR)(1 - q)\sin[\alpha_n(1 - q)]\}}\right\}$$

$$\theta_2 = \phi\left\{1 - 4\sum_{\alpha_n}\frac{\exp(-D\alpha_n^2 t/b^2).\cos q\alpha_n.\sin[\alpha_n(a + b - x)/b]}{\alpha_n\sin\alpha_n\{(1 + kR)(1 + q)\sin[\alpha_n(1 + q)] + (1 - kR)(1 - q)\sin[\alpha_n(1 - q)]\}}\right\}$$

where $q = a/bk = a/b\sqrt{(D/D^*)}$.

Now since we are supposing that $D^* \to \infty$, this implies that $q \to 0$ and θ_1 is independent of x. Moreover, the equation to determine the set of values α_n may then be simplified to $\alpha\tan\alpha = b/aR$, and only the smallest root $[\alpha_1 \simeq \sqrt{(b/aR)}]$ need be included in the summation for the other terms are relatively negligible on account of the smallness of the exponential factors.

Denoting by f the ratio:

$$\frac{\text{amount of solute in the permeable layer at time } t}{\text{equilibrium amount of solute in the permeable layer } (t \to \infty)}$$

after algebraic simplification one obtains

$$D/R = ab/t\log_e[1/(1 - f)]$$

The time t^* at which, say, 50% of the final solute uptake has occurred is consequently given by

$$t^* = ab.R/D.\log_e 2$$

† Carslaw, H. S., and Jaeger, J. C. *Conduction of Heat in Solids* (London: Oxford University Press, 1950).

Since this time specifies in a convenient way for many purposes the overall permeability of the film it follows that the ratio D/R is the appropriate physical magnitude to specify this permeability for given materials. It should be noted, however, that the mean rate of diffusion into the receiving layer remains independent of R, for in time t^* the amount of solute absorbed is clearly $\frac{1}{2}Ra\phi$, and consequently the mean rate of diffusion during this period $= D\phi/2b \log_e 2$. The derivation assumes, of course, that D^* is very large so that $q = (a/b)\sqrt{(D/D^*)}$ is sufficiently small.

Studies of the viscosity and sedimentation of suspensions

Part 3.—The sedimentation of isometric and compact particles†

By S. Gurel, B.Sc., Ph.D., Prof. S. G. Ward, M.Sc., Ph.D., D.I.C., and R. L. Whitmore, B.Sc., Ph.D., A.Inst.P.,‡
Department of Mining, University of Birmingham

[*Paper first received* 16 *May*, 1952, *and in final form* 8 *November*, 1954]

Series of experiments on the sedimentation of a variety of isometrically-shaped bodies are described and it is shown that the resistance to motion R, of a body moving with velocity v, in an infinite extent of fluid in the region of streamline flow is given by

$$R = v\eta K\sqrt{(\text{surface area of body})},$$

where η is the viscosity of the fluid and K a shape factor of the particle which varies from $\sqrt[3]{\pi}$ for spheres to $\sqrt[3]{2{\cdot}92}$ for tetrahedra. By using a value of $\sqrt[3]{3}$ for K the equation may be applied to isometric and other compact shapes, where the axial ratio does not exceed about 1·4 to 1, with an error not greater than $\pm 2\%$.

A more accurate, but less easily applied, empirical relationship for the settling rate of compact bodies is also given and an equation which satisfies the interference effects of the walls of a sedimentation vessel upon a falling body is developed experimentally.

Problems associated with the sedimentation of single particles are characterized by considerable theoretical and experimental difficulties, particularly when the fall of irregularly-shaped bodies is considered. With the exception of spheres, for which reliable information is available, the majority of particles investigated have been irregular in form, presumably because of the difficulties involved in producing accurate complex shapes. Shultz,[1] Pernolet[2] and Schmiedel,[3] however, have investigated the sedimentation of a number of shapes in the region of turbulent flow. Pettyjohn and Christiansen[4] made careful measurements of the settling rate of a number of well-defined, isometric bodies in the region of streamline flow and showed that Stokes' law could be extended to cover non-spherical particles by using Wadell's[5] concept of sphericity. They concluded that the terminal speed v_t of such a body under these conditions was given by

$$v_t = \frac{0{\cdot}843 \log \psi (\rho_b - \rho_l) d_s^2 g}{0{\cdot}065 \times 18\eta}$$

where ψ = (surface area of sphere having same volume as particle)/(surface area of particle)

ρ_b = density of particle

ρ_l = density of liquid

d_s = diameter of a sphere having the same volume as the particle

η = viscosity of the liquid.

Recently Kunkel[6] has investigated the magnitude of errors introduced by calculating the settling rate of dust particles from Stokes' law. The present investigations were undertaken to obtain basic data on the sedimentation of single compact particles as a basis for studying the effect of asymmetry and surface roughness upon the settling rate of single particles and suspensions in the region of streamline flow.

EXPERIMENTAL

The first experiments were made with cubes milled from polystyrene sheet and ground to exact size on a glass plate using abrasive materials of increasing fineness and softness. Fourteen were made; their dimensions (see Table 1), which ranged from 1·0 to 0·15 cm sides, were measured directly with a travelling microscope and a hand micrometer and were also calculated from density and weight determinations. The latter measurements were considered to give the more reliable

Table 1. *Properties of experimental cubes*

Cube colour	*Method of grinding**	*Density* (g/ml.)	*Length of side*		
			Hand micrometer (cm)	*Travelling microscope* (cm)	*Calculated from weight and density* (cm)
Red	*H*	1·0520	0·984	0·984	0·980
Light Green	*H*	1·0520	0·983	0·982	0·979
Dark Green	*H*	1·0522	0·993	0·993	0·988
Blue	*H*	1·0521	0·978	0·978	0·972
Brown	*M*	1·0516	0·995	0·995	0·994
Orange	*H*	1·0522	0·987	0·988	0·978
Yellow	*H*	1·0523	0·832	0·830	0·824
White 1	*H*	1·0524	0·998	0·994	0·989
White 2	*M*	1·0522	0·978	—	0·978
White 3	*M*	1·0522	0·371	—	0·370
White 4	*M*	1·0523	0·151	—	0·149
Colourless 1	*H*	1·0522	0·985	0·978	0·978
Colourless 2	*M*	1·0522	0·980	—	0·980
Colourless 3	*H*	1·0518	0·507	—	0·503

* *H* = hand ground; *M* = mechanically ground.

† Parts 1 and 2 of this paper, "The viscosity of suspensions of spherical particles" and "The viscosity and sedimentation of suspensions of rough powders," were published on pp. 286 and 325 of Volume 1 (1950) of this Journal.

‡ Now at the University of Nottingham.

values and were used in the subsequent calculations. The side-lengths of the hand-ground cubes varied by less than 0·7% and those of the mechanically-ground particles by less than 0·1%.

The sedimentation tank consisted of a cylindrical glass vessel 30·2 cm diameter and 46 cm high. Four open-ended glass cylinders of diameters 6·22, 8·04, 15·5 and 21·7 cm could be inserted axially in the tank, in order to alter the wall effect on the settling bodies. A few experiments were made also in vessels of 3·20 and 2·49 cm diameter, in which the wall effect was considerable. The tank was immersed in a water-bath, thermostatically controlled at 20° C ± 0·05°. Six mercury-in-glass thermometers capable of being read to 0·02° C showed no measurable temperature fluctuations during two days' observations when immersed at various depths and positions in the liquid. The sedimentation liquid was B.P. quality castor oil which had a viscosity of 9·86 P when measured in N.P.L.-calibrated Ostwald tubes used in accordance with B.S. Specification 188-1937. A pyknometer determination of density of the castor oil gave a value of 0·9615 g/ml.

The dropping apparatus allowed the cubes to be introduced into the sedimentation tank without removing the lid and to be released from below the level of the castor oil at any desired orientation after they had attained the temperature of the oil. Preliminary experiments showed that the particle had to fall at least ten diameters before constant velocity was attained and that retardation began when it was four to five diameters from the base of the vessel. The particles were viewed through a travelling microscope and timed over a distance of 17·0 cm in the middle of their fall to within 0·002 cm, with a stop-watch which could be read to 0·1 s. The Reynolds number did not exceed 0·07 in any experiment. The settling rate of each particle was measured at least five times and the arithmetic mean value was used for subsequent calculations.

RESULTS

The work of Stokes[7] and others has shown that the resistance to motion of a body moving under conditions of streamline flow is proportional to its linear dimensions, its velocity and the viscosity of the surrounding medium. For cubes, Pettyjohn and Christiansen[4] showed that the proportionality constant was about 12·7. For spheres, the proportionality constant is 18 when sphere diameter is used as the linear dimension in Stokes' equation. Assuming a value of 18, the settling velocity v_c of cubes should be given by the equation

$$v_c = [l_c^2(\rho_c - \rho_l)g]/18\eta \qquad (1)$$

where l_c = length of side of cube
ρ_c = density of cube
ρ_l = density of liquid
η = viscosity of liquid.

The settling velocity of each cube in each vessel was calculated from this equation (Table 2) and if the value of 18 selected for the constant had been correctly chosen, the calculated settling velocities would have equalled the measured velocities corrected to an infinite expanse of liquid. In Fig. 1 the ratio l/D of the length l, of the side of each cube to the diameter D, of the sedimentation vessel is plotted against the ratio v_m/v_c where v_m is the measured and v_c the calculated settling velocity. The extrapolated line intersects the velocity axis at a value of 1·418; if the correct value for the proportionality constant had been selected the line should

Table 2. *Sedimentation of cubes.*

Vessel diameter D (cm)	Cube colour	Ratio l_c/D	Average* observed velocity v_m (cm/s)	Velocity calculated from equation (1) v_c (cm/s)	Ratio v_m/v_c
30·2	Red	0·0324	0·634	0·480	1·321
	Light Green	0·0324	0·638	0·479	1·332
	Dark Green	0·0327	0·655	0·489	1·339
	Blue	0·0322	0·637	0·472	1·350
	Brown	0·0329	0·652	0·491	1·327
	Orange	0·0324	0·638	0·479	1·332
	Yellow	0·0273	0·447	0·340	1·314
	White 1	0·0327	0·658	0·491	1·340
	White 3	0·0122	0·0938	0·0687	1·365
	Colourless 1	0·0324	0·640	0·479	1·337
	Colourless 3	0·0166	0·173	0·126	1·373
21·7	Yellow	0·0380	0·432	0·340	1·271
	White 2	0·0451	0·598	0·479	1·248
	White 3	0·0170	0·0924	0·0687	1·345
	White 4	0·0069	0·0154	0·0111	1·378
	Colourless 2	0·0452	0·599	0·481	1·304
	Colourless 3	0·0232	0·168	0·126	1·333
15·5	Yellow	0·0532	0·413	0·340	1·214
	White 2	0·0631	0·567	0·479	1·184
	White 3	0·0239	0·0906	0·0687	1·319
	White 4	0·0096	0·0153	0·0111	1·352
	Colourless 2	0·0633	0·568	0·481	1·181
	Colourless 3	0·0324	0·165	0·126	1·309
8·04	Red	0·1218	0·463	0·480	0·965
	Light Green	0·1216	0·463	0·479	0·967
	Dark Green	0·1229	0·469	0·489	0·959
	Blue	0·1210	0·471	0·472	0·998
	Orange	0·1216	0·465	0·479	0·971
	Yellow	0·1024	0·352	0·340	1·035
	White 1	0·1230	0·480	0·491	0·977
	White 2	0·1216	0·465	0·479	0·971
	White 3	0·0460	0·085	0·0687	1·237
	White 4	0·0185	0·0149	0·0111	1·342
	Colourless 1	0·1216	0·469	0·479	0·979
	Colourless 2	0·1218	0·466	0·481	0·969
	Colourless 3	0·0626	0·151	0·126	1·199
6·22	Red	0·1573	0·422	0·480	0·879
	Dark Green	0·1588	0·426	0·489	0·871
	Blue	0·1563	0·417	0·472	0·883
	Orange	0·1572	0·426	0·479	0·889
	Yellow	0·1324	0·328	0·340	0·965
	White 1	0·1592	0·429	0·491	0·874
	White 3	0·0595	0·0816	0·0687	1·188
	White 4	0·0239	0·0148	0·0111	1·333
	Colourless 1	0·1572	0·427	0·479	0·892
	Colourless 3	0·0809	0·141	0·126	1·119
3·20	Colourless 2	0·306	0·213	0·481	0·443
2·49	Colourless 2	0·393	0·137	0·481	0·285

* Mean of not less than five determinations.

pass through the point 1·0, 0·0 where the calculated and the extrapolated settling velocities should be identical. By adjusting the value of the proportionality constant to the value 18·0/1·418 the correct proportionality constant 12·7 is obtained.

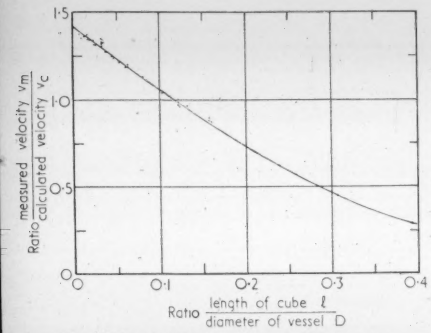

Fig. 1. Relationship between ratio l/D and v_m/v_c

Accordingly the resistance to motion R of a cube is given by

$$R = 12{\cdot}7\, v_c \eta l_c \qquad (2)$$

An empirical equation was developed to fit the line relating the ratio W of the observed settling rate to that calculated for settling in an infinite expanse of liquid from equation (2), to the diameter D, of the vessel. The best fit was given by

$$W = 1 - 2{\cdot}60\,(V^{1}/D) + 4{\cdot}0\,(V/D^{3}) \qquad (3)$$

where V = volume of the cube.

Table 3. *Sedimentation of isometric and other bodies*

Cube-octahedron: volume = 0·839 ml; length of side = 0·596 cm; density = 1·1065 g/ml.
Cylinder: volume = 0·785 ml; diameter = 1·00 cm; length = 1·00 cm.
Prism: volume = 0·225 ml; length = 1·00 cm; breadth and height = 0·475 cm.
Disk: volume = 0·024 ml; diameter = 0·422 cm; thickness = 0·172 cm.

Shape	*Vessel diameter* (cm)	*Observed settling velocity* (cm/s)	*Wall correction factor*	*Corrected settling velocity* (cm/s)
Cube-octahedron	6·22	0·506	0·618	0·819
	8·04	0·574	0·700	0·820
	15·51	0·695	0·842	0·825
Cylinder	6·22	0·535	0·627	0·853
	8·04	0·602	0·707	0·851
	15·51	0·727	0·847	0·858
	30·20	0·787	0·920	0·855
Prism	6·22	0·331	0·745	0·444
	8·04	0·385	0·803	0·446
	15·51	0·403	0·898	0·449
Disk	6·22	0·074	0·879	0·084
	8·04	0·076	0·907	0·084
	15·51	0·080	0·952	0·084

At dimension ratios below 8 to 1 an additional term $-2{\cdot}0\,(V^{5/3}/D^{5})$ was found necessary, the final equation giving the wall effect of a cube with one face horizontal, to an accuracy within about ±2% at dimension-ratios exceeding 3 to 1. When the ratio exceeds 10 to 1 the accuracy is believed to be within ±0·5%. The equation is similar in form to that of Faxen for spheres [see Barr[8]] but it may be slightly more accurate than his equation at dimension-ratios below 5 to 1.

The validity of the equation was tested on an isometric body (cube-octahedron) and three non-isometric bodies (cylinder, prism and disk). The bodies were allowed to sediment in vessels of different diameters and their settling velocities in an infinite expanse of liquid calculated from equation (3) with the additional term. Where the diameter of the vessel was sufficiently small for orientation to affect the falling speed, measurements were taken only with the largest face of the body horizontal. The results are shown in Table 3; the corrected values obtained from the different vessels vary by less than 2%.

The density ρ_{co} of the cube-octahedron was 1·049 g/ml. and its sedimentation rate was given by the equation:

$$v_{co} = [l_{co}^{2}(\rho_{co} - \rho_1)g]/6{\cdot}89\,\eta \qquad (4)$$

where l_{co} = length of the side of the cube-octahedron.

DISCUSSION

The resistance R to motion of a body moving through a medium under condition of streamline flow is given by

$$R = K_1 l v \eta \qquad (5)$$

where K_1 = constant (shape factor)
l = a linear dimension of the body
v = velocity of the body
η = viscosity of the medium.

For spheres

$$R_s = 3\pi d v_s \eta \qquad (6)$$

where d = diameter of the sphere, and
v_s = velocity of the sphere.

For other isometric bodies the length of the side of the particle may be used instead of d and the following values of the constant K_1 for certain isometric shapes would be obtained:

Shape	*Pettyjohn and Christiansen*[4a]	*Present work*
Cube octahedron	6·86	6·9
Octahedron	20·55	—
Cube	12·69	12·7
Tetrahedron	57·21	—

Other dimensions than the length of the side of the body may be used in equation (5) if a different value of K_1 is employed. For example, the perimeter of the projected area, the square root of the projected cross-sectional area of the particle when falling, the cube root of the volume or the square root of the surface area could be used.

From the work of Kunkel[6] it appears that the last mentioned may be the most significant. The resistance to motion may then be written

$$R = K\sqrt{(\text{surface area})}\, v\eta \qquad (7)$$

where K is a constant.

Equation (6) for a sphere may be rewritten

$$R_s = \sqrt[3]{\pi}\sqrt{(\text{surface area})\, v\eta} \qquad (8)$$

and the values for K for other isometric shapes would be

Shape	Pettyjohn and Christiansen[4]	Present work
Sphere	$\sqrt[3]{\pi}$	$\sqrt[3]{\pi}$
Cube-octahedron	$\sqrt[3]{3{\cdot}05}$	$\sqrt[3]{3{\cdot}08}$
Octahedron	$\sqrt[3]{3{\cdot}03}$	—
Cube	$\sqrt[3]{2{\cdot}98}$	$\sqrt[3]{3{\cdot}05}$
Tetrahedron	$\sqrt[3]{2{\cdot}92}$	—

Thus if a value of $K = \sqrt[3]{3{\cdot}00}$ were substituted in equation (7) it would satisfy the resistance to motion of all isometric shapes to within about 4% assuming that all intermediate isometric shapes had resistances between those of a sphere (highest order of symmetry) and a tetrahedron (lowest order of symmetry), as the above table suggests. Experiments were made in a vessel of 6·22 cm diameter to confirm this hypothesis.

The rate of sedimentation of a sphere 1·3 cm in diameter was measured. Six small equal caps were removed from it, in cube form, and the rate of fall retimed. The caps were progressively enlarged, the rate of fall being determined after each enlargement, until a cube, inscribed in the original sphere, was obtained. It was found, as indicated in Table 4, that the settling velocity of the shapes intermediate between the sphere and its inscribed cube, after correction for wall effect and allowing for the loss in weight of the body resulting from the removal of the caps, showed a close proportionality to square root of the surface area (compare last two columns).

The settling rate of a cube of 1·0 cm side was also measured and then prisms were removed from four parallel edges to leave a prism with a polygonal base. Further prisms were gradually removed in a symmetrical manner to yield forms which were compact but not isometric until finally a cylinder, inscribed in the original cube, was obtained. The settling

Table 4. *Effect of change of shape from sphere to cube on settling velocity*

Shape	Weight (g)	Ratio accelerating force to force due to gravity (A)	Surface area ($S.A.$) (cm^2)	Measured settling velocity (v) (cm/s)	Wall correction factor (W)	$\frac{v}{WA}$ (v_1) (cm/s)	$\frac{v_1\ (shape)}{v_1\ (sphere)}$	$\sqrt{\frac{S.A.\ sphere}{S.A.\ shape}}$
Sphere	1·2502	0·1059	5·437	0·675	0·575	11·10	1·000	1·000
	1·1714	0·1017	5·314	0·659	0·583	11·12	1·002	1·011
	1·1181	0·0965	5·231	0·633	0·589	11·14	1·004	1·019
	1·0832	0·0936	5·176	0·625	0·593	11·27	1·015	1·025
	0·8720	0·0735	4·834	0·537	0·621	11·77	1·061	1·060
	0·7130	0·0598	4·564	0·466	0·642	12·14	1·093	1·091
	0·6074	0·0508	4·377	0·420	0·659	12·54	1·130	1·117
Cube	0·4670	0·0395	3·464	0·387	0·689	14·41	1·283	1·253

Table 5. *Effect of change of shape from cube to cylinder on settling velocity*

Shape	Weight (g)	Ratio accelerating force to force due to gravity (A)	Surface area ($S.A.$) (cm^2)	Measured settling velocity (v) (cm/s)	Wall correction factor (W)	$\frac{v}{WA}$ (v_1) (cm/s)	$\frac{v_1\ (shape)}{v_1\ (cube)}$	$\sqrt{\frac{S.A.\ cube}{S.A.\ shape}}$
Cube	1·0816	0·1160	6·029	0·740	0·597	10·68	1·000	1·000
	1·0174	0·1107	5·467	0·741	0·605	11·06	1·035	1·049
	0·9587	0·1053	5·240	0·737	0·612	11·44	1·071	1·071
	0·9181	0·1017	5·108	0·721	0·616	11·51	1·076	1·085
	0·8932	0·0996	4·967	0·733	0·619	11·90	1·114	1·100
	0·8707	0·0976	4·830	0·730	0·621	12·05	1·128	1·116
Cylinder	0·8623	0·0966	4·729	0·743	0·624	12·33	1·154	1·128

Table 6. *Effect of deviation from compactness on settling velocity of a body*

(Compactness reduced by removing slices of the original cube parallel to one face.)

Shape	Weight (g)	Ratio accelerating force to force due to gravity (A)	Surface area ($S.A.$) (cm^2)	Measured settling velocity (v) (cm/s)	Wall correction factor (W)	$\frac{v}{WA}$ (v_1) (cm/s)	$\frac{v_1\ (shape)}{v_1\ (cube)}$	$\sqrt{\frac{S.A.\ cube}{S.A.\ shape}}$
Cube	0·9930	0·0538	5·917	0·343	0·599	10·65	1·000	1·000
compactness	0·9341	0·0487	5·687	0·318	0·606	10·78	1·012	1·020
being	0·9143	0·0470	5·611	0·309	0·609	10·80	1·014	1·027
reduced	0·8932	0·0452	5·530	0·300	0·612	10·85	1·019	1·034
	0·8549	0·0419	5·383	0·282	0·617	10·91	1·024	1·048
	0·8422	0·0408	5·335	0·276	0·618	10·95	1·028	1·053
	0·7940	0·0367	5·150	0·255	0·625	11·12	1·044	1·072
	0·7690	0·0346	5·054	0·242	0·629	11·12	1·044	1·085
	0·7458	0·0325	4·965	0·230	0·632	11·20	1·052	1·092
	0·7125	0·0297	4·837	0·214	0·637	11·31	1·062	1·106

rate of the body was measured after each alteration in shape and it was again found, as shown in Table 5, that the settling velocity, corrected for the effect of the walls, was very nearly proportional to the square root of the surface area, after allowing for the reduction in weight caused by removal of the prisms.

In another series of experiments, a cube of side 1·0 cm was altered in shape by removing, in stages, thin slices parallel to one face so that the height of one axis was ultimately reduced to two-thirds of its original value. The settling velocity, corrected for the wall effect, was determined at each stage in order to ascertain the variation of K with decreasing compactness. The results, as shown in Table 6, show that even for the final stage the change in value of K was only about 4%.

It appears, therefore, that the equation

$$R = \sqrt[3]{3{\cdot}00}\sqrt{(\text{surface area})}\,v\eta \qquad (9)$$

is applicable to the resistance to motion of isometric particles and other bodies to an accuracy of within about 4% providing they are compact in shape.

If values of K are plotted against values of β where

$$\beta = \sqrt{(\text{surface area of particle})}/\sqrt[3]{(\text{volume of particle})}$$

a line, shown in Fig. 2, is obtained having the equation

$$K = 3(2{\cdot}067 - 0{\cdot}136\beta) \qquad (10)$$

All values of K lie within $\pm 0{\cdot}5\%$ of the line.

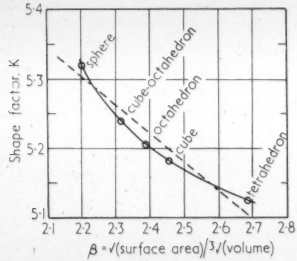

Fig. 2. Relationship between shape factor K and ratio $\beta = \sqrt{(\text{surface area of particle})}/\sqrt[3]{(\text{volume of particle})}$

Equation (9) may then be rewritten

$$R = 3(2{\cdot}067 - 0{\cdot}136\beta)\sqrt{(\text{surface area})}\,v\eta \qquad (11)$$

which will give, to within $\pm 0{\cdot}5\%$, the resistance to motion, in the streamline region of flow in an infinite expanse of liquid, of any smooth isometric shape and of other compact shapes the axial ratio of which does not exceed approximately 1·4 to 1.

CONCLUSIONS

The settling velocity v_p of any compact isometric particle, falling under conditions of streamline flow in an infinite liquid medium, can be calculated to within an accuracy of $\pm 2\%$ from the equation

$$v_p = \frac{V_p(\rho_p - \rho_1)g}{\sqrt[3]{3{\cdot}00}\sqrt{(S_p)}\eta} \qquad (12)$$

where V_p = volume of particle
ρ_p = density of particle
ρ_1 = density of liquid
S_p = surface area of particle.

The corresponding sedimentation velocity v_d in a vessel of diameter D is given by:

$$v_d = \frac{\left[V_p(\rho_p - \rho_1)g\left(1 - 2{\cdot}60\frac{V_p^{1/3}}{D} + 4{\cdot}0\,\frac{V_p}{D^3} - 2{\cdot}0\frac{V_p^{5/3}}{D^5}\right)\right]}{\left[\sqrt[3]{3{\cdot}00}\sqrt{(S_p)}\eta\right]} \qquad (13)$$

Because of its simplicity, equation (12) should be of assistance in calculating the sedimentation velocity of irregularly-shaped bodies.

It also appears that any deviation from isometry of a particle does not have a marked effect upon its falling speed under conditions of laminar flow until an axial ratio exceeding about 1·4 to 1 is attained. This is of considerable practical importance since perfectly isometric particles are seldom met in practice.

The limits of accuracy of the equations can be improved to $\pm 0{\cdot}5\%$ by substituting in equations (12) and (13) the value $(2{\cdot}067\text{–}0{\cdot}136\beta)$ for $\sqrt{3{\cdot}00}$ where

$$\beta = \frac{(S_p)^{1/2}}{(V_p)^{1/3}}$$

ACKNOWLEDGEMENT

The authors wish to acknowledge the assistance of Mr. H. Stanley in some of the experimental work.

REFERENCES

(1) SHULTZ, P. *Glückauf*, **51**, p. 458 (1915).
(2) PERNOLET, V. *Ann. Mines*, Series 4, **20**, pp. 379, 535 (1851).
(3) SCHMIEDEL, J. *Phys. Z.*, **29**, p. 593 (1928).
(4) PETTYJOHN, E. S., and CHRISTIANSEN, E. B. *Chem. Eng. Progr.*, **44**, p. 157 (1948).
(5) WADELL, M. *J. Franklin Inst.*, **217**, p. 459 (1934).
(6) KUNKEL, W. B. *J. Appl. Phys.*, **19**, p. 1056 (1948).
(7) STOKES, G. G. *Trans Cambridge Phil. Soc.*, **9**, p. 51 (1851).
(8) BARR, G. *A Monograph of Viscometry* (London: Oxford University Press, 1931).

The resistance of an elliptic plate

By E. E. Jones, B.Sc., Ph.D., University of Nottingham

[*Paper first received* 22 *June, and in final form* 20 *July*, 1954]

The resistance of a thin conducting plate, with an elliptic contour, is determined (i) when the current enters the plate at an internal electrode and flows out at the circumference of the plate, and (ii) when the current enters and leaves the plate at two internal electrodes. The formulae for the resistance are in the form of infinite series, capable of numerical evaluation to any degree of approximation. Examples are considered for both the current distributions.

1. INTRODUCTION

The resistance of an electrode system in the form of a circular conducting disk with internal electrodes of circular cross-section has been determined by Awbery,[1] and in the form of a rectangular conducting plate with its contour as one electrode and with an internal electrode of circular cross-section by Daymond.[2] The electrode system discussed here is that of an elliptic plate, with either two or more internal electrodes, or one internal electrode and one electrode coinciding with the contour of the plate. The internal electrodes in each case are of circular cross-section, with small radius compared with the dimensions of the plate. Electrode systems such as these have wide application as follows.

(i) In geophysical survey where it is of importance to measure the resistivity of geological formations. This is done by supplying electrical energy to the ground or to samples by means of small electrodes, and the change in the resistance for various positions of the electrodes is measured either directly or by investigating the distribution of potential throughout the formation.[3]

(ii) In vacuum tube electrode systems, e.g. a diode formed by an anode of elliptic section, and a cathode situated inside it. The relation between the anode voltage and the anode current is then important. An extension of the results is also possible to include grid systems, with wires assumed running parallel to the cathode.

(iii) In cables formed by sheathed conducting cores; the resistance in this case measures the leak resistance of the cable.

(iv) With a change in nomenclature, the results may be used to deduce the flux of viscous fluid flowing according to Darcy's law into a well of small bore, the outer boundary, which is in the form of an ellipse, being acted upon by constant fluid pressure.[4] An extension is also possible to multiple well systems.

The elliptic plate is assumed to be a right section of an infinite cylinder of elliptic section, with semi-major axis u, and semi-minor axis v. The line joining the foci of the ellipse has length $4c$, so that $4c^2 = u^2 - v^2$. Axes Ox, Oy define the z-plane, with origin O at the centre of the ellipse and axes Ox, Oy along the semi-major and semi-minor axes respectively. The region between the ellipse and the line of foci in the z-plane is mapped on to the annulus enclosed by the two circles $|\zeta| = 1$ and $|\zeta| = 1/t$, $(t > 1)$, in the ζ-plane, by the transformation

$$z = c(t\zeta + t^{-1}\zeta^{-1}) \tag{1}$$

where $z = x + iy$, and $t^2 = (u + v)/(u - v)$. It is noticed that the contour of the ellipse maps on to the circle $|\zeta| = 1$, and that the two sides of the line of foci of the ellipse map on to the circle $|\zeta| = 1/t$.

When a line electrode exists at the point $z = z_0$ in the z-plane, the corresponding position in the ζ-plane is $\zeta = \zeta_0$, where $1/t \leqslant |\zeta_0| < 1$. If ϕ is the field potential and ψ is the stream function, then a complex potential $w = \phi + i\psi$ can be determined in the ζ-plane (c.f. Rosenhead,[5] who deduced a complex potential in terms of elliptic functions). If I is the current leaving the electrode, and d is the thickness of the plate, and σ its conductivity, then

$$2\pi d\sigma w = -I \log(\zeta - \zeta_0) + \sum_{n=1}^{\infty}(a_n\zeta^n + b_n\zeta^{-n}) \tag{2}$$

Since the total current I flowing through a cylinder of length d is given by

$$I = -d\sigma(\psi)_s$$

where s is the circumference of a section of this cylinder, then equation (2) gives the correct value for w. For in describing the circuit s once in a positive direction, the only contribution to ψ is from the term $-I \log(\zeta - \zeta_0)$, and this is $-2\pi I$.

On the circle $|\zeta| = 1$, equation (2) can be written as

$$2\pi d\sigma w_1 = -I \log \zeta + \sum_{n=1}^{\infty} a_n\zeta^n + \sum_{n=1}^{\infty}\left(b_n + \frac{I}{n}\zeta_0^n\right)\zeta^{-n} \tag{3}$$

and on the circle $|\zeta| = 1/t$, it can be written as

$$2\pi d\sigma w_0 = -I \log(-\zeta_0) + \sum_{n=1}^{\infty}\left(a_n + \frac{I}{n}\zeta_0^{-n}\right)\zeta^n + \sum_{n=1}^{\infty} b_n\zeta^{-n} \tag{4}$$

2. THE CIRCUMFERENCE AS AN ELECTRODE

The first problem is one where a current I flows outwards through the boundary of the plate, i.e. the boundary is an electrode. Hence ϕ is a constant on the circle $|\zeta| = 1$, so there exists a boundary condition

$$Re\ w_1(\zeta) = 0 \tag{5}$$

Both ϕ and ψ are continuous across the line joining the foci of the ellipse, hence so is w. The two points in the ζ-plane corresponding to near points one on each side of the line of foci in the z-plane are ζ and $\overline{\zeta}$, where $\overline{\zeta} = 1/t^2\zeta$. Thus in order for w to be continuous across the line of foci, we must have

$$w_0(\zeta) = w_0(1/t^2\zeta) \tag{6}$$

From equation (5),

$$a_n + b_n + (I/n)\zeta_0^{-n} = 0$$

and from equation (6),

$$a_n + (I/n)\zeta_0^{-n} = b_n t^{2n}$$

Eliminating a_n, it is seen that

$$b_n t^{2n} + b_n = I(\zeta_0^{-n} - \overline{\zeta}_0^n)/n$$

Taking the conjugate of this equation, eliminating b_n leads to

$$b_n = I[(\zeta_0^{-n} - \overline{\zeta}_0^n)t^{2n} - (\overline{\zeta}_0^{-n} - \zeta_0^n)]/n(t^{4n} - 1)$$

and thus

$$a_n = I\{(t\zeta_0)^n + (t\overline{\zeta}_0)^{-n} - [(t\overline{\zeta}_0)^n + (t\overline{\zeta}_0)^{-n}]t^{2n}\}t^n/n(t^{4n} - 1)$$

Substituting for a_n and b_n in equation (2), and using equation (1), we have

$$(2\pi d\sigma/I)w = \log ct/(z - z_0) + \sum_{n=1}^{\infty} (\omega_n - \overline{\omega}_n t^{2n})[(t\zeta)^n + (t\zeta)^{-n}]/n(t^{4n} - 1) \quad (7)$$

where $$\omega_n = (t\zeta_0)^n + (t\zeta_0)^{-n}$$

The potential ϕ_0 on the inner electrode of small radius r is determined by substituting $z = z_0 + r\exp(i\theta)$, and $\zeta = \zeta_0$ in the real part of equation (7). Since the resistance R of the plate is defined by ϕ_0/I, then to the first order in r, we have

$$4\pi d\sigma R = 2\log(ct/r) + \sum_{n=1}^{\infty} (\omega_n^2 - 2\omega_n\overline{\omega}_n t^{2n} + \overline{\omega}_n^2)/n(t^{4n} - 1) \quad (8)$$

In order to reduce the expression for the resistance to a non-dimensional form, it is convenient to take the semi-major axis of the ellipse a as the unit of length. Then in order to indicate the order of magnitude of the resistance of the plate, and its variations as the dimensions of the ellipse and the position of the inner electrode are varied, a table is drawn for variations of v/u in the range $0 < v/u < 1$, and for z_0/u in the range $0 \leqslant |z_0|/u < 1$. Values of δ_1 are recorded, where

$$2\pi d\sigma R = \log(u/r) - \delta_1 \quad (9)$$

The upper set of numbers in each row correspond to the values when the inner electrode lies on the major axis of the ellipse, i.e. z_0 is real, and the lower set of numbers correspond to the values of δ_1 when the inner electrode lies on the minor axis of the ellipse, i.e. z_0 is purely imaginary. Only one set of numbers is required in the first column and the last row of Table 1, since in both the above cases the results are identical.

In order to evaluate ω_n the following recurrence formulae can be used:

$$\binom{z_0}{c}^n = \omega_n + \binom{n}{1}\omega_{n-2} + \cdots + \binom{n}{n/2}, \; n \text{ even},$$

$$= \omega_n + \binom{n}{1}\omega_{n-2} + \cdots + \left[\frac{n}{(n-1)/2}\right]\omega_1, \; n \text{ odd}.$$

Table 1. *The variation of* δ_1

r/u \ $\lvert z_0\rvert/u$	0	0·2	0·4	0·6	0·8
0·2	1·3746	1·3960	1·4658	1·6124	1·9236
		—	—	—	—
0·4	0·7044	0·7272	0·8096	0·9808	1·3751
		1·0454	—	—	—
0·6	0·3448	0·3747	0·4744	0·6857	1·1661
		0·4817	1·0081	—	—
0·8	0·1299	0·1659	0·2848	0·5317	1·0707
		0·2004	0·4415	1·0098	—
1·0	0·0000	0·0408	0·1743	0·4462	1·0216

For a given elliptic contour the resistance of the plate decreases as the inner electrode moves outwards away from the centre of the ellipse, and the rate of decrease is greater at larger distances of the electrode from this centre. Hence changes in the position of the inner electrode are less effective in altering the resistance of the plate at positions nearer the centre of the plate. For a given position of the inner electrode the resistance of the plate increases with increase of v/u, and the rate of increase is greater for smaller values of v/u.

Since δ_1 is independent of r, the radius of the electrode, then from equation (9) it is seen that the effect of an increase of the radius of the electrode is to decrease the resistance of the plate.

3. TWO INTERNAL ELECTRODES

In the second problem the outer boundary of the plate is a line of current flow, and for simplicity two electrodes only are assumed to be situated inside the plate. The electrode at $z = z_1$ has small radius r_1, and a total current I leaves it, whereas the electrode at $z = z_2$ of small radius r_2 has a current I entering it. The complex potential of the current flow in this case assumes the form

$$2\pi d\sigma w = I\log(\zeta - \zeta_2)/(\zeta - \zeta_1) + \sum_{n=1}^{\infty} (a_n\zeta^n + b_n\zeta^{-n}) \quad (10)$$

where ζ_1 and ζ_2 are the points in the ζ-plane corresponding respectively to the points z_1 and z_2 in the z-plane.

On the circle $|\zeta| = 1$, equation (10) reduces to

$$2\pi d\sigma w_1 = \sum_{n=1}^{\infty} a_n\zeta^n + \sum_{n=1}^{\infty}\left[b_n + \frac{I}{n}(\zeta_1^n - \zeta_2^n)\right]\zeta^{-n} \quad (11)$$

and on the circle $|\zeta| = 1/t$ to

$$2\pi d\sigma w_0 = I\log\frac{\zeta_2}{\zeta_1} + \sum_{n=1}^{\infty}\left[a_n + \frac{I}{n}(\zeta_1^{-n} - \zeta_2^{-n})\right]\zeta^n + \sum_{n=1}^{\infty} b_n\zeta^{-n} \quad (12)$$

The boundary condition on $|\zeta| = 1/t$ is as given by equation (6), but as the contour of the plate is a line of current flow, the second boundary condition is

$$Im\; w_1(\zeta) = 0 \quad (13)$$

From equations (6) and (12), we have

$$a_n + I(\zeta_1^{-n} - \zeta_2^{-n})/n = b_n t^{2n}$$

and from equations (11) and (13),

$$a_n - I(\overline{\zeta}_1^n - \overline{\zeta}_2^n)/n = b_n$$

Proceeding as in Section 2, it can be deduced that

$$b_n = I[\zeta_1^n + \overline{\zeta}_1^{-n} - \zeta_2^n - \overline{\zeta}_2^{-n} + (\overline{\zeta}_1^n + \zeta_1^{-n} - \overline{\zeta}_2^n - \zeta_2^{-n})t^{2n}]/n(t^{4n} - 1)$$

and $$a_n = I[\omega_{1n} - \omega_{2n} + (\overline{\omega}_{1n} - \overline{\omega}_{2n})t^{2n}]t^n/n(t^{4n} - 1)$$

where $$\omega_{sn} = (t\zeta_s)^n + (t\zeta_s)^{-n}, \quad (s = 1, 2)$$

The complex potential w is deduced from equation (10), and can be written in the form

$$(2\pi d\sigma/I)w = \log(z - z_2)/(z - z_1) + \sum_{n=1}^{\infty}[\omega_{1n} - \omega_{2n} + (\overline{\omega}_{1n} - \overline{\omega}_{2n})t^{2n}][(t\zeta)^n + (t\zeta)^{-n}]/n(t^{4n} - 1)$$

The potential ϕ_s $(s = 1, 2)$, on the surface of the sth electrode at $z = z_s$ of radius r_s is determined by substituting $z = z_s + r_s\exp(i\theta_s)$ and $\zeta = \zeta_s$ in the above equation, and considering only its real part. The resistance of the plate is determined by $R = (\phi_1 - \phi_2)/I$, and is given by

$$4\pi d\sigma R = 2\log(z_1 - z_2)(\bar{z}_1 - \bar{z}_2)/r_1 r_2 + \sum_{n=1}^{\infty}[(\omega_{1n} - \omega_{2n})^2 + 2(\omega_{1n} - \omega_{2n})(\overline{\omega}_{1n} - \overline{\omega}_{2n})t^{2n} + (\overline{\omega}_{1n} - \overline{\omega}_{2n})^2]/n(t^{4n} - 1)$$

A table can be drawn illustrating the variation in the resistance of the plate as the position of the electrodes is varied and the dimensions of the plate are changed, the semi-major axis of the ellipse being taken as the unit of length. In order to reduce the problem to its simplest form, it is assumed that the electrodes are confined to lie along the axes of the ellipse, symmetrically with respect to its centre. In each column of Table 2 the upper set of numbers are values of δ_2, where

$$2\pi d\sigma R = \log (u^2/r_1 r_2) + \delta_2$$

when the electrodes lie along the major axis with $z_1 = -z_2$, and the lower set of numbers correspond to the case when the electrodes lie along the minor axis, with $z_1 = -z_2$. In both cases the resistance has the same value for $v = u$.

For a given ellipse the resistance increases as the electrodes move further apart, the rate of increase being slightly greater at larger values of $|z|/u$. For a given position of the electrodes, i.e. given $|z|/u$, the resistance decreases as v/u increases, the rate of decrease being greater for smaller values of v/u. Changes in the distance between the electrodes are less effective at larger values of v/u in the range $0 < v \leqslant u$. An increase in the radii of the electrodes, whether separately or together, has the effect of decreasing the resistance of the plate.

Table 2. *The variation of* δ_2

v/u \ $\lvert z\rvert/u$	0·2	0·4	0·6	0·8
0·2	0·8029	7·3290	14·4451	22·9868
	—	—	—	—
0·4	−1·0512	2·3029	5·8946	10·1207
	−1·2929	—	—	—
0·6	−1·4563	0·9725	3·3939	6·3613
	−1·5694	0·8208	—	—
0·8	−1·6050	0·4429	2·3720	4·7661
	−1·6448	0·3468	2·4547	—
1·0	−1·6725	0·1992	1·8722	3·9727

REFERENCES

(1) Awbery, J. H. *Phil. Mag.*, **3**, p. 674 (1932).

(2) Daymond, S. D. *Quart. J. Mech. Appl. Math.*, **4**, p. 23 (1951).

(3) Heiland, C. A. *Geophysical Exploration* (New York: Prentice-Hall Inc., 1946).

(4) Muskat, M. *The Flow of Homogeneous Fluids through Porous Media* (New York: McGraw-Hill Book Co. Inc., 1937).

(5) Rosenhead, L. *Proc. Roy. Soc. A*, **140**, p. 579 (1933).

The estimation of the specific surface of a soil from mechanical analysis data

By J. R. H. Coutts, D.Sc., F.Inst.P., Department of Soil Science, University of Aberdeen

[*Paper first received* 15 *October, and in final form* 8 *November*, 1954]

A method by which an approximate value for the specific surface of a soil can be calculated from particle size distribution data is described. Factors affecting the accuracy of the results are discussed.

Methods for estimating the specific surface of a soil from mechanical analysis data have been derived by Krauss[1] and by Puri.[2] In the present paper, an alternative method is given, making use of a procedure which is a straightforward development of that used by van Bavel[3] for the determination of the weight mean radius of the structural aggregates in a soil.

Using notation similar to that adopted by van Bavel, let $f(r)$ be the (weight) distribution function of particle size, and $F(r)$ the accumulation function, which gives the ordinates in the familiar summation curve. Then, by definition,

$$[F(r)]_m^M = \int_m^M f(r).dr \qquad (1)$$

where the limits m and M denote the least and the greatest values of the independent variable [r in equation (1)]. The weight mean radius is $\bar{r}$, where

$$\bar{r} = \int_m^M r.f(r).dr \Big/ \int_m^M f(r).dr$$

Integrating the numerator by parts, and using equation (1)

$$\bar{r} = \frac{1}{[F(r)]_m^M}\left\{[r.F(r)]_m^M - \int_m^M F(r).dr\right\} \qquad (2)$$

which (with $m = 0$) is the equation applied by van Bavel.

In the summation curve, it is customary to plot $F(r)$ against a logarithmic scale for r or for the Stokes terminal velocity. If we use $\ln r$ as the independent variable, the calculation for $\bar{r}$ is conveniently made from the equation

$$\bar{r} = \frac{1}{[F(r)]_m^M}\left\{[r.F(r)]_m^M - \int_m^M r.F(r).d(\ln r)\right\} \qquad (3)$$

As explained by Dallavalle[4] the weight mean radius is the appropriate size parameter to use in the calculation of the specific surface S, and for spherical particles of density ρ g per cm^3

$$S = \frac{3000}{\rho\bar{r}} \text{ cm}^2/100 \text{ g} \qquad (4)$$

where $\bar{r}$ is expressed in millimetres.

The practical manipulation of equation (3) is illustrated by considering the two curves in the figure. The abscissae for these curves are the natural logarithms of r. For curve I (the summation curve), the ordinates are percentage values of $F(r)$, and for curve II they show the corresponding values of $r.F(r)$. (The two sets of ordinates have the same maximum

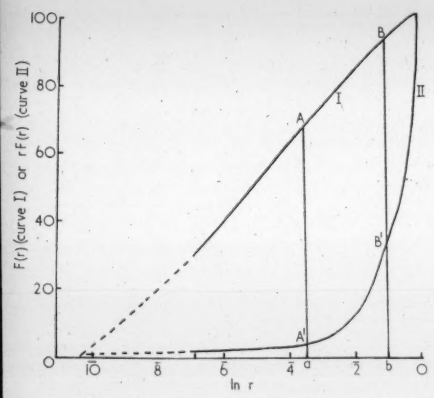

Curves of $F(r)$ and of $r.F(r)$ for a silty-clay loam

values in the case shown because the upper limit of the Stokes radius for coarse sand particles is 1 mm, it being customary to remove coarser material such as gravel and stones by sieving before carrying out the mechanical analysis of a soil.) Curve I can be constructed immediately from mechanical analysis data, and, in view of its simple form for most soils, it can be obtained with reasonable accuracy even though the routine mechanical analysis provides only four points upon it. By interpolation on curve I at suitable intervals of $\ln r$, the corresponding values of $F(r)$ are found, and the ordinate for curve II can be calculated for each specified value of $\ln r$.

If the specific surface is to be found for the soil fraction within the size limits defined by $\ln \alpha = a$ and $\ln \beta = b$, the terms on the right-hand side of equation (4) can be evaluated from the curves: $[F(r)]_a^b$ is the difference between the ordinates bB and aA erected to curve I; $[r.F(r)]_a^b$ is the difference between the ordinates bB' and aA' erected to curve II; and $\int_a^b r.F(r).d(\ln r)$ is given by the area $aA'B'b$ which can be measured with a planimeter.

The limits of size range determined in routine mechanical analysis are those covered by the full lines in the curves shown in the figure, but when the larger specific surfaces associated with smaller particles are of interest, these can be obtained approximately by extrapolation of curve I, and thence by constructing (on an enlarged ordinate scale) the curve for $r.F(r)$. (The extrapolation employed in Puri's method implies the assumption that there is a linear relationship between $F(r)$ and $1/r$.) It may be noted that the dotted extrapolation in the figure indicates that the smallest particles present have Stokes radii of approximately 3×10^{-5} mm, which is about the value suggested by Robinson.[5] Results for two soils of widely differing textures are shown in the table.

Values of specific surfaces of coarser and finer fractions of two soils and of the whole soils

Soil	S(cm²/100 g)		
	Fraction $\alpha =$	10^{-3}	3×10^{-5}
	$\beta =$	1	10^{-3}
Cruden Bay (silty-clay loam)	$9{\cdot}55 \times 10^3$	$4{\cdot}13 \times 10^5$	$1{\cdot}27 \times 10^5$
Craibstone (sandy loam)	$4{\cdot}38 \times 10^3$	$3{\cdot}64 \times 10^5$	$0{\cdot}41 \times 10^5$

In the calculation of these results, the value used for the density of the material is 2·65 g per cm³. While this is a good approximation for most mineral soils, it is probably rather too high for some of the clay minerals occurring in the fractions of the smallest particle size range; and it would also require modification in soils containing high proportions of humus. Further, a source of inaccuracy is necessarily introduced by the use of the extrapolated curves, but from the general form of curve II it will be seen that for a moderately large range of values of $\ln r$ the lower limits of the factors in equation (3) are very small compared with the upper limits and even relatively large errors in estimating the value of r for which $F(r) = 0$ will not appreciably alter the final values of $\bar{r}$.

There is also a source of error common to all estimates of specific surface from sedimentation analysis, namely that which arises from the non-sphericity of the particles. For this reason, the absolute values of S are of less significance than the relative values obtained in a comparison between different soils. In order to obtain valid absolute values, it would be necessary to apply appropriate shape factors. A considerable amount of work on this topic has been published for materials other than soils,[6,7] and Robins[8] has shown how to allow for the variations of shape factor that occur with varying Stokes radii of the particles. The relevant experimental data for soils are not readily available, but since the values for the finest particles are the most important, it should be possible to derive these from electron microscope investigations of the clay minerals.

REFERENCES

(1) KRAUSS, G. *Int. Mitt. Bodenk.*, **13**, pp. 147–160 (1923).

(2) PURI, A. N. *Soils*, pp. 316–322 (New York: Reinhold Publishing Corp., 1949).

(3) VAN BAVEL, C. H. M. *Proc. Soil Sci. Soc. Amer.*, **14**, pp. 20–23 (1950).

(4) DALLAVALLE, J. M. *Micromeritics*. 1st ed., p. 39 (London: Sir Isaac Pitman and Sons Ltd., 1943).

(5) ROBINSON, G. W. *Soils*. 3rd ed., p. 21 (London: T. Murby and Co., 1949).

(6) HEYWOOD, H. *Symposium on Particle Size Analysis*, Suppl. *Trans Instn Chem. Engrs*, **25**, p. 14 (1947).

(7) BEIRNE, T., and HUTCHEON, J. M. *Brit. J. Appl. Phys.*, **5**, *Supplement* 3, p. *S* 76 (1954).

(8) ROBINS, W. H. M. *Brit. J. Appl. Phys.*, **5**, *Supplement* 3, p. *S* 82 (1954).

Formulae for the transformation of indices in twinned crystals

By K. W. Andrews, D.Phil., F.I.M., F.Inst.P., and W. Johnson, M.A., The United Steel Cos. Ltd., Swinden Laboratories, Rotherham

[*Paper first received* 5 *August, and in final form* 11 *October*, 1954]

The interpretation of X-ray diffraction patterns from twinned crystals and the solution of other problems involving twin formation can be assisted by the use of certain formulae. Given the indices of the twin plane (HKL) or the twin axis $[UVW]$, it is possible to find the indices of a plane in the twinned part of a crystal in terms of those of the corresponding plane in the parent crystal, or to formulate the corresponding transformation for zone axes. A general relationship applicable to any crystal systems has been derived in matrix form. A particular form of the matrix and a new relationship follow for cubic crystals. Examples are given of the use of the matrix and formulae. These refer to twins on {111} planes in face-centred cubic metals and other cubic crystals and to twinning in titanium and in uranium.

In the interpretation of X-ray diffraction patterns of twinned crystals, particularly in connexion with certain orientation problems, the authors have derived and employed formulae which express the indices of a plane $(h_2k_2l_2)$ in the parent crystal in terms of $(h_1k_1l_1)$ in the twin. Otherwise, a plane $(h_1k_1l_1)$ in the twin may be considered to have been placed parallel to the plane $(h_2k_2l_2)$ in the parent crystal by the twinning process. Transformation formulae of this kind are not readily available in the literature and usually only refer to specific cases. It is of historical interest that Mügge[1] derived a formula as long ago as 1889. Subsequently occasional use has been made of such transformation relationships. Mügge[2] derived expressions for α-iron, Lewis and Hall[3] for pyrites, Mügge[4] for tin and Slawson[5] for diamond. A lengthy paper dealing with the geometry of twinned crystals was published by Friedel[6] and the morphology of mechanical twinning was considered by Bell.[7] Methods of interpreting X-ray diffraction patterns of twinned crystals have been described by Henry, Lipson and Wooster.[8] There appears, however, to have been no general treatment of the transformation formulae until a recent book by Hall.[9] Decker[10] has derived vector formulae for the identification of twinned crystals which can be shown to be equivalent to the formulae given by Hall and some of the other authors referred to.

The present authors have derived transformation formulae by a method which does not appear to have been used previously. This gives a new and concise general matrix expression for the transformation of planar indices applicable to all crystal systems. The corresponding formula for the transformation of zone axes is also given. When the formula is applied to the cubic case a completely new relationship can be derived and this enables the possible sets of planes $\{h_2k_2l_2\}$ to be obtained given the form of $\{h_1k_1l_1\}$. Three examples are given of the application of the matrix or formula to specific cases.

Relationships for the General Case

Planes. The problem reduces to finding $(h_2k_2l_2)$ in terms of $(h_1k_1l_1)$ so that these two planes make equal angles with a plane (HKL) as in the figure. Generally (HKL) is the twin plane or the composition plane and has simple integral indices. In certain cases twinning is related to an axis $[UVW]$ which rotates the plane $(h_1k_1l_1)$ through 180° to bring it into coincidence with $(h_2k_2l_2)$. In this case $[UVW]$ has simple integral indices but (HKL) is not necessarily represented by integral indices.

Given either (HKL) or $[UVW]$ it is possible to find the other by using relationships which can be derived as follows. The plane (HKL) contains the zone axes:

$$\left[\frac{1}{H}, \frac{-1}{K}, 0\right] \text{ which is parallel to the (001) plane}$$

and $$\left[0, \frac{-1}{K}, \frac{1}{L}\right] \text{ which is parallel to the (100) plane.}$$

The general formula for the angle between two zones is

$$\cos\rho = \frac{\left[\begin{array}{l} u_1u_2a^2 + v_1v_2b^2 + w_1w_2c^2 + bc(v_1w_2 + w_1v_2)\cos\alpha \\ + ca(w_1u_2 + u_1w_2)\cos\beta + ab(u_1v_2 + v_1u_2)\cos\gamma \end{array}\right]}{I_{u_1v_1w_1} \quad I_{u_2v_2w_2}} \qquad (1)$$

where $I_{uvw} = \sqrt{(a^2u^2 + b^2v^2 + c^2w^2 + 2bcvw.\cos\alpha + 2cawu.\cos\beta + 2abuw.\cos\gamma)}$

The two directions are perpendicular when the numerator is zero. Now $[UVW]$ is perpendicular to (HKL) and therefore to the two directions specified so that:

$$\frac{a^2U}{H} - \frac{b^2V}{K} - \frac{bcW.\cos\alpha}{K} + \frac{caW.\cos\beta}{H} + \frac{abV.\cos\gamma}{H} - \frac{abU.\cos\gamma}{K} = 0 \qquad (2)$$

and $$-\frac{b^2V}{K} + \frac{c^2W}{L} - \frac{bcW.\cos\alpha}{K} + \frac{bcV.\cos\alpha}{L} + \frac{caU.\cos\beta}{L} - \frac{abU.\cos\gamma}{K} = 0 \qquad (3)$$

The solution of these two equations enables $[UVW]$ to be found given (HKL), or (HKL) to be found given $[UVW]$. The complete solution for each of the seven crystal systems is given in Table 1. The above derivation is similar to that given by Niggli[11] who called $[UVW]$ the "quasi normal," but did not give fully general solutions.

The equations in Table 1 do not necessarily give integral indices but the indices obtained can be approximated to whole numbers. In the rhombohedral case $\cos\alpha$ can be approximated to the ratio of two whole numbers (see footnote to Table 1).

If now we take $[UVW]$, $\left[\frac{1}{H}, \frac{-1}{K}, 0\right]$ and $\left[0, \frac{-1}{K}, \frac{1}{L}\right]$, as a new set of axes, it follows by the usual matrix methods,

Table 1. *Formulae for zone axis perpendicular to plane*

Crystal system	*Equations for finding [UVW] given (HKL)*	*Equations for finding (HKL) given [UVW]*
Triclinic	$U/(HS_{11} + KS_{12} + LS_{13}) = V/(HS_{12} + KS_{22} + LS_{23}) = W/(HS_{13} + KS_{23} + LS_{33})$ where $S_{11} = b^2c^2 \sin^2\alpha$, etc. $S_{12} = abc^2(\cos\alpha\cos\beta - \cos\gamma)$, etc.	$H/(Ua^2 + Vab\,.\cos\gamma + Wca\,.\cos\beta) = K/(Uab\,.\cos\gamma + Vb^2 + Wbc\,.\cos\alpha) = L/(Uca\,.\cos\beta + Vbc\,.\cos\alpha + Wc^2)$
Monoclinic	$U/(Hb^2c^2 - Lab^2c\,.\cos\beta) = V/(Kc^2a^2\,.\sin^2\beta) = W/(-Hab^2c\,.\cos\beta + La^2b^2)$	$H/(Ua^2 + Wca\,.\cos\beta) = K/Vb^2 = L/(Uca\,.\cos\beta + Wc^2)$
Hexagonal	$U/(2H + K) = V/(H + 2K) = (2W/3L)(c/a)^2$	$H/(2U - V) = K/(2V - U) = L/[2W(c/a)^2]$
Rhombohedral*	$U/[H\,.\sin^2\alpha + (K + L)(\cos^2\alpha - \cos\alpha)] = V/[K\,.\sin^2\alpha + (L + H)(\cos^2\alpha - \cos\alpha)] = W/[L\,.\sin^2\alpha + (H + K)(\cos^2\alpha - \cos\alpha)]$	$H/[U + (V + W)\cos\alpha] = K/[V + (W + U)\cos\alpha] = L/[W + (U + V)\cos\alpha]$
Orthorhombic	$Ua^2/H = Vb^2/K = Wc^2/L$	$H/Ua^2 = K/Vb^2 = L/Wc^2$
Tetragonal	$U/H = V/K = (W/L)(c/a)^2$	$H/U = K/V = L/[W(c/a)^2]$
Cubic	$U/H = V/K = W/L$	$H/U = K/V = L/W$

* Also $\cos\alpha = \dfrac{(KU - HV)}{[H(U + W) - K(V + W)]} = \dfrac{(LV - KW)}{[K(V + U) - L(W + U)]} = \dfrac{(HW - LU)}{[L(W + V) - H(U + V)]}$

(e.g., as described in *International Tables for X-ray Crystallography*)[12] that a matrix given by

$$Q = \begin{bmatrix} U & V & W \\ \dfrac{1}{H}, & \dfrac{-1}{K}, & 0 \\ 0, & \dfrac{-1}{K}, & \dfrac{1}{L} \end{bmatrix}$$

will transform indices of planes referred to the crystallographic axes into indices corresponding to this new set of axes.

If these indices are $(h_1'k_1'l_1')$ it follows that, in this new axial system, the plane of indices $(h_2k_2l_2)$, now transformed to $(h_2'k_2'l_2')$ is related to $(h_1'k_1'l_1')$ by a simple reflexion process so that

$$h_2' = -h_1',\ k_2' = k_1',\ l_2' = l_1'$$

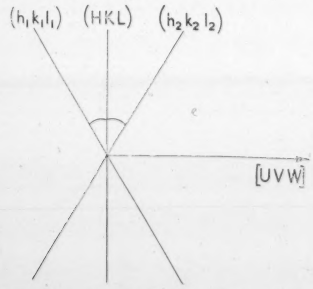

Relationship between twin plane, twin axis and crystallographic planes. [The planes (HKL), $(h_1k_1l_1)$, $(h_2k_2l_2)$ are perpendicular to the plane of the paper.]

Now $(h_2k_2l_2)$ can be found by transformation from $(h_2'k_2'l_2')$ by means of the matrix Q^{-1}. This process of reflexion of $(h_1k_1l_1)$ into $(h_2k_2l_2)$ is represented in the figure. Hence the complete expression of $(h_2k_2l_2)$ in terms of $(h_1k_1l_1)$ requires the matrix:

$$Q^{-1}\,.\,B\,.\,Q$$

where Q is defined as above

and $$B = \begin{bmatrix} -1 & 0 & 0 \\ 0 & 1 & 0 \\ 0 & 0 & 1 \end{bmatrix}$$

$$Q^{-1} = \frac{1}{\Delta}\begin{bmatrix} \dfrac{-1}{KL}, & -\left(\dfrac{W}{K} + \dfrac{V}{L}\right), & \dfrac{W}{K} \\ \dfrac{-1}{HL}, & \dfrac{U}{L}, & \dfrac{W}{H} \\ \dfrac{-1}{HK}, & \dfrac{U}{K}, & -\left(\dfrac{U}{K} + \dfrac{V}{H}\right) \end{bmatrix}$$

where $$\Delta = -(HU + KV + LW)/HKL$$

The product $Q^{-1}\,.\,B\,.\,Q$. required is therefore:

$$\frac{1}{(HU + KV + LW)}\begin{bmatrix} (-HU + KV + LW), & -2HV, & -2HW \\ -2KU, & (HU - KV + LW), & -2KW \\ -2LU, & -2LV, & (HU + KV - LW) \end{bmatrix}$$

or $$\begin{bmatrix} 1 & 0 & 0 \\ 0 & 1 & 0 \\ 0 & 0 & 1 \end{bmatrix} - \frac{2}{(HU + KV + LW)}\begin{bmatrix} HU & HV & HW \\ KU & KV & KW \\ LU & LV & LW \end{bmatrix} \quad (4)$$

which may be written formally as

$$\begin{bmatrix}1&0&0\\0&1&0\\0&0&1\end{bmatrix} - \frac{2\begin{bmatrix}H\\K\\L\end{bmatrix}[UVW]}{[UVW]\begin{bmatrix}H\\K\\L\end{bmatrix}}$$

From equation (4) the transformation formulae required are

$$\left.\begin{aligned} h_2 &= h_1 - \frac{2H(Uh_1 + Vk_1 + Wl_1)}{(HU + KV + LW)}\\ k_2 &= k_1 - \frac{2K(Uh_1 + Vk_1 + Wl_1)}{(HU + KV + LW)}\\ l_2 &= l_1 - \frac{2L(Uh_1 + Vk_1 + Wl_1)}{(HU + KV + LW)}\end{aligned}\right\} \quad (5)$$

An alternative set of expressions avoiding the fractional terms is given by

$$\left.\begin{aligned} h_2 &= (HU + KV + LW)h_1 - 2H(Uh_1 + Vk_1 + Wl_1)\\ k_2 &= (HU + KV + LW)k_1 - 2K(Uh_1 + Vk_1 + Wl_1)\\ l_2 &= (HU + KV + LW)l_1 - 2L(Uh_1 + Vk_1 + Wl_1)\end{aligned}\right\} \quad (6)$$

Zone axes. $[u_2v_2w_2]$ must be expressed in terms of $[u_1v_1w_1]$. In this case these two zone axes make equal angles (or direction cosines) respectively with the chosen transformation axes lying in (HKL), and only the sign of the direction cosine with $[UVW]$ (or Ox') is changed. Hence the matrix B can again be used to represent this reflexion through the plane (HKL).

If now the rows and columns of Q are interchanged we obtain the matrix:

$$Q' = \begin{bmatrix} U & \frac{1}{H} & 0\\ V & \frac{-1}{K} & \frac{-1}{K}\\ W & 0 & \frac{1}{L}\end{bmatrix}$$

and this matrix transforms vectors referred to the transformation set back into the original axes (e.g. [100] becomes $[uvw]$). Therefore for the transformation formula required, it is necessary to obtain the product:

$$Q' \,.\, B \,.\, (Q')^{-1}$$

It can easily be shown, however, that

$$(Q')^{-1} = (Q^{-1})' \text{ and it is clear that } B = B'$$

It follows from the "reversal rule" for transposition of products[13] that:

$$Q'B(Q')^{-1} = Q'B'(Q^{-1})' = (Q^{-1}BQ)'$$

Hence the matrix for the transformation of zone axes is simply the transpose of equation (4), i.e.

$$\begin{bmatrix}1&0&0\\0&1&0\\0&0&1\end{bmatrix} - \frac{2}{(HU + KV + LW)}\begin{bmatrix}HU&KU&LU\\HV&KV&LV\\HW&KW&LW\end{bmatrix} \quad (7)$$

$$= \begin{bmatrix}1&0&0\\0&1&0\\0&0&1\end{bmatrix} - \frac{2\begin{bmatrix}U\\V\\W\end{bmatrix}[HKL]}{[UVW]\begin{bmatrix}H\\K\\L\end{bmatrix}}$$

The transformation formulae are

$$\left.\begin{aligned} u_2 &= u_1 - \frac{2U(Hu_1 + Kv_1 + Lw_1)}{(HU + KV + LW)}\\ v_2 &= v_1 - \frac{2V(Hu_1 + Kv_1 + Lw_1)}{(HU + KV + LW)}\\ w_2 &= w_1 - \frac{2W(Hu_1 + Kv_1 + Lw_1)}{(HU + KV + LW)}\end{aligned}\right\} \quad (8)$$

or

$$\left.\begin{aligned} u_2 &= u_1(HU + KV + LW) - 2U(Hu_1 + Kv_1 + Lw_1)\\ v_2 &= v_1(HU + KV + LW) - 2V(Hu_1 + Kv_1 + Lw_1)\\ w_2 &= w_1(HU + KV + LW) - 2W(Hu_1 + Kv_1 + Lw_1)\end{aligned}\right\} \quad (9)$$

Application of formulae. To apply the formulae, Table 1 is first used to find values of one of the sets of indices H, K, L, or U, V, W, given the other. This is a very simple matter in all crystal systems except monoclinic or triclinic. The approximation to whole numbers can be made where necessary.

Equations (6) or (9) can then be used to calculate the transformed indices for any plane or zone axis. If HKL or UVW have been approximated to whole numbers it follows that $h_2k_2l_2$ or u_2, etc., must also be regarded as approximate. In these cases more exact non-integral indices can be found if desired, by using suitable fractional or decimal forms of UVW or HKL. The equations (6) or (9) are easy to use since the left-hand expression in brackets is the same for all the equations and the right-hand expression in brackets is the same for a given $(h_1k_1l_1)$ or $(u_1v_1w_1)$.

RELATIONSHIPS FOR CUBIC CRYSTALS

The matrix expressions (4) and (7) become identical on substituting $H = U$, $K = V$, $L = W$, $h_1 = u_1$, etc., and one set of equations results. Hence for the cubic case we have

$$h_2 = h_1 - \frac{2H(Hh_1 + Kk_1 + Ll_1)}{(H^2 + K^2 + L^2)}$$

with corresponding expressions for k_2 and l_2

$$\left.\begin{aligned} \text{or } h_2 &= (H^2 + K^2 + L^2)h_1 - 2H(Hh_1 + Kk_1 + Ll_1)\\ k_2 &= (H^2 + K^2 + L^2)k_1 - 2K(Hh_1 + Kk_1 + Ll_1)\\ l_2 &= (H^2 + K^2 + L^2)l_1 - 2L(Hh_1 + Kk_1 + Ll_1)\end{aligned}\right\} \quad (10)$$

From equations (10) it follows that

$$\begin{aligned}(h_2^2 + k_2^2 + l_2^2) &= (H^2 + K^2 + L^2)^2(h_1^2 + k_1^2 + l_1^2)\\ &\quad + 4(H^2 + K^2 + L^2)(Hh_1 + Kk_1 + Ll_1)^2\\ &\quad - 4(H^2 + K^2 + L^2)(Hh_1 + Kk_1 + Ll_1)(Hh_1 + Kk_1 + Ll_1)\end{aligned}$$

$$\text{i.e. } (h_2^2 + k_2^2 + l_2^2) = (H^2 + K^2 + L^2)^2(h_1^2 + k_1^2 + l_1^2) \quad (11)$$

This relationship appears to be new and indicates the possible forms to which $(h_2k_2l_2)$ can belong given $(h_1k_1l_1)$.

It will be appreciated that if equations (10) are used for the reverse operation of expressing $(h_1k_1l_1)$ in terms of

$(h_2k_2l_2)$, the same values of $h_1k_1l_1$ will be obtained after removal of a common factor.

APPLICATION TO SPECIFIC CASES

Cubic crystals with "spinel law" twins. The authors have employed the matrix and formulae in connexion with the occurrence of twins in face-centred cubic metals and diamonds. In the latter case the interpretation of stereographic projections of twinned diamonds was made considerably easier. In both cases the twin planes is one of the {111} set of planes—a type of twin described by the "spinel law."

From equation (11):

$$(h_2^2 + k_2^2 + l_2^2) = 9(h_1^2 + k_1^2 + l_1^2) \qquad (12)$$

Hence the sets of planes to which $(h_2k_2l_2)$ can belong is indicated in Table 2 for planes which correspond to the principle X-ray reflexions.

Table 2. *Cubic case: "spinel law" twins*

$\{h_1k_1l_1\}$	*Possible sets of planes for* $\{h_2k_2l_2\}$
{111}	{511} and {333} (= {111})
{100}	{221} and {300} (= {100})
{110}	{411} and {330} (= {110})
{311}	{755}; {771} and {933} (= {311})

For a particular plane $(\bar{1}11)$ the most convenient form of matrix (1) (omitting a factor of $\frac{1}{3}$) is

$$\begin{bmatrix} 1 & 2 & 2 \\ 2 & 1 & \bar{2} \\ 2 & \bar{2} & 1 \end{bmatrix}$$

and so
$$h_2 = h_1 + 2k_1 + 2l_1 = h_1 + 2(k_1 + l_1)$$
$$k_2 = 2h_1 + k_1 - 2l_1 = k_1 + 2(h_1 - l_1)$$
$$l_2 = 2h_1 - 2k_1 + l_1 = l_1 + 2(h_1 - k_1)$$

On applying these formulae to the individual planes in the set {100}, i.e. (100), (010), (001), only planes of the form {221} result. In the other cases in Table 2 $(h_2k_2l_2)$ is found to belong to planes of any of the possible forms indicated.

A hexagonal case—titanium. Titanium is a hexagonal metal with $c/a = 1{\cdot}591$. Twinning planes of the types {10, 2}, {11, 1} and {11, 2} have been reported.[14] In Table 3 the values of [*UVW*] corresponding to one plane from each of these sets are listed and the corresponding matrix for plane transformations. The matrix for zones can be found by interchanging rows and columns. Some comments are given in the right-hand section of Table 3 to indicate the new positions after twinning of certain planes or directions.

Table 3. *Data for titanium*

(*HKL*)	[*UVW*]	*Matrix (planes)*	*Comments*
(10, 2)	[10 5, 6]	$\begin{bmatrix} 1 & \bar{5} & \bar{6} \\ 0 & 11 & 0 \\ \bar{20} & \bar{10} & \bar{1} \end{bmatrix}$	(01, 0) near to $(\bar{1}2, \bar{2})$ after transformation [01, 0] unchanged
(11, 1)	[55, 4]	$\begin{bmatrix} 1 & \bar{10} & \bar{2} \\ \bar{10} & 1 & \bar{2} \\ \bar{10} & \bar{10} & 9 \end{bmatrix}$	(10, 0) near to (01, 1) after transformation (01, 0 near to (10, 1) [00, 1] near to $[\bar{11}, 1]$
(11, 2)	[55, 2]	$\begin{bmatrix} 2 & \bar{5} & \bar{1} \\ \bar{5} & 2 & \bar{1} \\ \bar{10} & \bar{10} & 5 \end{bmatrix}$	[00, 1] near to $[\bar{22}, 1]$ after transformation

An orthorhombic case—α-uranium. Twinning in α-uranium which is orthorhombic presents an interesting case as four different twin planes have been reported by Cahn.[15] The values of the lattice parameters are $a = 2{\cdot}852$ Å, $b = 5{\cdot}865$ Å and $c = 4{\cdot}945$ Å. The data relating to the four modes of twinning are listed in Table 4. The last column in this table gives the shear direction η_1 as listed by Cahn[15] and by Frank.[16] This direction lies in the plane (*HKL*) although in some cases the indices given for η_1 are approximations to integers (i.e. the true shear direction does not quite coincide with the simple indices). It is a convenient check on the matrix in Table 4 to apply it to (*HKL*) or (transposed) to these indices for η_1. In the former case (*HKL*) is transformed into $(\bar{H}\,\bar{K}\,\bar{L})$ apart from a common factor, but in the latter case there is no change in sign. That this should be so is also clear from equations (5) and (8).

Table 4. *Data for α-uranium*

(*HKL*)	[*UVW*]	*Matrix (planes)*	*Direction of shear* η_1
(112)	[17 4 11]	$\begin{bmatrix} \bar{1} & \bar{4} & \bar{11} \\ \bar{17} & 12 & \bar{11} \\ \bar{34} & \bar{8} & \bar{6} \end{bmatrix}$	$[3\bar{7}2]$
$(1\bar{7}2)$	[3 $\bar{5}$ 2]	$\begin{bmatrix} 18 & 5 & \bar{2} \\ 21 & \bar{14} & 14 \\ \bar{6} & 10 & 17 \end{bmatrix}$	[312]
(130)	[7 5 0]	$\begin{bmatrix} 4 & \bar{3} & 0 \\ \bar{21} & \bar{4} & 0 \\ 0 & 0 & 11 \end{bmatrix}$	$[3\bar{1}0]$
(121)	[21 10 7]	$\begin{bmatrix} 3 & \bar{10} & \bar{7} \\ \bar{42} & 4 & \bar{14} \\ \bar{21} & \bar{10} & 17 \end{bmatrix}$	$[3\bar{2}1]$

ACKNOWLEDGEMENTS

The authors thank Mr. F. H. Saniter, Director of Research, The United Steel Cos. Ltd., for permission to publish this paper. They also gratefully acknowledge assistance given by Mr. K. Lane with some of the mathematics.

REFERENCES

(1) MÜGGE, O. *Neues Jb. Miner., Mh.*, p. 98 (1889, 2nd Vol.).
(2) MÜGGE, O. *Neues Jb. Miner.*, p. 55 (1899, 2nd Vol.).
(3) LEWIS, W. J., and HALL, A. L. *Mineral Mag.*, **12**, p. 324 (1900).
(4) MÜGGE, O. *Zbl. Min.*, **18**, p. 233 (1917).
(5) SLAWSON, C. B. *Amer. Mineralogist*, **35**, p. 193 (1950).
(6) FRIEDEL, G. *Bull. Soc. Franç. Mineral*, **43**, p. 246 (1920).

(7) BELL, J. F. *Amer. Mineralogist*, **26**, p. 247 (1941).
(8) HENRY, N. F. M., LIPSON, H., and WOOSTER, W. A. *The Interpretation of X-ray Diffraction Photographs*, p. 110 (London: Macmillan and Co. Ltd., 1951).
(9) HALL, E. O. *Twinning and Diffusionless Transformations in Metals*, Chapter 3 (London: Butterworths Scientific Publications, 1954).
(10) DECKER, B. F. *Amer. Mineralogist*, **29**, p. 226 (1944).
(11) NIGGLI, P. *Geometrische Kristallographie des Diskontinuums*, p. 517 (Leipzig: Borntraeger, 1919).
(12) HENRY, N. F. M., and LONSDALE, K. (editors). *International Tables for X-ray Crystallography*, Vol. 1 (Birmingham: Kynoch Press, for International Union of Crystallography, 1952).
(13) AITKEN, A. C. *Determinants and Matrices*, p. 16 (Edinburgh and London: Oliver and Boyd, 1946).
(14) ROSI, F. D., DUBE, C. A., and ALEXANDER, B. H. *Trans Amer. Instn Min. Met. Engrs*, **197**, p. 257 (1953).
(15) CAHN, R. W. *Acta Metallurgica*, **1**, p. 49 (1953).
(16) FRANK, F. C. *Acta Metallurgica*, **1**, p. 71 (1953).

Ionic bombardment heating of magnetron cathodes

By A. E. BARRINGTON, Ph.D., B.Sc., A.M.I.E.E., Services Electronics Research Laboratory Extension, Admiralty, Harlow, Essex

[*Paper received 2 June*, 1954]

A novel method of heating thermionic cathodes in transverse electric and magnetic fields is described. Hydrogen at an accurately controlled pressure is admitted into the vacuum envelope from a hydride replenisher (consisting of an indirectly heated nickel pellet coated with a suspension of zirconium hydride). Following the initiation of a low-pressure gas discharge in the inter-electrode space, the cathode is heated by positive ion bombardment until it reaches the temperature required for thermionic electron emission. The hydrogen is then reabsorbed by the replenisher and high-vacuum conditions are restored, while the cathode is maintained hot by electron back-bombardment alone. Following a section dealing with physical phenomena, practical applications of the method are discussed, such as the processing and starting of oxide-coated as well as high-temperature magnetron cathodes.

Indirectly heated oxide-coated cathodes have been widely used in microwave magnetrons since 1940. Other cathode types, relying on secondary emission initiated by primary electrons from a thermionic pilot cathode or by a gas discharge in the inter-electrode space have been described[1] but not used on a large scale. With increasing mean-power requirements in recent years, high-temperature cathodes[2] heated indirectly or by means of electron bombardment[3] from an auxiliary electron gun have undergone considerable development.

In magnetrons operating at wavelengths below 1 cm, limitations of space may impair the effectiveness of any of the above heating methods, and restrict the choice of cathode materials, which in turn may prevent full exploitation of a given magnetron design. Even in cases where cathodes can be heated to normal operating temperature by conventional methods, these may be inadequate for activation and processing of such cathodes.

A simple method to overcome these difficulties has been devised recently.[4] Hydrogen from a heated replenisher, consisting of an indirectly heated nickel pellet coated with a suspension of zirconium hydride, is introduced in the valve envelope, the gas pressure depending on the replenisher temperature. A gas discharge is then initiated in the transverse magnetic field provided by the magnetron magnet. Over a limited range of gas pressure it is possible to heat the magnetron cathode by positive ion bombardment to any desired temperature. When the cathode reaches the temperature required for thermionic electron emission, the hydrogen is reabsorbed by the replenisher and high-vacuum conditions are restored. For a particular heating cycle depending on the thermal design of the cathode structure, the cathode can then be maintained at the emitting temperature by electron back-bombardment alone.

THEORY

The behaviour of gases at low pressure in transverse electric and magnetic fields has been studied by a number of investigators,[5-7] who found that breakdown occurred at pressures far below those observed in the absence of the magnetic field. The effects of various parameters governing the initiation of a self-sustained discharge, i.e. electrode geometry, gas pressure, electric and magnetic intensity, have also been analysed in some detail. Once breakdown occurs, the movements of the charged particles in the discharge are somewhat complex. It is possible, however, to examine the mechanisms leading to the production of charge carriers, and to describe their subsequent behaviour. The following discussion applies particularly to a hydrogen discharge in a concentric cylindrical electrode structure.

(i) *Production of charged particles*

The following mechanisms may lead to the production of electrons and positive ions:

(*a*) *Field emission.* The number of electrons produced in this way is probably small, particularly in the case of smooth metallic cathodes where surface irregularities are unlikely to result in a voltage gradient of sufficient magnitude for this type of emission ($>10^6$ V/cm).

(*b*) *Secondary emission at the cathode.* This process greatly depends on the material and condition of the cathode surface. Both electrons and positive ions colliding with the cathode may liberate secondary electrons.

(*c*) *Secondary emission at the anode.* While this type of emission again depends largely on the material and condition of the anode surface, the overall contribution to the number of electrons produced may be assumed to be negligible.

(*d*) *Collisions between electrons and neutral gas molecules.* This is probably the most important source of free electrons. Each ionizing collision results, in the simplest case, in the production of an electron and a positively charged molecule. More complex ionization phenomena, resulting in the production of atomic or multi-atomic ions and a corresponding number of electrons have been reported.[8,9] However, according to Finch,[10] hydrogen is not dissociated by a discharge, except in the presence of water vapour. In a

carefully outgassed sealed-off system molecular ions may therefore be expected to predominate.

(ii) *Motion of charged particles*

(*a*) *Electrons.* In the absence of collisions, electrons produced at the cathode describe epicycloidal orbits round the cathode, the radial displacement depending on the initial velocity. Following a collision with a gas molecule, an electron can no longer return to the cathode, but, together with electrons produced by ionizing collisions, will move along a succession of epicycloids until it either reaches the anode or collides with another gas molecule. In a practical multi-cavity magnetron the electron orbits will be modified considerably by the presence of radio-frequency fields which build up owing to the motion of charged particles in the inter-electrode space. A number of electrons, accelerated by the radio-frequency field near the anode, will then, in fact, return to the cathode.

(*b*) *Positive ions.* The radius of curvature of the orbit of a charged particle in transverse electric and magnetic fields depends on the mass of the particle and, for a given electric and magnetic intensity, is a minimum for electrons. The lightest positive ion, with a mass 1837 times that of an electron, therefore experiences a comparatively small magnetic deflexion during its passage to the cathode. As a first approximation, ions may thus be considered travelling in rectilinear motion across the inter-electrode space. Provided no collision takes place between ions and molecules, the energy dissipated at the cathode due to ion impact for a given electric field depends only on the site of ionization, i.e. the potential drop experienced by the ion.

If the gas pressure is too low, the number of ions reaching the cathode will be insufficient to raise its temperature appreciably. On the other hand, if the pressure is too high, ions will collide with neutral molecules and eventually arrive at the cathode with too little energy to heat it. It is to be expected therefore, that, depending on the electrode geometry and applied electric and magnetic fields, an optimum pressure range exists, where cathode heating by ion impact occurs with maximum efficiency.

In practical magnetrons, the electric field distribution due to the presence of cathode end-hats minimizes diffusion of charged particles from the inter-electrode space. It ensures that maximum electron density and ionization probability occur in the inter-electrode space, resulting in maximum ion bombardment at the active cathode surface.

THE HYDROGEN SOURCE

The theoretical possibility of a bombardment-heated thermionic cathode in transverse electric and magnetic fields was recognized several years ago.[11] It was found in practice, however, that accurate permanent control of the gas pressure was the limiting factor which could not be attained in the equipment used at the time. It follows, therefore, that in order to meet operational requirements in a practical magnetron a number of conditions must be satisfied.

(*a*) The hydrogen pressure must be accurately controllable within a narrow pressure range (found experimentally of the order of 10^{-2} mm of mercury).

(*b*) The temperature-pressure characteristic of the source must be constant throughout the life of the magnetron.

(*c*) When the cathode reaches the operating temperature required, the source must reabsorb the hydrogen quickly and the pressure in the envelope be reduced such as not to affect the efficient operation of the valve.

Several materials are available whose characteristics are suitable for this application,[12] i.e. titanium, zirconium, thorium. It was found in practice that these metals when coated on a base of tungsten or nickel lose their activity after a comparatively small number of heating cycles owing to alloying with the base material. Good results, however, were obtained when the base was pre-alloyed with the metal in question before a final application of the active coating. No deterioration of performance was observed with indirectly heated replenishers of this type after more than 1000 temperature cycles. Equally promising results have been obtained with a replenisher consisting of indirectly heated nickel mesh coated with a suspension of the active metal. Zirconium has so far been found the most satisfactory material.

RESULTS

Ionic bombardment heating has been applied in a number of rising sun magnetrons, operating in the 3 cm and 8 mm band, containing oxide as well as high-temperature cathodes. The hydrogen replenisher was mounted in an extension of the glass envelope and indirectly heated by means of a tungsten coil. The optimum hydrogen pressure varied from 5×10^{-3} to 30×10^{-3} mm of mercury, depending on the geometry of the valves and operating conditions. The electronic mean free path at these pressures was of the same order as the mean inter-electrode space perimeter. Following the heating of the hydrogen source to the required temperature, the discharge could be initiated by application of either high voltage pulses (0·2–1·0 μs) or a medium voltage direct potential. Cathodes were thus heated to emitting temperature in about 10 sec after which the hydrogen source was allowed to cool and hydrogen was reabsorbed. High-vacuum conditions were restored after another 10 sec. No difficulty was experienced in heating cathodes to over 2000° C in this way. When direct current was used for starting, it was found advisable to use a current-stabilized supply as the anode current tended to increase extremely rapidly as the emitting temperature was reached. Owing to electron back-bombardment of the cathode this effect was cumulative and, with increasing cathode temperature, eventually led to the destruction of the cathode.

The duty cycle range over which a given structure can be maintained at optimum operating temperature by back bombardment alone is comparatively small, particularly when cathode life depends critically on cathode temperature. It is possible, without appreciably affecting pulsed magnetron operation, to supply sufficient back-bombardment power by means of a medium-voltage direct current supply to obtain considerable extension of the duty cycle range. A practical method which was used successfully is shown in the figure. The direct current supply is adjusted by varying the screen voltage of the tetrodes V_3 and V_4, and stabilized by the voltage developed across the resistor R_7 between grid and cathode. Condenser C_1 isolates the direct current supply from the pulse transformer and provides a low-impedance path for the high-voltage pulse applied to the magnetron; diode V_1 provides pulse isolation of the direct current supply. Between pulses, C_1 can discharge through diodes V_1 and V_2. As the direct voltage applied to the magnetron is of the same polarity as the high-voltage pulse, a conventional average pulse current meter reads the sum of continuous and average pulse currents. These can be separated, however, as shown in the diagram. The choke L_1 provides a low resistance direct current path but presents a very high impedance to the 0·2 μs pulse. The direct current resistance of the branch

containing the neon tube V_7 and the copper oxide rectifier is high, while the pulse impedance is low. Meter M_1 therefore reads the average pulse current, while meter M_2 reads the continuous current.

Ion bombardment heating has also been used successfully for processing and outgassing of cathodes prior to seal-off. The valves, in permanent or electromagnets, were isolated from the vacuum pump while hydrogen was admitted from a replenisher sealed into the vacuum system. When, following initiation of the discharge, the cathode attained the temperature required for thermionic emission, the pump was reconnected and any gases evolved from the cathode structure were then pumped away while the cathodes were maintained hot by electron back-bombardment alone.

ACKNOWLEDGEMENTS

This paper is published with the approval of the Admiralty. The author wishes to thank Mr. C. M. Cade and Mr. F. T. Turner for establishing processing techniques of the hydrogen replenisher.

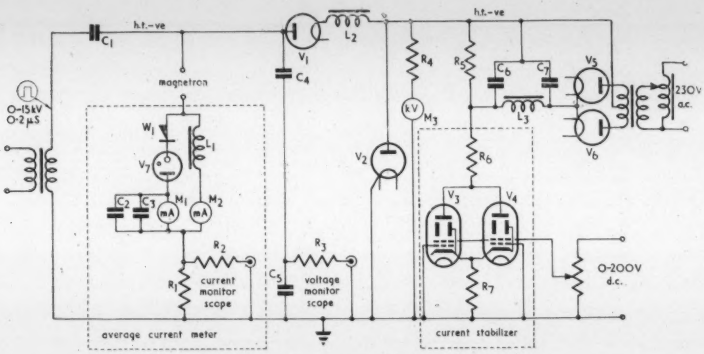

Circuit for combined direct current and pulse operation

R_1 = 20 Ω, 10 W high stability
R_2 = 50 Ω
R_3 = 70 Ω
R_4 = 3 MΩ
R_5 = 600 kΩ
R_6 = 10 kΩ
R_7 = 1·8 kΩ, 5 W

C_1 = 0·1 μF, 5 kV
C_2 = 0·1 μF mica
C_3 = 4 μF
C_4 = 50 pF, 10 kV
C_5 = 200 pF
C_6 = 4 μF, 5 kV
C_7 = 1 μF, 5 kV

L_1 = 1 H, 20 Ω
L_2 = 20 H
L_3 = 8 H

V_1 = CV74
V_2 = CV1111
V_3, V_4 = CV124
V_5, V_6 = CV1111
V_7 = CV188 (striking voltage 140 V, running voltage 70 V)

W_1 = copper oxide rectifier

M_1 = meter 0–10 mA
M_2 = meter 0–50 mA
M_3 = meter 0–3 kV

DISCUSSION OF RESULTS

Several factors may be expected to govern the life of a valve incorporating ion bombardment heating:

(*a*) Clean-up of hydrogen and absorption in other parts of the valve.

(*b*) Aging effects reducing the solubility and rate of absorption of hydrogen by the replenisher.

(*c*) Deterioration of the replenisher due to contamination by other gases in the valve.

None of these effects has been observed after life-testing a number of valves, all of which, after more than 1000 starting cycles, eventually failed from other causes. Clean-up of hydrogen by other valve components was negligible. This was probably due to the fact that, since the inter-electrode space represents a small fraction of the total valve volume, only a very limited number of the hydrogen molecules in the valve envelope were ionized during the short starting period. With careful processing and outgassing prior to seal-off, the evolution of gases from the cathode structure during life was minimized and no deterioration of the replenishers has been observed in practice.

REFERENCES

(1) Boot, H. A. H., and Randall, J. T. *J. Instn Elect. Engrs*, **93**, Part IIIA, p. 931 (1946).

(2) Collins, G. B. *Microwave Magnetrons*, M.I.T. Radiation Laboratory Series, Vol. VI, p. 515 (New York: McGraw-Hill Book Company, 1948).

(3) Harrison, A. E. *Klystron Tubes*, p. 210 (New York: McGraw-Hill Book Company, 1947).

(4) Barrington, A. E., and Buckingham, J. Provisional British patent specification, application No. 8686/53.

(5) Penning, F. M. *Physica*, **3**, p. 873 (1936).

(6) Somerville, J. M. *Proc. Phys. Soc.* [*London*], **63 (B)**, p. 620 (1952).

(7) Haefer, R. *Acta Phys. Austriaca*, **7** (No. 1), p. 52 (1953).

(8) Cobine, J. D. *Gaseous Conductors*, p. 84 (New York: McGraw-Hill Book Company, 1941).

(9) Massey, H. S. W., and Burhop, E. H. S. *Electronic and Ionic Impact Phenomena*, p. 245 (Oxford: Clarendon Press, 1952).

(10) Finch, G. I. *Proc. Phys. Soc.* [*London*], **62 (B)**, p. 533 (1949).

(11) Guthrie, A., and Wakerling, R. K. *The Characteristics of the Electrical Discharges in Magnetic Fields*, p. 343 (New York: McGraw-Hill Book Company, 1949).

(12) Smith, D. P. *Hydrogen in Metals*, p. 156 (Chicago: The University of Chicago Press, 1948).

Single exposure photography of a high speed event

By K. R. Tuson, Admiralty Materials Laboratory, Holton Heath, Poole, Dorset

[*Paper received* 8 *September*, 1954]

A method is described whereby conventional stroboflash and photoflash equipment can be used to provide a series of photographs of a recurrent event which cannot be mechanically linked to trigger the flash. Photoelectric triggering capable of accurate visual control and adjustment is therefore provided and the method has been satisfactorily applied to a study of the formation and behaviour of bubbles rising from a submerged orifice.

The normal photography of a selected event occurring within a single period of a rapidly recurrent process presents difficulties if the process is not one that is mechanically linked. The problem is apparent when trying to record the detachment of an air bubble from its jet under water. If the bubble rate is about thirty-three per second, the period is 30 ms; the time, however, between the moment of detachment and when the bottom of the bubble is, say, 1 mm above the jet, may be of the order of 100 μs. Since bubbles do not form in practice with such mechanical regularity that the bottom of each one is 1 mm above the jet every 30 ms, many exposures may have to be made in the endeavour to record this precise event. The ultra-high speed camera is wasteful of film when only a few frames are required from several feet, therefore another method was evolved. This uses a single exposure camera in conjunction with standard stroboflash equipment. Certain modifications are, however, necessary if the stroboflash is to control the photoflash exposure, because of the slight irregularity in the emission of the bubbles which are normally illuminated at precise intervals. The modification consists in arranging for the flashing rate to be controlled by the event to be recorded, and synchronizing this with the photoflash unit used to take the picture.

The illuminating system is shown in Fig. 1 and a block diagram of the complete arrangement is illustrated in Fig. 2.

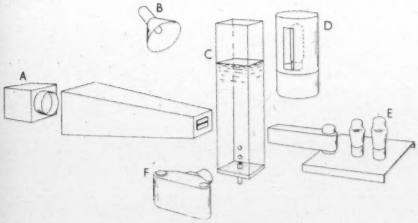

Fig. 1. Method of illumination

A, light source; *B*, stroboflash; *C*, observation cell; *D*, photoflash; *E*, photocell and amplifier; *F*, camera.

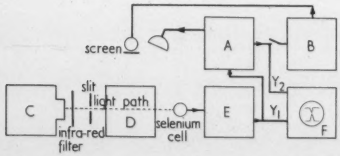

Fig. 2. Block diagram of stroboflash equipment

A, stroboflash unit; *B*, photoflash unit; *C*, light source; *D*, observation cell; *E*, amplifier; *F*, cathode-ray oscilloscope.

A parallel beam of light from a light-tight projector passes, first, through an infra-red filter in order to avoid specular reflexion. The beam passes on through a tube fitted with a slit at the end nearest the observation cell in which bubbles are generated. The very thin horizontal beam then traverses the liquid and impinges on to a selenium resistance cell. The latter is connected to a conventional amplifying and pulse-shaping circuit, the signal from which passes to the input of the stroboflash unit, which in turn is coupled, *via* a switch, to the photoflash unit. Thus the stroboflash unit is supplied with the necessary steep-fronted pulse each time a bubble interrupts the beam of light. The apparatus on either side of the observation cell is mounted on a platform so that the beam can traverse any position between the jet and the surface of the liquid. Since the flash is now triggered by the arrival of the top of a bubble at the light beam, it is possible to record any event within the precision of movement of the platform. For convenience in observing regularity of performance of the apparatus a double-beam oscilloscope may be used to monitor the signals. Plate Y_1 is connected to the amplifier output and Y_2 is connected to the stroboscope output, the scanning rate being adjusted to the bubble rate. To reduce specular reflexion from the photoflash, a piece of thin paper is placed between it and the observation cell. In this connexion, a few remarks are necessary on illuminating technique if the best photographic prints are to be obtained. The observation cell is made from perspex sheet. The thickness of the front and back is 1/16 in., the sides $\frac{1}{4}$ in. and the bottom $\frac{3}{8}$ in. Use is made of the property of perspex whereby light is transmitted through a reasonable length without much loss of intensity. A photograph, taken without any screening of the cell whatever, is flat and shows considerable specular reflexion. This is due to the high power flash passing through the rear edge of each side and the resultant reflexions illuminating the sides of the bubble. By using black tape of various widths, placed in different positions, almost any form of optical contrast can be recorded. In the case of the photographs illustrated here (Fig. 3), the tape was placed at the edges of the two sides and round the back so as to cover the thickness of the side pieces of perspex. The thickness of the bottom piece of perspex was also covered to avoid undesirable illumination of the glass jet and underside of the bubble. It will be seen that good boundary contrast is obtainable; the light tone in the middle of the bubble is from the open space between the side tapes, the parallel lines being distorted, of course, by the shape of the bubble. The tapes are seen to better advantage in the bore of the jet, the diameter of which is clearly indicated by the outer edges of the two black streaks. By combining a good optical contrast with a paper of appropriate photographic contrast, one is able to make dimensional measurements from the print to a considerable degree of accuracy.

The procedure for obtaining records is both simple and rapid. In a darkened room the stroboflash is switched on and the bubble rate adjusted. The bubbles are "arrested" in

the first place by manual control and the beam moved to its approximate position. The stroboflash is switched to the external, i.e. automatic, control and final adjustments made to the bubble rate and beam position in order to hold steady the exact picture required, which can now be continuously observed. The camera is swung into position, focused, and the shutter opened. Exposure of film, such as Pan F (by Ilford Ltd.), to the relatively weak red light of the stroboflash for a few seconds, does not affect the clarity of the final pictures. The switch controlling the photoflash is closed and a record is obtained the next time the stroboflash discharges, the two flashes being simultaneous. The process can be repeated by slightly raising the platform and a record is obtained of the phenomenon a fraction of its period later.

The type of record obtained is shown in Figs. 3(*a*), (*b*) and (*c*); the marks on the background are small bubbles arising from the turbulence of the liquid at the high bubble rate in operation. It will be observed that while the major part of the outline is sharp the point of the bubble is blurred, as seen more clearly in the enlargement, Fig. 3(*c*). The duration of the flash was about one hundred microseconds and it shows, therefore, that there is a very fast movement of the bottom of the bubble compared with the top. Since knowledge of these relative movements of the bubble envelope was required, a photoflash of shorter duration was not used. Experimental data combined with measurements on the photograph showed that the time between events shown in

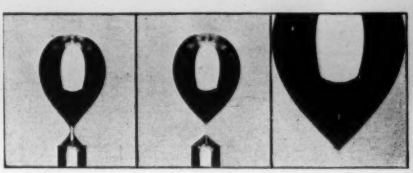

(*a*) (*b*) (*c*)

Fig. 3. (*a*) Bubble just prior to release. (*b*) Bubble just after release. (*c*) Tail of (*b*) enlarged

Fig. 3(*a*) and Fig. 3(*b*) was of the order of 50 μs while the actual bubble period was about 100 ms.

ACKNOWLEDGEMENT

This paper is published by permission of the Admiralty.

A method of measuring the intensity distributions of radio-frequency electric and magnetic fields in resonant cavities

By J. G. LINHART, Ph.D., Dipl.Ing., and T. H. B. BAKER, B.A., Grad.Inst.P., Research Laboratory, British Thomson-Houston Co. Ltd., Rugby

[*Paper received* 18 *October*, 1954]

A method is described whereby the intensity distributions of the radio-frequency electric and magnetic fields in a resonant cavity may be determined in terms of the changes in both the resonant frequency and the Q-factor, caused by the placing of a small spherical bead of dielectric or ferromagnetic material at the relevant points in the cavity.

The standard method of exploring radio-frequency field patterns in a resonant structure uses movable aerial or loop probes which couple out a certain amount of power, the latter being proportional to the square of the field intensity (E^2 or H^2) in the region occupied by the probe. It is evident that in order to couple power out of the resonant cavity (except when the investigation of the field is confined to the region close to the cavity walls), it is necessary to introduce into it a piece of coaxial cable connecting the probe to the detector. This may perturb the radio-frequency pattern and may detune the cavity by an amount sufficient to invalidate the intensity measurement.

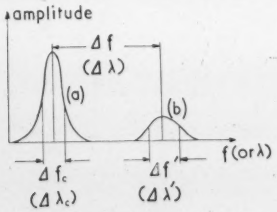

Fig. 1. Resonant curves of a cavity
(*a*) empty; (*b*) containing a bead.

A method will be described which dispenses with the link connecting the actual probe to the detector. The method is based on the well-known effect that a piece of dielectric or ferromagnetic material when introduced in a resonant cavity, displaces the resonant frequency f of the empty cavity and in most cases also lowers its Q-factor. (A similar method, using conducting materials has been described by L. C. Maier and J. C. Slater.[1])

In this case use is made of the dependence of both the resonant frequency displacement Δf and of the increase in the width of the resonance curve $\Delta f'$ (see Fig. 1), on both the electric field strength E and the magnetic field strength H, according to expressions of the form:

$$|E| = \phi(\Delta f, \Delta f')$$
$$|H| = \psi(\Delta f, \Delta f')$$

The nature of these relations will now be explained.

THEORY OF MEASUREMENT

Consider the effect of a small body within a resonant cavity on the resonance curve of the cavity. The effect is twofold.

(i) The resonant frequency f of the empty cavity is changed by an amount

$$\Delta f = \Delta f_e + \Delta f_m \qquad (1a)$$

where, for a small spherical body having volume V, dielectric constant ϵ and permeability μ[2]:

$$\left.\begin{aligned} -\frac{\Delta f_e}{f} &= \frac{\pi V}{3}\,\frac{\epsilon-1}{\epsilon+2}\,\frac{E^2}{W} \\ -\frac{\Delta f_m}{f} &= \frac{\pi V}{3}\,\frac{\mu-1}{\mu+2}\,\frac{H^2}{W} \end{aligned}\right\}$$

where W is the energy stored in the cavity. (It is assumed that Δf is small compared with f, so that we may use f throughout for the frequency.)

Now let $$E = A_e F_e(xyz)$$

and $$H = A_m F_m(xyz)$$

where F_e and F_m are normalized as follows:

$$\int_\Omega F_e^2 d\Omega = \int_\Omega F_m^2 d\Omega = 1$$

(Ω is the volume of the cavity).

Then
$$-\frac{\Delta f_e}{f} = \frac{\pi V}{3}\,\frac{\epsilon-1}{\epsilon+2}F_e^2(xyz) \qquad (1b)$$

$$-\frac{\Delta f_m}{f} = \frac{\pi V}{3}\,\frac{\mu-1}{\mu+2}F_m^2(xyz) \qquad (1c)$$

where xyz are the co-ordinates of the centre of the test-body.

If the material of the test-body has conductivity σ

$$\sigma > 0$$

it is necessary to define new ϵ and μ (the effective ϵ and effective μ).

The effect of non-zero conductivity on the effective ϵ is merely to increase its value. Thus

$$\epsilon \to \infty \quad \text{as} \quad \sigma \to \infty$$

and
$$\frac{\epsilon-1}{\epsilon+2} \to 1.$$

The effect of a conducting sphere on the magnetic field is to expulse the magnetic field lines from its interior, without becoming a terminus of these lines. Thus

$$\mu \to 0 \quad \text{as} \quad \sigma \to \infty,$$

and therefore
$$\frac{\mu-1}{\mu+2} \to -\frac{1}{2}.$$

If we take the ϵ and μ in the formulae (1*b*) and (1*c*) to be the effective ϵ and μ of the sample it follows that $(-\Delta f_m)$ may in some cases become positive.

The total relative displacement of the resonant frequency is

$$-\frac{\Delta f}{f} = \frac{\pi V}{3}\left(\frac{\epsilon-1}{\epsilon+2}F_e^2 + \frac{\mu-1}{\mu+2}F_m^2\right) \qquad (1d)$$

(ii) The other effect is due to the electric and magnetic losses within the body. These may be represented as follows:

$T = \epsilon_0 C_e V E^2$ – electric loss (watts)

$U = \mu_0 C_m V H^2$ – magnetic loss (watts).

where C_e and C_m are constants.

These losses alter the Q-factor of the cavity. Thus

$$1/Q = 1/Q_e + 1/Q_m + 1/Q_c$$

where $1/Q_e$ represents electric loss;
$1/Q_m$ represents magnetic loss; and
$1/Q_c$ represents losses in the walls of the cavity.

Now since $1/Q = \Delta f'/f$ (where $\Delta f'$ is the frequency interval between half-power points on the resonance curve), the equation for the Q's may be written in terms of $\Delta f'$.

Thus $$\Delta f'/f = \Delta f_e'/f + \Delta f_m'/f + \Delta f_c'/f \qquad (2a)$$

or $$\Delta f' = \Delta f_e' + \Delta f_m' + \Delta f_c'.$$

Q_e and Q_m follow from their respective definitions.

$$Q_e = \left(2\pi f \epsilon_0 \int_\Omega E^2 d\Omega\right) \Big/ T$$

$$= (2\pi f/VC_e)F_e^{-2}(xyz) = f/\Delta f_e' \qquad (2b)$$

and similarly

$$Q_m = (2\pi f/VC_m)F_m^{-2}(xyz) = f/\Delta f_m' \qquad (2c)$$

Substituting (2*b*) and (2*c*) into equation (2*a*) one obtains

$$\Delta f'/f = 1/Q_c + V(C_e F_e^2 + C_m F_m^2)/2\pi f$$

Introducing the change in breadth $\Delta f''$ of the resonance curve, the last equation may be written as

$$\Delta f''/f = V(C_e F_e^2 + C_m F_m^2)/2\pi f \qquad (2d$$

The equations (1*d*) and (2*d*) express Δf and $\Delta f''$ (both directly measurable quantities) in terms of the normalized electric and magnetic field strengths. Let us write these equations as

$$\Delta f = \alpha F_e^2 + \beta F_m^2 \qquad (3)$$

$$\Delta f'' = a F_e^2 + b F_m^2 \qquad (4)$$

$$\left(\text{where } \alpha = \frac{\pi V}{3}\,\frac{\epsilon-1}{\epsilon+2} f, \quad \beta = \frac{\pi V}{3}\,\frac{\mu-1}{\mu+2} f,\right.$$

$$\left. a = \frac{VC_e}{2\pi}, \quad b = \frac{VC_m}{2\pi}\right)$$

and let us solve these for F_e and F_m.

One obtains:

$$F_e = \sqrt{\left(\frac{b\Delta f - \beta \Delta f''}{\alpha b - \beta a}\right)} \qquad (5)$$

$$F_m = \sqrt{\left(\frac{\alpha \Delta f'' - a\Delta f}{\alpha b - \beta a}\right)} \qquad (6)$$

or more concisely

$$F_e = L\sqrt{(\Delta f - q\Delta f'')} \qquad (7)$$

$$F_m = M\sqrt{(\Delta f'' - p\Delta f)} \qquad (8)$$

where $q = \beta/b$, $p = a/\alpha$, $L = (\alpha - qa)^{-1}$, $M = (b - p\beta)^{-1}$.

We have thus obtained the required field strengths F_e and F_m in terms of the measurable quantities Δf and $\Delta f''$. It is not necessary to determine L and M since only the relative field strengths at different points in the cavity are required; p and q are determined by a separate experiment (Appendix I).

EXPERIMENTAL TECHNIQUE

(i) *Apparatus.* To check the formulae (7) and (8), use can be made of a cylindrical cavity oscillating in the E_{010} mode, for which the distribution of electric and magnetic field is known. Power from a tunable oscillator is fed into the cavity through a coaxial cable and a loop probe. Another probe couples out power, which is rectified and amplified, and measured on a meter (Fig. 2).

A small ferrite bead is suspended on a thread which passes through two diametrically opposed holes in the cavity wall. (In this case the ferrite had the composition 70% ferric oxide, 20% zinc oxide, 10% manganese dioxide, with a small amount of copper oxide added to aid sintering.) The ends of the

thread pass over pulleys and are joined to weights. The bead can be moved through the cavity by raising or lowering the weights, and the position of the bead is indicated by the position with respect to a fixed scale of a pointer attached to the thread (Fig. 3).

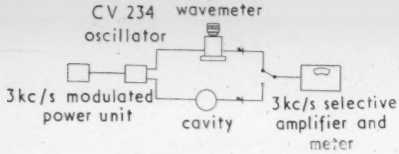

Fig. 2. Block diagram of the measuring gear

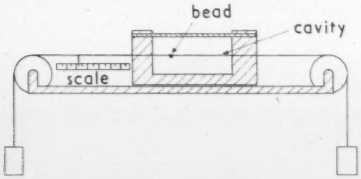

Fig. 3. Section through the cavity

(ii) *Procedure*

(*a*) The resonant wavelength λ of the empty cavity, and the wavelength separation $\Delta\lambda$ of the half power points are measured, using a sensitive wavemeter (λ and $\Delta\lambda$ can be used in formulae (7) and (8) instead of f and Δf, since $|\Delta f/f| = |\Delta\lambda/\lambda|$).

(*b*) The change in resonant wavelength, due to the introduction of the ferrite bead at suitable points in the cavity, is measured. The wavelength separation of the half power points at each of these positions is also measured.

(*c*) The constants p and q are determined for the test body as in Appendix 1.

(*d*) The electric field strength is calculated from expression (7) and the magnetic field strength from expression (8).

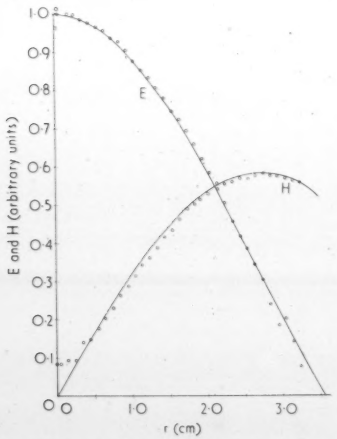

Fig. 4. Electric and magnetic field distribution in a cavity excited in the E_{010} mode

Resonant wavelength of empty cavity = 9·3 cm; diameter of bead = 6 mm; radius of cavity = 3·55 cm; $p = 0{\cdot}075$; $q = 0{\cdot}020$.

——— = theoretical distribution;
○○○○ = experimental values.

CONCLUSIONS AND APPLICATIONS

(i) The method has been used to measure the field distribution in an E_{010} cavity, and good agreement was obtained with the theoretical distribution (Fig. 4). The slight discrepancy at the centre may have been due to the finite radius (3 mm) of the bead.

(ii) Using a ceramic bead, the electric field distribution in a cavity oscillating in the H_{410} mode has been investigated, and found to agree well with the theoretical distribution (Fig. 5).

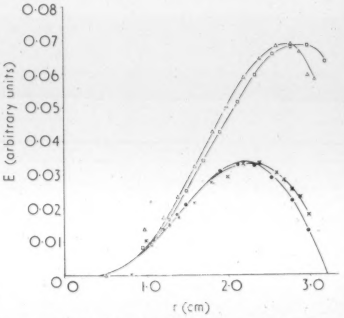

Fig. 5. Electric field distribution for a cavity excited in the H_{410} mode

Resonant wavelength of empty cavity = 3·05 cm; diameter of bead = 3 mm; radius of cavity = 3·2 cm; height of cavity = 2·7 cm.

● = E_ϕ } theoretical distribution.
□ = E_r } for simple cylindrical cavity
× = E_ϕ } experimental distribution.
△ = E_r } for actual cavity.

(iii) Using a ceramic rod inserted into the slots of a magnetron anode block, the resonant field patterns of the block have been investigated. This suggests that the method may be used in place of rotating probe measurements on magnetron anodes.

(iv) The method is also helpful in calculating the current excitation of cavities having complicated geometrical shapes. (See Appendix 3.)

ACKNOWLEDGEMENTS

This work was undertaken in connexion with a contract placed by the Department of Physical Research, Admiralty. The authors wish to thank the Admiralty, and also Mr. L. J. Davies, the Director of Research of The British Thomson-Houston Company Ltd., for permission to publish this article.

APPENDIX 1

Measurement of p and q

In order to find p and q, we use the bead in a cavity which has a known distribution of E and H, and measure Δf and $\Delta f''$ at two points.

Then using equation (8)

$$H_1^2/H_2^2 = r_1 \text{ (say)} = (\Delta f_1'' - p\Delta f_1)/(\Delta f_2'' - p\Delta f_2)$$

whence $$p = (\Delta f_1'' - r_1\Delta f_2'')/(\Delta f_1 - r_1\Delta f_2) \qquad (9)$$

Similarly, using equation (7)

$$E_1^2/E_2^2 = r_2 \text{ (say)} = (\Delta f_1 - q\Delta f_1'')/(\Delta f_2 - q\Delta f_2'')$$

whence $$q = (\Delta f_1 - r_2\Delta f_2)/(\Delta f_1'' - r_2\Delta f_2'') \qquad (10)$$

If one measurement is taken at a point where the magnetic field is zero, then $r_1 = 0$ and

$$p = (\Delta f''/\Delta f)_{H=0}$$

Similarly, if a measurement is taken at a point where the electric field is zero, then $r_2 = 0$ and

$$q = (\Delta f/\Delta f'')_{E=0}$$

APPENDIX 2

Accuracy of measurement

The fidelity of the measurement is limited by two factors.

(1) The volume of the bead. The larger the test-body the smaller is the accuracy with which one may relate the unperturbed E and H to a particular point xyz, as the measured field F is in fact the E-field (or H-field) integrated and averaged over the volume V.

(2) The ratio $\Delta f/f$. The accuracy of frequency measurements is proportional to $\Delta f/f$.

It is thus obvious that a compromise must be found between the volume of the test-body and the relative frequency shift $\Delta f/f$.

It is also interesting to note that this problem illustrates the principle of complementarity well known in information theory and quantum mechanics. As the product of two complementary quantities must yield a constant of the measurement, we find in the case of a dielectric non-lossy sphere that:

$$\frac{\Delta f}{f}\cdot\frac{1}{V} = \frac{\pi}{3}\cdot\frac{\epsilon - 1}{\epsilon + 2}\cdot F^2 = \text{constant}$$

In this constant only ϵ is at our disposal and thus one chooses ϵ as high as possible. It is important to remember that the function $F(xyz)$ derived from measurements using a spherical test-body does not give any information as regards the vector character of the $E(xyz)$.

Such information may be gained either from the knowledge of the general form of the pattern investigated or one may use a disk-shaped test-body. In most cases, however, the latter refinement of the measurement is not necessary.

APPENDIX 3

Comparison of mode patterns in different cavities

The method of measuring the field strength in a resonant system described in Appendix 2 is eminently suitable for making a comparison of the field strengths in metrically different but topologically identical cavities, given equivalent excitations.

Let us consider two cavities, the second of which may be evolved from the first by a continuous deformation of the walls. Let us also consider a mode M_1 (frequency f_1) of the first cavity which due to the deformation of the walls will pass into a mode M_2 (frequency f_2) of the second cavity. If the excitation of both modes is the same, i.e. if the input radio-frequency energy $\dot{W}$ in both cases is the same, we shall have for the stored energies $W_{1,2}$

$$W_1 = \dot{W}Q_1/2\pi f_1$$

$$W_2 = \dot{W}Q_2/2\pi f_2$$

where $Q_{1,2}$ are the Q-factors of the respective cavities.

According to equation (1*b*) the field strengths are:

$$E_1^2 = C_0 . W_1 . \Delta\lambda_1/\lambda_1$$

$$E_2^2 = C_0 . W_2 . \Delta\lambda_2/\lambda_2$$

where $C_0 = \dfrac{3(\epsilon + 2)}{\pi V(\epsilon - 1)}$ = constant, depending only on the volume and dielectric constant of the test-body.

Thus $$E_1/E_2 = \sqrt{\left(\frac{\Delta\lambda_1/\lambda_1}{\Delta\lambda_2/\lambda_2}\cdot\frac{Q_1/f_1}{Q_2/f_2}\right)}$$

Therefore $$E_1/E_2 = \sqrt{\left(\frac{\Delta\lambda_1 . Q_1}{\Delta\lambda_2 . Q_2}\right)}$$

One may also consider an excitation by a constant current element Il, where I is the magnitude of the current and l is the length of the current element. Then

$$\dot{W}_1 = I\,\boldsymbol{e}_1 . \boldsymbol{l}_1$$

$$\dot{W}_2 = I . \boldsymbol{e}_2 . \boldsymbol{l}_2$$

where e_1, e_2 are the electric field strengths at the place of the current element $Il_{1,2}$. As before the e_1 and e_2 are given by:

$$e_1^2 = C_0 . W_1\Delta\lambda_1/\lambda_1$$

$$e_2^2 = C_0 . W_2\Delta\lambda_2/\lambda_2$$

but now the stored energies are

(assuming that $\boldsymbol{e}_1 \wedge \boldsymbol{l}_1 = 0$, $\boldsymbol{e}_2 \wedge \boldsymbol{l}_2 = 0$).

$$W_1 = \dot{W}_1Q_1/2\pi f_1 = e_1l_1Q_1/2\pi f_1$$

$$W_2 = \dot{W}_2Q_2/2\pi f_2 = e_2l_2Q_2/2\pi f_2$$

from which the ratio $e_1/e_2 = l_1Q_1\Delta\lambda_1/l_2Q_2\Delta\lambda_2$.

These formulae may be used with advantage in cases where the output power W_1 (in a given mode) is known for a particular system (usually a single resonant structure excited by a linear or circular current I) and one desires to calculate the output W_2 for the same current excitation I but for a different shape of the resonant cavity.

Then

$$W_1/W_2 = Ie_1l_1/Ie_2l_2 = \Delta\lambda_1Q_1l_1^2/\Delta\lambda_2Q_2l_2^2 = \gamma$$

and therefore $$W_2 = \gamma W_1.$$

REFERENCES

(1) MAIER, L. C., and SLATER, J. C. *J. Appl. Phys.*, **23**, p. 78 (1952).

(2) CASIMIR, H. B. G. *Philips Res Rep.*, **6**, pp. 162–82 (1951).

Some lithium iodide phosphors for slow neutron detection

By K. P. NICHOLSON, M.Sc., Grad.Inst.P., and G. F. SNELLING, M.Sc., Atomic Energy Research Establishment, Harwell, Berks.

[*Paper received* 5 *August*, 1954]

An account is given of the growing of single crystals of lithium iodide for use as scintillation detectors of slow and resonance energy neutrons. Tin, europium and samarium activators have been tested and their relative merits are presented. Where possible the phosphor properties are compared with a standard sodium iodide crystal. The practical application of lithium iodide crystals to neutron counting and the limitations imposed by their sensitivity to γ-radiation are discussed.

Lithium iodide, when suitably activated, will scintillate under slow neutron irradiation as a result of the $^6Li(n, \alpha)^3H$ reaction in which the α-particle and triton share an energy of 4·79 MeV. By analogy with NaI(Tl), which is an efficient phosphor, the first activator to be tried was thallium[1]; however, the phosphor produced had a very non-uniform activator concentration resulting in poor energy resolution. As will be explained later, a practical lithium iodide neutron detector must exhibit good energy resolution to facilitate discrimination against the background of γ-radiation encountered in most neutron measurements, so that this phosphor is of little use. Subsequently uniform activation was achieved with tin,[2,3] europium[4] and samarium. The present work is concerned with the growing and testing of these three phosphors.

CRYSTAL GROWING

Using vertical growing ovens of the type introduced by Stockbarger,[5] single crystals of lithium iodide up to 5 cm diameter by 7 cm long have been grown in this laboratory. A commercial grade of lithium iodide is vacuum dehydrated[6] and the product ground to a powder to facilitate filling the Pyrex glass capsule or growing tube. This capsule is tapered to a capillary at the base to initiate single crystal growth. The appropriate quantity of activator is added and the capsule placed in a vertical cylindrical oven where the contents are melted under vacuum and kept at 500° C for an hour before sealing off. It is then transferred to the growing oven and lowered through the temperature gradient at a suitable rate, this being 1·0 mm per hour for 5 cm diameter crystals.

After the growing is complete the capsule is placed inverted in a large glass test tube, which in turn is evacuated and placed vertically in an oven held at 550° C. Here the surface of the crystal melts and the latter slides down into a wider portion of the capsule. The crystal is then ready for annealing, which takes twenty-four hours in a controlled run down from 350° C to room temperature.

Prior to canning, the crystal is cut to shape with a wet string cutter and the surfaces dry-ground with grade 0 emery paper. It is then mounted in a thin-walled aluminium can which has a glass window sealed in with cold-setting Araldite type 101, the optical joint between the crystal and the quartz being made with silicone oil type MS 200. The space remaining in the can is packed with the magnesium oxide reflector, after which the lid of the can is sealed with Araldite.

PHOSPHOR PROPERTIES

The salient properties of the lithium iodide phosphors activated with tin, europium and samarium are summarized in Table 1 and compared with data for a standard sodium iodide crystal. The tests were made with a scanning kick-sorter similar to that described by Owen.[7] A 200 mc polonium–beryllium source was used for neutron measurements and a ^{137}Cs γ-ray source was used for energy calibration purposes.

Table 1. *Summary of crystal characteristics*

Crystal	LiI(Sn)	LiI(Eu)	LiI(Sm)	NaI(Tl)
Activator concentration (mole %)	0·05	0·03	0·02	0·05
Colour of fluorescence	Green	Blue	Blue	Blue
Appearance in daylight	Yellow-Green	Almost colourless: fluoresces with blue tinge at edges	Colourless	Colourless
Average energy resolution for neutrons	15% (6260) 12% (5819)	12%	Insufficient data	—
Best recorded energy resolution for neutrons	11% (5819)	11·5%	13·8%	—
Equivalent neutron energy release (MeV)	4·0	4·1	3·6	—
Relative pulse heights using NaI(Tl) as standard and ^{137}Cs source	7·5	35	3·3	100
Decay time (μs)	0·8	1·4	0·25	0·34
Stability of crystal (after canning)	Chemical change with time under storage: accelerated by radiation	Stable	Deteriorates under irradiation	Stable

Referring to the table it can be seen that LiI(Eu) has a light output five times greater than that of LiI(Sn). Therefore it is reasonable to expect a better energy resolution for the europium-activated crystal. Schenck[4] reports a resolution of 6%; in our case 11·5% is the best so far achieved.

The decay times were determined by plotting neutron kicksorter curves, for a series of amplifier differentiation time constants. It may be shown that

$$V/V_0 = 1/e$$

where V is the output pulse amplitude when the differentiation time constant equals the phosphor decay time and V_0 is the output pulse amplitude when the differentiation time constant of the amplifier is large. (An A.E.R.E. type 1049 B amplifier, with a differentiating time constant adjustable between 0·08 and 8 μs was used in these experiments. All other differentiating time constants, e.g. the photomultiplier anode circuit, were greater than 50 μs.) By plotting the pulse height against the differentiation time constant a curve is obtained which asymptotically approaches V_0. The decay time constant may then be obtained using the condition stated above.

The short decay time of the samarium-activated phosphor would facilitate fast counting if its light output could be increased, but at present equivalent results may be obtained from LiI(Eu) using a short amplifier differentiation time.

Two types of photomultiplier were used, the EMI 6260 and the RCA 5819. Li(Sn) gave better energy resolution with the type 5819 than with the type 6260. This is to be expected as the type 5819 has a higher sensitivity in the green and affords a better match with the emission spectrum of LiI(Sn). The other phosphors, however, have emission spectra which have a peak in the blue, where these photomultipliers have approximately equal sensitivities.

It is seen from the table that when an energy calibration is made with the 0·66 MeV γ-rays of ^{137}Cs, the recorded energy release of the ^{6}Li(n, α)^{3}H reaction is in the region of 4·0 MeV, which is 20% lower than the accepted value. This result is due to a saturation effect in the phosphor, whereby the light output is no longer linearly related to the energy lost by the incident particle.

PROPERTIES AS A NEUTRON DETECTOR

The chief advantage of a scintillation detector over other forms of counter is its high efficiency per unit volume. The theoretical counting efficiency as a function of crystal thickness for a number of neutron energies is given in Fig. 1 where it is seen that a 1 cm thick crystal is 65% efficient for thermal neutrons. It is important to note, however, that lithium iodide has the same γ-detecting efficiency as a sodium iodide crystal of equal weight, and this will limit its applications. In order to discriminate against interference pulses of comparable height arising either from attendant γ-radiation of 4 MeV energy, or indirectly from the pile-up of large numbers of pulses corresponding to a lower energy, the pulses arising from neutron capture need to be sharply defined in amplitude. As pointed out in the literature[8] this necessitates the maximum light output per pulse in addition to the uniform activator concentration mentioned above.

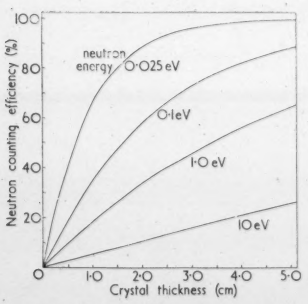

Fig. 1. Calculated neutron counting efficiency as a function of crystal thickness for energies between thermal and 10 eV. Neutron capture by the iodine has been included in the calculations

DISCRIMINATION BETWEEN NEUTRONS AND γ-BACKGROUND

If a lithium iodide crystal is tested under more realistic conditions, i.e. with both neutrons and γ-radiation present, the channel count rate rises rapidly at a pulse amplitude below the neutron peak as shown in Fig. 2. As the γ-flux

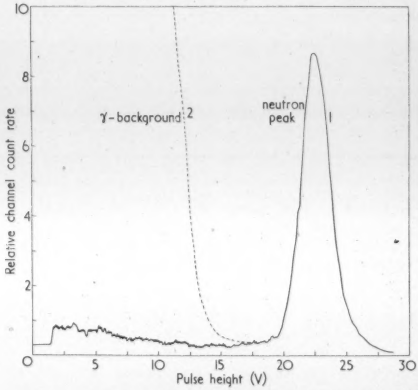

Fig. 2. (1) Typical kicksorter curve for a LiI(Eu) crystal irradiated by thermalized neutrons from a polonium–beryllium source. (2) Curve showing the count rate, at pulse heights less than the neutron peak, due to γ-radiation from an unshielded radium source. The composite curve is for a total neutron rate of 10 counts/s and a γ-radiation dose rate at the crystal of 10 mr/h

is increased pile-up will become noticeable and the situation may well arise where the γ-count at the neutron pulse height is comparable with the neutron count itself. The degree of pile-up is a function of the pulse width and may be reduced by shortening the differentiation time. However, when the latter is reduced to a value less than the phosphor decay time, serious attenuation of pulse height occurs with a consequent worsening of the resolution.

Due to the wide range of γ-energies existing in practice it is very difficult to calculate the point at which the build-up becomes significant, so an experiment was performed using a LiI(Sn) crystal and an unshielded radium source. The amplifier differentiation time was set equal to the phosphor decay time, in this case 0·8 μs. A polonium–beryllium source provided neutrons for an initial bias curve in the

absence of γ-radiation. The radium source was then moved in steps toward the crystal and a bias curve obtained for each γ-intensity. The data obtained is presented in Table 2. It must be noted that these results are accurate only for a LiI(Sn) crystal 2 cm diameter by 2 cm long placed in the chemical instability makes them unsuited to long-term use. The samarium-activated crystal matches the type 6260 and has the advantage of a short decay time, but is difficult to grow and appears to have a small light output. On the other hand the europium-activated phosphor is fairly easy to

Table 2. *Integrated γ-radiation interference rate (counts/s) as a function of pulse height for a number of γ-radiation dose rates*

(In the case considered the corresponding neutron "peak" occurred at 15 V)

Dose rate (mr/h)		5	10	20	50	100	200	500	1000
Pulse height (V)	10	12	22	40	100	—	—	—	—
	12·5	0·7	1·5	3·5	10	23	45	—	—
	15	0·06	0·15	0·4	1·4	3·8	10	37	—
	17·5	—	—	0·02	0·09	0·30	1·2	7	26
	20	—	—	—	—	0·02	0·08	0·7	4

γ-flux from a radium source. However, they should provide a useful guide where the conditions do not differ too drastically.

It may also be noted that neutron-induced iodine activity contributes to the background count, but in a constant neutron flux is not important for energies less than 20 eV.

CONCLUSIONS

An assessment of the lithium iodide phosphors may now be made. It has been pointed out that in addition to being efficient neutron detectors, they have a γ-response similar to that of a sodium iodide crystal of equal weight. For γ-radiation of energy less than 2 to 3 MeV, an intensity of 20 mr/h is the most that can be tolerated for a neutron count of the order of ten per second. Where the γ-energy exceeds 3·5 MeV direct interference occurs and the ratio of γ-radiation to neutrons must be small.

The γ-sensitivity could be reduced by using a lithium-bearing phosphor of lower atomic weight. In this regard crystals of pure lithium fluoride have been tested[9] and give weak scintillations under thermal neutron irradiation, but no suitable activator has so far been reported. A further improvement would result from the use of ^{6}Li enriched material. For a given neutron efficiency the crystal volume could be decreased with a corresponding reduction of the γ-interference.

Summarizing the relative merits of the crystals at present available, one concludes that LiI(Eu) is the most useful. The tin-activated crystals may be fairly readily grown and are capable of good energy resolution if used with a type 5819 photomultiplier. Conversely their emission spectrum does not match the type 6260 photomultiplier and also their grow, has a resolution at least as good as LiI(Sn) and matches the type 6260 very well. In addition it appears to be chemically stable in the sense that it does not deteriorate once canned, making it suitable for long-term use. Provided that its γ-radiation sensitivity can be tolerated LiI(Eu) constitutes a first-class scintillation detector for slow and resonance energy neutrons.

ACKNOWLEDGEMENTS

The authors wish to thank Mr. D. W. S. Smout and Mr. R. B. Owen for their valuable advice and assistance.

REFERENCES

(1) HOFSTADTER, R., MCINTYRE, J. A., RODERICK, H., and WEST, H. I., JR. *Phys. Rev.*, **82**, p. 749 (1951).
(2) BERNSTEIN, W., and SCHARDT, A. W. *Phys. Rev.*, **85**, p. 919 (1952).
(3) SCHENCK, J., and HEATH, R. L. *Phys. Rev.*, **85**, p. 923 (1952).
(4) SCHENCK, J. *Oak Ridge National Laboratory Progress Report* (ORNL 1365, 20 June, 1952).
(5) STOCKBARGER, D. C. *Rev. Sci. Instrum.*, **7**, p. 133 (1936).
(6) HARSHAW, J. A., KREMERS, H. C., STEWART, E. C., WARBURTON, E. K., and HAY, J. O. *United States Atomic Energy Commission Report* (NYO-1577, Sept., 1952).
(7) OWEN, R. B. *Atomics* [*London*], **4**, p. 34 (1953).
(8) GARLICK, G. F. J., and WRIGHT, G. T. *Proc. Phys. Soc.* [*London*], *B*, **65**, p. 415 (1952).
(9) FARMER, E. C., MOORE, H. B., and GOODMAN, C. *Phys. Rev.*, **76**, p. 454 (1949).

Correspondence

Electrical breakdown at very low gas pressures

Gas discharge phenomena at the pressures used in particle accelerators differ, in general, from those encountered in the normal discharge, since they occur at the pressures for which the mean free paths of the gas particles are comparable with the dimensions of the apparatus. It is the purpose of this note to examine, in terms of atomic collision data, two problems arising in connexion with such low pressure discharges. The first problem concerns the validity of a proposed interpretation of an observed breakdown anomaly, the second is to estimate at what pressure breakdown would occur if it were due solely to ionizing collisions in the body of the gas. Other effects, such as those due to X-rays, which must be considered in a general solution of the problem of breakdown, have been ignored in order to obtain order of magnitude estimates relating to one simple process.

An anomalous gas-discharge phenomenon has been reported in which the electrical breakdown strength increases with increasing pressure at unusually low pressures. Specifically the breakdown voltage increased from 60–70 kV with increasing pressure in the region of 10^{-4} mm of mercury in one case[1] where the electrodes were spaced 2 cm apart in air; in another case[2] it rose from 130 kV at 5×10^{-5} mm of mercury to 500 kV at 25×10^{-5} mm of mercury with a 40 cm air gap. The effect has also been noted in hydrogen.

An explanation has been advanced[3] in the following terms: a thin column of particles, presumably emanating from some local electrode irregularity (though no precise mechanism is postulated), strikes the second electrode and maintains a small "hot-spot." Secondary emission takes place from this area and provides the breakdown current. At pressures greater than a critical value the bombarding particles are all scattered out of the column, thus preventing the maintenance of the "hot-spot" and increasing the breakdown strength.

For calculation purposes it will be assumed that 50 kV is applied between plane electrodes with a spacing of 5 cm.

If a particle leaves one electrode with zero energy, is accelerated over a distance s by a uniform electric field maintained between the electrodes and then undergoes a collision in which it loses an amount of energy $e\Delta V$ and is deflected through an angle θ then, assuming it makes no further collisions, a relation may be found connecting the various parameters with r, the distance from the original target point to the actual point of impact with the second electrode. If r is to have a certain minimum value r_0 this equation will determine minimum and maximum values, θ_1 and θ_2, of the angle θ.

The total probability that the particle is scattered outside the circle of radius r_0 is given, to a good approximation when P is small, by:

$$P(r_0) = 2\pi N \frac{p}{760} d(\Sigma + \int) \int_0^1 dx \int_{\theta_1}^{\theta_2} I_n(\theta) \sin\theta d\theta \qquad (1)$$

where N is the number of molecules/cm^3 at S.T.P., p is the gas pressure in mm of mercury, d is the electrode spacing, $x = s/d$, $I_n(\theta)$ is the partial cross-section for collision between the charged particle and a gas molecule as defined in reference (4) and $(\Sigma + \int)$ denotes summation over all types of collision.

Equation (1) is invalid for $P(r_0) > 1$. For values approaching unity a correcting factor is necessary, this factor approximates to $\frac{1}{2}$ when $P(r_0) = 1$.

The evaluation of equation (1) in the general case presents some difficulty and further simplifying assumptions are necessary. For elastic collisions between electrons and hydrogen atoms the calculation was carried out for the three cases $r_0 = 0$, 0·0005 and 0·005 cm, corresponding to defocusing areas of 0, 8×10^{-7} and 8×10^{-5} cm^2, the relative probabilities being 11, 10·5 and 9. Since we are dealing with a diffraction phenomenon the same relative probabilities apply to the case of elastic collisions between protons and hydrogen atoms if the areas are scaled down in the ratio $m_e : m_p = 1 : 1860$.

The actual size of the postulated "hot-spots" is a matter for speculation, but the view is here advanced that they would certainly be no larger than 10^{-8} cm^2 and probably much smaller. Since the probability of defocusing by elastic collision is so little dependent upon the defocusing area within this upper limit, and assuming that the angular dependence for other types of collision is not vastly different, it is possible to simplify the calculations by evaluating for zero area in each case. This means that we are now dealing with the total collision cross-sections Q_n and equation (1) becomes:

$$P(o) = \frac{Np}{760}(\Sigma + \int)\frac{d}{V_0}\int_0^{V_0} Q_n(V)dV = d\frac{Np}{760}\bar{Q}_{total} \qquad (2)$$

Using published data[4, 5] we find for electrons in hydrogen:

$$\bar{Q}_{total} \simeq 0{\cdot}12\pi a_0^2 \quad (\pi a_0^2 \simeq 8{\cdot}8 \times 10^{-17}\ \text{cm}^2)$$

hence, assuming that $P = 1$ corresponds to complete defocusing, our estimate for the critical pressure in this case is:

$$p_c \simeq 1{\cdot}2 \text{ mm of mercury.}$$

Data is less complete in other cases but for electrons in oxygen or nitrogen we estimate:

$$\bar{Q}_{total} \simeq 0{\cdot}7\pi a_0^2 \quad \text{and} \quad p_c \simeq 0{\cdot}2 \text{ mm of mercury.}$$

In the case of positive ions, available information is still more meagre and a new process, charge exchange, has to be taken into account. Slightly extrapolating experimental results obtained by Keene[6] for ionization and charge exchange cross-sections, and assuming that the relative importance of elastic, excitation and ionization collisions is much as for the electron case, we find:

for H_2^+ in hydrogen: $\bar{Q}_{total} \simeq 8\pi a_0^2$ $p_c \simeq 16 \times 10^{-3}$ mm of mercury

N_2^+ in nitrogen: $\bar{Q}_{total} \simeq 20\pi a_0^2$ $p_c \simeq 6 \times 10^{-3}$ mm of mercury.

Comparison of these figures with the experimental results quoted above shows that the proposed mechanism is ruled out altogether if electrons are to constitute the particles of the defocused beam. Using the results for N_2^+ in nitrogen the estimated critical pressure is more than an order of magnitude greater than the observed value. In view of the

approximate nature of the calculations, the possibility that the collision cross-section data may be in error, that the criterion employed (complete scattering of the column of particles) is certainly too severe and that unknown contaminants may affect the experimental values, this is not an impossibly large difference, but we conclude that it is improbable that positive ions could be defocused in the way suggested and give rise to the observed increase in breakdown strength.

A process that must be taken into account in certain circumstances is the catastrophic reproduction of charged particles due to ionizing collisions. An estimate (relating to the same electrode spacing and applied voltage as mentioned earlier) of the pressure at which this form of "avalanching" would occur is an interesting by-product of the above calculations.

With electrons the probability of ionizing collisions falls off very rapidly at energies exceeding 100 eV (see Fig. 1) and

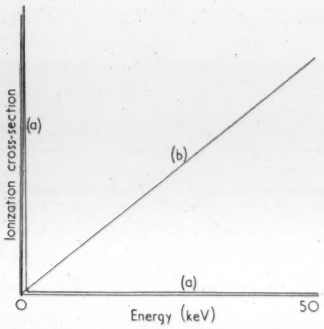

Fig. 1. General form of ionization cross-section/energy curves; (*a*) for electron/neutral collisions; (*b*) for positive ion/neutral collisions. (Curves are schematic only and vertical scales are not identical)

it will be a good approximation to assume that the integrated probability over the whole path, $P_i^{(e)}$, is concentrated very near the beginning of the path. Assuming the liberated electrons to have zero energy, and ignoring effects due to the liberated positive ions, the number of electrons deriving from an initial electron will be given approximately by:

$$1 + [P_i^{(e)}] + [P_i^{(e)}]^2 + [P_i^{(e)}]^3 + \ldots = [1 - P_i^{(e)}]^{-1} \quad (3)$$

This expression is obviously inexact since (*a*) the number of terms in the series must in fact be finite, and (*b*) $P_i^{(e)}$ will decrease, though very slowly. However, a fair deduction is that there will be a large multiplication factor when $P_i^{(e)}$ exceeds unity [see Fig. 2(*a*)].

For positive ions the position is very different. Here the ionization cross-section increases nearly linearly with energy up to 50 keV (see Fig. 1). To gain a crude estimate of the number of ions resulting from one original positive ion starting at rest from the anode, we again assume that the integrated probability of collision over the whole path is concentrated at the centroid of the cross-section/position curve. On this assumption the original positive ion produces $P_i^{(+)}$ new ions at a point $2d/3$ from the anode. Extending the argument these $P_i^{(+)}$ new ions produce $[P_i^{(+)}]^2/3^2$ further ions at a point $8d/9$ from the anode and so on [see Fig. 2(*b*)]. Thus, ignoring effects due to the liberated electrons, the number of positive ions per initial ion is given by:

$$1 + [P_i^{(+)}] + a[P_i^{(+)}]^2 + b[P_i^{(+)}]^3 + \ldots \quad (4)$$

where:

$$a = 3^{-2}, \quad b = (3 \times 9)^{-2}, \quad c = (3 \times 9 \times 27)^{-2} \ldots$$

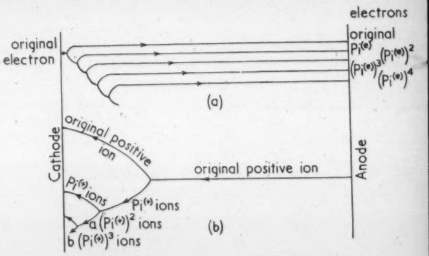

Fig. 2. Idealized representation of sequence of ionizing collisions assuming: (*a*) an electron starts from cathode with zero velocity and ignoring effects due to positive ions; (*b*) a positive ion starts from anode with zero velocity and ignoring effects due to electrons

The argument has been over-simplified by assuming that the new ions produced at each collision have zero energies. The values of the coefficients are less obvious in the more general case but we estimate for the other extreme case, in which all the energy is transferred to the new ions, that:

$$a \simeq (2)^{-1}, b \simeq (6)^{-1}, c \simeq (6 \times 6)^{-1}, d \simeq (6 \times 6 \times 12)^{-1} \ldots$$

Since both series are highly convergent and since the actual energy must be somewhere between these extremes it follows that multiplication of positive ions by this process can hardly be termed catastrophic unless $P_i^{(+)}$ itself is very large.

So far we have considered separately collisions between electrons and neutral atoms and between positive ions and neutral atoms. We may, however, combine the arguments and find that a single positive ion starting from rest at the anode produces approximately:

$$\frac{P_i^{(+)}}{[1 - P_i^{(e)}]} + \frac{a[P_i^{(+)}]^2}{[1 - P_i^{(e)}]^2} + \frac{b[P_i^{(+)}]^3}{[1 - P_i^{(e)}]^3} + \ldots \quad (5)$$

further ions and electrons, the coefficients being as above. This expression introduces no new features and it is obvious that multiplication becomes very large only for $P_i^{(e)} \simeq 1$ or for large values of $P_i^{(+)}$.

From calculations related to the previous ones it is found that, for hydrogen, $P_i^{(e)} \simeq 1$ corresponds to a pressure of 1·5 mm of mercury and $P_i^{(+)} \simeq 1$ to one of 0·05 mm of mercury. It is evident that the critical pressure for "avalanching" must be between these limits. To an order of magnitude we thus estimate the critical pressure for "avalanching" in hydrogen due solely to ionization by collision at 0·5 mm of mercury. In the case of oxygen or nitrogen the estimate is 0·1 mm of mercury.

It should again be emphasized that these estimates relate to the specific discharge conditions stated above (50 kV applied between plane electrodes with a spacing 5 cm). For other conditions the upper limit estimate can be modified by applying Paschen's law; the lower limit could also be determined but this is a more lengthy process.

Thanks are due to Mr. Fortescue and members of the Nuclear Particle Laboratory at Queen Mary College for drawing attention to the problems considered in this paper and for many helpful discussions.

Queen Mary College, J. W. LEECH
University of London,
London, E.1.

REFERENCES

(1) CLIFFORD, D. S. *Ph.D. Thesis* (London, 1952).
(2) HARRIS, D. J. *Ph.D. Thesis* (London, 1953).
(3) FORTESCUE, R. L. Private communication.
(4) MOTT, N. F., and MASSEY, H. S. W. *Theory of Atomic Collisions* (London: Oxford University Press, 1949).
(5) BATES, D. R., FUNDAMINSKY, A., LEECH, J. W., and MASSEY, H. S. W. *Phil. Trans A*, **243**, p. 93 (1950).
(6) KEENE, J. P. *Phil. Mag.*, Series 7, **40**, p. 369 (1949).

A method of making silicon junction diodes

A new and simple method of producing silicon *p–n* junction diodes is described. These diodes have particular applications as circuit elements in transistor circuits.

Briefly, the method is to oxidize the surface of a silicon crystal until an oxide layer is produced which is sufficiently thick to give a blue interference colour. A probe of suitable composition is pressed on the oxide layer and a current pulse of large amplitude and short duration is passed through the contact. The oxide layer is pierced and the probe welds to the silicon making a *p–n* junction of high mechanical stability.

Various details of the process are now described. The crystal is ground, polished and etched prior to the oxidizing treatment. A suitable oxidizing agent is a 3% solution of oxalic acid. This is contained in an electrolytic bath and alternating current is passed between two electrodes, each electrode consisting of a silicon crystal to be oxidized. With a *p*-type silicon crystal the probe must contain an element from Group V of the Periodic Table, e.g. phosphorus. Conversely, with an *n*-type crystal, the probe must contain an element from Group III, e.g. aluminium. The amplitude of the current pulse depends on the resistivity of the silicon. With 0·05 Ω cm silicon, a 5 ms pulse of amplitude 150 V is suitable. The oxide layer is an essential part of the process, without it a *p–n* junction is not produced. This layer is an insulator and it is considered that it permits a build-up of charge until the applied voltage is sufficiently high to arc through the layer. The area of the *p–n* junction is of the order 10^{-5} cm^2.

The figure shows voltage current characteristics of representative silicon diodes produced by the method. The table gives some data associated with these characteristics. The forward slope, Zener voltage* and Zener resistance increase as the resistivity of the silicon is increased. The onset of the Zener slope becomes less abrupt as the resistivity of the silicon increases. The minority carrier storage is very small, as would be expected in low resistivity short lifetime material. Only the diodes made with *n*-type silicon have a satisfactory working life.

Some circuit applications of these diodes are given in the following. (1) In transistor computor circuits of the type described by Williams and Chaplin,* widespread use is made of "catching diodes" which are returned to comparatively low catching voltages in the range 1 to 15 V. In practice two germanium point contact diodes are used. Each is biased

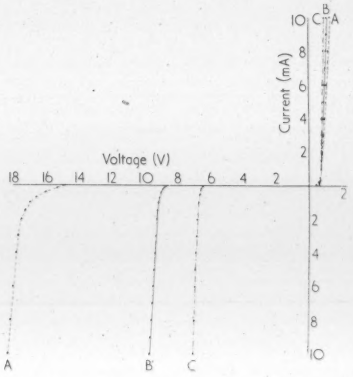

Voltage current characteristics of silicon junction diodes

Silicon junction diode parameters

	Diode A *p-type Si* 0·6 Ω cm. *Phosphor-bronze probe*	*Diode B* *n-type Si* 0·09 Ω cm. *Duralumin probe*	*Diode C* *p-type Si* 0·05 Ω cm. *Phosphor-bronze probe*
Forward slope resistance	54 Ω	33 Ω	18 Ω
Zener voltage	17·3 V	9·2 V	6·7 V
Zener slope resistance	122 Ω	59 Ω	58 Ω
Back resistance at 2 V	30 MΩ	180 MΩ	3 MΩ

appropriately and connected in parallel and in opposition to the collector, the emitter or the base of the transistor depending on the circuit application. A device with characteristics shown in the figure will replace the two germanium diodes and one bias supply. (2) The diode can be used as a voltage stabilizer to provide two "catching" levels. (3) The diode can be used for d.c. coupling between stages.

I thank my colleagues and Mr. G. B. B. Chaplin of the University of Manchester for helpful discussions and am indebted to the Chief Scientist, Ministry of Supply, and to the Controller, H.M. Stationery Office, for permission to publish this letter.

Radar Research Establishment, J. W. GRANVILLE
Great Malvern,
Worcestershire.

* MCAFEE, K. B., RYDER, E. J., SHOCKLEY, W., and SPARKS, M. *Phys. Rev.*, **83**, p. 650 (1951).

* WILLIAMS, F. C., and CHAPLIN, G. B. B. *J. Instn Elect. Engrs*, **100**, III, No. 66, p. 228 (1953).

New books

Theory of lenses. By E. W. H. SELWYN. (London: The Institute of Physics, 1955.) Pp. 62. Price 5*s*.

This little book is the fifth in The Institute of Physics' Monographs for Students Series, which is intended for general reading by students such as those in the first two years of a degree course in either science or engineering or for those reading for Higher National Certificates.

Although the book is about theory, its object is practical; the author has attempted to deal with the subject with not much, if any, more mathematics than is acquired at a grammar school. There are four chapters: Theory of light; First approximation; Second approximation, Seidel aberrations; Correction for colour and high order aberrations. A bibliography and a set of problems are included; none of the latter can be solved by merely substituting numerical values in a correctly remembered formula.

Radioisotope conference 1954 (sponsored by the Atomic Energy Research Establishment, Harwell), **Vol. 2,** Physical sciences and industrial applications. Edited by J. E. JOHNSTON, R. A. FAIRES and R. J. MILLETT. (London: Butterworths Scientific Publications, 1954.) Pp. ix + 223. Price 45*s*.

The publication in book form of all the papers presented at a conference gives a very rapid availability to the material and is in this case certainly very useful, although there is no attempt to survey or take stock of the field which one would expect in a normal book. This collection of papers deals mainly with the techniques of applying radioactive materials as tracers (the movement of wool fibres, diffusion in metals, the flow of water in pipes and in sewage tanks, carbide cutting tool wear); as sources of radiation for radiography (ranging from α-gauges for material of thickness 0–25 g/m^2 to γ-rays for 22 cm of steel and for measuring pipe thicknesses from the outside, including the measurement of moisture in soil by neutron scattering) and finally for determining the age of archeological samples from the concentration of ^{14}C. In some papers the results of the researches are also given, but, in general, the usefulness of the book is to show how many problems can be explored by radioactive tracers although by no means all important examples are included here (for example, the use of radon for gas flow studies in blast furnaces and open hearth furnaces). Only one paper has a summary at the beginning; a summary for each paper would certainly help the reader to find what he wants, as would a subject index.

M. W. THRING

Molecular theory of gases and liquids. By J. O. HIRSHFELDER, C. F. CURTISS and R. BYRON BIRD. (New York: John Wiley and Sons Inc.; London: Chapman and Hall Ltd., 1954.) Pp. xxvi + 1219. Price 160*s*.

As its name implies, this book provides a discussion of the properties of gases and liquids from the molecular standpoint. It is an astonishing account, for everything that could possibly be included finds its place here. At one end there is a discussion of general thermodynamics and statistical mechanics: and at the other end there is an almost complete account of transport properties, dispersion forces between large molecules, distribution functions in liquids and even a full description of what happens in a Bunsen burner. The text itself is supplemented by many tables of numerical magnitudes, and collected results. All the formulae that could possibly be needed are shown in full, and in a form suitable for immediate use.

When one meets a book of this size (over 1200 pages) there are three questions that have to be answered. First, who will want to use it? Second, how much prior knowledge does it presuppose? Third, is it clear and is it reasonably complete? Let us consider these questions one by one.

To begin with, this is not a book to read straight through, or even to take as a class text. It is a book of reference, with the additional property that the relation between each phenomenon and its basic explanation in terms of molecular forces, is always made apparent. For that reason it is most suitable for the research worker who wants to have a reasoned account of the interconnexions of his own particular piece of research and the wider field.

Next, the book presupposes that the reader has some prior acquaintance with the subject. It is true that it gives some elementary results, but unless the student had covered at least a year's course in quantum theory and statistical mechanics, he would find his progress pretty slow.

The answer to the third question is that the book is clearly written (though some of the formulae could be reduced in complexity of appearance with profit) and—at least to the present reviewer—it seems as complete as it could be. There is no doubt but that it contains some material not yet found in any other text-book and other material not readily available. An example of the first is the solution of the integral equation of Kirkwood–Yvon–Born for molecular distribution functions. An example of the second is the discussion of the complete Hamiltonian for a closed system such as a molecule in the presence of electric and magnetic fields.

The writing of a book as comprehensive as this is a tremendous job. The three chief authors have fitted their contributions together in a most satisfactory fashion. There is no doubt but that this book will not remain long on the library shelf: it will be in constant use for reference and similar purposes.

C. A. COULSON

Progress in metal physics, Vol. 5. Editors: B. CHALMERS, Ph.D., D.Sc., and R. KING, B.Sc. (London: Pergamon Press Ltd., 1954.) Pp. vii + 324. Price 60*s*.

The scientist who writes a review of recent progress may either cater for the specialist in his own subject and in closely related subjects, or he may endeavour to describe the principal results for the benefit of workers in other parts of the field. Previous reviewers of this series have deservedly praised most of the individual articles, but have sometimes complained that they did not fulfil the editor's declared intention (thrice repeated) of providing the second kind of report. Volume 5, the first to be produced under the joint editorship of Professor Chalmers and Mr. King, is honoured by a new foreword, and although phrased in general terms, this seems to imply that many of the reviews are now intended for the semi-specialist. This, if true, is no more than a recognition of the *de facto* situation, but many readers will continue to deplore the change in emphasis. The present reviewer does not subscribe wholeheartedly to this viewpoint; the need for good general surveys is obvious, but these more specialized reviews are of immense value to the active research worker.

Of the five articles in the present volume, those on *Liquid metals* by B. R. T. Frost and on *Solidification* by Ursula M. Martius are perhaps the least specialized. Dr. Frost's article is clear and interesting, but the review of solidification seems rather superficial, and the method of writing, which involves much repetition, is not a success. The important subject of *Fracture* is very well treated by N. J. Petch, and R. Maddin and N. K. Chen review recent experiments on the *Geometrical aspects of the plastic deformation of single crystals*. Both these articles are at about semi-specialist level, but may be read with profit and without undue effort by the less well informed. There remains the *Report on precipitation* by

H. K. Hardy and T. J. Heal, and this is definitely for the specialist only. The theoretical treatment of the thermodynamics and kinetics of precipitation is very good indeed, but the major portion of this very long and important review is given to a detailed discussion of the interpretation of the X-ray diffraction results obtained for all the reactions so far investigated. Even the specialist needs some guidance in this difficult and controversial topic, but the authors would have been better advised to stick to principles and to try to generalize the important conclusions; after fifty pages on the X-ray effects, it comes as rather a shock to read on p. 261 that "only for the aluminium-copper alloy may a qualitative understanding of the decomposition be taken as proved."

The standards of printing, reproduction and binding remain very high. The price is correspondingly stiff, but as indicated above, the book is extremely good value. Constant readers of the series, who have digested all the previous articles, must now be in the happy position of super-specialists, who know more and more about more and more.

J. W. CHRISTIAN

International Scientific Radio Union (URSI): Special Report No. 4. The distribution of radio brightness on the solar disk. Special Report No. 5. Interstellar hydrogen. (Brussels: URSI, 1954.) Pp. 71. Price 14*s*. 6*d*.

These two monographs, bound together, are a tribute to the stage now reached by radio-astronomy, of contributing powerfully to problems which already existed in solar physics and astrophysics, but which had been studied in a fog (as it were) when only optical wavelengths were available. Distribution of intensity and colour across the sun's disk had long been a question of importance, both in the information afforded as to depth of origin and in the localizing of the disturbances which give rise to spots and flares; recent development of radio receivers recording similarly the "brightness" in centimetre, decimetre and metre waves has enormously widened the range of weapons, and is rapidly accumulating evidence on chromosphere, corona, and isolated transient eruptions. Australian, American, British and European contributions are here discussed.

The second monograph describes the investigation of interstellar gas, especially by 21 cm wavelength (1420 Mc/s), which arises from transitions between hyperfine levels of the ground state of atomic hydrogen. The use of this frequency has become a prime method of finding the distribution of the extremely rarefied matter between the stars. There is even a "1420 Mc/s newsletter" edited from Leyden Observatory correlating the world's researches.

MARTIN JOHNSON

Radio. Vol. 2. By J. D. TUCKER and D. WILKINSON. (London: English Universities Press Ltd., 1954.) Pp. ix + 252. Price 10*s*. 6*d*.

This is the second volume of three intended to cater for the City and Guilds Radio examinations. It follows the City and Guilds syllabus for Radio II fairly closely, and can be recommended for the use of students preparing for this examination.

The book gives a selection of examination questions at the end of each chapter; some of them are from Institution of Electrical Engineers or British Institution of Radio Engineers papers, but students preparing for these, or for the Higher National Certificate, would need to supplement the book with others of a more analytical character.

The book is well produced and few misprints were noticed. Most of the treatment is non-mathematical, with frequent diagrams, but simple analyses (using the symbolic notation) are given in a number of cases. Specimen answers are given to some questions, and these are used to supplement the text, for example, to give typical component values. It is a pity that such typical values are not given much more often, especially as some readers will be studying at home. One or two of the photographs are of doubtful value (for example, those of a vibrator and of a cathode-ray oscilloscope), although others are good.

M. D. ARMITAGE

Noise and stochastic processes. Edited by NELSON WAX. (New York: Dover Publications Inc., 1954.) Pp. 337. Price $3.50 (cloth), $2.00 (paper).

It becomes increasingly clear that a knowledge of the theory of random processes and fluctuation phenomena is necessary to a complete understanding of most branches of science and technology. This book, the third in a series issued by the Dover Publications, each dealing with a particular branch of science, gives an excellent appraisal of the present state of the subject. It is a collection of six reprinted papers and reviews; two of these, "Stochastic problems" by S. Chandrasekhar, and "Mathematical analysis of random noise" by S. O. Rice, are almost complete treatises in themselves. The other four shorter papers by G. E. Uhlenbeck and L. S. Ornstein, by Ming Chen Wang and G. E. Uhlenbeck, by Mark Kac and by J. L. Doob, deal with various aspects of Brownian Motion.

The book does not make light reading—no proper treatment could—but those who wish to study this subject seriously could not do better than to do so with the aid of this book.

V. J. FRANCIS

Mathematics of engineering systems. By DEREK F. LAWDEN. (London: Methuen and Co. Ltd., 1954.) Pp. viii + 380. Price 30*s*.

There are a great number of text-books on engineering mathematics and new books on this subject appear fairly regularly. It is, however, not often that a book appears in this field that covers new ground in as lucid a manner as the book under review, or deals with the more familiar ground as refreshingly.

The book assumes a knowledge of the calculus, but in a brief introductory chapter the author revises a certain amount of ground which he expects his readers to have covered. Chapter 2 deals with the solution of linear differential equations with constant coefficients by the use of the D operator; many of the worked-out examples in this and other chapters relate to practical problems drawn from the servo-mechanisms and electrical fields. The next chapter deals with the same types of equations by modern methods. The response of stable linear systems to the input of a unit step function and of a sinusoidal function are discussed in detail, and the method of the Laplace transform is introduced. Chapter 4 covers Fourier analysis in a very lucid manner, particularly emphasizing the points students often find difficult.

The last chapter deals with non-linear differential equations. It contains a clear and concise section on phase plane methods, deals with van der Pol's equation with and without forcing terms, and concludes with a section on approximate solutions.

The book is pleasantly printed with clear diagrams of reasonable size. It is undoubtedly a valuable addition to the literature of engineering mathematics and should prove helpful, not only to students, but also to practising engineers and physicists who need an introduction to the solution of the linear and non-linear differential equations which govern many problems in electricity and mechanics.

E. K. FRANKL

Notes and comments

The Physical Society's annual exhibition of instruments and apparatus

As announced in the January issue of this *Journal* The Physical Society's 39th Annual Exhibition of Instruments and apparatus will be held in the New Hall of the Royal Horticultural Society, Westminster, London, S.W.1, from 25 to 28 April, 1955 (inclusive). The exhibition will be open from 10 a.m. to 8 p.m. on 26 and 27 April and from 10 a.m. to 5 p.m. on 28 April. Although it will also be open until 8 p.m. on the first day (25 April) the morning (10 a.m. to 2 p.m.) has been reserved for members of the Society and sister bodies.

It has been agreed to offer special tickets to members of sister institutions to enable them to visit the exhibition on The Physical Society members' morning, Monday, 25 April, when the exhibition is not so crowded. Tickets, available for any one day, may be obtained from The Physical Society, 1 Lowther Gardens, Prince Consort Road, London, S.W.7. Members of The Institute of Physics may obtain tickets from the Institute's office.

Meteorological Office Annual Report for 1953–4

The annual report of the Director of the Meteorological Office for the year ending 31 March, 1954 (H.M. Stationery Office, price 2*s*. 3*d*. including postage), summarizes the services which have been provided in weather forecasting, climatology and research and development. Probably the new service which has been most appreciated by the general public is the television weather forecast presented by the forecasters themselves.

Work in the instrument field again included further development of radio and radar sounding techniques for the measurement of pressure, temperature and humidity to heights of 20 km and above. There were also investigations, involving much instrumentation for high speed and high altitude aircraft, into the physical processes of cloud and precipitation and of ice accretion. Progress was made in the design of searchlight methods of measuring the height of cloud base by day. One method uses a modulated beam and the other a light-pulse timing system. Measurements of factors likely to influence fog formation were continued during last winter. The development of a bi-metallic actinometer of simple design for recording solar radiation was completed.

The report includes appendices giving details of the organization, estimates of expenditure and a list of publications issued during the year.

Joint conference on combustion

The Institution of Mechanical Engineers announces that it has arranged a joint conference on combustion with the American Society of Mechanical Engineers which will be held in Boston, Massachusetts, from 15 to 17 June next and in London from 25 to 27 October next. Bearing in mind the inherent difficulty in applying theory to practice in the sphere of combustion, the objects of the conference will be:

(i) to link theory and practice in this sphere by presenting the results of theoretical work to practical engineers in America, Great Britain and other countries; and

(ii) to provide an opportunity for practical engineers in these countries to meet together to discuss practical application of theory in the fields of boilers, furnaces, internal combustion engines and gas turbines.

Some thirty other institutions and societies, including The Institute of Physics, are supporting the conference and their members may obtain particulars and preliminary reply forms through these bodies. Others should apply to the Secretary of The Institution of Mechanical Engineers, 1 Birdcage Walk, London, S.W.1.

Errata in Supplement No. 3

The Physics of Particle Size Analysis

Fig. 3 on page *S* 140 is incorrect as the corrections requested by the authors in proof were not made. Also, on page *S* 139 in line 21 of the left-hand column, for 20° read 24°. Errata slips will be inserted in further copies of the Supplement distributed and will be sent (gratis) to anyone wishing to correct his own copy.

Requests should be sent on a post card to Editorial Section, The Institute of Physics, 47 Belgrave Square, London, S.W.1.

Journal of Scientific Instruments

Contents of the March issue

ORIGINAL CONTRIBUTIONS

Papers

The measurement and display of the current gain (α) of a transistor as a function of emitter current. By R. A. Hilbourne.

A reflexion electron microscope. By V. E. Cosslett and D. Jones.

A Pirani gauge circuit. By C. N. W. Litting.

A dielectric heating and test unit for the study of sand properties at elevated temperatures. By R. Rew and R. G. Godding.

An apparatus for measuring the elastic properties of gels. By L. J. Hastewell and R. Roscoe.

Investigation of the heterodyne beat method of measurement of magnetic susceptibility. By H. G. Effemey, D. F. Parsons and J. O'M. Bockris.

The theory and design of rotating mirror cameras. By H. Edels and D. Whittaker.

A driving unit for a "time-lapse" ciné camera. By A. F. Hughes and W. R. Hughes.

An adiabatic calorimeter for measuring the specific heats of liquids in the range 0 to 100° C. By L. W. Phipps.

A compact monochromator employing rhombic, constant deviation prisms. By J. W. Gates and S. P. Middleton.

Laboratory and workshop notes

A simple reflexion-transmission stage for an electron microscope. By K. Amboss.

A laboratory gas-flow control device. By R. A. Hall.

Simple extrusion press for preparation of specimens of optimum thickness for X-ray diffraction powder photographs. By M. Kossenberg.

An optical system for use in conjunction with glass spiral pressure gauges. By V. C. Ewing.

A coaxial line suitable for low-temperature work. By D. Bijl and H. Pullan.

NOTES AND NEWS

Correspondence

Modifications to the omnidirectional ionization anemometer. From W. L. Welman.

A versatile top terminal equipment for an electrostatic accelerator. From B. Millar, K. Firth and D. R. Chick.

A note on the hole, slot and plane method. From E. A. Neppiras.

Straightening curvilinear records. From C. A. Shain

New instruments, materials and tools

Notes and comments

THIS JOURNAL is produced monthly by The Institute of Physics, in London.

It deals with all branches of applied physics (including theory and technique). All rights reserved. Responsibility for the statements contained herein attaches only to the writers.

EDITORIAL MATTER. Communications concerning editorial matter should be addressed to the Editor, The Institute of Physics, 47 Belgrave Square, London, S.W.1. (*Telephone*: Sloane 9806.) Prospective authors are invited to prepare their scripts in accordance with the *Notes on the preparation of contributions*. (Price 2*s*. 6*d*. including postage.)

REPRODUCTION. The Institute of Physics is a signatory to The Royal Society's Fair Copying Declaration. Details may be obtained upon application from The Royal Society, London, W.1.

ADVERTISEMENTS. Communications concerning advertisements should be addressed to the agents, Messrs. Walter Judd Ltd., 47 Gresham Street, London, E.C.2. (*Telephone*: Monarch 7644.)

CLAIMS FOR MISSING JOURNALS. Claims from regular subscribers to this *Journal* for missing numbers will only be considered if received within 60 days of the date of mailing plus normal outward time of transit and time for lodging the claim. Losses attributable to failure to notify a change of address or to similar omissions will not be considered.

SUBSCRIPTION RATES. A new volume commences each January. The charge is £4 per volume ($11.50 U.S.A.), including index (post paid), payable in advance. Single parts, so far as available, may be purchased at 8*s*. each ($1.15 U.S.A.), post paid, cash with order. Orders should be sent to The Institute of Physics, 47 Belgrave Square, London, S.W.1, or to any bookseller.

The electrical conductivity and permittivity of mixtures, with special reference to emulsions of water in fuel oil

By C. A. R. PEARCE, M.Sc.(Eng.), A.M.I.Mech.E., A.M.I.E.E.,* Fuel Research Station, Greenwich, London, S.E.10

[*Paper received* 2 *December*, 1954]

The electrical characteristics of a mixture of two substances are dependent only in part on the electrical characteristics of the individual phases. In addition to the volume ratio of the components of the mixture other factors such as particle shape and distribution have important effects on the characteristics. In this connexion an emulsion formed of a liquid with a high conductivity in one of low conductivity is free from the complications of many practical mixtures. The droplets are spheres and the system approaches the case which has been attacked theoretically with the greatest success.

The characteristics of water in fuel oil emulsions have been studied both directly and indirectly by means of an electrolytic analogue. The work has drawn attention to the importance of the size distribution of the dispersed phase and has confirmed the theoretical treatments of Wiener and Bruggeman at the same time emphasizing the limitations of their formulae. This has given the work a value in applications outside the narrow field of the specialized emulsions in which it originated.

LIST OF SYMBOLS

ν and ϵ are the general symbols for electrical conductivity and permittivity.

ν_1 and ϵ_1 refer to the discontinuous phase of an emulsion or suspension.

ν_2 and ϵ_2 refer to the continuous phase.

ν_m and ϵ_m are the values of the mixture.

${}_2\nu_1 = \nu_1/\nu_2$ and ${}_2\nu_m = \nu_m/\nu_2$;

similarly with ${}_2\epsilon_1$ and ${}_2\epsilon_m$.

p_1, the volume ratio, is the fraction of the total volume represented by the discontinuous phase.

1. INTRODUCTION

Work at the Fuel Research Station on emulsions of sea water in fuel oil entailed an examination of their electrical properties and led to a study of the general problem of the electrical conductivity and permittivity of such mixtures. Part of this study provides the subject-matter of this paper.

The relationships between the electrical properties of heterogeneous dielectrics and those of the respective phases have been the subject of many theoretical and practical investigations since 1873 when Maxwell[1] published his treatment for the case of spheres immersed in a medium of different conductivity. It is unnecessary to detail the work of Maxwell, Lorentz,[2] Lorenz[3] or Rayleigh[4] because their results conform with the more general treatment of Wiener[5] who gave expressions for the permittivities of arrangements of spheres and cylinders in terms of the permittivities of the dispersed bodies and the continuous medium and the volume ratios.

At this stage it may be well to remark on the identity of the relationships for permittivity and for conductivity. Provided that the two properties are considered independently the same form of equation relates the properties of the phases with the property of the mixture. A similar remark applies to permeability in the magnetic case.

Wiener also examined special cases of other shapes besides the sphere and the cylinder but his results relate to formal arrangements exemplified in Fig. 1(*a*) and (*c*) as do those of Rayleigh and Maxwell.

For spheres, see Fig. 1(*a*), Wiener's equation is:

$$\frac{\epsilon_m - \epsilon_2}{\epsilon_m + 2.\epsilon_2} = p_1 \frac{\epsilon_1 - \epsilon_2}{\epsilon_1 + 2.\epsilon_2} \qquad (1)$$

The corresponding expression for conductivity, in accordance with what has already been written, is:

$$\frac{\nu_m - \nu_2}{\nu_m + 2.\nu_2} = p_1 \cdot \frac{\nu_1 - \nu_2}{\nu_1 + 2.\nu_2} \qquad (1a)$$

For cylinders with axes perpendicular to the field, see Fig. 1(*c*), his equation is:

$$\frac{\epsilon_m - \epsilon_2}{\epsilon_m + \epsilon_2} = p_1 \cdot \frac{\epsilon_1 - \epsilon_2}{\epsilon_1 + \epsilon_2} \qquad (2)$$

Although Ficker[6] attempted an experimental confirmation of Wiener's treatment his results are inconclusive and the present author has been unable to trace any other measurements aimed at the confirmation of equations (1) and (2) within the limits postulated by Wiener, Rayleigh and Maxwell. On the other hand no error has been pointed out in the derivation of the formulae which would cast any doubt on the validity of the findings of these authors. Instead, the expressions have been tested by application to the practical cases of emulsions, suspensions, powdered crystals, etc., which are far removed from the formal arrangements from which they are derived and they have been found by many workers not to agree well with the experimental findings, e.g. Guillien[7] and Voet.[8] These authors prefer the expression proposed by Bruggeman[9] for spherical particles arranged in a random fashion, namely:

$$1 - p_1 = \frac{\epsilon_1 - \epsilon_m}{\epsilon_1 - \epsilon_2} \times \sqrt[3]{\frac{\epsilon_2}{\epsilon_m}} \qquad (3)$$

Although this expression fits well with some experimental findings there are others, for example those of Voet, with which it can only be reconciled by the introduction of empirical factors alien to Bruggeman's treatment. The subject is thus in a somewhat unsatisfactory position. It was for this reason that the author devised the practical test for

* Now at National Coal Board, Central Research Establishment II, Isleworth, Middlesex.

Wiener's equations which will be described later, but the experimental work on emulsions will be dealt with first.

At this stage it is relevant to remark that in all expressions quoted above it is assumed that the particle size of the mixture may be ignored. A little consideration will suggest what has in fact been confirmed experimentally by Van Vessem and Bijvoet[10] that this may in any event only be done if the diameters falling within a fairly well defined range, about 2 to 40 μ. Such emulsions are in practice formed in ship's tanks by the rolling of the ship but are made in the laboratory by stirring. Prolonged stirring or the forcing of the mixture through a fine nozzle will reduce the mean droplet size and the range of diameters. This process is referred to as "homogenizing."

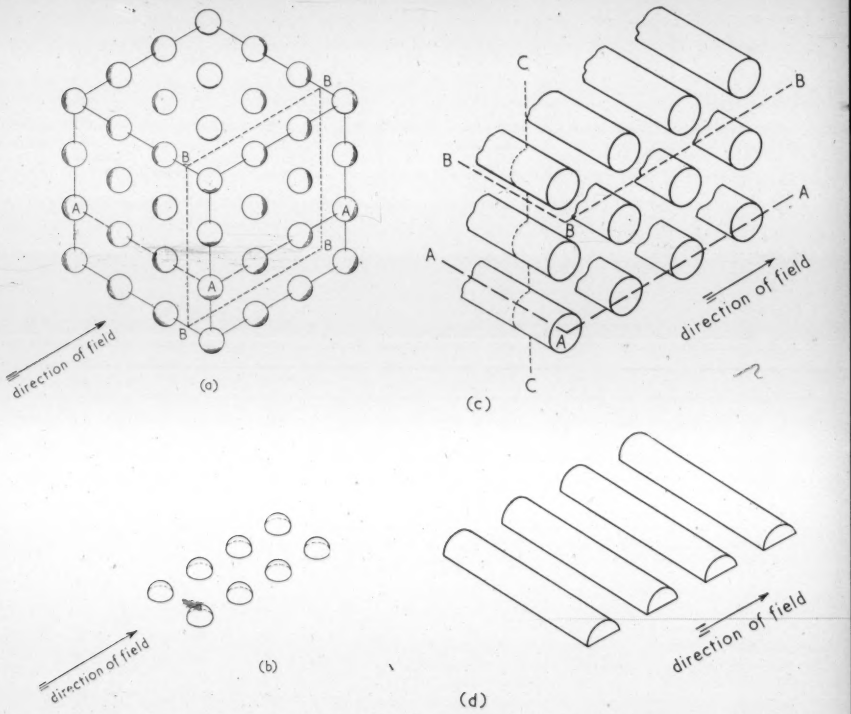

Fig. 1. (*a*) Arrangement of spheres as postulated by Maxwell, Rayleigh and Wiener. (*b*) Arrangement of hemispheres in electrolytic bath. (*c*) Arrangement of cylinders. (*d*) Arrangement of half cylinders in electrolytic bath

particle is very small in relation to the cell used in the measurement of the characteristic of the mixture. Bruggeman was aware of this factor but it is quite distinct from particle size distribution, the importance of which will later become apparent.

2. ELECTRICAL CHARACTERISTICS OF EMULSIONS

2.1. *Sea water in fuel oil.*

Fig. 2 is a photomicrograph of a typical emulsion of sea water in fuel oil and it will be seen to consist of a more or less random arrangement of spherical droplets of water with

Series of emulsions of varying water content were made up by simple stirring and by homogenizing with two Admiralty fuel oils, one from Trinidad petroleum and the other from Abadan. Once formed, the emulsions were quite stable over periods of hours. With the aid of a 1000 c/s bridge by H. W. Sullivan Ltd. and the cell illustrated in Fig. 3 the permittivity of the water-free oil and of each emulsion was measured at a fixed temperature. The recorded result was the mean of three taken on separate samples of the same emulsion. The sum of the end correction and stray capacity of the cell was estimated by subtracting the calculated capacity of the cylindrical annulus from the measured capacity of the empty cell.

Because they are conductors the permittivity of the droplets

for present purposes may be taken as infinite. In these circumstances equation (1) becomes:

$$\frac{\epsilon_m - \epsilon_2}{\epsilon_m + 2.\epsilon_2} = p_1 \qquad (4)$$

which can be rewritten:

$$_2\epsilon_m = \frac{\epsilon_m}{\epsilon_2} = \frac{1 + 2p_1}{1 - p_1} \qquad (4a)$$

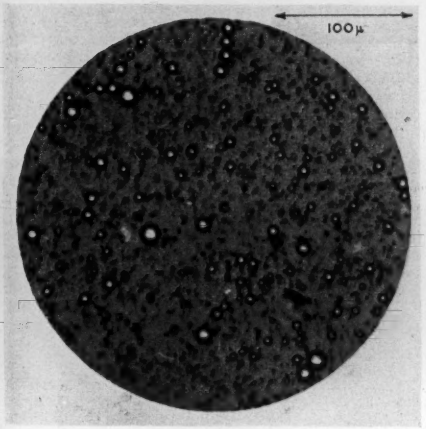

Fig. 2. Photomicrograph of an emulsion of one volume of sea water in nineteen of fuel oil

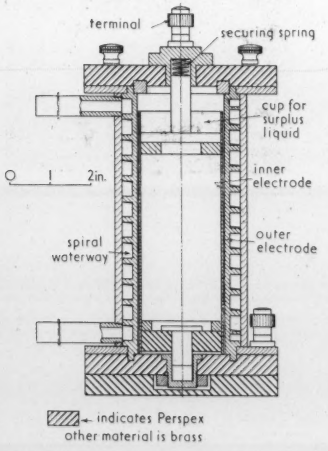

Fig. 3. Cell used for ϵ measurements on oils and emulsions

Equation (3) becomes:

$$_2\epsilon_m = (1 - p_1)^{-3} \qquad (5)$$

The experimental results and curves of equations (4) and (5) plotted on logarithmic scales are given in Fig. 4. The results were obtained with four different types of emulsions, namely:

1. Trinidad oil stirred.
2. Trinidad oil homogenized.
3. Abadan oil stirred.
4. Abadan oil homogenized.

The droplet sizes in types 1 and 3 were very similar to the sample from which Fig. 2 was obtained, whilst in types 2 and 4 the maximum droplet diameter was about 5 to 6 μ. The points plotted in Fig. 4 do not distinguish between the

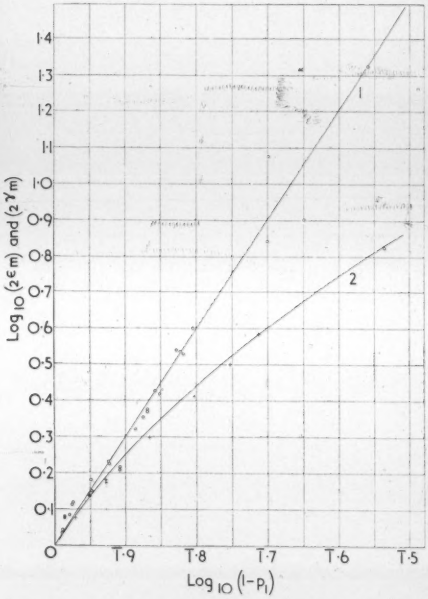

Fig. 4. Curve 1 is calculated from Bruggeman's formula and curve 2 from Wiener's formula for spheres. The points are the author's results

○ sea water in fuel oil emulsions.
+ electrolytic analogue of cubic arrangement of conducting spheres.

four cases and in fact when they were separated, no difference could be discerned between the general trends of the four sets of results.

2.2. *Results of Guillien with comparable dispersions.*

Guillien, in his investigations into the validity of the formulae of Wiener and Bruggeman, measured the permittivity of emulsions of mercury in oil. Electrically such a

system is similar to the emulsions of sea water in oil. His results are given in Fig. 5 together with the lower portion of Curve 1, Fig. 4.

Guillien also published the results he obtained with manufactured spheres of Wood's Metal in oil. He found, however, that such spheres being very soft were readily flattened by blows from the blades of the stirrer which he employed to ensure that they did not settle out and for this reason these results are not included in Fig. 5.

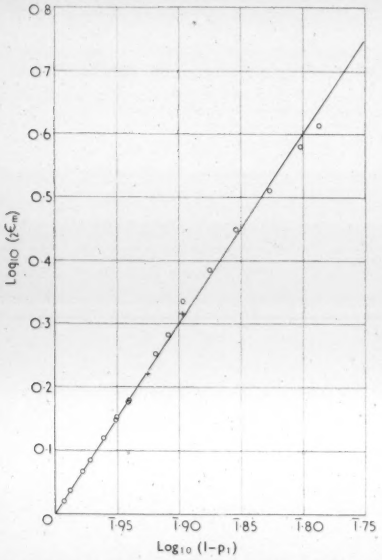

Fig. 5. The change in permittivity of an emulsion of mercury in oil, with mercury content as determined by Guillien. The curve was calculated from Bruggeman's formula

○ mercury in lubricating oil.
+ mercury in castor oil.

For a similar reason the results published by Voet for an emulsion of electrolyte in oil have also been omitted. To prevent agglomeration Voet subjected the emulsion under test to continuous shear, such as occurs in a cylindrical viscometer. It must be expected that such treatment will distort the suspended droplets and affect their distribution. Other results of this author are omitted because the conditions under which his measurements were made suggest that the results are likely to have been influenced by sedimentation or departures from sphericity in the shape of the suspended particles.

3. EXPERIMENTS WITH ELECTROLYTIC ANALOGUES

3.1. *General.*

The scatter of the results in Section 2.1 does not disguise the generally good agreement between them and Bruggeman's expression, whilst with Guillien's results in Section 2.2 the agreement is excellent. It would therefore seem that this expression adequately represents the conditions in emulsions consisting of random dispersions of spherical particles, which is precisely the case for which it was derived.

The next section will describe a device to test Wiener's formulae for the conditions for which they were derived and to examine their limitations and those of Bruggeman's formula.

3.2. *The principle and use of the electrolytic analogue.*

The infinite formal arrangements of spheres and cylinders illustrated in Fig. 1(*a*, *c*) can be examined by separation at certain chosen planes without affecting the contour of the electric field. Among such planes are those such as *AAA* which are perpendicular to the electrodes, i.e. planes parallel with the direction of maximum field strength and which pass through the centres of the spheres or cylinders. By symmetry no lines of electric force intersect such planes. *BBBB* typifies another set of such planes and with the cylinders shown in Fig. 1(*c*) *CC* is another such plane. It follows therefore that an arrangement of hemispheres such as is shown in Fig. 1(*b*) or half cylinders such as in Fig. 1(*d*) can be extracted and if bounded by planes of zero conductivity at faces such as *AAA*, *BBBB* and *CC* will have conductivity characteristics which are identical with those of the hypothetical unbounded arrangement.

The device used to test Wiener's formulae is illustrated in Fig. 6 and is based on the method explained in the preceding paragraph. An arrangement of brass hemispheres is shown

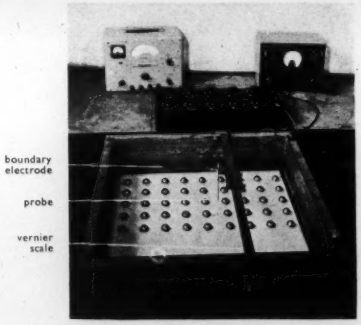

Fig. 6. Apparatus used in electrolytic analogue experiments. A formal arrangement of hemispheres is shown set out on the glass bottom of the tank. To facilitate the positioning of the hemispheres a sheet of squared paper has been mounted against the underside of the glass

set out in an electrolytic tank with a glass bottom. The electrolyte is tap water. The depth of water is one-half the lateral spacing. If now a voltage is impressed across the electrodes at the ends of the bath the ratio of the potential gradients in the part of the bath in which the spheres are set out and the part without spheres is effectively the ratio of their resistivities.

The potential gradient was measured by means of the circuit in Fig. 7. The probe, see Fig. 6, which was mounted on a vernier scale was set just to penetrate the surface of the water and R_1 and R_2 were adjusted to reduce the reading of

the valve voltmeter to a minimum. The ratio $R_1/(R_1 + R_2)$ was then a measure of the potential at the position of the probe. Fig. 8 is a typical plot of the potential along the bath. From this curve

$$_2\gamma_m = \tan\alpha/\tan\beta$$

In setting up the apparatus the glass bottom of the bath was carefully levelled and the brass hemispheres, etc., were

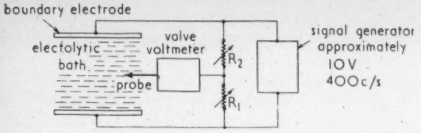

Fig. 7. Circuit employed for the electrolytic analogue

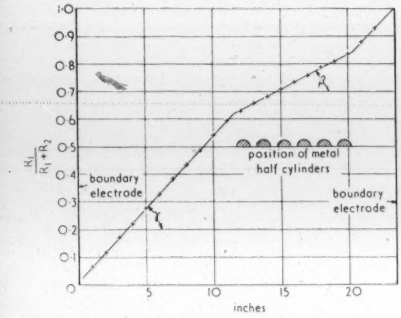

Fig. 8. Typical plot of the potential variation between the electrodes of the electrolytic analogue

cleaned in carbon tetrachloride and dilute nitric acid before use. The depth of the water was measured to the nearest 0·001 in. by means of a spherometer, the surface of the water being detected by the electrical contact which it made with the point of the micrometer head.

It will now be clear that by setting out in the electrolytic tank arrangements of hemispheres, etc., with various spacings between centres and appropriate depths of water, $_2\gamma_m$ can be measured for a series of values of p_1. There is, however, a restriction on the values of $_2\gamma_1$ which can be employed. Using brass hemispheres and half cylinders in water the ratio of conductivities is similar to that in the emulsions dealt with in Section 2, i.e. $_2\gamma_1$ is very great and by using hemispheres, etc., of Bakelite the case where $_2\gamma_1 = 0$ can be examined; there are serious practical difficulties in the way of using intermediate values of $_2\gamma_1$ and they were not attempted.

The Bakelite hemispheres used were weighted with lead disks sealed with a plastic cement, so as to keep them firmly on the glass bottom and at the same time to maintain the insulation.

3.3. *Results with formal arrangements in the electrolytic bath.*

In Figs. 4 and 9 the results obtained with formal arrangements of brass hemispheres and half cylinders are compared with the predictions of Wiener's formulae with good agreement, as is also the case for those for non-conducting hemispheres given in Fig. 10. In this case the substitution of $_2\gamma_1 = 0$ in equation (1*a*) gives:

$$_2\gamma_m = \frac{2(1-p_1)}{2+p_1} \qquad (6)$$

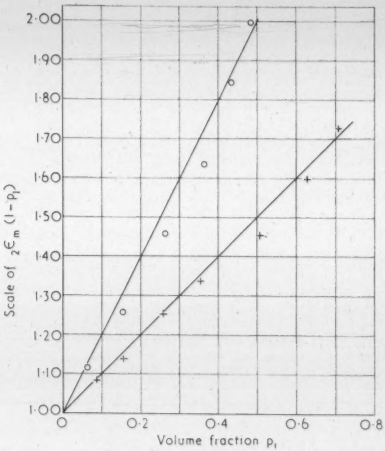

Fig. 9. Comparison between curves calculated from Wiener's formula and the results of the experiments with electrolytic analogues for the case in which $_1\gamma_2$ is very large

○ square pattern of hemispheres.
\+ parallel rows of half cylinders.

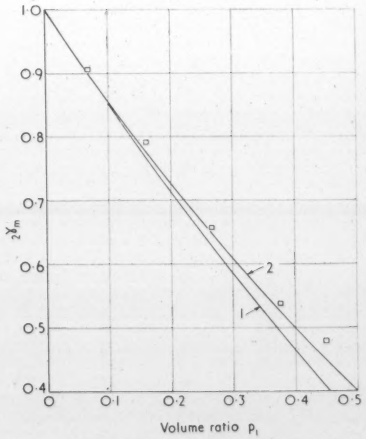

Fig. 10. Results obtained with electrolytic analogues of formal dispersions of non-conducting spheres. Curve 1: Bruggeman's formula. Curve 2: Wiener's formula

There is no equivalent to equation (6) with permittivity since ϵ_1 has a minimum value of one.

It has thus been established that whilst Bruggeman's expression holds for a certain type of random arrangement of spheres the formulae derived by Wiener, and indeed those due to Maxwell and Rayleigh, are valid for formal anisotropic arrangements.

In the next phase of the work the electrolytic bath was used to investigate random arrangements, in the hope that the limitations of the formulae could be more closely defined.

3.4. *Experiments with random arrangements in the electrolytic bath.*

3.4.1. *Method of setting out hemispheres.* The random distributions postulated by Bruggeman and those encountered in emulsions are three-dimensional but the analogue of such an arrangement could not be achieved with the apparatus used in the present study. Of necessity the randomness of the arrangements used was two-dimensional and to identify this type it will in future be referred to as quasi-random.

The method of setting out the hemispheres was based on the use of the set of random numbers compiled by Tippett.[11] A full-sized drawing of a convenient part of the electrolytic bath, measuring 16 in. × the full width 23½ in. was divided into 10000 rectangles, thus providing x and y axes each of 100 units. Random numbers were now taken in order, four at a time. The first pair was used for the value of x and the second for the corresponding value of y. In this manner a series of points was plotted, each point being numbered in sequence. The plot of these points was mounted on a board beneath the glass bottom of the electrolytic tank and wherever possible the hemispheres were placed with their centres over the points; where this was precluded by the proximity of the points, the hemispheres were arranged so that they touched but conformed in a general way with the disposition of the original points. The hemispheres were placed over the points in numerical order up to whatever quantity was necessary for the volume ratio required. When more than one size of hemisphere was used the respective sizes were taken in rotation.

The depth of water used for each measurement was that appropriate to the same numerical density of spheres in the tests made with the formal arrangements. In effect this depth is one-half the side of the cube having a volume equal to (the total volume of the dielectric)/(the total number of particles).

Fig. 11 illustrates the type of arrangement obtained by the method indicated and in it the same general characteristics may be observed as are to be seen in Fig. 2. This is a matter of interest in itself since the first impression of those examining Fig. 2 is that it reveals a marked tendency of the droplets to adhere, see Lewis.[12] On the evidence of Figs. 2 and 11 it seems that the forces examined by Lewis have little apparent effect on the dispositions of the droplets in the particular emulsions of sea water in fuel oil.

In measuring the potential gradients in the two parts of the electrolytic tank it was no longer possible to obtain a continuous straight line in the part occupied by the hemispheres. Instead, a boundary between the two sections was formed by rectangular section brass bars and its potential relative to the two end electrodes was measured. The potential gradient in each part of the bath was then determined from the potential differences and the distances between electrodes and the dividing bar.

It has already been mentioned that more than one size of hemisphere was used. This was done in order to study the effect of changes in size distribution. Three sizes of brass hemisphere were available, namely, 1 in., ¾ in. and ½ in. diameter. The 1 in. size was used exclusively for the formal arrangements but in the quasi-random arrangements measurements were also made with different proportions of the three sizes.

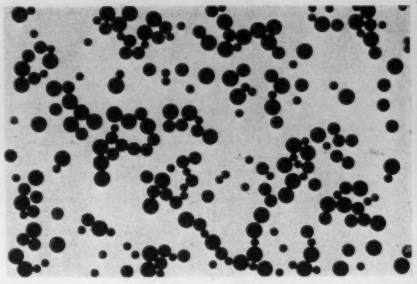

Fig. 11. Typical random arrangement of hemispheres

3.4.2. *Results with quasi-random arrangements of hemispheres in the electrolytic bath.* In Fig. 12 the predictions of

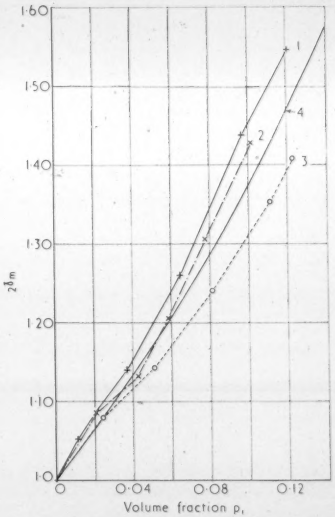

Fig. 12. Results obtained with electrolytic analogue of quasi-random dispersion of spherical conductors, showing the effect of size distribution. Curve 1 was obtained using only 1 in. diameter hemispheres; Curve 2 relates to 1, ¾ and ½ in. diameter hemispheres in the numerical ratio 2 : 1 : 1 and Curve 3 relates to equal numbers of the three sizes. Curve 4 is derived from Bruggeman's expression

Bruggeman's expression can be compared with the results obtained with quasi-random arrangements and three different size distributions of conducting spheres. It will be observed that $_2\gamma_m$ decreases with decreasing uniformity of the sphere diameters. The position of the calculated curve in relation to the practical results is not significant since, as will be readily apparent, in changing from three- to two-dimensional randomness, the mean distance between adjacent spheres is reduced and $_2\gamma_m$ is thus increased.

4. SIZE DISTRIBUTION OF DISPERSED PHASE

In the light of the foregoing results it was clearly of some interest to see how the size distribution of the droplets in emulsions of sea water in fuel oil compared with equivalent distributions in the arrangements employed in the electrolytic analogues. The diameters of the droplets appearing in Fig. 2 were measured and Fig. 13(*a*) was constructed from the results. Comparing this distribution with those given in Fig. 13(*b*) it is clear that in the arrangements used in the

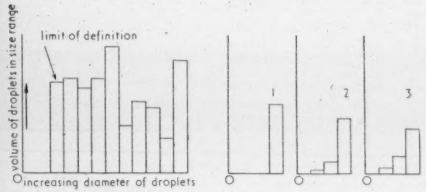

Fig. 13. Size distributions of droplets and spheres in emulsions and electrolytic analogues

(*a*) Size distribution of droplets in a typical sea water in fuel oil emulsion.
(*b*) Size distribution of spheres in electrolytic analogue experiments with quasi-random dispersions of spherical conductors. Numbers refer to curves in Fig. 12.

electrolytic analogues there was a much greater preponderance of the larger sizes. From a practical point of view this is inevitable.

A detailed study of droplet size distribution in emulsions would be inappropriate to the present work but references (13) and (14) give information on the subject.

5. CONCLUSIONS

Apart from confirming the theoretical work of Wiener the present study has made it clear that contrary to the tacit assumptions of Fricke,[15] Burton and Turnbull,[16] Scott and McPherson[17] and others the change from a formal arrangement to a random distribution may produce a major change in the relationship between the electrical properties of the component phases of a dielectric and the properties of the mixture. It has also drawn attention to the possible importance of particle size distribution as a factor in determining the properties of the mixture.

The good agreement between Bruggeman's formula and measurements on emulsions should not be interpreted to mean that the droplets in an emulsion are invariably arranged in random fashion. Voet's results indicate that this is not so. A number of factors operate to destroy the randomness, e.g. (i) sedimentation; (ii) adherence (see Lewis[12]); (iii) chain formation due to electric fields (see Pearce[18]).

The extent to which these are present in a particular case and their precise effect on the electrical characteristics of an emulsion are not easy to determine. On the other hand the limiting values of the characteristics can be readily estimated. Droplets of an emulsion produce their minimum effect on the electrical characteristics when they are disposed as a thin layer along an equipotential line (see Wiener). It can be shown that in these circumstances, for an emulsion of water in fuel oil:

$$_2\gamma_m \text{ and } {}_2\epsilon_m \simeq \left(1 - \frac{6}{5}p_1\right)^{-1}$$

or

$$\left(1 - \frac{63}{48}p_1\right)^{-1}$$

depending on whether the arrangement of the droplets within the layer is formal or random.

The maximum effect is obtained when such a layer is parallel to the electric field. Then

$$_2\epsilon_m \simeq 1 + 21p_1$$

Between these extremes lie the values given by the formulae of Wiener and Bruggeman. It therefore seems to be a doubtful assumption on the part of Voet that the addition of an empirical factor to Bruggeman's expression will adequately cover all cases. With emulsions of the sort now under consideration his suggested equation becomes:

$$_2\epsilon_m = (1 - \phi p_1)^{-3} \tag{7}$$

where ϕ is an agglomeration factor.

It is not difficult to find relationships of this type which appear to fit the results of a number of workers. For example, the author has tested the relationship between

$$(_2\epsilon_m - 1)/p_1 \quad \text{and} \quad {}_2\epsilon_m \tag{8}$$

and between

$$(_2\epsilon_m - 1)/(_2\epsilon_m)^{\frac{1}{3}} \quad \text{and} \quad p_1 \tag{9}$$

for a large number of results obtained by different workers with a variety of mixed dielectrics; generally satisfactory linear relationships can be established in most cases but such relationships are not fundamental and can be misleading. This is exemplified by the work of Burton and Turnbull[16] on the permittivity of a series of powdered salts. For the permittivity of a mixture they employed an expression very similar to Wiener's which it will be recalled applies only to certain anisotropic arrangements. Their expression was an adaptation of one due to Fricke.[10]

Burton and Turnbull's results depended on a linear relationship on the lines of equations (8) and (9) above, from which they derived a "form factor" for each salt. It is reasonable to expect that such factors should bear some relationship to the shape of the grains of the respective salts. The present author therefore sought to correlate the grain shapes revealed by photomicrographs with the "form factors." No such correlation could be discovered. Salts with the same particle shape had been allotted widely differing factors and salts allotted similar factors had very different particle shapes. The shape of the electric field in the neighbourhood of a body immersed in any liquid depends not only on the shape of the body but also on the ratios $_2\epsilon_1$ and $_2\gamma_1$ and on its superficial resistivity. The misapplication of the formula was confirmed by the work of Cheng[19] who, using another method, obtained values for the permittivities of some of the salts differing by up to 40% from the earlier values.

Another consideration which must be borne in mind in any electrical measurements made on mixtures is the ratio between the particle size and the dimensions of the measuring cell. Bruggeman drew attention to this factor and, as already

mentioned, its importance has been stressed more recently by Van Vessem and Bijvoet.[10]

ACKNOWLEDGEMENTS

This study was part of a programme of the Fuel Research Board of the Department of Scientific and Industrial Research and the paper is published by permission of the Director of Fuel Research.

The illustrations are Crown copyright and reproduced by permission of the Controller H.M. Stationery Office.

In conclusion, the author gratefully acknowledges the assistance rendered by Messrs. A. H. Perkin, H. A. Howe and D. W. Tims who made the measurements, and Mr. L. J. Edgecombe who was responsible for check determinations of the water content in the emulsions.

REFERENCES

(1) Clerk Maxwell. *Electricity and Magnetism*, first published 1873. Vol. 1, 3rd Ed., see Art. 314, p. 440 (Oxford: The Clarendon Press, 1892).
(2) Lorentz, H. A. *Ann. Phys.* [*Leipzig*], **9**, p. 641 (1880).
(3) Lorenz, L. *Ann. Phys.* [*Leipzig*], **11**, p. 70 (1880), and other publications.
(4) Lord Rayleigh. *Phil. Mag.*, **34** (5), p. 481 (1892).
(5) Wiener, O. *Leipziger Berichte*, **62**, p. 256 (1910).
(6) Ficker, E. *Ann. Phys.* [*Leipzig*], **31**, p. 365 (1910).
(7) Guillien, R. *Ann. Phys.* [*Paris*], **16**, p. 205 (1941).
(8) Voet, A. *J. Phys. Chem.*, **51**, p. 1037 (1947).
(9) Bruggeman, D. A. G. *Ann. Phys.* [*Leipzig*], **24**, p. 636 (1935).
(10) Van Vessem, J. C., and Bijvoet, J. M. *Receuil. Trav. Chim. pays-Bas*, **67**, p. 191 (1948).
(11) Tippett, L. H. C. *Random Sampling Numbers*, No. 15 of Tracts for Computors Series (London: University College, 1952).
(12) Lewis, W. C. M. *Trans Faraday Soc.*, **30**, p. 958 (1934).
(13) Cooper, F. A. *J. Soc. Chem. Ind.*, **56**, p. 447 (1937).
(14) Gaddum, H. *Nature* [*London*], **156**, p. 465 (1945).
(15) Fricke, H. *Phys. Rev.*, **24**, p. 575 (1924).
(16) Burton, E. F., and Turnbull, L. G. *Proc. Roy. Soc.* (*A*), **158**, p. 182 (1937).
(17) Scott, A. H., and McPherson, A. T. *J. Res. Nat. Bur. Stand.*, **28**, p. 279 (1942) R.P. 1457.
(18) Pearce, C. A. R. *Brit. J. Appl. Phys.*, **5**, p. 136 (1954).
(19) Cheng, C. K. *Phil. Mag.*, **30**, p. 505 (1940).

Effect of low temperature on the stability of permanent magnets

By A. G. Clegg, B.Sc., Permanent Magnet Association, Sheffield

[*Paper first received* 29 *October, and in final form* 6 *January*, 1955]

Magnetometer measurements have been made of the change in magnetization with temperature between +60 and −60° C for magnets with a range of dimension ratios. The materials tested were Alcomax III, Columax, Alnico, 35 and 15% cobalt steels. With decreasing temperatures the magnetization increases reversibly except for the shorter dimension ratio magnets in Alcomax III and Columax, for which losses occur. The influence of tempering on these losses is discussed. Losses occur in the lower coercivity materials only with increasing temperature. The losses, whether due to increase or decrease of temperature, can be minimized by a partial demagnetization by an alternating field. The results are correlated with the changes in the demagnetization curves of the materials with temperature.

Previous work has been carried out on the temperature variation of the general properties of Alcomax at elevated temperatures.[1] It was thought to be desirable to extend this work to the determination of magnetization change with temperature, particularly in its dependence on the alloy, its demagnetization curve and the working point of the test sample.

Preliminary experiments showed that peculiar effects occur in some cases when the temperature is decreased below room temperature. In view of these peculiarities, an attempt has been made in this paper to give a general idea of the variation of magnetization between +60 and −60° C for Alcomax III, Alnico, 35 and 15% cobalt steels and, in interesting cases, to extend the temperature range downwards to −180° C. The results have an important practical application in assessing the stability of magnets used for instruments in high-flying aircraft or in polar regions.

EXPERIMENTAL

Magnet samples. The magnet samples used for these experiments were ellipsoids of revolution. The working point of an ellipsoid of known *B*–*H* curve can be expressed as the ratio:[2]

$$-\frac{B}{H} = \frac{1}{D} - 1$$

Dimensions, demagnetization factors and values of B/H of the samples are shown in Table 1.

Table 1. *Sample dimensions and characteristics*

Length (*mm*)	*Diameter* (*mm*)	*Dimension ratio* L/D	*Demagnetization factor*	$-B/H$
66	5	13·2	0·014	70·3
66	8·3	7·9	0·028	34·7
47	9	5·2	0·053	17·9
68	15	4·5	0·066	14·15
53	15	3·5	0·088	10·35
40	15	2·66	0·127	6·78

Alcomax and Alnico magnets were cast and the cobalt steel magnets were turned from rolled bar. The composition and heat treatment of the samples are shown in Table 2; when other treatments were used this is stated in the text.

Table 2. *Compositions and heat treatments*

Material	*Average composition (weight %) (balance Fe)*	*Heat treatment*
Alcomax III and Columax	Al 7·8, Ni 13·5, Co 25, Cu 3, Nb 0·8	Cooled from 1250° C at 1·2° C/s in a magnetic field. Tempered 48 h at 590° C, 48 h at 560° C.
Alnico	Al 9·5, Ni 17, Co 12·5, Cu 6	Air-cooled from 1250° C. Tempered 2 h 600° C.
35% cobalt steel	C 0·9, Cr 5·5, W 4·5, Co 35	Oil-quenched from 950° C.
15% cobalt steel	C 1·1, Cr 9·0, Mo 1·5, Co 15	Air-cooled from 1000° C.

The Alcomax and Columax magnets were anisotropic, the preferred direction being the major axis. The magnets were magnetized with an applied field of at least 5000 oersteds in an electromagnet. Stabilization was achieved by reducing the magnetization by 5% using a 50 c/s alternating field.

Temperature control. For temperatures down to −75° C a mixture of solid carbon dioxide and methylated spirit was used. In certain cases a temperature of −180° C was obtained by the use of liquid air. For temperatures up to +60° C a non-inductive heater was placed in the vacuum flask containing methylated spirit. The temperature of the specimen was determined by a platinum-rhodium/gold-palladium thermocouple connected to a potentiometer for both the magnetometer and demagnetization curve experiments.

Measurement of temperature variation of magnetization. The magnetometer used for these experiments was of the Sucksmith[3] type made astatic to minimize the effects of external magnetic fields, the astatic pair of magnets being 20 cm apart. For calibration purposes, a Helmholtz coil system was fixed to the magnetometer so that the lower of the two magnets was at the centre of this system. The magnetometer, the specimen under test (fixed in a holder) and an adjustable control magnet (to give variable sensitivity and an offset zero), were all fixed rigidly on to a pair of parallel brass rails 80 cm in length. The average sensitivity of the magnetometer was about 5×10^{-4} oersteds/cm equivalent to 0·25% change in magnetization per centimetre deflexion.

The magnet under test was taken through the heating and cooling cycle 15, 60, 15, −60, 15° C in about 2½ h. Simultaneous readings were taken of temperature and magnetometer readings throughout the cycle. The percentage changes in moment were calculated from the magnetometer readings.

Measurement of the demagnetization curve at low temperatures. The *B–H* curves at −75 and −180° C were obtained by extraction of the magnet from a fixed coil at the centre of a solenoid. Before each reading the specimen was allowed to reach the temperature of the coolant contained in a vacuum flask. A calibration was obtained by comparison of the extraction method readings at room temperature with a *B–H* curve determined on the same fixed ellipsoid on open circuit in a solenoid. The extraction method has the advantages of giving readings directly proportional to $4\pi I$ in the specimen and of avoiding the necessity for maintaining the specimen at a steady low temperature within a solenoid dissipating up to 4 kW.

RESULTS

Alcomax (*including Columax*). The change in the magnetization of initially fully-magnetized ellipsoids of Alcomax III, when taken through the heating and cooling cycle +15 to +60 to −60 to +15° C is shown in Figs. 1, 2, 3 and 4. When the working point of the ellipsoid is above the BH_{max} point a normal negative temperature coefficient is obtained with a reversible change of magnetization (Fig. 1). If the working point is below the BH_{max} point, there is an irreversible change of magnetization as the temperature is lowered from 15 to −60° C. The changes in the magnetization of three different ellipsoids having working points below the BH_{max} point are shown in Figs. 2, 3 and 4. On heating to +60° C and allowing to cool to room temperature there is a small irreversible loss. As the temperature is decreased below room temperature the magnetization attains a maximum value and afterwards decreases. The loss is greater the larger the demagnetization factor and the lower the temperature to which the magnet is taken. When the temperature is allowed to increase again to room temperature, the magnetization again decreases but in a manner which is now reversible. The slope of this reversible magnetization curve varies quite considerably with dimension ratio and with the temperature at which the slope is measured. The loss in magnetization after return to room temperature can be regained by remagnetizing the specimen.

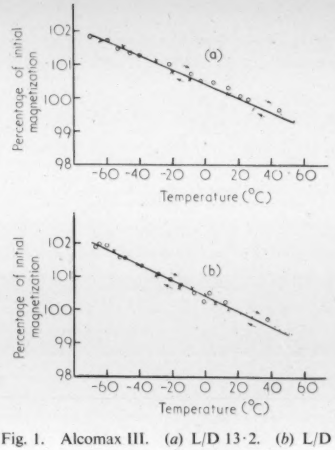

Fig. 1. Alcomax III. (*a*) L/D 13·2. (*b*) L/D 7·9

● = initial increasing temperature.
○ = decreasing temperature.
× = final increasing temperature.

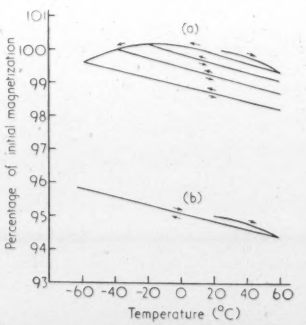

Fig. 2. Alcomax III. L/D 4·5

(*a*) fully magnetized; (*b*) reduced 5% by alternating field.

Magnets which are to be used in instruments are often stabilized by reducing the magnetization by a small amount in an alternating field. The effect of such stabilization on the magnetization-temperature changes of the shorter ellipsoids has been studied. The magnets were fully magnetized and the magnetization then reduced by 5% using a 50 c/s alternating field. The subsequent magnetization changes due

to the temperature cycle +15 to +60 to −60 to +15° C are shown in Figs. 2, 3 and 4, together with the changes in the unstabilized magnets. The results show that the irreversible loss of magnetization due to the first cooling to −60° C is very considerably reduced by stabilization.

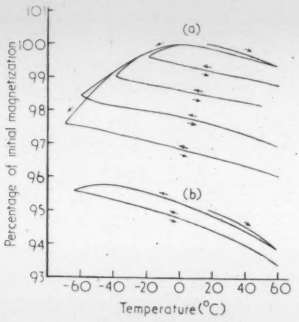

Fig. 3. Alcomax III. L/D 3·5

(*a*) fully magnetized; (*b*) reduced 5% by alternating field.

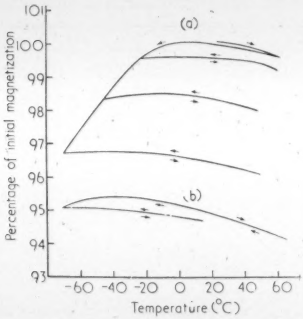

Fig. 4. Alcomax III. L/D 2·66

(*a*) fully magnetized; (*b*) reduced 5% by alternating field.

The effect of successive temperature cycles between room temperature and −65° C is shown in Fig. 5 for the fully magnetized and for a stabilized magnet. It can be seen that after the first complete cycle the magnetization change is reversible within the limits of experimental accuracy. It may be concluded that stability for practical purposes can be achieved by field stabilization, followed by one cooling cycle to a temperature lower than the lowest temperature to be subsequently used.

The effects found for Alcomax are also shown by Columax, i.e. Alcomax with a preferred crystal orientation. Tests taken on a Columax bar of dimension ratio 2/1 give curves similar to Alcomax III magnets having working points below the BH_{max} point. There is a permanent loss of 2·3% as a result of cooling to −70° C and reheating to room temperature, but this loss is almost eliminated after a previous stabilization. The properties of this Columax sample were $BH_{max} = 8{\cdot}2 \times 10^6$ G oersteds, $B_r = 14\,000$ G, $H_c = 738$ oersteds.

Alnico and cobalt steels. The changes in magnetization of fully-magnetized ellipsoids of Alnico and 35 and 15% cobalt steels have been similarly tested. With these materials there is a small irreversible change (less than 1·5%) on returning

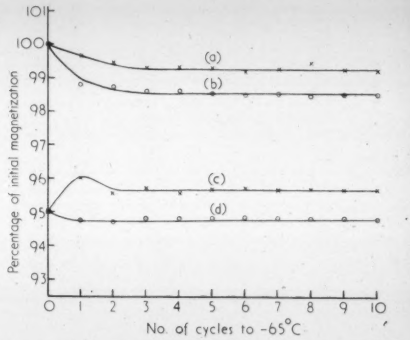

Fig. 5. Effect of repeated cycles of +15° C to −65° C on Alcomax III. L/D 4·5

(*a*) fully magnetized, measurements at −65° C; (*b*) fully magnetized, measurements at +15° C; (*c*) reduced 5% by alternating field, measured at −65° C; (*d*) reduced 5% by alternating field, measured at +15° C.

to room temperature after heating to +60° C. On cooling there is a reversible increase in magnetization, the slope of the curve being always less than −0·03% per °C but varying somewhat with magnets of different dimension ratio. The effect of alternating field stabilization is to eliminate the irreversible change on heating; the reversible changes are similar to those for fully-magnetized ellipsoids.

DEMAGNETIZATION CURVE RESULTS

The demagnetization curves of Alcomax III at 15, −75 and −180° C are shown in Fig. 6. It will be seen that the curves cross at H values just over −500, close to the BH_{max} point. The unit permeance lines of the five ellipsoids are also shown in this diagram.

In the cases of Alnico and cobalt steel there is an increase in the coercivity as well as B-values as the temperature is lowered with no crossing of the curves.

DISCUSSION

The demagnetization curves of Fig. 6 give the explanation of the magnetization temperature changes of Figs. 1 to 4. The intrinsic magnetization per domain increases with decreasing temperature, as indicated by the change of B_r and $4\pi I_s$ in Fig. 6. Therefore, magnetized ellipsoids with working points on the upper part of the demagnetization curve increase in strength on cooling and decrease in strength on reheating, without change in domain orientation. For ellipsoids with working points on the lower part of the curve, cooling gives a similar increase in intrinsic magnetization per domain, but, due to the reduced coercivity, the total magnetization at the working point is reduced. This change can only be achieved by partial domain re-orientation or boundary

movement and such changes are mainly irreversible, giving a magnetization loss on reheating to room temperature. If the ellipsoids are magnetized at low temperatures, the residual magnetization is less than after being magnetized at room

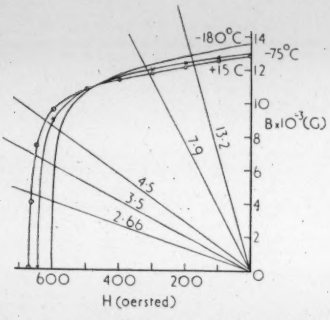

Fig. 6. Demagnetization curves of Alcomax III at +15, −75 and −180° C, showing also the unit permeance lines for the dimension ratios used

Saturation intensity $4\pi I_s$, 14 100 G at +15° C, 14 300 G at −75° C, 14 700 G at −180° C.

temperature by an amount which is in rough agreement with the change due to cooling the magnetized ellipsoid, as shown in Table 3.

Table 3. *Comparison of magnetometer measurements with the change in the residual magnetization*

Dimension ratio	*Decrease in $4\pi I$ at working point 15 to −75° C (%)*	*Loss by magnetometer 15 to −60° C (%)*	*Decrease in $4\pi I$ at working point 15 to −180° C (%)*	*Loss by magnetometer 15 to −180° C (%)*
4·5	1·02	0·5	5·8	5·25
3·5	3·5	2·3	9·9	7·6
2·66	4·56	3·3	14·8	9·9

In order to obtain further evidence for the explanation outlined above, an additional experiment was performed.

Untempered Alcomax has a coercive force which increases considerably at high temperatures. A magnet in this state magnetized at a high temperature should, therefore, lose much of its magnetization on cooling to room temperature. This was confirmed as shown by Table 4, which gives the losses in magnetization expressed as a percentage of the magnetization at 360° C.

Table 4. *Changes after magnetization at 360° C*

Dimension ratio	*Percentage loss in magnetization at:* 360° C	300° C	100° C	20° C
4·5	0	2·5	27	42
3·5	0	6·0	40	59
2·66	0	6·0	41	61

Since there is no apparent physical reason for the maximum in the magnetization at about 0° C shown in Figs. 2, 3 and 4, an experiment was performed to study this point. Fully-treated ellipsoids were magnetized at temperatures of 190 and 270° C and observations were taken of the magnetization variation on cooling. In each case there was an increase in strength over the greater part of the cooling range, followed by a decrease between 80° C and room temperature. The curves are similar to those obtained between room temperature and −10° C after magnetization at room temperature, except that the maximum strength is 1 to 2% higher than at the initial magnetization, and the final strength at 15° C is still somewhat higher than that obtained at the magnetization temperature.

The changes in the coercivity of Alcomax with temperature have no complete explanation as yet, although a correlation with the magneto-crystalline anisotropy has been previously discussed.(1) There is a maximum in the coercivity of Alcomax, in the untempered state, at about 450° C and in the normal tempered state at about room temperature; no such maximum has been found in the cases of Alnico or cobalt steel.

The normal tempering process for Alcomax is that which has been found to give the best room temperature properties. It is now clear that this process gives a maximum in the coercivity/temperature change at room temperature. It has been found that by extending the tempering treatment to 48 h at 590° C, 120 h at 560° C and 100 h at 530° C the percentage changes in magnetization between 15 and −75° C are as follows:

L/D 4·5	gain 0·23%
L/D 3·5	loss 0·65%
L/D 2·66	loss 0·81%
coercivity	685 oersteds

It is clear that the further treatment at 560 and 530° C gives a marked improvement in the temperature stability of the magnets, even though the room temperature coercivity value is not greatly changed.

CONCLUSIONS

There is a reversible increase in the magnetization of Alcomax III magnets with working points above the BH_{max} point as the temperature is decreased below room temperature.

There is an irreversible decrease in the magnetization of Alcomax III magnets with working points below the BH_{max} point as the temperature is decreased below room temperature; this effect also takes place with Columax. The irreversible decrease is greatly reduced by prestabilization or by a precooling cycle or by modification of the normal tempering treatment given to the alloy.

These changes can be correlated with the temperature changes of the demagnetization curve.

In the case of Alnico and the cobalt steels there is a reversible increase in the magnetization on cooling below room temperature which is independent of dimension ratio. For these materials, the irreversible decrease on heating to 60° C is much more evident than for Alcomax, but this loss is eliminated by prestabilization with an alternating field.

ACKNOWLEDGEMENTS

The author wishes to thank Mr. J. E. Gould and Dr. M. McCaig for constant advice and valuable discussion. This work was carried out at the Central Research Laboratory of the Permanent Magnet Association on behalf of the Electrical Research Association.

REFERENCES

(1) McCaig, M., and Clegg, A. G. *Electrical Research Association Report*, Ref. N/T67 (1954).
(2) Stoner, E. C. *Phil. Mag.*, **36** (7), p. 803 (1945).
(3) Sucksmith, W. *J. Sci. Instrum.*, **22**, p. 129 (1945).

The cracking of layers of brittle material by differential strains

By D. J. MILLARD, B.Sc., Ph.D., National Coal Board, Cheltenham, Glos.

[*Paper received* 6 *December*, 1954]

The cracking of a brittle layer of elastic material due to differential straining has been investigated with a view to discovering what factors govern the pattern of the cracks produced by a given strain pattern. An analysis of the stress equations leads to the conclusion that two dimensionless parameters only are involved, the ratio of the applied strains to the breaking strain and the ratio of the crack spacing to the layer thickness: the shape of the curve relating these parameters is deduced by physical argument. Evidence in support of the analysis is obtained from the observed cracking of brittle beams when subjected to a uniform strain gradient by bending.

The formation of cracks in a layer of brittle material suffering differential straining is of wide interest and has been studied from several standpoints, including work on the drying of clay,[1–3] the cracking of the lacquers used in brittle coating stress analysis,[4–6] and the crazing of the glaze on ceramics. The work described here, although perfectly general in nature, was carried out as part of a programme on the cracking that takes place in metallurgical coke due to differential shrinkage effects occurring in the coke oven. The stresses were considered in the material between cracks in a layer subjected to differential strain effects. These effects may occur, for instance, because of uneven temperature distribution in a sheet of ceramic or differential loss of volatile matter from a sheet of coke. The stress equations have been set up and studied to find the conditions prevailing when the stress relief due to the opening of cracks is just sufficient to reduce the maximum stress present to less than the breaking stress. The equations are not amenable to numerical solution but the factors influencing crack spacing have been deduced from them by dimensional arguments. The results of this analysis have been tested by experimental observations on the cracking of beams of brittle materials when differentially strained by bending in arcs of circles.

THE CASE OF PLANE STRAIN

Consider an infinite layer of homogeneous isotropic material of thickness t, the base of which is constrained so that it cannot change from its original form (Fig. 1). Let a

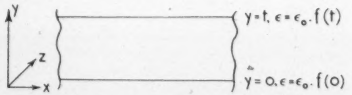

Fig. 1. Model for case of plane strain. Surface $y = 0$ constrained to pre-shrinkage condition

change take place in this material such that were any element free it would shrink, let this desired shrinkage have components in the x direction only ($\epsilon = \epsilon_x$, $\epsilon_y = \epsilon_z = 0$) and be of the form $\epsilon = \epsilon_0 . f(y)$ where $f(y)$ is an increasing monotonic function such that $f(0) = 0$ and $f(t) = 1$. Then it can be shown[7] that the stresses in the layer due to the suppression of these strains, that is due to the layer retaining its original form in spite of the desire to shrink, are given by the solution to the equations:

$$\nabla^2(\sigma_x + \sigma_y) = -[E\epsilon_0/(1-\nu)](\partial^2 f/\partial y^2) \quad \sigma_z = \nu(\sigma_x + \sigma_y)$$

$$(\partial\sigma_x/\partial x) + (\partial\tau_{xy}/\partial y) = 0 \quad (\partial\sigma_y/\partial y) + (\partial\tau_{xy}/\partial x) = 0$$

subject to the boundary conditions σ_y, $\tau_{xy} = 0$ at the free surface $y = t$ where σ_x, σ_y are normal and τ_{xy} shear stresses, E is Young's modulus, ν is Poisson's ratio and ∇^2 has its usual significance. Before cracking takes place (i.e. for $\partial/\partial x = 0$) these equations show the stress system present to be:

$$\sigma_x = [-E\epsilon_0/(1-\nu)]f(y) \quad \sigma_y = 0$$

$$\sigma_z = [-\nu E\epsilon_0/(1-\nu)].f(y) \quad \tau_{xy} = 0$$

Now consider what happens when the shrinkage is increased until σ_x locally reaches the tensile strength of the material at some point. A crack forms and stress magnification at its tip causes it to run through the thickness of the layer. This produces a new free boundary, and the stresses in the region of the crack are altered by the partial relief of the suppressed strains due to the opening of the crack. Such relief may best be considered in terms of the relief produced between two cracks and the possibility of such relief preventing further (intermediate) cracking. For reasons of symmetry it may be seen that the minimum stress relief occurs midway between two cracks, and that this minimum relief itself decreases as the spacing of the cracks increases until it becomes negligible for widely-spaced cracks. Thus, if the limits of the tensile strength of the material are known, it should be possible to produce an estimate of the maximum crack spacing to be expected for a given state of shrinkage, this being the spacing at which the stress midway between cracks may be regarded as just relieved. It follows that the minimum crack spacing to be expected under the same conditions is half this maximum spacing, and represents the final stage in a sequence, the penultimate stage of which was a crack spacing only just larger than the permitted maximum. Thus for a given state of strain in any one specimen the crack spacing produced may be expected to vary over a range of 2 : 1, depending on the manner of initiation of the first cracks.

To attempt to determine the spacing of cracks produced in the above manner, consider a layer of material bounded by the surfaces $y = 0$ and $y = t$, and containing two cracks running parallel to the z-axis at $x = \pm s$ (Fig. 2). We are

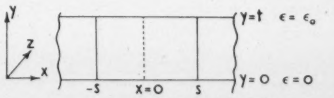

Fig. 2. Model for case of plane strain—two cracks

interested in obtaining the relationship between σ_x at points along the line ($x = 0$ $y = t$), s, the elastic constants of the material, and the shrinkage function ϵ, with a view to determining $2s$ as a function of all other variables for the special case of $(\sigma_x)_{0,t}$ equal to the lower limit of the tensile strength of the material. In this particular case the stresses between

cracks are given by the equations previously set out, subject to the boundary conditions that:

$$\sigma_x = 0 \quad \tau_{xy} = 0 \quad \text{at} \quad x = \pm s$$

$$\sigma_y = 0 \quad \tau_{xy} = 0 \quad \text{at} \quad y = t$$

σ_y, τ_{xy} = unknown constraining forces at $y = 0$.

The equations are not readily soluble, but their solution must be of the form

$$\sigma_x = [-E\epsilon_0/(1-\nu)] . f_1 (x, y, \text{constants})$$

where f_1 is some unknown function and the constants depend solely on the boundary conditions. Thus we may write

$$\sigma_x = [-E\epsilon_0/(1-\nu)] . f_1(xyst)$$

or, specifically considering the stress at points given by $x = 0, y = t$

$$(\sigma_x)_{0,t} = [-E\epsilon_0/(1-\nu)] \ f_2(s, t)$$

When conditions are such that $(\sigma_x)_{0,t} = \sigma_c$, the breaking stress of the material, we may then write

$$\sigma_c = [-E\epsilon_0/(1-\nu)] . f_2(s, t)$$

and this is the form of the equation relating the estimated crack spacing $2s$ with the other parameters in the problem. Now it can be seen from the stresses present in the layer before cracking starts that

$$[-\sigma_c(1-\nu)/E]$$

is the suppressed strain necessary to produce the first crack in the material. It is convenient to denote this quantity by the symbol ϵ_c the "breaking shrinkage," i.e. the breaking strain of the material as measured under the conditions of the problem. [This differs from the tensile test breaking strain for a rod by the factor $(1 - \nu)$.]

Thus we may write

$$\epsilon_c/\epsilon_0 = f_2(s, t)$$

The only other information obtainable is the statement of geometrical similarity. Since ϵ_0/ϵ_c is a numeric it follows that f_2 must be a function of s/t as required by geometrical similarity. Hence we may finally write

$$s = t f_3(\epsilon_0/\epsilon_c)$$

i.e. the crack spacing must be proportional to the thickness of the layer of material and a function of one other parameter only, this latter being the ratio of the total shrinkage that has taken place to the shrinkage necessary to produce the first crack.

It is not possible fully to evaluate the function f_3, which depends on the spatial pattern of the shrinkage strains, without solving the formal stress equations. Later in this paper an experimental determination of f_3 is given for the case of material subjected to a uniform strain gradient. This was obtained by observing the crack-strain relationship for brittle specimens as they were bent in arcs of circles.

At this stage of the argument, however, some indication as to the general nature of f_3 may be obtained by physical arguments. It is to be expected that the curve relating $2s/t$ to ϵ_0/ϵ_c will fall sharply in the region ϵ_0/ϵ_c just greater than unity as the first cracks appear and the major uncracked regions are reduced in size. It is also to be expected that when ϵ_0/ϵ_c is large the curve will tend to flatten, as when $2s/t$ is small the displacement needed to relieve even a large linear strain must be small compared with the thickness of the layer t. A stage must therefore be reached when the small displacement needed to accommodate any further shrinkage can readily be obtained by small permissible shear deformations of the material near the cracks. Thus increasing ϵ_0/ϵ_c will tend more and more to lead to the relief of x-stresses by shear deformation throughout the small uncracked regions, and less and less to the relief of stresses by cracking of the sort discussed above.

These arguments have so far been applied to a sheet of material kept flat by constraints applied to one surface, but the analysis is perfectly general and still holds even if the material be completely free. In this latter case, however, the strain pattern producing cracks must be regarded as only that part of the applied shrinkage that cannot be accommodated by simple bending.

CRACK PATTERNS DUE TO SHRINKAGE IN THREE DIMENSIONS

Consider now a layer of material in which the shrinkage pattern is given as

$$\epsilon_x = \epsilon_z = \epsilon_0 . f(y)$$

$f(y)$ being of the form previously considered. It is convenient to consider ϵ_y as zero since any shrinkage in the y-direction can be completely relieved by contraction of the layer without the production of elastic stresses. As ϵ_0 increases the stresses generated by suppression of the shrinkage increase until eventually, at some point on the surface, the stress reaches the tensile strength of the material and a crack is formed. This crack then allows local relief of the stress perpendicular to its length, any relief parallel to its length being a second order effect due to Poisson's ratio. Thus to relieve both x- and z-components of stress, cracking must take place in at least two directions. Once such cracking has started, consider the stress system near two cracks that happen to intersect. Taking one crack as a reference line and moving along it away from the point of intersection, the relief of stress components perpendicular to the reference remains constant, but the relief of stress components parallel to the reference decreases as the distance from the intersecting crack increases and the effect of that crack becomes less. Eventually a point is reached at which "parallel" stresses are virtually unrelieved and further cracking must take place both to relieve the stress components parallel to the reference and to continue relieving stress components perpendicular to the reference. It is sufficient that the original crack should divide into two branches, and, from the inherent symmetry of the system, it is to be expected that the two branches will form a symmetrical fork. The angle of formation of such a fork is not readily predictable, but once initiated, the cracks may be expected to assume a 120° configuration from strain energy considerations. Once a fork is formed the prongs then spread until they too must divide, the process continuing until a pattern of hexagons is built up.

Once the hexagonal crack pattern is formed, it is convenient to approximate individual hexagons by circles and to consider the stresses in one "island" of the crack pattern as shrinkage continues. The stress equations for a given island are now most conveniently expressed in cylindrical co-ordinates and, as in the case of plane strain, analysis of these equations leads to the conclusion that the "island diameter" $2s$ must be proportional to layer thickness t. Once the island pattern is formed, however, further cracking may take place in either of two different ways. The first possibility is that further cracks are initiated by stress magnification occurring at some irregularity in a crack bounding an "island." If this occurs, a crack will start from the edge

of an "island" and proceed in the manner already described, thus producing a secondary pattern of minor hexagons within each "island.' The second possibility, which might be expected to occur in a theoretically perfect material, is rather different from that previously mentioned. If there is no local irregularity to initiate cracking at an edge, then radial cracking is expected, producing a star pattern within each island. This follows from a consideration of the surface stresses in each cracked region. The radial and tangential stresses, σ_r and σ_θ are a maximum in the free surface of the island, and, for reasons of symmetry σ_r is a maximum at the centre of the island and decreases to zero at the edge ($r = s$) as required by the boundary conditions of the stress equations. However, σ_θ does not vary in this way. The equilibrium of segments of material near the origin requires that $\sigma_r = \sigma_\theta$ at the origin, but at all other points σ_θ is greater than σ_r. This follows from the fact that stress relief is, in general, greater for radial than for tangential stresses, since the relief of tangential strain at any point is, from simple geometry, proportional to the radial displacement at that point, and this radial displacement is itself proportional to the mean relief of radial strain taken over the radial length from the origin to the point considered. Thus as shrinkage proceeds σ_θ is greater than σ_r so cracks are propagated preferentially to the relief of σ_θ, i.e. under ideal conditions cracks spread radially producing a star pattern within each island.

SUMMARY OF THEORETICAL CONCLUSIONS

At this stage it is convenient to summarize the conclusions drawn from the foregoing argument. They are:

(1) the crack spacing produced by unidirectional differential suppressed shrinkages in a layer of brittle material is proportional to the thickness of the layer. It may vary by a factor of 2 : 1 depending on the position of initiation of the first cracks, and depends on the shrinkage pattern in a manner not readily determinable;

(2) in the more general case of isotropic shrinkage cracking takes place by the formation of a hexagonal crack pattern, the size of which is proportional to the thickness of the layer of material;

(3) the only parameter other than layer thickness affecting the crack pattern is the ratio of total shrinkage to breaking shrinkage. If this parameter is large a saturation condition may be reached and no further cracking may occur.

EXPERIMENTAL STUDY OF CRACK PATTERNS

The experimental work was designed to test three of the major conclusions drawn from the theoretical analysis, namely, that the spacing of cracks produced by differential straining is proportional to the thickness of the strained layer, depends on the total shrinkage divided by the breaking shrinkage, and tends to a saturation value for large shrinkages.

The strain system investigated was the constant strain gradient produced in a beam bent into an arc of a circle, the tensile stresses produced in the upper part of the beam then being analogous to the stress system produced by a constant suppressed shrinkage gradient. To prevent specimens falling apart once the first crack was formed, the bending was done either by constraining the specimen between curved jigs or by fixing it to a spring steel base and then constraining the base to a curved jig. When cracks had formed, the crack spacing was measured and compared with the "equivalent shrinkage" to which the beam had been subjected, i.e. with the strain the top surface of the beam would have suffered had it not cracked.

As wide a range of specimen size and material as possible was used to make the experimental testing of the theoretical conclusions as rigorous as possible, specimen thicknesses covering a range of 5 : 1 (4·0 to 0·8 cm) for four test materials, namely, glass, sealing wax, Bakelite X5337 and uncured Araldite. This latter is a thermo-curing resin adhesive. Details of the physical properties of these test materials are given in the table.

Physical constants of materials used in the experimental study of the cracking of brittle solids

Material	*Young's modulus in dyn/cm²* (measured)	*Breaking strain* (measured)	*Tensile strength in dyn/cm²* (calculated from columns 1 and 2)
Glass	$5{\cdot}4 \times 10^{11}$	$5{\cdot}8 \times 10^{-4}$	$3{\cdot}1 \times 10^{8}$
Sealing wax	$5{\cdot}4 \times 10^{10}$	$8{\cdot}0 \times 10^{-4}$	$4{\cdot}3 \times 10^{7}$
Bakelite X5337	$6{\cdot}0 \times 10^{11}$	44×10^{-4}	$2{\cdot}6 \times 10^{9}$
Uncured Araldite	$2{\cdot}8 \times 10^{10}$	$4{\cdot}8 \times 10^{-4}$	$1{\cdot}3 \times 10^{7}$

The testing of the theory lay in plotting the observed crack spacing using rational parameters deduced from the theoretical analysis and seeing that in spite of the wide variation in the properties of the materials used, essentially the same curve was obtained in all cases and that it tended to a saturation value as predicted.

For the jig experiments, specimen beams 18·0 × 1·3 cm were compressed between the male and female members of a series of jigs, the radii of these jigs varying in a geometrical progression of ratio $\sqrt{2}$ from 3·3 to 570 cm. Thus the conditions differed from those set out in the analysis of the case of plane strain in three respects; the constraint of the regions between cracks consisted of stresses on both upper and lower surfaces of the material and not of stresses on one surface only; there was a uniform surface pressure added to the conditions of the analysis; the specimens had tensile strains in the upper and compressive strains in the lower surface, whereas the analysis was for tensile strains in the upper and no strains in the lower surface. Fig. 3 shows the results of these experiments. It is a graph of crack spacing

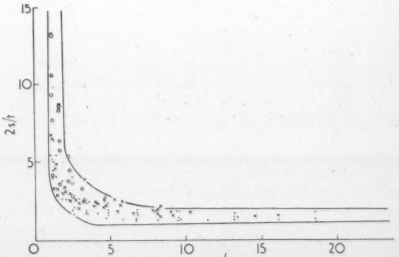

Fig. 3. Experiments on beams constrained between jigs. Plot of crack spacing divided by specimen thickness ($2s/t$) against strain parameter (ϵ_0/ϵ_c)

× = sealing wax; • = glass; ○ = Bakelite

divided by specimen thickness ($2\ s/t$) plotted against equivalent shrinkage divided by breaking shrinkage (ϵ_0/ϵ_c). It will be seen that for the three materials tested all points lie sub-

stantially on the same curve, and that this curve reaches a saturation value as predicted.

In the experiments with beams mounted on spring bases, specimen beams were mounted on strips of spring steel by

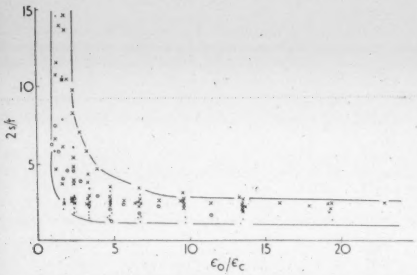

Fig. 4. Experiments on beams mounted on spring bases. Plot of crack spacing divided by specimen thickness ($2s/t$) against strain parameter (ϵ_0/ϵ_c)
× = sealing wax; • = glass; ○ = Araldite

means of Araldite cold-setting adhesive. These beams were then strained by bending the steel base to conform to the male portion of the various jigs described above. The conditions thus set up in the specimen differed from those set out in the analysis in one respect only; since the neutral axis of the compound beam was in the steel, the lower surface of the specimen was in tension. This would correspond to an overall shrinkage added to the conditions of the analysis, and so should not invalidate the application of the analysis to the results of these experiments. As before, the observed crack spacing was correlated with the applied deformation. Fig. 4 shows a plot of $2s\,t$ against ϵ_0/ϵ_c for the materials tested, and, as in the previous case, is of the predicted form.

ACKNOWLEDGEMENTS

The author would like to express his thanks to Mr. W. F. H. Howell who did much of the experimental work. Thanks are also due to the National Coal Board, for permission to publish this paper. The views expressed in it are those of the author and not necessarily those of the Board.

REFERENCES

(1) KINDLE, E. M. *Proc. Roy. Soc. Can.*, **20,** p. 71 (1926).
(2) KING, R. H. *J. Sediment. Pet.*, **16,** p. 14 (1946).
(3) HIND, S. R., and WHEELER, F. *Trans Brit. Ceram. Soc.*, **29,** pp. 10, 314 (1930).
(4) SMITH, C. W. *Paint*, **17,** p. 333 (1947).
(5) DEFOREST, A. V. *J. Appl. Mech.*, **9A,** p. 184 (1942).
(6) DURELLI, A. J., and OKUBOS, S. *Proc. Soc. Exper. Stress Anal.*, **11,** p. 153 (1954).
(7) TIMOSHENKO, S. *Theory of Elasticity*, pp. 203, 23, 27 (New York: McGraw-Hill Book Co. Inc., 1934).

High-frequency plasma-electron oscillations

By Prof. K. G. EMELEUS, Ph.D., F.Inst.P., and R. A. BAILEY, B.Sc., Ph.D.,* Physics Department, Queen's University, Belfast

[*Paper first received* 23 *December*, 1954, *and in final form* 20 *January*, 1955]

Methods are considered for increasing the concentration of plasma electrons and the plasma electron frequency in low pressure gaseous discharges traversed by electron beams. Two discharges are described which generate oscillations with a frequency of approximately 10^4 Mc/s.

There is now abundant evidence that a low pressure gaseous conductor, in which beams of electrons are present, can act as a source of high-frequency oscillations. The processes occurring are complicated,[1] but it is certain that the frequencies are not much different from those predicted for the free oscillations of the plasma electrons amongst a stationary matrix of positive ions. The frequency ν of such oscillations, in absence of friction and electron pressure effects, is

$$\nu = [Ne^2/(\pi m)]^{\frac{1}{2}} \qquad (1)$$

where N is the electron concentration, and e and m the charge and mass of an electron. The least electromagnetic wavelength obtained which has been reported, as far as the authors know, is 5 cm.[2] Brief descriptions are given below of some experiments in which 3 cm waves (10^4 Mc/s) have been obtained, although the power obtained was minute.

A fundamental difficulty in producing waves of very short wavelength is [equation (1)] that the frequency is proportional only to the square root of the electron concentration, and so, for example, a concentration of approximately 10^{13} per cm^3 would be needed for 1 cm waves. Methods available for increasing N in hot-cathode discharges include:

(i) increasing the electron emission from unit length or unit area of the filament;
(ii) concentrating the primary electron beams from a large area of cathode into a small volume;
(iii) increasing the amount of ionization produced per primary electron in that part of the discharge where the oscillations occur.

Method (i) is limited by the thermionic properties of available materials. Method (ii) is limited by the practical difficulty of removing the heat generated in a small volume, and by the fact that the authors have found that lower frequency ionic or relaxation oscillations often occur where primary electrons are focused, with accompanying irregularity of the plasma electron oscillations. Method (iii) might be applied (*a*) by using primary electrons with energy near that at which there is maximum chance of producing ionization in single impact with a gas molecule, or (*b*) by increasing the gas pressure. Condition (*a*) has not proved useful with the tubes used, in which the strongest oscillations have been consistently obtained under operating conditions not far from those near the saturation "knee" for the current *versus* voltage characteristic of a tube with a bright emitting filament, i.e. with electrons well below optimum ionizing energy. Best

* Now at Radar Research Establishment, Malvern.

results have so far been obtained with condition (*b*). At least in the pressure range for which each primary electron ionizes not more than once in the tube, the rate of production of ions per primary electron is proportional to the gas pressure, and although it cannot be stated, without detailed application of the plasma-balance equations, exactly how the equilibrium concentration N will be changed in this way, an increase of N and ν with increase in pressure would be expected, and has generally been found.

EXPERIMENTAL METHODS AND RESULTS

The oscillations were detected by two coaxial line wavemeters, having outer diameters of 2·2 and 0·64 cm respectively, with a crystal across the open end. The closed end was a piston, the position of which could be varied. The electrode picking up the high-frequency oscillations in the tube was connected to the central conductor by as short a length of shielded line as was practicable, but it was not possible to reduce the length of the connexion below 3 cm (tube *A*) or 8 cm (tube *B*). Since it is doubtful if any extended volume of plasma oscillates coherently, the pick-up arrangements in the tube are necessarily less standard and simple than in a cavity resonator, and the problem of matching the tube to the wavemeter presents difficulties which have not yet been satisfactorily overcome.

From the considerations set out above, the authors aimed at decreasing the wavelength by increasing the pressure. Most experiments were made with two tubes (*A* and *B*) containing argon, used on the pumping train. With tube *A* a minimum wavelength of 3·8 cm was reached, and with tube *B*, 3·0 cm.

The construction of *A*, a cylindrical diode without a probe, is shown in the figure. The arrangement on the left of the figure enabled the wavemeter to be connected through the

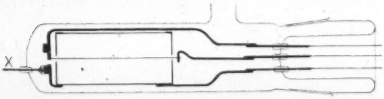

Tube *A* for generating short waves. Electrode supports and leads in the tube are shown by thick lines

rod *X* either to the end of the filament or to the anode, by rotating the ground joint at the right. The filament, made of 0·2 mm diameter tungsten, was 4·6 cm long. At an argon pressure of 3×10^{-2} mm of mercury, oscillations of wavelength between 10 and 20 cm were readily obtained, as before.(2) On increasing the pressure, the minimum wavelength obtained for a given emission current steadily decreased. Oscillations were generated up to a pressure of $1 \cdot 3 \times 10^{-1}$ mm of mercury, but were then so feeble as to be barely detectable. Typical discharge conditions for obtaining a wavelength of 3·8 cm were: pressure, $1 \cdot 22 \times 10^{-1}$ mm of mercury; tube voltage, 21·0 V; tube current, 0·30 A. The rectified crystal currents obtained with the wavemeter connected to the filament were about four times those obtained from the anode. It was otherwise immaterial which electrode was employed.

Although this tube yielded shorter wavelengths than had been hitherto reached, it was not considered entirely satisfactory, as the internal oscillation pattern probably had maxima at radial distances which did not coincide with the anode.(2) A modification of the convenient adjustable tube used by Neill(3) was therefore set up (tube *B*) in the form of a stemmed bulb 10·7 cm in diameter. The pick-up electrode was a movable flat probe, 4×3 mm, supported by a shielded wire. The shield was composed of a fine glass tube 3·9 cm in length, with above this a fine earthed metal tube. The probe could be set accurately and rapidly where it picked up the strongest oscillations.

The longer wavelength (10–40 cm) oscillations generated by this tube with argon at a pressure of a few 10^{-3} mm of mercury were similar to those described previously.(2, 3) The short wavelength oscillations generated at higher pressure were, however, of slightly higher frequency than those obtained with tube *A*. The tube generated oscillations for pressures up to $8 \cdot 5 \times 10^{-2}$ mm of mercury. They then occurred near the saturation "knee" of the current *versus* voltage characteristic curve of the tube, which was rounded, presumably because of the relatively high pressure. As anticipated from earlier work, the probe had to be set very close to the filament, at distances of the order of 1 mm, to obtain maximum pick-up. It probably intersected the equivalent for this discharge of the disturbed region of plasma, discovered by Druyvesteyn and Warmolz(4) and since studied in more detail for flat cathodes in this laboratory. Typical discharge conditions for which a wavelength of 3·0 cm was obtained were: pressure, $7 \cdot 0 \times 10^{-2}$ mm of mercury; tube voltage, 24·0 V; tube current, 0·235 A; probe, 0·6 mm from filament at its centre. The power withdrawable was again minute, and only of the order of a microwatt or less.

CONCLUSION

The conclusion drawn from these experiments concerning the possible use of plasma-electron oscillations as signal generators at about 10^4 Mc/s is the same as that drawn previously for oscillations of greater wavelength,(2) namely, that the small power available and the variability of gaseous discharges appear to rule them out, at least if tubes of conventional design are employed. The experiments have, however, been satisfactory in confirming the trend of the results predicted from theory as a result of an increase in pressure. The general accord with theory also extends to the amplitude of the oscillations, which would be expected to decrease with increase of pressure because of the disturbance of the regular oscillations of the plasma electrons by collisions with molecules, and because of the angular scattering of the beam electrons from the same cause. It would, nevertheless, be unsafe to assume that some other form of localized discharge, e.g. the plasma close to the cathode spot of a pool arc cathode, might not ultimately be found capable of giving oscillations of higher frequency, although with the increased density of ionization required by equation (1), disturbance of regular motion of electrons by ionic fields, as distinct from the fields of neutral molecules, might then prove to be a limiting factor.

ACKNOWLEDGEMENTS

We wish to thank Dr. C. S. Watt for his advice and interest in this work, and Mr. H. A. Menown for assistance with the experiments.

REFERENCES

(1) cf. GABOR, D. *Brit. J. Appl. Phys.*, **2**, p. 209 (1951). This reference contains a bibliography.
(2) ARMSTRONG, E. B., and EMELEUS, K. G. *Proc. Instn Elect. Engrs*, **96**, p. 390 (1949).
(3) NEILL, T. R., and EMELEUS, K. G. *Proc. Roy. Irish Acad. A*, **53**, p. 197 (1951).
(4) DRUYVESTEYN, M. J., and WARMOLZ, N. *Physica*, **4**, p. 51 (1937).

The solution of transient heat flow and heat transfer problems by relaxation

By G. LIEBMANN, D.Phil., F.Inst.P., Research Laboratory, Associated Electrical Industries Ltd., Aldermaston, Berks

[*Paper received* 14 *October*, 1954]

It is shown that by choosing a suitable finite difference approximation, parabolic partial differential equations, e.g. the *heat conduction equation*, can be converted into a series of boundary value problems of the Poisson type, each with specified boundary conditions, which can be easily solved by Southwell's relaxation technique. The method is first discussed with reference to the one-dimensional case, and is then generalized to problems in (x, y)- and (r, z)-co-ordinates. *Heat transfer* problems can be brought within the scope of the method. The outstanding characteristic of the method is the very stable nature of the solution for all values of the time interval; this permits the choice of relatively great time intervals, so that a complete solution, extending over a long period of time, may be obtained in a small number of steps without loss of accuracy. The required relaxation patterns are given and several numerical examples are included.

1. INTRODUCTION

The conduction of heat in a solid is described by the equation

$$\text{div } K \text{ grad } U = c\rho(\partial U/\partial t) \tag{1}$$

where U is the temperature, t the time, and K the thermal conductivity of the solid, c its specific heat and ρ its density. If K is constant, this equation simplifies to

$$\nabla^2 U = (1/D)(\partial U/\partial t) \tag{2}$$

where $D = K/c\rho$ is the diffusivity of the solid. If the flow of heat is one-dimensional, equation (2) becomes

$$\partial^2 U/\partial x^2 = (1/D)(\partial U/\partial t) \tag{3}$$

Formal solutions of these parabolic partial differential equations, for prescribed boundary conditions and given initial conditions, are often difficult and complicated, and in many practical problems a numerical method of solution is preferred, e.g. one in which the partial differential equation is approximated by a finite difference expression. For instance, equation (3) has often been replaced by

$$U_{m,n+1} = U_{m,n} + \alpha^{-1}(U_{m-1,n} - 2U_{m,n} + U_{m+1,n}) \tag{4}$$

where $U_{m,n}$ is the temperature at the point P_m (Fig. 1) at the time $t = n\delta t$, and

$$\alpha = (\delta x)^2/D\delta t \tag{5}$$

δx and δt being the space and time intervals in which the numerical solution is computed. Beginning with the known

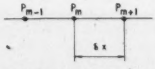

Fig. 1. Points at finite intervals δx used in difference approximation to partial differential equation

initial conditions (at $n = 0$), the temperature values for $n = 1$ can be evaluated from equation (4) for all points P_m, and then from these the temperature for $n = 2$, etc., until the solution for the whole time range $T = N\delta t$ has been built up. Equation (4) has, therefore, formed the basis of many computational or graphical methods for the solution of heat conduction problems (Schmidt,[1] Emmons,[2] Dusinberre,[3] and others). A well-known restriction (see, e.g. Price and Sarjant,[4] or O'Brien, Hyman and Kaplan[5]), however, lies in the condition that the time intervals have to be made small enough that

$$\alpha \geqslant 2 \tag{6}$$

to ensure "stability" or convergence of the solution.

The truncation errors of the approximation, equation (4), are of $0(\delta x)^2$ and $0(\delta t)$. A better approximation, in which the truncation errors are of $0(\delta x)^2$ and $0(\delta t)^2$, and which is stable for all values of α, has been given by Crank and Nicolson,[6] but their method involves more terms and requires an iterative procedure.

More recently, Allen and Severn[7] showed how one can bring the heat conduction equation within the range of the relaxation technique.[8] Their ingenious method consists in first transforming equation (3) into a fourth order differential equation for a substitute function w, containing only even orders of derivatives. By suitably choosing the transformation function, conditions are obtained for w at the end points $t = 0$ and $t = T$ of the required time range. In this way, the problem described by equation (3) is turned into a boundary value problem in the co-ordinates x and t, which is then solved by the usual methods of the relaxation technique. The higher order of the substitute partial differential equation necessitates, of course, a more complicated relaxation pattern than for the second order equation. Moreover, the one-dimensional equation (3) requires a two-dimensional relaxation net, and the two-dimensional forms of equations (1) or (2) would need three-dimensional relaxation systems.

In this paper, a method for the numerical solution of the equations (1), (2) or (3) by a more direct and rather simpler relaxation technique will be described.

2. AN ALTERNATIVE FINITE DIFFERENCE APPROXIMATION

The new method of solving the heat conduction equation by relaxation will be explained with reference to the one-dimensional equation (3). The generalization will be carried out in Section 7.

The finite difference approximation, equation (4), had been obtained by replacing $(\partial^2 U/\partial x^2)_n$ at the point P_m (Fig. 1) by $(U_{m-1,n} - 2U_{m,n} + U_{m+1,n})/\delta x^2$ and $(\partial U/\partial t)_m$ at the time $t = n\delta t$ by $(U_{m,n+1} - U_{m,n})/\delta t$. However, an equally good, and equally justified, first approximation to $(\partial U/\partial t)_m$ at the time $t = n\delta t$ is $(U_{m,n} - U_{m,n-1})/\delta t$. Using this latter approximation, the finite difference approximation to equation (3) becomes

$$U_{m-1,n} - 2U_{m,n} + U_{m+1,n} = \alpha(U_{m,n} - U_{m,n-1}) \tag{7}$$

The truncation errors of this approximation are of $0(\delta x)^2$ and $0(\delta t)$, as for the approximation, equation (4); the truncation error $0(\delta t)$ can be reduced to an error $0(\delta t)^2$ by a simple extrapolation technique given in Section 6.

Equation (7) has two important characteristics; first, while this equation gives a relation, at each point P_m at the time $n\delta t$, between four unknown and one known value of U, this relation is of exactly the same type as that used so successfully in the relaxation technique for solving Poisson type partial differential equations.[8] Hence, the usual relaxation technique can be applied in a very direct and simple manner. Second, the solution based on equation (7) is very stable, for any value of α; one can therefore choose relatively long time intervals δt, without the danger of finding an oscillating or diverging solution.

3. THE STABILITY OF THE RELAXATION SOLUTION

The stability of equation (7) for all values of α can be shown in several different ways, e.g. by the von Neumann–Hartree method.[5,6] A more elementary way of investigating the stability of equation (7), which also gives a more detailed insight into the effect of computational errors, is to introduce an error ϵ at the point P_m at the time $(n-1)\delta t$, and to evaluate from equation (7) the resulting errors $\Delta_{m,n}$ in the temperatures $U_{m,n}$ for different points P_m at the time $n\delta t$. The errors $\Delta_{m,n}$ also satisfy equation (7), with the values $\Delta = 0$ at the boundaries, i.e.

$$\Delta_{m,n} = (\Delta_{m-1,n} + \Delta_{m+1,n} + \alpha\Delta_{m,n-1})/(2+\alpha), \text{ with } \Delta_{m,n-1} = \epsilon.$$

In the first approximation of this evaluation of the resulting errors, one assumes, as a first step, $\Delta_{m-1,n} = \Delta_{m+1,n} = 0$. Then

$$\Delta_{m,n} = [\alpha/(2+\alpha)]\epsilon \qquad (8)$$

As the next step, one assumes $\Delta_{m-2,n} = \Delta_{m+2,n} = 0$, and evaluates $\Delta_{m-1,n}$ and $\Delta_{m+1,n}$ from equation (7) with the value of $\Delta_{m,n}$ from equation (8) and $\Delta_{m-1,n-1} = 0$. This gives

$$\Delta_{m-1,n} = \Delta_{m+1,n} = \alpha\epsilon/(2+\alpha)^2 = \Delta_{m,n}/(2+\alpha) \qquad (9)$$

and generally $\Delta_{m-r,n} = \Delta_{m+r,n} = \Delta_{m,n}/(2+\alpha)^r$.

In a second approximation, instead of assuming for the first step initial values of $\Delta_{m-1,n} = \ldots = 0$, one uses the values of the first approximation, which gives a correction factor $[1 + 2/(2+\alpha)^2]$ in equation (8) for $\Delta_{m,n}$, etc.

For $\alpha \to \infty$ (very short time intervals δt), all correction factors $\to 1$, and $\Delta_{m,n} = [\alpha/(2+\alpha)]\epsilon \simeq \epsilon$ and $\Delta_{m\pm r,n} \simeq 0$, i.e. the error ϵ remains localized at the point P_m, and is transmitted nearly unchanged to the temperature value at the next time interval. The smaller α, i.e. the larger the time interval, the more the error ϵ becomes distributed over neighbouring mesh points, its maximum value decreasing correspondingly; indeed, it can be shown that all errors $\Delta_{m,n}$ resulting from the error ϵ at $(n-1)\delta t$ have the same sign as ϵ, and that their sum is always smaller than, or at most equal to, ϵ. Hence, as the solution proceeds, numerical errors made will tend to disappear as $\Delta_{m,n} = 0$ at the boundaries, where values of $U_{m,n}$ are prescribed. In practice, error cancellation occurs quite rapidly if the final residuals of the relaxation process are always well distributed, such that positive and negative residuals, i.e. small negative and positive computational errors ϵ, are mixed, and of roughly equal value, as is anyway desirable in the application of the relaxation technique; then the ultimate "liquidation" of the numerical errors ϵ at the boundaries is much less important than the rapid mutual cancellation of errors of opposite sign at the interior mesh points.

4. THE RELAXATION PROCESS

Equation (7) can be put immediately into a form suitable for relaxation

$$\mathscr{R}_{m,n} = U_{m-1,n} + U_{m+1,n} - (2+\alpha)U_{m,n} + \alpha U_{m,n-1} \qquad (10)$$

where $\mathscr{R}_{m,n}$ represents the residual at the point P_m at the time $n\delta t$. The corresponding relaxation pattern is shown in Fig. 2, the numerals within the circles indicating, in the customary manner, the change in the residuals at the points represented by the circles due to a unit increment, $\Delta U_{m,n} = 1$, at P_m.

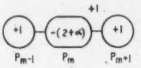

Fig. 2. Relaxation pattern used in solving one-dimensional heat conduction equation (3)

The relaxation pattern is of great simplicity and the relaxation process can therefore be carried out in a straightforward manner, starting from trial values of $U_{m,n}$ as usual in relaxation. When α is small (δt great), it can often be disregarded in the term $-(2+\alpha)$ during the relaxation, and only in the first working out of the residuals $\mathscr{R}_{m,n}$, or during any subsequent checking of the residuals, is the correct inclusion of the α terms needed.

As an example, Fig. 3 shows the temperature distribution in a thermally insulated infinitely long bar, computed by relaxation with $\alpha = 1$ ($D = 0{\cdot}125\ \mathrm{cm^2/s}$, $\delta t = 8$ s, $\delta x = 1$ cm). The initial temperature assumed is $U = 0$, the end of the bar, at $x = 0$, being raised at $t = 0$ to the temperature U_0 and kept thereafter at this temperature. In Fig. 3, the full lines give the exact solution [reference (9), p. 43] for $t = 64$ s and $t = 256$ s; the circles give the values computed by the method discussed here.

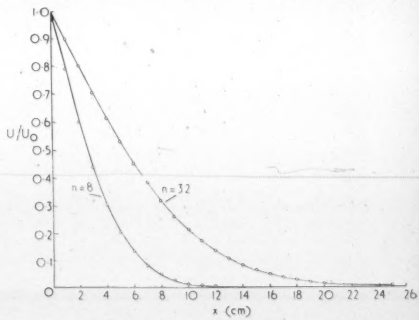

Fig. 3. Comparison of relaxation solution (circled points), using $\alpha = 1$, with exact solution (full lines) at times $8\delta t$ and $32\delta t$ [$\delta t = (\delta x)^2/(\alpha D)$], for problem of heat insulated bar initially at zero temperature, its end at $x = 0$ being raised to temperature U_0 at $t = 0$

5. THE CHOICE OF THE TIME INTERVAL

A point calling for further comment is the best choice of the time interval δt. The value of δt will mostly be a compromise, as a small value of δt may entail a great deal of work, whereas a too great value of δt may result in an undesirably great influence of the truncation error in the approximation for $(\partial U/\partial t)$. An experimental study of this question for a special case (infinitely long bar heated from one end) by a closely corresponding electrical analogue method[10] has shown that for values of $\alpha \leqslant 2$, the truncation error is greatest, in this type of problem, for the first time interval, $n = 1$. It is initially the greater the smaller α (i.e. the greater δt), the greatest error being of the order of several per cent. The truncation errors were found, in the case investigated, to fall monotonically such that their maximum value was reduced to about 2% for $n = 6$ (nearly independently of the value of α), to 1% for $n = 16$, and to less than 0·6% for $n = 30$ [see also Fig. 3 of this paper and Fig. 1.11 of reference (10)]. Owing to the uncertainty, in most practical problems, of the knowledge of the physical constants, K and c, entering into the value of D, it would seem that one should, in practice, subdivide the time range T studied into, say, five to forty time intervals, depending on whether one is interested in the final temperature distribution only, at $t = T$, or in the details of the solution at intermediate times as well. If this should be the case, it is often advisable to carry out the process with graded time intervals, e.g. taking five steps with an appropriate value of α, then a few more steps with a smaller value of α, etc. In this way, a very wide time range can be covered with relatively few steps, without appreciable loss of accuracy due to excessive truncation errors. (Compare Fig. 2.8 of reference (10), where a period, equal to 10000 of the smallest time intervals used, was covered in thirty-six steps, the deviation of the solution from the exact solution being always less than 2%, and mostly less than 1%.)

6. IMPROVEMENT OF CONVERGENCE BY EXTRAPOLATION

An alternative way of reducing the influence of the truncation error in t is the following easily applied extrapolation method, similar to Richardson's "deferred approach to the limit,"[11] which reduces the truncation error of the difference approximation, equation (7), from $0(\delta t)$ to $0(\delta t)^2$.

From

$$(\partial U/\partial t)_{m,n} = (U_{m,n} - U_{m,n-1})/\delta t - (\delta t/2)(\partial^2 U/\partial t^2) + 0(\delta t)^2$$

one can show that a better approximation to the correct temperature value is given by

$$U_{m,n}[1 + A\delta t(\partial^2 U/\partial t^2) + 0(\delta t)^2]$$

where A is a constant. Neglecting $0(\delta t)^2$ in the bracketed correction term, one can derive from the linearity of the correction term in δt this extrapolation formula

$$U_c(t) = U_2(t) + [U_2(t) - U_1(t)] \qquad (11)$$

Here $U_c(t)$ is the temperature at the time t corrected from the temperature $U_2(t)$, which is the temperature computed by relaxation with a time interval δt_2, by adding to $U_2(t)$ the difference between $U_2(t)$ and $U_1(t)$; $U_1(t)$ is the temperature found by relaxation using a time interval $\delta t_1 = 2\delta t_2$.

The usefulness of this extrapolation method is shown by the example given in the table. It is seen that the maximum of the truncation errors in U_2 is reduced by a factor of about 4 (the improvement factor varies mostly between 3 and 5). The improvement is most marked where the truncation errors are large. However, where the truncation errors are smaller than the numerical errors left in the temperature distribution as evaluated by relaxation, extrapolation may in some instances increase the error rather than reduce it, as the rounding-off errors of the two distributions U_1 and U_2 add as can be seen from equation (11). Hence, extrapolation should only be applied where the truncation errors predominate over the rounding-off errors.

Reduction of truncation errors through extrapolation

(Temperature distribution in infinitely long thermally insulated bar, initially at zero temperature, end raised to U_0 at $t = 0$)

$D = 0{\cdot}125\ \mathrm{cm^2/s}$, $\delta x = 1$ cm, $t = 16$ s, $\epsilon = (U/U_0)_{relax} - (U/U_0)_{exact}$

		$\delta t_1 = 4$ s $(n = 4)$		$\delta t_2 = 2$ s $(n = 8)$		*Extrapolated*	
x (cm)	$(U/U_0)_{exact}$	$(U/U_0)_{relax}$	ϵ	$(U/U_0)_{relax}$	ϵ	$(U/U_0)_{relax}$	ϵ
0	1	1	0	1	0	1	0
1	0·617	0·583	−0·034	0·599	−0·018	0·615	−0·002
2	0·317	0·294	−0·023	0·305	−0·012	0·316	−0·001
3	0·133	0·134	+0·001	0·136	+0·003	0·138	+0·005
4	0·046	0·056	+0·010	0·054	+0·008	0·052	+0·006
5	0·012	0·022	+0·010	0·020	+0·008	0·018	+0·006
6	0·003	0·008	+0·005	0·007	+0·004	0·006	+0·003
7	0·001	0·002	+0·001	0·002	+0·001	0·002	+0·001
8	0	0	0	0·001	+0·001	0·002	+0·002
9	0	0	0	0	0	0	0

Another way of reducing the initial error for $\alpha \leqslant 1$ is to employ for the first few steps Crank and Nicolson's[6] finite difference approximation to equation (3), put into a form suitable for relaxation. The equation for the residual then becomes

$$\mathscr{R}_{m,n} = U_{m-1,n} + U_{m+1,n} - 2(1 + \alpha)U_{m,n} + F_{m,n}$$

with

$$F_{m,n} = U_{m-1,n-1} + U_{m+1,n-1} - 2(1 - \alpha)U_{m,n-1}$$

Formula (11) can also serve the purpose of estimating the systematic error of the relaxation solution, by solving once with δt_1 and then with $\delta t_2 = \delta t_1/2$. The difference between these two solutions is approximately equal to the systematic error in the solution with δt_2.

being a contribution to the residual which can be evaluated at each point P_m at the time $n\delta t$ before the relaxation process proper is started. Comparative tests on the problem illustrated by Fig. 3 have shown that the amount of work required for solutions of approximately equal accuracy is slightly less for the extrapolation method.

7. THE GENERALIZATION OF THE METHOD

The technique described can be easily extended to deal with problems governed by the more general heat conduction equations (1) and (2). Considering first the application to equation (2), when $\nabla^2 U$ represents the Laplacian operator for two-dimensional (x, y)-problems, or three-dimensional problems of rotational symmetry, (r, z)-problems, the only change is the replacement of the finite difference approximation to $(\partial^2 U/\partial x^2)$ by the well-known difference approximations to $(\partial^2 U/\partial x^2 + \partial^2 U/\partial y^2)$ or $\partial^2 U/\partial z^2 + (1/r)(\partial/\partial r)[r(\partial U/\partial r)]$. Dividing the (x, y)-plane, or the meridian (r, z)-plane, into a net of square meshes with mesh length h, and numbering mesh points in the manner shown in Fig. 4, the residual formulae

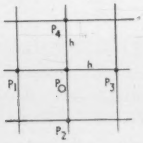

Fig. 4. Relaxation net of mesh length h for two-co-ordinate problems

at the mesh point P_0 (with off-axis distance r_0 in axially symmetric problems) replacing equation (10) are then for the (x, y) case

$$\mathscr{R}_{0,n} = \sum_{m=1}^{4} U_{m,n} - (4 + \alpha)U_{0,n} + \alpha U_{0,n-1} \tag{12}$$

and for the (r, z) case

$$\left.\begin{aligned} \mathscr{R}_{0,n} &= U_{1,n} + [1 - (h/2r_0)]U_{2,n} + U_{3,n} + [1 + (h/2r_0)]U_{4,n} \\ &\quad - (4 + \alpha)U_{0,n} + \alpha U_{0,n-1}, \quad r_0 \neq 0 \\ \mathscr{R}_{0,n} &= U_{1,n} + U_{3,n} + 4U_{4,n} - (6 + \alpha)U_{0,n} \\ &\quad + \alpha U_{0,n-1}, \quad r_0 = 0 \end{aligned}\right\} \tag{13}$$

with

$$\alpha = h^2/(D\delta t) \tag{14}$$

The corresponding relaxation patterns are given by Fig. 5 for the (x, y) case and by Fig. 6$(a$–$c)$ for the (r, z) case, with $r_0 = mh$, $m = 0, 1, 2, \ldots$ being written to give a more convenient representation.

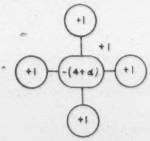

Fig. 5. Relaxation pattern used in solving heat conduction equation (2) for two-dimensional problems

In the extension of the method to the general heat conduction equation (1), governing the flow of heat in systems which are composed of several bodies, with different values of thermal conductivity K or thermal capacity $c\rho$, consider in an (x, y) problem the same subdivision into square meshes

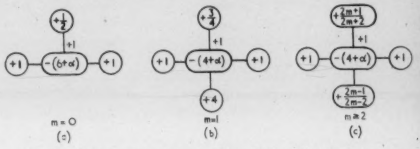

Fig. 6. Relaxation patterns used in solving heat conduction equation (2) for three-dimensional problems of rotational symmetry: (a) for points on axis; (b) for points one mesh length distant from axis; (c) for points more distant from axis

as before, but assume that the average value of K between mesh points P_0 and P_1 is K_1, and the average value of $c\rho$ is $(c\rho)_1$, etc., as shown schematically in Fig. 7.

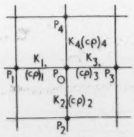

Fig. 7. Relaxation net for two-co-ordinate problems if the thermal conductivity K and the heat capacity $(c\rho)$ are functions of the space co-ordinates

Writing

$$k_m = K_m/K_0 \tag{15}$$

where

$$K_0 = \tfrac{1}{4}\sum_{m=1}^{4} K_m \tag{16}$$

and

$$\alpha_0 = \tfrac{1}{4}\sum_{m=1}^{4} \alpha_m \tag{17}$$

where

$$\alpha_m = h^2(c\rho)_m/K_0\delta t \tag{18}$$

the equation for the residual $\mathscr{R}_{0,n}$ at the point P_0 takes on this simple form within the previous degree of approximation

$$\mathscr{R}_{0,n} = \sum_{m=1}^{4} k_m U_{m,n} - (4 + \alpha_0)U_{m,n} + \alpha_0 U_{m,n-1} \tag{19}$$

The relaxation pattern corresponding to equation (19) is shown in Fig. 8 (note that $\sum_m k_m = 4$).

A similar formula applies for the residual in (r, z) problems with unequal thermal conductivities, etc.

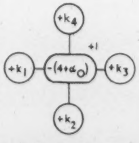

Fig. 8. Relaxation pattern for solving heat conduction equation (1) for two-dimensional problems in which thermal conductivity K and heat capacity $(c\rho)$ are functions of the co-ordinates

It is of course possible to generalize the technique further, solving heat conduction problems with unequal or graded meshes, or with modified boundaries, using the known methods established for this in the relaxation technique. The only point worth mentioning here is that it is then necessary to take account of the fact that the values of α_m in equation (18) have to be weighted accordingly.

The remarks made earlier in connexion with one-dimensional problems concerning the possibility of disregarding α in the actual relaxation process if α is small, and concerning the best choice of the time interval δt, or the extrapolation to reduce the truncation errors of $(\delta U/\delta t)$, apply equally well to the more general cases discussed in this section. It should also be noted that the short cuts of the relaxation technique, as "over-relaxation," and group and block relaxation, can be applied without modification.

8. A NUMERICAL EXAMPLE

As a numerical example, demonstrating the application of the method to a two-dimensional case, the heat flow through a model of the cavity brick wall shown in Fig. 9 was computed. The following assumptions were made to define the problem: initial temperature $U = 0$, the left surface of the wall being raised suddenly at the time $t = 0$ to the temperature $U_0 = 1000$, and kept thereafter at this temperature, the thermal constants of the material being uniform and constant, and the heat losses at the right surface of the wall being negligible. (This problem is artificial in so far as boundary values U_0 are prescribed for the left surface instead of heat transfer at a certain rate, and no loss of heat for the right surface, but the satisfaction of these more correct conditions would complicate the demonstration of a technique which is very simple in itself.) Owing to symmetry, only the part shown shaded in Fig. 9 need be considered. Fig. 10 shows this part and the relaxation net used.

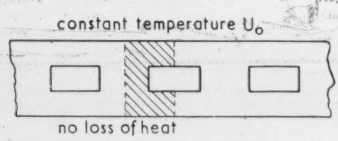

Fig. 9. Model of cavity brick wall

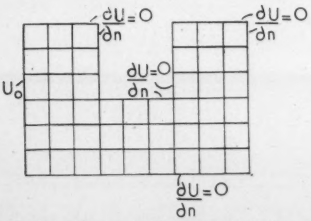

Fig. 10. Relaxation net, corresponding to shaded area in Fig. 9

The solution was worked with graded time intervals, using five intervals of length $\delta t_1 = h^2/D$, then four of $\delta t_2 = 5h^2/D$, and three of $\delta t_3 = 25h^2/D$, i.e. twelve steps were used to cover a time range which is equal to 200 of the maximum permissible time intervals $\delta t = h^2/2D$ in the older numerical techniques, based on equation (4). If the solution had been required for a considerably greater time range, a further step-up of δt would have been used for the final period. The values of δt used correspond to $\alpha = 1$, $\alpha = 0{\cdot}2$ and $\alpha = 0{\cdot}04$. The initial estimates of $U_{m,n}$ at each step before applying relaxation were made on the basis of the known solution for the infinitely long bar (see Fig. 3).

The isothermals within the cavity brick wall at the times $5\delta t$, $25\delta t$ and $100\delta t$ are shown in Fig. 11(*a–c*). It can be estimated that the maximum truncation errors in this figure are about 2%. The relaxation solution was continued at

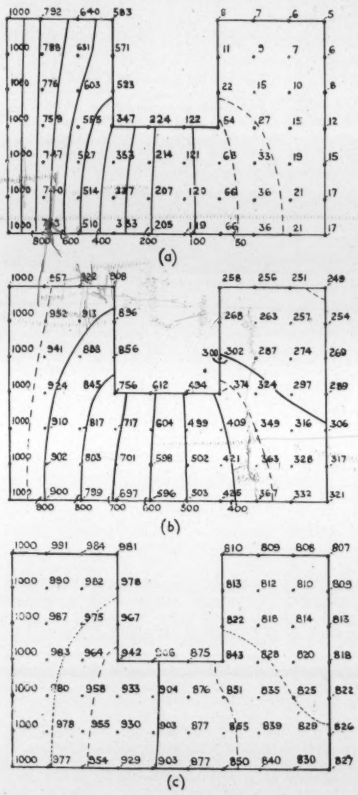

Fig. 11. Solution of problem illustrated by Figs. 9 and 10 for (*a*) $t = 5\delta t_1$; (*b*) $t = 25\delta t_1$; and (*c*) $t = 100\delta t_1$, where $\delta t_1 = h^2/D$. Numerals indicate temperatures at mesh points (boundary temperature at left surface $U_0 = 1000$)

——— isothermals at intervals of $\Delta U = 100$; – – – – isothermals at intervals of $\Delta U = 50$; ..... isothermals at intervals of $\Delta U = 25$.

each time interval until all residuals were within ± 2, and the sum of all residuals below ± 20, ensuring also alternation of the sign of the sum of all residuals at successive steps. It is therefore thought that the errors in $U_{m,n}$ due to the numerical work are not much greater than ± 2, i.e. $\pm 0{\cdot}002\ U_0$.

This accuracy is more than adequate in view of the systematic errors, and would be quite unnecessary for most practical problems, where the thermal data are often not known with any precision, and where less accuracy is sufficient. In that case, an increase in speed can be obtained as higher values of the residuals can be tolerated in the accepted solution. The main requirement would then be to keep the sum of the residuals small, or to alternate the sign of the sum of the residuals at successive time intervals, to avoid the building up of systematic error.

9. HEAT TRANSFER PROBLEMS

Heat transfer problems, in which heat is transferred to, or from, a surface by radiation or convection, as illustrated by Fig. 12, can easily be brought within the scope of the technique described, while retaining its simplicity of application, and the stable nature of the solution.

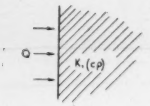

Fig. 12. Heat flux Q entering surface of body of thermal conductivity K and heat capacity $(c\rho)$

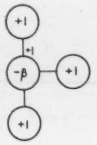

Fig. 13. Relaxation pattern at surface point $(\beta = 4 + \alpha + 2hH/K)$

The amount Q of heat transferred to a unit surface in unit time satisfies the condition [see reference (9), p. 7]

$$Q = K(\partial U/\partial n) \tag{20}$$

where n is the normal to the surface, pointing outward.

Referring back to Fig. 4, let it be assumed that in a two-dimensional problem the surface of the body, of unit height $\delta z = 1$, extends perpendicularly to the plane of the paper, along the line $P_2 - P_0 - P_4$, the body extending to the right and the heat flux Q crossing from the left. Using again finite difference approximations, based on a square mesh of length h, $\delta n = -\delta x \simeq -h$, and equation (20) is replaced by $Q \simeq -K(U_3 - U_1)/2h$; hence the "fictitious temperature" at the point P_1 outside the boundary is

$$U_1 = (2hQ/K) + U_3 \tag{21}$$

Inserting this value into the residual formula (12), one finds for the residual at the boundary point P_0

$$\mathscr{R}_{0,n} = U_{2,n} + 2U_{3,n} + U_{4,n} - (4 + \alpha)U_{0,n} + \alpha U_{0,n-1} + (2Qh/K) \tag{22}$$

One sees that the heat transfer term $2Qh/K$ enters into the computation of the residuals, but does not affect the relaxation pattern, if Q is not a function of the surface temperature $U_{0,n}$. In this case, the relaxation patterns at the surface point P_0 and the next interior point P_3 are the usual patterns applying to "free" surfaces $(\partial U/\partial n = 0)$, i.e. unit increment of $U_{3,n}$ at P_3 increases the residual $\mathscr{R}_{0,n}$ at P_0 by two units, etc. If Q depends on the surface temperature $U_{0,n}$, one has to work out the corresponding relaxation pattern; however, the change only affects the residuals at P_0 itself, and the rest of the relaxation pattern at P_0, as well as the whole relaxation pattern at P_3, etc., remain unchanged. For instance, a condition often met is

$$Q = H(U_A - U_{0,n}) \tag{23}$$

where H is the "heat transfer coefficient" and U_A the ambient temperature of the medium surrounding the body of surface temperature $U_{0,n}$. Equation (22) for the residual then becomes

$$\mathscr{R}_{0,n} = U_{2,n} + 2U_{3,n} + U_{4,n} - \beta U_{0,n} + F_{0,n} \tag{24}$$

where

$$\beta = 4 + \alpha + 2hH/K \tag{25}$$

is the increment factor to be used in relaxation at the point P_0, and

$$F_{0,n} = \alpha U_{0,n-1} + 2hHU_A/K \tag{26}$$

the constant contribution to the residual at P_0. (See Fig. 13.)

10. CONCLUSION

The method of solving heat flow problems discussed in this paper is well suited to practical problems, as it can easily be adapted to the various circumstances met in practice. In many practical problems, it may be sufficient to work with a relatively coarse net and to a limited numerical accuracy, leading to a relatively quick solution. While there is nothing gained over the older numerical methods if the time intervals are short [say $\delta t \simeq (\delta x)^2/D$], the saving of time will be considerable in most cases of practical interest, where the solution extends over periods which may be several hundred times longer than the greatest length of time interval $\delta t_0 = (\delta x)^2/2D$ allowable in the older methods based on equation (4); then full advantage can be taken of the stability of the relaxation solution, and long time intervals can be chosen to compute the solution.

The method can also be applied in slightly modified form to problems in which internal generation or absorption of heat is involved (including latent heat problems). This adaptation has been carried out in the paper describing the electrical analogue technique, related to the relaxation technique described here,[10] and has therefore not been discussed in this paper.

The method can obviously be applied to the solution of other problems governed by parabolic partial differential equations, with the appropriate modifications.

ACKNOWLEDGEMENTS

The author wishes to thank Miss P. Rush for help with the numerical work used in the examples given in the paper, and Dr. T. E. Allibone, the Director of the Laboratory, for permission to publish this paper. The author is indebted to Professor D. R. Hartree for furnishing the proof of the stability of equation (7) by the von Neumann–Hartree method.

REFERENCES

(1) SCHMIDT, E. Foeppl Festschrift "Beiträge zur techn. Mech. und techn. Phys." (1924), p. 179.
(2) EMMONS, H. W. *Trans Amer. Soc. Mech. Engrs*, **65**, p. 607 (1943).

(3) DUSINBERRE, G. M. *Trans Amer. Soc. Mech. Engrs*, **67**, p. 703 (1945).
(4) PRICE, P. H., and SARJANT, R. J. *Proc. Gen. Discuss. Heat Transfer*, p. 281 (London: Institution of Mechanical Engineers, 1951).
(5) O'BRIEN, G. G., HYMAN, M. A., and KAPLAN, S. *J. Math. Phys.*, **29**, p. 223 (1951).
(6) CRANK, J., and NICOLSON, P. *Proc. Cambridge Phil. Soc.*, **43**, p. 50 (1947).
(7) ALLEN, D. N. DE G., and SEVERN, R. T. *Quart. J. Mech. Appl. Math.*, **4**, p. 209 (1951); **5**, p. 447 (1952).
(8) SOUTHWELL, R. V. *Relaxation Methods in Theoretical Physics* (London: Oxford University Press, 1946).
(9) CARSLAW, A. S., and JAEGER, J. C. *Conduction of Heat in Solids* (London: Oxford University Press, 1947).
(10) LIEBMANN, G. *Trans Amer. Soc. Mech. Engrs*, to be published.
(11) RICHARDSON, L. F. *Math. Gazette*, **12**, p. 415 (1925).

Measurement of mass transfer by an electrical conductivity method

By E. W. GAYLORD, Ph.D., and W. FORSTALL, Sc.D., Carnegie Institute of Technology, Pittsburgh, Pennsylvania, U.S.A.

[*Paper received* 14 *December*, 1954]

A method has been developed to study the diffusion of fresh water into salt water using electrical conductivity cells in such a manner that it is possible to determine continuously, rapidly, and inexpensively what portion of any sample of the mixture came from the salt water, and what portion came from the fresh water. The method is one of comparison; an exact determination of the salt concentration of the salt water before mixing is not required. The method is restricted to the study of incompressible flow problems and subject to the limitations imposed by the use of water.

In turbulent flow, fluid is transported from one region to another region where it mixes with and becomes a part of the fluid of its new environment. If fluid from region A is transported to region X, where it mixes with the fluid of region X, this transport can be studied quantitatively in terms of the mass of fluid in region X that came from region A per unit mass of fluid in region X. In order to determine this ratio for fluids which are otherwise similar, the fluid from region A must transport with it to region X some tracer that remains with the fluid of region A during the transport and mixing process.

By means of tracers a number of studies of this type have been made, particularly in boundary layer mixing such as occurs in jets. Hinze and van der Hegge Zijnin[1] studied turbulent material diffusion for air jets issuing into a stationary stream, by introducing various gaseous tracers into the jet stream. Forstall and Shapiro[2] made a similar study of an air jet with moving secondary streams by using helium as a tracer. These methods, as well as the one which is the subject of this paper, require that samples of fluid be withdrawn from the flow region to be investigated. The concentration of tracer material in the withdrawn sample is determined by suitable analysis and compared with the concentration of tracer material in the unmixed portion of the stream.

The methods cited above were used to study the mass diffusion of gases. The authors sought to find a method which would be rapid and easily applied to studying mass diffusion in liquids. The method developed compares the electric conductivities of samples taken at points in the mixing region with the conductivity of either of the component liquids. Because of the comparison there is no need for accurate control of the concentration of tracer material in the unmixed stream. As a test of its usefulness, the electrical conductivity method for studying material diffusion was applied to the problem of a submerged water jet issuing into a stationary stream. The results of these measurements are described in an earlier paper[5] where they are compared with the work of others on diffusion in gases.

TRACER DETECTION BY ELECTRICAL CONDUCTIVITY

In Fig. 1 a jet issuing into a stationary stream is shown divided into three principal regions. Region A contains stationary unmixed fluid containing a grams of salt per litre. Region B, which includes the fluid in the nozzle and core of the jet, contains no salt. In the free turbulent boundary layer, region X, the mixing of fluids from regions A and B takes place. Let x equal the salt concentration of fluid at

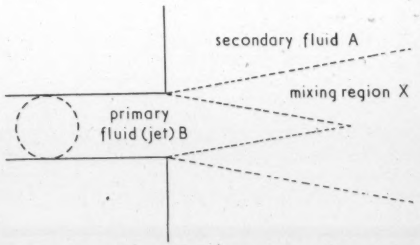

Fig. 1. Mixing pattern of a circular jet issuing into a stationary fluid

any point in region X and ξ equal the volume of fluid that came from region B per unit volume of fluid at the same point in X. Since water is incompressible, ξ is also the ratio of the respective masses when very low salt concentrations are used. If the salt dissolved in stream A remains with the fluid of stream A during the mixing process, then

$$\xi = 1 - (x/a) \qquad (1)$$

In the experiment to which this conductivity method was applied, the turbulent coefficient of diffusivity of water in water was found to be about 8 cm^2/s while the molecular

diffusivity of sodium chloride in water was $1{\cdot}3 \times 10^{-5}$ cm^2/s at 18° C. This is a ratio of something like one to a million, and it is therefore a valid assumption that the tracer salt ions travel with the water in which they were originally dissolved. The use of salt concentrations of less than 10 g/l. resulted in less than ½% change in density.

Since specific conductivity k is nearly proportional to the concentration of electrolyte, c gram equivalents per litre[3], the equivalent conductance Λ is defined by the equation

$$k = \Lambda c \tag{2}$$

Hence, for the mixing problem

$$1 - \xi = x/a = k_x\Lambda_a/k_a\Lambda_x \tag{3}$$

Λ depends on both the temperature and the concentration of the solution. The temperature function is

$$\Lambda_t = \Lambda_0[1 + \alpha(T - T_0)] \tag{4}$$

where α is the temperature coefficient. At 18° C, α is nearly independent of concentration and has a value of 0·024 per °C for sodium chloride. Hence, if liquids A and X are both at the same temperature,

$$\Lambda_a/\Lambda_x = \Lambda_{ao}/\Lambda_{xo} \tag{5}$$

and is a function only of concentration, so that equation (3) becomes:

$$1 - \xi = x/a = k_x\Lambda_{ao}/k_a\Lambda_{xo} = \phi(k_x/k_a) \tag{6}$$

This leads to the comparison method of measuring ξ. The ratio k_x/k_a is measured by placing conductivity cells containing samples of liquids X and A in two arms of a Wheatstone bridge, as shown in Fig. 2. The electrical resistance R of a

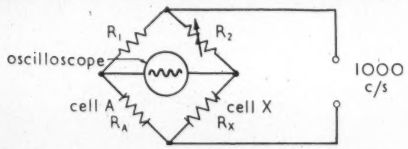

Fig. 2. Arrangement of cells in Wheatstone bridge circuit

properly designed conductivity cell is described with very little error by the equation

$$R = K/k \tag{7}$$

where K is the cell constant. If the two cells have the same cell constant, then

$$k_x/k_a = R_a/R_x \quad \text{and} \quad 1 - \xi = \phi(R_a/R_x) \tag{8}$$

As shown in Fig. 2, the other two arms of the bridge are a fixed resistance R_1 and a variable resistance R_2. Alternating current is used to reduce effects of polarization of the cells. Resistance R_2 is adjusted until a null balance is indicated on an oscilloscope. If the reactances in the bridge circuit are negligible, then

$$R_1/R_2 = R_a/R_x \quad \text{and} \quad 1 - \xi = \phi(R_1/R_2) \tag{9}$$

If the temperature of the two liquids X and A are the same, a calibration curve relating ξ to R_1/R_2 may be made that is independent of temperature and independent of the salt concentration of the salted stream. As shown earlier, this functional relationship is

$$1 - \xi = x/a = (\Lambda_{ao}/\Lambda_{xo})\ (R_1/R_2) \tag{10}$$

and can be found from values of Λ given in the International Critical Tables. Values of R_1/R_2 as a function of x/a were determined in this way for several values of x/a with a ranging from 4 to 10 g of sodium chloride per l. These values, Fig. 3,

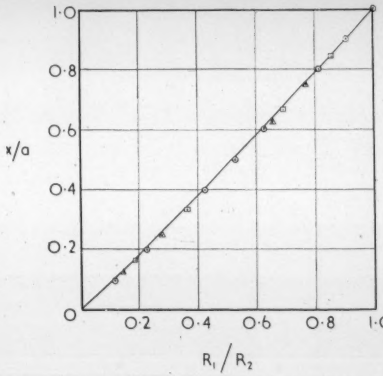

Fig. 3. Calibration of conductivity cells used in jet mixing study for reference solutions of 6, 8 and 10 g/l. ——— = theoretical; ○ = 10 g/l; □ = 8 g/l; △ = 6 g/l.

can be represented to a very good approximation by one curve, thus verifying equation (10). For comparison, an experimental calibration of two cells was made using test solutions of sodium chloride dissolved in distilled water. Discrepancies between the experimental values shown in Fig. 3 and the theoretical curve are within the probable range of experimental error in mixing the test solutions.

CAPACITANCE AND POLARIZATION

When alternating current is used, conductivity theory[3] assumes that the cell behaves like a capacitance in series with a resistance. This effect is caused by the alternate storing and releasing of energy within the cell. The phase angle of the voltage with respect to the current is $\theta = \arctan(1/R\omega c)$ and the impedance is (Fig. 4)

$$|Z| = R[1 + (1/R\omega c)^2]^{\frac{1}{2}}$$

Hence if one assumes that the cell forms this type of a circuit, the greater ωc the more closely the cell behaves like a pure ohmic resistance. Using a properly constructed cell having

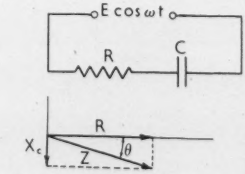

Fig. 4. Electrical characteristics of a conductivity cell

platinized electrodes, a frequency of 1000 c/s will make ωc sufficiently large so that the cell will behave like a pure resistance. Higher frequencies are not necessary, and may cause the cell to behave as though a parallel capacitance were shunted across it.

The current flowing in a conductivity cell forms gases at the electrodes resulting in the phenomenon called polarization. When the cell is polarized the resistance does not depend entirely on the specific conductivity of the solution surrounding the electrodes. Polarization is greatest with direct current; alternating current reduces, but does not entirely eliminate it. With alternating current the effect of polarization is to make the resistance dependent on the current, and to produce a large out-of-phase component of voltage. With alternating current having a frequency of 1000 c/s, polarization can be made negligible by platinizing the electrodes. This is a process of coating the electrodes with platinum black, thus greatly increasing the effective area of their surfaces.

The cells employed in this work were platinized, and their symmetrical arrangement in the bridge caused some cancellation of the out-of-phase voltage. There was still a small amount of voltage, however, that could not be balanced out by the variable resistance R. This was balanced by shunting a capacitance across one of the resistance arms of the bridge, R_1 or R_2. With these platinized cells no change in the voltage across the bridge would unbalance the bridge, but the ratio R_1/R_2 did vary slightly with frequency. However, the cells were calibrated and used with a fixed frequency of 1000 c/s.

A sketch of the cells is shown in Fig. 5. They have waterproof electrical connexions and are immersed in water, one

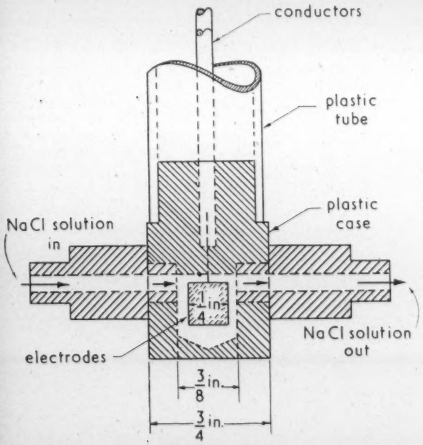

Fig. 5. Sectional view of a conductivity cell used with continuous sampling

in the mixing region and one in the stationary fluid. This keeps the cells at constant temperature and makes it possible for them to be placed close to the sampling probes with very little time delay between sampling and measuring the conductivity of the sample. It was possible to determine the value of ξ continuously by the steady syphoning of liquid from regions A and X through their respective cells.

USE OF A CONTAMINATED STREAM

In the experiment in which diffusion was measured by the salt tracer method, a sufficient quantity of distilled water was not easily available for the unsalted stream and so tap water was used. The contaminating minerals in the tap water caused the jet water, fluid B, to have a conductivity that was between 2 to 5% of the conductivity of the stationary salt water, fluid A. Hence, the method of determining ξ was modified.

The assumption is made that in the process of mixing, the contaminating minerals produce the same effect as that produced by water containing a concentration of sodium chloride such that its conductivity is equal to the conductivity of the tap water. Let stream B have a salt concentration b instead of 0. Conservation of salt gives the expression

$$(1 - \xi)a + \xi b = x \quad \xi = \left(1 - \frac{x}{a}\right)\Big/\left(1 - \frac{b}{a}\right) \qquad (11)$$

In the case of the jet diffusion experiment, this did not necessitate taking samples from stream A and B for each measurement to determine the value of a/b. A measurement of b_0/a_0 was taken at the beginning of the experiment; the concentration of stream B was held constant by storing sufficient water in a tank, and fluid A, the salted water, which was also in a tank, was being continually diluted with fluid B. Because of the very rapid mixing of fluid B with fluid A, the value of b/a could be computed from the value of b_0/a_0 at any later time, provided b was constant and equal to b_0.

To obtain ξ for the jet diffusion experiment using a contaminated fluid B, a factor with which to multiply the value of $[1 - (x/a)]$ as obtained from Fig. 3 is needed. This multiplying factor is derived as follows:

let q = volume rate of flow of jet water, V = total volume of fluid in the tank, and M = total mass of salt or its equivalent, in the tank.

Assuming complete and instantaneous mixing of the jet with the water in the tank, conservation of salt leads to the equation

$$qb - qa = dM/dt \qquad (12)$$

since $M = Va$

$$dM/dt = V(da/dt) = V(d/dt)(a - b) \text{ if } b \text{ is constant.}$$

Hence

$$(d/dt)(a - b) = -(q/V)(a - b) \qquad (13)$$

with $a = a_0$ at $t = 0$ and $b = b_0$ at all times.

The solution is

$$b/a = b_0/[b_0 + (a_0 - b_0)\exp(-qt/V)] \qquad (14)$$

Equation (14) is combined with equation (12) to give

$$\xi = (1 - x/a)\left[\frac{(b_0/a_0)\exp(qt/V)}{1 - (b_0/a_0)} + 1\right] \qquad (15)$$

During the experiments the time did not have to be recorded with great accuracy because the term

$$\frac{(b_0/a_0)\exp(qt/V)}{1 - (b_0/a_0)}$$

was never greater than 0·07.

CONCLUSION

While this method of studying turbulent material diffusion is limited to those situations where the use of water is feasible,

it might be useful in studying problems other than the jet problem. Moreover, it may not be necessary to withdraw samples as was done for the work described in this paper. Instead of withdrawing samples into a conductivity cell, the electrodes might be immersed directly in the flow region as described by Charow.[4]

Another possible use of the conductivity method would be to study temperature diffusion. In this approach, all fluids would have the same salt concentration but different temperatures. Because the conductivity of a salt solution is very sensitive to temperature, small temperature differences could be measured.

ACKNOWLEDGEMENTS

This paper is based in part on a thesis by one of us (E. W. G.) in partial fulfilment of the requirements for the degree of Doctor of Philosophy at Carnegie Institute of Technology.

REFERENCES

(1) Hinze, J. O., and van der Hegge Zijnin, B. G. *Heat and Mass Transfer in the Turbulent Mixing Zone of an Axially Symmetrical Jet* (London: Seventh International Congress for Applied Mechanics, 1948).
(2) Forstall, W., Jr and Shapiro, A. H. *J. Appl. Mech. Trans Amer. Soc. Mech. Engrs*, **72**, pp. 399–408 (1950).
(3) Jones, G., and Bollinger, G. M. *J. Amer. Chem. Soc.*, **53**, p. 411 (1931).
(4) Charow, W. J. *Pulse Integrator for Measuring Intensity of Turbulence by Salt Diffusion Method* (Washington: Alden Hydraulic Laboratory, Worcester Polytechnic; Technical Information Division, Report No. U22245, Library of Congress, 1952).
(5) Forstall, W., and Gaylord, E. W. *Momentum and Mass Transfer in a Submerged Water Jet. J. Appl. Mech.*, to be published.

Low-frequency dynamic response of photosensitive neon discharge tubes

By T. J. Dillon, M.Sc., F.Inst.P., Queen Elizabeth College, University of London

[*Paper received* 16 *December*, 1954]

The instantaneous response to illumination of photosensitive discharge tubes in relaxation oscillation circuits has been investigated, using light sources of periodically varying light output to irradiate the tubes. A brief theoretical outline is given of the effect of periodic variations on sawtooth oscillations and this is applied to the oscillations of neon discharge tubes illuminated by sources giving a light output of rectified sinusoidal waveform. Photographs are given of oscillation traces of tubes illuminated by light from mercury vapour lamps and by intermittent light pulses. It is shown that, under certain conditions, a complete delineation of the light output waveform is obtained. This method can be used for the determination of the light variation frequency or for studying the waveform of the light output from a source.

It has been shown that if photosensitive neon discharge tubes in relaxation oscillation circuits are subjected to irradiation, the consequent decrease in striking potential causes an increase in the frequency of the oscillation which can be used for illumination measurements.[1,2] When the light output of the irradiating source is periodic in character, as in the case of discharge lamps, or is intermittent, the striking potential for the charge-discharge cycles may vary with the instantaneous value of the illuminations on the tube, and thus irregularities are introduced into the time and amplitude of the cycles. With telephones in the circuit the effect can be discerned by the change from the fundamental pure note into a complex chord due to the presence of these irregularities. When the charge-discharge cycles of the condenser in the neon tube circuit are examined on a cathode-ray oscillograph a steady sawtooth waveform trace is seen in which the periods and amplitudes are unequal, giving the appearance of over-synchronization, as described by Builder and Roberts.[3] The inequalities in amplitude give a modulated effect to the envelope of the sawtooth waves, the depth of modulation pattern depending on the illumination.

THEORY

Consider the simple case of a linear charge-time sawtooth waveform, with negligible fly-back time, supplied from a relaxation oscillator. Let a periodic variation, of a rectified sinusoidal form, be applied to the striking potential of the sawtooth waves. Fig. 1 shows a sawtooth waveform represented by broken lines with V_B and V_A the normal striking and extinction potentials respectively. The variations which occur are negative, indicated by a decrease in striking potential, and these are represented diagrammatically by the dotted curve marked v_b below the V_B line, any instantaneous decrease being given by the perpendicular distance between the V_B line and the curve.

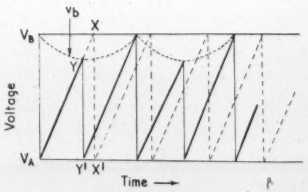

Fig. 1. The effect of periodic variations of striking potential on linear sawtooth waveforms

Consider the effect of the v_b curve on any sawtooth wave starting in phase with this curve. As the charge line rises it normally reaches the point X when the condenser discharges as indicated by XX'. If, however, the charge line cuts the v_b curve at Y, which is the reduced value of the striking potential, the condenser discharges along YY' when the charge line rises again at the same rate. In general, if n = free-running frequency of oscillations in c/s; n' = frequency of sinusoidal variations in c/s; and n_b = final oscillation frequency in c/s the oscillation waveform envelope is

modulated with a repetition pattern depending on the ratio n_b/n'.

In the example given in Fig. 1, the second charge line from Y' cuts the v_b curve when the amplitude is zero and the final effective sawtooth frequency is twice that of the voltage variation frequency, or $n_b = 2n'$ and the pattern repeats after time $1/n'$ s.

Applying these general considerations to the case of the relaxation oscillations of a photosensitive discharge tube, assume, for simplicity of treatment, a linear rate of charge for the condenser and suppose that the light output from a discharge lamp provides an external means of altering the striking potential in a sinusoidal manner. The light output from a discharge tube is closely related to the power input, but, as the light output lags behind the power and as there is also a thermal lag, light is being emitted even when the input power is zero. This must be taken into account when considering the illumination produced on a surface by such a lamp, as the effect is that of an equivalent steady source added to the fluctuations in the light output which produce a stroboscopic flicker of twice the frequency of the supply voltage.

In the diagram on the left of Fig. 2 a rectified sinusoidal wave (*a*) is given to indicate fluctuations in light output. The

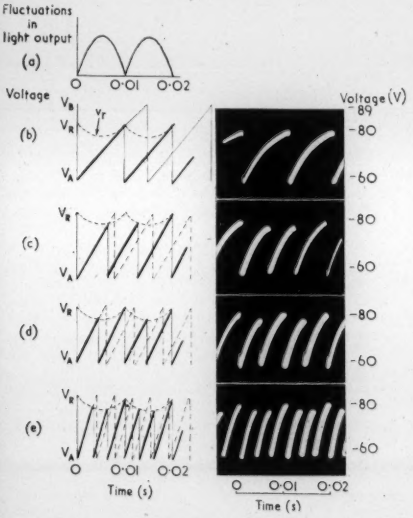

Fig. 2. (*a*) Sinusoidal fluctuations of frequency n' of light output. (*b–e*) Diagrams and traces of tube oscillations for frequency ratio n_b/n' of 1, 1·5, 2 and 3 respectively

sawtooth diagram (*b*) shows V_B as representing the normal striking potential for the unilluminated tube and V_R the striking potential under an illumination produced by the equivalent steady source. As in Fig. 1, the dotted curve v_r, which is now shown below the V_R line, indicates the fluctuating decreases in striking potential caused by the fluctuations in illumination. The shape of the v_r curve corresponds to that shown in (*a*). The free-running sawtooth oscillations with amplitude $(V_B - V_A)$ are shown by the fine lines in (*b*). The charge line starting from 0 cuts the v_r curve on the V_R line, where the fluctuating potential decrease is zero, so no irregularities are introduced and $n_b = n'$. In Fig. 2(*c–e*) the free-running oscillations have been omitted for clarity and the broken lines indicate the oscillations that would take place under illumination from an equivalent steady source which would reduce V_B to V_R, with consequent decrease of frequency from n to n_R. The heavy lines show the final frequencies n_b synchronized to multiples of n' and to odd multiples of $n'/2$. It is seen that in (*b*), (*d*) and (*e*) the period of the repetition pattern is $1/n'$, and in (*c*) the period is $2/n'$.

EXPERIMENTAL METHODS AND RESULTS

Steady oscillograph traces of the charge-discharge cycles were obtained using neon indicator tubes (types L7A and L10 by Siemens Electric Lamps and Supplies Ltd.) and the frequency determined either by including telephones in the circuit and tuning to an oscillator or by using the oscillograph calibrations.

A discharge lamp, having an oscillatory light output, was then used to irradiate the tube and the frequency of oscillations was tuned to the frequency of fluctuations of the source, or to one bearing a simple ratio to it. When the distance between the discharge lamp and the tube was fixed, this was done by altering the time constant. Alternatively, the tube could be moved nearer the source and the required change of frequency produced by the consequent increase of illumination. On the right side of Fig. 2 are given photographs of steady traces produced using a photosensitive tube placed at a distance of 7 in. from a 250 W high-pressure mercury vapour lamp (type ME by the General Electric Co. Ltd.). This source was chosen on account of the high degree of brightness and of the marked stroboscopic effect. Each photograph has been placed, for comparison, by the side of the diagram of a sawtooth wave having the same frequency as that of the tube. The similarity in variations of frequency and amplitude of the charge-discharge cycles confirms the simple theory and shows how the repetition pattern occurs according to the ratio n_b/n'.

In order to make sure that the modulation effect was not the result of mains pick-up, similar experiments were carried out using a cold cathode tetrode (type N.S.D.1 by Ferranti Ltd.) as a light source. With suitable triggering, short light pulses of any frequency up to 400 c/s were obtained which were quite independent of the mains supply voltage frequency. In Fig. 3 the upper trace shows the light pulses from the tetrode and the lower trace the synchronized oscillations of the tube. The voltage decreases in the wave traces corresponding to each light pulse can be seen.

A more accurate indication of the variations in light out-

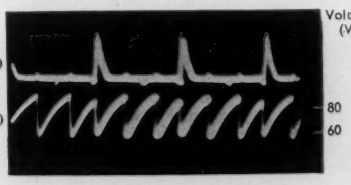

Fig. 3. (*a*) Short light pulses of frequency 290 c/s. (*b*) Oscillation frequency of tube 3 × 290 c/s

put is obtained when the tube is oscillating at higher frequencies. Traces given in Fig. 4 were taken as the illumination was gradually increased by moving the tube nearer to the

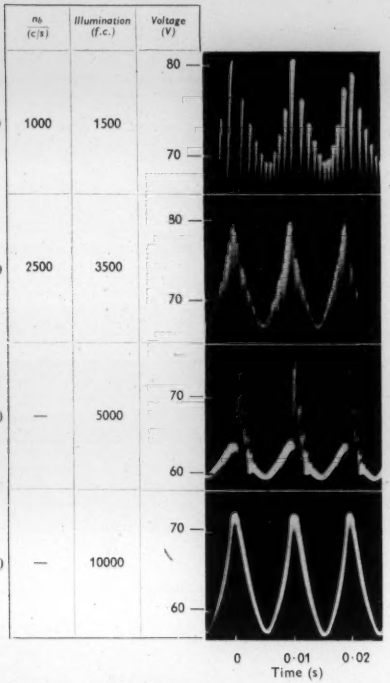

Fig. 4. Oscillograph traces at higher frequencies

mercury vapour lamp. The traces are amplified and show only the upper edge of the modulation envelope. In (*a*) and (*b*) the frequency ratio can be distinguished, in (*c*) the oscillations are intermittent, while in (*d*) only the light output wave trace is seen. A basic curve connecting illumination from a steady source and the striking potential of the tube is given in Fig. 5 to indicate the order of illumination necessary to produce the striking potential changes shown in Fig. 4; for example, in Fig. 4(*b*) a total decrease of 20 V requires an illumination of 5000 f.c.

The light output from sodium vapour discharge lamps, fluorescent daylight lamps, and ultra-violet lamps has also been examined by these methods. The mains flicker fluctuations can be detected, but the illumination received from these lamps on a tube placed quite close to them, is so much less than from a mercury vapour lamp that the shape of the light output waveform is not seen so clearly.

CONCLUSION

The response of photosensitive neon discharge tubes to low-frequency light fluctuations has been studied experimentally and the results conform to the outlined theory. Much work has been done in the past on the flickering of light sources by Bouma[4] and others, and it has been shown in this paper that these neon tubes will, under certain conditions of operation, behave as gas-filled photoelectric cells of comparable time lag in their response to fluctuations. This property renders them suitable for finding the frequency of oscillation of a source, for detecting a flicker or stroboscopic effect or for use in the examination of light output

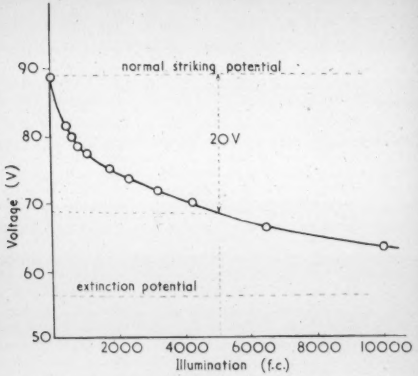

Fig. 5. Variation of striking potential with steady illumination

waveforms. The acoustical method for finding the frequency is simple as, in addition to the normal circuit components and telephones, no amplification is necessary and no subsidiary equipment is required. The oscillograph method of examining the light pulses can be compared with that described by Huxford and Engstrom[5] using photosensitive gas triodes.

The tubes vary considerably in sensitivity to light and in exhibition of fatigue, but some tubes have been in use for these photometric purposes over a period of two or three years without depreciation. However, when they have been subjected to intense illumination a recovery time of the order of a few seconds is necessary before oscillations start again. This temporary fatigue effect is being investigated and experiments are also being carried out on the spectral response of the tubes.

ACKNOWLEDGEMENTS

The author expresses thanks to her colleague, Dr. U. Andrewes, for helpful suggestions, and to Miss F. M. Spaull for technical assistance with the photographic traces.

REFERENCES

(1) Dillon, T. J. *Proc. Phys. Soc.* [*London*] *B*, **65**, p. 236 (1952).
(2) Dillon, T. J. *Brit. J. Appl. Phys.*, **4**, p. 245 (1953).
(3) Builder, G., and Roberts, N. F. *A.W.A. Tech. Rev.*, **4**, p. 170 (1939).
(4) Bouma, P. J. *Philips Tech. Rev.*, **6**, p. 295 (1941).
(5) Huxford, W. B., and Engstrom, R. W. *Rev. Sci. Instrum.*, **8**, p. 385 (1937).

Correspondence

A rubber-membrane model for axially-symmetric electric fields

It is well known[1,2] that small balls rolling over a rubber membrane stretched equally in two perpendicular directions follow paths approximately similar to those of electrons in a two-dimensional electric field (variation in a plane only), if the depression of the membrane at the "electrodes" is small and proportional to the potential, provided the charge of the electron beam is small.

In practical applications, however, three-dimensional fields having axial symmetry are probably more frequently encountered, but so far no method of using the membrane model for such systems has been proposed.

Recently it was shown[3] that the effect of the charge of the electron beam can be taken into account by applying a pressure by means of pads to the under surface of the membrane, the pressure being proportional to the charge density. This method can only be used in two-dimensional systems, but it is interesting to note that, using a similar kind of technique, a method of applying the rubber-membrane model to axially-symmetric field systems, with or without space charge, is possible.

Suppose we wish to investigate the potentials in an electrode system in a plane which contains the axis of symmetry. Fig. 1 illustrates an element, of area $\delta r \times \delta z$, of the corresponding rubber model; this element is a distance r from the z-axis. The z-axis corresponds to the axis of symmetry of the electrode system to be studied, and points on the surface of the membrane correspond to points on the section of the electrode system. It is now shown that the height of the membrane can be made to correspond to the potential of the electrode system.

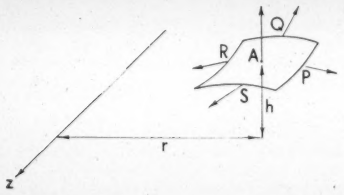

Fig. 1. Forces acting on an element of the membrane

We assume that there is an applied pressure p in the positive h direction given by

$$p = T.(1/r).(\partial h/\partial r) \qquad (1)$$

where T is the surface tension of the membrane and h is its height at any point. (It is also assumed that T is constant and, at all points on the membrane, the slope of the surface is small.) The result of resolving vertically upwards the surface tension forces acting at P, Q, R and S and the applied force $p\delta r\delta z$ (represented by the arrow at A, Fig. 1) is

$$T\delta z[(\partial h/\partial r)_P - (\partial h/\partial r)_R] + T\delta r[(\partial h/\partial z)_S - (\partial h/\partial z)_Q] + T.1/r(\partial h/\partial r)_A\delta r\delta z = 0 \qquad (2)$$

and for δr and $\delta z \to 0$, since

$$(\partial h/\partial r)_P - (\partial h/\partial r)_R = \delta r.(\partial^2 h/\partial r^2)$$

we obtain

$$(\partial^2 h/\partial r^2) + (\partial^2 h/\partial z^2) + (1/r)(\partial h/\partial r) = 0 \qquad (3)$$

If we now consider h to be proportional to a potential V (or $-V$ as is the case for ball-rolling experiments), this potential will obey Laplace's equation. Thus, if we apply at every point of the membrane a force proportional to $(1/r)(\partial h/\partial r)$, Laplace's equation for an axially-symmetric system will be satisfied.

If space-charge forces are to be considered it would be necessary to assume that the applied pressure p is given by

$$p = T.(1/r)(\partial h/\partial r) + \alpha T\rho \qquad (4)$$

in which ρ is the charge density of the beam and α a factor of proportionality. The factor α is defined by equation (6) of reference (3) and is negative for our purposes; therefore the pressure to represent the space charge is upwards all over the membrane.

Since $\partial h/\partial r$ can be positive or negative, the pressure p could be up or down. Even for simple arrangements of electrodes the membrane may have to be pushed in some regions and pulled in others. In order to push and pull the membrane and to leave the top of it free for the rolling balls, it might be convenient to reduce the air pressure on the under side of the membrane to produce a known uniform downward pressure, and oppose this, as required, by pads underneath.

To carry the method into effect $\partial h/\partial r$ must be measured at a number of points. This could be done optically, or by using some form of profile indicator, such as the one shown in Fig. 2 consisting of light rods of equal length resting on the membrane. Finding the slope of the membrane amounts to measuring the slope of the curve formed by the tops of the rods by means of a protractor, suitably placed. To measure the pressure produced by the rubber pads, and hence p, a method similar to that described in reference (3) could probably be employed. The indeterminacy of $(1/r).(\partial h/\partial r)$ on the axis can be avoided by arranging the pads symmetrically on either side of the axis. An iterative procedure would, of course, be necessary for setting up the system.

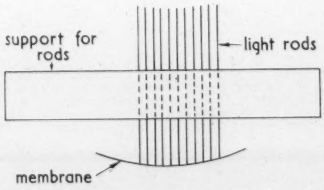

Fig. 2. A profile indicator

I wish to thank Mr. G. E. Condliffe, Managing Director of E.M.I. Research Laboratories, Ltd., for kind permission to publish this note.

E.M.I. Research Laboratories, Ltd., Hayes, Middlesex. B. J. MAYO

REFERENCES

(1) SMYTHE, W. R., RUMBAUGH, L. H., and WEST, S. S. *Phys. Rev.*, **45**, p. 724 (1934).
(2) KLEYNEN, P. *Philips Tech. Rev.*, **2**, p. 338 (1937).
(3) ALMA, G., DIEMER, G., and GROENDIJK, H. *Philips Tech. Rev.*, **14**, p. 336 (1953).

New books

The theory of cohesion. By M. A. JASWON, M.A., Ph.D. (London: Pergamon Press, Ltd., 1954.) Pp. viii + 245. Price 37*s*. 6*d*.

This is the second volume in the Pergamon science series on metal physics and physical metallurgy. It is concerned with cohesion, rather than with the general field of metal theory (though there is a full and useful account of the modern theories of ferromagnetism). The author tries to show how wave-mechanical ideas, originally or chiefly developed for atoms and molecules, play their part in an understanding of cohesion in solids. This is an interesting approach, not sufficiently stressed in the usual accounts, and it throws light on several otherwise puzzling features in the electronic description of a metal.

The book is almost wholly wave-mechanical, though it presupposes no previous knowledge of this subject. It is easy to read, and should be welcomed for the freshness of its approach. It is, unfortunately, not without a crop of minor errors, both in printing and in substance.

C. A. COULSON

Radioisotope conference 1954 (sponsored by the Atomic Energy Research Establishment, Harwell), Volume 1, Medical and physiological applications. Edited by J. E. JOHNSTON, R. A. FAIRES and R. J. MILLETT. (London: Butterworths Scientific Publications, 1954.) Pp. xi + 418. Price 65*s*.

The conference held at Oxford in July 1954, on the applications of radioisotopes, provided impressive evidence of the widespread use of these materials and of their great value as scientific tools. From a proffered total of about four times that number, forty-six papers on the medical and physiological applications were read and are now printed in this volume, together with a report of the discussion each paper provoked. The papers are divided into five main sections, namely, therapy, diagnosis, plant nutrition, animal physiology and pathology, and biochemistry; even within these groups the range of subjects is wide indeed.

Such a diversity of subjects, though impressive, is also a weakness of the book and will possibly limit its appeal. It may quite fairly be stated that the only aspect of the papers which is common to them all is the radioactivity of one of the materials used in the work reported, and it is to be doubted whether this thread is strong enough to hold the whole together for any single reader. Few of the papers have more than a short paragraph on the isotope technique, the bulk of each being devoted to the results obtained. In short, radioactive isotopes have taken their place alongside the microscope, the spectro-photometer and the like as important research tools, and we are passing into the phase where their use, like the use of any other equipment, calls for no special comment.

This does not, of course, reflect upon the standard of excellence of the papers, which is high, or their interest and value, which are considerable. As to which are the most interesting, each reader will have his own opinions. This reviewer would place the work of Ledlie and Baxter on the applications of tracer doses of ^{59}Fe in clinical investigation first on his list. High up, too, would be the paper by Veal and others on measurements of cardiac output, and the double tracer method used by Rowlands and his colleagues in blood volume measurements. Mention should also be made of the paper by Almond and others on the fate of intravenously injected antigenic proteins in immune and normal rabbits. On the technical side, the application of gamma-ray spectrometry to tumour localization by Allen and co-workers has great interest and possibilities, whilst Bowden and others have studied the surgically important problem of metallic transfer in screwing and bolting most elegantly.

The standard of the production of this book is high, the printing, illustrations and diagrams and the general clarity of layout are excellent. Only errors of a minor kind have been detected.

W. J. MEREDITH

Mass spectrometry (Methuen's monographs on chemical subjects). By A. J. B. ROBERTSON, M.A., Ph.D. (London: Methuen and Co., Ltd.; New York: John Wiley and Sons Inc., 1954.) Pp. 135. Price 8*s*. 6*d*.

With the rather severe limitations imposed in respect of size for monographs in this series, an author may perhaps be excused if he decides that it is not possible to produce a compact and balanced view of the whole field of work on his particular subject. Dr. Robertson has chosen to devote a substantial proportion of the space available to an exposition of work in which he is specially interested, namely, theoretical studies of the nature of excitation, ionization and dissociation processes in molecular gases on electron impact. Vibrational energy changes, as governed by the Franck–Condon principle, are considered in some detail with the aid of a number of potential energy diagrams. Discussions of experimental procedures and techniques of operation in different fields of application are hence very compressed. It is a pity that space has not been found to present an overall view of a modern analytical instrument, since the main value of this instrument is as a stable and sensitive comparator for analytical work.

However, the book should prove to be a useful addition to the steadily growing list of publications on this subject.

G. P. BARNARD

Magnetic cooling. By C. G. B. GARRETT (Cambridge, Mass: Harvard University Press; New York: John Wiley and Sons, Inc.; London: Chapman and Hall, Ltd., 1954.) Pp. x + 110. Price 36*s*.

This book tells how the low-temperature physicist uses paramagnetic salts to reach temperatures lower than 1° absolute. After a brief description of the experimental procedures, details are given of the establishment of the absolute temperature scale and of the properties of the paramagnetic salts used for magnetic cooling. These chapters

form a valuable review, with adequate references, of the work done up to the end of 1952.

Dr. Garrett has himself made significant contributions to the study of paramagnetic salts at very low temperatures and, perhaps as a consequence, his book tends to suggest that the chief importance of this new temperature region lies in the opportunities it offers for investigating the salts used in the cooling process. This is far from the case, and the last chapter is too brief to deal adequately with the wide range of experiments, including, for example, measurements of thermal and electrical conductivities and of specific heats, which are now being performed below 1° absolute.

However, within its limits, the monograph may be warmly recommended either to the general reader or to one of the steadily increasing number of specialists working in this field. It is well produced, but at 36*s*. is the most expensive 110 pages that this reviewer has yet come across. J. WILKS

An advance treatise on physical chemistry. Vol. 5. Molecular spectra and structure dielectrics and dipole moments. By Professor J. R. PARTINGTON, M.B.E., D.Sc. (London: New York: Toronto: Longmans, Green and Co., Ltd., 1954.) Pp. x + 565. Price 80*s*.

The latest volume of Partington's comprehensive and systematic treatise on physical chemistry is devoted to (*a*) molecular spectra and structure (286 pp.); (*b*) dielectrics and dipole moments (254 pp.); and (*c*) hyperelectrics (9 pp.). The first section is exhaustive and up to date. Special attention is given to valence and to the present-day theories of chemical structure. The inclusion of some photographs of actual spectra would add, however, to the presentation. The dielectric section covers the older methods as well as the modern ones. Subsections dealing with dipole moment and chemical constitution (comprising such topics as induction, resonance, bond moments, electronegativity, etc.) are also included. The text is now complete with the publication of the fifth volume. At an approximate cost of £18 for the five volumes it is probably too dear for most individual workers in the field, but it is an excellent reference book and has few rivals in any language. The treatise is the work of one author and has involved an enormous amount of concentration and scholarship. The outstanding characteristics may be summarized as follows:

(1) It is a treatise on a wide field of chemistry with full references and complete bibliography.

(2) The volumes are well illustrated with diagrams, graphs and figures of apparatus.

(3) The theoretical treatment is extensive and expounded in a lucid manner, yet only an elementary knowledge of mathematics is assumed.

(4) Most theoretical discussions are linked with practical formulae of use to the technologist. JOSEPH REILLY

Applied geophysics in the search for minerals. 4th Ed. By Professor A. S. EVE and Professor D. A. KEYS, M.A., D.Sc., F.R.S.C. (London: Cambridge University Press, 1954.) Pp. x + 382. Price 40*s*.

The teaching of geophysics to postgraduate students who intend to enter the profession is greatly hampered by the lack of modern textbooks dealing with the fundamental principles and their common applications. In the reviewer's opinion some of the large American books confuse new students and are out of date. The instruction of undergraduate geologists and petroleum technologists has to be performed solely by lectures because of their lack of mathematical training and they are in need of a readable account of modern techniques.

The revision of the 1938 edition of this textbook is welcome in so far as it will assist the geology student, but it is not sufficiently detailed to form more than an introduction for the geophysicist. The different subjects treated in the last chapter of the previous edition have been consigned to their proper places in the text and additional information has been supplied concerning estimates of the depth of the overburden (four pages), airborne magnetic surveys (four pages), airborne electrical surveys (two pages), gravimeters (nine pages) and seismic reflexion techniques for dipping strata (six pages). The chapter on radioactive methods has been expanded to give a general account of airborne scintillometer surveys, radioactive assaying and borehole exploration. A new chapter on well-logging methods has been added and some useful problems have been appended to the main chapters for the first time, but the answers have not been provided!

A. F. MOORE

The physics of experimental method. By H. J. J. BRADDICK, Ph.D. (London: Chapman and Hall Ltd., 1954). Pp. 392. Price 35*s*.

This is without question an exceptionally good book which, one feels, will be a standard work for many years to come.

The title provides the key to character: far from being a handbook of laboratory practice, it is a book which at all times emphasizes the physical principles underlying the choice of particular experimental methods and the design of apparatus. It is written clearly and concisely; and, indeed, the crispness and condensation sometimes achieved without detriment to the style, for example, in the opening of the chapter on vacuum technique, is a model of its kind.

The scope of the content is wide, including errors and the treatment of experimental results (with an appendix on numerical calculus); mechanical design; materials of construction; vacuum technique; electrical instruments; electronics; optics and photography; the natural limits of measurement (noise and fluctuation phenomena); and some techniques in nuclear physics, but the material has been selected with great care and forethought. The standard is high and is aimed at advanced students, but most research workers making physical measurements, whether in physics or other fields, will also profit from the author's knowledge and experience. A little confusion may perhaps arise among students from the use, on page 285, of the term resolving power where resolving limit is really meant. There is a comprehensive bibliography of selected references which is up to date.

The author has approached his subject and achieved his purpose in a manner which any experimenter possessing a healthy respect for fundamental simplicity and elegance cannot fail to admire. H. D. KEITH

Heat and cold, Part II. Descriptive catalogue of exhibits in the Science Museum. (London: H.M. Stationery Office, 1954.) Pp. 64. Price 3*s*.

This handbook contains detailed descriptions of part of the collection illustrating heat and thermal instruments in the Science Museum in London. The sections concerned are: thermal expansion; calorimetry; change of state and critical state; the nature of heat; heat transfer; refrigeration; very low temperatures; miscellaneous. There is also a list of nine portraits in the museum of some of the distinguished workers who have contributed to our knowledge of the science of heat.

Notes and comments

Elections to The Institute of Physics

The following elections have been made by the Board of The Institute of Physics:

Fellows: W. H. Dowland, J. V. Dunworth, J. R. Greening, F. Hirst, A. G. Peace, J. Walker.

Associates: A. W. Badcock, P. S. Baker, J. A. W. Huggill, D. S. Barmby, J. V. Bromiley, I. D. Brotherton, J. C. Cockram, A. R. Crathorn, M. F. Culpin, D. S. Dodd, I. Flinn, R. A. Granville, A. C. Ham, A. R. James, D. B. G. James, B. R. Malcolm, R. W. Pickard, W. P. F. Raffan, D. A. E. Roberts, P. M. Rolph, R. P. Rose, K. W. Scott, M. J. Sheehy, A. Turner, E. R. Wooding, N. R. Wynn.

Thirty-seven Graduates, fifty-eight Students and five Subscribers were also elected.

Conference on the production and utilization of electromagnetically enriched isotopes

A conference on the production and utilization of electromagnetically enriched isotopes will be held at the Atomic Energy Research Establishment, Harwell, from 13 to 16 September inclusive. Sessions on the following subjects will be included: design and operation of large mass separators; ion source and collector problems especially with high beam current; separation of radioactive materials; chemical aspects of production work; preparation of isotopic targets; developments in mass analysis of stable isotopes; utilization of electromagnetically enriched isotopes.

Although much of the available time will be occupied with problems of the electromagnetic separator itself, contributions will also be welcomed on applications of stable isotopes, especially those of an unusual type. The emphasis here should be on the principles involved and not on the details of the great variety of techniques which users may employ. On the other hand the great volume of work on the application of the isotopes of the lighter elements, particularly of hydrogen, carbon, nitrogen and oxygen which are more economically enriched by other methods, is specifically excluded.

The conference should provide an opportunity for bringing together people concerned with the production and use of stable isotopes and should stimulate further applications. Those wishing to attend should write immediately to Dr. M. L. Smith, Atomic Energy Research Establishment, Harwell, Didcot, Berks., indicating also, whether they will make a written contribution. Abstracts of papers must be submitted before 30 April, and complete manuscripts before 30 June, 1955, so that preprints of the papers can be made available before the conference. Fuller details of the arrangements will be sent to those who respond to this preliminary notice.

Award of the Duddell Medal

The 31st (1954) Duddell Medal has been awarded by The Physical Society to Professor A. C. B. Lovell who has, since 1945, built up an important centre of radio astronomy. The Jodrell Bank Experimental Station is perhaps best known for its contributions to the study of meteors by radar methods. In this field a number of entirely new methods of observations have been developed and their application has produced evidence which has, in the last few years, contributed much to meteor astronomy. The detailed survey of meteor-radiants carried out at Jodrell Bank led to the identification of intense day-time showers. The development of radio methods for determining the velocities of meteors has led to the study of the velocities of the sporadic (non-shower) meteors, which has shown that a negligible fraction of the incident meteors originates outside the solar system. Important contributions have also been made to the study of the physics of meteor ionization, and to the investigation of "winds" in the upper atmosphere by observations of persistent meteor trails.

In addition to these investigations of meteors, Professor Lovell has been responsible for an important series of observations on the "scintillation" of radio galactic nebulae. Recently a new type of interferometer has been developed at Jodrell Bank, and this has been used to measure the angular diameters of two of the intense radio stars.

Erratum

In the paper *A method of identifying double-flash exposures* by N. Dombrowski, published on page 17 of the January issue of this *Journal*, the legend for Fig. 2(*c*) should read: (*c*) Wratten 15G filter (light emitted by lamp *B*).

Journal of Scientific Instruments

Contents of the April issue

ORIGINAL CONTRIBUTIONS

Papers

An electronic phase-shift tube for microwave frequencies. By D. H. Pringle.
A generator for very small direct currents. By K. D. E. Crawford.
A hydrogen Pirani leak detector using a charcoal trap. By T. B. Kent.
A voltage stabilizer for a radio-frequency extra high tension set. By R. B. D. Knight, K. M. Poole and J. H. Sanders.
The application of shearing interferometry to routine optical testing. By D. S. Brown.
An isothermal bath for use in the temperature range 200–500° C. By W. H. Bridges, J. V. Cathcart and G. P. Smith.
A sensitive wave-front tilter. By M. De.
Photoconductive detectors for infra-red spectroscopy. By A. S. Young.
A modified pocket integrating ion chamber type B.D.11 of nearly uniform polar response. By B. W. Soole.
A thermocouple anemometer. By R. F. Benseman and H. R. Hart.

Laboratory and workshop notes

A magnetic pump for the laboratory. By J. S. George.
A simple chatter-proof electronic relay. By L. A. Cram.
An adjustable strut for use in measuring instruments. By L. W. Nickols.
An absorption coefficient calculator. By E. G. S. Paige.
A convenient way of heating a palladium osmosis tube. By A. Leemans.

NOTES AND NEWS

Correspondence

A proposed method of investigating the field distribution in a magnetron. From A. W. Aikin.
Fatigue of photomultipliers under pulsed operation. From R. Wilson.
Modifications to a sedimentation apparatus. From J. Kobak.
End-window radioactivity in photomultipliers. From A. G. Hester.
Maximum sensitivity in pneumatic gauging. From N. R. Wynn; N. Stolow.

Notes and comments

THIS JOURNAL is produced monthly by The Institute of Physics, in London. It deals with all branches of applied physics (including theory and technique).

All rights reserved. Responsibility for the statements contained herein attaches only to the writers.

EDITORIAL MATTER. Communications concerning editorial matter should be addressed to the Editor, The Institute of Physics, 47 Belgrave Square, London, S.W.1. (*Telephone:* Sloane 9806.) Prospective authors are invited to prepare their scripts in accordance with the *Notes on the preparation of contributions.* (Price 2*s.* 6*d.* including postage.)

REPRODUCTION. The Institute of Physics is a signatory to The Royal Society's Fair Copying Declaration. Details may be obtained upon application from The Royal Society, London, W.1.

ADVERTISEMENTS. Communications concerning advertisements should be addressed to the agents, Messrs. Walter Judd Ltd., 47 Gresham Street, London, E.C.2. (*Telephone:* Monarch 7644.)

CLAIMS FOR MISSING JOURNALS. Claims from regular subscribers to this *Journal* for missing numbers will only be considered if received within 60 days of the date of mailing plus normal outward time of transit and time for lodging the claim. Losses attributable to failure to notify a change of address or to similar omissions will not be considered.

SUBSCRIPTION RATES. A new volume commences each January. The charge is £4 per volume ($11.50 U.S.A.), including index (post paid), payable in advance. Single parts, so far as available, may be purchased at 8*s.* each ($1.15 U.S.A.), post paid, cash with order. Orders should be sent to The Institute of Physics, 47 Belgrave Square, London, S.W.1, or to any bookseller.

The solution of plane stress problems by an electrical analogue method

By G. LIEBMANN, D.Phil., F.Inst.P., Research Laboratory, Associated Electrical Industries, Ltd., Aldermaston, Berks

[*Paper first received* 17 *November*, 1954, *and in final form* 2 *February*, 1955]

It is shown that the biharmonic equation $\nabla^4\chi = 0$, which Airy's stress function has to satisfy, can be solved by an electrical analogue comprising two resistance networks in cascade. Apart from the requirement of high accuracy of the solution for χ, as the stresses are to be obtained by numerical differentiation of the measured analogue data, difficulties arise through the unfavourable nature of the boundary conditions which have to be satisfied in many practical problems. These difficulties have been overcome by an experimental iteration method. Details are given of the technique of solving the biharmonic equation in this way for prescribed shape of the stressed body and prescribed forces acting on it. The solution is of the same type as that found by numerical methods, e.g. by relaxation, but it is obtained with much greater speed and facility. An accuracy in the evaluation of the stresses of 1 to 2% can be obtained; agreement with photoelastic measurements is very good. Examples are given of several problems which have been solved by the new method. The "cascaded network" technique can also be applied to the solution of other problems in elasticity, described by equations of the type $\nabla^4 w = f(x, y)$, e.g. the bending and extension of flat plates.

1. INTRODUCTION

It is known that plane stress problems can be described by Airy's stress function $\chi = \chi(x, y)$, which satisfies the biharmonic equation:

$$\nabla^4\chi = 0 \tag{1}$$

for certain boundary conditions derived from the forces acting on the stressed body, the symbol ∇^4 representing the operator $\left(\frac{\partial^4}{\partial x^4} + 2\frac{\partial^4}{\partial x^2\partial y^2} + \frac{\partial^4}{\partial y^4}\right)$.

Once the biharmonic equation (1) is solved for a given plane stress problem, the stress distribution is completely determined, and can be readily evaluated. An equation similar to equation (1),

$$\nabla^4 w = f \tag{2}$$

appears in the problems of the bending or extension of flat plates, the displacement w taking the place of the stress function χ, and the function $f = f(x, y)$ being determined by the loading of the plate and its flexural rigidity.

As rigorous solutions of equations (1) or (2) are known in a few cases only, in general numerical methods of solving the biharmonic equation, e.g. the relaxation method,[1-3] have to be employed. The computational work usually proves laborious, as the convergence of the known mathematical techniques is slow, because the difference equations, which replace the fourth-order partial differential equations (1) or (2), are "ill-conditioned."

Some time ago, the author showed briefly[4,5] how the biharmonic equations (1) and (2) can be solved by a "cascaded" resistance-network analogue, and in this paper a fuller account of the new method will be given. (The idea of solving the biharmonic equation by a resistance-network analogue had occurred independently also to Redshaw[6] and to Boscher.[7])

2. THE BOUNDARY CONDITIONS OF THE STRESS FUNCTION

In a practical stress problem, the shape of the body, its elastic constants and the forces acting on it usually are the given data. In the following, the elastic constants will be assumed the same throughout the body, and it will be further assumed that the problem is one of "plane stress," or so-called "generalized plane stress," expressed in the Cartesian co-ordinates x and y. The stress tensor then has three components only, σ_x, σ_y and τ_{xy}, which can be derived from the Airy stress function χ satisfying the biharmonic equation (1) by the following relations:

$$\left.\begin{aligned} \sigma_x &= \partial^2\chi/\partial y^2 \\ \sigma_y &= \partial^2\chi/\partial x^2 \\ \tau_{xy} &= -\partial^2\chi/\partial x\partial y \end{aligned}\right\} \tag{3}$$

The principal stresses p_1 and p_2 are then given by:

$$p_{1,2} = \tfrac{1}{2}\left\{(\sigma_x + \sigma_y) \pm \sqrt{[(\sigma_x - \sigma_y)^2 + 4\tau_{xy}^2]}\right\} \tag{4}$$

and their directions by

$$\tan 2\theta = 2\tau_{xy}/(\sigma_x - \sigma_y) \tag{5}$$

θ being the angle with the x-axis.

The sum of the stress components $(\sigma_x + \sigma_y)$ or of the principal stresses $(p_1 + p_2)$ forms the Laplacian of the stress function χ, which will be denoted by $k\Phi = k\Phi(x, y)$:

$$\sigma_x + \sigma_y = p_1 + p_2 = (\partial^2\chi/\partial x^2) + (\partial^2\chi/\partial y^2) = k\Phi \tag{6}$$

The boundary conditions which the stress function χ has to satisfy are derived from the fact that, in equilibrium, the stresses at the boundary surface of the investigated body must be equal to the forces acting on it. Let, in Fig. 1, B be the boundary of the cross-section of the body in the

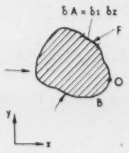

Fig. 1. Section through stressed body

x, y plane, the arrows indicating the forces. Over the area $\delta A = \delta s \delta z$, where δs is the line element of the boundary, and δz the height of the body (assumed henceforth to be unity), the force F per unit area may be acting. If the component of F normal to the boundary B at the surface element δA is F_n, and the tangential component is F_s, equations (3) give these conditions for $\chi = \chi_B(s)$ along the boundary B:

$$\left.\begin{aligned}[\partial\chi_B(s)]/\partial s &= \oint_0^s F_n\, ds \\ [\partial\chi_B(s)]/\partial n &= -\oint_0^s F_s\, ds\end{aligned}\right\} \tag{7}$$

The integrations are taken from a suitable point on the boundary B, e.g. the point $O(s = 0)$, in an anti-clockwise direction to the point with the line co-ordinate s, measured along the boundary from point O.

From equations (7), $\partial\chi_B/\partial s$ and $\partial\chi_B/\partial n$ can be evaluated, and then χ_B itself from $\partial\chi_B/\partial s$, using the fact that χ_B must be continuous. Hence, the biharmonic equation, equation (1), has to be solved mostly with prescribed simultaneous boundary conditions for χ_B and $\partial\chi_B/\partial n$. It is this circumstance which leads, together with the "ill-conditioning" referred to in the Introduction, to the practical difficulties in obtaining the solution.

3. THE PRINCIPLE OF THE NETWORK ANALOGUE METHOD

It is customary, in the numerical methods of solving the partial differential equations $\nabla^4\chi = f$ or $\nabla^2\Phi = g$, to divide the cross-sectional area enclosed by the boundary B in Fig. 1 by equidistant lines parallel to the x- and y-axes into meshes, of mesh size $\delta x = \delta y = h$, as shown in Fig. 2. The partial

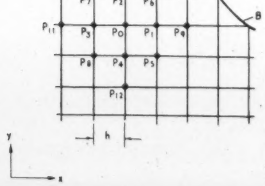

Fig. 2. Square mesh used in finite difference approximation

differential equations are then approximated by finite difference expressions, involving the functional values at the point P_0 and its four neighbouring points $P_1, \ldots P_4$, at distance h, in the case of the Laplace or Poisson equation, and the values at P_0 and its twelve nearest surrounding mesh points, in the case of the biharmonic equation.

It is known[8] that the difference equation:

$$\Phi_1 + \Phi_2 + \Phi_3 + \Phi_4 - 4\Phi_0 = h^2 g \tag{8}$$

which replaces the equation $\nabla^2\Phi = g$, is solved with high accuracy by an electrical resistance-network analogue; the voltages appearing at the network nodes correspond to the sought function Φ, and the known function, $g = g_0$ at the point P_0, is connected with the current I_0 fed in at the network node P_0 through the relation:

$$I_0 = -h^2 g_0/R \tag{9}$$

R being the value of the resistances used in the network.

The truncation error of the network analogue solution of the differential equation $\nabla^2\Phi = g$ is the same as that of the usual numerical solution, as both methods are based on the same finite difference approximation.

Now consider two geometrically similar resistance-networks N and N', the resistance values being R and R' in the two networks (Fig. 3). The corresponding network nodes

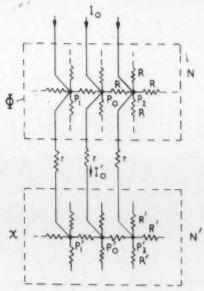

Fig. 3. Basic arrangement of cascaded networks

P_0 and P_0', etc., in the two networks are connected by "series resistances" of value r, $r \gg R$ and $r \gg R'$; let the current flowing into the node P_0 in network N (the "upper" network) from an external source be I_0, and the current flowing from P_0 to the corresponding node P_0' in network N' (the "lower" network) be I_0'. It will be assumed, for the present, that boundary values are given for the function χ, which satisfies the equation $\nabla^4\chi = f$, and for the function Φ, which satisfies the equation $\nabla^2\Phi = g$. Let the boundary values for Φ be applied to the upper network, and those for χ to the lower network.

The voltages appearing in the upper network then represent the solution Φ of the difference equation approximating the differential equation $\nabla^2\Phi = g$, and the voltages in the lower network represent the solution χ of the equation $\nabla^2\chi = g'$. The current I_0 flowing into the node P_0 of the upper network is determined by equation (9), whereas the current flowing into the corresponding node P_0' of the lower network is similarly given by:

$$I_0' = -h^2 g_0'/R' \tag{10}$$

However, the value of this current is:

$$I_0' = (\Phi_0 - \chi_0)/r$$

where the suffix 0 indicates that the voltages Φ and χ are measured at the nodes P_0 and P_0'. As the relative value r of the "series resistance" is assumed so high that $\Phi_0 \gg \chi_0$, one can write with sufficient approximation

$$I_0' = \Phi_0/r \tag{11}$$

[The errors arising from the finite values of (r/R) and (r/R')

will be discussed in Section 6. They can be made small enough in practice to be negligible.] Inserting this value into equation (10), one finds:

$$g' = \nabla^2\chi = -\Phi_0 R'/rh^2 \tag{12}$$

But the voltage distribution Φ satisfies the equation $\nabla^2\Phi = g$; hence operating with ∇^2 on equation (12):

$$\nabla^2(\nabla^2\chi)_0 = -\frac{R'}{rh^2}(\nabla^2\Phi)_0 = -\frac{R'g_0}{rh^2}$$

Eliminating g_0 through equation (9), there results, as I_0' is negligibly small in comparison with the currents in the upper network:

$$(\nabla^4\chi)_0 = RR'I_0/rh^4 \tag{13}$$

Hence, the "cascaded" resistance-network arrangement shown schematically in Fig. 3 solves the difference approximation to the fourth order partial differential equation $\nabla^4\chi = f$, if the currents I fed into the nodes of the upper network have the values:

$$I = rh^4 f/RR' \tag{14}$$

In the network solution of the biharmonic equation (1), governing the stress distribution in a plane problem, the right-hand side of equation (13) is identically zero, i.e. no currents are fed into the upper network.

It was assumed in the foregoing discussion that boundary values were given for both functions χ and $\Phi = (1/k)\nabla^2\chi$. If this were the case, the following simple steps would be needed in solving a plane stress problem by the analogue method: (i) two models of the stressed body would be set up on the two networks; (ii) the specified boundary conditions would be applied by impressing the required voltages, in both networks, at the network nodes lying along the boundary B (Figs. 1 and 2); (iii) the voltages at the nodes of the lower network would be measured, giving a record of the χ-values. The stress components $(\sigma_x)_0$, $(\sigma_y)_0$ and $(\tau_{xy})_0$ at the mesh point P_0 would then be evaluated from the usual difference formulae, the suffixes referring to the network points numbered as shown in Fig. 2:

$$\left.\begin{aligned}(\sigma_x)_0 &\simeq (\chi_2 + \chi_4 - 2\chi_0)/h^2\\ (\sigma_y)_0 &\simeq (\chi_1 + \chi_3 - 2\chi_0)/h^2\\ (\tau_{xy})_0 &\simeq (\chi_5 - \chi_6 + \chi_7 - \chi_8)/4h^2\end{aligned}\right\} \tag{15}$$

The measurement of the Φ-values would not be of interest in itself, but it serves a good purpose by giving an independent check on the numerical evaluation of the stress components and principal stresses from the recorded χ-values. The scaling constant k, which correlates the $(\nabla^2\chi)$-values computed from the χ-values measured in the lower network and those measured directly in the upper network, is found by comparing equations (6) and (12):

$$k = -R'/rh^2 \tag{16}$$

As mentioned in Section 2, the boundary conditions met in a practical problem usually prescribe boundary values χ_B for the χ-function, and its boundary gradients $(\partial\chi/\partial n)_B$, at least over part of the boundary. Thus, whereas one boundary condition is required for each of the two networks, two boundary conditions are given for the lower network, and none for the upper network. This difficulty can be overcome by applying only one boundary condition to the lower network, and varying the boundary voltages in the upper network until the second boundary condition in the lower network is also satisfied. Hence, an iterative approximation method, in which an adjustment to the upper network boundary voltage is made, its effect in the lower network measured, a further adjustment made, etc., is necessary. Unfortunately, the convergence of this method is very slow, owing to the "ill-conditioning," mentioned in the Introduction with reference to the numerical methods of solving the biharmonic equation. A method for observing simultaneously the effect, at all boundary points in the lower network, of small changes made in the boundary potentials of the upper network, has therefore been devised. In this way, it has been found possible to achieve quite rapid convergence of the analogue solution in spite of "ill-conditioning." The technique of this method will be described in Section 4.

In practice, it is often more convenient, or more accurate, to choose $(\partial\chi/\partial n)_B$ as the boundary condition to be set up initially, and χ_B as the second boundary condition which has to be approximated (see Appendix).

4. THE EXPERIMENTAL APPROXIMATION METHOD

It had been shown by the author[9] some years ago that equations of the type $\nabla^2\Phi = g(x, y, \Phi)$ can be solved by an iteration process applied to a resistance-network model, in which the currents fed into the network nodes are cyclically adjusted. It is possible to arrange the network model and the current feeding system in such a way that the relations governing the voltages at the network nodes (E_1) and at suitable corresponding points in the current feeding system (E_2) can be put in the form:

$$E_1 - E_2 = \epsilon \tag{17}$$

The error signal ϵ is a measure of the deviation of the actual condition in the network from the final state, representing the completed analogue solution of the problem. In a recent paper, Liebmann and Bailey[10] described an apparatus which, when connected to a resistance-network analogue and its current feeding system, extracts automatically the error signal ϵ and displays it simultaneously, according to value and sign, for a great number of network points. It is then very easy to adjust the currents fed into the network to make $\epsilon \to 0$ everywhere. In particular, if the problem is "ill-conditioned," it is possible to make a series of *small* and properly *planned* adjustments which make an approximate initial solution converge quite rapidly towards the final solution, as all error signals ("residuals") are in view, so that the sudden appearance of errors elsewhere can be avoided.

In the analogue solution of the biharmonic equation (1), the adjustments are not made directly to the currents flowing into the χ-network but to the boundary values of the Φ-network, but the method of directly observing the error voltages ϵ can be easily adapted to this. Fig. 4 shows a diagram of the arrangement used. The boundary value χ_B' in the χ-network, as it *exists* in the network at the particular stage reached in the solution, represents the potential E_1 in equation (17), whereas the *prescribed* values of χ_B are set up on an independent potentiometer strip. (This has often only the zero point in common with the network, the voltage at the other end of the potentiometer strip then being adjusted to equal that of the corresponding point in the χ-network.) The voltages E_1 and E_2 are passed through the "differencing unit" of the display apparatus, and the resulting error signal ϵ is amplified to a suitable level and displayed on a long-persistence cathode-ray tube screen. A fast running rotating multipole switch brings the various error voltages successively into view, but the long persistence of the tube screen retains them there until the next sweep of the switch.

Owing to the condition $r/R \gg 1$, already mentioned, a potential division between the Φ-network and the χ-network exists which reduces the signal level in the χ-network to a relatively low value. As the solution of the χ-function has to be correct to about 3 parts in 10000 to allow the numerical differentiation required in the evaluation of the stress components without the introduction of undesirably great errors,

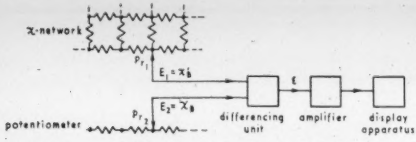

Fig. 4. Principle of boundary voltage comparison

it is necessary to detect quite small error signals ϵ, of the order of 2×10^{-6} of the maximum voltage applied to the Φ-network.

The display apparatus of Liebmann and Bailey, used in the work reported here, was built for a different type of problem, and it falls short of the present, more stringent requirement by a factor of about twenty, because a very small error signal becomes submerged in spurious voltages (hum, etc.). (An improved display apparatus is now under construction.) Fortunately, it was found that it was possible to make the final advance to an error of only 0·05% or less in the boundary values of the χ-function by a point-by-point adjustment along the boundary of the Φ-function, using a galvanometer to measure the error signal ϵ for each χ-boundary point, once the boundary values of the χ-function had all been brought within ±1% or better of their prescribed values with the help of the display apparatus. However, even when starting from an approximation as good as this, care and circumspection were needed in making the required small, local adjustments to avoid the introduction of appreciable errors elsewhere, leading to rapid divergence of the solution.

It might be mentioned here that another iterative method of establishing the required boundary values of the χ-function has failed so far. In this, a first trial solution Φ_0 is set up on the Φ-network [with the appropriate boundary condition for $(\partial\chi/\partial n)_B$ imposed on the χ-network], and the ensuing χ-distribution is measured. From this, a new set Φ_1 of boundary values for the Φ-function is computed, which can then be applied to the Φ-network, producing a new χ-distribution, etc. However, it was found that the rate of convergence was too slow in view of the errors introduced through the required numerical differentiation of the experimentally established trial values of the χ-function. Starting from trial values which made the boundary values χ_B correct to within ±1%, as mentioned above, it was not possible to improve on this, and the solution became rapidly worse in the two cases tried.

5. PRACTICAL REALIZATION OF THE ANALOGUE

The experimental "cascaded" network used by the author consists of a vertical board 4 ft square, carrying the Φ-network on its front and the χ-network on its back. The network nodes are 4 B.A. screw studs projecting through the board (¼ in. thick hardboard), with soldering lugs on either side, the screw studs being set in two square arrays of 2 in. pitch, the two arrays being "nested" within each other as shown in Fig. 5. In this figure, the circles indicate the screw studs, the solid circles being the nodes of the Φ-network and the open circles the nodes of the χ-network. The full lines represent the R-resistances of the Φ-network, the dashed lines the R'-resistances of the χ-network, and the dotted lines the interconnecting r-resistances. The r-resistances are arranged at the back of the board, to leave its front free for the measurement of the Φ- and χ-distributions, and for the setting-up of the boundary conditions.

In the earlier part of the investigation, 50 c/s a.c. excitation of the networks was used, the value of the R and R' resistances being 5 Ω, and that of the r-resistances several thousand ohms. This method of working, although convenient in

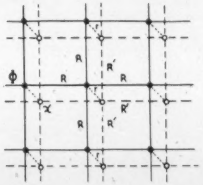

Fig. 5. "Nested" arrangement of Φ- and χ-networks

several respects, was later abandoned because the phase differences in the various parts of the χ-network were undesirably great, making a recording of the results to the required accuracy rather difficult. Nevertheless, useful results were obtained in this way.

In the later work, a value $R = R' = 100\ \Omega$ was used, the value of the r-resistances being varied between 25 and 200 kΩ, the network being mostly supplied by a d.c. voltage derived from a 12 V car battery, tapped such that positive and negative feeding voltages were available. A number of 30 Ω potentiometers, each in series with a 3 Ω rheostat for fine control, were connected across the appropriate terminals of the battery, the voltages at the potentiometer tapping points being the feeding voltages for the Φ-network.

A schematic circuit diagram of the final arrangement used is shown in Fig. 6. The battery is denoted by *Ba*, the 30 Ω feeding potentiometers by P_1, etc., and the 3 Ω rheostats by Rh_1, etc. The Φ- and χ-voltages are measured by a precision potentiometer bridge *Br* (connected by the probe *Pr* through the galvanometer *G* to the various network studs). The three-position switch S_2 allows connexion of the "1"-terminal of the bridge to the positive or negative end of the battery, to measure positive or negative Φ-values, or connexion to the positive battery terminal through the series resistances L_1 and L_2 ("level setters") to measure the χ-distribution. The potentiometer strip, on which the prescribed boundary potentials are set up, is represented by the resistance chain R_1, $R_2 \ldots R_n$, connected in parallel with the bridge *Br*. The ganged multipole switches MS_1, MS_2, MS_3 connect successively to the tapping points on the potentiometer strip, and the corresponding boundary points in the χ- and Φ-networks. The voltages at the terminals of switches MS_1 and MS_2 are fed through a double pre-amplifier A_1, each pre-amplifier comprising a single battery-operated stage of gain ×10, to the "differencing unit" *D* (a differential amplifier). The resulting voltage ϵ, being proportional to $\Delta\chi_B$, the error

of the boundary values in the χ-network, is further amplified by the unit A_2 and displayed on the long-persistence screen cathode-ray tube CRT_1; the bright dot on the screen, the vertical position of which represents the final error signal, is moved along by a horizontal deflexion voltage supplied through a fourth multipole switch ganged to $MS_1 \ldots MS_3$ (not shown in Fig. 6), such that the positions on the cathode-ray tube screen and along the network boundary are directly related.

The boundary potentials Φ_B are amplified by the amplifier A_3 and displayed on a second long-persistence screen cathode-ray tube CRT_2. The simultaneous display of the Φ_B-distribution is useful as it helps to obtain the required χ_B values to the degree of accuracy desired, whilst keeping the Φ_B distribution smooth. It also shows up quickly errors in the type of boundary conditions imposed. The link C, shown in Fig. 6, is sometimes used to fix the relative value of the

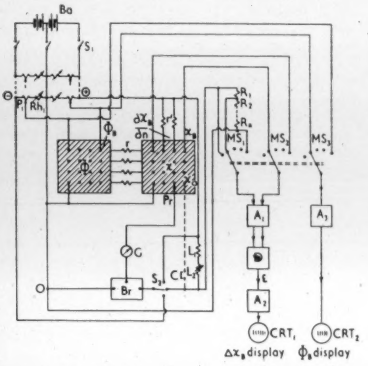

Fig. 6. Schematic diagram of complete cascaded network analogue and its measuring circuits

maximum voltage χ_m in the χ-network to $\chi_m = 1$ (in terms of the bridge setting); this may help to accelerate the process of establishing the correct χ_B values, as the effect of changes in the Φ_B-potentials made during the process of solution, which lead to a change in absolute signal level in the χ-network, is greatly reduced in this way.

The resistances r' are used to provide the required boundary gradients $(\partial\chi/\partial n) \neq 0$, being connected between the boundary studs of the χ-network and the positive or negative battery terminal, as may be required (see Appendix).

In solutions of problems described by equation (2), the currents I_r required to represent the function $f(x, y)$ as given by equation (14), are adjusted to their prescribed values in the way previously discussed by the author,[11] or they may be established by connecting the appropriate stud on the Φ-network to a voltage source of potential $V \gg \Phi$ through a resistance r'' of such a value that $I = (V - \Phi)/r'' \simeq V/r''$.

Suitable lengths of insulated resistance wire, wrapped round cardboard formers, were used for the R and R' resistances and for the potentiometer chain $R_1 \ldots R_n$ (resistance tolerances $\pm 0{\cdot}2\%$), whereas, for the r and r' (or r'') resistances high stability carbon resistors of $\frac{1}{2}$ to 1% tolerance were employed.

In setting up a model on the cascaded network analogue, *two identical models* are always set up, one on the lower network and one on the upper network. For example, if curved boundaries are represented, the same network modification is made in both networks. Details of the method of modifying a network to represent *irregular or curved boundaries* have been given before;[11,12] these apply directly to the analogue discussed in this paper. The frequently occurring boundary condition $\partial\chi/\partial n = 0$ is realized by cutting off both networks (see Appendix). If the boundary runs through a line of mesh nodes, the value of the resistances lying along the boundary have then to be doubled as has the value of the series resistance r.

6. FACTORS INFLUENCING THE ACCURACY OF THE METHOD

The accuracy of the resistance-network method for solving plane stress problems is affected by a number of factors, some of them of a technical nature and some of a more fundamental kind.

(*a*) *Truncation errors.* The difference approximations to the partial differential equations (1) and (2), which are solved by the cascaded network method, are of $0(h^4)$, and at interior points the lowest order of the neglected terms is $0(h^6)$, as in the relaxation method. At boundary points where a derivative is prescribed, or at boundary points where the network has been modified to represent a curved boundary, the lowest order of the neglected terms is $0(h^5)$ in the network method, as shown in the Appendix. While there is, therefore, necessarily a small loss of accuracy at the boundary in many cases, the position in this respect is not worse, and often better than is met in the numerical methods for solving partial differential equations by finite difference methods [unless higher order correction terms are introduced, as proposed by Fox[13,14]]. In fact, the correct and identical termination of both networks would be equivalent to the use in the relaxation method of *two* "fictitious" mesh points outside the boundary for each boundary point (see Appendix).

In problems involving curved boundaries, it is necessary to make the mesh size so small that $h \leqslant \frac{1}{2}\rho_{min}$, where ρ_{min} is the minimum radius of curvature of the boundary, to obtain a sufficiently faithful representation of the shape of the boundary.

A reduction in truncation errors can be obtained in the manner discussed by the author[8] in connexion with the resistance-network solution of the Laplace and Poisson equations, either by extrapolation or by feeding correcting currents into the network nodes, the correcting currents representing the next higher order terms of the finite difference approximation. The required values of the correcting currents could be determined with sufficient accuracy from the first approximate solution in which no correcting currents are used.

(*b*) *Resistance tolerance errors.* It has been shown before[8] that the errors in the measured network voltages due to the tolerances of the resistance values are relatively small. The formula for the expected error, given in the earlier paper, can be simply interpreted by saying that the error in the voltage distribution will be of the same order as the average resistance tolerance divided by the number of mesh intervals across the model. Assuming that the average number M of mesh intervals in the linear dimensions of the model used will be 10, say, and that the errors due to the resistance tolerances should be below the prescribed accuracy of $0{\cdot}03\%$ in the χ-distribution, a resistance tolerance in the networks

of 0·2% should be aimed at. The achievement of this tolerance in the R and R' values does not present any practical difficulties. The part played by the tolerances of the series resistances r is different. One sees from equation (12) that a tolerance error $\delta r/r$ leads to a corresponding error $-\delta(\nabla^2\chi)/\nabla^2\chi$ in $\nabla^2\chi = (p_1 + p_2)$; e.g., a value of $\delta r/r = 0{\cdot}01$ leads to a local error of 1% in the evaluated stresses. It is therefore necessary, when aiming at an accuracy of 1 to 2% in the values of the stresses to be computed from the χ-distribution, that the tolerance errors of the r-resistances are below 1%, and preferably not more than ½%, and similarly for the r'-resistances for the representation of boundary gradients.

(*c*) *Errors due to the finite* (r/R)*-ratio.* By following the argument of Section 3, without the simplifying assumption $\Phi_0 \gg \chi_0$, one finds, instead of equation (14), relation (18), which holds exactly, within the limitations discussed under paragraphs (*a*) and (*b*):

$$I = rh^4 f/RR' + (R + R')I'/R \tag{18}$$

As the second term on the right-hand side of relation (18) represents a small correction term, it is permissible to replace $I' = (\Phi - \chi)/r$ by $I' \simeq \Phi/r$, and equation (18) can therefore also be written:

$$I = rh^4 f/RR' + (R + R')\Phi/Rr \tag{19}$$

Relations (18) or (19) show that the error due to the finite (r/R)-ratio can be completely eliminated by feeding in correcting currents

$$I_c = (R + R')\Phi/Rr \tag{20}$$

at the nodes of the Φ-network. In practice, one would first obtain an approximate solution under the condition $I_c = 0$, and determine the required values of I_c from this approximate solution, repeating the process if necessary.

If correcting currents I_c are used, it may prove relatively little additional work to combine these correcting currents with those representing the higher order terms of the finite difference approximation discussed under paragraph (*a*).

Very often, one does not wish to go to the trouble of feeding in compensating currents, particularly in the case of the biharmonic equation $\nabla^4\chi = 0$, where then no currents are fed in at all into the upper network (except at boundary points). But it is not sufficient to rely on the fact that $r \gg R$ and $r \gg R'$, because all r-resistances are, in effect, in parallel. It is therefore desirable to have an estimate of the errors which result from the finite values of (r/R) and (r/R').

A useful way of assessing this error is to consider directly the error δp of the total stress $(p_1 + p_2)$ at the point P_0, referred to the maximum value p_m of $(p_1 + p_2)$, as a function of the ratio (χ_m/Φ_m) of the voltage levels in the two networks, χ_m and Φ_m being the maximum voltages in the two networks.

The ratio (χ_m/Φ_m), which is easily measured in practice, has the value:

$$(\chi_m/\Phi_m) = (R'/r)M^2A \tag{21}$$

where the numerical constant A measures the integrated effect of the (Φ/Φ_m) distribution. The value of A depends on the type of problem to be solved, but mostly does not vary over a very wide range. In simple cases, the constant A can be calculated, e.g. for a uniformly-stressed long rectangular bar of width $b = Mh$, $A = \frac{1}{4}$, the largest possible value for this constant. In other cases studied experimentally, A was found to be not far from ¼.

In view of equations (8)–(11), the local error $\delta\Phi_0$, due to the finite (r/R)-ratio, is proportional to $-RI'_0/h^2$, representing a measure of the "residual" in the upper network, and hence also proportional to $-(R'/r)(\Phi_0/h^2)$. As $(\delta p/p_m) = \delta\Phi_0/\Phi_m$, $(\delta p\ p_m)_0$ is proportional to $-(R'/r)(\Phi_0/\Phi)/h^2$. Replacing $(R'/r)/h^2$ by (χ_m/Φ_m) from equation (21), the required estimate for the systematic error becomes:

$$(\delta p/p_m)_0 = -\beta_0(\chi_m/\Phi_m) \tag{22}$$

The numerical factor β_0 in equation (22) depends on the type of problem studied and on the relative position of the mesh point P_0, and not on the scale of the model, except for the minor influence of the truncation errors. While the experience gathered so far shows that β_0 lines within the range 0·1 to 1·0, in several cases investigated systematically (mostly of the uniformly stressed parallel bar type), β_{max} was found to be between 0·2 and 0·3, depending on the actual nature of the conditions applied to the Φ-network. Hence, for the systematic error $(\delta p/p_m)_0$ to be smaller than 0·5%, say, at every mesh point P_0, requires that (χ_m/Φ_m) should not be greater than about 0·02.

(*d*) *Measurement errors and computational rounding-off errors.* The resistance networks for the solution of Laplace and Poisson type problems are mostly used under conditions where the measurement errors can be made so small (order of 10^{-5} of the impressed network voltage) that they can be disregarded. In the present analogue method, conditions are much less favourable for two reasons: (i) the relatively low signal level in the χ-network owing to the value of the (χ_m/Φ_m)-ratio required if no correcting currents are fed into the Φ-network, and (ii) the fact that the functional values of χ are not of interest, but only its second derivatives obtained by numerical differentiation. These two influences can be assessed together if the relative measurement error $\epsilon = \delta\chi/\chi_m$ is considered as if it were a numerical "rounding-off error."

When calculating, e.g. σ_x from the χ-distribution by formulae (15), the error $\delta\sigma$ in σ_x will be:

$$\delta\sigma = \gamma\epsilon\chi_m/h^2 \tag{23}$$

where γ is a statistical weighting factor. For instance, $\gamma = 4$ if equal measuring errors ϵ in χ_0, χ_2 and χ_4, and the worst possible combination of these errors are assumed. The relative error $\delta\sigma/p_m$, where p_m is the maximum stress value as used in paragraph (*c*), will then be:

$$\delta\sigma/p_m = (\gamma\epsilon/h^2)(\chi_m/p_m)$$

Replacing p_m in the factor (χ_m/p_m) through Φ_m by equations (6) and (16), and substituting (χ_m/Φ_m) from equation (21) gives:

$$\delta\sigma/p_m = \gamma M^2 A\epsilon$$

Assuming that, on the average, the product of the factor γ and of the constant A is about unity, the final estimate for the permissible relative measuring error ϵ becomes:

$$\epsilon = \delta\chi/\chi_m \simeq (\delta\sigma/p_m)/M^2 \tag{24}$$

Allowing an average error of $\delta\sigma/p_m$ of 1%, and assuming a model of linear dimensions (in mesh units) $M \simeq 7$, the permissible average measuring error would be $\epsilon \simeq 10^{-2}/50 = 2 \times 10^{-4}$; i.e. great accuracy in the determination of the χ-function is required to obtain a satisfactory accuracy in the finally evaluated stress components. It is also of some interest to estimate the permissible measurement error in terms of the maximum applied network voltage Φ_m. This is $\delta\chi/\Phi_m = \epsilon(\chi_m/\Phi_m)$. With $\epsilon \simeq 2 \times 10^{-4}$ and $(\chi_m/\Phi_m) \leqslant$

2×10^{-2}, the permissible error $\delta\chi$ would be $\delta\chi \leqslant 4 \times 10^{-6}\Phi_m$. In practice, Φ_m lies in the range of 5 to 10 V, hence the voltage discrimination required in the χ-measurement is about 20 μV.

(*e*) *The combination of the various errors.* It is evident from the above discussion that there are fairly closely defined optima for the scale $M = b/h$ of the model investigated by the resistance-network method, and for the ratio (r/R). The truncation errors require a large value of M, whereas the measurement errors ϵ require a small value of M, the dependence being quadratic in both cases. Similarly the reduction of systematic errors (in the absence of compensating currents) calls for a low (χ_m/Φ_m) ratio, i.e. for a high (r/R) value, whereas the measurement errors, on an absolute scale, require a high value of (χ_m/Φ_m), i.e. a low (r/R) value, to give a voltage of sufficiently high level for discrimination.

The examples given in Section 7 show, nevertheless, that accuracies of 1 to 2% in the evaluation of the stresses can be achieved in practice by careful attention to all the points discussed here. The best compromise values for the model data found by the author are: $M \simeq 5$ to 20, $r/R \simeq 500$ to 2000, and $(\chi_m/\Phi_m) \simeq 0{\cdot}01$ to $0{\cdot}02$. By the use of correcting currents as discussed earlier on, a different set of optimum values would be obtained and, in particular, it would be possible to work with relatively high (χ_m/Φ_m) values, and hence use larger scale models, but the required iterative technique would of course be more cumbersome.

7. EXPERIMENTAL TESTS OF ACCURACY

A check on how far the deductions of Section 6 can be used to evaluate the best conditions for studying a practical stress problem by the resistance-network analogue method was carried out, partly by the experimental investigation of trivial cases where the stress distribution is known exactly (e.g. an infinitely long parallel bar under tension), and partly by studying a few problems where the results could be compared with photoelastic measurements. Two such problems will be given as examples in Section 9. Only a few tests using the problem of the uniformly stressed parallel bar ($\sigma_y = 1$) of width $b = 8h$ will be mentioned here. Table 1 gives some typical analogue measurements of the values of the stress function χ in comparison with the theoretical solution $\chi/\chi_m = 2(x/b) - (x/b)^2$, the resultant stress component σ_y and the errors in σ_y. The experimental values (i), (ii), (iii) refer to three different models investigated at different times. The (χ_m/Φ_m) ratios used lay in the range 0·008 to 0·016.

Table 1. *Comparison of experimental and exact values for uniformly stressed infinite bar* ($\sigma_{y\,calc.} = 1{\cdot}000$)

		χ/χ_m			$\sigma_{y\,exp.}/\sigma_{y\,calc.}$			$\delta\sigma_{y\,exp.}$ (%)		
(x/h)	*Calculated*	*Experimental* (i)	*Experimental* (ii)	*Experimental* (iii)	*Experimental* (i)	*Experimental* (ii)	*Experimental* (iii)	*Experimental* (i)	*Experimental* (ii)	*Experimental* (iii)
0	0	0·0000	0·0001	0·0000	—	—	—	—	—	—
1	0·2344	0·2345	0·2346	0·2344	0·995	1·002	0·998	−0·5	0·2	−0·2
2	0·4375	0·4379	0·4379	0·4376	1·008	1·005	0·998	0·8	0·5	−0·2
3	0·6094	0·6098	0·6096	0·6096	1·011	1·008	1·018	1·1	0·8	1·8
4	0·7500	0·7501	0·7499	0·7498	0·995	0·979	0·976	−0·5	−2·1	−2·4
5	0·8594	0·8593	0·8596	0·8595	1·005	1·021	1·018	0·5	2·1	1·8
6	0·9375	0·9371	0·9374	0·9374	0·986	0·989	0·989	−1·4	−1·1	−1·1
7	0·9844	0·9841	0·9843	0·9844	1·002	1·002	1·005	0·2	2·0	0·5
8	1·0000	0·9998	0·9999	1·0000	—	—	—	—	—	—

This small sample shows already the characteristic features found in larger scale tests. That is, as truncation errors are absent owing to the trivial nature of the problem (uniform stress) and, as the systematic errors due to the finite (r/R)-ratio have been kept down to a negligibly small level by choosing a relatively small (χ_m/Φ_m)-ratio, the errors are statistically distributed, being caused by the combination of the errors discussed in Section 6 under paragraphs (*b*) and (*d*). The probable error in σ_y is here about 0·8%. An important feature, which already emerges in this small sample, is that the larger errors of one sign are usually surrounded by relatively large errors of opposite sign. It is therefore possible to improve the accuracy of the final result by "smoothing" (see also Section 8).

The largest error in the (χ/χ_m) distribution recorded in this sample is 4×10^{-4}, and formula (24) would predict a maximum error $\delta\sigma/p_m = 2{\cdot}6\%$. This happens to agree quite closely with the observed maximum error (2·4%), but the agreement is fortuitous; the maximum error in σ_y in Table 1 occurs where $(\delta\chi/\chi_m) = 2 \times 10^{-4}$ only, but where the distribution of adjacent errors $\delta\chi$ is more unfavourable than on the average. Nevertheless, formula (24) is a useful guide to the accuracy that can be expected in the presence of the unavoidable measuring errors.

The superposition of the statistically distributed measuring errors, and the systematic error due to the finite (r/R)-ratio, is demonstrated by the measurements shown in Fig. 7, in which the maximum observed relative error $(\delta p)_{max}/p_m$ is shown (circled points) as a function of the (χ_m/Φ_m) ratio. The models used were of relatively small size ($b = 4h$), to ensure that the experimentally found optimum would come to lie at a low enough (χ_m/Φ_m) value for ascertaining the relationship between the systematic error and the (χ_m/Φ_m)-ratio, in spite of the superposition of the measuring errors. The observed minimum value of the maximum total error occurring anywhere within the model is 0·75%, which agrees well with the data shown in Table 1, when making allowance for the scale factor M^2. The graph shows three curves. The two dashed lines represent the predictions based on equation (22) for the systematic error and equation (24) for the error due to the measuring error, assuming that the upper network voltage Φ_m has a constant value. The superposition of these two curves produces the full-line curve of Fig. 7. The constants of the two dashed curves were determined by the two extreme circled points on the right and on the left, and it is seen that the four intermediate measured points lie as closely to the composite theoretical error curve as can be expected.

The minimum of the composite curve in Fig. 7 lies at $(\chi_m/\Phi_m) = 0{\cdot}016$. Increasing the scale of the model would shift the minimum to the right, as would a lower discrimination

in the measurement of the χ-function, whereas an increase in the applied maximum voltage Φ_m would shift the minimum to the left. In practice, it is advisable to choose a (χ_m/Φ_m)-ratio such that the working point is on the minimum or

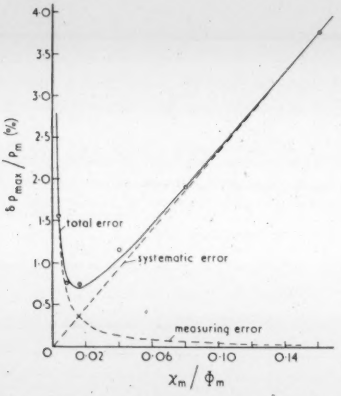

Fig. 7. Combination of systematic and statistical errors in the evaluated maximum stresses as a function of the (χ_m/Φ_m)-ratio

slightly left of it, so that the statistically-distributed errors outweigh the systematic errors (in view of the possibility of "smoothing").

8. CHECK OF SOLUTION BY RESIDUALS AND IMPROVEMENT OF ACCURACY BY RELAXATION

It was found useful in a number of cases to check the recorded analogue solutions for the absence of larger errors, e.g. due to a clerical error in the recording or transcribing of the measurements, or due to a fault in the resistance-network analogue apparatus, by evaluating the residuals $\mathscr{R}$ by the formula used in the relaxation technique:

$$\mathscr{R}_0 = 8\sum_1^4 X_n - 2\sum_5^8 X_n - \sum_9^{12} X_n - 20X_0 \qquad (25)$$

In equation (25), the suffixes denote the functional values χ at the correspondingly labelled mesh points in Fig. 2, and all χ-values are referred to the maximum value $\chi_m = 1$.

A typical distribution of the residuals calculated from the analogue solution [e.g., example (*a*), Section 9] is shown in Fig. 8. For the residuals at the interior points adjacent to the boundary, "fictitious" χ-values were computed for the next mesh points outside the boundary from the independently recorded Φ-distribution, measured in the upper network, by solving the equation

$$\sum_1^4 X_n - [4 + (R'/r)]X_0 + R'\Phi_0/r = 0$$

for the unknown "fictitious" χ-value, P_0 being the boundary points.

The residuals are seen to be fairly well distributed, the largest residuals mostly being surrounded by residuals of the opposite sign. For instance, the sum of all residuals over a "block" of nine mesh points centred on the point with the largest residual which occurs in Fig. 8 ($\mathscr{R} = 85 \times 10^{-4}$) i.e. the block centred on the point $x = 5$, $y = 10$ and marked by the dashed contour, amounts to only 11×10^{-4}, although the sum of the absolute values of the residuals in this block is 311×10^{-4}. Hence, the larger residuals will be due to *localized* inaccuracies in the recorded χ-distribution. It should be possible to remove these local errors by relaxation, and one would therefore expect that the accuracy of the recorded resistance-network analogue results could be improved through subsequent relaxation by a factor of two or three without very great expense of time and effort. The network method in itself ensures, of course, that the sum of all residuals is small.

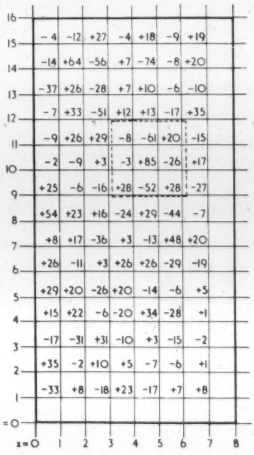

Fig. 8. Distribution of residuals for analogue solution of example (*a*), Fig. 9

$\mathscr{R} \times 10^4 (\chi_0 = 1)$

The residuals found for the analogue solutions have also been compared with those calculated from published relaxation solutions.[1] The residuals derived from the analogue solutions were found to be up to about 25% greater, but slightly better distributed. Hence, the accuracy of the analogue solutions reported in this paper, without subsequent improvement by relaxation, will be about the same as that of the published relaxation solutions referred to.

9. TWO PRACTICAL EXAMPLES

A fairly extensive study of the new method was carried out for two types of problem, (i) problems with uneven load distribution along the boundary but simple geometry of the boundary, and (ii) problems with simple loading conditions but more complicated geometry of the boundary. It was thought that once the best method of dealing with these two classes of problems were established, the way would be clear for treating more general problems. As a check on the new analogue method, mainly problems were investigated which had, at least partly, also been studied by the photoelastic method.

(*a*) *Square block loaded over part of its surface.* As examples of problems of type (i), several rectangular blocks,

loaded uniformly over *part* of their surface, were investigated. A typical case is that studied by Coker and Filon[15] in which a square block rests on a rigid surface and is loaded uniformly over the central quarter of its upper surface, as shown in Fig. 9.

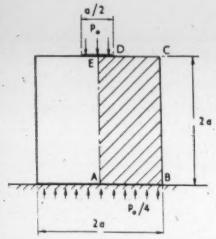

Fig. 9. Square block resting on rigid surface and loaded over central quarter of upper surface. Shaded area represents model set up on resistance-network analogue (153 mesh points)

Owing to symmetry, only the half which is shaded in Fig. 9 had to be represented on the resistance-network analogue. By preliminary investigations on the analogue, it was established that the stress in the neighbourhood of the base AB is uniform, of value $p_0/4$ if p_0 is the uniform pressure over the part DE of the upper surface.

Evaluating the boundary conditions from equations (7) along the line AB, where $s = x$, $F_n = p_0/4$ and $F_s = 0$, one finds $X_B = X_0[1 - (x/a)^2]$ and $(\partial X/\partial x)_B = -2X_0x/a^2$, $X_0 = p_0a^2/8$ being the value of X_B at the point A. Continuing the boundary integration along the line BC, where $ds = dy$ and $dn = dx$, and $F_n = F_s = 0$, one obtains along BC these values: $X_B = 0$ and $(\partial X/\partial x)_B = -2X_0/a$. Similarly for the section CD of the upper boundary line $X_B = 2X_0[1 - (x/a)]$, $(\partial X/\partial x)_B = -2X_0/a$, and for the section DE: $X_B = X_0[7/4 - 4(x/a)^2]$, $(\partial X/\partial x)_B = 8X_0x/a^2$. Finally, one has for the line EA on account of symmetry, $(\partial X/\partial x)_B = 0$ and $(\partial \Phi/\partial x)_B = 0$.

These boundary conditions are realized in the analogue by impressing the voltages V_0, corresponding to p_0, along the section DE of the upper edge, and $V_0/4$ along the edge AB of the Φ-network, the section CE of the upper edge of the Φ-network bring connected to the zero point of the voltage supply system. The network studs along the boundary BC of the Φ-network are connected to the adjustable voltage sources described in Section 5. The resistances along the edges BC and EA of both networks, and the series resistances r are doubled in value, to represent the "free edges" where $\partial X/\partial n = 0$. Along the edges AB and CE of the χ-network, a low value resistance chain and series resistances r of values lowered in the same ratio (1 : 400) are used to achieve the prescribed boundary potential distribution without the disturbance caused otherwise by the shunting effect of the network. (N.B. no manipulation of the χ-potentials along these boundaries is needed as the correct potential distribution is established there automatically by the current flow from the Φ-network into the χ-network.) The simultaneous conditions $(\partial X/\partial n)_B = -2X_0/a$ and $X_B = 0$ along the edge BC of the χ-network are satisfied by setting up the conditions for $(\partial X/\partial n)_B$ and then adjusting the Φ_B-potentials until $X_B = 0$ is also fulfilled, as discussed in Section 4. The prescribed boundary gradient $-2X_0/a$ is established (see Appendix) by feeding in currents of value $-2X_0h/aR'$ at each boundary node along the edge BC of the χ-network. This is most easily achieved by connecting each of the boundary nodes of the χ-network to the terminal $-V_0$ of the voltage supply system through a series resistance of value r'. From equations (6) and (16) and the value $X_0 = p_0a^2/8$, one finds $-2X_0h/aR' = -aV/4hr$, hence $r' = 4hr/a$. In the model used, $a = 8h$, and thus $r' = r/2$. The "level setter" resistances (L_1 and L_2 in Fig. 6) were set to such values that, in measuring the χ-potentials with the potentiometer bridge Br (Fig. 6), $X_0 = 0{\cdot}5000$, the maximum value of X (at point E) then being $0{\cdot}8750$.

The results of the investigation are shown in Figs. 10(a), 10(b).

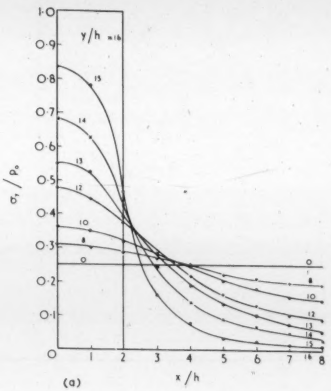

Fig. 10(a) Downward pressure distribution σ_y/p_0 for several planes y/h = constant for partially-loaded square block, as found by the resistance-network analogue method

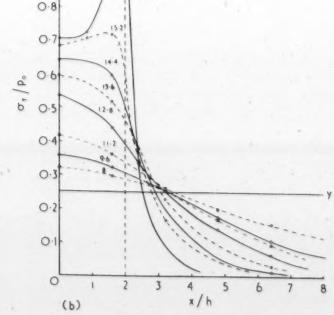

Fig. 10(b). Downward pressure distribution σ_y/p_0 for several planes y/h = constant for partially-loaded square block, as found by the photoelastic method (Coker and Filon)

– – – ○ – – – = Coker and Filon's measuring points.

11 and 12. In Fig. 10(*a*), the relative stress component σ_y/p_0 is plotted as a function of x/h for several values of y/h. It is instructive to compare the analogue solution with the solution of the same problem through the photoelastic method by

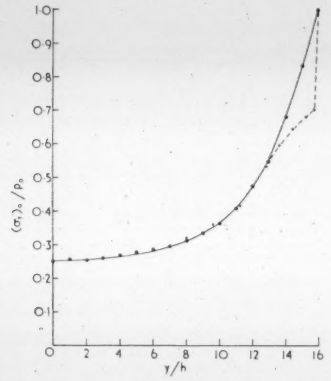

Fig. 11. Downward pressure distribution $(\sigma_y)_0/p_0$ along line of symmetry as function of height within partially-loaded square block, as found by the photoelastic method (– – + – –) (Coker and Filon), and by the resistance-network analogue method (— ○ —)

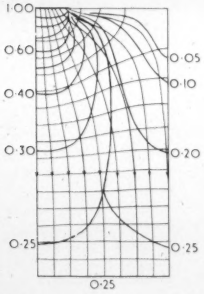

Fig. 12. Stress trajectories (thin lines) and contours of equal values of major principal stress p_1/p_0 (thick lines) for partially loaded square block, as computed from the resistance-network analogue solution ("arrowed" stress trajectories associated with p_1)

Coker and Filon.[15] Fig. 10(*b*) is Fig. 4·243 (p. 360) of their *Treatise on Photoelasticity*,[15] redrawn on a common base line, and with the same co-ordinates as in Fig. 10(*a*). It will be noticed that the two sets of curves resemble each other fairly closely. The most noticeable difference is the rise of the stress, in Coker and Filon's results, towards the edge of the loaded area; in the analogue result, the stress always drops away monotonically from a maximum located on the line of symmetry through the centre of the loaded area. Apparently, the desired condition of uniform loading of part of the top surface of the block was not completely achieved in Coker and Filon's experiments [see their remarks on p. 361, Ref. (15)]. Where the effect of the uneven loading in Coker and Filon's experiment has died away, the agreement between the two results is very good [compare, e.g. the curves $y/h = 13$ in Fig. 10(*a*) and $y/h = 12{\cdot}8$ in Fig. 10(*b*)].

A comparison of the stresses along the line of symmetry, as measured by the photoelastic and network analogue methods, is given in Fig. 11. A more complete picture of the state of stress due to the partial loading is given in Fig. 12, which shows the stress trajectories and lines of equal maximum principal stress, based on the computation of σ_x, σ_y and τ_{xy} from the analogue measurements for all mesh points. Again, there is a good agreement with the data given by Coker and Filon [their Fig. 4·242, p. 359 of Ref. (15)], the analogue results being rather more extensive.

As a further check on the evaluation of the results from the analogue solution of the χ-function, the integral $\int_0^a \sigma_y\,dx$, representing the total downward pressure transmitted by each plane $y =$ constant, was computed for all seventeen values of $y/h = 0$ to $y/h = 16$. The integral was found to be constant, as it should be, within better than 0·5%.

To confirm that the analogue boundary gradients $(\partial\chi/\partial x)_B$ are in fact 0 and $-2\chi_0/a = -0{\cdot}1250$, the values of $(\partial\chi/\partial x)_B$ were evaluated from the first and third differences, the missing "fictitious" χ-values outside the boundary needed for the formation of the third differences being inserted from the measurements on the Φ-network. The errors in $(\partial\chi/\partial n)_B$ were in the range $\pm 0{\cdot}0009$, consistent with an accuracy of about $\pm 0{\cdot}0003$ in the χ-measurement, and showing that the principle of the analogue representation of boundary gradients is correct.

(*b*) *Cross-bar under tension.* As a typical problem of type (ii), a cross-bar under uniform tension p_0, applied to the ends of the vertical member, as shown in Fig. 13(*a*), was investigated. On account of symmetry, one quarter only of the cross-bar (shown shaded) had to be represented on the resistance-network. At first, a relatively small-scale model was used, in which the half width a of the cross-bar was only $a = 3h$, but it was soon realized that this mesh is too coarse to allow a sufficiently good representation of the fillet (radius of curvature ρ), and the model was enlarged to the size shown in Fig. 13(*b*), for which $a = 6h$. Three cases,

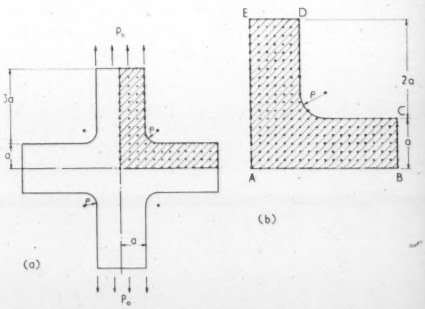

Fig. 13. (*a*) Cross-bar under tension (first model, 89 mesh points). (*b*) Investigated section of cross-bar (second model, 218 mesh points)

$\rho = a$, $\rho = a/2$ and $\rho = a/4$ were studied. The network modifications necessary to represent the fillet were computed by the rules given in earlier work, as mentioned at the end of Section 5. In the first case, the total number of mesh points in each network was 223, in the other two cases 218. The

resistance values used in the case $\rho = a/2$ are shown in Fig. 14.

The boundary conditions for this problem are derived as in the previous example. Along the line AB of Fig. 13(b), $(\partial\chi/\partial n)_B = 0$ and $(\partial\Phi/\partial n) = 0$, owing to symmetry. Along BC, $F_n = 0$ and $F_s = 0$, hence $(\partial X/\partial s)_B = (\partial X/\partial y) = 0$,

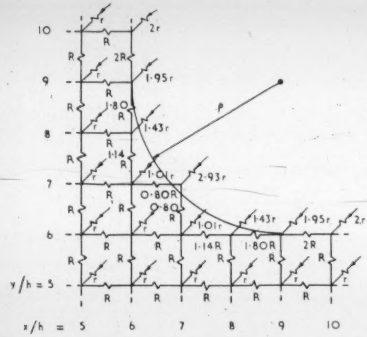

Fig. 14. Resistance-network representation of fillet ($\rho = a/2$)

and $\chi_B = \text{constant} = \chi_0$, with $(\partial X/\partial x)_B = 0$. Similarly, along CD, $(\partial X/\partial n)_B = 0$ and $(\partial X/\partial s)_B = 0$, whence $\chi_B = \text{constant} = \chi_0$. Along DE, $F_n = p_0$; upon integration with respect to $s = a - x$, here $\chi_B = \chi_0[2(x/a) - (x/a)^2]$, and $(\partial X/\partial x)_B = (2\chi_0/a)[1 - (x/a)]$. It also follows from $(\partial^2\chi/\partial x^2)_B = p_0$ that $\chi_0 = -p_0a^2/2$. Along EA, $(\partial\Phi/\partial n)_B = 0$ owing to symmetry and $F_s = 0$, hence $(\partial X/\partial n)_B = \text{constant} = -2\chi_0/a$.

The realization of these boundary conditions in the resistance-network analogue is similar to that of the previous example. The boundary gradients in the χ-network along EA are again established by feeding in currents, from the negative terminal of the voltage source ($V = -V_0$) through series resistances r'. It is then found, as in the other example, that $r' = (h/a)(V_0/\Phi_0)r$, where Φ_0 is the potential on the Φ-network corresponding to the traction p_0. In the present case, it is convenient to make $\Phi_0 = V_0/2$, say, and as $a = 6h$, $r' = r/3$. The simultaneous boundary conditions $\chi_B = \chi_0$ and $(\partial\chi/\partial n)_B = 0$ along BD are achieved by setting up $(\partial\chi/\partial n)_B = 0$, and adjusting the Φ_B values until $\chi_B = \chi_0$ everywhere. Along the edge DE, a low resistance potentiometer chain is connected, resulting in the establishment of the desired boundary values, and the level setter resistances L_1 and L_2 (Fig. 6) are always adjusted during the progress of the work to make the χ_B value at the corner D [Fig. 13(b)] equal to $\chi_0 = 1{\cdot}0000$ in terms of the potentiometer bridge reading, the zero point of the bridge being connected to point E of the model.

Two to four independent runs were taken for each different value of the corner radius ρ, starting each run with an arbitrary initial setting of the Φ_B-adjustment potentiometers along BD. Agreement between the solutions obtained in the separate runs for each value of ρ was very satisfactory, the difference of the solutions for χ being a few units in the fourth decimal place. It was invariably found that the mesh value at the centre of the fillet could not be brought more closely to the prescribed value χ_0 than about 0·8%, and that errors of about 0·2% have to be tolerated at its two neighbours along the boundary if the achievement of the correct value χ_0 within an accuracy of 0·05% at all other boundary points is required. These errors near the centre of the fillet appear to be of a systematic nature, and are thought to be due to the network inaccuracies caused by the modifications needed to represent the fillet. In evaluating the stress components from the χ-function, graphical smoothing was employed to eliminate the influence of these errors, and a cross-check of σ_y near the fillet from the constancy of $\int \sigma_y dx$, and of $(\sigma_x + \sigma_y)$ from the independently measured Φ-distribution, confirmed that the smoothed χ-values were reliable.

The reproducibility of results is illustrated by Table 2, which gives the maximum value of the sum of the stress components (or principal stresses) for two runs each for each value of ρ. The internal consistency is demonstrated by the comparison of $(\sigma_x + \sigma_y)/p_0$, calculated from the χ-distribution, and of Φ/Φ_0 measured directly in the Φ-network. The results given in Table 2 are typical for other points also;

Table 2. *Typical check of* $(\sigma_x + \sigma_y)$ *against* Φ (*at position opposite centre of curvature*)

Case	ρ/a	*Co-ordinate*	*Run*	$(\sigma_x + \sigma_y)/p_0$	Φ/Φ_0
I	0·25	$x/a = 1$, $y/a = 1{\cdot}25$	1st	1·71	1·69
			2nd	1·69	1·67
II	0·5	$x/a = 1$, $y/a = 1{\cdot}5$	1st	1·59	1·62
			2nd	1·56	1·59
III	1·0	$x/a = 1$, $y/a = 2$	1st	1·38	1·38
			2nd	1·41	1·39

from comparisons of this kind, the errors in the evaluated stress distribution can be estimated to be within ±2%.

The values of the maximum stresses found by the analogue method can be compared with those obtained by Willemze,[16] using the photoelastic method. He estimated his errors to be of the order of ±5%, and Table 3 shows that, within this

Table 3. *Comparison of maximum stresses by photoelastic and resistance-network methods*

Case	ρ/a	*By resistance-network* (±2%) p_1	*Photoelastic* (±5%) [*Willemze*[16]] p_1
I	0·25	1·60	1·64
II	0·5	1·52	1·47
III	1·0	1·33	(1·35)*

* By extrapolation.

accuracy, agreement between both methods is very satisfactory. The relatively low value of p_1 found by the analogue method for Case I may be partly due to the fact that the mesh size used is really too coarse for the radius $\rho = a/4$.

The result of the full analysis of the stress distribution, based on the analogue solution for the χ-function, is given for the case $\rho = a/2$ in Figs. 15 to 19. The same analysis has been carried out for the other two cases $\rho = a/4$ and $\rho = a$, but the results are of a sufficiently similar character to those obtained for $\rho = a/2$ (see Tables 2 and 3) that they do not justify reproduction here. Fig. 15 shows the lines of equal values of $(\sigma_x + \sigma_y)/p_0 = \Phi/\Phi_0$, obtained by interpolation along the curves $\Phi(x)$ for $y = \text{constant}$, and $\Phi(y)$ for $x = \text{constant}$, drawn from the Φ-values measured at the mesh points. The two stress components σ_x and σ_y are represented separately in a similar manner in Figs. 16 and 17, whereas the shear stress τ_{xy} is given in Fig. 18. From σ_x,

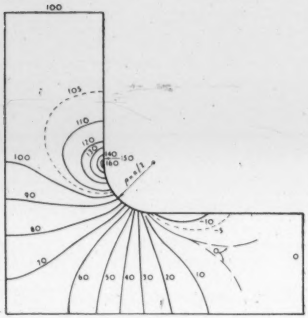

Fig. 15. Contours of equal values of $\Phi/\Phi_0 = (\sigma_x + \sigma_y)/p_0$ for cross-bar under tension with $\rho = a/2$

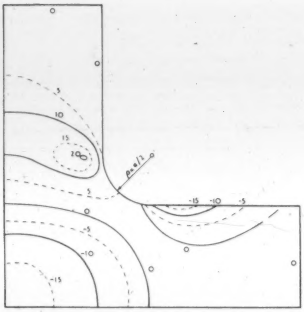

Fig. 16. Contours of equal values of σ_x/p_0 for cross-bar under tension, with $\rho = a/2$

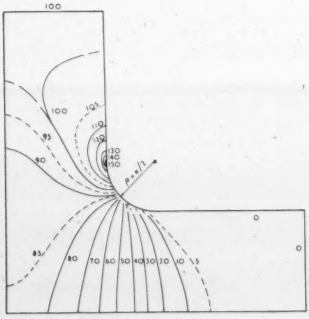

Fig. 17. Contours of equal values of σ_y/p_0 for cross-bar under tension, with $\rho = a/2$

σ_y and τ_{xy}, the values and directions of the principal stresses p_1/p_0 and p_2/p_0 were calculated. These are shown in Fig. 19 as stress trajectories (thin lines). The contours of equal values of the major principal stresses are shown by the heavy lines in Fig. 19. It is worth noting that the points of

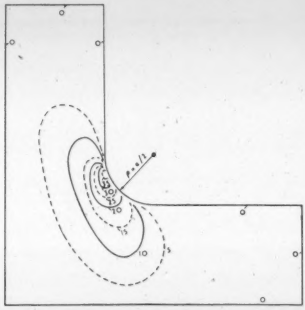

Fig. 18. Contours of equal values of shear stress τ_{xy}/p_0 for cross-bar under tension with $\rho = a/2$

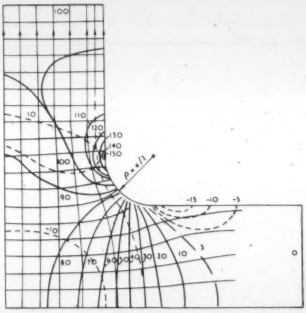

Fig. 19. Stress trajectories (thin lines) and contours of equal values (in per cent) of major principal stress p_1/p_0 (heavy full lines), and minor principal stress p_2/p_0 (heavy broken lines) for cross-bar under tension, with $\rho = a/2$ ("arrowed" stress trajectories associated with p_1)

the maximum values of σ_x, σ_y, τ_{xy} and p_1 are not coincident but closely grouped together at or near the boundary nearly opposite the centre of curvature of the fillet. The positions of these points are of course only approximately known, as they were obtained by graphical interpolation between the values at the mesh nodes.

10. CONCLUSION

In this paper, the principle of a new resistance-network analogue method for stress analysis has been discussed, and it has been shown how far the application of the method has progressed until now. The results of several investigations have demonstrated that the new method can give results as

reliable and as accurate as the previously known methods (numerical or photoelastic), whilst being faster and simpler to handle. It has also been indicated how measurement errors or truncation errors can be reduced, either by an extension of the analogue technique or by combining it with the existing numerical methods. While a more refined technique is required in this new field of application of the resistance-network analogue than was needed in the solution of the simpler second-order partial differential equations, the examples given demonstrate that the technique has been developed far enough already so that problems of moderate difficulty can be solved. There are obvious improvements in the analogue apparatus and its associated measuring technique which can be made. However, much remains to be learned about the best way of solving problems of greater complexity, and particularly about the establishment of the correct boundary conditions in problems where not tractions but displacements of the boundary are the given data.

The discussion of the network analogue relations has also indicated that the new analogue technique is applicable to the solution of many other problems in elasticity described by a fourth-order partial differential equation, like the bending or extension of plates. Here again, the main difficulty often resides in the enforcement of the required boundary conditions, as was shown by some exploratory experiments.

ACKNOWLEDGEMENTS

The author is indebted to Mr. P. J. Pollock, of the Research Department, Metropolitan-Vickers Electrical Co. Ltd., for many helpful discussions on various aspects of stress analysis, and for suggesting the investigation of the problem, example (*b*), Section 9. The author also wishes to thank Mr. A. C. Heath for his help in the construction of the analogue apparatus, and for taking many of the measurements, Miss P. Rush and Mr. R. K. Taylor for the numerical analysis of the measured data, and Dr. T. E. Allibone, Director of the Laboratory, for permission to publish this paper.

REFERENCES

(1) Fox, L., and Southwell, R. V. *Phil. Trans A*, **239,** p. 419 (1945).
(2) Christopherson, D. G. *Brit. J. Appl. Phys.*, **3**, p. 65 (1952).
(3) Allen, D. N. de G. *Relaxation Methods* (London: McGraw-Hill Publishing Co. Ltd., 1954).
(4) Liebmann, G. Lecture before the Stress Analysis Group of The Institute of Physics (March, 1953).
(5) Liebmann, G. *Nature* [*Lond.*], **172,** p. 78 (1953).
(6) Redshaw, S. C. *Aero. Res. Coun.* (*Min. of Supply*) *Rep., Mem.* 15335 (1952).
(7) Boscher, J. *C.R. Acad. Sci.* [*Paris*], **236,** p. 44 (1953).
(8) Liebmann, G. *Brit. J. Appl. Phys.*, **1,** p. 92 (1950).
(9) Liebmann, G. *Nature* [*London*], **164,** p. 149 (1949).
(10) Liebmann, G., and Bailey, R. *Brit. J. Appl. Phys.*, **5,** p. 32 (1954).
(11) Liebmann, G. *Proc. Instn Elect. Engrs*, **99** (IV), p. 260 (1952).
(12) Liebmann, G. *Brit. J. Appl. Phys.*, **5,** p. 362 (1954).
(13) Fox, L. *Proc. Roy. Soc. A*, **189**, p. 535 (1947).
(14) Fox, L. *Phil. Trans A*, **242,** p. 345 (1950).
(15) Coker, E. G., and Filon, L. N. G. *A Treatise on Photoelasticity* (London: Cambridge University Press, 1931).
(16) Willemze, F. G. *De Ingenieur*, No. 1, *Tech. Wetensch. Onderz.* 1 (T.N.O.) (1946).

APPENDIX

Boundary gradients in resistance-network analogues for solving the biharmonic equation $\nabla^4\chi = 0$. Consider the square mesh arrangement $P_0 \ldots P_{12}$ shown in the diagram, Fig. 2, and let P_0 be the boundary point where $\partial\chi/\partial n = \partial\chi/\partial x = 0$ is prescribed, the boundary passing parallel to the y-axis through the points $P_{10} \ldots P_{12}$. To represent the boundary condition $\partial\chi/\partial n = 0$, both networks are terminated along the boundary by breaking the resistance connexions to points outside the boundary, i.e. along line $P_0 - P_1$, etc., and doubling the resistance values along the boundary, between points P_0 and P_2, etc. This is equivalent to assigning values to the functions at the "fictitious" nearest points outside the boundary which are equal to those at the corresponding nearest points inside the boundary (as in relaxation), i.e.

$$\Phi_3 = \Phi_1, \quad \Phi_7 = \Phi_6, \quad \Phi_8 = \Phi_5 \tag{26}$$

and

$$\chi_3 = \chi_1, \quad \chi_7 = \chi_6, \quad \chi_8 = \chi_5 \tag{27}$$

Substitute in $\Phi_3 = \Phi_1$, i.e. $(\nabla^2\chi)_3 = (\nabla^2\chi)_1$, the usual finite difference approximation

$$\chi_0 + \chi_7 + \chi_{11} + \chi_8 - 4\chi_3 - \frac{h^2}{12}\left(\frac{\partial^4\chi}{\partial x^4} + \frac{\partial^4\chi}{\partial y^4}\right)_3 = \chi_0 + \chi_5 + \chi_9 + \chi_6 - 4\chi_1 - \frac{h^2}{12}\left(\frac{\partial^4\chi}{\partial x^4} + \frac{\partial^4\chi}{\partial y^4}\right)_1$$

In view of equation (27), this can be written

$$\chi_{11} - \chi_9 - 4\chi_3 + 4\chi_1 + 0\delta_0^{(5)} = 0 \tag{28}$$

where $\delta_0^{(n)}$ is the nth difference with respect to x of the function χ, taken at the point P_0. Equation (28) can be rewritten as

$$\delta_0''' - 4\delta_0' + 0\delta_0^{(5)} = 0 \tag{29}$$

As $\delta_0' = 0$, it follows that

$$\delta_0''' = 0\delta_0^{(5)} \tag{30}$$

Hence, the lowest order term neglected in the setting up of the boundary condition $\partial\chi/\partial n = 0$ in the resistance-network analogue for solving the biharmonic equation is of the order of the 5th difference, i.e. one order higher than the difference approximation of the biharmonic equation itself (as is the case with the Laplace equation). The use of the correct network termination at the boundary, as described, is therefore equivalent to the introduction of two "fictitious" external mesh points for each boundary point, and the smoothing technique,[1] required when only one "fictitious" external boundary point is used in relaxation, is not needed in the analogue method.

If $\partial\chi/\partial n \neq 0$, e.g. $\partial\chi/\partial n = g$, is prescribed, this can be established in the network method by feeding at the boundary points of the χ-network currents into the network of value $I_0 = g_0 h/R$, etc. By a similar reasoning as before, one establishes that, with $g_0 = (\chi_1 - \chi_3)/2h$,

$$(\partial\chi/\partial n)_0 = g_0 - \tfrac{1}{6}\Delta_0'' + 0\delta_0^{(5)}$$

where $\delta_0^{(5)}$ is the fifth difference of χ, as before, and Δ_0'' is the second difference of the boundary gradient taken along the boundary

$$\Delta_0'' = g_2 + g_4 - 2g_0$$

If this term should be of any significance, a correction for this can be made by modifying slightly the fed-in currents I_0.

The resistivity of thin metallic films

By D. E. CLARK, Ph.D., A.Inst.P., Physics Department, The Northern Polytechnic, London, N.7

[*Paper first received* 6 *December*, 1954, *and in final form* 11 *February*, 1955]

The resistivities of thin films of antimony and of bismuth have been measured by direct current and at frequencies of $0{\cdot}92 \times 10^{10}$ c/s and $2{\cdot}65 \times 10^{10}$ c/s. For bismuth films the resistivity measured by microwaves was found to be about 0·8 times that measured by direct current. For antimony films there appears to be no systematic difference between these values.

Considerable experimental work has been undertaken on the determination of the resistivities of thin metallic films. Most of the measurements have been made with direct current (see, for example, Van Itterbeek[1]), though more recently resistivities have been determined at high radiofrequencies.[2,3] The object of the present series of observations was to compare the resistivities of antimony and bismuth films at microwave frequencies with the values measured by direct current. Most of the previous measurements on the electrical properties of thin films have been made with the films in a vacuum chamber continuously evacuated. Because of the experimental difficulty of making microwave measurements in a vacuum with apparatus readily available, all the present observations were made with films removed from the coating unit.

EXPERIMENTAL METHODS

All films were prepared by evaporation under reduced pressure using a conventional vacuum evaporation unit, the substrate for each film being a glass cover slip about 0·1 mm thick. The pressure in the coating unit was allowed to fall to the same value (0·6 μ) before any evaporation process was commenced, and the rate of evaporation, about 4 mg of metal per min, was adjusted to be approximately the same for all films deposited. In general, for each mass of metal

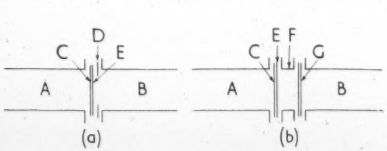

Fig. 1. Specimen mountings

(*a*) Method for measurement at $0{\cdot}92 \times 10^{10}$ c/s; (*b*) method for measurement at $2{\cdot}65 \times 10^{10}$ c/s.

A, standing wave detector; *B*, short-circuit section; *C*, metal film; *D*, diaphragm; *E*, glass substrate; *F*, quarter-wave section; *G*, cover slip compensator.

evaporated three films were prepared, one for each of the microwave measurements and one for direct current measurement. The film for direct current measurement was deposited between electrodes of silver which had been formed by a previous evaporation process.

For measurement at $0{\cdot}92 \times 10^{10}$ c/s the capacitative effect of the glass substrate was compensated by the use of an inductive diaphragm of aluminium foil, and, in the case of measurement at $2{\cdot}65 \times 10^{10}$ c/s, by the use of an identical cover slip separated from the test sample by a section of waveguide one-quarter of a guide wavelength long. Each waveguide test bench consisted of a klystron oscillator operated from a stabilized power supply, variable attentuator, wavemeter, standing-wave detector and an adjustable short-circuiting plunger, the distance of which from the film under test was adjusted to be one-quarter of a guide wavelength. The methods of mounting the specimens are shown in Fig. 1.

During all measurements the power used was sufficiently small for the observed resistivity to be independent of the current in the film.

CALCULATION OF RESULTS

The film under test was placed one-quarter of a wavelength from the short-circuit termination and was thus at a point of infinite impedance. Consequently, the nature of the standing-wave pattern existing on the generator side of this film gave directly the wave impedance, z_s, at that surface of the film nearer the generator. It is shown below [equation (9)] that the value of this impedance enables the resistivity of the metal to be calculated.

Let z_0, γ and l be respectively the characteristic wave impedance, propagation constant and thickness of the metal film. Then z_s, the wave impedance at the generator side of the film, is given by:

$$z_s = z_0 \coth \gamma l \tag{1}$$

For the H_{01} mode of vibration we have

$$\gamma^2 = (\pi/a)^2 - \omega^2\mu\epsilon[1 - (j\sigma/\omega\epsilon)] \tag{2}$$

also

$$z_0 = j\omega\mu/\gamma \tag{3}$$

where a is the width of the waveguide,

$\omega/2\pi$ is the frequency of vibration,

and μ, ϵ, σ are respectively the permeability, permittivity and conductivity of the metal.

Making the assumptions that $\sigma/\omega\epsilon \gg 1$ and $\omega\mu\sigma \gg (\pi/a)^2$ we have

$$\gamma = \sqrt{(j\omega\mu\sigma)} = \alpha + j\beta \tag{4}$$

and

$$z_0 = (1 + j)\sqrt{(\omega\mu/2\sigma)} \tag{5}$$

where

$$\alpha = \beta = \sqrt{(\omega\mu\sigma/2)} \tag{6}$$

Equation (1) may be written

$$z_s = z_0[\cosh(\alpha l + j\beta l)]/[\sinh(\alpha l + j\beta l)] \tag{7}$$

and making the assumption that for the films investigated $\alpha l \ll 1$ then

$$z_s \simeq z_0/\alpha l(1 + j) \tag{8}$$

Combining equations (3), (4), (5) and (8), we have

$$z_s = 1/\sigma l \tag{9}$$

To determine the thickness of any film, the piece of metal used in preparing that film was weighed before evaporation, and a film formed by the evaporation of about 2 g of metal was also weighed. The film thickness was assumed to be proportional to the mass of metal evaporated, and the density of the film was assumed to be that of the metal in bulk.

EXPERIMENTAL RESULTS

(i) *Antimony*. All the antimony films showed an initial decrease of resistance with time, and, in general, a small increase about an hour after formation. The initial decrease was greater for direct current than at microwave frequencies and in general was less marked the thicker the film. The results for two films are given in Table 1 and Fig. 2. In

Table 1. *Variation of resistance with time (antimony)*

Thickness of film = 98 Å				*Thickness of film* = 75 Å			
t (min)	R_1 (Ω)	R_2 (Ω)	R_3 (Ω)	*t* (min)	R_1 (Ω)	R_2 (Ω)	R_3 (Ω)
½	131	139	—	½	$>10^5$	—	—
1	—	—	126	2	10^4	416	—
2½	124	133	—	4	3000	350	320
3	—	—	121	6	1000	—	—
5	118	129	118	9	290	239	255
10	109	122	115	14	242	208	250
20	103	117	110	23	237	205	244
40	99	112	106	25	223	204	240
60	98·5	111	106·5	32	224	204	238
120	99	111	106	40	224	205	235
				60	225	206	235

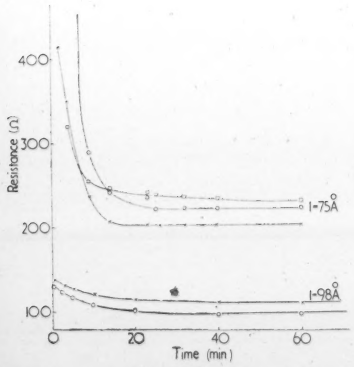

Fig. 2. Variation with time of resistances R_1, R_2 and R_3 (antimony films)

○ = d.c. values; × = values at $0{\cdot}92 \times 10^{10}$ c/s; □ = values at $2{\cdot}65 \times 10^{10}$ c/s.

Table 1, *t* is the time after formation of the film and R_1, R_2 and R_3 are the values of the film resistance per unit square obtained with direct current and at $0{\cdot}92 \times 10^{10}$ c/s and $2{\cdot}65 \times 10^{10}$ c/s respectively. The decrease of resistance with time is probably due to crystallization of these films deposited initially as amorphous layers.[4]

Table 2. *Variation of resistance with film thickness (antimony)*

Distance of films from heater = 26 cm. Assumed density of antimony = 6·68 g cm^{-3}

For 2·65 g evaporated, mass deposited on film (3·2 × 3·2 cm) = 7·8 mg

m (mg)	*l* (Å)	R_1 (Ω)	R_2 (Ω)	R_3 (Ω)	$\frac{1}{R_1} \times 10^5$ (Ω^{-1})	$\frac{1}{R_2} \times 10^5$ (Ω^{-1})	$\frac{1}{R_3} \times 10^5$ (Ω^{-1})
9·9	43	2000	2360	—	50	42·5	—
11·0	47	1690	1200	1410	59	83	71
11·8	51	893	847	1220	112	118	82
13·4	58	418	513	413	239	195	242
15·1	65	332	400	338	301	250	296
17·4	75	223	204	235	448	490	426
18·9	81	156	169	171	641	592	585
20·9	90	132	120·5	134	757	830	746
22·8	98	98·5	111	106·5	1016	901	940

The variation of the minimum resistance with film thickness is shown in Table 2 and Fig. 3. There appears no marked difference between the direct current and the microwave resistivities in the case of antimony. The resistivity of a film of thickness of 100 Å is approximately 1×10^{-4} Ω cm, that is greater than the resistivity of antimony in bulk by a factor of 2·5.

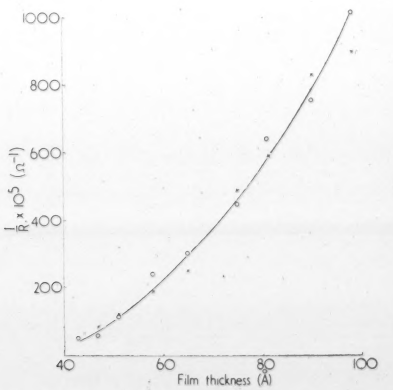

Fig. 3. Variation of resistance with film thickness (antimony)

○ = d.c. values; × = values at $0{\cdot}92 \times 10^{10}$ c/s.

In Tables 2 and 4, *m* is the mass of metal evaporated and *l* is the calculated thickness of the film.

(ii) *Bismuth*. Bismuth films of thickness less than about 45 Å showed an increase of resistance with time, the increase being greater for direct current than at microwave frequencies. An approximately linear relation between thickness and the reciprocal of film resistance was found to hold. The experimental results are expressed in Tables 3 and 4 and shown graphically in Figs. 4 and 5. For the 24 and the 42·5 Å films, the resistances given in Table 4 are those initially observed. The resistances of all other bismuth films appeared constant with time. The increase of resistance of the thin films may be due to their tendency to form small grains.

The resistivities calculated from Table 4 are approximately $43 \times 10^{-5}\ \Omega$ cm for direct current measurement and $36 \times 10^{-5}\ \Omega$ cm for measurement at $0{\cdot}92 \times 10^{10}$ c/s, that is the resistivities of the films are greater than the resistivity of bismuth in bulk by factors of 3·6 and 3·0 respectively for direct current and microwave determinations.

Table 3. *Variation of resistance with time (bismuth)*

Thickness of film = 42·5 Å

t (*min*)	2	5	10	15	26	46	61	74	101	130	160	200
R_1 (Ω)	829	842	858	863	893	941	958	982	1012	1026	1041	1056
R_2 (Ω)	706	710	716	719	735	748	753	—	759	761	765	771

Table 4. *Variation of resistance with film thickness (bismuth)*

Distance of films from heater = 17·3 cm. Assumed density of bismuth = 9·8 g cm^{-3}

For 2·09 g evaporated mass deposited on film (3·2 × 3·2 cm) = 13·5 mg

m (*mg*)	*l* (Å)	R_1 (Ω)	R_2 (Ω)	R_3 (Ω)	$\frac{1}{R_1} \times 10^5$ (Ω^{-1})	$\frac{1}{R_2} \times 10^5$ (Ω^{-1})	$\frac{1}{R_3} \times 10^5$ (Ω^{-1})
3·8	24	1160	1516	—	86	66	—
6·6	42·5	820	704	—	122	142	—
8·6	55	543	662	660	184	151	151
14·4	93	433	364	358	231	275	279
19·9	128	325	290	272	308	345	368
22·2	143	—	252	258	—	397	387
26·3	169	256	219	—	391	457	—
31·2	201	211	176	—	474	568	—
38·6	249	172	146	—	581	685	—
46·3	298	146	123	—	685	813	—
56·8	366	119	99	—	840	1010	—

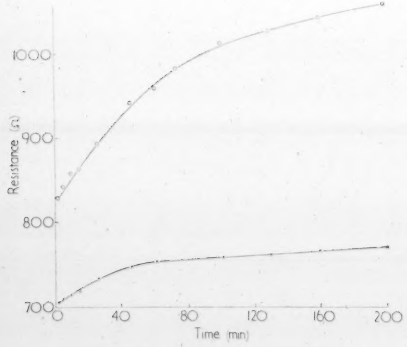

Fig. 4. Variation with time of resistances R_1 and R_2. Bismuth film thickness 42·5 Å

○ = d.c. values; × = values at $0{\cdot}92 \times 10^{10}$ c/s.

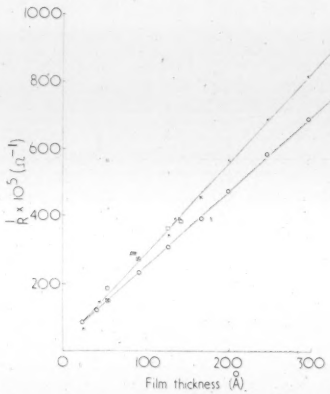

Fig. 5. Variation of resistance with film thickness (bismuth)

○ = d.c. values; × = values at $0{\cdot}92 \times 10^{10}$ c/s; □ = values at $2{\cdot}65 \times 10^{10}$ c/s.

ACKNOWLEDGEMENT

The author is indebted to the Director, Radar Research Establishment, for the loan of some of the 1·2 cm band equipment used in these observations.

REFERENCES

(1) VAN ITTERBEEK, A. *Low Temperatures*, p. 118 (London: Physical Society, 1947).

(2) TISCHER, F. J. *Z. Angew. Phys.*, **5**, p. 413 (1953).

(3) BROUDY, R., and LEVINSTEIN, M. *Phys. Rev.*, **94**, p. 285 (1954).

(4) SAKURAI, T., and MUNESUE, S. *Phys. Rev.*, **85**, p. 921 (1952).

Desorption of gas in the cold cathode ionization gauge

By E. Brown, B.Sc., and J. H. Leck, M.Eng., A.M.I.E.E., Department of Electrical Engineering, The University of Liverpool

[*Paper first received* 16 *December*, 1954, *and in final form* 4 *February*, 1955]

In this work desorption of gas in the cold cathode ionization gauge by positive ion bombardment has been studied. Mass spectrometer measurements have shown an interesting exchange process to take place at the cathode of the gauge. Incident ions with an energy of the order of 1000 eV drive off molecules already trapped at the surface and are themselves adsorbed. In addition to a careful study of this phenomenon a further clean-up mechanism has been noticed, in which gas is held in the interior of the electrodes. These two clean-up reactions take place simultaneously.

These phenomena are probably not confined to the cold cathode ionization gauge but take place whenever surfaces are exposed to ion bombardment and are therefore of fairly general interest.

The work described in this paper follows upon some earlier qualitative observations of gas clean-up in the Penning-type cold cathode ionization gauge.[1] In the previous work there was no apparatus available to study either the gas composition in the system or the desorption by the discharge. It was, however, observed that large quantities of gas, approximately the total quantity taken up by running the discharge, could be recovered by heating the gauge envelope. The present work has been undertaken to investigate the desorption which takes place both by heating and also by the ion bombardment itself. One improvement in the technique has been made by introducing a mass spectrometer to measure pressure. This enables the sorption and desorption of a single element in a complex gas mixture to be followed, because partial pressures down to 10^{-10} mm of mercury can be recorded even with the total pressure as high as 10^{-5} mm of mercury.

The work has been confined to a cylindrical anode gauge of the type described by Penning and Nienhuis in 1949.[2] This discharge tube is a simple and convenient ion source providing a positive ion current of the order of 10 μA at a pressure of 10^{-6} mm of mercury. Unfortunately results for various positive ion swarm energies cannot be obtained with this discharge because the ion energy distribution has not been measured and it is not easy to control the cathode temperature independently of the discharge.

APPARATUS

Penning gauges with electrodes of nickel, molybdenum and aluminium were used, each having an anode approximately 2 cm long and 2 cm in diameter. The envelopes were of Pyrex glass, connexion to the main vacuum manifold being by a glass tubulation and a glass-to-metal seal. The vacuum pumping system shown diagrammatically in Fig. 1 consisted of Metrovac O3B and O2 diffusion pumps (by Metropolitan-Vickers Electrical Co. Ltd.) in cascade with a small single-stage (Metrovac S.R.2) rotary pump, a solid carbon dioxide vapour trap being placed between the Penning gauge and the diffusion pumps. The gas composition and pressure in the Penning gauge could be controlled by passing gas from a two litre reservoir vessel through a porous plug into the main vacuum system, the pressure in the manifold being approximately proportional to that in the reservoir, 10^{-5} mm of mercury in the manifold corresponding to a reservoir pressure of the order of a few mm of mercury.

A 90° deflexion mass spectrometer with a Nier-type source and fixed magnetic field was used throughout this work. This instrument, which is similar in most respects to the commercial M.S.3 machine (manufactured by the Metropolitan-Vickers Electrical Co. Ltd.), resolved up to mass 90 and, with an automatically stabilized high-voltage supply and a high gain d.c. amplifier, proved capable of partial pressure measurements of less than 10^{-10} mm of mercury. The spectrometer tube connected directly to the pumping manifold without intermediate valves or constrictions. An

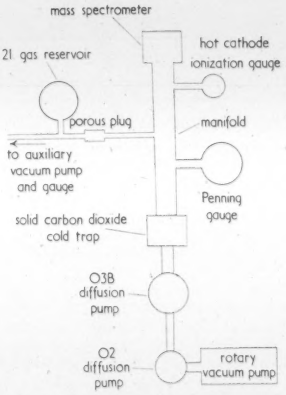

Fig. 1. Schematic diagram of apparatus

ordinary hot cathode ionization gauge, type 29D2 (by Edison Swan Electric Co. Ltd.), was included in the vacuum system to measure the total pressure, the pumping speed at the manifold and also for calibrating the mass spectrometer. [The pumping speed for any gas could be obtained by measuring the increase in pressure in the manifold due to a known flow of gas through the porous plug, the gas flow being calculated from an observation of the rate of fall of pressure in the reservoir. By definition, the pumping speed of the manifold is given by the ratio (gas throughout)/(gas partial pressure).]

The mass spectrometer and the connecting pipe work could be baked to 100° C and the glass bulb of the Penning gauge to 400° C. A radio-frequency induction heater enabled the gauge electrodes to be heated to about 1000° C. After 100 hours pumping with the mass spectrometer tube and the

gauge envelope baked continuously the residual gases were found, as expected, to consist largely of water and hydrocarbon vapours. Water vapour, the largest of the residuals, was of the order of 10^{-8} mm of mercury. The air pressure was negligibly small, always less than 10^{-9} mm of mercury. The residual spectrum was similar to that reported by Blears[3] for an almost identical vacuum system, the total pressure being a factor of two or three times greater in the present work, probably because of the rather less stringent pumping cycle.

In most cases spectroscopically pure gas samples were used in the following experiments. In every sample, mass spectrometer measurements showed the total impurity to be less than 0·1%, except for krypton which had a 1% xenon impurity.

EXPERIMENTAL PROCEDURE AND RESULTS

The following procedure was adopted to obtain successive sorption and desorption in the Penning gauge. Sorption was first achieved by running the discharge in a particular gas for a given time. Then, after switching off the discharge and removing the gas sample from the vacuum system, the molecules taken up by the discharge tube were recovered by restarting the discharge in another gas. The desorption rate, observed by means of the mass spectrometer, rose to a maximum immediately after restarting the discharge, and then fell off exponentially to zero in a period of from 20 to 60 min. If, after some minutes operation in the second gas, the gas composition in the discharge was changed, either to the original or some other gas, molecules of the second gas were immediately recovered from the Penning gauge. This desorption by the discharge was observed for all the gases used in these experiments, i.e. helium, neon, argon, krypton, hydrogen, nitrogen, oxygen and carbon dioxide.

The rate of outgassing did not depend to any appreciable extent upon either the applied voltage (between 500 and 4000 V), the magnetic field strength (between 300 and 600 G), or the gas composition in the discharge, with the exception of hydrogen. The outgassing was comparatively inefficient with hydrogen, even with 4 kV anode-cathode voltage drop. (The effect of voltage variation could only be observed down to 500 V as a stable discharge could not be maintained below this point.)

Although the desorption rate depended upon the discharge current the total quantity of gas recovered was independent of this current. Typical desorption characteristics of argon in a nitrogen discharge plotted in Fig. 2 illustrate the general shape of all characteristics, and in particular show that, with the reduced discharge current, desorption takes place at a reduced rate but for a longer time.

The total gas recovered depended almost entirely upon the previous sorption, both upon the type of gas taken up and also upon the discharge current and the operating time. The desorption characteristics obtained after having run the discharge in argon at 10 μA, for various times from 2 to 3000 min, are reproduced in Fig. 3. During the first few seconds of the desorption the argon pressure rose as high as 5×10^{-7} mm of mercury. After 30 min it was difficult to measure the desorption against the background pressure of argon in the spectrometer. The comparatively large background arises from the argon impurity in the nitrogen which, with the particular samples used in this experiment, was of the order of one part in ten thousand, thus giving a background pressure in the spectrometer of approximately 10^{-9} mm of mercury.

The total quantity of gas recovered in each desorption experiment (given by the area under the curves in Fig. 3 multiplied by the pumping speed) has been calculated and the

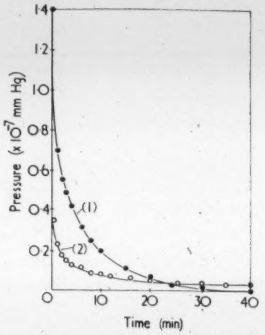

Fig. 2. Desorption of argon in a nitrogen discharge

Previous sorption of argon was in a discharge of 100 μA for 20 min. Discharge current in nitrogen: curve (1), 100 μA; curve (2), 15 μA.

values, expressed in units of litre microns, are tabulated with the curves in Fig. 3. Because of the difficulty in estimating the area under the curves these figures can only be approximate, the error probably being $\pm 10\%$. The main sources of error occur in estimating the gas removed during the first few seconds—when the pressure is high and changing

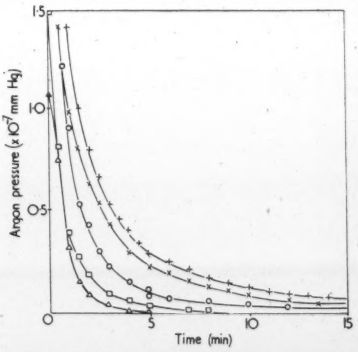

Fig. 3. Desorption of argon in a nitrogen discharge

The discharge current in the nitrogen was 100 μA. Previous sorption of argon was in a discharge of 10 μA for the times indicated in the key. The anode-cathode voltage of the Penning gauge was 2 kV for both sorption and desorption.

+ = 3000 min, 0·66 l.μ.; × 1000 min, 0·58 l.μ.; ○ = 20 min, 0·43 l.μ.; □ = 5 min, 0·19 l.μ.; △ = 2 min, 0·14 l.μ.

rapidly—and also in the long "tail," which may extend almost indefinitely. (The desorption curves are not sufficient approximations to the exponential to allow a simple formula to be used to calculate area.) The total quantity of gas

removed is plotted as a function of the product of discharge current × discharge time in Fig. 4, together with similar results for helium, neon, krypton, nitrogen and oxygen. The quantity of gas is here expressed in terms of the number of molecules rather than litre microns (1 l.μ at normal temperature contains $3{\cdot}54 \times 10^{16}$ molecules) and the discharge

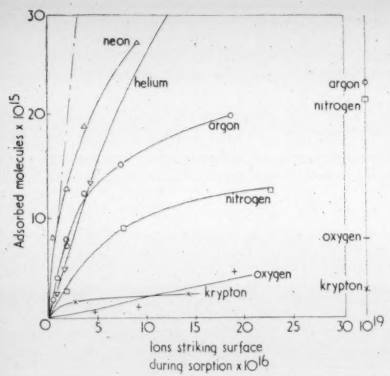

Fig. 4. The total number of molecules desorbed by positive ion bombardment in a nitrogen discharge

The values of ionic incidence quoted in Fig. 4 must be slightly high as the secondary electron emission has been neglected in estimating the ion current to the cathodes.

All the curves were obtained for a 2000 V discharge in the sorption and desorption.

current × time as the number of ions reaching the cathode (1 μA ion current for 1 min is equivalent to $3{\cdot}75 \times 10^{14}$ ions).

All the curves show a definite limit to the total quantity of gas which can be recovered. A large number of experiments have shown the maximum desorption to depend only upon the gas composition and not at all upon the discharge current, the anode-cathode voltage* or the magnetic field strength. The clean-up, however, only takes place in the presence of the discharge. Experiments with argon, nitrogen and oxygen showed that, even after leaving the gauge at a pressure of 10^{-5} mm of mercury for as long as 24 h, no measurable desorption could be observed either by ion bombardment or by radio-frequency heating. Thus, taking into account the limitations of the measuring equipment, the discharge increases the clean-up rate by at least four orders of magnitude.

The gas could be driven off by heating instead of by the ion bombardment. If, after sorption, the gauge envelope was heated to 100° C, desorption was just detectable. The rate of removal increased very rapidly with increasing temperature and at 200° C the total desorption could be completed in 20 min. The total quantity recovered was the same as that obtained by ion bombardment after the same sorption.

Radio-frequency heating showed that virtually all the gas was taken up at the cathodes. Either of the relatively small cathode disks could be heated to 1000° C without an appreciable rise in temperature of the anode. (The anode could not, however, be heated independently of the cathode.) After heating the cathodes for a few seconds to 1000° C no gas could be recovered in a subsequent ion bombardment. The gas must therefore be held at the cathodes, because during the heating the maximum temperature rise of the anode and gauge envelope was probably not more than 50° C.

Except for hydrogen and helium there was virtually no desorption at room temperature. The desorption characteristics were not affected by leaving the gauge under vacuum at room temperature for as long as 24 h between the sorption and the subsequent desorption, except for hydrogen and helium where the quantity recovered was only 50% of that expected. One particular experiment showed that allowing the gauge to reach atmospheric pressure for a few minutes immediately after the sorption of argon did not affect the subsequent desorption characteristic.

All the above experiments were carried out in turn for Penning gauges with the nickel, molybdenum and aluminium electrodes. The results were essentially the same in each case. The residual vacuum conditions were never of the highest order, and a significant residual of water vapour and hydrocarbon molecules was always present in the system. Thus clean cathode surfaces, such as are essential for the measurement of accommodation coefficient[4] and work function,[5] were never obtained. Throughout the period of the experimental work the residual vacuum varied appreciably; for example, in the initial stages some preliminary experiments were carried out under very poor vacuum conditions. The initial pump down and bake period was limited to 24 h and no radio-frequency heating of the electrodes carried out prior to starting the experiment. In the later work, however, a much longer bake time was allowed and the gauge cathodes heated to a dull red for 2 h before commencing the experiment. This change in the technique had no significant effect upon the results. During the early part of the work the discharge caused a continuous desorption of water vapour from the gauge, but in the later experiment—after thoroughly outgassing the electrodes—desorption of water vapour by the discharge fell almost to zero.

The sorption and desorption observed in the above experiments is almost certainly caused by a surface reaction. (This is discussed in the following section.) In addition to this adsorption there was seen to be an additional take-up of gas by the discharge, probably into the interior of the cathodes, these molecules being bound comparatively tightly to the metal so that they could not be dislodged by an ion bombardment or by a low temperature bake (to 200° C). Evidence of this second mechanism could be obtained with the present apparatus by heating the cathodes to a high temperature. For example, after sorption in argon for 24 h and subsequent desorption in nitrogen, a further quantity of argon could be driven out by heating the cathodes to 1000° C, the actual amount recovered depending upon the operation of the previous argon discharge. Fig. 5, showing the total quantity of gas taken up at the cathodes in the argon discharge (or more exactly that recovered by positive ion bombardment + a high temperature bake) plotted as a function of anode-cathode voltage, illustrates the dependence of the total clean-up upon the discharge voltage. The rate of clean-up by this second mechanism is initially slower than that at the surface, but even after 24 h there does not appear to be any saturation. Again in contrast to the surface reaction, the sorption rate depends upon the gas composition in the discharge. It is, for example, very much greater for nitrogen than for the inert gases. (This is in agreement with the previous experiments[1] which showed similar differences

* This is not exactly true for krypton or oxygen where the recoverable gas is 25% greater at 4 kV than at 2 kV.

of clean-up rate.) The different behaviour with respect to discharge voltage, current and time, and most important, to desorption by ion bombardment, suggests two very different

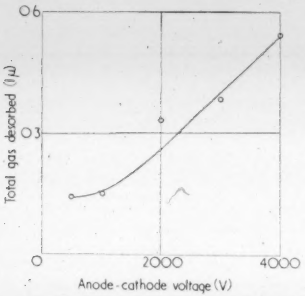

Fig. 5. Total quantity of argon recovered by heating the electrodes to 1000° C, after sorption in an argon discharge for 1000 min at 100 μA

(For these electrodes; molybdenum, the surface layer was 0·14 l.μ for all voltages between 0·5 and 4·0 kV.)

sorption mechanisms. Therefore, as it is both easy and convenient to separate the desorption mechanisms, only the surface clean-up is considered in this paper.

DISCUSSION OF RESULTS

The following deductions about the sorption–desorption mechanism can be made from the experimental results.

(*a*) Because the sorption and desorption is, to a first approximation, independent of the chemical nature of the gas or the metal surface, the molecules are probably bound to the cathode surfaces by Van der Waals forces. The relatively easy desorption is also consistent with physical rather than chemical bonds. With this simple physical picture it is difficult to understand why gas adsorbed from the ionic state is held much more strongly than that taken up as molecules. For the inert gases, for example, physical adsorption is only found at temperatures below about −80° C,[6, 7] whereas the surface layer formed from ion bombardment is stable up to approximately 100° C.

(*b*) The maximum quantity of gas recovered corresponds approximately to that needed to form a complete surface layer on the cathode. This strongly supports the model given above. The numbers of molecules needed to form a surface layer on the cathode disks are given in the table together with the maximum observed desorption so that a comparison can be made.

The number of molecules actually recovered from the cathodes and the number required to form a complete surface layer

Gas	*Maximum number of molecules adsorbed* $\times 10^{-15}$	*Number of molecules to form a surface layer* $\times 10^{-15}$
helium	10	4·7
neon	4	3·3
argon	2·3	1·7
krypton	0·17	1·3
nitrogen	2·18	1·7
oxygen	1·0	1·6

(*c*) Assuming the adsorption to be due entirely to molecules held at the cathode, the chances of an ion "sticking" approaches 100% for many gases. It can be seen from Fig. 4 that with a short bombardment of up to 10^{16} ions, the number of molecules adsorbed is of the same order as the number of ions striking the surface, oxygen, however, being a notable exception. It is not therefore unreasonable to assume that each ion on arrival at the surface is adsorbed, knocking off and taking the place of any other molecule held in the immediate neighbourhood. Thus, when the composition in the discharge is changed the gas on the surface changes from that of the old to that of the new gas.

This work confirms observations on the sorption of nitrogen and argon in a hot cathode ionization gauge by Schwarz[8] who found desorption of previously adsorbed molecules during the clean-up of either gas. In this present work, however, all the gas was taken up at the metal cathodes, whereas Schwarz, and also Von Meyeren[9] who measured clean-up in a hot cathode low voltage discharge, found most of the gas to be taken up by the glass. This is not inconsistent with the present work because in the Penning gauge the discharge is shielded from the glass.

CONCLUSIONS

By using a mass spectrometer to follow the desorption of individual components of a gas mixture, sorption and desorption have been shown to take place simultaneously in the cold cathode discharge. Positive ions adsorbed on striking the cathode at the same time dislodge any molecules already held there. Because the sorption and desorption is independent of gas composition the process is probably physical rather than chemical. The simplest physical explanation does not, however, account for the stability of the surface layers up to temperatures approaching 100° C.

The surface layer does not account for all the gas taken up in the discharge. Gas is also taken and bound very tightly to the cathodes by a mechanism depending very much on the gas composition. A more detailed investigation of this clean-up is being undertaken at the present time and will, it is hoped, be reported in a later paper.

ACKNOWLEDGEMENTS

The authors wish to thank Professor Meek and Dr. Craggs of The University of Liverpool for the continuous interest that they have taken in this work. The help of Mr. Blears of the Metropolitan-Vickers Electrical Co. Ltd., and the loan of equipment from this company are gratefully acknowledged.

REFERENCES

(1) Leck, J. H. *J. Sci. Instrum.*, **30**, p. 271 (1953).
(2) Penning, F. M., and Nienhuis, K. *Philips Tech. Rev.*, **11**, p. 116 (1949).
(3) Blears, J. *J. Sci. Instrum., Supplement No.* 1, **28**, p. 36 (1951).
(4) Roberts, J. K. *Proc. Roy. Soc. A*, **129**, p. 146 (1930).
(5) See, for example, Dushman, S. *Vacuum Technique*, p. 730 (New York: John Wiley and Sons, Inc., 1949).
(6) Miller, A. R. *Adsorption of Gases on Solids.* Chapter I (London: Cambridge University Press, 1949).
(7) Smithells, C. J. *Gases and Metals*, p. 21 (London: Chapman and Hall Ltd., 1938).
(8) Schwarz, H. *Z. Phys.*, **122**, p. 437 (1944).
(9) Von Meyeren, W. *Z. Phys.*, **84**, p. 531 (1933); **91**, p. 727 (1934).

The rheology of Portland cement pastes

By G. H. Tattersall, M.Sc., A.Inst.P., Research Committee for the Cast Stone and Cast Concrete Products Industry, Stoke Poges, Bucks

[*Paper first received* 14 *December*, 1954, *and in final form* 21 *February*, 1955]

Experiments with a rotation viscometer on the structural breakdown of Portland cement/water pastes are described. Hysteresis curves are shown and an empirical equation $T = T_E + (T_0 - T_E) \exp(-Bt)$ for the decay of torque T with time t, at constant rate of shear, is given. The equation is also derived theoretically by assuming that the "excess torque" is proportional to the number of linkages existing, and it is shown that the predicted dependence of B on the rate of shear is approximately fulfilled by the experimental results.

An understanding of the rheology of fresh concrete is of major importance to the efficient use of the material, and a great many methods have been devised in attempts to measure the flow properties. None of the methods so far proposed give a result in terms of fundamental physical quantities and none can claim success in practice over more than a very limited range. The study of cement pastes has been comparatively neglected, although it seems apparent that a knowledge of their properties is necessary to gain a knowledge of concrete itself.

It is now common practice to apply a vibratory force (frequency usually 50 to 100 c/s) in the placing of concrete, because it is found that the flow properties are profoundly modified so that a much drier mix can be used, and consequently a higher strength of the set concrete obtained. When a concrete mix is vibrated the material at first subsides and then an apparent "fusion" takes place, so that a previously stiff material will flow comparatively easily. This change at least suggests the possibility of a thixotropic change or breakdown of structure of the cement paste, so experiments were carried out to determine whether a breakdown under shear occurred, and if it did, to obtain some measure of it.

APPARATUS

The apparatus used was a coaxial cylinder viscometer in which the cylinders were made of brass and had dimensions similar to those used by Green,[1,2] namely, inner cylinder, radius 1·3 cm, height 5·0 cm; outer cylinder, radius 1·5 cm, height 6·0 cm. The gap was thus 2 mm. The speed of the outer cylinder could be controlled continuously up to 500 rev/min by means of an infinitely variable hydraulic transmission, so that the maximum average rate of shear was about 360 reciprocal seconds. (Average rate of shear in reciprocal seconds = 0·72 × speed in rev/min.) The inner cylinder was screwed on to the end of a vertical shaft which was supported by ball races, and the torque was measured by deflexion against various tension springs which were calibrated by means of weights. (The constants are given in the figures.) The cylinders were surrounded by a light oil, the temperature of which was controlled at 25° C (±0·1° C).

Since the gap was only 2 mm wide it was most important that the inner cylinder should be accurately centred, and this was accomplished by means of small adjustment screws and a specially-made feeler gauge. It was found that a slight displacement of the inner cylinder (of the order of 0·05 mm) had no effect on the torque/speed curve obtained for a Newtonian liquid, but might alter the measured torque by as much as 30% for a paste having a yield value. The tendency in this latter case was for the curve to be shifted parallel to itself.

To overcome difficulties caused by loss of paste during an experiment, Green used a cap which covered the gap while clearing the inner cylinder, but in the present work it was found that such a cap introduced more errors, by shear of the paste between itself and the inner cylinder, than it prevented by stopping escape of paste.

EXPERIMENTAL WORK

A sufficient quantity of ordinary Portland cement for the whole of the work was obtained from a thoroughly blended batch, and was stored in glass-stoppered bottles. The specific surface of the cement as measured by the Lea–Nurse method[3] was 3100 cm²/g. Each paste was made in the same way. 50·00 g of cement were weighed out into a crystallizing dish and the required quantity of distilled water was added from a burette during 1 min, a spatula being used to break up any lumps that formed and to expose fresh powder to the water stream. The paste was then stirred fairly vigorously for ½–¾ min and placed in the outer cylinder which was rotating at about 40 rev/min. The inner cylinder was lowered into position slowly, thus squeezing out excess paste which was removed with a spatula. Exactly 3½ min after the first drop of water was added to the cement the motor was switched off and the paste allowed to stand for 1 min, during which time the speed control was set to the speed at which measurement was to begin. At the end of the minute the motor was switched on and the measurement commenced.

It was found that a cement paste with a water/cement ratio by weight (W/C) of less than 0·28 was too thick to be used in the instrument because the inner cylinder could not be lowered into it, while at the other extreme, if the W/C ratio exceeded 0·35, pronounced sedimentation occurred. Full results were therefore obtained on pastes with W/C ratios of

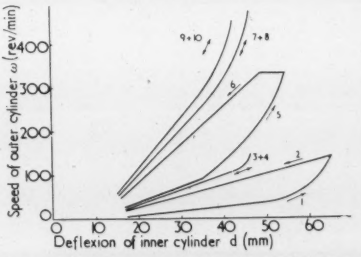

Fig. 1. Hysteresis curves obtained for 0·3 W/C paste
(Calibration constant 2·22 × 10³ dyn. cm/mm.)

0·28, 0·30 and 0·32 (i.e. 21·8, 23·1 and 24·2% water respectively).

Preliminary work was carried out on a paste of 0·30 *W/C* ratio and it was found that when torque was plotted against the speed of the outer cylinder, the up-curve (i.e. for increasing speed) and down-curve did not coincide, that is, a hysteresis curve was obtained. Fig. 1 was obtained as the result of a continuous experiment on one particular paste (0·30 *W/C*) in which the speed of rotation of the outer cylinder was increased to a maximum, reduced to zero, increased again and so on as shown on the graph. The curves were obtained in the order shown by the numbering and the arrows show whether the speed was being increased or decreased. For each curve, readings were taken of the deflexion as the speed was changed in small steps, the time of rotation at any particular speed being just long enough for a determination of the speed by means of the revolution counter and a reading of the deflexion. Conclusions which may be drawn from this experiment are as follows.

(1) The obtaining of hysteresis curves indicates that a structural breakdown of the paste takes place under shear. These curves are similar to those obtained by Green and Weltmann[2,4] working with printing inks.

(2) There appeared to be little or no tendency for the structure to build up again, at least in a time of the order of that taken for an experiment, since an up-curve was always displaced towards the speed axis relative to a previous down-curve. This was later confirmed by the fact that after breakdown had occurred in a paste, a period of rest of the order of 5 to 10 min did not result in an increase in torque at a given speed.

(3) All the curves when extrapolated intersect approximately at a point on the torque axis, indicating that there is little or no change in yield value during breakdown.

The main experiments on the breakdown were in measuring the torque as a function of time at constant rate of shear. After the filling procedure described above, the outer cylinder was started at the chosen speed and readings of the deflexion of the inner cylinder were taken every few seconds, and later every ten or twenty seconds until the torque reached a constant value. Results were obtained for speeds from about 200 to 500 rev/min (about 150 to 360 reciprocal seconds average rate of shear). In every case (except when trouble was experienced with friction in the bearings of the inner cylinder and the results were rejected) the curve was of the type shown in Fig. 2 where the torque decays at first rapidly and then more slowly, from an initial value T_0 to an equilibrium value T_E. The whole process occupied a time of the order of 2 to 3 min.

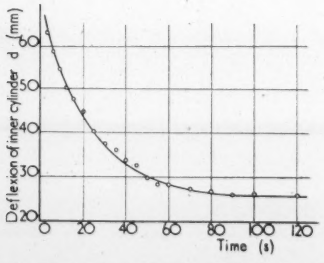

Fig. 2. Breakdown curve for 0·30 *W/C* paste at 386 rev/min

(Calibration constant $5{\cdot}82 \times 10^3$ dyn. cm/mm.)

By plotting the torque (or deflexion) logarithmically it can be shown that the experimental points show good agreement with the equation

$$T = T_E + (T_0 - T_E)\exp(-Bt) \qquad (1)$$

where T is the torque at time t. The numerical value of B, as determined from the slope of the line, was found to increase with increasing rate of shear, as illustrated in Fig. 3. Values of T_0 were obtained by extrapolating back to zero time, and when these values were plotted against ω a good straight line was obtained.

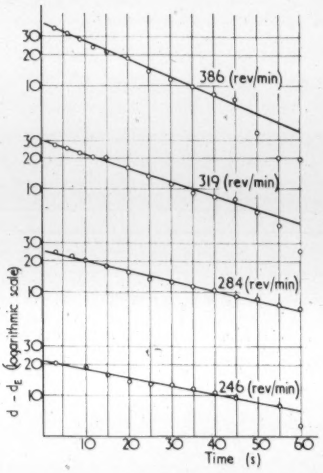

Fig. 3. Logarithmic breakdown curves for 0·30 *W/C* paste

The logarithmic formula given by Weltmann[5] for thixotropic breakdown with time, at constant rate of shear, does not fit the experimental results, particularly for small values of time. In addition, her equation gives no meaning to values of T for $t = 0$ and $t = \infty$.

THEORY

Equation (1), which was first obtained empirically, may be obtained theoretically as follows.

The work done in a rotation viscometer in a small time dt is $2\pi\omega T dt$ where ω is the speed of the outer cylinder in rev/min. Therefore, in a time t the total work done is

$$W = \int_0^t 2\pi\omega T \, . \, dt \qquad (2)$$

This work is used in: (*a*) overcoming normal viscous forces; (*b*) breaking the structure; and (*c*) keeping the structure broken.

It may be assumed that the work in keeping the structure broken is negligible, i.e. there is little or no tendency for a rebuilding of the structure to take place. It has been shown experimentally that this is at least approximately true for cement paste, during a time of the order of that required for an experiment, and it is thus necessary to consider only items (*a*) and (*b*).

At a constant rate of shear the torque decays from an initial value T_0 to a final value T_E. This torque T_E may be regarded as being independent of the "breakable structure" and as being that part of the torque used in overcoming normal viscous forces. Hence the work done against viscous forces in time t is

$$W_V = \int_0^t 2\pi\omega T_E \,.\, dt \tag{3}$$

Suppose that the structure consists of some type of linkages and that the torque in excess of the "viscous torque" is at any time proportional to the number of linkages still existing, then

$$T - T_E = Z(n_0 - n) \tag{4}$$

where n_0 is the number of linkages originally existing, n is the number broken at time t, and Z is a constant at constant rate of shear. Z will be dependent on rate of shear and may be written as $f(\omega)$ and therefore

$$n = -\left(\frac{T - T_E}{f(\omega)} - n_0\right) \tag{5}$$

If the work done in breaking one link is ϕ, the work done in breaking n linkages is $n\phi$ or

$$W_S = -\phi\left(\frac{T - T_E}{f(\omega)} - n_0\right) \tag{6}$$

Adding equations (3) and (6) and equating to equation (2)

$$\int_0^t 2\pi\omega T dt = -\phi\left(\frac{T - T_E}{f(\omega)} - n_0\right) + \int_0^t 2\pi\omega T_E \,.\, dt \tag{7}$$

and on differentiating

$$2\pi T\omega = -\frac{\phi}{f(\omega)} \cdot \frac{dT}{dt} + 2\pi T_E \,.\, \omega \tag{8}$$

The solution of this equation may be put in the form

$$T - T_E = (T_0 - T_E) \exp\left[-2\pi\omega \,.\, f(\omega) \,.\, t/\phi\right] \tag{9}$$

where $T = T_0$ when $t = 0$.

Equation (9) is identical with equation (1) if

$$B = [2\pi\omega \,.\, f(\omega)]/\phi \tag{10}$$

The function $f(\omega)$ was originally supposed to be equal to $K\omega$[6,7] but a better form may be deduced empirically as follows. When $n = 0$, $T = T_0$ and therefore from equation (4)

$$T_0 - T_E = f(\omega) \,.\, n_0 \tag{11}$$

The experimental values of T_0 and T_E when plotted against ω give straight lines which intersect at a point (ω_1, T_1), ω_1 for each W/C ratio being approximately 80 rev/min. Hence

$$T_0 - T_E = k(\omega - \omega_1) \tag{14}$$

where k is a constant. Therefore

$$f(\omega) = (k/n_0)(\omega - \omega_1) \tag{15}$$

and finally

$$B = (2\pi k/n_0\phi)\omega(\omega - \omega_1) \tag{16}$$

This indicates that B is a linear function of $\omega(\omega - \omega_1)$. Fig. 4 shows that the experimental points conform fairly well to this prediction, when it is considered that each point is the result of a completely separate experiment on a variable material. The slopes of the lines in Fig. 4 should show the variation of ϕ with concentration of paste, but the present results are not sufficient for any conclusions to be drawn. Further work is being done on this and it is thought that modifications to the instrument will allow the scatter of points on graphs such as Fig. 4 to be reduced. The existence of the intercept on the graph is not explained.

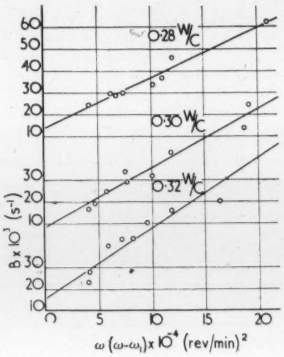

Fig. 4. B plotted against $\omega(\omega - \omega_1)$ for various W/C ratios

The lines shown were calculated by the method of least squares.

ACKNOWLEDGEMENT

The author wishes to thank the Research Committee for the Cast Stone and Cast Concrete Products Industry for permission to publish this paper.

This work was included in the author's M.Sc. thesis in the University of London.

REFERENCES

(1) GREEN, H. *Industr. Engng Chem.* (*Analyt.*), **14,** p. 576 (1942).

(2) GREEN, H. *Industrial Rheology and Rheological Structures* (London: Chapman and Hall Ltd., 1949).

(3) British Standard 12 (1947).

(4) GREEN, H., and WELTMANN, R. N. *Industr. Engng Chem.* (*Analyt.*), **15,** p. 201 (1943).

(5) WELTMANN, R. N. *J. Appl. Phys.*, **14,** p. 343 (1943).

(6) TATTERSALL, G. H. *M.Sc. Thesis*, University of London (1954).

(7) TATTERSALL, G. H. *Nature* [*London*], **175,** p. 166 (1955).

X-ray emission spectroscopy with electron excitation covering elements $_4Be$–$_{92}U$

By G. L. MACDONALD, M.A., B.Sc., and M. G. HARWOOD, B.Sc., A.Inst.P., Material Research Laboratory, Philips Electrical Ltd., Mitcham Junction, Surrey

[*Paper received* 4 *January*, 1955]

A plane glass optical diffraction grating has been used to disperse characteristic X-rays, of wavelengths 5–200 Å, produced by electron bombardment of materials. Advantages of an electron as opposed to an X-ray source for the analytical determination of the elements by X-ray spectroscopy are discussed. It is shown that almost any element throughout the periodic system can be detected with one photographic exposure, using K, L, M and N radiations. Light and heavy elements are recorded with equal facility. X-ray spectroscopy and electron diffraction have been combined to produce simultaneous elementary and compound analysis. The particular advantages of the method for the identification of surface films are noted.

In spite of the recent rapid advance in the use of X-ray emission spectroscopy for the analysis of the elements, little use appears to have been made of electron, as opposed to X-ray, excitation since the pioneer work of von Hevesy.[1] Castaing[2, 3] and Guinier[3] have recently combined electron microscopy and X-ray spectroscopy for metallurgical studies and cover elements $_{22}Ti$–$_{30}Zn$ and $_{55}Cs$–$_{75}Re$, but a more general application of the method does not seem to have been reported.

Another comparatively untouched aspect of the subject concerns the detection of elements of atomic number lower than $_{11}Na$. Several workers have employed ruled diffraction gratings for the detection of very soft X-rays while determining wavelengths or studying the electronic structure of materials. Siegbahn[4] was one of the pioneers in the former field, while the latter has been advanced by workers including Skinner,[5] and Piore, Harvey, Gyorgy and Kingston.[6] The application of such diffraction to the analysis of the elements, however, does not appear to have been carried out.

It is the purpose of this paper to describe investigations into some of the possibilities of electron excitation, and to show how almost all the elements in the periodic table can be potentially covered with one photographic exposure by means of a ruled diffraction grating. The combination of X-ray spectroscopy and electron diffraction is also discussed, particularly with reference to the detection of surface films.

THEORY

The range of wavelengths hitherto employed for X-ray spectroscopy (0·1–10 Å approximately) can readily be dispersed by utilizing the three-dimensional diffraction gratings of crystals. The spacing of the atomic planes used, however, must be at least half that of the longest wavelength to be detected, and it is difficult to obtain large stable crystals with a lattice parameter much greater than 10 Å. On the other hand, ruled gratings giving two-dimensional diffraction are usually employed for the dispersion of wavelengths much longer than X-rays. It is therefore necessary to consider the special conditions required if X-rays are to be dispersed by the latter.

For X-rays, unlike visible electromagnetic rays, materials in general have indices of refraction just less than one. In order, therefore, to achieve reasonable intensity of reflexion, it is necessary that the rays should strike the grating at a glancing angle, less than the critical angle for total reflexion (θ_c). When the reflecting material has no electrons of natural frequency of vibration close to the wavelength under consideration, this critical angle is proportional to wavelength and increases with the atomic numbers of the elements involved. Compton and Allison[7] give a theoretical equation and a comparative table of a few calculated and observed values. Table 1 based on these gives an idea of the critical angles for various materials.

Table 1. *Total reflexion angles*

Reflecting material	*Atomic number*	θ_c/λ (degrees/Å)
Al	13	0·15
Cr	24	0·24
Ni	28	0·28
Ag	47	0·29
W	74	0·37
Pt	78	0·39
Au	79	0·37
Glass		0·15
Calcite		0·15

It can be seen that the practical difficulties of grating dispersion increase with decrease in wavelength. This fact determines, to some extent, the short wavelength limit of a system such as described here.

A completely different consideration determines the long wavelength limit. The characteristic spectra used in X-ray spectroscopy with crystal dispersion (0·1–10 Å approximately) are simple, and since they arise from inner electron shells, their wavelengths are largely unaffected by changes in chemical combination of the elements. X-ray spectrograms can, therefore, be interpreted much more readily than their optical counterparts. In general, however, the longer the wavelength, the less well screened are the shells giving rise to X-rays, and the greater the wavelength differences and changes in line profile which occur with different states of chemical combination. This is liable to cause uncertainty in the assigning of a given line to its appropriate element for wavelengths longer than about 200 Å.

Fig. 1 shows that for every element heavier than $_3Li$ at least one Kα, Lα, Mα, or $N^{VII}O^{V}$ line occurs between 5 Å and 120 Å. A system capable of dispersing and detecting lines between these limits can, therefore, be used for elementary analysis. Since, with a ruled grating, the dispersion, when considered in terms of distance between lines from adjacent elements (Fig. 1), is lower at 5 Å than at 100 Å, it was considered desirable to increase the range under consideration to 200 Å. This allowed two lines from many elements to

appear, and increased the certainty of detection and correct interpretation.

With a glass grating the angle of incidence required to reflect 5 Å wavelength is 0·75° or less (Table 1). For 10 Å the critical angle is 1·5°. This latter would have been more convenient, but Fig. 1 shows that lines of wavelength considerably longer than 200 Å would, of necessity, have to be recorded if all the elements were to be included. As mentioned above, this was felt to be undesirable.

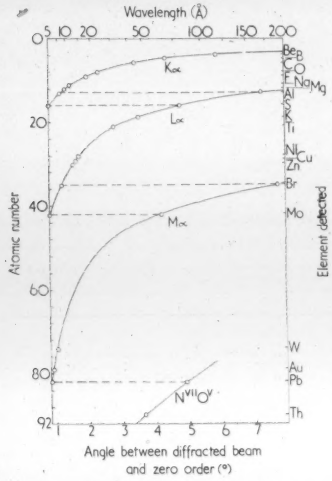
Wavelength (Å)
5 10 20 50 100 150 200
Kα
Lα
Mα
Be B C O F Na Mg Al Si K Ti Ni Cu Zn Br Mo W Au Pb Th
Nb Y
Atomic number
Element detected
0 20 40 60 80 92
1 2 3 4 5 6 7
Angle between diffracted beam and zero order (°)

Fig. 1. Dispersion by plane grating of chief X-ray lines 5–200 Å (571 lines per mm; angle of incidence, 0·75°)

Concave gratings are normally used for soft X-ray work but present serious problems for wavelengths as short as 5 Å. Table 2 makes a theoretical comparison of plane and concave gratings and lists some of the practical considerations arising therefrom.

The figures in part one of Table 2 are taken from papers by Petrie,[8] Bisacre,[9] and Mack, Stehn and Edlen.[10] Bisacre,[9] in a mathematical analysis of the diffraction of X-rays by a plane grating, shows that focusing can be obtained with a plane grating if the width is correctly chosen. A concave grating, focusing according to Rowland's principle, has certain aberrations which are considerably reduced by the choice of an optimum width calculated by Mack, Stehn and Edlen.[10] This width for both types varies according to wavelength, but for the concave grating is always six to nine times greater than for a plane grating. This means that the resolving powers and intensities are in much the same ratios. Petrie[8] points out, however, that for a concave grating spectrograph, a slit of width 0·01 mm has a resolving power of only 27 at 5 Å. At these wavelengths, therefore, the slit and not the grating determines the instrument's resolving power.

In other respects the plane grating appears to have advantages for the present purpose. Its dispersion below 20 Å is greater than for the concave grating and Fig. 1 shows

Table 2. *Comparison of plane and concave grating properties*

Description	*λ(Å)*	*Plane grating*	*Concave grating*
Number of lines per mm		571	571
Optimum width (mm)	20	0·725	5 (approximately)
Theoretical resolving power	20	670	4600
Relative intensity	20	1	7
Dispersion $\lambda/\delta\lambda$ ($\delta\lambda$ for 0·004 mm on plate)	5	1200	900
	20	2800	2900
	100	6600	10300
No. of lines possible in practice per mm		1800	1200
Difficulty of mounting for 0·75° angle of incidence		moderate	Very considerable, requires large radius of curvature
Precision required for slit		moderate	moderate
Precision required for grating mounting		moderate	considerable
Precision required for detector mounting		none	considerable
Angle of incidence on photographic plate (if used)		90° approximately	glancing

that this is the region where higher dispersion is desirable. The number of lines per millimetre affects the dispersion generally, and the small plane gratings of 1800 lines per mm ruled by Siegbahn and Magnusson[11] are probably more closely ruled than any concave grating. Finally, the practical difficulties involved in constructing and using a concave grating spectrograph with a 0·75° angle of incidence are considerable, while a plane one provides only moderate problems. For the present, therefore, it was considered that the intensity difference between the two types was outweighed by the other factors involved and a plane grating was used.

EQUIPMENT

General. The equipment consisted chiefly of an electron diffraction unit and a spectrograph originally intended for crystal dispersion. Most of the essentials are shown in the schematic diagram of Fig. 2. The electron beam was focused by a permanent magnet lens on to the specimen holder (*a*), shown in section, which could be viewed through a lead glass window (*w*). X-rays produced at the specimen passed through a vacuum "cut-off" (*c*) and slit system ($s_{1,2}$) on to a plane ruled diffraction grating (*g*). The dispersed rays were recorded on a film mounted in a cassette (*f*), or on a plate in a plate-holder (*h*).

Electron beam and specimen holder. The electron beam was operated at 30 kV and 0·5–3·0 mA. For the shortest wavelength in use, 5 Å, the excitation potential is about 2·5 kV. Above two or three times this value, the intensity of the spectral line ceases to be proportional to the square of the increase in voltage and approaches a limiting value. A 10 kV maximum would therefore have been ample, but the lens in use, designed for 50 kV, did not permit of focusing on to the sample at a lower value than 30 kV. This voltage was therefore temporarily accepted. The focal spot was usually maintained at about 5 × 2 mm, with the longer axis pointing towards the spectrograph.

In order that the highest power should be used, compatible with the non-destructive nature of the testing, it was necessary to arrange for cooling of the specimen. Two concentric brass tubes, led in through a double Wilson seal and brazed into a rectangular block (*a*, Fig. 2), allowed water to flow close to the specimen. Sylphon bellows (b_1) and associated tilting screws permitted adjustment of the specimen position. A small aluminium clamp gave rapid heat conduction from the top of the sample and provided easily recognizable X-ray lines when it was necessary for it to protrude into the electron irradiated area.

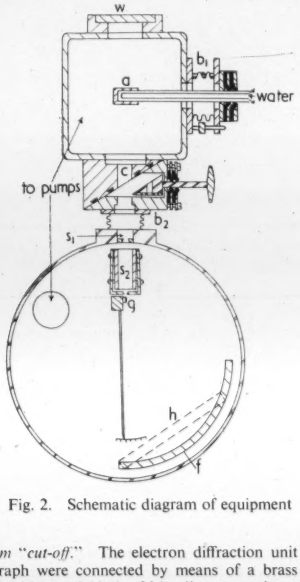

Fig. 2. Schematic diagram of equipment

Vacuum "cut-off." The electron diffraction unit and the spectrograph were connected by means of a brass cylinder (*c*, Fig. 2) with an axial hole of $\frac{5}{8}$ in. diameter and a trapezoidal central chamber. This permitted a triangular block to be pressed against a rubber O-ring by a shaft through a Wilson seal, or retracted, allowing free passage for X-rays through the central hole. The two main faces were lapped and held by low vapour pressure grease to the spectrograph bellows (b_2) on one side and the electron diffraction unit on the other. A cellophane window sealed into the triangular block made it possible for the harder X-rays to pass through the "cut-off" even when the two units were, for vacuum purposes, separated from one another.

Slit system. A broad slit (s_1), set in the spectrograph entrance, cut down scatter from the "cut-off" and bellows. The controlling slit (s_2), being originally intended for the higher dispersion of normal crystal methods, did not give very satisfactory results if reduced below about 0·1 mm. This width was therefore the one most commonly used throughout the experiments.

Grating. A plane glass optical grating ruled with 571 lines per mm and approximately 3 mm in width was used. It was mounted (Fig. 2) close to slit (s_2) to receive high incident intensity, and as far as possible from the detector (*f*, *h*) to provide high dispersion. It was fixed to a rotatable brass block, which had an arm projecting over a scale to allow small changes in angular setting to be measured.

EXPERIMENT

Detection. Various types of X-ray film including Kodak Industrex D and Ilford Ilfex and Industrial G were compared. The last was found to be most sensitive but, in company with the others, dropped rapidly in sensitivity for wavelengths greater than 10 Å. In consequence Kodak SWR film, Ilford G5, Q2 and Q3 plates, all with Schumann or nuclear type emulsions, were tried. Both G5 and Q3 plates showed high sensitivity in the region considered, but the former provided processing difficulties and the latter were therefore preferred. Fig. 3 shows the relative sensitivities of Industrial G film and Q3 plates for molybdenum Lα (5·4 Å) and molybdenum Mα (63 Å). Since the Q3 plates gave the highest average intensity over the whole region they were used throughout the experiments. Exposures varied from 15 min for major constituents to 180 min for trace elements.

Evacuation. A pressure of 10^{-4} mm of mercury was maintained throughout the system and appeared adequate. The use of a continuously evacuated path for the X-rays from specimen to emulsion led to an initial high background density which was found to be due to secondary electrons from the specimen. The placing of a small magnet on the spectrograph bellows (b_2, Fig. 2) deflected these so that they did not enter the spectrograph.

Source. In order to determine very approximately the relative intensities produced by X-ray and electron excitation respectively, a few experiments were carried out with a sealed-off X-ray tube (manufactured by the North American Philips Co. Inc.) with a W target. The power was 40 kV, 20 mA, and the beam was directed through a thin cellophane window on to the specimen which was in vacuum. The specimen was mounted at a small angle to the slit system and at a distance from it comparable with that used throughout the electron source experiments. In every case, exposures of the order of ten hours were required to produce just visible lines, as opposed to the few minutes to establish the same film density when an electron beam of only one-tenth the power was used.

RESULTS

Work was concentrated on the qualitative detection and identification of the elements involving if possible the whole of the periodic system. The following points were established.

(*a*) That elements of low atomic number could be detected. Fig. 4 shows O, C and Be K lines.

(*b*) That all elements except the lightest could be detected. Fig. 3 shows an overlap between the L and M series. Fig. 5 shows an overlap between the K and L, and the M and N series.

(*c*) That light and heavy elements when present in similar atomic percentages gave lines of the same order of intensity. Fig. 5 shows lines from a lead sulphide sample.

Fig. 1 shows the elements which have actually been detected, the horizontal dotted lines indicating where X-rays from two different series but from the same element have been registered on the same plate. In addition it was confirmed that X-ray spectrograms and electron diffraction patterns could be recorded simultaneously.

DISCUSSION

The desirability of maintaining the specimen without deterioration places a limitation on the power of the electron beam and therefore on the intensity of the X-rays produced. The more effective the cooling is, the more the power can be increased, and the temperature maintained at a reasonably low level. Several ways of achieving this are being considered, liquid air cooling or rotation of the sample being among them.

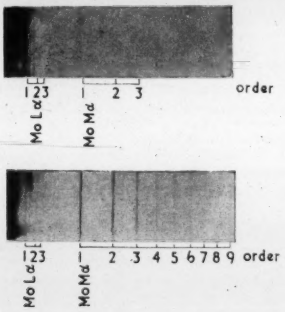

Fig. 3. Radiation from a molybdenum sample recorded on (*a*) Industrial G film; (*b*) Q3 plate

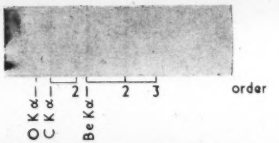

Fig. 4. Radiation from a carbon-contaminated beryllium oxide sample

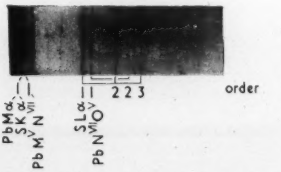

Fig. 5. Radiation from a lead sulphide sample

Other factors also affect the final intensity of the X-ray spectra. For instance, a large intensity increase could be obtained by reducing the distance between the specimen and the slit (at present 20 cm). As mentioned earlier, little gain in intensity is obtained if the voltage is increased to more than a few times the excitation potential. Since soft X-rays are being used it is, therefore, advantageous to raise the current and lower the voltage to about the previously suggested value of 10 kV. This allows the use of simpler electrical equipment than is normal for X-ray work.

Grating dispersion does not, of course, preclude the substitution of an X-ray source for the electron beam used here, if decomposition or contamination difficulties are likely to arise. It seems probable, however, that fluorescence coefficients will be extremely low for wavelengths greater than 5 Å and that exposure times will be correspondingly increased.

The long wavelengths employed make it necessary that all samples should be examined in vacuum. With other X-ray spectroscopic methods only elements lighter than about $_{16}S$ ($K\alpha = 5{\cdot}4$ Å) require this condition.

If quantitative analysis is considered the electron beam again offers an advantage over the X-ray source. Very approximately, the former has a penetration one-twohundredth that of the latter. Absorption corrections, necessary with X-ray bombardment, should, therefore, be eliminated to a large extent. Also it should be much easier to detect a small quantity of a light element within a matrix of a heavy element.

Little is known as yet about changes in intensity of lines in the region considered here with changes in state of combination, but it seems likely that quantitative measurements will be possible to a fair degree of accuracy. At present, the plates used can be subjected to microphotometer measurements, but direct-reading instruments, such as very thin-window Geiger counters, or, more probably, photomultipliers, can clearly be employed to advantage.

The low penetration affords considerable opportunity for the detection of surface films, a fact which is already utilized in electron diffraction studies. Difficulty often occurs in the identification of electron diffraction patterns from films of unknown composition, since layers of only a few molecules thick, at times possess abnormal crystal structure. In such cases, a knowledge of the elements present would be of considerable value. Many films which fail to provide electron diffraction patterns, because the surface roughness is not of the right order or because the material is amorphous, may still be subjected to elementary analysis.

It is possible, as Karlsson[12] has done, to use organic crystals with large lattice parameters, for the dispersion of soft X-rays. It seems likely, however, that the difficulties in preparing and maintaining such crystals would make their use impracticable for routine analysis. Ruled gratings, on the other hand, can readily be obtained and are very stable indeed. In addition, the two-dimensional character of the diffraction obviates the necessity for oscillation of the grating. With photographic detection, therefore, a stable source is not required for quantitative work. Since all the lines are being recorded simultaneously throughout the exposure, their relative intensities remain constant whatever the intensity of the source.

The wavelength region used seems to offer considerable advantages over the more normal one. Not only can most of the very important light elements be detected, but one comparatively short exposure is sufficient for the detection of all the elements in a sample of unknown composition with the exception of hydrogen and, possibly, lithium.

The dispersion and resolution obtained throughout these experiments were sufficient to show the practical possibilities of the method, but improvements could readily be effected to allow for more accurate analysis, and work is in hand with this end in view.

CONCLUSIONS

An electron source has been employed for X-ray spectroscopic analysis. For most samples, when used with care, it can be as non-destructive as an X-ray source and provides considerably higher intensity than the latter. The low penetration of electrons reduces "masking" of light elements

by heavy ones, permits the detection of elements in surface films and should diminish the difficulties of quantitative analysis. This type of source allows an electron diffraction pattern and an X-ray spectrogram to be recorded from the same sample, giving simultaneous compound and elementary analysis.

A small plane grating has been used successfully in the region 5–200 Å for the dispersion of spectra from elements throughout the periodic table from $_4$Be upwards. Only one photographic exposure is required.

ACKNOWLEDGEMENTS

The authors wish to thank Dr. J. A. M. van Moll of this Laboratory and the Directors of Philips Electrical Ltd. for permission to publish this paper.

REFERENCES

(1) Von Hevesy, G. *Chemical Analysis by X-rays and its Applications* (New York: McGraw-Hill Book Co. Inc., 1932).
(2) Castaing, R. *O.N.E.R.A. Pub.*, No. 55, 92 pp. (1952).
(3) Castaing, R., and Guinier, A. *Analyt. Chem.*, **25**, p. 724 (1953).
(4) Siegbahn, M. *Ergeb. Exact. Naturwissenschaften*, **16**, p. 104 (1937).
(5) Skinner, H. W. B. *Phil. Trans A*, **239**, p. 95 (1940–6).
(6) Piore, E. R., Harvey, G. G., Gyorgy, E. M., and Kingston, R. H. *Rev. Sci. Instrum.*, **23**, p. 8 (1952).
(7) Compton, A. H., and Allison, S. K. *X-rays in Theory and Experiment*. 2nd Ed., pp. 280 and 284 (New York: D. Van Nostrand Co. Inc., 1935).
(8) Petrie, D. P. R. *Proc. Phys. Soc.* [*London*], **47**, p. 626 (1935).
(9) Bisacre, F. F. P. *Proc. Phys. Soc.* [*London*], **47**, p. 948 (1935).
(10) Mack, J. E., Stehn, J. R., and Edlen, B. *J. Opt. Soc. Amer.*, **22**, p. 245 (1932); **23**, p. 184 (1933).
(11) Siegbahn, M., and Magnusson, T. *Z. Phys.*, **62**, p. 435 (1930).
(12) Karlsson, A. *Ark. Mat., Astron. Fys.*, **22**, No. A9 (1930).

A two-state light activated circuit element using germanium

By J. W. Granville, Ph.D., Radar Research Establishment, Great Malvern, Worcs

[*Paper received* 2 *February*, 1955]

A new germanium photo-switch with two stable states is described, each state being set by illumination of one or the other of two small germanium bars.

Germanium has been used to make a circuit element which has two stable states, each state being activated by a light beam. The device utilizes the double-base diode action.* To understand how the device works it will be helpful to describe first the action of the double-base diode.

The double-base diode consists of a rectifying contact on a bar of *n*-type germanium which carries non-injecting contacts at its ends. A sweep voltage V_s is applied to the bar as shown in Fig. 1. In these experiments, the rectifying

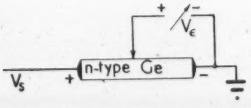

Fig. 1. Schematic diagram to illustrate double-base diode action

contact was a point-contact diode. Let the potential in the bar at the point contact be V when the point is returned to the negative sweep terminal through a bias V_ϵ. If $V_\epsilon < V$ the diode is biased in the reverse direction. Increasing V_ϵ so that it just exceeds V biases the diode in the forward direction. Holes are injected which drift into the right-hand region towards the negative sweep terminal and the conductivity of this region relative to that of the left-hand region is increased. The potential distribution in the bar is then no longer uniform and the potential at the point contact falls below V. This biases the diode further forward, the conductivity of the right-hand region increases still more and the action is cumulative until the diode is heavily biased in the forward direction. The reverse action is also cumulative. As a consequence, the voltage-current characteristic of the diode has a negative resistance region in the forward direction as shown in Fig. 2.

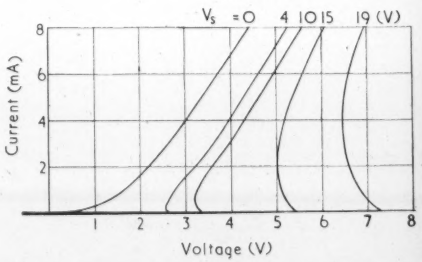

Fig. 2. Voltage-current characteristics of a double-base diode for different sweep voltages

THE TWO STATE PHOTO-SWITCH

The photo-switch consists of two bars of germanium, R_1 and R_2, with non-injecting end connexions and joined together as shown in Fig. 3. Near the positive terminal of

* Shea, R. F. (Ed.) *Principles of Transistor Circuits*, p, 466, (New York: John Wiley and Sons Inc., 1953).

R_2 is a point-contact diode which is connected to the negative sweep voltage terminal through a bias voltage and a load R_L. Evidently, this arrangement will show double-base diode action also.

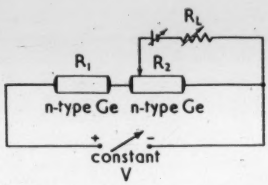

Fig. 3. Schematic diagram of the two-state photo-switch

Double-base diode action occurs when the conductivity of part of the germanium bar is increased by carrier injection. However, the conductivity of the bar may be equally well increased by illuminating the surface. This equivalence of light and contact injection is the basis of the action of the two-state photo-switch. The operation of the photo-switch may best be understood with the aid of the schematic diagram, Fig. 4. Let curve *OAB* be the static characteristic of the diode for the given sweep voltage and let the applied bias

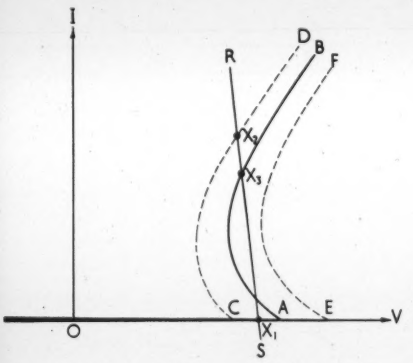

Fig. 4. Schematic voltage-current characteristics used to explain the operation of the photo-switch

be such that the diode is working in the reverse direction at the operating point X_1. *RS* is the load line determined by the resistance in the diode circuit. When bar R_2 (Fig. 3) is illuminated, its conductivity is increased and the voltage drop across the bar is reduced. This has the same effect on the diode characteristic as a decrease in sweep voltage and hence the characteristic moves to the left, taking up a new position given by the curve *OCD*. This displacement is a function of the light intensity. Double-base diode action occurs and the operating point switches over to X_2. When the light is removed the original characteristic is resumed and the operating point moves to X_3 which, being on a positive slope of the characteristic is a stable operating point and the diode remains conducting. This is the "on" state of the photo-switch. The load resistor R_L increases the positive slope of the diode characteristic and provides a current limiter. However, it must not be so large as to cancel out the negative resistance region. The device is turned off by illuminating bar R_1 (Fig. 3). The diode characteristic then moves to the right to take up a position such as curve *OEF*. This curve is not intersected by the load line in the positive quadrant and the diode switches back to its non-conducting state. Thus, illumination of bar R_2 gives the "on" state and illumination of bar R_1 gives the "off" state, *both states being stable when the light is removed.* Provided that the light intensity is sufficient, it is not difficult to set V_e, V_S and R_L so that switching action occurs. The speed of response of the photo-switch is of the order of the transit time of injected holes along bar R_2.

In principle, a single bar of germanium with the point-contact near its centre could be used for the photo-switch instead of two separate bars. However, it would then be necessary to ensure that the holes generated in the R_1 section by illumination recombined before reaching the R_2 section. If, instead of recombining, they were swept into the R_2 section the photo-switch would not turn off. The holes will recombine only if the germanium has a region of high recombination velocity just before the diode contact. The best region of high recombination velocity is a metallic conductor. Thus two separate bars with soldered end connexions and joined by a wire are necessary.

The optimum conditions to achieve maximum sensitivity of the photo-switch have been calculated and are as follows:

(1) the resistivity of the germanium should be as high as possible;
(2) the minority carrier liftime should be as long as possible;
(3) a constant voltage sweep source is necessary;
(4) the sweep voltage should be as large as possible, the limit being set by self-heating of the bars;
(5) R_1 should equal R_2;
(6) there should be negligible end injection into R_1 or R_2;
(7) if a spot of light less than the lengths of the bars is used, the regions nearest the positive terminals should be illuminated.

In the experimental arrangement, 40 Ω cm 80 μs lifetime *n*-type germanium was used in bars of dimensions 1·5 × 0·5 × 0·5 mm. With the voltages and R_L set to give maximum sensitivity, at least 5 mW of radiation were required to activate the device. At maximum sensitivity, some typical circuit values were $R_L = 1000\ \Omega$, diode-bias supply = 9 V, sweep voltage = 15 V, sweep current = 2 mA and the diode current in the "on" state = 0·5 mA.

CONCLUSIONS

The stability of the two states of the photo-switch suggests its use as a digital store. The device could also be used as a switch for gating a signal with a light beam. This is possible because the ratio of the a.c. resistances of the diode when switched from its high back resistance to its low forward resistance is of the order 1000 : 1.

ACKNOWLEDGEMENTS

The author is indebted to Dr. A. F. Gibson and Mr. J. B. Gunn for advice and help and to Dr. W. Bardsley for supplying the crystals. The paper is published by permission of the Chief Scientist, Ministry of Supply, and the Controller, H.M. Stationery Office. Crown copyright reserved.

An analogue study of the temperature distribution in cooled gas-turbine blades

By C. F. KETTLEBOROUGH, Ph.D., A.M.I.Mech.E., University of Melbourne, Australia

[*Paper first received* 30 *September, and in final form* 9 *December*, 1954]

A rapid method is described for determining the temperature distribution in cooled gas-turbine blades. Numerical results agree very closely with those obtained by more laborious methods.

LIST OF SYMBOLS

A_B = area of actual blade controlled per electrode.
A_M = area of model blade, immersed in electrolyte, controlled per electrode.
E = potential.
h_0 = surface coefficient of heat transfer between gas and blade.
h_1 = surface coefficient of heat transfer between blade and coolant.
k = thermal conductivity.
M = ratio of size of model to size of blade referred to linear dimensions.
n = direction normal to the boundary.
R_0 = electrical resistance representing heat flow resistance at the gas-blade boundary.
R_1 = electrical resistance representing heat flow resistance at the blade-coolant boundary.
T = temperature.
ρ = resistivity.

Suffixes B = blade. G = gas. L = liquid. GM = maximum gas. LM = minimum liquid.

INTRODUCTION

Thermodynamic analysis of the simple gas-turbine cycle shows that substantial increases in power and economy can be obtained by increasing the temperature of the working fluid at the turbine inlet. The utilization of increased turbine inlet temperature can be achieved by the development of suitable heat-resistant materials or by the use of turbine blade cooling. The latter method represents the more immediate and positive solution. The gas-turbine blade cooling problem has been more fully discussed elsewhere.[1,2]

HEAT FLOW EQUATIONS

The equation governing the temperature distribution in a body, assuming a constant value of the coefficient of thermal conductivity, and the equation governing the potential distribution in an electrolytic tank of constant depth both reduce to Laplaces' equation, and hence the potential distribution is proportional to the temperature distribution, provided the shape and boundary conditions are satisfied.

In the turbine blade, the boundary condition states that the heat flow across the boundary layer by convection is equal to the heat flow by conduction into the blade.

Hence
$$\partial T_B/\partial n = (h_0/k)(T_G - T_B) \tag{1}$$

at the outer boundary between the gas and blade and

$$\partial T_B/\partial n = (h_1/k)(T_B - T_L) \tag{2}$$

at the inner boundary between the blade and coolant.

THE ELECTROLYTIC TANK ANALOGY

For an electrode immersed along the boundary of an electrolyte, continuity of current flow across the outer boundary gives:

$$\partial E_B/\partial n = (\rho/A_B R_0)(E_G - E_B) \tag{3}$$

Comparing equations (1) and (3), the boundary resistance

$$R_0 = (\rho k/A_B h_0)$$

Similarly, at the coolant passage boundary

$$\partial E_B/\partial n = (\rho/A_B R_1)(E_B - E_L) \tag{4}$$

and

$$R_1 = (\rho k/A_B h_1)$$

Fig. 1 shows schematically the circuit for constant gas and coolant temperatures.

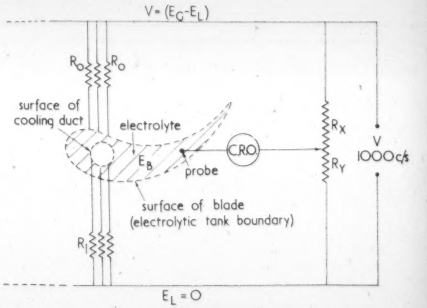

Fig. 1. Schematic diagram of electrolytic tank and circuit

By tying down the boundary resistances R_1 to zero potential, all temperatures, and hence potentials, are reduced throughout the system by T_L and E_L respectively. The supply voltage V is then equal to $(E_G - E_L)$ which is proportional to $(T_G - T_L)$.

The tank was built with linear dimensions 20·6 times larger than the original blade considered. The periphery was 67 in. and divided into inches, this being the effective width controlled per electrode. Hence the length of the periphery controlled per electrode in the model is 20·6 ($= M$) times the equivalent length in the actual blade. As the tank gives a two-dimensional distribution only, the depth is of no importance, hence:

$$R_0 = (\rho k M/A_M \,.\, h_0) \text{ and } R_1 = (\rho k M/A_M h_1)$$

see reference (3).

Copper electrodes were glued in position around the tank periphery, these being just slightly less than one inch wide so as to avoid short-circuiting.

The distribution of potential in the electrolyte is determined in the usual manner using a cathode-ray oscilloscope as a null indicator.[4]

The set up as shown in Fig. 1 is satisfactory for the case of constant gas and coolant temperatures. This is not the case in practice, but can be accommodated by inserting a voltage dropping series resistance in each electrode circuit. At the outer boundary these resistances are used to establish $(E_G - E_L)$ voltages differing from the supply voltage which represents the value $(E_{GM} - E_{LM})$. At the coolant boundaries these series resistances establish values of E_L greater than the minimum value. These resistances are adjusted relative to the maximum value of $(E_{GM} - E_{LM})$ using the potentiometer bridge $R_X R_Y$ and the cathode-ray oscilloscope.

EXPERIMENTAL RESULTS

Constant gas and coolant temperatures. For comparison the turbine blade with variable film coefficients[5] was considered. The same blade shape and position of the coolant holes were taken.

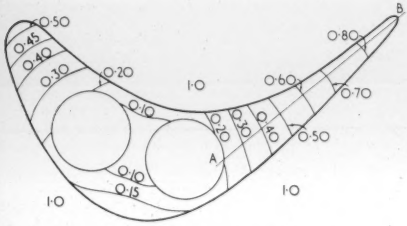

Fig. 2. Lines of equal value of the ratio $R_Y/(R_X + R_Y)$ for constant gas and coolant temperatures

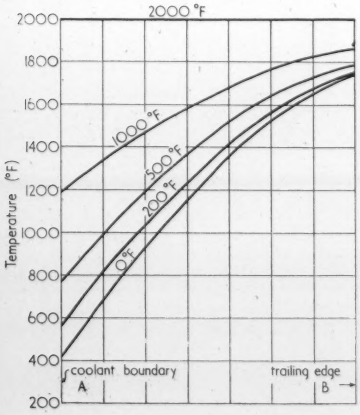

Fig. 3. Temperature distribution through blade trailing section. Constant effective gas temperature, 2000° F. Coolant temperature shown on each curve

The resistances in series with the R_0 and R_1 resistances were all set at zero to give constant gas and coolant temperatures. Fig. 2 gives values of the ratio $R_Y/(R_X + R_Y)$ and hence the voltage distribution in the electrolyte is given by

$$[R_Y/(R_X + R_Y)]V = [R_Y/(R_X + R_Y)](E_G - E_L) \quad (5)$$

To establish an actual temperature distribution, values of the actual gas and liquid temperatures have to be decided and hence the temperature at any point is given by

$$[R_Y/(R_X + R_Y)](T_G - T_L) + T_L \quad (6)$$

The temperature distribution along line AB is shown in Fig. 3 for an effective gas temperature of 2000° F and for coolant supply temperatures between 0 and 2000° F. It can be seen that at the blade trailing end the coolant has a relatively small effect.

Variable gas and coolant temperatures. In order to decrease the trailing section temperatures more coolant passages were provided (Fig. 4). The voltage dropping resistances were adjusted so that relative to the value of $(T_{GM} - T_{LM})$, the actual value of $(T_G - T_L)$ decreased linearly from unity at inlet to 0·72 at exit. The value of $R_X/(R_X + R_Y)$ at the coolant sources were fixed at 0·315, 0·168, 0, 0·028 and 0·056 respectively as in Fig. 4, which also gives lines of equal value

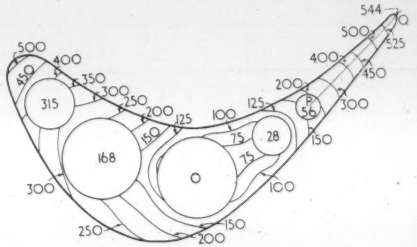

Fig. 4. Lines of equal value of the ratio $[R_Y/(R_X + R_Y)] \times 10^3$ for varying gas and coolant temperatures

of $R_Y/(R_X + R_Y)$. Any desired temperature distribution can be obtained from

$$T = [R_Y/(R_X + R_Y)](T_{GM} - T_{LM}) + T_{LM} \quad (7)$$

For an inlet temperature of 2000° F and a minimum coolant temperature of 50° F the temperature distribution is given in Fig. 5.

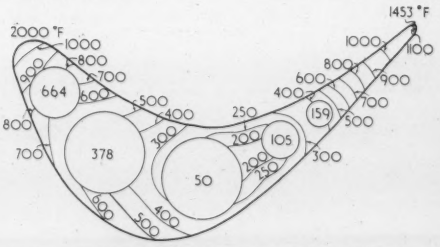

Fig. 5. Temperature distribution over blade section for varying gas and coolant temperatures

Temperature distributions along section PQ in the trailing section of the blade (see Fig. 4) for an inlet gas temperature of 2000° F and for a minimum coolant supply temperature increasing from zero upwards are shown in Fig. 6. Increasing the minimum temperature causes a general overall rise in temperature towards the maximum effective gas temperature. It is noted that the trailing edge blade temperature is less than for the simple case described previously. However, this is an unfair comparison as the trailing edge gas temperature is less than that of Fig. 3.

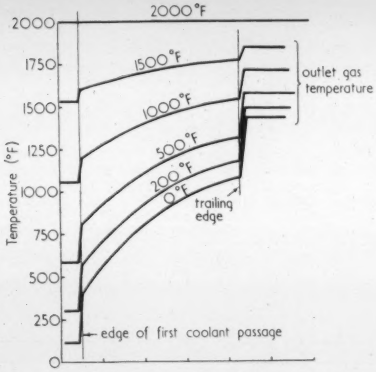

Fig. 6. Temperature distribution through blade trailing section for different coolant temperatures. Inlet gas temperature, 2000° F. Minimum coolant temperature shown on each curve

Still using the distribution of Fig. 4, a minimum coolant temperature of 200° F and an effective gas temperature at exit of 2000° F, the temperature distribution through the trailing section can be determined. It was found that the tip of the trailing section was at a temperature of 1560° F as compared with 1750° F for the case of constant gas and coolant temperatures as given in Fig. 3. The effective gas temperature at the entrance to the blade was 2700° F.

CONCLUSIONS

An analogue method has been described which gives a rapid solution to the governing equations. The examples quoted give the magnitude of the decrease in blade temperature due to the passage of coolant through the passages.

REFERENCES

(1) ELLERBROCK, H. H. *J. Aero. Sci.*, **15**, p. 721 (1948).
(2) LIVINGOOD, J. N. B., and BROWN, W. B. National Advisory Committee for Aeronautics (U.S.A.) Rep. 994 (1950).
(3) WEBER, M. *Forsch. Ing.-Wes.*, **11**, p. 49 (1940).
(4) LIEBMANN, G. *Brit. J. Appl. Phys.*, **4**, p. 193 (1953).
(5) LIVINGOOD, J. N. B., and BROWN, W. B. National Advisory Committee for Aeronautics (U.S.A.) Rep. 1066 (1952).

The orientation of fibres in an electric field

By J. O. ISARD, B.Sc., M.A., A.Inst.P., Nottingham and District Technical College, Nottingham

[*Paper received* 16 *December*, 1954]

Fibres dispersed in a liquid are observed to turn into the direction of an applied electric field. The effect is attributed to a difference of conductivity between fibre and liquid or, when both conductivities are very low, to a difference of dielectric constant. It is suggested that the effect might be used in microscopic examination of textiles.

A cell has been constructed by means of which short lengths of fibres may be observed under a microscope in an electric field. An alternating field is applied perpendicularly to the focal plane and the fibres rotate into the direction of the field so that they lie end-on to the microscope. By this means the transverse sections of the fibres can be observed rapidly and without the use of liquids or reagents which might cause swelling, and it is often possible to examine a given fibre both longitudinally and transversely, that is, before and after applying the field. It is thought that the method may be useful in the examination of fibres under the microscope, particularly for visual identification of fibres and for investigation of dye absorption. A description of the cell is given in the present paper and the results which have been obtained are discussed in terms of the theory of dielectric polarization.

DESCRIPTION OF THE CELL

The microscope slide B (Fig. 1) has a hole 1 cm diameter drilled through it and is cemented to the slide A, forming a cell about 1 mm deep. The top surfaces of A and B and the under surface of the cover glass C are coated with a transparent electrically conducting film, so that a uniform field can be maintained across the cell by connecting the supply

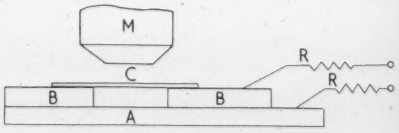

Fig. 1. Diagram of the cell

to A and B as shown. A convenient field strength is obtained by using the 230 V a.c. supply, in which case protective resistances R are inserted to prevent damage by accidental short circuits. The fibres are turned parallel to the field so

that they stand perpendicular to A and are viewed end-on in the microscope M.

The semi-conductor tin oxide was used for the transparent conducting films. They were produced by exposing the heated glass to stannic chloride.[1] The mechanical hardness and chemical durability of these films render them particularly suitable for this application and films showing second-order interference colours by reflexion, although nearly as transparent as glass, have sufficient conductivity to maintain the field across the cell even when it is filled with imperfectly insulating liquids.

Fibres about $\frac{1}{3}$ mm long are dispersed in a liquid in the cell. Shorter fibres can be used but the length must be greater than the diameter. The best liquids have been found to be those of approximately the same density as the fibres, having a moderately high viscosity and high boiling point. For instance, wool fibres have been dispersed in a mixture of paraffin oil (medicinal) and pentachlorethane of density 1·32 (denoted below W-mixture). Unless the density is approximately that of the fibres they tend to lie flat on the top or bottom of the cell and in this position there is no tendency to line up when the field is applied. A viscous liquid, such as paraffin oil, has been found to minimize swirling and movement of the fibres once they have lined up and so to improve the conditions for viewing under the microscope, but of course the viscosity must not be so high as to prevent the fibres turning in a reasonable time. Volatile liquids have been found unsuitable as bubbles may form in the cell during observations. The electrical properties of the liquid are discussed below, where it is shown from theory that the conductivity of the liquid should be different from that of the fibres, except that if both conductivities are extremely low the dielectric constants should be different.

EXPERIMENTAL OBSERVATIONS

Experiments have been carried out on a wide variety of fibres, including wool, Nylon, Terylene and glass, all of which had been in contact with laboratory atmosphere at about 65% r.h. All these fibres showed orientation in an alternating field in liquids of dielectric constant ranging from about 2 to 40. Table 1 lists the liquids used with the measured dielectric constants at 1000 c/s. The estimated dielectric constant of the glass used for the glass fibres is also shown.

Table 1. *Dielectric constants, k, and specific conductivities, σ*

	k	$\sigma\ (\Omega.m)^{-1}$
Paraffin oil	2·16	less than $5\cdot10^{-9}$
Carbon tetrachloride	2·30	
Pentachlorethane	3·69	
W-mixture of (*a*) and (*c*) at density 1·32 g/cm^3	2·98	
Aniline (dependent on sample)	7·7	$2\cdot10^{-5}$ to $5\cdot10^{-6}$
Nitrobenzene (dependent on sample)	30 to 40	10^{-4} to 10^{-5}
Glass	7·8	about 10^{-10}

The samples of aniline and nitrobenzene showed a variable conductivity, evidently depending on the moisture content, and the range of values found is given in Table 1. The other liquids showed no conductivity on the bridge used so their values must have been less than $5\cdot10^{-9}\ (\Omega.m)^{-1}$.

Alternating fields of frequencies 50 to 10000 c/s have been used but no dependence on frequency has been observed within this range. In general, field strengths of about 100 kV/m have been found necessary to obtain an appreciable effect; at less than 50 kV/m only a few fibres move, while at 200 kV/m the greater proportion usually line up. No effect was observed if the fibres were dispersed in air (up to 200 kV/m). However, the forces of adhesion between the fibres, and between the fibres and the walls of the cell are relatively stronger in air than in the liquids used, so that the absence of motion in the field is not conclusive proof of the absence of forces. In steady fields translational motions are observed, as well as orientation, and the fibres are more difficult to observe under the microscope.

FORCES DUE TO DIELECTRIC POLARIZATION

The orientation of the fibres takes place in an alternating field; hence the couple acting on the fibre must be an even function of the field strength. As this cannot arise from the presence of static charges on the fibres, the effect of dielectric polarization is considered.

The problem of an infinite cylinder of permittivity ϵ_2 and radius R lying at an angle α to an initially uniform infinite field E in a medium of permittivity ϵ_1 can be solved exactly. Cartesian axes are used with $0x$ along the cylinder axis (Fig. 2) and E in the x–y-plane at α to $0x$. Now the components of field parallel to the surface in the two media are equal at all points on the surface and div $D = 0$ everywhere; therefore the x component of the field is $E\cos\alpha$, both inside and outside the cylinder. On inserting the cylinder into the field the polarization is changed from $P_1 = (\epsilon_1 - 1)E\cos\alpha$ to $P_2 = (\epsilon_2 - 1)E\cos\alpha$, using rationalized units, and therefore the cylinder is equivalent to a dipole strength μ_x per unit length where

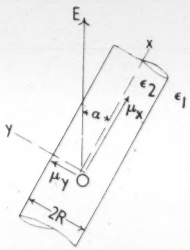

Fig. 2. Polarization of a dielectric cylinder inclined to an applied field E

$$\mu_x = (\epsilon_2 - \epsilon_1)\pi R^2 E\cos\alpha \qquad (1)$$

The y and z components of field can be obtained by treating the polarized cylinder as equivalent to a dipole strength μ_y per unit length for points outside the cylinder, and assuming a uniform field ${}_2E_y$ inside the cylinder. The potential field of an infinite line distribution of dipoles, μ_y, along $0x$ is given by $\mu_y.y/2\pi\epsilon_1(y^2 + z^2)$.

Therefore the complete potential functions are:

$$\phi_1 = -E\cos\alpha.x - E\sin\alpha.y + [\mu_y.y/2\pi\epsilon_1(y^2 + z^2)] \qquad (2)$$

$$\phi_2 = -E\cos\alpha.x - {}_2E_y.y \qquad (3)$$

The boundary conditions for non-conducting media are $\phi_1 = \phi_2$ and

$$\epsilon_1 \partial\phi_1/\partial r = \epsilon_2 \partial\phi_2/\partial r \quad \text{at} \quad r = \sqrt{(x^2 + y^2)} = R$$

Hence $${}_2E_y = \left\{1 - [(\epsilon_2 - \epsilon_1)/(\epsilon_1 + \epsilon_2)]\right\} E \sin\alpha \qquad (4)$$

and $$\mu_y = (\epsilon_2 - \epsilon_1)\left\{1 - [(\epsilon_2 - \epsilon_1)/(\epsilon_1 + \epsilon_2)]\right\} \pi R^2 E \sin\alpha \qquad (5)$$

The couple per unit length of the cylinder is given by

$$G = \mu_x E \sin\alpha - \mu_y E \cos\alpha \qquad (6)$$

taken as positive in the direction of α decreasing.

Hence $$G = [(\epsilon_2 - \epsilon_1)^2/(\epsilon_1 + \epsilon_2)] \pi R^2 E^2 \sin\alpha \cos\alpha \qquad (7)$$

i.e. $$G = [(k_2 - k_1)^2/(k_1 + k_2)] \epsilon_0 \pi R^2 E^2 \sin\alpha \cos\alpha \qquad (8)$$

where ϵ_0 is the permittivity of free space and k_1, k_2 are the dielectric constants. It is seen that G is proportional to E^2 so that it acts towards α decreasing in both alternating and steady fields. G is zero at $\alpha = 0$ or $\frac{1}{2}\pi$, and a maximum at $\alpha = \frac{1}{4}\pi$. It is proportional to $(k_2 - k_1)^2$ so that the cylinder turns parallel to the field whichever medium has the larger dielectric constant. Similarly, in magnetism, both para- and dia-magnetic bodies of elongated shape turn with their long axes parallel to a *uniform* field.[2]

The solution for a finite (long) cylinder in the finite field between two parallel plane conductors will differ from the solution for an infinite cylinder due to both the self-depolarization parallel to the axis of the cylinder, and the image force in the conducting plates. The self-depolarization along the axis will reduce the magnitude of μ_y without altering the sign. In fact, the orienting couple depends on the difference of depolarization factor in the directions perpendicular and parallel to the axis and is always towards α decreasing if the former is the greater; but no great reduction in the couple would be expected so long as the length is several diameters. On the other hand, the image force increases the magnitude of the couple. The couple on an infinite cylinder can be regarded as the resultant of the forces between each unit section and two infinitely distant plane parallel plates which are uniformly charged. The charge density on plates at a finite distance will be increased in the vicinity of the ends of the polarized cylinder, and therefore G will be increased.

Most of the experiments were carried out on fibres having a length at least ten times their diameter, so that the correction for finite length was probably small. The distance between the conducting plates was usually three or four times the fibre length, so there may have been a considerable image force. Expression (8) for the couple on an infinite cylinder probably gives an underestimate of the couple acting on the fibres.

Polarization of conducting media. If the two media have conductivities σ_1 and σ_2 and steady current conditions are attained, the current density J is given by σE and

$$\text{div}\, J = \text{div}\, \sigma E = 0 \qquad (9)$$

Hence the boundary conditions are

$$\phi_1 = \phi_2 \qquad (10)$$

$$\sigma_1 \partial\phi_1/\partial r = \sigma_2 \partial\phi_2/\partial r \qquad (11)$$

$$q_s = \epsilon_2 \partial\phi_2/\partial r - \epsilon_1 \partial\phi_1/\partial r \qquad (12)$$

where q_s is the surface density of real charges built up during the initial period of unsteady current. An approximate solution can be obtained for a long finite cylinder in an infinite field. In the y–z-plane the potential functions, equations (2) and (3), are combined with the new boundary conditions, equations (10)–(12), giving

$$\mu_y = [2\epsilon_1(\sigma_2 - \sigma_1)/(\sigma_2 + \sigma_1)] \pi R^2 E \sin\alpha \qquad (13)$$

and $${}_2E_y = [2\sigma_1/(\sigma_2 + \sigma_1)] E \sin\alpha \qquad (14)$$

The equivalent dipole μ_y gives the effect in the surrounding medium both of the dielectric polarization and of the surface

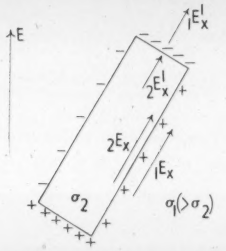

Fig. 3. Polarization of a conducting cylinder, in a conducting medium, inclined to an applied field E

charges. Parallel to the cylinder (Fig. 3) along the curved surface ${}_2E_x = {}_1E_x$ while at the plane end $\sigma_1\, {}_1E^1_x = \sigma_2\, {}_2E^1_x$ and

$$q_s = \epsilon_1\, {}_1E^1_x - \epsilon_2\, {}_2E^1_x = (\epsilon_1\sigma_2/\sigma_1 - \epsilon_2) {}_2E^1_x \qquad (15)$$

If the cylinder is long it is a reasonable approximation to assume ${}_2E^1_x = {}_2E_x = E\cos\alpha$ throughout the whole cylinder, as it would be for an infinite cylinder; this approximation ignores the depolarizing field due to q_s. The conditions at the plane ends then give

$$q_s = (\epsilon_1\sigma_2/\sigma_1 - \epsilon_2) E \cos\alpha \qquad (16)$$

The dielectric polarization gives rise to a dipole moment $(\epsilon_2 - \epsilon_1)\pi R^2 E \cos\alpha$ and the surface charges at the ends give rise to a total dipole moment $q_s \pi R^2$ per unit length. Hence the resultant dipole in the x-direction is given by

$$\begin{aligned}\mu_x &= (\epsilon_2 - \epsilon_1)\pi R^2 E \cos\alpha + (\epsilon_1\sigma_2/\sigma_1 - \epsilon_2)\pi R^2 E \cos\alpha \\ &= (\epsilon_1/\sigma_1)(\sigma_2 - \sigma_1)\pi R^2 E \cos\alpha \end{aligned} \qquad (17)$$

and the electrical couple on the cylinder per unit length by

$$\begin{aligned} G &= \mu_x E \sin\alpha - \mu_y E \cos\alpha \\ &= [\epsilon_1(\sigma_2 - \sigma_1)^2/\sigma_1(\sigma_2 + \sigma_1)] \pi R^2 E^2 \sin\alpha \cos\alpha \end{aligned} \qquad (18)$$

This equation can also be deduced from the expression given by Fürth[3] for the couple on an ellipsoid, by assuming an infinite axial ratio.

The couple is seen to be independent of ϵ_2 but proportional to the square of the difference of electrical conductivities, so that the cylinder turns into line with the field unless $\sigma_1 = \sigma_2$. When $\sigma_2 \gg \sigma_1$, the first factor becomes $\epsilon_1\sigma_2/\sigma_1$, i.e. G becomes very large; however, the approximate method of solution ignores the depolarizing effect of q_s on the fibre and q_s becomes very large when $\sigma_2 \gg \sigma_1$. The formula is therefore unsatisfactory for this condition. When $\sigma_2 \ll \sigma_1$, however, G becomes simply $\epsilon_1\pi R^2 E^2 \sin\alpha\cos\alpha$.

The order of magnitude of the time taken for the surface charges to build up is given by ϵ/σ for the more conducting medium.[4] Hence equations (9)–(18) are applicable for frequencies up to about σ/ϵ whilst equations (1)–(8) are applicable at higher frequencies, where no surface charges are built up.

COMPARISON WITH EXPERIMENTS

The vertical field strength, which will turn a fibre into the vertical position from an original inclination α, can be calculated. The gravitational restoring couple on a fibre of length l, assumed to have one end resting on the lower plate of the cell, is given by $\frac{1}{2}\pi R^2 l^2 |\rho_2 - \rho_1| g \sin\alpha$, where ρ_1, ρ_2 are the densities of the liquid and of the fibre. Using equation (8) for the electrical couple on the fibre, the condition for orientation becomes

$$E^2 \cos\alpha > [(k_1 + k_2)/(k_1 - k_2)^2].|\rho_2 - \rho_1| g/2\epsilon_0 \quad (19)$$

while using equation (18) for the electrical couple, the condition is

$$E^2 \cos\alpha > [\sigma_1(\sigma_2 + \sigma_1)/k_1(\sigma_2 - \sigma_1)^2].|\rho_2 - \rho_1| g/2\epsilon_0 \quad (20)$$

For $\sigma_2 < \sigma_1$, the latter becomes

$$E^2 \cos\alpha > [1/k_1].|\rho_2 - \rho_1| g/2\epsilon_0 \quad (21)$$

The values of E obtained are not very sensitive to the values chosen for l and $\cos\alpha$; in the following calculations l is taken as 0·3 mm and $\cos\alpha$ as 0·1 ($\alpha = 84°$). The field calculated would therefore be sufficient to orient fibres which were initially at 6° or more to the horizontal. For the glass fibres the dielectric constant was estimated from the composition as 7·8; values for the other fibres were not known. For the glass fibres $\sigma_2 < \sigma_1$ for nitrobenzene and aniline and probably also for the *W*-mixture. Values of E have been calculated for the glass fibres in these liquids from expressions (19) and (21) using the above data and they are shown in Table 2 together with the approximate experimental field strengths at which appreciable numbers of fibres oriented. The values of $f = \sigma/\epsilon$ for these liquids are also shown, and they indicate that expression (21) applies to the first two liquids at the experimental frequencies of up to 10^4 c/s. This is supported by the observed orientation of glass in aniline at 200 kV/m, which is over a thousand times less than that calculated from expression (19) but only three times less than that calculated from expression (21). The exceptional value for glass in aniline given by expression (19) is due to the near equality of the dielectric constants and is very sensitive to any errors in these, but the probable error is not sufficient to reduce the calculated field by a factor of ten. With glass in *W*-mixture, expression (19) is expected to apply at frequencies greater than 200 but a changeover to expression (21) is expected at some lower frequency; however, no significant change in the calculated orienting field accompanies the changeover. All the appropriate calculated fields are greater than the observed values but those for *W*-mixture particularly so. This may be due to having neglected the image force in the calculations of the electrical couple on a fibre.

Table 2. *Field strengths (kV/m) necessary to orient glass fibres*

	Experimental (at 1000 c/s)	Calculated from expression (19)	Calculated from expression (21)	f (c/s)
In nitrobenzene	100	355	250	10^5
In aniline	to	62 000	570	10^5
In *W*-mixture	200	960	810	<200

The data given by Hearle[5] suggest conductivities of about 10^{-5} for wool and 10^{-8} $(\Omega.m)^{-1}$ for Nylon at 65% r.h. For wool in nitrobenzene and aniline then, fibre and liquid have about the same conductivity, ignoring any dehydration of the fibre by the liquid and consequent lowering of the conductivity. However, it is unlikely that the conductivities will be so nearly equal as to cause an exceptionally high value of E from expression (20). Wool has a much greater conductivity than the other liquids of Table 1, which means that relatively low values of E would cause orientation. Nylon in nitrobenzene and aniline has $\sigma_2 < \sigma_1$ and the calculated fields from expression (21) will be similar to those for glass in Table 2, differing only by the change of density factor, $|\rho_2 - \rho_1|$, which would reduce the estimated field. Probably in the other liquids used, Nylon has $\sigma_2 > \sigma_1$. It is not possible to apply expression (19) to other fibres than glass in the absence of precise data on the dielectric constant. Errara and Sack[6] found the dielectric constant of dehydrated wool to range from 5·4 at 8 kc/s to 4·2 at 13 Mc/s but they reported a marked increase due to only 1% of moisture. New[7] and Murphy[8] found the capacity of cotton to increase very steeply with relative humidity at 1000 c/s and to decrease with increasing frequency, and Murphy suggests that the capacity is electrolytic in nature. These results suggest that the dielectric constant is high only if the moisture content is high, so that a much higher value would be expected for wool than for Nylon or Terylene at 65% r.h.

In general, the theory outlined requires fields of 100 to 1000 kV/m for most fibres in most liquids unless $k_1 = k_2$ fairly exactly and both conductivities are extremely low. The experimental fields are generally lower, but this discrepancy may be partly attributed to the neglected image force effects. However, another contribution to the couple on a fibre must be considered which may become important for very fine fibres. When any body is immersed in any liquid, an electrical double layer,[8] consisting of two concentric sheaths of oppositely charged electricity, is set up at the interface. Under the influence of an applied field there will be a displacement between the sheaths of charge, and, for a fibre, this displacement will be proportionately larger along the axis than perpendicularly to it, since this involves only a shearing between the sheaths of charge and not a separation of them. The polarization of the double layer gives a positive contribution to μ_{xx} and therefore to G, and acts towards α decreasing in both alternating and steady fields. In the absence of any data on the polarizability of a double layer no calculation can be made of the magnitude of this effect.

ACKNOWLEDGEMENTS

The author is indebted to Dr. H. A. Taylor of the Department of Glass Technology, Sheffield University, for information about the dielectric properties of glass, to Messrs. Pilkingtons Ltd. for supplying special samples of glass fibres, and to Mr. R. C. G. Williams of the Textile Department, Nottingham and District Technical College, for constant co-operation and enthusiasm.

REFERENCES

(1) Mochel, J. M. U.S. Patent 2522531 (1950).
(2) Stoner, E. C. *Phil. Mag.*, **23**, p. 833 (1937).
(3) Fürth, R. *Z. Phys.*, **22**, p. 98 (1924); **44**, p. 256 (1927).
(4) Abraham, M., and Becker, R. *Classical Electricity and Magnetism*, p. 115 (London: Blackie and Son, Ltd., 1932).
(5) Hearle, J. W. S. *J. Text. Inst.* [*Manchester*], **43**, p. 194 (1952).
(6) Errara, J., and Sack, H. S. *Industr. Engng Chem.*, **35**, p. 712 (1943).
(7) New, A. A. *Elect. Commun.*, **19**, p. 71 (1940).
(8) Murphy, E. J. *J. Phys. Chem.*, **33**, p. 200 (1929).
(9) Alexander, A. E., and Johnson, P. *Colloid Science*, Vol. 1, p. 295 (Oxford: Clarendon Press, 1949).

Correspondence

The study of semiconductor crystal perfection by X-ray diffraction methods

The electrical properties of semiconductors have been shown to be affected by certain types of crystal defects.* These may be studied by means of a high-resolution X-ray diffraction method, the essential feature of which is the use of a micro-focus X-ray source in conjunction with a collimator giving a narrow, near-parallel beam. This combination avoids the "pinhole camera" effect obtained by using a normal-sized

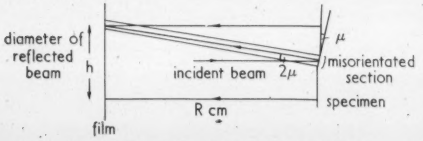

Fig. 1. Resolution of small misorientations

X-ray focus with a small aperture, and causes the appearance of a back-reflexion Laue diffraction spot to depend simply on the character of the crystal under examination. Although the parallel beam only gives spots of the same dimensions as the beam diameter, photographic enlargements can be prepared, and the limit of resolution is set by the grain of the X-ray film employed. The Laue method is chosen because of its great versatility: both orientation and perfection of a crystal can be obtained from a single photograph.

It is often necessary to know the angles between two crystallites which have a slight relative inclination, and the minimum angle which can be resolved depends on the beam diameter (Fig. 1). If a normally reflecting matrix contains, at its centre, a small included region of slightly different orientation, in which the reflecting plane is mis-orientated by an angle μ, the reflected beam from this region will be turned through an angle 2μ. This will be resolved (i.e. will strike the film outside the main reflexion) if $\mu > h/4R$ (where h is the beam diameter and R is the specimen-film distance). With a parallel beam, then, the angular resolution is thus directly proportional to the collimator diameter. Whether or not the two reflexions are distinguishable will then depend on how much they are broadened by the divergence of the beam. This factor is also controlled by the collimator diameter, so that to resolve small misorientations, the latter dimension should be made as small as is convenient for rapid alinement of the apparatus. (With a microfocus unit, the exposure time required is independent of the fraction of the total output of the tube employed.) The ultimate limit of angular resolution is set by the angle of convergence of the X-ray beam to a point on the specimen surface.

Fig. 4. Reflexions from lineage "fibres" parallel to the growth direction of a silicon ingot (total spread of orientation 3·2°) (× 10)

Fig. 2. Reflexion from an area of silicon crystal crossed by twin lamellae 0·05 mm or less in width (× 20)

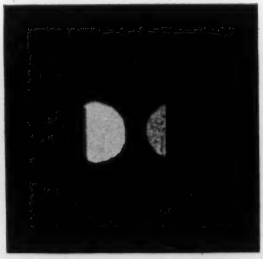

Fig. 3. Reflexion from regions on either side of a low-angle (1·1°) boundary in germanium (× 10)

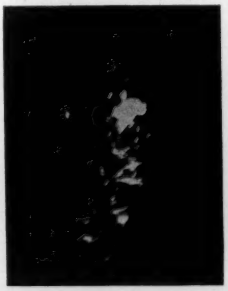

Fig. 5. Reflexions from a fragmented lattice in silicon (maximum spread of orientation from growth axis ± 2°) (× 10)

* Taylor, W. E., Odell, N. H., and Fan, H. Y. *Phys. Rev.*, **88**, p. 867 (1952).
Tweet, A. G. *Bull. Amer. Phys. Soc.*, **29** (5), p. 17 (1954).
Vogel, F. L., Read, W. T., and Lovell, L. C. *Phys. Rev.*, **94**, p. 1791 (1954).

Provided the collimator is such that there is no specular reflexion of X-rays from its walls, this angle will be proportional to the dimensions of the focal spot, and may easily be reduced to less than a minute of arc.

Figs. 2–5 show various enlarged examples of diffraction spots from defective crystals, obtained by application of the above principles. ($h = 1$ mm, $R = 3$ cm, focal spot diameter $= 0{\cdot}04$ mm for each of these photographs.)

For routine examination of specimens for the presence of defects, it is possible to use a fine beam and still study a large area of crystal by using a scanning mechanism. In this, the surface to be studied is carefully mounted parallel to the film, and by means of a suitably geared clock motor, it is drawn across the beam on a smooth-running carriage at a rate of 1 or 2 cm/h. By this means a line is scanned, and if the crystal is perfect the Laue photograph will be indistinguishable from one taken with the crystal stationary. Any defects occurring along the line, on the other hand, will give rise to distortions of the spots. To enable a larger area to be studied, a parallel-sided slit collimator may be employed, with its length perpendicular to the direction of traverse. Having once discovered the existence of defects by this means, stationary-crystal methods can be used to study them individually.

The details which can be revealed by these methods are:

(1) bulk defects, such as lineage and fragmentation;
(2) curvature of lattice;
(3) surface damage overlying a perfect structure.

The method is not sensitive to variations in lattice parameter, since white X-rays are employed, but the impurity densities normally occurring in semiconductor work are in any case so small as to have no appreciable effect on the parameter.

I am indebted to Dr. T. E. Allibone, and to the Admiralty, for permission to publish this note.

Research Laboratory, P. J. HOLMES
Associated Electrical Industries Ltd.,
Aldermaston, Berks.

A simple and rapid method of measuring the complex permittivity of a liquid

In a recent paper an apparatus was described for investigating the dielectric properties of liquids in the wavelength range of 4 to 50 cm.* For particular cases a method has since been developed which requires neither a phase-changer nor a cut-off attenuator, the complex permittivity being completely determined in terms of the positions of particular points in the standing wave set up in a short-circuited line.

If a short-circuited coaxial line contains liquid of propagation constant $\gamma = \alpha + j\beta$, the electric vector E at any point distant x from the short circuit may be written

$$E = E_0(e^{\gamma x} - e^{-\gamma x}) \qquad (1)$$

from which it follows that the amplitude $|E|$ is given by

$$|E| = E_0(\cosh 2\alpha x - \cos 2\beta x)^{\frac{1}{2}} \qquad (2)$$

If now two points with equal amplitudes are found at positions x_1 and x_2 from the short circuit, then

$$\cosh 2\alpha x_1 - \cos 2\beta x_1 = \cosh 2\alpha x_2 - \cos 2\beta x_2 \qquad (3)$$

and providing β is known, then, in principle, equation (3) can be solved for α. β is determined from the positions of the minima.*

Experimentally, therefore, it is only necessary to find two points where equal signal strengths are detected and then to measure their distances from the short-circuit with a micrometer. It will be noticed that the method is independent of the law obeyed by the detector.

To put the method to its best practical use, x_1 and x_2 must be chosen so as to facilitate the solution of equation (3) and to satisfy the condition that the error in α due to errors in measuring x_1 and x_2 be as small as possible. This is done as follows.

Differentiation of equation (3) gives the result,

$$\frac{\delta\alpha}{\alpha} = \frac{[\sinh 2\alpha x_1 + (\beta/\alpha)\sin 2\beta x_1]|\delta x_1| + [\sinh 2\alpha x_2 + (\beta/\alpha)\sin 2\beta x_2]|\delta x_2|}{x_1 \sinh 2\alpha x_1 - x_2 \sinh 2\alpha x_2} \qquad (4)$$

Hence for best results the following criteria must be satisfied:

(*a*) the two points be as far apart as possible; and
(*b*) one must be approximately at a minimum and the other approximately at a maximum.

Consideration of equation (4) also shows that the method is only suitable for medium- or high-loss liquids.

Thus a pair of points such as P and Q (see figure) should be chosen, with corresponding distances equal to x_2 and x_1

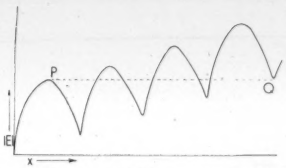

Variation of amplitude with distance along a short-circuited line

respectively. This also facilitates the solution of equation (3) since the approximations $\cos 2\beta x_1 = 1$ and $\cos 2\beta x_2 = -1$ may be written leading to

$$\cosh 2\alpha x_1 - 1 \simeq \cosh 2\alpha x_2 + 1 \qquad (5)$$

or

$$\sinh \alpha x_1 \simeq \cosh \alpha x_2 \qquad (6)$$

Equation (6) can be solved readily from tables of hyperbolic functions and the value of α so obtained substituted into equation (3) to obtain a more accurate result.

The method has been used successfully for water at a wavelength of 17 cm and it was found that usually at least two pairs of points could be observed, giving a useful check on each other.

Department of Physics Applied to Medicine, E. H. GRANT
Middlesex Hospital Medical School,
London, W.1.

The thermal conductivity of some technical materials at low temperatures

We have, at various times, determined the thermal conductivities of several substances which are of technical interest. Some of these have not been reported elsewhere and, as the results may be useful to other workers in the low temperature field, we give them below. The apparatus used for the measurements was the same as has been described previously.[1]

* BUCHANAN, T. J., and GRANT, E. H. *Brit. J. Appl. Phys.*, **6**, p. 64 (1955).

The relevant details of the materials are as follows.

Brass. A rod $\frac{1}{8}$ in. in diameter and conforming to B.S. 249, supplied by Henry Righton and Co. Ltd. (copper 55–60%, lead 2·0–3·5%, impurities 0·75%, remainder—about 40%—zinc). It was measured as received and also after being heated to a dull red heat for ten minutes and being allowed to cool slowly. The electrical resistivity was unchanged, with values of $7{\cdot}2 \times 10^{-6}\,\Omega$ cm at room temperature and $3{\cdot}5 \times 10^{-6}\,\Omega$ cm at 20° K.

As the temperature variation of thermal conductivity is, in each case, similar to that previously found for substances of the same types, the results will not be discussed further. Detailed reviews of heat conduction in metals and non-metals are given by Olsen and Rosenberg[3] and Berman[4] respectively.

The greatest use for these values is probably in the calculation of the heat flow down rods or tubes when the ends are at different temperatures. As before,[5] we therefore

Table 1. *Thermal conductivity of technical materials (W/cm.°C)*

Temperature (°K)	Brass as received	Brass annealed	Beryllium copper	Soft glass	Nylon	Soft solder	Wood's metal
2	$1{\cdot}3 \times 10^{-2}$	$1{\cdot}5 \times 10^{-2}$	$9{\cdot}0 \times 10^{-3}$	$5{\cdot}3 \times 10^{-4}$	$6{\cdot}5 \times 10^{-5}$	$5{\cdot}0 \times 10^{-2}$	$1{\cdot}0 \times 10^{-2}$
3	$2{\cdot}1$	$2{\cdot}3$	$1{\cdot}4 \times 10^{-2}$	$8{\cdot}3$	$9{\cdot}5$	$1{\cdot}15 \times 10^{-1}$	$2{\cdot}4$
4	$2{\cdot}9$	$3{\cdot}4$	$1{\cdot}9$	$1{\cdot}19 \times 10^{-3}$	$1{\cdot}2_5 \times 10^{-4}$	$1{\cdot}6$	$4{\cdot}0$
5	$3{\cdot}7$	$4{\cdot}4$	$2{\cdot}3$	$1{\cdot}44$	$1{\cdot}6$	$2{\cdot}2$	$5{\cdot}6$
6	$4{\cdot}6$	$5{\cdot}4$	$2{\cdot}9$		$2{\cdot}0$	$2{\cdot}6_5$	$7{\cdot}3$
8	$6{\cdot}4$	$7{\cdot}5$	$3{\cdot}9$		$2{\cdot}8$	$3{\cdot}6_5$	$1{\cdot}0 \times 10^{-1}$
10	$8{\cdot}2$	$9{\cdot}6$	$4{\cdot}9$		$3{\cdot}9$	$4{\cdot}2_5$	$1{\cdot}2$
15	$1{\cdot}3 \times 10^{-1}$	$1{\cdot}46 \times 10^{-1}$	$7{\cdot}8$		$6{\cdot}8$	$5{\cdot}1$	$1{\cdot}5_5$
20	$1{\cdot}7_5$	$1{\cdot}93$	$1{\cdot}07 \times 10^{-1}$		$9{\cdot}8$	$5{\cdot}6$	$1{\cdot}7$
25	$2{\cdot}1_5$		$1{\cdot}35$			$5{\cdot}7_5$	$1{\cdot}8$
30	$2{\cdot}5_5$		$1{\cdot}62$			$5{\cdot}6_5$	$1{\cdot}9$
40	$3{\cdot}3$		$2{\cdot}15$			$5{\cdot}2_5$	$2{\cdot}0$
50	$4{\cdot}0$		$2{\cdot}62$			$5{\cdot}2$	$2{\cdot}1$
60	$4{\cdot}6$		$3{\cdot}04$			$5{\cdot}1_5$	$2{\cdot}2$
70	$5{\cdot}0$		$3{\cdot}40$			$5{\cdot}2$	$2{\cdot}2_5$
80	$5{\cdot}3$		$3{\cdot}71$			$5{\cdot}2_5$	$2{\cdot}3$
90	$5{\cdot}4$	$5{\cdot}4$				$5{\cdot}3$	$2{\cdot}3$

Table 2. *Heat flow in watts along specimens 10 cm long, 1 mm² cross-sectional area*

Temperatures at ends (°K)	Brass (annealed)	Beryllium copper	Nylon	Glass
80–20	$2{\cdot}3 \times 10^{-2}$	$1{\cdot}6 \times 10^{-2}$		$2{\cdot}1 \times 10^{-4}$*
60–20	$1{\cdot}3 \times 10^{-2}$	$9{\cdot}4 \times 10^{-3}$		$1{\cdot}2 \times 10^{-4}$*
20–4	$1{\cdot}7 \times 10^{-3}$	$9{\cdot}7 \times 10^{-4}$	$8{\cdot}3 \times 10^{-6}$	$2{\cdot}9 \times 10^{-5}$*
10–4	$3{\cdot}3 \times 10^{-4}$	$2{\cdot}0 \times 10^{-4}$	$1{\cdot}5 \times 10^{-6}$	$9{\cdot}4 \times 10^{-6}$*
4–1	$5{\cdot}2 \times 10^{-5}$	$3{\cdot}5 \times 10^{-5}$	$2{\cdot}3 \times 10^{-7}$	$2{\cdot}1 \times 10^{-6}$
1–0	$2{\cdot}7 \times 10^{-6}$	$2{\cdot}0 \times 10^{-6}$	$1{\cdot}4 \times 10^{-8}$	$1{\cdot}3 \times 10^{-7}$

* Extrapolated according to relation found for quartz glass and Phoenix glass, which are, respectively, about 10 and 20% lower.

Beryllium copper. An alloy containing 2% beryllium was held at 300° C for two hours. The resulting hardness was about 41 Rockwell units. The electrical resistivity was $8{\cdot}25 \times 10^{-6}\,\Omega$ cm at room temperature, $6{\cdot}2 \times 10^{-6}\,\Omega$ cm at 77° K and $5{\cdot}5_4 \times 10^{-6}\,\Omega$ cm at 4·2° K.

Soft glass. Supplied by General Electric Company, Ltd., type X8 (SiO_2 70·12%, Al_2O_3 2·58, CaO 5·40, MgO 3·6, Na_2O 16·82, K_2O 0·35, B_2O_3 0·78, SO_3 0·20). Density 2·50 g/cm³.

Nylon. A drawn monofilament, 2 mm in diameter, supplied by Imperial Chemical Industries Ltd.

Soft solder. Tin 60%, lead 40%. Made up in the laboratory.

Wood's metal. Supplied by May and Baker, Ltd., without any specification. (Normal composition is bismuth 48%, lead 26%, tin 13%, cadmium 13%.)

Application of the Wiedemann–Franz–Lorenz law shows that for brass and for beryllium copper the electronic component represents 80–90% of the measured thermal conductivity. It will be noted that the annealing of the brass rod increased the thermal conductivity without altering the electrical resistance. This shows that only the lattice thermal conductivity is affected, in agreement with the results of Estermann and Zimmerman.[2]

append Table 2 giving heat flow along specimens 10 cm long and 1 mm² cross-sectional area, when the temperatures at the ends vary from 80 to 0° K. If the evaporation rate of liquid hydrogen or liquid helium produced by these heat flows is to be calculated, it should be noted that 1 W evaporates about 100 cm³ of liquid hydrogen per hour and about 1 l. of liquid helium per hour.

The measurements on beryllium copper were made at the Cryogenic Engineering Laboratory, Massachusetts Institute of Technology, Cambridge, Mass., while one of us (R. B.) was on leave of absence from Oxford.

Clarendon Laboratory,
University of Oxford.

R. Berman
E. L. Foster
H. M. Rosenberg

REFERENCES

(1) Berman, R. *Proc. Roy. Soc. A*, **208**, p. 90 (1951).
(2) Estermann, I., and Zimmerman, J. E. *J. Appl. Phys.*, **23**, p. 578 (1952).
(3) Olsen, J. L., and Rosenberg, H. M. *Adv. Phys.*, **2**, p. 28 (1953).
(4) Berman, R. *Adv. Phys.*, **2**, p. 103 (1953).
(5) Berman, R. *Phil. Mag.*, **42**, p. 642 (1951).

New books

X-ray diffraction by polycrystalline materials. Edited by H. S. PEISER, M.A., A.R.I.C., F.Inst.P., H. P. ROOKSBY, B.Sc., F.Inst.P., and A. J. C. WILSON, M.Sc., Ph.D., A.I.M., F.Inst.P. (London: The Institute of Physics, 1955.) Pp. 725. Price 63*s*.

This volume is the latest addition to the Physics in Industry series of monographs.

It is divided into three parts: experimental techniques, interpretation of data, and practical uses of the techniques in different fields. It contains over 250 figures, many references and an Appendix which includes useful tables.

Its contents and purpose are well described by Sir Lawrence Bragg in his foreword:

"For anyone who has been concerned with X-ray analysis since its early days, it is fascinating to see how the subject continues to grow and ramify. The present book is a striking illustration of this development. Although it deals with only one branch of crystal analysis, the study of polycrystalline materials, it has been found desirable to invite some thirty experts to make their contributions in order that each aspect of the subject might be covered in an authoritative way. That it has been possible to weld contributions from so many authors into a coherent scheme is both a tribute to the editors and an excellent example of that happy collaboration that has existed from the very beginning amongst X-ray crystallographers and continues so manifestly at the present time.

"The subject of this book is an important branch of X-ray crystallography because so many crystalline substances are only available in a microcrystalline form and because a 'powder photograph' is a ready way of obtaining a record characteristic of all the diffraction effects with a single exposure. It is not surprising that, in industrial applications especially, powder photographs are used to a far greater extent than the examination of single crystals.

"An interesting feature of this book is the series of essays at the end, which show how the methods described in the earlier chapters can be applied in many different scientific fields. The earlier chapters deal with tactics, the latter with strategy. These essays, in addition to their interest to the expert, should also have a particular appeal to all who wish to assess the potentialities of X-ray techniques in many branches of science.

"The lore of X-ray analysis by powder photographs, only to be found otherwise in many journals and books, is here collected into a form in which it is readily accessible, and this book will be warmly welcomed by an ever-increasing number of scientists."

Optics; lectures in theoretical physics (Vol. 4). By ARNOLD SOMMERFELD, translated by OTTO LAPORE and PETER A. MOLDANER. (London: Academic Books Ltd.; New York: Academic Press Inc., 1954.) Pp. xii + 383. Price $6.80.

This is an English translation of the well-known German text, the changes and additions being very slight. It assumes Maxwell's equations, and then treats the whole field of physical optics. The mathematical treatment is delightful in its directness and elegance. Much of the text would be suitable for the honours student in physics, but a number of topics would not be appropriate, for example, the rigorous treatment of the diffraction by a straight edge.

The translation reads well, and the rendering of this masterly work more accessible to English-speaking physicists is something for which many will be very grateful. The book is somewhat expensive, but well worth the price.

H. H. HOPKINS

Notes on applied science No. 8. Audio frequency power measurements. (London: H.M. Stationery Office, 1954.) Pp. iv + 16. Price 1*s*.

This is one of a series of booklets issued by the National Physical Laboratory and describes the measurement of power at frequencies over the audio frequency range, including, of course, mains frequencies. Three types of wattmeter are discussed and the limitations and advantages of each are outlined: these are the electrostatic, the thermal, and the electrodynamic wattmeters.

It is probably because the N.P.L. is concerned mainly with precision measurements that only these three types are described. Whilst the applications of electronic techniques are mentioned as possibilities, no word is given about any calorimetric methods and more might have been said about three-phase power measurements.

A. J. MADDOCK

Principles of modern acoustics. By G. W. SWENSON, Jr., Ph.D. (New York: D. van Nostrand Co. Inc.; London: Macmillan and Co. Ltd., 1954.) Pp. vii + 222. Price 30*s*.

In this work, sound is treated mainly from the view-point of the engineer, particularly the electrical engineer. The author plunges straightway into electrical networks and their mechanical analogues, from which the electro-acoustic transducer emerges. Then follow the vibrating string and membrane, plane and spherical waves of sound, normal modes and horns. These chapters lead on to architectural acoustics and subjective sound. Except in the last chapters, the treatment is almost entirely mathematical. Useful problems are set at the chapter ends. A helpful feature not usually met in books of this type is an appendix on methods of approximation to the solutions of wave problems, with some examples in the calculation of natural frequencies.

E. G. RICHARDSON

Massbalancing of aircraft control surfaces (Aeronautical). By H. TEMPLETON, B.Sc., F.R.Ae.S. (London: Chapman and Hall, Ltd., published under the authority of the Royal Aeronautical Society, 1954.) Pp. x + 241. Price 35*s*.

Mr. Templeton's monograph, the first book to deal specifically with massbalancing, is intended for students of aeronautics specializing in flutter. It is divided into three parts. The first deals very clearly with the basic principles of massbalancing, whilst the second part is devoted to their application. The numerous parameters that influence flutter characteristics, and thus determine the amount of mass-balance necessary for safety are enumerated and their effects are considered by the inclusion of brief accounts of a number of theoretical and experimental investigations that have been made. An account is then given of the "rules of thumb," the design criteria for avoiding flutter, and an outline is also given of the procedure to be followed during the design and development stage for ensuring, by detailed calculations, ground resonance tests and flight tests, that a prototype is flutter-free. The third part of the monograph looks for future trends and alternative means of prevention.

Except for the omission of any references to sources of information both on the general methods of flutter calculation and on the practical details of resonance and flight testing, the monograph is a thorough treatment of the subject. It will doubtless be of great value to those in design offices who are responsible for ensuring that their aircraft do not flutter.

N. C. LAMBOURNE

Notes and comments

Noise Control

We have received a copy of the first issue of a new bi-monthly magazine called *Noise Control*. It is produced by The Acoustical Society of America and like the Society's *Journal* it is published for it by the American Institute of Physics (57 East 55th Street, New York 22, New York), from where details of the various subscription rates can be obtained. The magazine "is directed to the reader who needs to know about noise control—whether he is an engineer, the manager of a factory, an 'audiologist,' or an architect." The copy before us is produced in what we should call a characteristically American semi-popular style, with copious illustrations, some of a cartoon nature, and practically no mathematics.

The contents in this issue are: Fundamentals of noise control; What does the ASA "Z24–X–2 Report" mean?; Twenty-five years' research in outdoor noise; How quiet must it be to measure normal hearing?; Noise reduction of machinery and vehicles; Quieting of apartments and houses; Measurement techniques for special noise problems; Control of interior noise; A community's reaction to noise: can it be forecast? In addition there are sections entitled: Legal aspects of noise; They are doing something about noise; Books; Noise in the news; New products, and Letters to the Editor.

Plastics exhibition and convention

The third biennial British Plastics Exhibition will be held at Olympia, London, from 1 to 11 June, 1955, and there will be nearly 100 exhibitors.

The associated convention which opens on 2 June and ends on 9 June will discuss twenty-one papers on the following subjects: Polymer structure and properties; Polymer formation; Expanded plastics; Thermoplastics; Extrusion; Work study; Injection moulding; Patents; Foundry resins; Glass reinforced plastics.

The exhibition is being organized by the journal *British Plastics* with the full co-operation of the British Plastics Federation. Further details may be obtained from the publishers: Associated Iliffe Press, Dorset House, Stamford Street, London, S.E.1.

Electronics exhibition

The Tenth Annual Exhibition organized by the Northern Division of the Institution of Electronics will be held at the College of Technology, Sackville Street, Manchester, 1, during the period 14–20 July, 1955. The exhibition will be open from 2 p.m. to 10 p.m. on 14 July, from 10 a.m. to 10 p.m. on 15, 18, 19 and 20 July and from 10 a.m. to 6 p.m. on 16 July.

Programmes of the lectures and film show (post free price 4½*d.*) will be available in June and catalogues (post free price 2*s.*) will be on sale early in July. Tickets are obtainable, free of charge, from the Honorary Exhibition Organizing Secretary, Mr. W. Birtwistle, 78 Shaw Road, Rochdale, Lancs., or from any of the exhibitors. A stamped and addressed envelope should be enclosed.

Semiconducting materials and transistors—a bibliography

A thirty-eight-page bibliography has been produced of work on semiconducting materials and transistors which has been published over the past ten years. The entries have been classified into the following groups: semiconductors—theory and measurements; processing of semiconductors; transistors; new forms of transistors; rectifiers and diodes; other semiconducting devices.

Copies of this bibliography are available free of charge from Pye Industrial Electronics Ltd., Exning Road, Newmarket, Suffolk.

Post-graduate courses in instrument technology

The National College of Horology and Instrument Technology, in conjunction with the Instrument Engineering Department of Northampton Polytechnic, conducts single-session (October–July) full-time courses in instrument technology for students holding either a university degree in science or engineering, or a Higher National Certificate (or diploma) in engineering, or an equivalent qualification. The aim of the course is to provide specialized or supplementary training in the field of instrument technology.

The next session commences in October. Application forms and prospectuses may be obtained from the Secretary, National College of Horology and Instrument Technology, Northampton Polytechnic, St. John Street, London, E.C.1.

Journal of Scientific Instruments

Contents of the May issue

SPECIAL ARTICLE

History of electrical devices for measuring strains and small movements. By B. E. Noltingk.

ORIGINAL CONTRIBUTIONS

Papers

The use of the milling machine for preparing bone sections for microradiography and microautoradiography. By Jenifer Jowsey.

A simple, sensitive, saturated-core recording magnetometer. By V. B. Gerard.

An infra-red radiation pyrometer. By J. D. Harmer and B. N. Watts.

A microscope hot stage using electron bombardment. By G. J. Ogilvie and G. Brinson.

A superconducting reversing switch. By I. M. Templeton.

A tilting micromanometer with continuous sensitivity control. By L. R. Taylor.

An automatic monitor for measuring tritium contamination in air. By D. F. Shaw.

Apparatus for the measurement of the lifetime of phosphorescence phenomena. By A. van Roggen and R. A. Vroom.

A single-profile crystal extensometer adjustable for orientation. By A. J. Kennedy.

A computing microphotometer for cell analyses. By S. Bourghardt, H. Hyden and B. Nyquist.

Laboratory and workshop notes

A stabilized current supply for a mass spectrometer, surface ionization, source. By K. L. Aitken, F. Hart and P. Reynolds.

Controlled water flows. By G. T. P. Tarrant.

A simple metal-to-metal vacuum valve. By G. W. Green.

Pneumatic micro-tweezers. By J. I. Pankove.

NOTES AND NEWS

New books

New instruments, materials and tools

Notes and comments

THIS JOURNAL is produced monthly by The Institute of Physics, in London. It deals with all branches of applied physics (including theory and technique).

All rights reserved. Responsibility for the statements contained herein attaches only to the writers.

EDITORIAL MATTER. Communications concerning editorial matter should be addressed to the Editor, The Institute of Physics, 47 Belgrave Square, London, S.W.1. (*Telephone:* Sloane 9806.) Prospective authors are invited to prepare their scripts in accordance with the *Notes on the preparation of contributions*. (Price 2*s.* 6*d.* including postage.)

REPRODUCTION. The Institute of Physics is a signatory to The Royal Society's Fair Copying Declaration. Details may be obtained upon application from The Royal Society, London, W.1.

ADVERTISEMENTS. Communications concerning advertisements should be addressed to the agents, Messrs. Walter Judd Ltd., 47 Gresham Street, London E.C.2. (*Telephone:* Monarch 7644.)

CLAIMS FOR MISSING JOURNALS. Claims from regular subscribers to this *Journal* for missing numbers will only be considered if received within 60 days of the date of mailing plus normal outward time of transit and time for lodging the claim. Losses attributable to failure to notify a change of address or to similar omissions will not be considered.

SUBSCRIPTION RATES. A new volume commences each January. The charge is £4 per volume ($11.50 U.S.A.), including index (post paid), payable in advance. Single parts, so far as available, may be purchased at 8*s.* each ($1.15 U.S.A.), post paid, cash with order. Orders should be sent to The Institute of Physics, 47 Belgrave Square, London, S.W.1, or to any bookseller.

Electronic fluctuations in semiconductors*

By Prof. R. E. Burgess, B.Sc., A.M.I.E.E.,† Radio Research Station, Slough, Bucks.

Electrical fluctuations which occur in semiconductors, particularly on the passage of current, are of considerable fundamental and technological significance. In many systems the limiting sensitivity is determined almost entirely by the noise of a semiconductor device. The present paper reviews the various types of spontaneous fluctuation which arise and comparison is made with the corresponding processes in a vacuum tube.

Particular attention is paid to modulation noise which is conspicuous in semiconductors at low frequencies, especially when current-carrying contacts or barriers occur.

Electrical fluctuations in semiconductors have attracted considerable attention over the last fifteen years, for two main reasons; because many radio and electronic devices depend essentially for their operation on the properties of a semiconductor and because the noise exhibited by these devices when carrying current can be considerably in excess of the thermal and shot noise components. Usually the spectral density of the noise decreases with increasing frequency and for this reason it is particularly a limitation at the lower frequencies; for instance, the transistor cannot compete with the vacuum tube at audio frequency in respect of signal/noise ratio, and this limitation in the performance of a new device has been responsible for increased attention to the general problem.

Empirically it has been observed that devices which are accurately reproducible in their macroscopic parameters (current-voltage-temperature characteristics) may exhibit noise levels which differ greatly from one sample to another. It is accordingly believed that the fluctuation processes may be markedly structure-sensitive and depend upon certain types of imperfection to a much greater extent than the macroscopic characteristics. It is also known experimentally that there is a particular tendency for noise to be generated in transition regions such as occur between a metal electrode and a semiconductor or between semiconductors having opposing types of conductivity. Since one or both of these types of transition region are inevitably present in practical devices it is particularly important that contact and junction noise should be understood.

There is little doubt that further improvements will result from more refined techniques of preparing semiconducting materials so as to eliminate chemical and physical imperfections and from advances in methods of fabrication so as to control the conditions existing at the surfaces and at electrode contacts.

In the present paper the various sources of noise in semiconductors are considered. Where possible the individual processes are compared with those which are analogous and familiar in the vacuum tube. We shall not be greatly concerned with *purely* spatial fluctuations, i.e. variations from point to point of the properties of the semiconductor as might arise from a random distribution of impurities; so long as such a distribution is invariant in time it would not of itself provoke temporal fluctuations which are our concern here.

It is appropriate to consider some of the terminology used to describe the fluctuations and for this purpose we regard the fluctuating variable x in which we are interested as a statistically stationary time series having certain well defined attributes; mean value $\bar{x}$, variance σ^2, autocorrelation coefficient $r(t)$, and the spectral density $S(f)$.

The spectral density may be defined as follows: if a fluctuating voltage be transmitted by a narrow band pass filter centred on frequency f and having unity transmission over a bandwidth Δf, the mean square voltage at the output would be given by $S(f)\ \Delta f$ when averaged over a time long compared with $1/\Delta f$. If the variable under examination contained a d.c. component $\bar{x}$ or a discrete sine-wave component of a certain frequency f_0, these would give rise to spectral lines at $f = 0$ or f_0 and would correspond to delta function terms in $S(f)$. In the fluctuations we are considering there may in general be a non-zero mean value of the quantity but not usually any discrete frequencies. The relations between the autocorrelation coefficient and the spectral density of the continuum may therefore be written

$$\sigma^2 r(t) = \int_0^\infty S(f) \cos(2\pi f t) df \qquad (1)$$

$$S(f) = 4\sigma^2 \int_0^\infty r(t) \cos(2\pi f t) dt \qquad (2)$$

The latter relation is frequently of convenience in the calculation of the spectral density of processes in which the statistical behaviour in time is readily formulated.

In more physical terms, the variables whose fluctuations are of interest include: current, voltage, resistance or conductance, number of carriers, number of ions, number of occupied traps, rates of generation and recombination of carriers, temperature, and height of a potential barrier.

A phenomenological description of the noise current and voltage of a two-terminal device connected in a circuit may be attempted in terms of the "fluctuating characteristic" concept. It is worthwhile to examine this in a little detail since the question of representation of noise generators in non-linear systems is involved. Consider a simple circuit having a battery of e.m.f. E in series with a source resistance S and a noisy element of resistance $R(t)$ which will be assumed for generality to have a non-linear current-voltage characteristic. Let it be possible to speak of an instantaneous characteristic, so that the characteristic at time t in general differs from the mean characteristic (as observed macroscopically). The fluctuations will always be regarded as sufficiently small for first-order effects only to be important. On account of the non-linearity the d.c. resistance R and the a.c. differential resistance ρ differ. The following relations then hold for the fluctuations of voltage current and resistance:

$$V = -S\Delta I = \frac{SE}{(S+R)^2}\Delta R = \frac{SI}{S+R}\Delta R \qquad (3)$$

* Based on a lecture given before the Electronics Group of The Institute of Physics in London on 18 September, 1954.

† Now at Department of Physics, University of British Columbia, Vancouver.

whereas the equivalent noise generators are

$$e = -\rho i = \frac{S+\rho}{S+R} I\Delta R \tag{4}$$

It is important to note that the noise e.m.f. e is not in general equal to $I\Delta R$. Equality only obtains when the noisy element R is linear ($R = \rho$) or when the impedance of the external circuit is very large compared with both R and ρ. Similarly the noise current generator i is not in general equal to $-I\Delta R/R$ unless R is linear or the impedance of the external circuit is very small compared with both R and ρ. It is also clear that thermal noise, which arises purely spontaneously in the absence of any current flow from an external circuit cannot be represented in terms of a fluctuating characteristic.

The types of noise which will be considered in order are: thermal noise, shot noise, partition noise, avalanche noise, and modulation noise. Much of the discussion is a review of previous work but some original contributions are included which it is intended to treat more fully elsewhere.

THERMAL NOISE

In any two-terminal passive element in thermodynamical equilibrium at absolute temperature T the fluctuation e.m.f. appearing at the terminals has the spectral density

$$S_e(f) = 4kTR(f) \tag{5}$$

where $R(f)$ is the real part of the impedance presented at the terminals at frequency f and k is Boltzmann's constant; this result, due to Nyquist is valid so long as $hf \ll kT$, or $f \ll 2 \times 10^{10}\, T\,\mathrm{sec}^{-1}$. This equation relates the electrical manifestation of the thermal energy of the current carriers (electrons, holes, ions) to the atoms of the material as a whole through the dissipative mechanism represented by R. Its proof rests on purely thermodynamical arguments and is therefore independent of mechanisms of conduction. However, proofs based on particular models of conduction-electron distribution and scattering have been given[1,2] and lead to the same result.

The noise current spectral density is given by

$$S_i(f) = 4kTG(f) \tag{6}$$

where $G(f)$ is the real part of the admittance at frequency f.

Although the thermal noise of a semiconductor or a semiconductor device is a well-defined quantity when equilibrium is established, this does not correspond to the practical conditions in which the devices normally operate. Usually there will be current flowing and thus additional types of noise can arise. Nevertheless, if the applied electrical field is everywhere such that the velocity distribution of the current carriers is unchanged apart from the linear superposition of a drift velocity in the direction of the field it is reasonable to assume that to a first approximation the thermal noise component is still given by Nyquist's equation. Physically we are saying that the thermal noise originates from the random discontinuities in the motions of the carriers due to their collisions with the atoms and its value is intimately connected with the appearance of the term kT in the energy distribution function for the carriers. In silicon and germanium at room temperature it seems that the superposition of drift and thermal velocities is valid for electric fields such that the drift velocity does not exceed 3×10^6 cm/s.[3,4]

SHOT NOISE

The term "shot noise" was originally applied to the fluctuations of current in a saturated vacuum diode due to the randomness of electron emission from the cathode. If the electrons are emitted at an average rate $\nu(=I/e)$ per second and each electron travels to the anode without interaction with the other electrons, the spectral density of the current is given by

$$S_i(f) = 2\nu|F(f)|^2 = 2(I/e)|F(f)|^2 \tag{7}$$

where $F(f)$ is the Fourier transform of the current impulse due to the passage of a single electron:

$$F(f) = \int_0^\tau i(t) \exp(-j\omega t)dt \tag{8}$$

At low frequencies such that the electron transit time τ is small compared with $1/\omega$, the transform $F(f) \simeq e$ and the spectral density assumes the simple form $2eI$. The concept of randomness of rate of emission implies that the process is determined by a stationary Poisson distribution. The random distribution of emission *velocities* can for some purposes be regarded as contributing additional thermal noise.[5]

If the vacuum diode be replaced by a uniform semiconductor a number of important differences arise. In general there are two types of current carrier—electrons and holes; these carriers will undergo many collisions during their drift motion with the electric field and furthermore they may be generated and may recombine at points throughout the bulk and on the surface of the semiconductor as well as at the electrodes. Thus the current impulses due to individual transits may vary widely in their duration and their integrated value $F(0) < e$ since it is only equal to the electronic charge for a carrier which passes completely from one electrode to the other. We here separate the carrier motion into the superposition of a drift motion and thermal agitation and to the latter we ascribe thermal noise given by Nyquist's equation to which must be added the shot noise due to drift which we now calculate.

Consider the case of an n-type semiconductor rod of cross-section A, length l and with uniform electric field E. If the electron mobility is μ and the mean lifetime τ we can assert that if N electrons are in motion at any given moment, the number of those still in motion at a time t later is, on the average

$$N \exp(-t/\tau)(1 - E\mu t/l) \text{ for } t \leqslant l/E\mu \tag{9}$$

and zero for greater values of t.

Thus

$$\overline{N_0 N_t} - (\overline{N})^2 = [\overline{N^2} - (\overline{N})^2] \exp(-t/\tau)(1 - E\mu t/l) \tag{10}$$

and since the instantaneous drift current is $Ne\mu E/l$ the spectral density of the shot noise is

$$S(f) = 4\left(\frac{e\mu E}{l}\right)^2 [\overline{N^2} - (\overline{N})^2] \int_0^{l/E\mu} \exp(-t/\tau)(1 - E\mu t/l)\cos(\omega t)dt \tag{11}$$

$$= 2eI\left[\frac{\overline{N^2} - (\overline{N})^2}{\overline{N}}\right] W\left(\omega\tau, \frac{\omega l}{E\mu}\right) \tag{12}$$

where $W = \frac{2\theta^2/\phi^2}{1+\theta^2} \times$

$$\left\{\frac{\phi}{\theta} - \frac{1-\theta^2}{1+\theta^2} + \frac{\exp(-\phi/\theta)}{1+\theta^2}[(1-\theta^2)\cos\phi - 2\theta\sin\phi]\right\} \tag{13}$$

in which $\theta \equiv \omega\tau$ and $\phi = \omega l/E\mu$. Davydov and Gurevich[6] also considered this particular case but derived an erroneous result. A number of special cases may now be considered:

(i) If the frequency is sufficiently low for both θ and ϕ to be small compared with unity

$$W = \frac{2\theta^2}{\phi^2}\left(\frac{\phi}{\theta} - 1 + \exp\frac{-\phi}{\theta}\right) \tag{14}$$
$$\simeq 1 \text{ if } l \ll E\mu\tau$$

as expected since we now have all the carriers traversing the semiconductor and full shot noise results.

(ii) If $l \gg E\mu\tau$ so that the life-path along the field is negligible compared with the length of the specimen

$$W = \frac{2\theta/\phi}{1+\theta^2} = \frac{2E\mu\tau}{l}\,\frac{1}{1+\omega^2\tau^2} \tag{15}$$

in which the shot effect is reduced by both a path factor and a frequency term.

(iii) If $l \ll E\mu\tau$

$$W = 2(1-\cos\phi)/\phi^2 \tag{16}$$

which corresponds to electrons crossing the distance l with uniform drift velocity $E\mu$ and is analogous to the noise induced by an electron beam in a klystron gap.

The ratio of the variance of N to its mean value which occurs in the spectral density depends upon the mechanism of carrier generation and recombination or trapping.[7] It is not unity as is commonly assumed.

Another important instance of shot noise arises in the other extreme from a uniform semiconductor, namely the motion of carriers across a high-field transition region, e.g. at a metallic contact or at a *p–n* junction. Normally the carrier velocities in such a region would be of the order of 10^7 cm/s and the width of the region would lie in the range 10^{-5} to 10^{-3} cm so that the transit time would be negligible except at the highest microwave frequencies. Furthermore it may be readily shown that since the change in quasi-Fermi level for the carriers across the transition region is very nearly equal to the applied voltage, the effect of each electron transit is effectively to induce a current impulse $e\delta(t)$, and thus full shot noise may be attributed to the flow.

In a semiconductor diode *at zero bias* there is no net current across the barrier layer, but since the noise induced by carrier transits in independent of the direction of transit one may consider the noise to equal twice the shot noise attributable to the flow I_0 in either direction. Then it is clear that since the noise must also be given by Nyquist's formula the zero-voltage conductance of the diode is

$$G_0 = eI_0/kT \tag{17}$$

If a biased semiconductor diode be illuminated a photo-current in the reverse direction is added to whatever current is already flowing due to the bias. Experimental data[8] may be interpreted to show that the increase of noise on illuminating a reverse-biased diode is equal to the shot noise associated with the increase of current *at a constant bias voltage*. This shot noise behaviour occurs even at low frequencies where the dark current may exhibit appreciable modulation noise. This result is very significant from the theoretical point of view, and is discussed elsewhere.[9]

The zero-bias condition is of importance in the video-detector type of receiver in which the low-level signals (usually received over a broad band at microwaves) are directly rectified and passed to a video amplifier. The r.m.s. noise current is inversely proportional to the square root of the crystal conductance, while the signal current is proportional to the applied signal power, the factor of proportionality being $e/2kT$ for an ideal detector. In this system there is no theoretical noise problem and the practical problem is to make the rectification coefficient approach the ideal as nearly as possible.

In a microwave superheterodyne receiver using a crystal diode mixer the noise appearing at the intermediate frequency is approximately given by the shot noise which one would attribute to the mean current flow through the diode. In good diodes at 30 or 45 Mc/s this is fairly closely true although in poor diodes there is a vestige of the modulation noise spectrum. The experimental work of Miller[10] and Nicoll[11] with both d.c. and a.c. excitation of silicon diodes illustrates the relative importance of shot and modulation noise at different frequencies.

If a diode has a reverse characteristic of the form

$$I = I_0[1 - \exp(-eV/kT)] \tag{18}$$

where I_0 in general increases slowly with the reverse voltage V, and if the h.f. noise be attributed wholly to the sum of the shot noises of two components of current:

$$S_i(f) = 2eI_0[1 + \exp(-eV/kT)] \tag{19}$$

then this may be expressed also in the following manner:

$$S_i(f) = 4kTG + 2eI\left(1 - \frac{2kT}{eI_0}\,\frac{dI_0}{dV}\right) \tag{20}$$

showing that the noise could be represented as the sum of thermal noise and a shot noise term which is somewhat reduced below the full value of the effect of non-saturation of the reverse current.

PARTITION NOISE

If a current *in vacuo* or in a semiconductor has the possibility of dividing between two or more electrodes, the process of partition will, because it is a statistical process, influence the noise in the resulting components of the current.

Let us first consider the case of a vacuum tube in which a cathode current I_0 having mean square noise $2eI_0F^2$ per unit bandwidth (F^2 = space-charge reduction factor) can divide between two electrodes (1) and (2). Then if I_1 and I_2 are the mean currents to these electrodes ($I_1 + I_2 = I_0$) the probabilities that an electron arrives at one or the other are I_1/I_0 and I_2/I_0 respectively. The noise in the current to electrode (1) will have the component $i_{01}^2 = 2eI_0F^2(I_1/I_0)^2$ due to the original cathode noise and a partition noise component given by $i_{p1}^2 = 2eI_1.I_2/I_0$ as determined from the variance of a binomial distribution. Thus the total noise in electrode (1) is

$$\overline{(i_{01} + i_{p1})^2} = \overline{i_1^2} = 2eI_1(I_1F^2 + I_2)/I_0 \tag{21}$$

The noise in electrode (2) may be similarly expressed with $i_{p2} = -i_{p1}$:

$$\overline{(i_{02} + i_{p2})^2} = \overline{i_2^2} = 2eI_2(I_2F^2 + I_1)/I_0 \tag{22}$$

As might be expected, if the cathode current exhibits full shot noise ($F^2 = 1$) the currents I_1 and I_2 will likewise do so since partition leaves unaffected the randomness of the original electron stream.

The noises of the two currents are correlated since they have equal and opposite partition components (electrons which do not go to one electrode go to the other) and also have related fractions of the initial cathode current noise. Thus

$$\overline{i_1 i_2} = \overline{(i_{01} + i_{p1})(i_{02} + i_{p2})} = -2e(I_1 I_2 / I_0)(1 - F^2) \quad (23)$$

Hence negative correlation always exists between the current fluctuations at the two electrodes. This correlation must be taken into account when circuital or electronic coupling exists between the two electrodes. Only when $F^2 = 1$ does the correlation become zero and the noises in (1) and (2) can be regarded as completely independent.

Now an analogous situation arises in an NPN junction transistor. The cathode current corresponds to the electron stream passing from the emitter into the base, the recombination of injected carriers in the base region corresponds to the current passing to electrode (1) and the current carried to the collector to that at electrode (2). Thus if the emitter be assumed to have unity electron injection efficiency we identify α with the ratio I_2/I_0. Since for normal current densities in semiconductors space charge effects are negligible we put $F^2 = 1$. The presence of a non-zero resistance in the base circuit results in a common impedance carrying the base current which will influence both the impedance and the noise appearing at the other electrodes. A further feature which does not arise in the vacuum tube is that not all of the collector current I_0 arises from carriers transmitted from the emitter across the base; a relatively small component I_{c0} is due to electrons thermally generated in the base region diffusing across to the collector junction. This component generates shot noise in the base-collector circuit independently of the current contribution from the emitter. On the basis of the shot noise of the emitter current and of I_{c0} and the partition noise associated with current division between base and collector together with the thermal noise of the base resistance it is possible to construct a reasonably satisfactory model for the noise behaviour of a junction transistor at frequencies sufficiently high that the $1/f$ component is unimportant yet not so high that the phase angle of the current transmission factor α is significant.[12]

AVALANCHE NOISE

When a barrier region is subjected to reverse bias the electric field may reach the order of 10^5 V/cm or greater, and at these fields there occur phenomena which cause a rapid increase of current and eventual breakdown; it has furthermore been observed that the current is "noisy" in this region, becoming increasingly impulsive as breakdown is approached.

One possible phenomenon is analogous to field emission and consists of the excitation of electrons from the valence band to the conduction band across the forbidden gap. It was first discussed by Zener in connection with dielectric breakdown in crystals. Similar excitation may also occur between impurity atoms and the valence or conduction band.

The second type of phenomenon is the electron multiplication process which arises from collision ionization of neutral atoms by electrons which have acquired appreciable energy from the field between collisions. This process is analogous to the electron avalanches which can occur in electrical discharges in gases, and the theory for the ionization rate per unit path length has been given by Wolff.[13]

McKay[14] has studied the processes of reverse voltage breakdown in silicon and germanium p–n junctions while Tomura and Abiko[15] have investigated selenium rectifiers. McKay concluded that electron and hole multiplication is the important process in silicon and germanium junctions while only in narrow germanium junctions is the Zener emission likely to be of significance.

As a first approximation the noise of electron avalanches may be treated from the point of view of the shot effect and it is somewhat analogous to the noise of a secondary emission multiplier. If n is the number of electrons in any one avalanche, the current it carries is nev where ν is the average frequency of such avalanches while the low frequency Fourier transform of the current impulse $F(0) = ne$. Thus the shot noise spectral density at frequencies low compared with the reciprocal of the transit time is given by:

$$S = 2\nu\overline{n^2}e^2 = 2eI(\overline{n^2}/\bar{n}) \quad (24)$$

This is the formula used by Haworth and Bozorth[16] in their study of electron multiplication in Pyrex, and they inferred values of $\overline{n^2}/\bar{n}$ ranging from 10 to 10^6 as the electric field was increased by a factor of 4.

Noise measurements[15] at 600 kc/s on reverse-biased selenium rectifiers were interpreted as corresponding to values of $\overline{n^2}/\bar{n}$ ranging from unity (corresponding to normal shot noise without electron multiplication) up to 100.

In silicon junctions McKay[14] observed that at the onset of breakdown there appears a distinctive form of impulsive noise consisting of a random sequence of rectangular current pulses of variable duration but of constant amplitude. The spectral density of such a pulse train would be expected to be of the form $S_0/(1 + \omega^2\tau^2)$ where $1/\tau$ is the sum of the transition probabilities corresponding to the on-and-off processes.[17] It is possible that the inevitable inhomogeneity of the semiconductor in the neighbourhood of the junction gives rise to small regions (or "weak spots") in which breakdown occurs for lower applied voltages than elsewhere and this localized breakdown will switch from an "off" to an "on" condition and back again, triggered by random fluctuations.

MODULATION NOISE

The term modulation noise is applied to those processes in which some controlling parameter (such as temperature, barrier height or rate of generation of carriers) undergoes fluctuations and thereby influences the flow of current on a collective or semi-macroscopic scale. To illustrate this concept by means of an analogy, consider a vacuum triode having a floating grid capable of capturing electrons which can leak away slowly through a high-resistance path to the cathode. Then in addition to the normal shot effect of the electron stream to the anode there will be grosser fluctuations of current due to modulation of the anode current by the fluctuations of grid potential; these fluctuations are an example of modulation noise and they have the typical characteristics of being able to exceed greatly the shot effect and having a spectral density which increases with decreasing frequency.

Similarly the flicker effect in a vacuum tube is due to the slow random variations in emissivity of small patches of the cathode surface; here the modulation is effectively one of a barrier height, i.e. of the work function of localized regions of the cathode.

In both these examples involving tubes the physical

mechanism involves the random arrival and departure of electrons or ions at a controlling region (the grid or the cathode surface). Similar effects can occur in a semiconductor due to the motion of carriers and the diffusion of ions, causing a variation in the effectiveness of potential barriers to influence the flow of current. This implies that co-operative effects are occurring and that the motion of carriers is no longer truly random.

Experimentally[10,11,18–22] the appearance of modulation noise becomes most marked at the lower frequencies (i.e. below about 10 kc/s) since it has a spectral density which increases with decreasing frequency.

These low frequency studies have been made in systems ranging from the simplest, namely bars of single-crystal germanium with potential probes, to the complicated in the form of point-contact diodes and transistors. In all these cases there is evidence of the presence of a component having a $1/f^n$ variation where n is usually in the range 1·0 to 1·1 together with components having the form appropriate to processes with a well-defined relaxation time τ:

$$S = \frac{A}{f^n} + \frac{B}{1 + \omega^2\tau^2} \tag{25}$$

The dependence of A and B on current (or voltage) and temperature has not been established but there is evidence that they are not in general proportional to I^2 as is suggested by unsophisticated theories. Not all experimenters have used the same noise generator representation. The preferable spectral density is that of the mean square current generator $S_i(f)$; sometimes the e.m.f. density $S_e(f)$ is used and sometimes the available power density $S_p(f)$.

These various forms are related by

$$S_e(f) = |Z(f)^2|S_i(f) \tag{26}$$

$$S_p(f) = S_e(f)/4R(f) = S_i(f)/4G(f) \tag{27}$$

where Z, R and G are the impedance, resistance and conductance of the device at frequency f. An alternative to the available power spectrum is that of the equivalent noise temperature ratio defined by

$$t(f) = S_e(f)/4kTR(f) = S_i(f)/4kTG(f) \tag{28}$$

These representations lead to spectral densities which vary with frequency, applied voltage and temperature. Thus when testing any specific model of noise generation it is important to choose the appropriate form in order that such phrases as "a $1/f$ component" or "temperature-independent noise" shall be meaningful.

In the simplest model for modulation noise the current I depends upon a barrier height ϕ by a factor of the form $\exp(-e\phi/kT)$. Thus if ϕ fluctuates due to some controlling parameter x fluctuating, the current fluctuations are given by

$$\overline{(\Delta I)^2} = \left(\frac{e}{kT}\right)^2 I^2 \left(\frac{d\phi}{dx}\right)^2 \overline{(\Delta x)^2} \tag{29}$$

Now only if $d\phi/dx$ is independent of I (or the applied voltage V) will the noise spectral density be proportional to I^2. In many physical systems, however, $d\phi/dx$ will depend on I or V; for example in a metal-semiconductor contact the barrier height is influenced by image force or by the surface state space charge. Each of these controls depends upon both the applied voltage and the ionic density in the barrier layer. Hence if the ionic density fluctuates so will the barrier height but to an extent which depends upon the field at the contact and thus on the applied voltage. The measurements of Hyde[19] on point-contact germanium rectifiers may be interpreted to suggest that the modulation noise current spectral density varies more nearly as I^2V rather than as I^2 and this type of dependence can be understood in terms of the model just discussed.

In bulk semiconductors such as the germanium filaments which have been examined experimentally in some detail, the mechanism for the modulation noise appears to be a variation of the rate at which carriers (or carrier pairs) are generated and recombine. Surface conditions have a marked effect suggesting that the modulation centres are primarily associated with superficial physical or chemical imperfections whose electrical state changes either by transitions in the state of ionization or by surface migration. The observed effect of magnetic fields on filament noise confirms at least qualitatively that surface sources and sinks for minority carriers are largely responsible for filament noise.[20,23]

A very general analysis of the noise due to diffusional mechanisms has been given by Richardson.[24] It is particularly applicable to the diffusion of ions in and out of a barrier region; the "coupling" between the current and the spatial location of the ions is determined completely generally by a vector function and the diffusion of the ions may take place in the volume or over the surface. Various specific models which lead to convergent spectra do not exhibit a $1/f$ behaviour over a wide range of frequency. This type of behaviour can be obtained by a rather special diffusional model but ensuring convergence at $f = o$ and $f = \infty$ requires the introduction of suitable boundary conditions for the coupling function.

A different approach to the $1/f$ type of spectrum is to consider the distribution in energy of modulation processes, and this treatment is now presented by considering electronic transitions between a modulation centre and a continuous band.

Consider a process in which a single modulation centre makes alternate random transitions between two states 1 and 2 (e.g. unionized and ionized) and let p_{12} and p_{21} be the transition probabilities per unit time. If such a transition causes a change A in the current flow in the system the relevant spectrum is that of a random rectangular wave. The resulting spectral density of the current may be derived from Machlup's analysis[17] (which was applied to a different problem) and is found to be

$$S(f) = \frac{4A^2\nu(\tau)\tau^2}{1 + \omega^2\tau^2} \tag{30}$$

where $1/\tau = p_{12} + p_{21}$ and $1/\nu(\tau) = 1/p_{12} + 1/p_{21}$.

If the transitions involve an energy difference E, the probabilities will be both proportional to $\exp(-E/kT)$; the ratio of the probabilities p_{12}/p_{21} is clearly the ratio r of the average time spent in state 2 to that spent in state 1, and is independent of E. If now E can have values lying between E_1 and E_2 the probability distribution of τ is proportional to $\exp(-E/kT)$ and thus to $1/\tau$ whence

$$P(\tau) = \frac{kT}{(E_2 - E_1)\tau} = \frac{1}{\tau \ln(\tau_2/\tau_1)} \tag{31}$$

and

$$\nu(\tau) = \frac{r}{(1 + r)^2\tau} \tag{32}$$

Thus the composite spectrum is

$$S(f) = 4A^2 \frac{kT}{E_2 - E_1} \frac{r}{(1+r)^2} \int_{\tau_1}^{\tau_2} \frac{d\tau}{1+\omega^2\tau^2} \quad (33)$$

$$= 4A^2 \frac{kT}{E_2 - E_1} \frac{r}{(1+r)^2} \frac{\tan^{-1}\omega\tau_2 - \tan^{-1}\omega\tau_1}{\omega} \quad (34)$$

where τ_1 and τ_2 correspond to the extreme cases of the allowable transitions with energy differences E_1 and E_2.

Thus for frequencies such that $1/\tau_1 \gg \omega \gg 1/\tau_2$ we have a $1/f$ spectrum. At extreme low frequencies S becomes constant while at high frequencies it behaves as $1/f^2$. The $1/f$ behaviour at intermediate frequencies depends on the Boltzmann factor in the transition probabilities, and since this is a general attribute it is not surprising that the $1/f$ spectral component has been found so ubiquitously in a wide variety of types of current noise. Note that it is *not* dependent on any assumed distribution of energy levels of centres. Since in fact the spectrum departs at the extremes from the $1/f$ form (and this could occur within the experimental range of frequencies) it is proposed that the generic form of equation (34) should be termed the "arctan" type of spectrum. Nothing generally can be asserted about the temperature since, in addition to the factor T, the parameters A and r will also depend on temperature.

The model just discussed may be illustrated by an example. Let the modulation centre be a hole trap which is either neutral (state 1) or negative (state 2) due to transitions between the centre and the valence band. Then we identify E_1 with the difference in energy level between the centre and the top of the valence band and $E_2 - E_1$ with the width of the valence band. The ratio r is simply $b \exp(-E_0/kT)$ where E_0 is the height of the trapping level above the Fermi level, and b is a spin factor which will be $\frac{1}{2}$ or 2. The factor $r/(1+r)^2$ will be small if $|E_0|$ is large compared with kT and consequently only levels near the Fermi level will experience appreciable fluctuations. In this connection it should be noted that the total mean square current fluctuation integrated over all frequencies is

$$\overline{(\Delta I)^2} = \int_0^\infty S(f)df = A^2 r/(1+r)^2 \quad (35)$$

which is, as expected, the variance of a quantity which can assume the values 0 or A with probabilities $1/(1+r)$ and $r/(1+r)$ respectively.

The mean square fluctuations in the number of carriers or ions in a semiconductor can also be calculated either by a purely statistical argument using the Fokker–Planck approach, or in the case where thermodynamical equilibrium applies by, the application of the Einstein free-energy method. These methods have been discussed in a recent paper[7] and shown to be consistent; particularly simple asymptotic results may be derived when the numbers involved are large as is usually the case.

If a variety of modulation centre levels occur, the spectrum will contain as many terms each having the form of equation (34). But so long as ω is between but remote from $1/\tau_1$ or $1/\tau_2$ for each of these levels the $1/f$ type of spectrum is obtained for each individual centre as well as for the aggregate. The distribution of relaxation times necessary for this type of spectrum arises simply from the existence of continuous bands (conduction or valence) to which transitions can be made, be it only from a single bound level or several. However as mentioned above the greatest weight will be given to those levels which lie near the Fermi level.

ACKNOWLEDGEMENTS

The work described above was carried out as part of the programme of the Radio Research Board. This paper is published by permission of the Director of Radio Research of the Department of Scientific and Industrial Research.

REFERENCES

(1) Bakker, C. J., and Heller, G. *Physica*, **6**, p. 262 (1939).
(2) Bernamont, J. *Ann. Phys.* [*Paris*], **7**, p. 71 (1937).
(3) Ryder, E. J. *Phys. Rev.*, **90**, p. 766 (1953).
(4) Shockley, W. *Bell. Syst. Tech. J.*, **30**, p. 990 (1951).
(5) Freeman, J. J. *J. Appl. Phys.*, **23**, p. 1223 (1952).
(6) Davydov, B., and Gurevich, B. *J. Phys. USSR*, **7**, p. 138 (1943).
(7) Burgess, R. E. *Physica*, **20**, p. 1007 (1954).
(8) Slocum, A., and Shive, J. N. *J. Appl. Phys.*, **25**, p. 406 (1954).
(9) Burgess, R. E. *Proc. Phys. Soc.* [*London*] (in course of publication).
(10) Miller, P. H. *Proc. Instn Radio Engrs*, **35**, p. 252 (1947).
(11) Nicoll, G. *Proc. Instn Elect. Engrs*, **101** (Pt. III), p. 317 (1954).
(12) Van der Ziel, A. *J. Appl. Phys.*, **25**, p. 815 (1954).
(13) Wolff, P. A. *Phys. Rev.*, **95**, p. 1415 (1954).
(14) McKay, K. G. *Phys. Rev.*, **94**, p. 877 (1954).
(15) Tomura, M., and Abiko, Y. *J. Phys. Soc. Japan*, **7**, p. 524 (1952).
(16) Haworth, F. E., and Bozorth, R. M. *Physics*, **5**, p. 15 (1934).
(17) Machlup, S. *J. Appl. Phys.*, **25**, p. 341 (1954).
(18) Brophy, J. *J. Appl. Phys.*, **25**, p. 222 (1954).
(19) Hyde, F. J. *Proc. Phys. Soc.* [*London*] *B*, **66**, p. 1017 (1953).
(20) Montgomery, H. C. *Bell Syst. Tech. J.*, **31**, p. 950 (1952).
(21) Van Vliet, K. M., and others. *Physica*, **20**, p. 481 (1954).
(22) Van der Ziel, A. *Noise* (New York: Prentice-Hall, Inc., 1954).
(23) Suhl, H. *Bell Syst. Tech. J.*, **32**, p. 647 (1953).
(24) Richardson, J. M. *Bell Syst. Tech. J.*, **29**, p. 117 (1950).

A replica technique for "reflexion" electron microscopy*

By D. E. Bradley, Associated Electrical Industries, Ltd., Aldermaston, Berks.

[*Paper first received* 10 *February, and in final form* 11 *March*, 1955]

Specimens of low thermal conductivity which are damaged by heat cannot easily be examined in the reflexion electron microscope. The paper describes a replica technique which allows the surface topography of such specimens to be reproduced in a silver surface. This can then be observed at the full intensity of the electron beam by the reflexion technique.

The application of the new technique to the examination of fibres, crystals and biological specimens is considered. The results obtained show that the use of replicas considerably widens the scope of reflexion electron microscopy, and simplifies the examination of specimens in some already established fields.

A rising interest has been shown in reflexion electron microscopy during the past few years, and it has been found that the technique has a number of definite advantages in several specialized fields. One of the most important advantages lies in the examination of surface finish, where the asperities encountered often have a very low angle of slope and so cannot be revealed by transmission replicas.[1, 2] Reflexion electron microscopy could also be used in the examination of crystal surfaces, e.g. for measuring the slopes of cleavage steps. A further advantage is to be found when examining fibres. Chapman and Menter have shown that it is desirable to be able to view a fibre in its entirety in order to gain a clear picture of its general topography.[3] They pointed out that the limited resolution and depth of focus of the light microscope renders it unsuitable for this purpose, and that the small field and higher resolution of the transmission electron microscope only allows an examination of the fine surface detail without giving a clear picture of the fibre as a whole.

The reflexion technique embraces the additional advantage that the actual specimen can be examined, but this factor can itself impose severe limitations, because it is not possible to place many objects in the electron microscope. For example, no crystal which is volatile in a vacuum can be examined; a specimen of low thermal conductivity will overheat in the intense electron beam required to give adequate image intensity, and large specimens must be cut up before they can be mounted in the electron microscope, so preventing their examination at subsequent stages in any experiment. Thus, in many cases where the unique advantages of the reflexion method are required, they may well be precluded because, for one reason or another, it may not be possible to examine the specimen directly. With a suitable replica technique, these difficulties could be overcome, hence increasing the field of application of reflexion electron microscopy, and simplifying its use in fields already established.

The requirements which a reflexion replica has to satisfy are, of course, quite different from those of a transmission replica. Firstly, the reproducibility of the replica need not be so highly accurate as that of the transmission replica, since, at present, the reflexion method itself has a limit of resolution of about 250 Å. Secondly, the replica must be a good electrical conductor in order to prevent the accumulation of charges. Thirdly, it must be as thick as possible so that it can conduct away the heat generated when the electron beam impinges on it. Fourthly, the general plane of the replica must be perfectly flat, otherwise much of the specimen will be shielded from the low-angle electron illumination. Finally, it must be mechanically stable so that there is no distortion due to thermal expansion effects. The technique described below produces a replica which satisfies all of these conditions.

THE METHOD

The replica is of the two-stage type, with a plastic first impression and a silver final replica, which is subsequently thickened with electro-deposited copper.[4] The various stages are described in detail below.

(i) A preliminary mould is made in a plastic block. The most satisfactory material so far encountered is Celastoid (a proprietary brand of cellulose acetate manufactured by British Celanese Ltd.), which is supplied in sheet form, the most suitable thickness being 0·040 in. A small square is cut from the sheet and moistened with acetone. The specimen, also moistened with acetone, is then pressed on to the plastic with sufficient force to exclude all air bubbles. After about ten minutes, the specimen is pulled away from the plastic. This setting period is very short because the acetone appears to disperse into the Celastoid in some manner, rather than dry by evaporation; it is this property which makes the material particularly suitable for the purpose.

(ii) The final replica, which is of silver, is now deposited on to the Celastoid by vacuum evaporation. In this operation, it is important that the Celastoid blocks are thoroughly degassed, and that the vacuum in the evaporating apparatus is good. The layer of silver should be as thick as possible. A suitable deposit is given by evaporating 0·15 g of metal from a molybdenum boat at a distance of 5 cm from the specimen. Heat radiation from the boat must be kept as low as possible during the initial stages of the evaporation, otherwise the first cast may be damaged.

(iii) The silver replica must now be strengthened so that it is sufficiently robust for examination by reflexion. This is carried out by electro-depositing copper on to the back surface while it is still mounted on the Celastoid. A copper sulphate–sulphuric acid electrolyte is used, and the replica is suspended in it with the silvered surface facing the copper anode. The cell should be electrically connected before the specimen is immersed, and adjusted to give a current density of about 4 mA/cm^2 of cathode. After half an hour, this value is increased to 10 mA/cm^2. The final thickness of the copper deposit should be about 0·005 in.; this is achieved after about four hours at the higher current density.

* It has been pointed out that strictly the term "reflexion" electron microscope is incorrect, as the instrument is a "dark-field" electron microscope operating at grazing incidence. It has been retained here at the author's request in view of its general adoption in the literature.—Editor.

(iv) After the deposition of the copper, the combined replicas are removed from the plating bath and washed in distilled water. The silver-copper foil is then separated from the Celastoid by cutting round the edges of the plastic block with a sharp knife, teasing up the edge of the replica and then peeling it away by means of a pair of forceps. Afterwards, the silver surface is carefully rinsed in distilled water followed by methylated spirits, and then dried in a hot air stream.

Sometimes a fine copper deposit may be found on the structure surface of the foil. This can be caused either by (*a*) a porous silver deposit due to a poor vacuum in the evaporating apparatus; (*b*) the distortion of the Celastoid before it is immersed in the plating bath, causing the loosening of the silver layer; (*c*) the use of too high a current density during the initial stages of the plating; or (*d*) the use of too thin a sheet of Celastoid, also causing loosening of the silver but, in this case, after immersion in the bath (the reason for this being that the plastic bends slightly when it has been in water for a long period). This copper deposit appears as a very fine structure in the electron microscope. It can, however, be removed by returning the foil to the plating bath after separating it from the Celastoid. The replica is made the anode of the cell, which is run at a current density of 2 mA/cm^2 of anode. The foil should be immersed in the bath for half-minute intervals until the deposit has disappeared. No residual structure has yet been observed after carrying out this operation, but the silver layer may be loosened from the copper backing if too high a current density is used.

(v) The only satisfactory method of mounting the foil has been found to be mechanical; if solder is used, the flux generally spreads over the silver surface, from which it is very difficult to remove. Wood's metal melts after a short time in the microscope due to heating in the electron beam. Other adhesives, such as Formvar and Collodion, have been tried, but they do not give a sufficiently good thermal contact between the foil and the peg upon which it is mounted. As a result, the plastics become charred and the replica falls off its support.

The specimen stage of the electron microscope used for this work was designed to accommodate a short $\frac{1}{4}$ in. diameter metal rod as a reflexion specimen. Such a rod was used as the support for the reflexion replica. A flat was filed on either side of the circumference of the rod, and each flat drilled and tapped for a 10 B.A. clamping screw, as shown in Figs. 1(*a*) and (*b*). The foil is most easily mounted in close contact with the flat end of the rod by cutting it into a strip $\frac{1}{4}$ in. wide, attaching one end of this to a clamping screw

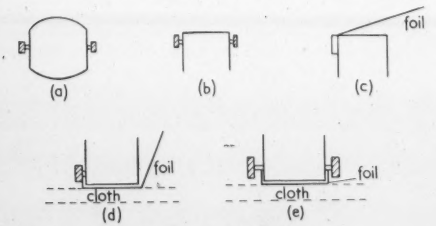

Fig. 1. Replica holder

(*a*) Plan view. (*b*) Side view.
(*c*) Foil attached at one end. (*d*) Foil flattened against cloth.
(*e*) Foil correctly mounted.

[Fig. 1(*c*)], bending the foil over the edge of the peg and pressing it on to the flat surface against a soft cloth (Selvyt, by Hollins Mill Co.), as in Fig. 1(*d*). The loose end of the foil is cut short and attached to the holder, as shown in Fig. 1(*e*).

Before examining the replica in the electron microscope, it should be washed in water and then in methylated spirits. If desired, a more efficient method of cleaning can be employed: a thin film of Formvar may be cast on the surface and removed with cellulose tape as soon as it is dry. It should be pointed out, however, that this procedure may possibly break off large, fragile portions of the replica. The replica can then be examined in the electron microscope like any ordinary metal specimen.

A slight modification to the method of preparing the Celastoid cast is necessary when replicating fibres. The block of Celastoid is first moistened with acetone, and the fibre is placed on it. A circular metal disk is now pressed on to the fibre, thus pushing it into the softened plastic. The casting is allowed to dry as before, and then the metal disk is removed. After the fibre has been pulled away from the Celastoid, the deposition of the silver is carried out as described above. In the case of weak fibres, best results are obtained by twisting several filaments together and adopting the procedure for thick fibres, but a single strand may be replicated by moistening the Celastoid, placing the fibre on it, and allowing it to dry without using the metal disk; it is then possible to remove the filament without breaking it.

The examination of fibres by this method is, of course, limited to those which are not soluble in acetone. However, it is possible to use glacial acetic acid in place of the acetone, and if necessary the Celastoid might be replaced by another plastic such as Perspex.

EXPERIMENTAL RESULTS

Fig. 2 illustrates the correlation between the replica and the original surface. The feature examined in this case was a scratch made with a sharp needle on an abraded copper surface. Such a feature is particularly suitable for the purpose of assessing the fidelity of the replica, since both fine and coarse structures are present. Fig. 2(*a*) is a micrograph of the original, and Fig. 2(*b*) shows the same area on a replica. It can be seen that even the finest detail resolved is accurately reproduced; at the same time, the coarse structure on the edge of the track is present in an identical form in each case. There is a slight difference in the appearance of the two pictures, but this is due to a small difference in the respective angles of illumination.

The application of the method to the examination of specimens which cannot be viewed directly in the microscope is illustrated in the remaining figures. Fig. 3 shows a replica taken from the surface of a cleaved sugar crystal (supplied by Tate and Lyle Ltd.). The cleavage steps are clearly shown, while the remainder of the surface is extremely smooth. In this case, the cleavage face was very uneven, so that only a limited portion of the replica could be examined under low-angle illumination, the remainder being obscured in shadow.

The use of replicas in examining fibres by reflexion electron microscopy overcomes the severe practical difficulties encountered when this type of specimen is examined directly.[3] Because there is no possibility of false structure being produced by the action of the electron beam, the full intensity can be employed. This permits a higher resolution to be attained, since a much smaller objective aperture can be used in the microscope, and also the elimination of very long

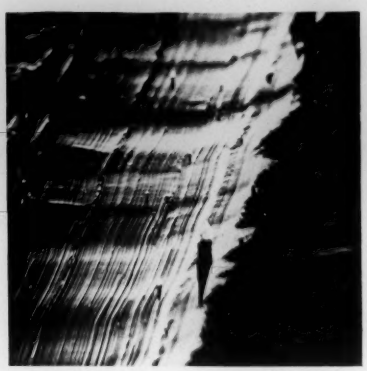

(*a*) Original specimen (×950).

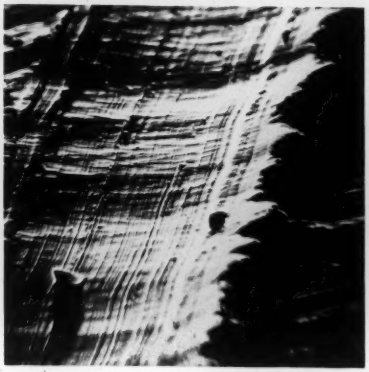

(*b*) Celastoid-silver replica (×950).

Fig. 2. Needle scratch on abraded copper.
$\theta_1 = 2°$, $\theta_2 = 6°$

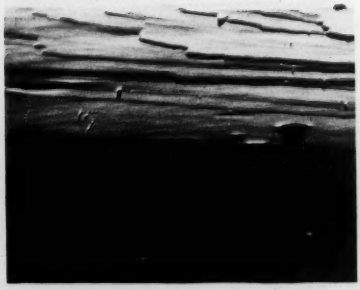

Fig. 3. Reflexion replica of the cleavage face of a sugar crystal
$\theta_1 = 2°$; $\theta_2 = 6°$. (×1400).

Fig. 4. Reflexion replica of a Nylon fibre
$\theta_1 = 1\frac{1}{2}^\circ$; $\theta_2 = 6\frac{1}{2}^\circ$. (×1000).

Fig. 5. Reflexion replica of a cluster of Bemberg filaments
$\theta_1 = 3^\circ$; $\theta_2 = 5^\circ$. (×1000).

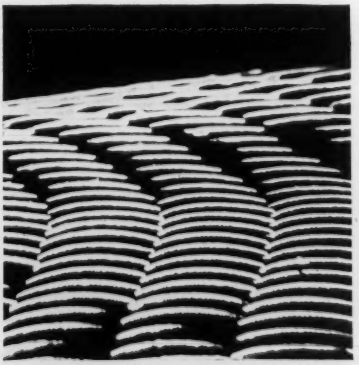

Fig. 6. Reflexion replica of the compound eye of a housefly
$\theta_1 = 2^\circ$; $\theta_2 = 6^\circ$. (×1000).

photographic exposures prevents loss of resolution by specimen movement.

Figs. 4 and 5 show replicas of two different types of fibre. Fig. 4 illustrates a 25 μ filament of Nylon, and Fig. 5 shows several Bemberg filaments twisted together.

The reflexion replica should permit the examination of certain biological specimens. To demonstrate the possibilities, a replica of the surface of the compound eye of a housefly was prepared in the manner described for weak fibres. Under optical examination, the eye appears as a large number of hexagonal, light-sensitive cells arranged in a manner similar to a honeycomb. The surface of each cell is curved, and should it be desirable to measure the radius of curvature, the simplest method would clearly to be to obtain the value from a reflexion electron micrograph such as that shown in Fig. 6.

CONCLUSIONS

The use of replicas in reflexion electron microscopy considerably widens the scope of the method. Many specimens which cannot be subjected to electron bombardment can be examined and the cutting-up or demounting of large mechanical objects is avoided. This allows the examination of a given area of a specimen to be carried out at successive stages during, for example, wear experiments or chemical etching. In addition, the direct examination of the specimens produces a carbon deposit[5] over the area under consideration, which seriously affects the mechanical or chemical treatment, but the use of a replica avoids such difficulties.

ACKNOWLEDGEMENTS

The author wishes to thank the British Rayon Research Association for supplying the fibre specimens, Mr. M. E. Haine, Dr. W. Hirst and Dr. J. S. Halliday for their interest and encouragement during this work, and Dr. T. E. Allibone, Director of this Laboratory, for permission to publish this paper.

REFERENCES

(1) HALLIDAY, J. S. *Proc. Inst. Mech. Engrs.* To be published. See also *Machinery*, **86**, p. 869 (1955).
(2) HAINE, M. E., and HIRST, W. *Brit. J. Appl. Phys.*, **4**, p. 239 (1953).
(3) CHAPMAN, J. A., and MENTER, J. *Proc. Roy. Soc. A*, **226**, p. 400 (1954).
(4) ZWORYKIN, V. K., and RAMBERG, E. G. *J. Appl. Phys.*, **12**, pp. 692–5 (1941).
(5) ENNOS, A. E. *Brit. J. Appl. Phys.*, **4**, pp. 101–6 (1953).

Conditions for aperiodicity in linear systems

By A. T. FULLER, M.A.,* Waymouth Gauges and Instruments Ltd., Godalming, Surrey

[*Paper first received* 23 *June, and in final form* 10 *December*, 1954]

The necessary and sufficient conditions which a linear system must satisfy to be completely aperiodic are derived. They may be expressed in terms of either the roots or the coefficients of the characteristic equation. In the latter case, the conditions take the form of a number of simple determinantal inequalities which are closely analogous to the Routh–Hurwitz stability criteria.

The problem of avoiding resonance occurs in many fields of contemporary engineering. For example, electronic amplifiers must be free from tendency to sustain parasitic oscillations. Again, anti-vibration mountings should be well damped to be fully effective. The problem is particularly relevant to systems incorporating negative feedback, such as automatic control systems. These are well known to be prone to undesirable hunting, and it has recently been suggested that they should be not merely stable but also aperiodic.[1,2]

The present paper is intended to contribute to the theory of such systems, by giving the necessary and sufficient conditions for complete aperiodicity. The usual assumption is made that the systems can be treated as linear. It emerges incidentally that the conditions required are also those for the absence of complex roots from a polynomial equation. They are thus of academic interest as well as practical importance. They were mentioned[3] in connexion with stability problems as long ago as 1879.

The solution is given in terms of a number of simple determinants involving the coefficients of the polynomial. It is interesting to note that these determinants are closely analogous to those of the Routh–Hurwitz criteria,[4,5] which express the conditions for stability.

DEFINITION OF APERIODICITY

The response, $R(t)$, of a linear system to an input may be put in the well-known general form:

$$R(t) = C_1e^{\alpha_1 t} + C_2e^{\alpha_2 t} + C_3e^{\alpha_3 t} + \ldots + D_1e^{\beta_1 t}\sin(\omega_1 t + \theta_1) + D_2e^{\beta_2 t}\sin(\omega_2 t + \theta_2) + D_3e^{\beta_3 t}\sin(\omega_3 t + \theta_3) + \ldots \quad (1)$$

where t is time, and the other symbols represent real constants which may be readily calculated by Laplace transform methods.[6] Let us call the separate terms such as $C_3e^{\alpha_3 t}$ and $D_1e^{\beta_1 t}\sin(\omega_1 t + \theta_1)$ the *exponential-components* of the response. Equation (1) shows that, in general, these are of two types: (*a*) those that vary exponentially with time; and (*b*) those that vary both exponentially and periodically with time. When type (*b*) are absent it is appropriate to call the response an *aperiodic response*.

* Now at Department of Engineering, University of Cambridge.

A further result from simple Laplace transform theory[6] is that some of the exponential-components in the response are contributed by the input, and some by the system. Hence an *aperiodic system* may be defined as *a system which contributes no periodic exponential-components to its response to an input*. The adoption of this definition is to some extent justified by the following consequent properties:

(i) an aperiodic system has aperiodic response to any aperiodic input;

(ii) the alternative and intuitively acceptable definition, that an aperiodic system is one which has aperiodic response to an impulse function, is mathematically equivalent to the adopted definition (since the response to an impulse function contains only exponential-components contributed by the system);

(iii) aperiodicity is a state of the system as a whole, its presence or absence being unaffected by the choice of the points at which the input is applied and the response measured.

To prove this, note that each aperiodic exponential component $Ce^{\alpha t}$ contributed by the system corresponds to a real pole α of the transfer function between input and output; and similarly each periodic exponential-component $De^{\beta t}\sin(\omega t + \theta)$ corresponds to a pair of complex conjugate poles $(\beta + j\omega)$ and $(\beta - j\omega)$. (This follows from elementary Laplace transform theory.[6]) Hence aperiodicity is determined only by the poles of the transfer function and is independent of the zeros. Now the transfer functions for the various possible sets of input and output points may be found by solving the simultaneous linear equations of the system. The usual process of elimination (Cramer's rule) then gives each transfer function as a ratio of two determinants, the one in the denominator being the same for all the transfer functions. Hence all transfer functions in a given system have the same poles, so that the determination of aperiodicity is independent of which particular set of input and output terminals is used.

Incidentally, instability has the same property of being a state of the system as a whole; and therefore the present definition is especially appropriate when aperiodicity is being considered as an indication of remoteness from instability.

It is as well to point out that aperiodicity does not ensure that responses to step or impulse functions will be free from *overshoots*. This is because the occurrence of overshoots depends not only on the poles but also on the zeros of the transfer function. (At first sight it might appear that a criterion of aperiodicity based on overshoot would be preferable. But examination of such criteria shows that they cannot retain the above property (iii), owing to their dependence on the zeros.)

BASIC CONDITIONS FOR APERIODICITY

Since any periodic exponential-components contributed by the system are due to the complex poles of the transfer function, it follows from the above definition that: *the necessary and sufficient conditions for a system to be aperiodic are that each of the poles of its transfer function should be real.*

For comparison, the well-known conditions for a system to be *stable* are that each of the poles should have its real part negative.

The basic conditions for aperiodicity obtained above are not usually suitable for direct application to practical problems, as they require the poles of the transfer function, i.e. the *roots* of the characteristic equation, to be evaluated. This is a tedious process if the order of the equation is more than two; and it is well-known that an exact formula for the roots is not available if the order is more than four. The difficulty may be overcome by expressing the conditions for aperiodicity in terms of the polynomial *coefficients* in the characteristic equation, as will be shown in the next section. (It is easy to evaluate these coefficients by conventional rules, e.g. Kirchhoff's laws in the case of electrical systems.)

DERIVED CONDITIONS FOR APERIODICITY

The characteristic equation, $f(p) = 0$, is obtained by equating the denominator of the transfer function to zero, so that

$$f(p) = a_0 + a_1 p + a_2 p^2 + \ldots + a_n p^n \qquad (2)$$

where p is the operator representing differentiation and $a_0, a_1, \ldots, a_n$ are known real constants.

The nature of the roots of a polynomial may be investigated by means of Sturm's theorem.[7] As applied to equation (2) this states: the number of distinct real roots between $p = u$ and $p = v$ (where $v > u$), is equal to the excess of the number of changes of sign in the sequence $f_0, f_1, \ldots, f_n$ when $p = u$ over the number of changes of sign when $p = v$; where

$$\left.\begin{aligned} f_0 &= f(p) \\ f_1 &= f'(p) \\ f_2 &= -\text{ (remainder obtained on dividing } f_0 \text{ by } f_1) \\ f_3 &= -\text{ (remainder obtained on dividing } f_1 \text{ by } f_2) \\ &\text{etc.} \end{aligned}\right\} \qquad (3)$$

It has been shown that the sequence $f_0, f_1, \ldots, f_n$ may be replaced by various other simpler sequences, involving the use of determinants.[8] Cayley[9] in 1848 was the first to give such a sequence; but that due to Trudi[10] is slightly more convenient for the present application. According to Trudi we may replace the sequence $f_0, f_1, \ldots, f_n$ by the sequence $F_0, F_1, \ldots, F_n$, where:

$$\left.\begin{aligned} F_0 &= 1 \\ F_1 &= \begin{vmatrix} a_n & a_{n-1} & \cdot \\ \cdot & na_n & 1 \\ na_n & (n-1)a_{n-1} & p \end{vmatrix} \\ F_2 &= \begin{vmatrix} a_n & a_{n-1} & a_{n-2} & a_{n-3} & \cdot \\ \cdot & a_n & a_{n-1} & a_{n-2} & \cdot \\ \cdot & \cdot & na_n & (n-1)a_{n-1} & 1 \\ \cdot & na_n & (n-1)a_{n-1} & (n-2)a_{n-2} & p \\ na_n & (n-1)a_{n-1} & (n-2)a_{n-2} & (n-3)a_{n-3} & p^2 \end{vmatrix} \\ &\text{etc.} \end{aligned}\right\} \qquad (4)$$

Now it follows from the previous section that, for aperiodicity, the number of real roots between $p = -\infty$ and $p = +\infty$ must be equal to n. Hence the conditions for aperiodicity are that there must be n more changes of sign in the sequence $F_0, F_1, \ldots, F_n$ when $p = -\infty$ than when $p = +\infty$.

When $|p| \to \infty$, only the highest power of p in each determinant need be considered, i.e. the sequence approaches:

$$A_0, A_1 p, A_2 p^2, \ldots, A_n p^n \qquad (5)$$

where, from equations (4):

$$\left.\begin{aligned} A_0 &= 1 \\ A_1 &= \begin{vmatrix} a_n & a_{n-1} \\ \cdot & na_n \end{vmatrix} \\ A_2 &= \begin{vmatrix} a_n & a_{n-1} & a_{n-2} & a_{n-3} \\ \cdot & a_n & a_{n-1} & a_{n-2} \\ \cdot & \cdot & na_n & (n-1)a_{n-1} \\ \cdot & na_n & (n-1)a_{n-1} & (n-2)a_{n-2} \end{vmatrix} \end{aligned}\right\} \quad (6)$$

etc.

Consider first the case when $A_0, A_1, \ldots, A_n$ are all positive. Then the signs of the sequence $F_0, F_1, \ldots, F_n$ are, from expression (5):

$$\text{for } p = -\infty\text{: } +, -, +, -, +, -, \ldots$$

and $$\text{for } p = +\infty\text{: } +, +, +, +, +, +, \ldots$$

Here, there are n changes of sign in the sequence for $p = -\infty$, and none for $p = +\infty$. Hence $f(p)$ has n real roots, so that the system is aperiodic. Note that, in this case, the number of changes of sign in the sequence for $p = -\infty$ is the maximum obtainable, since a change of sign occurs in every pair of adjacent terms.

When, on the other hand, some of $A_0, A_1, \ldots, A_n$ are negative, there are some pairs of adjacent members, in the sequence for $p = -\infty$, that have no change of sign. Hence, in this case, $f(p)$ must have less than n real roots, so that the system is periodic.

Thus the conditions for aperiodicity are that $A_0 > 0$, $A_1 > 0, \ldots, A_n > 0$. From equations (6) the first of these is always satisfied. Further, the other inequalities may be divided by a_n since this is a factor of $A_1, A_2, \ldots, A_n$. Hence the conditions are:

$$\left.\begin{aligned} &\text{if} \quad a_n > 0\text{: } A_1/a_n > 0,\ A_2/a_n > 0,\ \ldots,\ A_n/a_n > 0 \\ &\text{and} \\ &\text{if} \quad a_n < 0\text{: } A_1/a_n < 0,\ A_2/a_n < 0,\ \ldots,\ A_n/a_n < 0 \end{aligned}\right\} \quad (7)$$

From equations (6), $A_1/a_n = na_n$. Therefore the inequalities involving A_1/a_n in expressions (7) are always satisfied, and are hence redundant. Also, it is superfluous to specify the conditions when $a_n < 0$; since a_n may always be made positive,[5] if necessary by multiplying the characteristic equation by (-1). Considering the remaining conditions in expressions (7) and substituting from equations (6) we have: *the $(n-1)$ necessary and sufficient conditions for aperiodicity are:*

$$\begin{vmatrix} a_n & a_{n-1} & a_{n-2} \\ \cdot & na_n & (n-1)a_{n-1} \\ na_n & (n-1)a_{n-1} & (n-2)a_{n-2} \end{vmatrix} > 0,$$

$$\begin{vmatrix} a_n & a_{n-1} & a_{n-2} & a_{n-3} & a_{n-4} \\ \cdot & a_n & a_{n-1} & a_{n-2} & a_{n-3} \\ \cdot & \cdot & na_n & (n-1)a_{n-1} & (n-2)a_{n-2} \\ \cdot & na_n & (n-1)a_{n-1} & (n-2)a_{n-2} & (n-3)a_{n-3} \\ na_n & (n-1)a_{n-1} & (n-2)a_{n-2} & (n-3)a_{n-3} & (n-4)a_{n-4} \end{vmatrix} > 0,$$

$$\vdots$$

$$\begin{vmatrix} a_n & a_{n-1} & \cdots & \cdots & \cdots & \cdots & \cdots \\ \cdot & a_n & & & & & \\ \vdots & & \ddots & & & & \\ & & & a_1 & a_0 & & \\ & & & & a_1 & a_0 & \\ & & & 2a_2 & a_1 & \cdot & \\ & & & & & & \\ \vdots & & & & & & \\ \cdot & na_n & & & & & \\ na_n & (n-1)a_{n-1} & \cdots & \cdots & \cdots & \cdots & \cdots \end{vmatrix} > 0, \quad (8)$$

where the sign of a_n is to be taken as positive [if necessary by multiplying the characteristic equation by (-1)].

It is interesting to note that the first of these determinants is a minor of the second, the second is a minor of the third, and so on. Thus, for a fourth-order system, each determinant is formed of all the terms inside one of the dotted frames of the following array:

$$\begin{array}{ccccccc} a_4 & a_3 & a_2 & a_1 & a_0 & \cdot & \cdot \\ \cdot & a_4 & a_3 & a_2 & a_1 & a_0 & \cdot \\ \cdot & \cdot & a_4 & a_3 & a_2 & a_1 & a_0 \\ \cdot & \cdot & \cdot & 4a_4 & 3a_3 & 2a_2 & a_1 \\ \cdot & \cdot & 4a_4 & 3a_3 & 2a_2 & a_1 & \cdot \\ \cdot & 4a_4 & 3a_3 & 2a_2 & a_1 & \cdot & \cdot \\ 4a_4 & 3a_3 & 2a_2 & a_1 & \cdot & \cdot & \cdot \end{array} \quad (9)$$

(The innermost frame of array (9) corresponds, not to one of the necessary conditions, but to the premise that $a_n > 0$.)

By rearranging rows and columns, other arrays which are equivalent to array (9) may be derived. Possibly the most preferable is array (12) (in the next section) since this has the terms in each row arranged in order of subscript.

Finally, by applying Descartes rule of signs[7] to the characteristic equation, we find: the necessary and sufficient conditions for a system to be *both aperiodic and stable* are that the determinants in expressions (8) and $a_0, a_1, \ldots, a_n$ must all be positive.

COMPARISON WITH OTHER CONDITIONS

The necessary and sufficient conditions for a system to be *stable* are given by the well-known Routh–Hurwitz criteria.[4,5] For a fourth-order system (by way of example) these state that the four determinants, each formed of the elements inside a dotted frame of the following array, must be positive:

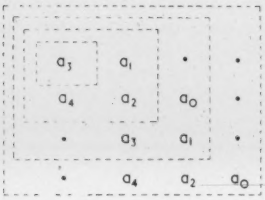

(10)

To facilitate comparison of arrays (9) and (10), the rows of the former may be rearranged, as follows (array 11):

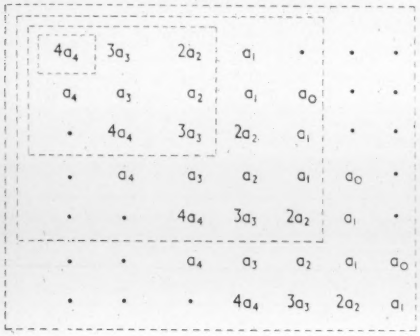

The similarities between arrays (10) and (11) show that the criteria for aperiodicity are closely analogous to those for stability.

Another condition of interest in linear systems is that of *quasi-critical damping*. This has been discussed in a previous paper,[2] where it was shown, for a typical control system application, that the relevant mathematical requirement was the vanishing of a certain determinant. The latter is, in fact, the same as the last determinant appearing in expressions (8), though with a trivial rearrangement of rows and columns. As applied to a fourth-order system, this rearrangement corresponds to turning array (11) through two right-angles in its own plane, as follows (array 12):

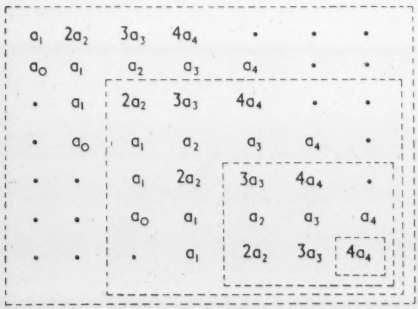

CONCLUSIONS

The necessary and sufficient conditions for a system to be aperiodic are that each of the roots of the characteristic equation should be real. Alternatively, expressed in terms of the polynomial coefficients, the same conditions are that the $(n-1)$ determinants

$$\begin{vmatrix} a_n & a_{n-1} & a_{n-2} \\ . & na_n & (n-1)a_{n-1} \\ na_n & (n-1)a_{n-1} & (n-2)a_{n-2} \end{vmatrix},$$

$$\begin{vmatrix} a_n & a_{n-1} & a_{n-2} & a_{n-3} & a_{n-4} \\ . & a_n & a_{n-1} & a_{n-2} & a_{n-3} \\ . & . & na_n & (n-1)a_{n-1} & (n-2)a_{n-2} \\ . & na_n & (n-1)a_{n-1} & (n-2)a_{n-2} & (n-3)a_{n-3} \\ na_n & (n-1)a_{n-1} & (n-2)a_{n-2} & (n-3)a_{n-3} & (n-4)a_{n-4} \end{vmatrix},$$

etc.,

should be positive (where a_n is to be taken as positive). For a system to be both aperiodic and stable, it is necessary and sufficient that the same conditions should be satisfied and that, further, $a_0, a_1, \ldots, a_n$ should all be positive. Other convenient forms of these determinants may be derived.

The conditions for aperiodicity are closely analogous to the Routh–Hurwitz criteria for stability. One of them is applicable to the determination of quasi-critical damping in certain systems.

ACKNOWLEDGEMENT

Thanks are due to the Directors of Waymouth Gauges and Instruments Ltd. for permission to publish this paper.

REFERENCES

(1) OLDENBOURG, R. C., and SARTORIUS, H. *The Dynamics of Automatic Controls* (Translated by Mason, H. C.), (New York: American Society of Mechanical Engineers, 1948).

(2) FULLER, A. T. *Brit. J. Appl. Phys.*, **5**, p. 174 (1954).

(3) THOMSON, W., and TAIT, P. G. *Treatise on Natural Philosophy*, Vol. I, 2nd Ed., p. 390 (Cambridge: University Press, 1879).

(4) ROUTH, E. J. *Advanced Rigid Dynamics*, Vol. 2 (London: Macmillan and Co., Ltd., 1930).

(5) HURWITZ, A. *Math. Ann.*, **46**, p. 273 (1895).

(6) GARDNER, M. F., and BARNES, J. L. *Transients in Linear Systems*, Vol. I (New York: John Wiley and Sons Inc., 1942).

(7) TURNBULL, H. W. *Theory of Equations* (London: Oliver and Boyd, Ltd., 1939).

(8) MUIR, T. *Theory of Determinants*, Vol. II, p. 362; Vol. III, p. 329 (London: Macmillan and Co., Ltd., 1920).

(9) CAYLEY, A. *J. (de Liouville) Math.*, **13**, p. 269 (1848).

(10) TRUDI, N. *Teoria de' Determinanti*, p. 192 (Naples: B. Pellerano, 1862).

Rheological behaviour of continuously sheared polythene

By W. F. O. Pollett, M.Sc., A.R.I.C., W. T. Henley's Telegraph Works Co. Ltd., Research Laboratories, Gravesend, Kent

[*Paper first received* 10 *January, and in final form* 28 *March*, 1955]

A commercial grade of polythene has been tested between its melting point and 190° C at constant shear rates from 0·1 to 9·8 s^{-1}. A disk-and-cone rheometer was used, and an improved technique introduced to provide a complete picture of the pressure distribution in the flowing melt by measuring each normal and tangential stress component individually. Changes of great complexity occurred with increasing shear, and varied with temperature and rate of shear, but simple relations could be established between the stress components and the measured strain recovery. These relations were not much affected by the imposed conditions and were in reasonable agreement with Weissenberg's theory when account was taken of an appropriate correction to his calculated recoverable strain. Moreover, the normal stress component in the axial direction was shown to be equal to that in the radial direction, in quantitative agreement with Weissenberg's theory. Changes occurred in the material during shearing, and increased with the applied shear and with the stress, but were reversible and vanished on resting. The observed behaviour is attributed to successive structural changes in the polymer, and an attempt is made to define equivalent structural states produced at different rates of shear.

1. INTRODUCTION

The fabrication of goods from polythene by extrusion and other processes involves continuous shearing above its melting point, and it was the object of the present investigation to study its rheological behaviour under such conditions. Previously published work on the shearing of high polymer melts has usually been conducted at non-uniform rates of shear, and has taken no account of the normal component of stress, but Pollett and Cross[1] have described a rheometer intended to rectify these shortcomings, and this has been used for the present investigation.

2. EXPERIMENTAL PROCEDURE

All experiments were carried out on a commercial grade of polythene (Alkathene grade 7) containing 0·1% of antioxidant. The sample at the desired temperature was sheared at a substantially uniform rate between a conical rotor and plane stator, on which the torque and axial thrust could be measured by their action on calibrated helical and leaf springs respectively. Shear recovery was measured by the angular recoil of the rotor when the drive was suddenly disengaged. Temperatures ranged from 117·5 to 190° C, and shear rates from 0·1 to 9·8 s^{-1}. The rotor used in nearly all the tests had an apical angle of about 170°; in a few instances one was employed having an angle of 177°, but was less satisfactory because of the reduced axial movement that could be tolerated. The polythene was allowed to stand for at least ten minutes after being moulded in the test space, before commencement of a test, and consistent results were obtained when this procedure was followed. In tests involving prolonged heating above 140° C the sample was protected from oxidation by a surrounding atmosphere of nitrogen.

In the original version of the rheometer a manually-operated micrometer head was used to maintain the stator substantially in its initial position. This was used in most of the present work, but did not permit the rapid changes of stress to be followed during the early stages of shearing at the higher rates. For the later experiments the apparatus was therefore modified to enable stiffer leaf springs to be used, which limited axial movement of the stator to less than 0·005 cm, and the effect of this on the mean rate of shear could be ignored. The friction acting on the stator spindle was reduced to a low level by the introduction of air bearings, and an optical lever replaced the dial gauge, enabling stator displacements to be measured to about 10^{-5} cm. By the inclusion of a rotating shutter in front of the lamp, a series of light spots, corresponding to a rapid change of normal stress, could be projected on to the scale, and photographed by a suitable time exposure. As rotation of the stator against the helical springs at the start of shearing reduced the rate of shear, this was prevented in tests concerned with this stage by the replacement of the springs by inextensible links, or, if torque too was to be measured, by pre-tensioning the helical springs.

Generally, the chief source of error was loss of sample from the test gap owing to departures from a completely symmetrical stress distribution (at the higher stresses) or to flow under gravity (mainly at the higher temperatures). Often it was necessary to counter this by occasionally pushing the material back with a spatula warmed to the test temperature. Errors from this cause produced some scatter in the results, especially at high shears, and this was more pronounced for the tangential traction, since torque varies as the cube of the sample radius, whereas axial thrust depends only on its square. Slip between the polymer and metal was shown to be absent by including in a sample a sector of pigmented polythene. Following a known number of revolutions of the rotor, the material was cooled and sectioned, and the number of coloured layers counted under the microscope. This also served as a rough check on the uniformity of shearing. If after a few turns of the rotor, the stator was allowed to drop, say, 0·01 cm, the uniformity of spacing of the coloured layers was unaffected, indicating that flow due to the axial movement was essentially towards the apex of the cone. The temperature rise due to shearing was generally negligible, but, under the most severe conditions, a maximum rise of approximately 1° was observed, in fair agreement with the calculated value.

3. DETERMINATION OF STRESS COMPONENTS

3.1 *Theory*. When an element of material is deformed in simple shear in the x direction and in the xy plane, normal tractions p_{xx}, p_{yy} and p_{zz} may develop. Under the conditions of the experiments the compressibility of polythene may be ignored, so that it is immaterial if a hydrostatic pressure equal to $-p_{zz}$ is imagined to be superimposed, making the normal tractions $p_{xx} - p_{zz}$; $p_{yy} - p_{zz}$ and 0. It will be convenient to put: $p_{xx} - p_{zz} = p_n$; $p_{yy} - p_{zz} = p_c$; $p_{xy} = p_s$. The value of p_s is directly calculable from the

torque, but the axial thrust on the stator depends on both p_n and p_c.

Equation (4*h*) in reference (5) may be written:

$$\partial p_{zz}/\partial \ln r = p_n + p_c \qquad (1)$$

Since the rate of shear and therefore the values of p_n and p_c are independent of the radius r, equation (1) may be integrated, and the boundary condition introduced that $p_{zz} = -p'$ at $r = R$, where p' is the atmospheric pressure and R is the radius of the stator. This gives:

$$p_{zz} = (p_n + p_c) \ln (r/R) - p' \qquad (2)$$

Substituting this expression for p_{zz} in the relationship $p_{yy} = p_c + p_{zz}$ and integrating over a circular area of radius r_1 concentric with the stator, gives the thrust F_{r1} acting on it as:

$$F_{r1} = \pi r_1^2[(p_n + p_c) \ln (R/r_1) + \tfrac{1}{2}(p_n - p_c) + p'] \qquad (3)$$

For $r_1 = R$ the logarithmic term vanishes. Thus p_n and p_c may be determined separately if the thrust on the whole stator, and on a smaller circle concentric with it, can be measured simultaneously.

3.2 *Measurement of p_n and p_c.* This was done by means of a special stator having a central disk of radius $R/2$ fitted into a circular cavity and supported by three symmetrically-disposed radial steel wires. The radial gap between the disk and the main part of the stator was only about 0·002 cm so that flow of polythene through it was negligible. The wire supports were adjusted so that the upper surface of the disk should be practically coplanar with that of the stator body at the working load. The disk formed one plate of an air condenser, being separated by about 0·025 cm from an insulated ring inside the stator. The variation in capacity accordingly enabled the thrust on the central disk to be determined at the same time as the total thrust on the stator was measured by means of the leaf spring in the usual way. Some difficulty was experienced in gripping the wire supports securely because of the limitations of space, but the method proved adequate for values of p_n up to 4×10^5 dyn/cm^2. In view of equation (2) this technique permits the determination of the complete pressure distribution in the flowing melt, which had not hitherto been possible with material of such high viscosity.

Weissenberg's theory[2,3] predicts that $p_c = p_{yy} - p_{zz} = 0$ for all temperatures, rates and amounts of shear. In a series of tests at 3·5 and at 1·0 s^{-1} at temperatures between 128 and 143° C, this was confirmed for molten polythene within the limits of experimental error ($\pm$ 3% of p_n). The relationship had previously been confirmed by Russell[4] and by Roberts[5,6] for various viscoelastic solutions subjected to stationary rates of shear, while evidence of a finite difference between p_{yy} and p_{zz} had been reported by Rivlin[7] and by Treloar[8] for vulcanized rubber subjected to large static shears.

In the main series of tests the normal stator was used, and p_c was then assumed to be zero, so that $p_n = 2F/\pi R^2$, where F is the measured thrust.

3.3 *Effect of axial stator movement.* When appreciable axial movement of the stator occurs during a test, this superimposes on the main shearing a variable shear velocity in a radial direction. If can be shown for a Newtonian material that when the apex of the cone is close to the disk and the angle α between the surfaces is small, the mean magnitude of the radial shear velocity throughout the sample is $9u/4R\alpha^2$, where u is the axial velocity. This may be taken as very roughly true for polythene, and suggests that the mean rate of radial shear at peak values of u did not exceed about 2% of the rotational shear velocity, so that the imposed conditions were not seriously vitiated, although the measured thrust could be appreciably in error. Conditions were too complex for the contribution of radial shearing to the thrust to be calculated, and recourse was had to an approximate experimental method. With the sample in position the stator was lowered, say, 0·005 cm, and the leaf spring then suddenly flexed by means of the micrometer head, the subsequent stator displacement being recorded against time. From these readings axial force was plotted against stator velocity, and the curve used to apply a correction to the measured thrust on the basis of the axial velocity. This procedure would be strictly admissible for Newtonian materials but is likely to give too high a correction with polythene, because the stress increases less rapidly than the rate of shear. A comparison of thrust/stator velocity curves, obtained with and without the rotor turning, after equilibrium conditions had been approached (see Section 4.1), indicated that the correction adopted might be as much as double its true value, though a considerable part of the discrepancy was probably due to the increase in consistency of polythene which occurs on the cessation of shearing (see Section 4.3). The form of the curves was similar, so that the corrections have a qualitative significance even though quantitatively they are rather unsatisfactory. Owing to the viscoelastic character of the material the thrust/stator velocity curve was appreciably dependent on the initial spring flexure, which was somewhat arbitrarily taken approximately equal to the maximum flexure occurring in the determination of p_n. In principle the correction can be reduced by increasing the stiffness of the leaf spring, but a limit is set by the deformability of the rheometer itself.

4. EXPERIMENTAL RESULTS

4.1 *Stress and strain recovery.* A constant rate of shear did not produce a constant stress, and it was found convenient to plot the stress components against logarithm of applied shear. Typical results are shown in Figs. 1 and 2 for a series of different temperatures, and in Figs. 3 and 4 for different rates of shear. The tangential traction p_s rose to its full value almost instantly when shearing commenced, but then dropped gradually till the applied shear σ was of the order of 100. Beyond this it again rose, but passed through a maximum at a shear which tended to be lower the higher the stress, and finally fell till, at sufficiently high shears, it seemed to approach a limiting value. In any particular test the rate of shear and range of times covered by the readings determined which of these features were observed, but all the curves conformed to this general pattern. At the lower applied shears the normal traction p_n was subject to the approximate correction described in Section 3.3. The main features of the corrected curves, which are shown as dotted lines, were independent of the leaf spring used, and may be accepted as real effects. It is seen that p_n rose rapidly to a sharply defined maximum at a shear of 10–25. The subsequent decline, which was most marked at the higher stresses, showed an interruption at moderate shears, with a second, rather indefinite maximum, before continuing apparently towards a limiting value. The minor fluctuations in the uncorrected and corrected curves in Figs. 2 and 4 were not sufficiently reproducible for any definite significance to be attached to them, though there was a hint that certain of them may not have been due to experimental error. An increase in temperature reduced the value of both stress

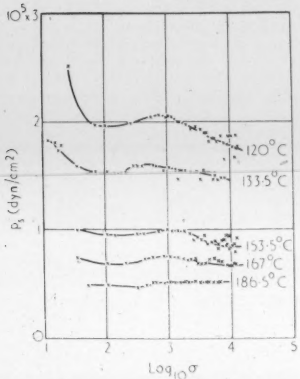

Fig. 1. Variation of p_s with applied shear at $3{\cdot}5\ s^{-1}$; effect of temperature

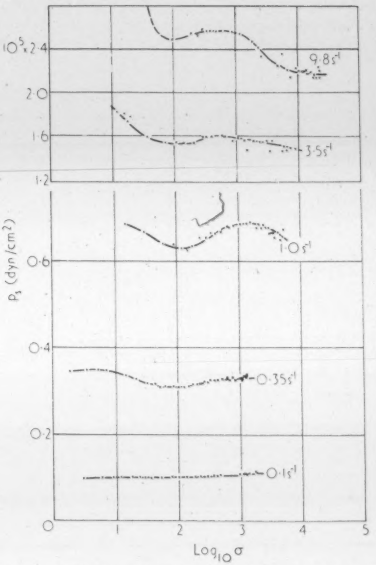

Fig. 3. Variation of p_s with applied shear at 133·5° C; effect of shear rate

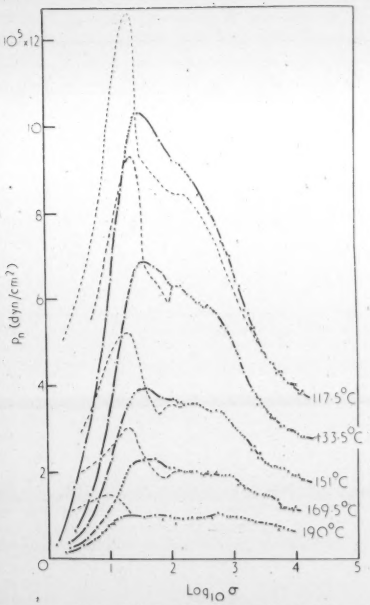

Fig. 2. Variation of p_n with applied shear at $3{\cdot}5\ s^{-1}$; effect of temperature. Dotted lines show values corrected for axial stator velocity

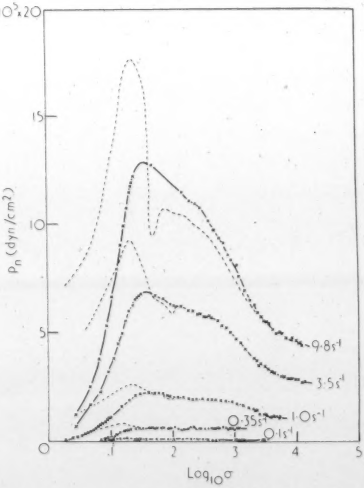

Fig. 4. Variation of p_n with applied shear at 133·5° C; effect of shear rate. Dotted lines show values corrected for axial stator velocity

components and a similar effect was produced by a reduction in the rate of shear.

When p_s was suddenly reduced to a low value, determined (after decay of the inertia forces) by the friction in the rotor bearings, shear recovery at first increased nearly linearly with logarithmic time, but subsequently tailed off to a steady value as shown by typical examples in Fig. 5, or sometimes decreased very slightly. The period of increasing recovery varied according to the conditions from a few seconds to fifteen minutes or so, and the maximum recovery was taken as the *recovery value*. Recovery values are shown as a function of log σ at various temperatures in Fig. 6, and at a series of shear rates in Fig. 7. They show an initial rise with increasing shear, followed by a rather sharp drop, then a

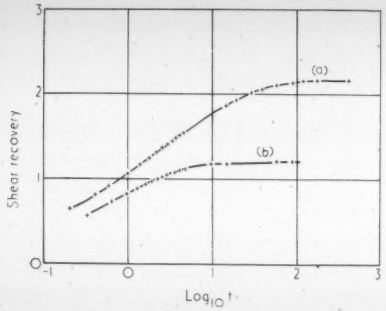

Fig. 5. Shear strain recovery at zero stress *versus* log time (seconds)

	σ	$\dot{\sigma}$	*Temperature*
(*a*)	38·5	3·5s^{-1}	133·5 °C
(*b*)	2112	3·2s^{-1}	136 °C

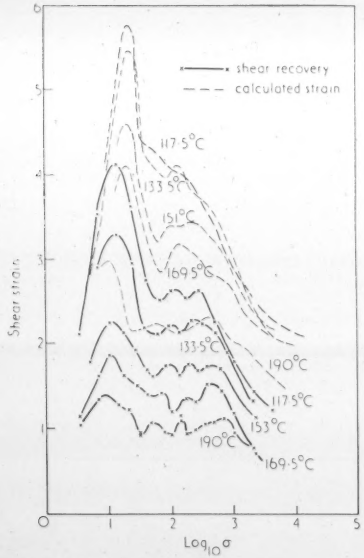

Fig. 6. Variation of shear recovery with applied shear at 3·5 s^{-1} and comparison with calculated strain at a series of temperatures

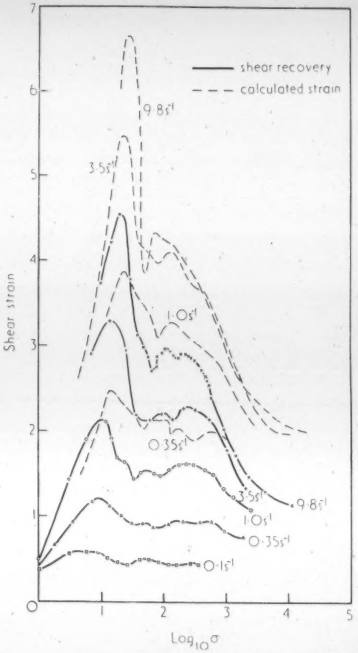

Fig. 7. Variation of shear recovery with applied shear at 133·5° C and comparison with calculated strain at various shear rates

series of minor fluctuations, and finally a reduction in recovery value at still higher shears. The first maximum and first minimum tended to occur at higher shears the higher the rate of shear and the lower the temperature (i.e. the greater the stress), whereas the final decline, as in the case of p_s, set in at a lower shear the greater the stress.

4.2 *Calculated elastic strain and shear modulus.* Weissenberg's theory [2, 3] requires that:

$$p_s = Gs \tag{4}$$

$$p_n = Gs^2 \tag{5}$$

where s is the recoverable shear strain, referred to below simply as "strain," and G is an elastic modulus. Mooney,[9] too, starting from the assumption that equation (4) holds for any isotropic plane, derives expressions for the normal tractions which give rise to equation (5) when p_c vanishes.

The stress components have accordingly been used to calculate values of s and G from equations (4) and (5).

For comparison with the recovery values, curves for the strain calculated from the corrected values of p_n are included in Figs. 6 and 7 as broken lines. The similarity in the form of the two sets of curves is quite striking, though the minor fluctuations in the recovery values are not apparent in the strain curves, probably because the accuracy of the stress measurements was insufficient. The first strain maxima were reached at slightly higher shears than the corresponding recovery maxima. In Fig. 8 the modulus G (given by p_s^2/p_n)

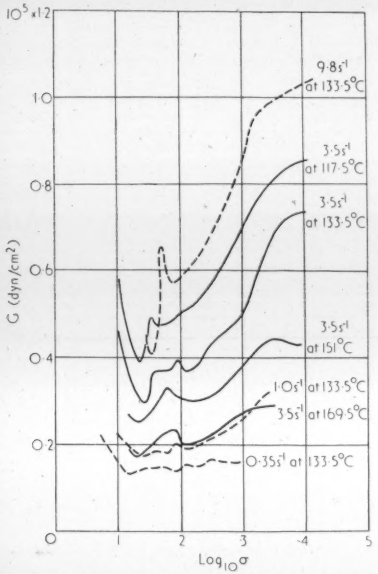

Fig. 8. Variation of G with applied shear and its dependence on temperature and shear rate

is shown as a function of log σ for several temperatures and rates of shear. Broadly, its dependence on applied shear was the inverse of that of the strain. On the other hand it diminished with increasing temperature and decreasing rate of shear just as stress and strain did.

4.3 *Reversibility of structural breakdown.* It is difficult to account for the observed complex changes in the rheological properties of the polythene as shearing proceeds, unless it is assumed that structural alterations occur in the material. Numerous experiments have shown beyond doubt that the changes are reversible. Thus the reduction in recovery value produced by shearing has been utilized to follow the reverse change, and Fig. 9 shows how the recovery from a small auxiliary shear gradually increased with the interval since more intense shearing, finally reverting to its normal value. Stress measurements at a low rate of shear following "breakdown" showed a similar tendency, but, if the shearing was continuous, an equilibrium condition was reached short of complete reversion to the initial state. Thus in Fig. 10 the continuous curves show the change in stress when a sample of polythene was sheared at $1{\cdot}0\,s^{-1}$, the elastic strain instead of applied shear being taken as abscissae. The arrows indicate the direction of the change. When further breakdown had become slow the rate of shear was increased to $9{\cdot}8\,s^{-1}$ for 15 min to take it to a more advanced stage. Shearing was then continued at the original rate, whereupon

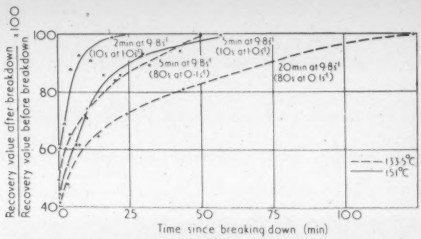

Fig. 9. Reversion of polythene to its initial state after shearing, as indicated by recovery values for the auxiliary shears shown in brackets

the stress and strain gradually increased as shown by the broken lines. They not only tended to the same equilibrium values as before, but approached this condition by curves substantially continuous with the original ones. Polythene took longer to revert to its initial condition the greater the degree of breakdown. At room temperature the broken-down condition was stable over periods of at least several

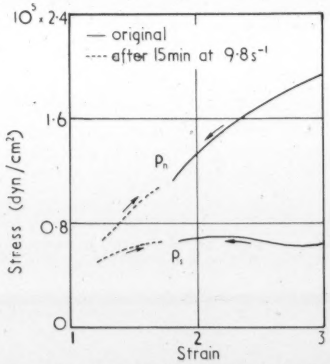

Fig. 10. Approach to equilibrium state, during shearing at $1{\cdot}0\,s^{-1}$, from initial and broken-down conditions. (133·5° C)

months. The whole cycle of breakdown and reversion has been repeated a considerable number of times without any evidence of a significant permanent effect.

In the measurement of recovery values, slightly more consistent results were obtained if the same specimen was used for the different periods of shearing under given conditions. It was therefore necessary to allow sufficient rest

periods at the test temperature between successive measurements.

5. STRUCTURAL INTERPRETATION OF RESULTS

5.1 *Recoverable strain.* The parallelism between the experimental recovery/log σ curves and the strain/log σ curves calculated from the stress by means of equations (4) and (5), provides considerable support for the validity of these equations, and this is not lessened by the fact that the observed recovery was less than the calculated strain. For one thing, inertia prevents p_s from being instantly reduced to zero, and p_n in any case does not immediately vanish. Hence, macroscopic relaxation of stress could occur simultaneously with recovery. Experiments, however, in which the moment of inertia of the rotor was varied between 654 and 2470 g.cm^2 indicated that this had very little influence on the recovery. In the second place, it is in line with current theory to suppose that a loose network of chains exists in the molten polythene. During shearing the secondary linkages responsible for the network structure continually break and re-form, so that there is a distribution of stresses at junction points from the most fully stressed to the completely relaxed. One can regard the *recoverable strain* as the amount of recovery that would ultimately occur, on removal of external stresses, if the cross linkages were stabilized at the instant in question. Actually, however, these junctions will continue to break and reform during the course of recovery, and because of this the observed recovery will be less than the recoverable strain defined as above. Weissenberg's is a continuum theory, and hence takes no account of this distinction, but, inasmuch as a change in the network structure is an alteration in the material itself, it appears that "recoverable strain" rather than recovery value should be identified with s.

5.2 *Nature of structural changes.* The main features of the recovery/log σ curves are shown by many high polymers,[10, 11] and a variation of shear stress with applied shear, similar to that exhibited by polythene, has been recorded for synthetic rubbers by Taylor, Fielding and Mooney[12] and by Fensom.[13,14] Any explanation must therefore be capable of fairly wide application.

The strain changes during shearing at a rate $\dot{s}$, given by the difference between $\dot{\sigma}$ and the rate at which strain decays through rupture of stressed cross linkages and formation of relaxed ones. The change of sign of $\dot{s}$ at a shear of 10–25 therefore represents a rapid increase in this rate of decay, probably due to the final disruption of the initial network, i.e. of the most stable of the original secondary linkages. Owing to the temporary rise in the rate of bond rupture, recovery at this stage will be less complete, since there is an increased number of free positions which can form cross linkages during the process. The first recovery maximum is therefore displaced to a lower shear than the corresponding strain maximum.

The value of G at constant strain increases with σ even at shears as low as 30, and this is interpreted as a change towards a visco-inelastic system caused by some kind of structural breakdown. The temporary interruption, at a shear of 50 or so, of the macroscopic manifestation of this process has been tentatively ascribed to mechanical interference between the branch chains as the molecules slide past one another,[10,11] the multiple peaks in the recovery/log σ curves apparently being due to the existence of more than one important branch spacing. The progressive increase in modulus and reduction in stress and strain are ultimately resumed, but there is probably no interruption of the structural change which they represent. Thus the last peak in the recovery/log σ curves is obliterated at the higher stresses which produce more intense breakdown, and similarly at the higher stresses the final decline in stress starts at lower shears. The nature of this breakdown is not known, but may be connected with a reduction in the intensity of the molecular entanglements.

6. EQUIVALENT STATES

Because of the difficulty of specifying the rheological properties of a system undergoing such complex changes during shearing, it is desirable to see whether states of equal breakdown can be defined. It cannot be assumed *a priori* that a given state of the polythene can be reached by shearing under two different sets of conditions, but some support for such a view is provided by the following considerations.

The kinetic theory and the nature of the polythene molecule suggest that the free energy of deformation is almost entirely due to a reduction in entropy, whence at constant temperature:

$$p_s = -T\partial\Phi/\partial s \qquad (6)$$

where Φ is entropy. At a given strain $\partial\Phi/\partial s$, and therefore p_s/T, should be constant, provided the state of the material is unchanged. A plot of s against p_s/T for all temperatures and rates of shear (Fig. 11) to a first approximation yields a

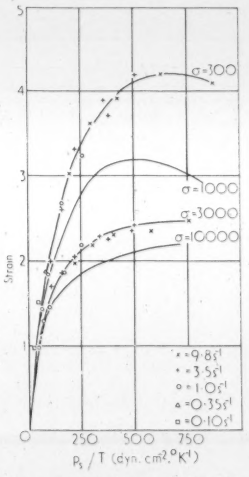

Fig. 11. Relationship between s and p_s/T at constant applied shear. (Experimental points are shown for only two values of shear to avoid confusion)

separate curve for each value of σ, so that shearing at a constant rate under two sets of conditions can produce the same strain and breakdown in the polythene only if the applied shear is the same. That it will then do so is a reasonable inference. The state of the material may therefore be defined by the values of p_s/T and σ. The convergence of the curves in Fig. 11 at $p_s/T \simeq 50$ dyn.cm^{-2}.°K^{-1} indicates that there is little structural change below this value. In so far as p_s/T and σ together determine s they also determine

p_n/T (i.e. sp_s/T), but it is interesting to observe that the data approximate equally well to a unique relationship between p_s and p_n at constant σ (Fig. 12). This emphasizes the equivalence of changes in shear rate and in temperature.

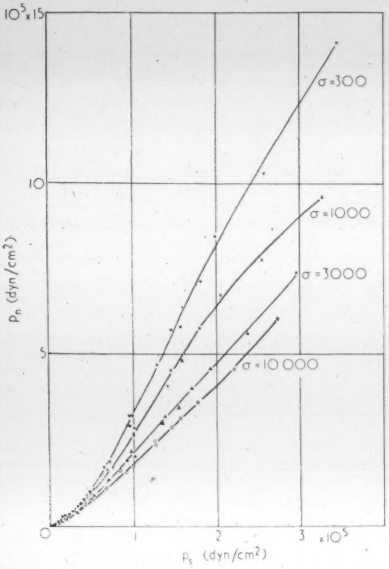

Fig. 12. Relationship between p_n and p_s at constant applied shear

7. VISCOUS PROPERTIES

In Fig. 13 the relationship between shear rate and tangential traction is plotted logarithmically for an applied shear of 1000, and is of the usual type shown by high polymers.[15] Similar series of curves are obtained at other values of σ. Their non-linearity indicates that even at constant shear the data do not conform to the Ostwald-de Waele relationship $\dot{\sigma} = (p_s/\eta^*)^n$ where η^* and n are constants. The curves are capable of being superimposed reasonably accurately by translation parallel to the log $\dot{\sigma}$ axis, which means that b in the Andrade equation $\eta = A \exp(b/T)$ (applied to conditions of constant shear and stress) is substantially independent of stress. The values shown in the table for the activation energy for viscous flow confirm this. However, activation energy should—to have even a limited physical meaning—be determined at a constant degree of breakdown and at a constant mean molecular configuration (i.e. constant strain). It has been shown that both requirements are probably satisfied if p_s/T and σ are fixed. That log $(p_s/\dot{\sigma})$ is a linear function of $1/T$ for these conditions may be seen from Fig. 14 for $\sigma = 1000$. The corresponding values for the activation energy determined at this and other shears are included in the table, and are mostly a little higher than at constant stress, with a mean of 12·4 kcal/mole. Dienes[16] has given a figure of 11·0 kcal/mole for polythene, while Dexter[17] has recently reported values of 12·9, 13·95 and 11·9 kcal/mole at constant stress for three different grades.

It will be seen from the table that there was a tendency

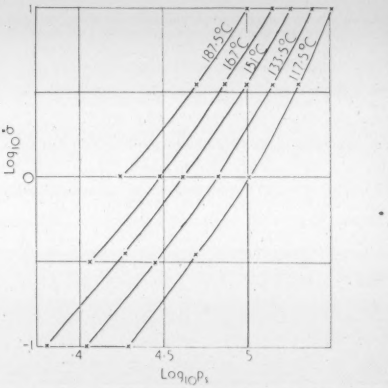

Fig. 13. Relationship between rate of shear and shear stress, plotted logarithmically, for applied shear of 1000

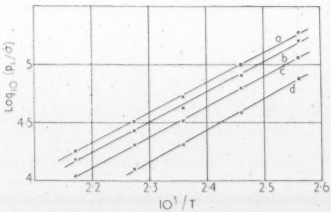

Fig. 14. Logarithm of apparent viscosity at applied shear of 1000 and at constant p_s/T, as a function of reciprocal absolute temperature

p_s/T
(*a*) 50 dyn.cm^{-2}, °K^{-1}.
(*b*) 100 dyn.cm^{-2}, °K^{-1}.
(*c*) 200 dyn.cm^{-2}, °K^{-1}.
(*d*) 400 dyn.cm^{-2}, °K^{-1}.

Activation energy for viscous flow (kcal/mole) determined at constant tangential traction and at constant p_s/T

		Applied shear 300	1000	3000
p_s	2×10^4 dyn.cm^2	12·6	11·6	11·8
	5×10^4 dyn.cm^2	13·0	11·45	12·1
	10×10^4 dyn.cm^2	12·9	11·4	12·3
	20×10^4 dyn.cm^2	12·9	11·3	11·7
p_s/T	50 dyn cm^{-2} °K^{-1}	11·7	12·1	12·0
	100 dyn cm^{-2} °K^{-1}	11·7	12·3	12·9
	200 dyn cm^{-2} °K^{-1}	12·1	12·2	13·0
	400 dyn cm^{-2} °K^{-1}	13·2	12·3	13·2

for the activation energy determined at constant stress to drop as the shear increased beyond 300, but at constant p_s/T this was no longer so. If the slight variations in slope of the curves in Fig. 14 are attributed to experimental error, their relative positions would, on Eyring's theory, represent a reduction in the magnitude of the entropy of activation with increasing strain. The validity of this treatment is open to question, but it is interesting to note that the conclusion corresponds to what would be expected if Spencer's view[18] is accepted that in the activated state the molecules are oriented in the direction of shear. The value of p_s passed through a minimum at a higher shear than the recovery value and continued to rise after p_n and s had started finally to decline. These effects may result from the change in entropy of activation accompanying the alterations in strain.

ACKNOWLEDGEMENTS

The author wishes to record his thanks to Dr. K. Weissenberg and to Mr. J. E. Roberts for helpful suggestions and discussions relating to the apparatus and the results obtained; also to Mr. W. C. Barry, Manager of the Research Laboratories, to Mr. S. E. Goodall, Chief Engineer of W. T. Henley's Telegraph Works Co. Ltd., and to the Company for permission to publish this paper.

REFERENCES

(1) POLLETT, W. F. O., and CROSS, A. H. *J. Sci. Instrum.*, **27**, p. 209 (1950).
(2) WEISSENBERG, K. *Arch. Sci. Phys. Nat.*, **17**, p. 1 (1934).
(3) WEISSENBERG, K. *Report of the General Conference of the British Rheologists' Club, London*, 1946, p. 36 (London: Thomas Nelson and Sons, Ltd., 1949).
(4) RUSSELL, R. J. *The Determination of the Basic Rheological Constants Governing the Flow of Pseudo-Plastic Substances.* (Doctorate Thesis, University of London, 1946).
(5) ROBERTS, J. E. *Ministry of Supply Report*, No. A.D.E.13/52 (1952).
(6) ROBERTS, J. E. *Proceedings of the 2nd International Congress on Rheology*, Oxford, 1953, p. 91 (London: Butterworths Scientific Publications, 1954).
(7) RIVLIN, R. S. *J. Appl. Phys.*, **18**, p. 444 (1947).
(8) TRELOAR, L. R. G. *Proc. Phys. Soc.* [*London*], **60**, p. 135 (1948).
(9) MOONEY, M. *J. Appl. Phys.*, **11**, p. 582 (1940).
(10) POLLETT, W. F. O. *Research*, **6**, p. 3*S* (1953).
(11) POLLETT, W. F. O. *Proceedings of the 2nd International Congress on Rheology*, Oxford, 1953, p. 85 (London: Butterworths Scientific Publications, 1954).
(12) TAYLOR, R. H., FIELDING, J. H., and MOONEY, M. *Rubber Age, N.Y.*, **61**, p. 567 (1947).
(13) FENSOM, D. S. *Rubber Age, N.Y.*, **73**, p. 795 (1953).
(14) FENSOM, D. S. *Research*, **6**, p. 63*S* (1953).
(15) See, for example, SAUNDERS, D. W., and TRELOAR, L. R. G. *Trans Instn Rubber Industr.*, **24**, p. 92 (1948).
(16) DIENES, J. G. *J. Colloid Sci.*, **2**, p. 131 (1947).
(17) DEXTER, F. D. *J. Appl. Phys.*, **25**, p. 1124 (1954).
(18) SPENCER, R. S. *J. Polymer Sci.*, **5**, p. 591 (1950).

Forming procedures for silicon point-contact transistors

By J. W. GRANVILLE, Ph.D., W. BARDSLEY, Ph.D., A.Inst.P., and A. F. GIBSON, Ph.D., Radar Research Establishment, Great Malvern, Worcs.

[*Paper received* 11 *March*, 1955]

Methods of forming silicon point-contact transistors have been established. Suitable whisker materials for use as emitters and collectors on n- and p-type silicon and the necessary pulsing techniques are described. Using these forming procedures, silicon transistors have been made with increased power gains and with output characteristics of the correct type. The performance figures of typical formed silicon transistors are quoted.

Silicon transistors are important because, unlike germanium transistors, they will give stable operation at high ambient temperatures. Silicon n-p-n junction transistors are now produced commercially in large quantities and to specification limits. On the other hand, point-contact silicon transistors are not available and very little information about them has appeared in the literature. There are some applications, for instance in transistor trigger circuits, where the point-contact transistor with its current gain exceeding unity is superior to the junction transistor. For this reason, an investigation of the properties of silicon point-contact transistors was thought to be worthwhile.

In a recent paper,[1] Jacobs, Brand, Matthei and Ramsa describe a method of forming the emitter contacts of n- and p-type silicon point-contact transistors. This method is rather different from that developed in this laboratory and it will be helpful to describe it briefly so that the two techniques can be contrasted.

To form an emitter by the technique of Jacobs and others a small pellet of antimony (for p-type transistors) or aluminium (for n-type transistors) is pressed on to the prepared silicon surface with a 0·080 in. pointed tungsten probe, the whole assembly being in an atmosphere of nitrogen. A large current is passed through the probe and some of the pellet material diffuses into the silicon making a p–n junction at the surface. The probe is then removed and the crystal is etched to remove the surplus pellet material. The transistor is made by placing emitter and collector contacts of 0·004 in. tungsten wire on the crystal with the emitter contact on the contaminated region of the surface. Because of the improved emitter injection efficiency, the current and power gains of the transistor are increased.

A different approach to the problem was adopted by the present authors. During the initial investigation it was found that the output characteristics of silicon transistors were not of the saturation type associated with formed germanium point-contact transistors. Transistor circuitry has been developed on the basis of a saturation type output characteristic, and if silicon transistors were to be useful it appeared to be of primary importance to give them the type of characteristic by some forming process. This was achieved by using collector whisker materials of suitable composition

and pulsing the contact. Having obtained the correct output characteristics, attention was then given to improving the emitter efficiency, again by using suitable whisker materials and forming pulses.

Jacobs and others do not give the output characteristics of silicon transistors formed by their technique so a strict comparison between the two methods is not possible. However, it does appear that the forming procedures described in this paper are simpler than those of Jacobs and others and more suitable for quantity production.

THE TRANSISTOR PARAMETERS

The transistor, being a three-terminal device, requires the specification of two voltages and two currents to describe its operating conditions. Thus, at low frequencies, a transistor may be represented by a network of four dynamic resistances. A knowledge of these resistances enables the performance of the transistor to be assessed. The dynamic resistances are defined in terms of the voltages and currents between the emitter and the base and collector and base as follows, the symbols ϵ, c and b being used for emitter, collector and base respectively:

$$r_{11} = \left(\frac{\partial V_\epsilon}{\partial I_\epsilon}\right)_{I_c=\text{const.}} \quad \text{input resistance}$$

$$r_{12} = \left(\frac{\partial V_\epsilon}{\partial I_c}\right)_{I_\epsilon=\text{const.}} \quad \text{base resistance}$$

$$r_{21} = \left(\frac{\partial V_c}{\partial I_\epsilon}\right)_{I_c=\text{const.}} \quad \text{mutual resistance}$$

$$r_{22} = \left(\frac{\partial V_c}{\partial I_c}\right)_{I_\epsilon=\text{const.}} \quad \text{output resistance}$$

where V_c and I_c are the collector voltage and current and V_ϵ and I_ϵ are the emitter voltage and current at the chosen operating point.

THE TRANSISTOR CHARACTERISTICS

The collector or output characteristics, three sets of which are shown in Fig. 1, will be discussed first. Fig. 1(*a*) shows an idealized set of output characteristics. These are, in fact, pentode type characteristics and typified by a large value of the output resistance, r_{22}. Fig. 1(*b*) shows the output characteristics of a formed germanium point-contact transistor. These characteristics are a fair approximation to the ideal ones but here r_{22} is typically only 15 kΩ and the curves do not coalesce but go separately to the origin. This non-coalescence of the output characteristics is fundamental in a transistor and cannot be changed by forming. Fig. 1(*c*) shows the output characteristics of an unformed silicon point-contact transistor and their totally different nature compared with the two previous sets is evident at a glance. It should be pointed out that output characteristics of this form are obtained for unformed *germanium* transistors. The object of collector forming is to change the non-saturation characteristics of the type in Fig. 1(*c*) to saturation characteristics of the types in Figs. 1(*a*) or 1(*b*).

The maximum available power gain of a grounded base transistor is given approximately by $\alpha^2 r_{22}/4r_{11}$ where α is the incremental current gain defined as $(\partial I_c/\partial I_\epsilon)_{V_c=\text{const.}} = r_{21}/r_{22}$. The value of r_{22} is normally fixed by the forming procedure adopted to obtain an output characteristic of the correct shape. However, in principle the power gain can still be improved by reducing r_{11}, which indicates the need for an emitter forming procedure. α is in part a function of the emitter efficiency and collector efficiency and would be expected to be dependent on both the forming procedures.

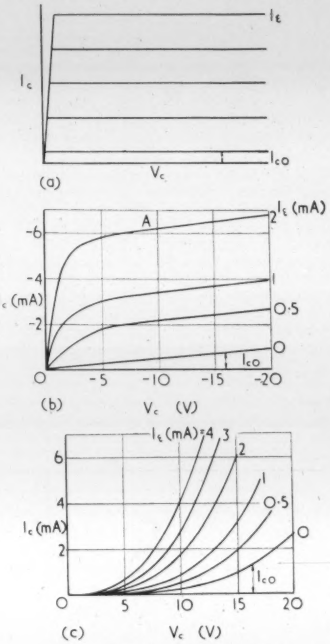

Fig. 1. Transistor characteristics

I_{c0} for an arbitrary collector voltage is indicated on each graph.

(*a*) Ideal output characteristics.

(*b*) Output characteristics of a germanium transistor of modern manufacture.

(*c*) Output characteristics of an unformed p-type silicon transistor; phosphor bronze used for both emitter and collector.

THE EXPERIMENTAL CONDITIONS

The silicon used in the transistor tests was mainly single-crystal material prepared in this laboratory. Silicon specimens with resistivities in the range 4 to 30 Ω . cm were used having minority carrier lifetimes in the range 1 to 10 μs as measured by the method of Arthur and others.[2] Small specimens cut from the silicon ingots were nickel-plated and soldered to brass base plates. The free surfaces were ground, polished and etched with the standard germanium etch CP4.[3] It is possible that a different etch would have improved the transistor action of these specimens, but a systematic investigation on suitable etching techniques for silicon was not undertaken. The transistors were tested on micro-manipulators.

The emitter and collector contacts were formed using a single pulse of controlled duration and amplitude applied

between the contact and the base. This pulse could be varied from 1 to 10 ms duration and up to 600 V amplitude and was delivered from a 500 Ω impedance. The transistor characteristics were observed on a calibrated oscilloscope before and after forming.

THE FORMING TESTS

Some thirty different whisker materials of various compositions were tested as emitter and collector contacts on n- and p-type silicon. These included a range of copper based alloys in wire form of 0·005 in. diameter containing 2% of aluminium, indium, gallium, phosphorus, arsenic or antimony. The first three elements are in Group 3 of the Periodic Table and the last three are in Group 5.

Each whisker material was tested as a collector contact of a given silicon specimen and the shape of the output characteristics after various forming pulses had been passed through the contact was observed. Those whiskers which gave saturation-type output characteristics were noted. One of these was selected as a collector and then a range of emitter contacts was tested, the change in r_{11} and α on forming being noted. It was found that suitable whisker materials which gave a decrease in r_{11} also gave an increase in α. The procedure was repeated for a silicon specimen of the opposite conduction type. Then, suitable emitter and collector contacts for n- and p-type silicon having been established, these were tested on a series of specimens with different resistivities.

Suitable whisker materials and forming procedures for silicon transistors are now given.

p-type silicon

(*a*) *Collectors.* Saturation output characteristics were obtained with whisker materials containing an element from Group 3 of the Periodic Table. Aluminium, indium- and gallium-bronze wires gave equally good results. A 5 ms forming pulse of 200 V amplitude applied in the forward direction of the contact was satisfactory. Fig. 2(*b*) shows a typical collector diode characteristic on 10 Ω . cm, 1 μs lifetime p-type silicon before and after forming. It will be seen that collector forming reduces the rectification ratio of the collector diode and near the origin the sign of rectification is reversed.

(*b*) *Emitters.* An increase in α and a reduction in r_{11} were obtained if the whisker material contained an element from Group 5 of the Periodic Table. Phosphorus-, arsenic-, and antimony-bronze wires made equally good emitters. It was essential to form the emitter to bring about these changes, a pulse of 5 ms duration and 200 V amplitude applied in the forward direction being suitable. It should be pointed out that in some cases, emitter forming alone was sufficient to give a reduced value of r_{11}, an increased α and saturation output characteristics, collector forming being unnecessary. However, it was essential that a suitable collector whisker material was used. Fig. 2(*a*) shows a typical emitter diode characteristic on 10 Ω . cm, 1 μs lifetime p-type silicon before and after forming. It will be seen that forming decreases r_{11} and increases the reverse resistance. Thus, the rectification ratio of the emitter diode is increased.

n-type silicon

(*a*) *Collectors.* Saturation output characteristics were obtained with whisker materials containing elements from Group 5 of the Periodic Table. Phosphorus-, arsenic- and antimony-bronze wires made equally good collectors. A pulse of 5 ms duration and 100 V amplitude applied in the forward direction was suitable to form the contact. Unlike the p-type case, it was always necessary to form the contact to obtain a saturation output characteristic. Tantalum, also of Group 5, made a suitable collector whisker, but a forming pulse of about 400 V was necessary to form the contact. Fig. 3(*b*) shows a typical collector diode characteristic on

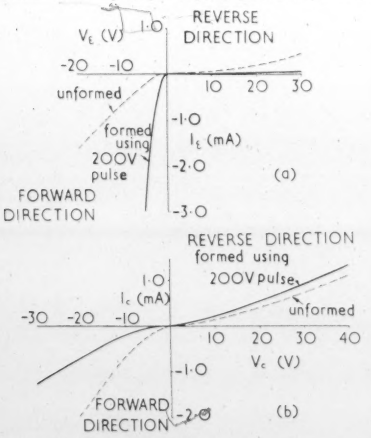

Fig. 2. Diode characteristics of unformed and formed transistor point contacts on p-type silicon

(*a*) Antimony-bronze emitter.
(*b*) Gallium-bronze collector.

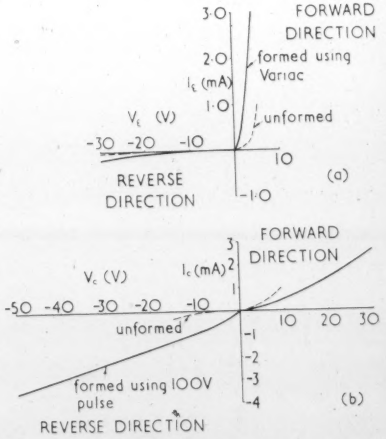

Fig. 3. Diode characteristics of unformed and formed transistor point contacts on n-type silicon

(*a*) Gallium-bronze emitter.
(*b*) Antimony-bronze collector.

15 Ω . cm, 10 μs lifetime n-type silicon before and after forming. It will be seen that after forming the rectification ratio is reduced and the sign of rectification near the origin is reversed. This is similar to the change observed with collectors on p-type silicon. However, in contrast with the p-type transistor, the characteristic is discontinuous at the origin. This is an unusual type of voltage-current characteristic but typical of these collectors.

(*b*) *Emitters.* An increase in α and a decrease in r_{11} was obtained for whisker materials containing an element from Group 3 of the Periodic Table. Aluminium-, indium- and gallium-bronze probes were found to be equally satisfactory. Contrary to the previous methods, forming with a single pulse impaired the transistor performance, α being halved in typical instances. By trial and error, it was found that a 50 c/s signal applied to the contact and of sufficient magnitude to pass about 30 mA in the forward direction would produce the desired change. It is not understood why an n-type emitter should require different forming but it is possible that pulse forming would be satisfactory with a pulse duration outside the available range of 1–10 ms. Fig. 3(*a*) shows a typical emitter diode characteristic on 15 Ω . cm, 10 μs lifetime silicon before and after forming. It will be seen that after forming, the current for a given applied voltage is increased in both the forward and the reverse directions. Comparison with Fig. 2(*a*) shows that the reverse characteristics of emitters on n- and p-type silicon move in opposite directions on forming.

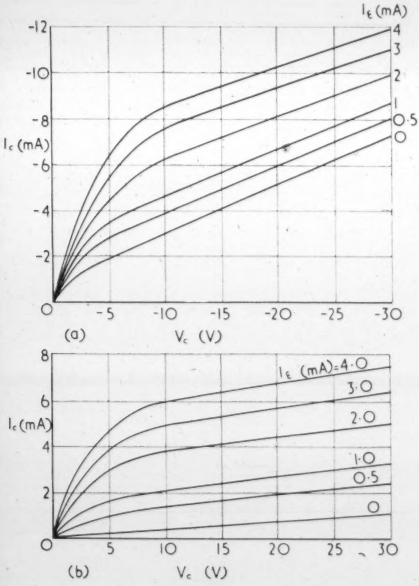

Fig. 4. Output characteristics of formed silicon transistors

(*a*) n-type transistor.
(*b*) p-type transistor.

The whisker materials mentioned above form symmetrical groups. Thus, wires containing Group 5 elements make suitable emitters on p-type silicon and suitable collectors on n-type silicon while wires containing Group 3 elements make suitable emitters on n-type silicon and suitable collectors on p-type silicon. However, a number of satisfactory whisker materials were found which did not contain elements from either of these groups. Thus, gold (Group 1) and nickel and platinum (Group 8) made satisfactory collector wires for n-type silicon provided that large forming pulses of about 400 V were used. Similarly, platinum (Group 8) made a good emitter on n-type silicon. It was only for n-type silicon that suitable whiskers were found which did not contain elements from Group 3 or Group 5 but it must be stressed that the number of wires tested was very limited.

Fig. 4 shows two sets of output characteristics for silicon transistors which were formed as described above. Fig. 4(*a*) refers to 32 Ω . cm, 3 μs lifetime n-type silicon and Fig. 4(*b*) refers to 12 Ω . cm, 1 μs lifetime p-type silicon. Each set saturates in a satisfactory manner. It will be noticed that the collector current for zero emitter current, I_{c0} (see Fig. 1), is largest for the n-type transistor. This was typical for the units tested.

DISCUSSION OF THE FORMING PROCESS

It is not possible at the present stage to advance a generalized theory of forming to explain all the varied experimental results. However, a symmetry does exist in that wires containing Group 3 or Group 5 elements make satisfactory emitters or collectors on n- or p-type silicon and this will now be discussed.

Elements from Group 3 are acceptor impurities in silicon while those from Group 5 are donor impurities. Consider first emitter forming. A suitable emitter for p-type silicon is one which contains a donor impurity from Group 5. It is reasonable to suppose that during forming, this impurity diffuses from the wire into the silicon making a p–n junction beneath the contact. This would be expected to increase the injection efficiency of the emitter and hence the value of α of the transistor. An increase of injection efficiency would also lower r_{11} as observed experimentally. A similar explanation has been offered by Jacobs and others for their type of emitter forming.

A suitable collector for p-type silicon is one which contains an element from Group 3. On forming, some of this impurity would be expected to enter the silicon and produce a region of low resistivity in the neighbourhood of the contact or a p/p^+ junction. A transistor functions by virtue of the minority carriers which are injected at the emitter and travel to the collector. From geometrical considerations it is clear that only a small fraction of the injected carriers will reach the collector, unless they are influenced by the electric field due to the standing collector current I_{c0}. The presence of the p^+ region is expected to increase I_{c0} for all collector voltages and in particular, at low collector voltages, the electric field would be sufficiently strong to attract most of the minority carriers from the emitter to the collector. This would result in saturation type output characteristics. These considerations should also apply, with the appropriate changes, to n-type silicon transistors. However, the differences found to exist between the experimental results for formed n- and p-type transistors indicate that the above explanations are not complete.

An explanation can be given for the fact that it is frequently only necessary to form the emitter of a p-type silicon tran-

sistor, collector forming being unnecessary. Reference to Fig. 2(*b*) shows that, even without forming, I_{c0} is quite large at low collector voltages. Thus, saturation characteristics would be obtained with an unformed collector on this material. On the other hand, for n-type silicon transistors, I_{c0} is small at low collector voltages [see Fig. 3(*b*)] and hence collector forming is essential.

SOME RESULTS ON FORMED SILICON TRANSISTORS

Formed n- and p-type silicon transistors were tested at room temperature and at about 100° C. No significant change in the transistor parameters was found over this temperature range.

Table 1 lists some of the results obtained for a p-type silicon transistor. 12 Ω . cm, 1 μs lifetime material was used with a phosphor-bronze emitter and an aluminium-bronze collector. These results were typical of the better transistors. This transistor, whose output characteristics are shown in Fig. 4(*b*), was measured at 105° C. The current gain, voltage gain and maximum power gain[4] are calculated for three values of emitter current at a constant collector voltage.

Similarly, the results listed in Table 2 are typical of those obtained for n-type silicon transistors. This particular transistor was made with 32 Ω . cm, 3 μs lifetime material, an aluminium-bronze emitter and a tantalum collector. Its output characteristics are shown in Fig. 4(*a*).

The power gains of the p-type silicon transistor at 105° C compare quite favourably with those of a typical germanium point-contact transistor at room temperature. In general, the performance figures of the p-type transistors were better than those of the n-type transistors as illustrated by the two tables. It will be noted from the tables that α decreases with increasing emitter current. This behaviour is characteristic of silicon transistors.

With normal bias voltages applied, n-type silicon transistors were stable when operated in air at 100° C. On the other hand, the p-type units deteriorated rapidly under similar conditions, the power gain being halved after 24 hours. The cause of the failure has not been investigated, but it is likely to be associated with the crystal surface. It is probable that more suitable etches and proper encapsulation of the unit would prevent the deterioration.

CONCLUSIONS

It has been established that silicon transistors with improved power gains and saturation output characteristics can be produced by using specific whisker materials and pulsing techniques. The power gains are not markedly inferior to those of germanium point-contact transistors. The results of the forming tests are of considerable physical interest and indicate the kind of work which must be done if other semiconductors, for instance semiconducting compounds, show promise as transistor materials.

ACKNOWLEDGEMENTS

The authors are indebted to their colleagues in the transistor group of this establishment for their advice and help. The copper-based whisker materials were kindly supplied by Dr. W. E. Alkins of Thomas Bolton and Sons Ltd. The paper is published by permission of the Chief Scientist, Ministry of Supply, and the Controller, H.M. Stationery Office.

Table 1. *Operating conditions for p-type silicon transistor*

Operating point										
V_c V	I_E mA	V_g V	I_c mA	r_{11} Ω	r_{22} Ω	r_{21} Ω	r_{12} Ω	α	*Max. voltage gain emitter load = 400 Ω*	*Max. power gain*
+25	−0·1	0	2	1100	22 000	50 000	350	2·27	33	42
+25	−0·5	−0·15	2·4	700	18 500	35 000	330	1·9	32	53
+25	−1·0	−0·2	3·1	540	16 000	30 000	270	1·9	32	66

Table 2. *Operating conditions for n-type silicon transistor*

Operating point										
V_c V	I_E mA	V_g V	I_c mA	r_{11} Ω	r_{22} Ω	r_{21} Ω	r_{12} Ω	α	*Max. voltage gain emitter load = 400 Ω*	*Max. power gain*
−8	+0·2	+0·1	−3	920	5000	11 000	205	2·2	8·5	11
−8	+0·5	+0·15	−4	600	5000	7000	230	1·4	7	5·5
−8	+1·0	+0·25	−5	400	5000	5700	230	1·1	7	8

REFERENCES

(1) JACOBS, H., BRAND, F. A., MATTHEI, W., and RAMSA, A. P. *J. Appl. Phys.*, **25**, p. 1046 (1954).

(2) ARTHUR, J. B., BARDSLEY, W., GIBSON, A. F., and HOGARTH, C. A. *Proc. Phys. Soc.* [*London*], *B*, **68**, p. 121 (1955).

(3) HAYNES, J. R., and SHOCKLEY, W. *Phys. Rev.*, **81**, p. 835 (1951).

(4) SHOCKLEY, W. *Electrons and Holes in Semiconductors*, p. 45 (New York: D. Van Nostrand Co. Inc., 1950).

Measurement of the statistical time lag of breakdown in gases and liquids

By R. F. Saxe, Ph.D., and T. J. Lewis, Ph.D., Queen Mary College, University of London, London, E.1

[*Paper first received* 17 *November, and in final form* 13 *December*, 1954]

It has been shown by earlier workers that the observation of the statistical distribution of time lags to breakdown of small spark gaps may provide information concerning the emission of electrons from the cathode. This paper discusses the restrictions imposed by this method of measurement of cathode emission. Since the measuring technique causes the surface being investigated to undergo a change, efficient spark quenching should be provided to reduce this change to a minimum. A circuit which provides efficient spark quenching is described, together with a novel circuit to record a set of time lags automatically. Preliminary experiments show that "conditioning" of the cathode surface in air is now more rapid than that obtained by previous workers, and the reasons for this are discussed. Further, application of the method to the breakdown of small gaps in *n*-hexane indicates that the behaviour is similar to that of a gap in air in that "conditioning" of the cathode surface and a statistical variation of time lags occur.

1. INTRODUCTION

The statistical time lag of the breakdown of small gaps between metal electrodes in a gas when subjected to an impulse voltage has been investigated by several workers[1–8] who have shown that the distribution of such lags is, under certain conditions, exponential. The average time lag of this distribution can be related to the electron current from the cathode[9,10] and, as a result, the method may be used to investigate the factors affecting such a cathode emission.

As will be shown later, however, the process of measurement, since it involves a spark, causes a modification of the emissive properties of the cathode surface and, unless care is exercised, the results cannot be analysed statistically. Difficulties are further increased by the fact that, in order to obtain results of reasonable accuracy, large numbers (of the order of 10^3) of time lags must be measured. Such difficulties become serious when the method is extended to measurements in liquid dielectrics. The damage caused by a spark in a liquid is normally so great that more than one time lag measurement for a given gap and liquid sample is impossible without serious change of the gap characteristics.

In an attempt to overcome these difficulties, equipment has been developed in which the modification of the emission due to sparks has been reduced to an amount which is probably smaller than that which has been obtained previously.

Before a description of the equipment is attempted, an analysis of the assumptions and limitations of the method will be given since these are important in any later interpretation of results. Preliminary results, to be discussed later, show that the reduction in damage achieved by efficient spark quenching enables the "conditioning" of such gaps to proceed more rapidly and to a higher stress.

2. THEORY OF THE MEASUREMENT

The generally accepted conception of the spark breakdown process in a gas envisages an initial electron which, in the electric field, multiplies by avalanche ionization processes and finally causes an instability in the gap. Thus the observation of a spark is taken to indicate the prior appearance of an initiating electron and the spark gap is an electron counter. Not every electron appearing in the gap may be counted in this way since the probability W that a primary electron causes a spark may be less than unity. The value of W will depend on such factors as field strength, gap geometry and the nature of the gas. If $W < 1$, more than one electron may appear in the gap before a spark occurs and thus, if W_n is the probability of the occurrence of a spark due to the appearance of the nth electron in the gap after a step-function voltage is applied to the gap, then

$$W_n = W(1 - W)^{n-1}$$

It can be shown that the probability, $P(n, t)$, that this nth electron appears in the time interval t to $(t + \delta t)$ is

$$P(n, t) = [I^n t^{n-1}/(n - 1)!] \exp(-It)\delta t$$

where I is the mean rate of electron production and time is measured from the instant of voltage application. Thus the probability that a spark will occur in the interval t to $(t + \delta t)$ is

$$\sum_{n=1}^{\infty} W_n P(n, t) = WI \exp(-WIt)\delta t \qquad (1)$$

It follows that the average time lag, $\bar{t}$ is given by

$$\bar{t} = 1/WI \qquad (2)$$

It is easy to show from equation (1) that the probability of a time lag greater than t is $\exp(-WIt)$ and thus if, in a particular experiment of N measurements, the number of recorded lags greater than t is n, then

$$\log_e (N/n) = WIt \qquad (3)$$

and a graphical plot of $\log_e (N/n)$ against t gives an estimate of WI which may be more convenient than equation (2).

Equations (2) and (3) may be used to obtain the rate of electron production provided certain conditions concerning W and I are satisfied. These conditions, which are vital to the interpretation of the experimental results, will now be discussed.

3. CONDITIONS NECESSARY FOR RELIABLE MEASUREMENT

3.1. *The probability function W.* As already stated, W is field dependent, and in uniform field gaps it is likely to be small when the static breakdown field (E_s) is applied, but is expected to increase rapidly for field strengths greater than E_s. The calculations of W by Wijsman[11] are based on the assumption that the breakdown mechanism is described by the Townsend theory. There is reason[12] to suspect that this

theory is not necessarily applicable to the gaps being discussed here, and there appears to be, as yet, no calculation of the probability function W which can be applied.

While it is considered probable that $W = 1$ for values of $E \geqslant 1{\cdot}5E_s$, it must be emphasized that this has not been proved, and that the measurements give only the product WI.

It should also be noted that, since W is field dependent, it will vary during the finite rise time τ of the voltage applied to the gap. This will produce a distortion of the distribution given by equation (1) but the error will not be serious provided $\bar{t} \gg \tau$.

3.2. *Rate of electron production I.* The analysis above has assumed that I remains constant, not only throughout a particular time lag measurement, but also throughout the series of N measurements required to obtain the time lag distribution. This constancy will depend on the source of electrons which in general will be either (i) cosmic radiation and radioactivity in the gas or (ii) emission from the cathode. If the gap volume is small, the first process will produce only a small electron current and a correspondingly large value of $\bar{t}$. The occurrence of a shorter average time lag than this may be taken as an indication of cathode emission. Provided this emission is great enough, the contributions from process (i) may be neglected.

If, as has been indicated by several authors, I is field dependent, conditions for the constancy of I during a particular time lag measurement will be similar to those already discussed for W. Although it is possible to visualize other processes by which I may be caused to vary during a time-lag measurement, it is considered reasonable to assume that, provided the field (i.e. the voltage wave), remains constant, I remains constant also.

The further condition that I remains constant over all N measurements requires that the emissive properties of the cathode should remain constant and that the spark accompanying each measurement should not alter the subsequent cathode emission appreciably. While it is obviously impossible to eliminate all damage, efficient limitation of the spark discharge may reduce it significantly, and methods of achieving this spark limitation or quenching will be discussed below.

The cathode damage is reduced if comparatively few measurements are made, although the accuracy with which $\bar{t}$ and I may be computed will be reduced. While Llewellyn Jones and de la Perrelle[6] have shown that a coefficient of variation of 3% is obtained in the value of I if N is 1100, this will only be true if cathode conditions do not vary significantly during a set of measurements. If variations are appreciable, then a more reliable value of I for a given cathode state might be obtained from a far smaller set of measurements.

While the above restrictions apply essentially to breakdown in a gas, similar restrictions will apply to liquid breakdown. Since there is little information concerning collision processes in liquids, the value of W is not known, and therefore at the moment, equations (2) and (3) can only yield values of the product WI. Thus at present, time lag measurements in liquids can only indicate relative surface conditions and cannot be used to evaluate the cathode emission current. In spite of this, such measurements are important in providing information about the breakdown processes in a liquid.

The equipment used for spark quenching and time-lag measurement, designed with the above restrictions in mind, will now be described.

4. SPARK QUENCHING

Once a spark begins, the impedance of the gap falls rapidly and a discharge current flows. This current will have two components, that arising from the energy stored in the capacity of the gap and that which is drawn from the voltage source. The first component may be reduced by ensuring that the gap capacitance (including any stray capacitance) is a minimum. It must be emphasized, however, that no modification to the external circuit can affect this current or modify the damage it produces, unless a parallel path of impedance low compared with that of the gap is established in a time shorter than the formative time of the spark in the gap, which is about 10^{-8} s for the small gaps used. Since the stored energy of the gap depends on the square of the voltage, it will be seen that its effect on the cathode will rise rapidly as the voltage is increased. This becomes very troublesome when the electric strength of the gap is very high, e.g. for liquid dielectrics, and reduces the overall efficiency of any limiting device.

The spark may be maintained by current drawn from the source of voltage; and the magnitude and duration of this current depends on the impedance of this supply. By suitable circuits this component of the current may be limited considerably and a consequent reduction in damage achieved.

4.1. *Diversion by a parallel device.* In the past limitation of the spark current, for an applied d.c. voltage, has been achieved by using the initial current pulse through the gap as a trigger pulse to close a switch which short-circuits the supply, thereby quenching the spark in the gap. As a further aid to limitation a large resistance may be employed in series with the gap to lower the magnitude of the current which can be drawn from the source. The switching operation should be rapid and it is unlikely that the mechanical devices employed for instance by Salvage[13] and Maksiejewski and Tropper[14] were very efficient.

Trigatrons, which are certainly much faster than mechanical switches, have been employed by Watson and Higham[15] and by Lewis.[16] They require, however, a considerable triggering pulse and have an undesirably long and variable delay in operation.

More efficient operation is obtained at present by using a hydrogen thyratron (type BT83), which may be triggered by a pulse of a few hundred volts amplitude with a delay of approximately 10^{-7} s. With care, diversion of the current in the gap should be achieved in approximately 2×10^{-7} s. A serious limitation is that the maximum voltage rating of available types is of the order of 10 kV and although Young[17] has shown that such devices may be operated in cascade, the overall time delay is greater.

The role of the high series resistor in limiting the charge transfer Q in the gap is illustrated by equation (4) which expresses this charge as the sum of two components:

(a) the charge stored in the gap capacitance,
and
(b) the charge due to the flow of current from the generator for a time T before diversion is achieved.

$$Q = CV + VT/R \tag{4}$$

where C = the gap capacitance (plus stray capacitance), V = breakdown voltage, and R = series resistance.

Taking, as representative values,

$C = 3 \times 10^{-12}$ F, $V = 5 \times 10^3$ V, $R = 10^7\,\Omega$, and $T = 2 \times 10^{-7}$ s.

$$Q = 1{\cdot}5 \times 10^{-8} + 10^{-10}\,\text{C} \tag{5}$$

It will be seen from equation (5) that the charge transfer due to the current from the generator is negligible in comparison with that arising from the gap capacitance. Provided, therefore, that diversion is achieved within about 10^{-6} s, it may be considered that efficient spark quenching is occurring.

The efficacy of the simple parallel diverter for d.c. conditions is due to the use of a high value of series resistor in the circuit. Under impulse conditions, however, a series resistor of high value may not be tolerated since it makes the voltage rise time too large. For impulse conditions, the value of R can rarely exceed $10^4\,\Omega$ and Q becomes [with the other parameters as for equation (5)]:

$$Q = 1{\cdot}5 \times 10^{-8} + 10^{-7}\,\mathrm{C} \qquad (6)$$

It will be seen that the charge flow from the voltage source is now greater than the charge stored in the gap by a factor of about ten. It would therefore appear that the use of a parallel device for impulse conditions is inefficient and other means for reducing the energy must be found.

4.2. *Series-parallel limiters.* Limitation may be achieved by inserting, in series with the test gap, a device which, while normally of low impedance, becomes of infinite impedance within a short time after the formation of a spark in the test gap. Such a series device, the use of which appears to be novel, can be obtained approximately by changing a hard valve from the conducting to the non-conducting state. In practice, such a device may be most easily incorporated into the circuit by inserting it on the "earthy" side of the test gap and Fig. 1 shows the complete circuit of such an arrangement.

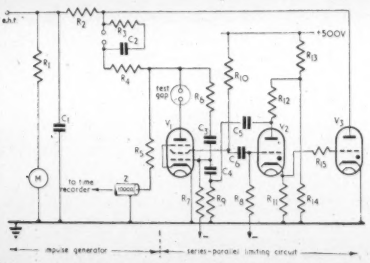

Fig. 1. Impulse generator and series-parallel limiter circuit

The operation of the circuit is as follows. A positive-going pulse from the impulse generator is applied as shown to the test-gap and series valve V_1, which is arranged to be conducting in the waiting period, with its anode at earth potential. At the same time a portion of the test pulse is fed by the capacitance divider C_3, C_4 to the grid of V_1, thereby ensuring that the valve remains conducting during the flow of capacitance current in the test gap, i.e. for the duration of the pulse front. When a spark starts to develop in the test gap, the voltage on the upper electrode will start to fall towards earth, and this negative voltage swing is communicated by the divider C_3, C_4 to the grid of V_1, which then becomes non-conducting. The anode of V_1, and hence the lower electrode of the test gap, is now isolated and will rapidly rise in potential until the potential difference across the test gap is zero and the spark extinguishes.

When the valve V_1 becomes non-conducting, the voltage across the screen resistor R_{10} will collapse, the resulting positive pulse being applied to the grid of a thyratron V_2, causing it to strike. The discharge circuit of V_2 consists of C_5, R_{11} and R_9, and by including R_9 in the lower end of the capacitance divider, as shown, the negative pulse appearing across R_9 ensures that V_1 remains non-conducting. At the same time, the positive pulse developed across R_{11} causes a hydrogen thyratron V_3 to conduct, making the voltage on the system collapse rapidly to zero.

It will be noticed that during the initial stages of the spark discharge, current flows to the anode of V_1 which causes the screen current to drop to a small fraction of its initial value. This action alone is sufficient to fire the valve V_2, but does not, in itself, render V_1 non-conducting. The use of the capacitance divider C_3, C_4 is necessary both to render V_1 non-conducting when a spark develops and to prevent the screen potential of V_1 from rising when capacitance current flows during the front of the test pulse.

It will be seen that this circuit will operate with the same efficiency when steady, rather than impulse, voltages are applied to the test gap.

5. THE TIME CONVERTER

The principles of an analogue time converter have been stated[18] and an expansion circuit has previously been designed which converts a time interval of between 10^{-8} and 10^{-7} s between two pulses, into a square pulse the duration of which is greater than this time interval by a known factor of the order of 10^3 or 10^4.

The converter to be described here (Fig. 2), is intended to accept a square pulse of duration in the range 10^{-6} to 10^{-3} s, and to display this time duration as a slowly decaying voltage, the rate of decay being such that ample time is available to record the peak value.

The positive pulse from the lower arm of the potential divider (R_5, Z, Fig. 1) is applied, *via* the $1000\,\Omega$ cable, to the grid of a valve which amplifies and inverts it. The resultant negative pulse is impressed on the grid of V_5 (Fig. 2), causing this valve to become non-conducting. In the waiting period, valve V_5 is arranged to be conducting with the anode clamped at earth potential by the diode D_1. The grid of V_6 is held at earth potential due to the current flowing through R_{21} and D_2.

When V_5 becomes non-conducting the potential of its anode begins to rise from earth towards h.t. potential at a rate governed by the h.t. potential and the values of R_{19}, L_1 and C_9, since the grid of V_6 is held at earth potential by the diode D_2. This rate is arranged to be approximately constant over the range of times used.

When the test gap breaks down, the negative voltage applied to the grid of V_5 collapses to zero, and the anode of V_5 returns rapidly to earth potential. This forces the grid potential of V_6 negative by a voltage $v = q/C_9$ where q is the charge accumulated by C_9 during the time for which V_5 was non-conducting. Since the rate of charging of C_9 was arranged to be constant, the grid of V_6 is forced negative by the voltage v which is proportional to the pulse duration, t. This charge on C_9 then leaks away towards h.t. at a rate governed by C_9 and R_{21} and until earth potential is reached, valve V_6 is rendered non-conducting. For values of v small compared with the h.t. potential, the discharge rate of C_9 may be considered to be constant and therefore the time for which V_6 is non-conducting will be proportional to v and hence to t. The use of suitable components enables a time expansion of the order of 10^2 to be achieved.

In a similar manner, stages V_6 and V_7 further increase the time expansion, until the rate of decrease of the voltage on C_{15} is so slow that a meter indication is possible. In order, however, to enable a meter reading to be obtained without affecting the slow rate of decrease of voltage, a two-valve "see-saw" circuit, consisting of V_8 and V_9, is used as an impedance transformer to supply the meter V. The voltage on the meter decays so slowly that providing a reading is taken within a few seconds, the loss of accuracy is negligible. The contacts K are inserted to enable the circuit to be reset when the reading has been taken.

Since it will be necessary to make a series of measurements in any time lag experiment, it is desirable that some form of automatic recording and resetting should be employed. To

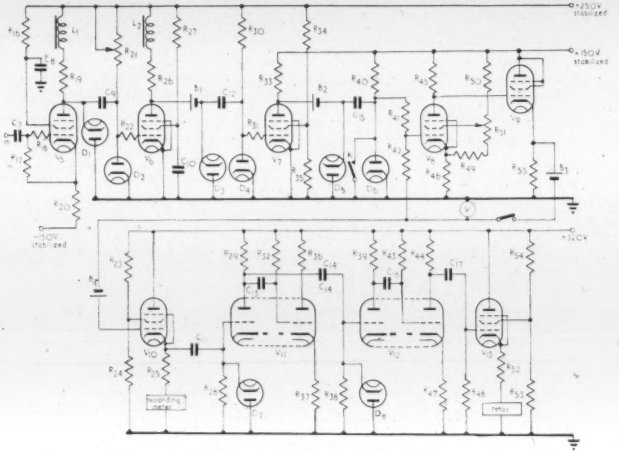

Fig. 2. Time converter circuit

R_{15} = 22 kΩ
R_{17} = 1 MΩ
R_{18} = 100 Ω
R_{19} = 25 kΩ
R_{20} = 6·2 kΩ
R_{21} = 8 × 3·9 MΩ high stability (switching)
R_{22} = 100 Ω
R_{23} = 15 kΩ
R_{24} = 25 kΩ
R_{25} = 2 kΩ
R_{26}, R_{27} = 220 kΩ
R_{28} = 1 MΩ
R_{29} = 40 kΩ
R_{30} = 100 MΩ high stability
R_{31} = 1 kΩ
R_{32} = 2·5 MΩ
R_{33} = 1·2 MΩ
R_{34} = 270 kΩ
R_{35} = 33 kΩ
R_{36} = 32 kΩ
R_{37} = 1·5 kΩ
R_{38} = 1 MΩ
R_{39} = 40 kΩ
R_{40} = 1000 MΩ high stability
R_{41} = 100 MΩ high stability
R_{42} = 1000 MΩ high stability
R_{43} = 2·5 MΩ
R_{44} = 32 kΩ
R_{45} = 1·2 MΩ
R_{46} = 1 kΩ
R_{47} = 1·5 kΩ
R_{48} = 5 MΩ
R_{49} = 36 kΩ
R_{50} = 56 kΩ
R_{51} = 50 kΩ
R_{52} = 2 kΩ
R_{53} = 25 kΩ
R_{54} = 15 kΩ
R_{55} = 22 kΩ
C_5 = 0·01 μF
C_8 = 0·1 μF
C_9 = 0·002 μF
C_{10} = 0·1 μF
C_{11} = 0·01 μF
C_{12} = 0·01 μF
C_{13} = 4 μF
C_{14} = 0·01 μF
C_{15} = 1·5 μF
C_{16} = 1 μF
C_{17} = 0·5 μF
V_5 = CV1065
V_6 = CV1065
V_7 = EF37A
V_8 = EF37A
V_9 = EF37A
V_{10} = CV2127
V_{11} = CV858
V_{12} = CV858
V_{13} = CV138
B_1 = 6V
B_2 = 3V
B_3 = 48 V
B_4 = 3 V

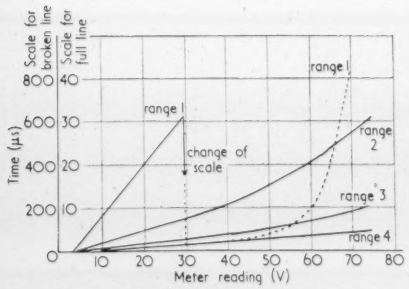

Fig. 3. Calibration curves of time converter

do this the voltage output of the converter is applied to the grid of a cathode follower V_{10} which drives a recording milliammeter. The change in cathode voltage of V_{10} also triggers a flip-flop V_{11}, which produces two square waves each having a duration of approximately two seconds. The negative square wave is differentiated and applied to a second flip-flop V_{12}, which therefore triggers approximately two seconds after the appearance of a reading on the recording milliammeter. The pulse from V_{12}, through the cathode follower V_{13} closes the relay contacts K for about 0·3 s, thereby resetting the time converter. Provided the test impulses are arranged to occur at a rate not exceeding about fifteen per minute, the equipment will record each time lag automatically.

The switching resistance R_{21} allows different ranges of time intervals to be expanded and calibration curves for the different ranges are given in Fig. 3. Non-linearity of these curves is due to the voltage on the integrating capacitors

becoming appreciable compared with the h.t. voltage, and could be removed by switching in different values of capacitance. However, this non-linearity was considered to be an advantage for the longer time-intervals since a greater range of time lags could then be recorded with a particular switch setting.

It is of interest to note that the time expander described above is designed to record the duration of square pulses in the range 10^{-6} to 10^{-3} s as a meter reading, while the time expander designed by Moody[18] converts time intervals in the range 1–100 mμs into square pulses of duration proportional to the input time interval and of the order of 10^{-5} s. Therefore by using the two converters together it is possible to display, as a voltmeter reading, time intervals from 10^{-9} to 10^{-3} s with an accuracy of approximately $\frac{1}{2}$ mμs or 2 per cent, whichever is the greater.

6. THE IMPULSE GENERATOR

The single-stage impulse generator employed (Fig. 1), has a discharge resistor R_5 such that the voltage wave applied to the test gap, in the absence of a breakdown, falls to half value in $2{\cdot}8 \times 10^{-2}$ s, and for the range of time lags measured, i.e. up to 10^{-3} s the applied voltage decays by not more than 2·5 per cent. The series resistors ($R_2 + R_4$) have a value of 10 kΩ, giving a wave front of approximately 0·2 μs duration at the test gap.

The resistor R_5 also serves as the upper arm of a voltage divider of which the lower arm consists of the matched cable of 1000 Ω impedance. This cable is used to take the voltage pulse to the time converter, and is less than two metres long so that the distortion introduced should not be great and would probably only significantly affect short time lag measurements (i.e. less than 1 μs). The distortion by the cable would certainly not introduce appreciable error in the measurements to be described below.

7. PRELIMINARY RESULTS

Using the equipment described above, preliminary results concerning the conditioning process of small gaps both in air and in liquid *n*-hexane have been obtained. While these results are not extensive they are felt to be sufficiently interesting to warrant inclusion at this point. The most important result is that conditioning, i.e. the process in which sparking of the gap produces progressively increasing time lags, is extremely rapid when efficient spark quenching is employed.

For instance, copper electrodes of 1·25 cm diameter were finely turned, degreased in *n*-hexane and left in dry air for twelve hours so that the surface had a definite oxide layer. When set at a gap of 0·033 cm (i.e. a geometry corresponding to that used by Llewellyn Jones and de la Perrelle[6]) the static breakdown field strength (E_s) was $6{\cdot}95 \times 10^4$ V/cm. A series of time lag measurements was then made; a conditioned state at any particular voltage being indicated by the virtual absence of breakdown. In this way it was possible to condition up to a field strength of $1{\cdot}5 \times 10^5$ V/cm after only 2200 pulse applications. On resuming measurements after a further period of twelve hours, E_s was unchanged, while the conditioned state at $1{\cdot}5 \times 10^5$ V/cm (greater than $2\,E_s$) was regained after twenty pulses. Increase of the stress to $1{\cdot}6 \times 10^5$ V/cm did not produce any further conditioning and a series of measurements at this stress yielded a linear $\log_e (N/n)/t$ relation from which a cathode emission current $I = 2{\cdot}8 \times 10^4$ electrons/s was deduced, assuming $W = 1$. Subsequent tests showed these results to be repeatable.

The rate of conditioning was even more rapid for nickel electrodes. Such electrodes, smoothly turned and degreased, gave, for air, the same value of E_s as for copper above. The gap was able to withstand a stress of $1{\cdot}9 \times 10^5$ V/cm ($2{\cdot}7\,E_s$) after 1800 pulses and it was possible to continue the conditioning up to 2×10^5 V/cm ($2{\cdot}9\,E_s$). As for copper electrodes this behaviour was reproducible. The conditioning rate for nickel electrodes given above should be compared with that quoted by Llewellyn Jones and de la Perrelle[6] in which conditioning to $1{\cdot}5\,E_s$ required 45 000 pulse applications.

At the stress of 2×10^5 V/cm, the emission rate was certainly less than 10^4 electrons/s ($W = 1$) for nickel electrodes, and this should be compared with the expected rate of approximately 6×10^6 electrons/s at a similar stress for a comparable oxidized nickel surface investigated by Llewellyn Jones and de la Perrelle,[6] obtained by a linear extrapolation of their curve showing the field dependence of the emission current.

It seems likely that the increased rates of conditioning and the higher stresses achieved are due to highly efficient diversion of the spark energy. In order to test this, time lag measurements were made in which the energy dissipated in each discharge was increased by an additional gap capacitance. The rate of conditioning was not only slowed down but in some cases ceased altogether. This latter type of behaviour has also been described by Llewellyn Jones and de la Perrelle,[6] who showed that heavy sparking of the electrodes resulted in a shortened time lag. The reason why the normal conditioning rate quoted by Llewellyn Jones and de la Perrelle[6] was much less than that found by the present authors, is probably that less efficient spark quenching was used by the former workers. One further difference may also be important. The present technique employs a pulse repetition frequency of approximately fifteen per minute, whereas the former workers employed a rate of fifty per second. At the higher frequency, the rate of sparking may be such that stable conditions are not reached and a more rapid conditioning process thus prevented.

Further conditioning experiments were performed with gaps of 5×10^{-3} cm between 1 cm diameter, spherical electrodes having highly-polished surfaces. Such gaps are of interest since similar arrangements have been used in investigations of liquid breakdown. Using highly-polished chromium electrodes in air, it was found possible to condition to a stress of $1{\cdot}1 \times 10^6$ V/cm (approximately $2\,E_s$) using about 300 pulses. Obvious conditioning ceased at stresses above this value and measurements at a stress of $1{\cdot}2 \times 10^6$ V/cm and $1{\cdot}5 \times 10^6$ V/cm yielded mean electron currents of $2{\cdot}5 \times 10^4$ and $1{\cdot}0 \times 10^5$ electrons/s respectively. Although it is true that the emitting area is smaller than for a parallel plate arrangement, nevertheless, the low electron yield at such a high stress is surprising, especially as W [equation (2)] is unlikely to be greatly different from unity. Phosphor-bronze spheres with a lower degree of polish produced a lower value of E_s ($3{\cdot}4 \times 10^5$ V/cm), but conditioned rapidly to a stress of $1{\cdot}0 \times 10^6$ V/cm with less than 150 pulses.

If such a gap is placed in purified liquid *n*-hexane it should be possible to measure the statistical lag in the same way as for the gap in air. In this application it is very essential that efficient spark limitation should occur, since rapid deterioration in the insulating properties of the gap due to deposits from the discharges will occur if the energy dissipated

is large. Conditions are also made more difficult by the greater breakdown strength of the gap and by the increase in gap capacitance resulting from the increased dielectric constant of the medium. Preliminary measurements with chromium electrodes as above and gaps up to 5×10^{-3} cm have shown that it is possible to achieve a fair degree of conditioning in a manner similar to that in a gas. Ultimately, however, damage and deposits on the electrodes cause all the time lags to become short and prevent any further conditioning. As for a gas, the conditioning process is rapid, but sufficient time (5–10 s) must elapse between sparks in order that any disturbance in the liquid caused by a spark may die out.

With a gap of $3{\cdot}4 \times 10^{-3}$ cm in pure *n*-hexane it was found possible to condition upwards from the static stress E_s of $1{\cdot}2 \times 10^6$ V/cm to a stress of $1{\cdot}8_4 \times 10^6$ V/cm and at this latter stress there was a statistical variation in the time lag with a preponderance of long lags (greater than 10^{-3} s). Even at a stress of $1{\cdot}9_2 \times 10^6$ V/cm although the lags were generally shorter, individual lags greater than 100 μs were recorded. It is impossible to give any reliable estimate of the cathode electron emission at such stresses since insufficient measurements could be made owing to final deterioration of the gap due to discharge damage. While it may prove to be impossible to make a sufficiently long series of measurements to estimate $\bar{t}$ and I under the conditions stated in Section 3, the method does allow qualitative comparison of cathode surfaces and also indicates a statistical variation in the time lag. It is interesting to note that it is possible to achieve at least a limited amount of conditioning for electrodes in *n*-hexane and further that statistical variation of the time lag is found even at stresses of $1{\cdot}9_2 \times 10^6$ V/cm where lags greater than 100 μs have been recorded. At this stress, Goodwin and MacFadyen[19] found a constant time lag of $0{\cdot}4$ μs, and interpreted this in terms of mechanisms occurring in the liquid. However, it would now appear that this short lag was due to the technique employed by these authors in which a virgin, i.e. unconditioned, electrode surface was used for each individual time lag measurement. As shown above, long time lags are observed when conditioned electrodes are used, and it is therefore suggested that the values of the time lags provide information on the state of the cathode, and are not apparently related to mechanisms in the liquid.

8. CONCLUSIONS

The "conditioning" process appears to be facilitated when the energy dissipated in the gap by a single spark is reduced. It is suggested that the conditioning observed is the result of two opposing effects caused by the spark. It is conceivable that extremely low energy sparks would produce "ideal" conditioning, but that sparks of higher energy produce damage which lessens and may even annul this conditioning. As conditioning proceeds and the gap voltage is raised, energy dissipation increases as the square of the voltage, and eventually a voltage is reached at which the "ideal" conditioning is annulled by spark damage and further conditioning ceases.

It has been suggested that, in the case of gases, conditioning results in the removal by the discharge of any "high spots" on the cathode. This is not supported by the present evidence since reduction in the energy dissipation during a spark increases rather than decreases the conditioning rate. Further, the electrodes used in the above experiments were microscopically extremely rough and conditioning was so rapid that it is unlikely that any appreciable change in the surface micro-geometry occurred. Certainly, no evidence of such changes could be found by microscopic examination. It seems likely, therefore, that the conditioning process is a complicated one in which the reduction of high spots may not be the only or even the most important change. The nature of the spark is such that vigorous electro-chemical processes probably occur on the cathode and in the gas. If the emission occurs mainly from a few active sites of small dimensions, comparatively few sparks may suffice to reduce the activity of these sites and thereby cause a large reduction in the emission.

The experiments performed by the authors, although not exhaustive, seem to indicate that both the conditioning process and the subsequent rate of electron emission are greatly influenced by the experimental technique. In view of the discussion in Section 3·2 it would seem that, until the exact nature of the conditioning process is understood, experimental results should be treated with caution.

ACKNOWLEDGEMENTS

The authors wish to thank Professor W. J. John, in whose laboratories this work was carried out.

They also wish to acknowledge the award of an I.C.I. Research Fellowship to one of the authors (R.F.S.) and the award of the W.T. Henley Fellowship to the other (T.J.L.), during the tenures of which this work was performed.

REFERENCES

(1) STRIGEL, R. *Elektrische Stossfestigkeit* (Berlin: J. Springer, 1939).

(2) STRIGEL, R. *Arch. Elektrotech*, **26**, p. 803 (1932); **27**, pp. 137, 397 (1933).

(3) STRIGEL, R. *Wiss. Veröff. Siemens-Werk*, **11**, p. 52 (1932); **15**, p. 15 (1936).

(4) STRIGEL, R. *Elektrotech. Z.* [*ETZ*], **59**, p. 31 (1938).

(5) LLEWELLYN JONES, F. J. *Proc. Phys. Soc.* [*London*] *B*, **62**, p. 366 (1949).

(6) LLEWELLYN JONES, F. J., and DE LA PERRELLE, E. T. *Proc. Roy. Soc. A*, **216**, p. 267 (1953).

(7) LLEWELLYN JONES, F. J., and MORGAN, C. G. *Proc. Roy. Soc. A*, **218**, p. 88 (1953).

(8) GREY MORGAN, C., and HARCOMBE, D. *Proc. Phys. Soc.* [*London*] *B*, **66**, p. 665 (1953).

(9) VON LAUE, M. *Ann. Phys.* [*Leipzig*], **76**, p. 261 (1925).

(10) ZUBER, K. *Ann. Phys.* [*Leipzig*], **76**, 231 (1925).

(11) WIJSMAN, R. A. *Phys. Rev.*, **75**, 833 (1949).

(12) SAXE, R. F. To be published.

(13) SALVAGE, B. *Proc. Instn Elect. Engrs*, **98**, IV, p. 15 (1951).

(14) MAKSIEJEWSKI, J. L., and TROPPER, H. *Proc. Instn Elect. Engrs*, **101**, II, p. 183 (1954).

(15) WATSON, P. K., and HIGHAM. J. B. *Proc. Instn Elect. Engrs*, **100**, IIA, p. 168 (1953).

(16) LEWIS, T. J. *Proc. Instn Elect. Engrs*, **100**, IIA, p. 141 (1953).

(17) YOUNG, D. R. *J. Appl. Phys.*, **21**, p. 222 (1950).

(18) MOODY, N. F. *Electronic Engng*, **24**, p. 289 (1952).

(19) GOODWIN, D. W., and MACFADYEN, K. A. *Proc. Phys. Soc.* [*London*] *B*, **66**, p. 85 (1953).

Indium antimonide as a fluxmeter material

By E. W. Saker, Ph.D., A.Inst.P., F. A. Cunnell, Ph.D., and J. T. Edmond, M.A., A.Inst.P.,
Services Electronics Research Laboratory, Baldock, Herts.

General principles in the measurement of magnetic fields by use of the Hall effect are considered, and it is shown that the efficiency of Hall generator devices is proportional to the square of the carrier mobility in the material used. Indium antimonide, a semi-conductor with a very high carrier mobility, is therefore very useful for such a purpose. The construction of fluxmeter probe units using indium antimonide is described. Sensitivity and linearity are discussed, and methods are given for temperature compensation.

The large Hall effect in certain semi-conductors has led to the use of germanium as a fluxmeter material for the measurement of magnetic fields.[1] The advantages of fluxmeters of this type are: (1) direct and stable reading; (2) linear scale; (3) small probe size, which will measure the field over a very small area and in narrow gaps; (4) robust output meter. Analysis of the requirements for a fluxmeter material show that the main requirement is a high carrier mobility, and in this respect indium antimonide, a semi-conductor possessing the highest known mobility of over 60 000 $cm^2/V.s$, compared with 3600 $cm^2/V.s$ for germanium, has important advantages over the latter substance. An account is given of the various points which have arisen in the use of indium antimonide as a fluxmeter material.

General considerations

For a specimen of length L, breadth b, and thickness t cm, the magnitude of the Hall voltage is given by

$$V_H = 10^{-8}(RHi/t) \text{ volts} \qquad (1)$$

where R is the Hall constant (cm^3/coulomb), H is the magnetic field in gauss, and i is the total current in amperes. If the Hall probes are connected directly to an external load, such as a milliammeter, experiment shows that considerable current may be drawn from the contacts, and the current flowing in the external circuit is given accurately by the expression

$$i_{out} = V_H/(Z_{ext} + Z_{int})$$

where Z_{ext} is the external load and Z_{int} is the internal resistance of the specimen measured between the Hall probes. Z_{int} depends on the method of making contact and on the geometry of the specimen, but for the low resistance soldered contacts of the type with which we are concerned, we may take $Z_{int} = K\rho b/Lt$, where ρ is the resistivity and K has a value between 2 and 5 usually. If the specimen is matched to the load so that $Z_{ext} = Z_{int}$, the power output is given by

$$W_0 = (V_H^2/4Z_{ext}) = (V_H^2 Lt/4K\rho b)$$

The power supplied to the specimen is $W_i = (i^2\rho L/bt)$ so that the efficiency of the device, defined as the ratio of output power to input power, is

$$\eta = \frac{V_H^2 t^2}{4K\rho^2 i^2} = \frac{10^{-16}R^2H^2}{4K\rho^2} \qquad (2)$$

The value of the Hall constant R is given by

$$R = -\frac{3\pi}{8|e|}\frac{n\mu_n^2 - p\mu_p^2}{(n\mu_n + p\mu_p)^2} \text{ cm}^3\text{/coulomb}$$

where n and p are electron and hole concentrations, μ_n and μ_p are electron and hole mobilities ($cm^2/V.s$) and e is the electronic charge in coulombs. If germanium is used in the device the material is extrinsic ($n \gg p$) for two reasons: (1) to reduce the resistance of the specimen; (2) to reduce the temperature sensitivity of n and therefore of R. In this case the expression for R reduces to the simple form

$$R = 3\pi/8ne$$

for not too impure material. If indium antimonide is used the material is actually intrinsic ($n = p$), but since μ_n is greater than μ_p by a factor of approximately eighty[2] the presence of the holes may be ignored and the expression for R again reduces to the simple equation. Using the expression $\rho = (ne\mu)^{-1}$ we have that $R/\rho = (3\pi/8)\mu$, so that in equation (2)

$$\eta = \frac{9\pi^2}{256}\frac{1}{K}10^{-16}H^2\mu^2 \qquad (3)$$

For sensitivity the input power will be made as large as possible, the limit being set by that dissipation which will cause a significant temperature rise in the specimen. For similar substances like germanium and indium antimonide this will depend only on the surface area and hence for identical geometry will be the same in both cases. Hence it is shown that in a given field the available power depends only on the square of the mobility. The power available from indium antimonide will therefore be approximately $(60\,000/3600)^2 = 280$ times greater than that available from germanium. The input current will be much greater in the case of indium antimonide, but since the material has low resistivity this causes no embarrassment.

The available power is only obtained in practice if the meter is matched to the Hall impedance Z_{int}. With germanium this is easy to arrange; if the resistivity of the material is such that it is not temperature sensitive, the resistance of a specimen of the required dimensions is such that it can easily be matched to a milliammeter of normal resistance. With indium antimonide this is not so easy as the resistivity of the intrinsic material is approximately $5 \times 10^{-3}\ \Omega$.cm. The resistance of the specimen is made as high as possible by reducing the thickness, but the brittleness of the material precludes the use of specimens thinner than about $\frac{1}{4}$ mm without the use of elaborate care. The resistance between the Hall probes of such a specimen is about $0{\cdot}5\ \Omega$ using soldered contacts. Milliammeters are not usually made with such low resistance; one which has been in use in this laboratory has a resistance of $3{\cdot}5\ \Omega$. It can be shown that in this case the power delivered to the meter is 44% of that available with perfect matching. Such a mismatch still leaves a large factor in favour of indium antimonide, and improvements may be expected with better techniques.

The calculation of efficiency performed above is the most fundamental, but different considerations may apply under different operating conditions. If, for example, the specimen is used in conjunction with an amplifier of high input impedance the important consideration will be Hall voltage and not Hall power. In this case it may be shown by an

argument similar to the one above that the output voltage in terms of input power is

$$V_H = 10^{-8} H \left(\frac{3\pi}{8} \frac{W_i b}{tL}\right)^{\frac{1}{2}} (\mu R)^{\frac{1}{2}}$$

For specimens of similar geometry and equal input power the significant factor is $(\mu R)^{\frac{1}{2}}$. For pure indium antimonide $R = 350\ \text{cm}^3/\text{C}$, $\mu = 60\,000\ \text{cm}^2/\text{V.s}$, and $(\mu R)^{\frac{1}{2}}$ has the numerical value $4{\cdot}6 \times 10^3$. For germanium of resistivity $1\ \Omega.\text{cm}$ ($R = 4200\ \text{cm}^3/\text{C}$) the value is $3{\cdot}9 \times 10^3$, and for $5\ \Omega.\text{cm}$ material ($R = 21\,000\ \text{cm}^3/\text{C}$) the value is $8{\cdot}6 \times 10^3$. Germanium of resistivity greater than about $1{\cdot}5\ \Omega.\text{cm}$ therefore has an advantage for this type of application, which is however less usual. If alternating current is used for the primary supply the Hall voltage may be fed into an amplifier by means of an input transformer. The ratio of this transformer may be considerably higher in the case of indium antimonide than for germanium because of the low output impedance, so that the advantage of indium antimonide is regained.

PRACTICAL CONSIDERATIONS

(*a*) *Construction of probe unit.* For the construction of fluxmeter probes using indium antimonide, the material must first be purified by zone-melting until it is intrinsic. The specimens used for the fluxmeter are ground to the approximate size 5–10 mm × 2–4 mm × ~ 0·25 mm. The ratio L/b should not be less than 3 or the Hall voltage will be reduced by the short-circuiting effect of the current electrodes. It is advantageous to make the specimens as thin as possible, but as stated it is difficult to handle specimens thinner than about $\frac{1}{4}$ mm without risk of fracture. The specimen is copper plated and the electrodes are soldered on, after which the excess copper is removed by immersion in nitric acid. If necessary, contacts may be soldered on directly using ordinary soft solder. The specimen is then embedded in cold-setting resin or otherwise protected against mechanical shock. Fluxmeter specimens of indium antimonide embedded in transparent resin and encased in Perspex holders were demonstrated at the 1954 Physical Society Exhibition. Currents of 100 mA may be passed through fully enclosed specimens of the size quoted without undue heating.

Due to inaccuracy in alinement of the Hall probes, a voltage usually appears at the probes when current is passed through the specimen in the absence of a magnetic field. This may be compensated in a number of ways, of which the most simple and elegant is that described by Kuhrt.[3] The Hall probes are joined to their respective points of equipotential on a potentiometer wire in parallel with the specimen, the output meter being in one lead (Fig. 1). This method has the advantage of keeping the output resistance down to a minimum.

(*b*) *Sensitivity.* The sensitivity of the device is such that, using a current of 100 mA, a deflexion of about $\frac{1}{4}$th division is produced on the measuring meter (1 mA full scale, 100 divisions, $3{\cdot}5\ \Omega$) if the probe is held so that the vertical component of the earth's field passes normally through the specimen and is then rotated through 180° about a horizontal axis. This corresponds to a change in field of about 1 oersted. Hence fields upwards of 10 G can be measured with accuracy. If the output from the Hall probes is amplified instead of being fed directly into a meter, much smaller fields can be measured. The noise appearing at the Hall probes is low and it appears that fields of the order of 1/1000 G could be detected. Difficulties might arise from thermomagnetic effects in the specimen (Ettinghausen and Nernst effects), but these could be eliminated by the use of alternating current for the primary supply. This would also make amplification easier.

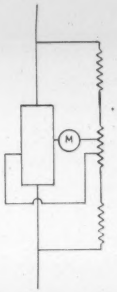

Fig. 1. Compensation of zero-field voltage between Hall contacts

(*c*) *Linearity.* Provided that the material used is intrinsic or *n*-type, the Hall voltage depends linearly on H and i. Fig. 2 shows V_H and V_A (where V_A is the voltage across the current electrodes of the specimen for constant i) for an intrinsic specimen using fields up to 26 kG. The ratio V_H/V_A is also shown. Since the Hall voltage arises from the rotation of the lines of equipotential in the specimen in a magnetic field, it is obvious that V_H cannot exceed V_A. For fields of

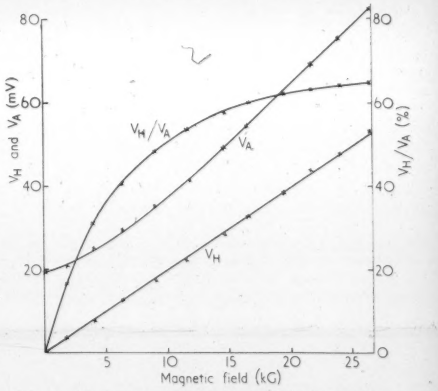

Fig. 2. Hall voltage V_H and applied voltage V_A as functions of H for constant input current

only a few kG V_H is an appreciable fraction of V_A, and linearity of V_H with H is only possible because in high fields V_A (for constant current) also increases linearly with H due to the magneto-resistive effect. Owing to the increase in resistance of the specimen, the total resistance of the output circuit increases in high fields and the output current will not be completely linear with H. For this reason it is desirable to cut down the sensitivity in high fields by putting a resistance in series with the output meter rather than by cutting down the primary current.

If *p*-type material is used, R is a function of field and the gaussmeter is not linear.[4]

(*d*) *Temperature compensation.* Whereas the Hall constant of germanium of a few Ω.cm resistivity is independent of temperature up to about 50° C, the Hall constant of indium antimonide is temperature dependent and a gaussmeter must be compensated against temperature changes if accurate measurements are to be obtained. Compensation can be applied in the following manner by simple methods.

Elimination of R in equation (1) by the substitutions $R = (3\pi/8)(1/ne)$ and $i = V_A ne\mu tb/L$ leads to the expression

$$V_H = 10^{-8}\frac{3\pi}{8}\frac{V_A H\mu b}{L} \tag{4}$$

Compensation is then applied in two stages:

(1) by maintaining a constant voltage across the specimen at every temperature. This corrects for the fall in resistance due to the increasing number of carriers as the temperature rises. The voltage applied can conveniently be monitored using the output meter and a suitable series resistor;

(2) by correcting for the fall in mobility with increase of T. This can be done in two ways:

(*a*) by using a piece of germanium in series with the meter with which the voltage applied to the specimen is monitored. The germanium should be *n*-type and extrinsic (constant number of carriers) and of such resistivity that lattice scattering is dominant. If V_M is the voltage across the meter then

$$V_A = V_M\frac{Z_{Ge} + Z_M}{Z_M} \simeq V_M\frac{Z_{Ge}}{Z_M} \text{ if } Z_{Ge} \gg Z_M \tag{5}$$

so that in equation (4)

$$V_H = 10^{-8}\frac{3\pi}{8}\frac{V_M Z_{Ge}}{L Z_M} H\mu b \tag{6}$$

Now $Z_{Ge} \propto T^{3/2}$ for lattice scattering and $\mu \propto T^{-3/2}$ so that V_H is independent of T;

(*b*) by inserting a variable resistor in series with the measuring meter (Fig. 3). This resistor R_2 is ganged to the variable resistor R_1 with which the current is adjusted to give constant voltage across the specimen. If the temperature rises, the resistance of the specimen falls and the current must be increased by operation of R_1 to give constant voltage. This adjustment automatically decreases R_2 to an extent which compensates for the fall in mobility so that the output current for a given field remains constant and independent of temperature.

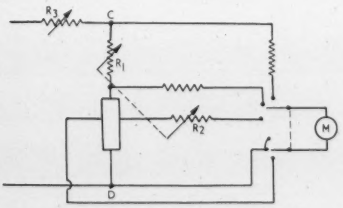

Fig. 3. Method of compensating fluxmeter against temperature changes

These methods of compensation have certain disadvantages. In method (*a*) it is assumed that the temperature of the germanium is the same as that of the indium antimonide. The germanium should be mounted in the same holder as the specimen, but even so the current passing through the latter may cause a temperature difference. The exponent in the mobility relation is actually greater than 3/2 for both materials, but the values for the two are sufficiently close to each other for practical purposes. The method described gives constant voltage and not constant output current for a given field, and it is therefore desirable that the resistance of the output meter should be higher than that of the specimen. In method (*b*) it is necessary to measure the resistance-temperature and mobility-temperature characteristics of the sample so that the amount of resistance required in the output circuit as a function of temperature can be calculated. However, this method can, in principle, correct for any form of mobility-temperature behaviour, and does not assume that the temperature of the specimen is the same as that of the ambient. Since a fall in the voltage of the source would cause a fall in V_A which could not be compensated by R_1 without upsetting the calibration, it is necessary to provide a third variable resistor R_3 which is adjusted to give a specified voltage (e.g. 1·8 V if an accumulator is used) between points C and D. The output meter, with suitable series resistor, may again be used to monitor this voltage.

Using these methods, the output for a given magnetic field has been maintained constant within 2% for temperatures in the range 0–40° C, and within 1% for temperatures in the range 10–30° C.

CONCLUSIONS

It is seen that the efficiency of Hall generator devices is proportional to the square of the carrier mobility in the material used, and is independent of the Hall constant. A fairly high Hall constant (in the region of a few thousand) is, however, desirable in order that the resistance of specimens shall be high enough to facilitate matching of the output circuit. The efficiency of indium antimonide, when properly matched, is approximately 280 times that of germanium. Linear low-resistance contacts may be made on indium antimonide using soft solder and without preparation of the surface. It is necessary to compensate indium antimonide against temperature changes if accurate measurements of field are to be made, but this can be done by simple circuits. (If power is taken from a germanium specimen this also needs temperature compensation for accurate measurements, for although the Hall voltage is independent of temperature the resistance of the specimen is not, owing to mobility changes.) Indium antimonide gives a sensitivity of 10 G without amplification and using a portable and robust output meter. For the detection of low fields, efficient use could be made of the low output resistance by using an a.c. supply and transforming the output voltage with a transformer of about 1000 : 1 ratio. Alternatively a magnetic amplifier of low input resistance could be used.

ACKNOWLEDGEMENT

Thanks are due to the Admiralty for permission to publish this paper.

REFERENCES

(1) PEARSON, G. L. *Rev. Sci. Instrum.*, **19**, p. 263 (1948).
(2) TANENBAUM, M., and MAITA, J. P. *Phys. Rev.*, **91**, p. 1009 (1953).
(3) KUHRT, F. *Siemens-Z.*, **28**, p. 370 (1954).
(4) MADELUNG, O. *Z. Naturforsch.*, **8A**, p. 791 (1953).

APPENDIX

The magneto-resistive effect in indium antimonide may also be used as a means of measuring magnetic fields. The effect is larger than in bismuth, and by a suitable choice of the dimensions of the specimen, may be larger by a factor of ten or more. Calculation shows that in fields greater than about 5 kG a bridge network using the magneto-resistive effect would give greater output than the Hall fluxmeter, but in low fields the operation of the H^2 law in the magneto-resistive effect reduces the output to below that of the Hall fluxmeter. The device would also suffer from non-linearity with H for small values of H and would be more complicated in temperature compensation.

The disturbance of stress in an infinite plate by a lemniscate-shaped hole

By W. SNOWDON, M.Sc., University of Nottingham

[*Paper received* 16 *February*, 1955]

Curvilinear co-ordinates are used to determine the functions of a complex variable, from which may be deduced the components of stress and displacement for an infinite plate perforated by a double hole, the boundary of which is the lemniscate of Bernoulli. Four cases are considered; in the first, the plate is assumed to be under simple tension in any direction; in the second, the plate is assumed to be in a state of uniform all-round tension; in the third, it is supposed to be in a state of pure shear having any orientation to the lemniscate; and in the fourth, the hole is assumed to be an area of compression in an otherwise undisturbed plate. In each case, expressions are obtained for the stress at the edge of the hole, and numerical values of this stress are tabulated and displayed graphically.

1. SUMMARY OF THEORY IN CARTESIAN CO-ORDINATES

The problem of finding the stresses and strains in a thin plate caused by forces in its plane applied at its boundary depends upon the determination of a stress function ϕ satisfying the equation[1]

$$(\partial^4\phi/\partial x^4) + 2(\partial^4\phi/\partial x^2\partial y^2) + (\partial^4\phi/\partial y^4) = 0 \qquad (1)$$

The two normal components of stress σ_x and σ_y, and the shearing stress τ_{xy} at any point are obtained from the stress function by the use of the equations

$$\sigma_x = \partial^2\phi/\partial y^2, \quad \sigma_y = \partial^2\phi/\partial x^2, \quad \tau_{xy} = -(\partial^2\phi/\partial x\partial y) \qquad (2)$$

No account is taken here of body forces such as the force of gravity. Now it may be shown[2] that any solution of equation (1) may be expressed in the form

$$\phi = Re[\bar{z}\psi(z) + \chi(z)] \qquad (3)$$

where $\psi(z)$ and $\chi(z)$ are analytic functions, and that the converse of this is true, so that the stress function ϕ is determined when $\psi(z)$ and $\chi(z)$ are chosen to satisfy the boundary conditions. The boundary conditions are usually expressible in terms of specific values of the stress components, which are defined in terms of the above analytic functions by the equations

$$\begin{aligned} \sigma_x + \sigma_y &= 4Re[\psi'(z)] \\ \sigma_y - \sigma_x + 2i\tau_{xy} &= 2[\bar{z}\psi''(z) + \chi''(z)] \end{aligned} \qquad (4)$$

the latter being equivalent to two equations by a separation into real and imaginary parts. The components of displacement u and v of a point of the plate from the position it occupied before the external forces were applied are given by the following equation

$$2G(u + iv) = \frac{3 - \nu}{1 + \nu}\psi(z) - z\overline{\psi'}(\bar{z}) - \overline{\chi'}(\bar{z}) \qquad (5)$$

where ν is Poisson's ratio, and G is the modulus of elasticity in shear (or modulus of rigidity).

2. SUMMARY OF THEORY IN CURVILINEAR CO-ORDINATES

The reasoning of Section 1 has been adapted (Ref. 1, p. 197) to solve the case of a figure defined by constant values of curvilinear co-ordinates (ξ, η) defined by a transformation $z = f(\zeta)$ where $\zeta = \xi + i\eta$. The values of $\psi(z)$ and $\chi(z)$ are obtained by substitution of the boundary values of the stress components in the following relations.

$$\begin{aligned} \sigma_\xi + \sigma_\eta &= 4Re[\psi'(z)] \\ \sigma_\eta - \sigma_\xi + 2i\tau_{\xi\eta} &= 2\exp(2i\alpha)[\bar{z}\psi''(z) + \chi''(z)] \end{aligned} \qquad (6)$$

where

$$\exp(2i\alpha) = f'(\zeta)/\overline{f'}(\bar{\zeta}) \qquad (7)$$

The theory, of which the above is the merest outline, is illustrated by Timoshenko and Goodier (Ref. 1, pp. 197–201) by a solution of the case of an elliptic hole in an infinite plate. The object of the present work is to provide a second illustration using different curvilinear co-ordinates, and to obtain numerical results from the formulae proved.

3. THE PROBLEM APPLIED TO A PLATE UNDER SIMPLE TENSION

The curvilinear co-ordinates used are defined by

$$\zeta = \log_e(z^2 - 1) \qquad (8)$$

giving, in bipolar form, $\xi = \log_e r_1 r_2$ and $\eta = \theta_1 + \theta_2$,

where $z - 1 = r_1 \exp(i\theta_1)$ and $z + 1 = r_2 \exp(i\theta_2)$. $\xi = \xi_0$ defines an oval of Cassini when $\xi_0 > 0$, and the lemniscate of Bernoulli when $\xi_0 = 0$, while when $\xi_0 < 0$, the curve consists of two detached ovals surrounding the points (1, 0) and (−1, 0).

The curve of particular interest in this work is the lemniscate $\xi = 0$, i.e. $r_1 r_2 = 1$ which is drawn in Fig. 1. Consider an infinite plate in a state of simple tensile stress S, the direction of which is inclined at an angle β to the x-axis in the manner

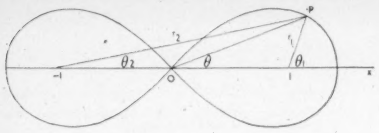

Fig. 1. The lemniscate of Bernoulli

shown in Fig. 2. Suppose this plate is perforated by a double hole, the outline of which is the complete lemniscate. The aim here is to find the potential functions for such a plate from which it is possible to deduce formulae for the components of stress and the components of displacement at any

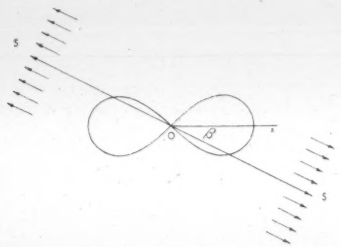

Fig. 2. Plate under simple tension, showing the meaning of the angle β

point of the plate, and to investigate the stress round the boundary of the hole.

4. THE CONDITIONS TO BE SATISFIED

By a rotation of the axes through an angle β, it may be shown (Ref. 1, pp. 201–4) that the stress components at infinity (i.e. where $\xi \to \infty$) must satisfy the relations

$$\sigma_x + \sigma_y = S, \quad \sigma_y - \sigma_x + 2i\tau_{xy} = -S\exp(-2i\beta)$$

Therefore, from equations (4), the complex potentials $\psi(z)$ and $\chi(z)$ sought as a solution of the present problem must satisfy the conditions

$$4Re[\psi'(z)] = S \qquad \text{at infinity} \quad (9)$$

and $$2[\bar{z}\psi''(z) + \chi''(z)] = -S\exp(-2i\beta) \qquad \text{at infinity} \quad (10)$$

In addition, it is necessary that $\sigma_\xi = \tau_{\xi\eta} = 0$ on the boundary of the hole (i.e. where $\xi = 0$). Therefore, from equations (6), the following condition must be satisfied along the lemniscate $\xi = 0$.

$$2Re[\psi'(z)] - \exp(2i\alpha)[\bar{z}\psi''(z) + \chi''(z)] = 0 \quad (11)$$

the factor $\exp(2i\alpha)$ being defined as in equation (7), where $f(\zeta) = [\exp(\zeta) + 1]^{\frac{1}{2}}$.

In going round the lemniscate, η goes from zero to 4π. Thus displacement and stress components must be periodic in η with period 4π, since they must have the same value for $\eta = 0$ as for $\eta = 4\pi$. This means that $\psi(z)$ and $\chi(z)$ may be made up of functions of $\exp(n\zeta/2)$ where n may take positive or negative integral values, while in addition, from equations (3) and (5), $\chi(z)$ may include a term $C\zeta$ where C is some constant. The usual method (Ref. 1, pp. 197–201) of obtaining these functions is a tentative one, in which both $\psi(z)$ and $\chi(z)$ are evolved by trial at the same time. The procedure used successfully in Section 5 is to choose a suitable function for $\psi(z)$, and to obtain the corresponding expression for $\chi(z)$ by two integrations, modifying $\psi(z)$ where necessary until the functions together satisfy the required boundary conditions.

5. SOLUTION OF THE PROBLEM

Let

$$\psi(z) = A\exp(\zeta/2) + B\exp(-\zeta/2)$$

Then

$$\psi'(z) = [1 + \exp(\zeta)]^{\frac{1}{2}}[A\exp(-\zeta/2) + B\exp(-3\zeta/2)]$$

Condition (9) is satisfied by taking $A = S/4$. Also

$$\psi''(z) = -A\exp(-3\zeta/2) + B[3\exp(-5\zeta/2) + 2\exp(-3\zeta/2)]$$

Now along the lemniscate, $\xi = 0$, so that $\bar{\zeta} = -\zeta$ and making this substitution in equation (11), the result is

$$\chi''(z) = A[1 + \exp(\zeta)]^{\frac{1}{2}}[\exp(-3\zeta/2) + 2\exp(-2\zeta)] - B[1 + \exp(\zeta)]^{\frac{1}{2}}[4\exp(-3\zeta) + 2\exp(-2\zeta) + \exp(-\zeta/2)] \quad (12)$$

If this expression is taken to apply to the whole plate, condition (11) at the edge of the hole is satisfied. Now for this value of $\chi''(z)$,

$$2[\bar{z}\psi''(z) + \chi''(z)] = 2[1 + \exp(\bar{\zeta})]^{\frac{1}{2}} \{-A\exp(-3\zeta/2) + B[3\exp(-5\zeta/2) + 2\exp(-3\zeta/2)]\} + 2[1 + \exp(\zeta)]^{\frac{1}{2}}\{A[\exp(-3\zeta/2) + 2\exp(-2\zeta)] - B[4\exp(-3\zeta) + 2\exp(-2\zeta) + \exp(-\zeta/2)]\}$$

As ξ tends to infinity, every term except the last in this expression tends to zero, so that the whole expression tends to the value $-2B$. Thus condition (10) is satisfied by taking $B = \frac{1}{2}S\exp(-2i\beta)$. Therefore the first of the required potential functions is

$$\psi(z) = (S/4)[\exp(\zeta/2) + 2\exp(-2i\beta)\exp(-\zeta/2)] \quad (13)$$

Substituting for A and B in equation (12) and integrating twice, the results are

$$\chi'(z) = -(S/4)[\exp(-\zeta) + \exp(-\zeta/2)] + (S/2)\exp(-2i\beta)[\exp(-2\zeta) + \exp(-\zeta) - \exp(\zeta/2)] \quad (14)$$

and

$$\chi(z) = -(S/4)\{(1 - \exp(-2i\beta)\log \{[1 + \exp(\zeta)]^{\frac{1}{2}} - 1\}\{[1 + \exp(-\zeta)]^{\frac{1}{2}} + 1\} + [1 + \exp(\zeta)]^{\frac{1}{2}}\exp(-2i\beta)\exp(-\zeta)\} \quad (15)$$

It is necessary at this stage to ensure that the functions $\psi(z)$ and $\chi(z)$ obtained above imply no discontinuity in the displacement. The displacement function defined by equation (5) is found to be

$$u + iv = (S/8G)\{(3 - \nu)[\exp(\zeta/2) + 2\exp(-2i\beta)\exp(-\bar{\zeta}/2)](1 + \nu) - [1 + 2\exp(\xi)\cos\eta + \exp(2\xi)]^{\frac{1}{2}}[\exp(-\bar{\zeta}/2) - 2\exp(-2i\beta)\exp(-3\bar{\zeta}/2)] + \exp(-\bar{\zeta}) + \exp(-\bar{\zeta}/2) - 2\exp(-2i\beta)[\exp(-2\bar{\zeta}) + \exp(-\bar{\zeta}) - \exp(\bar{\zeta}/2)]\}$$

Since this expression involves ζ only in exponential form, having real and imaginary parts periodic in η of period 4π, 2π or $4\pi/3$, it follows that in a circuit of any oval or lemniscate ξ = constant, the displacements u and v return to their original values at the starting point. Thus the formulae for the displacement components are continuous, and this verifies that expressions (13) and (15) constitute a solution of the problem.

6. CALCULATION OF STRESS AT THE EDGE OF THE HOLE

On the boundary of the hole, $\sigma_{r_1} = \tau_{\xi r_1} = 0$, and so the component of stress there is σ_t which from equations (6) is

$$\begin{aligned}(\sigma_t)_{\xi=0} &= 4Re[\psi'(z)] \\ &= SRe[z(z^2 - 1)^{-\frac{1}{2}} - 2z\exp(-2i\beta)(z^2 - 1)^{-\frac{1}{2}}] \\ &= S[r/(r_1r_2)^{\frac{1}{2}}]Re\{\exp\{i[\theta - \tfrac{1}{2}(\theta_1 + \theta_2)]\} \\ &\quad - (2/r_1r_2)\exp\{i[\theta - 2\beta - \tfrac{1}{2}(\theta_1 + \theta_2)]\}\}\end{aligned}$$

Using the facts that along the lemniscate, $r^2 = 2\cos 2\theta$, $r_1r_2 = 1$, and $\theta_1 + \theta_2 = 4\theta$ in the first quadrant, this simplifies to

$$(\sigma_t)_{\xi=0} = S(2\cos 2\theta)^{\frac{1}{2}}[\cos\theta - 2\cos(2\beta + 5\theta)] \quad (16)$$

The variation of the stress along the edge of the hole in the first quadrant, for values of β from 0° to 165°, at intervals of 15°, is shown in Fig. 3.

It will be observed that the stress at the centre of the lemniscate ($\theta = 45°$) is zero for all values of β. The envelope of the family of curves is $(\sigma_t)_{\xi=0} = S(2\cos 2\theta)^{\frac{1}{2}}(\cos\theta \pm 2)$ which is of interest as indicating the limits between which the value of the stress varies at any point of the boundary, irrespective of the value of β. These limits may be expressed in the concise form $S(x \pm 2r)$. Noting that the variation of stress round the whole lemniscate for a given inclination of tension is covered by the pair of curves $\beta = \beta_1$ and $\beta = \pi - \beta_1$, the range of values of stress is greatest for $\beta = 90°$ ($-0{\cdot}98S$ to $4{\cdot}24S$) and least for $\beta = 0$ ($-1{\cdot}41S$ to $2{\cdot}60S$). The stress at any point of the boundary may be made zero by inclining the tension at either of two angles to the x-axis; in particular, the stress at the point where the curve cuts the x-axis is zero for $\beta = 30°$ and $\beta = 150°$.

For all values of β except two, the value of $d(\sigma_t)/d\theta$ at the centre of the lemniscate is infinite. It is easy to show that the exceptional values are $\beta = \pi/8 + \frac{1}{2}\sin^{-1}[\sqrt{(2)}/4] = 32° 51'$, and $\beta = 5\pi/8 - \frac{1}{2}\sin^{-1}[\sqrt{(2)}/4] = 102° 9'$, and that for these values of β, $d(\sigma_t)/d\theta = 0$ when $\theta = 45°$. One physical significance of these two angles concerns the occurrence of points of zero and maximum or minimum stress on

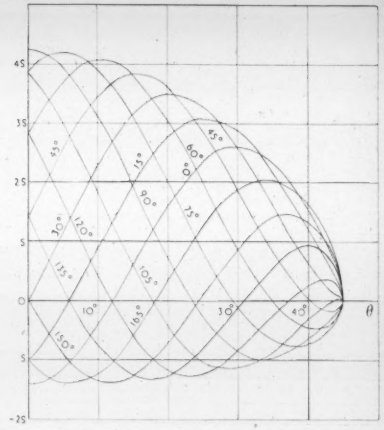

Fig. 3. Variation of stress along the edge of the hole in the first quadrant for a plate under simple tension in a direction at an angle β to the x-axis, for different values of β marked on the curves

the edge of the hole. This is best expressed in the following tabulated form. The numbers refer to the whole lemniscate.

Value of β	No. of points of zero stress	No. of turning values of stress
$0 \leqslant \beta < 32° 51'$	4 + centre 0	4 + ve and 2 − ve
$32° 51' < \beta < 77° 51'$	6 + centre 0	4 + ve and 4 − ve
$77° 51' < \beta \leqslant 90°$	4 + centre 0	2 + ve and 4 − ve

7. FURTHER DEDUCTIONS BY SUPERPOSITION

By combining the potential functions obtained as a solution of the above problem for the two cases $\beta = \beta_1$ and $\beta = \pi/2 + \beta_1$, where β_1 may have any value, the potential functions appropriate to the problem of finding the disturbance of stress produced by a lemniscate-shaped hole in a plate in a state of uniform all-round tension S is obtained. The solution is

$$\begin{aligned}\psi(z) &= (S/2)\exp(\zeta/2) \\ \chi(z) &= -(S/2)\log\{[1 + \exp(\zeta)]^{\frac{1}{2}} - 1\}\{[1 + \exp(-\zeta)]^{\frac{1}{2}} + 1\} \quad (17)\end{aligned}$$

and the stress round the edge of the hole in the first quadrant is

$$(\sigma_t)_{\xi=0} = 2S\cos\theta(2\cos 2\theta)^{\frac{1}{2}} = 2Sx \quad (18)$$

The maximum value of this occurs when $\theta = 0$ so that the maximum stress on the boundary of the hole occurs at its intersection with the x-axis. Fig. 4 shows graphically the variation of the stress along the edge of the hole in the first quadrant.

By combining the potential functions (17) obtained as a solution of the problem for a uniformly stressed perforated plate, and the potential functions for a state of undisturbed uniform stress of magnitude $-S$, the solution of the problem of finding the stress functions for uniform pressure S within

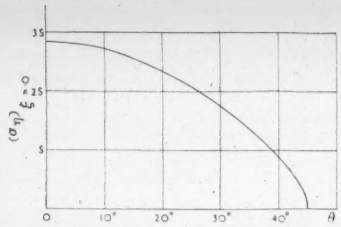

Fig. 4. Variation of stress along the edge of the hole in one quadrant for a uniformly stressed plate

a lemniscate-shaped hole in an otherwise unstressed plate is obtained. This requires the addition of $-Sz/2$ to $\psi(z)$ as given by formula (17), $\chi(z)$ being left unaltered, so that

$$\psi(z) = (S/2)[(z^2 - 1)^{\frac{1}{2}} - z]$$

At the boundary of the hole, in the first quadrant,

$$(\sigma_r)_{\xi=0} = 2S\cos\theta(2\cos 2\theta)^{\frac{1}{2}} - S = S(2x - 1)$$

and

$$(\sigma_\xi)_{\xi=0} = -S$$

Finally by superposing the results of the original problem solved in Sections 3 to 6 for the two cases $\beta = \beta_1$ with negative S, and $\beta = \beta_1 + \pi/2$ with positive S, the result is the solution for a lemniscate-shaped hole in a plate in a state of pure shear in any direction. The potential functions are

$$\psi(z) = -S\exp(-2i\beta)\exp(-\zeta/2)$$

$$\chi(z) = -(S/2)\exp(-2i\beta)\Big(\big[1 + \exp(\zeta)\big]^{\frac{1}{2}}\exp(-\zeta) + \log\Big\{\big[1 + \exp(\zeta)\big]^{\frac{1}{2}} - 1\Big\}\Big\{\big[1 + \exp(-\zeta)\big]^{\frac{1}{2}} + 1\Big\}\Big) \tag{19}$$

and the stress component on the boundary of the hole is

$$(\sigma_r)_{\xi=0} = 4S\cos(2\beta + 5\theta)(2\cos 2\theta)^{\frac{1}{2}} \tag{20}$$

Fig. 5 shows the variation of the stress along the edge of the hole in the first quadrant for values of β between 0 and 165° at 15° intervals. The envelope of the family of curves is $(\sigma_\eta)_{\xi=0} = \pm 4S(2\cos 2\theta)^{\frac{1}{2}}$, giving the limits between which the stress varies at any point of the boundary. Expressed in terms of r these limits are $\pm 4Sr$.

Taken in pairs, the curves give the stress round the complete lemniscate for a given direction of pure shear. In the first and third quadrants, the appropriate curve is that for $-S$ along $\beta = \beta_1$ and $+S$ along $\beta = \pi/2 + \beta_1$; in the second and fourth quadrants, the curve for $-S$ along $\beta = \pi - \beta_1$ and $+S$ along $\beta = \pi/2 - \beta_1$ must be taken. It will be seen that the stress may be made zero at any point on the boundary by taking one suitable pair of directions of pure shear.

The value of $d(\sigma_r)/d\theta$ is infinite at the centre of the lemniscate, except for the case of pure shear corresponding to $\mp S$ along $\beta = 22\frac{1}{2}°$ and $\pm S$ along $\beta = 112\frac{1}{2}°$, when the curve is a tangent to the θ-axis when $\theta = 45°$. The significance of this as regards points of maximum and minimum stress is that when one direction of the tension or compression S is at an angle less than or equal to $22\frac{1}{2}°$ to the x-axis, there are, round the whole lemniscate, four points of negative and two of positive turning stress separated by the origin and four other points of zero stress; but when one direction of $\pm S$ is

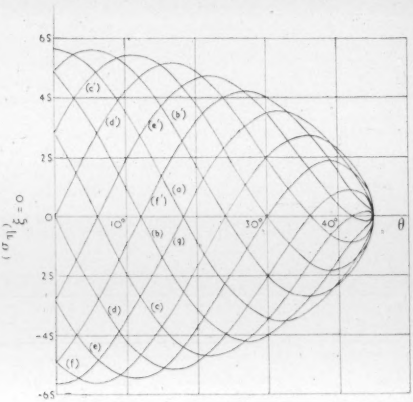

Fig. 5. Variation of stress along the lemniscate in the first quadrant for a plate in a state of pure shear, the tension and compression being orientated as below

(*a*) $(-S)\beta = 0°$ $(+S)\beta = 90°$	(*b*) $(-S)\beta = 15°$ $(+S)\beta = 105°$	(*b'*) $(-S)\beta = 165°$ $(+S)\beta = 75°$
(*c*) $(-S)\beta = 30°$ $(+S)\beta = 120°$	(*c'*) $(-S)\beta = 150°$ $(+S)\beta = 60°$	(*d*) $(-S)\beta = 45°$ $(+S)\beta = 135°$
(*d'*) $(-S)\beta = 135°$ $(+S)\beta = 45°$	(*e*) $(-S)\beta = 60$ $(+S)\beta = 150°$	(*e'*) $(-S)\beta = 120°$ $(+S)\beta = 30°$
(*f*) $(-S)\beta = 75°$ $(+S)\beta = 165°$	(*f'*) $(-S)\beta = 105°$ $(+S)\beta = 15°$	(*g*) $(-S)\beta = 90°$ $(+S)\beta = 0°$

at an angle greater than $22\frac{1}{2}°$ to the x-axis, the turning values are increased to four negative and four positive, and the points of zero stress to six, in addition to the origin.

ACKNOWLEDGEMENT

The author thanks Dr. N. Davy of the University of Nottingham for his patient supervision of the above work.

REFERENCES

(1) TIMOSHENKO, S., and GOODIER, J. N. *Theory of elasticity*, pp. 26, 34, 183–9 and 192–7 (New York: McGraw-Hill Book Co. Inc., 1951).

(2) MUSKHELISHVILI, N. I. *Some basic problems of the mathematical theory of elasticity*, pp. 110–11 (Groningen: P. Noordhoff Ltd., 1953).

Correspondence

Motion of water droplets of an emulsion in a non-uniform field

In an interesting paper by Pearce describing microscopic studies on "The mechanism of the resolution of water in oil emulsions by electrical treatment," published in this *Journal*,[1] an inconsistency between theory and observation in the motion of water droplets in a non-uniform electric field was reported. Although a spherical conductor in a non-uniform electric field is subject to a force in the direction of increasing field strength, migration of water droplets towards the strongest part of a radial field was on no occasion observed. The conclusion drawn by Pearce was that this force is ineffective, though the reason for the inconsistency was not revealed.

The explanation of Pearce's results was found to lie in the fact that his observations were carried out on a concentrated emulsion (10%) in a microscope cell with an extremely small sample thickness (0·1 mm), circumstances which cause hindrance of the movement of the droplets owing to chain formation and coalescence to larger droplets.

By using a microscope cell with a sample thickness of 3 mm and employing very dilute emulsions (0·1%), observations on free floating droplets could be performed. Using this arrangement it was found that:

1. The water droplets move in the direction of maximum field strength.
2. Large droplets move faster than small ones, other conditions being kept constant.
3. The velocity of a droplet increases rapidly with decreasing distance from the central electrode and/or with increasing voltage over the electrodes.
4. Droplets collect around the central electrode and form radial projections.
5. Chains of droplets are formed after some time in the bulk of the liquid.

Observations 1, 2 and 3 are in qualitative agreement with the equation of motion, which reads:

$$\frac{d\bar{r}}{dt} = C\frac{V^2}{(\log_e f)^2}\cdot\frac{a^2}{r^3}\bar{l}$$

where

$$C = \frac{\epsilon_1-\epsilon_2}{2\epsilon_2+\epsilon_1}\frac{1}{6\pi\eta}$$

ϵ_1 = dielectric constant of disperse phase,
ϵ_2 = dielectric constant of continuous phase,
η = viscosity of continuous phase,
V = voltage over the electrodes,
$f = r_0/r_i$,
r_0 = radius of outer electrode,
r_i = radius of inner electrode,
a = radius of droplet,
r = distance from centre,
$\bar{l}$ = unit vector in the direction of field gradient.

The following examples show that the observed and calculated particle velocities are of the same order of magnitude.

Velocity (μ/s)	
observed	*calculated*
0·2	0·1
6·9	2·6

Since large droplets overtake smaller ones by their more rapid motion (observation 2), an additional mechanism of chain formation and subsequent coalescence is involved.

From the above it can be concluded that a general movement of droplets in the direction of maximum field strength takes place. The photographs opposite demonstrate the phenomena described. Similar observations were made on carbon black suspensions. It may be mentioned here that Pohl[2] applied a non-uniform electric field for removing carbon black filler from diluted samples of polyvinylchloride.

The authors wish to thank the Management of the Koninklijke/Shell-Laboratorium, Amsterdam (N.V. De Bataafsche Petroleum Maatschappij) for permission to publish this work.

Koninklijke Shell-Laboratorium, Badhuisweg 3, Amsterdam, Holland.
C. BEZEMER
G. A. CROES

REFERENCES

(1) PEARCE, C. A. R. *Brit. J. Appl. Phys.*, **5**, p. 136 (1954).
(2) POHL, H. A. *J. Appl. Phys.*, **22**, p. 869 (1951).

The results described by Bezemer and Croes form an interesting extension of my work. By using emulsions of low water content they have so far reduced the chain forming forces to which I drew attention, that they have been able to observe and measure the effect of non-uniformity of the electric field. In my own experiments this effect was masked, not so much by the "hindrance" to droplet movement as by the rapid formation of droplet chains.

The authors have not given the value of the field strength used in their experiments, but the droplet velocities which they observed are much lower than those occuring in my own and I estimate that this must in general be so. Again, the non-uniformity of the electric field can only bring about coalescence when the droplets arrive at the central electrode or overtake one another on the way and thus the mean distance travelled by each droplet, before coalescence, must generally be greater than when chains are formed. These two factors combine to produce a very much slower action than occurs when chain formation is present.

An emulsion containing only 0·1% of water would, in terms of my own work, have been a "dry oil" and I think that there can be little doubt that in practice the force on a droplet due to the non-uniformity of the field can play no major part in the electrical dehydration of emulsions of fuel oils.

Fuel Research Station, London, S.E.10.
C. A. R. PEARCE*

* Now at National Coal Board, Central Research Establishment II, Worton Hall, Isleworth, Middlesex.

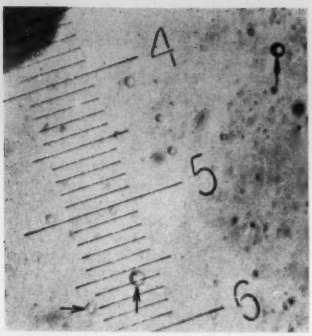

0 s

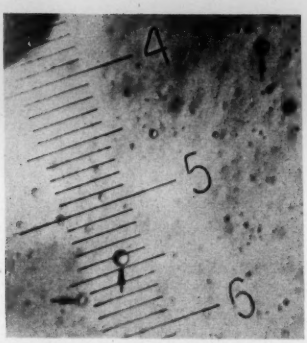

6 s

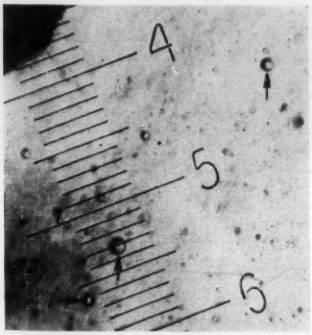

12 s

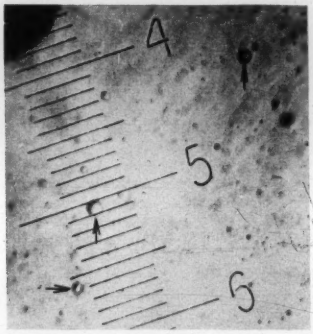

18 s

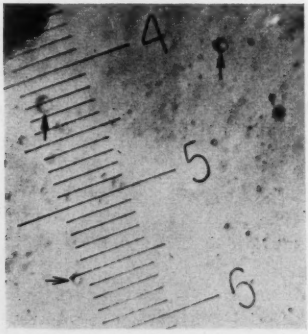

24 s

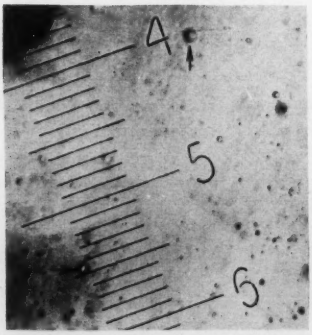

30 s

Sequence of photomicrographs demonstrating the movement of droplets in the direction of maximum field strength; times are indicated under each photomicrograph. The dark spot in the top left corner is the central electrode of the concentric cell. The positions of three droplets are indicated by arrows (1 scale division = 16·6 μ)

Notes and comments

The Institute of Physics

At the Annual General Meeting of The Institute of Physics held on 17 May, 1955, Sir John Cockcroft (Director of the Atomic Energy Research Establishment, Harwell) was re-elected President. Dr. W. H. Taylor was elected a Vice-President, Dr. S. Whitehead was re-elected Honorary Treasurer and Dr. B. P. Dudding was re-elected Honorary Secretary. The three new Ordinary Members of the Board elected were Dr. M. R. Hopkins, Dr. J. M. A. Lenihan and Dr. J. Taylor.

The Report for 1954, which was adopted at the meeting, shows that the total membership in the several grades continues to increase steadily and reached 4749 at the end of the year. The newly established Graduate examination was held in London, Birmingham and Paisley, and of the 54 candidates who sat only 19 satisfied the examiners in those papers they were required to take. The number of candidates taking the final examinations for National Certificates in Applied Physics was 206 at the Ordinary level and 75 for the Higher Certificate; these figures compare with 151 and 55 respectively in 1953. The Institute has continued to take an active part in discussions on higher technological education and has not changed the views it expressed in its 1948 Report on this subject. Arising from reports to the Membership Committee indicating that there were several vacancies for undergraduates in departments of physics in some universities and large technical colleges, the Board decided that an inquiry should be made covering the physics departments of all universities in Great Britain and all the colleges recognized by the Institute.

The work involved in the production and distribution of the Institute's publications has continued to increase and now forms about half of the total work of the Institute, the principal part being its monthly Journals, the *Journal of Scientific Instruments* and the *British Journal of Applied Physics* which was established in 1950 and "is rapidly obtaining for itself a place among the leading scientific journals." A third selection of Laboratory and Workshop Notes from the *Journal of Scientific Instruments* was published by Messrs. Edward Arnold (Publishers) Ltd. for the Institute. As with the first two volumes in this series the royalties are credited to the Institute's Benevolent Fund.

The Report states that the day-to-day inquiries on professional matters have included such items as advice on consulting fees and salaries, deferment from military service, appropriate education and training in physics and its special branches and its ancillary subjects, and on sources of technical information. For the second year an inquiry was addressed to all new graduates in physics of universities in the United Kingdom. They were again asked to provide information about their present occupations and, if appropriate, the source of any maintenance grant. There was a good response. It is proposed to carry out such a survey in each of the next few years and to follow up the returns by making a subsequent inquiry of those at present engaged on research leading to higher degrees. In this way it should be possible to obtain information that will indicate clearly the way in which the services of physics graduates are being used.

In addition to the several specialist conferences held by the Institute's branches and subject groups, a conference on "The physics of particle size analysis" was held in Nottingham in April 1954, the proceedings of which were published as a supplement to this *Journal* in October. The Report shows that the Institute's sixteen local branches and subject groups again held many meetings and visited various laboratories and works, and in some instances carried out other functions in connexion with their members' special interests. Brief reports from the Institute's representatives on many outside Committees and Councils conclude the Report of another active year.

Elections to The Institute of Physics

The following elections have been made by the Board of The Institute of Physics:

Fellows: C. F. Bruce, T. J. Buchanan, B. Donovan, J. W. Menter, R. Oliver, R. L. Woolley, L. Wright.

Associates: G. R. Antell, S. R. Armsdon, C. Bowness, E. J. Burge, L. Cartz, D. A. Davies, J. C. Evans, F. C. Fenton, J. Graham, R. C. Gupta, D. O. C. Harker, R. G. Harlow, T. E. Heslop, R. C. Holloway, R. H. Holloway, S. Hope, G. Howells, D. Jeffcock, J. T. Johnston, D. W. Kahan, D. Macfie, P. M. McGregor, S. C. Nyburg, D. W. Payn, A. E. Ranger, E. F. W. Seymour, S. P. Thong, F. C. J. Tildsley, J. M. Valentine, J. Walters, R. A. Wilson.

Twenty-three graduates, thirteen Students and three Subscribers were also elected.

Journal of Scientific Instruments

Contents of the June issue

SPECIAL ARTICLE

Precision measurement of time. By H. M. Smith.

ORIGINAL CONTRIBUTIONS

Papers

A centrifuge permitting continuous observation of the spinning tube. By B. B. Marsh.

The final vacua of oil diffusion pumps. By R. F. Coe and L. Riddiford.

An improved construction of the Smith bridge type 3. By C. R. Barber, A. Gridley and J. A. Hall.

A demountable vacuum system for secondary emission studies. By A. Lempicki.

A photoelectric sampling switch for use in double-beam optical instruments. By D. M. Neale.

Apparatus for measuring the intensity of cosmic radiation at great depths in the sea. By J. C. Barton.

A high-temperature X-ray diffraction powder camera. By E. Matuyama.

Laboratory and workshop notes

A rapid and simple method for obtaining permanent records from cathode-ray oscilloscopes. By H. D. Rathgeber.

Holes of small diameter in stainless steel. By H. G. Jerrard.

A low-temperature microscope stage for metal specimens. By D. Hull and R. D. Garwood.

A constant pressure gas storage vessel. By G. W. Green.

NOTES AND NEWS

British Instrument Industries Exhibition—A preview

Notes and comments

THIS JOURNAL is produced monthly by The Institute of Physics, in London.

It deals with all branches of applied physics (including theory and technique). All rights reserved. Responsibility for the statements contained herein attaches only to the writers.

EDITORIAL MATTER. Communications concerning editorial matter should be addressed to the Editor, The Institute of Physics, 47 Belgrave Square, London, S.W.1. (*Telephone*: Sloane 9806.) Prospective authors are invited to prepare their scripts in accordance with the *Notes on the preparation of contributions*. (Price 2*s.* 6*d.* including postage.)

REPRODUCTION. The Institute of Physics is a signatory to The Royal Society's Fair Copying Declaration. Details may be obtained upon application from The Royal Society, London, W.1.

ADVERTISEMENTS. Communications concerning advertisements should be addressed to the agents, Messrs. Walter Judd Ltd., 47 Gresham Street, London, E.C.2. (*Telephone*: Monarch 7644.)

CLAIMS FOR MISSING JOURNALS. Claims from regular subscribers to this *Journal* for missing numbers will only be considered if received within 60 days of the date of mailing plus normal outward time of transit and time for lodging the claim. Losses attributable to failure to notify a change of address or to similar omissions will not be considered.

SUBSCRIPTION RATES. A new volume commences each January. The charge is £4 per volume ($11.50 U.S.A.), including index (post paid), payable in advance. Single parts, so far as available, may be purchased at 8*s.* each ($1.15 U.S.A.), post paid, cash with order. Orders should be sent to The Institute of Physics, 47 Belgrave Square, London, S.W.1, or to any bookseller.

Čerenkov radiation and its applications*

By J. V. JELLEY, Ph.D., Atomic Energy Research Establishment, Harwell, Berkshire

The paper opens with a brief review of the original discovery of the radiation and the physical principles of the process that gives rise to it. This is followed by an elementary account of the theory of the effect. A general survey of the practical applications to cosmic-ray and high-energy physics is then presented, with two examples of modern detectors discussed in greater detail.

The article concludes with an account of recent experiments carried out on light pulses from the night-sky associated with cosmic-ray showers, found to be due to Čerenkov radiation in the atmosphere.

HISTORICAL INTRODUCTION

It was observed by many workers in the early days of the study of radioactivity that a faint visible light was sometimes emitted from strong sources of β- and γ-radiation. This light, which was bluish-white in colour, was particularly evident when the sources were in the form of a solution. It seemed natural, at the time, to attribute the radiation to ionization caused either by β-particles or secondary electrons from γ-rays. However, this explanation was soon found to be unsatisfactory for a number of reasons. In the first place the colour and intensity of the light were found to be markedly independent of the medium from which it emanated; this property, and one discovered later, namely that the spectrum of the radiation was continuous, were at variance with the general properties of luminescence produced by ionization, properties already well known at the time. It was found, furthermore, that the light could not be quenched by the addition of impurities in the solutions, neither did its intensity depend on the temperature, two properties again in contrast to those normally found in the phenomena of luminescence.

The first serious attempt to study the phenomenon on a quantitative basis appears to have been due to Mallet[1,2,3] who describes, in three papers, results of experiments carried out with a spectrograph to try and resolve the observed continuous spectrum. Though perhaps Mallet deserves more credit for his part in the early investigations, his work was not developed on the experimental side, neither was there any attempt to explain the phenomenon theoretically.

Some years later, however, and quite independently, a long series of experiments were carried out by Čerenkov[4] who proved conclusively that this mechanism of light production by the passage of fast charged particles through transparent media was indeed very different from luminescence. In addition to the properties already mentioned, Čerenkov discovered two other features by which the effect could be distinguished, namely that the light has unique polarization and directional properties. In view of the considerable work carried out by Čerenkov on the experimental side, the radiation has appropriately been named after him. About the same time, Frank and Tamm[5] brought out a theory of the effect based entirely upon classical electromagnetic theory.

Following these early experiments, there was a lapse of some years during which very little work was done; since 1945 however, there have been great strides in the field. The advent of the photomultiplier, the most sensitive detector known for the study of faint pulses of light, has been largely responsible for the more recent developments. At the same time, accelerating machines have appeared in nuclear physics laboratories all over the world; these, year by year, are producing beams of charged particles of ever higher and higher energies and fluxes. It will be seen later how the unique properties of Čerenkov radiation may be used in radiation detectors having special features, enabling one to distinguish between different types of particles and to measure directly their velocities. Čerenkov detectors are also being used in the field of cosmic-ray physics to an ever-increasing extent.

ELEMENTARY THEORY OF THE ČERENKOV EFFECT

When a fast charged particle travels at a uniform velocity in a dielectric medium, the associated electromagnetic field close to the particle polarizes the medium along its track, so that the electrons attached to the atoms follow the wave-form of the pulse as the particle goes by. It is most important to realize in this process that the atoms are not *excited* by the electron and neither are they *removed* from their bound states (ionization). It is true that there is in *addition* ionization, when the impacts are sufficiently close, but the process with which we are concerned here arises from only very small displacements by a very large number of electrons. Now, in the general case, when the particle is slow, the radiation from these displaced electrons, which return immediately to their normal positions after the particle has passed, is not observed, owing to destructive interference. If, however, the velocity of the particle in the medium is faster than the phase velocity of light in the medium, the wavelets from all portions of the track are in phase with one another on a wavefront inclined to the direction of the track, and a coherent radiation is then observed. Referring now to Fig. 1, if a particle traverses a distance AB inside a dielectric medium at a high velocity βc, where c is the velocity of light *in vacuo*, and we denote separate points $P_1P_2P_3$ as sources of spherical wavelets, then the resulting wavefront will lie along the line BC, and the direction of emission of the radiation will be along the line AC, at right angles to BC. Now, the distance the particles will have gone in a time Δt, will be $AB = \beta c.\Delta t$; in the same time the light will have travelled a distance $AC = (c/n)\Delta t$ where n is the refractive index of the medium. From these two equalities it is at once seen that there is a very fundamental relation between the velocity of the particle, the refractive index of the medium, and the angle at which the light is emitted. This, known as the Čerenkov relation, is:

$$\cos\theta = 1/\beta n \qquad (1)$$

For those unfamiliar with the relativistic equations, the

* Based on a lecture given before the Electronics Group of The Institute of Physics in London on 16 November, 1954.

quantity β is related to the kinetic energy E of the particle, and to its rest mass m, by the equation:

$$E = mc^2\left[\frac{1}{\sqrt{(1-\beta^2)}} - 1\right] \tag{2}$$

Thus we see that the Čerenkov effect is the electromagnetic or optical analogue of the "supersonic bang," or the bow wave from a ship travelling through water faster than the natural velocity of surface waves on the water. From equation (1) it is at once seen that there are two special

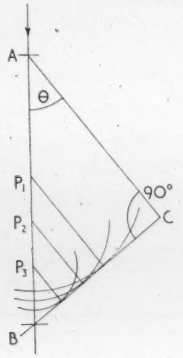

Fig. 1. A diagram to illustrate the coherent nature of Čerenkov radiation

conditions in limiting cases. First, there is a *threshold condition*, namely when $\beta = 1/n$ and $\theta = 0$. This implies a kinetic energy for the particle below which no radiation takes place. Secondly, there is a *maximum angle* at which the light may be emitted, when the particle is travelling at ultra relativistic velocities. This arises when $\beta \to 1$, in which case $\theta_{max} \to \cos^{-1}(1/n)$.

Fig. 1 has only been drawn in one plane and in practice the light is of course emitted over a conical surface, the axis of which coincides with that of the particle, and the semi-apex angle of which is the angle θ; this is shown better in Fig. 2. The radiation has unique polarization properties, the electric vector E is always at right angles to the direction of propagation of the light, and the magnetic vector H is always tangential to the surface of the cone, as in Fig. 2.

Those interested in the theory of the effect should consult either the original paper by Frank and Tamm[5] or a later and more comprehensive one by Tamm.[6] Next in importance to the condition of coherence, equation (1), is the expression for the rate of production of the light. The amount of light produced, in ergs per centimetre of path, is given by:

$$\frac{dW}{dl} = \frac{e^2}{c^2}\int_{\beta n>1} \omega\, d\omega\left(1 - \frac{1}{\beta^2 n^2}\right) \tag{3}$$

where e is the charge of the particle and ω is the angular frequency of the light in question. This rate of loss of energy (over the whole spectrum) amounts to about 0·5% of that due to ionization, for a minimum ionizing particle, so some idea may be gained of the weakness of the radiation.

We see from equation (3) that the spectrum is continuous; the spectral distribution, neglecting dispersion (i.e. $n =$ constant), is seen to be of the form:

$$\frac{dW}{d\omega} \propto \omega \tag{4a}$$

which, expressed on a wavelength scale, is:

$$\frac{dW}{d\lambda} \propto \frac{1}{\lambda 3} \tag{4b}$$

These equations illustrate why the light appears bluish-white in colour. The continuous spectrum, which extends over quite a wide range of frequencies, is cut off on the short wave side in the X-ray region, when n becomes less than unity and equation (1) cannot then be satisfied. The long-wave cut-off arises due to self-absorption of the radiation in the

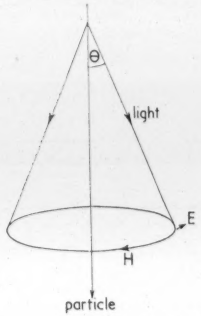

Fig. 2. The formation of the Čerenkov cone of radiation, and the disposition of electric and magnetic field vectors.

medium by the presence of atomic and molecular absorption bands. On the question of long-wave radiation, Ginsburg[7] has discussed how it might be feasible to generate microwaves by the Čerenkov effect, in the wavelength region of a few millimetres or less, a region involving considerable technical difficulties by the usual radio techniques. The possible production of radio waves in this way, and in particular how line spectra might be produced, has been developed further by Abele.[8]

Returning to consider the Čerenkov effect in the optical region, the table below gives the numerical values for the various quantities for water and dry air.

Čerenkov radiation for water and dry air

	Water	*Air (N.T.P.)*
Refractive index n	1·33	1·00029
θ_{max} (i.e. when $\beta \to 1$)	41°	1·3°
Threshold energies $E_T(\theta = 0)$	260 keV electrons	21 MeV
	54 MeV μ-mesons	4·4 BeV
	475 MeV protons	39 BeV
$\frac{dW}{dl}$ (photons/cm, between 3500–5500 Å)	250	0·3

Before concluding remarks on the theory of the Čerenkov effect, it is well to emphasize that the process should not be confused with that of Bremsstrahlung. The latter process,

which for example is responsible for the emission of the continuous spectrum of X-rays when a heavy material is bombarded by fast electrons, arises owing to an acceleration or deceleration when the fast particle interacts strongly with the electric field near an atomic nucleus. Without going into details, it may be stated that the two phenomena have markedly different properties and in general will not be confused. Lawson[9] has shown recently that under *certain* circumstances it might be hard to distinguish between the two outwardly; the underlying physical processes, however, are essentially different. Classical and quantum treatments of the Bremsstrahlung process may be found in the work of Heitler in 1944, while a quantum treatment of the Čerenkov effect has been carried out by Ginsburg.[10] One result obtained by Ginsburg is that there is an additional term to the radiation equations which arises if the charged particle has in addition a magnetic moment. There is in fact also "magnetic" Čerenkov radiation from a pure magnetic dipole having no net electric charge; the predicted intensities for both these cases, however, are so minute that it would seem very unlikely that they could be detected by present techniques. It is interesting that the condition of coherence, equation (1), has been obtained by Cox[11] by simple arguments of conservation of momentum and energy when a fast electron in a dielectric is deflected, and a light quantum emitted; this treatment is very similar to that carried out in the case of the Compton effect.

Having discussed the essential features of the theory we will consider some typical practical applications of the Čerenkov effect. In passing, however, it should be mentioned that in the intervening years from about 1938 to about 1951 a large number of purely experimental studies of the effect were carried out, and for a comprehensive review of these, the reader is referred to an article by Jelley[12]; this article in addition contains some details of the early experiments of Čerenkov's, whose work is not always readily accessible.

PRACTICAL APPLICATIONS TO THE DETECTION OF FAST CHARGED PARTICLES

The practical applications of the Čerenkov effect may be classified roughly under the following headings:

(i) The efficient detection and fast counting of single charged particles at energies in excess of the Čerenkov threshold (Čerenkov counters have an extremely rapid rate of response and at the same time suffer no paralysis effects).

(ii) The direct determination of the velocity of the particle over a limited range of β above the threshold. This in turn implies a direct measurement of the energy of the particle if its mass is known.

(iii) The discrimination between particles of different mass when they have the same energy.

(iv) The ability to determine in which sense a fast particle is travelling, by virtue of the directional features of the light.

The exceptionally high speed of response of a Čerenkov counter arises because the particle and the light travel along together, the wavefront of the light retaining its thin shell-like structure while increasing in intensity as the particle passes through the medium. The light pulse may thus have a duration considerably shorter than the time required for the particle to traverse the counter, and if the light can be focused, its duration is limited by dispersion. This high intrinsic speed of a Čerenkov counter, which may be about 10^{-11}s or less, cannot unfortunately be used, since in general the photomultiplier and subsequent electronics will be much slower, taking a time of about 10^{-8} or 10^{-9} s to respond.

In view of the unique directional characteristics of the light in Čerenov radiation, and also its very low intensity, necessitating efficient means of gathering the light at the detector, rather special considerations have to be given to the optical arrangements used. In general, Čerenkov detectors are either of the focusing type or non-focusing type, depending on the optical system used. Applications under the headings (ii), (iii) and (iv) above, use focusing, while those under heading (i) use non-focusing detectors. Getting[13] and Marshall[14] have outlined the principles and design of the optics of focusing detectors. It is obvious that if the Čerenkov angle θ is required, then it is necessary to design the optical system with care and use focusing, so as to concentrate the light emitted at one definite angle into an area defined by the detector, and thus to differentiate as strongly as possible against light emitted at other angles. One severe limitation of focused counters is that in an optical system having cylindrical symmetry, it is never possible to focus the light into an area smaller than the effective area of the dielectric medium through which the particles are travelling. This point, which arises from quite fundamental considerations, is discussed in the paper by Marshall.

The optics of non-focusing Čerenkov counters has been discussed recently by Mandò[15] who works out the light-gathering efficiency, time of response and uniformity of efficiency, for detectors of various shapes and sizes. In the non-focusing type of detector it is usual to integrate the light from all parts of the track of the particle by surrounding the "radiator" (as we shall henceforward call the dielectric) by some matt white scattering material of high reflectivity, such as magnesium oxide powder. The photomultiplier is then inserted somewhere inside, and collects a proportion of the total light produced.

An example of a counter of the focusing type is shown in Fig. 3. In this particular design, due to Marshall,[14] the

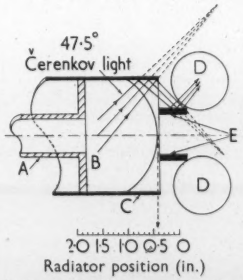

[Reproduced from *Physical Review*]

Fig. 3. One of the counters designed and built by Marshall[14] having focusing properties

A, brass tube for positioning radiator; *B*, Lucite radiator lens; *C*, cylindrical mirror; *D*, photomultiplier tube, type 1P28; *E*, plane mirrors for splitting image

radiator and lens are combined into a single unit. The primary focused image is a ring of rather large radius, so in order to gather the light into a smaller area, a cylindrical mirror surrounds the radiator, to concentrate the light close

to the optic axis. Since, however, the instrument was used with a rather intense beam of particles from a synchrocyclotron, the beam passing down the axis of the system, the new image was split by two small plane mirrors so that the light was divided between two photomultipliers connected in a fast coincidence circuit. In this way the phototubes are to the side of the main beam of particles, and the coincidence arrangement helps to distinguish between the desired pulses of light from the particles in the beam, and the general high background rate of pulses from the tubes in proximity to the machine. By adjusting the position of the radiator in the cylindrical mirror, it is possible to focus rays of differing Čerenkov angle in turn on to the cathodes of the phototubes.

A typical result obtained with this instrument is shown in Fig. 4, for which it was possible to measure the energy of a beam of π-mesons. The taller curve shows the variation in

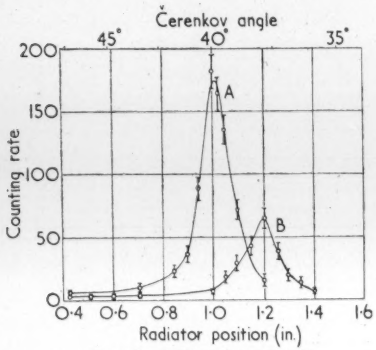

[Reproduced from *Physical Review*]

Fig. 4. Typical results obtained with the instrument shown in Fig. 3 using a beam of π-mesons

response of the counter for 145 MeV π-mesons as the radiator position is altered, while the smaller curve was obtained after the mesons had been slowed down to 121 MeV by passing through a graphite absorber of thickness 7·6 cm. From these curves, some idea may be obtained of the resolution possible with a simple device of this type. Estimating from these curves that one could locate the position of maximum response to say about 0·3 of the separation of the two peaks, this corresponds to a resolution of about 8 MeV in 145 MeV, i.e. $\pm 6\%$.

Another example of a detector of the focusing type is shown in Fig. 5. This instrument, which uses direct photographic recording of the light, was designed by Mather[16] to obtain absolute calibrations of the velocity of the proton beam in the 184-inch synchrocyclotron at Berkeley, California. It is a precision instrument of extreme simplicity and elegance and had an energy resolution of approximately $\pm 1\%$ at a proton energy of 340 MeV.

The radiator, in this case, consists of a thin glass plate 0·7 mm thick and of refractive index 1·88. This is mounted in the proton beam at an angle such that a portion of the conical shell of Čerenkov light leaving the back of the plate normal to its surface, is reflected at this surface (which is aluminized) and in turn enters the lens of a Leica camera *via* a small prism. With this arrangement, refraction effects at the surface of the glass plate can be eliminated; the prism is inserted to cancel the first-order dispersion in the Čerenkov radiation, which results from the variation of n, and hence θ, with ω. The instrument is completed by the addition of an

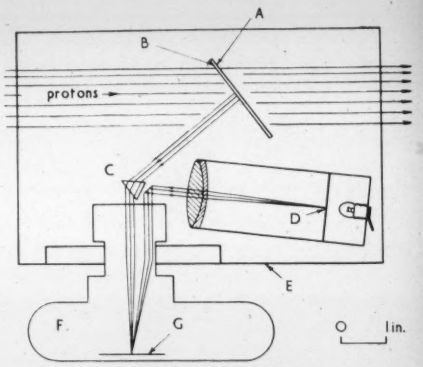

[Reproduced from *Physical Review*]

Fig. 5. A precision photographic instrument constructed by Mather[16]

A, aluminized surface; *B*, glass sheet; *C*, glass prism; *D*, scale; *E*, light-tight box; *F*, Leica camera; *G*, 35 mm film.

illuminated scale for purposes of calibration and measurements. In general, long exposures are required with such a device, often of the order of an hour or more, to obtain images of sufficient intensity.

A microphotometer trace of a typical image obtained with this instrument is shown in Fig. 6, on which scales of θ, E and β are included. In the example shown, the resolution is

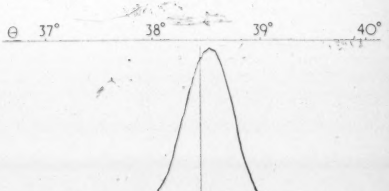

[Reproduced from *Physical Review*]

Fig. 6. A typical result obtained with Mather's instrument

approximately 3 MeV in 340 MeV, i.e. about $\pm 1\%$, while the theoretical limit for such a detector has been shown by Mather to be about $\pm 0{\cdot}1\%$.

Some brief references will now be made to other applications of Čerenkov radiation. Duerden and Hyams[17] have used a non-focusing detector as a threshold instrument

for selecting the very small flux of cosmic-ray protons at sea-level, against the large background of particles of other types. Anderson and Belcher[18] have developed solutions of radioactive isotopes as standard sources of very weak light, using the Čerenkov radiation from β-particles in the solvent. The cosmic-ray "albedo"* in the upper atmosphere has been investigated by Winckler and Anderson,[19] using Čerenkov radiation detectors carried up in a balloon. In this, the directional property of the radiation was used to distinguish in which sense the particles were travelling. These detectors are essentially a development of the water detector originally used by Jelley[20] to count individual μ-mesons.

ČERENKOV RADIATION IN THE ATMOSPHERE

In 1948 Blackett[21] worked out that a small fraction of the total light of the night sky should arise from the Čerenkov radiation produced by the passage of cosmic-ray particles through the earth's atmosphere. This contribution was calculated to be extremely small, of the order of 10^{-4} of the total intensity; it would be very difficult to measure such a low mean intensity in view of the continual fluctuations of atmospheric origin, and in any case there is no way of eliminating the effect for comparison purposes.

If, however, we select *individual* cosmic-ray events of exceptionally high energy, such as give rise to the extensive air showers (or Auger showers[22] as they are frequently termed), and at the same time use a pulse technique, in order to differentiate against the mean light intensity of the night sky, then it appeared possible that *individual* light pulses might be observable which could then be correlated with the individual air showers.

It was with these considerations in mind that Galbraith and Jelley[23] were first able to detect quite large pulses of light with very simple apparatus. Their apparatus consisted of a simple parabolic mirror (diameter 25 cm and focal length 10 cm), mounted at the bottom of a standard domestic dustbin, and a photomultiplier (type 6260 by Electric and Musical Industries Ltd.) with its photocathode at the focus. The phototube was connected to a video frequency amplifier of bandwidth about 5 Mc/sec and thence to a recording oscilloscope *via* a discriminator. The light intensity is such that, even on the darkest night, the rate of emission of photoelectrons from the cathode of the phototube is so high that the amplifier output observed on the oscilloscope has the appearance of thermionic noise, the above bandwidth being insufficient to resolve it into separate pulses. However, it was possible to set the discriminator at a level just above the "noise" so that the rate of trigger of the oscilloscope by noise pulses was negligibly low.

Under these conditions, with this light receiver pointing to the zenith and a field of view of $\pm 11°$ with respect to the vertical, light pulses were observed at a rate of 1 or 2 per minute. These pulses were not spurious, since by closing the dustbin and lighting a small lamp inside to an intensity such that the noise level was the same as before, no light pulses were then observed. The confirmation that the pulses were in fact associated with the air showers followed a few nights later when it was shown that they occurred in coincidence with the firing of one or more Geiger counters of an air-shower array used by Cranshaw and Galbraith[24] for other work.

A series of experiments was continued at Harwell during the winter of 1952–53, but work was severely restricted by the low frequency of occurrence of clear nights and, worse, by the fluctuations in brightness of the night sky over a few hours on any single night. In view of this, it was decided to transfer the work to the Pic du Midi observatory in the Pyrénées where it was known the clarity of the night sky was exceptionally good, and during three months in the summer of 1953 really excellent observing conditions were found for the continuation of the experiments. The apparatus taken to the observatory was essentially similar to that used at Harwell though there were some restrictions imposed by the number of Geiger counter units that could be taken, and the available space for arranging these along the mountain ridge on which the observatory is situated.

Two improvements were made in the light receivers since the earlier experiments; the mirrors were larger, of diameter 60 cm (focal length 25 cm) and the photomultipliers had a cathode diameter of 12·5 cm, giving therefore a field of view of approximately $\pm 15°$. With this combination, and the same criterion of bias levels, the rate of arrival of light flashes was about 7 per minute at the zenith.

Since the mean brightness of the night sky, within the field of view of the light receiver, was found to change by a factor of about two during the night, as the Milky Way passed overhead, it was necessary to enhance artificially the mean light intensity falling on the phototube during the darker periods of the night, so as to maintain a constant noise level. The necessity of this arose because the light pulses were found to have a steep power law spectrum and were superimposed on the noise pulses; it was achieved by manually controlling a small filament lamp mounted at the edge of the mirror so that the mean current in the phototube remained constant.

The details of the results of these experiments have recently become available[25] and the essential findings are outlined here.

Studies of the polarization of the light were made first, in an attempt to identify it with Čerenkov radiation; these experiments were carried out using polaroid over the photocathode, first with its axis parallel and then perpendicular to a line of counters spread out along the mountain ridge to a distance of 100 m. The results of these experiments gave evidence in favour of Čerenkov radiation. This evidence was strengthened when it was found in a later experiment that the light was highly directional. The latter experiment consisted of running two light receivers side by side, each having a small field of view, and counting the number of times that a pulse was observed simultaneously in both units for different settings of the angle between their optic axes.

Until these experiments had been carried out, there had been a suspicion that perhaps the light might be associated with ionization. The most conclusive evidence that the light pulses from the night sky arise from Čerenkov radiation comes from a later laboratory experiment in which Jelley has detected Čerenkov radiation from individual cosmic-ray μ-mesons in a 6 metre air path, the apparatus in this case being in total darkness. This work, not yet published,[26] has shown that the rate of production of light associated with the ionization of fast particles in air, is at least $< 10^{-2}$ of that due to Čerenkov radiation.

It is interesting to reflect that the detection of light pulses from the night sky was therefore probably the first time in which Čerenkov radiation had been detected in a gas; the first laboratory experiments on the radiation in gases were carried out later, by Balzanelli and Ascoli.[27]

* The "albedo" is defined as the ratio of the number of particles travelling upwards, to the number travelling downwards, at a given point in the atmosphere.

Continuing the survey of the work at the Pic du Midi, the following main results were obtained. The pulse-height distribution was found to obey a power law of the form $N(>h) \propto h^{-1.6}$ where N and h are the pulse rates and heights respectively; this form of the spectrum follows closely the numbers-energy distribution of the incoming primary cosmic-ray particles.

The rate of frequency of arrival of light flashes at different zenith angles Z, was studied with a light receiver that could be tilted to set positions. It was found that the light pulse rate $N(Z)$ varied approximately as $\cos^2 Z$ or $\cos^3 Z$, which was a slower rate of variation than that for the showers themselves, which is known to vary approximately as $\cos^6 Z$. This is consistent with the idea that the light pulses behave as a penetrating component of the air showers, which is indeed natural in such a clear atmosphere; the much steeper law for the air showers arises from the much greater absorption for the shower particles (mostly electrons) as the zenith angle is increased.

Absolute light fluxes were estimated by comparison with pulses from a radioactive source and a crystal scintillator. For those pulses at the threshold level of bias imposed by the noise, and those therefore arriving at the rate of a few a minute, were found to have a flux at sea-level of about 3 photons per square centimetre per flash. (This particular experiment was carried out later, at Harwell.)

Experiments in conjunction with the Geiger counters, showed that the variation in probability of a given counter firing in coincidence with a flash from the light receiver, fell away slowly as a function of the distance of the counter from the receiver.

In general, larger air showers (i.e. those firing more than one, two, etc., counters simultaneously) were associated with larger light pulses, but the correlation here was not very strong.

The most obvious practical application of the new instrument was to attempt to find if these high energy showers appear to originate from "points" or restricted areas of the sky. There were two characteristics of the light receivers that made them ideally suited for this type of experiment. The first of these is that by choice of the field of view (controlled by placing stops over the photocathode), one has a very simple instrument with excellent directional features. The second is that a *single* light receiver is a shower detector by itself, since it is sensitive to a shower falling anywhere within quite a large radius from the position where it is situated.* Ryle,[28] among others, had suggested that possibly the radio "stars" might in addition be emitters of cosmic-ray particles, and it was therefore thought worth while to look at some of these "objects" with a light receiver of small field of view; runs were therefore carried out on the regions of sky containing the strong radio sources in Cygnus, Casseiopeia and Taurus, the technique being to count flashes for half an hour with the instrument pointing at the "object," and then for half an hour away from it. With none of these sources, nor with the Andromeda nebula, was there any significant increase in counting rate. Now it can be shown that the average shower energy responsible for our light pulses was probably about 10^{14} eV (i.e. that the incoming primary particles have this energy); it was, however, not surprising that these experiments gave a negative result since Cranshaw and Galbraith[24] have found the cosmic radiation isotropic up to much higher energies, namely about 10^{16} eV and higher. If the supposed magnetic fields in the universe are such as to even out the spacial distribution of particles of energies of about 10^{16} eV, it is clear that one would be unlikely to find "point" sources at the lower energies around 10^{14} eV. However, if light receivers can be developed which are both more sensitive and can detect still higher energy showers at a reasonable rate, over large areas of ground, the technique may one day reveal anisotropies in the cosmic radiation.

In conclusion it should be emphasized that even in such a restricted field in physics, as is the topic of Čerenkov radiation, this article covers only the main features; the reader will find the list of references lead him to a much wider scope, in cosmic-ray and high-energy physics generally.

* It can be shown from quite simple arguments on the variation of refractive index of air with height above the ground, that for a shower having no lateral spread or appreciable angular scattering of its electrons, the "pool" of Čerenkov light on the ground has a maximum radius of about 130 m at sea-level.

REFERENCES

(1) MALLET, L. *C.R. Acad. Sci.* [*Paris*], **183**, p. 274 (1926).

(2) MALLET, L. *C.R. Acad. Sci.* [*Paris*], **187**, p. 222 (1928).

(3) MALLET, L. *C.R. Acad. Sci.* [*Paris*], **188**, p. 445 (1929).

(4) ČERENKOV, P. A. *C.R. Acad. Sci. U.S.S.R.*, **2**, p. 451 (1934).

(5) FRANK, I., and TAMM IG. *C.R. Acad. Sci. U.S.S.R.*, **14**, p. 109 (1937).

(6) TAMM, IG. *J. Phys. U.S.S.R.*, **1**, p. 439 (1939).

(7) GINSBURG, V. L. *Dokl. Acad. Nauk. SSSR*, **56**, p. 253 (1947).

(8) ABELE, M. *Nuovo Cimento*, Supp. **9** [3], p. 207 (1952).

(9) LAWSON, J. D. *Phil. Mag.*, **45**, p. 748 (1954).

(10) GINSBURG, V. L. *J. Phys. U.S.S.R.*, **2**, p. 441 (1940).

(11) COX, R. T. *Phys. Rev.*, **66**, p. 106 (1944).

(12) JELLEY, J. V. *Prog. Nuclear Phys.*, **3**, p. 84 (1953).

(13) GETTING, I. A. *Phys. Rev.*, **71**, p. 123 (1947).

(14) MARSHALL, J. *Phys. Rev.*, **86**, p. 685 (1952).

(15) MANDÒ, M. *Nuovo Cimento*, **12**, [1], p. 5 (1954).

(16) MATHER, R. L. *Phys. Rev.*, **84**, p. 181 (1951).

(17) DUERDEN, T., and HYAMS, B. D. *Phil. Mag.*, **43**, p. 717 (1952).

(18) ANDERSON, W., and BELCHER, E. H. *Brit. J. Appl. Phys.*, **5**, p. 53 (1954).

(19) WINCKLER, J. R., and ANDERSON, K. *Phys. Rev.*, **93**, p. 596 (1954).

(20) JELLEY, J. V. *Proc. Phys. Soc. A*, **64**, p. 82 (1951).

(21) BLACKETT, P. M. S. *Gassiot. Comm. Rep. Phys. Soc.*, p. 34 (1948).

(22) AUGER, P., MAZE, R., and GRIVET-MEYER, T. *C.R. Acad. Sci.* [*Paris*], **234**, p. 1551 (1952).

(23) GALBRAITH, W., and JELLEY, J. V. *Nature* [*London*], **171**, p. 349 (1953).

(24) CRANSHAW, T. E., and GALBRAITH, W. *Phil. Mag.*, **45**, p. 1109 (1954).

(25) *J. Atmos. Terrest. Phys.*, **6**, p. 250 (1955).

(26) *Nuovo Cimento*. To be published.

(27) ASCOLI BALZANELLI, A., and ASCOLI, R. *Nuovo Cimento*, **11**, [5], p. 562 (1954).

(28) RYLE, M. *Rep. Progr. Phys.*, **13**, p. 184 (1950).

Time-lag data for spark discharges in uniform field gaps

By A. Aked, B.Sc., F. M. Bruce, M.Sc., Ph.D., M.I.E.E., A.Inst.P., and D. J. Tedford, B.Sc., A.R.T.C.,
The Royal Technical College, Glasgow

[*Paper first received* 21 *March, and in final form* 26 *April*, 1955]

Formative time-lags of spark breakdown have been measured for air in uniform fields with static applied voltages up to 63 kV; and the very long time lags (greater than 10^{-4} s) predicted by theory for such conditions have been recorded. Time-lag data have also been obtained for air in uniform fields with impulse spark voltages up to 150 kV for standard impulse waveforms, and also for lower voltages with non-standard impulse waveforms. For the latter condition the data indicate an impulse ratio of the order of 1·01. Comparative data for sphere gaps are included.

Characteristics of the spark discharge provide the experimental data which must be satisfied by any theory of the spark mechanism, and the sparkover voltage under given conditions between spherical electrodes in air is a recognized standard[1] for high voltage measurement. With increasing knowledge of the factors that influence the sparkover voltage, and data for alternating, static and impulse voltages, it has become necessary to define more precisely the conditions appertaining to experimental data to be used to assess the validity of spark theory,[2] or to compile calibration tables. Two important factors are the irradiation of the gap to eliminate statistical time-lag T_s by providing an adequate supply of initiatory electrons, and the subsequent formative time-lag T_F required for the development of the discharge across the gap. The latter not only provides some indication of the active secondary ionization processes,[3] but must be taken into account when using a spark gap to measure rapidly varying voltages such as impulse waveforms. The present data relate to spark breakdown in the uniform field between parallel plane electrodes with suitably curved edges,[4] using static voltages and impulse voltages of various waveforms.

When impulse voltages of increasing magnitudes are applied to a gap, a value is first reached at which repeated impulses will produce only an occasional sparkover; at some higher value still there will be sparkover for each impulse applied. This change in voltage ($\Delta V\%$) between 0 and 100% frequency of sparkover is reduced by irradiation of the gap to eliminate T_s and consequently time-lags that are excessive relative to the time that an impulse voltage wave is maintained above a given voltage level. For present purposes, the requisite level of irradiation for uniform field gaps, whether by exposure to ultra-violet light or to the presence of a radioactive salt, has been taken as that giving the minimum value of $\Delta V\%$. Ultra-violet irradiation was obtained by mounting the gap in a fixed position relative to the trigger gaps of a multi-stage impulse plant, and radioactive irradiation by inserting a capsule of 0·5 mg radium equivalent in one of the electrodes. It was confirmed that either source alone, or both acting together, gave a value for ΔV of 0·8% for uniform field gaps, and this condition was frequently checked.[5] The same sources of irradiation were employed in comparative observations on a sphere gap, using spheres 6·25 cm in diameter. Uniform field electrodes having nominal voltage ranges up to 100 or 140 kV were used, but as sparkover up to these limits occurs in the uniform field region, no significant variation in the observed phenomena for the two sizes was found or was to be expected.

1/50 IMPULSE WAVEFORM DATA

Standard 1/50* waveforms[6] of either polarity were applied to irradiated uniform field gaps. By discharging the impulse generator when the stage capacitors were charged to a given voltage, which could be measured to an accuracy of about ±0·1%, it was possible to measure small changes in output voltage, and hence in ΔV, much more accurately than the determination of the peak impulse voltage which includes oscillography errors. The datum sparkover voltage was taken as that corresponding to the 0% limit of the ΔV range, and higher voltages within that range are expressed as corresponding percentage overvoltages.

The results for three gap spacings are shown in Fig. 1, in which the broken vertical lines denote typical scatter in the values of T_F. There is no observable variation with polarity or spacing. The full line gives the time for which the applied impulse waveform exceeded the datum level corresponding to 0% sparkover frequency, and most of the observed time-lags are in excess of this, indicating that a breakdown, which was presumably initiated during the overvoltage period, was completed after the wave tail had fallen slightly below the assumed datum. These results cannot include the long time-lags predicted by the Townsend theory[3] for low overvoltages

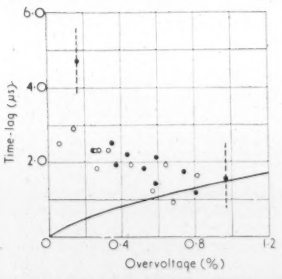

Fig. 1. Uniform field gap data for 1/50 impulse waves

○ = positive polarity
● = negative polarity

Gap spacings 1·34, 3·19, 5·68 cm (about 40 to 150 kV).

* A T_1/T_2 waveform is an impulse wave which reaches the crest value in T_1 μs and decays to half the crest value in T_2 μs.

because of the limitation imposed by the fall of voltage on the wave tail, and the mean values shown by the points can apply only to 1/50 waves, but this is a case of particular interest in high voltage testing procedure.

EFFECT OF IMPULSE WAVEFORM

0·2/240 and 1·2/240 waveforms were applied to a given gap; the results are shown by curves of mean values plotted in Fig. 2, and remarkably good curves were obtained, despite the range covered by the individual observations. The non-irradiated gap gave longer time-lags than for the irradiated

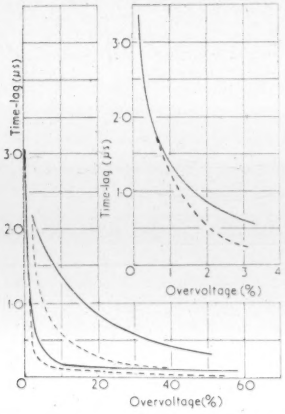

Fig. 2. Uniform field gap data for 2 cm spacing

—— = 1·2/240 waves
- - - = 0·2/240 waves

For each waveform the upper curve is for the non-irradiated gap, and the inset diagram is an enlarged portion of the curves for the irradiated gap.

condition, but the mean values were still very close to the curves drawn. An increased consistency in this respect relative to the sphere gap is to be expected, since uniformity of the field is maintained over a much greater area of cross-section, and the probability that fortuitous ionization will reduce T_s is thereby increased. There was no significant difference due to polarity, or for ultra-violet as compared with radium irradiation. The observations were extended to very high overvoltages giving the extremely low values of T_F frequently mentioned in the literature. Because of the very high overvoltages used, which are much in excess of the 100% sparkover criterion, the percentage overvoltage is defined as the ratio of the prospective peak value to the datum value, and the curves show that, for a given overvoltage, T_F is lower for the 0·2 μs wavefront, as would be expected from the greater rate of rise of voltage.

Comparative data for a sphere gap are shown in Fig. 3. Without irradiation the points are widely scattered; time-lag values for negative waves are greater than those for positive waves, and two of these lie outside the boundary of the figure. The inset figure shows reasonable consistency in the performance of the irradiated gap, with no apparent difference due to polarity or the method of irradiation.

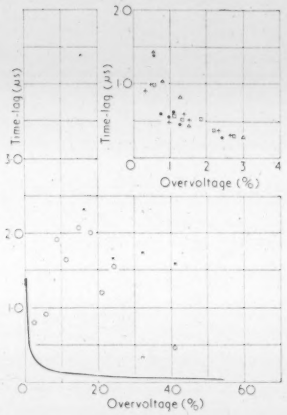

Fig. 3. Data for 6·25 cm diameter spheres at 2·0 cm spacing for 0·2/240 waves

—— = radium or ultra-violet irradiation
○ = positive waves, non-irradiated
× = negative waves, non-irradiated

The inset figure is an enlargement of the curve showing individual points for both polarities and both forms of irradiation.

STATIC TIME-LAG DATA

The use of static voltages overcomes the limitations imposed by an impulse waveform on the range of possible time-lags, and the static sparking potential is easily determined as a datum to which overvoltages can be related. A stabilized and smoothed static approach voltage some 2 kV below the sparking potential was applied to the gap, and on this was superimposed a pulse voltage of relatively low magnitude, and having a rise time of 0·16 μs on the front and a decay time-constant of about 0·2 s. The magnitudes of the approach voltage and the pulse voltage were measured independently by potentiometer methods having sensitivities of the order of 0·01%. The amplitude of the pulse voltage was increased at intervals of ten applications, the datum voltage being taken as the sum of the approach voltage and pulse voltage which just failed to give an occasional sparkover. The mean values of T_F for three gap spacings are indicated by the points on Fig. 4, the scatter of individual observations lying within a range of half to twice the mean value. For the smallest spacing the data link with those of Fisher and Bederson.[7] At very low percentage overvoltages long time-lags are obtained, and within the present range of values appear to increase without limit as the overvoltage approaches zero. The time-lags decrease rapidly at higher overvoltages, being of the order of 1 μs at 2% overvoltage. These values are of the nature and order that has been predicted by theory.[3]

The alternative plot of the data shown in Fig. 5 reveals a linear relationship between T_F and gap spacing for a constant

percentage overvoltage, and the very high values of T_F at low overvoltages. Individual values of T_F up to some 400 μs were observed in the course of this work.

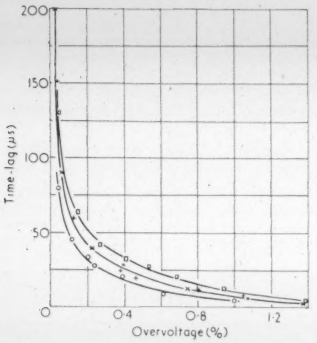

Fig. 4. Static data for irradiated uniform field gap, positive voltages

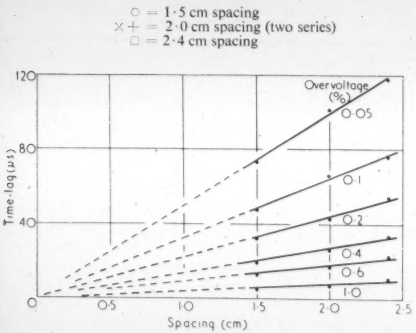

Fig. 5. Time-lag/spacing characteristics derived from Fig. 4

COMPARISON OF DATA FOR STATIC AND IMPULSE VOLTAGE

Corresponding values for a 2·0 cm gap are shown in Fig. 6. For a given impulse wave, the overvoltage will have to be sustained for a time of the order of the minimum T_F before breakdown can occur, and the 0% sparkover criterion taken as the datum sparking voltage in this work will therefore be in excess of the static datum, for which there is no imposed time limit due to waveform. In the inset figure, the horizontal full line represents the impulse datum voltage; the static datum will be at some lower value as indicated by the dotted line. A given impulse overvoltage, as defined in the above data, therefore corresponds to a higher overvoltage when referred to the static datum; an effect which can be termed the impulse ratio of the gap, and accounts for the difference between the curves of Fig. 6. If the difference between the impulse and static datum voltages is assumed to be 1·15%, and the impulse overvoltages are adjusted to the static datum, the characteristic then coincides exactly with that obtained with static voltages, as shown by the transfer points on Fig. 6. For the 0·2/240 waveform used, therefore, the impulse ratio of the gap relative to static sparkover is of the order of 1·01.

In most laboratories, the impulse voltages available are much in excess of the static voltages, and the only measurable datum for specifying overvoltage is that used in the present impulse tests—the 0% sparkover criterion. This has been shown to be greater than the static sparking potential, which is the datum used for static measurements, and that which

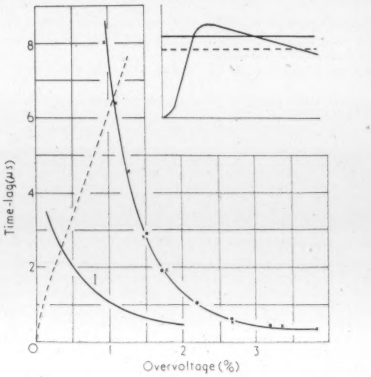

Fig. 6. Comparison of static and impulse time-lag data for an irradiated uniform field gap (2 cm spacing)

I = impulse characteristic for 0·2/240 waveform
× = observed points from d.c. characteristic
● = points transferred from *I*
- - - = duration of impulse waveform overvoltage

On the inset figure, the full and dotted horizontal lines illustrate relative levels for minimum sparking voltage on impulse and static voltages respectively.

must be considered when relating the data to the theory of the spark mechanism. In the impulse case, a low percentage overvoltage with a steep wavefront has to be written as some 1% higher when referred to the static datum. Irrespective of waveform restrictions, work which is confined to impulse voltage measurements could not therefore be expected to reveal the high values for T_F predicted by theory for very small overvoltages. Nevertheless, the impulse data do give the conditions, however restricted, that will be encountered in impulse voltage measurements.

CONCLUSIONS

Data for three impulse waveforms, including the 1/50 wave, have shown that the uniform field gap in air has sparkover characteristics that are independent of polarity, and that they can be repeated with consistent results. The time-lag characteristic gives a smooth curve even in the absence of external irradiation, although the time-lag values are then

greater. Comparative data for a sphere gap show that irradiation is essential to consistent performance on impulse voltages. The level of irradiation required to obtain minimum time-lags with a uniform field gap is conveniently defined as that giving the minimum voltage range between 0 and 100% frequency of sparkover, and this is not difficult to check, in practice.

The impulse waveform restricts the maximum values of T_F that can be observed, owing to the fall of voltage on the wave tail. For analytical purposes, the values of T_F must be observed down to very low overvoltages with respect to the static sparking potential, and this has been done by static voltage measurements, and with results that agree with the order of values predicted by theory. All aspects of the work described in this paper are now being studied at considerably higher voltages.

ACKNOWLEDGEMENT

The authors are indebted to the Sir James Caird Travelling Scholarship Trust for awards to two of them which enabled the work described to be undertaken.

REFERENCES

(1) *Brit. Stand.* 358: 1939. *Measurement of Voltage with Sphere-Gaps.*
(2) LLEWELLYN-JONES, F. *Brit. J. Appl. Phys.*, **5**, p. 49 (1954).
(3) DUTTON, J., HAYDON, S. C., LLEWELLYN-JONES, F., and DAVIDSON, P. M. *Brit. J. Appl. Phys.*, **4**, p. 170 (1953).
(4) BRUCE, F. M. *J. Instn Elect. Engrs*, **94**, p. 138 (1947).
(5) BRUCE, F. M. *Endeavour*, **13**, p. 61 (1954).
(6) *Brit. Stand.* 923: 1940. *Impulse-Voltage Testing.*
(7) FISHER, L. H., and BEDERSON, B. *Phys. Rev.*, **81**, p. 109 (1951).

The resistance of the oxide-coated cathode at ultra high frequencies

By L. J. HERBST, B.Sc., A.Inst.P., and J. E. HOULDIN, Ph.D., F.Inst.P., Department of Physics and Mathematics, College of Technology, Birmingham

[*Paper first received* 11 *February, and in final form* 4 *April*, 1955]

The impedance of the oxide-coated cathode of disk seal triodes has been measured at frequencies from 730 to 2360 Mc/s and with cathode temperatures from 1250 to 1400° K. The main feature of the method is the use of a photocell for indicating constancy of cathode temperature. Changes of 0·5° K could be measured. The behaviour of the coating is consistent with an equivalent circuit consisting of the grid-cathode capacitance C_1 in series with the coating resistance R.

Measurements of the d.c. coating resistance have also been made and the values agree approximately with those obtained at radio frequency. Values of R correspond to specific conductivities of between 0·3 and 0·4 Ω^{-1} m^{-1} at a cathode temperature of 1250° K, and R is found to decrease with temperature.

Finally a method is outlined which utilizes the change of heater resistance with cathode temperature to determine the power dissipated in the coating under oscillatory conditions.

LIST OF SYMBOLS

R_0 = d.c. cathode coating resistance (Ω)
R = radio frequency cathode coating resistance (Ω)
G = equivalent conductance across terminals A and B in Fig. 2(*b*)
T = cathode temperature (° K)
P = filament power in the absence of cathode current (W)
$P - \delta P$ = filament power required to keep the temperature of coating at the same value as P when cathode passes d.c. or radio frequency current (W)
I = steady cathode current (A)
f = frequency (c/s) ($\omega = 2\pi f$)
V = peak radio frequency voltage between grid and cathode
σ = specific conductivity of coating (Ω^{-1} m^{-1})
S = cathode coating area (cm^2)

1. INTRODUCTION

The resistance of the oxide-coated cathode under d.c. and pulse conditions has been the subject of thorough investigation in recent years.(1) On the other hand, little has been published on the behaviour of the coating at high frequencies, though some unpublished work was done by one of the authors (J. E. H.) some years ago. The present paper describes an attempt to determine the coating resistance by observing the surface where radio frequency heating takes place.

The valves investigated were disk seal triodes similar to type CV273.(2) The experimental arrangement of the valve and circuit is shown in Fig. 1. The grid-cathode and grid-anode circuits were tunable coaxial transmission lines, the tuning being effected by adjusting the position of the shorting bridges of those lines. With this type of valve it was possible to view the cathode surface through the grid wires as shown. A hole was drilled through the anode cap and the adjacent

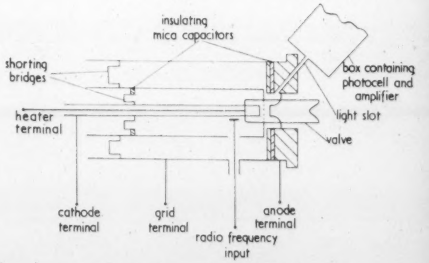

Fig. 1. Arrangement of circuit apparatus

brass structure so that there was a direct line of view from the cathode surface to a photocell. Approximately half the total cathode area was viewed by the photocell. The heater filament was immediately behind the cathode and surrounded by a nickel cylinder. Hence, in observing the cathode as shown, the only light reaching the photocell from inside the valve came from the coating surface. The photocell and d.c. amplifier were provided with double screening for both electrical and optical purposes. Even in a well-lit room no measurable light reached the photocell other than that from the cathode.

2. METHODS OF MEASUREMENT

2.1. *Determination of R.* A radio frequency voltage from a separate oscillator was applied between the grid and the cathode of the valve *via* an adjustable probe (Fig. 1). A high resistance voltmeter was connected across the external grid and cathode terminals (grid and anode terminals were joined together) of the circuit and gave the peak value of the applied radio frequency voltage with the valve itself acting as the rectifier. The following cycle of operations was then carried out.

First, the coating surface was observed in the absence of radio frequency power. The heater power was then P. Next, with some radio frequency power applied, the heater power supplied was adjusted so as to restore the coating temperature to its original value. (The heater power was then $P - \delta P$.) Finally, the radio frequency power was removed, the initial heater conditions restored, and a check made to see that the coating temperature was still the same. The coating took about half a minute to reach a steady temperature after a sudden change in heating, and a complete cycle as just described took about two minutes.

It is assumed that nearly all the heater power was transferred to the cathode and that the change in heater power resulted in an equal change in the power reaching the coating. Thus δP was equal to the radio frequency power dissipated in the coating. This assumption was checked by using a similar procedure to that described in Section 2.2. At normal filament temperatures the cooling of the cathode due to emission greatly exceeds the heating effect due to the resistance of the coating [see equation (4)]. Thus it was possible to compare directly the calculated cooling of the cathode surface due to electron emission with the increase in heater power necessary to keep the cathode at constant temperature. The agreement was well within experimental error.

The actual value of the coating resistance was determined by calculation using the circuit shown in Fig. 2 in which C_1 is the capacitance between the grid wires and the coating

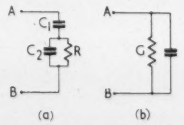

Fig. 2. (*a*) Circuit between grid and cathode.
(*b*) Equivalent admittance between A and B

surface; C_2 and R represent the impedance of the actual coating. In this circuit the interface impedance between the coating and the metal base has been ignored. The interface capacitance is such that the impedance is negligible at the frequencies of the measurements.

From Fig. 2 it can be shown that the equivalent conductance G, across the terminals A and B is given by

$$G = \omega^2 C_1^2 R/[1 + \omega^2(C_1 + C_2)^2 R^2] \quad (1)$$

G may then be determined from

$$G = 2\delta P/V^2 \quad (2)$$

using the measured values of δP and V.

The use of equation (2) implies that all the radio frequency heating of the cathode was due to losses in the coating arising from the circulating radio frequency current. Back bombardment from excess energy electrons has been ignored. The mean rectified current was about 1 μA.

Finally, R may be found from equation (1). The value of C_1 may be calculated from the valve dimensions. It is shown in Section 3.1 that under certain conditions, $\omega^2(C_1 + C_2)^2 R^2$ is much less than unity, and then

$$R = G/\omega^2 C_1^2 \quad (3)$$

2.2. *Determination of* R_0. The method consisted in passing a steady cathode current I through the coating and keeping the surface temperature T constant by altering the filament power as before. The theoretical formula dealing with the temperature of the coating under space charge limited conditions gives a value of R_0 as follows[3]

$$R_0 = \left\{\delta P + I \times 10^{-4} T[1{\cdot}72 + 1{\cdot}98 \log (SAT^2/I)]\right\}/I^2 \quad (4)$$

where A is the constant in Richardson's equation

$$I = SAT^2 \exp(-b/T)$$

The term involving I in the numerator of equation (4) arises because of the cooling effect of the electron evaporation from the cathode which generally exceeds the heating effect $I^2 R_0$.

Determination of R_0 thus depends on a knowledge of the value of A, which is known to vary between wide limits. As a result of pulse measurements on a large number of valves A was found to vary from 15 to 95 A/cm$^2 \times (^\circ\text{K})^2$. Thus accurate determination of d.c. coating resistance is not possible. The accuracy of the measurements increases as the coating resistance increases. Only one valve out of about forty had a sufficiently high coating resistance to give reasonably accurate measurements. Details of the measurements on that valve and two others are given in Section 3.2.

2.3. *Determination of T.* The cathode temperatures have been determined in all cases by retarding field plots. It has been found on a number of valves that

$$T \propto P^{1/4} \quad (5)$$

over the range of measurement. The usual procedure was to determine one value of T by a retarding field plot and then to calculate the others from equation (5). The sensitivity of the photocell and d.c. amplifier was such that temperature changes of $\pm 0{\cdot}5^\circ$ K could be detected. The comparable accuracy obtainable with a high-grade disappearing filament pyrometer was about $\pm 10^\circ$ K. The photocell method has the additional advantage that it can be used at temperatures below the range of the pyrometer.

3. RESULTS

3.1. *Radio frequency measurements.* For valves with small grid-cathode clearances it was found that the values of G were independent of the radio frequency voltage at a given frequency. Typical results for one valve are given in Tables 1(*a*) and (*b*) for two widely different frequencies. It will

be seen that G is constant at each frequency. The effect of transit time on voltage readings has been neglected.

The voltage V is that across the electrodes which are acting as the peak diode rectifier. Thus the usual error in diode voltmeters due to the impedance of connecting leads is in this case zero.

Table 1. *Variation of G with V*

(*a*) *Valve No.* 3

Frequency, 730 Mc/s; cathode temperature, 1150° K; mean value of G, $1{\cdot}8 \times 10^{-4}(\Omega^{-1})$

V	$\delta P(W)$	$G(\Omega^{-1})$
23·8	0·051	$1{\cdot}8 \times 10^{-4}$
31·8	0·097	$1{\cdot}9 \times 10^{-4}$
41·8	0·145	$1{\cdot}7 \times 10^{-4}$
54·8	0·260	$1{\cdot}7 \times 10^{-4}$
64·8	0·370	$1{\cdot}8 \times 10^{-4}$

(*b*) *Valve No.* 3

Frequency, 2360 Mc/s; cathode temperature, 1140° K; mean value of G, $1{\cdot}8 \times 10^{-3}(\Omega^{-1})$

V	$\delta P(W)$	$G(\Omega^{-1})$
8·6	0·068	$1{\cdot}8 \times 10^{-3}$
10·6	0·106	$1{\cdot}9 \times 10^{-3}$
12·6	0·131	$1{\cdot}7 \times 10^{-3}$
15·0	0·195	$1{\cdot}7 \times 10^{-3}$

From Tables 1(*a*) and (*b*) it may also be seen that the ratio of the conductances, G_1 and G_2, at the two frequencies f_1 and f_2, is given by $G_2/G_1 = 10$. Since $(f_2/f_1)^2 = 10{\cdot}5$, it may be concluded from equation (1) that under the conditions of the measurements $\omega^2(C_1 + C_2)^2R^2 \ll 1$. Values of R and σ determined with the aid of equation (3) are shown in Table 2.

Table 2. *Values of R and σ for four different valves at* 730 Mc/s

Valve	$T(°K)$	$R(\Omega)$	$\sigma(\Omega^{-1}m^{-1})$
1	1222	10	0·4
2	1168	13	0·3
3	1148	10	0·4
4	1181	16	0·3

It was found for other valves with larger electrode clearances that the values of G varied with the radio frequency voltage. These results, which are being investigated further, may be attributable to electron inertia.

3.2. *D.C. measurements.* Table 3 gives the measured values for R_0 for valves Nos. 1 to 3.

Table 3. *Cathode coating resistances at d.c.*

Valve No.	$T(°K)$	$\delta P(W)$	$I(mA)$	$R_0(\Omega)$	*Estimated accuracy of* R_0 (%)
1	1098	0	44	45	±15
	1162	0	62	34	±20
	1214	−0·058	41	23	±20
2	1050	−0·058	40	11	±30
3	1067	−0·049	30	11	±40

(No measurements were made on valve No. 4.)

It will be seen by comparison with Table 2 that there is reasonable agreement between the values of R and R_0 in the case of valves Nos. 2 and 3. Valve No. 1 had an abnormally high value of R_0 and this was attributed to interface resistance. For the reasons mentioned in Section 2.2 the values of R_0 are difficult to determine. In Table 3 the last column gives the range of values of R_0 allowing for the possible spread in A (see Section 2.2).

3.3. *Variation of R with T.* Table 4 shows the measured variation of R with cathode temperature.

Table 4. *Variation of R with temperature at* 730 *Mc/s*

Valve	$T_1(°K)$	$T_2(°K)$	R_1/R_2	$T_2 - T_1$	$\log_{10}\frac{R_1}{R_2}/10^4\left(\frac{1}{T_1} - \frac{1}{T_2}\right)$
1	1222	1372	1·4 (1)	150	0·17
2	1168	1314	1·4 (2)	146	0·16
3	1148	1288	1·4 (6)	140	0·17
4	1181	1331	1·4 (2)	150	0·16

It will be seen that R decreases with increasing temperature and the fractional change in R over a given temperature range is very much the same for all valves.

4. EXTENSION OF METHOD TO OSCILLATOR

It has been found that a change in cathode temperature produces a readily detectable change of heater resistance; the heater may therefore be used as a resistance thermometer. Accordingly, the following method may prove to be useful for investigating power dissipation in the coating under oscillatory conditions. First, values of δP for various values of V are found in the manner already described. At the same time the changes in heater resistance are measured. Then, the valve is made to oscillate at the same frequency and the measurement of change in heater resistance allows deduction of the dissipation in the coating. It has to be remembered that evaporation cooling and I^2R_0 heating due to d.c. current, and possible back bombardment of returning electrons will all affect the coating temperature. However, the change of heater resistance should give some useful indication of the power dissipated in the coating under oscillatory conditions. The method may also give an indication of the radio frequency voltage between grid and cathode.

ACKNOWLEDGEMENTS

The authors are indebted to the Board of Admiralty for financial assistance and permission to publish. Thanks are due to the Research Laboratories of the General Electric Co. Ltd., for the provision of the disk seal triodes. Finally, the authors wish to thank Dr. M. R. Gavin, under whose supervision the work was carried out, their colleagues for their co-operation, and the workshop staff, Mr. L. Brierley and the late Mr. A. Darby for construction of the equipment.

REFERENCES

(1) WRIGHT, D. A. *Proc. Instn Elect. Engrs*, **100**, p. 125 (1953).

(2) BELL, J., GAVIN, M. R., JAMES, E. G., and WARREN, G. W. *J. Instn Elect. Engrs*, **93** *A*, p. 833 (1946).

(3) HERRMANN, G., and WAGENER, S. *The Oxide Coated Cathode* (London: Chapman and Hall Ltd., 1951).

The sedimentation of suspensions of spheres

By R. L. Whitmore, B.Sc., Ph.D., A.Inst.P., Department of Mining and Fuels, University of Nottingham

[*Paper first received* 5 *October*, 1954, *and in final form* 7 *March*, 1955]

An experimental investigation of Hawksley's equation for the sedimentation of suspensions of spheres has shown close agreement with the theory, except that the derived value of Einstein's viscosity constant appears to vary with the size range, possibly exceeding 3·4 for equi-sized spheres. When spheres of the same density as the sedimentary fluid were added to the suspension, a slight decrease in settling rate was produced at total volume concentrations not exceeding about 10%. Above this figure, appreciable increases in settling rate were found and were attributed to hydrodynamic attractive-forces between the spheres leading to the development of vertical streams in the suspension.

Many attempts have been made from time to time to develop a reliable theoretical relationship between the concentration and the settling rate of solid, undeformable particles falling in a fluid.[1-4] The falling speeds of many powders are sufficiently small for viscous-flow conditions to prevail and as this premise leads, at infinite dilution, to their following Stokes' law, many of the relationships have been derived from it for low concentrations of solids. Extensions to cover concentrated suspensions have been fewer in number, the most satisfactory probably being those of Steinour[5] and Hawksley.[6] The former, however, requires the inclusion of an experimentally determined constant, and as all the theories are developed basically for equi-sized spherical particles, the problems of producing equivalent practical suspensions on which constants may be measured are obvious. Hawksley, who developed his equations from the theoretical work of Burgers[2] on the sedimentation of dilute suspensions and of Vand[7] on the viscosity of suspensions, concluded that

$$U_c = \frac{(\sigma - \rho)gd_s^2}{18\,\eta_0}(1 - c)^2 \exp - \left(\frac{kc}{1 - Qc}\right) \qquad (1)$$

where U_c = settling rate of a suspension at concentration c;
c = volume concentration of spheres per unit volume of suspension;
σ = density of spheres;
ρ = density of pure fluid;
d_s = diameter of spheres;
η_0 = absolute viscosity of pure fluid;
k = Einstein's viscosity constant;
Q = Vand's interaction constant (39/64 for spheres).

If U_0 is equal to the Stokes' settling rate of a single sphere, then the settling rate of a suspension relative to that of a single constituent sphere is

$$U_c/U_0 = (1 - c)^2 \exp -[kc/(1 - Qc)] \qquad (2)$$

or

$$\log_e \frac{U_c}{(1 - c)^2} = -\left(\frac{kc}{1 - Qc}\right) + \log_e U_0 \qquad (3)$$

and

$$y = bx + a \qquad (4)$$

where

$$y = \log_{10} \frac{Uc}{(1 - c)^2},\ x = \frac{c}{1 - Qc},\ b = \frac{-k}{\log_{e10}},\ a = \log_{10} U_0 \qquad (5)$$

A plot of y against x should give a straight line of slope

$$b = -\frac{k}{\log_e 10} = -\frac{k}{2{\cdot}3} \qquad (6)$$

In developing these equations it is assumed that there is no relative motion between the falling particles as they are all of identical size and weight. This condition does not generally apply in practice and some interaction is probably inevitable. When the particles are in contact, the fluid adjacent to them will be withdrawn from active participation in the suspension, giving an apparent increase in the volume concentration of solids, and a corresponding reduction in the settling rate would be expected. Moreover, during contact the particles would be deflected from their vertical path, further reducing the average settling rate. The effect could, to some extent, be examined experimentally by altering the size range of the falling particles, but this would also produce an indeterminate "head" to the falling suspension, and make the settling-rate determination less reliable. An alternative method, which has been explored in the experiments to be described, is to introduce into the fluid a known volume of particles of the same size as the falling particles but of the same density as the fluid, so that they produce interactions but do not take part in the sedimentation process.

THE SUSPENSIONS

The theoretical requirement of equi-sized spheres is very difficult to achieve in practice, particularly as they must be small enough to fall under streamline-flow conditions. As the size of particle is increased, the size of vessel must be increased correspondingly and it is necessary to use a highly-viscous sedimentary fluid (giving stirring difficulties) or a small density difference between the particles and fluid (making the suspension sensitive to slight evaporation if, as is usual, a solution or a mixture of liquids is employed).

In the experiments to be described, the sedimenting particles were of methyl-methacrylate polymer, a material which has already been used satisfactorily for making model suspensions,[8,9] and the suspended particles of polystyrene, the fluids consisting of aqueous solutions of lead nitrate.

(*a*) *The particles*. The samples were obtained from unsized material by mechanical dry-sieving on new B.S.S. sieves, the procedure being continued with frequent cleaning of the sieves until less than 0·5% of the weight of each batch passed the 200 B.S.S. screen in 2 min. The 150–170 B.S.S. mesh fractions were then sieved separately in water, dried and density separated by adding them to solutions of lead nitrate of known density to give spheres of a narrow size and density range, the average density being taken as that at which equal volumes of the fraction floated and sank (Table 1). Since the polystyrene spheres were from a fraction smaller than the modal fraction of the bulk sample and the methyl-methacrylate polymer spheres from a fraction larger, there was a preponderance, by weight, of large over small spheres in the polystyrene sample and of small over large in the methacrylate. The diameter of the sphere which fell at the average rate of all the spheres in the fraction was calculated by assuming a linear variation of the weight of sub-fractions of the particles with the diameter over the range

150–170 B.S.S. (which the sieve analysis showed to be substantially correct), and integrating over the size range with respect to weight and the (particle diameter)^2, which is proportional to the settling rate. On dividing through by the integrated weight over the size range, the average (particle diameter)^2 was obtained and hence the average particle diameter. A check was obtained microscopically by setting a circular eyepiece-graticule to the mean diameter of the fraction and counting the number of particles within the range 0·089–0·095 mm, 0·095–0·098 mm and 0·098–0·104 mm. The results were then summed on a weight and (particle diameter)^2 basis as before and the results are compared in Table 1. Photomicrographs of the two materials are shown in Fig. 1.

Table 1. *Spheres used in experiments*

Material	*Size range (mm)*	*Average size*		*Density range (g/ml.)*	*Average density (g/ml.)*
		Sieve (mm)	*Microscope (mm)*		
Polystyrene	0·089–0·104	0·0980	0·0982	1·0543–1·0572	1·0553
Methyl-methacrylate polymer	0·089–0·104	0·0961	0·0954	1·1871–1·1956	1·1881

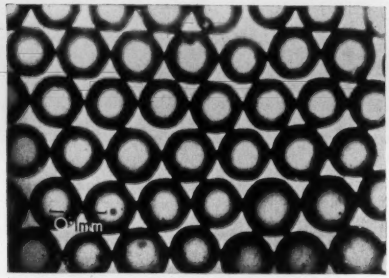

(*a*)

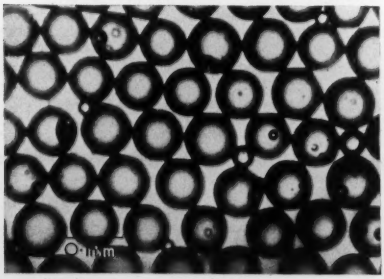

(*b*)

Fig. 1 (*a*) Photomicrograph of polystyrene spheres (*b*) Photomicrograph of methyl-methacrylate polymer spheres

(*b*) *The fluids.* Aqueous solutions of lead nitrate, with the addition of 0·1% Dispersol VL (by I.C.I. Ltd.) to inhibit flocculation, were employed. A wide range of dispersants was found which would disperse either one powder or the other but not both, and some compromise was necessary. The fluid finally chosen produced no flocculation of dilute suspensions of methacrylate spheres after standing overnight but slight flocculation of dilute suspensions of polystyrene spheres was observed after about 5 h. Details of the fluids are given in Table 2.

Table 2. *Sedimentary fluids*

Spheres used	*Density of fluid (g/ml.)*	*Viscosity of fluid (P)*
Polystyrene	1·0266	0·01024
Methyl-methacrylate polymer	1·0558	0·01046

(*c*) *The apparatus.* Two sizes of glass cylinders were used for containing the suspensions. One was a 100 ml. Nessler tube, 30 mm in diameter and 130 mm from the base to the 100 ml. mark and graduated in 1 ml. divisions. The other was 16 mm in diameter and 440 mm to the 0 mm mark, graduations reading downwards in 5 mm divisions. The majority of the experiments were made in the long tube, but some were made in both to confirm observations, reported elsewhere by Gurel,[10] that for particles of 0·15 mm diameter, the settling rate is unaffected by changes of the vessel diameter within the range 30 to 12 mm.

Each tube was provided with a simple stirrer, consisting of a horizontal, circular, perforated brass plate attached at one point on the perimeter to a 1½ mm diameter, vertical brass rod which could be clipped to the side of the settling tube when not in use. The tubes were mounted in cradles which could be levelled and were immersed in a glass-sided water thermostat maintained accurately at 20° C ± 0·05.

Illumination was obtained from a Regulite projector-type microscope lamp (by W. Watson and Sons, Ltd.) which was mounted above the tank. The horizontal light-beam was reflected vertically downwards behind the tank on to a second mirror attached to a racking mechanism so that a narrow, horizontal light-beam could be shone through the suspensions at any desired height. A simple sighting tube, 20 mm in diameter by 150 mm in length, was used for viewing the falling suspensions in order to reduce parallax errors.

Attempts to follow the fall of one suspension through the other by differences in light intensity were not successful and it was found that greater accuracy and sensitivity could be achieved by using divers of a density intermediate between that of the settling suspension and the pure fluid. Berg[11] has reported using glass divers in particle-size analysis work, but greater versatility in their design was possible by turning them out of Alkathene rod (density 0·92 g/ml. approximately) and weighting them with tinned copper wire. A simple disk was unsatisfactory at low concentrations as particles tended to be deposited upon its upper surface and increase its effective density. The most suitable shape was found to

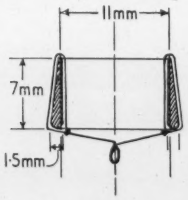

Fig. 2. Cross-section through diver

be a narrow annulus of streamline section, the dimensions of which are given in Fig. 2 and other details in Table 3.

Table 3. *Annular diver*

Weight	0·1311 g
Density	1·0600 g/ml.
Volume concentration of methyl-methacrylate spheres which just balanced diver	3·2%

TWO-COMPONENT SYSTEMS

The first experiments were made separately with polystyrene and methyl-methacrylate spheres so that their individual settling characteristics could be ascertained and the effects of tube diameter and diver behaviour examined. The method employed was to run a known volume of the sedimentary fluid (usually 50 ml.) into the tube and to add a known weight of powder to bring the volume concentration to 5%. The tube was then carefully levelled (if the distance from the vertical exceeded about 1 mm in 200 mm a difference in the settling rate was just discernible) in the constant temperature bath and the suspension well mixed by giving seventy strokes with the stirrer in 100–110 s. The stirrer was then clipped to the side of the tube with the perforated disk at the bottom of the tube, the light switched on and timings taken from when the head of the falling spheres passed the first engraved line on the tube. Readings were taken at at least twenty levels during each test, after which the suspension was restirred and the procedure repeated, at least three runs being taken. Finally, the stirrer was lifted clear of the suspension and the settled volume of the powder measured.

Additional powder was then added to bring the total volume concentration of spheres to 10% and the settling procedure described above repeated. The concentration was increased further in steps of 5% to a maximum value of 25%. The particles were then filtered off, washed, dried, reweighed and rebottled.

The stirring action caused some spheres to be deposited on the walls of the tube above the suspension level and it was necessary before each run to work them down into the suspension with the aid of the stirrer rod.

Experiments with the diver were made without removing it from the suspension. It was added to the suspension of lowest concentration and remained in the tube during all mixing and concentration-changing operations. This eliminated possible errors caused by removing suspension particles and fluid from the tube with the diver.

In practically all cases the variation between the times recorded for the head to reach a given level on duplicated suspensions was less than 3% and the averaged slopes of the settling rate/volume concentration curves differed by slightly less than ±1%. This error arose from weighing the powder and transferring it to the tube, adding the fluid, and making the settling-rate measurement. Another small error was introduced by the adhesion of some particles to the settling-tube sides above the level of the suspension. The effect was just discernible at high concentrations from repeat measurements made with the walls well covered with particles and clear of them, the increase in settling rate not exceeding 1%. The density of fluid increased slightly through the experiment (see next section) leading to a slight, compensating decrease in the settling velocity. A reasonable estimate for the errors from these two effects is ±½%, giving an overall uncertainty in the measurement of the settling rate of ±1½%.

The settling rates at each concentration were grouped and the results tested in Hawksley's[1] equation (Tables 4 and 5).

Table 4. *Settling rate of two-component systems*

Volume concentration of spheres (%)	*Material*			
	Polystyrene	*Methyl-methacrylate polymer*		
	Settling of head	*Settling of head*		*Settling of diver*
	Short tube (mm/s)	*Short tube (mm/s)*	*Long tube (mm/s)*	*Long tube (mm/s)*
5	0·0975	0·405	0·408	0·470
10	0·0762	0·306	0·309	0·337
15	0·0573	0·235	0·237	0·250
20	0·0416	0·177	0·178	0·183
25	0·0308	0·129	0·129	0·130
0	0·147*	0·627†		0·637‡

* Calculated from average particle size (Table 1).
† Calculated from average particle size from microscopic analysis (Table 1).
‡ Calculated from average particle size from sieve analysis (Table 1).

Table 5. *Values of constants from Hawksley's equation*

Material	Polystyrene	Methyl-methacrylate polymer	
Method of measurement	Head	Head*	Diver†
Regression coefficient y on x (b)	−1·390	−1·396	−1·475
Intercept (a)	$\bar{1}$·133	$\bar{1}$·755	$\bar{1}$·790
Degrees of freedom	16	34	34
Standard error of coefficient	0·0491	0·0447	0·0149
Standard error of residuals	0·0210	0·0270	0·0090

* Includes results obtained in long and short tube.
† Includes check results obtained with three-component system (see Table 7).

Note.—Difference of coefficient between columns 1 and 2 not significant at 50% level; between columns 2 and 3 just significant at 10% level; between columns 1 and 3 just significant at 5% level.

The mean regression-coefficient for the sedimentation of both materials [the constant "*b*" of equation (6)], when measured by the head of the falling particles is −1·394, and on solving in equation (6), a value of Einstein's constant k of 3·21 is obtained. With the diver (which, in effect, measured the settling rate of the portion of the suspension which had reached a volume concentration of 3·2%), k equals 3·39, with a greatly reduced standard error in the regression coefficient. It is apparent that the head of a dilute suspension of spheres, if not of absolutely identical size and density, will fall at a slower rate than the bulk of the spheres, and if the settling rate at the nominal concentration could have been measured, an even higher value of k might have been expected.

The values of k from the sedimentation experiments are compared with those obtained from viscosity measurements and theory in Table 6.

Hawksley's analysis of Steinour's data for the sedimentation of glass spheres (measured by the fall of the head) sized 75·6% within a range of 1·39 : 1 gives a regression coefficient of −1·16 and a value of k of 2·67. Viscosity measurements reported on an approximately similarly-sized suspension[8] (1·4 : 1) give k equal to 2·8.

Table 6. *Values of Einstein's constant*

Method of measurement	*Size ratio of spheres*	*Einstein's constant*
Sedimentation (head)	1·2 : 1	3·21
Sedimentation (diver)	1·2 : 1	3·39
Viscosity (falling sphere method)[8]	1·2 : 1	3·50
Theory[12]	1 : 1	3·37

For Steinour's tapioca spheres, Hawksley obtains a value of k of 2·58 which would suggest that they covered a wider size-range than the glass spheres. Steinour, however, claims that 80% were within the ratio 1·1 : 1, but an inspection of his micrograph of these particles shows numbers of them to have marked deviations from spheres, with an unknown effect on the settling rate. The general confirmation of Hawksley's theory can, therefore, be considered satisfactory.

THREE-COMPONENT SYSTEMS

All experiments made on the sedimentation of methyl-methacrylate polymer spheres through suspensions of polystyrene spheres were made with the diver. A few check experiments were made in the short tube, but the majority were carried out in the long tube. The general technique was similar to that used for the two-component systems, but for each series of tests the methyl-methacrylate polymer concentration was fixed and the polystyrene concentration increased in steps of 2·5% or 5% to a maximum of 20%. With each addition of polystyrene (suspended) spheres a small quantity of methacrylate polymer (falling) spheres was added to keep their proportion of the suspended particles plus suspension fluid constant. At the end of each series, the two sets of spheres were separated in a lead nitrate

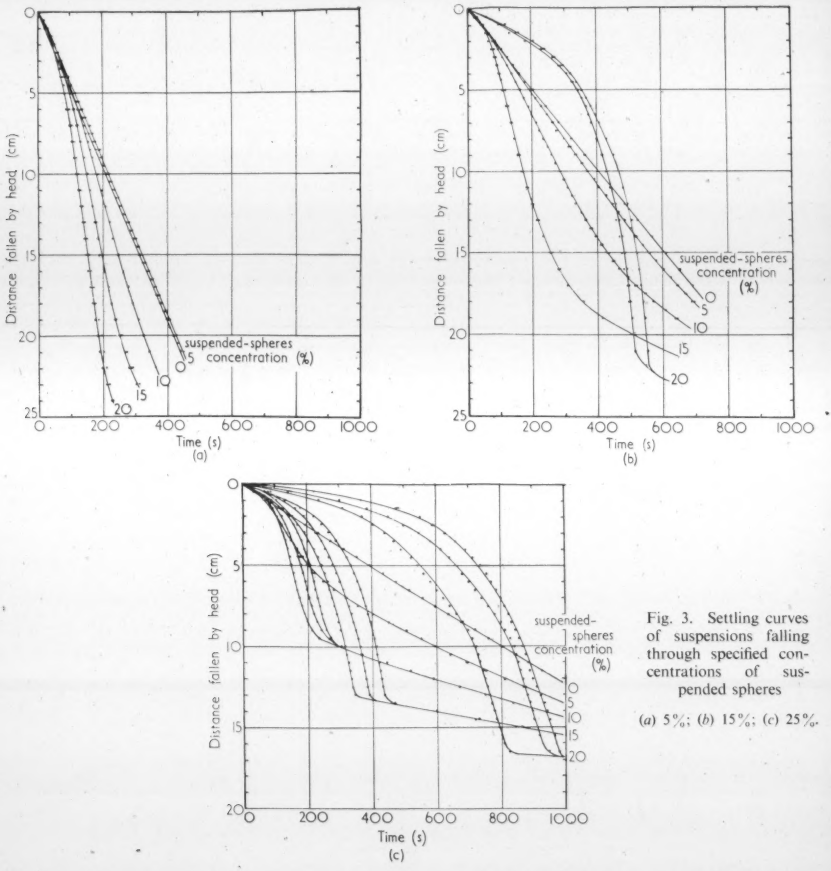

Fig. 3. Settling curves of suspensions falling through specified concentrations of suspended spheres

(*a*) 5%; (*b*) 15%; (*c*) 25%.

solution of intermediate density, washed, dried and re-weighed.

The total loss in weight of particles was found to be less than 1% in all cases. The average density of the suspension fluid collected from all the experiments was 1·0568 g/ml., an increase of 0·1% over the initial value.

Figs. 3 (*a*, *b*, and *c*) show typical sets of settling curves obtained with a constant proportion of falling particles and varied suspended-particles/total-volume ratios in the sedimentary fluid. The most striking characteristic is the marked deviation from linearity which occurs with increasing suspended-particle concentration, the effect being most marked at the higher falling-particle concentrations. It appears that an appreciable time, which is not always exactly reproducible, is necessary for the suspension head to reach its maximum settling-velocity which is, in almost all cases over the range of concentration examined, greater than that of the falling spheres alone and frequently in excess of that of a single falling sphere in an infinite expanse of fluid. The exception is at low falling-particle concentration where a slight decrease in settling rate is apparent for small additions of suspended spheres. The high settling rates are not generally maintained until the suspension is completely consolidated and, as the distance over which the maximum settling rates are constant are short compared with those of the two-component systems, the accuracy of measuring them is correspondingly reduced and only reaches approximately ±5% at the highest concentrations of suspended and falling spheres.

The sedimentation characteristics exhibited in the short tube were very similar to those in the long one, except that the falling spheres had insufficient distance in which to achieve the true maximum velocity. As the concentration of suspended spheres was increased, the initial rate of change of settling rate with time became slightly higher in the short than in the long tube.

The maximum settling rates in the long tube are summarized in Table 7, and in Fig. 4 the maximum settling rate of each three-component suspension is plotted as a ratio of the settling rate of the two-component suspension having the same falling-sphere concentration. It will be referred to subsequently as the relative settling rate.

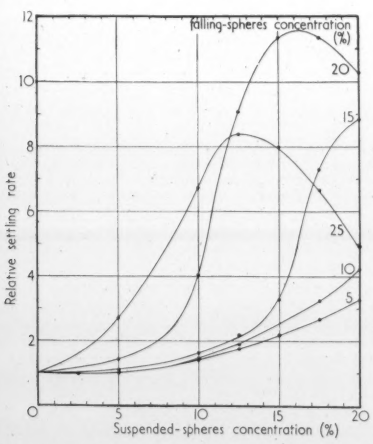

Fig. 4. Settling rate of three-component systems relative to two-component systems of same falling-sphere concentration

Table 7. *Maximum settling rates of suspensions*

Suspended-spheres concentration (%)	*Falling-spheres concentration* (%) 5 (*mm/s*)	10 (*mm/s*)	15 (*mm/s*)	20 (*mm/s*)	25 (*mm/s*)
0	0·470	0·339	0·248	0·183	0·130
2·5	0·46	—	—	—	—
5	0·47	0·34	0·27	0·26	0·35
10	0·67	0·50	0·41	0·74	0·87
12·5	—	0·64	0·54	1·67	1·09
15	1·03	0·85	0·81	2·09	1·04
17·5	—	1·10	1·81	2·09	0·87
20	1·54	1·43	2·20	1·89	0·64

DISCUSSION

It is improbable that the effects described are due to flocculation which can also increase the settling rate of a suspension. Flocculation is most effective at low concentrations and at values exceeding 15–20% is likely to lead to a decrease in the settling rate compared with the dispersed suspension.[6,13] Moreover, flocculated suspensions are more bulky when settled out than dispersed particles. Assuming that the sediment consisted entirely of falling spheres with no trapped suspended particles, the settled volumes from forty-eight experiments were calculated to have a solids content varying from 52·4–59·2%, the higher figures being obtained in general from the long tube. The highest solids-content figures reported by Rose,[14] Mott[15] and others[16] with large, equi-sized spheres well tamped down are 60–62%, suggesting that only the falling spheres were in fact concentrated in the sediment and were well consolidated.

From Fig. 4 it may be observed that at the lowest concentration of falling spheres (5%) there was a slight diminution in the relative settling rate as sedimentary fluid was replaced by suspended spheres until they accounted for approximately 5% of the total volume. Above this value the relative settling rate of the falling spheres increased steadily with increasing concentration of suspended spheres. With falling-sphere concentrations of 10 and 15%, the relative settling rate of the head always increased with increasing proportions of suspended particles over the range of concentrations employed. At falling-sphere concentrations of 20 and 25%, however, the relative settling rate attained a peak value beyond which the replacement of further fluid by suspended spheres led to a diminution in the relative settling rate.

It is apparent from Fig. 4 that, except at the lowest concentration of falling spheres, the initial rate of increase of the relative settling velocity with increasing concentration of

Table 8. *Concentrations of spheres at which a rapid increase in relative settling rate commences*

Sphere concentration (%) *Falling*	*Suspended*	*Total*
5	conditions not attained	
10	17	27
15	13	28
20	7	27
25	2½	27½

suspended spheres is positive, and rises rapidly when the suspended spheres exceed a certain concentration. If this rate is taken as 0·3 relative settling-rate increase per unit increase in volume concentration, the corresponding concentrations of spheres will be as in Table 8.

Thus the concentration conditions under which rapid settling is achieved appear to depend upon the total volume of spheres present rather than on their relative proportions, provided that both suspended and falling spheres are present.

The concentrations at which the maximum relative settling rates are achieved are summarized in Table 9.

Table 9. *Concentrations of spheres which produce maximum relative settling rate*

Sphere concentration (%)		
Falling	*Suspended*	*Total*
5	maximum not reached	
10	maximum not reached	
15	21*	36
20	16½	36½
25	12½	37½

* Extrapolated value.

The figures suggest that the total concentration is more important than the relative proportions of the two solid components in determining maximum settling rate.

It is apparent from Figs. 3 (*a*, *b* and *c*) that the high settling rates are not attained immediately stirring of the suspension ceases. An appreciable time is required for them to develop and, moreover, they are not maintained until consolidation is complete. There is an intermediate stage of slow sedimentation before the final consolidation and it is believed to occur after the expulsion of all stable particles from the consolidating mass, which finishes its settling as a simple two-component system.

A close examination of the suspensions, which were translucent under transmitted light, showed that in the three-component systems which exhibited high settling rates, vertical currents developed in the tube. Moreover, a re-examination of the two-component systems showed them to be present to a small extent when the concentration exceeded about 15% and careful relevelling of the tube would not eliminate them. When sufficient stable spheres had been added to any suspension, except the 5%, vertical streams developed randomly, the streams fluctuating in position round the tube and flowing alternately upwards and downwards in any one place. When the total concentration exceeded 30–35%, the streams became increasingly granular in appearance as though the particles were forming into loose conglomerates while falling. The intensity of the effect diminished from the bottom to the top of the tube and the last 5 mm or so of suspension below the diver was comparatively free from internal motion. The period of slow settling immediately before the final consolidation corresponded to a great reduction in interparticular motion and the disappearance of the vertical streams.

A tentative explanation of the phenomenon is that when the stirring ceases and the sedimenting particles commence to fall and the stable particles to rise slowly in the return stream, the hydrodynamic equilibrium between the parallel-moving particles is disturbed. Particles moving in the same direction develop attractive forces; those moving in opposite directions exhibit repulsive forces. An accurate calculation of the effect is difficult but a rough estimate, assuming an attraction inversely proportional to the fourth power of the distance between the spheres and proportional to the square of their parallel velocity,[17] balanced by a Stokes' resistance, gives a collision time between the falling spheres of the same order of magnitude as the settling time, assuming their initial distance apart to be less than half diameter (corresponding to total concentrations exceeding approximately 30%). Once grouping commences, vertical instability develops in the tube, producing streams of particles moving vertically through the fluid. Experiments[18] have shown that groups of particles fall considerably faster than the separate individual particles. The effect will take some time to reach equilibrium but should then be maintained until the interaction between streams becomes sufficiently great to reduce their intensity or all the stable particles are lifted clear of the sediment, leaving it to complete its fall as a two-component system.

CONCLUSIONS

From an examination of the settling of suspensions of closely-sized, spherical particles it appears that when the volume concentration of the falling spheres is less than approximately 10%, a slight decrease in settling rate is achieved by the introduction of small quantities of stable spheres in place of sedimentary fluid. As the volume concentration of either solid component is increased, however, instability develops, leading to vertical streaming and a considerable increase in the settling rate of the falling spheres relative to that of the same concentration falling in pure fluid. The instability takes some time to attain a maximum and the greatest settling rate is not achieved immediately the falling particles begin sedimenting. The consolidated sediment appears to consist only of the falling particles, the stable spheres being lifted clear by the streaming action.

ACKNOWLEDGEMENTS

The author's thanks are due to Imperial Chemical Industries, Ltd. (Plastics Division), and British Resin Products Ltd., for gifts of plastic materials, and to Professor F. B. Hinsley for helpful discussions during the course of the work.

REFERENCES

(1) BRINKMAN, H. C. *Appl. Sci. Res.*, *A*, **1**, p. 27 (1947); *Research*, **2**, p. 190 (1949).
(2) BURGERS, J. M. *Proc. K. Ned. Akad. Wetensch.*, **44**, pp. 1045, 1177 (1941); **45**, pp. 9, 126 (1942).
(3) CUNNINGHAM, E. *Proc. Roy. Soc. A*, **83**, p. 357 (1910).
(4) SMOLUCHOWSKI, M. S. *Proceedings 5th International Congress of Mathematicians*, 1912, **2**, p. 192 (London: Cambridge University Press, 1912).
(5) STEINOUR, H. H. *Industr. Engng Chem.*, **36**, p. 618 (1944).
(6) HAWKSLEY, P. G. W. *Conference on Some Aspects of Fluid Flow*, 1950, p. 114 (London: Edward Arnold and Co., 1951).
(7) VAND, V. *J. Phys. Coll. Chem.*, **52**, p. 277 (1948).
(8) WARD, S. G., and WHITMORE, R. L. *Brit. J. Appl. Phys.*, **1**, p. 286 (1950).
(9) EVESON, G. F., WARD, S. G., and WHITMORE, R. L. *Disc. Faraday Soc.*, **11**, p. 11 (1951).
(10) GUREL, S. *Ph.D. Thesis*, University of Birmingham (1951).
(11) BERG, S. *IngenVidensk. Skr.*, No. 2 (1940). See HERDAN, G., *Small Particle Statistics*, p. 86 (Amsterdam: Elsevier Publishing Co., 1953).

(12) ROSCOE, R. *Brit. J. Appl. Phy.*, **3**, p. 267 (1952).
(13) STEINOUR, H. H. *Industr. Engng Chem.*, **36**, p. 840 (1944).
(14) ROSE, H. E. *Conference on Some Aspects of Fluid Flow*, 1950, p. 136 (London: Edward Arnold and Co., 1951).
(15) MOTT, R. A. *Conference on Some Aspects of Fluid Flow*, 1950, p. 242 (London: Edward Arnold and Co., 1951).
(16) DALLAVALLE, J. M. *Micromeritics*, Chapter 6 (London: Sir Isaac Pitman and Sons, Ltd., 1948).
(17) RAMSAY, A. S. *Hydrodynamics*, Part II, 4th ed., p. 208 (London: Bell and Sons, Ltd., 1947).
(18) TIMBRELL, V. *Brit. J. Appl. Phys. Supplement No.* 3, **5**, p. S12 (1954).

A general mathematical treatment applicable to certain electrode systems

By G. POWER, M.A., Ph.D., University of Nottingham

[*Paper first received* 21 *January, and in final form* 7 *February*, 1955]

Some general formulae are obtained concerning the perturbation effects on certain two-dimensional electric fields of dielectric cylinders, assumed homogeneous and isotropic, with various boundary shapes. By taking particular values for the dielectric constants, these formulae lead to results of interest for particular electrode systems

1. SYSTEM OF CIRCULAR DIELECTRIC CYLINDERS

The application of electrode systems to certain branches of science is now well known, and the resistance of such systems in the form of circular,[1] rectangular[2] and elliptic[3] plates has been determined. By starting with a system of two concentric circular dielectric cylinders of different homogeneous and isotropic media containing an embedded line-charge, we are able to develop further useful formulae of a general nature for various boundary shapes with internal singularities. By taking particular values for the dielectric constants, these formulae lead to interesting results for certain types of electrode systems.

Let us assume an inner circular cylinder of radius b, dielectric constant k_1, a concentric cylinder of radius $a(>b)$, dielectric constant k_2, and suppose that this system is placed with the common centre at the origin of co-ordinates in a medium of dielectric constant k_3. A line-charge of strength m per unit length is taken to be embedded in the medium k_2 at the point $z = z_0$, the complex z-plane being defined in the usual manner.

If ϕ is the electric potential, ψ the current function, then $w = \phi + i\psi$ is the complex potential, so that, with the obvious notation, the perturbed fields in the various media can be represented in the form

$$w_1 = \sum_{n=1}^{\infty} a_{1,n} z^n, \qquad (|z| < b)$$

$$w_2 = \Omega + \sum_{n=1}^{\infty} a_{2,n} z^n + \sum_{n=1}^{\infty} b_{2,n} z^{-n}, \quad (b < |z| < a)$$

$$w_3 = \sum_{n=0}^{\infty} b_{3,n} z^{-n} + c_3 \log z, \qquad (a < |z|)$$

where (omitting the constant term)

$$\Omega = -\frac{2m}{k_2}\log(z - z_0) = \begin{cases} \dfrac{2m}{k_2}\displaystyle\sum_{n=1}^{\infty}\frac{z^n}{nz_0^n}, & \text{if } \left|\frac{z}{z_0}\right| < 1, \\ \dfrac{2m}{k_2}\displaystyle\sum_{n=1}^{\infty}\frac{z_0^n}{nz^n} - \frac{2m}{k_2}\log z, & \text{if } \left|\frac{z_0}{z}\right| < 1. \end{cases}$$

The boundary conditions are

$$\mathscr{R}(w_1) = \mathscr{R}(w_2), \quad k_1\mathscr{I}(w_1) = k_2\mathscr{I}(w_2) \quad \text{on} \quad |z| = b,$$

and

$$\mathscr{R}(w_2) = \mathscr{R}(w_3), \quad k_2\mathscr{I}(w_2) = k_3\mathscr{I}(w_3) \quad \text{on} \quad |z| = a.$$

Applying these conditions and solving we get

$$\alpha_n a_{1,n} = (4m/nz_0^n)[(k_2 + k_3)a^{2n} + (k_2 - k_3)z_0^{n}z^{n}],$$
$$\alpha_n a_{2,n} = (2m/nk_2z_0^n)(k_2 - k_3)[(k_1 + k_2)z_0^{n}z^{n} + (k_2 - k_1)b^{2n}],$$
$$\alpha_n b_{2,n} = (2m/nk_2z_0^n)(k_2 - k_1)[(k_2 + k_3)a^{2n} - (k_3 - k_2)z_0^{n}z^{n}]b^{2n},$$
$$\alpha_n b_{3,n} = (4m/nz_0^n)[(k_2 - k_1)b^{2n} + (k_2 + k_1)z_0^{n}z^{n}]a^{2n},$$
$$b_{3,0} = [m(k_2 - k_3)/k_2k_3]\log a^2, \quad c_3 = -2m/k_3,$$

where

$$\alpha_n = (k_3 + k_2)(k_2 + k_1)a^{2n} + (k_3 - k_2)(k_2 - k_1)b^{2n}.$$

2. CIRCULAR ELECTRODE SYSTEM

Setting $k_1 = k_2 = k_i$, $k_3 = k_0$, we immediately obtain in series form the complex potentials for the fields inside and outside a circular cylinder of radius a and dielectric constant k_i placed, with its centre at the origin of co-ordinates, in a medium of constant k_0. Noting the form of these series, we can generalize the results as follows. If we have an undisturbed field $f(z)$, caused by singularities placed inside the cylinder, then the perturbed fields outside and inside the cylinder are respectively

$$w_0 = \frac{2k_i}{(k_0 + k_i)}f(z), \quad w_i = f(z) + \frac{(k_i - k_0)}{(k_i + k_0)}f\left(\frac{a^2}{z}\right)$$

provided $f(z)$ has no logarithmic singularity at infinity.

These formulae can now be adapted to an electrode system in the form of a circular conducting disk with internal electrodes, by letting $k_i \to \infty$. The potential distribution throughout the disk is thus given by

$$w = f(z) + f(a^2/z)$$

If, however, the boundary of the disk is itself an electrode, we let $k_0 \to \infty$, thus obtaining $w = f(z) - f(a^2/z)$.

3. FURTHER CIRCULAR ELECTRODE SYSTEMS

If in the results of Section 1 we set $k = k_2/k_3$ and let $k_1 \to \infty$, we then obtain

$$\left.\begin{aligned}
a_{2,n} &= \frac{2m}{k_2 n z_0^n}\,\frac{(k-1)(z_0^n\bar{z}^n - b^{2n})}{[(1+k)a^{2n} - (1-k)b^{2n}]} \\
&= -\frac{2m\bar{z}_0^n\lambda}{k_2 n a^{2n}}\left(1 - \frac{b^{2n}}{z_0^n\bar{z}^n}\right) \\
&\qquad \left(1 + \lambda\frac{b^{2n}}{a^{2n}} + \ldots + \lambda^p\frac{b^{2np}}{a^{2np}} + \ldots\right) \\
b_{2,n} &= -\frac{2m}{k_2 n z_0^n}\,\frac{[(1+k)a^{2n} - z_0^n\bar{z}^n(1-k)]b^{2n}}{[(1+k)a^{2n} - (1-k)b^{2n}]} \\
&= -\frac{2mb^{2n}}{k_2 n z_0^n}\left(1 - \lambda\frac{z_0^n\bar{z}^n}{a^{2n}}\right) \\
&\qquad \left(1 + \lambda\frac{b^{2n}}{a^{2n}} + \ldots + \lambda^p\frac{b^{2np}}{a^{2np}} + \ldots\right) \\
b_{3,n} &= \frac{4m}{k_3 n z_0^n}\,\frac{(z_0^n\bar{z}^n - b^{2n})a^{2n}}{[(1+k)a^{2n} - (1-k)b^{2n}]} \\
&= \frac{4mz_0^n}{k_3 n(1+k)}\left(1 - \frac{b^{2n}}{z_0^n\bar{z}^n}\right) \\
&\qquad \left(1 + \lambda\frac{b^{2n}}{a^{2n}} + \ldots + \lambda^p\frac{b^{2np}}{a^{2np}} + \ldots\right) \\
c_3 &= -2m/k_3
\end{aligned}\right\} \quad (1)$$

where

$$\lambda = (1-k)/(1+k).$$

Thus if $|z| = b$ is a conducting surface, the fields outside and inside the cylinder $|z| = a$ are expressible as

$$\left.\begin{aligned}
w_0 &= -\frac{4m}{k_3(1+k)}\sum_{p=0}^{\infty}\lambda^p \log\left[z - \frac{b^{2p}z_0}{a^{2p}}\right] \\
&\quad + \frac{4m}{k_3(1+k)}\sum_{p=0}^{\infty}\lambda^p \log\left[z - \frac{b^{2(p+1)}}{a^{2p}\bar{z}_0}\right] - \frac{2m}{k_3}\log z, \\
\text{and} \quad w_i &= \frac{2m}{k_2}\left\{\sum_{p=0}^{\infty}\lambda^p \log\left[z - \frac{b^{2(p+1)}}{a^{2p}\bar{z}_0}\right]\right. \\
&\quad - \sum_{p=0}^{\infty}\lambda^{p+1}\log\left[z - \frac{b^{2(p+1)}z_0}{a^{2(p+1)}}\right] \\
&\quad + \sum_{p=0}^{\infty}\lambda^{p+1}\log\left[z - \frac{a^{2(p+1)}}{b^{2p}\bar{z}_0}\right] \\
&\quad \left. - \sum_{p=0}^{\infty}\lambda^{p+1}\log\left[z - \frac{a^{2(p+1)}z_o}{b^{2(p+1)}}\right] - \log[z - z_0] - \log z\right\}
\end{aligned}\right\} \quad (2)$$

If now we let $k_3 \to \infty$, $\lambda = 1$ and w_i will give the potential distribution throughout the annulus when the boundaries $|z| = a$, $|z| = b$ are electrodes.

It is to be noted that equations (2) give an infinite image system, but usually only one or two of these images need be considered in numerical calculation, since the series concerned will be fairly rapidly convergent. Equations (1) will give results in the form of infinite series capable of approximation to any degree required.

The expansions of Section 1 can be used to give immediately the distribution inside an electrode system in the form of the annulus $a \geqslant |z| \geqslant b$, simply by setting $k_1 = k_3 = 0$. By inspection of the result, we see that we may generalize in the following manner. If the field is due to internal electrodes so that its undisturbed complex potential $f(z)$ has no logarithmic singularity at infinity, then the perturbed complex potential inside the annulus is

$$w = f(z) + \sum_{p=0}^{\infty}\left\{f\left[\frac{a^{2(p+1)}}{b^{2p}z}\right] + f\left[\frac{b^{2(p+1)}}{a^{2p}z}\right] + f\left[\frac{b^{2(p+1)}z}{a^{2(p+1)}}\right] + f\left[\frac{a^{2(p+1)}z}{b^{2(p+1)}}\right]\right\} \quad (3)$$

This form will again give an image system which can be employed in numerical approximation. Alternatively, the results of Section 1 may be used to give an infinite series directly.

Suppose now we require $|z| = b$ to be a line of flow, then we let $k_1 = 0$ in Section 1, thus obtaining the fields outside and inside the annulus respectively in the form

$$\left.\begin{aligned}
w_0 &= -\frac{4m}{k_3(1+k)}\left\{\sum_{p=0}^{\infty}\mu^p \log\left[z - \frac{b^{2p}z_0}{a^{2p}}\right]\right. \\
&\quad \left. + \sum_{p=0}^{\infty}\mu^p \log\left[z - \frac{b^{2(p+1)}}{a^{2p}\bar{z}_0}\right]\right\} + \frac{2m}{k_3}\log z, \\
\text{and} \quad w_i &= -\frac{2m}{k_2}\left\{\sum_{p=0}^{\infty}\mu^p \log\left[z - \frac{b^{2(p+1)}}{a^{2p}\bar{z}_0}\right]\right. \\
&\quad + \sum_{p=0}^{\infty}\mu^{p+1}\log\left[z - \frac{b^{2(p+1)}z_0}{a^{2(p+1)}}\right] \\
&\quad + \sum_{p=0}^{\infty}\mu^{p+1}\log\left[z - \frac{a^{2(p+1)}}{b^{2p}\bar{z}_0}\right] \\
&\quad \left. + \sum_{p=0}^{\infty}\mu^{p+1}\log\left[z - \frac{a^{2(p+1)}z_o}{b^{2(p+1)}}\right]\right\} \\
&\quad - \frac{2m}{k_2}\log[z - z_0] + \frac{2m}{k_3}\log z
\end{aligned}\right\} \quad (4)$$

where $\mu = (k-1)/(k+1)$

We shall use these equations later in discussing further electrode systems.

4. ELECTRODE IN THE FORM OF A SEMI-INFINITE STRIP

If we set $z = e^{-it}$, $t = \alpha + i\beta$, $b = 1$, $a = e^{\beta_1}$, the dielectric annulus becomes a semi-infinite dielectric strip of width β_1. Further, if in the results of Section 1 we put $k_1 = k_3 = k_0$, $k_2 = k_i$, then the perturbed fields due to an internal line charge at $t = t_0$ in the parts of the t-plane given respectively by $0 \geqslant \beta$, $\beta_1 \geqslant \beta \geqslant 0$, $\beta \geqslant \beta_1$ become

$$w_1 = -\frac{4m}{k_0(1+k)}\left\{\sum_{p=0}^{\infty}\lambda^{2p}\log[t - t_0 - 2ip\beta_1] - \sum_{p=0}^{\infty}\lambda^{2p+1}\log[t - \bar{t}_0 + 2i(p+1)\beta_1]\right\}$$

$$w_2 = \frac{2m}{k_i}\left\{\sum_{p=0}^{\infty}\lambda^{2p+1}\log[t - \bar{t}_0 - 2i(p+1)\beta_1][t - \bar{t}_0 + 2ip\beta_1] - \sum_{p=0}^{\infty}\lambda^{2(p+1)}\log[t - t_0 - 2i(p+1)\beta_1][t - t_0 + 2i(p+1)\beta_1] - \log(t - t_0)\right\}$$

$$w_3 = -\frac{4m}{k_0(1+k)}\left\{\sum_{p=0}^{\infty}\lambda^{2p}\log\left[t-t_0+2ip\beta_1\right] - \sum_{p=0}^{\infty}\lambda^{2p+1}\log\left[t-\bar{t}_0+2ip\beta_1\right]\right\}$$

where

$$k = k_i/k_0, \quad \lambda = (1-k)/(1+k).$$

These formulae can obviously be generalized for the case of several singularities inside the strip by replacing $-\frac{2m}{k_i}\log(t-t_0)$ by $f(t)$, the undisturbed complex potential, so that $\log(t-t_0-2ip\beta_1)$ becomes $f(t-2ip\beta_1)$, $\log[t-\bar{t}_0-2i(p+1)\beta_1]$ becomes $f[t-2i(p+1)\beta_1]$ and so on. For an electrode system in the form of a semi-infinite strip, we can adapt the result for ω_2 by putting $\lambda = -1$ for internal electrodes, or $\lambda = 1$ if the boundaries of the strip are themselves an electrode.

5. ELLIPTIC ELECTRODE SYSTEM

The problem of an elliptic conductor in a general external field has long been solved. The case of the elliptic dielectric cylinder, however, has not received a great deal of attention, due to difficulties arising from the singularities of transformation. These difficulties can be overcome in a number of ways, but here we make use of the results of Section 3.

Consider the transformation

$$z = \frac{c}{2}(\zeta + 1/\zeta) \quad z = c\sin w \quad w = u + iv.$$

The region outside a slit AB in the z-plane transforms into the region outside the unit circle in the ζ-plane. The ellipse $v = \text{constant} = v_1$ say, of semi-axes $c\cosh v_1$, $c\sinh v_1$ in the z-plane, having A, B as foci, becomes the circle $|\zeta| = e^{v_1} = a$, say. Let this ellipse be set in the general field

$$g(z) \equiv g\left[\frac{c}{2}(\zeta + 1/\zeta)\right] = h(\zeta)$$

Split the function $h(\zeta)$ into

$$G(\zeta) = \tfrac{1}{2}[h(\zeta) + \overline{h}(\zeta)] \text{ and } H(\zeta) = \tfrac{1}{2}[h(\zeta) - \overline{h}(\zeta)],$$

so that $h(\zeta) = G(\zeta) + H(\zeta)$.

The component of $g(z)$ corresponding to $G(\zeta)$ will contain the real axis as a line of flow, so that inside the ellipse, AB will be a line of flow. Thus the formulae (4) of Section 3 are relevant with $b = 1$ and $a = e^{v_1}$.

Now inside the ellipse the electric potential is continuous in crossing the line of foci AB. This means that in the ζ-plane the values of the potential on $|\zeta| = 1$ are the same at $\pm am\zeta$, so that formulae (2) of Section 3 can be used for the terms derived from $H(\zeta)$. Splitting $h(\zeta) = -(2m/k_2)\log(\zeta - \zeta_0)$ into the two parts as indicated above, we obtain on addition the external and internal fields respectively in the form

$$w_0 = -\frac{4m}{k_3(1+k)}\left[\sum_{p=0}^{\infty}\mu^p\log\left[\zeta - \frac{\zeta_0}{e^{2pv_1}}\right]\left[\zeta - \frac{1}{e^{2pv_1}\zeta_0}\right]\right] - \frac{4m}{k_3(1+k)}\left[\sum_{q=1}^{\infty}{}'\mu^q\log\left[\zeta - \frac{\overline{\zeta}_0}{e^{2qv_1}}\right]\left[\zeta - \frac{1}{e^{2qv_1}\overline{\zeta}_0}\right]\right] + \frac{2m}{k_3}\log\zeta,$$

$$w_i = -\frac{2m}{k_2}\left\{\sum_{p=0}^{\infty}\mu^p\log\left[\zeta - \frac{1}{e^{2pv_1}\zeta_0}\right] + \sum_{p=0}^{\infty}\mu^{p+1}\log\left[\zeta - \frac{\overline{\zeta}_0}{e^{2(p+1)v_1}}\right]\left[\zeta - \frac{e^{2(p+1)v_1}}{\overline{\zeta}_0}\right][\zeta - e^{2(p+1)v_1}\overline{\zeta}_0]\right\} - \frac{2m}{k_2}\left\{\sum_{q=1}^{\infty}{}'\mu^q\log\left[\zeta - \frac{1}{e^{2qv_1}\overline{\zeta}_0}\right] + \sum_{q=1}^{\infty}{}'\mu^{q+1}\log\left[\zeta - \frac{\zeta_0}{e^{2(q+1)v_1}}\right]\left[\zeta - \frac{e^{2(q+1)v_1}}{\zeta_0}\right][\zeta - e^{2(q+1)v_1}\zeta_0]\right\} - \frac{2m}{k_2}\log[\zeta - \zeta_0] + \frac{2m}{k_3}\log\zeta$$

where Σ refers to even powers, Σ' to odd powers, $\mu = (k-1)/(k+1)$, $k = k_2/k_3$, $\zeta = ie^{v-iu}$, and ζ_0 is the point in the ζ-plane corresponding to the point z_0 in the z-plane.

These formulae give an infinite image system for the fields due to a line-charge inside a dielectric elliptic cylinder, and can be generalized for several such internal singularities in a manner similar to that indicated in Section 4.

For an elliptic conducting system with internal electrodes, we set $\mu = 1$ in the result for w_i, but if the boundary is itself an electrode we put $\mu = -1$, $k_3 = \infty$.

6. PARABOLIC ELECTRODE SYSTEM

The method described in Section 5 can also be applied to obtain corresponding expressions for a parabolic cylinder. The transformations

$$z = t^2, \quad \zeta = e^{-it}, \quad \text{where} \quad t = \alpha + i\beta,$$

are such that $\beta = \text{constant} = \beta_1$, say, gives a parabola in the z-plane which becomes a circle of radius e^{β_1} in the ζ-plane. The limits of α, β are given respectively by

$$-\infty \leqslant \alpha \leqslant \infty \quad \text{and} \quad 0 \leqslant \beta \leqslant \infty.$$

The limiting case $\beta = 0$ becomes the positive x-axis in the z-plane and the unit circle in the ζ-plane.

Let there be a line-charge m inside the parabola $\beta = \beta_1$ at the point $z = z_0$, then using the procedure of Section 5, we have to split into two parts the function $h(\zeta) = -(2m/k_2)\log(t-t_0)$, where t_0 is the point corresponding to z_0.

The results, which again involve infinite series of logarithmic functions, will not be given here as they follow the same pattern as those of Section 5. As before, for an electrode system in which the parabolic boundary is an electrode we set $k_3 = \infty$, $\mu = -1$ in the expression obtained for w_i, and for internal electrodes, we put $\mu = 1$.

In conclusion, it should be noted that whilst the solutions to some of the cases discussed can be obtained directly by the usual methods of images and inversion, the approach indicated in this paper gives a simple treatment of a more general character. All the results given normally converge with reasonable rapidity, although it may be found that certain problems can lead to slowly convergent series.

REFERENCES

(1) AWBERY, J. H. *Phil. Mag.*, **3**, p. 674 (1932).
(2) DAYMOND, S. D. *Quart. J. Mech. Appl. Math.*, **4**, p. 23 (1951).
(3) JONES, E. E. *Brit. J. Appl. Phys.*, **6**, p. 88 (1955).

Electrode shapes for a cylindrical electron beam

By P. N. Daykin, M.A., Ph.D., Research Laboratories, The General Electric Co. Ltd., Wembley, Middlesex

[*Paper first received* 22 *December, and in final form* 5 *April*, 1955]

The problem of obtaining the electrode shapes which will maintain a cylindrical beam of space-charge limited current reduces to the problem of solving Laplace's equation for the electrostatic potential outside the space-charge region, with the appropriate boundary conditions on the surface of the beam. A new approximate analytical solution of the Laplace equation has been obtained, and numerical tables have been developed for designing the electrode shapes. A plot of the electrode shapes, which is applicable to either hollow or solid beams, has been drawn up. The shape of the outside electrodes is the same for either type of beam, but the hollow beam requires an additional set of electrodes located inside the beam. The shape of the outside electrodes agrees fairly well with that obtained previously by Pierce,(1) Harrison,(2) and Kuo Chu Ho and Moon.(3)

The problem of obtaining the electrostatic field configuration which will maintain a constant-radius cylindrical beam of space-charge limited electron current may be restated briefly as follows. Within the beam the potential and the charge density are determined by the equations:

$$|d^2V(z)/dz^2 = 4\pi|\rho(z)| \tag{1}$$

$$J = |\rho|v_z = \text{constant} \tag{2}$$

$$v_z = \sqrt{(2e/m)}\sqrt{V} \tag{3}$$

In these equations and the following equations z is the axial distance from the cathode and r is the cylindrical radius. Equation (3) is valid provided initial thermal velocities can be neglected. The potential V then follows the well-known 4/3 power law.

$$V = Az^{4/3} \tag{4}$$

$$A = [9\pi J(m/2e)^{1/2}]^{2/3} \tag{5}$$

Outside the space-charge region the potential is a solution of Laplace's equation with the boundary conditions from equation (4)

$$V = Az^{4/3}, \quad \partial V/\partial r = 0 \tag{6}$$

on the surface of the beam. In the case of a hollow beam, the boundary conditions apply to both the inner and outer surfaces of the beam.

The solid beam problem was first stated, and solved approximately in the electrolytic tank, by Pierce.(1) A rather approximate analytic formula for the electrodes has been given by Harrison.(2) Further, a non-iterative numerical method has been described by Kuo Chu Ho and Moon.(3) However, an analytical solution, applicable where considerable accuracy is required, would be desirable. The desired solution, which has not before been available, is given here for both the solid and hollow beam.

THE SOLID CYLINDRICAL BEAM

For the region near the beam edge we can use an expansion of the form

$$V = Az^m\left[F_0\left(\frac{r}{a}\right) + \left(\frac{a}{z}\right)F_1\left(\frac{r}{a}\right) + \left(\frac{a}{z}\right)^2F_2\left(\frac{r}{a}\right) + \ldots\right]; \quad m = 4/3 \tag{7}$$

where a is the beam radius.

By substituting the series into Laplace's equation,

$$\frac{1}{r}\frac{\partial}{\partial r}r\frac{\partial V}{\partial r} + \frac{\partial^2 V}{\partial z^2} = 0 \tag{8}$$

and equating coefficients of like powers of z to zero, we find

$$\frac{1}{r}\frac{d}{dr}r\frac{dF_n}{dr} = 0; \quad n = 0, 1$$

$$\frac{1}{r}\frac{d}{dr}r\frac{dF_n + 2}{dr} = -(m-n)(m-n-1)F_n; \quad n = 0, 1, 2 \tag{9}$$

The boundary conditions are found from equation (6) to be:

$$F_0(1) = 1, \quad F_{n+1}(1) = 0, \quad (dF_n/dr)(1) = 0; \quad n = 0, 1, 2 \tag{10}$$

These equations can be solved exactly in order, giving

$$\left.\begin{aligned} &F_0\left(\frac{r}{a}\right) = 1, \quad F_{2n+1}\left(\frac{r}{a}\right) = 0 \\ &F_2\left(\frac{r}{a}\right) = \frac{-m(m-1)}{2^2}\left[\left(\frac{r}{a}\right)^2 - 2\log\left(\frac{r}{a}\right) - 1\right] \\ &F_4\left(\frac{r}{a}\right) = \frac{m(m-1)(m-2)(m-3)}{2^2.4^2} \times \\ &\quad\left\{\left(\frac{r}{a}\right)^4 - 8\left(\frac{r}{a}\right)^2\left[\log\left(\frac{r}{a}\right) - \frac{1}{2}\right] - 4\log\left(\frac{r}{a}\right) - 5\right\} \end{aligned}\right\} \tag{11}$$

The functions F_2 and F_4 are listed in Table 1. These do not agree with the corresponding approximate functions given by Harrison,(2) but a comparison of numerical values indicates

Table 1. *Cylindrical functions* F_2 *and* F_4

ξ	$F_2(\xi)$ (−)	$F_4(\xi)$ (+)
0·1	0·4016	0·0342
0·2	0·2508	0·0166
0·4	0·1103	0·0039
0·6	0·0423	0·0006
0·8	0·0096	0·0002
1·0	0·0000	0·0000
1·5	0·0488	0·0088
2·0	0·1793	0·0158
3·0	0·6448	0·2219
4·0	1·3586	1·020
5·0	2·309	3·022

that the corresponding functions approach equality for large r. With the aid of Table 1 and equation (7) the equipotential surfaces can be found near the beam edge. At the

beam edge the potential $V = Az_0^m$; the equipotential which cuts the beam at z_0 is then defined by the equation

$$z_0^m = z^m\left[1 + \left(\frac{a}{z}\right)^2 F_2\left(\frac{r}{a}\right) + \left(\frac{a}{z}\right)^4 F_4\left(\frac{r}{a}\right) + \ldots\right] \quad (12)$$

The simplest procedure seems to be to choose values of z_0 and r and solve equation (12) by trial for z.

Unfortunately, the expansion in cylindrical co-ordinates is divergent for large $(r - a)/z$. For the cathode surface it is quite useless and a different solution must be used. We note that the leading terms of the $a^n z^{m-n} F_n(r/a)$ are the expansion of the spherical harmonic:

$$(r^2 + z^2)^{2/3} P_{4/3}(\cos\theta)$$

where $P_{4/3}(\cos\theta)$ is the Legendre function of the first kind of order 4/3 and θ is arc tan (r/z). The spherical harmonic is well defined, although its expansion in powers of r/z is divergent for $r/z > 1$. These two facts suggest that we try a solution in spherical polar co-ordinates of the form

$$V = A\left\{R^m P_m(\cos\theta) + a^2 R^{m-2}[a_2 P_{m-2}(\cos\theta) + b_2 Q_{m-2}(R\cos\theta)] + \ldots\right\} \quad (13)$$

Here $R = (r^2 + z^2)^{1/2}$ and $R^{m-2}Q_{m-2}$ is any solution of Laplace's equation with a singularity of the form $\log(R\sin\theta)$. (It is not a spherical harmonic of the second kind since the latter has a singularity of the form $\log z$ as well.) Physically the meaning of the term in Q_{m-2} is clear; it is the potential which would arise from the space-charge if it were concentrated on the axis. The terms in the P_{m-n} represent the potential due to the electrodes and are non-singular on the axis (except at $z = 0$).

If we try the form

$$Q_m = \log\left(\frac{R\sin\theta}{a}\right) P_m(\cos\theta) + G_m(\cos\theta) \quad (14)$$

and substitute $R^m Q_m$ into Laplace's equation, we find that G_m must satisfy the inhomogeneous Legendre equation:

$$(1 - x^2)\frac{d^2G_m}{dx^2} - 2x\frac{dG_m}{dx} + m(m+1)G_m = -2_m P_m(x) + 2x\frac{dP_m}{dx} \quad (15)$$

where $x = \cos\theta$. In solving for G we can, without loss of generality, choose the boundary condition $G(1) = 0$. Any other boundary condition, $G(1) = \alpha$, would be equivalent to replacing Q_m by $Q_m + \alpha P_m$, and would alter the coefficient a_2 in equation (12).

The first two terms of the expansion (13) will be sufficient to allow an accurate joining on with the expansion (7). To find a_2 and b_2 we expand equation (11) in r/z to order z^{m-2}. We obtain

$$V = Az^m\left[1 - m\frac{(m-1)}{4}\left(\frac{r}{z}\right)^2 + a_2\left(\frac{a}{z}\right)^2 + b_2\left(\frac{a}{z}\right)^2 \log\left(\frac{r}{a}\right) + \ldots\right] \quad (16)$$

The boundary conditions (6) for $r = a$ determine a_2 and b_2:

$$a_2 = m\frac{(m-1)}{4} = \frac{1}{9}; \quad b_2 = m\frac{(m-1)}{2} = \frac{2}{9} \quad (17)$$

The functions $P_{4/3}(\cos\theta)$, $P_{-2/3}(\cos\theta)$ and $G_{-2/3}(\cos\theta)$ are listed in Table 2. In Table 2 the first and second derivatives of $P_{4/3}$, computed by the central difference method, are included for reasons which appear below. The functions were computed from the Taylor series which was obtained from the corresponding Legendre equation. Up to nine terms were used and the remainder of the series was replaced, with sufficient accuracy, by a geometrical series and summed to infinity. The calculation of the coefficients in the Taylor series was verified, for the $P_{4/3}$ and $P_{-2/3}$, by comparison with the formula[4]

$$P_m(0) = -\tfrac{1}{2}\pi^{-3/2}\sin m\pi\,\Gamma\left(\frac{m+1}{2}\right)\Gamma\left(-\frac{m}{2}\right) \quad (18)$$

The asymptotic form of the equipotentials, for large R, is found by dropping all but the first term in (13). By a second order interpolation the root of the equation

$$P_{4/3}(\cos\theta) = 0 \quad (19)$$

is found for θ equal to 74° 10′. The cathode electrode is therefore asymptotic to a cone with this half angle. This agrees with the asymptotic value of approximately 75° found by Pierce.[1] The remaining asymptotes are found by solving the equation

$$V = Az_0^{4/3} = AR^{4/3}P_{4/3}(\cos\theta) \quad (20)$$

which gives

$$R = (r^2 + z^2)^{1/2} = z_0[P_{4/3}(\cos\theta)]^{-3/4} \quad (21)$$

Here z_0 is the intercept of the asymptote with the z-axis. Values of r/z_0 and z/z_0 are given in Table 3, with $\cos\theta$ as argument.

Table 2. *Legendre functions of order 4/3 and −2/3*

x	$P_{4/3}(x)$	$P'_{4/3}(x)$	$P''_{4/3}(x)$	$P_{-2/3}(x)$	$G_{-2/3}(x)$
1·0	1·0000	1·556	0·43	1·0000	0·000
0·9	0·8466½	1·511	0·45	1·0114½	0·062
0·8	0·6978	1·464	0·48	1·0235½	0·137
0·7	0·5538	1·414	0·50	1·0364½	0·227
0·6	0·4148½	1·363	0·53	1·0502	0·335
0·5	0·2813	1·308	0·57	1·0649	0·462
0·4	0·1535	1·248	0·62	1·0807½	0·610
0·3	0·0319½	1·183	0·67	1·0979½	0·785
0·2	−0·0829½	1·113	0·74	1·1166	0·990
0·1	−0·1905	1·035	—	1·1370½	—
0·0	−0·2898	—	—	1·1596	—
0·2728	0·0000	1·165	—	1·1030	0·839

Table 3. *Asymptotic form of the equipotential surfaces*

$\cos\theta$	r/z_0	z/z_0
1·00	0·000	1·000
0·90	0·548	1·020
0·80	0·785	1·048
0·70	1·110	1·090
0·60	1·550	1·161
0·55	1·847	1·216
0·50	2·245	1·295
0·45	2·812	1·417
0·40	3·72	1·627
0·35	5·63	2·10
0·325	7·70	2·63
0·30	12·62	3·97

Since the second term in equation (13) is less than 10% of the leading term for $R > 2a$, it may be treated as a small correction. If we regard equation (20) as determining the value of θ for given R, z_0, then the correction $d\theta$ due to the inclusion of the second term in equation (13) is given by

$$\frac{Rd\theta}{a} = \left(\frac{a}{r}\right)[P'_{4/3}(\cos\theta)]^{-1}\left[\frac{1}{9}P_{-2/3}(\cos\theta) + \frac{2}{9}Q_{-2/3}(\cos\theta)\right] \tag{22}$$

Having plotted first the asymptotes, the corrected equipotential surfaces are obtained by using equation (22). The corrected surfaces join on with the portions computed from equation (7); the plotted surfaces are shown in the figure. For the solid beam, the continuation of the surfaces inside the beam should be ignored.

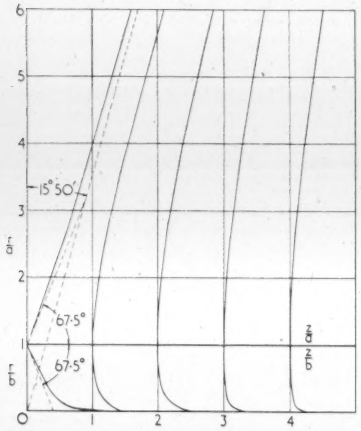

Electrode shapes for the solid and hollow cylindrical beam

The plot refers to a hollow beam with outer radius a and inner radius b. The electrode shapes are plotted in terms of r/a and z/a for $r > a$ and in terms of r/b and z/b for $r < b$. Broken lines are asymptotes or tangents. For the solid beam the inner electrodes should be omitted.

A solution is still required for the part of the cathode surface near the edge of the beam. It is convenient to introduce the polar co-ordinates:

$$R^* = [z^2 + (r-a)^2]^{1/2}, \quad \theta^* = \arctan(r-a)/z \tag{23}$$

so that Laplace's equation becomes

$$\frac{1}{R^*}\frac{\partial}{\partial R^*}R^*\frac{\partial V}{\partial R^*} + \frac{1}{R^{*2}}\frac{\partial^2 V}{\partial \theta^{*2}} = -(a + R^*\sin\theta)^{-1}\left(\sin\theta^*\frac{\partial V}{\partial R^*} + \frac{\cos\theta^*}{R^*}\frac{\partial V}{\partial \theta^*}\right) \tag{24}$$

A solution in ascending powers of R^* has the form

$$V = R^{*m}\cos m\theta^* + R^{*+1}(4a)^{-1} \times \left[\sin(m-1)\theta^* - \frac{m-1}{m+1}\sin(m+1)\theta^*\right] + (2a)^{-2}R^{*m+2}\left[\frac{1}{m(m+1)}\cos(m+2)\theta^* + \frac{1}{m+1}\cos m\theta^* - \frac{1}{m}\cos(m-2)\theta^*\right] + \ldots; \quad m = 4/3 \tag{25}$$

which is valid for $R^* < a$. The cathode surface is therefore tangent to a cone of half angle 67·5° as previously found by Pierce, and the half angle gradually increases to 74° 10′. The correction $d\theta^*$ to be added to the value of 67·5° is given for small R^*/a, by

$$md\theta^* = \frac{R^*}{2a}(m+1)^{-1}\sin 22{\cdot}5^\circ - \left(\frac{R^*}{2a}\right)^2\frac{m+2}{m(m+1)}\cos 45^\circ \tag{26}$$

The final plot appears to agree fairly well with the previous results of Pierce, Harrison, and Kuo Chu Ho and Moon.

THE HOLLOW CYLINDRICAL BEAM

For a hollow beam of outer radius a and inner radius b the outer equipotential surfaces are identical with those shown for the solid beam, but there must be an additional set of electrodes located in the charge-free space inside the beam. For the inner equipotentials the expansions (7) and (25) can be used if a is replaced by b. In using equation (25) it should be noted that θ^* is negative and therefore the correction $d\theta^*$ has the effect of reducing $|\theta^*|$ from the 67·5° value. The differential formula corresponding to equation (26) is

$$md\theta^* = \frac{R^*}{2b}(m+1)^{-1}\sin 22{\cdot}5^\circ + \left(\frac{R^*}{2b}\right)^2\frac{m+2}{m(m+1)}\cos 45^\circ \tag{27}$$

The inner equipotentials have the shape of a cone with a spike of decreasing radius extending along the z-axis. For small r/b the radius of the spike is given by

$$r/b = \exp\left\{\frac{9}{2}\left(\frac{z}{b}\right)^2\left[1 - \left(\frac{z_0}{z}\right)^{4/3}\right] + \frac{1}{2}\right\} \tag{28}$$

which is obtained from equations (7) and (11).

The complete set of equipotentials for the charge-free regions is exhibited for convenience as a single plot in the figure. It should be noted, however, that the scales of the plot are different for $r > a$ and $r < b$. In practice the cathode spike could probably be replaced by a self-supporting cylinder cut off short of the anode without introducing appreciable error into the field.

REFERENCES

(1) Pierce, J. R. *J. Appl. Phys.*, **11**, p. 548 (1940).
(2) Harrison, E. R. *Brit. J. Appl. Phys.*, **5**, p. 40 (1954).
(3) Kuo Chu Ho and Moon, R. J. *J. Appl. Phys.*, **24**, p. 1186, 1953.
(4) Magnus, W., and Oberhettinger, F. *Formeln und sätze fur die speziellen functionen der mathematischen physik*, p. 79 (Berlin: Springer-Verlag, 1948).

A germanium point-contact transistor to operate at high ambient temperatures

By A. F. Gibson, Ph.D., J. W. Granville, Ph.D., and W. Bardsley, Ph.D., A.Inst.P., Grad.I.E.E., Radar Research Establishment, Great Malvern, Worcs.

[*Paper first received* 4 *March, and in final form* 1 *April*, 1955]

Under suitable conditions, minority carriers can be swept out of a bar of germanium by application of an electric field. The density of minority carriers is kept small and one of the causes of the large temperature coefficients of transistor characteristics, namely the rapidly increasing density of minority carriers with increasing temperature, is suppressed. This paper describes the application of this technique to germanium point-contact transistors. A significant improvement in high temperature performance and speed of operation is obtained at the cost of increased complexity in assembly.

In a previous paper[1] a process called 'carrier extraction' is described. Since this paper was written it has been pointed out that the term 'extraction' was used originally by Banbury[2] to describe another phenomenon also associated with the reduction in density of minority carriers in semiconductors. To prevent confusion, it has been decided to rename the process described by the above authors 'carrier exclusion.' Briefly this process is as follows.

If a voltage is applied to a bar of *n*-type germanium the minority carriers (holes) are swept out at the negative electrode and an equal number of electrons at the positive electrode. Provided that holes are *excluded* from entering at the positive electrode, i.e. the injection ratio is nearly zero, and that the transit time of holes along the bar is less than the hole lifetime, the hole density in the bar is considerably reduced. Thus, the minority carrier exclusion technique maintains a hole density small compared with the electron density (due to impurities) at all temperatures.

In both junction and point-contact transistors the most troublesome effect at high temperatures is the rapid increase with temperature of the collector current at zero emitter current (i_{c0}). This causes a shift of the operating point of the transistor, a reduced 'on' to 'off' collector current ratio in point-contact switching transistors and ultimately a self-cumulative increase in collector current which burns out the collector contact. As the increase of i_{c0} at high temperature is caused by an increase in the minority carrier density, it is clear that these disadvantages can be overcome by the use of exclusion techniques.

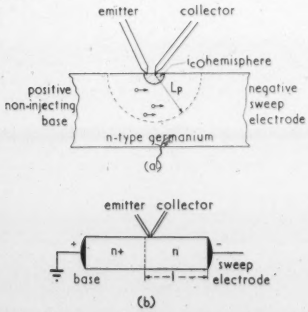

Fig. 1. (*a*) Schematic diagram illustrating the i_{c0} hemisphere and the diffusion length hemisphere

(*b*) The experimental arrangement used in the transistor tests

The application of carrier exclusion to a point-contact transistor is illustrated in Fig. 1(*a*). The collector contact collects holes by two main processes, namely field flow and diffusion flow. Within the smaller hemisphere the current density (due to i_{c0}) is large and hence the electric field is large. All holes generated in or injected into this region reach the collector quickly without significant recombination. Outside this hemisphere the holes travel mainly by diffusion, and in the absence of external fields the collector receives holes generated within a diffusion length of the contact. This division of the collector region into an i_{c0} hemisphere and a diffusion length hemisphere is rather arbitrary, but is convenient for the present discussion. Holes that are thermally generated within the i_{c0} hemisphere are controlled by the strong collector field and are not influenced by the comparatively weak sweep field when this is applied. On the other hand, in the diffusion length hemisphere where the collector field is weak, the thermally generated holes are removed by the sweep field.

An "exclusion point-contact transistor" has the structure shown in Fig. 1(*b*). A region of very low resistivity is necessary at the positive terminal to reduce end injection to negligible proportions.

On the Design of Transistors Utilizing the Principle of Carrier Exclusion

The approximate voltage required to reduce the hole density in *n*-type germanium to half its original value is given in the previous paper[1] as

$$V_s = (kT/q)(l/L_p)^2$$

where $kT/q = 0{\cdot}026$ V at room temperature, l is the length of the germanium bar [see Fig. 1(*b*)] and L_p is the diffusion length of holes in the *n*-type germanium. Despite the approximations made, the equation has been found to be in good agreement with experiment over a wide range of resistivity, diffusion length, specimen length and temperature.

When a sweep voltage is applied to a transistor so as to cause carrier exclusion, it is desirable that this voltage should be several times larger than V_s. The sweep current is, of course, a function of the sample dimensions, resistivity and temperature, and was typically a few milliamperes in the units studied.

The density of the holes not swept out of the bar by the field is not uniform but increases towards the negative terminal. For sweep voltages appreciably greater than V_s

the hole density increases from zero (ideally) at the non-injecting positive base terminal to $p_0 t/\tau$ at the negative base terminal, where p_0 is the initial hole density without exclusion, t is the transit time and τ is the hole lifetime. This effect makes it desirable to place the emitter and collector contacts as near as possible to the positive base terminal, typically within 0·5 mm. Furthermore, a line joining the emitter and collector contacts should be parallel to the long edge of the bar with the emitter nearest to the positive base terminal. The results of these arrangements are that (i) the sweep field has the maximum effect on the transistor, (ii) the current gain α is maintained as large as possible, (iii) the base resistance r_b is reduced and (iv) the biasing of the emitter and collector relative to the base by the sweep field is kept to a low value.

In germanium specimens of the dimensions used, the lifetime τ, and hence the diffusion length L_p, are primarily determined by the surface recombination velocity. It was found that the surface recombination velocity increased markedly with time of exposure to air at elevated temperatures (of the order of 100° C). For this reason, the surfaces were allowed to "age" to obtain consistent results. Thus the performances of the experimental transistors to be described could be improved by using suitable encapsulation techniques.

EXPERIMENTAL CONDITIONS

Germanium bars of rectangular cross-section were used in the transistor tests as the voltages and currents necessary to reduce the hole density could be calculated simply. Other geometrical configurations are possible for exclusion transistors but these were not investigated.

Comprehensive tests of the performances of exclusion transistors were made using 8 Ω.cm, 50 μs hole lifetime n-type germanium on to which a heavily doped 0·01 Ω.cm n-type region had been grown. Specimens of bar form with pure regions of typical dimensions $2 \times 0{\cdot}5 \times 0{\cdot}5$ mm were cut from this material so that in each bar the $n/n+$ junction was normal to the axis of the bar. The $n+$ region was connected to the positive terminal of the sweep voltage. This terminal was also the "base terminal" of the transistor. The sweep voltage was 2 V in all the tests unless otherwise stated. It might be pointed out that non-injecting end connexions can be made by using antimony/lead alloy solders. However, these were not tested in the transistor experiments.

All the transistors were made on a micro-manipulator. The point assembly and the germanium were enclosed under a small glass dome to exclude draughts, but otherwise were open to the air.

HIGH TEMPERATURE TESTS

Fig. 2 shows i_{c0} as a function of temperature for a transistor with and without carrier exclusion. Taking the maximum allowed value of i_{c0} as say 1 mA, the effect of exclusion is to increase the maximum temperature limit of the transistor by about 30° C.

Fig. 3 shows a full set of characteristics for a typical transistor at 105° C with and without carrier exclusion. The collector was formed in the usual manner. The displacement of the characteristics from the origin when the sweep field is applied is caused by the voltage gradient along the bar. The transistor parameters for this set of characteristics are given for the swept condition taking as an operating point: $V_c = -8$ V, $I_c = -2$ mA, $V_e = 0{\cdot}11$ V and $I_e = 0{\cdot}5$ mA.

$$
\begin{aligned}
r_{11} &= 400\ \Omega \\
r_{22} &= 15\,000\ \Omega \\
r_{21} &= 36\,000\ \Omega \\
r_{12} &= 50\ \Omega \\
\alpha &= 2{\cdot}4 \\
\text{maximum power gain}^{(3)} &= 60 \\
\text{voltage gain} &= 49
\end{aligned}
$$

This is an excellent performance for a germanium transistor at 105° C when i_{c0} for this operating point is only 1·1 mA and the transistor has been aged in air to obtain consistent results.

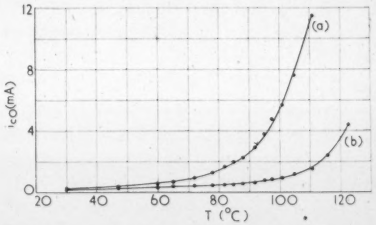

Fig. 2. i_{c0} as a function of temperature for a transistor (b) with, and (a) without carrier exclusion. $V_c = 8$ V

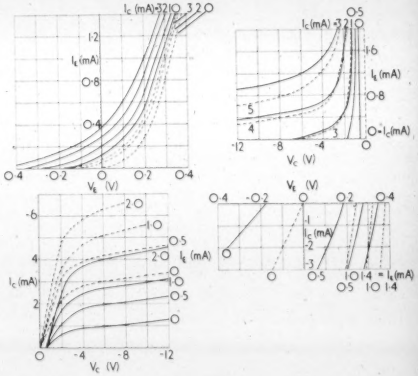

Fig. 3. A set of characteristics of a germanium transistor at 105° C with and without exclusion
——— = with exclusion; - - - - - = without exclusion.

HOLE STORAGE MEASUREMENTS

When the emitter current of a transistor is suddenly reduced to zero, the collector current does not decrease instantaneously but suffers a delay which can be several microseconds in point type transistors. This effect is known as hole storage and arises in the following manner. Consider an emitter which is suddenly turned off with a small negative pulse. At

the time of turn off, the holes from the emitter are travelling by various paths to the collector and those outside the i_{c0} hemisphere are travelling mainly by diffusion. It is the relatively slow diffusion of these holes to the collector which maintains a collector current greater than i_{c0} for several microseconds when the emitter current is zero. If a sweep field exists in the transistor, the holes which would have travelled to the collector by diffusion are swept out at the negative electrode and the hole storage effect is reduced. This reduction has been confirmed experimentally.

Relative changes in the hole storage effect were observed using the circuit shown in Fig. 4. The emitter is grounded

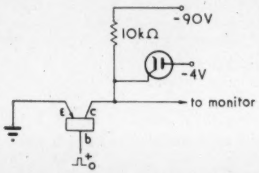

Fig. 4. Circuit used to test the hole storage effect

and a positive going pulse of about 4 V is applied to the base. The collector is connected to a thermionic catching diode to limit the collector voltage swing. Fig. 5 shows voltage waveforms obtained at the collector of a typical

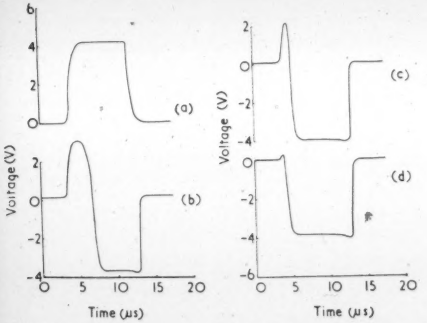

Fig. 5. Waveforms obtained in the hole storage tests

(*a*) Input pulse to base. (*b*) Collector pulse, no exclusion. (*c*) Collector pulse; sweep voltage = 1·5 V, sweep current = 2 mA. (*d*) Collector pulse; sweep voltage = 6 V, sweep current = 7 mA.

transistor with different sweep voltages applied. The magnitude of the pip which follows the leading edge of the pulse is a function of the hole storage. With no sweep field a large pip is obtained and its reduction is proportional to the magnitude of the applied sweep voltage.

SMALL SIGNAL FREQUENCY RESPONSE

The cut-off frequency of a transistor is usually defined as the frequency at which the current gain α, falls to $1/\sqrt{2}$ of its low frequency value. In a point-contact transistor the decrease of α at high frequencies is caused by the random phase of the holes arriving at the collector. Holes leaving the emitter set out in all directions and those leaving the emitter in the opposite direction to that of the collector will have longer paths to travel before reaching the collector. The sweep field in an exclusion transistor is of the correct polarity to assist the transfer of these long path length holes to the collector and should improve the frequency response of the transistor. This improvement has been confirmed experimentally.

Fig. 6 shows the α *versus* frequency curves for a transistor with and without carrier exclusion. When the sweep field is

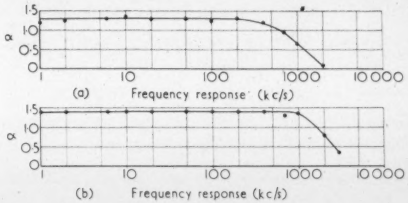

Fig. 6. Frequency response of α for a transistor with and without carrier exclusion. Point separation = 6×10^{-3} in.

(*a*) Without exclusion. (*b*) With exclusion.

applied, α remains constant up to higher frequencies and the cut-off frequency is raised. The degree of improvement is a function of the point spacing as shown in Fig. 7. For point spacings less than about 0·002 in. the cut-off frequency is not improved by the use of carrier exclusion. This limitation

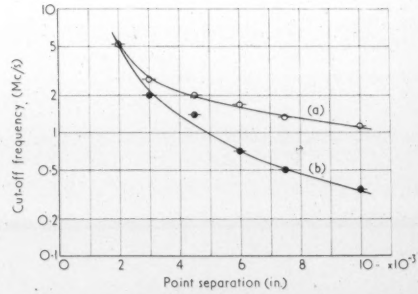

Fig. 7. The cut-off frequency as a function of point spacing for transistors, (*a*) with, and (*b*) without carrier exclusion. (8 Ω.cm germanium)

can be explained by assuming that when the points are very close together the emitter contact lies within the i_{c0} hemisphere so that all the holes travel to the collector under the influence of the collector field. This field is large compared with that due to the sweep voltage and the effect of the latter on the path lengths of the emitted holes is negligible.

NOISE

The reason for the large noise factor of a point-contact transistor is not known at present. There was the possibility that the sweep current used in an exclusion transistor might provide an additional source of noise. Therefore, the noise factors of several transistors were measured at room temperature and at elevated temperatures for various values of sweep current. The test frequency was 1 kc/s. It was found that exclusion did not cause any change in the noise factor which was of the order of 50 dB under all test conditions. The invariance of the noise factor with sweep voltage suggests that it is independent of the minority carrier density outside the i_{c0} hemisphere.

DISCUSSION AND CONCLUSIONS

Although the technique of exclusion improves the performance of point-contact transistors, it cannot be successfully applied to junction transistors. For point-contact transistors, the majority of the emitted holes flow to the collector in the strong electric field set up by i_{c0} and the comparatively weak sweep field has negligible effect on them. Thus, the transistor performance is not impaired. On the other hand, in a junction transistor holes flow from emitter to collector primarily by diffusion, and if a sweep field existed in the base region they would be swept out and the current gain α of the transistor would be reduced. Even a small decrease of α in a junction transistor would seriously impair its performance. It may be noted, however, that the exclusion technique can be applied successfully to a junction *diode* and a marked decrease in its hole storage is obtained.

Exclusion point-contact transistors have the following advantages:

(i) a point-contact transistor capable of safe operation up to at least 100° C can be made using germanium;

(ii) Compared with a conventional germanium point-contact transistor, an exclusion transistor with the same point spacing has reduced hole storage;

(iii) the cut-off frequency is increased by carrier exclusion for point spacings greater than 0·002 in.;

(iv) the techniques necessary to produce exclusion germanium transistors in quantity are all well known.

These advantages are obtained, however, at the following costs:

(*a*) it is necessary to have an additional power supply of a few volts (typically 2 V) delivering a few milliamperes (typically 1·5 to 6 mA) to each transistor. This power consumption is about 20% of the total power consumption of the transistor under typical operating conditions;

(*b*) the construction of each transistor is made more complicated in that, not only must the points be closely spaced, but they must be placed near a particular part of the crystal.

ACKNOWLEDGEMENTS

The authors are indebted to their colleagues in the transistor group of this establishment for their advice and help. The paper is published by permission of the Chief Scientist, Ministry of Supply, and the Controller, H.M. Stationery Office.

REFERENCES

(1) ARTHUR, J. B., BROWN, M. A. C. S., BARDSLEY, W., and GIBSON, A. F. *Proc. Phys. Soc.* [*London*] *B*, **68**, p. 43 (1955).

(2) BANBURY, P. C. *Proc. Phys. Soc.* [*London*] *B*, **66**, p. 50 (1953).

(3) SHOCKLEY, W. *Electrons and Holes in Semiconductors*, p. 45 (New York: D. Van Nostrand Co. Inc., 1950).

The determination of the dynamic properties of crystal diodes

By G. STUART-MONTEITH, B.Sc., A.M.I.I.A., Grad.Inst.P., Royal Naval Scientific Service

[*Paper received* 15 *February*, 1955]

The a.c. properties of a crystal diode biased in the forward direction are discussed, and are shown to depend both on the frequency and magnitude of the applied voltage. A method is given for determining the dynamic resistance, the results obtained agreeing with the theory.

There are three methods by which crystal diodes have been used in amplifiers to impart non-linear characteristics. The first method makes use of the property that the dynamic or a.c. resistance of a crystal varies with the quiescent or d.c. current passing through it, and hence the transmission loss of an attenuation pad, in which crystals are incorporated, may be varied by means of a d.c. control current.[1,2] The second application merely uses the diode as a voltage-controlled switch to introduce either an attenuating resistance or feedback.[3] The third method combines both properties, the crystal shunting a high resistance so that when the diode is conducting the high resistance is by-passed by the low resistance of the crystal, and when the control voltage causes conduction to cease, the high resistance is introduced.[4]

In all these methods the dynamic properties of the crystal are important, and this paper briefly discusses these properties, and gives a method of determining the dynamic resistance for low values of bias current, so that this parameter may be measured under the same conditions under which the crystal will be working.

GENERAL PROPERTIES OF A CRYSTAL DIODE

The simplest equivalent circuit for a crystal diode[5] that takes into account the known physical parameters is shown in Fig. 1. The circuit consists of a non-linear resistance R, shunted by a non-linear capacitance C (the barrier resistance and capacitance), these being in series with a linear resistance r, which is the "spreading resistance" in the semi-conductor, and which depends on the construction of the crystal. At zero bias the barrier resistance $R \gg r$ but it decreases as the current in the forward direction is increased, and ultimately becomes small compared with r.

Consideration of the voltage-current characteristic of a

crystal diode in the forward direction shows that it approaches closely to the ideal d.c. characteristic for small values of the applied voltage, that is, in the region where R is appreciable. The ideal characteristic is of the exponential form

$$i = A\left[\exp(\alpha E') - 1\right] \tag{1}$$

where i is the direct current, A and α are constants, and E' is the voltage across the barrier. The voltage E' is given by

$$E' = E - ir \tag{2}$$

where E is the voltage applied to the rectifier and r is the spreading resistance.

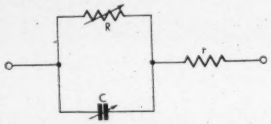

Fig. 1. Equivalent circuit of a crystal diode when biased in the forward direction

Differentiating equation (1), to obtain the dynamic barrier resistance R'

$$1/R' = di/dE' = \alpha A \exp(\alpha E') \tag{3}$$

but from equation (2)

$$dE' = dE - r.di \tag{4}$$

Therefore $R' = dE'/di = (1/\alpha A)\exp(-\alpha E')$ (5)

$$= (dE/di) - r = (1/\alpha A)\exp\left[-\alpha(E - ir)\right] \tag{6}$$

i.e. dynamic resistance of the diode

$$dE/di = R' + r = (1/\alpha A)\exp\left[-\alpha(E - ir)\right] + r. \tag{7}$$

Thus when the applied voltage is a periodic function, the dynamic resistance will depend upon frequency, and in general will not be the value obtained by determining the slope of the static characteristic curve.

This dependence of the dynamic resistance on frequency has in the past been investigated at radio frequencies; furthermore, it has been shown that the dynamic resistance is dependent upon the power expended in the crystal, that is, if $E' = E'' + E'''f(t)$ where E'' is a d.c. voltage and $E'''f(t)$ is a periodic voltage, then the value of dynamic resistance will depend on $E'''f(t)$.

When R becomes small compared with r the characteristic is no longer exponential and approaches a constant slope determined by the value of the spreading resistance.

The barrier capacitance C arises from the storage of charge in the boundary layer. Since the magnitude of the capacitance depends upon the thickness of the barrier layer, which in turn is a function of the applied voltage, the capacitance is non-linear. The large forward conductance and the presence of the spreading resistance makes a quantitative determination of the effect difficult, but in general it lies in the range 0·2 to 2·0 pF. Hence the shunting effect of its impedance may be neglected, except at very high frequencies.

DETERMINATION OF THE DYNAMIC RESISTANCE

A Wien's bridge circuit described in the literature[1] was first used, but as a meter for determining the quiescent current through the crystal was required, and also since the barrier capacitance made the balance point difficult to determine, the variation of the Schering bridge shown in Fig. 2 was used and found to be satisfactory for low values of the bias current where $R \gg r$.

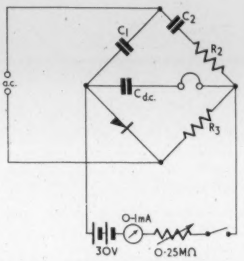

Fig. 2. Bridge circuit for determining the dynamic resistance. $C_{d.c.}$ is a d.c. blocking condenser having a high capacitance

Referring to Figs. (1) and (2) and neglecting r, then for balance:

$$\frac{1}{j\omega C_1}\Big/\left(R_2 + \frac{1}{j\omega C_2}\right) = \left(\frac{1}{1/R + j\omega C}\right)\Big/R_3 \tag{8}$$

i.e.
$$j\omega C_1\left(R_2 + \frac{1}{j\omega C_2}\right) = R_3\left(\frac{1}{R} + j\omega C\right). \tag{9}$$

Equating real and imaginary parts

$$R = (C_2/C_1) \times R_3; \quad \text{and} \quad C = (R_2/R_3) \times C_1 \tag{10}$$

thus the conditions for balance do not depend on frequency and, by making the variables C_2 and R_2, are independent of each other. In practice it was found that a very sharp and accurate measurement of R could be made by varying R_3, but the determination of C was, as predicted above, most difficult, only the order of the capacitance being determined.

With increase in the bias current R became comparable with r and a sharp minimum could no longer be detected, but the dynamic resistance could be plotted to show the asymptotic value of r.

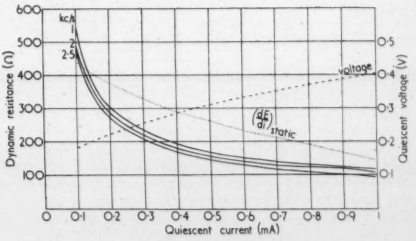

Fig. 3. Variation of dynamic resistance with current, for applied voltages of different frequency. The static voltage current characteristic is also shown, together with the dynamic resistance characteristic (dE/di) obtained from this curve

a.c. input to bridge = 1V r.m.s.

RESULTS

Using crystal diodes type CV425, the static voltage current characteristic together with the dynamic resistance obtained from the curve were plotted for a number of crystals. The dynamic resistance was then plotted against bias current at a number of audio-frequencies, a family of curves such as those shown in Fig. 3 being obtained in each case.

It will be observed that the dynamic resistance obtained experimentally is considerably less than that obtained from the static curves. In addition, it was also determined that the dynamic resistance depended upon the magnitude of the applied voltage. (It should be noted that in the bridge circuit C_1 was chosen to have a sufficiently high impedance so that the a.c. voltage across the crystal did not vary appreciably with frequency.)

ACKNOWLEDGEMENT

The work described in this paper was carried out at the Admiralty Signal and Radar Establishment, and the writer is indebted to the Admiralty for permission to publish this paper.

REFERENCES

(1) STANSEL, F. R. *Bell Lab. Record*, **31**, p. 501 (1953).
(2) FRACASSI, R. D. *Bell Lab. Record*, **31**, p. 452 (1953).
(3) BAXTER, I. G. *Electronic Engng*, **26**, pp. 97–99 (1954).
(4) HOLBROOK, G. W. *Electronics*, **25**, p. 200 (1952).
(5) TORRY, H. C., and WHITMER, C. A. *Crystal Rectifiers*, Radiation Laboratory Series, Vol. 15 (New York: McGraw-Hill Book Co. Inc., 1948).

Measurement of the pressure distribution between rollers in contact

By G. J. PARISH, B.Sc., The British Cotton Industry Research Association, Shirley Institute, Manchester, 20

[*Paper first received* 11 *January, and in final form* 11 *February*, 1955]

The measurement of pressure distribution in industrial rolling processes has hitherto been carried out only on roller systems of the fixed gap type. The apparatus described here extends the measurement to processes in which there is no fixed gap between the rollers, and also to appreciably lower loads than any previously studied. A radial pressure pin is mounted in one of the rollers and transmits the load on its outer end to a pressure-sensitive device situated within the roller. Provision has been made for the investigation by actual pressure-distribution measurement of the effect on recorded pressure of the height of the pressure pin relative to the roller surface and of depression of the pin under load. Pin depression has been found to cause erroneous pressure recording, and a method of correction has been developed.

The processes of calendering and mangling are used for a variety of purposes in the finishing section of the textile industry. However, the two processes are essentially similar in that in both the textile material is subjected to pressure by being passed between two rollers which are pressed together. A knowledge of the distribution of pressure between the rollers is therefore of fundamental importance to a study of these processes. Measurements of pressure distribution have been made in other industrial rolling processes[1–4]; but only in processes of the type having a fixed gap between the rollers. In the textile processes, on the other hand, there is no roller gap, which means that the nip (the area over which the roller load is distributed) is obtained in quite a different manner, as shown in Fig. 1. If there is no gap one of the rollers must be relatively soft, and the nip is formed largely by the indentation of this roller. The conditions in the nip depend not only on the properties of the rolled material, but also to a considerable extent on the composition of the soft roller. Calendering and mangling differ mechanically only in the load applied to the rollers and in soft roller composition; pressure distributions in both processes may thus be investigated on one machine.

The method of pressure-distribution measurement originated by Siebel and Lueg[1] consists in mounting a pressure-transmitting pin in a radial hole in one of the rollers, with its outer end flush with the roller surface and its inner end in contact with some pressure-sensitive device inside the roller. As the outer end of the pin passes through the nip the variations in load on it are transmitted to the pressure-sensitive device where they are converted into some form (such as electric current variations) which may be extracted from the roller and displayed to represent the original distribution of pressure. The accuracy of the method depends primarily upon the pressure pin, and errors may be expected to arise

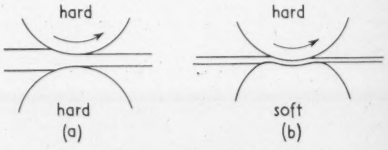

Fig. 1. The two types of nipping process
(*a*) fixed gap between rollers.
(*b*) no fixed gap.

both from a pin height differing from zero (flush with the roller surface) and from a relative movement of the pin face and the roller surface under load. An effect is to be expected from the first of these factors even though the compressibilities of pin and roller are equal. However, it is reasonable to assume that a pin having the same compressibility as the roller and set flush with the roller surface will correctly record the pressure distribution; this, indeed, has been the basis of

the previous investigations, pains being taken to reduce the relative compression of pin and roller to as small a value as possible. A few measurements have been reported by Smith, Scott and Sylwestrowicz[3] in which the pin, after calibration, instead of being ground flush with the roller surface was left slightly proud, but until the present investigation no systematic study of the effect of deviations from the ideal conditions had been made. To study these effects in the present apparatus the height of the pin is adjustable.

To convert the variations in load transmitted by the pressure pin into a form suitable for recording, the photoelastic method devised by Orowan, Scott and Smith[2] has been adopted. In this method a glass block situated at the roller axis is used as the pressure-sensitive device. Polarized light is passed down an axial bore in the roller, the source being stationary and mounted outside the roller. The light transmitted through the block is passed through an analyser and collected by a stationary photocell. The polarizer and analyser with their axes suitably orientated are fixed to the roller and rotate with it. In this way the load variations on the glass block are converted into intensity variations in the transmitted light. The high mechanical strength and negligible creep of glass make it the ideal photoelastic material for this purpose, and its low sensitivity is no disadvantage.

In their paper, Orowan, Scott and Smith derive the relationship between light intensity and applied load for the arrangement in which the polarizer and analyser are crossed and have their axes inclined at 45° to the axes of principal stress in the glass block. In the present application use has been made of some features of the general relationship for any analyser position. It is sufficient to quote this general relationship, which is

$$I = 4A^2[1 + \cos 2\theta \cos (KL/b)] \qquad (1)$$

Here I denotes the intensity of the light falling on the photocell, and A the amplitude of each of the polarized beams emerging from the glass block; L denotes the load on the block, b its breadth, and θ the angle between analyser and polarizer; K is a constant dependent upon the photoelastic properties of the glass. If the analyser is crossed with the polarizer ($\theta = \pi/2$)

$$I = 8A^2 \sin^2(KL/2b)$$

which is the relation given (with different notation) by Orowan, Scott and Smith. This is the working position of the analyser, and in order to obtain an approximately linear light intensity/load relationship the glass block must be pre-loaded to bring the working range into the central portion of this curve.

THE EXPERIMENTAL CALENDER

In an apparatus designed to give a quantitative measure of the pressure distribution in the nip it is desirable to be able to check the accuracy of the results obtained from direct calibration of the pressure pin by comparing them with some other measure of the load present; this will generally be the total load on the nip. In order to compare this total load with a single measurement of pressure distribution made at the centre of the roller face, it is necessary to ensure an even distribution of pressure along the nip. In the experimental calender, which has been built to house the pressure-recording equipment, roller deformation, the most serious cause of uneven pressure distribution in conventional machines, is overcome and an even distribution of pressure obtained by reducing the length of the working faces of the rollers to 15 in.

The experimental calender has three rollers, the outer two of which are of metal and remain permanently part of the machine. The centre position is occupied by the soft roller; soft rollers of various sizes can be accommodated. The 14 in. diameter mild steel top roller contains the pressure pin and glass block assembly, and the bearings in which it runs are fixed in position on the calender frame; load is applied hydraulically, the bottom and centre rollers being pushed up into contact with the top one. The drive to the machine is applied directly to a gear on the top roller shaft, the other rollers being driven through the forces at the nips.

THE PRESSURE RECORDING APPARATUS

The apparatus (Fig. 2) is required to cover mean nip pressures ranging from 100 to 8000 lb/in.^{2}, with nip widths between $\frac{1}{4}$ and $1\frac{1}{2}$ in. A rectangular pressure pin is used,

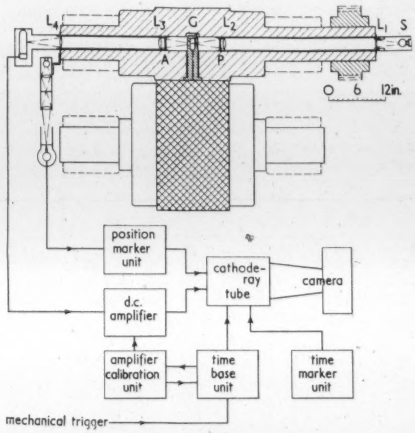

Fig. 2. Schematic diagram of the apparatus

S, light source; L_1–L_4, lenses; *P*, polarizer; *A*, analyser; *G*, glass block.

having a width (in the direction of rolling) of $\frac{1}{32}$ in. and a length of $\frac{1}{2}$ in. With these pin dimensions a glass block 1 in. wide with a stress optical coefficient of 2·5 brewsters will give a satisfactorily linear response at the highest load.

The time of passage of the pressure pin through the nip varies from $\frac{1}{30}$ to $1\frac{1}{2}$ s, and d.c. amplification between the photocell and the cathode-ray tube is essential. By using an efficient optical system it has been found possible, with a 12 V, 24 W bulb as the light source, to cover the required load range with an amplifier gain variable between 30 and 500 (a further range of gain may be obtained by varying the lamp voltage). The use of d.c. amplification also permits calibration of the apparatus by static loading of the pressure pin.

The functions of the auxiliary apparatus may be described briefly. The mechanical trigger to the time-base unit is obtained from a cam on the top roller. The time-marker unit provides periodic interruptions of the time-base trace in the usual manner. The position-marker unit provides three

equally-spaced markers on the trace, giving a scale in terms of peripheral or angular position of the top roller. The pulses are initially obtained by sweeping with a rotating narrow light beam across three slits mounted in front of a photocell, the units being so positioned that the centre pulse indicates the line of centres of the rollers. For display, twin pulses are generated from each of the primary pulses in such a way that the centre line of each pair corresponds to the peak of the primary pulse. To avoid confusion with the time-marker pulses the display pulses are applied not to the cathode-ray tube modulating electrode but to one of the Y-plates.

The amplifier calibration circuit is necessary because the gain of a d.c. amplifier varies appreciably with the operating conditions; the way in which the calibration is applied is described below.

THE PRESSURE PIN ASSEMBLY AND OPTICAL SYSTEM

As there is no fixed gap between the rollers of the experimental calender, the assembly of pressure pin and glass block must be mounted in the top roller in such a way that there are no sharp edges to damage the surface of the soft middle roller. This has been achieved by building the assembly into an insert unit which fits into a radial hole in the top roller surface, the upper surface of the insert forming a part of the roller surface. The insert is held in place by being bolted to the roller, and the recesses which take the bolt heads are filled in with a low melting-point alloy.

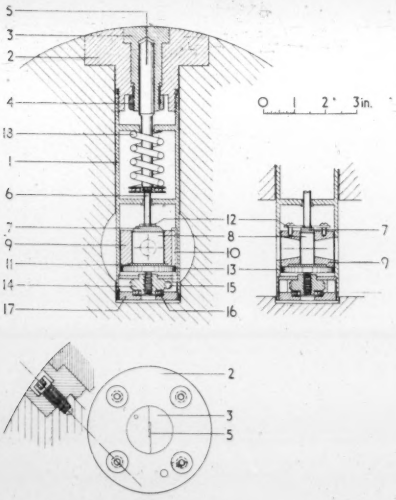

Fig. 3. Simplified diagram of the pressure pin and glass block assembly

The details of the pin assembly are shown in Fig. 3. The cylindrical tube (1), which contains the assembly, screws on to the cap (2), the pin turning in its bearings since its upper end is constrained by the slot through which it passes. This slot is cut in the minor cap (3), which is split for this purpose; this cap is held in the larger cap by the nut (4), its position being determined by a dowel pin. A similar pin locates the main cap on the roller.

The pin blade (5), of tool steel, protrudes $\frac{1}{2}$ in. from the pressure rod (6); the bottom end of this rod transmits the load to the glass block (8) through the cover plate (7). Pre-loading of the block is also applied through this cover plate by means of the stiff leaf spring (12).

The glass block itself is contained in the cylindrical block (9) which is free to slide in the tube (1) but is restrained by the guide (10) from rotating. This cylindrical member has conical holes drilled in it to allow the light beam to pass through. The bottom plate (11) on which the glass block rests, is firmly fixed to the cylindrical block, and pre-loading is accomplished by adjusting the screws which hold the leaf spring (12). Since this part of the assembly forms a single, removable unit, the pre-loading can be adjusted on an optical bench.

The plate (11), which supports the glass block, is itself supported by the plate (13), which is part of the pin-raising mechanism. This plate is continued below as a threaded rod on to which the pinion (14) is screwed. The pinion engages with a worm (15) and therefore, since the plate (13) is prevented from rotating by the guide (10), rotation of the worm raises or lowers this plate and hence the whole pin assembly. The combination of worm, pinion and thread gives a movement of $0{\cdot}9 \times 10^{-3}$ in. per turn of the worm. The thrust from the pressure pin, which is transmitted through the assembly to the pinion (14), is taken through the thrust race (16) to the bottom plate (17) which screws into the tube (1) to complete the assembly.

The mechanism for altering the pin height acts against the spring (18), which keeps the pressure rod in contact with the cover plate and the glass block unit in contact with the raising plate (13). This spring is of just sufficient strength to hold the units in position against their own weight. For calibration the pin must be raised slightly, but it is not necessary to raise it more than $\frac{1}{2000}$ in. above the roller surface; any increase of pre-loading due to compression of the spring is therefore negligible, as is the effect of movement of the centre of the glass block from the axis of the roller. The end of the worm shaft is of square section to enable the pin to be raised and lowered with the insert in the roller, and can be engaged by a control rod inserted down the axial bore of the roller.

The lenses and polarizers of the optical system are mounted in tubes which slip into the axial bore (see Fig. 2). The tube on the source side is permanently locked in position, but that on the photocell side is removable to enable the pin height control rod to be inserted; the photocell is mounted so that it can be swung to one side for this purpose. The flange on this tube has a simple locking device to locate the analyser in its correct angular position when replaced. A simple device is quite sufficient, since, at the crossed position, the analyser setting is not critical [equation (1)]. The position of the photocell also is not critical providing that all the light falls on its cathode; the calibration procedure adopted will correct for small changes in sensitivity due to changes in the response of the cell.

CALIBRATION PROCEDURE

The calibration of the apparatus consists in applying known loads to the pressure pin from a simple lever system and

measuring the deflexion obtained on the cathode-ray tube; the deflexion produced by a given pressure distribution can then be related to the load on the pin. This simple procedure can be invalidated by variations, in the interval between calibration and use, in the optical or the electronic part of the circuit. For this reason it is necessary to keep a check on the gain of the whole apparatus, which is done in the following manner. First, the photocell is made to act as its own monitor, by using the displacement from zero of the trace obtained with the pin not loaded as a measure of the light intensity. It is convenient to refer to this as the "standing light." In this way variations in the intensity of the light from the source and any variations in the optical system which affect the general intensity are allowed for. This includes compensation for variation in sensitivity of the cell itself, providing its response remains linear.

The gain of the electronic circuit is measured by the amplifier calibration unit, the calibration being carried out automatically after each time-base sweep. A series of stepped voltages is applied to the amplifier input and the time base is retriggered at each level. Six traces are obtained in this way and are photographed with the pressure-distribution record. The six equally spaced voltages are obtained from a chain of wire-wound resistors, the voltage applied to the chain being measured by a meter. Two potentiometers are used to adjust the zero level voltage and the magnitude of the voltage steps. The selection of the various calibration voltages in turn and the necessary time-base triggering are carried out by a relay circuit.

The monitoring of the optical system as so far described assumes that any variations will affect the general light intensity; that is, will affect equally both the "standing light" and the slope of the linear portion of the light intensity/load curve. However, there is one possible variation in the glass block assembly which will not have this effect; this is an alteration in the amount of pre-loading. A small reduction in the pre-loading would reduce the standing light but not alter appreciably the slope at the working point. Constancy of pre-loading can be checked by recording the light intensity with the analyser in the parallel position [which gives a cosine-squared relation, see equation (1)] as well as in the crossed position, since the ratio of parallel and crossed readings is dependent upon the amount of pre-loading.

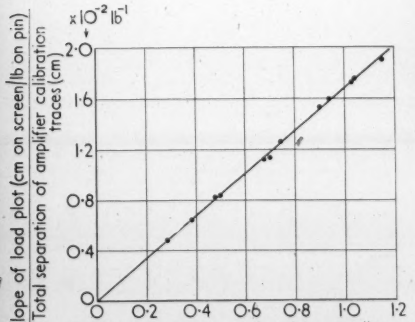

Fig. 4. Calibration curve

EXPERIMENTAL RESULTS

A typical calibration curve of the apparatus is shown in Fig. 4; this relates the slope of the load plot to the standing light value, both being expressed in terms of the amplifier calibration trace separations, for a given calibration input voltage. If the same voltage is used for amplifier calibration during pressure-distribution measurements this curve is used directly; if a different voltage must be used the appropriate correction is made.

Figs. 5(*a*) and (*b*) show two typical photographs of pressure distributions, the former being obtained with a soft roller of compressed cotton, the latter with a roller having a thin

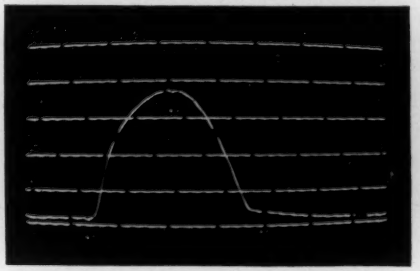

(*a*)

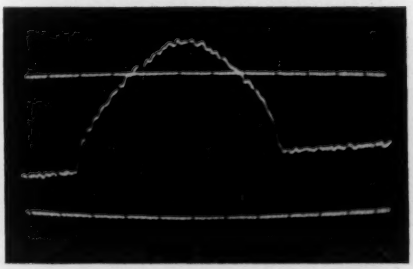

(*b*)

Fig. 5. Typical pressure records

Soft roller	(*a*) Compressed cotton	(*b*) Rubber layer on metal shell
Indicated roller loading (lb/linear in.)	1550	220
Roller speed (ft/min)	7	7
Pin height (in.)	−0·15	$-0{\cdot}05 \times 10^{-3}$
Amplifier calibration trace separations (lb)	20·5	7·15
Recorded peak load (lb on pin)	70·0	5·9
≡ (lb/in.²)	4480	380
Time marker period (ms)	80	80
Position marker horizontal separations (in.)	0·202	0·202

rubber covering on a metal shell. The slope of the base line in Fig. 5(*b*) represents a true variation in response of the photocell with rotation of the roller; it is due partly to polarization of the light from the source and partly to polarization sensitivity in the cell itself. The effect is a very small fraction of the mean value of the standing light, and it has not been found possible to reduce it significantly. The curvature of the calibration traces is due to the curvature of the cathode-ray tube screen affecting the linearity of photographic reproduction.

EFFECT OF HEIGHT OF THE PRESSURE PIN

It has been found that the height of the pin has a pronounced effect on the magnitude of the pressure record obtained. Fig. 6 shows a plot of recorded peak load against pin height, and it will be seen that for a small range of pin height about zero the relationship is effectively linear. The pin height on this graph is the height to which the face of the pin is set, relative to the roller surface, before each set of pressure measurements. The heights were measured with a dial gauge and are the means of readings taken before and after each set of measurements; they are repeatable to $0{\cdot}1 \times 10^{-3}$ in.

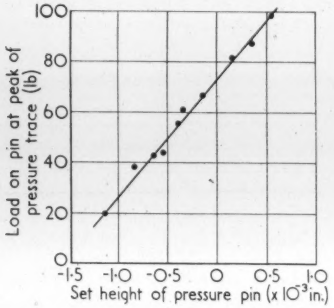

Fig. 6. Plot of peak recorded load against set height of pressure pin at a given roller loading

Each point is the mean of five records.

This variation of recorded peak load with pin height means that any depression of the pin under load will result in a distorted picture of the pressure distribution, and the effect may well be appreciable.

In addition to increasing the height of the pressure curve, an increase in pin height increases the base length of the curve (owing to earlier contact of the pin with the soft roller), but this second effect is very small and may be neglected. Furthermore, inspection of the curves recorded at different pin heights showed that the general shape of the curves is not affected by pin height in the small region about zero height. All the pressure curves recorded with a given roller loading can then be regarded as being on the same base and having the same general shape, differing from one another only in a vertical scale factor. As shown in Fig. 6, this scale factor varies linearly with the height of the pin. With this information it is possible to arrive at a correction for the effect of pin compression. Details of the correction are given in the appendix; the result is the following equation:

$$Pf(x) = p_0\phi(x)[1 - \alpha m\phi(x)]^{-1} \qquad (2)$$

where

$f(x)$ is the normalized true pressure distribution function,
$\phi(x)$ is the normalized recorded pressure distribution function,
P is the true peak pressure,
p_0 is the recorded peak pressure with the pin set to zero height,
α is the compressibility of the pin assembly,
and m is the slope of the straight line relating recorded peak load and pin height.

The value of α is determined from direct tests on the pin using the static loading system; the measured value of $5{\cdot}5 \times 10^{-6}$ in. depression per pound load on the pin is in good agreement with the value calculated from the compressibilities of the various units of the pin assembly. The values of p_0 and m are obtained for each set of measurements from a curve similar to that shown in Fig. 6, and the correction is applied point by point to the recorded pressure curve. The result of such a correction is indicated in Fig. 7 which

Comparison of loads per linear inch

The probable errors in the recorded measurements with the pin are increased in the corrected curves because of the relatively large errors in the determination of α and m. The errors in the pressure gauge measurements are affected considerably at lower loads by the reading accuracy of the gauge; pistons of smaller area were used in sets I, III and IV than in II, V, VI and VII. The value of α is $5{\cdot}5 \times 10^{-6}$ in./lb.

Soft roller composition		*Recorded peak pressure for zero pin height* (lb/in.²)	*Value of slope m* (lb/in.)	*Value of correction factor αm*	*Corrected peak pressure* (lb/in.²)	*Load per linear inch* (lb/in.) *A From recorded curve*	*B From corrected curve*	*C From pressure gauge on hydraulic line*	*Ratio B/C*
Rubber cover on metal shell	I	270	—	—	(270)	125 ± 5	(125 ± 5)	135 ± 10	0·93 ± 0·08
	II	415	$3{\cdot}6 \times 10^3$	—	(415)	235 ± 10	(235 ± 10)	210 ± 30	1·12 ± 0·16
	III	705	$6{\cdot}0 \times 10^3$	0·03	725	460 ± 15	470 ± 15	445 ± 15	1·05 ± 0·05
	IV	915	$7{\cdot}9 \times 10^3$	0·04	955	665 ± 20	690 ± 25	670 ± 15	1·03 ± 0·04
Compressed cotton	V	3400	$4{\cdot}9 \times 10^4$	0·27	4650	630 ± 20	820 ± 45	880 ± 50	0·93 ± 0·07
	VI	4800	$4{\cdot}3 \times 10^4$	0·24	6300	1250 ± 40	1550 ± 70	1600 ± 50	0·97 ± 0·06
	VII	5800	$6{\cdot}0 \times 10^4$	0·33	8650	1640 ± 50	2220 ± 130	2350 ± 60	0·95 ± 0·06

shows the pressure distribution of which Fig. 5(*a*) is one record.

The reliability of the apparatus and of the correction formula can be tested by comparing the integrated area under the corrected curve with the load per linear inch on the

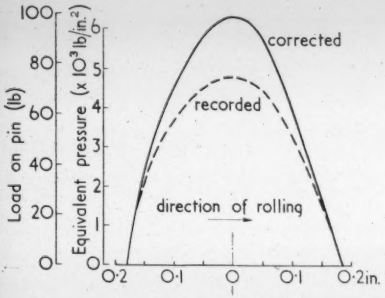

Fig. 7. Recorded and corrected pressure distributions

These distributions correspond to the photograph shown in Fig. 5(*a*) and to set VI of the measurements in the table.

nip (this load is simply the total roller loading divided by the length of the nip). A series of results is shown in the table, and satisfactory agreement is obtained in view of the errors in the system. The probable errors in the pressure curves arise largely from errors in α and m, neither of which can be measured with accuracy; the error in the product of the two is about $\pm 20\%$.

ACKNOWLEDGEMENTS

The author is indebted to many colleagues for assistance and helpful discussions in the course of the present work, particularly to Mr. A. P. Stainforth and to Mr. G. V. Bond. Acknowledgement is also due to the Director of the Shirley Institute for permission to publish this paper.

REFERENCES

(1) SIEBEL, E., and LUEG, W. *Mitt. K-Wilh-Inst. Eisenforsch.* **15**, p. 1 (1933).
(2) OROWAN, E., SCOTT, F. H., and SMITH, C. L. *J. Sci. Instrum.*, **27**, p. 118 (1950).
(3) SMITH, C. L., SCOTT, F. H., and SYLWESTROWICZ, W. *J. Iron Steel Inst.*, **170**, p. 347 (1952).
(4) BERGEN, J. T., and SCOTT, G. W. *J. Appl. Mech.*, **18**, p. 101 (1951).

APPENDIX

Correction for depression of pin under load

It is assumed that an "ideal" pin, having the same compressibility as the roller, would record the true distribution if set with its surface flush with the roller surface, and also that the real pin, although it records a pressure distribution differing from the true one, has a negligible effect on the true distribution; the small size of the pin makes this assumption reasonable.

Let x denote position through the nip; then the true pressure distribution may be written as

$$L(x) = Pf(x) \tag{3}$$

and the actually recorded distribution as

$$l_H(x, H) = p_H\phi(x, H) \tag{4}$$

where H is the set height of the pin. Since the pin is compressible it will not remain at this height under load.

The experimentally observed facts, on which the correction is based, are as follows:

(1) The recorded peak load has a linear relationship with set pin height

$$p_H = mH + p_0 \tag{5}$$

(2) The shape of the recorded pressure curve is independent of the set pin height. Equation (4) may thus be written

$$l_H(x, H) = p_H\phi(x) \tag{6}$$

since the function ϕ is independent of H.

Now consider the pin at any point in the nip; the pin depresses under load to a height h relative to the roller surface, and it records the load l_H. The depression $H-h$ is the difference between the true depression of the pin and the depression of adjacent parts of the roller surface. It is safe to assume that in the present apparatus the depression of the roller is always negligible, and we may write

$$H-h = \alpha l_H \tag{7}$$

where α is the compressibility of the pin assembly.

Now the pin is in equilibrium, at this point in the nip, at the height h. The load it records is therefore that which would be recorded by an ideal pin set to this height. Setting h equal to zero we obtain the condition that, at this particular point, the recorded load shall equal the true load; that is, $l_H = L$ for $H = \alpha l_H$. The problem is thus effectively to find for each point in the nip the load corresponding to the value of H such that under load the pin shall depress to a position flush with the roller face.

We have, from equations (5) and (7), putting $h = 0$

$$\begin{aligned} p_H &= \alpha m l_H + p_0 \\ &= \alpha m p_H\phi(x) + p_0 \end{aligned}$$

Hence
$$p_H = p_0/[1 - \alpha m\phi(x)] \tag{8}$$

Putting $L = Pf(x) = l_H = p_H\phi(x)$ we get:

$$Pf(x) = p_0\phi(x)[1 - \alpha m\phi(x)]^{-1} \tag{9}$$

which is the desired correction equation.

Correspondence

Thulium 170 for industrial radiography

In his recently published paper[1] R. Halmshaw states in the summary: "The exact nature of the γ-ray spectrum does not appear to be agreed and the absorption curves which have been obtained suggest the presence of some high energy radiation, probably due to *Bremsstrahlung*."

For the last two years published values have been in full agreement concerning the γ-ray spectrum of ^{170}Tm; only one γ-ray line exists and its energy is 84·1 keV. The γ-rays at 205 and 430 keV given in Table 1 of the paper do not exist; see Graham, Wolfson and Bell,[2] Hollander, Perlman and Seaborg.[3] and more recently Pohm, Lewis, Talboy, and Jensen.[4] According to Graham and others, only about 3% of the ^{170}Tm disintegrations give 84 keV γ-ray photons while 5% give Yb K X-ray photons at about 54 keV, and 17% give Yb L and M X-ray photons with energies less than 10 keV and some Auger electrons. There is also a weak, continuous γ-radiation, namely, the internal *Bremsstrahlung*.

Furthermore, using the scintillation spectrometer method, we have investigated the spectral distribution and absolute amount of the *internal* and *external Bremsstrahlung* accompanying the β-rays from ^{170}Tm sources of various thicknesses.[5] For instance, for the source, used by Mr. Halmshaw, we estimate the composition of the electromagnetic radiation, leaving the source with photon energies above 30 keV, to be about 10% 84 keV photons, 45 Yb and Tm K X-ray photons, and 45% *Bremsstrahlung* photons. The spectral distribution of this continuous *Bremsstrahlung* (maximum energy 968 keV) decreases rapidly with increasing energy; the mean energy is found to be almost independent of source thickness and equal to about 150–160 keV.

Department of Radiation Physics, University Hospital, Lund, Sweden.

KURT LIDÉN
NILS STARFELT

Unfortunately I had not seen Dr. Lidén's paper at the time of writing my article on the use of ^{170}Tm, and the work of Pohm and Lewis was noticed too late to be referenced.

In spite of these papers and the data given by Williamson, Rossiter and Bentley[6] thulium is still frequently referred to as emitting radiation of energy 0·084 MeV, and the harder radiation is not indicated. One of the purposes of my article was to emphasize the presence of this harder radiation and show its relative importance when thulium is used for industrial radiography.

The high figure obtained by Drs. Lidén and Starfelt for *Bremsstrahlung* photons would appear to confirm my findings.

Finally I would like to emphasize that 150–160 keV is not the same quality of energy as generated by an X-ray set operating at 150–160 kV (peak voltage), as is sometimes assumed.

Armament Research and Development Establishment, Woolwich, London.

R. HALMSHAW

REFERENCES

(1) HALMSHAW. *Brit. J. Appl. Phys.*, **6**, p. 8 (1955).
(2) GRAHAM, WOLFSON and BELL. *Canad. J. Phys.*, **30**, p. 459 (1952).
(3) HOLLANDER, PERLMAN and SEABORG. *Rev. Mod. Phys.*, **25**, p. 469 (1953).
(4) POHM, LEWIS, TALBOY and JENSEN. *Phys. Rev.*, **95**, p. 1523 (1954).
(5) LIDÉN and STARFELT. *Ark. Fys.*, **7**, p. 109 (1953–54); see also *Phys. Abstr.*, No. 727 (1954).
(6) *Radioisotope Conference* 1954 (London: Butterworths Scientific Publications Ltd., 1954).

Radiation from a hollow cylinder

D. W. Stops[1] has recently pointed out the value of treating problems of energy radiation and molecular flow by analogous methods. Consequently, the radiation emitted by a hollow cylinder, closed at one end, is considered here by a treatment which has already been applied to a molecular flow problem.[2] This type of radiator is very frequently used as a black body in high temperature measurements.

The cylindrical hollow cylinder, closed at one end

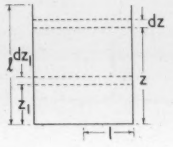

It has been shown[2] that (see figure)

$$\Phi(z_1) = \phi_0(z_1) + \frac{1-\beta}{2} e^{-z_1} \int_0^{z_1} \Phi(z) e^{z} dz + \frac{1-\beta}{2} e^{z_1} \int_{z_1}^{l} \Phi(z)\, e^{-z}\, dz \quad (1)$$

Where $\Phi(z_1)$ is the total radiation emitted from the walls of a cylinder of length l and unit radius, from an annulus of width dz_1, at height z_1 above the base of the cylinder; β is the emissivity of the walls of the cylinder; and

$$\phi_0(z_1) = b + (1-\beta)\tfrac{1}{2} a\, e^{-z_1} \quad (2)$$

The initial radiation emitted by the walls per unit area in unit time is b and the initial radiation emitted by the base per unit area in unit time is a.

Thus in the case of radiation

$$b = \beta\sigma T^4 \quad \text{and} \quad a = \alpha\sigma T^4 \quad \text{(Stefan's law)}$$

where T is the temperature of the cylinder in degrees Kelvin, σ is Stefan's constant, and α is the emissivity of the cylinder's base.

It has also been shown[2] that by differentiating the equation (1) twice with respect to z_1, we have

$$\frac{d^2\Phi(z_1)}{dz_1^2} = \beta\Phi(z_1) - b$$

or in general, putting z for z_1

$$\frac{d^2\Phi(z)}{dz} = \beta\Phi(z) - b \quad (3)$$

The solution of this differential equation is

$$\Phi^1(z) = A_2^1 e^{z\sqrt{\beta}} + B_2^1 e^{-z\sqrt{\beta}} + \frac{b}{\beta},$$

or $$\Phi^1(z) = A_2^1 e^{z\sqrt{\beta}} + B_2^1 e^{-z\sqrt{\beta}} + \sigma T^4$$

A_2' and B_2' being arbitrary constants.

If A_2', B_2' and $\Phi'(z)$ are expressed as fractions of σT^4 we have

$$\Phi(z) = A_2 e^{z\sqrt{\beta}} + B_2 e^{-z\sqrt{\beta}} + 1 \tag{4}$$

When this solution is substituted back into the integral equation (1) two simultaneous equations for A_2 and B_2 are obtained. On solving these it is found that

$$A_2 = \frac{(1-\sqrt{\beta})[(1-\alpha)(1-\beta) - (1+\sqrt{\beta})^2 e^{l\sqrt{\beta}}]}{e^{2l\sqrt{\beta}}[(1+\sqrt{\beta})^2 - (1-\sqrt{\beta})^2 e^{-2l\sqrt{\beta}}]} \tag{5a}$$

$$B_2 = -\frac{(1+\sqrt{\beta})[(1-\alpha)(1-\beta) - (1-\sqrt{\beta})^2 e^{-l\sqrt{\beta}}]}{(1+\sqrt{\beta})^2 - (1-\sqrt{\beta})^2 e^{-l\sqrt{\beta}}} \tag{5b}$$

From reference (2) [equation (12)]

$$n\alpha = \int_0^l \Phi(z) e^{-z}\, dz \tag{6}$$

where n is the fraction of radiation which, after inter-reflexion on the walls of the cylinder, is eventually reflected back onto unit area of the base.

Thus substituting the solution (4) in equation (6)

$$n = \frac{1}{\alpha}\left(\frac{A_2}{1-\sqrt{\beta}} + \frac{B_2}{1+\sqrt{\beta}} + 1\right) \tag{7}$$

But values of A_2 and B_2 have been found in terms of α, β and l, therefore

$$n = \frac{1}{\alpha} \cdot \frac{[(1+\sqrt{\beta})^2 - (1-\alpha)(1-\beta)] - [(1-\sqrt{\beta})^2 - (1-\alpha)(1-\beta)]e^{-2l\sqrt{\beta}} - 4\sqrt{\beta}e^{-l\sqrt{\beta}}}{(1+\sqrt{\beta})^2 - (1-\sqrt{\beta})^2 e^{-2l\sqrt{\beta}}} \tag{8}$$

Initially radiation of value α leaves unit area of the base in unit time (since we are expressing a as a fraction of σT^4), of which radiation of value $n\alpha$ returns after inter-reflexion.

Thus radiation of $(1-\alpha)n\alpha$ is again reflected from the base per unit area.

Let radiation n' of $(1-\alpha)n\alpha$ return after another set of inter-reflexions with the cylinder's walls. This is a pure set of reflexions in which we are not concerned with emission from the walls. Thus $b = 0$. Hence n' may be found as a solution of the integral equation (1) where

$$\phi_0(z) = (1-\beta)\tfrac{1}{2}\alpha e^{-z} \tag{9}$$

Equations (1) and (9) give rise to the differential equation

$$\frac{d^2\Phi(z)}{dz^2} = \beta\Phi(z)$$

and the solution is of the form

$$\Phi(z) = A_3 e^{z\sqrt{\beta}} + B_3 e^{-z\sqrt{\beta}} \tag{10}$$

Thus on substituting back into the integral equation (1) we obtain two simultaneous equations in A_3 and B_3. Solving these equations we find that

$$A_3 = -\frac{\alpha(1-\beta)(1-\sqrt{\beta})e^{-2l\sqrt{\beta}}}{(1+\sqrt{\beta})^2 - (1-\sqrt{\beta})^2 e^{-2l\sqrt{\beta}}} \tag{11a}$$

$$B_3 = \frac{\alpha(1-\beta)(1+\sqrt{\beta})}{(1+\sqrt{\beta})^2 - (1-\sqrt{\beta})^2 e^{-2l\sqrt{\beta}}} \tag{11b}$$

But from equation (6)

$$n' = \frac{1}{\alpha}\int_0^l \Phi(z) e^{-z} dz$$

where $\Phi(z)$ is given by equation (10). On performing the integration we see that

$$n' = \frac{1}{\alpha}\left(\frac{A_3}{1-\sqrt{\beta}} + \frac{B_3}{1+\sqrt{\beta}}\right) \tag{12}$$

Substituting for A_3 and B_3

$$n' = \frac{(1-\beta)(1-e^{-2l\sqrt{\beta}})}{(1+\sqrt{\beta})^2 - (1-\sqrt{\beta})^2 e^{-2l\sqrt{\beta}}} \tag{13}$$

Now radiation of amount α leaves unit area of the base initially in unit time and an amount of radiation $n\alpha$ returns after inter-reflexion, of this radiation $(1-\alpha)n\alpha$ is reflected again per unit area. Thus $n'(1-\alpha)n\alpha$ radiation returns again and hence $(1-\alpha)n'(1-\alpha)n\alpha$ is reflected per unit area.

After another set of inter-reflexions and reflexion from base, an amount $(1-\alpha)n'$ of $(1-\alpha)n'(1-\alpha)n\alpha$ leaves the base per unit area, etc.

If Φ_0 is the final total distribution of the radiation leaving the base per unit area in unit time,

$$\Phi_0 = \alpha + (1-\alpha)n\alpha + (1-\alpha)^2 nn'\alpha + (1-\alpha)^3 nn'\alpha + \ldots = \alpha + \frac{(1-\alpha)n\alpha}{1-(1-\alpha)n'}$$

Substituting for n and n' with equations (8) and (13) respectively, we have, on simplifying

$$\Phi_0 = 1 + \frac{(1-\alpha)4\sqrt{\beta}e^{-l\sqrt{\beta}}}{[(1-\alpha)(1-\beta) - (1+\sqrt{\beta})^2] - [(1-\alpha)(1-\beta) - (1-\sqrt{\beta})^2]^{-2l\sqrt{\beta}}} \tag{14}$$

This is the expression for the radiation of the cylinder's base. If the base and wall are made of the same material of emissivity ϵ say, put $\alpha = \beta = \epsilon$. Then

$$\Phi_0 = 1 + \frac{4\sqrt{\epsilon}(1-\epsilon)e^{-l\sqrt{\beta}}}{[(1-\epsilon)^2 - (1+\sqrt{\epsilon})^2] - [(1-\epsilon)^2 - (1-\sqrt{\epsilon})^2]e^{-2l\sqrt{\beta}}} \tag{15}$$

The above expression is identical to that which has already been obtained by Buckley[3] by a different method of approach.

In order to calculate the actual distribution $\Phi''(z)$ on the walls of the cylinder, it must be remembered that the "apparent" emission from the base is $\Phi_0\sigma T^4$ not $\alpha\sigma T^4$. Thus α must be replaced by Φ_0 in the expressions for A_2 and B_2.

Thus $$\Phi''(z) = A_4 e^{z\sqrt{\beta}} + B_4 e^{-z\sqrt{\beta}} + 1 \tag{16}$$

where

$$A_4 = \frac{(1-\sqrt{\beta})[(1-\Phi_0)(1-\beta)-(1+\sqrt{\beta})^2 e^{l\sqrt{\beta}}]}{e^{2l\sqrt{\beta}}[(1+\sqrt{\beta})^2-(1-\sqrt{\beta})^2 e^{-2l\sqrt{\beta}}]} \quad (17a)$$

and

$$B_4 = -\frac{(1+\sqrt{\beta})[(1-\Phi_0)(1-\beta)-(1-\sqrt{\beta})^2 e^{-l\sqrt{\beta}}]}{(1+\sqrt{\beta})^2-(1-\sqrt{\beta})^2 e^{-2l\sqrt{\beta}}} \quad (17b)$$

Substituting for Φ_0 given by equation (14) and simplifying

$$A_4 = \frac{(1-\beta)e^{-l\sqrt{\beta}}[(1+\sqrt{\beta})-(1-\alpha)(1-\sqrt{\beta})]}{D} \quad (18a)$$

and

$$B_4 = \frac{(1-\beta)e^{-l\sqrt{\beta}}[(1-\alpha)(1+\sqrt{\beta})-(1-\sqrt{\beta})]}{D} \quad (18b)$$

where

$$D = [(1-\alpha)(1-\beta)-(1+\sqrt{\beta})^2] - [(1-\alpha)(1-\beta)-(1-\sqrt{\beta})^2 e^{-2l\sqrt{\beta}}] \quad (19)$$

Thus the wall distribution of radiation of the cylinder is given by equation (10) whose constants A_4 and B_4 are given in terms of α, β and l above. This is again in complete agreement with Buckley.[3] When comparing the result of Buckley and the writer's result it should be realized that Buckley measures his distances from the open end of the cylinder, while the writer measures his distances from the opposite end.

Department of Natural Philosophy,
The Royal Technical College,
Glasgow, C.1.

M. G. ROSSMANN

REFERENCES

(1) STOPS, D. W. *Brit. J. Appl. Phys.*, **5**, p. 269 (1954).

(2) ROSSMANN, M. G., and YARWOOD, J. *Brit. J. Appl. Phys.*, **5**, p. 7 (1954).

(3) BUCKLEY, H. F. *Phil. Mag.*, **17**, p. 576 (1934).

New books

X-ray diffraction procedures for polycrystalline and amorphous materials. By H. P. KLUG and L. E. ALEXANDER. (New York: John Wiley and Sons, Inc., 1954; London: Chapman and Hall Ltd.) Pp. xiv + 716. Price 120*s*.

One responsibility that a reviewer often undertakes is to compare a new publication with previous books covering similar ground. In spite of the great practical importance of X-ray diffraction by powders and polycrystalline substances however, no other book is available at present which attempts such a detailed survey of the subject, though as it happens the reviewer has himself been connected with the preparation of a book recently published with a very similar title.*

Messrs. Klug and Alexander are well-known figures in the X-ray diffraction sphere and have made many original contributions of their own to the X-ray study of powders. They remark in their preface that the book is the "outgrowth of more than twenty-five years of research and teaching of X-ray diffraction and a varied consulting experience." Thus we are led to expect an authoritative and expert treatment of the subject, and broadly speaking this is what we obtain.

The scope of the book is deliberately confined to polycrystalline and amorphous materials and no attempt is made to include matter about single-crystal analysis. Even so, the volume is of very considerable size. Basic introductions to elementary crystallography, the properties and production of X-rays, and the principles of X-ray diffraction are provided in the first three chapters. Next the various techniques of examining polycrystalline substances are described. The chapter on the diffractometer technique (in the book it has been thought advisable to retain the use of the "unnatural designation 'X-ray spectrometer' ") is of special interest because of the authors' own contributions in this field. Later chapters embrace the subjects of interpretation, qualitative and quantitative analysis, precision lattice-parameter measurements, crystallite-size determination from line broadening, preferred orientation, and radial distribution analysis. Small-angle scattering and long spacings are not forgotten and hints about the lay-out of an X-ray diffraction laboratory and the handling of film are included in an Appendix.

* PEISER, H. S., ROOKSBY, H. P., and WILSON, A. J. C. *X-ray diffraction by polycrystalline materials* (London: The Institute of Physics, 1955).

Having regard to the wealth of valuable information that this book does contain, it may appear a little ungrateful to draw attention to items that have received only scant treatment. Nevertheless many will think that microbeam techniques, in view of their growing practical importance, deserve more than the few paragraphs they are awarded. The microfocus tube is merely given a literature reference. The discussion of high- and low-temperature techniques is also rather less than adequate, and the omission of all but a paragraph or two on organic fibre patterns is excused on the grounds that the analysis of them depends on single-crystal techniques. Although a very full account of lattice-parameter measurement is given, and a helpful tabulation of the possible methods appears on p. 488, many will feel that the authors are not sufficiently critical of the exaggerated claims for high accuracy that are made in some quarters.

These are, however, very minor criticisms of an excellent and interesting text. The book is an admirable testimony to continued expansion in the use of X-ray diffraction techniques, and it may be read with benefit by all those concerned directly or indirectly with X-ray crystallography. Although it is expensive by British standards, the printing and binding are of the very high quality that appears to be so effortlessly maintained by the main American publishing houses.

H. P. ROOKSBY

Dynamical theory of crystal lattices. By MAX BORN and KUN HUANG. (Oxford: London: Oxford University Press, 1954.) Pp. xii + 420. Price 50*s*.

It is just forty years since Max Born's first book on the dynamics of crystal lattices was published. Since that time the subject has been extensively developed and the present book may be regarded as a final account of the dynamic properties of perfect non-conducting crystals. The main (second) part of the book is divided into four sections. The first of these is very general in nature and deals with the general statistical mechanics of ideal lattices (with and without external forces), leading to the electric polarizability and to the scattering of light. In the second section properties of long lattice waves are investigated. The third section deals with thermal and the fourth with optical properties. The presentation of these sections is very elegant and often novel

but they require of the reader more than elementary mathematical knowledge. The book should nevertheless be also of great value to the reader with less mathematical knowledge because the main part is preceded by an elementary (first) part. The latter is subdivided into three sections dealing with atomic forces, lattice vibrations and elasticity respectively. They also contain many references to experimental data. The book can be highly recommended not only for its excellent survey on the particular subject but also for the clear presentation of important mathematical methods which should be of use in other subjects as well. H. FRÖHLICH

Notes on applied science No. 9. Measurements of pressure with the mercury barometer. (London: H.M. Stationery Office, 1955.) Pp. iv + 15. Price 1*s*.

This pamphlet, prepared by the National Physical Laboratory, explains very clearly what is involved in the correct use of mercury barometers for measuring gas pressure.

It appears at an opportune time, since at the beginning of the year new international barometer conventions for the definitions of pressure units and for the standard instrumental conditions were introduced. The essential features of the Kew and Fortin types of barometer are described and concise but adequate instructions are given on installation, observational procedure and the correction of readings. No correction tables are, however, included in the pamphlet, the reader being referred to the tables recently issued in British Standard 2520. It is good to see that the basic unit, the millibar, is strongly recommended in preference to the millimetre and inch of mercury for the expression of barometric pressure. F. J. SCRASE

The design and analysis of industrial experiments. Edited by OWEN L. DAVIES, M.Sc., Ph.D. (Edinburgh: Oliver and Boyd, Ltd., 1954.) Pp. xii + 636. Price 63*s*.

This book is an outstanding contribution to the literature concerned with the use of statistical methods in industry which has appeared since the end of the second world war. The theme of the book is the efficient planning of industrial experiments in the light of the statistical methods which were admirably treated in a book published in 1947.* Both books have been edited by Dr. Davies and are the work of teams of authors not identical in membership. The new work is an ambitious volume; it describes experimental designs which have been introduced quite recently. It is not concerned with the methods of statistics and the reader is frequently referred to the earlier book; advice that he should certainly follow.

Few industrial organizations are fortunate enough to have a team of scientists and statisticians who could readily comprehend and utilize the more advanced designs contained in the latter half of the volume. Readers who have had industrial experience in this experimental field may be inclined to the view that the more complicated experimental designs have their pitfalls even for able and gifted workers, owing to the length of time that would often be required to carry the experiment through in an industrial organization. However, these experienced readers will applaud the ability and welcome the thoroughness with which the compilation of this book has been done. To appreciate its potential value it should be recalled what a large proportion of British industrial effort is sustained by small organizations. These small organizations produce large quantities of components used by others. The users expend much effort in inspecting the product supplied and they also suffer from inconvenience leading to increased manufacturing costs due either to delays caused by having to return unsuitable products or by the use of products not wholly satisfactory.

If the principles laid down in Chapter 2, "The planning of simple comparative experiments," and in Chapter 4, "Investigation of sampling and testing methods," were fully comprehended and utilized there is no doubt whatever that very considerable economies could be effected in production. Fortified with practical experience based on these two chapters, the worker in industry would pave the way for a study of the later chapters. More important still, he would place himself in the position to take advantage of the opportunities provided to-day by open meetings in many important industrial centres to meet persons highly qualified in the use of statistical methods.

The use of trained men in small organizations has increased considerably in recent years, but as the Editor points out in the Introduction, it is still true that most chemists and physicists graduate without a knowledge of statistical methods, and are often unaware of the value of such methods in their work.

Readers having little acquaintance with the application of statistical methods should read the Introduction with care, particularly paragraph 1.2 on the nature and value of experimental design. The authors necessarily refer frequently to chemical processes, but the mode of thought which characterizes this book is of quite general application.

The authors have again provided great assistance to the conscientious enquirer and student by including fully worked out examples in Appendices at the end of the chapters. Rarely are industrialists offered an investment which is capable of earning so large dividends. B. P. DUDDING

Applied mass spectrometry. (London: The Institute of Petroleum, 1954.) Pp. vii + 333. Price 50*s*.

The principles of mass spectroscopy were first enunciated in this country; but for too many years since Astor's pioneer work they have found their development and application abroad. It is encouraging therefore to read in this report of papers presented at the Second conference of applied mass spectrometry (organized by The Institute of Petroleum last October) of some British progress employing this fruitful and expanding technique. Some contributions by overseas visitors are also included.

The scope of the book is strictly limited. Some problems in hydrocarbon analysis are thoroughly discussed, including one complete section on the computing methods involved in the analysis of spectral data. Fundamental physical chemical investigations are described in a number of papers on free radicals and molecular structure. Only a few contributions go beyond these bounds.

One section is devoted to instrument design; but small mention is made of two aspects of mass spectrometer development which will prove extremely useful in many fields of application. These are the ability of instruments to handle solid materials, and to attain high resolving power by the double focusing principle. No doubt the instrument designers will consider these points before the next conference.

The discussions following each paper are well edited; and the book also contains a supplement to the useful bibliography on mass spectrometry issued earlier, which brings it up to June 1953. K. I. MAYNE

* *Statistical methods in research and production.* Edited by OWEN L. DAVIES. (Edinburgh: Oliver and Boyd, Ltd., 1947.)

Transistors, theory and applications. By ABRAHAM COBLENZ and HARRY L. OWENS. (London: McGraw-Hill Publishing Co. Ltd., 1955.) Pp. xv + 313. Price 42*s*. 6*d*.

This book is a valuable addition to the rapidly increasing literature of the subject. It is directed to technicians in the electronics field and makes provision, by way of commentaries, for those whose knowledge of mathematics is restricted. The physicist must therefore expect to find the fundamentals of semiconductor physics treated in a comparatively simple manner, but he will probably agree that the exposition is clear, concise and stimulating. An account is given of the preparation of single-crystal germanium and silicon material and of the manufacturing processes by which crystal valve diodes and triodes are made from it. This account is as full and up to date as could reasonably be expected. It should assist the readers to obtain a sympathetic understanding of the new devices which are available to them. The design and operation of transistor circuits is treated extensively with many practical examples. Some of this treatment is a little academic and, occasionally, the circuit values quoted should be treated with caution. There is no doubt, however, that this well-produced and illustrated book should successfully achieve its stated purpose of initiating technical people with varied backgrounds in electronics into this fascinating new subject.

N. L. HARRIS

Electroacoustics—the analysis of transduction, and its historical background. By PROFESSOR FREDERICK V. HUNT. (London: Chapman and Hall Ltd.; New York: John Wiley and Sons, Inc.; Cambridge, Mass.: Harvard University Press, 1954.) Pp. viii + 260. Price 48*s*.

Professor Hunt has given us two distinct studies in this book (No. 5 in the Harvard monographs in applied science): both are excellent and may be read quite independently.

In the first part, which occupies two-fifths of the whole, a complete historical survey is given of the origin and growth of electroacoustics and in it are described developments of the various aspects of the subject, such as the telegraph, telephone, echo ranging, control of frequency, the phonograph, loud speakers, microphones. This section is a fascinating narrative and one enjoys the author's style, the insights into personal relationships existing at the time and the descriptions of the patent wrangles that have occurred: a nice sense of humour of the author adds much to the pleasure of reading. At the same time the work is well documented with references to papers, patents and private correspondence, 250 in all.

The technical part of the book comprises analytical studies of some of the major subdivisions enumerated above, all treated in a manner which shows the fundamental similarities between them. All these transducer types can be represented by the same form of equivalent circuit. As indicated by the title, the author does not go beyond these analyses and the book is the better for not continuing into practical applications, descriptions of various makers' products and the like. Altogether it is a work to be recommended.

A. J. MADDOCK

Wool research 1918–1954. Volume 3—Testing and control. (Leeds: Wool Industries Research Association, 1955.) Pp. v + 227. Price 25*s*.

This volume deals with testing for controlled purposes from the fibre to the finished fabric—from the determination of fibre length to the measurement of fabric strength, wearing properties, air permeability and shrinkage. The book is, however, more than a testing manual, for it summarizes the research results and considerations which have led to the adoption of appropriate techniques and the design of special instruments. References to the original papers are given.

Textile fibres and their products are variable, and measures of the variabilities of their properties are often as important as average values. Methods of sampling the materials and of analysing the results of tests are therefore subjects of first importance which receive adequate attention throughout the book. A chapter is given to methods and apparatus for characterizing the variation in linear density of yarns and rovings.

The scope of this book and the method of presentation, including the liberal use of graphs, nomograms, and illustrations, will enable the textile reader to understand the basic principles of the methods recommended. Those who lack knowledge of wool technology need not be deterred from reading this book. They will find it of general interest and of importance as an illustration of the way in which the work of a research association can provide an industry with means for controlling the quality of its products.

J. POLLITT

Fatigue tests on rolled alloy steels made in electric and open-hearth furnaces. By P. H. FRITH. Special Report No. 50 of the British Iron and Steel Research Association. (London: Iron and Steel Institute, 1954.) Pp. xxii + 129. Price 25*s*. 0*d*.

This report gives the results of the vast amount of work carried out by Mr. Frith on the fatigue properties of alloy steels (mainly nickel–chromium–molybdenum and carbon–chromium steels) heat treated to different ranges of tensile strengths and made by different melting procedures. The main conclusions are that the fatigue properties of the steels are not improved when they are heat treated to above about 60 tons/in^2 tensile strength, and may even be reduced, especially in the transverse direction. Steels made by certain procedures, e.g. the neutral open hearth, gave better fatigue properties than others and an attempt was made to explain this by the nature, form and size of the non-metallic inclusions present in the steels.

THIS JOURNAL is produced monthly by The Institute of Physics, in London. It deals with all branches of applied physics (including theory and technique).
All rights reserved. Responsibility for the statements contained herein attaches only to the writers.
EDITORIAL MATTER. Communications concerning editorial matter should be addressed to the Editor, The Institute of Physics, 47 Belgrave Square, London, S.W.1. (*Telephone:* Sloane 9806.) Prospective authors are invited to prepare their scripts in accordance with the *Notes on the preparation of contributions*. (Price 2*s*. 6*d*. including postage.)
REPRODUCTION. The Institute of Physics is a signatory to The Royal Society's Fair Copying Declaration. Details may be obtained upon application from The Royal Society, London, W.1.
ADVERTISEMENTS. Communications concerning advertisements should be addressed to the agents, Messrs. Walter Judd Ltd., 47 Gresham Street, London, E.C.2. (*Telephone:* Monarch 7644.)
CLAIMS FOR MISSING JOURNALS. Claims from regular subscribers to this *Journal* for missing numbers will only be considered if received within 60 days of the date of mailing plus normal outward time of transit and time for lodging the claim. Losses attributable to failure to notify a change of address or to similar omissions will not be considered.
SUBSCRIPTION RATES. A new volume commences each January. The charge is £4 per volume ($11.50 U.S.A.), including index (post paid), payable in advance. Single parts, so far as available, may be purchased at 8*s*. each ($1.15 U.S.A.), post paid, cash with order. Orders should be sent to The Institute of Physics, 47 Belgrave Square, London, S.W.1, or to any bookseller.

SPECIAL ARTICLE

Mass transfer theories of fuel bed combustion

By R. S. Silver, D.Sc., M.I.Mech.E., F.Inst.P., and R. W. Mackay, B.Sc., A.Inst.P., John Brown Land Boilers Ltd., Clydebank, Dunbartonshire

[*Paper received* 18 *April*, 1955]

Considerable interest in the possibilities of developing theories of combustion based on mass transfer ideas has resulted in a number of attempts which are not immediately capable of comparison. The purpose of the present paper is to clarify the general position reached as a result of previously published work with particular reference to combustion of carbon in solid fuel beds, and to enumerate the points on which certain of the more recent approaches agree or differ theoretically. The papers so chosen by Thring, Silver, and Spalding respectively are used not because these were thought to be exhaustive, nor necessarily final, but because each uses a different approach and is amenable to the process of intercomparison. In this way it is hoped that an improved appreciation of the general theory will facilitate further advance. In terms of this basic general theory a method of evaluating an accurate transport parameter to describe a live fuel bed is suggested as a logical beginning for further progress.

LIST OF SYMBOLS

d	fuel particle effective diameter	$[L]$
D	carbon channel effective diameter	$[L]$
D_F	diffusion coefficient assumed to be the same for oxygen, carbon monoxide and carbon dioxide in nitrogen	$[L^2/T]$
g	gravitational acceleration	$[L/T^2]$
$\frac{K'}{0{\cdot}034\,m}$	group used as transport parameter by Thring	$[1/L]$
l	length of path through fuel bed	$[L]$
m	mass air flow per unit bed area per unit time	$[M/L^2T]$
Δp	pressure drop across fuel bed	$[M/L^2]$
R_e	Reynolds number	—
S_c	Schmidt number	—
u	bed depth in characteristic units $= \alpha l$	$[L/L]$
v	air velocity through carbon channels	$[L/T]$
x	proportion of oxygen collisions with carbon surface, which yield carbon monoxide	—
α	general symbol for transport parameter	$[1/L]$
β	transport parameter used by Silver	$[1/L]$
ϵ	fractional voidage	—
μ	coefficient of absolute viscosity	$[M/LT]$
ν^2	number of channels per unit area of bed	$[1/L^2]$
ρ	density of air	$[M/L^3]$

1. INTRODUCTION

In recent years there has been considerable interest in the possibilities of developing theories of combustion based on mass transfer ideas. Papers by Nusselt,[1] by Tu, Davis and Hottel,[2] by Thring,[3] by Silver,[4] and by Spalding,[5] are examples of that trend of interest. The purpose of the present paper is to clarify the general position reached as a result of such work, particularly in relation to combustion of carbon in fuel beds. The clarification intended is not so much in regard to questions of agreement with experimental observation, as to give an account of the inter-relations between the more recent theoretical approaches, and therefore a description of the existing position of general theory. From some points of view, questions of agreement with experiment are less important than clear appreciation of the theoretical position. This situation happens to be especially true in the field of our present interests, because the fact is that any theoretician can aline a range of experimental results with his theory by suitable choice of parameters. Now the practical situation is also that he is entitled to a choice of parameter because there are no independent sources of information regarding values of such relevant properties as thermal conductivity, viscosity, etc., at the temperatures and non-equilibrium conditions which occur in the combustion process. For these reasons it can be expected that further advances can only be made by clarification of theory, so that the different, or apparently different, current approaches can be merged into one logical and self-consistent approach. If one such general approach becomes available, and is logically satisfactory, there will then be no objection to the necessary choice of parameters to agree with experimental results, provided the range covered is comprehensive.

In any theory of the type which we are discussing, the rates of change in the concentrations of calculated species require to be specified in terms of certain transport rates. We therefore have three main sources of difference between one author and another, namely:

(*a*) Different sets of assumed chemical reactions.

(*b*) Different qualitative sets of assumed physical processes.

(*c*) Different arithmetical values for transport parameters, which should refer to the same physical processes.

Since there are naturally many possibilities of individual differences in each of these three types, the total number of possible differences of approach and resultant theory and calculation is bewildering. The first object of the present paper is to indicate how some of the less important differences can be discounted in order to compare satisfactorily their essential points.

In choosing, for our discussion, the respective published theories of Thring, Silver, and Spalding, it is not suggested that these are exhaustive, nor that any one of them is necessarily correct, nor worked out yet to its best and final form. For the purposes of the present paper, we are taking the three theories just as they are published as examples with which to discuss the methods of inter-comparison. The clarification which this can give of general theoretical principles to be observed in the combustion field is a necessary preliminary to further advance.

2. THE ELIMINATION OF TYPE (*c*) DIFFERENCES; THE CHARACTERISTIC LENGTH IN A FIREBED

It is suggested that it is primarily desirable to remove, if possible, all differences of type (*c*) which arise only from the choice of different transport parameters. These are necessarily extraneous to the formal body of theory, and differences in choice introduce confusion which may be quite unnecessary if the respective theories can be developed in a formal way without inclusion of specific values for such parameters. On examination of the general underlying concepts, it becomes apparent that such formal treatment is certainly possible, because all theories of this mass transfer type necessarily lead in the first place to gas concentrations (or composite functions equivalent to gas concentrations), expressed as functions of length of travel through the firebed. Moreover, it is also the case that in such functions the variable l representing the length of travel through the firebed, appears only in combination with, and multiplied by, a parameter arising from the transport parameters, and which has the dimensions of $(\text{length})^{-1}$, i.e. the product of this parameter by the path length is non-dimensional. Furthermore, this is the only point in which the transport parameters enter.

For example, according to Thring, the gas concentrations in a firebed are a function of the group $K'l/0{\cdot}034\,m$, while Silver gives them as a function of a group βl. It is clear that $K'/0{\cdot}034\,m$ in Thring is completely analogous to β in Silver, although the arithmetic values, which they indicate by their different choice of transport parameters and experiments, may be substantially different—in fact the former tends to be from two to three times the latter arithmetically.

Again, Spalding finds the gas concentration to be a function of still another group of the same kind, his coefficient of l being different in form from both Thring's and Silver's, and also different in arithmetical value.

It is therefore suggested that we are entitled to recognize, in the dimensionless product appearing in the different theories, merely different expressions for something which should really be identical in all the theories, and which is the characteristic independent variable of firebed phenomena. We are led to the belief that there must be one correct parameter, which we may denote by α, having the dimensions of $(\text{length})^{-1}$ such that the governing variable for the firebed is αl. This quantity α will be dependent on particle size, on rate of air flow, on viscosity, and in general on the "flow field." The different values which the above different authors have used in place of α have been derived by adopting different sets of non-combustion experimental results (or different interpretations thereof) for mass transfer data (see Section 4). It must be accepted that some of these must be wrong, both formally and numerically, and that only one of them may happen to be correct arithmetically. More probably none of them is correct, since we have no independent knowledge of transport parameters under the high-temperature and non-equilibrium conditions which occur in combustion.

On this basis, the really important differences between different theories such as those of Thring, Spalding, and Silver, are that each derives entirely different gas concentrations as functions of αl. The fact that they have used different values of α is relatively "accidental," and unimportant from the standpoint of logical theory. They should all have used the same value. Since in all the functional expressions α appears only in the dimensionless group αl, it is not necessary to choose *any* value of α, in order to calculate gas concentrations, according to the different theories as functions of αl. We need merely substitute a suitable numerical range of αl between 0 and ∞.

This point was made to some extent in Silver's paper where he gave his group βl the symbol u, and showed that a full discussion of combustion problems could be made by considering gas concentrations, firebed temperatures, etc., all as functions of u, and emphasized that it was only when attempting to translate values of u into actual fuel bed depths that he had to decide on a method of evaluating his β. From the foregoing it is seen that this circumstance applies still more generally, and we may therefore, for convenience in future discussion, use the same symbol u to denote the more general group αl.

It is clear that $1/\alpha$ corresponds to some length dimension in the firebed, whose magnitude is governed by the complex of factors operating in the firebed field, i.e. particle size, packing, possibly shape, airflow rate, viscosity, etc. We may think of $1/\alpha$ as the characteristic length unit of the field, so that a length l as measured in ordinary units is actually αl or u, characteristic units; what happens successively in the firebed being dependent on the distance when expressed in these natural units.

The next step is to compare the results which different theories give in terms of u, which will be quite independent of any errors which may have been made, or of differences which may have arisen, in choice of transport parameters, i.e. ultimately of α.

3. INTER-COMPARISON OF THEORIES OF THRING, OF SPALDING, AND OF SILVER

In Figs. 1, 2 and 3 are shown respectively the curves of oxygen, carbon dioxide and carbon monoxide which are obtained when the theoretical expressions derived by the

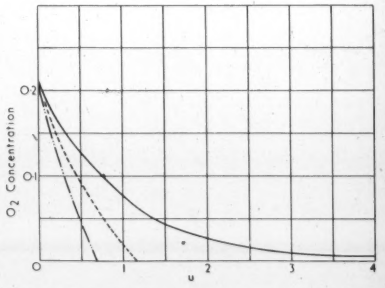

Fig. 1. Comparative oxygen concentrations as function of u

Thring —·—·—
Silver ————
Spalding - - - - - -

aforementioned authors are regarded as functions of the same argument u. In the case of Silver's theory which is general, we have to choose some particular value of x and we have used the case of $x = 0$, i.e. when the primary product of the oxygen/solid carbon reaction is supposed to form entirely carbon dioxide.

One major difference between the theories is shown in Fig. 1 in that according to Silver the oxygen is asymptotic

to zero, whereas, according to the others, it vanishes in a finite length, namely, at $u = 1{\cdot}14$ for Spalding and $u = 0{\cdot}69$ for Thring.

In Fig. 2, the chief distinction is that Silver's theory gives a smooth carbon dioxide curve with a maximum of 7½%

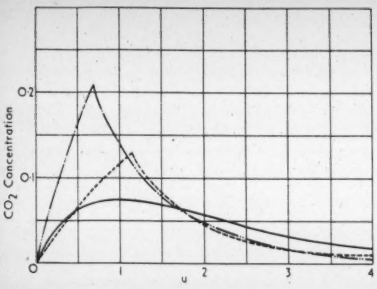

Fig. 2. Comparative carbon dioxide concentrations as functions of u

Thring —·—·—
Silver ————
Spalding - - - - - -

carbon dioxide at u approximately equal to 1, whereas both Thring's and Spalding's give carbon dioxide curves with pronounced discontinuities. Thring's shows a discontinuous maximum of 21% at $u = 0{\cdot}69$, and Spalding shows a discontinuous maximum of $13{\cdot}1\%$ at $u = 1{\cdot}14$.

In Fig. 3, Thring's curve is distinct from the other two in indicating no formation of carbon monoxide at all until

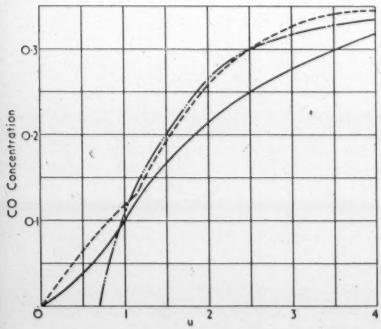

Fig. 3. Comparative carbon monoxide concentrations as functions of u

Thring —·—·—
Silver ————
Spalding - - - - - -

after $u = 0{\cdot}69$. Both Silver and Spalding show formation of carbon monoxide right from the start, but Silver's is a continuous curve, while Spalding's again has a discontinuity at $u = 1{\cdot}14$ at which the carbon monoxide concentration is $13{\cdot}1\%$.

Another distinction between Silver and Spalding, however, is that Silver's theory gives actual calculated values of carbon monoxide and carbon dioxide separately. Such separate values are not calculable on Spalding's theory so long as oxygen is present, and he makes the arbitrary assumption that the concentrations of these two gases are equal.

Naturally, for large values of u, the curves given by all three authors tend to the same asymptote, 35% of carbon monoxide.

The curves of Figs. 1, 2 and 3, while very useful for formal comparison, are not directly comparable against experimental results since values of u are not directly known for experiment. There is, however, one method by which check against experiment can be made even without attempt to interpret u in relation to firebed path length. The method consists in taking any one of the three combustion gases as independent variable, and plotting against it the values of the other two read from Figs. 1, 2, and 3 for identical values of u. In Figs. 4 and 5 we have plotted in this way concentrations of oxygen against carbon dioxide and concentrations of carbon monoxide against carbon dioxide. The arrows on the curves indicate the direction of variation with direction through the firebed.

Thus, suppose in an experiment the gas analysis at the point in the firebed gives 6% carbon dioxide. Fig. 4 shows that

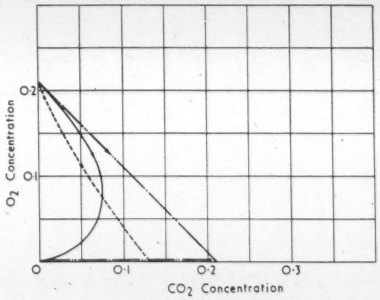

Fig. 4. Comparative oxygen concentration at a given carbon dioxide concentration

Thring —·—·—
Silver ————
Spalding - - - - - -

according to Thring the oxygen concentration should either be 15% or zero; according to Spalding, either 11% or zero, and, according to Silver, either $13{\cdot}2\%$ or $3{\cdot}1\%$. In each case the respective figures refer to a lower and a higher position, in a firebed through which gases ascend. Similarly, Fig. 5 shows that when a carbon dioxide concentration of 6% is found, the carbon monoxide concentration should be, according to Thring, either zero or 25%; according to Spalding, either 6% or 25%, and, according to Silver, either $3{\cdot}2\%$ or $20{\cdot}2\%$.

Hence, if sufficiently accurate experimental gas analysis from various positions in firebeds were available, it should be possible to discriminate to some extent between the validity of different theories even without knowing the actual values

of u. One difficulty which arises is, however, as pointed out by Silver, that it is very difficult to rely on the accuracy of firebed gas samples because of the high probability of some reaction between carbon monoxide and oxygen in the sampling tube, if these gases are simultaneously present. It is worth noting in this connexion that Thring's curves in Figs. 4 and 5 would be quite unaffected, since on no occasion, according to his theory, are carbon monoxide and oxygen simultaneously

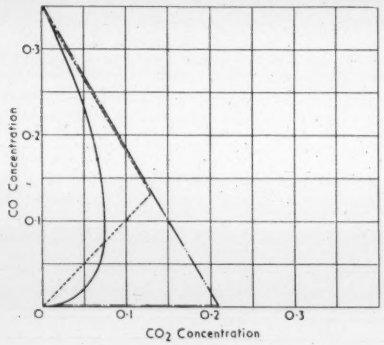

Fig. 5. Comparative carbon monoxide concentration at a given carbon dioxide concentration

Thring
Silver
Spalding

present. On the other hand, both Silver and Spalding have carbon monoxide and oxygen simultaneously present, Silver at all times, and Spalding for part of the time, so that if sampling tube reaction occurs, the apparent experimental results would show disagreement with their theories even if the actual firebed conditions have been in agreement. Such experimental results would be displaced to the right, i.e. towards greater concentrations of carbon dioxide. It follows, therefore, that when the formal calculations of a theory have been made in this way, a comparison against experimental results can give the following amount of information.

(*a*) If the experimental points when entered on graphs such as Figs. 4 and 5 lie to the *right* of the theoretical curve, the theory is not necessarily disproved but may be correct.

(*b*) If the experimental points lie to the *left* of the theoretical curve, the theory must be incorrect.

4. RANGE OF VALUES OF α

The preceding section established in principle the possibility of inter-comparison of theories on a formal basis. In the long run, however, and for practical purposes, the calculations must be related to actual path lengths in a firebed; i.e. we must be able to give an arithmetic value to α as a number per foot or per centimetre. The purpose of this section is to illustrate how in fact different authors have used different values of α, the origins of these differences being quite distinct from and quite independent of the chemical and qualitative physical assumptions in their respective theories. It is also hoped to show that, despite the different choices of α, there is sufficient common ground to suggest a basis of procedure for further work.

The methods of correlating the transport parameter with the physical constants of the system under consideration differ quite widely. We shall again exemplify with reference to the same three authors, Thring, Silver and Spalding.

In Thring's notation $\alpha = K'/0{\cdot}034\,m$ and K' is evaluated on the basis of an empirical expression obtained by Gamson[6] for correlating experimental data on mass transfer factors in fixed beds. This yields

$$\alpha = 10{\cdot}2(1-\epsilon)^{1{\cdot}61}(S_c)^{-\frac{1}{3}}(R_e)^{-0{\cdot}41}d^{-1} \tag{1}$$

Silver denotes his transport parameter by β and evaluates it by equating the rate of momentum lost at the surface to the frictional resistance of that surface. This is assumed to contribute to a total pressure drop in the form

$$\Delta p = \frac{\rho v^2}{2g}(1 + 2\beta l) \tag{2}$$

He assumed that β could be obtained for streamline flow within a carbon channel by using the Poiseuille formula. This leads to

$$\alpha = \beta = \frac{8\pi\mu v^2}{m} \tag{3}$$

A subsidiary approach still using Silver's main concepts, is to use experimentally determined pressure drop results, as for example those found by Ergun[7] which can be expressed in the form

$$\Delta p = \frac{\rho v^2}{2g}\left(2{\cdot}3\frac{l}{D} + 2{\cdot}08.2\beta l\right) \tag{4}$$

This gives $\alpha = 2{\cdot}08\ \beta$.

In his paper Spalding does not state explicitly how he evaluated his α but in a private communication indicated his method which then yields

$$\alpha = \left(\frac{1-\epsilon}{\epsilon}\right)\frac{1}{d}(S_c)^{-1}\,1{\cdot}15\left(\frac{R_e}{1-\epsilon}\right)^{-0{\cdot}29} \tag{5}$$

It should be noted that in the treatments of Thring and Spalding there is an explicit dependence on ϵ the voidage fraction. In Silver's original treatment the concept of carbon channels was used, the number of these per unit area being equated to the 2/3 power of the number of particles per unit volume. This number ν^2 per unit area of cross-section of firebed is determined by counting the number of particles and so can be readily evaluated.

For comparison purposes Silver's formulae have been written in the others' notation as

$$(a)\quad \alpha = \left(\frac{72}{d}\right)\left(\frac{1-\epsilon}{\epsilon}\right)\left(\frac{R_e}{1-\epsilon}\right)^{-1} \tag{6a}$$

$$(b)\quad \alpha = \left(\frac{150}{d}\right)\left(\frac{1-\epsilon}{\epsilon}\right)\left(\frac{R_e}{1-\epsilon}\right)^{-1} \tag{6b}$$

The expressions are therefore

Thring
$$\alpha = \left(\frac{10{\cdot}2}{d}\right)(1-\epsilon)^{1{\cdot}2}(S_c)^{-\frac{1}{3}}\left(\frac{R_e}{1-\epsilon}\right)^{-0{\cdot}41} \tag{7}$$

Silver (*a*)
$$\alpha = \left(\frac{72}{d}\right)\left(\frac{1-\epsilon}{\epsilon}\right)\left(\frac{R_e}{1-\epsilon}\right)^{-1} \tag{8a}$$

$$(b)\quad \alpha = \left(\frac{150}{d}\right)\left(\frac{1-\epsilon}{\epsilon}\right)\left(\frac{R_e}{1-\epsilon}\right)^{-1} \qquad (8b)$$

$$\text{Spalding}\quad \alpha = \left(\frac{1{\cdot}15}{d}\right)\left(\frac{1-\epsilon}{\epsilon}\right)(S_c)^{-1}\left(\frac{R_e}{1-\epsilon}\right)^{-0{\cdot}29} \qquad (9)$$

The effect of these differences inherent in the transport parameters mentioned above can be seen in the variation in arithmetical values obtained for the same experimental conditions. Experimental conditions instanced by the three authors are listed below with their corresponding arithmetical values for α.

Example quoted by	Thring	Silver		Spalding
Particle size (in.)	1·18	1·75		0·125
Estimated gas temperature (°C)	1200	600		600
Mass air flow (lb ft^{-2} s^{-1})	0·063	0·024		0·398
Voidage fraction ϵ	0·4	(*a*)	(*b*)	0·4
α per foot	6·9	1·3	2·7	45

To illustrate the differences most satisfactorily it is useful to determine the value of α which each author's method gives both for his own experimental conditions and for the conditions of the other two. These are shown in the following table which gives the values of α per foot.

Theory of	Thring	Silver		Spalding
		(*a*)	(*b*)	
Example quoted by Thring	6·9	1·2	2·4	5·4
Silver	5·2	1·3	2·7	3·4
Spalding	67·5	20	41·6	45

It is seen that for the same conditions, the estimated values of α vary by as much as five to one. This situation is quite unacceptable. Its existence reveals the futility of attempting to estimate the validity of a combustion theory by comparison with experimental observations in terms of firebed path lengths. It is only if values of α could be specified with much greater uniformity, acceptability, and accuracy that such comparisons can hope to be fruitful. Until this can be done, it would appear that the method of formal comparison outlined in the previous section would be a preferable guide to development of theory.

The question arises as to whether there is any reason to believe that any one of the above-mentioned four methods of determining α is likely to be more correct than the other. This would appear to be doubtful. Thring's, Silver's (*b*) and Spalding's values are all based on experimental results, to each of which must be accorded some validity. The ways in which they are derived from the experimental results are different, but each way is logically plausible and not self-evidently incorrect. The most important point is, however, that for the reasons mentioned in Sections 1 and 2, it is very doubtful whether true values of α, which must be dependent on the transport of material under *non-equilibrium combustion conditions*, can reasonably be expected to be derived from any experiments on cold packed beds. All the above authors have implicitly assumed that it was legitimate to derive values of α from cold experiments although they have adjusted the values of viscosity to suit supposed temperature conditions.

In view of this situation, it is suggested that it may be more profitable in the long run to use a reverse method of approach in which the procedure would be as follows. Suppose that a series of accurate experimental results is available for gas composition at various points in a fuel bed, i.e. the concentration of any of the three combustion gases has been experimentally determined as a function of path length. If a series of arbitrary values of α is assumed, the known experimental results for each of the combustion gases can be translated into a family of curves for each combustion gas, since by multiplying a known path length by the assumed values of α a series of values of u will be obtained. Thus for each gas we obtain a family of curves in which the concentration is shown against u. In this form the predicted theoretical curve can be shown upon the same graph and it will be possible to see directly whether its form agrees with the general form of the family derived from the experimental results and, if so, to see whether any one particular member of the family is in close agreement with the theoretical curve. If this is so, the value of α corresponding to that member of the family will be indicated as relevant. This procedure can be carried out for the three combustion gases and a further criterion of judgment will be that not only must a member of each family agree closely with the corresponding theoretical curve for the particular gas, but the indicated values of α from the three different gases should be equal or nearly so. If this is found to be the case, then there will be very good reason to believe that the theory is correct, and the value of α can then be regarded as inductively established. If such agreement is not possible, then the theory must be suspect.

If, by such means, an acceptable theory is found, it should then be investigated over many different experimental conditions to see if formal agreement in all respects is continued, and, if so, to derive by the above means the various values of α. In this way it will be possible to establish the way in which α does actually vary with particle diameter, rate of air flow, etc.

ACKNOWLEDGEMENTS

The authors are grateful to Professor M. W. Thring and to Dr. D. B. Spalding for discussion in correspondence although the views expressed are their own. The authors are also indebted to the Directors of John Brown Land Boilers Ltd. for permission to publish this paper, and to Mr. M. J. Young for assistance in computation.

REFERENCES

(1) Nusselt, W. *Z. Verein. Dtsch. Ingen.* [*VDI*], **60**, p. 102 (1916).

(2) Tu, Davis and Hottel. *Industr. Engng Chem.*, **26**, p. 749 (1934).

(3) Thring, M. W. *Fuel*, **31**, p. 355 (1952).

(4) Silver, R. S. *Fuel*, **32**, p. 121 (1953).

(5) Spalding, D. *Proc. Mech. Engrs.* To be published.

(6) Gamson, B. W. *Chem. Engng Progr.*, **47**, p. 19 (1951).

(7) Ergun, S. *Chem. Engng Progr.*, **48**, pp. 89, 227 (1952).

Changes in the structure of oxide cathodes at high temperatures

By H. P. Rooksby, B.Sc., F.Inst.P., The M.O. Valve Co. Ltd., at the Research Laboratories of The General Electric Co., Ltd., Wembley, Middlesex

[*Paper first received* 6 *April, and in final form* 27 *April*, 1955]

The effect of heat treatment on barium oxide and strontium oxide thermionic cathodes has been examined by X-ray diffraction methods. Crystal growth in these cathodes has been studied by a simple microbeam technique. It has been shown that in the temperature range 900–1150° C, crystallites of barium oxide between 2 and 5 μ in size are normally developed. This size is considerably greater than had been estimated previously by X-ray line broadening methods. Similar sizes develop in strontium oxide in the temperature range 1100–1250° C.

It has also been found that in both oxides a gradual decrease in the structure-cell dimensions takes place with increasing temperature of heating in a vacuum. This change is attributed to a progressive increase in the numbers of defects in the lattice and, in the case of barium oxide, appears to correspond with the process of thermionic activation.

Recent studies by Yamaka[1] on the alkaline earth oxide coatings of thermionic cathodes have indicated average crystallite dimensions in the order 0·1 μ. Yamaka used X-ray line broadening phenomena as a measure of the crystal dimensions, and suggested that the changes of X-ray reflexion definition with heat-treatment temperature provided evidence about crystal growth. This X-ray method of assessment of crystal size, however, is open to criticism on the grounds that there are other factors besides small crystal size that contribute to X-ray line broadening. With solid solutions, for example, such as exist in the alkaline earth oxide systems used as cathode coatings, some point-to-point variability in composition may be expected, and its contribution to X-ray line broadening would be difficult or impossible to separate from that due to particle size.

In this paper a more direct assessment of the textural character of oxide coatings has been made by using a microbeam technique. By a simple reduction of the X-ray beam to a diameter of about 50 μ as compared with the more usual 500 μ, resolution on the X-ray diffraction pattern has been improved so that reflexions from individual crystallites have become distinguishable. Ambiguities in interpretation, such as arise in the line-broadening method, are thus completely eliminated. The method is analogous to that developed by Hirsch and others[2,3] for the study of textural detail in metals on plastic deformation.

In parallel with the evaluation of crystal size, it has been found possible to measure the lattice parameters of pure barium and strontium oxides with considerable accuracy, and as a result it has been discovered that the mean interatomic distances alter on heating at high temperatures in a vacuum. Both results are of considerable importance in the development of an understanding of the thermionic properties of barium oxide and related oxide coatings.

EXPERIMENTAL PROCEDURE

The samples examined were mainly in the form of oxide coated box-type nickel cathodes, which had been processed in experimental diodes. The oxide coating is sprayed on to the nickel base in the form of carbonate, this being subsequently heated in a vacuum at various temperatures. The sample cathodes had been prepared in the course of the thermionic investigations described elsewhere by Wright.[4]

Since the alkaline earth oxides, particularly barium and strontium oxides, take up moisture and carbon dioxide very quickly on exposure to the atmosphere, the method developed by Eisenstein[5] of opening the diode in a nitrogen-filled box and overcoating the cathode specimen with wax to prevent weathering was adopted. This was successful in preserving the barium oxide specimens for a period sufficiently long to take the required X-ray diffraction patterns. With strontium oxide and solid solutions containing only about 50 molar per cent of barium oxide the wax was effective for several weeks.

The X-ray diffraction examinations were made in two different ways. For the microbeam investigation a 50 μ diameter lead-glass collimator was used, and the distance from specimen-to-film fixed at 2·5 cm. Reflexion patterns were obtained with the X-ray beam incident at an angle of approximately 10° on the flat cathode surface. Strong smooth rings for the paraffin wax appear on each pattern, but the reflexions for the alkaline earth oxide generally showed a detectable degree of spottiness. Unfiltered CuKα radiation was used.

In addition to the microbeam photographs, diffraction patterns were also taken in a Straumanis-type 11·46 cm diameter camera. No special collimation of the X-ray beam was required in this case, since the patterns were required primarily for lattice-parameter determinations. Both back-reflexion and glancing-angle settings of the specimens were tried.

CRYSTALLITE SIZE OF BARIUM AND STRONTIUM OXIDE CATHODES

Cathode processing schedules were chosen to compare oxides formed under several different conditions in the range in which thermionic emission is usually measured.

Barium oxide. It is difficult to decompose barium carbonate at a temperature much below 900° C, so the mildest treatment given was 900° C for 15 min. Even at this comparatively low temperature the microbeam reflexion pattern shows spotty Debye–Scherrer rings. Numerical calculations based upon the number of spots in a ring show the crystal size to be in the neighbourhood of 2 μ. The calculations have been confirmed by obtaining reference patterns of powders whose crystal sizes have been determined independently.

Table 1 shows the effect of increasing severity of heat treatment on the crystal size. Although other changes in

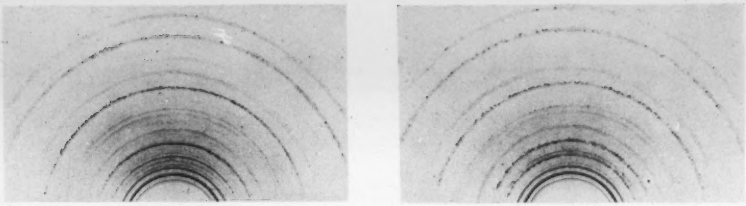

900° C 1150° C

Fig. 1. X-ray microbeam reflexion patterns of barium oxide cathodes

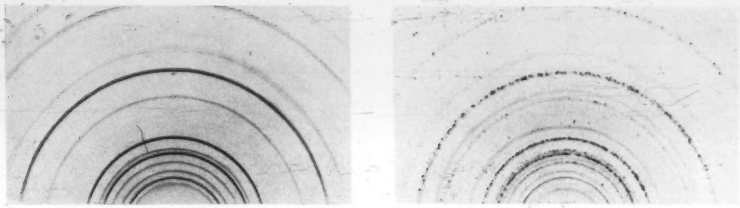

1030° C 1250° C

Fig. 2. X-ray microbeam reflexion patterns of strontium oxide cathodes

900° C 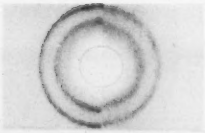 1150° C

Fig. 3. X-ray powder ring 51 for barium oxide after heating in a vacuum at different temperatures

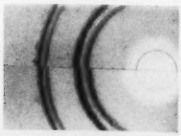

1030° C

1250° C

Fig. 4. X-ray powder rings 43 and 44 for strontium oxide heated in a vacuum at different temperatures

Identification of materials by electron diffraction in the electron microscope

By H. I. MATTHEWS, O.B.E., M.C., B.Sc., A.M.I.Mech.E., and H. WILMAN, D.Sc., Ph.D., F.Inst.P.

See pages 277–280

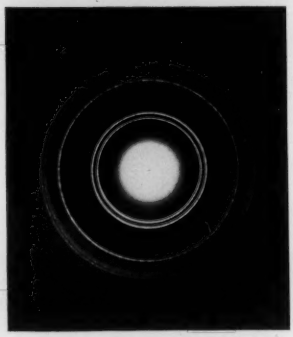

Fig. 1. Pattern corresponding to zinc; only slight orientation; 75 kV

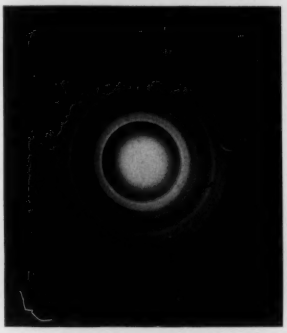

Fig. 2. Pattern corresponding to zinc oxide, with some zinc

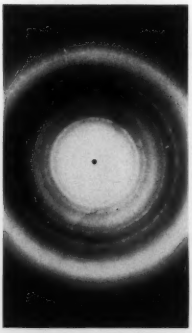

Fig. 3. F.C. cubic pattern, corresponding to lead

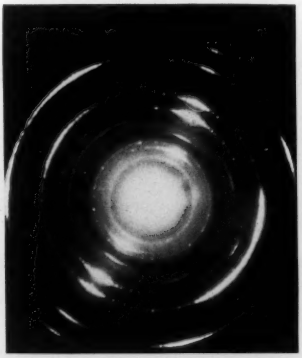

Fig. 4. Pattern due mainly to zinc, strongly orientated with (001) planes parallel to the substrate; also some zinc oxide and lead present; substrate inclined 15° from normal setting

barium oxide, described below, take place, crystal growth does not occur to any noticeable extent until temperatures above 1100° C for relatively long periods of time are reached. Then sizes of 5 to 10 μ develop. X-ray patterns of barium oxide coatings heated at 900 and 1150° C respectively are compared in Fig. 1.

Table 1. *X-ray data on barium oxide cathodes*

Cathode No.	*Heat treatment*	*Crystal size* (μ)	*Lattice parameter* (Å)
11	900° C for 9 min	2	5·5304
7	960° C for 4 min	2	$5{\cdot}529_5$
6	1030° C for 2 min + 1050° C for 30 min	2	$5{\cdot}528_5$
12	900° C for 9 min + 1150° C for 6 min	—	$5{\cdot}527_5$
10	1100° C for 5 min + 1200° C for 5 min	5	$5{\cdot}526_5$
15	1100° C for 1½ min + 1150° C for 10 min + 980° C for 1 h	5	$5{\cdot}526_2$

Unusually drastic growth of the oxide is promoted, however, when the carbonate is decomposed by raising its temperature rapidly to 1150° C or more. Crystals of barium oxide as large as 50 μ are found. The most likely explanation of this extreme condition is that, on heating to high temperature rapidly, fusion of barium carbonate occurs before decomposition is complete. In that event the first-formed crystallites of barium oxide can grow quickly in a flux of molten barium carbonate. This particularly rapid growth has not been observed with the other alkaline earth oxide compositions investigated, and with such coatings conditions under which part of the carbonate may fuse are probably unlikely to arise.

Apart from this unusual growth, the results show that the sizes of barium oxide crystals formed on cathodes subjected to more ordinary processing conditions fall in the range 1 to 5 μ. The values are thus several times larger than those estimated by Yamaka, and it appears that X-ray line broadening does not give a true measure of crystal size, in these "oxide" cathodes.

Strontium oxide. Table 2 shows the effect on crystal size of increasing severity of heat treatment. As would be expected from the more refractory character of strontium oxide, the sizes developed at temperatures below 1100° C are considerably smaller than for barium oxide. Individual spots cannot be distinguished, for example, on the microbeam pattern for strontium oxide heated at 1030° C for 15 min (Fig. 2). Indeed, for very short periods of heating below 1100° C reflexion broadening phenomena show small crystallites no larger than 0·1 μ; the first example in Table 2 is of such a strontium oxide specimen.

At higher temperatures substantial crystal growth does occur, though even prolonged heating at 1200° C does not induce growth much above 2 μ. Still higher temperatures could not be used with safety on the cathode devices, since the heaters generally burn out after a minute or two at 1250° C. One specimen was, however, maintained at 1250° C for 4 min and further crystal growth to a size near 5 μ is indicated (Fig. 2).

LATTICE PARAMETER CHANGES IN BARIUM AND STRONTIUM OXIDES

There is no novelty about the basic crystal structure of barium and strontium oxides. The oxides possess the face-centred cubic, sodium chloride type, crystal structure and lattice parameters of approximately 5·53 Å for barium oxide and 5·16 Å for strontium oxide have been recorded by several observers.[6] In the course of the present studies of barium oxide cathodes subjected to various heat treatments, however, the somewhat unexpected result became apparent that the lattice parameter of the barium oxide was not constant but depended upon the thermal history of the cathode. Indeed, under most conditions of preparation, barium oxide cathodes give X-ray powder photographs, the lines of which are perceptibly broadened; the investigations have shown that this line broadening originates with point-to-point or crystal-to-crystal variations in lattice parameter.

Table 2. *X-ray data on strontium oxide cathodes*

Cathode No.	*Heat treatment*	*Crystal size* (μ)	*Lattice parameter* (Å)
8	1100° C for 2 min	≃ 0·1	—
6	900° C for ½ min + 1100° C for 1 min	0·5	5·1610
3	900° C for ½ min + 1100° C for 1 min + 1050° C for 1½ min	0·5	5·1613
11	1100° C for 15 min	0·5	$5{\cdot}159_4$
5	900° C for ½ min + 1100° C for 1 min + 1200° C for 30 min	2	5·158
9	1200° C for 54 min	2	$5{\cdot}157_3$
7	1250° C for 4 min	4	$5{\cdot}157_5$

Variations in lattice parameter of barium oxide. It should be possible to measure the lattice parameter of barium oxide with considerable accuracy. On the X-ray Debye–Scherrer pattern with copper radiation, line 51 occurs at a Bragg angle of approximately 85°, so that with a Straumanis film arrangement the usual errors in lattice-parameter determinations become very small. Unfortunately, in the present measurements the possible accuracy is reduced because most of the cathode specimens give more or less broadened lines.

Comparatively sharp lines were obtained on the X-ray diffraction pattern from a barium oxide cathode prepared by careful decomposition of the carbonate at 900° C (Fig. 3). From this the lattice parameter was calculated to be 5·5304 ± 0·0005 Å. This is the maximum value obtained for any of the series of barium oxide preparations. As the temperature of processing was raised it was found that, in addition to some deterioration in line sharpness, the line position shifted progressively towards higher Bragg angles. Thus the mean lattice parameter decreases with increasing temperature. The magnitude of the changes is shown by the values listed in Table 2. Line 51 of the X-ray pattern of a

cathode heated at 1150° C is compared with the corresponding line from the 900° C specimen in Fig. 3.

At the higher temperatures, 1150 and 1200° C for example, the time of heating probably also has an influence on the lattice changes. But this aspect has not been investigated in any detail.

Such decreases in lattice spacings caused by heating in a vacuum reflect considerable perturbations of the atomic arrangement. They take place at temperatures at which the barium oxide is dissociating and beginning to volatilize. If in this way a number of defects in the structure are created, some change in the average interatomic distances may be expected. If an analogy with ferrous oxide is valid, the observed decrease in atomic spacings is consistent with a deficiency of barium atoms. In ferrous oxides, in which the iron concentration can vary over a wide range below the stoichiometric amount, it has been shown that the lattice parameter decreases as the iron concentration decreases.[7]

The observed X-ray line broadening is also explained by the lattice-parameter changes. The particular conditions under which the polycrystalline barium oxide specimens have been formed make it probable that the lattice disturbances do not take place uniformly, as between one crystallite and another, or even throughout a given crystal fragment. Thus some variability in the mean interatomic distances will be likely, and this variability will manifest itself as X-ray line broadening.

These changes in the barium oxide lattice have been shown by Wright[4] to be an important factor in influencing the thermionic behaviour. A rise in thermionic emission from barium oxide cathodes occurs with increasing temperature of heating, and it is the development of the lattice defects described which appear to be primarily responsible for this rise.

Variations in lattice parameter of strontium oxide. X-ray powder diffraction patterns of strontium oxide taken with copper radiation reveal lines 43 and 44 at Bragg angles near 80°, conveniently placed for moderately accurate lattice parameter determination. For strontium oxide cathodes processed at temperatures in the range 900 to 1100° C, measurements show the cubic structure cell to have an a_0 value of 5·1609 ± 0·0005 Å (see also Fig. 4). The crystallite size of the strontium oxide formed in this temperature range, as indicated by microbeam photographs, is not appreciably below 0·5 μ, but for specimens given only a short heating the size is still lower, since there is noticeable broadening of the high-order lines 43 and 44.

A decrease in structure-cell dimensions, as shown by the figures listed in Table 2, takes place on heating at 1200° C and above. The observed decrease is of the same order as was established for barium oxide. The short heat treatment at 1250° C gave a similar result to prolonged heating at 1200° C. As previously mentioned, attempts to use more severe processing conditions with the present cathode devices had to be abandoned.

As for barium oxide, the changes in the measured lattice parameter of strontium oxide entail some increase in variability of the lattice spacings, sufficient to give rise to perceptible X-ray line broadening. The effect is most manifest in the case of specimen 7 (Table 2), heated at the highest temperature. Even in this example, however, the effect remains much smaller than was found for barium oxide.

Back-reflexion microbeam patterns suggest that reflexion spots from individual crystallites are not abnormally extended, but that they occur over a larger than usual angular range. If this is true, then the variability in lattice parameter arises between one crystallite and its neighbours rather than within a given crystallite. It has not so far proved possible to investigate barium oxide in a similar way.

SUMMARY AND CONCLUSIONS

The investigations have established that the average crystal size developed in a barium oxide cathode formed in the temperature range 900 to 1100° C lies between 2 and 5 μ. This is several times greater than the figure deduced by Yamaka[1] from X-ray line-broadening measurements. A relatively small increase in crystal size occurs with increase of temperature of heating. Excessive growth to sizes as large as 50 or 100 μ can be promoted, however, in the unusual circumstances in which too rapid heating leads to melting of the original barium carbonate before decomposition is complete.

Another significant effect is the progressive decrease in the mean value of the interatomic spacings as the temperature of heating in a vacuum increases. This change, which approaches 0·1% at 1150–1200° C, appears to be associated with outward diffusion and evaporation of barium oxide from the crystallites, which partially disrupts the crystal structure and leads to a considerable increase in the number of defects. It is likely that this process corresponds with development of a thermionically "active" state in the barium oxide coating.

Similar observations have been made on strontium oxide cathodes, but, as is to be expected, the temperature range in which the lattice disturbances become apparent is considerably higher than for barium oxide. Up to 1250° C, the upper limit of temperature reached in the present work, the maximum measured change in lattice spacing is 0·07%. The maximum size of strontium oxide crystal observed in the temperature range investigated is about 4 μ.

In the polycrystalline specimens studied the lattice changes induced by heating are not effected uniformly and homogeneously. In a given specimen there is thus a small variability in the mean lattice parameters as between one crystallite and another, with the consequence that X-ray diffraction line broadening will be observed under some experimental conditions. This is one factor which must make X-ray line broadening an unsatisfactory measure of crystallite size, and could account, at least in part, for the incorrect small values obtained by earlier workers.

ACKNOWLEDGEMENTS

The author desires to tender his acknowledgement to the M.O. Valve Co. Ltd., on whose behalf the work described in this paper was carried out.

REFERENCES

(1) YAMAKA, E. *J. Appl. Phys.*, **22**, p. 1087 (1951); **23**, pp. 498, 937 (1952).
(2) HIRSCH, P. B., and KELLAR, J. N. *Acta Cryst.*, **5**, p. 162 (1952).
(3) GAY, P., HIRSCH, P. B., and KELLY, A. *Acta Cryst.*, **7**, p. 41 (1954).
(4) WRIGHT, D. A. *Vide*, **9**, p. 58 (1954).
(5) EISENSTEIN, A. *J. Appl. Phys.*, **17**, p. 434 (1946).
(6) WYCKOFF, R. W. G. *Crystal Structures*, Vol. I (New York: Interscience Publishers Inc., 1949).
(7) ROOKSBY, H. P., and WILLIS, B. T. M. *Acta Cryst.*, **6**, p. 827 (1953).

Identification of materials by electron diffraction in the electron microscope

By H. I. Matthews, O.B.E., M.C., B.Sc., A.M.I.Mech.E., and H. Wilman, D.Sc., Ph.D., F.Inst.P., Chemical Engineering Department, Imperial College, London, S.W.7

[*Paper first received* 2 *March, and in final form* 30 *March*, 1955]

The recognition and avoidance of impurities are briefly discussed. It is shown that in the use of electron microscopes for the electron diffraction identification of specimen nature, the minute particles worn off the brass specimen holder during the mounting of the specimen sometimes give rise to deposits of zinc, zinc oxide and lead. Specimen holders should therefore be of a material harder and less volatile than brass.

It is emphasized that in order to use diffraction intensities reliably for identification, or to assist in determination of lattice form and dimensions, patterns should be obtained with the specimen film inclined to the electron beam. In the identification of electron diffraction patterns valid use can be made of X-ray powder-pattern data, although the relative ring intensities differ appreciably from those in electron diffraction.

Although electron microscopes are still, in some ways, not so efficient and versatile for diffraction as are electron diffraction cameras, their use of a condenser lens to focus a high-intensity beam on to a small area of specimen is often a valuable feature, although not always desirable. In particular, this can often assist the identification of the components in intimate mixtures of two or more materials. For this purpose it is important to recognize, and preferably avoid, adventitious impurities, the pattern from which might be wrongly attributed to the specimen under investigation. It is also sometimes necessary to make use of the relative intensities of the diffractions, or to determine the lattice form and dimensions of the specimen material, as an aid to its identification, and appropriate specimen mounting is then required as described below.

Recognition and Avoidance of Impurities

Impurities may arise in (i) preparation of the specimen or the substrate film; (ii) exposure of the specimen or film during conveyance to the microscope; (iii) abrasion of the inner wall of the specimen cap in the process of mounting it on the holder; (iv) contamination of specimen or film in the microscope, particularly during exposure to the beam.

Examples of type (i) are the avoidable traces of the greases or waxes from finger-prints or inadequate cleaning of glass vessels or tweezers.[1] The main rings are the *hk*0 diffractions of the orthorhombic cell ($a = 7{\cdot}49$, $b = 4{\cdot}97$, $c > 20$ Å), with net-plane spacings (d) of 4·19, 3·74, 2·48, 2·23, 2·07, 1·87 Å, etc.

Sodium chloride (f.c. cubic with $a = 5{\cdot}628$ kX) is another frequent but water-soluble impurity associated with finger-prints (or perspiration), also often present in appreciable amount in chemicals of less than the highest grades of purity.

The type of impurity (ii) includes products of reaction of the specimen with the atmosphere, for example, oxidation, especially in humid atmospheres; and sulphides or halides produced by exposure of thin films or particles of reactive metals (silver, copper, etc.) to laboratory air containing hydrogen sulphide, sulphuric dioxide halogens or halogen acids. Plasticine (though not Apiezon "Q" compound) has an appreciable sulphur content which rapidly forms sulphide films on certain metals (e.g. copper) in its vicinity; and benzene may contain enough thiophene to lead to rapid formation of sulphide films on copper immersed in it. If metal specimens have been exposed to mercury vapour and amalgamation is suspected, it may be useful to compare the diffraction patterns obtained with those described by Aylmer, Finch and Fordham.[2]

Of the impurities originating in the microscope, type (iv), the contamination of the specimen which occurs as a progressively thickening deposit (possibly carbon from the charring of the grease deposit) on it during its examination in the beam is probably the best known.[3] We have now brought to light a further source of confusion which appears not to have been recognized before. Both in our own microscopes and elsewhere, we have found that the diffraction pattern of rings shown in Fig. 1. (p. 274) occurred sometimes, besides those which can be ascribed to the known nature of the specimens. These rings are mainly due to zinc, since all the strong ones correspond to a close-packed hexagonal structure with basal axis $a = 2{\cdot}66$ Å and $c/a = 1{\cdot}86$. In some cases the arcing of the rings, and their relative intensities, indicate that the zinc crystals are orientated with the (001) plane parallel to the substrate film. Patterns such as Fig. 2 (p. 274) have only occasionally been noticed, and are evidently due mainly to zinc oxide, since the strongest rings correspond to a close-packed hexagonal structure with $a = 3{\cdot}24$ Å and $c/a = 1{\cdot}60$, the main additional rings being those of zinc.

It is found that the zinc originates from small particles of brass which fall on to the specimen film when the cylindrical brass cap normally used slides on to the split end-cylinder of the specimen holder, which in our microscopes is made of stainless steel. The brass particles become heated by even short exposure to high beam intensity, to such an extent that the zinc vaporizes and condenses on the surrounding parts of the substrate film. Since it would be difficult to avoid such particles entirely when using brass caps sliding over the holder, it is concluded that both the caps and the holder should be made of some material harder and less volatile than brass.

The zinc oxide presumably arises when such zinc deposits are heated further by the beam for a sufficiently long period in the residual air in the evacuated apparatus.

The pattern usually contains other rings of weak to medium intensity, which correspond to a face-centred cubic material with $a = 4{\cdot}95$ Å. This pattern is rarely found in the absence of the zinc pattern, as in Fig. 3 (p. 274). This is evidently due to lead, since extremely few materials are known having this size of f.c. cubic cell, and the ring intensities suggest that only one atom is associated with each lattice point. Chemical analysis of the brass caps has confirmed that they contain 1–2% of lead. Lead is often added to brass to give free-

machining properties, the lead being present mainly as small globules separating the grains of the zinc–copper phase.

Fig. 4 (p. 274) is from an inclined Formvar substrate on which zinc had become deposited in the above way, and shows intense spotty arcs indicating zinc crystals with strong (001) orientation on the substrate, medium-strong spotty arcs due to (110)- or (111)-orientated lead (especially the innermost 111 arc of radius 0·85 cm, and the 220 arc of radius 1·39 cm), and more diffuse weaker continuous arcs due to zinc oxide (100 almost coincident with the lead 111 arc, 110 at 1·50 cm radius, and 200 at 1·74 cm within the zinc 110 ring).

PROCEDURE FOR IDENTIFICATION OF MATERIALS FROM THEIR ELECTRON DIFFRACTION PATTERN

Specimens formed on the supporting substrate by condensation, by crystallization from solution, or by adsorption usually show more or less strong orientation with a densely populated net plane parallel to the substrate. The ring pattern obtained with the beam normal to the substrate thus often differs much from that from the random crystals, some rings being abnormally weak or even absent.

To detect whether or not the pattern is affected in this way it is necessary to obtain patterns with the specimen film inclined, and this can be easily arranged by a minor modification of the specimen-mounting arrangements. As Fig. 4 shows, an inclination of even only 15° from the setting normal to the beam will sometimes suffice to show the arcing of the rings when orientation is present, in view of the small extent of the (thus almost perfectly flat) specimen film in the path of the electron beam. At least 45° is preferable, however, especially for lattice-determination purposes.

A pattern such as Fig. 4 can also be used to determine the amount of rotation of the diffraction pattern (about the microscope axis) relative to the specimen. The "equator-line" row of arcs on a locus through the central spot has a well-marked curvature, and in the absence of rotation the orientation axis (the normal to the specimen film) would meet the photographic plate on a line joining the centre of curvature of this locus to the central spot, and would lie on the concave side of the locus. Comparison with the known direction of inclination of the specimen therefore gives the amount of rotation. Azimuthal correlation of the diffraction pattern with the microphotograph can thus be achieved, since the amount of rotation of the image relative to the specimen is readily obtained by observing the direction of response of the image to movement of the specimen.

(*a*) *Identification when orientation is absent.* It is usually easy to see (and test by measurement) whether the ring pattern is of the cubic or hexagonal (or rhombohedral) type. In the latter case, $\sqrt{3}$ ratios of certain of the plane spacings (e.g. 100 : 110) afford a clue to the identification and indexing of the *hk*0 rings, and then by trial the axial ratio *c*/*a* can be found, using the Hull–Davey[4] or Bunn–Bjurström (Bunn[5]) type of charts. Similarly $\sqrt{2}$ ratios (e.g. 100 : 110, or 110 : 200, etc.) may indicate tetragonal symmetry and identify the *hk*0 rings, and then the *c*/*a* may be found by trial as above.

Identification is then often possible by comparison of the lattice dimensions with the data listed in the well-known *Strukturbericht* and *Structure Reports*, or by Wyckoff.[6] The tabulations of the known data for cubic, tetragonal and hexagonal crystals by Frevel, Rinn and Anderson[7] can also be consulted. When the elements present in the material are known (e.g. from spectroscopic data) or suspected, these data, and also those in *Dana's Mineralogy*[8] for possible compounds, can be compared with that from the pattern, which may also be compared with the patterns obtained from any available compounds suspected to be present.

If the pattern cannot be recognized by these means, or if further evidence of the structure type is required to differentiate between materials of nearly the same lattice dimension (e.g. if f.c. cubic, whether sodium chloride, zinc sulphide or calcium fluoride type, etc.), then it is necessary to use the relative intensities of the diffraction rings, at least qualitatively, as follows.

First, if the crystals are several hundred ångströms or more in diameter, as indicated by the sharpness of some or all of the rings, it is important to consider whether the crystals are roughly spherical or are more or less plate-shaped or needle-shaped, as shown by the equality or otherwise of the breadths of the various rings, or by the shape observed in the image in microscopy. Due allowance can then be made to some extent for the different absorption of the electron beam in the directions in the crystals at which the various Bragg reflexions occur. Plate-shaped crystals include those of materials having a "layer-lattice" structure, such as cadmium iodide or cadmium chloride type, clays and micaceous crystals (for data see Brindley[9]). If the crystals have smooth faces, as in the cleavage faces of these layer-type structures, then refraction of the incident beam and the emergent diffracted beams occurs and some of the diffraction rings show a displacement to smaller radii, accompanied by a more or less extensive broadening and diffusion and often much weakening by absorption.[10] Certain rings may arise only by entry and emergence of the primary and diffracted beams at grazing incidence on a smooth extensive face, and some orders, such as 002 of graphite, may be entirely forbidden owing to total internal reflexion of the diffracted beams, owing to the magnitude of the inner potential and the Bragg angle concerned.[11]

It must be remembered that crystals greater than about 1000 Å thick will contribute little diffracted intensity apart from background scattering, unless made of very light atoms (carbon, oxygen, hydrogen, etc.); and that such thick parts of the specimen could be of some material other than that yielding the main pattern. In "reflexion" it is essential to use low grazing incidence to record the diagnostically most valuable inner rings, and if the surface is flat and atomically smooth the depth of penetration may be as low as 10 Å.[12]

If absorption affects all the rings about equally, or can be allowed for from the evidence of the crystal shape as above, then the plane spacings of the three strongest rings can be found and search made in the A.S.T.M. file of X-ray diffraction powder photograph data,[13] with allowance made for the fact that appreciable intensity differences may occur due to the different relative structure factors (S^2) in X-ray and electron diffraction. The differences arise because the ratio of the scattering powers of two different atoms at any given $(\sin\theta)/\lambda$ value, i.e. for any particular ring, is not the same for electron as for X-ray diffraction. For example, the ratios of the copper scattering amplitude to that of sulphur at $(\sin\theta)/\lambda = 0{\cdot}1,\ 0{\cdot}2,\ 0{\cdot}3,\ 0{\cdot}4,\ 0{\cdot}5$, are, for X-rays,[14] 1·90, 2·00, 2·00, 1·94, and 1·94, while for electrons[15] they are 1·42, 1·43, 1·56, 1·71 and 1·61, respectively.

Nevertheless, in at least the simpler structures, S^2 can only take one of a small number of forms, such as the square of the sum of the scattering powers of two atoms or the square of their difference, giving strong or weak rings respectively, so that in most such cases there is still a rough correspondence of the relative intensities of neighbouring rings in the X-ray and electron diffraction patterns. In general, strong and

weak rings in the X-ray pattern are also strong or weak respectively in electron diffraction patterns, because the wavelets from the various atoms are in phase (or nearly so) for in anti-phase (or nearly so) in these two cases. It is thus seen that the identification from electron diffraction patterns depends most on the comparison of net-plane spacings with those of known materials, but that with the above proviso as to crystal size and shape, the comparison of the ring intensities with the standard X-ray intensity data can also be used, qualitatively, as a somewhat less stringent test of identification. Direct comparison with electron diffraction patterns from known suspected materials is, of course, not always easily available, but can sometimes be arranged.

(*b*) *Identification when orientation is present.* When the crystal size, shape and preferred orientation are not favourable for using the spacings and relative ring intensities as above, then, if the orientation is strong enough, the arc positions (obtained with the specimen inclined) can be used in one of the ways described by Wilman[16] to show the spatial relationships between the net planes and thus to define the unit cell. Comparison with the above-mentioned reference data may then permit identification of the material.

ESTIMATION OF LATTICE DIMENSIONS

For identification purposes it usually suffices to estimate lattice dimensions to within about 1%, which can be done by calibration of the apparatus using graphite patterns[17–19] obtained at the same lens-current settings as those used to record the pattern to be identified. However, there is usually an appreciable distortion of the pattern, both radial and circumferential, the amount depending on the degree of centring of the apertures limiting the beam, and on the lens characteristics. It is thus preferable to add a trace of very fine graphite powder to the specimen, e.g. by very gently scraping the "lead" of a pencil above it, or by forming a thin layer of aquadag colloidal graphite on the substrate initially. A composite diffraction pattern of graphite and the material investigated can then be obtained, either in a single exposure or a double exposure superposing the two separate patterns if these are obtained at slightly laterally displaced positions of the specimen. This direct method will thus allow interpolation to be applied between the known spacings of the graphite *hk*0 rings, so as to give spacing estimates accurate to the order of 0·1% when the pattern contains sharp rings.

Using the (*hk*0) graphite spacings as a standard amounts, in effect, to comparing lattice dimensions with the *C–C* spacing, i.e. the carbon atom "diameter," and has the advantage that the basal axis *a* of graphite varies scarcely appreciably between room temperature and 1000° C.[20] The X-ray diffraction measurements of Trzebiatowski[21] and Nelson and Riley[20] showed that at room temperature $a = 2{\cdot}4563$ kX, $c/a = 2{\cdot}626$; and $a = 2{\cdot}4562$ kX, $c/a = 2{\cdot}626$, respectively, thus $d_{110} = 1{\cdot}2281$ kX $= 1{\cdot}2301$ Å.

Though Finch and Fordham[17] had initially suggested using gold foil as a standard, its lattice dimension is subject to considerable variation, as work by Garrod[22] and by Lu and Malmberg[23] has shown. Garrod demonstrated that it was this that led to the apparently abnormal *a* value obtained for sodium chloride by Finch and Fordham, and that when graphite was used as the common reference, the sodium chloride was found to have as lattice dimension the normal X-ray diffraction value, while the gold had sometimes abnormal dimensions. It can now be said that alkali halides, when of reasonably high purity, can be used as sub-standards (e.g. for sodium chloride $a = 5{\cdot}628$ kX $= 5{\cdot}640$ Å at room temperature).

Finally, it should be noted that much evidence has shown that for pure materials, when the heating caused by the electron beam is negligible, the lattice dimensions are the same as those found by X-ray diffraction, at least when the crystals are larger than 120 Å diameter.[24] Slight deviations may occur in the case of smaller crystals, according to Boswell's results,[25] though further confirmation of this is desirable, since other observations (e.g. Boochs[26]) have shown no appreciable deviation in small-crystal metal deposits. In the electron microscope, where high beam intensities are used at times, the specimen temperature may often be so much raised as to lead to appreciable (though only small) discrepancies between calculated lattice dimensions and the room-temperature measurements given in the literature.

ACKNOWLEDGEMENT

The authors thank Mr. M. L. Levin, of this laboratory, for Figs. 1 and 2.

REFERENCES

(1) MARK, H., MOTZ, H., and TRILLAT, J. J. *Naturwissenschaften*, **20**, p. 319 (1935); TRILLAT, J. J., and MOTZ, H. *Trans Faraday Soc.*, **31**, p. 1127 (1935); MOTZ, H., and TRILLAT, J. J. *Z. Krist.*, **91**, p. 248 (1935).

(2) AYLMER, A. E., FINCH, G. I., and FORDHAM, S. *Trans Faraday Soc.*, **32**, p. 864 (1936) (note that Fig. 6 there is now known to be due to Ag + Ag_2S); see also PINSKER, Z. G. *Electron Diffraction*, translated by SPINK, J. A., and FEIGL, E. (London: Butterworths Scientific Publications, 1953), but note that Plate IX Figs. *a* and *b* are also largely due to Ag_2S.

(3) WATSON, J. H. L. *J. Appl. Phys.*, **18**, p. 153 (1947); BURTON, E. F., SENNETT, R. S., and ELLIS, S. G. *Nature* [*London*], **160**, p. 565 (1947); MENTER, J. W. *J. Inst. Metals*, **81**, 163 (1952); HAINE, M. E., and HIRST, W. *Brit. J. Appl. Phys.*, **4**, p. 239 (1953).

(4) HULL, A. W. *Phys. Rev.*, **10**, p. 661 (1917); HULL, A. W., and DAVEY, W. P. *Phys. Rev.*, **17**, p. 549 (1921); DAVEY, W. P. *Gen. Elect. Rev.*, **25**, p. 565 (1922).

(5) BUNN, C. W. *Chemical Crystallography* (Oxford: Clarendon Press, 1945).

(6) WYCKOFF, R. W. G. *The Structure of Crystals* (New York: Reinhold Publishing Corporation, 2nd Ed., 1931, and Supplement, 1934); *Crystal Structures*, Vols. 1–3 (London: Interscience Publishers Ltd., 1948–53).

(7) FREVEL, L. K. *Industr. Engng Chem., Analyt. Ed.*, **14**, p. 687 (1942); FREVEL, L. K., RINN, H. W., and ANDERSON, H. C. *Industr. Engng Chem., Analyt. Ed.*, **18**, p. 83 (1946); FREVEL, L. K., and RINN, H. W. *Analyt. Chem.*, **25**, p. 1697 (1953).

(8) PALACHE, C., BERMAN, H., and FRONDEL, C. *Dana's System of Mineralogy*, 7th Ed., 2 Vols (London: Chapman and Hall Ltd., 1944, 1951).

(9) BRINDLEY, G. W. (Editor). *X-Ray Identification and Crystal Structures of Clay Minerals* (London: The Mineralogical Society, 1951).

(10) TRENDELENBURG, F. *Naturwissenschaften*, **20**, p. 655 (1922); **21**, p. 173 (1933); TRENDELENBURG, F., FRANZ, E., and WIELAND, O. *Z. Tech. Phys.*, **14**, p. 489 (1933); TRENDELENBURG, F., and WIELAND, O. *Wiss. Veröff. Siemens-Konz.*, **13**, pp. 31, 41 (1934).

(11) YAMAGUTI, T. *Proc. Phys. Math. Soc. Japan*, **16**, p. 95 (1934); MIYAKE, S. *Proc. Phys. Math. Soc. Japan*, **22**, p. 666 (1940).

(12) FINCH, G. I., and WILMAN, H. *Trans Faraday Soc.*, **33**, p. 337 (1937); FINCH, G. I., LEWIS, H. C., and WEBB, D. P. D. *Proc. Phys. Soc.* [*London*] *B*, **66**, p. 949 (1953).
(13) *Alphabetical and Numerical Indexes of X-Ray Diffraction Data*, 1953 Ed. (Philadelphia, U.S.A.: American Society for Testing Materials, 1954: Sole U.K. agents: The Institute of Physics, London).
(14) See *Internationale Tabellen zur Bestimmung von Kristallstrukturen*, **2**, (Berlin: Borntraeger, 1935).
(15) See, e.g. THOMSON, G. P., and COCHRANE, W. *Theory and Practice of Electron Diffraction* (London: Macmillan and Co. Ltd., 1939).
(16) WILMAN, H. *Acta Cryst.*, **5**, p. 782 (1952).
(17) FINCH, G. I., and FORDHAM, S. *Proc. Phys. Soc.* [*London*], **48**, p. 85 (1936).
(18) FINCH, G. I., and WILMAN, H. *Proc. Roy. Soc. A*, **155**, p. 345 (1936).
(19) FINCH, G. I., and WILMAN, H. *Ergebn. Exakt. Naturwiss.*, **16**, p. 353 (1937).
(20) NELSON, J. B., and RILEY, D. P. *Proc. Phys. Soc.* [*London*], **57**, p. 477 (1945).
(21) TRZEBIATOWSKI, W. *Roczniki Chem.*, **17**, p. 73 (1937).
(22) GARROD, R. I. *Proc. Phys. Soc.* [*London*] *A*, **65**, p. 292 (1952).
(23) LU, C. S., and MALMBERG, E. W. *Rev. Sci. Instrum.*, **14**, p. 271 (1943).
(24) ELLEMAN, A. J., and WILMAN, H. *Proc. Phys. Soc.*, [*London*] *A*, **62**, p. 344 (1949).
(25) BOSWELL, F. W. C. *Proc. Phys. Soc.* [*London*] *A*, **64**, p. 465 (1951).
(26) BOOCHS, H. *Ann. Phys.* [*Leipzig*], **35**, p. 333 (1939).

The flexural vibrations of an end-loaded vertical strip

By R. F. S. HEARMON, F.Inst.P., and E. H. ADAMS, Forest Products Research Laboratory, Princes Risborough, Bucks

[*Paper received* 18 *March*, 1955]

An approximate equation is derived for the frequency of vibration of an end-loaded fixed-free strip having the loaded end vertically below the fixed end. This equation, which is an improvement on previous results, is compared with experiment, and a comparison is also made between the observed and predicted deflexion curve of the vibrating strip. In both cases the agreement is satisfactory.

(1) INTRODUCTION

The system considered in the present paper is shown in Fig. 1, in which Ox and Oy are respectively the vertical and horizontal directions. An elastic strip, regarded for the present as of negligible mass, is clamped at O and carries at its lower, free end a mass m. This lower end oscillates between the limits m^1 and m, along the arc $m^1 L\, m$.

If the system is turned through a right angle, so that Ox is horizontal and Oy vertical, the strip becomes an end-loaded cantilever, the vibrations of which have been studied theoretically by Davies,[1] with special reference to the measurement of Young's modulus. One advantage which the arrangement of Fig. 1 has over the cantilever for this purpose is that, however great the load, there is no initial static deflexion. It is thus possible to carry out the measurements in the absence of static deflexion, and, by increasing the load, to study the behaviour of the material of the strip at very low frequencies; these advantages may be quite important for materials in which the modulus varies with stress and frequency.

The system of Fig. 1 is more complicated in one respect than the simple cantilever because, when the mass is displaced to the position m, there are two restoring forces acting on it, namely (i) the elastic restoring force of the bent strip and (ii) the component of the weight mg, resolved along mL.

The second component is analogous to the restoring force acting on the bob of a simple pendulum displaced from its rest position, and is absent when the strip vibrates as a cantilever. Under some circumstances this component can appreciably influence the frequency of vibration of the strip when vibrating as shown in Fig. 1.

In 1940, one of the present authors attempted to take this effect into account by assuming that the length L of the equivalent pendulum was the same as the length l of the strip, and the result was published in 1948[2] in the form of a correction to be applied to the Young's modulus calculated from the usual cantilever formula.[2, 3]

However, Balinkin[4] had earlier considered the same problem, but his paper was overlooked until recently. Balinkin, following the usual treatment appropriate to the cantilever,[3] assumed that the deflexion curve Om (Fig. 1)

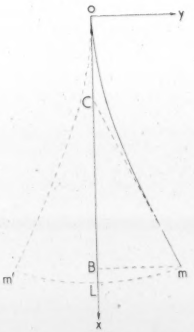

Fig. 1. Diagram of system

of the strip was the same as that of a statically deflected end-loaded cantilever:

$$y = (W/6EI)(3lx^2 - x^3) \qquad (1)$$

where y = deflexion of a point x on the strip,
W = end load,
E = Young's modulus,
I = moment of inertia of cross-section.

He further assumed that the length of the equivalent pendulum was CL (Fig. 1), where C is the point at which the tangent to the deflected strip at its end point m meets the vertical axis. It is easily shown from equation (1) that this assumption leads to an equivalent length for the pendulum of $2l/3$, provided the deflexion is small.

The assumption that $L = l$ leads to the dimensionless equation

$$\omega\sqrt{(l/g)} = \sqrt{(3r + 1)} \tag{2}$$

where ω = angular frequency,
g = gravitational acceleration,
$r = EI/mgl^2$ (3)

Balinkin's assumption that $L = 2l/3$ leads to the equation

$$\omega\sqrt{(l/g)} = \sqrt{(3r + 1{\cdot}5)} \tag{4}$$

It will be seen that equations (2) and (4) differ in the constant term under the right-hand square root sign, and the present investigation was carried out in an attempt to resolve this discrepancy.

(2) THEORETICAL ANALYSIS

The Rayleigh method[5] has been applied here to obtain an approximate solution of the problem. It is assumed as a first approximation that the deflexion curve of the vibrating strip is given by equation (1) and thus, for simple harmonic motion

$$y = k(3lx^2 - x^3)\cos\omega t \tag{5}$$

where $k = W/6EI$.

The potential energy of the system is made up of two parts:

(i) the potential energy of bending

$$V_1 = \tfrac{1}{2}EI\int_0^l \left(\frac{d^2y}{dx}\right)^2 dx \tag{6}$$

(ii) the potential energy (V_2) of raising the mass m through the distance BL (Fig. 1), where BL is perpendicular to mB. Considering any element ds of the curve Om,

$$ds^2 = [1 + (dy/dx)^2]dx^2$$

and since the deflexions are assumed small, the slope is also small, and

$$ds = [1 + \tfrac{1}{2}(dy/dx)^2]dx \text{ approx.} \tag{7}$$

The length BL is $l - OB$, or approximately,

$$BL = \left(\int_{x=0}^{x=l} ds\right) - l = \tfrac{1}{2}\int_0^l \left(\frac{dy}{dx}\right)^2 dx \text{ from equation (7)}$$

Thus

$$V_2 = \frac{mg}{2}\int_0^l \left(\frac{dy}{dx}\right)^2 dx \tag{8}$$

The kinetic energy

$$T = \tfrac{1}{2}m(dy_0/dt)^2 \tag{9}$$

y_0 being the deflexion at free end of the strip, where $x = l$. Substituting equation (5) in equations (6), (8) and (9), gives

$$V_1 = 6\,EIl^3k^2\cos^2\omega t$$
$$V_2 = (12mgl^5/5)k^2\cos^2\omega t$$
$$T = 2m\omega^2l^6k^2\sin^2\omega t$$

Equating the maximum value of T to the maximum of $(V_1 + V_2)$ leads to the equation

$$\omega\sqrt{(l/g)} = \sqrt{(3r + 1{\cdot}2)} \tag{10}$$

Comparison of equation (10) with equations (2) and (4) shows that the constant term is now 1·2, corresponding to $L = 5l/6$. It should be noted that it is not necessary to assume a value for L, because, on the above analysis, this value follows from, and is implicit in, the expression chosen to represent the deflexion of the strip.

The solution given by equation (10) can be improved by applying the Ritz modification of the Rayleigh method.[6] A better approximation than equation (5) to the deflexion of the strip will be given by including a term in x^4, and in order that the resulting expression may still satisfy the boundary conditions it is taken in the form

$$y = [k_1(3lx^2 - x^3) + k_3(3lx^3 - x^4)]\cos\omega t$$

or, writing $k_2 = k_3l$, by

$$y = \{k_1(3lx^2 - x^3) + k_2[3x^3 - (x^4/l)]\}\cos\omega t \tag{11}$$

where k_1 and k_2 are arbitrary parameters.

Equation (11) is then substituted in equations (6), (8) and (9) as before; the result is

$$\omega\sqrt{(l/g)} = \sqrt{(ar + b)} \tag{12}$$

where

$$a = \frac{3(5k_1^2 + 10k_1k_2 + 12k_2^2)}{5(k_1 + k_2)^2} \tag{13}$$

$$b = \frac{168k_1^2 + 371k_1k_2 + 227k_2^2}{140(k_1 + k_2)^2} \tag{14}$$

Finally, the frequency is minimized with respect to k_1 and k_2, so that

$$\partial\omega/\partial k_1 = \partial\omega/\partial k_2 = 0$$

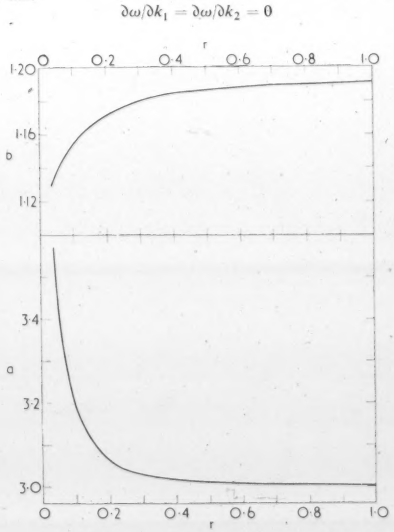

Fig. 2. Variation of a and b [equation (12)] with r

leading to

$$1176\,rk_2 = -35\,k_1 - 83\,k_2 \qquad (15)$$

Fig. 2 shows the variation of a and b in equation (12) with r. This figure was constructed by inserting appropriate values of r in equation (15) and finding the corresponding ratios k_2/k_1. These values of k_2/k_1 were then put into equations (13) and (14) to find a and b; since the equations are homogeneous the k's disappear and the a's and b's are left as simple numbers. For instance, when $r = 1$, $k_2/k_1 = -0{\cdot}02779$, $a = 3{\cdot}003$, $b = 1{\cdot}191$. Inspection of Fig. 2 shows that as r increases, a falls asymptotically to 3 and b rises asymptotically to $1{\cdot}2$, the values found for these quantities in equation (10).

(3) EXPERIMENTAL

In order to test the above analyses, experiments have been carried out on strips of mild steel, brass and boxwood. The strips were clamped at their upper end, a platform fastened to the lower end, and weights, in the form of sheet lead, were attached to the platform. Fig. 3 shows the general arrangement; this is a double-exposure photograph, the first exposure being made with the strip stationary, and the second with the strip moving, near the extremity of its swing. All the frequencies were measured by timing fifty swings with a stop watch.

Fig. 3. Double-exposure photograph of vibrating strip

The Young's modulus E of each material was found by supporting the strips on two knife edges and loading symmetrically on two lines near the ends of the strips. Under these circumstances the state of stress in the span between the supports is one of pure bending, and by measuring the deflexion at the centre of the span when a load is applied, the Young's modulus can be calculated.[7]

The strips were of rectangular cross-section and therefore

$$I = wt^3/12 \qquad (16)$$

where w is the width and t the thickness of the strip. Values of w and t were measured at a number of points along the strips and I calculated from equation (16).

The resulting values of E and I are given in the table; these are the values which were used in the calculations of Section 4(*a*) below.

The measurements on the vibrating strips are subject to correction for rotatory inertia and shear in the strip, for the finite mass of the strip and for the rotatory inertia of the load. Only the last two corrections were appreciable in the present experiments and were taken into account by replacing m wherever it occurs in the equations by

$$M = \frac{m}{1 - (9i^2/4l^2)} + \frac{33m_0 l}{140} \qquad (17)$$

where i is the radius of gyration of the load about its line of attachment to the specimen and m_0 is the mass per unit length of the specimen. Thus, in place of equation (3), r is calculated from

$$r = EI/Mgl^2 \qquad (18)$$

Both corrections are applied in the approximate form given by Rayleigh.[5] The second term in equation (17) allows for the mass of the strip; in the present experiments the magnitude of the correction varied from about 13% of M on the lightly loaded long brass strip to about 1% of M on the heavily loaded short boxwood strip. The denominator of the first term allows for rotatory inertia of the load. The value of i^2 in the present experiments was about $5{\cdot}5\ \mathrm{cm}^2$; the value of $9i^2/4l^2$ was accordingly never greater than $0{\cdot}01$ and was usually less than $0{\cdot}005$.

(4) RESULTS

(*a*) *Frequencies.* A selection of the results is given in the table and compared with values calculated from equations (10) and (12). For each material, measurements were made at intermediate values of M and l, but to save space, these additional results are not reproduced here. In each set of experiments, the values of m in ascending order were 873·0,

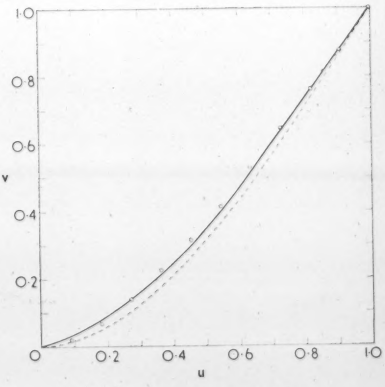

Fig. 4. Calculated and observed deflexions
– – – – = calculated [equation (20)]
——— = calculated [equation (22)]
○ = observed (Fig. 3)

Values of observed $\omega\sqrt{(l/g)}$ *compared with* $\sqrt{(ar+b)}$ [*equation* (12)] *and* $\sqrt{(3r+1{\cdot}2)}$ [*equation* (10)]

(i) *Mild Steel*—$E = 20{\cdot}3 \times 10^{11}$, $I = 8{\cdot}50 \times 10^{-4}$.

$l = 40$ cm					$l = 65$ cm				
M (g)	r	$\omega\sqrt{(l/g)}$ observed	$\sqrt{(ar+b)}$ equation (12)	$\sqrt{(3r+1{\cdot}2)}$ equation (10)	M (g)	r	$\omega\sqrt{(l/g)}$ observed	$\sqrt{(ar+b)}$ equation (12)	$\sqrt{(3r+1{\cdot}2)}$ equation (10)
908·8	1·209	2·14	2·19	2·20	922·8	0·4511	1·58	1·59	1·60
2082	0·5279	1·63	1·67	1·67	2091	0·1991	1·32	1·33	1·34
3244	0·3389	1·45	1·49	1·49	3247	0·1282	1·23	1·25	1·26
4391	0·2503	1·36	1·39	1·40	4388	0·0949	1·19	1·21	1·22
5518	0·1991	1·31	1·33	1·34	5510	0·0755	1·16	1·18	1·19
6073	0·1810	1·28	1·31	1·32	6062	0·0687	1·15	1·17	1·18

(ii) *Brass*—$E = 8{\cdot}95 \times 10^{11}$, $I = 7{\cdot}52 \times 10^{-3}$.

$l = 50$ cm					$l = 80$ cm				
M (g)	r	$\omega\sqrt{(l/g)}$ observed	$\sqrt{(ar+b)}$ equation (12)	$\sqrt{(3r+1{\cdot}2)}$ equation (10)	M (g)	r	$\omega\sqrt{(l/g)}$ observed	$\sqrt{(ar+b)}$ equation (12)	$\sqrt{(3r+1{\cdot}2)}$ equation (10)
958·4	2·863	3·08	3·13	3·13	1005	1·067	2·07	2·10	2·10
2128	1·290	2·22	2·25	2·25	2170	0·4940	1·62	1·63	1·64
3285	0·8356	1·90	1·92	1·93	3325	0·3224	1·45	1·47	1·47
4429	0·6198	1·72	1·75	1·75	4466	0·2400	1·37	1·38	1·39
5554	0·4942	1·62	1·63	1·64	5587	0·1918	1·31	1·33	1·33

(iii) *Boxwood*—$E = 1{\cdot}47 \times 10^{11}$, $I = 2{\cdot}28 \times 10^{-2}$.

$l = 40$ cm					$l = 95$ cm				
M (g)	r	$\omega\sqrt{(l/g)}$ observed	$\sqrt{(ar+b)}$ equation (12)	$\sqrt{(3r+1{\cdot}2)}$ equation (10)	M (g)	r	$\omega\sqrt{(l/g)}$ observed	$\sqrt{(ar+b)}$ equation (12)	$\sqrt{(3r+1{\cdot}2)}$ equation (10)
888·8	2·402	2·94	2·90	2·90	896·2	0·4223	1·57	1·57	1·57
2062	1·035	2·09	2·07	2·07	2062	0·1836	1·32	1·32	1·32
3223	0·6624	1·79	1·78	1·78	3217	0·1176	1·23	1·24	1·25
4371	0·4885	1·64	1·63	1·63	4357	0·0869	1·19	1·20	1·21
5498	0·3883	1·53	1·53	1·54	5477	0·0691	1·17	1·17	1·19
6053	0·3527	1·49	1·49	1·50	6029	0·0628	1·16	1·16	1·18

2038, 3190, 4329, 5448 g and, in the case of the mild steel and boxwood, 5998 g.

It will be seen that equation (10) gives reasonable agreement with experiment in most cases, and that this agreement is slightly improved by the use of equation (12). However, even when equation (12) is used, discrepancies of the order of 1–2% still remain. These may be due partly to the approximate nature of the analysis, and of the corrections represented by equation (17), and partly to experimental errors associated with the measurements.

Calculations were also made using equations (2) and (4). Equations (10) and (12) invariably gave better agreement with experiment than equation (4). In a few instances on the lightly loaded steel and brass strips the agreement with experiment of equation (2) was slightly better than equations (10) and (12) but in the great majority of cases, equations (10) and (12) gave better results. Thus it appears from the evidence of the frequencies that the best available equations are (10), or (12) if the increase in accuracy justifies the extra calculations involved in the use of the latter equation.

(*b*) *The deflexion curve.* The deflexion curve of the vibrating strip was obtained by measuring on photographs such as Fig. 3 the deflexion as a function of position along the strips; the accuracy of the measurements was, of course, increased by having the stationary strip on the print to serve as a datum for the measurements.

Introducing the variables

$$u = x/l,\ v = y/y_0 \tag{19}$$

equation (5) becomes,

$$v = (3u^2/2) - (u^3/2) \tag{20}$$

The photograph of Fig. 3 refers to the boxwood strip with $M = 3760$ g, $l = 95$ cm. Thus $r = 0{\cdot}1006$, and equation (15) gives

$$k_2 = -0{\cdot}174\, k_2 \tag{21}$$

Inserting equations (19) and (21) in equation (11) leads to

$$v = 1{\cdot}82\, u^2 - 0{\cdot}92\, u^3 + 0{\cdot}10\, u^4 \tag{22}$$

The curves corresponding to equations (20) and (22) are drawn on Fig. 4, which also contains the measured values derived from Fig. 3. It is evident that equation (22) gives a better representation of the observed deflexion curve than does equation (20). Thus, in the particular case illustrated in Fig. 3 there is an appreciable departure of the deflexion curve from that appropriate to an end-loaded cantilever [equations (1) and (20)]. The extent of this departure in any instance will depend on the value of r; equation (15) shows that as r increases, the ratio k_2/k_1 approaches zero, and for large values of r the difference between equation (1) and the more accurate equation (11) will be negligible.

ACKNOWLEDGEMENT

This paper is published by permission of the Department of Scientific and Industrial Research.

REFERENCES

(1) DAVIES, R. M. *Phil. Mag.*, **22**, p. 892 (1936); **23**, pp. 464, 563, 1129 (1937).
(2) HEARMON, R. F. S. *Elasticity of Wood and Plywood.* Spec. Rep. For. Prod. Res., London. No. 7 (London: H.M. Stationery Office, 1948).
(3) WORSNOP, B. L., and FLINT, H. T. *Advanced Practical Physics for Students.* 2nd ed. (London: Methuen and Co. Ltd., 1927).
(4) BALINKIN, I. A. *Phil. Mag.*, **21**, p. 283 (1936).
(5) RAYLEIGH, LORD. *Theory of Sound* (London: Macmillan and Co., Ltd., 1877).
(6) TIMOSHENKO, S. *Vibration Problems in Engineering* (London: Constable and Co., 1937).
(7) MORLEY, A. *Strength of Materials.* Section 57, p. 127, and Section 76, p. 183 (London: Longmans, Green and Co., Ltd., 1943).

Phenomenological approach to "current noise"

By D. A. BELL, M.A., Ph.D., Electrical Engineering Department, University of Birmingham

[*Paper first received* 26 *October*, 1954, *and in final form* 1 *April*, 1955]

There is no satisfactory theory of the noise additional to Johnson noise which is found when a steady current is passed through resistors made of any kind of semi-conducting material. Experiments by various workers have failed to show conclusively that it is an interface phenomenon. Rough estimates are given of the total fluctuation (all frequencies) and the number N of charge carriers present in three examples, and the relative fluctuations are shown to be much greater than $1/N$. The inverse-frequency spectrum cannot be a result of a particular pulse shape, but could possibly be due either to a complicated diffusion process or more probably to the law relating mean-square perturbation and time for the whole population of carriers which is not to be regarded as an equilibrium system.

It is little exaggeration to say that throughout the years since Schottky's flicker theory was first applied to semi-conductor noise the several theories which have been proposed for the latter have been mathematical models which were not based on any detailed examination of the experimental evidence. It is, of course, mathematically possible to represent any spectrum by a sufficiently extensive distribution of relaxation times, each of which has a spectrum of the form $(1 + \omega^2\tau^2)^{-1}$ but it is not physically plausible to suggest that such a range of relaxation times occurs in all the varied substances which exhibit current-noise, from carbon granules and metal films to single-crystal germanium.

It is therefore an urgent necessity to review the available experimental data, and the principal sources of information are the effects on noise of current-density, resistivity and temperature, and the spectral distribution of the noise.

THE EFFECTS OF RESISTIVITY AND CURRENT DENSITY

A law of the type $\overline{dV^2} \propto i^2R^2$ is dimensionally correct, and $\overline{dV^2} \propto i^2$ is supported by much of the experimental evidence. Departures from this law may be due to changes in the internal state of the semi-conductor at high values of current-density or field-strength. Variation of noise with "resistance" is difficult to interpret, since a change of resistance requires *either* a change of material *or* a change of size or shape: resistance is not an independent variable. Otto[1] found that the parameter which appeared to be specific to the material was one equivalent to $\overline{dV^2}/R$, and the same form applies to the combination of resistors in series and parallel. If one passes a constant steady current through two separate resistors in series, the fluctuation voltages arising in each will be uncorrelated and the total squared voltage will be only *twice* that of one resistor, though R has been increased by a factor of *four*. Similarly, if one has a number of resistors in parallel or a number of parallel paths in one resistor, the total noise will be found by summing squares. In Fig. 1, the total resistance r is supposed to be made up of n parallel resistors each of magnitude nr and each carrying $1/n^{th}$ of the current i. Each branch is expected to be the seat of a voltage of the form

$$\overline{dv^2} = I^2\overline{dR^2} = I^2R^2(\overline{dR^2}/R^2) \qquad (1)$$

which is effectively in series with the unit resistance, and since in each branch I is $1/n^{th}$ of the total current while r is n times the total resistance, $I^2R^2 = i^2r^2$. This voltage is divided between its source resistance nr and the remainder of the circuit of resistance $nr/(n-1)$, a fraction $1/n$ appearing across the terminals of the whole resistor. The contribution from one constituent path is therefore

$$\overline{dV_1^2} = (1/n^2)I^2R^2(\overline{dR^2}/R^2) \qquad (2)$$

The combination of n uncorrelated constituents will give an output

$$\overline{dV^2} = (1/n)I^2R^2(\overline{dR^2}/R^2) \qquad (3)$$

i.e. in a composite body having n constituent parts, the total mean-square fluctuation voltage will be $1/n^{th}$ of the value which would otherwise be found for the given material, resistance and current. On this basis one might expect to find (and one often does find) that the carbon film resistor is less noisy than the carbon-composition resistor, and the metal film resistor (which may possibly be regarded as a structure of extremely fine grain) is quieter than the carbon film.

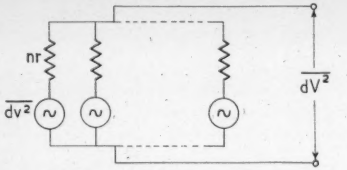

Fig. 1. Equivalent circuit of composite resistor

THE EFFECT OF TEMPERATURE

Published data on the effect of temperature on semiconductor noise have been sparse and inconclusive, but a recent set of measurements by Barber[2] on a lead-sulphide film is capable of systematic interpretation. If instead of plotting noise power against temperature in the usual way one plots the logarithm of noise power against the reciprocal of temperature, and simultaneously plots the logarithm of resistance against temperature, straight lines are obtained as shown in Fig. 2. There is a slight change in slope of the noise line at about the same temperature as the changeover point of the resistance characteristic, which may be significant of a relationship between noise and mechanisms of excitation of charge carrier. Application of the same type of plot to noise/temperature data published by Montgomery[3] for a single-crystal germanium filament is shown in Fig. 3. (Resistance/temperature data were unfortunately not published.) Although this graph is complex, it does now approximate to a group of straight lines whereas the original noise/temperature plot could only be described as an irregular wave.

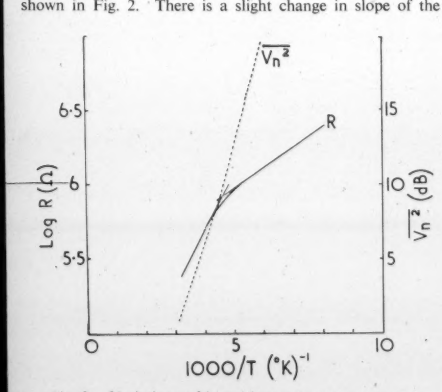

Fig. 2. Variations of logarithms of noise power and resistance with the reciprocal of temperature

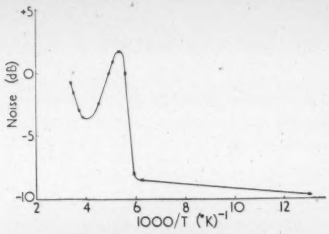

Fig. 3. Application of type of plot used in Fig. 2 to data published by Montgomery[3]

THE INVERSE-FREQUENCY SPECTRUM

The outstanding feature of current-noise is that its power spectrum (i.e. the spectrum of squared amplitudes of the Fourier components) varies as f^{-n}, with n constant and of the order of unity, over as wide a range of frequencies as can be observed. All the theoretical formulae proposed in the past show a departure from this law at low frequencies on the ground that if with $n \geqslant 1$ the f^{-n} spectrum extended over *all* frequencies the total noise power would be infinite. No such low-frequency departure from the constant index has ever been substantiated, and the work of Bernamont[4] on metal films,* Rollin and Templeton on carbon,[6] Barber on a lead-sulphide film[2] and Rollin and Templeton on germanium[7] are good examples of constancy of index over wide frequency bands which, in the case of both studies of Rollin and Templeton, extended down to about 10^{-3} c/s. Since power is constantly being fed into the resistor *via* the steady current which sets up the current-noise, and practical values are such that even in the noisiest semi-conductor the f^{-n} spectrum could extend over scores of *decades* of frequency without the total noise power reaching 1% of the input power, one need not be over-anxious about the theoretical divergence of the integral of a formula for the spectrum.

At one time it appeared that departure from $n = 1$ might be due to experimental error, but the evidence now appears sufficient to establish other values of n. Some of Bernamont's metal films[4] appeared to show $n = 0{\cdot}95$ and $n = 1{\cdot}06$ as significant departures from $n = 1$. Harris[8] found $n = 1{\cdot}45$ for lead-sulphide films (though Barber[2] subsequently found $n = 1$ for another specimen). Finally, Rollin and Templeton[7] found $n = 1{\cdot}35$ for germanium using the same techniques which had demonstrated $n = 1$ for carbon.[6] It does now appear that n is rather precisely unity in carbon but may have other values in other substances; this may be a function of the excitation energy, or of the complexity of the generation and recombination processes, or may be affected by the presence of minority carriers.

* Adjustment of Bernamont's data to eliminate an obvious discrepancy[5] makes his indices even more constant than originally appeared, though the difference is mainly at the high-frequency end.

THE EVIDENCE FOR A VOLUME EFFECT

Current-noise was at one time known as "contact noise," and both the direct transfer to this field of Schottky's theory of flicker effect in thermionic emission and the application of diffusion theories implies that current-noise arises at interfaces which have to be crossed by the steady current; yet various experiments designed to test this point have failed to give positive evidence of an interface effect. Otto[1] failed to prove interface effect in carbon granules, and found current-noise in a carbon filament. Schönwald[9] failed to eliminate current-noise from photoconductive cuprous oxide, even when he used a single crystal and terminals formed by reducing the end surfaces to pure copper. Montgomery,[10] adopting a technique of separate current and potential terminals which has now become standard practice in semi-conductor noise research, showed that current-noise was generated in the main part of a single-crystal germanium filament, away from the terminal faces. The suggestion of undetectable microscopic interfaces between different parts of a nominally single-crystal specimen is untenable because such thin layers would be bypassed by their capacitances at quite low frequencies and hence distort the f^{-n} spectrum.

THE SEARCH FOR A MECHANISM

Diffusion theories of the f^{-n} spectrum appear to be eliminated for the following reasons:

(i) they require a complicated system of *two-dimensional* diffusion to give even a rough approximation to a constant index, and the previous section shows lack of evidence for interface effects;

(ii) they have not given a constant index over a range of several decades of frequency;

(iii) their predictions of temperature-dependence are not supported by the experimental evidence.

There are mathematical grounds for saying that no single type of event can be responsible for a $1/f$ spectrum. In a Fourier-series analysis of any function which is of bounded variation, the amplitude of the n^{th} harmonic tends to decrease at least as fast as $1/n$[11] so that the power spectrum would decrease at least as fast as $1/n^2$. (This has been found to hold well for the time-average of the spectrum of a television signal, which represents a fairly random wave-form.) The author has examined several systematic decay processes, but while it is possible to devise special arrangements which give a $1/f$ spectrum *in relation to the early part of the decay of a large perturbation*, they are all found to approximate to an exponential decay (with the relaxation spectrum) when one considers small perturbations of large populations and long periods. Since the measured life-times and transit times of carriers in some semi-conductors are very small compared with the periods of spectrum analysis for the low-frequency part of the current noise, one would have to consider the later part of the decay curve; and in all practical cases the total population N is so large that a fluctuation of order $\sqrt{N}$ would be a small fractional perturbation.

A *uniform* distribution of relaxation times from $\tau = 0$ to $\tau = \infty$ would give a precisely f^{-1} spectrum, but the upper limit of τ would need to extend far beyond 10^3 s (since a constant index has been found to hold down to 10^{-3} c/s): and this is not consistent with the observed *mean* life of carriers which in germanium is a few microseconds.

The fact that current-noise occurs in semi-conductors, i.e. bodies in which the number of available charge-carriers is a random variable, suggests the idea first published by Brillouin[12] that the current noise represents merely the resistance-modulation which arises from statistical fluctuations in the number of available charge carriers. The idea seems to have been abandoned at this stage because it would not account for the magnitude of the observed resistance fluctuations. It would usually be expected that the total (i.e. all-frequency) mean-square relative fluctuation, $\overline{\Delta N^2}/N^2$, would be of the order of $1/N$. Estimates of the total numbers of carriers involved are very difficult; and the total fluctuation is undefined because the low-frequency limit of the f^{-n} distribution has not been found, but for a first approach it will be assumed that this distribution holds over ten decades of frequency, and that contributions from outside this range can be neglected. Rough estimates (to the nearest power of ten) for three different experiments are as follows, the bases of the estimates of numbers of carriers being given in the Appendix.

Estimates of total fluctuation

Resistor	*Ten-decade fluctuation*	*No. of carriers*
Lead sulphide, Barber[2]	10^{-8}	10^{12}
Carbon composition, Rollin and Templeton[6]	10^{-11}	10^{21}
Platinum film, Bernamont[4]	10^{-12}	10^{16}

Although these figures are only very rough orders of magnitude, it appears definite that the total fluctuation is substantially greater than $1/N$. But it is probable that lead sulphide and carbon-composition resistors cannot be regarded as unitary bodies, and one must also consider the effect of compounding separate noise sources within the body of a resistor.

Recently detailed analyses[13, 14] have shown that the statistical distribution of numbers of charge carriers on an equilibrium basis does not follow strictly either a Poisson or Gaussian law and the variance is not equal to the number in population. But on an equilibrium basis the distribution for large numbers is very nearly Gaussian; and for a simple model of an intrinsic semi-conductor, assuming square-law recombination, the variance is merely halved. The variances thus calculated on an equilibrium basis are therefore of the same order of magnitude as the simple assumption of a variance equal to the number in the population.

The case for a "variable-number" theory is so strong in comparison with the others outlined above, particularly in view of the correlation between noise and resistance when referred to inverse temperatures, that the author thinks this the most profitable line to pursue. The apparent dependence of the value of index on the conduction mechanism also supports the view[15] that an explanation is to be sought in the detailed mechanism of the fluctuations in number of charge-carriers, although the conventional approaches, which give values of the variances defined as equilibrium values averaged over infinite time, always lead to relaxation spectra. But the fact that reducing the lower frequency limit of the spectrum (i.e. increasing the time of observation) has always increased the noise intensity shows that the spectrum *cannot be treated in terms of infinite-time averages:* if the time of observation could be made long enough to be effectively infinite, and to correspond to the full restoration of equilibrium after all perturbations, the intensity of the spectrum would remain constant when examined over longer periods than this. The requirement is, therefore, to determine not the variance but the mean-square perturbation as a function of time; and the latter corresponds to the squared displace-

ment which in Brownian motion increases uniformly with time. The power "spectrum" of Brownian motion would therefore follow a law f^{-2}; and it appears that a spectrum law f^{-1} would result from a mean-square perturbation increasing logarithmically with time, but it has not yet been possible to show that precisely this law of perturbation is to be expected in semi-conductors.

CONCLUSIONS

The author's deductions from the experimental evidence are as follows:

(i) Current-noise in semi-conductors is a true conduction phenomenon, i.e. associated with bulk conduction rather than with contact phenomena.

(ii) When experimental results give different values of noise for different objects, the interpretation of the relation between noise and *resistance* as a function of *resistivity* requires knowledge of the internal structure of the object. There is, in fact, insufficient experimental evidence to state any general relation between noise and resistivity.

(iii) The main feature of the inverse-frequency spectrum is constancy of the index of f over a wide frequency range, whether or not the index is precisely unity.

(iv) It seems to be established that the index is precisely unity for carbon, but greater than unity for some other semi-conductors.

(v) In at least one case the noise *versus* temperature characteristic can be simplified by plotting the logarithm of noise power *versus* the reciprocal of temperature.

(vi) There is no reasonable identification of time-constants of traps, etc. with the range of relaxation times which would be needed to fit the spectrum.

(vii) Of the two general hypotheses not involving specific relaxation times, namely diffusion and statistical properties of a variable population, the latter is qualitatively supported by items (i), (iv) and (v) above.

REFERENCES

(1) OTTO, R. *Hochf. Tech. u. Elektroakus.*, **45**, p. 187 (1935).

(2) BARBER, D. *T.R.E. Technical Note No.* 168 (1954); also *Proc. Phys. Soc.* [*London*] *B*. To be published.

(3) MONTGOMERY, H. C. *Bell Syst. Tech. J.*, **31**, p. 950 (1952).

(4) BERNAMONT, J. *Ann. Phys.* [*Paris*], **7**, p. 71 (1937).

(5) BELL, D. A. *Phil. Mag.*, **43**, p. 1107 (1952).

(6) ROELIN, B. V., and TEMPLETON, I. M. *Proc. Phys. Soc.* [*London*] *B*, **66**, p. 259 (1953).

(7) ROLLIN, B. V., and TEMPLETON, I. M. *Proc. Phys. Soc.* [*London*] *B*, **67**, p. 271 (1954).

(8) HARRIS, E. J. *Electronic Engng*, **20**, p. 145 (1948).

(9) SCHÖNWALD, B. *Ann. Phys.* [*Leipzig*], **15**, p. 395 (1932).

(10) MONTGOMERY, H. C. Reported in a review article in *Electrical Engng*, **68**, p. 865 (1949).

(11) JEFFREYS, H., and JEFFREYS, B. S. *Methods of Mathematical Physics*, 2nd Ed., p. 430 (London: Cambridge University Press, 1950).

(12) BRILLOUIN, L. *Helv. Phys. Acta*, **7** (Suppl.), p. 47 (1934).

(13) BELL, D. A. *Proc. Phys. Soc.* [*London*] *B*, **77**, p. 227 (1954).

(14) BURGESS, R. E. *Physica*, **20**, p. 1007 (1954).

(15) BELL, D. A. *Wireless Engr*, **30**, p. 23 (1953).

APPENDIX

Estimates of the numbers of charge carriers in certain experiments

(i) The lead sulphide film used for noise measurements by Barber[2] was about 1 cm square, and the estimated thickness was 1 to 2×10^{-4} cm, giving a volume of 10^{-4} cm^3. A typical value for carrier concentration in such material at room temperature is 10^{16} per cm^3, resulting in 10^{12} for this film.

If we assume a mobility of 1 cm^2/V-s, a carrier density 10^{16} gives a specific conductivity of $1{\cdot}6 \times 10^{-3}$ and a resistance for the film of 6 MΩ. The measured value at room temperature was about 0·4 MΩ, so there is an uncertainty of about one power of ten in the estimate of number of charge-carriers.

(ii) A typical composition resistor weighs about 1·5 g gross, but less than a tenth of this is likely to be carbon which participates in the conduction. This may be, say, less than 1/100th g-atom (C = 12), and on this basis 10^{21} atoms is a possible estimate. It is assumed that there will be approximately one charge-carrier per atom at room temperature where the carbon has semi-metallic properties.

(iii) One of Bernamont's sputtered platinum films[4] was 4 cm long by 1 mm wide and approximately 4×10^{-7} cm thick, i.e. a volume of $4{\cdot}6 \times 10^{-7}$ cm^3. If the annealed film had approximately the density of metallic platinum, 21·3 g/cm^3, the weight of film would be $3{\cdot}4 \times 10^{-6}$ g, and with an atomic weight of 195 there would be approximately 10^{16} atoms in the film.

Electron liberation by low energy ions at metal surfaces and in gases

By H. Fetz, Institute of Physics, University of Würzburg

[*Paper first received* 15 *January*, 1954, *and in final form* 15 *December*, 1954]

Two methods are described for the production of electrons by the impact of slow moving ions with metallic surfaces as well as gas molecules of the same type. In the first method, which is the simpler of the two, a steady d.c. discharge provides the ion source but corrections are necessary for the effects of ultra-violet light. The second method, which uses a more complicated impulse technique, enables the electron emissions due to photons and positive ions to be measured separately.

The experiments have shown that with copper surfaces, cleaned by reduction, the impact of nitrogen and argon ions give yields up to 1%, whilst for hydrogen and oxygen ions the yield is below 10^{-6}. When the kinetic energy E/p is increased beyond approximately a few 100 V/cm mm of mercury, ionization by collision of the gas atoms with the positive ions is noticeable for all gases examined. This indicates that for volume ionization by ion impact, a minimum energy of twice the ionization energy is required.

The occurrence of a self-maintained discharge in a gas is dependent on ionization in the bulk of the gas by electron collisions as well as on the production of electrons by other processes. Accordingly the conventional expressions for the discharge current

$$\frac{i}{i_0} = \frac{\exp(\rho\alpha dx)}{1 - \gamma[\exp(\rho\alpha dx - 1)]}$$

and for the breakdown condition

$$\gamma \exp(\rho\alpha dx - 1) = 1$$

contain two coefficients α and γ. The first coefficient α describes the ionization by electrons and the second coefficient γ takes into account a number of other mechanisms, namely: photoelectric emission from the cathode, photoionization of the gas molecules, impact of positive ions at the cathode and the ionization by collision of these ions in the gas.

Provided the ionization coefficient $\alpha/p = f(E/p)$ is known with sufficient accuracy for a particular gas, it is not difficult to calculate γ from the sparking potential, and numerous publications have appeared which deal with this coefficient. Among the more important should be mentioned those of Posin,[1] Bowles[2] and Llewellyn Jones.[3] More recently this method was applied by Llewellyn Jones and Davies[4] and Llewellyn Jones and Williams.[5] Although it is not possible in this way to separate in a reliable manner the individual contributions to γ due to the different mechanisms, the investigations have nevertheless shown the great importance of photoemission at the cathode, apart from the ion impact at this electrode.

The ionization of the gas by ion collisions has been examined by Loeb,[6] who arrives at the conclusion that the contribution to the γ-mechanism from this source is not very marked. His argument is based on theoretical considerations and on the results of experiments with ion-rays, which showed no appreciable ionization cross-section when energies below about 100 eV were used. (For comprehensive references, see Loeb.[6]) A contribution due to this mechanism was reported by Townsend and Llewellyn Jones,[7] but with the test procedure used it is possible that their results may have been affected by ultra-violet irradiation from the ionization region. In this connexion the important work by Horton and Millest[8] should be mentioned, who found that the threshold energy for ionization by impact of two equally heavy neutral particles (helium atom → helium atom) was exactly twice the normal ionization potential.

For the study of ionic collision processes by themselves, only experiments using ion-rays are suitable and such experiments were performed as early as 1930, for example by Oliphant.[9] For low-pressure discharges, however, the ions involved have extremely small kinetic energies and for such low-energy ions it becomes extremely difficult to produce rays of sufficient intensities. Hagstrum[10] has recently overcome these difficulties to a large extent and was able to produce He^+ rays of energies down to 10 eV.

In the experiments described in this paper the disturbing influence of photoionization was completely eliminated and it is, therefore, concluded that the observed ionization effects are solely due to ion collisions. Accordingly, it is suggested, contrary to the view expressed by Loeb, that in certain cases ionization in the gas by collisions of ions may be important.

Two methods were developed for the investigation of the intensity of the electrons liberated by ion impact and experiments were made with four different ions, which impinged either on very clean or on oxidized copper surfaces. This was done for pressures varying from 5 to 15 mm of mercury.

D.C. METHOD

In this method, which is illustrated in Fig. 1(*a*), a steady Townsend discharge fed from a d.c. supply served as ion source. The discharge was maintained between a wire anode

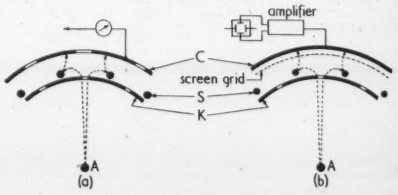

Fig. 1. Experimental arrangements

A and the concentric cylinder *K* which formed the cathode. This cylinder was provided with twelve rows of holes through which ions could escape into the surrounding space. Between two rows of holes copper rods *S* were arranged and the whole system was surrounded by another cylindrical electrode *C* which served to collect the electrons liberated by the ions

which entered the anular region between K and C. These two electrodes were maintained at the same potential, while the rods were kept at a negative potential with respect to K and C, which could be varied in order to change the energy of the impinging ions. In this way a potential barrier was provided between K and C which prevented electrons which were photoelectrically released from K and ions which passed through the holes, from being collected by C. This electrode, therefore, collected only electrons which were produced either at the surface of the rods facing C, or liberated in the gas between S and C. The electrons liberated by ions impinging the surface of S opposite to K had no chance of reaching C.

The electrodes were mounted between two ceramic plates and enclosed in a hard-glass cylinder. The whole arrangement could be heated to 500° C by placing an oven over it. The geometrical dimensions were found to be not very critical. The cathode had a diameter of 40 mm and the clearance between this electrode and K was about 5 mm. With these dimensions a rod diameter of 1·5 mm was found to be satisfactory. The rods were not arranged mid-way between the two cylindrical electrodes but slightly nearer to C. A suitable pressure range with these dimensions was between 5 and 20 mm of mercury. The potential of the rod is determined by the electric field at the rod surface which must be of the order of 100 to 500 V/cm. An upper limit to the field is set by sparkover from the rods to the cathode. The ion source was operated with currents of 0·5 to 1×10^{-3} A and the total ion current passing through the twelve rows of holes was from 1 to 30×10^{-6} A.

The rods were made of copper, since with this metal the conditions of the surface could be changed conveniently and in a reproducible manner. Using hydrogen, for example, a quick and complete reduction took place at a temperature of 250° C, whilst an oxygen discharge between A and K deposited oxygen-ions on the copper surface, so that a very thin oxide layer could easily be obtained which was invisible to the eye.

Great attention was paid to the purity of the gases used for the experiments. Hydrogen was introduced over palladium, and argon and nitrogen of high purity were supplied in high-pressure cylinders. Tests made on samples of these gases showed that only 10^{-4}% of other gases were present. Only the nitrogen content of argon was appreciably greater and amounted to approximately 0·1%. To remove condensible admixtures, such as water, the gases were cooled with liquid air before being introduced into the apparatus.

Because of the chosen layout of the apparatus no direct light from the gas discharge reached the rods and the effect of reflected light was small, since ultra-violet light, on which photoionization depends, is only weakly reflected. Also, as shown in Fig. 1, to reduce the reflexion, holes were provided in the electrode C opposite to those of K. Moreover, for correction purposes the photoionization at the surface of S could be independently measured by applying a positive potential to C and making S negative with respect to K. No ions will then pass through K so that a galvanometer connected to S will indicate only current produced photoelectrically.

For hydrogen, nitrogen and argon only surface photoelectric effects were observed and no volume photoionization. For oxygen, on the other hand, conditions were reversed and the surface effect on the rods was negligibly small and the photoelectrons produced in the gas between K and C were appreciable. This was shown in the experiments by the observation that decreasing the rod potential resulted in a residual current from the collector electrode which did not vary with this potential. The explanation is that the volume photoionization occurs in a region of weak electric field so that any electrons produced are not multiplied by gaseous ionization.

Another disturbing effect is due to ionization by collision of those electrons which were initially liberated at the surfaces of the rods. This will occur as soon as E/p adjacent to S exceeds a critical value (assuming that electron liberation takes place in proximity of S). The measured ionization yield has been corrected for this effect by subtracting values for the electron ionization which were calculated from accepted α/p values. [For nitrogen and oxygen the data given by Masch[11], and for argon those of Penning and Kruithoff[12] were used. The correction for hydrogen was more difficult, since the results published by Ayres[13], Fucks and Kettel,[14] and Hale[15] do not agree very well.]

IMPULSE METHOD

With the impulse method the ion source operated only in short pulses of about 10^{-5} s duration. As a result, two successive current pulses were observed. The first coincided with the discharge pulse and is due to photoelectric effects, while the second originates from ion collisions and hence is delayed by the travelling time of the ions.

The experimental arrangement, which is shown in Fig. 1(*b*), differed from that used in the d.c. method only by the insertion of a screen grid of about 8000 meshes/cm^2 between C and S. The purpose of this screen was to eliminate induced charges on S due to the voltage pulse. However, the screen captures most of the electrons liberated at or near S, and only a small fraction of these electrons will reach C. To compensate for this loss, a positive potential was applied to C sufficient to produce electron multiplication in the gas between C and the screen. The gain achieved in this way was determined experimentally by replacing one of the rods S by a tungsten wire of known thermal emission intensity, so that a calibration could be made.

An oscillogram of the emission current obtained with the impulse method is shown in Fig. 2. As can be seen there are two distinctly displaced current pulses. The first pulse, which is produced by photoelectric effects is surprisingly high and this, no doubt, is due to the presence of the additional screen,

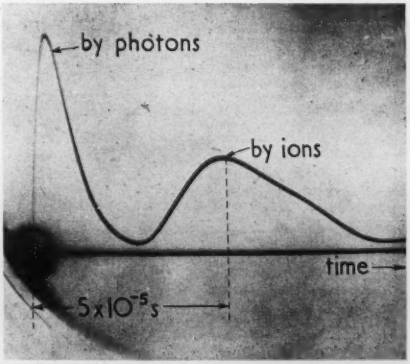

Fig. 2. Oscillogram of electron yield by impulse method

which is exposed to direct radiation coming from the holes of K. The second pulse gives a true indication of the ionization yield, which consists both of the electrons liberated at the surface as well as those formed in the gas between K and C and the screen respectively.

SEPARATION OF SURFACE AND VOLUME IONIZATION

From the current measurements obtained by either method the ionization yield η can be derived, which is the number of electrons produced per impinging ion. Plotting the value of η against E/p (where E is the field at the surface of S), graphs were obtained, which were of widely different character for different ranges of E/p. This difference made it possible to distinguish between volume and surface effects, using the following considerations.

(1) The surface effect will depend on the energy of the impinging ion, or what amounts to the same, on the E/p value at the surface of S. This dependence on E/p is expected to be relatively small for small E/p values, when, as in the present experiments, the kinetic energy is of the order of 1 eV.

(2) When η is plotted as a function of E/p, neither gas pressure nor rod diameter should influence the surface yield.

(3) Characteristics of different heights are to be expected for different surface conditions.

(4) The volume effect, on the other hand, will make η strongly dependent on E/p, the gas pressure and the rod diameter, for the number of collisions will increase with the pressure and similarly increasing the rod diameter will increase the volume of the region of sufficiently high E/p values. The quantity η/pr (where r is the rod diameter) is therefore expected to increase strongly with E/p. However, the volume effect should not be affected by the surface conditions of the target.

EXPERIMENTAL RESULTS

Surface ionization. The yield due to surface ionization determined by the above consideration is given in Table 1.

Table 1. *η for surface ionization*

Kind of ion	*Energy level*	*η for clean copper surface*	*η for oxidized copper surface*
hydrogen	1 eV	$<3 \times 10^{-6}$	$<3 \times 10^{-6}$
oxygen		—	$<10^{-6}$
nitrogen		$\simeq 10^{-2}$	$\simeq 10^{-5}$
argon		$\simeq 10^{-2}$	$\simeq 10^{-4}$

As can be seen from this table, for clean as well as oxidized copper surfaces, neither oxygen nor hydrogen ions produced appreciable surface ionization, whilst nitrogen and argon ions were very effective, particularly when clean surfaces were used.

Volume ionization. When the electron yield is plotted as a function of E/p as shown in Fig. 3, a sudden change occurs at a critical value of E/p. Beyond this value the current due to ion collisions increases strongly, and at the same time the influence of the surface conditions disappears. As pointed out, in this region the electron yield depends on E/p, the gas pressure as well as on the rod diameter.

Keeping E/p constant and varying p for the rod diameter results in a proportional variation of the current from which it may be concluded that the volume ionization predominates. Calculation shows that the corresponding coefficient of ionization varies exponentially with E/p and can be written in the form $A \exp(-Bp/E)$. The value for B in this expression is given in Table 2. It is about 10 or even more times as great as the corresponding values for electrons.

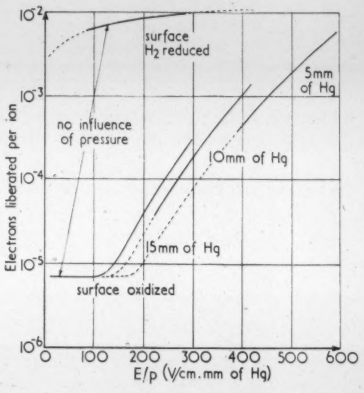

Fig. 3. Electron yield as function of E/p, with nitrogen and $r_5 = 0{\cdot}75$ mm

Table 2. *B-coefficient for various gases*

Kind of ions	*B*
hydrogen	1000 to 1400
nitrogen	2300 to 2600
argon	1500 (approx.)
oxygen	4000 (approx.)

The B-values for ions must obviously be much higher than those for electrons because of the shorter mean free path of the ions and because of the smaller energy transfer (only half) during collisions of particles having the same weight. Hence, the experimental results are in agreement with what is to be expected from theoretical considerations. No effective ionization can be expected as long as the collisions do not occur with velocities corresponding to at least twice the ionization energy.

For the coefficient A in the above expression, no reliable values can be given at present. However, the results so far obtained seem to indicate that the A-values for ions are smaller than, or at most equal to the corresponding A-values for electrons.

It is as yet not possible to state definitely whether the volume ionization is due to direct ion collision or whether it is caused by an electron exchange mechanism (Wolf,[16] Kallmann and Rosen[17]). According to this the ions gain energy during their flight in the electric field and become neutralized by resonant electron exchange and finally liberate electrons by impinging as neutral particles. Several investigators[18–22] are inclined to contribute the bulk of the ionization by ion impact to such a two-stage mechanism, since from theoretical considerations, this would require less energy than a single-stage mechanism.

ACKNOWLEDGEMENTS

The author wishes to thank his co-workers Messrs. A. Diener and W. Mahr for their care and patience in carrying out the

experiments and Professor H. Kulenkampff for providing facilities in the Institute of Physics at the University of Würzburg. He is especially indebted to Dr. H. von Bertele for providing him with the relevant English literature and to Dr. H. Tropper for his help in preparing the English text.

REFERENCES

(1) Posin, D. Q. *Phys. Rev.*, **50**, p. 650 (1936).
(2) Bowles, W. E. *Phys. Rev.*, **53**, p. 293 (1938).
(3) Llewellyn Jones, F. *Phil. Mag.*, **28**, p. 192 (1939); *Proc. Phys. Soc.* [*London*], **48**, p. 513 (1939).
(4) Llewellyn Jones, F., and Davies, D. E. *Proc. Phys. Soc.* [*London*], **64**, pp. 397 and 519 (1951).
(5) Llewellyn Jones, F., and Williams, G. C. *Proc. Phys. Soc.* [*London*] *B*, **66**, pp. 17 and 345 (1953).
(6) Loeb, L. B. *Fundamental Processes of Electric Discharges in Gases*, p. 374 (New York: John Wiley and Sons, Inc., 1939).
(7) Townsend, J. S., and Llewellyn Jones, F. *Phil. Mag.*, **15**, p. 282 (1933).
(8) Horton, F., and Millest, D. M. *Proc. Roy. Soc. A*, **185**, p. 381 (1946).
(9) Oliphant, M. L. E. *Proc. Roy. Soc. A*, **127**, p. 373 (1930).
(10) Hagstrum, H. D. *Phys. Rev.*, **89**, p. 244; **91**, p. 543 (1953).
(11) Masch. *Arch. Elektrotech.*, **26**, p. 587 (1932).
(12) Penning, and Kruithoff. *Physica*, **7**, p. 657 (1940).
(13) Ayres, T. L. R. *Phil. Mag.*, **45**, p. 353 (1923).
(14) Fucks, and Kettel. *Z. Phys.*, **116**, p. 657 (1940).
(15) Hale, D. H. *Phys. Rev.*, **54**, p. 241 (1938); **56**, pp. 815 and 1199 (1939).
(16) Wolf, F. *Ann. Phys.* [*Paris*], **29**, p. 33 (1937).
(17) Kallmann, H., and Rosen, B. *Z. Phys.*, **61**, p. 61 (1930).
(18) Beek, O., and Wayland, H. *Ann. Phys.* [*Paris*], **19**, p. 129 (1934).
(19) Berry, H. W., Varney, R. N., and Newberry, S. *Phys. Rev.*, **61**, p. 63 (1942).
(20) Berry, H. W. *Phys. Rev.*, **62**, p. 378 (1942).
(21) Varney, R. N. *Phys. Rev.*, **50**, p. 159 (1936).
(22) Wayland, H. *Phys. Rev.*, **52**, p. 31 (1937).

The square wave response method of analysing process control systems

By L. Mandel, B.Sc., Ph.D., A.Inst.P.,* Imperial Chemical Industries Ltd., Welwyn, Herts

[*Paper first received* 21 *February, and in final form* 18 *April*, 1955]

The response of a process to a periodic square wave train is examined. By introducing parameters analogous to attenuation and phase lag and making certain approximations, it is shown how the frequency response may be derived from the square wave response with little computation. The technique is seen to have much of the accuracy of the direct sinusoidal method, but requires no special signal-generating equipment.

Automatic control systems are now generally synthesized on the basis of their frequency response[1–4] and the derivation of this frequency response has therefore been the subject of much thought. As the analytical treatment of the unit processes is still in its infancy, it is usual to measure the response of the system directly.

This can be done in a variety of ways. The most direct method is to inject small sinusoidal signals of various frequencies and measure the attenuation and phase lag of the resulting sinusoidal (suitably normalized) process output.[1, 5] This is the most accurate method, but it calls for special equipment to generate pneumatic sine waves at very low frequencies.[6]

Alternatively, the same information can be obtained from a record of the time response of the system to a sudden change of input. Since the time and frequency response functions are related by a Fourier transform it is then possible to derive the latter from the former. This procedure requires no special equipment, but the results depend rather critically on the exact shape of the recorded response curve, which is usually distorted by extraneous disturbances.[5] Furthermore, considerable computational work is necessary, although a number of simplifications involving numerical approximations[7–10] or the use of the planimeter[11] have been suggested.

The square wave method of analysis seeks to combine the directness and greater accuracy of the first procedure with the experimental simplicity of the second. It calls for no equipment other than the usual recorder and appears to have been first seriously put forward by Bane.[12] The frequency response function has, of course, to be derived from the measured square wave response. Unfortunately, the exact relationship is rather complicated and leads to considerable computational work.

In this paper an attempt is made to simplify the approach by introducing two parameters analogous to attenuation and phase lag and making certain approximations. The formulae then allow the frequency response to be rapidly computed from these parameters. The analysis will be confined to systems the responses of which decrease with increasing frequency, but it is thought that there are few processes which do not satisfy this condition.

THE PRINCIPLE OF SQUARE WAVE ANALYSIS

In this method repeated step changes in the form of a square wave train are injected into the process [Fig. 1(*a*)], for example, by setting a control valve alternately above and

* Now at Department of Physics, Imperial College of Science and Technology, London, S.W.7.

below its normal working point. After a few cycles the process output becomes stationary, with a waveform depending on the repetition rate. The problem is then to relate this waveform at different periods to the sinusoidal response function.

At very low frequencies the output clearly consists of alternate positive and negative process reaction curves [e.g. as in Fig. 1(*b*)]. But, as the frequency is raised, the response generally tends to become increasingly sinusoidal [see Fig. 1(*c*)]. The Fourier series corresponding to the waveform of Fig. 1(*a*) has the form:

$$g(\omega, t) = \frac{2}{\pi} \sum_{n=1,3,\text{etc.}}^{\infty} \frac{\sin(n\omega t)}{n} \tag{1}$$

i.e. it consists of a fundamental with period $T = 2\pi/\omega$, together with odd harmonics of gradually diminishing amplitude. And, since the process is assumed to attenuate the higher frequencies increasingly, the fundamental is dominant in the output.

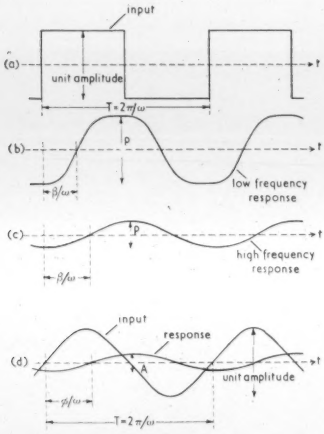

Fig. 1. Illustrating the definitions of response amplitude and phase lag

Between these frequency extremes lies the region of greatest interest, in which the waveform is approximately sinusoidal with some harmonic distortion. In the following sections we shall obtain some approximate formulae for the sinusoidal response function which take due note of this distortion. But first it will be necessary to derive an exact relationship between the sinusoidal and square wave responses.

ITERATIVE DERIVATION OF THE EXACT SERIES

Let the input $g(\omega, t)$ to the process be a rectangular wave train, with zero mean and period $T = 2\pi/\omega$, as shown in Fig. 1(*a*). Then this will be represented by the Fourier series (1). At this point it is convenient to introduce an abbreviated notation using subscripts, by writing $g(n\omega, t)$ as $g_n(t)$, etc.

When the initial transients have died down and the process output is stationary, it will be given by:

$$f(\omega, t) \equiv f_1(t) = \frac{2}{\pi} \sum_{n=1,3,5,\ldots}^{\infty} \frac{A_n}{n} \sin(n\omega t - \phi_n) \tag{2}$$

where $A(\omega)$ and $\phi(\omega)$ (or A_1 and ϕ_1) are the sinusoidal response amplitude and phase lag at the frequency $\omega/2\pi$ [Fig. 1(*d*)].

We now postulate that $A(\omega) \to 0$ with increasing ω at least as quickly as $1/\omega$, so that the successive terms in the series (2) decrease fairly rapidly. In the language of process control this will normally imply that the process contains at least one exponential stage, or, if it has no inherent self-regulation, the equivalent of at least one integration.

We require to transform equation (2) into a relationship between A_1, ϕ_1 and the f_n's and it is instructive to derive this by an iterative procedure, although a more rigorous proof is given later. The iteration will help to draw attention to the level of the subsequent approximations.

If we first neglect the higher harmonics in equation (2), we have approximately:

$$(2/\pi)A_1 \sin(\omega t - \phi_1) \simeq f_1(t)$$

and hence also:

$$(2/\pi)A_n \sin(n\omega t - \phi_n) \simeq f_n(t) \tag{3}$$

This relation (3) can now be used to obtain approximate values of the higher order terms in equation (2) and hence to derive a better estimate of $A_1 \sin(\omega t - \phi_1)$. Thus:

$$f_1(t) = \frac{2}{\pi} A_1 \sin(\omega t - \phi_1) + \frac{2}{\pi} \sum_{n=3,5,\ldots}^{\infty} \frac{A_n}{n} \sin(n\omega t - \phi_n)$$

and therefore,

$$\frac{2}{\pi} A_1 \sin(\omega t - \phi_1) \simeq f_1(t) - \sum_{n=3,5,\ldots}^{\infty} \frac{f_n(t)}{n} \tag{4}$$

From equation (4) it now follows that:

$$\frac{2}{\pi} A_n \sin(n\omega t - \phi_n) \simeq f_n(t) - \sum_{r=3,5,\ldots}^{\infty} \frac{f_{rn}(t)}{r}$$

and this improved estimate of the higher harmonics in the series (2) can again be substituted to give a still better approximation to $A_1 \sin(\omega t - \phi_1)$. By proceeding thus iteratively we obtain finally:

$$\frac{2}{\pi} A_1 \sin(\omega t - \phi_1) = f_1(t) - \sum_{i=3,5,\ldots}^{\infty} \frac{f_i(t)}{i} + \sum_{i,j=3,5,\ldots}^{\infty} \sum \frac{f_{ij}(t)}{ij} - \sum_{i,j,k=3,5,\ldots}^{\infty} \sum \sum \frac{f_{ijk}(t)}{ijk} + \text{, etc. ...} \tag{5}$$

We have therefore derived a relation between A_1, ϕ_1 and the square wave response at different frequencies, which holds at all times t. The equation looks formidable, but, in view of the initial assumptions, the individual terms of each series, and more particularly the successive sums, decrease rapidly.

It should be understood that, although equation (5) was obtained by a process of successive approximation, it holds exactly. The proof of the convergence of the series and a formal derivation are given in the Appendix.

THE SQUARE WAVE RESPONSE PARAMETERS

Equation (5) allows A_1 and ϕ_1 to be calculated, but it presumes a knowledge of the functions $f_n(t)$ at least at certain

fixed times t. These will correspond to different phases for the different $f_n(t)$ and since, ultimately, A and ϕ are to be determined over a whole range of frequencies, it is virtually true to say that the complete functions $f_n(t)$ need to be known. This involves recording and making repeated measurements of all the square wave response functions and leads to many of the disadvantages of the step response method of analysis.

From an experimental point of view it would be more satisfactory to measure only certain easily identifiable parameters, such as the maximum amplitude of the waveform, and to compute A and ϕ from these. This will, in general, lead to rather more complicated analytic relationships. However, if the experimental accuracy is such that approximations can be tolerated, it is possible to introduce considerable simplifications into the formulae.

We shall define two parameters which are analogous to the amplitude and phase lag normally associated with sine waves. Let $P(\omega)$ be the maximum amplitude of the output at the frequency $\omega/2\pi$, when the input is of unit amplitude [Figs. 1(*b*) and (*c*)]. Let $\beta(\omega)$ be the lag, expressed in radians, between the mean crossover points of the output and input waveforms [Figs. 1(*b*) and (*c*)]. These quantities can be measured with an accuracy not very much worse than for sine waves and we shall now show how good approximations to $A(\omega)$ and $\phi(\omega)$ may be derived from measurements of $P(\omega)$ and $\beta(\omega)$.

THE APPROXIMATION SERIES FOR A AND ϕ

From the approximate equation (3), $f_n(t)$ has the maximum value $(2/\pi)A_n$ and is zero at time $t = \phi_n/(n\omega)$. But, by definition, these quantities are $\frac{1}{2}P_n$ and $\beta_n/n\omega$ respectively. Hence we have:

$$f_n(t) \simeq \tfrac{1}{2}P_n \sin(n\omega t - \beta_n) \tag{6}$$

We now substitute this approximation for $f_n(t)$ into the exact series (5) for all n except $n = 1$. Thus:

$$\frac{2}{\pi}A_1 \sin(\omega t - \phi_1) \simeq f_1(t) - \tfrac{1}{2}\sum_{i=3,5,\ldots}^{\infty}\frac{P_i}{i}\sin(i\omega t - \beta_i) + \tfrac{1}{2}\sum_{i,j=3,5,\ldots}^{\infty}\sum_{ij}^{\infty}\frac{P_{ij}}{ij}\sin(ij\omega t - \beta_{ij}) -, \text{ etc.} \tag{7}$$

Now let $t = \beta_1/\omega$. Since, by definition, $f_1(\beta_1/\omega) = 0$, we obtain:

$$\phi_1 \simeq \beta_1 + \sin^{-1}\left(\frac{\pi}{4A_1}\right)\left[\sum_{i=3,5,\ldots}^{\infty}\frac{P_i}{i}\sin(i\beta_1 - \beta_i) - \sum_{i,j=3,5,\ldots}^{\infty}\sum_{ij}^{\infty}\frac{P_{ij}}{ij}\sin(ij\beta_1 - \beta_{ij}) +, \text{ etc.}\right] \tag{8}$$

It is worth noting that, to a first approximation, $\phi_1 = \beta_1$ and that the subsequent series which has been approximated represents a correction. The only unknown in the equation is A_1 but, since the term involving A_1 is a correcting term and hence small, it is adequate to use the simple approximation $A_1 \simeq (\pi/4)P_1$, so that finally,

$$\phi_1 \simeq \beta_1 + \sin^{-1}\frac{1}{P_1}\left[\sum_{i=3,5,\ldots}^{\infty}\frac{P_i}{i}\sin(i\beta_1 - \beta_i) - \sum_{i,j=3,5,\ldots}^{\infty}\sum_{ij}^{\infty}\frac{P_{ij}}{ij}\sin(ij\beta_1 - \beta_{ij}) + \ldots \text{ etc.}\right] \tag{9}$$

Thus, at any chosen frequency ω, ϕ is derivable from measurements of P and β at ω and odd multiples of ω. In practice, P and β would be plotted against frequency and the appropriate values read off from the graph.

There remains the problem of finding A_1. Let $f_1(t) = \frac{1}{2}P_1$ when $\omega t = \alpha_1$. Then, from equation (7):

$$\frac{2}{\pi}A_1 \sin(\alpha_1 - \phi_1) \simeq \tfrac{1}{2}P_1 - \tfrac{1}{2}\sum_{i=3,5,\ldots}^{\infty}\frac{P_i}{i}\sin(i\alpha_1 - \beta_i) + \tfrac{1}{2}\sum_{i,j=3,5,\ldots}^{\infty}\sum_{ij}^{\infty}\frac{P_{ij}}{ij}\sin(ij\alpha_1 - \beta_{ij}) - \ldots, \text{ etc.} \tag{10}$$

This series depends on a knowledge of α_1, i.e. the position of the output peak, which is generally less easy to measure than the position of the zero β_1. However, if we assume an approximately sinusoidal output waveform, we can put $\alpha_1 \simeq \beta_1 + (\pi/2)$. This substitution will not affect the dominant term $\frac{1}{2}P_1$ on the right-hand side of equation (10), but only the subsequent terms which are essentially corrections. The left-hand side now reduces to $(2/\pi)A_1 \cos(\beta_1 - \phi_1)$ and, since $\beta_1 \simeq \phi_1$ and the cosine is very nearly unity for small arguments, this simplifies to $(2/\pi)A_1$. Hence, finally:

$$A_1 \simeq \frac{\pi}{4}\left[P_1 - \sum_{i=3,5,\ldots}^{\infty}(-1)^{(i-1)/2}\frac{P_i}{i}\cos(i\beta_1 - \beta_i) + \sum_{i,j=3,5,\ldots}^{\infty}\sum_{ij}^{\infty}(-1)^{(ij-1)/2}\frac{P_{ij}}{ij}\cos(ij\beta_1 - \beta_{ij}) - \ldots, \text{etc.}\right] \tag{11}$$

For convenience, the first half-dozen terms of the two series (9) and (11) are given in full below, but, with experimental accuracies of a few per cent, two or three terms will usually suffice. The series themselves are, of course, approximate and the summation of too many terms only leads to a spurious impression of accuracy.

$$\phi_1 \simeq \beta_1 + \sin^{-1}\frac{1}{P_1}\left[\frac{P_3}{3}\sin(3\beta_1 - \beta_3) + \frac{P_5}{5}\sin(5\beta_1 - \beta_5) + \frac{P_7}{7}\sin(7\beta_1 - \beta_7) + \frac{P_{11}}{11}\sin(11\beta_1 - \beta_{11}) + \frac{P_{13}}{13}\sin(13\beta_1 - \beta_{13}) \ldots\right] \tag{12}$$

$$A_1 \simeq \frac{\pi}{4}\left[P_1 + \frac{P_3}{3}\cos(3\beta_1 - \beta_3) - \frac{P_5}{5}\cos(5\beta_1 - \beta_5) + \frac{P_7}{7}\cos(7\beta_1 - \beta_7) + \frac{P_{11}}{11}\cos(11\beta_1 - \beta_{11}) - \frac{P_{13}}{13}\cos(13\beta_1 - \beta_{13}) \ldots\right] \tag{13}$$

When the process under examination attenuates the higher frequencies so rapidly that the output is nearly sinusoidal, it will be found that the successive amplitudes P_1, P_3, P_5, etc., decrease very quickly. In that case it follows from the equations that: $\phi_1 \simeq \beta_1$ and $A_1 \simeq (\pi/4)P_1$, so that the results of this method are as direct as those of a sinusoidal analysis.

THE ACCURACY OF THE APPROXIMATION

In view of the several approximations involved in the derivation of the series (12) and (13), it is important to have some measure of the errors. Unfortunately, these are not easy to evaluate analytically and the expressions lead to considerable numerical work in each case. A more straight-

forward procedure is to calculate the errors in an example in which the approximations are known to be particularly weak.

The basis of the approximations is the rapid attenuation of the higher frequencies by the process; in other words, the square wave response is assumed to be roughly sinusoidal. The less rapid the attenuation, the greater are the expected errors. Since we have postulated that the frequency response falls off at least as $1/\omega$, it seems likely that the approximations will be weakest for a process consisting of a single exponential stage. The high frequency response then tends to zero as $1/\omega$, while the square wave response tends to become triangular with increasing ω.

Fortunately, it is not difficult to compute the output $f(\omega, t)$ for such a stage with given time constant τ and hence to derive the functions $P(\omega)$ and $\beta(\omega)$. If $h(t)$ is the response to a single step and $nT \leqslant t \leqslant (n + \frac{1}{2})T$, then

$$f(\omega, t) = \tfrac{1}{2}h(t) + \sum_{r=1}^{n} \left[h(t - rT) - h(t - r - \tfrac{1}{2}T)\right] \quad (14)$$

It is well known that $h(t) = 1 - \exp(-t/\tau)$ and, on substituting $t = x + nT$ and letting $n \to \infty$, we obtain:

$$f(\omega, x) = \frac{1}{2} - \left[\frac{\exp(-x/\tau)}{1 + \exp(-T/2\tau)}\right] \quad (15)$$

This function has its maximum value $\frac{1}{2}P(\omega)$ when $x = \frac{1}{2}T$ and it is zero when $2\exp(-x/\tau) = 1 + \exp(-T/2\tau)$. Thus, on replacing T by $2\pi/\omega$, we have finally:

$$P(\omega) = 1 - \left[\frac{2\exp(-\pi/\omega\tau)}{1 + \exp(-\pi/\omega\tau)}\right] \quad (16)$$

and

$$\beta(\omega) = \omega\tau \log\left[\frac{2}{1 + \exp(-\pi/\omega\tau)}\right] \quad (17)$$

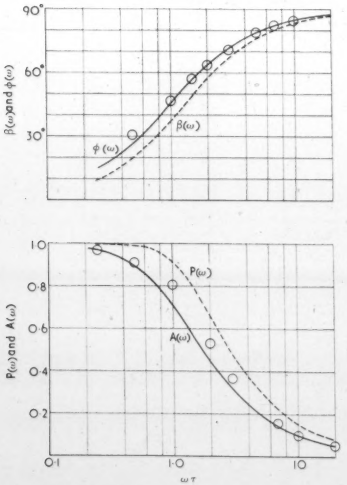

Fig. 2. Illustrating the accuracy of the approximation for a single transfer stage
(Values calculated from the series are shown as circles.)

These functions are plotted as broken curves in Fig. 2. Also shown as full curves are the well-known sinusoidal response functions:

$$A(\omega) = 1/\sqrt{(1 + \omega^2\tau^2)} \quad (18)$$

and

$$\phi(\omega) = \tan^{-1}(\omega\tau) \quad (19)$$

We can now attempt to derive the forms (18) and (19) from the functions (16) and (17) by the use of the series (12) and (13). The series converge relatively slowly for a single exponential stage and, occasionally, more than six terms are required. The calculated points are shown by the circles in Fig. 2. It will be seen that the phase angles agree very reasonably with the theoretical curve, but the weaker approximations involved in deriving equation (11) are reflected in the lower accuracy of the calculated amplitudes.

However, when we consider the very formidable test imposed on the formulae (the response is at no time even roughly sinusoidal), the resulting accuracy appears reasonable. It is probably fair to say that the errors of the approximation will never be greater and generally very much less. In practice, there will of course be experimental errors of measurement and these will normally be the more significant.

TWO EXAMPLES OF THE METHOD APPLIED IN PRACTICE

As the technique must ultimately prove its value in practice, it was decided to analyse two small pneumatic model plants by injecting both sinusoidal and rectangular pressure signals. These plants consisted of up to four non-interacting transfer stages, which were synthesized by combinations of needle valves and air chambers. The details are shown in Fig. 3.

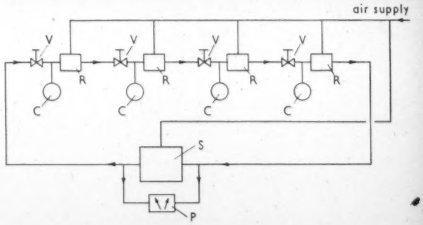

Fig. 3. The experimental set up for the analysis of the model plants
V, needle valve; *C*, air chamber; *R*, pneumatic relay; *S*, pneumatic signal generator; *P*, two-pen chart recorder.

Each stage was followed by a Kent pilot relay, the sole function of which was to isolate the stage and reproduce at low impedance the pressure at the relay input.

Use was made of the pneumatic analyser developed by Aikman[13] and Halsall.[14] This not only provided sinusoidal pneumatic signals of varying frequency, but also served as a convenient waveform recorder in both tests. In order to make the two experiments strictly comparable the plants were driven from the same source at all times and the rectangular input signals were generated by resetting the mean analyser output level at regular intervals. The following combinations of transfer stages were chosen:

(*a*) two stages with equal time constants of one minute, which we shall call plant I;

(*b*) four stages with time constants in geometric progression, namely four minutes, two minutes, one minute, half minute, which we shall call plant II.

Fig. 4 shows two actual records of the rectangular wave response of model plant II. The first one is a typical low-frequency response in which alternate half-cycles resemble the step response curve. The second record illustrates the sinusoidal form of the output at higher frequencies.

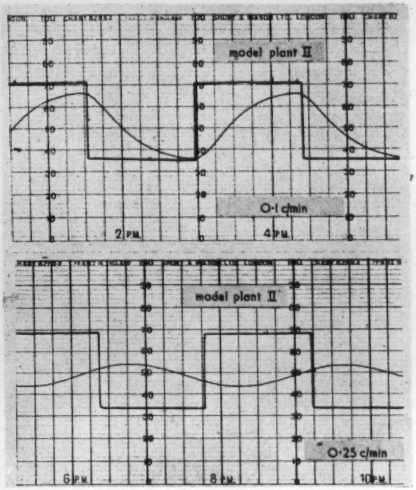

Fig. 4. Typical response curves of model plant II

The results of the measurements are contained in Figs. 5 and 6. The broken curves connect the experimental points obtained from the rectangular wave analysis and the full curves the corresponding points for sine waves. It will be seen that the two methods yield very similar phase angles and indeed, the results were practically indistinguishable for model plant II. Only the measured angles ϕ are therefore shown in Fig. 6.

The application of equations (12) and (13) yielded the values shown as open circles in Figs. 5 and 6. For the majority of points the corrections embodied in the series were, in fact, negligible. Except at very low frequencies, when there is virtually no attenuation and the rectangular wave response is not even remotely sinusoidal, the results show good agreement. When due note is taken of the decreasing accuracy of measurement (particularly phase angles) with increasing frequency, it is probably fair to attribute any differences between the measured and calculated values at the upper frequencies to experimental errors. In the analysis of real processes the measurements are complicated by disturbances superimposed on the signals and, in such cases, the inaccuracies of measurement will undoubtedly predominate.

Finally, it should be stressed that, although a pneumatic signal generator was used for all the above tests, the multiple step response analysis can be performed simply by adjusting

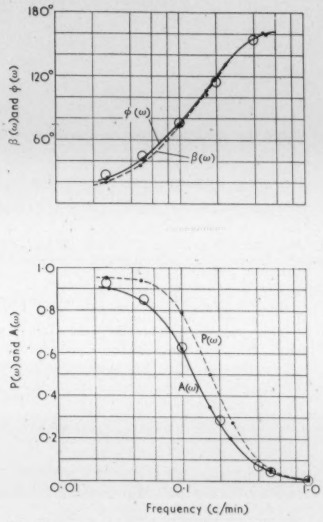

Fig. 5. The experimental and the derived response of model plant I

(Values calculated from the series are shown as circles.)

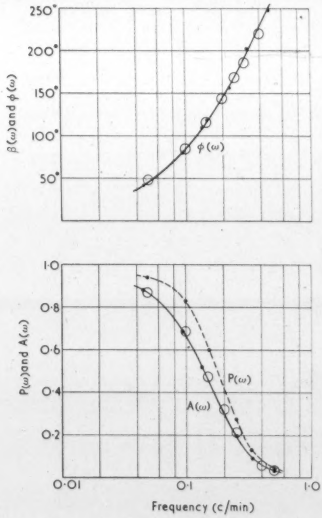

Fig. 6. The experimental and the derived response of model plant II

(Values calculated from the series are shown as circles.)

a control valve at the plant input. The only additional equipment required is a watch.

CONCLUSIONS

The square wave response method of analysing processes has been described. It has been demonstrated to have much of the directness and accuracy of the frequency response technique, without demanding special pneumatic signal generating equipment.

By introducing two easily measured parameters analogous to amplitude and phase lag, it has been shown that the frequency response function may be simply obtained from the square wave response with little calculation. In particular, the two methods of analysis become equivalent when the plant output tends to a sinusoidal form with increasing frequency.

ACKNOWLEDGEMENT

The writer wishes to thank W. M. Law for carrying out much of the experimental and computational work.

REFERENCES

(1) RUTHERFORD, C. I. *Proc. Instn Mech. Engrs*, **162**, p. 334 (1950).

(2) WESTCOTT, J. H. *Trans Soc. Instrum. Techn*, **4**, p. 113 (1952).

(3) SYRBE, M. *Regelungstechnik*, **1**, p. 160 (1953).

(4) REAM, N. *Trans Soc. Instrum. Techn*, **6**, p. 19 (1954).

(5) OPPELT, W. *Regelungstechnik*, **1**, p. 56 (1953).

(6) ST. CLAIR, D. W., ERATH, L. W., and GILLESPIE, S. L. *Frequency Response Symposium*, Paper No. 53–A–12 (New York: American Society of Mechanical Engineers, 1953).

(7) SAMULON, H. A. *Proc. Inst. Radio Engrs*, **39**, p. 175 (1951).

(8) ST. CLAIR, D. W. Instrument Society of America, Techn. Paper 52–9–3 (1952).

(9) LUDBROOK, L. C. *Electronic Engng*, **26**, p. 27 (1954).

(10) WALTERS, E. R., and REA, J. B. *J. Aero. Sci.*, **17**, p. 446 (1950).

(11) SINGER, D. *Slaboproudý Obzor.*, **14**, p. 20 (1953).

(12) BANE, W. T. Discussion on a paper by AIKMAN, A. R., *Trans Soc. Instrum. Techn.*, **3**, p. 2 (1951).

(13) AIKMAN, A. R. *Instrum. Pract.*, **5**, p. 393 (1951).

(14) HALSALL, J. R. *Instrum. Pract.*, **5**, p. 793 (1951).

APPENDIX

The formal proof of equation (5). We begin by postulating that $A_n \leqslant c/n$ for all positive integral values of n and then show that $f_n(t)$ is bounded. From equation (2):

$$f_n(t) = \frac{2}{\pi} \sum_{r=1,3,5,\ldots}^{\infty} \frac{A_{rn}}{r} \sin(rn\omega t - \phi_{rn}) \tag{20}$$

$$\leqslant \frac{2c}{\pi n} \sum_{r=1,3,5,\ldots}^{\infty} \frac{1}{r^2} = \frac{\pi c}{4n} \tag{21}$$

Consider now the $(s+1)$th term $T(s+1)$ as written in equation (5). This is given by:

$$T(s+1) = \sum_{i,j,k,\ldots s=3,5,\ldots}^{\infty} \sum^{\infty} \cdots \sum^{\infty} \frac{f_{ijk\ldots s}(t)}{ijk\ldots s} \tag{22}$$

and, using the inequality (21),

$$\leqslant \frac{\pi c}{4} \sum_{i,j,k,\ldots s=3,5,\ldots}^{\infty} \sum^{\infty} \cdots \sum^{\infty} \frac{1}{i^2 j^2 k^2 \ldots s^2}$$

$$\leqslant \frac{\pi c}{4} \left(\frac{\pi^2}{8} - 1\right)^s \tag{23}$$

It follows that the series (5) converges. To prove the relation we divide the summation (20) into two parts, namely:

$$f_n(t) = \frac{2}{\pi} A_n \sin(n\omega t - \phi_n) + \frac{2}{\pi} \sum_{r=3,5,\ldots}^{\infty} \frac{A_{rn}}{r} \sin(rn\omega t - \phi_{rn})$$

and then substitute in expression (22). Thus:

$$T(s+1) = \frac{2}{\pi} \sum_{i,j,k,\ldots s=3,5,\ldots}^{\infty} \sum^{\infty} \cdots \sum^{\infty} \frac{A_{ijk\ldots s}}{ijk\ldots s} \sin(ijk\ldots s\omega t - \phi_{ijk\ldots s})$$

$$+ \frac{2}{\pi} \sum_{i,j,k,\ldots s,r=3,5,\ldots}^{\infty} \sum^{\infty} \cdots \sum^{\infty} \sum^{\infty} \frac{A_{ijk\ldots sr}}{ijk\ldots sr} \sin(ijk\ldots sr\omega t - \phi_{ijk\ldots sr}) \tag{24}$$

On summing the terms $T(s+1)$ with due regard to sign according to the right-hand side of equation (5) we find that the first part of $T(s+1)$ cancels the second part of $T(s)$, etc. Finally there remains:

$$f_1(t) = \frac{2}{\pi} \sum_{i=3,5,\ldots}^{\infty} \frac{A_i}{i} \sin(i\omega t - \phi_i)$$

and this equals $(2/\pi)A_1 \sin(\omega t - \phi_1)$ from equation (2).

New books

Advances in electronics and electron physics, Vol. 6. Edited by L. MARTON. (London: Academic Books Ltd.; New York: Academic Press Inc., 1955). Pp. xi + 538. Price $11.80.

One looks forward, each year, to the issue of these valuable reviews, but a high price has to be paid for adding this year's volume to the series. The title has been extended by the addition of "electron physics," which brings it more into line with the normal subject matter of the volumes.

At high frequencies a superconductor is no longer without resistance and even in non-superconductors, where the electronic free path is large (i.e. at low temperatures), anomalous effects occur. These are reviewed by A. B. Pippard in "Metallic conduction at high frequencies and low temperatures." W. M. Webster, in "A comparison of analogous semiconductor and gaseous electronics devices" sets out to show that transistors (notably of the junction-type) are more analogous to gas tubes than to vacuum valves: comparisons are made between conduction processes in, and the electrical ratings of, existing devices. The behaviour of space-charge-limited currents has been investigated generally, only in cases which are simplified: H. F. Ivey in "Space charge limited currents" summarizes these results and points out the large number of problems still awaiting solution.

"The electron microscope—a review," by M. E. Haine, outlines the present state of knowledge of the instrument (apart from its applications) and indicates where further improvements may yet be sought. R. G. E. Hutter, in "Travelling-wave tubes," deals with them on the basis of a simple theory permitting common, as well as distinctive, features of the various members of the family to be brought out.

There are three articles on magnetism; the first, by E. Abrahams, deals with "Relaxation processes in ferro-magnetism," whilst J. Smit and H. P. J. Wijn discuss the "Physical properties of ferrites." It is only fitting that a review article on these types of ferromagnetic materials should come from the Philips Research Laboratories where the modern work on them originated. Lastly, J. Van den Handel, in "Paramagnetism," outlines experimental methods, gives results on certain materials and follows with theoretical treatments of the various magnetic phenomena.

A. J. MADDOCK

The inventor of the valve. By J. T. MCGREGOR-MORRIS. (London: The Television Society 1954.) Pp. 141. Price 10*s*.

This little book is a valuable factual summary of Sir Ambrose Fleming's life and achievements, spanning the years from his early days with Guthrie and Maxwell up to the time of his last scientific communication, which was to the Physical Society in 1939, when he was ninety-two. Fleming's fame will rest mainly on his introduction of the thermionic diode into wireless telegraphy, but the author makes it clear how even without this Fleming will be regarded as one of the foremost scientist-engineers of his time. In spite of his high admiration the author does not quite bring to life Fleming the man, but this deficiency is largely made good by the reproduction as an appendix of Arthur Blok's Third Fleming Memorial Lecture, delivered in 1948.

D. H. FOLLETT

Dielectric materials and applications. Edited by A. R. VON HIPPEL. (Published jointly by The Technology Press of the Massachusetts Institute of Technology, John Wiley and Sons, Inc., New York, and Chapman and Hall Ltd., London, 1955.) Pp. xii + 438. Price 140*s*.

The avowed aim of this book is the description of macroscopic dielectric phenomena, their interpretation by molecular theory, their measurement, and the properties and applications of present-day dielectric materials. So ambitious a programme is rather beyond the scope even of nearly 450 large-sized pages from 22 distinguished contributors. About a third of the book is devoted to the tables of dielectric materials which have appeared in various forms and parts over some 10 years, but are here brought up to date and given completely. Admittedly all such tables have limitations in that it is difficult to specify unambiguously materials like dielectrics, new materials or new variants continually appear and it is impracticable to give anything more than indicative values for every dielectric. This last difficulty has to a large extent been overcome by listing some 600 materials with their permittivities and loss tangents at a number of frequencies in decades and at room temperature, sometimes two or, rarely, more temperatures. The list is supplemented by curves which give the same properties of nearly 60 typical dielectrics over a range of temperature at various frequencies. It is hard to improve on this method of presentation of a unique and impressive compilation.

In the remaining two-thirds of the book the first chapter by Professor von Hippel, the Editor, provides a brief and elementary survey of macroscopic properties, in which the sections on waves are more interesting, and a survey of the theory of dielectric structure in relation to these properties, including ferro-electricity. This chapter is a mixture of very elementary first principles on the one hand and on the other hand some valuable observations on the introduction of quantum mechanics and other advanced concepts. Chapter 2 on dielectric measuring techniques is too cursory in the lower ranges of frequency or on magnetic permeability where methods are fairly well established, but contains more lengthy and attractive discussions on measurements at the very high frequencies and also on microwave spectrometry and magnetic resonance. Chapter 3 is in three parts. Part A comprises sections on gases, liquids, plastics and ceramics, which are detailed within a narrow range so as to approach contributed articles rather than parts of a book. Part B considers in a brief but competent manner the use of dielectrics in power equipment, such as transformers, switchgear, capacitors and machines, in electronic equipment, in capacitors for light-current equipment, and in cables. Part C enters the field of semi-conductors by short notes on rectifiers, returns to dielectrics with piezo-electric transducers and resonators, goes to magnetism with the magnetic amplifier and comes back again with the dielectric amplifier: similarly a final section on memory devices includes both magnetic and dielectric methods. Chapter 4, the last of the book proper, mentions some special requirements in dielectrics for the air force, army and navy. It is very brief because little can, of course, be disclosed. For this reason the chapter is rather scrappy, but it gives an indication of the onerous demands which fighting services make and often manage to secure.

This book is very uneven in its treatment and is, therefore, but too easy to criticize. It is hardly suitable nor is it probably intended for general consumption but, regarded as a work of reference, the tables of dielectric materials (separately indexed) would alone earn it a place on the shelves of any library or private collection which includes the subject of dielectrics. In addition, a reader new to the subject will gain quite a good general picture of dielectrics in theory and practice and the informed reader is likely to find quite a few stimulating ideas.

S. WHITEHEAD

Nuclear physics. By ALEX E. S. GREEN. (London: McGraw-Hill Publishing Co. Ltd., 1955.) Pp. xv + 535. Price 64*s*. 6*d*.

This book presents a thorough and detailed account of the physics of atomic nuclei. The approach is that of a theoretician: only about one-fifth of the book is devoted to a description of experimental methods (which is clear and competent and sufficiently detailed for the purpose). But in most other parts, if you open the book at random, you find a good deal of quantum mechanical formalism. For those who are not familiar with this, the first chapter, giving an introduction into relativity theory and atomic physics, will be very welcome; but it would be a bold student who tried to work through this book from cover to cover. However, it should be a most valuable companion to a lecturer preparing a course in nuclear physics or to an experimenter wishing to look up a point in theory. It is all pure physics, no applications; for instance, the fission process is discussed in great detail, but only a couple of pages are given to chain reactions. The treatment of nuclear models is fairly up-to-date, but the collective model is only briefly mentioned. All the same, the book contains a great deal of detailed and valuable information and is on the whole well-balanced and likely to be of lasting value.

O. R. FRISCH

Linearized theory of steady high-speed flow. By G. N. WARD. (London: Cambridge University Press, 1955.) Pp. xv + 243. Price 30*s*.

This book is the third to be published in the new series of Cambridge monographs on mechanics and applied mathematics. One of the reviewers of the high-speed flow volumes of modern developments in fluid dynamics, to which Professor Ward contributed the chapter on approximate methods, spoke of a vision he had had in which the authors had been allowed to forget about the space restrictions imposed on them in a composite work. One feels that, in writing this book on what is after all only part of the material of his chapter, Professor Ward has been able to go some way towards the realization of this vision.

In his preface the author says that the possibility of working entirely in terms of the particle velocity appealed to him as "giving a more physically satisfying approach to the subject than to work in terms of potentials," and he adds that "it turns out that this approach has many advantages over the more conventional treatment, and actually simplifies the analysis in many cases." I must say that I found this notation eminently satisfying and I entirely applaud the author's decision.

The book is a book of methods rather than of specific results for particular shapes. The reader who wants such results is referred to the original papers which are set out in a bibliography at the end of the book. Briefly the contents are as follows: in Part 1, after an introductory chapter dealing with the linearization of the equations, the author goes on to consider the general solutions of the linearized equations of subsonic and supersonic flow, boundary conditions, aerodynamic forces and uniqueness and flow-reversal theorems. Part 2, which deals with special methods, lays emphasis on subsonic flow past thin bodies, supersonic flow past nearly plane wings, cone fields and the application of operational methods to supersonic flow. The final part (Part 3) is devoted to the flow past slender bodies at both subsonic and supersonic speeds. The author has firmly put on one side what must have been a considerable temptation to say something about higher order approximations. It is in fact only when he discusses slender bodies, when the higher order terms are of paramount importance, that he permits himself, and obviously quite rightly, to depart from the strictest interpretation of his title.

The whole book in the reviewer's opinion forms a very satisfying work; it is relatively short and yet it contains the essence of the important contributions to the theory. The author is to be congratulated on producing a work which is eminently suited to the properly equipped beginner as well as being stimulating to the established worker.

L. HOWARTH

Progress in low temperature physics. Edited by C. J. GORTER. (Amsterdam: North-Holland Publishing Co., 1955.) Pp. xii + 418. Price 61*s*. (30.50 guilders).

This book consists of eighteen articles on various aspects of low temperature physics, each written by a worker actively engaged in the work he describes. It gives a very good picture of many recent developments, particularly in the three main fields of magnetism, liquid helium and superconductivity.

As is perhaps not surprising in a work produced by so many authors, the general impression is of a collection of papers rather than a volume dealing with its subject in a methodical manner. However, this is probably the inevitable result of the ever increasing scope of the low temperature field.

With the notable exception of Feynman's paper on liquid helium, most of the articles either review or recapitulate work already published. In the latter case, the result is often a much clearer account than has appeared previously. However, the great merit of the book is that it is a veritable mine of information for anyone interested in this field. There are, for example, over 800 references in it.

The book is well produced, and the price quite reasonable. There is no doubt that it will be a valuable addition to the library of all low temperature physicists.

J. WILKS

Behaviour of metals under impulsive loads. By JOHN S. RINEHART and JOHN PEARSON. (Cleveland, Ohio: American Society for Metals, 1954.) Pp. 256. Price $5.50.

Although research workers in this field have been quite active for some considerable time and particularly in recent years, there has been a surprising lack of authoritative books on the subject. Therefore any new book which adequately fulfils this need is to be welcomed.

The present book attempts to be comprehensive in scope, covering both physical and engineering aspects and consequently most topics are only treated in a broad, general way. Whilst the specialist in any particular aspect of the field will be disappointed by the brevity and generality of treatment, other readers will find this book useful as a broad survey of the subject. Whilst this kind of treatment is

unavoidable in a book of limited size, the reviewer feels that some chapters such as those on "Explosives and explosions" and "The practical application of explosives" could have been omitted without great loss and replaced by a more comprehensive treatment of the more relevant aspects of the subject and particularly of the recent work on such topics as delayed yielding and plastic wave propagation in pre-strained materials which are scarcely mentioned.

The book is in general well written and reproduced although improvements could be effected in the arrangement of the text which is heavily biased on explosives research. However, despite its shortcomings, it does provide a good introduction to the subject and is a useful reference book containing some 250 references which enable any particular topic to be followed up. The approach to the subject given in this book is largely experimental and in many senses it is complementary to H. Kolsky's book *Stress waves in solids*. The chapters devoted to the survey of the experimental techniques used in this field will be of particular interest to experimentalists and are perhaps the best in the book. H. Ll. D. PUGH

Proceedings of the third meeting of the joint commission on radiometeorology. Published by Union Radio-Scientifique International, 42 Rue des Minimes, Brussels (1955). Pp. 30. Price 4*s*.

This report on a meeting of the commission, held at Brussels in 1954, gives a brief account of the discussions on fluctuations of properties of the atmosphere affecting radio propagation, the diffusion of radio waves, refractive index profiles and ray theory, the use of radar in precipitation studies and the location of thunderstorms by direction-finding and analyses of atmospherics. The report concludes with recommendations for further activities, and the need for exchange of ideas by radio scientists, meteorologists and other physicists is emphasized. F. J. SCRASE

The gyroscope applied. By K. I. T. RICHARDSON, M.A. (London: Hutchinson and Co. (Publishers) Ltd., 1954.) Pp. 384. Price 30*s*.

The purpose of this book, to quote from the preface, is to explain the theory of the gyroscope in a manner understandable by all with any interest in the subject, and the book itself is a revised and much-expanded issue, by one author, of the well-known book *The gyroscope and its applications* published in 1946. The present issue is excellently printed and illustrated and is at a price which, by modern standards, is very reasonable.

The book explains practically all the "commercial" applications of gyroscopes and is sub-divided appropriately, about half of it being devoted to their various aeronautical applications. This is no doubt in keeping with the relative importance of such applications in these days, but it is a little salutary to one of the old school to note the corresponding reduction in the space devoted to the marine gyroscopic compass and to the numerous problems, such as the overcoming of the "inter-cardinal error," which had to be faced in the early days in designing this compass. However, it is probably felt by the author that this aspect has been fully treated hitherto in the standard works of Rawlings and Ferry.

In order that the book may be made of interest to a wide variety of readers, considerable space is devoted to elementary explanations of the action of the gyroscope and to elementary mathematics which will of course be familiar to physicists. Despite this it is felt that to non-physicists the descriptive matter would in some cases be somewhat difficult to follow, and this especially relates to the section dealing with automatic pilots for aircraft, necessarily complicated as the latter are. Nevertheless, this minor criticism does not detract from an otherwise excellent work upon which the author and publishers are to be congratulated. W. G. BIRD

Engineering dynamics, Vol. 1, Theory of elasticity: analytical and experimental methods. By Prof. C. B. BIEZENO and Prof. R. GRAMMEL. (London and Glasgow: Blackie and Sons Ltd., 1955.) Pp. viii + 307. Price 50*s*.

In this English translation no major revision has been attempted. The treatment of the laws of elastomechanics is still extremely pedestrian. The cautionary remarks on uniqueness theorems, and the treatment of St. Venant's principle, both very welcome, are still new to English text books.

The most serious weakness of the book lies probably in the section on two-dimensional stress functions. The authors deal very inadequately with generalized plane stress under the heading "the plane state of stress," and add still further to the confusion by referring to "Filon's generalized plane stresses and strains." The student will find it very difficult to distinguish between plane stress which involves three space co-ordinates, and generalized plane stress, and the often analagous plane strain each of which involves only two. Also, the consideration of the shear centre is very superficial. It is not shown that $V = V_1 + V_2$ is a possible condition, nor is it shown that this relation is the condition for minimum strain energy.

Part 3 on methods of solution is of immense scope and though necessarily incomplete is of a high standard. The description of the photoelastic method is highly theoretical. It contains no reference to the methods mainly in use at the present, and the discussion on the merits of glass or Bakelite has a pleasant old-fashioned ring.

References are adequate and up to date. The book is well produced, with few printer's errors, but a fuller index would have increased its value. C. SNELL

Optical properties of thin solid films. By O. S. HEAVENS, Ph.D. (London: Butterworths Scientific Publications, 1955.) Pp. vii + 261. Price 35*s*.

At this moment advances in the science of thin solid films are still being made at a rate which Dr. Heavens himself would characteristically call alarming. His success in covering so thoroughly the groundwork of his subject and in presenting so fully the most modern developments of theory and practice is all the more praiseworthy.

The style of writing is pleasant, and is particularly appreciated in the excellent chapter on theory and methods of calculation (but surely table 4.1 is in error—the reflectivity of a supported $\lambda/2$ film is independent of its refractive index). Equal weight is given to methods of measurement of film thickness and optical constants, the results of these measurements, and the practical applications of films. Film structure is ostensibly dealt with in Chapter 3 on microscopical and electron diffraction evidence; perhaps in the next edition it might be made clear at that point that much important information is also derived from the optical measurements analysed in Chapter 6. The opportunity might also be taken to reconcile apparent contradictions in the various assessments of the degree of mobility of condensed atoms.

The whole subject has been skillfully compressed into a well-printed book which can be recommended with confidence. K. M. GREENLAND

Notes and comments

Prizes for original contributions published in the *Journal of Scientific Instruments*

The Board of The Institute of Physics has awarded the following Bowen Prizes for papers published in last year's volume of the *Journal of Scientific Instruments*.

Dr. K. P. Norris, of the Wheatstone Physics Laboratory, King's College, London, for his paper on *A reflecting microscope for infra-red absorption measurements* (p. 284, August 1954). A prize of twenty guineas.

Mr. G. Revesz, of the British Rayon Research Association, Manchester, for his paper on *An autocorrelogram computer* (p. 406, November 1954). A prize of fifteen guineas.

Mr. J. H. Welch, of the Building Research Station, Watford, Herts, for his paper on *A simple microscope attachment for observing high-temperature phenomena* (p. 458, December 1954). A prize of fifteen guineas.

These prizes are awarded to authors who are not more than 35 years of age and whose papers are judged to be the best in respect of originality, scientific value, practical utility to instrument makers and users, and presentation including the standard of presentation of the manuscript. Money for prizes is provided by the Scientific Instrument Manufacturers' Association of Great Britain Ltd., from the Bowen Trust Fund established by the late Mr. William Bowen.

British Nuclear Energy Conference

In the light of recent rapid developments in the technology of nuclear energy, and the increasing demand for a common ground between scientists and engineers where these developments can be discussed, an organization has been formed by the Institutions of Civil, Mechanical, Electrical and Chemical Engineers, and The Institute of Physics, to satisfy this need. This will be known as the British Nuclear Energy Conference, the affairs of which will be managed by a Board consisting of three representatives from each of these institutions. The Chairman is Sir Christopher Hinton, and Sir John Cockcroft is one of its distinguished members. The Secretary is Mr. Alexander McDonald (Secretary of The Institution of Civil Engineers, Great George Street, London, S.W.1).

The five institutions will arrange for the presentation of papers dealing with nuclear energy subjects, and all their members will be able to attend and take part in the discussions. The Conference will publish a Journal about four times a year containing records of the papers, discussions, symposia and conferences conducted by the Board. This Journal will be offered for sale.

The Board proposes to hold its inaugural meeting in the autumn at which a symposium of lectures will be delivered on the technology of nuclear energy and its applications. The Board also proposes to promote national and international conferences from time to time, and to arrange for British participation in international meetings.

The expenses of the Conference will be met by the institutions, although it should be self-supporting once it is fully established.

Radiological protection

The recommendations of the International Commission on Radiological Protection (revised 1 December, 1954) have been published as Supplement No. 6 of the *British Journal of Radiology*. They cover general principles of protection from ionizing radiations, including definitions of the scientific terms used, a report on permissible dose for internal radiation and a report on protection against X-rays generated at potentials of 5 kV up to 2 MV. The latter report includes a section on protection against X-rays from apparatus for non-medical applications. This section contains protection-data in the form of broad-beam attenuation curves, tables of barrier thicknesses and tables giving equivalent thicknesses of protecting material. Most of this data is given in terms of the thickness of material required to reduce the dose rate to 6 mr/h, this value being based on a permissible dose of 300 mr/week, assuming a 48-hour week.

No detailed protection-data are given for the gamma-rays from radio-isotopes, nor are the data on radium protective recommendations given in the 1950 recommendations reproduced.

The Supplement is available in paper covers from the British Institute of Radiology, 32 Welbeck Street, London, W.1, at 10*s*. 6*d*.

Journal of Scientific Instruments

Contents of the August issue

SPECIAL ARTICLE

The physics of clocks and watches. By J. F. W. Bishop.

ORIGINAL CONTRIBUTIONS

Papers

An optical absorption cell for use at low temperatures. By V. Roberts.

A simple method of measuring the dynamic Young's modulus of concrete. By J. P. A. Lochner and W. de V. Keet.

Low-cost, battery-operated oscillators and detectors for a.c. bridges. By M. D. Armitage.

A portable twenty-four-channel kicksorter. G. F. von Dardel.

A slide rule technique for calculating neutron energies from tracks in nuclear emulsions. By J. P. Scanlon.

A simple microcalorimeter for heat of solution measurements. By W. P. Hutchinson and A. G. White.

A superconducting modulator. By I. M. Templeton.

Dosimetry of X- and γ-rays by alkali-halide crystals containing U-centres. By W. G. Burns and R. Lockyer.

Laboratory and workshop notes

A simply constructed electron-optical bench. By W. Fishwick.

Preparation of copper-constantan thermocouples. By E. F. Kiernan.

A beam current stabilizer for an X-ray generator. By R. G. Stone.

A thermal conductivity gauge for use in gas-liquid partition chromatography. By D. Ambrose and R. R. Collerson.

NOTES AND NEWS

Correspondence

A laboratory gas-flow control device. From W. J. Gooderham; R. A. Hall.

A bent crystal X-ray spectrometer with roller bearing rotation mechanism. From H. R. Moore.

Modification of an apparatus for preparing small sodium chloride crystals. From F. W. Thompson, G. S. Rose and J. A. Morrison.

New books

New instruments, materials and tools

A.C. differential current meter. Stabilized power supply unit. Electric "Bunsen." Miniature potentiometer.

Notes and comments

THIS JOURNAL is produced monthly by The Institute of Physics, in London. It deals with all branches of applied physics (including theory and technique).

All rights reserved. Responsibility for the statements contained herein attaches only to the writers.

EDITORIAL MATTER. Communications concerning editorial matter should be addressed to the Editor, The Institute of Physics, 47 Belgrave Square, London, S.W.1. (*Telephone:* Sloane 9806.) Prospective authors are invited to prepare their scripts in accordance with the *Notes on the preparation of contributions*. (Price 2*s*. 6*d*. including postage.)

REPRODUCTION. The Institute of Physics is a signatory to The Royal Society's Fair Copying Declaration. Details may be obtained upon application from The Royal Society, London, W.1.

ADVERTISEMENTS. Communications concerning advertisements should be addressed to the agents, Messrs. Walter Judd Ltd., 47 Gresham Street, London, E.C.2. (*Telephone:* Monarch 7644.)

CLAIMS FOR MISSING JOURNALS. Claims from regular subscribers to this *Journal* for missing numbers will only be considered if received within 60 days of the date of mailing plus normal outward time of transit and time for lodging the claim. Losses attributable to failure to notify a change of address or to similar omissions will not be considered.

SUBSCRIPTION RATES. A new volume commences each January. The charge is £4 per volume ($11.50 U.S.A.), including index (post paid), payable in advance. Single parts, so far as available, may be purchased at 8*s*. each ($1.15 U.S.A.), post paid, cash with order. Orders should be sent to The Institute of Physics, 47 Belgrave Square, London, S.W.1, or to any bookseller.

SPECIAL ARTICLE

Alloys for use at high temperatures*

By W. BETTERIDGE, Ph.D., F.Inst.P.

The properties necessary in metallic materials intended for service at high temperatures are outlined and the characteristics of nickel-base alloys for such applications are particularly described. The materials are dealt with in two classes: those primarily of value because of their resistance to oxidation and those characterized by high strength at elevated temperatures.

One of the most important technical factors in the maintenance and advancement of civilization is man's ability to generate heat and to use temperature differences as a source of power. For many centuries man's use of heat was confined to the provision of bodily comfort and of cooked food—and this is surely still the ultimate aim of the more complicated uses to which thermal energy is now put. With such primitive aims there were no major problems with regard to the materials used to contain and restrict the combustible material used as the heat source—stones and refractory earths were readily available and the common metals copper, and eventually iron, were suitable for cooking vessels. Even with the extension of the use of heat to the firing of pottery and to the extraction of metals from ores, refractory materials satisfactorily met the requirements for the construction of kilns and furnaces. The introduction of heat as a source of power, however, has led to the demand for materials capable of withstanding considerably elevated temperatures without deterioration—at least without rapid deterioration—and having the characteristic metallic properties of ductility, malleability, etc., which make them suitable for the construction of a wide variety of components or operating parts of various devices. Typical examples of metallic parts which operate at considerably elevated temperatures will readily come to mind: in the home, the elements of electric fires and cooking stoves; in automobile engines, the valves and sparking plugs; in steam engines, the boiler tubes; various components of gas turbine engines; parts of industrial furnaces used for heat-treating metals and for firing pottery—in fact metals operating at elevated temperatures are ubiquitous.

The properties required of an alloy for such service are primarily twofold: ability to resist chemical reaction, which usually means resistance to atmospheric oxidation; and adequate strength, to resist deformation and fracture. These two properties are fundamentally different, although, as will be mentioned later, some interaction between the two does occur, and it is therefore proposed in this article to review separately these two aspects of high-temperature alloys.

CORROSION RESISTANCE

Thermodynamic data for the stabilities of metallic compounds show clearly that no metals other than the noble metals can remain completely unaffected by a gaseous environment and the problem of resistance to surface attack is therefore reduced to one of the rate at which reaction takes place. For any particular alloy this is, as would be expected, strongly dependent on temperature, but the characteristic behaviour of any alloy is essentially dependent on the manner of growth of the film of reaction product which forms on the surface and on the rates at which the various reacting ions diffuse through this film. Experimental studies of the rates of growth of oxide layers have shown that any one of a number of relationships can apply: a linear increase of weight per unit surface area with time indicates that the oxide film produced offers no obstacle to further growth, and from the point of view of a high-temperature material such a case is of no interest. Pilling and Bedworth[1] showed in 1923 that such behaviour could be predicted from a study of the relative molecular volumes of metal and oxide; if the oxide has a smaller specific volume than the metal from which it is formed it cannot form a coherent layer to protect the underlying metal. Most of the alkaline and alkaline-earth metals follow this law. Other metals show parabolic, cubic, or logarithmic laws of oxidation and various theories introducing the diffusion of the reacting ions through the protective film have been proposed to explain these laws. When the case of even a simple binary alloy is considered, however, it is readily seen that the possible processes which could contribute to a determination of the reaction rate are so numerous that a satisfactory simple theory is very unlikely. The diffusion rates of the two metallic atoms in the alloy, and of the metallic and oxygen ions in the oxide, the possibilities of multilayers of scale consisting of oxides of both constituents, reactions between the different oxides, and evaporation of either metal or oxide are all processes which could in some way affect the rate of oxidation. At the present state of knowledge it is therefore found that the experimental approach provides the fastest progress in the development of oxidation-resistant alloys. It is proposed, therefore, to describe the properties and the developments which have taken place in commercially available alloys.

By far the greatest proportion of technically important alloys are based on the ternary system iron–nickel–chromium, but even in this system the iron may be considered as a diluent present only for economic reasons. The iron-free alloys are always more resistant to simple oxidation than are the corresponding iron-containing alloys. The effect of variation of the chromium content of nickel–chromium alloys has been described by Hessenbruch.[2] After an initial fall, with a minimum at about 5% chromium, which can be explained on the basis of the relative valencies of the nickel and chromium ions,[3] the resistance to scaling of the binary alloys increases progressively with increasing chromium content. The alloy containing 20% of chromium has been selected as the basis for the most widely used high-temperature oxidation-resistant alloy, the choice being a compromise between oxidation-resistance and ease of fabrication into the common forms of wire, strip and tape in which the alloy is required. Working difficulties increase considerably with higher chromium contents. However, the simple binary

* Based on the Chairman's Address given to the Midland Branch of The Institute of Physics in Birmingham on 9 November, 1954.

alloy has a drawback which becomes evident when intermittent testing conditions simulating service operation are adopted. The alloys are widely used in the form of wire for electrical heating elements and in this form are frequently tested in the manner described in A.S.T.M. Specification B76—39. A sample of the wire, usually about 20 s.w.g., is suspended vertically in a draught-proof enclosure and is heated electrically to a stipulated temperature in the region of 1100–1200° C. The temperature is measured with an optical pyrometer and the current is adjusted to maintain the wire at the required temperature. The current is switched on or off every 2 min and the test is continued until the wire burns out. In the initial stages of the test the temperature is re-set two or three times, to compensate for the changing emissivity of the surface as the scale layer builds up, but after the first 24 hours the temperature is neglected and the applied voltage is maintained constant. Failure of the wire is finally brought about by flaking of the scale at a localized point, which then becomes overheated and eventually melts. The behaviour of nickel–chromium alloy wires in this test has been found to be very much influenced by small proportions of certain very reactive metals added to the alloy. Particularly notable in their effect on the life are calcium, cerium, zirconium, thorium and silicon, and considerable improvement in the life of wires has been obtained over the last 20 years or so by selection of the optimum balance of these minor additions. This improvement is shown by the fact that the temperature at which an average life of about 100 hours is obtained has been raised, during this period, from 1060 to 1232° C.

Interesting work has been carried out with the object of determining the mechanism by which this improvement of life is obtained.[4] Determinations of the rates of oxidation under conditions of steadily maintained temperature have shown that alloys untreated with particular reactive elements, i.e. short-life materials, have a very similar oxidation rate, particularly in the early stages of the test, to that of specially treated long-life alloys, and indeed the life of a test wire heated continuously instead of being repeatedly switched on and off is not very different for the two classes of wire. In order to explore the difference between continuous tests and intermittent tests a series of tests has been carried out in which, instead of completely switching off the heating current every 2 min, it was reduced from the value required to maintain the wire at the normal test temperature to a value maintaining the wire at a lower temperature. A number of tests, in which the wires were cycled between two temperatures, the upper one remaining constant, but the lower one varying from almost room temperature up to close to the upper temperature, have shown very different behaviour for short-life wires and for long-life wires. Figs. 1 and 2 illustrate the

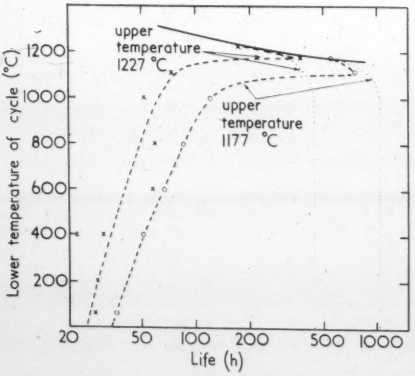

Fig. 1. Life-test results for short-life, nickel–chromium wire

——— constant-temperature test
— — — cycling-temperature test
..... calculated from constant-temperature test

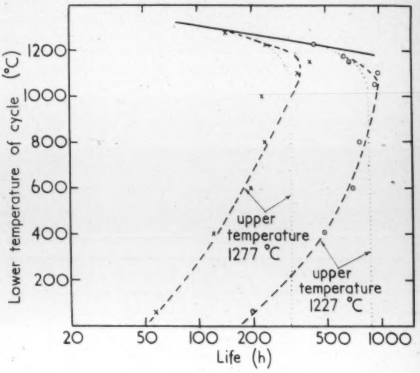

Fig. 2. Life-test results for long-life, nickel–chromium wire

——— constant-temperature test
— — — cycling-temperature test
..... calculated from constant-temperature test

behaviour of two wires which had lives under the normal intermittent test conditions at a temperature of 1177° C of 37 h and 606 h. It is to be noted that the life at first increases as the lower temperature is reduced, on account of the lower rate of oxidation, but later the life is seriously reduced, by the cracking and flaking of the scale due to thermal stresses. The difference between the two wires is to be associated with the greater adhesion or cohesion of the scale layer on the longer-life wire. Photomicrographs of the wires after a constant period of test, Fig. 3, indicate that the improved adhesion is probably due to the more irregular interface between scale and metal, which can give a much stronger mechanical key to the scale. The reason for the small additions of reactive metals producing such an interlocked phase boundary is most probably to be found in the phenomenon of internal oxidation. Oxygen diffuses into the alloy to a very small degree and, although the effective pressure of oxygen within the alloy is insufficient to produce an oxide of the major constituents, the highly reactive metals are oxidized within the alloy, and dispersed globules of their oxides are deposited ahead of the normal scale layer, causing formation of the irregular interface. However, the effect of additions of reactive elements cannot be due solely to this effect, as the

following experiment has indicated. Wires of an untreated, and therefore short-life, alloy were submitted to the normal type of life test, but before commencing the test half of the length of the wire was coated with a cerium salt. The effect

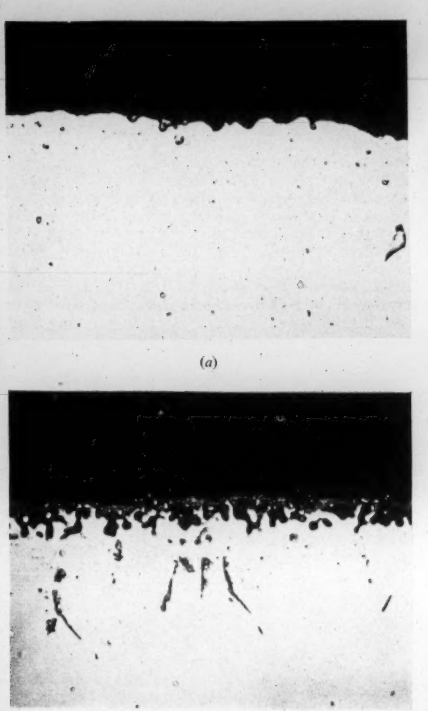

(*a*)

(*b*)

Fig. 3. Structures of scale-metal interface for (*a*) short-life and (*b*) long-life, nickel–chromium wires (×500)

produced is shown in Fig. 4; the uncoated half has lost a good deal of the scale by flaking but the coated half has a smooth layer of adherent scale. Since the cerium in this case has been added only to the scale and not to the alloy the effect cannot be one of internal oxidation.

Nickel–chromium alloys are not the only ones suitable for applications requiring oxidation-resistance at high temperatures. In fact, although nickel–chromium alloys will give good service at temperatures up to 1200° C, or thereabouts, an iron–chromium–aluminium alloy can give useful service at temperatures up to about 100° C higher than this. The alloys contain about 20–25% chromium, 4–6% aluminium and small amounts of other elements and are sufficiently ductile to be drawn into wires for electrical heating purposes. They suffer from two main disadvantages, however, which make them rather less favoured than nickel–chromium alloys for most applications. In the first place their strength at high temperatures is low and in many cases insufficient for the wire to support its own weight. Modified designs providing full support for the elements are usually necessary. Secondly, they become seriously embrittled after service at elevated temperatures and no adjustment to the shape of elements can be made after a period of use, without danger of fracture.

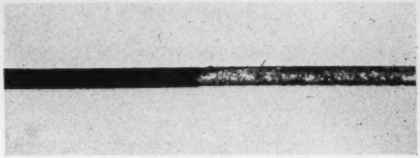

Fig. 4. Effect of coating of cerium nitrate on flaking of scale on nickel–chromium wire

In many applications resistance to oxidation in air is the only requirement, but in other fields additional corrosive media are present. Perhaps most important of these are the carbonaceous gases which are frequently present in industrial furnaces, either on account of oil fumes from quenching baths or from articles charged into the furnace, or because of the use of coal gas. Characteristic attack of nickel–chromium or nickel–chromium–iron alloys can then occur at temperatures in the region of 900–1100° C, associated with the formation of chromium carbide in the alloys.[5] Particular corrosion problems also occur in connection with sulphur, and with vanadium, both of which are present in the ashes of crude mineral oils.

CREEP AND FRACTURE RESISTANCE

The second important property required in a material to operate at high temperatures is the ability to resist deformation and fracture under the stresses to which it is submitted. Even in the applications in which scaling-resistance is the primary requisite, some alloys are so lacking in strength as to distort under their own weight. The same phenomenon occurs over a wide range of temperatures and stresses for any material and, particularly when taking place slowly over a period of hundreds or thousands of hours, is referred to as creep. From the engineering aspect, the range of strains which are regarded as important are usually between 0·1 and 1%. Scientific study of creep has been carried out mainly under conditions of simple tensile stress at a constant temperature and the type of deformation-time curve obtained (the creep curve) is one showing an initial decelerating portion (the primary stage), followed by a period of essentially constant creep rate (the secondary stage), and finally succeeded by a period of accelerating creep rate (the tertiary stage), which leads to eventual fracture. Qualitatively speaking, increase of stress and increase of temperature have a similar effect in increasing the rate of creep and reducing the life before fracture, but no simple relationship between these variables has yet been found, although numerous empirical formulae have been proposed. It is important to appreciate that the time of fracture in a creep test of the type described is not dependent solely on the rate of creep and, indeed, in some alloys it can be varied by special methods of heat-

treatment without affecting the shape of the creep curve, except for a relatively short period immediately prior to fracture. Fig. 5 shows the appearance of two broken test

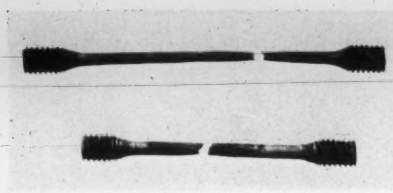

Fig. 5. Ductile and brittle creep fractures of creep-resistant, nickel–chromium alloy

bars of the same alloy and initially of the same dimensions, the first having failed by intercrystalline fracture at a total elongation of only about 5% and the second having extended a total of about 80% and finally failed in a ductile manner. Creep and fracture are, therefore, to be regarded as associated rather than completely interdependent properties, and the practice which is sometimes adopted of comparing different alloys solely on the basis, for example, of the stress to produce fracture in a given time at a certain temperature, must be realized to be applicable to those conditions only. However, in order to compare the different classes of high-temperature materials which have been developed it is necessary to follow such a line. Fig. 6 illustrates the properties of three important

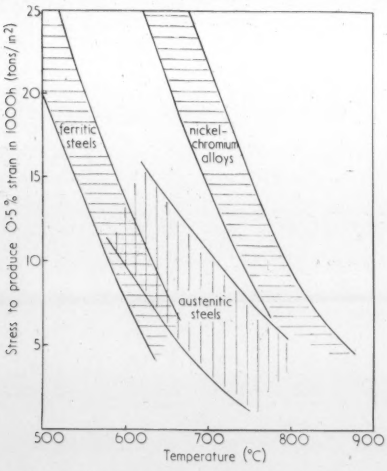

Fig. 6. Creep resistance of different types of alloy

classes of materials, the stress to produce a creep strain of 0·5% in 1000 hours being plotted against temperature. Relatively wide bands of properties are indicated for each group, although in each case the materials represented are only those specially developed for creep resistance. In the ferritic steel group, for instance, all normal alloy constructional steels are excluded, and the band represents mainly the 3% Cr–½% Mo–¼% V or 0·7% Mo–0·4% V steels and the 11% Cr–½% Mo–¾% V steels. The austenitic steel group includes a wide range of types suitable for use in sheet form or as bars or stampings and the properties are consequently fairly widely scattered. Those at the top of the band are mostly rather complicated steels, consisting of a matrix of iron–nickel–cobalt–chromium hardened with carbides of stable-carbide-forming elements such as molybdenum, tungsten, niobium or titanium. The nickel–chromium alloys have all been developed from the 80% Ni–20% Cr alloy referred to earlier as predominantly an oxidation-resisting alloy, the high creep properties being obtained by the hardening effects of a dispersed phase, namely a nickel–titanium–aluminium compound. Some of these alloys also contain additions of cobalt. There is still another class of alloy not represented in this figure, since its main field of application is one in which the creep strain is of lesser importance and the life-to-rupture is most important. Consequently the data available are mostly concerned with rupture properties. These alloys are cobalt-rich materials containing also nickel and chromium and hardened by molybdenum or tungsten carbides. They are, in general, unforgeable and are used in the cast form, although some of the less fully hardened varieties can be forged, but their high-temperature properties are to some extent reduced. Fig. 7 illustrates the

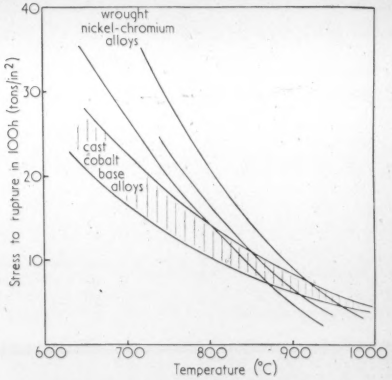

Fig. 7. Rupture strengths of different alloys

stress-rupture properties of such alloys, plotted against temperature; typical curves for wrought nickel–chromium base alloys are included for comparison. It is, as yet, uncertain to what factor the crossing of the curves for the two types of alloy curves is to be ascribed. Some workers have suggested that it is due to the change of the major constituent from nickel to cobalt, others attribute it to the change from an alloy hardened by a nickel–titanium–aluminium compound to one hardened by carbides. For the further development of improved alloys it is important to answer this question, but an answer is not so readily forthcoming as might be

supposed, for it is not easy to change one characteristic of a complex alloy without changing the alloy also in other ways, and work on this problem is still proceeding.

It was stated earlier that creep-resistance and fracture-resistance are to some extent separately variable properties of a high-temperature alloy and it is interesting to examine the effect of variations in heat-treatment procedure on the characteristics of the creep curve of a typical alloy of the nickel–chromium type, Nimonic 95. Fig. 8 shows curves

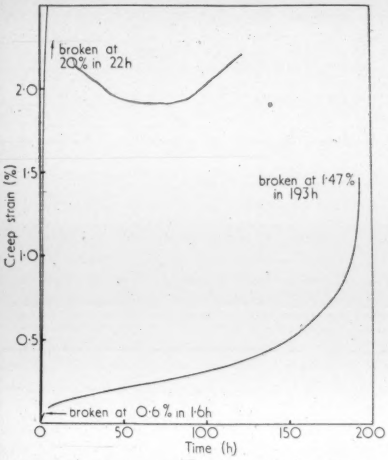

Fig. 8. Creep curves of Nimonic 95 after different heat-treatments (9 tons/in.^{2} at 870° C)

obtained on samples of the same alloy after heat-treatment in different ways. The best creep properties and the longest life to fracture are obtained by solution-treating at 1200° C, air-cooling, reheating to 1080° C and air-cooling, and aging at 700° C. If the material is solution-treated at a lower temperature, say 1000° C, or for too short a time, in spite of the solution treatment being satisfactory so far as precipitation-hardening is concerned, the creep-resistance is poor and the test bar extends rapidly and fractures in a short time. On the other hand, if solution treatment is carried out at a high temperature and the bar is cooled at a fast rate, such as by quenching, there is an unsatisfactory condition of precipitation at the grain boundaries, and, although the minimum creep rate is then low, fracture occurs at a very low elongation and with a short life.

The materials already referred to have been developed by essentially empirical methods guided by the experience of metallurgists, and it must be emphasized that so far in this field, progress has owed little to fundamental studies. Nevertheless, such studies are being widely made and the following section indicates fairly briefly, and in a descriptive rather than a mathematical manner, the present trend of this work. The earliest studies of the subject were carried out by Andrade,[6] on pure metals, and he introduced a formula which is now very familiar. With pure metals the tertiary or accelerating stage of creep does not appear at all readily and in most cases in which it does occur the strain is then so high that the distortion of the specimen makes it difficult to ensure conditions of constant stress. Various devices have been proposed to reduce the load on a specimen in proportion to its extension, so that the creep takes place under conditions of constant stress, but these, of course, are only valid if the extension of the specimen is quite uniform along the length of the test bar. Andrade's results did not include the tertiary stage and for a long time there was some doubt as to whether accelerating creep did occur in a constant-stress test, or whether it was only observed in constant-load tensile tests, in which progressive extension leads to reduction of the cross-section of the test-bar and consequent increase of stress. However, Sully and his colleagues[7] observed it for a creep-resisting alloy in compression tests, for which the stress is reduced by increasing strain, and its existence is therefore established.

Andrade's formula for the first two stages of creep was as follows:

$$l = l_0(1 + \beta t^{1/3})e^{kt}$$

where l and l_0 are the instantaneous and initial lengths of the material, t is the time, and β and k are constants.

This can be rewritten for small amounts of strain, ϵ,

as $$\epsilon = \beta t^{1/3} + kt$$

This formula was derived empirically, but numerous attempts have been made, with varying degrees of success, to establish a theoretical basis for the expression. These have all been based on the now commonly accepted mechanism by which metals deform, either rapidly at normal temperatures or in a time-dependent manner as in creep, namely the movement of dislocations along slip planes of the crystal lattice. A dislocation is a line discontinuity in the crystal, which by movement across a lattice plane produces a shift of one atom distance between the parts of the crystal on either side of the plane swept out. The study of the generation and movement of dislocations is now quite an extensive subject,[8] but for the present purpose it is sufficient to say that creep is now accepted as being primarily due to the temperature-activated movement of dislocations. Primary creep is thought to be due to the relatively easy movement of the dislocations existing in the material in its initial condition, the decreasing creep rate being due to the gradual exhaustion of dislocations free to move. Secondary creep, the steady-state creep represented by the term kt in Andrade's expression, is sometimes described as quasi-viscous creep (quasi-viscous since although the velocity of displacement is independent of time it is not linearly proportional to the applied stress), and attempts have been made to identify it with the displacements which are observed to occur at grain boundaries, at least in pure metals and simple solid-solution alloys. The photomicrograph shown in Fig. 9 illustrates some of the types of distortion which can be observed in metals distorted in creep.[9] It shows the appearance of a tin–antimony alloy which has strained 1·4% in 71 hours under a constant load of 1300 lb/in.^{2} at normal temperature. Two major types of distortion are visible: deformation of the grains revealed by slip lines or rumpling of the surface, and grain-boundary displacement shown by the displacement of scratches as they cross the boundaries. Further evidence of grain-boundary flow is given by the signs of severe distortion of the grains in directions which form prolongations of the boundaries; this is also evidence that the two mechanisms of strain usually occur in an associated manner. Measurements by McLean[10] of the magnitudes of the creep strains produced by grain

distortion and by grain-boundary flow have, however, shown that direct identification of the $\beta t^{\frac{1}{3}}$ term with grain distortion and the kt term with boundary flow is far from the truth.

A number of investigators who have made careful measurements of creep have come to the conclusion that, although the Andrade equation can be made, by suitable choice of the constants, to represent the initial stages of an observed curve very closely, it is by no means exactly true. A closer fit appears to be given by a simple power law in which the exponent differs from $\frac{1}{3}$. Torsion creep tests carried out on pure aluminium at very low stresses[11] have shown that in some cases this formula gives a much closer fit than the Andrade equation, but it is nevertheless surprising that the Andrade expression gives a good approximation for many different materials and under various conditions of testing.

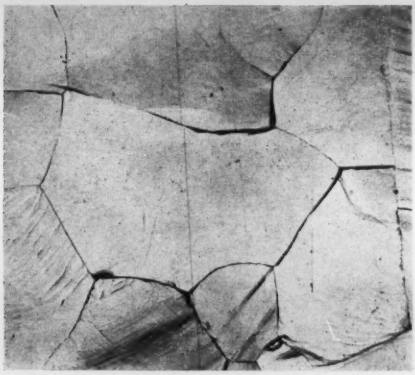

[Reproduced from *Journal of The Institute of Metals*]

Fig. 9. Surface appearance of Sn–5% Sb alloy after creep

Study of the creep process is, however, making it increasingly clear that the observed overall strain is compounded of a number of partial strains due to differing mechanisms, and since these are likely to be dependent on time, stress and temperature according to different laws, it is not to be expected that the total strain can be expressed by a simple formula. Simple laws will be found to apply only in conditions in which a single mechanism is predominant.

ACKNOWLEDGEMENTS

The author's thanks are due to The Mond Nickel Co. Ltd. for permission to publish this article.

REFERENCES

(1) PILLING, N. B., and BEDWORTH, R. E. *J. Inst. Metals*, **29**, p. 529 (1923).

(2) HESSENBRUCH, W. *Zunderfeste Legierungen*, pp. 82–84 (Berlin: Springer, 1940).

(3) WAGNER, C., and ZIMENS, K. E. *Acta Chem. Scand.*, **1**, p. 547 (1947).

(4) BETTERIDGE, W. *Fourth International Congress on Industrial Heating*, Paper No. 18 (Paris: Chaleur et Industrie, 1952).

(5) BUCKNALL, E. H., and PRICE, L. E. *Rev. Mét.*, **45**, p. 129 (1948).

(6) ANDRADE, E. N. DA C. *Proc. Roy. Soc. A*, **90**, p. 329 (1914).

(7) SULLY, A. H., CALE, G. N., and WILLOUGHBY, G. *Nature* [*London*], **162**, p. 411 (1948).

(8) COTTRELL, A. H. *Dislocations and Plastic Flow in Crystals* (London: Oxford University Press, 1953).

(9) BETTERIDGE, W., and FRANKLIN, A. W. *J. Inst. Metals*, **80**, p. 147 (1951–52).

(10) MCLEAN, D. *J. Inst. Metals*, **81**, p. 293 (1952–53).

(11) BETTERIDGE, W. *J. Inst. Metals*, **82**, p. 149 (1953–54).

An attempt to simplify coding for the Manchester electronic computer

By R. A. Brooker, M.A., A.R.C.S., Department of Electrical Engineering, University of Manchester

[*Paper received* 24 *March*, 1954]

This paper outlines some of the difficulties encountered in attempting to simplify the task of preparing programmes for a large scale digital computer. In general this is most simply achieved at the price of increasing the machine time consumed by the resulting programme. Such a compromise is nevertheless worth while for many "small" problems and a means is described for treating such problems on the Manchester University Computer (Ferranti MK I computer). The method is also applicable to any of the Ferranti range of machines, several of which are now available in this country.

The task of preparing programmes for large scale digital computers has always been recognized as a bottleneck to the use of these machines by persons whose main interest lies only in the results and not in the techniques of coding. For this reason several proposals have been made for converting into precise machine instructions, programmes originally drawn up in a more convenient and general form.[1,2] In all these proposals the conversion is done by the machine itself in the following way. The ordered aggregate of symbols which constitute the original programme are presented to the machine on the input medium. It is then scanned by the machine under the operation of an input-conversion routine which translates the symbols on the input medium into a corresponding programme of words which are recorded in the store. These words may be the final instructions which are subsequently obeyed directly by the machine, or they may be words which serve as "instructions" for a further interpretive routine. The purpose of this report is to describe a means for writing programmes which the use of conversion and interpretive techniques has made possible on the Manchester University Electronic Computer MK I. This is a typical two-level storage machine and has the following characteristics:

working store (electrostatic): 512 words each of 20 bits;
auxiliary store (magnetic drum): 256 tracks each of 128 words;
fixed binary point arithmetic on 40 bit words: addition time 1·2 ms, multiplication time 2 ms;
time to transfer contents of any track to working store: 40 ms, reverse operation: 90 ms;
input-output medium: 5-hole teleprint tape, page printer.

STRATEGICAL CONSIDERATIONS

In coding directly for such a machine two main difficulties are encountered which should be taken into account in any proposals for simplifying the coder's task.

The first is the scale factor difficulty of arranging the calculation so that all the quantities involved are represented to the required accuracy and yet remain within the capacity of the registers. This difficulty can be alleviated to some extent by working throughout with double length arithmetic keeping, say, 40 binary digits for the fractional part of a number, and 40 digits for the integral part. Another solution to the problem is to associate every number occurring in the calculation with its own adjustable scale factor: an interpretive scheme for doing this has been described by Brooker and Wheeler.[3] This so-called floating-point technique requires the use of routines for carrying out operations of the form $a.2^p \pm b.2^q$, etc., and for this reason the time of execution of a floating-point instruction is very long (addition 50 ms, multiplication 40 ms, division 100 ms) compared to that of the corresponding fixed point machine instructions. This is partly offset by the fact that, in general, fewer of the floating variety are needed. It is this second solution which has been adopted in the scheme developed for the Manchester machine.

The second difficulty relates to the physical nature of the storage facilities. The coder's task would be made easier if, instead of two levels of storage with their corresponding accessibility features, there was a single storage medium of indefinitely large capacity and rapid accessibility. Any proposals for simplifying coding ought therefore to include some means for converting a programme written for a hypothetical one-level store into a programme suitable for a two-level store. The real problem is to do this efficiently, so that the computation time spent on the "fast" level approximately matches the time spent in gaining access to material (numbers and instructions) on the "slow" level. As in the case of the scale factor problem an optimum solution really requires an insight into the calculation being programmed. Thus, for example, when allocating magnetic storage to the elements of a vector one would try to keep them as far as possible on the same track so that the entire vector could then be transferred to the working store in a single operation; in other words, the experienced programmer tries to take advantage of any natural ordering that exists in the numerical material. When a machine has been educated to do this it will have gone some way towards being able to think! Nothing so ambitious has been attempted in the scheme adopted, mainly because the use of floating arithmetic does not make it worth while to improve on the method described below for gaining access to numerical material.

The strategy adopted for using the two levels of storage is as follows. After input, the programme of converted "instructions" is recorded on consecutive lines and tracks of the magnetic store. The capacity of the working store is limited to four tracks of the auxiliary store. At any stage, therefore, in the execution of the programme there is only room for one trackful of "instructions" and one trackful of numbers, the remaining space (one-half) being taken up by the interpretive routine. The "instructions" are normally used consecutively and when the trackful has been exhausted arrangements are made to replace it by the contents of the next track, or in the case of a jump "instruction," by whichever new track is involved. This track changing business is

also a feature of the conventional programming technique used with the Manchester machine and has been described by Hume[4]: supplemented by suitable facilities in the input conversion stage it enables the instructions to be written out originally as if for a one-level instruction store. This means of access to "instructions" is efficient because the time taken to transfer each trackful of "instructions" is negligible compared with the time taken to execute them: the ratio is still quite reasonable even where ordinary (machine) instructions are concerned.

The situation is not so favourable, however, in the case of numbers because the order in which access to them is required depends on the nature of the calculation. The conversion problem is simplified if the operands are selected directly from the auxiliary drum store—the capacity is virtually infinite—by the interpretive routine. To do this the routine has first to determine the track involved, then transfer the content of the track to the working store, and finally select the particular line required. The access time for any operand is then at least 40 ms, the time for a magnetic reading transfer. Similarly the corresponding recording operation would take at least 90 ms. These figures about match the times of floating operations so that in this case not much advantage is to be gained by improving the access time.

The position would be very different, however, if the arithmetical operations took only a few milliseconds or less, for in that case most of the time would be spent in selecting and recording numbers on the drum. To achieve any sort of balance in these circumstances it is essential to take advantage of any natural ordering of the numbers. Now, however crudely the original programme is written, any such ordering would almost certainly be reflected in the allocation of storage in the hypothetical one-level store, and the correspondence between this store and the magnetic drum store means that in many cases successive operands will be found on the same track. Unnecessary magnetic transfers can therefore be eliminated by testing whether the magnetic address of each operand involves the same track as the previous operand. This can be done either by the interpretive routine as each operand is required, or once and for all before the programme is executed. The former device has been incorporated in the Manchester scheme because it is simpler and the rewards are just worth while. The second and ultimately more rewarding method would involve examining the context of each "instruction," which, in the case of an "instruction" immediately following a "control" junction, means searching through all possible alternative "control" paths to find the previous operand. This can only be done after input when the whole programme—or at least the important parts, the inner loops—are available for scanning. This stage will be called *secondary conversion*; such conversion as it is convenient to do during input proper will be called *primary conversion*. Primary conversion will include all those techniques usually associated with compiler routines, i.e. use of algebraic symbols, floating addresses,[5] specification of subroutines by a symbol, etc.

[With most machines the floating address facility usually involves secondary conversion, or its equivalent, the "two-pass" technique. Applied to control transfers, however, this is unnecessary with the Manchester machine because of the particular way in which control transfer instructions work. They involve a double reference: instead of giving directly the address of the next instruction (*the control number*) it is the address of this address which is given. Thus for each control transfer instruction a spare location must be found to hold the control number, the address of the next instruction. The associated locations, which are arbitrary, can be allocated as each transfer instruction is read from the tape and the corresponding control numbers filled in as the instructions to which control is transferred are read from the tape.]

CONCLUSION

It can thus be seen that with the aid of routines for the calculation of the elementary functions, and input and output of numerical data, the above techniques enable the machine to be transformed, at the price of considerable loss of speed, into a programmer's conception of an "ideal machine." The total material involved in the transformation of the Manchester machine occupies about twenty tracks of the magnetic store. It is usually run into the machine when required by means of the conventional input routine which is kept permanently on the magnetic drum.

It remains to consider the "ideal machine." In designing the code described below the following points were considered. The price paid in the terms of speed rules out the possibility of using the "machine" for problems involving $0(n^3)$ or more operations where n is large, e.g. partial differential equations. Its use will therefore be confined to *ad hoc* problems and problems which might otherwise have been considered as too small for a large scale computer; a typical example is given later on. Extending the class of problems that can be treated by the machine in this way may mean extending the class of user. The occasional user with a small problem will not, naturally, be very keen to learn the conventional programming techniques, more especially if this means digesting the contents of a hundred-page manual. For this reason the principal consideration in the choice of the "ideal machine" has been economy of description: what the author aimed at was two sides of a foolscap sheet with possibly a third side to describe an example. The psychological advantages which such an economy of description brings to the prospective reader makes the attempt worth while, even at the expense of considerable compression of the material. How far this has been achieved can be judged from the following standard account which is similar to one we hand out to prospective occasional users.

The "machine" used at present differs from that described here in certain minor respects (e.g. the accuracy is limited to nine significant decimals) but will shortly be modified to conform with the following account. Further details can be obtained on application to this laboratory.

THE STANDARD ACCOUNT OF THE "SIMPLE MACHINE"

By the means described above the electronic computer can be made to accept programmes written in the simplified form described below. In this form a programme of calculation consists of an ordered sequence of *instructions* arranged in a

List of permissible symbols employed

FS	*FS* (Blank)	*K*	—	*V*	6
A	1	*L*	*v*	*W*	/
B	2	*M*	*LF*	*X*	⊗
C	*	*N*	*SP*	*Y*	9
D	4	*O*	,	*Z*	+
E	(	*P*	0	*LS*	*LS*
F	)	*Q*	>	.	.
G	7	*R*	≥	?	*n*
H	8	*S*	3	£	*CR*
I	≠	*T*	*j*	■	■ (Erase)
J	=	*U*	5		

single column. These instructions are chosen from a permissible set and employ only the symbols given in the table. Ultimately the programme is presented to the machine in the form of a length of perforated paper tape which is scanned by a photoelectric tape reader, the input unit of the machine. This programme tape is prepared on a keyboard perforator in a manner to be described later. The machine gives its results on a page printer.

The instructions mostly take the form of equations giving the new value of a computed quantity in terms of one or two previously calculated quantities or parameters. Instructions are also necessary, however, for selecting between alternative courses of action, for printing results, and for the input of further data. The instructions involve the following kinds of quantities.

(*a*) *Variables*. The quantities or intermediate quantities which it is necessary to compute. These are denoted by $v1$, $v2$, $v3$, etc. The number of variables which can be introduced is for practical purposes unlimited: it is in fact about 12000. The range of magnitudes of a variable is virtually infinite, $10^{\pm 10^{5}}$: the precision is limited to eleven significant decimal figures.

(*b*) *Constants*, or variables of which the value is known in advance. For these quantities the permissible range and precision is limited in order that numerical values may be written in the form:

integral part, decimal point, fractional part.

A certain lack of preciseness is inevitable here, e.g. to six significant figures π may be written 3·14159, 03·14159, 03·141590, +03·141590. All these and similar variations are accepted by the machine, provided the integral part does not exceed 10^{11}: in any case, as explained above, not more than eleven significant figures are recorded inside the machine. Negative numbers must be preceded by sign.

(*c*) *Indices*. These correspond to the subscripts of conventional mathematical notation. In order to take advantage of the repetitive nature of calculation it is desirable to have some means of specifying any of the elements of a sequence, e.g. the components of a vector. For this purpose the notation $vn1$, $vn2$, $vn3$, etc., is introduced where $n1$, $n2$, $n3$, etc., are indices restricted to integral values but otherwise computable like variables. Thus, for example, if $n1 = 5$, then $vn1$ is identified as $v5$. The number of indices which can be introduced is limited to 64. The possible range of values of an index quantity is $-2^{-39} \leqslant x < 2^{39}$, which, of course, far exceeds its usefulness as an index proper. In writing down the numerical value of an index the decimal point and fractional part can be omitted.

Those instructions which take the form of equations are given below as (i), (ii) and (iii). Permissible instructions are obtained from these basic forms by replacing x, y and z by the group of symbols denoting a variable (v), or, except in the case of (iii), an index (n), or a combination (vn). In particular x and y may also be replaced by constants.

(i) $z = x$
(ii) $z = x\theta y$ θ is replaced by one of the symbols $+ \; - \; \otimes \; /$
(iii) $z = Ax$ A is replaced by one of the letters

A ($\equiv \arctan x$)
C ($\equiv \cos 2\pi x$)
E ($\equiv \exp x$)
L ($\equiv \log_e x$)
S ($\equiv \sqrt{x}$)

Instructions are normally obeyed in the order in which they are written down until a jump instruction is encountered. This may be conditional or unconditional and takes the form (iv) or (v) as follows.

(iv) *jm* means "jump to instruction labelled m"
(v) *jm*, $x\phi y$ means "jump to instruction labelled m if $x\phi y$," where ϕ denotes one of the symbols $\geqslant \; > \; = \; \neq$.

The *label* is a positive whole number which is written immediately before (i.e. to the left of) the instruction concerned. The remaining instructions are as follows.

(vi) The letter P inserted before any of the instructions (i), (ii) or (iii) causes the computed value of z to be printed in the style described earlier, namely, integral part, decimal point, fractional part. The number of decimal places is determined manually by setting a row of hand switches on the console. Insignificant zeros are suppressed. The machine prints 0·0 if $z < 10^{-11}$; and * if $z > 10^{11}$.

(vii) The following single letter instructions can be inserted at any point in the programme to control the layout of results.

X carriage return
Y line feed
Z space.

(viii) The letter H is a stop instruction: the machine halts. It can be made to resume operation by pressing a key on the console.

As a simple exercise in coding write down instructions for evaluating the sum of squares of $v1, v2, \ldots, v100$. A suitable sequence is:

$$\begin{aligned} n1 &= 1 \\ v101 &= 0 \\ 2\,v102 &= vn1 \otimes vn1 \\ v101 &= v101 + v102 \\ n1 &= n1 + 1 \\ j2,\ 100 &\geqslant n1 \end{aligned}$$

Such a group of instructions may form part of a larger programme involving the variables in question.

A complete programme of instructions and numbers is normally recorded *inside* the machine before being executed: it is therefore necessary to explain the *input* procedure.

The programme tape is prepared on a keyboard perforator on which are engraved the standard symbols. The material is "punched" in the conventional fashion, namely from left to right and down the column. Each instruction is followed by the symbols *CR* (carriage return) and *LF* (line feed). The keyboard is normally on "figures" which means that capital letters have to be preceded by *LS* (letter shift) and followed by *FS* (figure shift). Blank tape corresponds to blank paper and any number of blanks may separate the symbols provided their order is preserved. About six inches of blank should be left at the head of the tape. Associated with the keyboard is a printer which gives a printed copy of whatever is punched; this should agree with the original manuscript.

As the programme tape is scanned the instructions are normally recorded in the store where ultimately they will be obeyed. The rate of scanning is approximately one instruction per second and the rate of execution about eight per second. In the case of instructions included between brackets each instruction is executed immediately after it has been read and is not recorded in the programme proper. This facility is used to start the programme simply by including an unconditional jump instruction between brackets, e.g. (*j*1) which means "stop reading the tape and start obeying the programme at the instruction labelled 1."

Having got the programme started it may be necessary to call on the input medium for further numerical data. This

may be done in two ways for which it is necessary to introduce two further instructions. These are:

(ix) $z = I$, which means "replace z (which has the same significance as before) by the number formed by the next group of symbols on the tape";

(x) the letter T which causes the machine to start reading further instructions from the tape adding them to those already recorded in the store.

The former instruction may be used to read a tape bearing numbers only.

The T instruction, combined with the "bracket" facility, allows data to be input in the form (z = constant). This is a convenient method of altering parameters in between different runs. Thus, for example, if the supplementary instructions take the form

$$\begin{aligned} v23 &= 0{\cdot}012 \\ v24 &= 0{\cdot}965 \\ n3 &= 12 \\ j1) & \end{aligned}$$

then the effect will be to repeat the run with these new values of the quantities $v23$, $v24$ and $n3$.

To illustrate the coding scheme described above, the following calculation is programmed.

It is required to compute.

$$t = \frac{1-(p_2/p_1)^{2/7}}{1-(p_2/p_3)^{2/7}} \text{ where } p_2 = 30,\ p_3 = 40$$

$$r_e = 1{\cdot}3 + 2\left[1 - \frac{t^{3/2}(p_2/p_3)^{2/7}}{(p_2/p_1)^{2/7}}\right]$$

$$r_m = 1{\cdot}3 + 2\left[1 - \frac{t^{1/2}(p_2/p_3)^{2/7}}{(p_2/p_1)^{2/7}}\right]$$

for values of p_1 of the form $40 - (10n/156{\cdot}4)$, where $n = 0(1)156$.

The programme which required about 10 min to draw up is given below. For each value of p the time of execution is approximately $2\frac{1}{2}$ s plus the time to print the results—about a further $2\frac{1}{2}$ s. If the calculation is treated conventionally the time of execution could be reduced almost to the printing time above but the coding time might well run into several hours.

$2v1 = 40$	$(p_1 = 40)$
$v2 = 30$	$(p_2 = 30)$
$v3 = 40$	$(p_3 = 40)$
$v4 = 10/156{\cdot}4$	
$v5 = v2/v3$	(p_2/p_3)
$v6 = Lv5$	
$v7 = 2/7$	
$v8 = v7 \otimes v6$	
$v9 = Ev8$	$(p_2/p_3)^{2/7}$
$1v10 = v2/v1$	
$v11 = Lv10$	
$v12 = v7 \otimes v11$	
$v13 = Ev12$	$(p_2/p_1)^{2/7}$
$v14 = 1 - v13$	
$v15 = 1 - v9$	
$XYPv16 = v14/v15$	forms and prints t on a new line
$v17 = Sv16$	
$v18 = v17 \otimes v9$	
$v19 = v18/v13$	
$v20 = v/16 \otimes v19$	
$v21 = 1 - v20$	
$v22 = 2 \otimes v21$	
$ZPv23 = 1{\cdot}3 + v22$	forms and prints r_e
$v24 = 1 - v19$	
$v25 = 2 \otimes v24$	
$ZPv26 = 1{\cdot}3 + v25$	forms and prints r_m
$v1 = v1 - v4$	adjusts p_1
$j1, v1 > 29$	tests for last cycle
$(j2)$	starts programme

The following notes are of interest.

(1) The maximum number of instructions allowed cannot be given very precisely but a safe estimate is 500, which, in view of their comprehensive nature, should be adequate for the class of problems envisaged.

(2) No attempt has been made to economize on the use of variables. Thus, for example, instead of $v9 = Ev8$ we could write $v8 = Ev8$ since the argument is no longer needed. However, nothing is gained by so doing since space is virtually infinite for problems of this kind.

(3) A further example of laziness is the means adopted for evaluating 2/7. Instead of bothering to evaluate the fraction we have simply included an instruction for doing so, namely $v7 = 2/7$.

(4) The value of any intermediate quantity can be printed simply by inserting a P before the appropriate instruction. This may be useful in locating mistakes: the P can afterwards be erased by turning it into a ■.

(5) Rounding off. In general the "machine" rounds off only where necessary; in particular the following rules are observed.

(*a*) During input. Constants, which appear in decimal form on the input medium, are converted to the scale of two inside the machine. Whole numbers are converted exactly but terminating decimal fractions, which may or may not have terminating binary equivalents, are replaced by an approximately equivalent binary fraction. (It is, of course, possible to arrange that those fractions which, like 0·125, do have an exact binary equivalent are converted exactly.)

(*b*) During the subsequent calculations. In the instructions (ii) rounding off takes place only where the result extends beyond 39 significant binary digits. In the instructions (iii) the accuracy obtainable depends on the nature of the function and argument. For example, in forming the cosine of an angle of about 1000 rev, three significant decimals are unavoidably lost. The jump instruction (v) involves taking the difference $x - y$, an operation which is identical with the corresponding form of instruction (ii).

(*c*) During output. Numbers are first converted from floating binary to fixed binary form, digits beyond 2^{-40} being discarded. The resulting number can be converted to decimal form exactly since a terminating binary fraction has a corresponding decimal equivalent; but in fact conversion is carried only as far as the number of decimal places required—set on the hand-switches.

This completes the standard account. The "simple machine" is not necessarily the ideal machine for all purposes. For example, the coding of repetitive work could be made more economical in instructions by introducing variables whose index is a general linear function of one or more index quantities. However, this facility would not be appreciated in the kind of problems to which the "simple machine" is restricted. Moreover the inclusion of such facilities would

tend to destroy the main advantage of the "simple machine," namely its simplicity.

REFERENCES

(1) MUTCH, E. N., and GILL, S. *Proceedings of a Symposium on Automatic Digital Computation*, Paper No. 11, National Physical Laboratory, March, 1953 (London: H.M. Stationery Office, 1954).

(2) *Symposium on Automatic Programming for Digital Computers.* Sponsored by the Navy Mathematical Computing Advisory Panel at Washington, D.C., May, 1954.

(3) BROOKER, R. A., and WHEELER, D. J. Floating operations on the Edsac, *Math. Tables Aids Comput.*, **7**, p. 37 (1953).

(4) HUME, J. N. P. Input and Organisation of Subroutines for FERUT, *Math. Tables Aids Comput.*, **8**, p. 30 (1954).

(5) WILKES, M. V. *Proc. Cambridge Phil. Soc.*, **49**, p. 84 (1953).

Instability of photomultipliers

By L. P. DE VALENCÉ, M.Sc., A.Inst.P., Institute of Cancer Research, Royal Cancer Hospital, London, S.W.3

[*Paper first received* 1 *April, and in final form* 1 *June*, 1955]

A phenomenon of dark current instability in specified types of electrostatically focused photomultiplier tubes is described. Particular attention is drawn to the variation with glass envelope potential of dark current fluctuation under fixed circuit constant conditions. The degree of instability does not appear to be related to the relative photometric sensitivity on the tube. A possible explanation of the phenomenon on the basis of electron defocusing is suggested, and a satisfactory method of eliminating the disturbance is described.

This paper describes an investigation into a phenomenon of photomultiplier dark current instability, under conditions obtaining in many experimental procedures where the tube is housed in an earthed metallic casing and operated at room temperature with its anode at approximately earth potential and its cathode at a potential of -1000 V. Under such conditions, it has been found that should the glass envelope either touch, or come into close proximity with, the earthed metallic housing, both the level and the fluctuation in the dark current increase, in some cases by a very large factor. The fluctuation is here defined as the maximum variation in dark current under fixed circuit constant conditions.

An investigation into the effect of glass envelope potential on the dark current *level* has been reported by Taylor,[1] and Morton and Mitchell,[2] whose results are confirmed in the present work. These authors, however, do not deal with the influence on dark current *fluctuation*, which effect is stressed here.

This phenomenon of instability is clearly of importance in experiments concerned with the detection of small changes in light flux, using sensitive scintillation dosemeters of the type described by Belcher.[3] The effect was first observed in optical experiments designed to study the behaviour of light pipes in clinical scintillation dosemeters. In these experiments the photomultiplier and its dynode resistor chain were mounted in a light-tight brass housing of about twice the diameter of the photomultiplier, provision being made for a lateral positional adjustment of the photomultiplier for centring purposes on an optical bench. It was observed that in an extreme setting of the photomultiplier, when the glass envelope either touched or was very close to the metallic housing, the dark current increased considerably and, even of greater importance (since the dark current itself could be "backed off" electronically) there was a considerable increase in the dark current fluctuation. This markedly reduced the accuracy with which small changes of light flux could be detected above the noise level.

EXPERIMENTAL

In the experiments described below, measurement of dark current was made using a valve voltmeter of very high input impedance, based on a circuit suggested by Scroggie.[4] This instrument measures the potential developed by the photomultiplier output current, across a high stability resistor of $10^8\ \Omega$. In all the investigations that follow the time constant of the associated electrical circuits was 10^{-1} s.

In a preliminary investigation, the photomultiplier was supported horizontally, free from any earthed screens, in a large light-tight box. The dark current measured under these conditions is hereafter referred to as "normal." A single turn of naked copper wire was then loosely suspended around the glass envelope and the dark current was again found to be normal, provided that the wire was electrically floating. If, however, the wire was earthed the dark current and dark current fluctuation increased noticeably.

The same phenomenon was observed when the single turn of wire was replaced by a turn of insulated wire. In this case, however, a capacitive effect was apparent in that immediately the photomultiplier e.h.t. was switched on, the dark current and fluctuation was excessively high, and then gradually decreased to an equilibrium value which was higher than normal. The time taken to reach the equilibrium value could be increased by increasing the number of turns of wire. Further, the actual position of the wire on the glass

envelope seemed to have no observable influence on the degree of instability induced when the wire was earthed.

In order to measure the degree of instability two Terry clips were rigidly connected together and fitted over the glass envelope of the photomultiplier so that their open ends were in front of the photocathode, thereby allowing sensitivity tests to be carried out. By connecting the clips to selected points in the dynode resistor chain, the potential of the envelope could be varied from 0 to −1000 V in 100 V steps.

Using this arrangement eight photomultipliers of types 27M1, 931A and 1P21 were investigated. The electrode arrangements of these types, and the effect of current fluctuations has been discussed by several authors (see, for example, Morton and Mitchell[2] and Rhodda[5,6]). At each value of glass potential the dark current, dark current fluctuation and photometric sensitivity were measured, the latter to test for any possible relation between changes in sensitivity and changes in dark current fluctuation. Further, the relative photometric sensitivities of all eight photomultipliers were measured under "normal" conditions (i.e. glass envelope electrically floating) for the purpose of establishing any possible relation between tube sensitivity and the degree of instability induced by earthing the envelope. The possibility of a hysteresis effect was investigated by varying cyclically the envelope potential between −1000 and 0 V. No such effect was observed.

All the photomultipliers investigated exhibited the phenomenon described, the degree of instability increasing as the envelope potential approached zero. The results of these experiments are discussed below.

In the case of one of the photomultipliers (a type 27M1 tube) an experiment was performed extending the envelope potential range to voltages outside those at which the photomultiplier is operated. A Dynatron type 200 (0 to 4 kV) power unit was used to provide the necessary potentials and the experiment was carried out for potentials varying from −1460 to +2000 V.

RESULTS

Fig. 1 shows a typical curve of dark current plotted against envelope potential over the range 0 to −1000 V. The arrow indicates the "normal" dark current level. In this particular

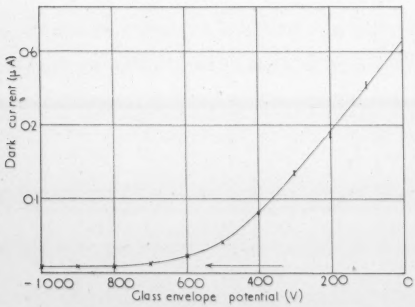

Fig. 1. Variation of dark current with envelope potential

case (a type 27M1 tube) the dark current when the envelope is earthed is some thirty times that when the envelope is electrically floating. The dark current fluctuation in this tube also increased by a similar factor, while its photometric sensitivity was found to increase by a factor of only 1·1. It is seen that the dark current remains sensibly constant over an envelope potential range extending from about −750 to −1000 V, and this is the region of most stable behaviour. This "range of stability" is arbitrarily taken as that range of envelope potentials over which the dark current remains within 20% of its "normal" value.

The plots of dark current against envelope potential for all eight tubes investigated were of a similar shape to that of Fig. 1, although the factors by which dark current and fluctuation increased, varied markedly from tube to tube. The following table summarizes the behaviour of the tubes investigated.

	Factors of increase in:				
Tube	*Relative photometric sensitivity*	*Dark current*	*Dark current fluctuation*	*Sensitivity*	*Range of stability* (V)
27M1 (A)	1·20	7	50	1·05	−700 to −1000
27M1 (B)	0·88	5	14	—	−600 to −1000
IP21	0·87	2	3	1·00	−600 to −1000
931A (A)	0·74	72	140	1·10	−700 to −1000
931A (B)	0·61	4	30	1·00	−600 to −1000
27M1 (C)	0·55	2	2	1·00	−600 to −1000
27M1 (D)*	0·33	30	30	1·10	−750 to −1000
931A (C)	0·06	8	30	—	−600 to −1000

* The behaviour of this tube is shown graphically in Figs. 1, 2 and 3.

The "factors of increase" quoted in columns 3 to 5 are the ratios of the quantities measured at zero envelope potential to those with the envelope electrically floating. The relative photometric sensitivities of the tubes investigated varied over a wide range (column 2), and from these results there does not appear to be any relation between photometric sensitivity and the degree of instability (particularly column 4) induced by earthing the glass envelope. In most cases the factor by which the dark current increases is different from that by which the fluctuation increases and there seems to be no simple relation between these factors.

In the experiment over an extended voltage range the tube used was the one, the behaviour of which is shown in Fig. 1. Figs. 2 and 3 show the variation of dark current and fluctuation respectively with envelope potential over the range −1460 to +2000 V. It is seen that as the envelope potential is increased negatively beyond −1000 V the dark current rises very sharply and the tube displays abnormally high instability in this region. Also, for a given value of dark current in this region, the fluctuation is far more marked than that for the same value of dark current in the positive potential region of the curve.

DISCUSSION

Two possible explanations of the observed effects may be tentatively suggested:

(*a*) increased evaporation of electrons from the photocathode due to glass envelope potentials which are sufficiently positive with respect to the photocathode. Such potentials may also have the effect of attracting some of the electrons out of the dynode system, thereby influencing the noise level;

(*b*) a defocusing effect between photocathode and first dynode. Since the photocathode is at a potential of −1000 V,

the resulting electrostatic field on earthing the envelope is greatest in this region.

If electron attraction alone were the cause of this phenomenon it would be expected that as the envelope potential is increased negatively beyond −1000 V the curve would either fall very gradually or remain parallel to the abscissa. It is

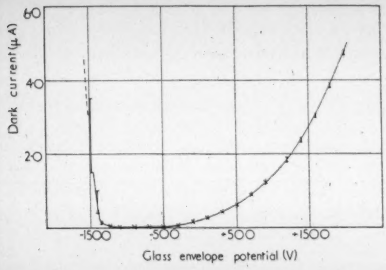

Fig. 2. Variation of dark current with envelope potential

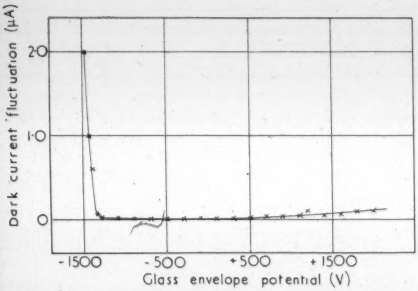

Fig. 3. Variation of dark current fluctuation with envelope potential

seen in Fig. 2, however, that it rises very sharply. Further, it is observed that the rise for potentials between about −1300 and −1460 V (i.e. 300 to 460 V negative with respect to cathode) is very much sharper than that for potentials between about −700 and −500 V (300 to 500 V positive with respect to the cathode). This is precisely what might be expected from a combination of both defocusing and electron attraction, since the overall noise level in a photomultiplier is determined primarily by that at its first stage, i.e. the photocathode. Envelope potentials differing from that of the photocathode either positively or negatively would give rise to extraneous electrostatic fields which could, if sufficiently large, produce a defocusing of electrons and this would become manifest as an increase in noise level. Such an increase produced by a positive envelope potential (relative to the photocathode) would probably not be as great as that produced by an equally negative envelope potential since, in the latter case, the electrons would be repelled into the dynode system, giving rise to an even greater increase in dark current and not attracted out of the system as would be the case for positive envelope potentials. The non-symmetrical nature of the curve shown in Fig. 2 can thus be explained on this basis.

It would appear from this analysis that from the point of view of most stable operation it would be of some advantage to connect the glass envelope of a photomultiplier to its cathode, thereby minimizing electrostatic disturbances. In practice, however, since all tubes investigated have a range of stability extending over a few hundred volts in the region of the cathode potential, the actual envelope potential giving maximum stability is not critical and the envelope may be connected to, say, the second dynode (−800 V) with equal advantage. This can be carried out in the following manner.

A fine wire is wound a few times around the glass envelope where the latter enters the base, and is soldered on to the top of the second dynode pin. The coil of wire is then covered with Aquadag and two Aquadag strips painted over the glass, each beginning at the coil, continuing over the top of the tube and ending at the coil on the opposite side, care being taken that each strip is well clear of the "field of vision" of the photocathode.

(A similar method of surrounding the glass envelope, by a screen which is maintained at a potential substantially negative with respect to the anode, has been patented by Rhodda and Heath.[7])

This method has proved very successful in achieving good stability. It should be pointed out, however, that this treatment of photomultipliers is only likely to increase stability in experimental arrangements where there exist disturbing electrostatic fields such as, for example, in apparatus where the photomultiplier is very close to an electrical screen, the potential of which differs by at least a few hundred volts from that of the photocathode.

ACKNOWLEDGEMENTS

I would like to express my gratitude to Professor W. V. Mayneord, Director of the Physics Department, for his interest and encouragement during this work, and to Drs. L. F. Lamerton and E. H. Belcher for helpful criticism in the preparation of the script. I would also like to record my thanks to Mr. S. P. Newbery and other members of the Electronics Staff for much helpful discussion.

Acknowledgement is also due to the South African Council for Scientific and Industrial Research for the award of a bursary.

REFERENCES

(1) TAYLOR, M. C. *J. Phys. Radium*, **10**, p. 255 (1949).

(2) MORTON, G. A., and MITCHELL, J. A. *R.C.A. Rev.*, **9**, p. 632 (1948).

(3) BELCHER, E. H. *Brit. J. Radiol.*, **26**, p. 455 (1953).

(4) SCROGGIE, M. G. *Wireless Wld*, **58**, p. 14 (1952).

(5) RHODDA, S. *J. Sci. Instrum.*, **26**, p. 65 (1949).

(6) RHODDA, S. *Photo-electric Multipliers* (London: Macdonald and Co. Ltd., 1953).

(7) RHODDA, S., and HEATH, F. G. British Patent Specification 645,763.

A polarized light study of glass fibre laminates

By G. A. Horridge, M.A., Ph.D.,* Royal Aircraft Establishment, Farnborough

[*Paper received* 16 *April*, 1955]

The use of a stress sensitive resin (Marco 28C) in the formation of a glass-fibre-resin laminate makes possible a photoelastic stress analysis of a highly anisotropic material. This will have an application in conjunction with theoretical stress analysis in anisotropic materials; it is hoped that it will also be of value to the designer of reinforced plastic structures. The relation between the resin and the fibres in a laminate under load has been studied with the aid of a polarizing microscope. A disconcerting feature is the discovery of a pattern of cracks which open under relatively small stress, and which may provide a pathway for erosion by water.

Glass-fibre-resin laminates are reinforced plastics in which the reinforcement is a mat or cloth of glass fibre and the matrix is one of the large range of synthetic resins now available. The high strength-weight ratio of these materials has led to a great interest from the aircraft industry but their applications are best known from the boats and sports-car bodies that are beginning to appear. The materials themselves are expensive but fabrication costs are relatively low and, if design problems can be overcome, it seems that the use of these materials for complicated moulded shapes will continue to increase. The present work is an attempt to study the interaction of the resin with the fibre and at the same time to initiate photoelastic analysis of anisotropic materials as an aid to design.

The use of reinforced plastic laminates for photoelastic observations is important from three points of view. First, for the designer of plastic structures, any assistance in the calculation of the state of stress and stress concentrations in an anisotropic material is welcome because the theory is embryonic and extremely cumbersome. Even in isotropic materials it is an advantage to make use of photoelastic models, but in these anisotropic laminates an actual structure itself may often be examined in this way.

Secondly, for the manufacturer of either resin, fibre or surface treatment, information about the behaviour of laminates under load is useful in the search for better materials. Improvement of the laminate and the effect of the surface treatment of the glass fibre is at first sight brought about by a better adhesion of resin to fibre, but the failure to achieve theoretical strengths at all orientations is very likely due to stress concentrations at this interface, and the effect is augmented by better adhesion. The photoelastic effect is due to stress in the resin, and the observations given here, that at a given strain this is the same for all orientations, shows that it arises from resin that is straining with the fibre and acting as a mere passenger. Exploiting the stiffness of the resin at 45° to the fibres merely means that the overall Young's modulus is so much lower in this direction that the stiffness of the passenger is felt. This justifies the methods used elsewhere for calculating the stiffness of these materials.† It is futile to eliminate resin, though much of it only adds to the weight, because in it are neutralized all the secondary stresses that hold the fibres in place relative to each other. The existence of these is shown after removal of primary stress effects by a suitable alinement of the polaroids.

Thirdly, it is important to be able to check photoelastically the predictions of any theory of anisotropic materials. Such a theory is necessarily complicated by an excessive burden of coefficients and the calculation of photoelastic results will also be long and tedious. So far as the author is aware a complete photoelastic solution for an anisotropic material is not available.

TECHNIQUES

To obtain a glass-fibre laminate sufficiently transparent for photoelastic work it is important to follow certain recommendations. The materials and the moulding surfaces must be absolutely clean. The surface of the fibres must be treated with vinyl di-chlorsilane after burning off all the size, or be volanized by the manufacturer. The birefringence of the starch grains normally used in sizing the fibre interferes with the measurement of retardation and a poor adhesion of resin to glass produces an opaque laminate. The refractive index of the resin (Marco 28C by Scott Bader and Co. Ltd.) used in the present work was sufficiently near that of the glass to give the laminate a blue appearance by transmitted light because it is impossible to match the dispersive powers of the two materials. To avoid gas bubbles in the final product it may be necessary to remove dissolved gas from the resin with a vacuum pump, but satisfactory results are generally obtained without this precaution, as long as a temperature rise of more than 10° C is prevented by high thermal capacity of the moulding surfaces.

The moulding technique is important. The cloth is cut along the line of a pulled-out thread. For flat laminates a plate-glass surface is used for moulding, coated with a commercially available cellulose-ester parting agent. The plate-glass is mounted on a frame and illuminated from below, so that air bubbles may be clearly seen. Starting with twice the weight of mixed resin as cloth, about 20 ml. of resin is poured on the glass and a piece of clean, treated cloth laid carefully over. The resin is slowly pushed outward from the centre with a finger, progressively wetting the cloth, and air bubbles are stroked out. This is repeated for ten to twelve layers of cloth to a thickness of ¼ in. or so. The threads of all layers must run in the same line unless a crossed arrangement is intended. When sufficient cloth has been smoothed down, a sheet of cellophane is laid over with an overlap of about 12 in. all round. This must be stout, dry, without creases, and preferably not treated with cellulose nitrate as are some brands of "moisture-proof" cellophane. Working from the centre the laminate is then firmly rolled with a rubber roller and all visible bubbles pushed out. The large overlap of the cellophane prevents the return of air into the laminate. It is best to arrange the concentration of catalyst to give a setting-time of four to six hours. To avoid extensive creep, see Fig. 1, it is an advantage to harden off the resin the next day by warming to 80° C for an hour. The best results have been obtained with satin-weave cloth, thirty-two threads per inch; so-called unidirectional materials always produced an opaque

* Now at St. John's College, Cambridge

† Gordon, J. E. *J. Roy. Aero. Soc.*, **56**, pp. 705–728 (1952).

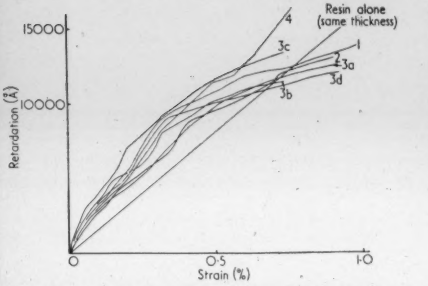

Fig. 1. A calibration of four test pieces (No. 3 is repeated four times) cut in different directions from a laminate in which the resin is insufficiently cured and shows considerable creep. Volan-treated eight-strand satin weave

Test piece	*Thickness (in.)*	*Young's modulus (lb/in.²) × 10⁻⁶*	*Angle to warp (degrees)*
1	0·170	1·1	70
2	0·165	2·0	90
3	0·170	0·75	40
4	0·165	2·5	0

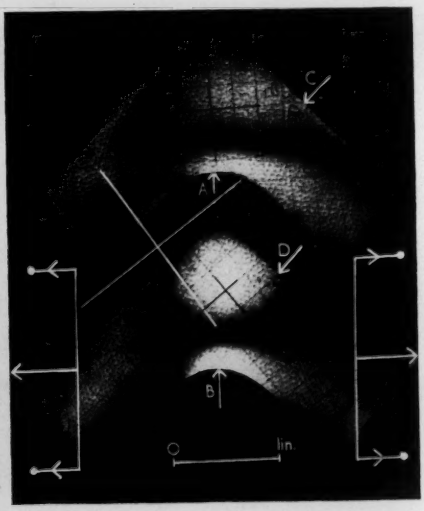

Fig. 2. Two shapes cut from an eight-strand satin-weave laminate, similar in all respects and in loading conditions but that the warp and weft of the reinforcement run in the directions shown by the black lines. The white cross shows the direction of the polaroids. The maximum retardation at the edges is given in the table. No quarter-wave plates were used and a slight difference can be seen between the isoclinics of the two test pieces

product. Analysis by ashing the final laminate after the experiment should give a resin content of about 50%.

The stress in the resin is only a fraction of that in the fibre. This, and the fact that the maximum thickness is about ¼ in., means that retardations are obtained which are relatively small for photoelastic work. A compensator must therefore be used for quantitative work. Using monochromatic light (sodium light) the fifth or sixth fringe can be reached in simple tension but the danger of buckling in compression test pieces prevents such high stresses. An example with a more complicated test piece, Fig. 2, shows a typical picture.

Ordinary straight-waisted test pieces in simple tension are used, cut at a variety of angles to the direction of the warp. They must be at least an inch wide to ensure that load is transferred into fibres which do not run along the axis of the test piece. To retain the transparency, the front and back surfaces are not machined and in general it is not necessary to grease the surface or work in oil. It is expected that the usual procedure in photoelastic work, e.g. axiality, uniform illumination, direction of machining, will be followed. Time-edge effects are not likely to arise.

For the microscopical work, thin laminates of a single thickness of cloth are cast on glass. Straight strips 6 × ½ in. cut at various angles to the fibre are fitted symmetrically with metal ends, fixed with Araldite. With a simple miniature testing machine, mounted on the revolving microscope stage, the test piece is observed and photographed by polarized light. The directions of the stresses are found by revolving the stage and plotting isoclinics in the usual way.

CALIBRATION RESULTS

The basic result, which is interesting from several points of view, is that the retardation per unit strain is independent of the orientation of the fibres with respect to the test piece. This is shown in Fig. 3, in which are plotted results from three test pieces cut in different directions from the same laminate. In laminates of this kind the Young's modulus varies from $0{\cdot}75 \times 10^6$ lb/in.^{2} at 45° to the grain to $3{\cdot}0 \times 10^6$ lb/in.^{2} along the grain, and for a given photoelastic effect the loads are inversely proportional to these values. In the samples made as described a retardation of 10000 Å for 0·5% strain was usual for a laminate ¼ in. thick.

This result makes it possible to use this method in quantitative work, at least in determining stress concentrations at an edge (see the table), and must form the basis for a theory of photoelasticity of these anisotropic materials.

The values of the retardation observed at the points marked in Fig. 2 and the corresponding stresses calculated from the data on Fig. 10

		Retardation (Å)	*Calculated stress (lb/in.²)*
A	tension	4050	3800
B	tension	5900	2400
C	compression	−3660	−1400
D	compression	−2560	−2500

On a maximum tensile-strain theory the upper test piece will be stronger than the lower. The greater compression at *D* than at *C* shows the tendency to transfer the load into the parts of the structure where the fibres are better orientated.

Calibrations of laminates containing so-called "unidirectional" reinforcement (warp: weft = 9 : 1) show that test pieces cut parallel to the warp behave in the normal way, with a fringe strain coefficient similar to that for satin-weave materials; but for those at an angle to the warp the retardation per unit strain is much lower, in fact less than half. It is not

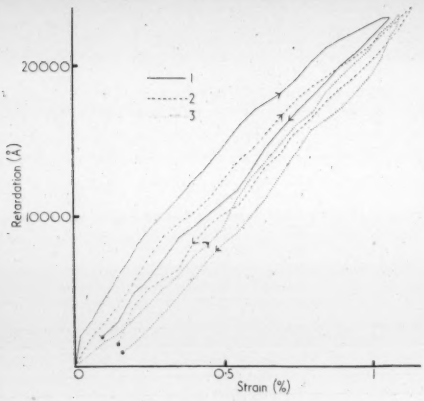

Fig. 3. Calibration of three straight test pieces in simple axial tension. The retardation is proportional to strain, independent of the direction relative to warp of the cloth. Eight-strand satin weave cloth, vinyl dichlorsilane-treated

Test piece	*Thickness (in.)*	*Young's modulus* $(lb/in.^2) \times 10^{-6}$	*Angle to warp (degrees)*
1	0·236	0·9	40
2	0·235	1·95	22
3	0·229	2·5	9

clear what is happening in these cases, but certainly "unidirectional" reinforcements cannot be treated under the simple rule.

DISCUSSION OF PRIMARY RESULT

A glance at the procedure for making a laminate shows that a great many variables may be changed at will. The stress birefringence of the resin depends to some extent on the conditions at the time when it was mixed, e.g. exact percentage of catalyst, temperature, rate of hardening, and the resin varies from batch to batch. If a model is cut from a flat laminate this does not matter, for a calibration piece may be taken from the same sheet. But it is a valuable characteristic of reinforced plastic that complicated shapes are moulded, not assembled or machined; in this case a flat laminate for calibration must be made at the same time under the same conditions. As long as a reasonable transparency is obtainable by use of treated fibre, there seems no reason why large structures should not be tested in a qualitative way for points of high stress in the plane of the laminate while under load. However, the method would not necessarily give a warning of high interlaminar shear, which is a common cause of failure in these materials.

MICROSCOPICAL OBSERVATIONS

For an understanding of the changes when a reinforced plastic is loaded, the use of a polarizing microscope is essential, but this is a technique that has been rarely used in the field of stress analysis. Models of a more convenient size cannot be used in this case, in which both the initial stresses which arise from shrinkage of the resin and those which appear under load, depend on the absolute dimensions of the reinforcement. For example, when a large straight "fibre" such as a glass rod 12 in. long and 0·1 in. diameter is embedded in Marco polyester resin, the tensile stresses which appear when it sets are sufficient to fracture the resin. The crosswise compressive forces on such a rod are sufficient to give the appearance of a powerful adhesion which is not found when this resin sets on a clear flat sheet of glass. The case of the fibre a thousand times smaller must be similar but, though looked for, the compressive forces in the resin have not been seen. The resin gives approximately 20 Å retardation per inch thickness per $lb/in.^2$, so that for a glass fibre of usual size a simple compressive stress of 1000 $lb/in.^2$ at the interface would be about the limit of sensitivity.

The directions of the principal stresses (P and Q) in a loaded laminate as shown in Figs. 4 and 5 are obtained by

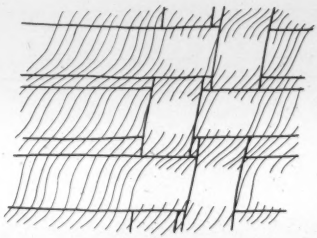

Fig. 4. The directions of the greater principal stress in the resin plotted from isoclinics obtained by rotating the microscope stage. This is impregnated "unidirectional" fabric with the main axis horizontal and twelve horizontal threads per inch

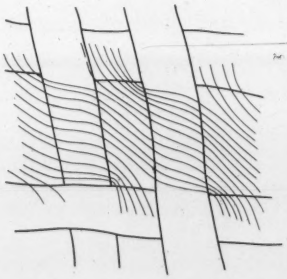

Fig. 5. The directions of the greater principal stress in the resin plotted from isoclinics as in Fig. 4. This is "satin weave" fabric which has been opened out to make large spaces between bundles

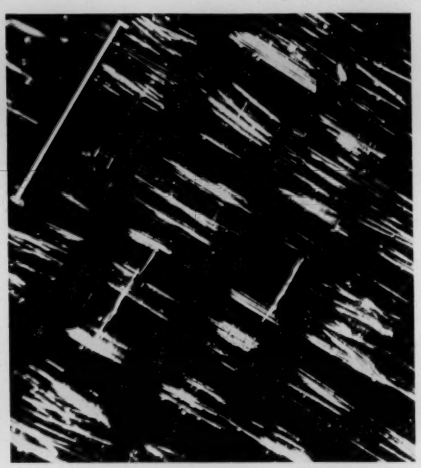

Fig. 6. Cracks between the fibres of the weft photographed after partial removal of a former load of approximately 6000 lb/in.^{2}. The polaroids are orientated to cut out the stress birefringence of the resin. The white line (0·03 in.) shows the scale and the direction of the loading

Fig. 7. Satin weave volanized cloth under a load that is 45° to the fibre directions. Note the neutral axes where the fibres cross and the light areas caused by curving of the lines of principal stress in the outside of the bundles. The arrows indicate the points where failure is initiated. Stress 3000 lb/in.^{2}. The white line (0·03 in.) shows the scale and the direction of the loading

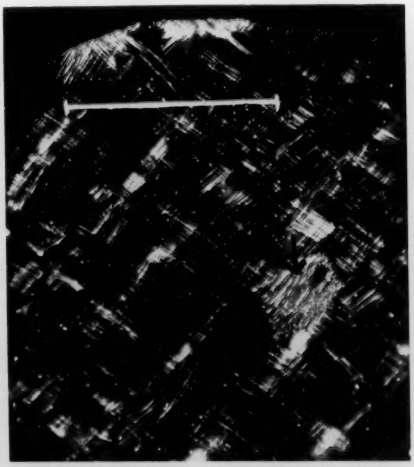

Fig. 8. The black arrow indicates a small failure where warp crosses weft, as a result of a former load of 8000 lb/in.^{2} at 45° to the directions of the fibres. The white line (0·03 in.) shows the scale and the direction of the loading

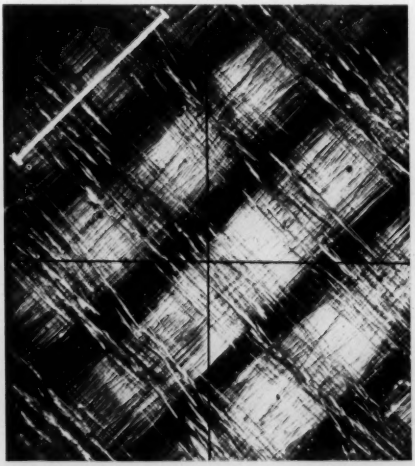

Fig. 9. Square weave volanized cloth under load that is parallel to the warp. Note the stress in the resin round the warp bundles and the cracks between the threads of the weft. Stress approximately 5000 lb/in.^{2}. The white line (0·03 in.) shows the scale and the direction of the loading

The appearance of some oscillating discharges

By T. K. Allen, Ph.D., R. A. Bailey, Ph.D., and Prof. K. G. Emeleus, M.A., Ph.D., F.Inst.P.

See pages 320–322

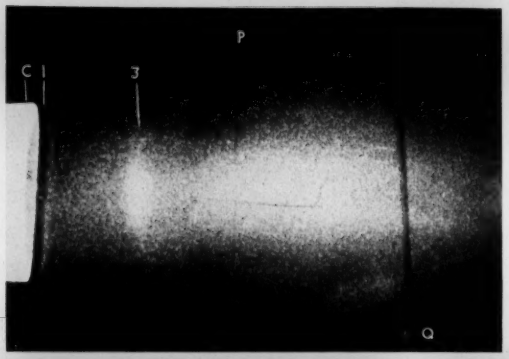

Fig. 2. Cathode sheath (1) and meniscus (3). The anode was just beyond the right-hand edge of the photograph. There is slight convergence visible of the beam to the anode side of (3). The patch of light near the base of the right-hand probe is a reflexion from the tube wall

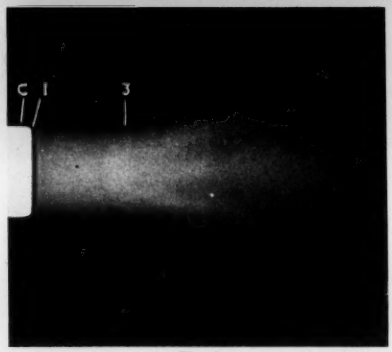

Fig. 3

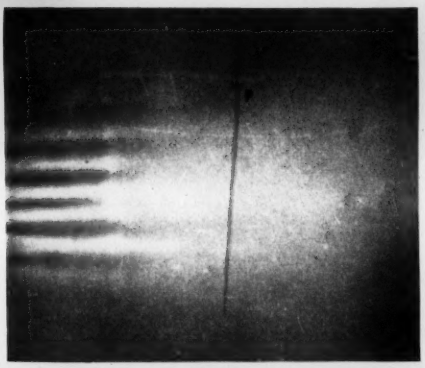

Fig. 4

Fig. 3. Beams deviated beyond (3). The convergence of the central beam was often more marked than in this instance. The cathode sheath (1) is clearly visible

Fig. 4. Collapse of ribbon beams at (3). The dark line is a large probe the presence of which was without effect. The cathode shield was at the left-hand edge of the photograph

Fig. 5. Broadening of narrow beam by oscillation. The flat probe is near the right of the photograph. A wire probe, not in use at the time, is behind the flat probe

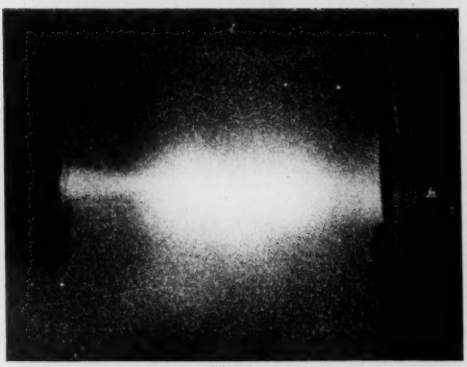

Fig. 5

plotting isoclinics. The method gives only the resolved directions of P and Q in the plane of the laminate and hence the shear stresses where the bundles cross do not appear. The crowding of stress lines at the corners of the resin window is shown and also the interesting fact that load is transferred progressively from the resin to the fibres as we move along a stress line from the periphery of a bundle to its centre. This is accompanied by the curving of the stress lines in this region and it immediately suggests that an optimum bundle size will exist for given conditions.

Besides giving the directions of the stresses and intensity of stress concentrations in a reinforced plastic under load, polarized light may be used to show minute cracks which appear in the resin between the threads of the weft when tensile loads are applied in the direction of the warp, Fig. 6. The stress at which these appear (4000 lb/in.^{2}) is much less than normal working stresses of these materials and about a tenth of the ultimate. This shows the uselessness of absolute data on erosion tests and sea-water resistance from observations on unstressed material, though such tests may be valuable for rapid comparison of alternative methods and materials. The position of these cracks shows that even in extension parallel to the warp, the straightening out of the crimp in the fibre produces an irregular distribution of load in the resin, sufficient to produce a pattern of small failure points.

The picture obtained with plain stress at 45° to warp and weft is shown in Fig. 7. Small failure points, Fig. 8, appear at the areas where the warp crosses the weft, as a result of shear stresses where one overlies the other. Being in the plane of the principal stresses, these patches are not responsible for failure, although their progressive multiplication is the basis of the creep, always pronounced where the stresses are at an angle to the fibres. This process can be followed in a test piece loaded under the microscope. Failure is initiated by cracks in the resin at the points shown by the arrows in Fig. 7, where there is the maximum tensile strain in the resin. Very roughly, reinforced plastics fail at a given breaking strain, irrespective of fibre orientation, and the above results lead one to think that the breaking strain of a resin is the property that determines its effectiveness as a bonding agent for glass fibres.

With the load parallel to the warp there is quite a different distribution of stress in the resin, particularly noticeable at relatively small stresses (Fig. 9). The resin windows between the fibre bundles now appear unstressed because the fibres take the load but the birefringence largely originates in the resin between the individual fibres. This is thought to arise from unequal strains of the individual fibres and a consequent fibre to fibre redistribution of the load at all points throughout the bundle.

The mechanism of creep can be shown indirectly. In Fig. 10 the values of retardation $(P - Q)$ in the resin are plotted against load for three orientations. As a result of creep the return path does not follow the loading path. However, for test pieces cut at an angle greater than 20° to the fibres, the retardation per unit *stress* increases after creep has occured but parallel to the fibres it decreases. The first case is interpreted as a transfer of stress into the resin by sliding of fibres over each other, and has no limit. The second case is interpreted as a transfer of load from the resin to the fibres, because the progressive removal of crimp from the fibre bundles increases their stiffness relative to the resin. The retardation per unit *strain* (Fig. 3) is always lower in the unloading part of the curve. This is a property of the resin, which has

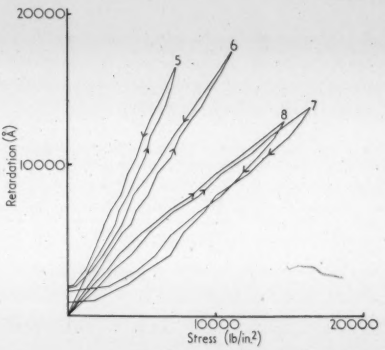

Fig. 10. The retardation plotted against the stress shows that the mechanism of creep depends on the direction of the fibres relative to the stress. In Nos. 5 and 6 the retardation at a given load is greater after creep; in 7 and 8 it is less

Test piece	*Thickness (in.)*	*Young's modulus (lb/in.^{2}) × 10^{-6}*	*Angle to warp (degrees)*
5	0·12	0·95	40
6	0·12	1·75	25
7	0·12	2·2	0
8	0·12	2·1	90

approximately a constant retardation for a given stress $(P - Q)$ even after a 0·5% creep.

CONCLUSION

Some apology must be given for the qualitative nature of many of the results given here. However, in the exploration of a new subject, particularly one so full of arbitrary recipes and variable materials, the biological methods of selection and description are better adapted to produce order. It is hoped that the topics raised in this paper will at least point to the great lack of more fundamental work on these new engineering materials, reinforced plastics.

ACKNOWLEDGEMENTS

I acknowledge with thanks the assistance given by Messrs. L. N. Phillips, A. Cornwell and especially by my assistant, S. A. Thompson, in the preparation of the laminates by the techniques developed at the Royal Aircraft Establishment. I should also like to thank Mr. J. E. Gordon of Tube Investments Ltd. for all his help and encouragement during this and related work.

The appearance of some oscillating discharges

By T. K. Allen, Ph.D., R. A. Bailey, Ph.D.,* and Prof. K. G. Emeleus, M.A., Ph.D., F.Inst.P., Physics Department, Queen's University, Belfast

[*Paper received* 1 *April*, 1955]

An account is given of the appearance of some low voltage, hot-cathode discharges generating high-frequency oscillations internally in gas at a pressure of the order of 10^{-3} mm of mercury. The primary electrons are deviated laterally, as well as being accelerated or retarded in their longitudinal motion, at a distance of a few millimetres from the cathode, in or close to a layer of ionized gas which is brighter than the neighbouring plasma. The position of this layer changes discontinuously when a probe is moved through it, giving rise to an apparent abrupt alteration of the electrical properties of the discharge along a line normal to the cathode which is partly spurious. The layer becomes unstable if large currents are passed, and the tube then also generates oscillations with frequencies below 1 Mc/s. The discharge can be stabilized to higher currents by a longitudinal magnetic field. Two other instances are recorded of a close association of high-frequency and low-frequency oscillations.

Hot cathode rectifiers and thyratrons containing gas at low pressure are commonly found to be generators of electromagnetic oscillations in the centimetre and decimetre bands.[1] The processes responsible, which involve large amplitude, non-linear disturbances of the discharge, have not yet been fully analysed mathematically.[2, 3] In their pioneer work on these oscillations, Merrill and Webb[4] noted that the discharge had an unusual visual structure, somewhat similar to that previously described by Druyvesteyn and Warmolz[5] in other hot-cathode discharges, but did not investigate it in detail. The present paper is a fuller account of the appearance of oscillating discharges of these and similar types. Most of the observations were made incidentally to electrical investigations of plasma-electron oscillations[6, 7] of which an account has been given elsewhere.[8, 9]

EXPERIMENTAL ARRANGEMENTS AND RESULTS

As the structure of discharges cannot be seen clearly with bare cathodes, on account of the glare, oxide-coated cathodes have been used. Disks (with diameters of 3–15 mm) have been employed in preference to cylinders, since the symmetry of the discharge from the latter hinders observation of effects transverse to the primary electron beams. The discharges were passed through mercury vapour saturated at room temperature (usually 18–21° C) in large demountable tubes[8, 10] used on the pumps. Similar results were obtained with argon at comparable pressures of a few 10^{-3} mm of mercury.

The main structural units of an oscillating discharge at low voltage (15–50 V) are shown diagrammatically in Fig. 1. *C* is the cathode, emitting from its right-hand face, and *A* the anode, the position of which is largely immaterial so long as it is sufficiently far from *C* for the intermediate structure to develop. The principal static fall of potential takes place across the thin dark space charge sheath (1) on the cathode, the rest of the discharge being nearly at anode potential. The primary electrons leave (1) normally, forming a cylindrical region (2), brighter than and of different colour from the plasma round its lateral surface, and terminated at the right-hand side at a distance of a few millimetres by a bright meniscus (3), slightly convex to *C*. The meniscus is often bounded on its anode side by a dark layer. After passing through (3) the primary electrons are deviated laterally into approximately conical converging (4) and diverging (5) beams. Between (1) and (3) the primary electrons acquire a range of energies centred roughly on their original energy (Dittmer's "scattering"[11]), most of the dispersion taking place in (3)[4] or just to the cathode side of it.[10] The occurrence of (4) and (5) shows that there are transverse components of field in (3) as well as longitudinal fields. Strong oscillations can be picked up by a probe only in and to the right-hand side of (3).

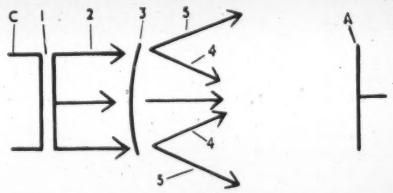

Fig. 1. Sections of high-frequency oscillating discharge

C, cathode; (1) cathode sheath; (2) unscattered beam section of discharge; (3) meniscus; (4), (5) scattered beams; *A*, anode.

Owing to differences of colour and brightness it has not been found possible to obtain photographs showing both the meniscus (3), and the beams (4) and (5) well simultaneously. Fig. 2 (p. 318) shows (3) and (1) for the following discharge parameters; diameter of cathode 15 mm, tube voltage 17·1 V, tube current 35 mA. (The exact temperature was not recorded for the discharges shown in Figs. 2 and 4.) The outer edge of (1) appears brighter than the plasma immediately to its right. *P* and *Q* are two probes on opposite sides of (2). Fig. 3 (p. 318) shows the beams (4) and (5); the position of (3) is indicated. The discharge parameters were: diameter of cathode 5 mm, tube voltage 17·3 V, tube current 29 mA, pressure $1{\cdot}55 \times 10^{-3}$ mm. Close inspection of these and other photographs, and of actual discharges, reveals a number of other details. In particular, (4) tends to form an axial line at its apex, without necessarily crossing over to form a new divergent beam, and (5) seems to diverge from a small region, narrower than the primary beam, on the anode side of (3), rather than from (3) itself. These require further investigation, as well as the dependence of the angles of (4) and (5) on discharge parameters.

* Now at Radar Research Establishment, Malvern, Worcs.

With increase in current and pressure, the plasma electron concentration and the oscillation frequency increase, and (3) moves nearer to the cathode. The variation of distance with current may account partly for the curvature of (3), as the current density in the discharge will be greatest opposite the centre of a uniformly activated cathode, but part of the curvature may be associated with lateral loss of oscillatory energy.

At constant pressure, the current can be increased only up to a certain limit without a change in the character of the discharge.[8] Below this the meniscus is fairly well defined, and the oscillations have a definite frequency, with, under some circumstances, harmonics. Above the limiting current the meniscus becomes blurred, several high frequency oscillations not obviously related to one another are recorded, and "noisy" lower frequency oscillations appear in the kc/s to Mc/s range. The discharge can be stabilized to higher currents by a magnetic field (e.g. 50 G), perpendicular to the cathode. This simultaneously decreases the curvature of (3) and the divergence of (5).

The existence of a transverse field component in the meniscus (3) has been shown in another way. A number of parallel wires, 0·1 mm in diameter, were mounted on a frame 1 mm in front of a flat cathode 15 mm in diameter. By making the wires positive to the cathode in an otherwise normal discharge, the primary beam passing the wires was split into a set of parallel ribbons. Viewed edge-on, these were seen to retain their original shape fairly closely for a short distance, but then to become diffuse abruptly, as if they had burst sideways perpendicular to their planes. The place where they became broad was about where a meniscus would have formed in an ordinary discharge. This effect is shown in Fig. 4 (p. 318) for an anode current of 30 mA, anode voltage 40 V, and potential of the wires +20 V relative to the cathode.

The appearances described so far are independent of the presence of a probe. Even a small cylindrical probe at near floating potential may, however, affect the meniscus (3) considerably when in its neighbourhood, repelling it and making it brighter locally, with accompanying frequency pulling effects in the oscillation intensity and frequency *versus* probe position curves.[8, 10] When two such probes are used, one on each side of (3), the probe nearer the cathode records more intense oscillations when the second probe is near (3) than when it is moved to a distance, or is absent. When a single probe is moved through (3) steadily, the latter jumps abruptly past the probe at a certain stage, or may flicker irregularly from one side of the probe to the other, the probe recording strong oscillations and marked energy scattering of the primary electrons only during the times when it is on the anode side of (3). These observations show that

(*a*) there is some form of feedback, probably oscillatory, from a probe to the discharge;

(*b*) the variation in properties of an undisturbed discharge along a line perpendicular to the cathode through (3) probably occurs less abruptly than is indicated by purely electrical measurements with a movable probe. Spectroscopic study of (3) in argon[10] indicates that the main growth of scattering nevertheless occurs in a space of not more than 1–2 mm.

A curious property of the well known small glow that forms on a probe held at more than the ionization potential of the gas positive to the space has been noticed. If the probe is in a part of the discharge where it can pick up high-frequency oscillations, e.g. between (4) and (5), the glow is several times larger than if the probe is in (2), under otherwise identical conditions. The large glow is in a state of low-frequency oscillation, like certain forms of anode glow.[12]

An association of high-frequency and low-frequency oscillations, which may show that plasma-electron and plasma-ion oscillations can react on one another, has also been found in a modified form of electron beam discharge, which appears similar to one at higher voltage investigated by Looney and Brown.[13] A flat cathode 7 mm in diameter was covered by a cylindrical shield 10 mm in diameter, with a hole 2 mm in diameter in the flat end opposite the emitting surface. With a positive shield voltage and anode voltage of the order of 100 V, a well-defined cylindrical beam with diameter about that of the hole was produced to the anode side of the shield. A wire probe placed in the beam detected no oscillations at any point. When, however, a flat probe 6 mm in diameter was moved into the beam, and rotated so that the beam was accurately perpendicular to its surface, high-frequency oscillations were detected for certain probe voltages. Simultaneously, a diffuse glow, about 8 mm wide, formed round the beam midway between cathode and probe, and low-frequency oscillations were found to be present. The latter were absent when high-frequency oscillations were not present. The frequency of the low-frequency oscillations was usually in the 10 kc/s to 1 Mc/s range, and the wave-form varied from nearly sinusoidal to untunable noise. Fig. 5 (p. 318) shows the appearance of an oscillating discharge, with anode current 3·1 mA, and anode voltage 138 V. The cap was at a potential of +20 V to the cathode, and the probe at cathode potential. The wavelength of the high-frequency oscillations was 46 cm. The pressure was 10^{-3} mm.

A few observations have also been made with the simple electrode system of Fig. 1 on discharges at 100–200 V. The most interesting effect noticed was the formation of a second meniscus a few millimetres from and convex to the anode. It was sometimes joined to the cathode meniscus (3) by a bright hollow cylinder with the two menisci as end caps. At these voltages the cathode disintegrates rapidly by ion bombardment, contaminating the gas; it would be necessary to use a Gabor-type gas cathode to avoid this. The discharges appear to be an intermediate stage between the low-voltage form, with its principal features near the cathode, and the higher-voltage form studied by Wehner,[14] which is more nearly symmetrical between the two electrodes.

CONCLUSION

The effects described in the previous section have been found to be sufficiently reproducible to serve as visual indicators of the presence or absence of oscillations in discharges of the types studied. In addition, they both supplement the information obtained by earlier electrical measurements in the discharges, and indicate some of the limitations of the latter. Some of the additional information, in particular the existence of transverse effects originating near the cathode meniscus (3), has been confirmed later by probe measurements, and spectroscopically.[10]. (It is perhaps worth pointing out that little modulation of the light emitted from these discharges can be brought about by the high-frequency oscillations, as their frequency is several orders of magnitude greater than the reciprocal of transition probabilities for dipole optical spectra.) The limitations discovered are also compatible with the results of a careful analysis of the probe data,[7] and, if anything, lead to a somewhat simpler picture of the discharge when it is undisturbed by a probe. The

main process occurring near the cathode—other than maintenance of the plasma by the primary electrons—seems most likely to be a slipping stream interaction between the primary and plasma electrons, producing oscillations which become catastrophic near the meniscus (3), where the disturbance of the discharge may be so violent that lower frequency ionic or relaxation oscillations can also occur.

REFERENCES

(1) ARMSTRONG, E. B., and EMELEUS, K. G. *Proc. Instn Elect. Engrs*, **96**, p. 390 (1949).

(2) GABOR, D. *Brit. J. Appl. Phys.*, **2**, p. 209 (1951).

(3) ECKER, G. *Z. Phys.*, **140**, p. 274 (1955).

(4) MERRILL, H. J., and WEBB, H. W. *Phys. Rev.*, **55**, p. 1191 (1939).

(5) DRUYVESTEYN, M. J., and WARMOLZ, N. *Physica*, **4**, p. 51 (1937).

(6) BAILEY, R. A. Thesis, University of Belfast (1951).

(7) ALLEN, T. K. Thesis, University of Belfast (1954).

(8) BAILEY, R. A., and EMELEUS, K. G. *Proc. Roy. Irish Acad., A*, **57**, p. 53 (1955).

(9) ALLEN, T. K., and EMELEUS, K. G. *Austral. J. Phys.* To be published (1955).

(10) ALLEN, T. K. *Proc. Phys. Soc.* [*London*]. To be published (1955).

(11) DITTMER, A. F. *Phys. Rev.*, **28**, p. 507 (1926).

(12) ARMSTRONG, E. B., EMELEUS, K. G., and NEILL, T. R. *Proc. Roy. Irish Acad. A*, **54**, p. 291 (1951).

(13) LOONEY, D. H., and BROWN, S. C. *Phys. Rev.*, **93**, p. 965 (1954).

(14) WEHNER, G. *J. Appl. Phys.*, **21**, p. 62 (1950).

The measurement of elastic wave velocity in small cylindrical specimens

By N. B. TERRY, Ph.D.,* and H. J. WOODS, M.A., F.Inst.P., Textile Physics Laboratory, University of Leeds

[*Paper received* 6 *April*, 1955]

A modification of the composite oscillator method is described in which the specimens, which have sizes ranging down to 5 mm in length and $\frac{1}{2}$ mm across, are cemented to nickel wire transducers. By exciting the nickel rod magnetostrictively, the resonant frequency of the composite rod can be measured and the elastic wave velocity in the specimen calculated. The behaviour of the composite oscillator when the areas of cross-section of the components are not matched is discussed. The selection of a transducer for a particular specimen with the object of reducing the errors due to the cement and to inaccurate frequency measurement is considered. Some results of measurements on mineral and keratin specimens are given.

Surprisingly few data are available for the elastic constants of common minerals; it was thought, therefore, that it would be useful if a method could be devised which would allow rapid measurements to be made for a variety of specimens. Since, as Hearmon[1] has pointed out, the elastic constants of many minerals are so dependent on the presence of impurities and the conditions governing growth that variations of the order of 10% are not uncommon, an experimental accuracy of the order of 1% would be sufficient for many purposes. The method described here, a modification of the composite oscillator method developed by Quimby,[2] is suitable for specimens with a natural rod-like shape or which can be prepared in such a form, and can give results with the required accuracy for specimens as small as 5 mm in length and 0·5 mm across.

THE COMPOSITE OSCILLATOR

If two rods of different materials, but of identical cross-section, are cemented together end-to-end and set into vibration under "free-free" conditions, the motion at resonance is subject to the condition

$$M_1\nu_1 \tan(\pi\nu/\nu_1) + M_2\nu_2 \tan(\pi\nu/\nu_2) = 0 \qquad (1)$$

where M and ν denote the mass and the natural resonant frequency of a rod and subscripts refer to the two components. The velocity c_i of elastic waves in a component is given by

$$c_i = 2l_i\nu_i \qquad (2)$$

where l_i is the length.

Quimby cemented his specimens to a quartz transducer which was excited piezoelectrically. For precise measurements the stable mechanical properties of quartz and its very low internal damping make it an ideal transducer, but for the type of work required here nickel, excited magnetostrictively, has some important advantages. For some degree of matching of the natural frequencies of the specimen and transducer is desirable, as will be shown below, and quartz transducers of the required dimensions would be expensive, fragile, and difficult to cut and handle. Nickel wire, on the other hand, can be obtained in a range of diameters, and is

* Now at the National Coal Board, Central Research Establishment II, Isleworth.

easily cut to any desired length. Because of its comparatively high density, however, nickel would have a somewhat higher acoustic impedance than most crystalline materials, so that its efficiency as a transducer would be low. Moreover, the energy of a magnetostrictive vibrator is low for frequencies greater than 60 kc/s, so that the oscillator circuit would have to be highly sensitive in order to maintain resonant vibrations and allow their detection and measurement. The circuit used in this work is shown in Fig. 1 and has been

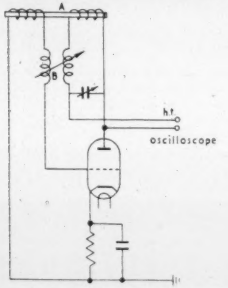

Fig. 1. Modified Pierce magnetostrictive oscillator circuit

found to be quite suitable;[3] it is a modification of Pierce's original circuit[4] giving greater sensitivity. The nickel transducer is introduced between the coil pair A which is arranged to give negative inductive feedback in order that the feedback due to the magnetostriction of the nickel should be positive. The compensating coil pair B gives positive inductive feedback which can be adjusted to balance out the negative inductive feedback from A. In this way, oscillations can be produced which are controlled solely by the resonant vibrations of the nickel rod, even when these are very feeble. The frequency could be measured with an accuracy of about 0·25% by feeding the output to one beam of a double-beam oscillograph and comparing it with a 500 kc/s quartz controlled oscillation on the other beam, making careful adjustment of the time of traverse in order to obtain stationary traces.

A test of the oscillator was made by measuring the frequency of vibration of seven nickel rods, cut from hard-drawn wire of diameter 0·91 mm, with lengths ranging from 1·596 to 6·871 cm. Each specimen was premagnetized in a field of about 180 oersted. The observed frequencies ranged from about 40 to 170 kc/s, and the values of the velocity c calculated from equation (2) all lay within the range from $5{\cdot}38 \times 10^5$ to $5{\cdot}40 \times 10^5$ cm/s. Various methods of suspending the rod in the coils were tried (e.g. by balancing it in a small hole in an ebonite disk, or by hanging it freely by a fine silk fibre attached at the central node) but these had no apparent advantage over placing the rod so that it rested on the inner surfaces of the coil formers, which was therefore done in all the subsequent work.

MISMATCHING OF SPECIMEN AND TRANSDUCER CROSS-SECTIONS

In the derivation of equation (1) the following boundary conditions are assumed: the pressure is zero at the ends of the composite rod, continuous at the interface, and uniform over the cross-section; and the linear displacement is continuous at the interface. When the transducer and specimen have different cross-sections the pressure cannot be uniform over the cross-section, so that the waves are no longer plane and equation (2) cannot hold.

Nevertheless, it has been found that the equation

$$\rho_1 c_1 A_1 \tan(\pi\nu/\nu_1) + \rho_2 c_2 A_2 \tan(\pi\nu/\nu_2) = 0 \qquad (3)$$

obtained from equations (1) and (2) by expressing the masses in terms of the lengths, cross-sectional areas A and densities ρ, gives consistent results for all the cases examined, that is, within the range $1 \leqslant A_1/A_2 \leqslant 3$, A_1 referring to the transducer and A_2 to the specimen. In one experiment, a nickel rod of length 4·058 cm and diameter 1·632 mm was ground in a high speed lathe to a diameter of 1·289 mm over about half its length, and its resonant frequency measured. The length of the portion of reduced diameter was then decreased in six steps to 1·245 cm, and the new frequency measured each time. From the frequency of the original rod the elastic wave velocity was calculated to be $4{\cdot}86 \times 10^5$ cm/s; assuming this to hold still for the larger component, the frequency ν_1 was 120 kc/s. Using equation (3), the frequency ν_2 of the reduced portion could then be found. The results are set out in Table 1, together with the velocity c_2 calculated from

Table 1. *Nickel rod with reduced cross-section over part of its length*

Length of reduced part (*cm*)	*Frequency of "composite" rod* (*kc/s*)	*Velocity of elastic waves in reduced part* (*cm/s*)
2·030	59·4	$4{\cdot}80 \times 10^5$
1·914	61·5	4·78
1·779	64·4	4·81
1·682	66·6	4·82
1·572	69·2	4·81
1·450	72·1	4·80
1·245	77·9	4·82

equation (2); the mean value of this, $4{\cdot}805 \times 10^5$ cm/s, is about 1·1% less than the value obtained for the original rod; surface changes brought about by grinding might account in part for this small discrepancy.

In a second experiment an aluminium rod of length 1·980 cm and cross-sectional area 0·9592 mm^2, having the form of a right circular cylinder, was cemented in turn to a number of nickel transducers having different diameters but approximately the same length; the natural frequencies of the transducers were measured separately. From the observed frequency of each composite oscillator a value for the frequency of the aluminium rod could be obtained from equation (3). These are tabulated in Table 2. It will be seen

Table 2. *Aluminium rod cemented to various transducers*

Length of transducer (*cm*)	*Ratio of cross-sections* A_1/A_2	*Frequency of composite rod* (*kc/s*)	*Frequency of specimen* (*kc/s*)
1·972	2·0	63·06	126·6
1·990	1·7	62·40	125·4
1·944	1·5	63·25	126·9
2·163	1·3	61·98	127·1
2·030	1·1	62·58	126·9
2·224	0·99	61·06	126·7

that the effects of mismatching are relatively slight, but it should be noted that in this experiment the value of ν/ν_2 is approximately 0·5, under which conditions the value obtained from equation (3) is not very sensitive to changes in the ratio A_1/A_2. Similar conclusions followed from an experiment in which the specimen was lithium fluoride, cut with its length parallel to one of the crystallographic axes and resonated with three different nickel transducers. The results are given in Table 3. The modulus of compliance $s_{11} = s_{22} = s_{33}$ for

Table 3. *Lithium fluoride rod of length 2·186 cm and cross-section 0·6825 mm² cemented to various transducers*

Length of transducer (cm)	*Ratio of cross-sections* A_1/A_2	*Frequency of composite rod* (kc/s)	*Frequency of specimen* (kc/s)
2·312	3·06	62·3	127·3
1·972	2·87	63·2	127·0
1·944	2·07	63·3	127·0

Mean velocity $c_2 = 5{\cdot}55 \times 10^5$ cm/s

lithium fluoride has been given by Hearmon[1] as $11{\cdot}6 \times 10^{-13}$ cm²/dyn; this is the mean of four independent results with a coefficient of variation of 13%. The value of $1/\rho_2 c_2^2$ when $\rho_2 = 2{\cdot}645$ g/cm³ and $c_2 = 5{\cdot}55 \times 10^5$ cm/s (as in Table 3) is $12{\cdot}3 \times 10^{-13}$ cm²/dyn; this is within the range of the results quoted by Hearmon, and gives a satisfactory external check of the accuracy of the present experiments.

THE MAGNITUDE OF CERTAIN ERRORS

(*i*) *Neglect of lateral motion.* In the theory leading to equation (1), it is assumed that the motion is such that the effect of lateral dilatation can be neglected, so that the velocity of elastic waves is given by the equation

$$c = (E/\rho)^{\frac{1}{2}} \tag{4}$$

where E is Young's modulus. The correction to be applied for lateral motion has been considered experimentally by Boyle and Sproule,[5] who found it to be entirely negligible if the length was greater than about twice the diameter. In this work all the transducers and specimens were cut to satisfy this condition, and equation (4) was used for calculating the value of E.

(*ii*) *Errors due to inaccurate frequency measurements.* As mentioned above, the frequency measurements were liable to errors of the order $\pm\frac{1}{4}$%. Consider first the effect of an error $\delta\nu$ in the measurement of ν, the frequency of the composite rod; let $\delta\nu_2$ be the corresponding error in the calculated value of ν_2. Then, if the ratio of the percentage errors is called R_1, we have

$$R_1 = \frac{\nu\delta\nu_2}{\nu_2\delta\nu} = \frac{2\theta_2 \sin 2\theta_1 - 2\theta_1 \sin 2\theta_2}{\sin 2\theta_1(2\theta_2 - \sin 2\theta_2)} \tag{5}$$

where

$$\theta_1 = \pi\nu/\nu_1 \quad \text{and} \quad \theta_2 = \pi\nu/\nu_2 \tag{6}$$

Using equation (1), it can be seen that R_1 depends on θ_2 and also on the value of the ratio

$$\mu = M_1\nu_1/M_2\nu_2 \tag{7}$$

For a fixed value of μ, R_1 is infinite when $\theta_2 = 0$, but decreases rapidly to $1 + 1/\mu$ at $\theta_2 = \pi/2$ and to 1 at $\theta_2 = \pi$. This behaviour is illustrated for $\mu = 1$ in Fig. 2, curve *B*. To reduce the error in ν_2 in importance it is desirable to have ν/ν_2 as large as possible, and at any rate greater than 0·5, with ν/ν_1 consequently less than 0·5.

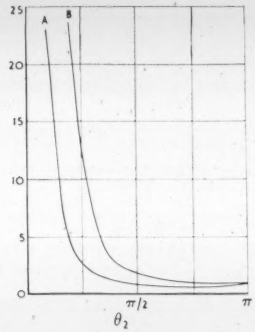

Fig. 2. R_1 for $\mu = 1$ (curve *B*) and $-R_3/K$ for $a_2 = a_3$ (curve *A*) as functions of θ_2

For an error of measurement in ν_1, the ratio of the percentage error in ν_2 to that in ν_1 is similarly found to be

$$R_2 = \frac{2\theta_1 - \sin 2\theta_1}{\sin 2\theta_1} \times \frac{\sin 2\theta_2}{2\theta_2 - \sin 2\theta_2} = 1 - R_1 \tag{8}$$

The desirable limitations on the value of ν/ν_2 are the same as before; they can be ensured by using a short transducer and a long specimen. Such requirements, however, are directly contrary to the considerations that the method is primarily designed for small specimens, and a long transducer is easier to handle. As a compromise, therefore, it would appear that the optimum conditions would be to have ν/ν_2 approximately equal to 0·5; the node of the composite vibrator would then be near the interface, and this would have the advantage mentioned above that mismatching in cross-section would be of little importance.

(*iii*) *Error due to the cement.* The transducer with a specimen of the same cross-section cemented to it may be regarded as a tripartite oscillator for which the equation

$$\Sigma a_i \tan\theta_i = (a_1 a_2/a_3)\tan\theta_1 \tan\theta_2 \tan\theta_3 \tag{9}$$

replaces equation (1). Here we have used the notation

$$a_i = \rho_i c_i \tag{10}$$

with i taking the values 1, 2, and 3 for transducer, specimen, and cement, respectively, and with the θ's defined as in equation (6). Equation (9) is equivalent to

$$\phi_1 + \phi_2 + \theta_3 = \pi \tag{11}$$

where $a_3 \tan\phi_1 = a_1 \tan\theta_1$ and $a_3 \tan\phi_2 = a_2 \tan\theta_2$ (12)

In fact, we use equation (1) instead of equation (9) to calculate a value ν_{20} of ν_2, so that equation (1) may be re-written

$$\left.\begin{aligned} a_{20}\tan\theta_{20} + a_1\tan\theta_1 &= 0 \\ \text{or} \qquad \tan\phi_{20} + \tan\phi_1 &= 0 \end{aligned}\right\} \tag{13}$$

where a_{20}, θ_{20}, and ϕ_{20} are the values of a_2, θ_2, and ϕ_2

corresponding to ν_{20}. From equation (13) ϕ_{20} and ϕ_1 are supplementary, so that

$$\phi_{20} - \phi_2 = \theta_3 \tag{14}$$

We shall suppose that θ_3 is a small quantity, as it will be if the cement layer is thin enough. Hence we obtain from equation (12)

$$a_3(\phi_{20} - \phi_2)\sec^2\phi_2 = a_2(\theta_{20} - \theta_2)\sec^2\theta_2 + (a_{20} - a_2)\tan\theta_2 \tag{15}$$

and thus, since the fractional changes in ν_2, θ_2, and a_2 are numerically equal,

$$R_3 = \frac{\nu_{20} - \nu_2}{\nu_2} = -\frac{\rho_3 l_3}{\rho_2 l_2}\left(\cos^2\theta_2 + \frac{a_2^2}{a_3^2}\sin^2\theta_2\right)\frac{2\theta_2}{2\theta_2 - \sin 2\theta_2}$$

$$= -K\left(\cos^2\theta_2 + \frac{a_2^2}{a_3^2}\sin^2\theta_2\right)\frac{2\theta_2}{2\theta_2 - \sin 2\theta_2} \tag{16}$$

where K = (mass of cement/mass of specimen).

The value of R_3/K is infinite at $\theta_2 = 0$, but for values of θ_2 between $\pi/2$ and π it is numerically less than the greater of 1 and a_2^2/a_3^2 (compare Fig. 2, curve *A*). Within this range, therefore, R_3 can be kept to a reasonable size by reducing the value of K. With the cements used in the present work (shellac and polyethylene pthalate) the thickness required to give good acoustical contact was small enough to ensure that no serious error was involved in neglecting the effect of the cement, for specimens longer than about 5 mm, provided that the conditions were such that ν/ν_2 was approximately 0·5.

EXPERIMENTAL RESULTS

The results obtained for a variety of specimens are summarized in Table 4. Cylindrical transducers were used, and the specimens were generally approximately square in cross-section; the asbestos specimens, however, had irregular cross-sections. There was no evidence that the elastic wave velocity depended upon the shape of the cross-section, but it was essential to cut the specimens so that the lateral dimensions were constant along the length. Specimen lengths ranged from 0·5 to 4 cm, and the lateral dimensions were of the order of 1 mm. The mineral specimens were cut with the length along one of the crystallographic axes, identified by X-ray analysis. The asbestos and keratin specimens were cut along the fibre axis.

Five specimens of each material were used; the mean values and coefficients of variation are given in Table 4. The variability of the keratin (cow's horn) is not excessive for a biological material of this kind, bearing in mind the possible variations in the degree of crystallinity and in the perfection of molecular orientation; the humidity and temperature were uncontrolled also. Static measurements of Young's modulus of cow's horn at room humidity give values near 4×10^{10} dyn/cm^2. The higher value obtained in these experiments agrees with the results of other experiments[6] in which the dynamic Young's modulus is measured. It is due to the decreased importance of relaxation processes for rapid deformations. The results for barite provide another independent check on the accuracy of the method, since they are in close agreement with those of Bergmann[7] and Voigt[8]:

Voigt $s_{11} = 1{\cdot}644 \times 10^{-12}$ cm^2/dyn; $s_{22} = 1{\cdot}892 \times 10^{-12}$ cm^2/dyn

Bergmann $s_{11} = 1{\cdot}72 \times 10^{-12}$ cm^2/dyn; $s_{22} = 1{\cdot}99 \times 10^{-12}$ cm^2/dyn

Composite oscillator $s_{11} = 1{\cdot}69 \times 10^{-12}$ cm^2/dyn; $s_{22} = 1{\cdot}975 \times 10^{-12}$ cm^2/dyn

Table 4. *Wave velocity and elastic moduli for some minerals and keratin*

Specimen and direction of measurement	*Elastic wave velocity* (cm/s)	*Modulus of compliance* (cm^2/dyn)	*Young's modulus* (dyn/cm^2)	*Coefficient of variation* (%)
Barite, *a*-axis	$3{\cdot}685 \times 10^5$	$1{\cdot}69 \times 10^{-12}$	—	1·3
Barite, *b*-axis	3·36	1·975	—	0·8
Gypsum, *c*-axis	5·91	1·235	—	1·1
Wollastonite, *b*-axis	6·46	0·848	—	3·0
Kyanite, *c*-axis	8·62	0·375	—	0·35
Crocidolite, fibre axis	7·36	—	$1{\cdot}75 \times 10^{12}$	1·2
Tremolite, fibre axis	7·39	—	1·66	0·21
Chrysotile, fibre axis	8·38	—	1·73	1·6
Keratin, fibre axis	2·145	—	0·060	4·1

CONCLUSION

The method described has been shown to be capable of measuring the elastic wave velocity in small rod-like specimens; it is reasonably rapid, and is accurate enough for most purposes. With more precise methods of measuring frequency, a high order of accuracy could be achieved.

ACKNOWLEDGEMENTS

The authors are grateful to Professor Cox, of the Department of Inorganic and Structural Chemistry, and to Mr. von Knorring, of the Department of Geology, for mineral specimens, and to Professor Quimby of Columbia University for helpful suggestions in a private communication.

REFERENCES

(1) HEARMON. *Brit. J. Appl. Phys.*, **3**, p. 120 (1952).
(2) QUIMBY. *Phys. Rev.*, **25**, p. 558 (1925).
(3) TERRY and WOODS. *Proc. Leeds Phil. Lit. Soc.*, **6**, 251 (1954).
(4) PIERCE. *Proc. Inst. Radio Engrs*, **17**, p. 42 (1929).
(5) BOYLE and SPROULE. *Nature* [*London*], **123**, p. 13 (1929).
(6) CHAIKIN and CHAMBERLAIN. *J. Text. Inst. Manchr*, **46**, p. T44 (1955).
(7) BERGMANN. *Ultrasonics* (London: G. Bell and Sons, 1938).
(8) VOIGT. *Lehrbuch der Kristallphysik*, p. 761 (Leipzig and Berlin: Teubuer, 1928).

Thermal constants of pyrophyllite and their change on heating

By A. E. Carte, M.Sc., National Physical Laboratory, South African Council for Scientific and Industrial Research

[*Paper received* 10 *March*, 1955]

Results are given for the thermal conductivity, thermal diffusivity and specific heat of pyrophyllite before and after heating to temperatures up to 1200° C. Before heating, the conductivity in directions parallel to the bedding planes is about 0·01 cal cm/cm² s °C (0·04 joule cm/cm² s °C) and at right angles to these planes it is half this value. The difference is attributed to the effects of bedding and to preferred orientation of the crystals. A method of finding the directions of maximum and minimum conduction is outlined. As the heating temperature is increased the two conductivities converge, until after heating to 1200° C the physical and chemical changes are such as to make the material thermally isotropic with a conductivity of about 0·003 cal cm/cm² s °C (0·01 joule cm/cm² s °C). Some other properties and uses of pyrophyllite are mentioned.

There are extensive deposits of a rock of sedimentary origin commonly known as Wonderstone to be found in the Lichtenburg district of the Transvaal. X-ray analyses have shown that this rock is comprised mainly of the mineral pyrophyllite, a hydrous aluminium silicate. Spectrochemical methods revealed traces of rutile (1·5%) and iron oxide (1%). Wonderstone has also been known as G-stone and Koranna stone and is sometimes sold under the erroneous name of soapstone, which it closely resembles in some properties. Pyrophyllite found in other parts of the world is referred to by a variety of names such as pencil stone, agalmatolite and pyrauxite. In this paper the term pyrophyllite will henceforth be used when referring to this rock since it is felt that the thermal properties are characteristic of pyrophyllite, and little influenced by the small amounts of other minerals present.

The physical properties of this rock are such as to make it an exceedingly useful material. It is fine-grained, usually bluish in colour, is easily worked on a lathe and takes a good polish. The natural rock is resistant to weathering and acids and on being baked it becomes an extremely hard substance, white to pink in appearance, resembling a ceramic. Apart from its use for ornaments and statues it is useful for making small crucibles and intricate electrical insulators, spacers and formers. In the South African National Physical Laboratory pyrophyllite has been used for components for the ion source of a mass spectrometer, heater formers, specially shaped porous plates and crucibles for establishing the melting point of gold. Further information on the properties has been given by Nel and others.[1]

The thermal conductivity of the naturally occurring rock was determined in the course of the compilation of data on thermal conductivity of rocks. It is of special interest because it is a practically pure monomineralic aggregate and shows extreme preferred orientation of the crystals. When it was realized how wide a variety of applications pyrophyllite has, many of which require a knowledge of its thermal constants, the investigation was extended to include thermal diffusivity and specific heat measurements and to the effect on these constants of heating to various temperatures.

EXPERIMENTAL METHODS

Test for anisotropy. Sedimentary rocks usually have anisotropic thermal properties as the result of schistosity, bedding or preferred orientation of the component crystals. The method that was used to test for anisotropy is a modification of the de Senarmont method as used by Powell.[2] Three thin plates of rock were cut from mutually perpendicular planes of the block being tested and coated on one face with a thin layer of wax by covering with a solution of beeswax in acetone. A point source of heat (the tip of a pencil-shaped copper rod which was heated at the thick end) was then applied to the centre of the waxed surface. Regions where the wax melted showed up dark whereas the rest of the surface was white. On isotropic planes the area of melted wax is circular; on anisotropic planes elliptical. From tests on the three plates and the orientation of the axes of the conductivity ellipses it is a straightforward matter to find the principal axes of conduction.

Pyrophyllite proved to have a maximum conductivity in directions parallel to the bedding planes and half this value perpendicular to these planes. The rock has an extremely fine-grained texture and the bedding planes cannot be detected by the naked eye unless there happen to be streaks of an impurity, such as haematite, present or unless the rock has been fired in which case coloured streaks parallel to the bedding planes usually appear. A plate cut from any direction perpendicular to the bedding planes and tested for anisotropy gave the ellipse of maximum eccentricity. The square of the ratio of the major axis to the minor axis of this ellipse was found to give the ratio of the principal conductivities to within about 10%.

Thermal conductivity. Measurements of thermal conductivity at a mean temperature of 40° C were made on samples in the form of $1\frac{1}{8}$ in. diameter disks in a divided-bar type of apparatus.[3] Samples which had been subjected to heat treatment usually distorted slightly even though heated slowly and were always resurfaced before testing. Tests at high temperatures were made on a 4 × 4 in. slab 1 in. in thickness, the heat flow being measured by a similar slab of steel of known conductivity made up in the form of a guard ring surrounding the $1\frac{1}{4}$ in. square central section and placed on top of the specimen.

Specific heat. Specific heat measurements were made by means of an adiabatic calorimeter,[3] the temperature range of the tests being from 96 to about 30° C. The specific heat of water-soaked specimens was found by calculation, knowing the amount of water absorbed.

Thermal diffusivity. The thermal diffusivity of disk specimens as used in the conductivity apparatus was determined from measurements of the change in temperature with time of one surface when the other surface was suddenly brought into contact with melting ice. The time taken for one complete observation was about 1 min so that water penetration was negligible. This method also enabled measurements to be made on samples with a known amount of moisture in them. The mean temperature of an observation was close to 10° C. The conductivity as found from the product of the diffusivity, specific heat and density agreed

with results obtained in the divided-bar apparatus to about 15% and if allowance was made for the different mean temperatures of the various measurements then agreement was substantially improved.

RESULTS

Measurements were made on specimens cut from five blocks from different sources; the only restriction on the selection of samples was that there should be no obvious heterogeneities such as red bands of haematite. The composition of the rock has been found to show little variation with its location in the quarry.[1] The results in the table are for the two blocks which differed most in bulk density. Spectrochemical analyses confirmed that the chemical composition was the same: density differences are thus to be attributed to porosity.

Specimens from Block *E* were then heated to successively higher temperatures after which diffusivity and specific heat measurements were made. The procedure was to heat slowly (about 3° C/min) to the final temperature which was maintained constant for 3 h, and then to cool slowly down to room temperature. Longer periods of heating did not bring about any significant changes in thermal properties. For example, the samples that had been baked at 600 and 900° C were both heated for a further period at these respective temperatures without causing further changes. The effect of very much prolonged heating was not investigated. The diffusivity changes are shown in Fig. 1, while densities and specific heats are given in Fig. 2. The conductivity results in Fig. 3 were calculated from the diffusivity, specific heat and density measurements, the results being corrected to a mean temperature of 40° C. Several of these points were confirmed by direct conductivity measurements. The utmost caution had to be exercised to obtain reliable results as the pyrophyllite becomes exceedingly porous after baking at high temperatures and it then tends to absorb the medium used to improve contact resistance between the specimen and the bars.

Negligibly small permanent changes in conductivity occur on exposure of pyrophyllite to temperatures up to 400° C. Thus the curves conductivity and resistivity in Fig. 4 show

Thermal constants of dry and water-saturated specimens

	Block B				Block E			
	Heat flow parallel to bedding planes		Heat flow perpendicular to bedding planes		Heat flow parallel to bedding planes		Heat flow perpendicular to bedding planes	
	Dry	% increase of water-saturated specimens	Dry	% increase of water-saturated specimens	Dry	% increase of water-saturated specimens	Dry	% increase of water saturated specimens
Bulk density: (g/cm²)	2·74	0·7	2·74	0·7	2·65	2	2·65	2
Volume porosity: (%)	2		2		5·5		5·5	
Thermal diffusivity at 10° C: (cm²/s)	$0{\cdot}025_2$	3	$0{\cdot}014_8$	7	$0{\cdot}021_8$	25	$0{\cdot}011_6$	27
Specific heat (96 to 30° C):								
(cal/g °C)	0·22	4	0·22	4	0·22	8	0·22	8
(joules/g °C)	0·92		0·92		0·92		0·92	
Calculated thermal conductivity:								
(cal cm/cm² s °C)	$0{\cdot}015_2$		$0{\cdot}008_9$		$0{\cdot}012_7$		$0{\cdot}006_7$	
(joules cm/cm² s °C)	$0{\cdot}063_6$		$0{\cdot}037_2$		$0{\cdot}053_2$		$0{\cdot}028_0$	
Calculated thermal conductivity corrected to 40° C:								
(cal cm/cm² s °C)	$0{\cdot}013_0$	7	$0{\cdot}007_6$	11	$0{\cdot}011_0$	36	$0{\cdot}005_9$	35
(joules cm/cm² s °C)	$0{\cdot}054_4$		$0{\cdot}031_8$		$0{\cdot}046_0$		$0{\cdot}024_7$	
Measured thermal conductivity at 40° C								
(cal cm/cm² s °C)	$0{\cdot}013_4$		$0{\cdot}007_4$		$0{\cdot}010_4$		$0{\cdot}005_4$	
(joules cm/cm² s °C)	$0{\cdot}056_1$		$0{\cdot}031_0$		$0{\cdot}043_5$		$0{\cdot}022_6$	

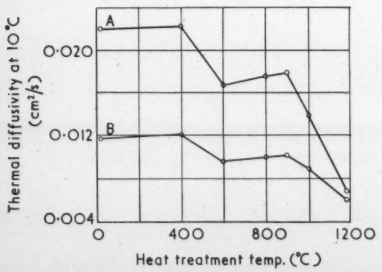

Fig. 1. Thermal diffusivity at 10° C after heating to successively higher temperatures; heat flow parallel (curve *A*) and perpendicular (curve *B*) to the bedding planes

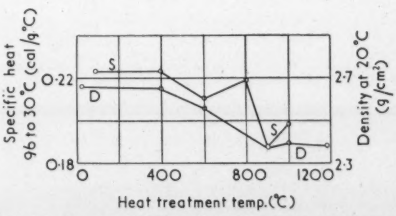

Fig. 2. Specific heat (96 to 30° C) (curve *S*) and density at 20° C (curve *D*) after heating to successively higher temperatures

the reversible changes that occur on heating to 400° C. Interpolation between the points is most readily effected using the resistivity points since the relationship between resistivity and mean temperature is virtually linear.

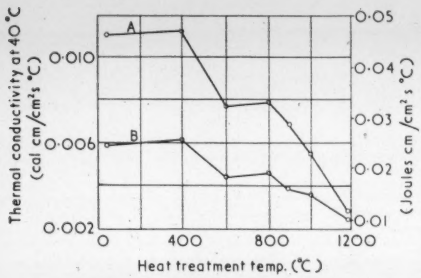

Fig. 3. Thermal conductivity at 40° C after heating to successively higher temperatures; heat flow parallel (curve *A*) and perpendicular (curve *B*) to the bedding planes

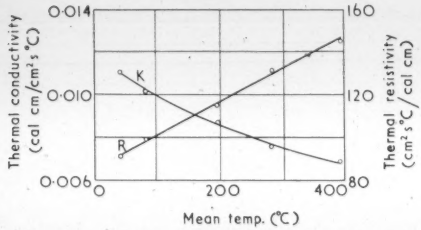

Fig. 4. Thermal conductivity (curve *K*) and thermal resistivity (curve *R*) at various mean temperatures; heat flow parallel to the bedding planes; unheat-treated material

DISCUSSION

Samples cut from the same block in the same direction relative to the bedding planes usually showed little variation in thermal conductivity, but differences of up to 20% were found for blocks having different bulk densities. These differences in conductivity are to be attributed to porosity and not to differences in chemical composition. From X-ray examinations of a powder sample and the comparative ease with which the powder could be compressed to bring about preferred orientation almost as pronounced as in the original rock, it was concluded that the crystals are plate- rather than rod-shaped. In the naturally occurring rock the crystals are mainly oriented with the plane of the plates parallel to the bedding planes. Since it is a general rule that the conductivity of plate-shaped crystals is a maximum in the plane of the plate, this coupled with the effects of bedding gives rise to the two-fold difference in the two principal conductivities. An interesting observation is that water, as well as heat, penetrates more readily in any direction parallel to the bedding planes or planes of preferred orientation than at right angles to them.

The physical and chemical changes that occur on heating the pyrophyllite bring about a continuous decrease in both the principal conductivities such that after being baked at 1200° C the material becomes very nearly thermally isotropic. A differential thermal analysis of pyrophyllite showed an endothermal reaction with a single peak at 870° C.(4) X-ray analysis showed that heating to temperatures between 600 and 1000° C produced an unidentified substance closely related to pyrophyllite. This is probably pyrophyllite with decreasing amounts of water of crystallization. After 1200° C no pyrophyllite is present but sillimanite and either corundum or mullite, or both, were detected. X-rays also revealed that no silica in crystalline form was present. The nature of the unit cells of sillimanite and corundum (it is considered unlikely that there would be mullite formed at 1200° C) are such that preferred orientation is not to be expected. The bulk density changes are the result of a continously increasing loss in weight, amounting to 6% at 1200° C, as the temperature is stepped up and a steady increase in volume up to 1000° C after which there is a slight contraction. Thus after heating to 1200° C the loss of preferred orientation, the chemical changes and the greatly increased porosity make the material isotropic with the exceedingly low conductivity of 0·003 cal. cm/cm² s °C. Another instance of irreversible changes in thermal conductivity after heat treatment of an anisotropic material is that found by Powell and Griffiths for phlogopite micas: this they attribute to tilting of the elementary crystals composing the mica laminae.(5)

The chances of a sample developing cracks, usually parallel to the bedding planes, during the firing process are greater the larger the sample and the higher the rate of heating and the final temperature are made. Above about 1000° C only thin samples can be baked with success and in the region of 1400° C exfoliation occurs. If it is desired to produce an article of the baked material of accurate dimensions the best procedure is to heat slowly to 800° C, cool, machine to the required dimensions and then heat to the final temperature. Fig. 3 shows that the density changes, and also the dimensional changes, that occur between 800 and 1200° C are small. This procedure has recently been confirmed.(6) The fine powder formed when pyrophyllite is worked would no doubt make an excellent high temperature insulating medium.

ACKNOWLEDGEMENTS

This paper is published with the permission of the South African Council for Scientific and Industrial Research.

It is a pleasure to acknowledge the care with which Mr. G. J. Viljoen carried out the experimental observations. My thanks are also due to Mr. G. Gafner who developed the method of making the diffusivity measurements, Dr. J. N. van Niekerk who was responsible for the X-ray analyses, Dr. A. Strasheim for the spectrochemical analyses and Ore and Metal Co. Ltd. for supplying some of the samples.

REFERENCES

(1) Nel, L. T., Jacobs, H., Allan, J. T., and Bozzoli, G. R. *Geol. Series Bull. No.* 8, Union of S. Afr. Geol. Survey (1937).
(2) Powell, R. W. *J. Sci. Instrum.*, **30,** p. 210 (1953).
(3) Mossop, S. C., and Gafner, G. *J. Chem. Soc. S. Afr.*, **52,** p. 61 (1951).
(4) Heystek, H., and Schmidt, E. R. *Trans Geol. Soc. S. Afr.*, **56,** p. 149 (1953).
(5) Powell, R. W., and Griffiths, E. *Proc. Roy. Soc. A*, **163,** p. 189 (1937).
(6) Dyke, V. E. *Brit. J. Appl. Phys.*, **5,** p. 270 (1954).

Discontinuities in the saturation curves of vacuum photocells

By J. S. Preston, M.A., M.I.E.E., F.I.E.S., F.Inst.P., and G. W. Gordon-Smith, A.M.I.E.E., National Physical Laboratory, Teddington, Middlesex

[*Paper received* 21 *March*, 1955]

Discontinuities have been observed in the saturation curves of most of a number of vacuum photoemissive cells of the special photometric types. In these cases, in certain circumstances, the cells can operate in either of two stable states for which the observed photo-currents, for the same light intensity, can differ by a significant amount. A reason is suggested, in terms of variations in potential of the inner bulb surface arising from secondary emission processes at the bulb and leakage of this surface to the anode. This is confirmed by a series of experiments. The main conclusion is that the best conditions, for saturation and freedom from irregular behaviour, are ensured if the bulb surface has high conductivity, and is in good connexion with the anode but well insulated from the cathode. Paradoxically, good saturation cannot be expected over the normal range of voltage if the bulb surface is highly insulating, partly because the bulb then remains at cathode potential and considerably depresses the field strength at the cathode, and partly because—at that potential—it can reflect an appreciable fraction of the photoelectrons back into the cathode.

1. Introduction

Campbell and his contemporaries[1] evolved a design of vacuum photoemissive cell which has long been favoured by British makers and users of special precision cells. The cathode is a central metal plate. The anode is a gauze cylinder or "Faraday cage" surrounding it and fitting inside a coaxial cylindrical bulb. The cage-construction is meant to ensure efficient collection of the photoelectrons, and screening of the cathode from any electrostatic charge on the inner bulb-surface. The saturation curve typical of a good cell of this design rises steeply near zero applied voltage, has a pronounced "knee" near 18 V, and thence is very flat rising only 2 or 3% from 20 to 100 V. For a voltage a little above the "knee," therefore, it is widely and reasonably assumed that the ratio of actual cell-current to the full possible photo-emission is constant and very nearly unity, under all ordinary conditions. Apparently there is no room for error or doubt in accepting the actual output as a linear and certain measure of light intensity.

However, small but significant irregularities in the saturation curves of the majority of such cells have now been observed, and form the subject of this paper. The conclusions reached have a general significance for all types of vacuum cell. They throw doubt on the earlier appraisal of Campbell's design.

2. Observed Saturation Curves

Fig. 1 shows part of the saturation curve of a typical cell (an Osram type KMV6), taken by slowly varying the applied voltage from 0 to 100 V and back again, the light intensity being held strictly constant throughout. Arrows show the sense of the cycle. There are two discontinuities, or jumps, in output, upward at 60 V and downward at 20 V, forming a "loop" between these voltages. In this range, either an "upper" or a "lower" stable state of the cell is possible, depending on past history. The two outputs differ by the loop height, about 1½%. In ordinary use there would thus be doubt about which reading would be given. The whole graph consists of sections of two different smooth curves, a lower limb from 0 to 60 V and an upper one from 20 to 100 V. If the upper one is the true saturation curve, what is the lower one?

Many precision cells of different makes and cathode types were examined. Most exhibited such loops. In the few that did not, the saturation curves did not flatten out well, and the "knee" was not very obvious. Much fascinating detail, especially effects of varying the light intensity, is omitted, and the main observations were (*a*) that loop heights ranged from a mere kink to some 10% of output, Fig. 1 representing a fair sample, (*b*) that the lower jump was almost always near an applied voltage of about 20 V, and (*c*) that the upper jump could be anywhere upwards of 20 V.

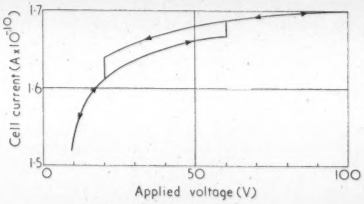

Fig. 1. Upper part of the saturation curve (current-voltage curve at constant illumination) of a type KMV6 cell, taken over a complete voltage cycle

The loops recalled the work of Penning and Moubis,[2] who described a rather similar effect due to secondary emission from the bulb, which had some surface conductivity and was leaky to cathode. They noted sharp and considerable changes in potential of the inner surface of the bulb during a saturation cycle, but the accompanying discontinuities in cell output were of a different kind from the present ones, and their origin a little more obvious.

In the present case, considerable changes in bulb potential were again quickly confirmed, using a small flat probe connected by screened cable to a quadrant electrometer. An explanation seemed possible, similar to that of Penning and Moubis, but on the changed assumption that the bulb was leaky to anode.

Two quite separate questions arise, (*a*) how and why does the bulb potential change, and (*b*) how do these changes affect cell output? We consider them in that order, putting hypothesis before experimental proof in each case, as the easier treatment.

3. ORIGIN OF CHANGES IN BULB POTENTIAL

We explain bulb-potential changes as follows using Fig. 3, in anticipation, to help visualize what happens. Assume the inner bulb surface to have slight conductivity, to be leaky to the anode (*via* the lead-in wire, say), and to be a secondary emitter. Neglect the small, though finite, emission energy of the photoelectrons, and let all potentials be referred to cathode as zero.

At low anode voltage, the bulb receives some negative photoelectrons shot through the holes in the anode gauze, and also some positive leakage from anode. The two balance with the bulb at a steady potential near cathode. The aforesaid photoelectrons, ending their paths at this potential, are too feeble for any secondary emission to upset the balance. This balance persists up to a considerable anode voltage (56 V in Fig. 3), but the increased leakage from anode raises the bulb potential a few volts. There will then also be some perceptible secondary emission from the bulb, also tending to drive it positive, the secondaries going to anode. We may at this stage safely assume the secondary-gain factor to be still well below unity. However, suppose that at this stage the *increment* in actual secondary emission, caused by any *increment* in bulb potential, just outweighs change in the other factors, so that it reinforces the increment in bulb potential. Onset of such a cumulative process will cause a sudden upward jump in bulb potential (*B*, Fig. 3).

A new equilibrium is now established. Neglecting the now smaller leakage from anode, the ruling condition is that the secondaries being drawn by anode from bulb must equal in number the primary photoelectrons being shot at the bulb. So, the bulb takes a potential quite near that of the anode, so that though the secondary gain is now considerable, the surplus secondaries are simply not drawn off. The equilibrium is stable because, for a small change in bulb potential, the large change in draw-off rate of secondaries by anode acts as a strong corrective. For further rise in applied anode voltage, this state persists. As the applied voltage is lowered, however, there eventually comes a point where the photoelectrons arriving at the bulb are too feeble to provide enough secondaries. The cell then reverts suddenly to its original state, with a sudden drop in bulb potential (*A*, Fig. 3).

It seems clear that this drop is "triggered" when the secondary gain at the bulb has fallen to a value quite near unity. Roughly, then, all the potentials just before the drop occurs are governed by the electron energy required for unit gain, which is a characteristic of the glass surface. This may well be similar from cell to cell, so accounting for the observation that the downward jumps in all saturation curves occurred at about the same applied voltage of 20 V (see Section 2). The upward jump, on the other hand, being governed by such a widely variable factor as bulb-surface resistivity, could clearly occur at any voltage over a wide range, in different cells.

Two practical cases can now be recognized when no loop would be observed.

(i) If the bulb wall is highly insulating, or is not leaky to anode, its potential will always be held very near cathode, by receipt of photoelectrons. The cell will then never jump to the upper state, but operate always in the lower.

(ii) When there is considerable bulb-anode leakage, the upward jump can, mathematically speaking, occur at a lower applied voltage than the downward one, i.e. no jumps at all will occur, and the cell will operate always in the higher state.

The cells mentioned in Section 2 as showing no loops, but having poor saturation curves, were probably examples of case (i). Paradoxically, then, it seems that good saturation is not to be expected in a "clean" cell. In case (ii), the bulb is always nearly at anode potential and can, as we have seen, freely pass on to the anode all the photoelectrons it receives, mostly by the secondary emission process and, to a small extent, by direct leakage. So the electric-field conditions are excellent, and so also is the efficiency of collection of the photoelectrons. We can, as a corollary, identify the upper, or "high state," limb of a looped saturation curve as the "truer" saturation curve.

4. EXPERIMENTS ON BULB POTENTIAL

We now seek experimental confirmation of the cycle of bulb potential arising from the hypothetical process of Section 3. With a regular cell, the anode often touches the bulb at several points. The behaviour of the cell is then liable to be more complicated than that of the simple model. A special Cintel type VS39 cell was therefore obtained, with standard electrodes but extra large bulb. This was set up as shown in Fig. 2. External guard-rings and other

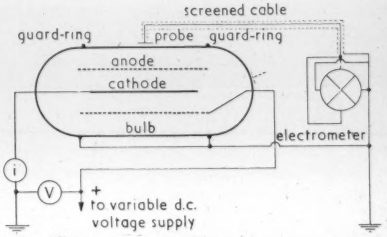

Fig. 2. Circuit for measuring potential changes of inner surface of bulb of a special type VS39 cell

precautions ensured that no variation of static charge occurred on the outside of the bulb near the probe. Calibration of probe and electrometer was done with a dummy "bulb" of metal. On taking this cell through a cycle of applied voltage, the results of Fig. 3 were obtained. They demonstrate all the features expected. The corresponding saturation curve is not given here, but it showed jumps in cell output simultaneous with the jumps *A* and *B* in bulb potential. They were of about 10%. We shall later suggest an accidental practical reason why, in the regular cells with smaller bulbs, the jumps are usually appreciably smaller than this.

This special cell served for another informative experiment. By using a second probe (dotted in Fig. 2), and connecting both to a detector having time-discrimination, it was found that the jump *B* in bulb potential occurred first near the anode lead-in, and only reached the original probe near the middle of the bulb about half a second later. As one would expect, the jump originated where the bulb potential was, for obvious reasons, higher than elsewhere just before the jump.

For the third experiment, another special Cintel type VS 39 cell was obtained, with standard cathode and anode, but with these enclosed in a slightly larger coaxial metal cylinder or "can" having only a tiny hole for admission of a focused pencil of light. The can formed an artificial "bulb," and had a separate lead-in. (There was, of course, an outer bulb of glass as well.) With this, the non-uniform potential

distribution over the "bulb," emphasized by the second experiment, was avoided, while the leak from anode to "bulb" was controllable according to what resistance was connected externally from anode to can. Caesium-contamination of the

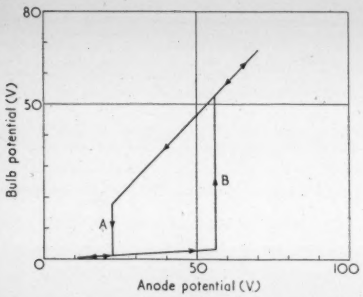

Fig. 3. Variation of bulb surface potential with anode potential, both referred to cathode, for a special type VS39 cell taken over a complete voltage cycle, at constant illumination

can was relied on for secondary emission. The set-up for loop-tests is shown in Fig. 4. Ordinary cell output was measured by meter M_1 in the cathode lead, while the reading of M_2 together with the known value of R enabled potential difference can-to-anode, and therefore also can-to-cathode,

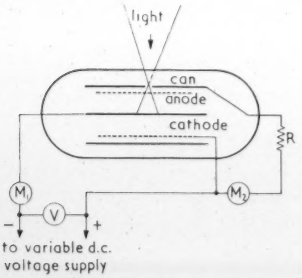

Fig. 4. Arrangement for simulating bulb potential characteristics of an ordinary photocell, using a special type VS39 cell, with extra electrode or "can" acting as an artificial bulb

to be found at the same time. Fig. 5 shows a typical looped saturation curve for this cell, as well as the can potential values taken at the same time, over a typical cycle. The value of R for this was 580 MΩ. Note, (*a*) the excellent form of the upper limb of the saturation curve, and the very poor shape of the lower one up to as much as 50 V, (*b*) the coincidence of jumps in cell current with those in can potential, and (*c*) that for the upward jump in current, the can goes from +3 to +62 V, while for the downward one the can goes from +21 to 0 V. With R considerably higher, no looping occurred, the can potential always remained near cathode, and the cell always in the lower state up to an applied voltage of 100 V, with a very unconvincing saturation curve. With R in a lower range, the cell always operated in the upper state, with can potential near anode. The characteristics of this special cell, operating as a photo-triode, were plotted in full. For brevity, we do not quote this large family of curves. They demonstrated clearly the existence of stable and unstable regions of operation, in full agreement with the hypothesis and the results here given. By suitable choice of resistance R, and light intensity, almost all of the observations on regular cells could be closely simulated.

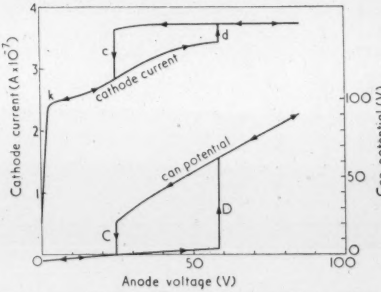

Fig. 5. Curves of cathode current, and potential taken up by the can, when the circuit of Fig. 4 is taken over a complete voltage cycle, with constant illumination

We close this section with a significant inference. It is that, generally, one simply cannot predict how even the best modern vacuum cell will behave, within the whole wide range noted in this last experiment and in those of Penning and Moubis. For who knows how much the bulb leaks to anode, or to cathode, or how good a secondary emitter it is? (Even for clean glass, the secondary-gain factor is unity for an energy as low as about 20 eV.) All that is usually observable and guaranteed is that leakage from anode to cathode is negligible. One can only look for probabilities. For instance, the generally good behaviour and saturation of the Osram type KMV6 cell is probably because the anode is a push-fit in the bulb giving high leakage from anode to bulb, while the latter is isolated from the cathode by a guard ring. It has been observed that in clean-looking cells of this type, in which the anode happened not to be a good fit in the bulb, bulb potential changes as well as saturation loops were larger than usual. Changes in characteristics with time, such as complete disappearance of a loop in a few weeks, have been noted. These are probably due to changes in surface resistivity of the bulb, owing to migration of minute amounts of alkali metal by vaporization.

5. INFLUENCE OF BULB POTENTIAL ON CURRENT OUTPUT

We now consider the influence of bulb potential on cell current. There are two mechanisms to consider. First, the emission from the cathode is determined by the electric field at its surface, and this is the resultant field due to bulb as well as anode. The bulb, being more distant and partially

screened by the anode, will be the less influential; but its effect cannot be ignored if its potential differs much from that of the anode, or is subject to large changes. Second, the bulb may reflect photoelectrons, and we postulate that such as are reflected mostly end their trajectories at the cathode and re-enter it. (Re-entry is possible because of the finite energy of emission.) The reflexion factor of the bulb is likely to be very small for all positive bulb potentials above a few volts, but will change from this to nearly unity as the bulb goes through zero to a small negative potential. This would mean a rather sharp increase in the return of photoelectrons to cathode, and a corresponding decrease in net emission or cell current. In this narrow potential-range, therefore, bulb potential should have a particularly marked influence on cell current.

This explanation is clinched by Fig. 6, which is a typical cell-current (cathode-current) characteristic of the "canned"

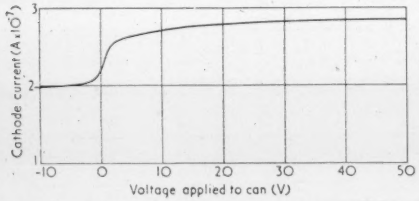

Fig. 6. Curve of cathode current of the special type VS39 cell of Fig. 4, with anode held at 55 V, and variation of the voltage applied to the "can" or artificial bulb. Illumination constant

cell, treated as an ordinary photo-triode, the anode voltage being fixed at 55 V, and the can or "bulb" voltage being varied from -4 to $+50$ V. The S-bend at the lower end shows the steep and appreciable change in the net photoemission, due chiefly to the steep change in reflexion factor of the "bulb" near zero volts, while the upper range shows the much smaller but definite effect of increase in field-strength due to increase in "bulb" potential. We see that generally any jump in "bulb" potential which includes all or most of the S-bend will produce a greater change in cell current than one that does not. This is why, in Fig. 5, the drop c is greater than the jump d, the former being determined by a drop in "bulb" potential right down to zero, while the latter is due to a jump in the "bulb" from $+3$ to $+62$ V which, though larger, does not include the large effect of the S-bend. We also see the effect of the reflexion mechanism in the shape of the range k-d of the output curve of Fig. 5. The general rise in the curve over this range is of course due to the increasing field strength, but the curve is slightly S-shaped and steepest in the middle of this range because the "bulb" is meanwhile changing steadily from about -3 to $+3$ V, and reflexion changes are added to effects of changing field strength.

6. SUMMARY AND CONCLUSIONS

Our conclusions may now be summarized. In a vacuum photoemissive cell it is generally unsafe to assume that the emission and the shape of the saturation curve are governed only by the field due to the anode. According to circumstances, the bulb may be a serious influential factor in that its potential may differ largely from that of the anode, and may undergo large discontinuous changes due to secondary emission. Three fairly distinct unsatisfactory cases may now be recognized. The first is that of Penning and Moubis where, with the bulb leaking to cathode, secondary emission from the bulb can give rise to appreciable spurious output *additional* to the photoemission. The second is where the bulb is highly insulated and so will almost certainly be kept near cathode potential by receipt of photoelectrons as necessary. Here, reflexion of electrons back to the cathode by the bulb may prohibit more than, say, 90% saturation over the normal range of anode voltage, while the adverse bulb-field effect will still further delay attainment of saturation with rising anode voltage. The third case is the one discussed at greater length in this paper. We assume that the case of bulb leaking to both anode and cathode is ruled out by the overall insulation requirements regularly attended to by the manufacturer. Any actual cell may, of course, present a sort of combination of the second with the first or third of these cases, depending on its particular geometrical form and the inevitable variations in conductivity of the bulb over its inner surface.

The only satisfactory case seems to be the one in which the bulb surface is isolated from the cathode, is in connexion with the anode, and has high enough conductivity everywhere to ensure that the cell operates always in the upper state. The ideal would be to have a transparent electrically-conductive coating over the inside of the bulb, itself serving as anode, and to omit the gauze anode altogether. Since the coating would then have to carry the whole cell current, however, its resistance would have to be low enough to avoid any trouble due simply to ohmic potential gradients. The special "canned" photocell, used with the can and anode connected directly together, is a replica of this ideal. Fig. 7

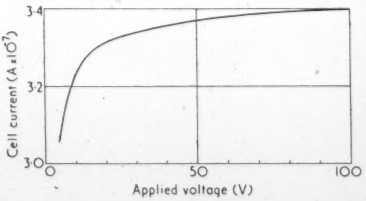

Fig. 7. Upper part of the saturation curve of the special type VS39 cell of Fig. 4, with the can and anode connected together and used as anode. For fair comparison, the scale of the diagram is the same as in Fig. 1. The saturation curve is more satisfactory, though the photocurrent is 2000 times greater

shows the excellent form of the upper part of the saturation curve under these conditions.

Using another special Cintel cell, a compromise along these lines was tried, by having the inside of the bulb fully metallized and connected to anode, except for an untreated window about 2 cm square. A saturation loop of 1% was still observable, however, due to potential jumps of the free window-area. No doubt this area happened to be clean and well insulating. The most certain remedy seems to be a deliberate conductive-film treatment, but this presents considerable problems, chiefly of a chemical nature, in a photocell.

Meanwhile, it seems advantageous to try to have the inside of the bulb as "dirty" as possible, and to make the anode a push-fit in it, touching it as intimately as possible. Good isolation of bulb surface from cathode is in all cases essential, to avoid the Penning–Moubis condition with its spurious augmentation of cell output.

Finally, it seems very likely that fatigue in a vacuum cell is simply another manifestation of the processes above described, as they may occur in an ordinary cell having large and ill-defined variations in conductivity over its inner bulb surface, and some very slight leakage between this surface and cathode as well as anode, perhaps. It has been shown that it may take as long as half a second for a major change in bulb potential to spread from one end to the middle of the bulb. There seems to be no reason why the time constant of such processes should not often be very much longer, depending on bulb surface resistivity. Their effects would then appear as a slow change, rather than a sudden jump, in cell output.

The irregularities of behaviour observed in some modern photocells, and herein discussed, are hardly to be laid at the door of the earlier pioneer workers responsible for their design. Rather, it is that the general cleanliness attainable by modern vacuum tube technique has made the irregularities clearly recognizable or—one may almost say—has caused their occurrence.

ACKNOWLEDGEMENTS

This research was prompted by some observations brought to our notice by Mr. J. H. Hodgson of Cinema Television Ltd., and thanks are due to this firm for supplying all the special photocells necessary for its completion. The work has also profited by discussions with Mr. G. T. Winch, of the Research Laboratories of the General Electric Co. Ltd.

The probable importance of electron-reflexion mechanisms was first pointed out by the authors' colleague Mr. E. J. Gillham of the Light Division, National Physical Laboratory, in which Division the work was done.

The work described above has been carried out as part of the research programme of the National Physical Laboratory and this paper is published by permission of the Director of the Laboratory.

REFERENCES

(1) CAMPBELL, N. R., and RITCHIE, D. *Photoelectric Cells*, 3rd Ed., pp. 24 and 25 (London: Sir Isaac Pitman and Sons Ltd., 1934).

(2) PENNING, F. M., and MOUBIS, J. *Physica*, **2**, p. 55 (1935).

Photoelectric recording of reflecting echelon fringes

By T. A. LITTLEFIELD, Ph.D., A.Inst.P., Physics Department, King's College, University of Durham, Newcastle upon Tyne

[*Paper received* 6 *April*, 1955]

The apparatus described consists of a reflecting echelon interferometer used in conjunction with a photomultiplier to measure the relative intensities of hyperfine structure components of spectral lines. The arrangement eliminates the troublesome "envelope effect" which leads to distortion and displacement. The choice of exit slit width is discussed and the dispersion of wave number along the pen recorder trace is shown to be almost linear. Tests with the cadmium triplet $2^3S_1 - 2^3P_{012}$ indicate that the method is reliable when the components are completely resolved.

Since its development by Williams,(1) the reflecting echelon has been largely used for precision vacuum wavelength measurements, a task for which it appears to be particularly well suited. Some hyperfine structure investigations have also been made, notably by Drinkwater, Richardson and Williams,(2) and by Foster and Richardson.(3) By comparison with the Fabry–Perot etalon, however, the reflecting echelon finds little favour with spectroscopists, largely on account of its high cost and fixed dispersion.

The development of the photomultiplier has rendered possible the direct recording of the intensities of hyperfine structure components of spectral lines. The Fabry–Perot interferometer has already been used in this manner by Jacquinot and Dufour,(4) and some indication has already been given by Barrell(5) and Jacquinot(6) that similar work is in progress in this laboratory. It will be shown that, despite the envelope effect, the measurement of intensities provides another promising field of activity for the echelon.

PRINCIPLE

Briefly the behaviour of a reflecting echelon may be considered in the following way. Each step behaves as a rectangular aperture so that the light, reflected from it, is distributed in a diffraction pattern, the shape of which is given by $\sin^2\alpha/\alpha^2$ where α is half the phase difference for light proceeding from opposite sides of the step. This is known as the envelope curve. When a number of such steps are arranged as an echelon, interference occurs so that only two fringes for each wavelength appear. The relative intensities of the two fringes are governed by the envelope curve. Thus fringes of appreciable breadth are not only reduced in intensity but also distorted in any position other than single order ($\alpha = 0$) at the centre of the envelope curve. The distortion depends upon the breadth of the fringe and its position within the envelope curve.

By arranging a photomultiplier behind a moving slit, the intensities of the fringe system could be recorded. Since, however, the echelon is already enclosed in a vacuum chamber it is more convenient to move the fringes across a fixed slit by adjusting the air pressure within the chamber. Moreover, when the photomultiplier slit is placed in the position of single order, the fringes are recorded not only at maximum intensity but also free from envelope distortion and displacement. The air pressure within the chamber is allowed to rise slowly by leakage from the atmosphere through a length of

capillary tube. Thus, with this simple arrangement, some of the most troublesome limitations of the echelon are removed and an entirely new field of activity has become available for it.

EXPERIMENTAL ARRANGEMENT

Two methods of crossing a reflecting echelon with auxiliary dispersion have been used in the past. The internal parallel beam mounting was advocated by Jackson[7] while the external parallel beam mounting was preferred by Williams.[1] Although the former is very economical of light, it has been criticized by Williams because it will only give full resolving power for the wavelength falling normally upon the echelon. A more serious disadvantage is that such an arrangement cannot be used for precision wavelength measurements, since different wavelengths, incident upon the echelon at different angles, implies a variation of interference path for different wavelengths. Since in the present arrangement only one wavelength at a time can be examined, Williams's objections no longer hold, and Jackson's arrangement is preferred on account of its greater economy of light and compactness.

Light is focused upon the first slit S (Fig. 1) which lies in the focal plane of the echelon lens L, so that a parallel beam

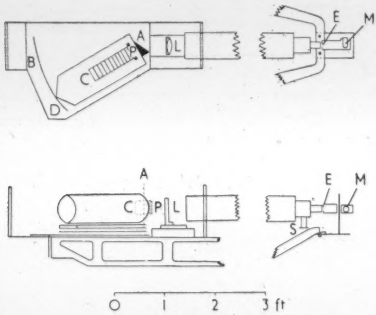

Fig. 1. Experimental arrangement

of light falls upon a prism P lying immediately in front of the echelon chamber C. Light of only one wavelength falls normally upon the echelon surface and thus after reflexion returns through the prism and echelon lens to be focused upon the fixed photomultiplier slit E. Behind this slit the photomultiplier M is placed at such a distance that the cone of light emerging from the slit almost fills the photosensitive surface. Rotation of the echelon chamber and prism about the vertical axis at A brings any desired wavelength on to the slit at E. A wavelength scale can therefore be attached to the arc BD.

To ensure that the photomultiplier slit lies at the centre of the envelope curve, a source having a continuous spectrum is first examined. Such a source containing all wavelengths, gives a light distribution corresponding to the envelope curve. The tilt of the echelon chamber mount is then carefully adjusted until a maximum response of the photomultiplier is recorded, corresponding to the single order position.

The source having the continuous spectrum is then replaced by one giving the line spectrum to be examined. Air is allowed to leak slowly into the echelon vacuum chamber, the rate of leakage being controlled by a suitable length of capillary tubing. A leakage rate such that it took 75 s for a whole order to pass across the exit slit was found to be satisfactory. Initially, galvanometer deflexions arising from the output current of the photomultiplier were recorded with a continuous paper camera running at constant speed, but recently the galvanometer has been replaced by a direct current amplifier and a pen recorder.

SLIT WIDTHS

Experience with photography of echelon fringes has shown that the optimum entrance slit width is about 0·002 cm. An exit slit of similar width was used in the present work, the choice being governed in the early stages by what was readily available. It is clear that the resolving power of the instrument used in the present way is closely linked with the width of the exit slit. It will be appreciated that when the slit is made too narrow, the sensitivity is reduced, while, if it is made too wide, the resolving power will be sacrificed.

Graphical investigation of slit width, plotted as a fraction of the half-width of the fringe, showed that, when the fraction was $\frac{1}{4}$, the recorded contour was indistinguishable from the original. This also applied to two fringes which were just resolved when the intensities were equal and also when they were in the ratio 1 : 5. It was a little surprising to find that even when the slit width was as much as $\frac{1}{2}$ the half-width, the recorded contours were just perceptibly different from the original. From this it is evident that there is no advantage in reducing the slit width below $\frac{1}{4}$ or $\frac{1}{5}$ of the half-width of the fringe.

Blackie and Littlefield[8] have shown how to calculate the width of an echelon fringe from a knowledge of the instrumental width and the Doppler width. This calculation yields a fringe half-width of 0·0042 cm for cadmium excited in an Osira lamp (by General Electric Co. Ltd.) at about 600°K. The slit should therefore be 0·0010 cm, but the above considerations showed that the records obtained, in which the ratio of exit slit to width to half fringe width was $\frac{1}{2}$, will not be significantly different from the original fringes. Even if this source were cooled with liquid air, the fringe width would be reduced to 0·0030 cm, so that a slit width of 0·0005 to 0·0010 cm would still be satisfactory. This is fortunate since it is difficult to construct slits with widths appreciably smaller than this.

DISPERSION

Although the most important function of this equipment remains an investigation of intensities of hyperfine structure components, some knowledge of the dispersion as measured along the pen recorder paper is desirable, even if only to facilitate the identification of components. It is clear that the dispersion cannot be linear, because the rate of leakage falls as the air pressure within the chamber rises towards atmospheric pressure. Moreover, to make the dispersion linear hardly seems worth while at this stage. Since spectroscopists are primarily interested in wave-number differences, the dispersion of wave-number between orders along the pen recorder trace was investigated.

For light of wave-number ν falling upon an echelon of step thickness t and step height s, $m/\nu = 2t - s\theta$ where m is the order of interference and θ is the angle of diffraction. In the present arrangement t, s and θ are all fixed. As air enters the chamber, ν and m increase proportionally so that the

above relationship is preserved. The wave-number difference $\Delta\nu$ corresponding to an order difference Δm is given by $\Delta\nu/\nu = \Delta m/m$, where $m = 2t\nu$. The distance between two successive orders in wave-numbers is obtained by setting $\Delta m = 1$, from which $\Delta\nu = 1/(2t)$. Let a be the linear distance between two successive orders of the main component of a line having hyperfine structure, and b be the distance of one of its satellites from the main component. Thus a corresponds to a wave-number difference of $1/(2t)$, and provided the dispersion of wave-number along the trace is linear, the wave-number difference of the satellite from the main component is given by $b/2at$.

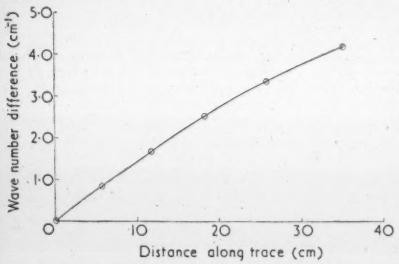

Fig. 2. Dispersion of wave-number along trace

The dispersion of wave-number along the pen recorder trace was examined experimentally by allowing air to leak into the pressure chamber until six orders had passed over the slit. The distances of these along the trace were measured. Since it has been shown that there is a constant wave-number difference between successive orders, a graph of wave-number and distance along the trace was plotted as shown in Fig. 2. If x is the distance of a satellite along the trace from the first fringe of the main component, the wave-number difference $\Delta\nu$ is given by the equation $\Delta\nu = 0{\cdot}145x - 0{\cdot}000021x^3$. This only applies to the particular echelon used for this experiment and for which there are thirty-five steps, each 6 mm thick. The cubic term represents the departure from linearity of the dispersion along the trace. The errors arising from the assumption of linearity for satellites situated at a half, one and two orders away from the main component can readily be calculated and amount to 0·13, 1·05 and 2·1% respectively. Since it is unlikely that the pattern over more than one order would be measured, it is evident that the error introduced by the assumption of linearity of dispersion is not likely to exceed 1%.

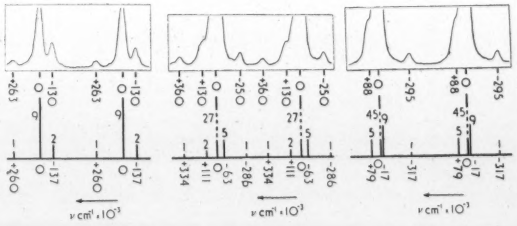

Fig. 3. Traces of the cadmium triplet
(*a*) $2^3S_1 - 2^3P_0$ at wavelength 4678 Å.
(*b*) $2^3S_1 - 2^3P_1$ at wavelength 4800 Å.
(*c*) $2^3S_1 - 2^3P_2$ at wavelength 5086 Å.

DISCUSSION OF RESULTS

Preliminary tests of the method were made using the cadmium triplet $2^3S_1 - 2^3P_{012}$ at wavelengths 4678, 4800, 5086 Å excited in an Osira cadmium lamp. The traces (Fig. 3) show successive orders of the main component due to the even isotopes with the less intense components arising from the odd isotopes lying between. Beneath each trace the structures reported by Schuler and Bruck[9] have been placed for comparison, the intensities being indicated in circles at the top of each component. The recorded structures agree reasonably well with them, but the temperature widths were too great to allow observation of all components.

To a large extent unresolved components can account for discrepancies between the recorded structures and those of Schuler and Bruck. Thus the main components of both wavelengths 4800 and 5086 Å appear to be displaced by about 0·030 and 0·020 cm^{-1} respectively towards the lower frequencies. No such displacement occurs with wavelength 4678 Å which has a simple structure with all components resolved. Only in this case has a comparison of intensities proved possible and inspection shows that these are in good agreement with those calculated theoretically. It is concluded that this method may be used to compare intensities of hyperfine structure components, but great care will be necessary in avoiding frequency and intensity errors arising from incompletely resolved neighbouring components.

ACKNOWLEDGEMENTS

The author wishes to thank Professor W. E. Curtis for the excellent laboratory facilities placed at his disposal and for many helpful discussions and suggestions. Acknowledgement is also due to Mr. H. Bolland who was responsible for much of the constructional work.

REFERENCES

(1) Williams, W. E. *Proc. Phys. Soc.* [*London*], **45**, p. 699 (1933).
(2) Drinkwater, J. W., Richardson, O., and Williams, W. E. *Proc. Roy. Soc. A*, **174**, p. 164 (1940).
(3) Foster, E. W., and Richardson, O. *Proc. Roy. Soc. A*, **189**, p. 149 (1947).
(4) Jacquinot, P., and Dufour, Ch. *J. Rech. Cent. Nat. Rech. Sci.* (No. 6), p. 91 (1949).
(5) Barrell, H. *Nature* [*London*], **164**, p. 599 (1949).
(6) Jacquinot, P. *J. Opt. Soc. Amer.*, **43**, p. 414 (1953).
(7) Jackson, D. A. *Proc. Roy. Soc. A*, **128**, p. 508 (1930).
(8) Blackie, J., and Littlefield, T. A. *J. Opt. Soc. Amer.* To be published.
(9) Schuler, H., and Bruck, H. *Z. Phys.*, **55**, p. 575 (1929).

Millimicrosecond exposures by image tubes

By R. F. Saxe, Ph.D., Queen Mary College, University of London, and R. A. Chippendale, B.Sc., Mullard Research Laboratories, Salfords, Surrey

[*Paper first received* 18 *March, and in final form* 13 *April*, 1955]

The technique whereby an image tube and a coaxial system may be used to obtain pictures with an exposure not exceeding 4 mμs is described. Pictures showing the growth of a streamer across a gap in approximately 4 mμs are given. The limitations of this technique are briefly discussed, and it is estimated that exposures of the order of 10^{-10} s should be possible.

The study of the spatial distribution of a body emitting an optical transient may be performed by taking a short-exposure picture of that body. If the spatial distribution which is to be studied is varying in time, then such a picture will record the integrated distributions existing while the exposure is being taken. If the duration of the exposure is made so short that the change in spatial distribution during the exposure is small, then effectively a single, "still" picture is obtained. The upper limit of exposure, for which the resultant picture may be regarded as a single, "still" picture, will obviously depend on the rate of change of spatial distribution to be studied.

In the case of certain gaseous discharge phenomena, the upper limit of exposure lies in the millimicrosecond range (1 mμs $\equiv 10^{-9}$ s), and it is therefore desirable to be able to record with an exposure of this order. An attempt was made by Dunnington and White[1,2] to achieve this end by means of a Kerr cell. The Kerr cell shutter is maintained open to light by the application of a voltage and the same voltage is applied to a spark gap through an open line.

When a spark is initiated in the spark gap, the resulting collapse of voltage is propagated along the line and causes the Kerr cell shutter to shut. The use of mirrors to delay the arrival at the Kerr cell of the light emitted by the spark enables the early stages of the spark to be studied. The transition time of the Kerr cell shutter from the open to the closed state was estimated to be 4 mμs. It is, however, doubtful if such a rapid closing was in fact achieved since an open line was used. No monitoring of the pulse shape was attempted.

By the use of a Blumlein system and a Kerr cell, Walker[3] claims to have achieved an exposure of 20 mμs, although the opening and closing of the cell occupied a large fraction of this time. Other workers[4,5] have obtained exposures of this order of magnitude using Kerr cells, the shortest exposure claimed being of the order of 7 mμs. In these cases, however, the cell was driven by an *LCR* circuit and the transition time of the shutter was limited to about 4 mμs. This limitation of minimum transition time is due to the high capacitance (of the order of 10^{-10} F) of a Kerr cell of reasonable aperture, and to the use of a circuit composed of lumped components.

It will be shown later that in uniform field conditions a streamer may cross a 1 cm gap in about 4 mμs, and it is obvious, therefore, that a shutter of higher performance is required to investigate this motion. The use of an image tube has enabled this higher performance to be achieved and the system will now be described.

THE ELECTRICAL SYSTEM

In order to generate transients of short duration and with rapid transitions, it is advisable to employ a coaxial system, and the system here employed to drive the image tube is shown in Fig. 1. It consists of a coaxial line, the centre of which is formed in two parts, *A* and *B*. The insulant is polythene and the characteristic impedance, Z, of the line is approximately 13 Ω.

Section *A* of the line is charged to approximately 30 kV through the high resistor *R*, and the gap between sections *A* and *B* is arranged so that a spark will pass when the section *A* is fully charged. If the spark is assumed to present a very low impedance in an infinitely short time after initiation, then a square electrical transient will travel along section *B* and will appear across the matching impedance, Z, at a time t after the initiation of the spark where t is the time of travel of an electrical wave along section *B* of the coaxial system.

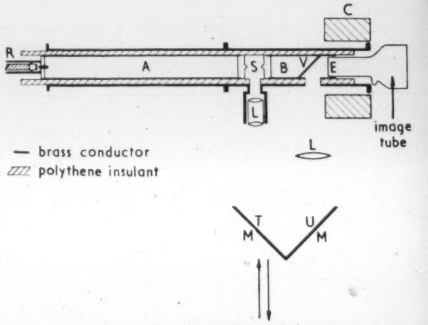

Fig. 1. Diagram of the coaxial line-image tube system used to study the growth of a spark

A, *B*, sections of centre conductor; *C*, focus coil; *S*, spark gap; *M*, mirrors; *V*, mirror; *L*, lenses; *R*, charging resistor; *STUVE*, optical path.
The arrows indicate the directions in which the mirrors *M* may be moved to vary the optical path *STUVE*.

The duration of the transient will be $2T$, where T is the time of travel of an electrical wave along section *A* of the coaxial line. The transient appearing across Z will not be perfectly square but will be degraded, both in the shape of the front and in amplitude, by attenuation in section *B*. The back of the transient will be degraded by attenuation suffered in travelling twice along section *A*, once along section *B* and by reflexion at the open end (left-hand end, Fig. 1) of section *A*.

These considerations are based, however, on the assumption that the impedance transition in the spark occurs in an infinitely short time, which does not obtain in fact. Analysis of the experimental evidence of the breakdown processes in a uniform field gap has shown[6] that the final stage of the initiation process is a streamer, and a theory has been advanced[7] in which the mechanism is shown to be essentially the same in uniform and non-uniform fields. Experiments

on long point/plane gaps[8] have shown that a charge dissipation occurs of the order of 1 μC/cm travel of the streamer.

In the breakdown of a gap, such as that shown in Fig. 1, this charge may be drawn only from the charge stored in the capacitance of section *A* of the line. If 1 μC of charge is stored in a length *l* of section *A*, then the maximum velocity at which the streamer may advance is 1 cm in a time $2l/v$, where v is the velocity of an electrical wave along the coaxial system. If we consider a 70 Ω coaxial system, it may be estimated that the streamer will cross a 1 cm gap in approximately 10 mμs, while in a 13 Ω system the streamer will cross the gap in approximately 2 mμs.

It is therefore obvious that, in order to obtain rapid transitions in the switching, the system must be coaxial and of low impedance.

The application of the square transient to the image tube must also be considered. In early experiments, the image tube was situated outside the coaxial line and was connected across the matching impedance by the shortest possible connexions. However, the inductive circuit which resulted deteriorated the transient applied to the image tube and a distorted picture resulted.

This defect was eliminated by the use of a coaxial tube and termination as shown in Fig. 2. The use of this tube, which has an internal capacitance of the order of 10 pF, gives a time constant of 10^{-10} s.

THE IMAGE TUBE

The first trials were made with a standard Mullard type ME 1201 AA image tube. This tube is fitted with a grid electrode to facilitate its use as an optical shutter[9] and has electrode connexions brought out to standard valve caps. The physical construction and position of these lead-out electrodes gives rise to an inductive mismatch when the tube is connected up as near as possible to the end of the coaxial line. For this reason the diode shown in Fig. 2 was constructed.

The tube (Figs. 2 and 3) is built of Phoenix glass and has a 1 in. diameter low resistance antimony–caesium cathode on

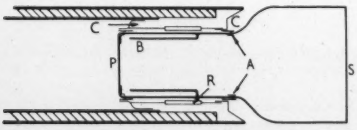

Fig. 2. Method of connexion of the image tube to the coaxial line to preserve the coaxial nature of the system

P, end plate on which the photocathode is formed; *B*, internal glass re-entrant; *S*, fluorescent screen; *A*, tungsten seals for connexion to the anode; *C*, spring contact bands; *R*, resistors.

the end plate *P* and a 4½ in. diameter fluorescent screen *S*. The internal glass re-entrant tube *B* provides an insulating path between the photocathode and the anode which consists of a conducting coating of aluminium covering the internal walls from *B* to the aluminium backed screen. The anode lead-out consists of four tungsten seals *A* equally spaced round the tube and joined externally by a ring of silver deposited on the glass. The cathode lead-out is identical and is brought out to a similar silver ring on to which the spring contact band *C* is clamped as in the case of the anode. The resistors *R* (40, ¼ W, 25 Ω in series parallel) are connected across the two contact bands *C*, and provide a reasonable termination across the inner and outer conductors of the coaxial system.

Care must be taken to ensure that connexions associated with the tube are of low impedance as it is estimated that the current which flows in the tube for an exposure such as that shown in Fig. 4(*a*) is in the range 0·1 to 1 A.

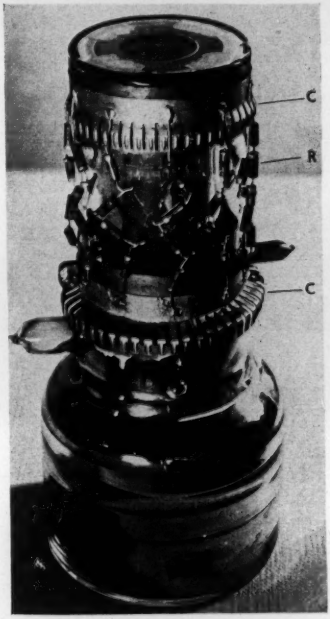

Fig. 3. Photograph of image tube showing spring contact bands *C* and matching resistors *R*

The tube works at an electron-optical magnification of four using the magnetic focus coil *C* (Fig. 1). Under d.c. conditions the maximum anode voltage is approximately 8 kV but the tube works satisfactorily up to 15 kV with transients of less than 10^{-8} s duration.

EXPERIMENTAL RESULTS

Lack of a travelling wave cathode-ray tube prevented accurate monitoring of the wave shape applied to the image tube, but the cathode-ray tube available (type GEC 958) showed that the wave was approximately square.

The study of the initiation processes of breakdown in a gap was performed using the experimental arrangement shown diagrammatically in Fig. 1. Light from the spark is taken along the optical path *STUVE* by means of lenses *L*, and mirrors *M*, and is focused on to the photocathode *E*, of the image tube. The mirrors *M* are mechanically connected and may be moved as shown by the arrows. The

length of the optical path may therefore be varied at will by a known amount. Since the velocity of light in air is known, the variation in the delay of arrival of light at the photocathode E, owing to a given change of path length, may be readily computed.

The electric transient operating the image tube is of duration $2T$, but the maximum exposure obtainable will be shorter than this owing to transit time effects. Electrons which have been accelerated by the electric transient will continue to move down the image tube after the termination of the electric transient and will reach the screen. Electrons which have been accelerated to velocities of less than 10 kV will not contribute significantly to the recorded picture on account of their lower energies. As the time t_2, taken for an electron from the cathode to reach 10 kV is approximately 0·5 mμs, the exposures may be considered to be shortened by this amount at the trailing edge.

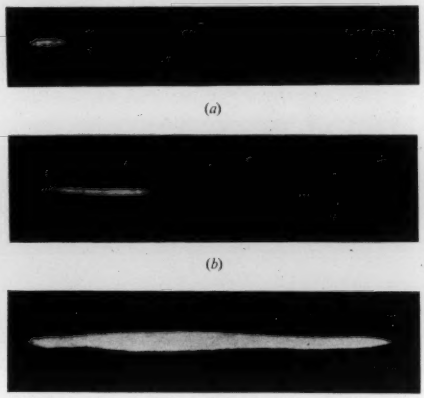

(*a*)

(*b*)

(*c*)

Fig. 4. The growth of a streamer across a spark gap

Duration of electric transient applied to image tube of the order of 4½ mμs.
Amplitude of electric transient applied to image tube of the order of 15 kV.
Relative times are (*a*) 0; (*b*) 1·3$_5$ mμs; (*c*) 3·4 mμs.

If the delay in the arrival of light from the spark at the image tube is t_1, then the conditions for photo-emission (i.e. a voltage established across the image tube and cathode-illuminated) will persist only for a time $(t + 2T - t_1 - t_2)$. Variation of t_1, by movement of the mirrors, enables the stages of growth of the spark to be studied, and if $t_1 > (t + 2T - t_2)$, the initiation processes may be observed.

The above analysis of the temporal range of the spark process observed is based on the assumption that no delay in the emission of light from the spark occurs, i.e. that the lifetimes of the excited states concerned are small compared with the time intervals considered. The results obtained indicate that this assumption is not valid, the delay in light emission being approximately 1·8 mμs.

When the initiation processes are being studied, the growth of visible luminosity across the gap is arrested on the resultant picture by the termination of the open condition of the image tube shutter and the rapidity of this termination will obviously be dependent on the shape of the back of the electric transient applied to the image tube.

Pictures of different stages of the growth of a streamer in the gap are shown in Fig. 4, and the relative times are indicated. It will be seen that the streamer crosses the gap in approximately 4 mμs. The duration of the electric transient for these pictures is of the order of 4½ mμs and the amplitude of the transient is of the order of 15 kV.

Normal methods were used to record the image on the fluorescent screen, i.e. Wray $f/1{\cdot}0$ lens, HPS emulsion developed in Johnson's contrast developer diluted 2 : 1 for 12 min at 20° C.

POSSIBLE FUTURE DEVELOPMENTS

The production of shorter exposures by means of an image tube should be possible. In the present image tube, the effective transit time is approximately 0·5 mμs, and this probably represents the shortest exposure obtainable. Further, the streamer transit time for the 15 Ω coaxial system used is about 4 mμs and during this time, since current flow is occurring in the gap, an increasing voltage is being propagated along section B of the line (Fig. 1). This increasing voltage will cause some low-level exposure to be obtained on the image tube.

To eliminate these limitations, it is suggested that a simple planar type of image tube (similar to the type CV 144 by Electric and Musical Industries Ltd.) with a small cathode-screen spacing could be driven by a line of impedance of, say, 1·5 Ω. The use of higher voltages is also to be recommended in order to increase the brilliance of the image on the screen of the image tube. Owing to the short duration of the electrical transient applied to the image tube, breakdown is not a serious limitation.

It is probable that exposures of the order of 10^{-10} s could be achieved by the use of the above suggestions.

ACKNOWLEDGEMENTS

One of us, R. F. S., wishes to acknowledge the grant of an I.C.I. Research Fellowship during the tenure of which the work was performed, while the other, R. C., wishes to thank the Directors of the Mullard Radio Valve Co. for permission to publish this work.

Both authors wish to thank the above Company for the generous facilities provided, and in particular to thank Mr. G. Knott for his interest and encouragement.

REFERENCES

(1) DUNNINGTON, F. G. *Phys. Rev.*, **38,** pp. 1506, 1535 (1931).
(2) WHITE, H. J. *Phys. Rev.*, **49,** p. 507 (1936).
(3) WALKER, E. Private communication.
(4) CADY, W. M., and ZAREM, A. M. *Nature* [*London*], **162,** p. 528 (1948).
(5) ZAREM, A. M., and MARSHALL, F. R. *Rev. Sci. Instrum.*, **21,** p. 514 (1950).
(6) SAXE, R. F. To be published.
(7) SAXE, R. F. To be published.
(8) SAXE, R. F., and MEEK, J. M. *Proc. Instn Elect. Engrs.* Monograph No. 124 M., April, 1955.
(9) CHIPPENDALE, R. A. *Photogr. J.*, **92B,** p. 149 (1952).

New books

Sensitometry. By L. LOBEL and N. DUBOIS. (London: The Focal Press Ltd., 1955.) Pp. 263. Price 25*s*.

From a practical, indeed in many ways from a theoretical, point of view the *H* and *D* curve of a photographic material, which relates the density produced to the exposure, is of fundamental importance. This book is concerned with the meaning, the measurement and the use of the *H* and *D* curve. It has been translated and somewhat modified from the *Manuel de sensitometrie* by the same authors, the first edition of which was published nearly 20 years ago. A chapter on the application of the *H* and *D* curve to colour materials and an index in the English fashion have been added. Considering the price the reviewer considers that the book might have been more attractively produced. The figures are heavy in comparison with the French version, but the photographs are better reproduced and rather more attractive in other respects. The treatment is at an elementary level but sound, so that it provides an excellent introduction to the subject.

E. W. H. SELWYN

Electrical characteristics of overhead lines (1954). By S. BUTTERWORTH, O.B.E., M.Sc. Pp. 238. Price 44*s*. **Handbook on electrical characteristics of overhead lines** (1953). Pp. 20. Price 15*s*. (Leatherhead: The British Electrical and Allied Industries Research Association.)

In the design and operation of overhead-line power systems it is necessary to know the electrical characteristics of various types of line; for example, the power-carrying capacity, the voltage drop and the fault current are determined largely by the line impedance, the power loss by the resistance, and the charging current by the capacitance. It is the aim of this book to give the transmission line engineer all the information he needs to calculate such characteristics for any design of line likely to be of practical importance.

The first three chapters of the book discuss the basic line constants; resistance, inductance, and capacitance. The following chapters deal with three-phase lines under balanced and unbalanced conditions, current-carrying capacity, corona and corona losses, multiple conductors and voltage regulation. Line calculations are rather tedious if they are carried out from the basic formulae, and valuable features of the book are the tables and alinement charts which reduce the calculations to very simple arithmetical operations.

The book is comprehensive and up-to-date; for example, it contains a useful treatment of multiple conductor lines, i.e. lines in which each phase consists of two, three or four conductors spaced about 12 in. apart. This type of line is becoming of increasing importance for high-voltage power transmission, and information on its characteristics is not yet available in most textbooks on the subject.

Although the book gives a full theoretical derivation of all the formulae used, the practical engineer will normally use only the tables and alinement charts. Accordingly, a separate handbook has been published containing the tables and alinement charts together with some practical examples illustrating their use, but without the theoretical treatment.

The author and the Electrical Research Association are to be congratulated on these two publications which should be of great service to overhead-line designers and operators and also to advanced students.

J. S. FORREST

Progress in biophysics and biophysical chemistry, Vol. 5. Edited by J. A. V. BUTLER and J. T. RANDALL. (London: Pergamon Press Ltd., 1955.) Pp. viii + 230. Price 55*s*.

This volume, in common with others of the series, contains a mixed bag of subject-matter. It is unlikely that the average biological scientist will have time to read all the sections however good these may be. The diversity renders it difficult for one person, including the reviewer, to judge equally the contributions. The volumes in their present compass resemble "annual reviews"; it is possible that the common interest might be better served if all sections in a given number bore on a particular subject.

Taking the sections in order: there is a discussion of the kinetics of bacterial growth by Dean and Hinshelwood. In this the process of adaptation of the cell enzymes to changes in the conditions is discussed and contrasted with the theory that mutant varieties take over following the change.

Schulman and collaborators discuss the adsorption of surface active agents and antibiotics on cells. Haemolytic activity is related to the penetration of a cholesterol monolayer by the substance, and the antibiotic activity of some substances may similarly be related to their effects on a monolayer.

Pollard and collaborators discuss the action of ionizing radiation on enzyme systems. It is possible to deduce the size and molecular weight from the inactivation caused by exposure to radiation. The structure and function of the photosynthetic centres, the chloroplasts, of plant cells, forms the subject of a section by J. B. Thomas. The formation of X-ray diagrams from fibres, and their interpretation, is dealt with in an elementary way by A. R. Stokes. Finally M. Joly discusses the denaturation of proteins, and its reversal. The latter includes a very extensive bibliography of this complex subject.

Following this list one can only concur with the editors' expression of the difficulty met in deciding upon the field covered by the title.

E. J. HARRIS

Sonics. Techniques for the use of sound and ultrasound in engineering and science. By THEODOR F. HUETER and RICHARD H. BOLT. (London: Chapman and Hall Ltd.; New York: John Wiley and Sons, Inc., 1955) Pp. xi + 456. Price 80*s*.

The authors of this book have set out to survey, for those who are interested in introducing new techniques into industry, the possible applications of devices using sound and ultrasonic vibrations. With their considerable experience as consultants and lecturers, they have fulfilled this task well. They take care to explain the fundamental bases of the techniques and give detailed descriptions of the various transducers and detectors that may be used, setting out the information in useful comparative tables.

There is a tendency when new devices using previously untried phenomena like ultrasonics are presented to claim more for their applications than is justified. The authors are careful to show what techniques have been brought to the plant stage and to distinguish them from those which have not progressed beyond the "test-tube" stage.

The book can be recommended to all who wish to consider the application of acoustic methods in all branches of engineering.

E. G. RICHARDSON

Fundamentals of radiobiology. By Z. M. BACQ and P. ALEXANDER. Pp. xii + 389. Price 40*s*. **Radiobiology symposium 1954.** Edited by Z. M. BACQ and P. ALEXANDER. Pp. v + 362. Price 60*s*. (London: Butterworths Scientific Publications, 1955.)

The development of the new science of radiobiology (should it not be "radiation biology"?) owes much to British physicists, notably to J. A. Crowther, to D. E. Lea and to L. H. Gray. It was Crowther who proposed the first definite, physical, hypothesis to explain the biological actions of ionizing radiations: ". . . action takes place whenever one of the biological structures is 'hit' by the radiation . . . a 'hit' is registered when a pair of ions is produced anywhere within the sensitive particle" he said in his Sylvanus Thompson Memorial Lecture in 1937. Lea, on the basis of a long sequence of beautifully designed and executed physical experiments on *biological* material developed this into the "target" theory, which was set out in the second edition of *Actions of radiations on living cells* (London: Cambridge University Press, 1954). He postulated that *in certain precisely defined cases*, biological changes resulted from ionization "in, or in the immediate vicinity of, some particular molecule or structure" vital to the life of the organism, the so-called "target." Lea emphatically disclaimed universality for this theory, and was quick to see the significance of the suggestion, made in this country by Weiss in 1944, that the process of ionization in water (and so in tissue) results in the liberation of free hydroxyl and hydrogen ions and sets in train a sequence of chemical reactions with the solutes present, a theme some biological aspects of which were discussed by Gray in the Sylvanus Thompson Lecture in 1953. Lea's work provided the foundations of the new science. This wider theory brought chemists to the aid of physicists and biologists and an increasingly voluminous literature has resulted. It is this literature which Prof. Bacq (a physiologist) and Dr. Alexander (a physical chemist) have set out to survey in their book. In the preface they say "We have selected certain investigations from the enormous mass of published material . . . we have deliberately chosen certain aspects of radiobiology for special emphasis." They must therefore not expect every reader to agree either with this selection nor with the conclusions they draw. These are clearly very personal opinions. The author index gives 57 references to Bacq, 48 to Herve (one of his collaborators), 41 to Alexander and 39 to L. H. Gray—the many others listed are "also rans." The title of the book is, in a way, misleading: it should have been *Some chemical aspects of radiobiology*. In this context it is valuable in showing the change of emphasis which has taken place since the appearance of the first edition of Lea's book in 1946; but the authors should have been more cautious in the predictions made in their "postcript." It is not wise to argue too soon from the test-tube to the patient. Nor are they fair in their reference to the "sterile pursuit of purely anatomical observations." If, by this, they mean the study of the effects of radiations on living organisms as compared with *in vitro* studies of radiation-induced chemical changes, the reviewer must beg to differ. This subject is biology, and the fundamental unit of biology is the cell. From it one can work inwards biochemically, or outwards, to living tissue; but the changes produced in the individual cell by the actions of radiations are the fundamental ones. Nevertheless, despite such criticism, this book will take its place as a source book in the radiological literature. Its writing has involved much labour—960 original papers are listed in the bibliography—and no mean scholarship. Any physicist who thinks he would like to find out for himself what radiobiology really is could do worse than to start on F. G. Spear's *Radiations and living cells*, continue with Lea's *Actions of radiations on living cells* and then read Bacq and Alexander to bring himself up-to-date.

Radiobiology symposium, edited by the same authors, is a collection of the papers read at a radiobiological symposium held in Liége in 1954. The topics are largely biological and cover a very diffuse field. This again has its main value as a source book.

C. B. ALLSOPP

Atomic energy research at Harwell. By K. E. B. JAY. (London: Butterworths Scientific Publications, 1955.) Pp. xii + 144. Price 5*s*.

This volume is in the nature of a progress report and gives the reader a good general picture of what has been happening at Harwell since the account published in 1952.* Some sections, however, deal with the work done over the whole of the Establishment's eight years of life, for it is only now that the information can be released.

The report is divided into two parts. The first (76 pp.) deals with the major programmes and is written primarily for non-technical readers. The second part (62 pp.) is written for "scientific readers who have not specialized in the various fields discussed" and deals with selected researches carried out in the last two or three years.

Part I, while a little uneven, is generally good and satisfying; the chapter on the development of electronic instruments which describes clearly and concisely the various counters in use and the associated equipment is an excellent piece of technical writing for the non-specialist. There are, however, occasional lapses, for example a phrase like "glass heavily loaded with lead . . . " (p. 63) may mislead a non-technical reader not familiar with lead-glass. The standard of technical knowledge assumed varies—some terms being explained, whilst others are not.

Part II opens with a paragraph on the importance of fundamental research, which is so good that it is worth quoting in full.

> "Right from the beginning it has been recognized that one of the main duties of the Establishment would be to consider the long-range planning of atomic energy, and to be alert to its every possibility, from the most general point of view. To do this the Establishment needs men of a vigorously independent turn of mind who will approach the subject from a fundamental viewpoint, untrammelled by the immediate problems of day-to-day research and development. To attract men of this kind and to create an atmosphere favourable to new ideas and a rebellious spirit of inquiry, opportunities must be provided for pure research in fields of international interest, up to the very frontiers of contemporary scientific inquiry. Without such research a laboratory slowly dies of intellectual stagnation. The stimulating influence of pure research at Harwell has more than justified the comparatively small proportion of the Establishment's effort devoted to such research; it has brought many distinguished visitors who have kept the scientists on their toes; it has rejuvenated men who had begun to lose sight of the wood for the trees in the daily worries of applied research; and it has provided unexpected bonuses in techniques that have turned out to be valuable for project applications unrelated to the fundamental work from which they were born."

The three chapters in this part deal with research in physics, in chemistry and chemical engineering, and in metallurgy. These divisions, let it be said, however, are not to be taken

* *Harwell—the British Atomic Energy Research Establishment, 1946–1951* (London: H.M. Stationery Office, 1952).

too seriously since one finds an account of the use of the plane grating in divergent light under chemistry and the effect of radiation on long chain polymers under metallurgy.

This book deserves to be widely read. It will make the reader generally, even if vaguely, aware of the remarkable advances in pure and applied physics resulting from the work at Harwell; it will show him how outsize scientific and technological problems are tackled; lastly, but by no means least, it contains some excellent examples of scientific writing.

H. R. LANG

Elektronische Halbleiter. By E. SPENKE. (Berlin: Springer-Verlag, 1955.) Pp. xx + 379. Price DM 34.50.

Dr. Spenke's book on electronic semiconductors may be regarded as a very timely and most valuable contribution to a deeper understanding of this important subject. Its usefulness for students, both beginners and advanced, is beyond question. What is more, the only existing "classic" on the subject, issuing from the Bell Laboratories, is now followed by a book from an entirely different school, centred around the person of W. Schottky. This leads to differences in emphasis and approach which will be found most refreshing and stimulating. The book is written in the form of ten lectures and is divided into two parts. The first part deals with a qualitative description of electronic semiconductors and presents the theories of rectification and transistor action. The second part gives a more advanced treatment of the physics of semiconductors.

The first chapter gives a qualitative discussion of the band model and an elementary discussion of electron motion in metals which is sometimes so much simplified as to be misleading. Chapter 2 gives a comprehensive discussion of imperfections and disorder including the ionic crystals, based to a large extent on thermodynamic principles. This chapter will be found very useful by students brought up primarily on Shockley's book. Chapter 3 deals with the concept of a positive hole and defends the idea of "negative mass" as both plausible and essential for the assumed physical model. Whether the notoriously tricky transition from $(-m, -e)$ to $(+m, +e)$ will be quite convincing to the beginner, and the more advanced student, is an open question. Chapter 4 gives a detailed treatment of rectification. Those familiar with the author's contributions to the physics of metal rectifiers will not be surprised that he should begin with and place main emphasis on metal-semiconductor contacts rather than on p–n junction. The importance attached to concentration gradients and Boltzmann distribution in equilibrium at the expense of band models is to be welcomed as a change. The principles of transistor action are the subject of Chapter 5. The filamentary transistor is discussed in considerable detail and the junction and point contact transistors are then compared with it. The equivalent circuits are derived.

Part 2 begins with a discussion of the Heitler–London and Hund–Mulliken approximations for hydrogen molecule, as a preliminary to the treatment of the band model. The author makes a strong plea against the uncritical acceptance of the latter and presents the case for the validity of the atomistic approach in certain circumstances, a point which is frequently overlooked. Chapter 7, accounting for 120 pages, gives a detailed treatment of the band model. The student should find the discussion of Bloch's model for strongly bound electrons and Brillouin's model for weakly bound ones very illuminating. The latter case is approached from the point of view of diffraction of waves in three dimensions. This is followed by derivation of formulae for momentum, velocity, acceleration, effective mass, etc. A novel and useful contribution is the detailed discussion of band-to-band transitions under the action of an electric field, leading to Zener breakdown.

The scattering by imperfections is discussed qualitatively, but no temperature dependence of mobility is derived. Fermi statistics of an electron gas is treated in a separate chapter. A very welcome extension of the scope of this book is a whole chapter devoted to the dynamics and inertia of impurity reactions in semiconductors, with detailed discussion of the relaxation time. The last chapter dealing with the barrier layers on semiconductors gives an excellent exposition of the potential relations near the surface and discusses in great detail much that is too often taken for granted.

It might be trivial, in so extensive a subject, to talk about omissions. However, accepting the limits set by the author himself which include only conduction phenomena, as distinct from photo-, thermo- and magneto-electric effects, one would expect some discussion of surface recombination velocity and a more detailed treatment of minority carrier transport phenomena.

There is a comprehensive author and subject index. The general standard of production is high, though some of the band model diagrams lack clarity.

A. K. JONSCHER

Progress in nuclear physics, Vol. 4. Edited by O. R. FRISCH, O.B.S., F.R.S. (London: Pergamon Press Ltd., 1955.) Pp. vii + 379. Price 70*s*.

The fourth volume in this well-established series maintains the high standard of its predecessors. The topics selected are, as usual, extremely diverse, and are discussed in authoritative fashion by the authors concerned.

In an article on "Isotopic spin and nuclear reactions," Professor W. E. Burcham provides a most welcome presentation for experimentalists of this important concept. Two articles devoted principally to techniques are those on "Scintillation spectrometer statistics" by E. Breitenberger, and "Focussing in high energy accelerators" by T. G. Pickavance. The former is directed at the specialist, and deals in detail with the many factors which affect line shape. The latter is a general introduction for the non-specialist, and emphasizes, amongst other things, the close inter-relation of the problems of focusing and economics in high-energy machine design.

The only theoretical article is by R. H. Dalitz on "Meson phenomena and meson theory," in which the interaction of pions and nucleons is discussed. Professor E. W. Titterton contributes an article on "Photodisintegration experiments with nuclear emulsion" containing reviews of experimental technique, photodisintegration theory and experimental results. "Heavy ions of high energy" are discussed by D. Walker in a short article. D. J. Hughes' review of "Neutron spectroscopy" deals with the experimental and interpretative aspects of this still developing subject.

The remaining two articles are on the "Nuclear properties of the very heavy elements" by J. O. Newton, and "The preparation and chemistry of the transuranium elements" by H. A. C. Mckay and J. Milsted. It is appropriate that these should appear together, for in few branches of physics is the physicist so dependent upon the chemist as in the study of the very heavy elements. Newton, however, discusses all nuclei heavier than ^{208}Pb in his review of present experimental and theoretical knowledge.

B. ROSE

Notes and comments

Journal of The Institution of Telecommunication Engineers

We have received the first issue of a new quarterly published in New Delhi by The Institution of Telecommunication Engineers which was established in India in connexion with the telegraph centenary celebrations in 1953. The issue before us has 58 pages of text measuring $7\frac{1}{4} \times 9\frac{3}{4}$ in. and is nicely printed and produced. Only twenty of these pages are devoted to scientific papers, the others recording the inaugural exercises of the Institution and other domestic news and reports. The titles of the three papers are: Line fault location by pulse technique; On radio measurements at Jabalpur during the Solar eclipse of 30th June, 1954; Power density diagrams of short-wave aerial arrays.

The annual subscription to the Journal is 15 Rs. and the address of the new Institution, to which subscriptions should be sent, is P.O. Box 481, New Delhi, India.

Glossary of terms used in radiology

The many new applications to radiology of discoveries in nuclear physics has made the need for a revised authoritative glossary long overdue. We therefore welcome the publication of British Standard 2597: 1955, *Glossary of terms used in radiology* which has been published by the British Standards Institution (price 10*s.* net). The 750 terms and definitions contained in it are divided into four main sections: General terms and physics; Sources of ionizing radiation; Radiography and fluoroscopy; Radiotherapy and radiation protection. The comprehensive nature of the glossary is indicated by the inclusion of terms relating to such subjects as, atomic physics, high voltage generating equipment, X-ray tubes and their accessories, particle accelerators, diffraction analysis and isotopes in medicine. Where appropriate, quantitative values and symbols are given for the various terms. A complete alphabetical index is included.

Review of electronic components for use in telecommunications

We have received a copy of the *Journal l'Onde Electrique* for March–April 1955. This is a special edition devoted exclusively to components for use in telecommunications equipment and has been sponsored by the French Society of Radio-Electricians. It comprises several papers by authorities in the field, on subjects ranging from resistors and capacitors to the recent developments on semiconductors. On the whole, the papers are intended for the general reader rather than the specialist, but even for the latter they constitute a useful review.

Copies of the Journal can be obtained from the publishers, Editions Chiron, 40 rue de Seine, Paris, 6e. The price is 600 francs.

Exhibition of electrical standards and metering

A special exhibition has been opened at The Science Museum to coincide with the current meeting of the International Electrotechnical Commission and will remain open until 31 October. Although the Exhibition is of particular interest to those concerned in the problems of metering bulk supplies of electrical energy to large industrial and commercial undertakings, it is intended also for the less specialized visitor and serves to demonstrate the care which is devoted to the accurate calibration of electricity meters.

One of the objects of the exhibition is to show the origin and derivation of the various electrical units. An exhibit of particular interest is the complete set of the original B.A. units of resistance which were made in 1864 for the British Association and constitutes the oldest set of accurate electrical standards now in existence. These "B.A. Units" have been stored for many years at the National Physical Laboratory. It is now hoped that they will be presented formally to The Science Museum, and thus become a part of the National Collection of historic scientific apparatus.

The Science Museum, to which admission is free, is open on weekdays from 10 a.m. to 6 p.m. and on Sundays from 2.30 to 6 p.m.

Symposium on magnetic materials

The electronics Group of The Institute of Physics will be holding a symposium on "Some recent developments in magnetic materials" in the Institute's House on 23 and 24 September, 1955. Seven papers will be read and discussed. Further details may be obtained from the Institute at 47 Belgrave Square, London, S.W.1.

Journal of Scientific Instruments

Contents of the September issue

ORIGINAL CONTRIBUTIONS

Papers

A short duration, double-flash system for simultaneous or delayed operation. By N. Dombrowski, R. P. Fraser and G. T. Peck.

A magslip isograph. By G. M. Parker and R. W. Williams.

Angle-spring hinges. By R. V. Jones.

The effect of eccentric loading of optical flats during grinding or polishing. By N. J. Rumsey.

Portable radiation detectors employing photoconductive cells. By J. C. S. Richards.

An automatic sample changer for radiometric work. By J. Rydberg.

Oscillographic measurement of the Penning-gauge characteristics. By M. Varičak and B. Vošicki.

A sensitive manometer for rapid chemical reactions. By E. Rideal and A. J. B. Robertson.

A recording water velocity meter. By M. J. Wilkie.

A simplified form of microwave interferometer for speed measurements. By G. W. G. Court.

A stress-strain machine for testing single crystals in alternating tension and compression. By M. S. Paterson.

An apparatus for measuring the visco-elastic properties of coal in the course of carbonization. By D. Fitzgerald.

Laboratory and workshop notes

The detection of the level of liquid sodium in stainless steel tubes. By E. W. Pulsford.

A circulation-system for ^3He. By K. E. A. Effat and J. H. Fremlin.

Heat treatment and sealing of metal electrodes into fragile glass bulbs under high vacuum. By N. Pentland, J. O'M. Bockris and E. Sheldon.

NOTES AND NEWS

Correspondence

A simple method of determining the shrinkage factor of nuclear research emulsions. From P. J. Duke, W. O. Lock, P. V. March and B. A. Munir.

The effect of the filter absorption edge in X-ray integrated intensity measurements. From R. F. Braybrook.

Device for use with a non-recording microphotometer. From G. L. Rogers.

The preparation of thin bone sections. From S. M. Clark and J. Iball.

An improved probe assembly for use with an electrolytic tank. From M. K. Weston.

Notes and comments

THIS JOURNAL is produced monthly by The Institute of Physics, in London.

All rights reserved. Responsibility for the statements contained herein attaches only to the writers.

EDITORIAL MATTER. Communications concerning editorial matter should be addressed to the Editor, The Institute of Physics, 47 Belgrave Square, London, S.W.1. (*Telephone:* Sloane 9806.) Prospective authors are invited to prepare their scripts in accordance with the *Notes on the preparation of contributions.* (Price 2*s.* 6*d.* including postage.)

REPRODUCTION. The Institute of Physics is a signatory to The Royal Society's Fair Copying Declaration. Details may be obtained upon application from The Royal Society, London, W.1.

ADVERTISEMENTS. Communications concerning advertisements should be addressed to the agents, Messrs. Walter Judd Ltd., 47 Gresham Street, London, E.C.2. (*Telephone:* Monarch 7644.)

CLAIMS FOR MISSING JOURNALS. Claims from regular subscribers to this *Journal* for missing numbers will only be considered if received within 60 days of the date of mailing plus normal outward time of transit and time for lodging the claim. Losses attributable to failure to notify a change of address or to similar omissions will not be considered.

SUBSCRIPTION RATES. A new volume commences each January. The charge is £4 per volume ($11.50 U.S.A.), including index (post paid), payable in advance. Single parts, so far as available, may be purchased at 8*s.* each ($1.15 U.S.A.), post paid, cash with order. Orders should be sent to The Institute of Physics, 47 Belgrave Square, London, S.W.1, or to any bookseller.

The diffuse reflexion of silver atoms at a metallic target at high temperature

By S. Chomet, M.Sc., and J. Yarwood, M.Sc., F.Inst.P., The Mathematics and Physics Department, The Polytechnic, W.1

[*Paper received 22 June*, 1955]

Experiments on the diffuse reflexion of metallic atoms at solid surfaces have hitherto been conducted only with mercury and the alkali metals, and at target temperatures not exceeding 600° C. To study such reflexion at temperatures of about 1000° C, using silver atoms, a special type of atom "gun" has been constructed and an autoradiographic technique employed where the silver used was highly enriched with radioactive silver, ^{110}Ag. The measurements show that Knudsen's cosine law applies at these elevated temperatures.

If a beam of molecules or atoms is reflected from a surface, then specular reflexion will occur if

$$h \sin \theta < \lambda$$

where h is the average height of inequalities on the reflecting surface, θ is the angle of incidence of the beam measured from the plane of the reflector, and λ is the De Broglie wavelength of the particles in the beam.

In the case of a beam of molecules or atoms impinging on a plane surface where $h \sin \theta > \lambda$, diffuse reflexion occurs. Such surfaces will be those in which the atoms, ions or molecules are in strong thermal agitation (i.e. the surface temperature is high) or where adsorbed gas layers are present, or where the surface is macroscopically rough. If the reflector is macroscopically rough, the incident molecules or atoms will emerge from its hills and valleys in random directions. According to Knudsen,[1] there is then an equal probability of a reflected particle travelling in any direction away from the surface. Analytical consideration of this case gives rise to the Knudsen cosine law, conveniently put in the form

$$\frac{dn}{n} = \frac{d\omega \cos \theta}{\pi}$$

where dn/n is the fraction of the molecules or atoms reflected into a solid angle $d\omega$ in a direction making an angle θ with the normal to an element of the surface.

This law was first investigated experimentally by Wood[2] and independently by Knudsen.[3] Wood studied the reflexion of mercury atoms and also cadmium atoms from polished glass. The experiments with mercury were only qualitative but did indicate a general agreement with the cosine law. The experiments on cadmium gave quantitative results, because they included a photometric determination of the reflected deposit on a receiver cooled with liquid air, which showed that the cosine law was obeyed "within the probable error of the experiment." At about the same time (1915) Knudsen devised a very ingenious method of testing the cosine law for mercury reflected from glass. He considered a hollow sphere in which an element of the inner surface was emitting a number of atoms per second. Application of the cosine law led simply to the result that the number of atoms hitting unit area of the sphere per second had the same value all over the sphere. From a gravimetric examination of the distribution of deposited mercury, Knudsen concluded that the cosine law was obeyed within the limits of experimental error.

In 1930, Taylor[4] reported accurate experiments on the reflexion of lithium, potassium and caesium atoms from the cleavage planes of crystals of rock salt and lithium fluoride. The temperatures of the evaporator crucibles were in the range 450 to 900° K, and the De Broglie wavelengths in the region of 0·2 to 0·07 Å. The reflected alkali metal atoms were detected by means of a surface ionization gauge. The Knudsen cosine law was found to apply for all angles of reflexion to the normal from 30 to 88° with an accuracy of 0·01%. The only possible process by which this type of reflexion could have occurred was by adsorption followed immediately by re-evaporation.

To establish this last point experimentally, Cohen and Ellett[5] used a magnetic velocity analyser to determine whether a beam of potassium atoms reflected diffusely from a crystal of magnesium oxide had a distribution of velocities characteristic of the source of the beam or of the magnesium oxide target. Definite evidence of the latter gave strong support to the postulated mechanism of adsorption and quick re-evaporation.

In view of the importance of the techniques of the evaporation *in vacuo* of metals such as aluminium and silver, and because the experiments in verification of the cosine law have been confined, in the case of metal atoms, to mercury and the alkalis, with targets at temperature not exceeding about 600° C, the experiments to be described have been conducted using atomic beams of silver at temperatures of 1000 and 1150° C with a molybdenum target at a temperature of 1100° C.

The amount of silver reflected from the target was very small. The films of silver deposited on a cooled receiver were too thin for gravimetric or direct photometric assay; moreover detectors such as the surface ionization gauge cannot be readily used with silver, which has a higher first ionization potential than the alkali metals, and also condenses quickly on any solid surface at a temperature lower than that of the heated reflector target. The problem of detecting the small amounts of reflected silver deposited on the cooled receiver was therefore solved by using the radioactive isotope of silver, ^{110}Ag. An autoradiographic method of measurement could then be used. Such methods have, in addition to high sensitivity, an additional advantage in that any material recorded must be from the original source of silver and cannot be due to any contamination.

THE PRODUCTION OF AN ATOMIC BEAM OF SILVER

In the production of a molecular (or atomic) beam in which the distribution of energies is a known function of the temperature of the source, effusion conditions must be satisfied. This implies that the substance must be heated to a uniform temperature in a crucible which is closed except for an aperture through which the molecules emerge. Furthermore, the diameter of a circular aperture must be less than the mean free path of the evaporating molecules in the residual gas pressure prevailing so that inter-molecular collisions in the beam produced have only a small probability of occurrence.

According to Saha,[6] the mean free path of silver is given by

$$p\lambda = 10 \text{ cm (approximately)}$$

where p is the pressure in microns and λ is the mean free path in centimetres.

From Dushman,[7] the vapour pressures of silver in the temperature region employed are:

Temperature (°C)	1047	1184	1353
Vapour pressure (microns)	10	100	1000

It is seen that an effusion aperture diameter of 1 mm is just satisfactory if the temperature of the silver is not in excess of 1184° C, but that a diameter of 0·1 mm would be preferable.

The use of aperture diameters of only 0·1 mm restricted severely the amount of silver available in the beam. The atom "gun" used was therefore constructed in the form shown in Fig. 1.

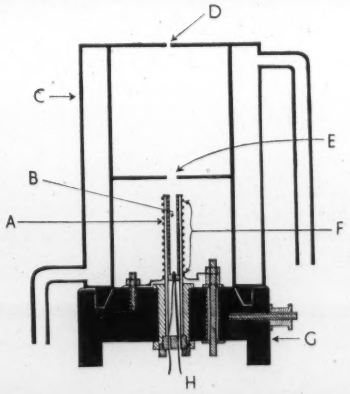

Fig. 1. Production of an atomic beam of silver atoms in the region of 1000° C

A, ceramic tube; *B*, carbon crucible; *C*, water-cooled heat shield; *D*, final aperture (1 mm diameter); *E*, intermediate aperture; *F*, tungsten wire heater; *G*, cylindrical steel block; *H*, thermocouple.

In the experiments it was essential to ensure a rigidly mounted evaporator crucible which was not moved or distorted on heating to temperatures in excess of 1000° C. To achieve this, the silver was placed in a cylindrical crucible of carbon (length: 24 mm; internal diameter: 3·5 mm) which was a close fit inside the upper half of a cylindrical ceramic tube. This ceramic tube was then mounted vertically in the central hole of a heavy, cylindrical, chromium-plated steel block (outside diameter of block: 8·5 cm) a tight fit being ensured, and a retaining steel ring being screwed in from the lower side of the block (Fig. 1). This steel block was then positioned in the centre of the vacuum chamber over the 2 in. diameter hole cut in the base plate where the oil diffusion pump was attached. Space around the base of the steel block, and a series of holes drilled through its thickness, enabled a low impedance to gas flow from the chamber to the pump to be maintained.

The electric heater was in the form of a tungsten wire 1 mm in diameter and 1 m long wound into a spiral closely round the outside of the ceramic tube. The free ends of this spiral were attached to steel terminals in the cylindrical steel block; one of them was earthed to the block and base plate and the other insulated by means of a small ceramic tube and mica washers. These terminals were then connected by a number of flexible copper strips to the main porcelain-insulated terminals which were inserted into the base plate, using O-rings for vacuum seals. Temperatures of the silver in the crucible of the order of 1000° C and above could then be maintained with currents of 15 to 20 A through the spiral.

To prevent the considerable heat radiated from the crucible from raising the temperature of the glass walls of the vacuum chamber, the crucible was surrounded by a heat shield in the form of a water-cooled, chromium-plated, steel jacket. Water cooling was found to be essential to prevent silver atoms which left the crucible from being reflected from the inner surfaces of the heat shield. Such reflected atoms collided with the beam emerging from the crucible and caused considerable departure from effusion conditions. With water cooling, most of the silver impinging on the heat-shield was condensed.

To define a beam, two apertures were supported by the heat shield, one intermediate aperture and a final top aperture of 1 mm diameter.

The temperature of the heated silver was measured by a calibrated platinum/13% rhodium–platinum thermocouple of which the junction was inserted into a small hole drilled in the base of the carbon crucible to give a very tight fit.

In preliminary experiments on the definition of the atomic beam of silver, a glass slide was mounted in the vacuum chamber vertically above the final aperture of the "gun" at a distance of 10 cm. If a carbon lid with a central $\frac{1}{2}$ mm diameter hole was put on the carbon crucible it was found that a spot of circular silver deposit about 1 mm in diameter could be obtained after a run of 3 to 10 min, depending on the temperature of the crucible. Subsequent experiments proved that the amount of silver available in such a beam was inadequate, so the crucible lid with $\frac{1}{2}$ mm aperture was omitted. The diameter of the silver spot obtained on the glass slide was then 5 mm approximately, and the sharpness of its edges indicated that effusion conditions were being maintained.

THE VACUUM CHAMBER, THE REFLECTOR AND THE RECEIVER

The vacuum chamber was in the form of a Pyrex glass cylinder 12 in. in diameter and 12 in. in height. L-section gaskets to a steel base plate and to a steel top cover plate ensured vacuum tightness and enabled a pressure of 10^{-5} mm

of mercury to be maintained by an oil diffusion pump and mechanical rotary pump combination.

The reflector was in the form of a strip of molybdenum 1 in. wide, 1·5 in. long and 0·0022 in. thick. This was mounted between steel clamps so that the reflector plane was at 60° to the horizontal (Fig. 2). Copper rods provided with cooling fins were screwed on to the steel rods to act as current

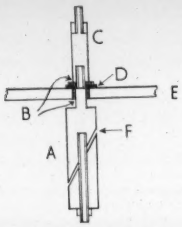

Fig. 2. Clamp for molybdenum strip target

A, steel; *B*, insulation; *C*, copper; *D*, rubber; *E*, top cover plate; *F*, one end of molybdenum strip clamped in slot at 60° to horizontal.

leads on the air side of the plate, O-ring vacuum seals being used. A current of 60 A. approximately through the molybdenum strip enabled it to be heated to a temperature of 1100° C, as determined by observation with an optical pyrometer through a central window in the cover lid.

By moving the top cover plate to the vacuum chamber, before pumping commenced, the centre of the molybdenum strip reflector could be arranged to be vertically above the final aperture of the atom "gun." Optical observation and an alinement mechanism were used to ensure accuracy in this respect.

After the beam was reflected from the heated strip, it was received on a glass plate (21·5 × 16·5 cm) in a vertical plane. This plate was kept cool by placing it in intimate contact with the surface of a water-cooled, flat, copper box, let through a Wilson seal in the top cover plate (Fig. 3). The temperature of this box was 15° C, as recorded by a copper-constantan thermocouple. The shortest distance between the centre of the molybdenum reflector strip and the glass plate was 9·50 cm.

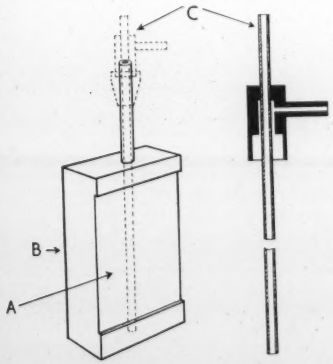

Fig. 3. Water-cooled box for supporting flat glass plate

A, glass plate clamped to this surface; *B*, copper box; *C*, arrangement for inlet and outlet of cooling water.

AUTORADIOGRAPHIC METHOD OF MEASURING THE DEPOSITED SILVER

The silver ^{110}Ag used was in the form of pieces of 1 mm diameter wire which had been irradiated in the Harwell pile for one week. The specific activity was then 320 microcuries per gram. Since ^{110}Ag has a half-life of 270 days, it is very convenient for this type of work. It emits β- and γ-radiation, the energies being β: 0·087 MeV (58%); 0·53 MeV (35%); 2·12 MeV (3%); 2·86 MeV (3%). γ: 10 lines over the range from 0·166 to 1·516 MeV.

The silver deposited on the cooled receiver plate after a run of some 7 hours was in the form of a thin film barely discernible by the naked eye. After removal from the vacuum chamber, this glass plate was placed with the silvered side in intimate contact with X-ray film (Ilfex film, by Ilford Ltd.), and wrapped in black paper. After an exposure of 14 days, the developed film gave minimum optical density readings of 0·3. According to Yagoda,[8] the blackening of the developed plate is very nearly proportional to the activity of the deposit, and hence to the mass of the radioactive silver, for densities above 0·3.

The optical density was measured by a Baldwin densitometer at equal intervals along the axis of symmetry of the plate (the vertical central axis for the plate when in the vacuum chamber). Readings were excellently reproducible. Davenport and Stevens[9] report that the autoradiographic method compares well with methods using counters.

THE GEOMETRY OF THE ARRANGEMENT OF SOURCE, REFLECTOR AND RECEIVER

To relate the observed optical density measurements to the reflexion conditions prevailing in the experiment, consider Fig. 4.

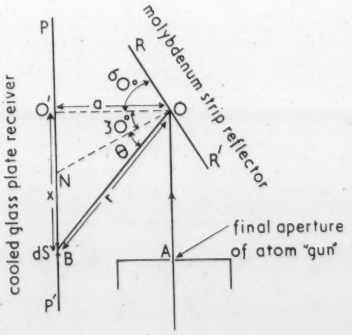

Fig. 4. Illustrating geometry of source, reflector and receiver

Suppose AO represents the incident vertical beam of silver atoms, and assume the cross-section of the beam is small. RR' represents the heated reflector, i.e. the molybdenum strip, assumed to be perpendicular to the plane of the paper. Consider an element of area dS at B on the receiver plane PP' (also perpendicular to paper plane) at a distance x below O', where O is the centre of the reflector RR' and OO' is perpendicular to PP'. The angle that the reflector makes with the horizontal was kept at 60° in the experiments, i.e. angle $O'OR$ was 60°. From O, a normal to RR' is drawn to meet PP' at N. Let the angle NOB be θ.

If the Knudsen cosine law is obeyed, then the amount of silver reaching dS must be proportional to $d\omega \cos\theta$, where $d\omega$ is the elementary solid angle subtended by dS at O. If $OO' = a$, then the distribution of the silver along the line PP' is such that the amount deposited on unit area around B is proportional to

$$\frac{\cos\theta \cos(\theta + 30^\circ)}{r^2} \quad \text{where } OB = r.$$

But $r^2 = a^2 + x^2$,

$$\cos(\theta + 30^\circ) = a/r$$

and $$\cos\theta = \frac{1}{r}[a \sec 30^\circ + (x - a \tan 30^\circ) \sin 30^\circ]$$

Therefore, after substitution, it is seen that the amount of silver per unit area at a distance x below O' is proportional, for a fixed value of a, to

$$(\sqrt{3}a + x)/(a^2 + x^2)^2$$

RESULTS

To determine whether the Knudsen cosine law applies, a theoretical curve derived from the above simplified expression was plotted. This was done by inserting $a = 9{\cdot}5$ cm (the distance used in all the experiments) into this equation, and, for convenience only, the figures obtained were "normalized" by multiplying them by a constant k such that

$$k\left[\frac{\sqrt{3}a + x}{(a^2 + x^2)^2}\right]_{max} = 41$$

This curve was then compared with the experimental results obtained, assuming the optical density of every point on the X-ray film (provided a correction is made for the unexposed film) is directly proportional to the mass of silver per unit area at the corresponding point on the glass plate. With the molybdenum strip reflector at 1100° C, and the crucible source of silver atoms at 1000° C, good agreement was obtained between the experimental curves and the theoretical one, except that the experimental curves were slightly narrower near the peak values than the theoretical curve (Fig. 5). This is probably due to the fact that the reflecting molybdenum strip expanded when heated between rigidly fixed supports and was always slightly concave rather than plane.

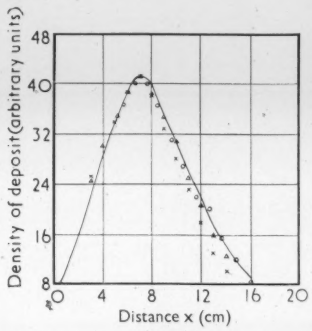

Fig. 5. Comparison of theoretical and experimental curves

——— theoretical curve;
○ × △ experimental points;
molybdenum reflector at 1100° C;
source of silver at 1000° C.

The conclusion is that the Knudsen cosine law is correct in the case of the reflexion of an atomic beam of silver atoms with a temperature of 1000° C impinging at an angle of incidence of 60° from the normal on a molybdenum target at 1100° C.

REFERENCES

(1) KNUDSEN, M. *Kinetic Theory of Gases* (London: Methuen and Co. Ltd., 1952).

(2) WOOD, R. W. *Phil. Mag.*, **30,** p. 300 (1915); **32,** p. 364 (1915).

(3) KNUDSEN, M. *Ann. Phys.* [*Leipzig*], **48,** p. 1113 (1915).

(4) TAYLOR, J. B. *Phys. Rev.*, **35,** p. 376 (1930).

(5) COHEN and ELLETT. *Phys. Rev.*, **52,** p. 509 (1937).

(6) SAHA and SRIVASTAVA. *A Treatise of Heat* (Allahabad: The Indian Press, 1950).

(7) DUSHMAN, S. *Scientific Foundations of Vacuum Technique* (New York: John Wiley and Sons, Inc., 1949).

(8) YAGODA, H. *Radioactive Measurements with Nuclear Emulsions* (New York: John Wiley and Sons, Inc., 1949).

(9) DAVENPORT and STEVENS. *Brit. J. Appl. Phys.*, **6,** p. 31 (1955).

Air circulations about a vibrating plate

By Mary D. Waller, Ph.D., F.Inst.P.,* London

[*Paper received* 10 *June*, 1955]

Fine powders are employed, as in Faraday's experiments, to observe the air circulations above a vibrating plate. The surface streaming, which occurs away from nodal lines and also inwards from the edges, is recorded by means of a mixed heterogeneous powder. Surface streamings from the side edges of a bar give rise to four circulations; compare results of other experiments in which there is relative oscillatory motion between a solid, e.g. a cylinder or reed, and a fluid. The senses of these circulations are, in the present instance, the same as those of Andrade's four-fold smoke vortices.

The circulations which occur as the result of relative oscillatory motion between solids and fluids is a subject which has lately attracted considerable attention, as, for example, in the recent discussion on first and second viscosities.[1]

But Faraday's experiments[2] on the movements of air above a vibrating plate, as watched or recorded by means of fine powders, are seldom referred to and observations based on his method are our present concern. For although information on the circulations around cylinders and spheres, disks and small reeds are more suitable for the theoretical development of the subject, studies of vibrating plates, or plate-like bodies, are of interest in connexion with the increasingly large number of practical problems which arise under hydraulic loose-boundary conditions.

The theory which is discussed in the report mentioned above derives largely from Rayleigh's paper,[3] in which is included a formal section diagram of circulation above a vibrating plate. The air, after leaving the surface at an antinode, proceeds towards the nodes on either side and returns along the surface to the point from which it started. This general circulation (compare Kundt's tube) is quite different from the sonic air vibration. Fig. 1(*a*) of the present paper, which shows the circulation below as well as above the plate, emphasizes that the diagram is only applicable to an interior vibrating segment. In practice, there are usually also edge effects to be considered, as suggested by the section diagram of Fig. 1(*b*).

Powders as Indicators of the Circulation and of the Surface Streaming

Distinction must be made between powders which may be used to observe the circulations of air and those which are suitable for obtaining a permanent record of the surface streaming.

Any of Faraday's "fine" powders, and many others, have been found suitable for the first purpose. A fine powder, for use with Chladni plates, may be defined as one in which the peak diameter of the particles is not far removed from the smallest sieve sizes, say about 55 μ. The fineness which is desirable increases with the frequency, but in the case of powders deemed "light," which term includes such properties as the shape, porosity and surface texture of the particles, in addition to the density of the solid matter, the fineness may be reduced without loss of efficiency. (We may note that since no two powders behave exactly in the same way above a vibrating plate, these circulation experiments provide a possibly useful method of studying the properties of powders; this is now being investigated.)

During the vibration a suitable powder forms a large revolving cloud with the air in each of the segments of the plate, the sense of which is in accordance with Fig. 1. Though gravity effects on the powder movements must not be ignored, it is generally clear that the distance which the

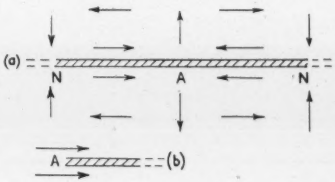

Fig. 1. (*a*) Circulations associated with one interior segment of a vibrating plate. (*b*) Surface edge streaming

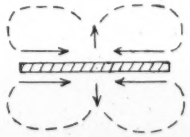

Fig. 2. Vertical section, illustrating streaming from sides but not from ends or nodes of a vibrating bar

air moves away from the surface is less than its travel in horizontal directions. Compare "quartz wind" which, formed at *ultrasonic* frequencies, is characterized by the streaming away from the surface.

As the vibration dies away the cloud diminishes in size; but it is noteworthy that final concentration into one or several or many small "humps" is occasioned by secondary reactions between the powder particles which would not exist on the bare plate. [This phenomenon, discernible in Fig. 4 (p. 350), is now receiving separate attention.]

For purposes of recording surface streaming the powder must be chosen much more carefully. Faraday's drawings illustrate the use of lycopodium spores, used also for the figure just mentioned, which are spheres about 20 μ in diameter. Heterogeneous fine powders of medium density, the particles of which are of irregular shapes, tend to move more sluggishly along the surface and to leave more noticeable tracks than a uniform powder. The present author has used heavy powders mentioned by Faraday, including

* Formerly at Royal Free Hospital School of Medicine, London.

stannic oxide (which is white and excellent for photographic purposes) and iron, but has adopted fine sand or silt (which can be collected at various peak fineness in any quantity at river estuaries) in preference to his powdered glass and silica. Portland cement, Gregory powder, and cork filings (which may be coarser) are among the other powders which have also been found useful. Best of all are powder *mixtures* which contain a considerable amount of dust in the sub-sieving range. Of these, dust from bomb explosions has proved superior to anything else so far tried. Records obtained with it (after removal of larger particles with suitable sieves) are to be seen in Figs. 3 and 5 (p. 350).

SURFACE STREAMING FROM NODAL LINES AND FROM EDGES

Fig. 3 shows surface streaming towards an interior point on the antinodal diameter of one of the four quadrants of a circular brass plate which was supported centrally and which, when excited by bowing, vibrated at 180 c/s. It will be observed that the streaming occurs inwards from the periphery, which includes the vibration of greatest amplitude, as well as away from the two nodal diameters.

The magnitude of the hydrodynamic forces involved at the periphery may be appreciated by repeating the experiment in which Faraday removed powder from the straight edge of a stationary surface on to a vibrating square plate, one side of which was situated parallel and near to it.

On narrower plates the edge streaming becomes even more prominent and the powder pattern then bears very little relation to the antinodal lines (referred to as "loops" in Rayleigh's paper). See, for instance, the rectangles of Fig. 4 (p. 350) where the two bands of unmoved lycopodium denote the two nodal lines of the 2|0 mode for which the ends and shorter median are antinodal. See also Fig. 5 which includes the central and part of the right-hand side of a 6 × 1 rectangular plate (3|1 mode, 330 c/s)

COMPARISON WITH OTHER CIRCULATION EXPERIMENTS

We may end this paper by pointing out the connexion between the present observations and those of other "circulation" experiments in which there are not (as in Kundt's dust tube or in most quartz wind experiments) any fixed boundaries.

Consider the case of a very narrow rectangle, in fact a free-free bar, which vibrates as in Fig. 4 (see legend). Then the vibration of the portion between one end and the nearest nodal line is similar to that of a free-fixed bar, which, if its dimensions are greatly reduced, becomes comparable to the vibrating reed of West's[4] or of Ghabrial and Richardson's[5] experiments. A vertical section through the powder concentration, at right angles to the length, includes the streaming from the two side edges, but not that from the free end or the nodal line (see Fig. 2). The senses of the four circulations shown will be recognized as being the same as those of West's four outer smoke vortices (compare also Skogen[6]), i.e. the same as in Andrade's[7] and Schlichting's[8] well-known photographic records of fourfold fluid vortices.

REFERENCES

(1) Rosenhead, L., Chairman of conference, and others. *Proc. Roy. Soc. A*, **226**, p. 1 (1954).
(2) Faraday, M. *Phil. Trans*, **121**, p. 299 (1831).
(3) Rayleigh, Lord. *Phil. Trans A*, **175**, p. 1 (1884).
(4) West, G. D. *Proc. Phys. Soc.* [*London*] *B*, **64**, p. 483 (1951).
(5) Ghabrial, A. M., and Richardson, E. G. *Acustica*, **5**, p. 28 (1955).
(6) Skogen, N. *K. Norske Vidensk. Selsk. Fördhandl.*, **24** p. 60 (1952).
(7) Andrade, E. N. da C. *Proc. Roy. Soc. A*, **134**, p. 4[illegible] (1931).
(8) Schlichting, H. *Phys. Z.*, **33**, p. 327 (1932).

Plastic flow in coal

By P. C. Newman, M.A., A.Inst.P.,* National Coal Board, Central Research Establishment, Stoke Orchard, Glos.

[*Paper first received* 25 *February, and in final form* 29 *April*, 1955]

During briquetting of coal, conditions favourable to plastic flow may be developed by the non-uniform stress system. Photographs of particles of coal removed intact from both rock salt and coal briquettes show that plastic flow has occurred at moderate briquetting pressures.

Much work has been done on the induction of plastic behaviour in materials which are normally considered brittle. Bridgman[1] has observed extensive plastic flow in corundum, rock salt and other materials, in the presence of very high pressures, applied hydrostatically. King and Tabor[2] have shown plastic flow of rock salt during Vickers pyramid hardness testing, whilst the use of potassium bromide for infra-red spectroscopy[3] depends on developing plastic properties in the material. Some results are now reported on inducing and observing extensive plastic flow in coal, which depends, like the above results, on the superposition of hydrostatic pressure on a non-uniform stress pattern.

Coal can be classed as a brittle material, being unable to suffer any permanent deformation without failure, when tested on a large scale in the normal manner. However, plastic flow of micron-sized particles has been observed[4] which leads one to expect a similar result on a larger scale under suitable conditions. The work reported here was carried out as an aid to understanding the processes occurring during the briquetting of coal, and this determined the techniques that were used.

During the formation of a briquette, any one particle of coal is stressed by the forces applied to it by its neighbours. It is generally legitimate to consider these stresses to consist of a hydrostatic pressure (equal to the mean normal stress along the axis of the briquetting plunger) to which are added particular non-uniform stresses. The calculation of these non-uniform stresses in one particle can not be attempted,

* Now at Mullard Research Laboratories, Salfords, Surrey.

unless the shapes and positions of its neighbours are known. However, due to the angularity of coal particles, it can be seen that some very high stresses may be developed.

A briquette, then, forms a system in which plastic flow of the normally brittle coal material may be expected to occur. In order better to observe any plastic deformation which might occur, a very few pieces of coal may be included in a briquette made from a transparent substance having about the same hardness as coal. If the substance is also easily soluble in a liquid which does not attack coal, the investigation is made simpler. This combination of requirements points to one of the alkali halides as the most suitable briquetting material.

Rock salt briquettes were made containing a few pieces of Windsor (301) or Sherwood (702) coal ($-30 + 36$ B.S.S., i.e. of about 0·5 mm size). Rock salt was chosen as the best edge-on in the photograph, and part (*c*) shows the cratered silhouette typical of particles after briquetting. A typical particle before briquetting is shown in part (*a*) for comparison.

Since these particles were briquetted individually in salt, and were found to be coherent afterwards, it is supposed that the deformation was produced by plastic deformation, and not by shattering followed by agglomeration.

Some briquettes were also made of -30 B.S.S. coal at $1{\cdot}55 \times 10^3$ kg/cm^2 with no binder, and subsequently disintegrated in ethyl alcohol. This disintegration occurs with many organic liquids and appears to separate each individual coal particle. The $+60$ B.S.S. fraction (i.e. those particles above 0·25 mm in size) from the disintegrated briquette showed the same evidence of plastic deformation as the particles from the rock salt briquettes, in a substantial proportion of the particles.

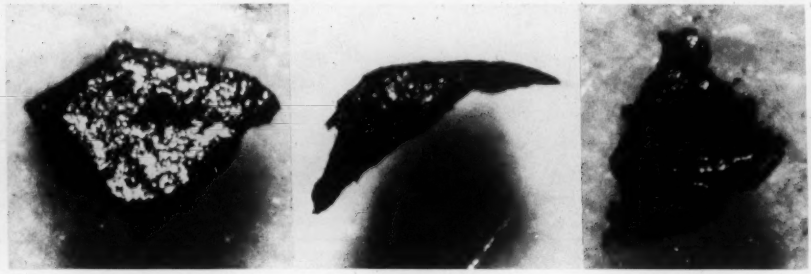

(*a*) (*b*) (*c*)

0·5 mm particles of Windsor coal

(*a*) Before briquetting. (*b*) Briquetted in rock salt at 10·85 kg/cm^2. (*c*) Briquetted in rock salt at 1·55 kg/cm^2.

compromise between salts that were softer than coal and easily gave transparent briquettes, such as potassium bromide, and those that were harder, but gave opaque briquettes, such as calcium chloride. However, it was not possible easily to distinguish the shape of the coal particles while still in the briquette, so the rock salt was dissolved in warm water and the coal particles washed in ethyl alcohol (the effects of ethyl alcohol are described below).

The evidence for plastic deformation is most convincingly presented in a three-dimensional display; in stereographic projection, for instance, the characteristic cavities in the coal are clearly seen, sometimes close together so that they are separated by thin vertical walls, and sometimes the coal is pierced through. In a two-dimensional display the best evidence is to be seen in the silhouette. In the figure, particles of Windsor coal about 0·5 mm in size are shown, the projection system being selected to give a large depth of focus. Parts (*b*) and (*c*) of the figure show coal after being briquetted in rock salt at 10·85 and $1{\cdot}55 \times 10^3$ kg/cm^2 respectively. It may be seen that the right-hand end of the particle in part (*b*) has been deformed into a broad curved tail, viewed

It is clear from this evidence that a high degree of plastic flow occurs in any coal briquetting process, even at relatively low pressures.

ACKNOWLEDGEMENTS

The permission of the Director-General of Research, National Coal Board, to publish this article is gratefully acknowledged. The opinions expressed are those of the author and not necessarily those of the Board.

REFERENCES

(1) BRIDGMAN, P. *Large Plastic Flow and Fracture* (New York: McGraw-Hill Book Co., Inc., 1952).
(2) KING, R. F., and TABOR, D. *Proc. Roy. Soc. A*, **223**, p. 225 (1954).
(3) GORDON, R. R., ADAMS, W. N., PITT, G. J., and WATSON, G. H. *Nature* [*London*], **174**, p. 1098 (1954).
(4) BANGHAM, D. H., and BERKOWITZ, N. *Coal Research*, p. 139 (1945).

Air circulations about a vibrating plate

By M. D. WALLER, Ph.D., F.Inst.P.

See pages 347–348

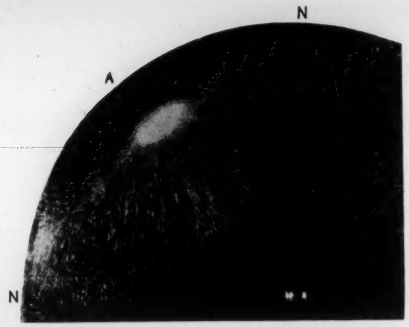

Fig. 3. Surface streaming from two nodal diameters and edge in one quadrant of a circular plate, 180 c/s (×0·5)

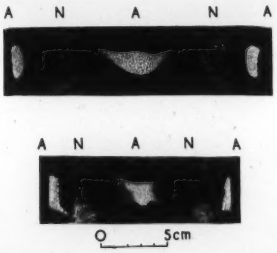

Fig. 4. Surface streaming on rectangular plates, 2|0 mode, 280 and 370 c/s respectively

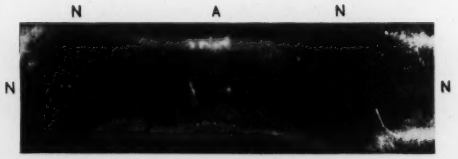

Fig. 5. Part of 6 × 1 rectangular plate, 3|1 mode, 330 c/s (×0·24)

The determination of the order of interference in white light

By R. C. Faust, M.Sc., Ph.D., A.Inst.P., and H. J. Marrinan, B.Sc., Ph.D., The British Rayon Research Association, Manchester

[*Paper first received* 3 *June, and in final form* 14 *July*, 1955]

The achromatic fringe observed in white light does not necessarily correspond to the position of zero path difference, the reason being that the optical paths of the two interfering beams do not usually have the same wavelength dispersion. A general theory of this effect is presented, and it is shown how it can be applied to a Rayleigh interference refractometer, a Babinet compensator, and an interference microscope. Experimental verification of these predictions is given.

1. Introduction

Many routine laboratory measurements employ optical instruments that depend for their operation upon the interference of two coherent light waves. The interference fringes formed in monochromatic light are indistinguishable one from another and, consequently, it is not normally possible to tell through how many orders the fringe system has been displaced when the phase difference between the two beams is suddenly altered. It is therefore customary to use white light in order to identify the zero-order fringe. This method is, however, uncertain, because the zero-order fringe will coincide with the position of strict achromatism only when the optical paths of the two beams have the same wavelength dispersion. This condition is not usually satisfied and there is thus a possibility of introducing an error. This was recognized by Airy[1] as early as 1833 and has since been appreciated by users of Jamin and Rayleigh interference refractometers. The general occurrence of this phenomenon has not, however, been fully realized. The first part of this paper, therefore, deals with the problem as presented by the interference refractometer, and the second part shows how this same treatment can be applied to other interference apparatus; particular reference is made to the Babinet compensator and to the Baker interference microscope.

2. Interference Refractometers

To this class of instrument belong the Jamin and the Rayleigh–Haber–Löwe interferometers,[2] in which a single light beam is split into two spatially separated beams represented in Fig. 1(*a*) by the wavefronts W_1 and W_2. One beam passes through a cell containing the medium under examination, whilst the other passes through an identical cell containing the comparison medium. The two beams are then re-united so as to form a fringe system.

When the cells contain identical media, the compensator is adjusted until the zero-order achromatic fringe seen in white light coincides with the centre of the field of view. (In the Rayleigh interferometer, the centre is defined by the achromatic fringe of a fiduciary system formed by the interference of two beams originating from the slits S_1 and S_2 but passing below the cells and the compensator plates.) If the index of the medium in one of the cells is then altered, the fringe system will undergo a displacement, and the compensator is therefore adjusted until an achromatic fringe is once again seen at the centre of the field of view. Unfortunately, this adjustment does not provide an unambiguous measurement of the displacement of the zero-order fringe. The reason for this is that the wavelength dispersion of the path difference introduced by the compensator is not usually the same as the dispersion of the path difference introduced by the two cells, and the achromatic fringe need not, therefore, necessarily coincide with the zero-order one.

A search of the literature suggests that Siertsema,[3] in 1890, was the first to observe the difference between the positions of the zero-order and achromatic fringes in this type of interferometer. Hallwachs[4] later made some

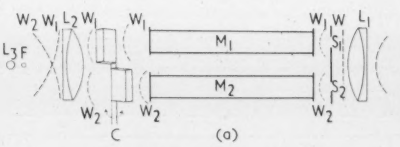

Fig. 1(*a*). Rayleigh refractometer (plan view)

S, slit source; S_1, S_2, parallel slits; M_1, M_2, identical cells; L_1, L_2, spherical lenses; *F*, focal plane of L_2; *C*, tilting compensator; L_3, cylindrical viewing lens; *W*, incident wavefront; W_1, W_2, wavefronts arising at S_1, S_2.

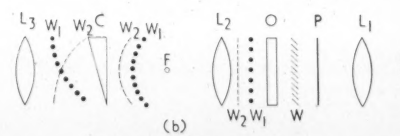

Fig. 1(*b*). Babinet compensator

S, source; L_1, collimating lens; *P*, polarizer; *O*, object; L_2, objective; *F*, back focal plane of L_2; *C*, quartz wedge compensator; L_3, eyepiece; *W*, incident wavefront; W_1, W_2, wavefronts leaving the object.

independent observations from which he was able to calculate the dispersion of the refractive index difference between the liquids in the two cells. Since these early experiments numerous workers have encountered this "jumping" of the position of the achromatic fringe.

The first mathematical treatment was by Adams,[5] but it unfortunately suffers from obscure reasoning and unwarranted assumptions. Although a satisfactory theory was later presented by Clack,[6] the equations were expressed in a form especially suitable for a Rayleigh interferometer with a tilting plate compensator, and in this way the general application to other forms of interference equipment was lost. The relevant equations are therefore derived for an interference refractometer with an arbitrary type of compensator.

Theory. At a distance X from the centre of the field of view, the phase difference between the two interfering beams is

$$\phi = (2\pi/\lambda)(qX - P) \tag{1}$$

Here q is an instrumental constant, P is the excess of path 2 over path 1 in passing through the cells and the compensator, and λ is the vacuum wavelength of the light. The experiment begins with identical media in the two cells and with equal compensator thicknesses in the two beams (i.e. $P = 0$). The zero-order fringe, defined by the condition $\phi = 0$, is then found at $X = 0$. Since this is true for all wavelengths, the zero-order fringe is achromatic. The refractive index of the medium in one of the cells is then changed, whereupon the zero-order fringe for wavelength λ is displaced to the point X_λ given by the expression

$$qX_\lambda = N_\lambda\lambda = (\mu_2 - \mu_1)l \tag{2}$$

where l is the cell length, and μ_1, μ_2 are the appropriate refractive indices of the media in the two cells. Ideally one would like to rotate the compensator drum until the zero-order fringe is again brought to the centre of the field of view; the drum reading, calibrated in terms of the wavelength λ, would then indicate a fringe displacement of N_λ orders as defined by equation (2). In general, however, one can only bring the achromatic fringe to the centre; the drum reading then indicates a fringe displacement of N_A orders for the wavelength λ.

A point in the fringe system may be regarded as achromatic provided that $d\phi/d\lambda = 0$ for some wavelength near the centre of the visible spectrum. (In the calculations below the sodium D line is selected, but the best choice of wavelength will depend upon the nature of the white-light source and the spectral sensitivity of the eye.) From equation (1) the co-ordinate X_A of the achromatic point is then found to be given by

$$qX_A = P - \lambda P' \tag{3}$$

where the dash notation denotes differentiation with respect to the wavelength. The achromatic position will therefore coincide with the centre of the field when $P = \lambda P'$. Under these conditions the zero-order fringe will have the co-ordinate X_0 determined by

$$qX_0 = P = \lambda P' \tag{4}$$

Consequently the desired fringe displacement, N_λ, is related to the measured one, N_A, by the expression

$$N_\lambda - N_A = P/\lambda = P' \tag{5}$$

The path difference P has the value

$$P = (\mu_2 - \mu_1)l - p \tag{6}$$

where p is the excess optical thickness of the compensator in beam 1. The expression for p depends upon whether the non-tilting or the tilting type of compensator is under discussion.[7] The first type consists of a fixed plate in one beam and a plate of variable thickness (two opposing wedges) in the other; the light usually falls upon the plates at normal incidence. The expression for p is then

$$p = (\mu_G - \mu_S)t \tag{7}$$

where t is the excess thickness of compensator in beam 1, μ_G is the refractive index of the compensator glass and μ_S that of the atmospheric surroundings. In the second class one or both of two equally thick plates can be so tilted as to alter the angle θ between the light beam and the normal to the plate. In this case p is dependent upon the angles θ_1 and θ_2 of the two plates as well as upon the refractive indices of the compensator glass and of its surroundings. Equation (7) will represent the action of this compensator provided that the symbols are redefined: the excess thickness t is equal to the actual thickness of the compensator plates, and the effective refractive index difference $(\mu_G - \mu_S)$ is a function of the angles θ_1 and θ_2.

One can now calculate from equations (3), (6) and (7) the compensator thickness t_A required in order to bring the achromatic position of the interference pattern back to the centre of the field. The result is

$$t_A[(\mu_G - \mu_S) - \lambda(\mu_G' - \mu_S')] = l[(\mu_2 - \mu_1) - \lambda(\mu_2' - \mu_1')] \tag{8}$$

the dash notation still signifying differentiation with respect to wavelength. It is thus seen that the achromatic position will lie at the centre of the field provided that the two interfering beams travel paths of equal "optical thickness," the "optical thickness" being here calculated from the group refractive indices[8] and not from the phase indices $(\mu_G - \mu_S)$ and $(\mu_2 - \mu_1)$.

Substitution of the above value of t_A in equations (5), (6) and (7) leads to

$$N_\lambda - N_A = P/\lambda = l(\mu_2 - \mu_1)\left[\frac{\mu_2' - \mu_1'}{\mu_2 - \mu_1} - \frac{\mu_G' - \mu_S'}{\mu_G - \mu_S}\right]\left[1 - \lambda\frac{(\mu_G' - \mu_S')}{\mu_G - \mu_S}\right]^{-1} \tag{9}$$

This gives the difference between the positions of the zero-order fringe and the achromatic fringe in terms of the optical properties of the compensator and the liquids. By employing the Cauchy dispersion formula $[\mu = a + (b/\lambda^2)]$ one can obtain an equation from which the differential coefficients have been eliminated, namely

$$N_\lambda - N_A = -\frac{2N_\lambda}{\lambda^2}\frac{\lambda_C^2\lambda_F^2}{\lambda_C^2 - \lambda_F^2}(\tau - \tau^*)\left[1 + \frac{2}{\lambda^2}\left(\frac{\lambda_C^2\lambda_F^2}{\lambda_C^2 - \lambda_F^2}\right)\tau^*\right]^{-1} \tag{10}$$

Here τ is the relative dispersion of the refractive index difference $(\mu_2 - \mu_1)$ of the media in the two cells; that is

$$\tau = \frac{(\mu_2 - \mu_1)_F - (\mu_2 - \mu_1)_C}{(\mu_2 - \mu_1)_\lambda} \tag{11}$$

The quantity τ^* is defined by an analogous equation in $(\mu_G - \mu_S)$. If λ is the sodium D line equation (10) becomes

$$N_D - N_A = -3{\cdot}01\,N_D(\tau - \tau^*)(1 + 3{\cdot}01\tau^*)^{-1} \tag{12}$$

If τ and τ^* were equal, then $(N_\lambda - N_A)$ would vanish and the achromatic fringe would also be the zero-order one. Different pairs of liquids do, however, possess such widely differing values of τ that it is not possible to design a compensator that will always fulfil the condition $\tau = \tau^*$.[7] Because of these difficulties Geffcken and Kruis[9] have dispensed with the use of white light. They have shown that it is possible to determine in monochromatic light the order of interference for a short (1 cm) cell provided that the cell can be gradually inclined relative to the incident light beam. This information permits them to predict the interference order for a longer cell; the prediction is then used

as a guide for the accurate experimental determination of this order. The method allows one to employ interference over several thousand orders, thereby greatly increasing the accuracy of the measured refractive index difference $(\mu_2 - \mu_1)$.

Application. The isotopic exchange reaction between deuterium oxide and the hydroxyl groups of cellulose,

$$3D_2O + 2R(OH)_3 \rightleftharpoons 2R(OD)_3 + 3H_2O$$

has been used to estimate the accessibility to water of various forms of cellulose.[10, 11] In these experiments the amount of H_2O in the D_2O after deuteration was measured by a density method, but Crist, Murphy and Urey[12] have shown that the Rayleigh refractometer can be used to estimate the amount of H_2O in water-heavy water mixtures with a precision equal to that obtainable with careful pycnometer methods. Accordingly the Rayleigh refractometer has been used in these laboratories.[13]

To calibrate the refractometer D_2O was placed in both cells and the compensator adjusted so that the achromatic fringe was coincident with the achromatic fringe of the fiduciary system. Under these conditions the achromatic fringe was also the zero-order fringe. H_2O was then slowly added to one of the cells and at the same time the zero-order fringe was kept central by turning the compensator. With increasing concentration of H_2O, the zero-order fringe gradually became coloured and an adjacent one became achromatic. Setting on this latter fringe would therefore have produced an error of one fringe in the zero-order shift. Further "fringe jumps" were observed as the concentration of H_2O was gradually increased. At each concentration readings were taken of the zero-order and the achromatic fringe positions, the results being shown in Fig. 2.

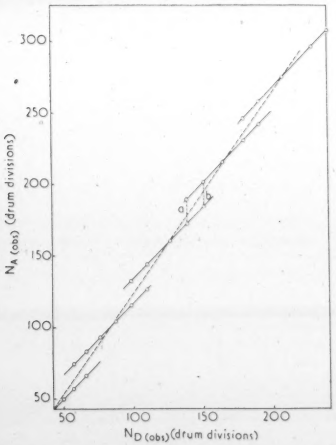

Fig. 2. Relationship between N_A(obs.) and N_D(obs.) for D_2O, H_2O mixtures

From equation (12) it can be seen that in theory a plot of N_A against N_λ would produce a straight line, such as the dotted one in Fig. 2, provided that both τ and τ^* are independent of N_λ. In practice, however, a regular series of straight lines of equal slope were obtained. These discontinuities arose because, although the true achromatic position did not usually coincide with a fringe, the observer considered the achromatic position to be determined by the most nearly achromatic fringe; when it was impossible to decide which of the two fringes was the least coloured, two readings were possible, e.g. region *ab* of Fig. 2. Since these discontinuities occurred approximately every three fringes, neglect of the "fringe jumping" would have led to appreciable errors.

From the linear form of Fig. 2 it must be concluded that $(\tau - \tau^*)$ was constant over the concentration range covered experimentally ($0 - 2\%$ H_2O). The measurements described above were carried out on a refractometer built by A. Hilger Ltd. This instrument incorporates a tilting plate compensator for which τ^* is a function of the angles θ_1 and θ_2, and therefore of the order N_λ. However, the maximum rotation of the compensator during these measurements was only 2°, and calculations have shown that the resultant variation of τ^* was sufficiently small (about 1%) for τ^* to be considered a constant of value 0·0080. Consequently τ itself can be regarded as constant. A constant value of τ is to be expected because one can reasonably assume that D_2O, H_2O mixtures obey the Gladstone–Dale refractivity addition formula

$$V(\mu - 1) = V_\alpha(\mu_\alpha - 1) + V_\beta(\mu_\beta - 1) \qquad (13)$$

and the volume addition formula

$$V = V_\alpha + V_\beta \qquad (14)$$

Under such conditions the value of τ is given by

$$\tau = \frac{(\mu_\alpha - \mu_\beta)_F - (\mu_\alpha - \mu_\beta)_C}{(\mu_\alpha - \mu_\beta)_\lambda} \qquad (15)$$

and is hence independent of the volume ratio V_α/V_β of the components.

It is now possible to use Fig. 2 and the known value of τ^* in order to calculate τ from equation (12); this gives $\tau = 0{\cdot}131$. In the experiment quoted above an excess of D_2O was present and this would react with the H_2O as follows

$$D_2O + H_2O \rightarrow 2HDO$$

Thus, the calculated value of τ is, in fact, that for a D_2O, HDO mixture. However, if it is assumed that the refractive index and dispersion of HDO lie midway between those of H_2O and D_2O, this value of τ is also that for a D_2O; H_2O mixture. This assumption was made in order to calculate the dispersion of D_2O from the known dispersion of H_2O, and a value of $0{\cdot}0053_9$ was found.

3. BIREFRINGENCE MEASUREMENTS

Fig. 1(*b*) illustrates the usual optical arrangement for the determination of the birefringence of a specimen. The birefringent compensator is so placed that its fast direction is parallel to the slow direction of the specimen, the latter being at 45° to the polarizer direction. The two beams (W_1, W_2) leaving the specimen are distinguished by their states of polarization and not necessarily, as in the Rayleigh refractometer, by any spatial separation. The resultant interference pattern, viewed on a plane conjugate to the specimen plane, is formed by components of these beams transmitted through an analyser.

It is possible to apply the equations of Section 2 to the present problem simply by redefining the terms: $(\mu_2 - \mu_1)$

is now the birefringence $\Delta\mu$ of the specimen, and $(\mu_G - \mu_S)$ is the effective birefringence $\Delta\mu^*$ of the compensator. [As with the refractometer there are tilting (e.g. Berek) and non-tilting (e.g. Babinet) compensators.] Equations (10), (11) and (12) are now applicable provided it is understood that τ and τ^* are now the relative dispersions of birefringence for the specimen and the compensator; that is, with sodium D radiation $\tau = (\Delta\mu_F - \Delta\mu_C)/\Delta\mu_D$, which is the relative dispersion of birefringence as introduced by Ehringhaus.[14]

The achromatic position and the zero-order fringe will not coincide unless $\tau = \tau^*$, a condition which is not usually fulfilled. There are, however, few references in the literature to observations of "fringe jumping" with birefringent compensators. The probable reason is that the majority of specimens examined under the microscope are thin and the order of interference N_λ is accordingly small. Nowadays, however, the laboratory worker in the macromolecular field is presented with large diameter fibres or thick plastic sheets prepared from materials of relatively high birefringence (e.g. rayon 0·03, Nylon 0·06, Terylene 0·2), and "fringe jumping" is much more likely to be encountered.

The use of a compensator of the same material as that under study will not always eliminate this "jumping." This is particularly well illustrated by the work of Savur[15] who was studying the birefringence of a strip of celluloid as a function of the strain. He realized that the use of white light with a quartz Babinet compensator would not yield a reliable figure for the order of interference. A compensator was therefore constructed by bending a bar of celluloid: a neutral line thus separated a region of compression from one of tension and, in consequence, one region of the bar was negatively, the other positively birefringent. When the elongated strip of celluloid was examined with this compensator, the position of the achromatic fringe indicated a negative birefringence for the strip, whereas independent observations had shown conclusively that the strip was of positive birefringence. Further experiments revealed the cause of this behaviour: the dispersion of birefringence of the celluloid was extremely strain sensitive and became anomalous when the strain exceeded the elastic limit.

Application. In many laboratories the determination of the birefringence of fibres is a routine operation, and it is therefore important to know whether or not the value of τ for a given material is independent of the birefringence. (The striking behaviour of celluloid is attributable to the camphor content.[16–18]) Table 1 shows the results obtained

Table 1. *Examples of "fringe jumping" in the Babinet compensator*

$\Delta\mu_D$	τ	$N_A/(N_D-N_A)$	N_A (obs.)	(N_D-N_A) (calc.)	N_D (obs.)
0·0035	0·0215	46·1	6·7	0·1	6·7
0·0065	0·0206	41·2	11·3	0·3	11·3
0·0124	0·0188	32·7	or 18·3 / 19·3	0·6	19·3
0·0171	0·0168	28·2	23·7	0·8	24·7
0·0238	0·0160	26·5	29·1	1·1	30·1
0·0308	0·0146	23·8	or 35·2 / 36·2	1·5	37·2

on a series of viscose rayon model filaments of different degrees of stretch. In the first column is given the birefringence at the sodium D line. The second column shows the corresponding τ-value obtained from a spectroscopic analysis of the interference colours; the absolute error in τ does not exceed $\pm$ 0·0006 and is generally much less.

From the International Critical Tables τ^* for crystalline quartz was found to be 0·0292. Equation (12) was then used in order to calculate the value of $N_A/(N_D - N_A)$ that applies to the examination of these fibres under a quartz Babinet compensator. This value, given in column 3, represents the order N_A that will correspond to $(N_D - N_A)$ equal to unity. In order to check this conclusion a fibre was viewed under a Babinet compensator (supplemented with quartz retardation plates) and the order of the achromatic fringe was measured on the fibre axis (column 4). From this information the difference $(N_D - N_A)$ was calculated (column 5). Furthermore, the true order N_D was determined unambiguously by means of a non-compensator method (column 6). It will be seen that these observations are consistent with the calculations; when, as in the third and final rows, $(N_D - N_A)$ is approximately 0·5 or 1·5, either of two fringes can be regarded as the achromatic one.

With cellulose fibres the birefringence is positive (i.e. N_D is positive) and $\tau < \tau^*$; consequently $(N_D - N_A)$ is also positive. If, however, one has a positively birefringent fibre for which $\tau > \tau^*$, then $(N_D - N_A)$ will be negative and the achromatic fringe will move towards higher, not lower, orders. An example of this is provided by a well stretched fibre of Nylon 610 ($\Delta\mu_D = 0{\cdot}0528$, $\tau = 0{\cdot}0335$). A much more striking illustration of the same phenomenon is observed when rubber is stretched, a "fringe jump" occurring every time the retardation N_D is increased by six orders[19]; from this it is concluded that $\tau \simeq 0{\cdot}09$.

Finally it should be mentioned that, when form birefringence is present, the dispersion of birefringence can be unusually large,[20] and the achromatic fringe might "jump" a whole order even though the retardation of the specimen be small.

4. INTERFERENCE MICROSCOPES

Interference microscopy, of which there are two classes, two-beam and multiple-beam, is now widely used for the examination of a wide field of objects, including textile fibres and living cells. The zero-order fringe is, however, not normally encountered in multiple-beam interferometry. Our interest is, therefore, confined to the two-beam type, in which the incident light is split into two beams, one of which passes through the object and the other through a reference medium. An early instrument of this type was the Linnik interferometer, which was in essence a Michelson interferometer with paired objectives, one in each beam. In recent designs of interference microscopes only one condenser and one objective are used. The incident beam is divided into two beams sheared relative to one another; one beam traverses the object, the other by-passes it, after which they are recombined in the objective so as to produce interference effects. In the Cooke, Troughton and Simm interference microscope[21] the compensator is a glass wedge, whereas in the Baker microscope[22] the two beams are polarized at right angles to one another and a quartz wedge, followed by an analyser, can be used as compensator. (The use of polarized light means that a shearing of the two beams is not essential, and a double-focus mode of operation has been introduced.)

Application. In order to show how the theory of Section 2 can be applied, a determination was made of the path difference introduced by a specimen immersed in a liquid. Two different liquids were used, their optical properties (denoted by the suffix 1) being given in the first two columns of Table 2. The properties of the specimen, a glass fibre of 0·052 mm diameter, are given in the next two columns under

the suffix 2. In the fifth column are the corresponding τ-values calculated from equation (11) for the sodium D line. The immersed fibre was examined under a Baker interference microscope to which was attached a quartz Babinet compensator ($\tau^* = 0{\cdot}0292$). The position of the achromatic fringe on the fibre axis was observed (column 6) and from this $(N_D - N_A)$ was calculated (column 7). It was easy to determine in sodium yellow light the correct order N_D on the fibre axis, and comparison of columns 6, 7 and 8 reveals a satisfactory agreement between calculated and observed values. It will also be seen how, even for low orders of interference, an extremely large error can occur if white light is used.

Table 2. *Examples of "fringe jumping" in the Baker interference microscope*

$(\mu_1)_D$	$(\mu_1)_F-(\mu_1)_C$	$(\mu_2)_D$	$(\mu_2)_F-(\mu_2)_C$	τ	N_A (obs.)	(N_D-N_A) (calc.)	N_D (obs.)
1·5610	0·0192			0·634	−3·7 or −4·7	2·3 or 2·9	−1·7
		1·5416	0·0065				
1·5311	0·0151			−0·818	−1·1	1·9	0·9

One of the fringe patterns seen in white light has been reproduced schematically in Fig. 3. The instrumental arrangement resulted in the extinction of light of any wavelength for which the order of interference was integral. The solid curves in Fig. 3 therefore correspond to regions of the specimen that appeared reddish in colour and the dotted curves to regions appearing blue-green. In Section 2 it was

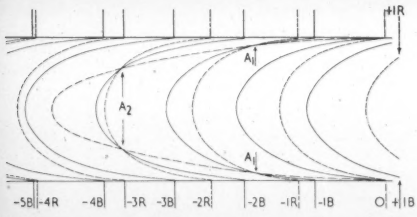

Fig. 3. The white light fringe pattern of an immersed fibre as seen in the interference microscope. On the fibre axis the order in sodium D light is $N_D = -1{\cdot}7$

—— locus in blue of a fringe of given order.
– – – locus in red of a fringe of given order.
–·–·– locus of achromatic position.
A_1, A_2, achromatic points in the fringes.

shown that, wherever τ and τ^* are constant, N_A is proportional to N_λ. With a fibre of circular cross-section the fringes, which are loci of constant N_λ, are half-ellipses. Consequently, the locus of the achromatic position N_A is also represented by a half-ellipse, and where this locus intersects a fringe, as at points A_1 and A_2, the fringe appears achromatic.

Whenever N_λ is zero two possibilities arise. The first is the trivial one that the specimen thickness l is zero; then $N_A = N_\lambda = 0$ and there is no jump in the achromatic fringe position. The other is that $(\mu_2 - \mu_1)_\lambda = 0$; in this instance N_A will be zero only if the dispersion of μ_2 is the same as that of μ_1, a condition that is unlikely to be fulfilled when a solid is immersed in a liquid. As an illustration, a piece of the glass fibre was placed in a liquid of such a refractive index that N_λ was zero for some wavelength in the middle of the visible spectrum; that is, the fringes were undisplaced upon crossing the fibre. Despite the straightness of the fringes, the zero-order fringe was highly coloured on the axis of the fibre, but this coloration diminished as the edges ($l = 0$) of the fibre were approached. The fringe of order −1 was coloured on the axis but was achromatic at a point between the axis and the edge of the fibre. The fringe of order −2, although nearly achromatic on the axis, was brightly coloured towards the edges.

The following points deserve emphasis. (1) These results are mainly due to the large difference in the dispersions of the fibre and of the liquid, and are but little influenced by the small contribution made by dispersion in the compensator. Equally marked results should therefore be observed with most forms of interference microscope. (2) If the fringes undergo an abrupt and not a gradual displacement at the specimen edge, there might be no evidence that a jump has occurred in the position of the achromatic fringe; it is thus unwise to use white light without careful consideration of this possibility.

ACKNOWLEDGEMENTS

Our thanks are due to Dr. G. A. J. Orchard for helpful discussions during the course of this work, which forms part of the fundamental research programme of The British Rayon Research Association.

REFERENCES

(1) AIRY, G. B. *Phil. Mag.*, **2**, p. 161 (1833).
(2) CANDLER, C. *Modern Interferometers* (London: Hilger and Watts Ltd., 1951).
(3) SIERTSEMA, L. A. *Beibl. Ann. Phys.*, **14**, p. 801 (1890).
(4) HALLWACHS, W. *Ann. Phys.* [*Leipzig*], **47**, p. 380 (1892).
(5) ADAMS, L. H. *J. Amer. Chem. Soc.*, **37**, p. 1181 (1915); *J. Washington Acad. Sci.*, **5**, p. 265 (1915).
(6) CLACK, B. W. *Proc. Phys. Soc.* [*London*], **37**, p. 116 (1925).
(7) HANSEN, G. *Z. Instrumkde.*, **50**, p. 460 (1930).
(8) CRAVEN, E. C. *Proc. Phys. Soc.* [*London*], **57**, p. 97 (1945).
(9) GEFFCKEN, W., and KRUIS, A. *Z. Phys. Chem. B*, **23**, p. 175 (1933).
(10) CHAMPETIER, G., and VIALLARD, R. *Bull. Soc. Chim. France*, **5**, p. 1042 (1938).
(11) FRILETTE, V. J., HANLE, J., and MARK, H. *J. Amer. Chem. Soc.*, **70**, p. 1107 (1948).
(12) CRIST, R. H., MURPHY, G. M., and UREY, H. C. *J. Chem. Phys.*, **2**, p. 112 (1934).
(13) MANN, J., and MARRINAN, H. J. Unpublished work.
(14) EHRINGHAUS, A. *Neues Jb. Min. Geol. Paläont.*, **41**, p. 342 (1917); **43**, p. 557 (1920).
(15) SAVUR, S. R. *Proc. Roy. Soc. A*, **109**, p. 338 (1925).
(16) WÄCHTLER, M. *Kolloidchem. Beih.*, **20**, p. 157 (1925).
(17) DERKSEN, J. C., KATZ, J. R., HESS, K., and TROGUS, C. *Z. Phys. Chem. A*, **149**, p. 371 (1930).
(18) HARRIS, F. C., and SETH, B. R. *Proc. Phys. Soc.* [*London*], **48**, p. 477 (1936).
(19) TRELOAR, L. R. G. *Trans Faraday Soc.*, **37**, p. 84 (1941).
(20) AMBRONN, H., and FREY, A. *Das Polarisationsmikroskop* (Leipzig: Akademische Verlag, 1926).
(21) DYSON, J. *Proc. Roy. Soc. A*, **204**, p. 170 (1950).
(22) SMITH, F. H. British Patent Specification 639014.

The use of electronic analogue computers with resistance network analogues

By W. J. KARPLUS, Ph.D., Department of Engineering, University of California, Los Angeles, U.S.A.

[*Paper first received* 19 *April, and in final form* 14 *June*, 1955]

A method is described whereby conventional d.c. electronic analogue computing units are used in conjunction with a resistance network to solve partial differential equations. These computing units are connected to the network nodes and supply automatically the required feed-in currents. The procedure eliminates iterative or trial-and-error adjustments, without impairing appreciably the high accuracy obtainable with resistance network analogues.

The solution of partial differential equations of the type

$$\nabla^2\phi = f(\phi) \tag{1}$$

by use of resistance network analogies has received considerable treatment in recent literature.[1,2] In this method the left-hand side of equation (1) is expanded in finite differences and represented by its analogue, a network of electrical resistors. A current corresponding to the factor $f(\phi)$ is then applied to each network node. Since the electrical potential at each node and the magnitude of the current applied to it are dependent upon each other, they cannot be determined separately. It is therefore necessary to employ iterative or trial-and-error methods. That is, the current applied to each node must be adjusted and readjusted until equation (1) is satisfied at every node of the network. It is the purpose of this paper to present a method whereby these iterations are performed automatically, in a fraction of a second, by means of analogue computing units connected to the nodes of the network.

PRINCIPLE OF THE METHOD

As an example, the computer method will be employed to obtain a solution of the equation

$$d^2\phi/dx^2 = k\phi^{-\frac{1}{2}} \tag{2}$$

subject to specified boundary conditions. This equation expresses the electrical potential ϕ in a plane diode, as a function of the distance x from the cathode, when the current is limited by a space charge. It was used by Liebman[3] to demonstrate the basic principle of the iterative method used in conjunction with the resistance network analogue. An exact solution of this equation, subject to the boundary conditions that $\phi = 0$ and $d\phi/dx = 0$ for $x = 0$, may be found by multiplying both sides of the expression by $2d\phi/dx$ and integrating twice; then

$$\phi = (9k/4)^{2/3}x^{4/3} \tag{3}$$

Equation (2) may be expanded

$$\frac{\phi_{+1} - \phi_0}{h^2} + \frac{\phi_{-1} - \phi_0}{h^2} = k\phi_0^{-\frac{1}{2}} \tag{4}$$

where h represents the mesh interval between adjacent nodes. The appropriate electrical analogue may therefore be represented as shown in Fig. 1. In this figure, i represents the current that must be applied to a typical network node, the potential of which is ϕ_0.

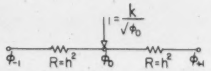

Fig. 1. Resistance network analogue for equation (4)

Since analogue computers work primarily with voltages, it is desirable to transform equation (4) into

$$\frac{\phi_{+1} - \phi_0}{R} + \frac{\phi_{-1} - \phi_0}{R} + \frac{(\phi_0 - kh^2\phi_0^{-\frac{1}{2}}) - \phi_0}{R} = 0 \tag{5}$$

where R is a resistor of arbitrary magnitude. According to equation (5), the node of potential ϕ_0 should be connected to three nodes with potentials ϕ_{+1}, ϕ_{-1} and $(\phi_0 - kh^2\phi_0^{-\frac{1}{2}})$ respectively, through three equal resistors R. Therefore equation (5) may be solved by attaching to each network node a resistor R, and applying a voltage $(\phi_0 - kh^2\phi_0^{-\frac{1}{2}})$ to its free end. This is illustrated in Fig. 2, where the rectangles represent the computer units supplying these voltages.

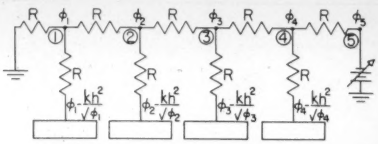

Fig. 2. Resistance network analogue for equation (5)

DESCRIPTION OF A TYPICAL COMPUTER UNIT

The purpose of each computer unit is to furnish the required voltage $(\phi_0 - kh^2\phi_0^{-\frac{1}{2}})$. One manner of accomplishing this with standard computing components is shown schematically in Fig. 3. The significance of the d.c. voltages appearing at various points of the circuit, in terms of the network variables, is indicated in the figure. The symbols indicated for the resistances connected to amplifiers (*A*), (*B*) and (*C*) denote the ratio between the feedback and input resistors for these amplifiers. For example, the feedback resistor of amplifier (*C*) is ten times as large as each of the two input resistors. Since adequate descriptions of commercially available analogue computers are to be found in the literature,[4] only a brief discussion of their operation will be presented here.

Amplifiers (*A*), (*B*) and (*C*) are standard high gain, d.c., operational amplifiers. The output voltage of such amplifiers is proportional to the magnitude of the feedback resistor. If the feedback resistor and the input resistors are all of equal magnitude, the output voltage is equal to minus the algebraic sum of the input voltages. Operational amplifier (*A*) therefore acts as a simple sign changer, while amplifier (*B*) serves as an adder as well as a sign changer. The combination of amplifier (*C*), the servo-amplifier, and the motor *M*, comprises

an error-sensing network. The motor shaft is coupled mechanically to the three ganged, precision ten-turn potentiometers I, II and III. Connected as shown the motor rotates in a direction to make the voltage appearing at the moving arm of potentiometer II equal to minus the fixed input voltage E_1. If the potentiometer ratios are equal to α, the voltage at the moving arm of potentiometer I is $(-\alpha\phi_0)$, and the voltage at the moving arm of potentiometer II is then equal to $(-\alpha^2\phi_0)$. This latter voltage is equated to $(-E_1)$, by the action of the servo-motor, so that $\alpha = (E_1/\phi_0)^{\frac{1}{2}}$. The voltage appearing at the moving arm of potentiometer III is then equal to $E_2(E_1/\phi_0)^{\frac{1}{2}}$, where E_2 is the fixed voltage applied to potentiometer III, and ϕ_0 is the voltage at the node of the resistance network. If the product of the fixed voltages $E_2(E_1)^{\frac{1}{2}}$ is made equal to the factor (kh^2), the output of potentiometer III is $kh^2\phi_0^{-\frac{1}{2}}$ as desired.

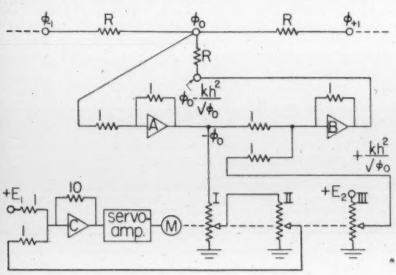

Fig. 3. Typical electronic analogue computer unit

By careful selection of the magnitudes of the resistances of the three potentiometers and the input resistors of amplifiers (*B*) and (*C*) all so-called potentiometer loading errors can be made to compensate each other and a high order of accuracy may be achieved. To assure overall stability care must be taken in the design of the computing units to make the gain around all closed loops less than unity. The voltages E_1 and E_2 for all computer units may come from common power supplies.

OPERATION OF ANALOGUE

The first step in applying the method to the solution of equation (3) involves the construction of computer units of the type shown in Fig. 3 for each of the network nodes. This task may be speeded considerably by using plug-in type equipment. The units are then connected to the resistance network, and the boundary potentials of the network as well as the two computer voltages, E_1 and E_2, are set to their correct values. These values must be selected with care to avoid exceeding the operating limits of the operational amplifiers. The computers will then "relax" automatically to the correct node voltages and currents, and the desired potentials may be measured and recorded.

The speed with which the solution becomes available extends greatly the applicability of the resistance network. For example, it may be used for determining the optimum value of design factors, by making a series of measurements and changing the system parameters in a systematic manner. An analogue of this type has also been used successfully to solve so-called free-surface problems, important in petroleum production engineering. Details of that research are presented elsewhere.[5]

The circuits shown in Figs. 2 and 3 were employed to solve equation (3) for $k = 4/9$. A comparison of the computer solution and the exact solution expressed by equation (4) is shown in the table. A considerable increase in accuracy is

Comparison of analytical and computer solutions

X (arbitrary units)	*ϕ (in volts) by equation (4)*	*ϕ (in volts) by analogue*
0	0	0
.1	1·00	1·03
2	2·50	2·52
3	4·28	4·25
4	6·28	6·26
5	8·46	8·46

possible by increasing the number of network nodes by reducing the factor h, and by making the network spacing more dense in those regions in which the potential gradient is most non-linear.

Howe and Hannerman[6] have shown that partial differential equations may be solved entirely by means of operational amplifiers. The present method represents an effort to combine the speed of the computer type of solution with the high inherent accuracy of the resistance network analogue. Liebman[7] has shown that accuracies approaching one part in 10000 are attainable with resistance networks using resistors with tolerances of $\pm 1\%$. The accuracy of analogue computer units of the type described can generally not be expected to exceed one part in 100. By employing them only for the purpose of introducing the required feed-in currents, however, the overall accuracy of the analogue process is only slightly impaired. This is particularly true if the magnitude of the feed-in currents is small compared to the currents flowing in the resistance network, as in the problem described above for small k.

ACKNOWLEDGEMENT

The author wishes to express his appreciation for the helpful advice offered by Mr. James R. Allder and Mr. Norman Friedman.

REFERENCES

(1) LIEBMAN, G. *Brit. J. Appl. Phys.*, **5**, p. 32 (1954).

(2) LIEBMAN, G. *Brit. J. Appl. Phys.*, **4**, p. 193 (1953).

(3) LIEBMAN, G. *Nature* [*London*], **164**, p. 149 (1949).

(4) KORN, G. A., and KORN, T. M. *Electronic Analog. Computers* (New York: McGraw-Hill Book Co., 1952).

(5) KARPLUS, W. J., Ph.D.Thesis, University of California, Los Angeles (1954).

(6) HOWE, R. M. and HANNEMAN, V. S. *Proc. Inst. Radio Engrs*, **41**, p. 1497 (1953).

(7) LIEBMAN, G. *Brit. J. Appl. Phys.*, **1**, p. 92 (1950).

The permittivity of two phase mixtures

By C. A. R. Pearce, M.Sc.(Eng.), A.M.I.Mech.E., A.M.I.E.E., National Coal Board, Central Research Establishment, Worton Hall, Isleworth, Middlesex

[*Paper first received* 18 *May, and in final form* 14 *July*, 1955]

The paper compares the results of a number of workers with the predictions of published formulae. It is shown that expressions due to Bruggeman accord with the observations but those due to Böttcher, and Van Vessem and Bijvoet are only valid over a limited range of permittivities. An empirical expression is given which is adequate for all available relevant results.

LIST OF SYMBOLS

ε is the general symbol for relative permittivity.

ε_1 and ε_2 refer to the discontinuous and continuous phases respectively of a porphyritic mixture.

ε_m is the value for the mixture.

${}_2\varepsilon_m = \varepsilon_m/\varepsilon_2$ and ${}_2\varepsilon_1 = \varepsilon_1/\varepsilon_2$.

p_1, the volume ratio, is the fraction of the total volume represented by the discontinuous phase.

INTRODUCTION

A number of formulae have been proposed which seek to relate the electrical properties of a mixture with the corresponding properties of the phases. Those by Maxwell,[1] Rayleigh,[2] and Wiener[3] relate to formal arrangements of bodies and as Pearce[4] has shown are inadequate when applied to random dispersions. Similar limitations can be presumed for those of Burgess,[5] Lewin[6] and Eckart[7] which can be shown to reduce to special cases of Maxwell's expression.

The first analysis of a specifically random mixture was by Bruggeman[8] in 1935. He derived a number of expressions but two are significant in the present context. Besides randomness Bruggeman's other postulates were homogeneous, isotropic elements all of which have the same general form and are small in relation to the total volume of the mixture or aggregate.

For a porphyritic dispersion of randomly orientated laminae of undefined profile, Bruggeman derived the expression:

$$\varepsilon_m = \varepsilon_1 \cdot \frac{3\varepsilon_2 + 2p_1(\varepsilon_1 - \varepsilon_2)}{3\varepsilon_1 - p_1(\varepsilon_1 - \varepsilon_2)} \qquad (1)$$

and for a similar dispersion of spheres:

$$1 - p_1 = \frac{\varepsilon_1 - \varepsilon_m}{\varepsilon_1 - \varepsilon_2} \sqrt[3]{\frac{\varepsilon_2}{\varepsilon_m}} \qquad (2)$$

These two expressions are given as the extreme values obtained with dispersions of all particle shapes, that for the spheres being the lower limit.

COMPARISON OF BRUGGEMAN'S FORMULA WITH PUBLISHED OBSERVATIONS

To compare the published observations of other workers with the predictions of formulae (1) and (2) the author has transformed the results, using the expression:

$$\varepsilon' = \frac{{}_2\varepsilon_m - 1}{{}_2\varepsilon_1 - 1} = \frac{\varepsilon_m - \varepsilon_2}{\varepsilon_1 - \varepsilon_2} \qquad (3)$$

so that $0 < \varepsilon' < 1$ for all cases.

Fig. 1 compares limiting curves from Bruggeman's formulae plotted for a number of values of ${}_2\varepsilon_1$ with points derived from published observations on the wide variety of "mixtures" listed in the table. The majority of the observations relating to mixtures for which $1 < {}_2\varepsilon_1 < 5$ lie between the limits set

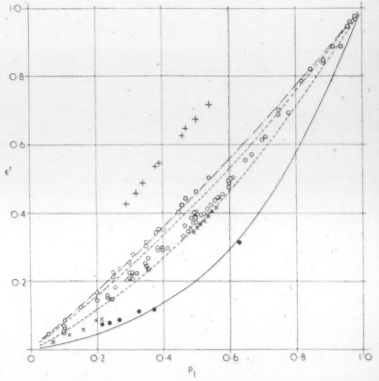

Fig. 1. Showing how the results of a number of observers compare with curves of Bruggeman's formulae for porphyritic mixtures

\+ ${}_2\varepsilon_1 < 1$ —·—·— laminae, ${}_2\varepsilon_1 = 2$.
○ $1 < {}_2\varepsilon_1 < 5$ } - - - - - upper curve laminae, ${}_2\varepsilon_1 = 4$.
× $5 < {}_2\varepsilon_1 < 15$ } - - - - - lower curve spheres, ${}_2\varepsilon_1 = 4$.
• ${}_2\varepsilon_1 > 15$ ———— spheres, ${}_2\varepsilon_1 = 16$.

by formula (1) with ${}_2\varepsilon_1 = 2$ and formula (2) with ${}_2\varepsilon_1 = 4$. The observations falling outside this region of the diagram are in the main those for which ${}_2\varepsilon_1 < 1$ or > 5 and these points generally fall into regions bounded by curves for appropriate values of ${}_2\varepsilon_1$. In Fig. 1 the curves for laminae with ${}_2\varepsilon_1 = 16$ and spheres ${}_2\varepsilon_1 = 2$ have been omitted in order to reduce the congestion in the diagram. The first lies between the middle two of the diagram and the second practically coincides with the curve for laminae with ${}_2\varepsilon_1 = 4$.

Fig. 1 not only provides general confirmation of the validity of Bruggeman's work on porphyritic mixtures but also serves to emphasize the limited value of his formulae in dealing with practical cases since they do not indicate even the form of the relationship between p_1 and ${}_2\varepsilon_m$ for given precise conditions. It is therefore inevitable that attempts to use these formulae have generally required the introduction of empirical

constants usually called "form" or "agglomeration" factors, see, for example, Voet.[9]

EMPIRICAL EXAMINATION OF PUBLISHED OBSERVATIONS

An examination of the observations listed in the table has revealed that the relationship between ε' and p_1 can be adequately represented by the family of curves:

$$\varepsilon' = \frac{(1-v)p_1}{1-vp_1} \qquad (4)$$

where parameter v is a constant for each condition. The sets of observations examined in this way were all those known to the author for finite values of ${}_2\varepsilon_1$ and for which the necessary conditions were available with a reasonable

Table giving details of observations used in Figs. 1, 3, 4 *and* 5

System	*Authority*	${}_2\varepsilon_1$	*Empirical factor* v
NaCl in oil	Burton and Turnbull[12]	2·605	0·375
$K_2Al_2(SO_4)_4$	Burton and Turnbull[12]	2·835	0·375
KCl in vacuum	Guillien[13]	4·57	0·35
$PbCl_2$ in vacuum	Guillien[13]	28	0·73
$PbCl_2$ in CCl_4	Guillien[13]	12·56	0·65
NaCl in air	Van Vessem and Bijvoet[11]	5·81	0·45
KCl in air	Van Vessem and Bijvoet[11]	4·68	0·39
NH_4Cl in $CCl_4 - C_6H_6$	Van Vessem and Bijvoet[11]	3·13	0·32
KCl in $CCl_4 - CBr_4$	Van Vessem and Bijvoet[11]	1·972	0·18
$CaCO_3$ in rubber	Scott and McPherson[14]	3·47	0·375
$CaCO_3$ in vistonex	Scott and McPherson[14]	3·87	0·45
KCl in air	Errera[15]	4·78	0·35
Powdered quartz in benzol	Mecke and Schill[16]	2·01	0·15
Powdered quartz in nitrobenzol	Mecke and Schill[16]	0·135	−0·90
TiO_2 in air sintered at 1500° C, 7 days	Stevels[17]	114	0·5
TiO_2 in air sintered at 1000–1300° C, 1 hour	Stevels[17]	114	0·87
TiO_2 in air unsintered	Stevels[17]	114	0·905

degree of certainty. They include the results of tests on powders in air and immersed in liquids and solids as well as compressed and sintered powders. A few sets of published results which might have otherwise been included were omitted because of uncertainties of one sort or another, e.g. those by Rushman and Strivens.[10] They worked with sintered $BaTiO_3$ and varied the sintering temperature at the same time as p_1 was varied. Their published curves indicate a major transition between 1150 and 1250° C ($p_1 = 0{\cdot}596$ to $0{\cdot}686$). The results above the transition are well represented by formula (4) with $v = 0{\cdot}4$, ${}_2\varepsilon_1 = 1650$ but the remainder are insufficient to establish a law.

Fig. 2 includes typical examples of the family of curves represented by formula (4) and Fig. 3 shows some of the results plotted with the curve derived from (4) which provides the best fit with the published data. The worst fit obtained was that shown for quartz in nitrobenzol.

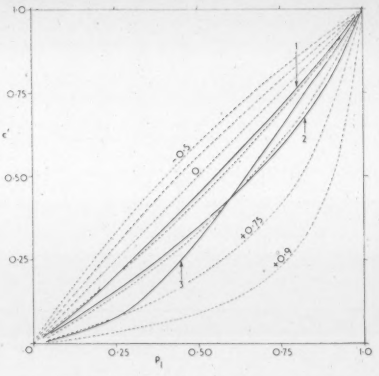

Fig. 2. The broken lines are examples of the family $\varepsilon' = \dfrac{(1-v)p_1}{1-vp_1}$, for $v = 0{\cdot}9$ and $-0{\cdot}5$ to $0{\cdot}75 \times 0{\cdot}25$.

The full lines are derived from Böttcher's expression

Curve 1 for ${}_2\varepsilon_1 = 2$, curve 2 for ${}_2\varepsilon_1 = \frac{1}{2}$ and curve 3 for ${}_2\varepsilon_1 = 16$.

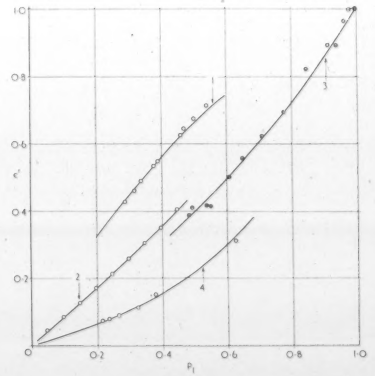

Fig. 3. Showing how the results of various workers fit curves of the family $\varepsilon' = \dfrac{(1-v)p_1}{1-vp_1}$

Curve 1, the points are for quartz in nitrobenzol and the curve is $v = -0{\cdot}9$. Curve 2, the points are for KCl in $CCl_4 - CBr_4$ and the curve is $v = +0{\cdot}18$. Curve 3, the points are for KCl in air[15] and the curve is $v = +0{\cdot}35$. Curve 4, the points are for $PbCl_2$ in vacuum and the curve is $v = +0{\cdot}73$.

In general, therefore, the available results of measurements of permittivity of mixtures with finite values for $_2\varepsilon_1$ fit expression (4) at least as well as the accuracy and repeatability of the original measurements allow.

The factor v fulfils some of the functions of the form factor u used by Wiener[3] but its value in any set of conditions depends on so many properties which are unrelated to shape that it will be referred to instead as the "empirical factor." The values obtained for v and quoted in the table are plotted in Fig. 4 for comparison with $_2\varepsilon_1$ and the wide scatter further emphasizes the way in which the characteristics of mixtures depend on factors not found in any published expression.

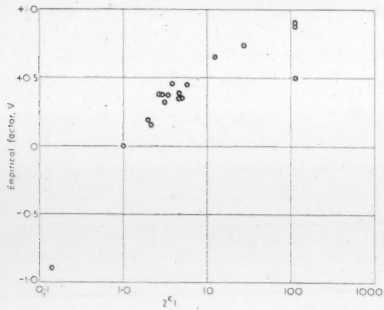

Fig. 4. Values of the empirical factor v plotted against a logarithmic scale of $_2\varepsilon_1$

The general empirical relationship for a porphyritic mixture can now be assembled, namely:

$$\frac{{}_2\varepsilon_m - 1}{{}_2\varepsilon_1 - 1} = \frac{\varepsilon_m - \varepsilon_2}{\varepsilon_1 - \varepsilon_2} = \frac{(1-v)p_1}{1 - vp_1} \qquad (5)$$

which differs from previously published expressions for mixtures in that the factor v is defined only in relation to test results.

THE WORK OF BÖTTCHER, AND POLDER AND VAN SANTEN

In a series of papers published between 1940 and 1945 Böttcher[18] dealt with the problem of mixtures and put forward the following expression for a powder in air:

$$\frac{{}_2\varepsilon_m - 1}{3\,{}_2\varepsilon_m} = p_1 \frac{{}_2\varepsilon_1 - 1}{{}_2\varepsilon_1 + 2\,{}_2\varepsilon_m} \qquad (6)$$

In the case of the observations which he quoted the predictions of the formula were in excellent agreement, but if the expression is tested against measurements made on mixtures for which $_2\varepsilon_1$ is high, say above 10, or on the other hand is fractional, agreement ceases to be so satisfactory. Fig. 5 indicates the sort of discrepancy that occurs in two such cases. There is, however, an alternative method of examining such formulae. Having, in the previous section, established empirically the general form of the relationship between ε' and p_1 this can be used to compare any formula with the observations on which the relationship is based.

The way in which the discrepancies of Böttcher's formula arise will be readily apparent from an examination of two sets of curves in Fig. 2. With $_2\varepsilon_1 = 2$ or 4 Böttcher's formula gives results conforming to the general shape of the curves of $(1-v)x/(1-vx)$ but for $_2\varepsilon_1 = 16$ the curve is quite different in form. There is also a marked difference with fractional values of $_2\varepsilon_1$.

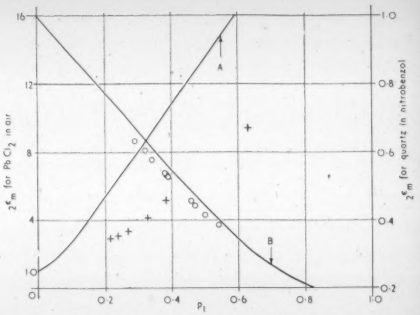

Fig. 5. Examples of the application of Böttcher's equation to mixtures with high and fractional values of $_2\varepsilon_1$

\+ Guillien[13] for $PbCl_2$ in air, $\varepsilon_1 = 28$, $\varepsilon_2 = 1$.
○ Mecke and Schill[16] for powdered quartz in nitrobenzol, $\varepsilon_1 = 4{\cdot}575$, $\varepsilon_2 = 33{\cdot}95$.
The curves are derived from equation (6), Böttcher's equation. Curve A with $_2\varepsilon_1 = 28$. Curve B with $_2\varepsilon_1 = 0{\cdot}135$.

Polder and Van Santen[19] also examined the general problem and derived a number of related formulae. The version applying to spheres is identical with Böttcher's equation. If their curves are transformed and compared directly with those derived from $(1-v)x/(1-vx)$, as has been done for Böttcher's formula, it will be found that once again those for $_2\varepsilon_1 \simeq 1$ to 4 fit fairly well with observations, whereas those for high values of $_2\varepsilon_1$ exhibit major discrepancies.

CONCLUSION

The most important outcome of the study has been to demonstrate the validity of Bruggeman's work and of formula (4) proposed by the author in relation to previously published observations made on a wide variety of mixtures.

REFERENCES

(1) Clerk Maxwell. *Electricity and Magnetism*, first published 1873. Vol. 1, 3rd Ed., see Art. 314, p. 440 (Oxford: The Clarendon Press, 1892).
(2) Lord Rayleigh. *Phil. Mag.*, **34** (5), p. 481 (1892).
(3) Wiener, O. *Leipziger Berichte*, **62**, p. 256 (1910).
(4) Pearce, C. A. R. *Brit. J. Appl. Phys.*, Vol. 6, p. 113 (April 1955).
(5) Burgess, R. E. *Wireless Engineer*, **23**, p. 156 (1946).
(6) Lewin, L. *Journ. Inst. E.E.*, **94** (3), Pt III, pp. 65 to 68 (1947).
(7) Eckart, G. *Z. agnew Phys.*, **4**, p. 134 (1952).
(8) Bruggeman, D. A. G. *Ann. Phys.* [*Leipzig*], **24**, p. 636 (1935).
(9) Voet, A. *J. Phys. Chem.*, **51**, p. 1037 (1947).

(10) RUSHMAN, D. F., and STRIVENS, M. A. *Proc. Phys. Soc.*, **59**, p. 1011 (1947).
(11) VAN VESSEM, J. C., and BIJVOET, J. M. *Receuil. Trav. Chim. pays-Bas*, **67**, p. 191 (1948).
(12) BURTON, E. F., and TURNBULL, L. G. *Proc. Roy. Soc. A*, **158**, p. 182 (1937).
(13) GUILLIEN, R. *Ann. Phys.* [*Paris*], **16**, p. 205 (1941).
(14) SCOTT, A. H., and MCPHERSON, A. T. *J. Res. Nat. Bur. Stand.*, **28**, p. 279 (1942), R.P. 1457.
(15) ERRERA, J. *Compt. Rend.*, **184**, p. 458 (1927).
(16) MECKE, R., and SCHILL, H. *Zeit. fur Electrochemie*, **57**, p. 270 (1953).
(17) STEVELS, J. M. *Receuil. Trav. Chim. pays-Bas*, **66**, p. 71 (1947).
(18) BÖTTCHER, C. F. *Receuil. Trav. Chim. pays-Bas*, **64**, p. 47 (1945), and others to which it refers.
(19) POLDER, D., and VAN SANTEN, J. H. *Physica*, **12**, p. 257 (1946).

Transient heat conduction in multiphase media

By J. H. WEINER, B.M.E., A.M., Ph.D., Columbia University, New York, U.S.A.

[*Paper first received* 31 *December*, 1954, *and in final form* 27 *May*, 1955]

An analytical solution is obtained for the problem of a semi-infinite mass of material initially at a uniform temperature, the surface of which is maintained at a different constant temperature, where the material may change phase an arbitrary number of times in passing from its initial to its final temperature. Each phase of the material may have distinct thermal properties. Each change of phase is assumed to take place at a given temperature and may be accompanied by the evolution or absorption of heat. The solution is obtained by a semi-inverse procedure.

A numerical example is given of the application of the solution to the analysis of the solidification of 0·2% carbon steel and comparison is made between the theoretical solution, experimental results and an electrical analogue solution of the same problem.

Transient heat conduction problems which involve one or more changes of phase arise in several fields of practical interest. Their mathematical formulation requires the specification of conditions on the boundaries separating the various phases; however, these boundaries move, as the temperature distribution changes, in a manner which is initially unknown. They represent, therefore, problems of considerable difficulty, and direct general methods of solution are not yet available.

The nature of this class of problems may be clarified by the consideration of the following typical example. A semi-infinite mass of pure metal is initially in the molten state at a uniform temperature $T_1 > T_S$, where T_S is the solidification temperature of the metal, Fig. 1(*a*). At time $t = 0$, the temperature of the surface of the metal is brought to

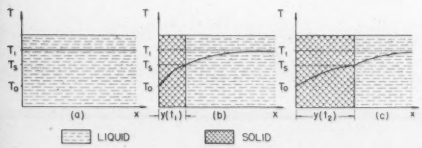

Fig. 1. Solidification of a pure metal

$T_0 < T_S$ and solidification begins immediately. At a later time, $t = t_1$, the temperature distribution appears as in Fig. 1(*b*), $y(t_1)$ representing the thickness of metal solidified up to this time. At a still later time, $t = t_2$, the temperature distribution appears as in Fig. 1(*c*). Since the thermal properties of the solid and liquid metal are different, and since latent heat is released when the metal solidifies, boundary conditions must be specified on the plane $x = y(t)$, although this function is initially unknown.

The solution to the above problem was obtained by Neumann[1] by a semi-inverse procedure; it is one of the few known exact solutions in this field. However, the following shortcoming of Neumann's and the other analytical procedures is clearly stated by Ruddle, in his excellent review monograph on solidification as follows: "A very serious disadvantage of all the mathematical methods is that they are only applicable to materials which freeze at constant temperatures and are not capable of dealing with alloys solidifying over a substantial range of temperature."[2]

An alloy undergoes at least two changes of phase during solidification; one when it drops below the liquidus temperature T_L, and one when it drops below the solidus temperature T_S. At a time $t = t_1$ after the start of solidification of a semi-infinite mass of an alloy, the temperature distribution appears as in Fig. 2. It is seen that, in contrast to the case of the

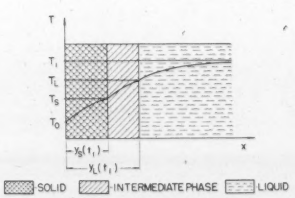

Fig. 2. Solidification of an alloy

pure metal, there are now two moving boundaries at positions $y_L(t)$ and $y_S(t)$ which correspond to the liquidus and solidus temperatures respectively. If other phase changes occur between these two temperatures there will be additional moving boundaries.

It is shown in this paper that Neumann's semi-inverse procedure may be extended to obtain the solution to the problem of a semi-infinite mass of material initially at a uniform temperature, the surface of which is maintained at a different constant temperature, where the material may change phase an arbitrary number of times in passing from its initial to its final temperature. Each phase may have

distinct thermal properties. A numerical example is given of the application of this solution to the study of the solidification of an alloy which undergoes three-phase changes. Comparison is made between the theoretical solution, experimental results and an electrical analogy solution of the same problem.

The above discussion has been phrased in terms of the solidification of metals in order to fix ideas. However, it will be clear from the mathematical formulation and the solution of the problem presented in the next section that the procedure is of broader application. It may be used, for example, in the analysis of melting, heat-treating, the propagation of chemical reactions, etc. The method may also serve to obtain approximate solutions to non-linear heat conduction problems by replacing the continuous dependence of thermal properties upon temperature by step-wise phase changes. It is also clear that the solution presented applies as well to other diffusion problems of this type, requiring merely a suitable change in terminology.

MATHEMATICAL FORMULATION OF THE PROBLEM

It is assumed that the substance under consideration occupies the region $x \geqslant 0$. For the temperature range $T_{i-1} < u < T_i$, $i = 1, 2, \ldots, n$ the material exists in a phase with thermal conductivity K_i, volumetric specific heat c_i, and thermal diffusivity $\alpha_i = K_i/c_i$. At time $t = 0$, the entire mass is at the uniform temperature T_n, and for $t > 0$ the surface $x = 0$ is maintained at the constant temperature T_0. (T_0 and T_n need not be phase change temperatures.) At the interface $y_i(t)$ separating the i phase from the $(i + 1)$ heat is generated at a rate proportional to the volumetric rate of conversion of the $(i + 1)$ phase to the i, that is at a rate $L_i(d\,y_i/d\,t)$. At a time $t > 0$, the temperature distribution will appear as in Fig. 3. Mathematically, the problem

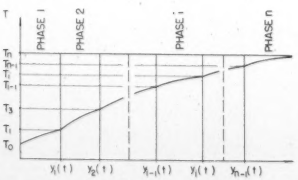

Fig. 3. Temperature distribution in n phase substance

is formulated as follows. [For compactness, the symbols $y_0(t)$ and $y_n(t)$ are used for 0 and ∞ respectively; by $f[y_n(t)]$ is meant $\lim_{x \to \infty} f(x)$]. Then the following equations obtain for $u_i(x, t)$, the temperature in the i phase.

$$\alpha_i \frac{\partial^2 u_i}{\partial x^2} = \frac{\partial u_i}{\partial t};\ y_{i-1}(t) < x < y_i(t),\ t > 0,\ i = 1, \ldots, n \qquad (1)$$

$$u_i(y_{i-1}(t), t) = T_{i-1},\ u_i(y_i(t), t) = T_i;\ t > 0,\ i = 1, \ldots, n \qquad (2)$$

$$K_i \frac{\partial u_i}{\partial x} - K_{i+1} \frac{\partial u_{i+1}}{\partial x} = L_i dy_i/dt;$$
$$x = y_i(t),\ t > 0,\ i = 1, \ldots, n-1 \qquad (3)$$

Only the n phase is present initially and for it

$$\lim_{t \to 0} u_n(x, t) = T_n;\quad x > 0 \qquad (4)$$

Solutions for the functions u_i are assumed to be of the form

$$u_i(x, t) = A_i \phi(\beta_i x/\sqrt{t}) + B_i,\quad i = 1, \ldots, n \qquad (5)$$

where A_i and B_i are constants,

$$\beta_i = 1/(2\sqrt{\alpha_i}) \text{ and } \phi(x) = \operatorname{erf} x = (2/\sqrt{\pi}) \int_0^x \exp(-u^2) du$$

It is seen by direct substitution that the functions defined by equations (5) satisfy equations (1). It is also seen that equations (2) require that $y_i(t)$ be of the form $y_i(t) = \gamma_i \sqrt{(t)}$, where γ_i is a constant, $i = 0, 1, \ldots, n$. Note that by the above convention, $\gamma_0 = 0$ and $f(\gamma_n) = \lim_{x \to \infty} f(x)$. The constants A_i and B_i are then determined from equations (2) as

$$\left.\begin{aligned} A_i &= \frac{T_i - T_{i-1}}{\phi(\beta_i \gamma_i) - \phi(\beta_i \gamma_{i-1})},\quad i = 1, \ldots, n \\ B_i &= \frac{T_{i-1}\phi(\beta_i \gamma_i) - T_i \phi(\beta_i \gamma_{i-1})}{\phi(\beta_i \gamma_i) - \phi(\beta_i \gamma_{i-1})},\quad i = 1, \ldots, n \end{aligned}\right\} \qquad (6)$$

Substitution of the functions $u_i(x, t)$ defined by equations (5) in equations (3), with the constants A_i defined by equations (6), leads to the following set of $n - 1$ equations for the $n - 1$ constants $\gamma_1, \ldots, \gamma_{n-1}$:

$$\frac{2}{\sqrt{\pi}} \left[\frac{K_i \beta_i (T_i - T_{i-1}) \exp(-\beta_i^2 \gamma_i^2)}{\phi(\beta_i \gamma_i) - \phi(\beta_i \gamma_{i-1})} - \frac{K_{i+1} \beta_{i+1} (T_{i+1} - T_i) \exp(-\beta_{i+1}^2 \gamma_i^2)}{\phi(\beta_{i+1} \gamma_{i+1}) - \phi(\beta_{i+1} \gamma_i)} \right] = \frac{L_i \gamma_i}{2};$$
$$i = 1, \ldots, n-1 \qquad (7)$$

Equation (4) is clearly satisfied. A complete solution to the problem is therefore given by the set of functions $u_i(x, t)$ defined by equations (5), with the constants A_i and B_i given by equations (6) and the constants γ_i determined as solution of equations (7), providing this solution exists with $\gamma_{i+1} > \gamma_i > 0$, $i = 1, \ldots, n-1$. The question of existence and uniqueness of the solution to the above system of equations is not considered here. For a particular system, if the solution exists, it may be found numerically by the procedure outlined in the following section.

METHOD OF SOLUTION OF EQUATIONS (7)

Although the system of equations (7) constitutes a set of $n - 1$ transcendental equations for the $n - 1$ constants γ_i, $i = 1, \ldots, n-1$, they are only loosely coupled and may be solved numerically without excessive computation. This may be accomplished as follows.

(1) The first equation, $(i = 1)$, is solved numerically for γ_1 as a function of γ_2.

(2) Using this relationship, the second equation, $(i = 2)$, is solved numerically for γ_2 as a function of γ_3; this process is continued through the $(n - 2)$ equation, $(i = n - 2)$ obtaining γ_{n-2} as a function of γ_{n-1}.

(3) The $(n - 1)$ equation, $(i = n - 1)$, is solved numerically for γ_{n-2} as a function of γ_{n-1}, yielding a second relationship which is solved simultaneously with that obtained in step (2) above to determine the values of γ_{n-2} and γ_{n-1}. The values of γ_1 through γ_{n-3} are then obtained directly by back substitution in the functional relationships previously established.

The labour involved in obtaining a solution for a problem involving n phases is therefore simply proportional to $(n - 1)$,

APPLICATION TO THE SOLIDIFICATION OF AN ALLOY

The manner in which a solidifying alloy releases its latent heat in passing from the liquidus to the solidus temperatures is not yet well understood. In a series of electrical analogy solutions at the Heat and Mass Flow Analyser Laboratory of Columbia University, Paschkis[3] found that good agreement with experiment was obtained by assuming that the latent heat may be represented as additional specific heat. He assumed further, that the alloy has the same thermal properties as the liquid metal until the temperature midway between liquidus and solidus temperatures is reached; at this point, the thermal properties change to those of the solid metal.

With this formulation, the problem is one of a four-phase medium. Letting T_3 be the liquidus temperature, T_1 the solidus temperature, L the latent heat release per unit volume of solidified metal, the equivalent volumetric specific heat increment, c_{eq}, is given by:

$$c_{eq} = L/(T_3 - T_1) \tag{8}$$

Letting $T_2 = \frac{1}{2}(T_1 + T_3)$, the thermal conductivity and volumetric specific heat of the four phases are assumed to be

$$\left.\begin{aligned} K_1 &= K_s; \quad c_1 = c_s \\ K_2 &= K_s; \quad c_2 = c_s + c_{eq} \\ K_3 &= K_L; \quad c_3 = c_L + c_{eq} \\ K_4 &= K_L; \quad c_4 = c_L \end{aligned}\right\} \tag{9}$$

In the above, K_s, c_s and K_L, c_L are the thermal properties of solid and liquid metal respectively.

The temperature distribution in a mass of liquid alloy occupying the region $x > 0$ initially at temperature $T_4 > T_3$ when suddenly brought into intimate contact at time $t = 0$ with a semi-infinite mould of thermal properties K_0, c_0 occupying the region $x < 0$ and initially at temperature T_{-1} will now be examined.

A solution to the above problem is attempted in which the mould-metal interface temperature is a constant T_0, for $t > 0$. The temperature distribution in the metal is then given by equations (5), (6) and (7) with $n = 4$ and $L_i = 0$, $i = 1, \ldots, 4$. To complete the solution, it is only necessary to determine the interface temperature, T_0. Under the above hypothesis, the temperature distribution in the mould, $u_0(x, t)$ is given by the equation

$$u_0(x, t) = (T_{-1} - T_0)\phi(-\beta_0 x/\sqrt{t}) + T_0 \tag{10}$$

From equations (5) and (6) for $i = 1$, it is seen that

$$u_1(x, t) = \frac{T_1 - T_0}{\phi(\beta_1\gamma_1)}\phi(\beta_1 x/\sqrt{t}) + T_0$$

By the substitution of the above functions, $u_0(x, t)$ and $u_1(x, t)$ in the additional boundary condition at $x = 0$,

$$K_0 \partial u_0/\partial x = K_1 \partial u_1/\partial x \tag{11}$$

the interface temperature T_0 is found to be

$$T_0 = T_1 - \frac{K_0\beta_0\phi(\beta_1\gamma_1)(T_1 - T_{-1})}{K_0\beta_0\phi(\beta_1\gamma_1) + K_1\beta_1} \tag{12}$$

If a solution to the system of equations (7) exists for this value of T_0, then a solution to the solidification problem of the postulated form exists. The constants $\gamma_1, \ldots, \gamma_4$ may be determined numerically as described above.

NUMERICAL EXAMPLE

The above procedure was applied to a problem studied experimentally by Clarke[4] and, using an electrical analogy, by Paschkis.[3] The problem is that of the solidification of 0·2% carbon steel in contact with a chill (a metallic mould insert used to accelerate solidification) of the same material. With the above notation, the data used in the electrical analogy experiments as representing the conditions of the actual experiments, are as follows:

$K_0 = K_s = 18{\cdot}4$ B.t.u./ft h °F $c_0 = c_s = 77{\cdot}2$ B.t.u./ft³
$K_L = 9{\cdot}2$ B.t.u./ft h °F $c_L = 90{\cdot}0$ B.t.u./ft³
$T_{-1} = 70°$ F, $T_1 = 2600°$ F, $T_3 = 2700°$ F, $T_4 = 2845°$ F
$L = 58\,000$ B.t.u./ft³

A theoretical solution to this problem was obtained using the procedure described above. As indicated there, the latent heat was represented as additional specific heat. A comparison of the progress of the liquidus and solidus isothermals as given by the analytical and analogue solutions is shown in Fig. 4 for the first 81 seconds. Further comparison is not

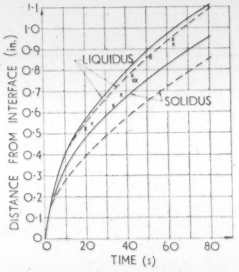

Fig. 4. Comparison of theoretical, experimental and analogy solutions

——— = theoretical.
- - - - = electrical analogy (Paschkis).
× = experimental (Clarke).

possible since the formation of an air gap between metal and chill was assumed at this time in the analogue experiments. Also shown are values of the solidified thickness at various times obtained experimentally by Clark by pour-out tests. The agreement between the three results is seen to be reasonably good.

REFERENCES

(1) CARSLAW, H. S., and JAEGER, J. C. *Conduction of Heat in Solids*, p. 71 (London: Oxford University Press, 1948).
(2) RUDDLE, R. W. *The Solidification of Castings*, p. 29 (London: The Institute of Metals, 1950).
(3) PASCHKIS, V. *Trans Amer. Foundrymen's Assoc.*, **53**, pp. 90–101 (1945).
(4) CLARKE, K. L. *Trans Amer. Foundrymen's Assoc.*, **53**, pp. 88–89 (1945).

Measurement of metallurgical equilibria by thermal conductivity gas analysis

By J. W. Evans, Ph.D.,* International Nickel Co. of Canada, Ltd., Copper Cliff, Ontario, Canada

[*Paper received 9 June*, 1955]

A gas thermal conductivity cell is used to measure the high temperature equilibria between metal oxides and carbon monoxide/carbon dioxide gas mixtures.

In the extraction and refining of metals the high temperature thermodynamic properties of substances such as oxides and sulphides are essential data for the understanding of the processes involved. Of particular interest is the free energy of formation which is frequently obtained by high temperature equilibrium measurements of the substance with an appropriate gas phase.

For example, with oxides, sulphides and carbides the following equilibria have been widely used:

(1) $MeO + CO = Me + CO_2$.
(2) $MeS + H_2 = Me + H_2S$.
(3) $MeC + 2H_2 = Me + CH_4$.

For each of these reactions at any one temperature, the equilibrium is determined by the gas compositions in contact with the solid phases. The measurement of the equilibria then depends essentially on some form of accurate gas analysis.

A variety of methods which are comprehensively described by Kubaschewski and Evans[1] have been used and will not be discussed here. In practice, the equilibrium gas ratios vary over a wide range depending on the system and any method usually involves the careful determination of one component of the gas mixture which may be present at quite low concentrations.

The thermal conductivity method of gas analysis is very suitable for the determination of these gas compositions since the method, apart from its great potential sensitivity (especially with hydrogen as one component), has the advantage of almost continuous measurement without disturbing the equilibrium. The principles of thermal conductivity methods are well known and an excellent account together with many industrial and research applications is given by Daynes.[2] However, little use has been made of thermal conductivity methods in studying metallurgical equilibria and the apparatus described here deals with its application to oxide equilibria at about 1000° C.

The metal oxide is brought to equilibrium with a gas phase of carbon monoxide/carbon dioxide, the gases being continuously circulated through the furnace tube and the thermal conductivity cell to avoid thermal diffusion errors. The approach to equilibrium can be followed continuously without in any way disturbing the equilibrium.

THE APPARATUS

A schematic drawing of the apparatus is shown in Fig. 1. *F* is a fused silica tube, of 1 in. outside diameter, mounted centrally in a Nichrome-wound tubular furnace, of 2½ in. internal diameter. The silica tube is baffled externally with refractory brick to concentrate a uniform temperature zone in the centre. A chromel-alumel thermocouple (not shown) is secured outside the tube with the tip of the thermocouple at the centre of the tube. The furnace is hand-controlled by a Variac type autotransformer to within ±2° C. One end of the silica tube is drawn down to 3 mm diameter and this end is connected to glass tubing at J_1 with pressure tubing coated with deKhotinsky cement; at the other end a large standard taper Pyrex joint is connected at J_2 with cement. The use of the taper joint enables the sample boat *S* to be taken in and out of the tube.

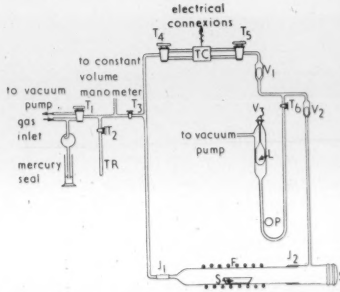

Fig. 1. Thermal conductivity apparatus for equilibrium measurements

TC is the thermal conductivity cell (described in detail below) connected between two double-oblique taps T_4 and T_5. The connexions to the cell are metal-glass joints sealed with deKhotinsky cement.

OP is an oscillating mercury-column pump. The oscillating column alternately operates valves V_1 and V_2 and circulates gas continuously in a closed circuit through the furnace and the thermal conductivity cell.

THERMAL CONDUCTIVITY CELL

The cell *TC* consists of four separate platinum resistance elements mounted in a single stainless steel block which is enclosed in a steel case packed with glass wool to protect the cell from sudden temperature changes. Two of the elements are in the reference gas line which contains pure carbon dioxide. The other two elements are in the gas line through which the unknown gas mixture of carbon dioxide and carbon monoxide passes. The resistance elements are arranged in a Wheatstone bridge network. A constant current of 60 mA is maintained across the bridge and the out-of-balance condition set up by the unknown gas mixture creates a potential difference which is accurately measured with a null-point potentiometer using a mirror galvanometer.

* Now at Department of Metallurgy, University of Manchester.

CALIBRATION

Pure carbon dioxide is obtained by freezing out dry cylinder gas in a liquid nitrogen trap and pumping off the residual air which is the chief impurity. Pure carbon monoxide is obtained by condensing commercial cylinder carbon monoxide to liquid in a liquid nitrogen trap, allowing about half to evaporate to eliminate uncondensed nitrogen, oxygen and hydrogen and finally passing the remaining half through a liquid oxygen trap to remove water, hydrocarbons and carbon dioxide.

The entire system is evacuated and then filled with pure carbon dioxide at atmospheric pressure, both the reference and unknown gas lines being filled with carbon dioxide. The current through the cell is adjusted to 60 mA and the off-balance voltage determined with the potentiometer. Ideally, when both lines are filled with the same gas, the bridge should be balanced; this deviation is caused by the physical asymmetry of the resistance wires in the cell block. One line of the cell is sealed with pure carbon dioxide at atmospheric pressure to serve as the reference gas. The remainder of the system is evacuated. Tap T_2 is closed and the apparatus filled with pure carbon dioxide at a definite pressure and volume by means of the constant volume manometer. Tap T_2 is then opened and the carbon dioxide condensed in the trap *TR* with liquid nitrogen. Tap T_2 is closed and carbon monoxide gas is passed into the same volume at the required pressure by manipulation of the constant volume manometer. Tap T_2 is opened and the liquid nitrogen removed from the trap *TR*. The required carbon dioxide/carbon monoxide ratio is simply the ratio of the pressures at constant volume. Tap T_3 is now closed.

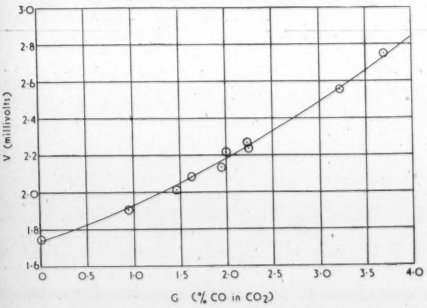

Fig. 2. Calibration curve for thermal conductivity cell *TC*

The off-balance voltage is determined and checked for constancy with time by pumping the gases around the system with the oscillating pump. The off-balance voltage is plotted for different volume percentages of carbon monoxide in carbon dioxide and a calibration curve constructed as shown in Fig. 2.

The "best" curve through the experimental points was obtained by the method of least squares assuming that the curve could be represented by the function $V = 1{\cdot}731 + 0{\cdot}173G + 0{\cdot}0263G^2$, where V is in millivolts and G is volume percentage of carbon monoxide in carbon dioxide.

PROCEDURE

A sample of the metal oxide weighing about 1 g, contained in a fused alumina boat, is placed in the furnace and brought to the required temperature in air. The system is evacuated and a carbon monoxide/carbon dioxide gas mixture introduced in the manner already discussed in the calibration section. The amount of carbon monoxide in the gas mixture is adjusted on the basis of preliminary experiments to give about 10% reduction. The use of a carbon monoxide/carbon dioxide mixture rather than pure carbon monoxide is to prevent the possible initial thermal decomposition of pure carbon monoxide in the cooler parts of the furnace tube according to the equation

$$2CO = CO_2 + C$$

This gas mixture is then circulated continuously for some hours in the closed system at about 1 litre/min and the approach to equilibrium observed by means of the potentiometer readings of the thermal conductivity bridge. The approach to equilibrium is also made from the oxidizing side with pure carbon dioxide after previous partial reduction.

The method is very sensitive; as little as 0·005% carbon monoxide by volume in carbon dioxide can be detected. It is, however, limited by the accuracy with which the thermal conductivity cell can be calibrated. With appropriate modifications other metallurgical equilibria involving a binary gas mixture can be investigated. For reactive gases, e.g. hydrogen sulphide/hydrogen mixtures in sulphide systems, a glass cell with glass-coated platinum wires would be suitable and the oscillating mercury pump could be replaced by an electromagnetic glass-solenoid pump such as that described by Leake[3] for corrosive gases.

ACKNOWLEDGEMENTS

This work was carried out in the Copper Cliff Research Laboratory of the International Nickel Co. of Canada Ltd., and is published by permission of the management. The author wishes to thank Messrs. W. Buchanan and A. Thornborough for help in conducting the tests and in construction of the apparatus.

REFERENCES

(1) KUBASCHEWSKI, O., and EVANS, E. LL. *Metallurgical Thermochemistry*, p. 146 ff. (London: Butterworth–Springer Ltd., 1951).

(2) DAYNES, H. A. *Gas Analysis by Measurement of Thermal Conductivity* (London: Cambridge University Press, 1933).

(3) LEAKE, L. E. *J. Sci. Instrum.*, **30**, p. 434 (1953).

An X-ray method for studying radial current distributions in electron beams

By J. S. THORP, Ph.D., B.Sc., A.Inst.P.,* Services Electronics Research Laboratory, Admiralty, Baldock, Hertfordshire

[*Paper received* 3 *May*, 1955]

An X-ray method is described for studying the radial distribution of current in low-voltage electron beams. The continuous X-ray spectrum is used. X-rays generated where the beam impinges on a thin foil are transmitted and produce an image of the transverse section of the beam on a film pressed against the foil. One application is in connexion with millimetre wave klystron development, and the potentialities of the method are illustrated by reference to beam studies with internally coated cathodes.

In assessing the value of new forms of cathode[1,2,3] for use in millimetre wave klystrons information is required about the diameters of the beams which can be produced and the current distributions in them so that estimates of interception and coupling factor for given designs of r.f. structure may be made. Similar problems are encountered in estimating the performances of X-ray tubes, and in this connexion the use of the pin-hole camera for beam cross-section studies is well known.[4] In X-ray tubes the anode is normally a water-cooled block and X-rays enter the camera through a window in the side of the tube. The characteristic radiation from the target is employed and the operating voltage is raised to about four times the threshold voltage to increase the X-ray intensity.† A typical arrangement might involve a target-film distance of 10 cm and a pin-hole diameter of 0·1 mm, and under normal loading conditions, e.g. 20 mA at 40 kV for a copper target, exposure times might be a few seconds.

Several factors make pin-hole camera techniques unsuitable for beam studies relating to millimetre wave valves. These devices often operate at beam voltages of a few kilovolts which may be too low for excitation of characteristic radiation. The continuous spectrum must therefore be used and because of its low intensity the exposure times would be prohibitively long. Moreover, the beam diameters are generally an order of magnitude smaller than in X-ray tubes, and to obtain good resolution very small pin-holes would be needed; this would again lead to long exposures, and would also make alinement critical. Finally, space restrictions may be severe if measurements are to be made in magnetic confining fields. A simple transmission X-ray method has therefore been developed. The cathode to be studied is mounted in a small valve whose anode is a thin foil. Soft X-rays, generated where electrons impinge on the foil, are transmitted, and produce an image of the transverse section of the beam on a film pressed against the outer surface of the foil; the blackness at any point in this image is proportional to the current density at the corresponding point in the electron beam. Pulsed voltages are used to reduce the anode loading, but because of the high power density in the beams and the small target-film distance exposure times are short.

VALVE DESIGN AND TECHNIQUES

Techniques for using foil anodes have been developed in connexion with the X-ray microscope.[5,6] In this instrument currents of about 10 μA at voltages between 3 and 13 kV are concentrated into a spot of 10^{-3} mm diameter, and X-rays generated at this source pass through the specimen to the photographic plate. In the present technique, however, the X-ray distribution in the source itself is used to derive information about the electron beam and both the beam current and diameter are several orders of magnitude higher than in the microscope.

The type of valve used is shown schematically in Fig. 1. Sealed-off valves have been used exclusively to avoid gas

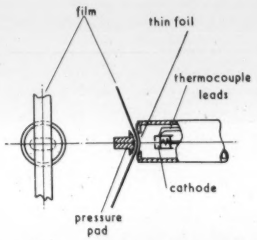

Fig. 1. Valve with foil anode

focusing effects, and the pumping procedure follows standard practice. The foil, usually of copper, is brazed over a rectangular slot in the anode block and the cathode system is subsequently sealed in at the appropriate spacing. In alternative designs the foil is supported by a fine mesh grid. A major requirement is that the exposure time should be short, both for convenience and to avoid errors due to changes in cathode activity over long periods. However, the foil must withstand atmospheric pressure over an area of several square millimetres and thus the thickness chosen is that giving the lowest absorption with the requisite mechanical strength.

The absorption introduced by a foil can be expressed by the relation

$$I/I_0 = \exp(-\mu_\lambda . x)$$

where I = transmitted X-ray intensity, I_0 = incident X-ray intensity, μ_λ = linear absorption coefficient at wavelength λ, and x = foil thickness. In this expression μ_λ increases as the cube of the wavelength and, as the table shows, there is a large spread in the short wavelength limits below 10 kV.

The Kα characteristic radiation from copper has a wavelength of 1·54 Å. It thus appears that near 8 kV the absorption will be similar to that obtained in normal X-ray crystallographic practice, but that it will rise rapidly at lower voltages.

* Now at Radar Research Establishment, Great Malvern, Worcs.

† For characteristic radiation $I = ki(V - V_0)^{1\cdot5}$, where I = X-ray intensity, k = constant, i = beam current, V = applied voltage, V_0 = threshold voltage.

This suggests that foils 25 μ thick would be practicable; these are sufficiently strong, and foils of thickness 25 μ to 100 μ were used to cover the voltage range 4 kV to 10 kV.

Short wavelength limits below 10 kV

Voltage (kV)	1	2	3	4	5
Wavelength (Å)	12·39	6·18	4·13	3·09	2·47
Voltage (kV)	6	7	8	9	10
Wavelength (Å)	2·06	1·77	1·54	1·37	1·23

The beam diameters likely to be encountered are an order of magnitude greater than these foil thicknesses. Relations for heat flow under these conditions have been given by Oosterkamp.[7] Assuming inner and outer surface temperatures of 300° C and 20° C respectively, calculations show that the maximum loading which such foils can withstand continuously is about 4 kW mm^{-2}. This is less than the energy density likely to be found in some high current, small diameter beams; for example, the average power density is about 5 kW mm^{-2} in a 50 mA, 5 kV beam of diameter 0·25 mm. For this reason pulsed voltages are used to reduce the anode loading. Millisecond pulses are sufficiently long to simulate d.c. conditions and with low-duty cycles, of about 0·002, a range of conditions of beam current, voltage and diameter can be explored.

Standard photographic techniques are adequate for most purposes. Strip films are used so that a sequence of exposures can be processed simultaneously. The film must be closely pressed to the foil, as the resolution obtainable is determined by the distance between them. The exposure time necessary under given beam conditions is found by trial. For constant current and voltage it decreases with decreasing beam diameter, and in the present work was usually between 5 min and 1 s; these times correspond to 600 pulses and 2 pulses respectively. Further details are given in the next section. It is convenient to take several different exposures for a given beam so that comparisons can always be made on images of equal density. In some cases the exposure required may be less than the pulse duration; additional absorbing foils may then be inserted between the valve and the film as necessary. The smallest beam diameter which can usefully be studied is about 0·25 mm because of the resolution obtainable with the simple techniques outlined.

APPLICATIONS

The technique can, in principle, be applied to study the radial current distribution in beams produced by any electron gun system operating at suitable voltages. Here it has been used to investigate beams produced by internally coated cathodes.[1,2,3] These cathodes are of special interest in connexion with millimetre wave valves because preliminary experiments suggested that annular beams of high current density could be obtained. The form of the cathode used is shown in Fig. 2. In many klystrons and travelling wave devices beam interception is minimized by using magnetic confining fields, while the power output and tuning range depend on the beam current and voltage. The beam cross-section was therefore studied for various values of these parameters.

The type of information which can be obtained is illustrated by Fig. 3, which reproduces part of a sequence obtained with increasing field at constant voltage and temperature. Visual inspection shows the form of the radial and peripheral current density distributions and quantitative data can be derived from photometric measurements of the record. Low-current beams are annular in low fields but the current density is not uniform round the annulus. Beam parameters which are useful in calculations of the beam interception and coupling

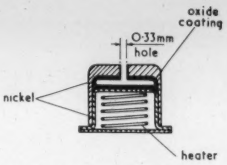

Fig. 2. Geometry of an internally coated cathode

Fig. 3. Current distributions in a 6 kV, 12 mA beam

Cathode temperature 820° C. Left to right, 0, 500, 1000 gauss; exposures 30, 15, 8 s (50 μ foil, millisecond pulses, duty cycle 0·002).

factor for a given r.f. structure are the overall diameter d, the peak-to-peak diameter p, and a shape factor s, defined as the percentage ratio of the current density on the axis to the peak value in the annulus. Fig. 4 shows these parameters

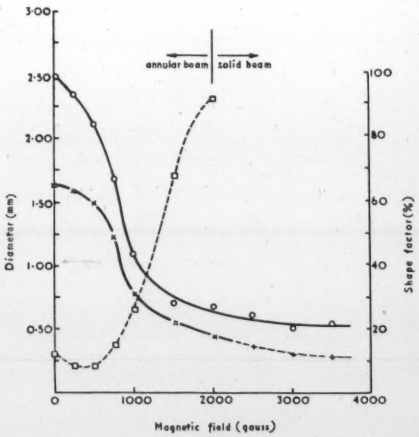

Fig. 4. Variation of beam parameters with magnetic field

Anode voltage 6 kV. Cathode temperature 820° C. Current 12 mA. (□ overall diameter, × peak-to-peak diameter, + half peak width, □ shape factor.)

plotted as functions of field for a low-current 6 kV beam. With increasing field d falls to an approximately constant value which is slightly greater than the cathode diameter. Initially s falls to a minimum value of about 10% but subsequently rises until, when the sides of the annulus begin to overlap, the beam is no longer annular. The difference in the values of d and p shows clearly the departure from an ideal straight-edged beam. Similar experiments of this kind enable a comprehensive knowledge of the current distribution in the beam to be obtained under a wide range of operating conditions.

ACKNOWLEDGEMENTS

The author wishes to thank Mr. P. O. Hawkins and colleagues at the Services Electronics Research Laboratory for helpful advice. This paper is published by permission of the Admiralty.

REFERENCES

(1) MUELLER, G. E. *Trans Inst. Radio Engrs (P.G.E.D.)*, **4**, p. 33 (1953).
(2) KUMPFER, B. D., and BRETT, H. *Convention Record Instn Radio Engrs*, Part III, p. 66 (1954).
(3) HAWKINS, P. O. *Nature [London]*, **174**, p. 1177 (1954).
(4) GAY, P., HIRSCH, P. B., THORP, J. S., and KELLAR, J. N. *Proc. Phys. Soc. [London]*, **64**, p. 374 (1951).
(5) COSSLETT, V. E. *Proc. Phys. Soc. [London] B*, **65**, p. 782 (1952).
(6) COSSLETT, V. E., and NIXON, W. C. *J. Appl. Phys.*, **24**, p. 616 (1953).
(7) OOSTERKAMP, W. J. *Philips Res. Rep.*, **3**, p. 49 (1948).

A thermally triggered spark gap

By T. E. BROADBENT, M.Sc., and J. K. WOOD, M.Sc., Electrical Engineering Department, University of Manchester

[*Paper first received* 20 *June, and in final form* 4 *July*, 1955]

A new effect is described in which the presence of a small source of heat at one electrode of a spark gap considerably reduces its breakdown voltage. The performance of the gap is investigated.

INTRODUCTION

It is well known that a double electrode spark gap can be made to break down at voltages considerably less than the direct breakdown voltage, by the application of a pulse of a few kilovolts to a third electrode, which projects into a small hole in the sparking surface of one of the main electrodes.[1] This system is used as a means of triggering high voltage spark gaps.

Recent work[2] has shown that self-illuminating gaps of this type can be made to break down at voltages as low as half the direct breakdown voltage. It has also been shown that the time lag between the application of the trigger pulse and the breakdown of the main gap depends upon the magnitude and polarities of the pulse and main gap charging voltage. When both the trigger pulse and main gap polarities are positive, time lags of the order of 50 μs, with small scatter, were observed. The breakdown process under these conditions is generally attributed to field distortion, ionization and photo-ionization. The present work was undertaken with a view to investigating the relative importance of these effects.

The term "direct breakdown voltage" is used to denote the breakdown voltage of the gap when the triggering mechanism is not in operation.

EXPERIMENTAL WORK

Preliminary experiments. It was first decided to establish a source of electrons at the cathode, without field distortion. This was accomplished by replacing the third electrode[1] with a tungsten wire, heated electrically to incandescence (Fig. 1). This was found to give a voltage lowering equivalent to that of the self-illuminating gap[2] for both charging polarities. It was noticed that considerable lowering of the breakdown voltage was obtained when the temperature of the tungsten wire was too low to allow appreciable thermionic emission. A large quantity of tungsten oxide smoke was generated as the wire burnt away, and it was thought that this might be affecting the breakdown potential. The hot wire was therefore mounted inside the hemisphere (Fig. 1),

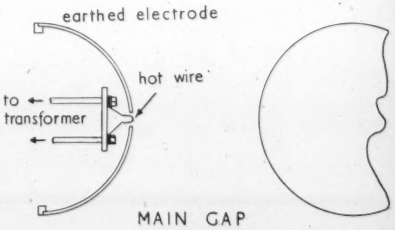

Fig. 1. The thermally triggered spark gap
15 cm diameter electrodes.

the back of which was sealed so that smoke escaped only through the hole in the sparking surface. This test showed that the presence of the smoke did not affect the direct breakdown potential.

It would appear from these results that field distortion did not account for the voltage lowering effect to any great extent in this type of gap. As the effect seemed to be independent of appreciable thermionic emission, it was decided to carry out a series of experiments using Nichrome wire instead of tungsten. This wire forms an oxide layer which protects the surface from further oxidation and can be used up to red heat.

RESULTS WITH NICHROME WIRE

Effect of wire current. Fig. 2 shows the variation of breakdown voltage lowering (expressed as a percentage of the direct breakdown voltage) with current in the Nichrome wire, for a variety of gap lengths, and with both charging polarities. An approximate scale of temperature has been added; the higher temperatures were measured with an optical pyrometer, and the lower ones obtained by interpolation. In view of the high percentage lowering of breakdown voltage obtained with relatively low wire temperatures, it would appear that thermionic emission is not responsible for this effect.

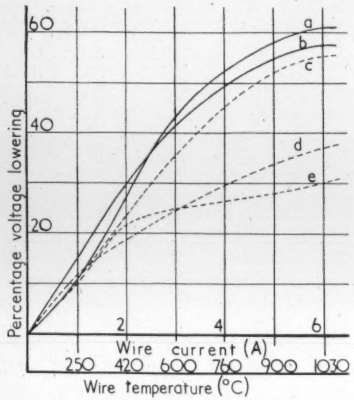

Fig. 2. Voltage lowering curves for the hot wire gap

——— negative charging: a = 2 cm gap.
b = 8 cm gap.

..... positive charging: c = 2 cm gap.
d = 6 cm gap.
e = 10 cm gap.

(intermediate gap lengths are omitted for clarity)

Effect of position of wire. Experiments were carried out with the tip of the Nichrome wire loop in various axial positions relative to the hole in the main electrode. Breakdown voltage is plotted against position of the wire at wire temperatures ranging from cold to red heat (1030° C) in Fig. 3. It may be seen from these curves that the greatest percentage lowering of breakdown voltage occurs when the tip of the Nichrome wire is level with the sparking surface. The curves also show that the hot wire rapidly becomes ineffective as it is withdrawn through the hole.

Effect of wire diameter. Experiments carried out with various wire diameters, ranging from 0·2 to 1·46 mm, showed that the percentage lowering of breakdown voltage did not vary appreciably with wire size.

Tests with a thin foil placed over the hole in place of the wire, and heated from behind, gave similar results to those obtained with the hot wire.

Corona measurements. It was observed that with positive charging voltages less than those required to produce breakdown, and with wire temperatures greater than about 700° C, a fine, needle-shaped discharge occurred at the cathode. The length of this discharge increased with voltage up to about 25% of the gap length just below the breakdown potential. This corona occurred in a series of bursts, ranging in frequency from less than one to about ten bursts per second. The frequency of these bursts varied with both wire temperature and charging voltage. The effect may be explained as follows: a corona burst causes a draught towards the hot

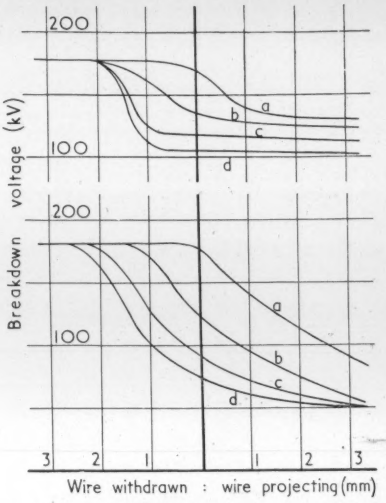

Fig. 3. Breakdown voltage curves for 8 cm gap with various axial wire-tip positions

Above: positive charging.
Below: negative charging.

In each case: a = zero wire current.
b = 2 A wire current.
c = 4 A wire current.
d = 6 A wire current.

wire; this cools the wire and thus reduces corona; the draught decreases and the temperature of the wire increases, which results in an increase in corona. This cycle is repeated.

An audible whistle was occasionally noticed when corona was present. On investigation, each corona burst proved to be composed of a succession of Trichel pulses.[3] The frequency of these pulses was considerably lower than that obtained by Trichel at atmospheric pressure. When the hot wire was replaced by a cold, slightly projecting point, pulses were obtained which agreed closely in frequency and current to those observed by Trichel. Mean corona current is plotted against frequency for both cases in Fig. 4: Trichel's curves for atmospheric pressure and 20 mm of mercury are added for comparison.

Effect of hot air. In order to determine whether the presence of a heated metal surface was necessary to initiate the process of breakdown, tests were carried out in which a small gas flame inside the hemisphere caused hot air to escape from the hole in the sparking surface. In order to prevent the possibility of a strongly ionized channel being produced in the main gap, the flame was arranged so that

the visible part ended well over a centimetre behind the hole. A large percentage lowering of the breakdown potential was observed.

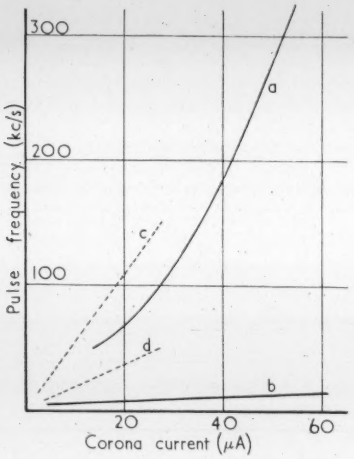

Fig. 4. Corona current and pulse frequency curves

——— observed results at atmospheric pressure.
a = gap with projecting point replacing hot wire.
b = hot wire gap.
..... Trichel's results.
c = 760 mm of mercury pressure.
d = 20 mm of mercury pressure.

CONCLUSIONS

From the results obtained with the hot wire gap it would appear that the mode of action of the self-illuminating gap described in the Introduction depends upon the production of a small region of hot air as well as ionization, the presence of this region of hot air being mainly responsible for the breakdown voltage lowering effect. In the case of positive charging and trigger polarities, the long time lags which were obtained were of the same order as the intervals between the corona pulses observed under similar conditions with the hot wire system. These time lags may represent the time required to sweep the gap more or less free of positive ions produced by the trigger discharge. Investigations into the mechanism of breakdown in these gaps are now in progress.

The hot wire gap provides a simple and cheap method of triggering a high voltage spark gap. Where synchronization with an oscillograph is required, delay cables are needed. An advantage over mechanical tripping systems is that no moving parts are required.

ACKNOWLEDGEMENTS

The authors wish to thank Professor F. C. Williams of the Electrical Engineering Department of Manchester University for facilities provided and for his interest in this work. One of us (J. K. W.) also expresses his gratitude to the Department of Scientific and Industrial Research for a maintenance grant.

REFERENCES

(1) Craggs, J. D., Haine, M. E., and Meek, J. M. *J. Instn Elect. Engrs*, **93** (3A), p. 963 (1946).
Wilkinson, K. J. R. *J. Instn Elect. Engrs*, **93** (3A), p. 1090 (1946).
(2) Hardy, D. R., and Broadbent, T. E. *Proc. Instn Elect. Engrs*. To be published.
(3) Trichel, G. W. *Phys. Rev.*, **54**, p. 1078 (1938).

Initiation of hot-cathode discharges

By N. R. Daly, Ph.D., and Professor K. G. Emeleus, Ph.D., F.Inst.P., Queen's University, Belfast

[*Paper received* 1 *July*, 1955]

An experimental study has been made of the effect of a voltage fall along a hot cathode on the initiation of a gas discharge in a diode at low pressure. Plasma forms first near the negative end of the cathode and spreads along the cathode with increase in tube current. Positive ions diffuse in the inter-electrode space towards the positive end of the cathode, where the potential difference between cathode and anode when plasma is present may be well below the ionization potential of the gas. Observations have been made on the appearance of the discharge before and after plasma forms, and on oscillations generated by the discharge.

Although a large amount of work has been done on low-voltage arcs,[1,2,3] no systematic investigation appears to have been made of the effect on these of a voltage drop along the cathode. This occurs commonly in both commercial and experimental tubes. The present work was undertaken to study its effect on the initiation of the discharge. Initiation is here taken to mean the stages leading to production of a plasma in some part of the discharge space, and the growth of the plasma to its final form with the electron current from the cathode saturated, or nearly so. By a plasma we mean in the present connexion a region of quasineutral ionized gas, giving current *v* voltage characteristic curves of regular shape for a small Langmuir probe.

Most of our measurements have been made in mercury vapour at room temperature (about 20° C), with electron free paths greater than the linear dimensions of the electrodes. It has been found that plasma first appears abruptly over a short section of the negative end of the cathode, and spreads with increasing current along its length. Oscillations occur immediately before the plasma forms, and whilst it is spreading. When the current was just saturated, the potential difference between the positive end of the cathode and the neighbouring plasma was still less than the ionization potential.

A few measurements have been made in argon. The discharges at low pressure (about 10^{-3} mm of mercury) were

similar to those in mercury vapour; at higher pressure (about 1 mm of mercury) plasmas with more complex structure were obtained.

EXPERIMENTAL ARRANGEMENTS

Most of the measurements were made with five demountable tubes connected to the pumps. The first tube (I) had an open-ended cylindrical anode 6 cm long and 2 cm in diameter, in four identical cylindrical sections almost touching one another, with separate leads, and an axial 100 μ bare straight tungsten cathode 6 cm long. The second tube (II) was similar, but had a continuous anode, and two 100 μ tungsten probes, each 8 mm long, half-way between the cathode and anode at each end of the tube. The third tube (III) was similar to tube II, with a single 100 μ tungsten probe 2 mm long which could be moved to any position between the cathode and anode. The fourth tube (IV) was similar to tube II, but had its cathode interrupted at its middle point by a 2 cm length of thicker wire, which did not become hot enough to emit electrons; it had probes like those in tube II. The fifth tube (V) had a straight oxide-coated cathode 6 cm long and approximately 50 μ in diameter, parallel to and 7 mm from a rectangular ($6 \times 1{\cdot}5$ cm) plate anode, with a fixed probe like that in tube II at the negative end. The position of the filament leads was found to have practically no effect; all the data given are for tubes with filament leads outside the anode, usually taken to opposite ends of the tube. It was also found that addition of caps at anode potential to the anode cylinders produced no change in the general nature of the results. The probes were cleaned by electron bombardment from the plasma before taking measurements.

The cathode, tube and probe currents were drawn from accumulators. The fall of potential along the bare cathodes (I–IV) was about 12 V, and along the oxide-coated cathode (V), 6 V. The tube and probe current v voltage characteristic curves were either obtained with sensitive galvanometers with low-resistance shunts ($<1\ \Omega$), or displayed on a cathode-ray oscillograph with a persistent screen and photographed on microfilm. Plasma-electron oscillations were detected with a cavity resonator, and lower frequency plasma-ion or relaxation oscillations with a cathode-ray oscillograph.

EXPERIMENTAL RESULTS

Typical semi-logarithmic characteristic curves for three of the four anode sections of tube I, measured simultaneously with galvanometers, are shown in Fig. 1. The numbers 1, 3 and 4 refer to different sections, starting with 1 at the negative end of the filament. The curve for section 2 was almost identical in shape with that for section 1. Potentials were measured relative to the negative end of the cathode. The characteristics show the following main features:

(*a*) On initially increasing the voltage from small values, the currents to all segments are small up to nearly 14 V. The smallest currents (not shown) give nearly straight lines, with abrupt increases of slope at 10·5, 12·0, 13·5 and 13·7 V for sections 1, 2, 3 and 4 respectively, as in the space-charge method for measuring ionization potentials.

(*b*) At 14 V discontinuous changes in current occur to all segments, and the voltage falls. Each curve then shows a further rise in current with increase in voltage. After this the curve for section 1 rises to approximate saturation, with an initial section of negative slope. The curve for section 3 is similar, with a shorter section with large negative slope, but an almost horizontal low-current section. The latter is further developed for section 4, and the main section with negative slope almost absent. The final rise with positive slope occurs for voltages of 10·6 V upward for each segment and approximate saturation is reached for sections 1 and 3 at the same voltage; section 4 is saturated a little later.

(*c*) When an abrupt change in current occurs for one segment it occurs for all others. This applies both to the large changes shown in Fig. 1, and to smaller changes smoothed out in drawing the curves.

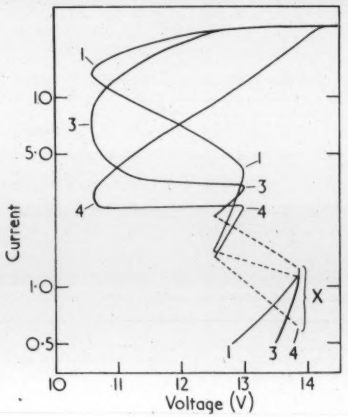

Fig. 1. Current/voltage characteristics for sections of tube I. Current is on a logarithmic scale

Temperature of mercury 18·5° C. Filament voltage 12·3 V. The saturation currents have been reduced to a common maximum: actual values for the four sections were: 1, 75 mA (2, 100 mA), 3, 63 mA, 4, 38 mA.

The shapes of the tube characteristics for tubes II and III were roughly means between those for the segments of tube I. That for tube IV was like those for tubes II and III, with an almost vertical rise to saturation, interrupted by a discontinuity half-way up.

The probe characteristics obtained with tubes II–V were regular, showing the presence of electron groups[4] with drift velocity, when the tube current was saturated. Above the first low-current discontinuity on the tube characteristic (X, Fig. 1), and below saturation, the probe characteristics were regular only opposite the negative end of the cathode, and for a distance towards the positive end which increased with tube current. When plasma was present, it was usually 2–3 V positive to the anode, with radial changes in potential less than 0·5 V. There was a small field parallel to the cathode in the plasma, of opposite sign to that in the cathode material, of the order of 1–2 V in 5 cm. The "ultimate" electron concentrations (n_1, n_2) at any two points were related to the potential difference between the points (V) and the electron temperature T, by the formula

$$V = \frac{kT}{e} \ln (n_1/n_2)$$

within the accuracy of measurement (0·25 V).

The appearance of the discharge, which could not be seen clearly in tubes I–IV because of the glare from the cathode and obstruction by the anode, was examined in detail with tube V; the brighter parts of the discharge appeared to be similar in all the tubes. On increasing the tube voltage from zero with a filament current of 1·4 A, a thin blue luminous layer, covering the entire anode, was first noticed at about 14 V. The appearance at 14 V is shown in Fig. 2(*a*). On increasing the voltage further the layer became thicker, bulging a little at the ends, and at 24 V extended almost to the cathode [Fig. 2(*b*)]. On reaching 25 V the current

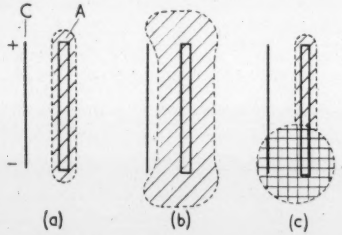

Fig. 2. Diagrams showing appearance of developing discharge at various stages in tube V

Temperature of mercury 16·5° C. Filament voltage 6·0 V. Anode (*A*) and cathode (*C*) are marked in *a*. The faint glow is shown by diagonal shading, and plasma by square shading.

increased abruptly from 3 mA to 18 mA, the voltage fell to 18 V, and a brilliant plasma formed near the negative end of the cathode. The faint glow covering the rest of the anode persisted, but was reduced in thickness to about 2 mm. The appearance is shown in Fig. 2(*c*). With further increase in current, the voltage rose slightly and the plasma extended along the cathode. A thin blue glow remained on that part of the anode not covered by plasma, until the whole of the cathode and anode were enveloped in plasma at 20 V and 150 mA. The spread of plasma occurred by small jumps when there were small discontinuities in the tube characteristic, but otherwise proceeded smoothly. With tube I, a similar spread of plasma was noticed outside the anode, marked bulging from the negative end of the cathode first occurring about where the characteristics started to have positive slope prior to saturation.

The high-frequency oscillatory behaviour of the tubes was like that of the cylindrical tubes studied by Armstrong and Emeleus,[5] and their low-frequency behaviour like that of similar tubes studied by Martin and Woods.[6] Low-frequency oscillations occurred consistently for currents below the first discontinuity (*X*, Fig. 1), both for the individual sections of tube I, and for the continuous anodes. In each case they were first detected at about the voltage for which the change of slope occurred in the linear part of the semi-logarithmic anode characteristic. The frequency changed very little with voltage, but the amplitude increased as point *X* was approached, monotonically for continuous anodes and for sections 3 and 4 of tube I, but with several discontinuities for sections 1 and 2, thought to be connected with the discharge jumping gaps between sections. The waveform was sinusoidal, except near *X*. A typical frequency was 60 kc/s, and a typical amplitude of the oscillations measured between anode and cathode, immediately below *X*, was 0·06 V. These oscillations disappeared above point *X*.

DISCUSSION

The special features of the low-current discharges prior to "firing" (*X*, Fig. 1) are the oscillations, and the uniformity of appearance of the discharge over the anode. As the current from the cathode is not saturated, there will be a potential minimum between the cathode and anode. In addition, once the potential is sufficiently large for ionization to occur, a potential maximum may develop.[7] If a maximum is present, it will move towards the cathode as the current increases, whilst the minimum becomes shallower. The observations with tube V indicate that firing occurs when the layer where the potential is a maximum has reached a critical distance from cathode *C* (Fig. 2). A similar spread of a faint glow from anode to cathode prior to firing was noticed with the discharges in argon at pressures between 0·1 and 1 mm of mercury. The oscillations could be either those of positive ions trapped in the minimum, or of electrons trapped in the maximum. If both types of oscillations occur, their frequencies might be of the same order, the greater mass of the ions being compensated for by the larger curvature of the potential curve at its minimum; it is conceivable that firing is ultimately due to resonance between the two modes. The uniformity of the glow over the anode in tube V was surprising, considering the fall of potential along the cathode and the fact that primary electrons could not reach the back of anode *A* direct, and requires further investigation.[8]

The curves above point *X* after firing are the result of the effects due to the voltage drop along the cathode, superposed on the effects due to changes in cathode field at any one region. The measurements with tubes I and IV, the probe measurements, and the appearance of tube V, together show that plasma forms initially over a restricted length of cathode at the negative end and spreads with increasing current towards the positive end. The shapes of the characteristic curves for the individual sections of tube I are generally similar to those recorded by Pengelly and Wright[3] for nearly equipotential cathodes. They are explicable in the same way as the curves of Pengelly and Wright, with the differences that: (i) there was no detachment of a "ball of fire" in the present investigation, on account of the lower pressure, and (ii) much of the neutralization of electron space-space near the positive end of the cathode, in at least tubes I–IV, must have been due to positive ions which had been formed near the negative end of the filament and subsequently diffused axially, the primary electrons from the positive end of the cathode having insufficient energy to ionize.

REFERENCES

(1) Druyvesteyn, M. J., and Penning, F. M. *Rev. Mod. Phys.*, **12**, p. 87 (1940).
(2) Malter, L., Johnson, E. O., and Webster, W. M. *R.C.A. Rev.*, **12**, p. 415 (1951).
(3) Pengelly, A. E., and Wright, D. A. *Brit. J. Appl. Phys.*, **5**, p. 391 (1954).
(4) Langmuir, I., and Jones, H. A. *Phys. Rev.*, **31**, p. 357 (1928).
(5) Armstrong, E. B., and Emeleus, K. G. *Proc. Instn Elect. Engrs*, III, **96**, p. 390 (1949).
(6) Martin, H., and Woods, H. A. *Proc. Phys. Soc. [London] B*, **65**, p. 281 (1951).
(7) Langmuir, I. *Phys. Rev.*, **33**, p. 954 (1929).
(8) Daly, N. R. Thesis, Queen's University, Belfast (1953).

New books

Introduction to atomic and nuclear physics, 3rd edition. By PROF. H. SEMAT. (London: Chapman and Hall Ltd., 1954.) Pp. xii + 561. Price 50*s*.

This third edition of Professor Semat's *Introduction to atomic physics* has, as the new title indicates, been expanded to include much more nuclear physics, which now occupies about half of the book.

It retains the feature, so characteristic of modern American texts, of being designed to bring students rapidly from a state of low to a state of high information content. This is achieved by providing introductory summaries of basic electricity and magnetism, by concentration upon the factual rather than upon the philosophical aspects of the subject, and by very careful planning of such aids to study as the diagrams and the numerical exercises that are liberally provided. Thus the student who at the beginning has to be reminded about the electrification of a rod rubbed with cat's fur is at grips with the anomalous Zeeman effect midway through the book.

Though it is not usual to lead the British second-year undergraduate up such steep but well-fenced roads to the hill-tops, he will find this book extremely useful near the end of his course when he is preparing for his final examination.

Professor Semat has prepared his text with great care and thoroughness and has arranged to include quite recent work, so the book should rank as a reliable and modern work for several years to come.

P. B. MOON

Applied X-rays. Fourth edition. By PROF. GEORGE L. CLARK. (New York: McGraw-Hill Book Co., Inc., 1955.) Pp. ix + 843. Price 89*s*. 6*d*.

Books about the many and varied applications of X-rays nowadays make a quite impressive list. The present volume is, however, not strictly an addition to the number; the first edition was published as far back as 1927, whilst subsequent editions appeared in 1932 and 1940. Nevertheless the last fifteen years have seen such advances in the X-ray sciences that the author has had to undertake very far-reaching changes and this fourth edition is almost a new publication. The basic plan of surveying all the principal branches of applied X-rays is maintained, but a great part of the text has been revised, or is new.

Professor Clark has had a profound interest in X-rays since the early nineteen-twenties. He could claim to have been one of the original advocates of the use of X-ray techniques for practical purposes and in 1927 attempted to portray X-rays as "a practical research tool in industry." Since then experience of the many different contributions that for example X-ray crystallography and radiology have made to knowledge and scientific progress has provided ample justification for many of the author's views.

There are 843 pages in this fourth edition compared with 673 pages in the third. But the format is also enlarged, so that the increase in size is in fact greater than this simple page number comparison indicates. Part I on the general physics and applications of X-radiation includes an entirely new chapter on microradiography, as well as considerably expanded texts under the old chapter headings. The new chapter is a concise but useful account of a subject of growing importance to physical metallurgists and others.

The second and major part of the book deals with the applications of X-ray diffraction. Although methods and interpretation are discussed, the main emphasis is on results, and the chapters on crystal chemistry, alloys, the texture of metals, organic compounds, and glasses and liquids comprise an excellent survey of the achievements of X-ray analysis. The whole account is sufficiently up-to-date to include references to counter diffractometers, to recent discussions about the statistical treatment of structure factors, and to current models of protein structure, to mention only three examples.

Earlier editions were open to criticism because so few literature references were given. The situation is much improved in this respect by the addition of many references to the literature of the last fifteen years. There is also a better subject index than in earlier editions, though since names are not listed in the subject index, it is surprising to find no author index.

This is a book that should appeal to a very wide circle. The experienced crystallographer may think that individual branches of X-ray analysis are covered more completely and fundamentally in other texts. As a broad and stimulating survey of all the applications of X-rays, however, Professor Clark's account is hardly likely to be bettered in the immediate future.

H. P. ROOKSBY

Strömung durch Rohre, Umströmung von Körpern bei zweidimensionaler Strömung, Umströmung von Körpern bei räumlicher Strömung. By L. SCHILLER (part of volume 4 of the sixth edition of Landolt–Börnstein's tables). (Berlin: Springer-Verlag, 1955.) Pp. 134. Price (Vol. 4) DM 288.

This part, which is concerned with fluid flow, is in three divisions: pipe flow, two-dimensional flow, three-dimensional flow. Prepared by L. Schiller and others, it comprises a vast collection of aero- and hydro-dynamic data in graphical or tabular form (with concise verbal explanations of detail) and is copiously documented with references to original sources. Data for compressible flow are included. The wide range covered is indicated by the following selection from the contents.

Pipe flow. Smooth and rough walls; laminar and turbulent flow; various shapes of cross-section, divergent and convergent channels; orifice plates; corners and branches. Flow resistance; velocity distributions. Pulsating flow.

Two-dimensional flow. Flat plates, smooth and rough; ridges, protuberances, hollows; flat plates at various angles of incidence; circular and elliptic cylinders, prisms; streamline shapes; aerofoils, including scale effect, compressibility effects, and cavitation; high-lift devices—flaps, slots and suction.

Three-dimensional flow. Spheres and circular plates; rectangular plates and wings, including sweep-back; ellipsoids and airship shapes; cylinders, prisms, hemispheres, cones, parachutes, ropes; buildings; beams and lattice girders; snow fences; aeroplanes, fuselages, undercarriages; airscrews; vehicles; projectiles.

The material is attractively presented and well produced; and constitutes a useful reference work and data source.

R. C. PANKHURST

Progress in photography. Vol. 2. Editor-in-Chief, Dr. D. A. SPENCER, Hon. F.R.P.S. (London: The Focal Press, 1954.) Pp. 336. Price 50*s*.

The first volume of *Progress in photography* covered the period 1940–1950, and the volume under review brings the story up to 1954. It contains 63 articles, mainly by British and American authors, though Germany, France and Italy are also represented. Articles which largely supplement material covered in the earlier volume are set in small type, and it is noteworthy that these only account for some 25 pages out of 310.

Most of the articles deal with scientific or technical aspects of photography, though about a fifth of the volume is concerned with the commercial side. The subjects dealt with include emulsion theory, developments in apparatus, colour photography, cinematography and radiography, while under the headings of "Special techniques" and "Special applications" we find articles on high-speed and stereoscopic photography, various aspects of photomicrography and the applications of photography to various fields of research and industry.

The book has considerable value as a work of reference, and this is enhanced by the large number of references which are given. The index comprises some 700 entries, but a few spot checks revealed some omissions.

J. AINGER HALL

Engineering dynamics, Vol. 4: Internal-combustion engines. By PROF. C. B. BIEZENO and PROF. R. GRAMMEL. (Translated by M. P. WHITE.) (Glasgow: Blackie and Son, Ltd., 1954.) Pp. ix + 282. Price 50*s*.

This book is the translation of a classical work which was originally published in German before the war.

Part I deals mainly with the balancing of engines and does so most thoroughly for all conceivable types of in-line, V-, W-type and radial engines, and this section provides interesting suggestions as to possible departures from the conventional standard engine designs. However, the present work resembles most others in that it makes no attempt to deal with the very practical problem of assessing the effects of the residual out-of-balance.

Part II investigates the factors causing cyclic variations in engine speed and cyclic angular deviation. All types of engines are considered, with several methods for determining the moment of inertia required for a flywheel to obtain a specified value of cyclic speed variation.

Part III considers the problems presented by torsional vibration. It begins by considering the torsional stiffness of a crankthrow for the two cases: (*a*) torques acting at the journals, and (*b*) tangential forces at the crankpins. The authors state that the analysis for case (*a*) gives adequate results in most cases, but claim that case (*b*) requires consideration for higher modes of vibration. The authors assume that the basic problems of vibration are already well known to the reader, and obtain natural frequencies by means of recurrence formulae, based on methods for determining characteristic values which are described in Vol. 1. There is little on damping and hence on finite values of peak amplitudes.

For a reader prepared to follow protracted reasoning and unfamiliar symbols, this is a valuable reference book on theoretical engine dynamics.

E. J. NESTORIDES

Introduction to nuclear engineering. By Prof. R. L. MURRAY. (London: George Allen and Unwin Ltd., 1955.) Pp. xiv + 418. Price 30*s*.

This book was written to serve as an introduction to the atomic energy field for engineering students, and it fulfils this purpose admirably. The scope of the subject matter is extensive, and almost all aspects of atomic energy are dealt with, except the chemical processing of irradiated fuel elements. Because of the wide range of topics covered, the engineer obtains a balanced picture of the new science.

Since so many facets of atomic energy are described, the treatment of the subject must necessarily be sketchy in a number of places. However, the book is well supported by references, and the reader should have no difficulty in following up his particular interest in a more comprehensive work. The examples given at the ends of the chapters are simple but illustrative, and because of their simplicity the engineer will be encouraged to work through all of them. The dimensions of most of the physical constants used are quoted in the text, and the author uses the c.g.s. system of units in some places to remind the reader that it is not impossible for an engineer to work in this system.

Two minor criticisms of the book are that the section on the flow of fluids through particle beds seems to intrude rather unnecessarily into the middle of Chapter 10, and the reader is left with the impression at the end of Chapter 11 that electrical power can be produced remarkably cheaply by a reactor, since the author does not stress the fact that the chemical processing of irradiated rods containing plutonium (in order to remove the fission products) may be quite a costly business.

In Section 12.6, it is stated that the temperature effect on resonance capture is principally dependent on moderator temperature, and numerical values are given for the temperature coefficient of reactivity in support of this statement. However, the temperature coefficient found for the B.E.P.O. at Harwell when the uranium temperature only is raised, is in close agreement with the one quoted in the book, which would suggest that the temperature effect due to Doppler broadening is by no means as unimportant as the author suggests.

The reviewer was surprised to find a reference in Appendix A to some simple approximate formulae for Bessel functions quoting a Master's thesis at the North Carolina State College, rather than the more easily obtainable and previously published results of Guggenheim and Pryce in *Nucleonics*.

However, these are only small points, and the book is to be heartily commended as a first reading to all engineers now entering the field of nuclear energy. It is published at a price which is low for a technical work of this kind.

D. J. LITTLER

Protective wrappings. By C. R. OSWIN, M.A., F.R.I.C. (London: Cam Publications Ltd., 1954.) Pp. 268. Price 32*s*.

This is a textbook prepared from articles previously published in *The British Packer* dealing with commercial wrapping materials, their selection and application. The opinions expressed are at times controversial, nevertheless the book does provide a useful and needed source of reference. The author deserves a better vehicle for his work: the published volume abounds in misprints and the printing is abominable.

V. G. W. HARRISON

Notes and comments

Length of papers for publication

The Editor believes that the view is widely held in some laboratories that papers exceeding 3000 words cannot be considered for publication by The Institute of Physics in either this or its other Journal (*Journal of Scientific Instruments*). This is not so. Indeed, papers of nearly double this length have recently been published. To be acceptable, however, papers must be as concise as clarity allows.

The availability of places for physics students in universities and technical colleges

The September *Bulletin* of The Institute of Physics contains a report on the availability of places for physics students in universities and technical colleges. It is based on a survey made by the Institute after the Board decided in November 1954 to investigate the facilities existing in universities and technical colleges for the education of physicists and of the extent to which these were at present being used. Among the reasons which led to this decision were the public discussion of the need to develop facilities for higher technological education (to which discussion the Institute has contributed over the past few years), and various reports that had been presented to the Board on the difficulty experienced by certain technical colleges in securing students for courses in physics for which the colleges were well equipped and which had been running, in some cases, for several years. The report is based on information supplied by twenty-seven universities and fifty-three technical colleges.

The report is followed by the comments of two of the Institute's committees, the Education Committee and the Membership and Examinations Committee. These comments begin by stating: "The data presented in the accompanying report clearly indicate that existing facilities for the education of physicists in universities and technical colleges in Great Britain are more than adequate for the number of students who wish to read for an honours degree in physics and who leave school with qualifications normally regarded as essential for admission to the honours course."

The report and comments have been reprinted with the title *The availability of places for physics students in universities and technical colleges* and copies are available free of charge from The Institute of Physics, 47 Belgrave Square, London, S.W.1.

Exhibition of X-ray photography

A selection of X-ray photographs will be exhibited at The Royal Photographic Society's house, 16 Princes Gate, London, S.W.7, from 13 to 22 December. In addition, ciné films will be shown and several lectures have been arranged. The exhibition will be opened by Mr. W. E. Schall at 4.30 p.m., and at 7 p.m. Mr. Schall and Mr. Cuthbert Andrews will speak on the development of X-ray photography in industry and medicine.

The final date for the receipt of entries is 4 November; entry forms are available from the above address.

Proceedings of the Geneva conference on the peaceful uses of atomic energy

The United Nations have announced that the proceedings of the international conference on the peaceful uses of atomic energy, held in Geneva in August 1955, will be published in sixteen volumes of approximately 500 pages each. There will thus be available the complete, unabridged record of the conference which will comprise all papers, whether presented orally or in written form, together with a record of the discussions on each paper.

These volumes will be published in several languages; the English edition will be available in the beginning of 1956, the others at a later date.

The pre-publication price will be £39 (418 guilders or the equivalent in other currencies) for the full series of sixteen volumes. Advance orders must be received before 31 December, 1955. Orders for the full set of sixteen volumes or for individual volumes (the prices of individual volumes will be announced later) may be placed with any sales agent for United Nations publications including H.M. Stationery Office, P.O. Box 569, London, S.E.1, and N. V. Martinus Nijhoff, Lange Voorhout 9, The Hague, Holland.

Mimeographed copies of most of the individual papers read at the conference are now available at 1*s.* 9*d.* each, 1.00 guilder or the equivalent in other currencies. Orders for individual papers, giving the full title and author, may be ordered through H.M. Stationery Office or through N. V. Martinus Nijhoff. These agents do not carry stocks of the individual papers but will forward orders to the European Office of the United Nations for execution and will accept payment for the papers in national currencies.

Semiconductor symposium

The Fourth Annual Semiconductor Symposium of the Electrochemical Society will be held from 29 April to 3 May, 1956, at the Mark Hopkins Hotel in San Francisco, California. At present it is planned to include two half-day sessions on semiconducting materials, elemental alloys and compounds; a half-day session on surface-controlled phenomena; and a half-day session on chemical process technology. It is hoped to present a balanced agenda including one review paper of the state of each field, 30-minute presentations (including discussion time) of new information which can be scheduled by mid-winter 1955, and a number of shorter presentations of about 10 minutes' duration of the "late news" type.

Persons wishing to present papers are requested to submit to the Chairman the titles of proposed papers as early as possible and no later than 15 November, 1955; submit an abstract of approximately 75 words no later than 15 January, 1956; and submit a second "extended abstract" of about 1000 words with brief pertinent data, illustrations, curves, etc., not later than 1 February, 1956.

Persons wishing to present 10-minute "late news" type of papers are requested to notify the Chairman as soon as possible, giving relevant details and submit 75-word abstracts no later than 8 April, 1956.

The Chairman is J. W. Faust, Jr., Westinghouse Research Laboratories, Beulah Road, Churchill Borough, Pittsburgh 35, Pennsylvania, U.S.A.

Journal of Electronics

We have received the first issue of a journal "devoted to electron sciences," entitled *Journal of Electronics* and associated with *The Philosophical Magazine*. The Editor is Dr. J. Thomson and the Consultant Editor is Professor N. F. Mott. The following comment is taken from the editorial: "The field of this journal is not easy to define. In a very real sense we shall be concerned with phenomena directly attributable to the electron, but since most of the properties of matter fall into this category, it is necessary to make some distinction between the field of the journal and the field of the rest of natural science. In the brochure distributed by

the publishers the field was defined as 'electron science . . . interpreted to mean the description of the behaviour of electrons in the free state or in states where their binding energy is low,' which we had hoped describes what the editors had in mind."

In this first issue of 102 pages measuring 10 × 7 in. there are nine papers with the following titles:

On the initial space charge distribution in a cylindrical magnetron diode; The space charge distribution in the pre-oscillation magnetron; Theory of the preoscillating magnetron I; Factors in the design of power amplifiers for ultra high frequencies; Some experiments on a cylindrical electron beam constrained by a magnetic field; On the solution of an equation of electron optics; Note on moving striations; A review of the structure and some magnetic properties of ferrites; Recent research with an experimental mass spectrometer.

The format and typography of this journal are similar to those of its parent journal (*The Philosophical Magazine*); although adequate, they are perhaps a little dull and unimaginative for so promising an offspring. The journal is to be issued every other month at £1 per issue and the subscription price for the volume of six issues is £5 10*s*. 0*d*. The publishers are Taylor and Francis, Ltd., Red Lion Court, Fleet Street, London, E.C.4.

Safe transport of scientific instruments

For purposes of comparison it is often necessary for laboratories in different countries to exchange scientific instruments. To enable these transfers to be made safely and quickly the United Nations Educational, Scientific and Cultural Organisation has introduced a scheme in which customs officials are present when the instruments are packed and unpacked. An internationally recognized label is attached to such packages which are then exempt from normal customs procedure.

The governments of those laboratories using the scheme provide the Director-General of Unesco, Paris, with a list of the laboratories and details of the methods, including customs procedure, by which they propose to operate the scheme. At present, twenty-two governments have named more than 180 laboratories as participants in the scheme.

Conference on lubrication and wear

The Council of The Institution of Mechanical Engineers is arranging a conference on lubrication and wear to be held in London from 1 to 3 October, 1957, inclusive. Meetings for the presentation of papers will be held each day, as much time as possible being allowed for discussion. It is hoped to obtain papers covering the whole field of lubrication and wear, and the Council invite both members and non-members of the Institution to contribute papers to the conference. Those interested are invited to submit a brief synopsis of about 200 words setting out the proposed title and contents of their contributions. These should be received by the secretary of the Institution at the latest by 1 April, 1956, but notification before this date of intention to submit a synopsis would be very helpful.

Copies of the papers will be available before the conference; the proceedings, including papers and discussion, will be published by the Institution in due course.

Further information may be obtained from the Secretary, The Institution of Mechanical Engineers, 1 Birdcage Walk, London, S.W.1.

British Journal of Applied Physics

Original contributions accepted for publication in future issues of this Journal

Propagation of transient fields from dipoles near the ground. By H. Poritsky.
The corona resisting property of polytetrafluoroethylene. By Shigeo Nagao.
Determination of the velocity of ultrasonic sound in molten salts. By N. E. Richards, E. J. Brauner and J. O'M. Bockris.
Creep and static friction. By R. T. Spurr.
The effect of standing wave pattern changes in the virtual cathode of an electron emitter on the emission characteristics. By W. W. H. Clarke.
The capacity and field of a cylindrical trough with a plane conductor in the axial plane of symmetry. By H. J. Peake and N. Davy.
Reduction of noise in photoconductive cells. By R. E. Burgess.
Technical properties of iron powder magnets. By E. H. Carman.
The thermal conductivity of liquid and gaseous oxygen. By H. Ziebland and J. T. A. Burton.
Stability inertia for an electrical network with distributed parameters. By A. S. Gladwin.
The scanning electron microscope and its fields of application. By K. C. A. Smith and C. W. Oatley.
A simple adaptation of the carbon replica technique for the examination of selected areas in the electron microscope. By D. E. Bradley.
The deposition of thin films of gold on cylindrical specimens by sputtering. By F. R. Lipsett.
The gamma-ray spectrum of fission products from slow neutron irradiation of uranium 135. By D. H. Peirson.

Journal of Scientific Instruments

Contents of the October issue

SPECIAL ARTICLE

The physics of the scintillation counter. By G. F. J. Garlick.

ORIGINAL CONTRIBUTIONS

Papers

Simplified apparatus and procedure for freezing-point determinations upon small volumes of fluid. By J. A. Ramsay and R. H. J. Brown.
A furnace for obtaining optical spectra of radioactive elements. By L. F. H. Bovey.
An apparatus for the measurement of γ-radiation from the human body. By J. Rundo.
An electronic magnetometer. By B. G. Cragg.
A photoelectric light-spot-displacement detector. By A. Thulin.
An analogue computer for nuclear reactions. By E. S. Shire.
A fraction collector for chromatography. By E. T. Sanders.
Tube wall thickness gauge with selection of backscattered γ-radiations. By J. L. Putman, S. Jefferson, J. F. Cameron, J. P. Kerry and E. W. Pulsford.

Laboratory and workshop notes

A method of machining slits and pinholes. By S. P. Middleton.
An improved high-conductance cold-trap. By A. J. Martin.
An automatic cathode-ray oscilloscope beam brightening device for transient recordings. By J. Wood.
Modifications to an air-driven ultra-centrifuge. By I. J. O'Donnell.
A resistance thermometer with a high speed of response. By W. T. Bane and E. R. Dymott.
A simple achromatic doublet for spectroscopic purposes. By N. J. Rumsey.

NOTES AND NEWS

Correspondence

Logarithmic device for a densitometer. From D. T. R. Dighton.
Adaptation of a projection microscope for microphotometry. From D. H. Tomlin and F. J. Fayers.
Realizable light gain in photoelectronic image intensifiers. From L. Mandel.

New instruments, materials and tools

Small analogue computer. High-speed vibration mill. An ionizing unit for discharging non-conductive specimens in an electron diffractograph. Painted circuit kit.

Notes and comments

THIS JOURNAL is produced monthly by The Institute of Physics, in London. It deals with all branches of applied physics (including theory and technique).
All rights reserved. Responsibility for the statements contained herein attaches only to the writers.
EDITORIAL MATTER. Communications concerning editorial matter should be addressed to the Editor, The Institute of Physics, 47 Belgrave Square, London, S.W.1. (*Telephone*: Sloane 9806.) Prospective authors are invited to prepare their scripts in accordance with the *Notes on the preparation of contributions*. (Price 2*s*. 6*d*. including postage.)
REPRODUCTION. The Institute of Physics is a signatory to The Royal Society's Fair Copying Declaration. Details may be obtained upon application from The Royal Society, London, W.1.
ADVERTISEMENTS. Communications concerning advertisements should be addressed to the agents, Messrs. Walter Judd Ltd., 47 Gresham Street, London, E.C.2. (*Telephone*: Monarch 7644.)
CLAIMS FOR MISSING JOURNALS. Claims from regular subscribers to this *Journal* for missing numbers will only be considered if received within 60 days of the date of mailing plus normal outward time of transit and time for lodging the claim. Losses attributable to failure to notify a change of address or to similar omissions will not be considered.
SUBSCRIPTION RATES. A new volume commences each January. The charge is £4 per volume ($11.50 U.S.A.), including index (post paid), payable in advance. Single parts, so far as available, may be purchased at 8*s*. each ($1.15 U.S.A.), post paid, cash with order. Orders should be sent to The Institute of Physics, 47 Belgrave Square, London, S.W.1, or to any bookseller.

CONFERENCE REPORT

Summarized proceedings of a conference on the structures and textures of metals—London, October, 1954

The annual Autumn Conference of the X-ray Analysis Group of The Institute of Physics was held in the Royal Institution, London, on 22 and 23 October, 1954. The first day's discussion centred on the structure of metals and alloys, whilst on the second day their texture was discussed. An evening lecture on dislocations was given by Prof. A. H. Cottrell (University of Birmingham).

THE STRUCTURE OF METALS

The first paper, given by DR. W. H. TAYLOR (Cavendish Laboratory, Cambridge), dealt with some aspects of the electron distribution in complex alloys. Although confining his remarks to aluminium-rich compounds with transition metals, Dr. Taylor said that they were of general application. The usual elementary treatment of the Brillouin zones of the structures of these compounds gives good agreement, for specified "effective valencies," between "calculated" and "observed" electron to atom ratios in some cases,[1–4] but poor agreement in others.[5, 6] This naïve treatment is, in fact, of doubtful validity for complex structures, and in particular in these structures, because of what appears to be a strong interaction between the transition metal atoms and aluminiums; also there is often a wide spread of possible "calculated" values according to the choice of energy stabilizing conditions.

The results of accurate structure analyses show that the tructures may be derived from stacking of simple aluminium heets of from regions of close packing with misfits. The ransition metal atoms occur in 9- or 10-co-ordination with ome of their aluminium neighbours remarkably close, but these near aluminium atoms themselves appear to be small. Using F_0 and $(F_0 - F_c)$ syntheses there appears to be some electron transfer from aluminium atoms to transition metal atoms in the structures of Co_2Al_9,[7] Mn_3SiAl_9,[2] $MnAl_6$[5] and $Cr_4Si_4Al_{13}$,[3] but the structure of $FeAl_3$[6] is too complicated for the small transfer found in it to be significant.

Dr. Taylor then considered some of the assumptions and approximations which may give possible sources of error in electron counts, e.g. variable composition, incoherent scattering, the use of two-dimensional Fourier projections, diffraction ripples, extinction effects in the critical low-angle reflexions, lack of *absolute* intensities, and difficulties due to atomic *f*-curves. Examples were given of the influence of these last two effects on the results for Co_2Al_9, $MnAl_6$ and Mn_3SiAl_9.[8] In Co_2Al_9 the presence or absence of electron transfer depends on whether the background electron density is zero or not, and in the other cases there is an overall deficiency in the atomic scattering factor used for manganese[9] in $(F_0 - F_c)$ syntheses, which would reduce the electron transfer found by these syntheses.

DR. W. HUME-ROTHERY (Inorganic Chemistry Laboratory, University of Oxford) then considered the meaning of valency in metallic crystals. He gave the original chemical definition of the term valency in terms of the power of combination with hydrogen atoms, and showed how the development of the electronic theory of valency focused attention on the number of electrons concerned in atomic cohesion in different types of molecule. In the structures of some solid crystals molecules can still be identified, e.g. in selenium, whilst in others, e.g. diamond, the whole crystal is a giant molecule in which atoms exert their normal valency. Even in inorganic chemistry, however, we meet difficulties, e.g. we speak of co-ordination number rather than valency in sodium chloride, and the structure of cuprous bromide has been treated as ionic Cu^+ Br^- and as covalent, both with and without transfer of electrons from copper to bromine.

In metals, the whole crystal may be regarded as a molecule in which some electrons belong to the crystal as a whole, and in this connexion the term valency has been used with a new meaning, i.e. the number of electrons per atom contributing to metallic cohesion. The fact that the electrical conductivity of nickel is due mainly to about 0·6 *s* state electrons per atom is sometimes described in terms of a "valency" of 0·6, and this is using the word "valency" in yet another sense. Supporters of the Pauling resonating bond theory[10] would say that nickel has a valency of 5·78 to indicate the number of electrons in hybrid *s*, *p*, *d* orbitals concerned in the bonding, and the numbers 0·6 and 5·78 are not directly comparable.

Alloys of some elements of well defined chemical valency tend to form characteristic structures at certain ratios of valence electrons to atoms,[11] and their occurrence has been interpreted in terms of Brillouin zone theories.[12] Some authors have attempted to choose "valencies" which would satisfy either a constant electron to atom ratio for a series of compounds or would fill a Brillouin zone up to some specified limit. In either case this is a new definition of "valency," and in some cases its meaning is obscure. In the case of transition metals magnetic evidence may help, but, for example, the reported diamagnetism of $MnAl_6$[13] may be reconciled with any $(3d)^{2n}$ electron groups and not only $(3d)^{10}$ groups.

Dr. Hume-Rothery suggested that for metals and alloys it may be well to cease using the term valency, and to speak of *electron number*, abbreviated to Elno or to E.N., and qualified where necessary, e.g. bonding E.N., conductivity E.N., etc.

The final paper of the first morning was given by PROF. H. W. B. SKINNER (The University of Liverpool), who spoke on the determination of electron distribution in metals by soft X-ray spectroscopy. After giving some details of the experimental technique,[14, 15] including the information that targets could be cleaned satisfactorily by scraping with a steel wire brush, and after outlining the relationship between the intensity distribution in emission and absorption spectra in the region of 10–500 Å and the distribution of electrons in the conduction bands, Prof. Skinner showed results obtained from metals of the first and second groups of the periodic table.[14] The kinks on the bands could be associated with Brillouin zone overlaps, and these become more numerous when the bands from the non-metals carbon, boron, silicon, phosphorus and sulphur are examined.

Prof. Skinner also showed the L and M emission bands obtained before the war from the iron group metals.[16] These bands show no sharp edges in contradiction with the results published by Gyorgy and Harvey,[17,18] and it is possible that these authors' edges may have been produced spuriously by their method of continuous evaporation. The L and resolved components of the M bands are thought to represent substantially the structure of the 3d band of these metals and seem to show that this band is without any appreciable structure except in the case of zinc and, possibly, copper.

Finally the L spectra from binary magnesium–aluminium alloys were shown. Both the aluminium and magnesium emission edges become less sharp than from the pure metals, in the former case the edge width becoming greater than that from molten aluminium. The aluminium band width narrows appreciably in the alloy, but it is not possible to note any change in the width of the magnesium band, although the dip in this band has moved to a lower energy. The results of these experiments therefore differ somewhat from those obtained by Farineau[19] on the K emission spectra from magnesium–aluminium alloys.

Opening the discussion to this section Dr. K. Robinson (The University of Reading) supported Dr. Hume-Rothery's suggestion for avoiding the term valence, but did not care for the abbreviated forms. He suggested to Prof. Skinner that a study of the L spectra from aluminium in the complex aluminium-transition metal compounds might be very useful, and asked Dr. Taylor whether it might not be better to study the spatial electron distribution in simpler compounds before considering those of greater complexity. Dr. Taylor replied that the increased number of low-angle reflexions from structures of medium complexity made this doubtful.

Prof. G. V. Raynor (The University of Birmingham) could not see why the diamagnetism of $MnAl_6$ should be interpreted in any way other than by $(3d)^{10}$ electron groups and suggested that this filling of the (3d) shell results from a building-up of electron pressure, since an alloy of composition $MnCu_6$ is strongly paramagnetic and $MnAl_4$ has appreciable paramagnetism.

Prof. Sir Lawrence Bragg (The Royal Institution, London) emphasized the difficulty of knowing where to draw a boundary between atoms in attempts to make electron counts.

Dr. E. Billig (Associated Electrical Industries Ltd., Aldermaston) suggested that the soft X-ray emission from doped germanium or silicon should be examined, but Prof. Skinner said that the impurity concentration would be too small.

Dr. T. Ll. Richards (Imperial Chemical Industries Ltd., Metals Division) asked if the outer Brillouin zones of aluminium-rich complex compounds had been examined as in the γ-structures.[20] Dr. Taylor replied that they were much less prominent.

Opening the afternoon session Dr. J. W. Christian (Inorganic Chemistry Laboratory, University of Oxford) gave a paper on the crystallography of transformations, confining his remarks to those of a martensitic type. Recent theories assume that the total atomic movements are equivalent to a physical deformation of one structure into another. Except for a few very simple transformations, the lattice deformations involved in the production of a single martensitic plate are not homogeneous. Adjacent very small regions are assumed to form by different homogeneous deformations, the effects of which partially cancel and partially add to give the observed change of shape. Many transformations can be explained by assuming the habit plane to be an invariant plane of the observed deformation, and the macroscopically inhomogeneous part of the change to be a shear on the twinning plane and in the twinning direction of the final structure.[21,22]

In other reactions, the theories (*a*) retain the assumption that the habit plane is macroscopically invariant and modify the plane of the "invisible" shear,[23,24] or (*b*) assume that the homogeneous part of the total strain is an invariant plane strain with the addition of a small dilatation[25] or a uniaxial expansion in the invariant plane.[26,27] Scatter of experimental results makes it difficult to distinguish between the predictions of these theories, but twins would not be expected within a single martensite plate in (*a*), whereas this is quite possible in (*b*). Microbeam experiments on single plates of {225} martensite might possibly provide such a distinction. Single interface transformations of the type observed in indium–thallium alloys[28] would not be probable unless the habit plane were macroscopically invariant. Work on single crystals in this system shows the importance of avoiding accumulating long range stresses. The phenomena of interpenetrating bands in polycrystals and other transformation effects may be explained on this basis. The concept of "surface dislocation" introduced by Bilby[29] may be used to rationalize the interactions of many types of interface.

The structures of uranium alloys were surveyed by Dr. P. C. L. Pfeil (Atomic Energy Research Establishment, Harwell), who remarked that although our information is by no means complete, it is clear that the alloying behaviour of uranium is strongly influenced by atomic size considerations, e.g. in the solid solubility of the body-centred cubic elements niobium, titanium, zirconium, molybdenum, chromium and vanadium in γ-uranium (Fig. 1). The solid solubility of

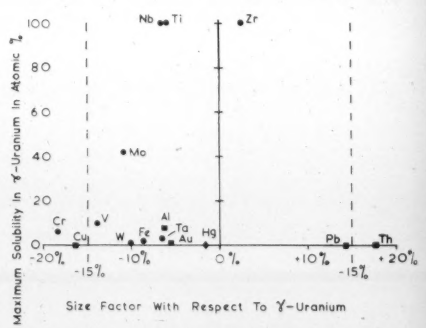

Fig. 1. Maximum solubility in γ-uranium as a function of size factor

● = body-centred cubic; ■ = face-centred cubic; ♦ = rhombohedral.

molybdenum in uranium is particularly interesting in that there appears to be a sorting out of molybdenum and uranium atoms in the body-centred tetragonal cell to form a superlattice. The variation with composition of lattice parameters of the γ'-phase in this system shows a very marked increase in c/a at about 30 atomic % molybdenum corresponding to an overlap of the {002} Brillouin zone faces.

A summary of the types of compound found in uranium

alloy systems was shown as in Fig. 2, emphasis being laid on the fact that no compounds are found with niobium, tantalum, chromium, molybdenum and tungsten, whilst manganese, iron, cobalt and nickel all form tetragonal U_6X-type compounds. Dr. Pfeil concluded by reviewing the interatomic distances in the UX_3 (LI_2-type) structures, showing that although there is a marked contraction on *formation*, in almost all cases the interatomic distances

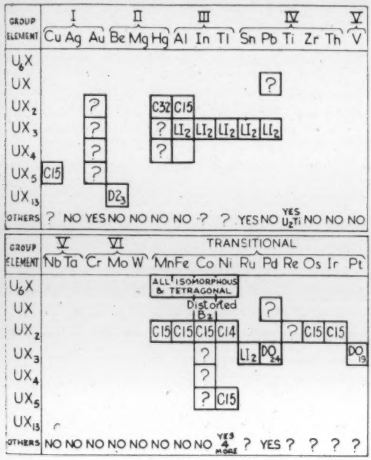

Fig. 2. Compounds in uranium alloy systems

(X–X, X–U and U–U) are greater than would be expected on the basis of calculations similar to those of Berry and Raynor.[30]

The discussion of these two papers followed. In reply to a query by MR. A. P. MIODOWNIK (Battersea College of Technology) Dr. Christian said that Geisler's theory[31] might be correct for a nucleation stage, but at the growth stage, with which the above theories are concerned, he believed it to be either incorrect or indistinguishable from these theories. The theory is difficult to discuss, since it is not formulated in a quantitative manner, and predictions cannot be made from it.

Dr. T. Ll. Richards pointed out that the condition of atomic correspondence existing between untransformed and transformed structures implies that the operative shear systems and habit plane might be derived by straightforward crystal geometry, ignoring changes in interatomic distances, providing these were small. In this way it can be shown that the {225} and {259} austenite habit planes have corresponding martensite planes all close to {112} and {111} respectively. The first of these planes contains a common glide direction in austenite and martensite, and the {112} planes are twin planes of the body-centred cubic lattice. Hence it is likely that strains developed in the surrounding matrix by shear in the martensite plate may be relieved by a counter shear associated with twinning. The mid-rib often seen in martensite plates may well be evidence of such twinning.

MR. T. J. HEAL (Fulmer Research Institute, Stoke Poges) spoke on the structure of liquid metals and began by describing the general analysis of the diffraction patterns from liquid metals in terms of atomic or electronic radial distribution functions.

Subtraction from the experimentally observed intensity of calculated incoherent and coherent scattering necessitates curve matching at high values of s $[=4\pi(\sin\theta)/\lambda]$ where interference effects can be assumed to vanish. To obtain a wide range of s, both Cu Kα and Mo Kα radiations are used and this necessitates further curve matching. These processes, together with correction for absorption and polarization, lead to errors in the final intensity curve of the interference effects. In the Fourier transformation of this curve the limited range of s gives false ripples.[32] False peaks may result from the various errors in $I(s)$.

The essential difference between electronic and atomic distribution curves is the inclusion in the latter of a term $1/f^2$ which sharpens the peaks but which, for finite limits of integration, materially enhances the false ripples.

Mr. Heal gave a number of examples of atomic and electronic distribution curves, and pointed out examples in the curves of peaks which could be false.[33] Finally the following table was presented. This summarizes the published data on liquid metals, and Mr. Heal drew attention to the fact that by treating a number of subsidiary maxima in the distribution curves as spurious, a striking similarity in the structures of the metals becomes evident.

Published data on liquid metals

m.p. (°C)	*Metal*	*Temp. expt.* (°C)	*Relative diameters of co-ordination shells* 1st	2nd	3rd	*No. of atoms in 1st shell*
659	Al	700	1	1·86		10·6
321	Cd	350	1*	1·86		8·3
30	Ga	45	1	2·0	2·9	
155	In	160	1	2·0		8·5
155	In	390	1*	2·0		8·4
186	Li	200	1*	1·8		9·8
− 38·9	Hg	− 38	1*	2·0		
62·3	K	70	1	1·9		8
62·3	K	395	1	1·9		8
97·5	Na	100	1*	1·9		
97·5	Na	400	1	1·9		
232	Sn	280	1*	1·9	2·8	10
419	Zn	460	1	1·8		10·8
−189·3	Ar	−188·6	1	2·0		10·5

* Peaks regarded as probably spurious have been omitted from these results.

The final paper of the afternoon session was given by DR. B. FROST (Atomic Energy Research Establishment, Harwell) on the structure of liquid alloys. Liquid alloys have many practical applications and in developing alloy casting techniques, for example, a knowledge of how physical properties of the liquid alloy vary with composition is required. If the structure changes which accompany these property variations were known, it might be possible, ultimately, to formulate a theory relating the liquid-state structure to physical properties.

When two elements of widely differing electrochemical

potentials are alloyed together, compounds are usually formed which display heteropolar bonding. A number of investigators[34–37] have shown that these compounds, on melting, retain some of their solid-state characteristics. No direct evidence of incipient compound formation in liquid alloys has, however, been forthcoming from X-ray work. This is due to the difficulty in assessing the relative contributions to scattering of the two different types of atom present.

Dr. Frost briefly reviewed the possible methods of approach to the problem, and then described the work in progress at Harwell using the method in which two elements are chosen, having almost identical scattering factors (e.g. mercury–thallium, magnesium–aluminium, antimony–cadmium); this enables the analysis to proceed as for a liquid element.

Although it is eventually intended to use an X-ray beam directed at a free liquid surface, and to use focusing at all θ-values, preliminary experiments on mercury–thallium alloys have been made using a conventional diffractometer and a specimen cell having a cellophane window.

Alloys containing 8·5%, 30%, 34% and 40% thallium were prepared. Intensity *versus* θ curves for these alloys and for pure mercury were obtained and corrected for absorption in the cellophane and for polarization of the beam. A first peak was obtained at the same value of θ in all cases except 30% thallium where a slightly lower value indicates a closer packing. Variation of peak intensity with composition was observed which, since all exposures were made at 17° C, may be due to the variable distances above the liquidus.

A radial distribution analysis has so far only been made for pure mercury, and the d-value corresponding to the first peak is 2·69 Å compared with 2·70 Å obtained by Sauerwald and Osswald.[38]

The discussion on the above two papers was opened by Dr. U. W. Arndt (The Royal Institution, London). He said that the reliability of radial distribution functions is always difficult to assess, since they are calculated from actual intensities whose accuracy may be good at medium scattering angles but much less at very low and, more particularly, at high angles. In addition, the values of the atomic scattering factors and the calculated incoherent scattering are only imperfectly known. When the radial distribution curve is obtained by Fourier inversion it is difficult to see which of its features are related to the more reliable parts of the intensity curve and which peaks must be regarded as doubtful. Waser and Schomaker[39] recommend multiplying the experimental curves by modification functions, whose transforms are known and which suppress parts of the intensity functions at the expense of others without introducing "cut-off" and diffraction effects. Dr. Arndt described a simpler procedure in which the experimental curve is inverted part by part so that the effects of each step can be assessed separately.

Even with these precautions any reasoning based on radial distribution curves, especially from hetero-atomic materials such as liquid alloys, should be done with care. Whenever possible it is preferable to compute an intensity curve from a model of the structure and compare this with the observed scattering.[40]

The actual process of Fourier inversion can be carried out conveniently using 3° Beevers–Lipson strips as described by Ross[41] and Whittaker.[42] It is convenient to sample the intensity curve at intervals of $(\sin\theta)/\lambda = 1/120$; the radial distribution function is then given at 0·5 Å intervals. Sometimes closer intervals of r are required; Dr. Arndt found the interpolation method due to Danielson and Lanczos[43] very rapid in use.

Dr. R. E. Smallman (Atomic Energy Research Establishment, Harwell) referred to the subsidiary maxima which occur on many atomic distribution curves for liquid metals, and which, as Mr. Heal had pointed out, are probably spurious.

Although the use of Mo Kα radiation to obtain higher integration limits and the adoption of an electronic distribution function in preference to an atomic one are sound in principle, the errors introduced in practice are likely to be more serious than those being corrected. The use of Mo Kα in addition to Cu Kα radiation, simply moves subsidiary peaks nearer the main maxima; this, though lessening the tendency to ghost formation, may lead to their being included in the area under the main maxima thus giving a false value for the co-ordination number. The use of the electronic distribution function results in reduced resolution.

Dr. Smallman drew attention to the need for caution in deducing the existence of molecular formation from the appearance of discrete peaks in the distribution function. He concluded by pointing out that errors due to finite integration limits can be calculated, and that it is the "unknown" errors, such as absorption, which are serious.

DISLOCATIONS

In the evening discourse, Prof. A. H. Cottrell (University of Birmingham) reviewed the general subject of dislocations.

After enumerating the various methods by which dislocations can be detected, Prof. Cottrell continued by describing how certain foreign atoms are strongly attracted to dislocations and segregate to them even when present in minute amounts. In covalent crystals these atoms attach themselves firmly to unsatisfied chemical bonds at the centres of dislocations, thereby immobilizing the dislocations. Silicon and germanium, for example, are ductile at temperatures at which the impurity atoms "evaporate" off the dislocations and are brittle at temperatures at which they "condense" on to them. At intermediate temperatures plastic yielding occurs abruptly at stresses sufficient to pull the dislocations away from their impurity atoms. In metals the impurities are bound less strongly to dislocations, by forces of an elastic rather than a chemical nature, which may be one reason why metals are generally more ductile than non-metals. Certain impurities are highly potent even in metals, however, and produce striking effects on mechanical properties. The well-known brittleness of chromium, for example, appears to be caused by minute amounts of nitrogen, an impurity which is known to be strongly attracted to dislocations in several metals.

THE TEXTURE OF METALS

The papers on the second day of the Conference were devoted to the texture of metals, the opening paper being given by Dr. P. B. Hirsch (Cavendish Laboratory, Cambridge) on some observations on the cold-worked state.

Dr. Hirsch first reviewed the evidence on dislocation density and distribution in unworked crystals. Observations on growth spirals have shown that the density of screw dislocations in metal crystals grown from the vapour is approximately 10^4 per cm^2; in non-metallic crystals it varies from 0 to 10^6 per cm^2.[44] On germanium crystals grown

from the melt, rows of etch pits of density approximately 10^6–10^8 per cm^2, have been interpreted as walls of edge dislocations, and the agreement between the calculated and measured angles of tilt across the boundaries is excellent.[45] More complicated types of boundaries have been detected in aluminium crystals,[46] but these have not been analysed in terms of a definite distribution of dislocations. X-ray measurements of dislocation densities in annealed metal crystals grown from the melt have so far shown densities not exceeding 10^6–10^8 dislocations per cm^2.[47]

Turning to worked crystals, Dr. Hirsch referred to the direct evidence on distributions of dislocations derived from visual observation on slightly worked and partially annealed crystals of silver bromide subsequently exposed to light. The density of dislocations is found to be approximately 10^6–10^7 per cm^2.[48] Indirect evidence is derived from X-ray microbeam experiments on metals, which have shown that the dislocations are not randomly distributed but are concentrated in certain boundary regions with densities of dislocations between 10^9 and 10^{11} lines per cm^2.[47]

Dr. Hirsch concluded by comparing briefly the various kinds of studies that can be made in this field with the various available techniques, such as electron transmission microscopy, dark field microscopy, low-angle X-ray scattering, and X-ray microbeams.

Prof. A. J. C. Wilson (University College, Cardiff) spoke next, on the effects of dislocations on X-ray diffraction.*

No satisfactory general theory of the effect of dislocations on X-ray diffraction exists. In Wilson's treatment,[49] which provides integral breadths for a powder consisting of cylindrical particles each with a single axial screw dislocation, the actual expressions, though complex, lead to breadths increasing almost linearly with l, the index of reflexion corresponding to the dislocation axis. Although the results can be generalized to give approximate breadths for similar particles with edge dislocations,[50, 51] expressions for (*a*) the line profile for a crystal with a single dislocation, and (*b*) breadths and profiles for crystals with more than one dislocation, have not been obtained.

Prof. Wilson then turned to the general problem of interpreting the line profiles observed with cold-worked metals. Williamson and his collaborators have found that these are approximately of the Cauchy form. This tends to zero rather slowly, as the inverse square of the distance from the centre of the line, and Williamson and his collaborators[52, 53] have suggested that this long tail is associated with the region of high distortion near the dislocation axis. A calculation of the line profile, based on the approximate treatment of strain broadening by Stokes and Wilson,[54] offers no support for this, but suggests an approach to zero as the inverse cube of the distance from the centre of the line. Eastabrook and Wilson[55] have devised general arguments to show that, if the distorted crystal is large enough to contain several positive and negative cycles of strain, the line profile is likely to be one of the Cauchy type. In all probability, therefore, the Cauchy distribution does not specifically indicate the effect of dislocations.

In the paper dealing with deformation faults in cold-worked copper given by Dr. G. B. Greenough (Department of Metallurgy, University of Sheffield) and Mrs. E. M. Smith (Royal Aircraft Establishment, Farnborough), Dr. Greenough spoke of some experiments[56] on cold-worked copper which had become of interest since the publication of the more recent theoretical work of Paterson[57] on the effect of "deformation faults" in a face-centred cubic lattice on the positions and breadths of diffraction lines.

X-ray photographs had been taken of copper filings, the broad diffraction lines photometered and separated into their α_1 and α_2 components, and the Bragg angle for the α_1 peaks determined. Comparison with the Bragg angles determined in the same way for annealed filings showed that the difference between the θ-values for lines having $(h^2 + k^2 + l^2) = 19$ and 20, was significantly less in the cold-worked copper than in the annealed. This result agrees with the theoretical prediction made by Paterson for stacking faults parallel to (111).

Since in the experimental work it was probable that deformation faults existed parallel to all possible {111}, whereas the theory was developed for one particular set of (111) planes only, a detailed quantitative comparison between theory and experiment is not possible. However, Dr. Greenough had found that if the effects of faults on various {111} planes are linearly additive, the results indicate that there is 1 stacking fault every 600 planes. If it is assumed that, on average, slip stops in the faulted position on half the planes, then the average distance between slip planes is 300 planes (600 Å). Dr. Greenough compared this figure with the size of the crystallites (6000 Å) deduced by Gay and Kelly[58] from microbeam photographs and with the spacing of the lines of "elementary slip structure" (300 Å) observed by Kuhlmann–Wilsdorf and Wilsdorf[59] by electron microscopy. The stacking fault and microscope values appear to be in agreement, but the crystallites of Gay and Kelly are larger than the distance between operative slip planes.

The discussion on these three papers was opened by Dr. G. K. Williamson (Atomic Energy Research Establishment, Harwell), who paid particular attention to Dr. Hirsch's paper. Estimates of dislocation densities from microbeam experiments appeared to be lower than the generally accepted values, and a recent analysis of X-ray extinction by Dr. Smallman and himself had suggested that the density must exceed 10^7 dislocations per cm^2 in annealed filings. Referring to the various difficulties in the different methods, Dr. Williamson asked whether in the microbeam method, allowance was made for screw dislocations and how the one-dimensional nature of the results was taken into account.

In reply, Dr. Hirsch pointed out that estimates of dislocation densities based on extinction cannot be relied upon. In the microbeam analysis, screw dislocations had been taken into account and although the analysis was one-dimensional, Dr. Hirsch felt that correction to three-dimensions was not likely to alter the order of magnitude. He agreed, however, that the averaging process used is crude and should be improved. The accuracy of the estimates derived from microbeam methods was limited to a factor of the order of three.

In connexion with Dr. Greenough's paper, Dr. Hirsch said that the theory of X-ray diffraction from stacking faults applies only to the case of planes of stacking faults of infinite extent, and requires extension to the case of stacking faults of limited extent.

Dr. T. Ll. Richards asked whether Dr. Greenough had considered if elastic anisotropy could account for the difference in spacings derived from the 19 and 20 reflexions of cold-worked copper. Stokes, Pascoe and Lipson[60] had shown that differences in line broadening of the different reflexions could be almost wholly explained by elastic anisotropy. Furthermore, Williams[61] had shown, by electron diffraction measurements, that there were significant

* This paper has now been published in full in *Nuovo Cimento*, **1**, pp. 277–283 (1955).

differences in the lattice spacings of the various planes near to the free surfaces of evaporated metal particles. In this instance also the differences could be accounted for on the basis of elastic anisotropy.

In reply Dr. Greenough said that he could not visualize a mechanism whereby elastic anisotropy might account for his results.

DR. J. S. HALLIDAY (Associated Electrical Industries Ltd., Aldermaston) drew attention to the work of Wright[62] who found by electron diffraction, a hexagonal modification of gold in some evaporated films. These films were composed of the normal face-centred cubic gold which was strongly oriented with the {111} planes lying in the plane of the film, and the hexagonal modification which was oriented with the basal plane in the plane of the specimen. Precision measurements[63, 64] showed that the face-centred cubic reflexions were displaced from their normal positions. The general character of these displacements was similar to those found in gold leaf[64] and in lithium fluoride and copper specimens.[65] The displacements of the evaporated gold face-centred cubic reflexions, which were in an opposite sense to those previously found for gold leaf, are most certainly due either to strains in the crystallites or perhaps to faults which may be similar to the stacking faults described by Paterson.[57]

In reply to questions by DR. K. W. ANDREWS (The United Steel Companies Ltd., Sheffield), Dr. Greenough confirmed that deformation faults would cause points to fall off lattice parameter *versus* $f(\theta)$ plots and made some observations about the connexion between changes in lattice parameter and line broadening due to cold work.

The last part of the session on the texture of metals consisted of three papers, the first being given by DR. E. A. CALNAN (National Physical Laboratory, Teddington) on the development of deformation textures.

After briefly reviewing previous treatments for the explanation of deformation textures, Dr. Calnan outlined the method of Calnan and Clews[66] which, though not rigorous, has the advantage of not involving too great an amount of computation and is applicable to all structure types. The starting point is that a grain in a polycrystalline aggregate does not slip immediately the applied stress resolved on the most favourable slip system reaches the critical value, otherwise cohesion could not be maintained at the grain boundaries. Therefore the constraints imposed by neighbouring grains must be such as to give an effective stress at a slightly different orientation so that the critical value is not attained. The probable paths along which the effective stress will move are considered, these involving regions where single, duplex or multiple slip systems are most favourable. Since the deformation is visualized as a step-like process with successive elements of slip occurring at varying positions of the effective stress along its path, there will be corresponding amounts of single, duplex and multiple slip. Associated with each of these will be the appropriate rotation of the crystal. From a consideration of these component rotations the general trends of rotation are obtained, so leading to the deformation textures.

Examples of the derived rolling textures and the corresponding experimental determinations, were given for uranium rods and magnesium, zinc and titanium sheets. Dr. Calnan also considered copper and α-brass which although having the same slip systems, develop different textures.

Finally, Dr. Calnan referred to the evidence of Hibbard[67] of drawing texture differences in copper alloys. If one considers the stresses in drawing through a circular die as simulated by a circular array of compressive radial stresses together with the main tension, then the treatment he had described gives an explanation in agreement with experiment. An important point to note here, however, is that the brass type texture is obtained with various solute elements. The amount of solute required appears to depend on an atomic size factor.

The next paper, on practical texture investigations, was read by DR. K. W. ANDREWS (The United Steel Companies Ltd., Sheffield).

With the term "texture" used in the broad sense and including the size, shape and possible internal strain of grains, as well as their orientation, Dr. Andrews gave a general survey of some of the developments in techniques and methods of interpretation which have been reported in recent years.

In crystal size determination, the microbeam technique has nearly bridged the previously existing gap between 10^{-3} and 10^{-5} cm, and Hirsch[68] has recently described an extrapolation method capable of high accuracy, in which the number of spots on a ring is a function of the ratio of two exposure times. Information has also been obtained by microbeam methods of particle shape and distortion from tangential and radial breadths of spots.

Sub-grain structures can be studied by the X-ray microscope of Berg,[69] Barrett[70] and Honeycombe[71] and, in certain cases, by a technique due to Goldschmidt[72] which uses synchronism between specimen rotation and pulse frequency of the X-ray beam.

Much of the recent work on deformation of metals has employed either Laue patterns or spotty Debye–Scherrer rings. Altogether these techniques are not new, they are being used with greater certainty in interpretation.

The widest applications of these various techniques have been in the study of the effects of plastic deformation on metals and the understanding of their mechanical strength. This fundamental understanding will undoubtedly have practical industrial applications, especially, perhaps, in regard to creep and fatigue. Dr. Andrews emphasized that the same techniques and methods of interpretation can also assist in the elucidation of *ad hoc* industrial problems, e.g. in the determination of grain size, "degree of cold work," recovery and recrystallization. As examples, Dr. Andrews referred to some recent examinations made in his laboratory of the degree of cold work in sand-blasted surfaces and the recovery and recrystallization of bent tube.

In the study of preferred orientation, a number of special cameras and goniometers have been reported.[73–77] Dr. Andrews described some important work on preferred orientation determinations on titanium[78, 79] and uranium.[77, 80, 81] Of particular interest is the result that the textures found for α-uranium under certain conditions of deformation, can be explained on the basis that α-uranium, though orthorhombic, is very nearly close-packed hexagonal.[77]

Dr. Andrews finally reported an X-ray examination he has made of annealed stainless steel wire. Such material is known from microscopic examination to be twinned and the X-ray examination has now for the first time shown faint extra intensity peaks which are probably accounted for by this twinning.

The final paper of the Conference was by DR. T. LL. RICHARDS and MR. D. E. YEOMANS (Imperial Chemical Industries Ltd., Metals Division) on the principle of the unextended cone in the plastic deformation of metal crystals.

Dr. Richards, in presenting the paper, said that the principle of the unextended cone is well known in elasticity theory

where strains are usually small or, as Dr. Christian had shown in an earlier paper, in the theory of transformations where strains are quite specific. The application to plastic deformation, however, where the magnitude of strain is varying, was, he believed, novel.

Dr. Richards then indicated the significance of the unextended cone in relation to the various possible forms of shear in metals of cubic symmetry under simple tension and compression. The unextended cone of plastic deformation can be defined for any small increment of finite strain on the basis that, with no change in volume, an extension increment e is accompanied by a lateral contraction $\frac{1}{2}e$.

Most metals having a face-centred or body-centred cubic structure are elastically and plastically anisotropic with a minimum Young's modulus in a ⟨100⟩ direction, so that a stress applied to a single crystal in any direction extends the crystal preferentially along the nearest ⟨100⟩ direction. Also if one assumes that in cubic metals the atoms are most strongly bonded in directions of closest atomic packing, then such directions would be expected to be the least extensible and thus be directions of shear in plastic deformation. Dr. Richards demonstrated how, for the purpose of considering the plastic behaviour of metal crystals, one may regard the close-packed directions as being almost rigid and the crystal lattice simply as a three-dimensional "garden trellis" which is most easily extended along one of the cube axes.

Considering face-centred and body-centred cubic crystals in turn, Dr. Richards showed that for all the various modes of crystallographic shear, the shear direction and/or normal to the shear plane lie in or near the surface of the unextended cone of strain along the nearest ⟨100⟩ direction.

While not wishing to detract from the theory of deformation textures developed by Calnan and Clews, Dr. Richards felt that a theory based on the unextended cone was more rational and simpler to understand. The Calnan and Clews treatment makes no reference to actual tension textures of face-centred cubic metals which are usually composed of various proportions of ⟨100⟩ and ⟨111⟩ textures. On the unextended cone theory, the ⟨100⟩ texture is one in which the normals to the four possible (111) slip planes are tangential to the unextended cone of extension in ⟨100⟩, whereas for the ⟨111⟩ texture, the normals to the three (100) planes are tangential to the cone of tension in ⟨111⟩. ⟨110⟩ {100} has been shown to be a secondary mode of slip in aluminium crystals.

In reply to Dr. Richards, Dr. Calnan said that wire and rod textures are not strictly comparable with tension textures since the radial compressive stresses exerted by the die or the rolls influence the texture development. Dr. Calnan felt that there was need for more measurements of pure tension textures; his own measurements[82] gave some evidence that the tension end-points were not [100] or [111] but were somewhere between.

In discussion of the last three papers, Dr. R. E. Smallman spoke of the considerable interest in the problem of determining to what extent fundamental properties on an atomic scale may be predicted from microscopic properties. To investigate this, deformation textures for many common face-centred cubic metals have been determined using a quantitative counter technique. All exhibit approximately (123) [1$\bar{2}$1] texture in contrast to the usually quoted (110) [$\bar{1}$12] texture for face-centred cubic alloys having the same deformation modes as the pure metal.

From studies of the variation in texture with increasing solute content in copper, aluminium, nickel, gold and silver, the work to date indicates that it is the interaction of solute atoms in solution which governs the texture transition from (123) [1$\bar{2}$1] to (110) [$\bar{1}$12]; any physical property such as yield point formation, the extent of the region of low work hardening, the degree of overshoot or hardenability of active and latent slip planes, are all related to the transition.

K. Robinson
E. G. Steward

REFERENCES

(1) Raynor, G. V., and Waldron, M. B. *Phil. Mag.*, **40**, p. 198 (1949).
(2) Robinson, K. *Acta Cryst.*, **5**, p. 397 (1952).
(3) Robinson, K. *Acta Cryst.*, **6**, p. 854 (1953).
(4) Robinson, K. *Phil. Mag.*, **43**, p. 775 (1952).
(5) Nicol, A. D. I. *Acta Cryst.*, **6**, p. 285 (1953).
(6) Black, P. J. *Acta Cryst.*, **8**, p. 175 (1955).
(7) Douglas, A. M. B. *Acta Cryst.*, **3**, p. 19 (1950).
(8) Black, P. J. *Phil. Mag.*, **46**, p. 155 (1955).
(9) Viervoll, H., and Ogrim, O. *Acta Cryst.*, **2**, p. 277 (1949).
(10) Pauling, L. *Phys. Rev.*, **54**, p. 899 (1938).
(11) Hume-Rothery, W. *J. Inst. Metals*, **35**, p. 309 (1926).
(12) Jones, H. *Proc. Roy. Soc. A*, **144**, p. 225 (1934).
(13) Vogt, E. *Appl. Sci. Res. B*, **4**, p. 34 (1954).
(14) Skinner, H. W. B. *Phil. Trans Roy. Soc. A*, **239**, p. 95 (1940).
(15) O'Bryan, H. M., and Skinner, H. W. B. *Proc. Roy. Soc. A*, **176**, p. 229 (1940).
(16) Skinner, H. W. B., Bullen, T. G., and Johnston, J. E. *Phil. Mag.*, **45**, p. 1070 (1954).
(17) Gyorgy, E. M., and Harvey, G. G. *Phys. Rev.*, **87**, p. 861 (1952).
(18) Gyorgy, E. M., and Harvey, G. G. *Phys. Rev.*, **93**, p. 365 (1954).
(19) Farineau, J. *Ann. Phys.* [*Paris*], **10**, p. 20 (1938).
(20) Pauling, L., and Ewing, F. J. *Rev. Mod. Phys.*, **20**, p. 112 (1948).
(21) Bowles, J. S., Barrett, C. S., and Guttman, L. *Trans A.I.M.E.*, **188**, p. 1487 (1950).
(22) Weschler, M. S., Lieberman, D. S., and Read, T. A. *J. Metals*, **5**, p. 1503 (1953).
(23) Machlin, E. S., and Cohen, M. *Trans Amer. Inst. Min. Met. Eng.*, **191**, p. 1019 (1951).
(24) Weschler, M. S., Lieberman, D. S., and Read, T. A. *J. Metals*, **6**, p. 676 (1954).
(25) Bowles, J. S., and Mackenzie, J. K. *Acta Met.*, **2**, pp. 129, 138, 224 (1954).
(26) Frank, F. C. *Acta Met.*, **1**, p. 15 (1953).
(27) Suzuki, H. *Sci. Rep. Tôhoku Univ.*, **6**, p. 30 (1954).
(28) Basinski, Z. S., and Christian, J. W. *Acta Met.*, **2**, pp. 101, 148 (1954).
(29) Bilby, B. A. *Report on the Conference on Defects in Crystalline Solids*, p. 124 (London: Physical Society, 1955).

(30) BERRY, R. L., and RAYNOR, G. V. *Acta Cryst.*, **6**, p. 178 (1953).

(31) GEISLER, A. H. *Acta Met.*, **1**, p. 260 (1953).

(32) BRAGG, W. L., and WEST, J. *Phil. Mag.*, **10**, p. 823 (1930).

(33) FINBAK, CHR. *Acta Chem. Scand.*, **3**, p. 1272 (1949).

(34) HEYMANN, E., MARTIN, R. J. L., and MULCAHY, M. F. R. *J. Phys. Chem.*, **47**, p. 473 (1943).

(35) FRIESEN, A. P. *Phys. Rev.*, **49**, p. 414 (1936).

(36) KLEMM, W., and HAUSCHULZ, B. *Z. Elektrochem.*, **45**, p. 346 (1939).

(37) FISHER, H. J., and PHILLIPS, A. *J. Metals*, **6**, p. 1060 (1954).

(38) SAUERWALD, F., and OSSWALD, E. *Z. Anorg. Chem.*, **257**, p. 195 (1948).

(39) WASER, J., and SCHOMAKER, V. *Rev. Mod. Phys.*, **25**, p. 671 (1953).

(40) ARNDT, U. W., and RILEY, D. P. *Phil. Trans*, **247**, p. 409 (1955).

(41) ROSS, M. A. S. *Nature* [*London*], **152**, p. 302 (1943).

(42) WHITTAKER, E. J. W. *Acta Cryst.*, **1**, p. 165 (1948).

(43) DANIELSON, G. C., and LANCZOS, C. *J. Franklin Inst.*, **233**, pp. 365 and 435 (1942).

(44) FORTY, A. J. *Advances in Phys.*, **3**, p. 1 (1954).

(45) VOGEL, F. L., PFANN, W. G., COREY, H. E., and THOMAS, E. E. *Phys. Rev.*, **90**, p. 489 (1953).

(46) LACOMBE, P., and BEAUJARD, L. *C.R. Acad. Sci.* [*Paris*], **218**, p. 878 (1944).

(47) GAY, P., HIRSCH, P. B., and KELLY, A. *Acta Met.*, **1**, p. 315 (1953).

(48) HEDGES, J. M., and MITCHELL, J. W. *Phil. Mag.*, **44**, p. 223 (1953).

(49) WILSON, A. J. C. *Acta Cryst.*, **5**, p. 318 (1952).

(50) WILSON, A. J. C. *Research*, **3**, p. 387 (1950).

(51) LI, Y. Y. Private communications (1954).

(52) WILLIAMSON, G. K., and HALL, W. H. *Acta Met.*, **1**, p. 22 (1953).

(53) WILLIAMSON, G. K., and SMALLMAN, R. E. *Acta Cryst.*, **7**, p. 574 (1954).

(54) STOKES, A. R., and WILSON, A. J. C. *Proc. Phys. Soc.* [*London*], **56**, p. 174 (1944).

(55) EASTABROOK, J. N., and WILSON, A. J. C. *Proc. Phys. Soc.* [*London*] *B*, **65**, p. 67 (1952).

(56) GREENOUGH, G. B., and SMITH, E. M. *Proc. Phys. Soc.* [*London*] *B*, **68**, p. 51 (1955).

(57) PATERSON, M. S. *J. Appl. Phys.*, **23**, p. 805 (1952).

(58) GAY, P., and KELLY, A. *Acta Cryst.*, **6**, p. 172 (1953).

(59) KUHLMANN-WILSDORF, D., and WILSDORF, H. *Acta Met.*, **1**, p. 394 (1953).

(60) STOKES, A. R., PASCOE, K. J., and LIPSON, H. *Nature* [*London*], **151**, p. 137 (1943).

(61) WILLIAMS, E. C. *Research*, **5**, p. 392 (1952).

(62) WRIGHT, K. H. R. *Ph.D. Thesis* (University of Reading, 1950).

(63) RYMER, T. B., and BUTLER, C. C. *Phil. Mag.*, **36**, p. 515 (1945).

(64) RYMER, T. B., and BUTLER, C. C. *Proc. Phys. Soc.* [*London*], **59**, p. 541 (1947).

(65) HALLIDAY, J. S., RYMER, T. B., and WRIGHT, K. H. R. *Proc. Roy. Soc. A*, **225**, p. 548 (1954).

(66) CALNAN, E. A., and CLEWS, C. J. B. *Phil. Mag.*, **41**, p. 1085 (1950); **42**, p. 616 (1951); **43**, p. 93 (1952).

(67) HIBBARD, W. R. *J. Inst. Metals*, **77**, p. 581 (1950).

(68) HIRSCH, P. B. *Brit. J. Appl. Phys.*, **5**, p. 257 (1954).

(69) BERG, W. *Z. Krist.*, **89**, p. 286 (1934).

(70) BARRETT, C. S. *Trans Amer. Inst. Min. Met. Eng.*, **161**, p. 15 (1945).

(71) HONEYCOMBE, R. W. K. *J. Inst. Metals*, **80**, p. 39 (1951–52).

(72) GOLDSCHMIDT, H. J. *Acta Cryst.*, **5**, p. 256 (1952).

(73) WOOSTER, W. A. *J. Sci. Instrum.*, **25**, p. 129 (1948).

(74) CUSTERS, J. F. H. *Physica*, **14**, p. 453 (1948).

(75) JETTER, L. K., and BORIE, B. S. *J. Appl. Phys.*, **24**, p. 532 (1953).

(76) MITCHELL, C. M., and ROWLAND, J. F. *Acta Met.*, **2**, p. 559 (1954).

(77) SEYMOUR, W. *Trans Amer. Inst. Min. Met. Eng.*, **200**, p. 999 (1954).

(78) MCHARGUE, C. J., and HAMMOND, J. P. *Trans Amer. Inst. Min. Met. Eng.*, **197**, p. 57 (1953).

(79) WILLIAMS, D. N., and EPPELSHEIMER, D. S. *Trans Amer. Inst. Min. Met. Eng.*, **194**, p. 615 (1952); *J. Inst. Metals*, **81**, p. 553 (1952–53).

(80) HARRIS, G. B. *Phil. Mag.*, **43**, p. 113 (1952).

(81) ADAM, J., and STEPHENSON, J. *J. Inst. Metals*, **82**, p. 561 (1953–54).

(82) CALNAN, E. A., and WILLIAMS, B. E. *Trans Amer. Inst. Min. Met. Eng.*, **194**, p. 743 (1952).

Reduction of noise in photoconductive cells

By R. E. Burgess, B.Sc., A.M.I.E.E.,* Radio Research Station, Slough, Bucks.

[*Paper first received* 18 *April, and in final form* 15 *August*, 1955]

The factors determining the signal/noise ratio of photoconductive cells are briefly discussed and attention is drawn to the importance of the noise generated at the electrode contacts when current is flowing through the cell. Means are described for reducing or eliminating this component of noise by means of potential probes near the electrodes combined with suitable external circuits.

A photoconductive cell consists essentially of a strip of semiconductive material with metallic electrodes; the increase of its conductance on illumination permits the detection and measurement of the incident radiation. The excitation of carriers by the radiation may either be extrinsic (involving impurity or imperfection levels) or may be intrinsic corresponding to electron transitions from the valence to the conduction band. For extrinsic excitation, carriers of one sign only are liberated while the intrinsic process produces equal numbers of electrons and holes. The type of process which is important in any given case depends upon the electronic energy level structure of the semiconductor and upon the wavelength (i.e. the photon energy) of the incident light. The transient and the steady-state response will depend upon the reaction kinetics of the carrier densities under illumination, and this will be determined by the nature of traps and recombination centres present in the material and on its surface.[1]

The sensitivity of such a device for the detection of weak radiation is limited by the noise generated by the cell under the conditions of measurement of its conductance.[2] Usually direct current is passed through the cell in order that the increase of conductance will appear as a voltage change in the circuit. The incident radiation is commonly "chopped" (e.g., by a perforated disk or shutter) and the signal voltage is amplified in a resonant system tuned to the chopping frequency, which will usually lie within the audio-frequency range.

Certain components of the cell noise may be regarded as fundamental, i.e. thermal noise and those due to temperature fluctuations in the cell and photon fluctuations in the incident radiation. Other components of noise (termed "excess noise") arise from the passage of current through the cell and may be classed as shot noise and modulation noise.[3] Shot noise arises from the drift motion of the carriers under the applied field and has a spectral intensity which depends upon the density, lifetime and mobility of the carriers, as well as on the applied field and the geometry of the cell. Modulation noise is the term applied to the gross variation of the current flow due to fluctuations in the generation rates of the carriers or in the transmission properties of the barriers through which the carriers must pass. These effects can arise at the surface of the semiconductor, at barriers which occur between crystallites in polycrystalline material and particularly at the junction between the metal electrodes and the semiconductor.

The experimental attributes of the excess noise are that: (i) its spectral density decreases with increasing frequency; (ii) its intensity increases with increasing current, at first slowly then more rapidly; and (iii) its intensity depends very markedly on the fabrication, structure, surface treatment, and contact conditions of the cell to such an extent that noise reproducibility from one sample to another, nominally identical, is very poor.

The signal sensitivity of a cell expressed as the ratio of the fractional increase of conductance to the intensity of illumination ($\Delta G/G_0L$) will depend upon the wavelength of the light and will decrease with increasing frequency of modulation of the light intensity.

Thus the signal/noise ratio tends to its maximum when: (i) the frequency of the light modulation has the optimum value at which the decrease of sensitivity and the decrease of noise with increase of frequency offset each other; and (ii) the current through the cell is given the optimum value at which the increases of signal voltage and of noise voltage with current offset each other. For such an optimum to exist, if the noise voltage depends upon the current as I^n then n must be less than unity for low currents and greater than unity for large currents.

Fabrication of the cell to minimize its noise is at present largely an empirical process. In view of the earlier remarks on modulation noise it is clear that a cell would ideally be made from a monocrystal whose surface condition (both physical and chemical) had been carefully treated and with electrodes applied such that ohmic (barrier-free) contacts were obtained. There is experimental evidence[4,5] that photocells with a good *bulk* signal/noise ratio are handicapped by very considerable noise at the electrodes, even when these are carefully made. It is therefore relevant to examine means of reducing or eliminating electrode noise since such a step should result in the limiting noise being only that of the bulk photoconductor which is inextricably associated with the signal generation process.

Two methods of achieving this are described and involve the use of potential probes applied to the cell.

USE OF POTENTIAL PROBES TO REDUCE OR ELIMINATE ELECTRODE NOISE

First let us consider the simple scheme shown in Fig. 1(*a*). If illumination changes the cell resistance R from R_0 to $R_0 - \Delta R$ (where $\Delta R \ll R_0$) the signal voltage is given by

$$V_s = \frac{ES \,.\, \Delta R}{(R_0 + S)^2} = I_0 \frac{SR_0}{(S + R_0)} \frac{\Delta R}{R_0} \qquad (1)$$

For a given cell current I_0 the greatest output voltage is obtained by making S as large as possible. It is not correct to assert that the greatest voltage is obtained in the matched condition ($S = R_0$) since this only maximizes V_s if E is regarded as constant, whereas in fact the appropriate parameter in practice is the cell current, since for maximum response the cell current would be maintained at its optimum value under conditions of variable load resistance.

The noise will have three components: the cell noise, the noise of the load resistance S and the amplifier noise. The

* Now at University of British Columbia, Vancouver, Canada.

**

latter two should be minimized and this means using, if possible, a wire-wound resistor for S or, failing that, a film resistor which does not generate noise comparable with the cell under the relevant conditions of current and frequency. It will be assumed that the noise of S and the amplifier have been reduced below cell noise so that we have only the signal/noise ratio of the cell itself to consider.

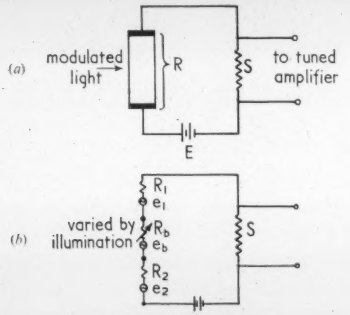

Fig. 1. Simple two-electrode cell

(*a*) Basic photoconductive cell circuit.
(*b*) Equivalent signal and noise circuit.

The cell noise is assumed to consist of two e.m.f.'s e_1 and e_2 at the two ends and a third e.m.f. e_b in the bulk [Fig. 1(*b*)]. Although the resistances R_1 and R_2 of the contact regions at the end may be very small (e.g. one thousandth) of the bulk resistance R_b between the electrodes, one or both of the noise e.m.f.'s e_1 and e_2 may appreciably exceed e_b. The signal/noise ratio of the cell is given by

$$\frac{V_s}{e_b + e_1 + e_2} \cdot \frac{R_0 + S}{S} = \frac{I_0 \Delta R}{e_b + e_1 + e_2} \qquad (2)$$

which is independent of S for a given cell current I_0.

Now let two low-resistance potential probes be applied to the cell near the electrodes so that the major part of the bulk resistance is included between them [Fig. 2(*a*)]. The signal is taken off from between these probes and the circuit is arranged so that no direct current flows in the probes and hence they generate no additional noise. The battery voltage E is applied through an impedor Z which transmits direct current but has a high impedance at the frequency of operation (i.e. the light modulation frequency). The equivalent a.c. circuit is shown in Fig. 2(*b*) in which R_{p1} and R_{p2} represent the spreading or contact resistances of the two probes. If the thermal noise of the probe resistances is negligible then the signal/noise ratio at the probe terminals becomes

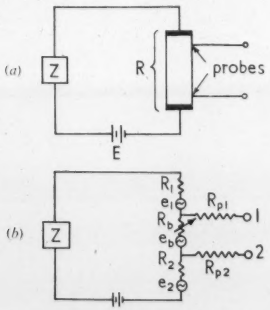

Fig. 2. Electrode noise reduction using potential probes [with $|Z(f)| \gg R$]

(*a*) Scheme using potential probes.
(*b*) Equivalent signal and noise circuit.

$$\frac{I_0 \cdot \Delta R}{e_b + K(e_1 + e_2)} \qquad (3)$$

where

$$K = R_b/(R_1 + R_2 + Z) \qquad (4)$$

which is a factor determining the extent to which the noise at the electrodes is reduced relatively to the bulk noise. Clearly if $|Z|$ is sufficiently large compared with the cell resistance the electrode noise is effectively suppressed. Thus ideally Z would consist of a parallel resonant circuit tuned to the measuring frequency. Practical considerations may, however, prevent the attainment of a sufficiently large value of Z, especially if the cell resistance is high. In this case a method of balancing out the e.m.f.'s e_1 and e_2 by a bridge-like circuit is desirable and this may be achieved in the following way.

In Fig. 3(*a*) a resistor Q_1 connected between electrode 1 and probe 1 through a capacitor C_1 will, if suitably adjusted,

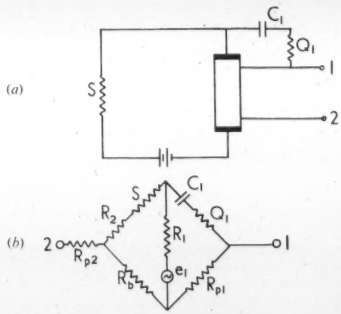

Fig. 3. Electrode noise cancellation using potential probes (illustrated for cancellation of noise e.m.f. e_1; similar technique may be simultaneously applied to cancellation of noise e.m.f. e_2)

(*a*) Scheme using potential probes with balancing circuit.
(*b*) Equivalent noise circuit showing bridge cancellation of e_1.

balance out the effect of the electrode noise e.m.f. as Fig. 3(*b*) indicates. The capacitor C_1 is included to prevent the flow of direct current in the probe circuit and it must be sufficiently large to make its impedance small compared with Q_1. Then the probe potential difference contains no noise from e_1 when

$$Q_1 = [R_{p1}(R_2 + S)]/R_b \qquad (5)$$

This technique has been tried experimentally in the Department of Physics, University of British Columbia. The following numerical values are typical of a monocrystal of

silicon or germanium of 50 Ω cm resistivity, 2 cm long and 1 mm square cross-section. $R_b = 10\,000\ \Omega$, $R_{p1} = 100\ \Omega$, $R_2 + S \simeq S = 100\,000\ \Omega$ whence $Q_1 = 1000\ \Omega$. Thus for an operating frequency of 1000 c/s the capacitance C_1 should be about 1 μF. Alternatively S can be shunted by a capacitance C_0 such that the phase angle of the $S + R_2$ arm is equal to that of the Q_1 arm.

Exactly the same procedure may be simultaneously applied to the other electrode so that neither of the noise e.m.f.'s e_1 and e_2 contributes to the output voltage between the probes. This technique may also be applied in the study of noise in semiconductor filaments in which it is desired to avoid the effects of conductance modulation produced at the electrode contacts.

ACKNOWLEDGEMENTS

The work described above was carried out as part of the programme of the Radio Research Board, and this paper is published by permission of the Director of Radio Research of the Department of Scientific and Industrial Research.

REFERENCES

(1) FAN, H. Y. *Phys. Rev.*, **92**, p. 1424 (1953).
(2) JONES, R. C. *Advances in Electronics*, **5**, pp. 1–96 (New York: Academic Press Inc., 1953).
(3) BURGESS, R. E. *Brit. J. Appl. Phys.*, **6**, p. 185 (1955).
(4) BROPHY, J. *J. Appl. Phys.*, **25**, p. 222 (1954).
(5) SMITH, R. W.: *Phys. Rev.*, **97**, p. 1525 (1955).

Determination of the velocity of ultrasonic vibrations in molten salts

By N. E. RICHARDS, M.Sc., A.N.Z.I.C., E. J. BRAUNER, B.S., and J. O'M. BOCKRIS, D.Sc., Ph.D., F.R.I.C.,
University of Pennsylvania, U.S.A.

[*Paper first received* 13 *June, and in final form* 11 *July*, 1955]

An apparatus for the direct measurement of the velocity of sound in molten liquids at temperatures up to 1000° C is described. The technique depends upon the phase interference of two wave trains, one passing through the liquid and the other a reference signal. The apparatus gives results to within 0·5% of accepted values. The theory of the method is investigated.

Earlier methods for the measurement of the velocity of ultrasonic vibrations in liquids[1–7] involved techniques with contacts between the sound source and test liquid and are thus not to be considered at high temperatures. A pulse reflexion method[8] has been used up to 450° C but results from it appear to be inaccurate in respect of temperature coefficients.[9,10] The main problem in devising a technique applicable to molten liquids is the elimination of contact between the sound source and the liquid. Consequently, it was decided to use a phase interference approach[11] and to propagate the ultrasonic longitudinal waves in and out of the liquid along quartz rods on which the source and receiving transducers were mounted out of contact with the melt.

APPARATUS

The furnace used for these experiments is shown in Fig. 1. The furnace tube *P*, was a stainless steel cylinder which was supported on a stainless steel plate *D*, soapstone block *C*, and the asbestos base plate *B*. The tube was wound with six separate windings *F*, which were connected to terminals *Q* mounted on the case. These heating coils were encased with a layer of alumina refractory cement *E*. Each coil was provided with a shunt for smoothing out temperature gradients. By appropriate settings of the shunts it was possible to obtain a 2½–3 in. zone where the temperature gradient was less than 0·4° C in.$^{-1}$. With a variable transformer control the temperature could be held constant to within ±1° C in the range 400–1000° C. Water cooling for the top and lower furnace case plates was provided by the tube coils *J*, whilst the silica tube *H* gave access to the furnace tube. The furnace case *A* was lagged with insulation *G*.

A screw control *L* was mounted on the steel plate *I*, by means of the aluminium rod *K*. This threaded control terminated in a chuck *M*, on which the threaded collar *N* fitted, thus clamping the upper quartz rod perfectly central with respect to the furnace tube. (The upper and lower controls were alined centrally during the construction.) A similar clamp and threaded control was mounted on an aluminium post at the base of the furnace to hold the lower quartz rod.

The fused quartz ultrasonic cell contained a cylindrical platinum crucible, 4 in. high, 1·4 in. diameter and with a wall of 0·005 in. supported by a platform inside the 1·6 in. outer tube so that a melt in the crucible was within the region of uniform temperature. The lower quartz rod on which the generating transducer was mounted passed through a fused quartz tube sealed to the 1·6 in. tube and the sliding fit was made vacuum-tight by means of a double O-ring seal. (Mechanical support for the vibrating rods should not be completely rigid; elasticity is provided by the compressible O-ring seals.) This rod was brought into contact with the base of the platinum crucible by means of the thread control. A tapered ground joint was sealed to the top of the cell. A matching ground glass stopper was fitted with four entry tubes to accommodate two pre-electrolysis electrodes,* a quartz thermocouple sheath (the temperature was measured from the e.m.f. of a chromel-alumel thermocouple) and the upper quartz rod on which the receiving transducer was mounted. The whole system was made vacuum-tight and could be filled with an inert atmosphere.

* The pre-electrolysis electrodes served to remove the last traces of absorbed water from the melt by electrolyzing at a potential difference greater than the decomposition potential of water but less than that for the molten liquid. The pre-electrolysis electrodes consisted of spectroscopically pure graphite rods, which could be retracted from the melt before velocity measurements were commenced since they passed through a double O-ring seal in the guide tubes of the stopper.

The transducers were silver-plated, X-cut quartz crystals with a resonant frequency of 1000 kc/s. The diameter of the rods was much greater than the wavelength of sound in the liquid; hence the emitted beam of sound waves was effectively planar.

In the electrical circuit (see Ref. 16, p. 374) a radiofrequency oscillator and pulse modulator generated a train of pulses

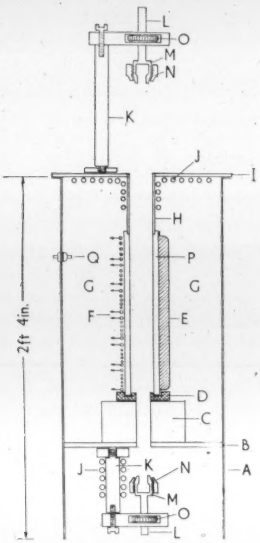

Fig. 1. Diagram of the furnace and clamps for the quartz rods

with a 1000 kc/s carrier frequency, a pulse repetition rate of 200 pulses/s and each with a duration of about 25 μs. The pulses were applied to the source transducer and, after passage through rods and the liquid, the received signal was amplified, added to an attenuated reference signal from the oscillator, further amplified and observed on a cathode-ray oscilloscope.

EXPERIMENTAL

To measure the velocity of sound in molten salts the apparatus was partially assembled before the furnace was heated to a temperature just below that of the melting point of the pure salt. The crucible was then lowered on to the platform with platinum suspension wires. The stopper with the rod, thermocouple sheath, and electrodes was then fitted, the upper clamp secured and the salt melted under a pressure of approximately 1 mm of mercury. Pre-electrolysis was carried out and while transmission of sound pulses continued, the upper and lower chucks (Fig. 1, *M*) were rotated slightly until the amplitude of the first pulse on the screen appeared greatest. (This condition meant that faces of the quartz rods were as closely parallel as possible.) When constant temperature was attained, both the position of the upper quartz rod and the setting of the reference signal attenuator were adjusted until a minimum (or null in the vertical Y-axis) was obtained on the screen at the point in the pattern where the pulse nearest to the origin of the horizontal sweep appeared, before the reference signal was added to the output of the detecting transducer. This condition indicated complete phase interference between the wave trains propagated through the cell and the direct reference signal. The position of the thread control (Fig. 1, *L*) was recorded with a cathetometer when such a minimum was obtained. The phase angle difference of π-radians was again achieved after moving the rod through such a distance that the phase of the propagated sound changed by 2π. This distance represented one wavelength. Thus, the upper rod was moved by means of the thumbscrew (Fig. 1, *O*) through about five wavelengths as indicated by the sequence of maxima and minima at the X-displacement corresponding to the former minimum on the oscilloscope. The position of the rod control giving the new minimum was noted and further measurements made by moving the rod both up and down. The frequency f was measured by a zero beat method to within ± 10 c/s in the range $f = 980$–1010 kc/s. The frequency of the oscillator varied less than the limits of accuracy of the frequency meter, i.e. ± 10 c/s, during the time required for a determination of λ. If h_1 and h_2 are the respective settings of the cathetometer for the passage of the upper rod through n nodes (minima), then $\lambda = (h_2 - h_1)/n$ and knowing the frequency, the velocity v was thus calculated. λ may be measured and reproduced to within 0·0005 cm, i.e. within 0·4%.

RESULTS

Velocity measurements were made on several liquids and the results are compared with those of room temperature accepted methods in Table 1. The liquids were either of analytical quality or redistilled.

Table 1. *Comparison of sound velocity results in common liquids with those obtained by present method*

Liquid	*Temperature* (°C)	*Velocity* (obs.) (m/s)	*Freyer*[4] (m/s)	*Passynski*[5] (m/s)	*Willard*[12] (m/s)
Acetone	22·5	1178 ± 10	1179	—	1170
	24·0	1168 ± 10	1172	1170	—
Benzene	25	1295 ± 20	1301	1303	1295
Carbon tetrachloride	23·5	924 ± 4	924	927	930
	58	815 ± 9	818	821	—
Ethyl alcohol	23	1155 ± 20	1158	1160	1150
Glycerol	22	1927 ± 20	1920	—	1986
Water	20	1484 ± 6	1484·2	1484	1500
	24	1490 ± 10	—	—	—

The agreement is better than 0·5%. The deviation listed in column 3 is the maximum experimental deviation from the mean result.

The velocity of sound in the molten salts listed in Table 2 was found to be a linear function of temperature in the ranges investigated. The following are the results for v_T, the velocity of sound at T° C in the range listed, together with the value of C_p/C_v. For the measurements in molten

salts the mean maximum deviation was 11 m/s; while the mean deviation was 5 m/s.

Table 2. *Velocity of sound in certain molten salts as a function of temperature*

Salt	v_T((m/s)	*Range* (°C)	C_p/C_v
Lithium nitrate	1796 − 1·3 (T-300)	260–500	1·14
Sodium nitrate	1812 − 1·23 (T-310)	310–440	1·14
Potassium nitrate	1748 − 1·184 (T-340)	333–535	1·18
Potassium chloride	1562 − 0·88 (T-800)	780–1010	1·31
Potassium bromide	1278 − 0·72 (T-750)	750–1008	1·36

DISCUSSION

From the agreement between observed and accepted sound velocities for common liquids recorded in Table 1, it can be seen that the apparatus yields reliable results at low temperatures. However, at high temperatures there is no existing data on the velocity of sound in liquids with which comparison may be made. A criterion of the validity of the results for high temperature liquids would be the agreement between C_p/C_v as calculated from the velocity results in Table 2 and the value obtained theoretically.

Now,

$$C_p - C_v = \alpha^2 VT/\beta_I \tag{1}$$

$$C_p/C_v = \gamma \tag{2}$$

when α is the coefficient of thermal expansion, V is the specific volume, T the absolute temperature and β_I the isothermal compressibility. C_p and C_v are the specific heats at constant pressure and constant volume respectively.

Then,

$$\gamma - 1 = \alpha^2 VT/C_v\beta_I \tag{3}$$

The velocity of sound in a liquid is given by

$$v_T^2 = \gamma/\beta_I\rho \tag{4}$$

where ρ is the density.

From equations (3) and (4),

$$\gamma - 1 = \alpha^2 v_T^2 T/\gamma C_v = \alpha^2 v_T^2 T/C_p \tag{5}$$

Thus, from a knowledge of α,[13] C_p,[14] γ was calculated from the present results and is listed in column 4 of Table 2.

For the liquid alkali metal nitrates there is a total of six translational, three rotational, and six vibrational degrees of freedom. Since $\gamma = 1 + (2/n)$ where n is the total number of degrees of freedom, γ may be expected to equal 1·13 in good agreement with the values based on the present results.

Goodwin and Kalmus[14] applied Kopp's law to solid and molten halides (e.g. silver chloride, thallium chloride, lead chloride, silver bromide, thallium bromide and lead bromide) at temperatures in the vicinity of 500° C and found that the atomic heat was 7·1 cal/g. atom. The extrapolated values[13] of $C_p(s)$ for solid potassium chloride and potassium bromide give values for the molecular heat at 800° C of 13·80 cal and 13·76 cal/mole respectively. The value of $C_p(l)$ was found to be greater than $C_p(s)$ by a factor varying between the limits 1·01–1·3.[14] Assuming this ratio to be applicable at 800° C, then the molecular heat capacity of both potassium chloride and potassium bromide is 14·2 cal, i.e. 1·03 $C_p(s)$. Substituting the derived value of C_p in equation (5) results in the values for γ listed in Table 2 which agree well with theoretical value of 1·33. In obtaining the above results the first of several (five to eight) pulses appearing in the sweep across the cathode-ray screen was used since the first must traverse the sound path in the shortest time interval. However, trial showed that for organic liquids at room temperatures velocity measurements made by using subsequent pulses along the X-axis gave results in fair agreement (within 2%) with those obtained on the first pulse, indicating that the wave trains which gave rise to subsequent pulses, pass through liquid once. For molten potassium bromide, however, the velocities measured on the first two pulses were in agreement but subsequent pulses gave rise to velocities of approximately $\frac{1}{3}$ and $\frac{1}{5}$ of the true velocity as measured by the first pulse. This suggests that wave trains involving multiple reflexions of the sound waves within the liquid contribute to the phase summation of pulses at the receiving crystal.*

The time taken (time delay) by each pulse appearing on the screen to travel through the two rods and the liquid sample can be determined experimentally to within 5% by use of the equation: 1000[(X-co-ordinate of centre of a pulse) − (X-co-ordinate of the origin of sweep)]/(length of sweep) μs since a 1000 μs sweep was used. In Fig. 2, *AB*, length l_1 cm, represents the lower quartz rod in the apparatus; *BC*, length l_2 cm, the mean path through the liquid, and *CD*, length l_3 cm, the upper quartz rod. If v_q cm/μs is the velocity of sound in quartz[15] and v_1 cm/μs that in the liquid, the time for the leading edge (or centre) of a pulse to travel from the sound source directly to the detecting transducer is

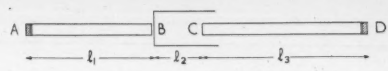

Fig. 2. Plan of the path of the ultrasonic vibrations through the system of rods and liquid

$$t = (l_1/v_q + l_2/v_1 + l_3/v_q)\mu s \tag{6}$$

For reflexions such as $AB + (BC + CB + BC) + CD$; $(AB + BA + AB) + BC + CD$, the respective times t_2 and t_3 are

$$t_2 = (l_1/v_q + 3l_2/v_1 + l_3/v_q)\mu s \tag{7}$$

$$t_3 = (3l_1/v_q + l_2/v_1 + l_3/v_q)\mu s \tag{8}$$

The times for propagation of additional postulated reflexions can be similarly determined. A comparison between the calculated propagation times and the observed delay times assuming various reflexions shows that there are times for the former agreeing to within 5% of the latter.

A comparison of observed and calculated times for propagation through the apparatus is made in Table 3, for benzene (25° C) and potassium bromide (1000° C).

A further check on this theory of reflexions can be provided by the evaluation of the relative amplitudes of vibrations in

* The estimated attentuation (from the classical equation[16]) for potassium bromide expressed in the form $Aff^2 \times 10^{15}$ nepers/cm is 0·2 which is much less than the experimentally obtained value for benzene of 8·3,[12] so that sound reflexions within molten potassium bromide are not so strongly damped as in benzene.

Table 3. *Comparison of the propagation times through the cell for benzene and potassium bromide*

Benzene—						
Observed (μs)	162	254	288	384	470	
Calculated (μs)	159	253	282	353 375	441, 469 497	
Type of reflexion assumed in calculated times	$AB+BC+CD$	$3AB+BC+CD$	$AB+BC+3CD$	$3AB+BC+3CD$ $5AB+BC+CD$	$7AB+BC+CD$ $5AB+BC+3CD$ $3AB+BC+5CD$	
Potassium bromide—						
Observed (μs)	183	276	344	462	525	650
Calculated (μs)	186	289	322, 316	458, 453 430, 485	529, 524 490, 550	630, 660 665
Type of reflexion assumed in calculated times	$AB+BC+CD$	$3AB+BC+CD$	$AB+3BC+CD$ $AB+BC+3CD$	$AB+5BC+CD$ $AB+3BC+3CD$ $3AB+3BC+CD$ $7AB+BC+CD$	$5AB+3BC+CD$ $5AB+BC+3CD$ $AB+5BC+3CD$ $3AB+BC+5CD$	$7AB+BC+3CD$ $5AB+3BC+3CD$ $5AB+5BC+CD$

the pulses from theoretical considerations which may then be compared with the observed ratios.

From an equation in Ref. 17:

$$(E_r/E_i) = (\rho_1 v_1 - \rho_2 v_2)^2/(\rho_1 v_1 + \rho_2 v_2)^2 \qquad (9)$$

where E_r and E_i are the reflected and incident energies for normal waves; ρ_1, ρ_2 are the densities of the two media and v_1, v_2 are the sound velocities in the media, the fraction of sound intensity transmitted at an interface can be calculated if it is assumed that no energy is lost at an interface, i.e.

$$E_r/E_i + E_t/E_i = 1 \qquad (10)$$

E_t being the transmitted energy. After suffering a normal reflexion at, or passage through, a liquid-quartz or quartz-liquid interface the new energy becomes the "incident" energy with respect to the next change, either a reflexion or a refraction. In the ideal case for a group of sound waves travelling normally through n interfaces and suffering m reflexions at the same type of boundaries, the fraction of the initial energy emerging is $(E_t/E_i)^n(E_r/E_i)^m$. The direct pulse would pass through a quartz-liquid and a liquid-quartz interface which is equivalent to two quartz-liquid boundaries. Therefore, $E_{final}/E_{initial}$ in this case is $(E_t/E_i)^2$. Since the intensity or energy of a wave is proportional to the square of the amplitude, it follows that

$$\frac{\text{amplitude of indirect pulse}}{\text{amplitude of direct pulse}} = \left[\frac{(E_t/E_i)^n(E_r/E_i)^m}{(E_t/E_i)^2}\right]^{\frac{1}{2}} \qquad (11)$$

Table 4. *Comparison of calculated and observed relative maximum amplitudes of consecutive pulses on the screen*

Benzene—						
Observed relative amplitude	1	1·2	0·9	0·7	0·37	
Calculated relative amplitude	1	0·84	0·82	0·8	0·7	
Potassium bromide—						
Observed relative amplitude	1	0·7	0·87	0·6	0·55	0·4
Calculated relative amplitude	1	0·60	0·84	0·53	0·43	0·15

The relative amplitudes are then determined according to equation (11). In the instances where the pulses reinforce according to their phase, the resultant intensity is the sum of the respective intensities. Table 4 shows the satisfactory comparison of the observed and calculated relative amplitudes of pulses appearing across the screen.

REFERENCES

(1) Pellam and Galt. *J. Chem. Phys.*, **14,** p. 608 (1946).

(2) Pierce. *Proc. Amer. Acad.*, **60,** p. 269 (1925).

(3) Hubbard and Loomis. *Phys. Rev.*, **31,** p. 158 (1928); *Nature* [*London*], **120,** p. 189 (1927).

(4) Freyer, Hubbard and Andrews. *J. Amer. Chem. Soc.*, **51,** p. 759 (1929).

(5) Passynski. *Acta Physicochimica, URSS*, **8,** p. 385 (1938).

(6) McMillan and Lagemann. *J. Acoust. Soc. Amer.*, **19,** p. 956 (1947).

(7) Lagemann, McMillan and Woolf. *J. Chem. Phys.*, **17,** p. 369 (1949).

(8) Kleppa. *J. Chem. Phys.*, **18,** pp. 1303, 1331 (1950).

(9) Fox and Rock. *Rev. Sci. Instrum.*, **10,** p. 345 (1939).

(10) Telfair and Peilmeier. *Rev. Sci. Instrum.*, **13,** p. 122 (1942).

(11) Carstensen. *J. Acoust. Soc. Amer.*, **26,** p. 858 (1954).

(12) Willard. *J. Acoust. Soc. Amer.*, **12,** p. 438 (1941).

(13) *International Critical Tables*, Vol. V, p. 100 (1929).

(14) Goodwin and Kalmus. *Phys. Rev.*, **28,** p. 1 (1909).

(15) Sosman. *The Properties of Silica* (New York: The Chemical Catalog Co., 1927).

(16) Mason. *Piezoelectric Crystals and Their Application to Ultrasonics*, p. 338 (New York: D. Van Nostrand Co. Inc., 1950).

(17) Rayleigh. *Theory of Sound*, Vol. II, p. 91 (London: Macmillan and Co. Ltd., 1929).

The scanning electron microscope and its fields of application

By K. C. A. Smith, B.A., and C. W. Oatley, M.A., M.Sc., Engineering Laboratory, University of Cambridge

[*Paper received* 3 *August*, 1955]

Experience with the scanning electron microscope has shown that there are fields of application where this instrument has distinct advantages over the conventional transmission microscope (with or without replicas) and the reflexion electron microscope. For example, there are specimens which are too thick to be viewed by direct transmission and which nevertheless do not lend themselves readily to the construction of replicas, either because they are too fragile, because their surfaces are undercut so that the replica would be keyed to them or because observation of the specimen at high temperatures is desired. The paper gives examples of the use of the scanning microscope in such cases and shows that the images produced are very similar in character to those obtained with optical microscopes. In particular, a pronounced three-dimensional effect is observed.

In the work described the specimens have been mounted so that the mean surface under observation is at a glancing angle of about 25° to the incident electron beam. Contrast is provided by the variation of the local angle of incidence as the scanning electron beam moves over the surface, and does not depend on secondary emission. With the present apparatus a resolution of about 200 Å has been attained, but there appears to be no reason why this performance should not be substantially improved.

It is shown that, with the scanning microscope, bombardment of the specimen is much less severe than with other electron microscopes.

1. Introduction

In the scanning electron microscope a beam of electrons, which is focused to a very small spot, is caused to move in turn over each point of the object. The electron current leaving the object is collected and amplified and is then used to modulate the brightness of a cathode-ray tube whose spot is moving over the screen in correspondence with the motion of the electron beam over the object. If, then, any property of the object causes the electron current which leaves it to change from point to point, the picture built up on the cathode-ray tube will constitute a record of the variation of this property over the area of the object which is scanned. It does not follow that this picture will bear any resemblance to the one which would be seen through an optical microscope, although it may do so.

A microscope based on the above principles was first proposed by Knoll[1] in 1935 and a few years later an actual instrument, in which mechanical scanning was employed, was described by von Ardenne.[2, 3] In 1942, Zworykin, Hillier and Snyder[4] gave an account of a scanning microscope which is much more closely related to the present work. This instrument made use of the variation of secondary emission over the surface of the specimen and was employed chiefly for the examination of metals. One of the greatest difficulties encountered in this work was the very low signal-to-noise ratio that it was found possible to achieve.

Soon after the end of the war, electron multipliers with beryllium–copper dynodes came into general use. Unlike earlier multipliers, these devices could be used in demountable vacuum systems and it seemed probable that they could profitably be employed for the detection of electrons in a scanning microscope. Work along these lines was therefore put in hand in this laboratory and in 1953 McMullan[5] was able to report the construction of a successful instrument. He also showed that it is unnecessary to rely on variation of secondary emission to provide contrast. If the mean plane of the surface under examination is set at an angle of about 25° to the incident electron beam and the scattered electrons (including secondaries) are collected by the multiplier, it is found that the multiplier current depends strongly on the angle between the incident beam and the portion of the surface on which it is falling. This angle normally varies from point to point of the surface, so the picture finally built up on the cathode-ray tube is related to the topographical structure of the surface rather than to its secondary-emission properties.

The scanning electron microscope constructed by McMullan has now been in use for several years and sufficient experience has been gained with it to make possible an appraisal of the probable fields of usefulness of instruments of this kind. The original apparatus has been modified in several ways but the modifications are not of a fundamental nature and will not be considered in any detail here. In the present paper an attempt is made to compare the performance and possibilities of the scanning electron microscope with those of the conventional transmission electron microscope (with or without the use of replicas) and with the reflexion electron microscope.

At the present time the conventional transmission instrument is firmly established as the most useful type of electron microscope for general work. Furthermore, it is usually possible to modify such microscopes quite simply to allow examination of opaque specimens to be carried out by reflected electrons. Thus the conventional instrument is likely to be used whenever it can be made to give satisfactory results. By comparison, the scanning electron microscope involves the use of a good deal of additional apparatus and is inherently a more complicated instrument. Its use can therefore be justified only in cases where ordinary electron microscopes are unsatisfactory, and it is one object of the present paper to indicate where such cases may arise.

2. Formation of the Image in the Scanning Electron Microscope

As has been indicated above, contrast in the image formed by a scanning electron can be made to depend either on variation of secondary emission over the surface of the object or on the surface topography of the object. In the former case the range of objects that can be examined is severely

limited, since for most surfaces the secondary emission coefficient is unlikely to show sufficient variation. Furthermore, this coefficient almost always falls to a low value when the primary electrons have energies of a few ten thousands of electron volts so that, to obtain sufficient secondary emission, it may become necessary to work with a primary energy of about 1 keV. This in turn brings other difficulties; surface contamination of the object is likely to be serious and it is not easy to obtain good resolution with electrons of such low energy. For these reasons the work described below was done under conditions such that contrast depended on the surface topography of the object and the angle between the incident beam and mean surface was usually about 25°, though angles up to 45° have been found satisfactory. The energy of the incident electrons was about 20 keV; this is sufficient to penetrate thin contaminating films on the object and no serious trouble from such films has been encountered.

Since the number of electrons scattered from the object varies with the local angle of incidence of the primary beam, the final image built up on the cathode-ray tube will be related to this variation, but it is not obvious that the image will be a recognizable picture of the surface. However, this proves to be the case as is clearly shown by Fig. 1 which is an image of a portion of a grid from a television camera tube. The marked three-dimensional effect is particularly noteworthy and is also found in the examples to be discussed later.

In the present instrument the collection of scattered electrons is performed in a relatively crude manner. The first dynode of the electron multiplier is placed as close to the object as is convenient and is maintained at a positive potential of about 500 V with respect to the object. Of the electrons leaving the object, some have nearly the full energy of the primary beam, while others are relatively slow. Because the secondary emission coefficient of the first dynode falls to a low value for high primary energies, the slow electrons may have a disproportionately large effect in the formation of the image. This is suggested by the fact that the signal strength is considerably reduced if the potential of the first dynode is made equal to that of the object. This change would be unlikely to alter the number of swift electrons collected but it might seriously reduce the number of slow ones. Relatively little work has so far been done on the investigation of these factors and it seems unlikely that the present arrangement of the collector is the best that can be devised. It is, however, good enough to give very satisfactory results.

Scintillation counters have now been brought to a high state of efficiency and they might have numerous advantages for the detection of the scattered electrons in a scanning microscope. Work is in hand to test this possibility. A rather special example of this technique is shown in Fig. 2 (obtained by Dr. McMullan), where the object itself consisted of grains of a silver-activated zinc sulphide phosphor and the normal electron multiplier was replaced by a photomultiplier. In this particular phosphor most of the light comes from active regions which occupy only small portions of the grains within which they occur.

3. SPECIMENS FOR WHICH THE SCANNING ELECTRON MICROSCOPE OFFERS ADVANTAGES

The most obvious field of application for electron microscopes of the scanning or reflexion types is for the examination of opaque objects when replica techniques cannot be used. For example, the object might have indentations which were undercut so that a replica would be keyed to the surface. Again it might be desired to examine the surface at a temperature at which the replica would be destroyed; or to watch the changes in structure as the surface was heated. Although relatively little work along these lines has so far been done, there are clearly many situations in which a scanning or a reflexion microscope is the only instrument that can be used.

A rather different case occurs with many biological specimens where the object is too thick to be viewed by transmission, but too small for the preparation of replicas to be at all easy. Two examples of results obtained with the scanning microscope in such cases are shown in Figs. 3 and 4(*a*, *b*). They represent respectively an amoeba and part of the skin of a meal-worm grub. A somewhat similar situation arises in the microscopy of fibres and Fig. 5 shows the result obtained with a fibre of Orlon.

With specimens of this kind which are insulators, difficulties may be caused by charging of the object. These troubles can usually be overcome by coating the object with a thin evaporated layer of metal.

Although the above photographs were obtained with a scanning electron microscope, the objects belong to a class for which the use of a reflexion microscope might be contemplated (e.g. Holdgate, Menter and Seal[6]) and it is therefore necessary to consider whether the former instrument has any advantages to justify its greater complexity. From this point of view the chief difference between the microscopes lies in the angles at which the electrons strike the object and are collected from it. In the reflexion microscope a glancing angle of incidence of 5° or less has hitherto proved essential and most workers have collected electrons lying in a narrow pencil which makes an angle of 10° or less with the mean surface. An obvious disadvantage of such a small glancing angle of reflexion is the very large foreshortening of the final picture, and a ratio of maximum to minimum magnification of ten or more is not uncommon. An even more serious difficulty lies in the fact that some asperities on the surface cast large shadows and the deeper depressions are not illuminated at all. Thus, on rough surfaces, much of the detail is concealed.

Recent work in France by Fert[7] suggests that it may be possible to work with glancing angles of reflexion up to 35° and thus lessen the troubles due to foreshortening. However, unless the glancing angle of incidence can also be increased, the other difficulties will remain.

The scanning electron microscope is inherently free from the above disadvantages since large glancing angles of incidence and reflexion can be used without difficulty. In fact, careful examination of some of the photographs (e.g. those shown in Figs. 1 and 6) shows that electrons must have been reaching the collector by indirect paths since detail is revealed at some points from which there was no direct path to the multiplier. This effect is likely to prove extremely valuable and further investigation of it is planned.

The ability of a scanning electron microscope to operate with very irregular surfaces, coupled with the large depth of focus which is characteristic of most electron microscopes, makes it possible to carry out certain types of manipulation on a specimen while it is actually under observation. An example of this is shown in Fig. 6, which shows a tungsten point contact on a germanium crystal, (*a*) before and (*b*) after the discharge of a condenser through the contact. The process was carried out while the contact was under observation and the electrical rectification characteristics could also be measured.

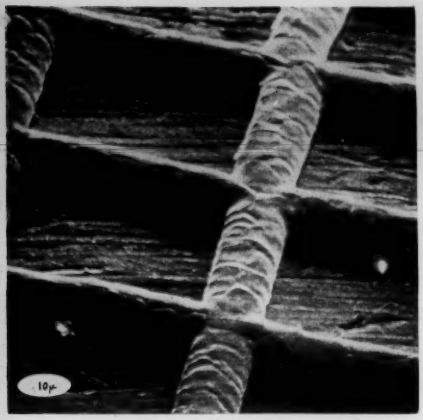

Fig. 1. Portion of aluminized copper grid from a television-camera tube

Fig. 2. Grains of silver-activated zinc sulphide phosphor

Fig. 3. Amoeba, fixed with osmic acid (no metal coating) on nickel surface

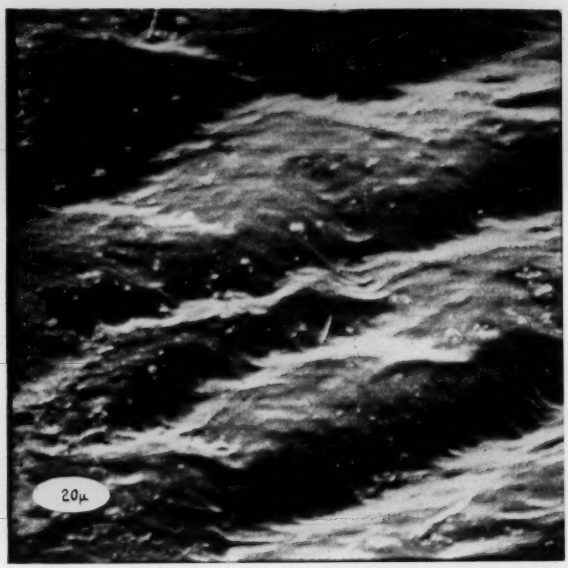

Fig. 4(*a*). Surface of meal worm grub, *Tenebrio molitor* (silver coated)

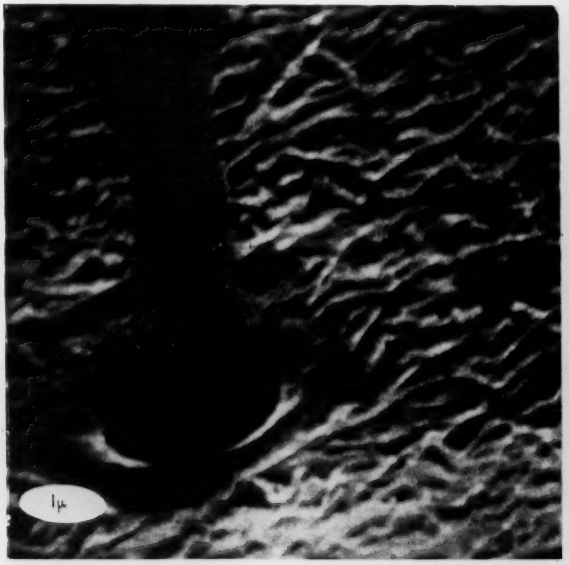

Fig. 4(*b*). Bristle on meal worm grub

Fig. 5. Orlon fibre (gold-palladium coated)

Fig. 6. Tungsten–germanium point contact

(*a*) Before discharge of condenser through contact.

Fig. 6. Tungsten–germanium point contact
(*b*) After discharge.

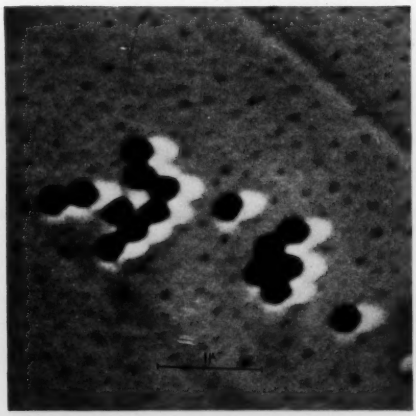

(*a*)

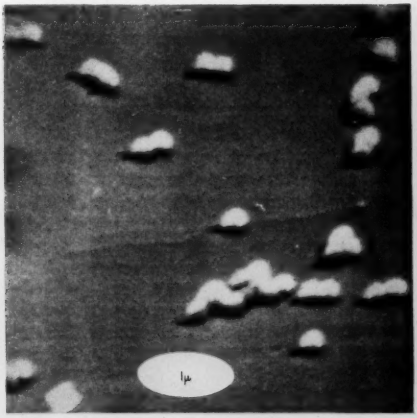

(*b*)

Fig. 7. Latex particles
(*a*) Transmission micrograph. (*b*) Reflexion micrograph.

4. FUNDAMENTAL LIMITATIONS

There are certain fundamental principles which set a limit to the performance of any electron microscope, but their application to the scanning microscope is rather different from what it is with conventional electron microscopes. Before making further comparisons between the different types it is therefore necessary to establish some basic equations which are of general application.

Suppose a square area of the object of side D cm to be under observation and let d cm be the smallest distance that it is desired to resolve. For the time being, electron-optical aberrations of the instrument are assumed to be negligible. Then the object may be divided into D^2/d^2 square elements, each one of which must be resolved from its neighbours. Following the principles laid down by Rose,[8] there must fall on each element of the object a certain minimum number N of electrons, which can be calculated as follows. Because the arrival of electrons is a random process, there will be associated with N a fluctuation of r.m.s. magnitude $\sqrt{N}$ and $N/\sqrt{N} = \sqrt{N}$ represents the basic signal-to-noise ratio from the element. Subsequent stages in the production of the final picture cannot improve this basic ratio, though they may make it worse. Consider two adjacent elements such that all the electrons striking the first go to form the corresponding bright area of the image, while those striking the second are removed by absorption or scattering so that the corresponding area in this case is completely black. This represents the most favourable case for resolution of the two elements and experiment shows that, in the final picture, the eye will be unable to distinguish the black area from the adjacent area, which is speckled as a result of the random fluctuations, unless N exceeds a value of about 5. Thus in this case a minimum of twenty-five electrons per element would be needed. In general it will be desirable for the eye to be able to distinguish much smaller changes of contrast in the final picture than the complete change from "white" to "black" in adjacent elements. If, for example, an element of brightness B is to be distinguishable from one of brightness $B \pm \Delta B$, the relevant equation becomes

$$\sqrt{N} \geqslant 5B/\Delta B \tag{1}$$

so that for 5% contrast to be detectable a minimum of about 10^4 electrons per element is required.

So far it has been assumed that randomness in the primary electron stream is the limiting factor, but this may not be the case. For example, in the conventional electron microscope used visually, electrons leaving the object strike a fluorescent screen where each electron produces, on the average, several quanta of light. A fraction of these quanta enter the eye of the observer and are absorbed by the retina. Several quanta are required to produce a visual stimulus, so the number of stimuli conveyed to the brain is less than the number of quanta absorbed. Thus the number N' of independent events per element varies from point to point of the apparatus. So long as N' is, on the average, always greater than N, no additional noise is introduced since complete randomness was already associated with the original number N. If, however, N' falls below N at any stage, the stage with the lowest value of N' will become the limiting one and this value of N' should replace N in equation (1). This point will be discussed further in Section 5.

Let j A/cm^2 be the useful electron current density arriving at the object, i.e. that portion of the total current density which is contained in a solid angle small enough to allow it to pass through the complete electron-optical system of the instrument, and let t be the effective time during which electrons from each element are collected. Then, if e coulombs is the electronic charge,

$$N = jd^2t/e \tag{2}$$

and from equation (1)

$$j \geqslant 25B^2e/d^2t\Delta B^2 \tag{3}$$

However, j is limited by the maximum emission density j_0 A/cm^2 of the cathode from which the electrons originate and according to Langmuir's theorem

$$j \leqslant j_0 \sin^2 \alpha(1 + Ve/kT) \tag{4}$$

where k J/degree is Boltzmann's constant, T the absolute temperature of the cathode, V volts the potential difference between object and cathode and α radians the semi-angle of the cone within which lies the useful electron current striking a point of the object. Since $Ve/kT \gg 1$ and $\sin \alpha \doteqdot \alpha$, equations (3) and (4) can be combined to give

$$j_0 \geqslant 25(B/\Delta B)^2 \frac{kT}{Vtd^2\alpha^2} \text{A/cm}^2 \tag{5}$$

5. RESOLUTION

Equation (5) is valid for the conventional transmission microscope as well as for the scanning electron microscope and for the purpose of comparison it will be convenient to use the following typical values

$$B/\Delta B = 20$$
$$T = 3000^\circ \text{K}$$
$$j_0 = 10 \text{ A/cm}^2$$
$$V = 30 \text{ kV}$$
$$k = 1{\cdot}38 \times 10^{-23} \text{ J/degree}$$

to give

$$\alpha^2 \geqslant 1{\cdot}38 \times 10^{-21}/td^2 \tag{6}$$

In the conventional transmission microscope used visually, t is determined by the properties of the eye, and experiment shows that the time over which effective integration takes place is about 0·2 s. Haine and Einstein[9] have shown that practical electron guns approach quite closely to the maximum theoretical efficiency indicated by equation (4) so that, even if a resolution of 5 Å is required, equation (6) merely requires α to be greater than $1{\cdot}7 \times 10^{-3}$ rad. However, the designer would in any case wish to exceed this limit to obtain the best compromise between spherical aberration and diffraction effects. If the image is recorded photographically, t can readily be made much greater than 0·2 s, and the minimum value of α is correspondingly smaller. Thus, with this type of instrument, the random nature of the beam current does not impose any practical limitations on design.

For the scanning microscope the case is quite different. Here the elements of the object are scanned sequentially and t is found by dividing the total scan period T by the number of elements $(D/d)^2$. To cover a reasonable field of view D/d must be of the order of 1000 and for visual work T cannot be much greater than 2 s, giving, for a resolution of 5 Å,

$$\alpha \geqslant 0{\cdot}53 \text{ rad.} \tag{7}$$

For photographic work T can, in principle, be increased without limit, but the practical problem of ensuring that the object does not move sets a limit of, say five minutes. A

longer period would, in any case, be extremely inconvenient. This gives, for a resolution of 5 Å,

$$\alpha \geqslant 4{\cdot}3 \times 10^{-2}\,\text{rad}. \qquad (8)$$

The limit for α set by equation (7) is impossibly high and even that given by equation (8) is much larger than that required to give the best compromise of aberrations in the electron-optical system.

The above figures represent limiting cases and are given merely by way of example since the equations cannot, in the nature of things, yield an exact limit for α. For example, it has been tacitly assumed that the collection of electrons scattered from a "white" element of the object is 100% efficient, and this is certainly not the case. Again, many of the electrons striking the first dynode of the collector have such high velocities that they contribute little to the secondary emission. On the other side of the picture it would be possible, by accepting a smaller field of view, to reduce the number of elements very considerably and thus increase the value of t. Similarly, for some specimens, a value of $B/\Delta B$ less than twenty might be acceptable. A great deal more work is needed to provide further information on these various factors but it is clear that, for visual work, the random nature of the beam will be an important factor in setting a limit to the resolution that can be obtained. It may also limit the resolution in photographic work.

A quite different factor which may set a limit to the attainable resolution is the penetration of the incident electrons into the object. Suppose, for example, the object to consist of a rectangular solid and let the incident beam fall on the top surface and be moving towards the edge formed by the top and one of the sides. If the top surface is perfectly smooth and the beam is not near the edge, electrons will penetrate the surface to various depths, will be deflected by collision and a proportion of them will re-emerge from an area of the surface much larger than the original spot. However, under the conditions stated above, the electron current flowing to the multiplier will have a definite constant value. Similarly when the incident beam has passed the edge by a considerable distance and is falling on the side of the object, the current to the multiplier will have a different constant value. In the vicinity of the edge, however, it is possible for electrons to enter the surface and emerge from the side or *vice versa*, and the transition of the multiplier current from the value characteristic of the surface to that characteristic of the side will thus be gradual and the edge may appear blurred in the final image. The extent to which this effect will limit resolution would be expected to vary with the nature of the object and the energy of the incident electrons. Once again, detailed information on these points is not yet available.

The scanning microscope at present in use is not very suitable for tests on resolution, since it was designed to give a Gaussian spot-diameter of about 150 Å. Now that a stigmator has been added and the efficiency of collection of the scattered electrons greatly improved, a reduction of the diameter of the spot would be advantageous and the electron lenses will shortly be modified to make this change possible. With the aperture at present in use in the second demagnifying lens, the calculated spherical aberration, $C_s\alpha^3$, amounts to 70 Å and the diffraction aberration to about 30 Å.

A photograph of latex particles taken with the microscope used as a scanning transmission instrument (the latex being mounted on a collodion film) is shown in Fig. 7(*a*), and suggests a resolution of between 200 and 250 Å, i.e. approximately the theoretical value. It was hoped that, with this arrangement and with such small objects, penetration of the primary electrons into the object would not have such serious consequences as in the more normal arrangement. However, a photograph of similar particles taken with the instrument used as a scanning reflexion microscope, is shown in Fig. 7(*b*) and the resolution is about the same as before.

At the present time it is difficult to hazard a guess at the ultimate resolution that it will be possible to attain with the scanning microscope, but a value less than 100 Å would seem to be within reach.

6. BOMBARDMENT OF THE OBJECT

There are many objects which are partially or totally destroyed by excessive electron bombardment, so it is of interest to compare different types of electron microscope from this point of view. The reflexion microscope is known to be very much worse than the ordinary transmission microscope because, in the former instrument, only a very small proportion of the electrons striking the specimen pass through the object lens and thus contribute to the final image. In what follows, therefore, a comparison will be made between the transmission microscope and the scanning microscope.

In the light of the principles laid down in Section 4, consider first what the situation would be if a perfect instrument of each type were available. In the case of the transmission microscope, every electron striking a "white" element of the object would subsequently enter the object lens and, in the scanning microscope, every electron striking a white element would be collected by the multiplier. Furthermore, in each instrument the number of independent events per white element of the object, at each subsequent stage of observation, would be greater than the number of electrons striking that element. Under these conditions it should be possible to obtain an image, in each case, when the number of electrons per element was as great as N in equation (1). Thus the performances of the two instruments would be equal from the point of view of the bombardment of the specimen.

Practical instruments may fall short of the ideal in two respects. In the first place the collection of electrons from a "white" element is not perfect. Quantitative measurements are lacking but it is probable that the efficiency of collection could be made to approach 100% in both types of instrument. In any case, the difference between them is unlikely to be very large.

Consider next the assumption that the number of individual events per element, at each stage in the production of the image, is greater than the number of electrons per element. In the scanning microscope this will be true if the average secondary emission coefficient at the first dynode is greater than unity, since enough dynodes can be used to counteract inefficiency in any subsequent process. In the existing instrument the average secondary emission coefficient probably does not fall short of unity by a large factor, and there is certainly room for improvements in the design so that electrons shall strike the first dynode with the optimum energy. Thus the scanning microscope approaches the ideal quite closely.

For the transmission microscope used visually the case is quite different. Each electron entering the object lens strikes the fluorescent screen and, in a good screen, rather less than 10% of the energy of the electron is converted into light so that a 50 keV electron might produce about 2000 quanta. Only about 2 in 10^4 of the total number of quanta enter the eye of the observer; furthermore, according to the work of Hecht[10] about 100 quanta must enter the eye to produce a

single visual signal to the brain. Thus the processes subsequent to the entry of the electrons into the object lens reduce the number of individual events per element by a factor of about 250 and the initial bombardment of the object must therefore be increased in this ratio.

An additional factor of ten in favour of the scanning microscope arises from the fact that the effective integration period of the eye is about 0·2 s. Thus if, as is usually the case, the image is to be viewed continuously for at least a few seconds, the required number of electrons must fall on the object in the transmission microscope every 0·2 s. In the scanning microscope, however, the integration is carried out by a long-persistance screen on the cathode-ray tube and the effective integration period may easily be as high as 2 s.

It is interesting to note that the poor performance of the transmission microscope is not fundamental. In principle it could be greatly improved by the use of a long-persistance screen and/or an image intensifier, but this would entail considerable additional complication. Again, the performance is greatly improved when photographic recording with suitable plates is used. There remains, however, the practical difficulty of selecting and focusing the image if it cannot be observed visually.

It appears, therefore, that the scanning microscope offers material advantages when bombardment of the object is to be kept to a minimum.

7. CONCLUSIONS

It will be apparent from what has been written that relatively little is yet known about many of the factors affecting the performance of the scanning electron microscope and it is reasonable to expect that, when these factors are better understood, an improved instrument will result. Even now, however, there is a wide range of objects with which the scanning microscope will yield results that cannot be obtained in any other way.

ACKNOWLEDGEMENTS

We wish to express our thanks to the Admiralty for a grant to cover the cost of apparatus. One of us (K. C. A. S.) is also indebted to the Department of Scientific and Industrial Research for a maintenance grant.

REFERENCES

(1) KNOLL, M. *Z. Tech. Phys.*, **16**, p. 767 (1935).

(2) VON ARDENNE, M. *Z. Phys.*, **109**, p. 553 (1938).

(3) VON ARDENNE, M. *Z. Tech. Phys.*, **19**, p. 407 (1938).

(4) ZWORYKIN, V. K., HILLIER, J., and SNYDER, R. L. *Bull. Amer. Soc. Test. Mater.*, **117**, p. 15 (1942).

(5) MCMULLAN, D. *Proc. Instn Elect. Engrs*, **100**, (II) p. 245 (1953).

(6) HOLDGATE, H. W., MENTER, J. W., and SEAL, M. *International Electron Microscopy Conference, London* (Royal Microscopical Society, 1954).

(7) FERT, C. *Conference on Recent Progress in Corpuscular Microscopic Techniques*, Toulouse, 1955.

(8) ROSE, A. *Advances in Electronics*, Vol. 1, p. 131 (New York: Academic Press, 1948).

(9) HAINE, M. E., and EINSTEIN, P. A. *Brit. J. Appl. Phys.*, **3**, p. 40 (1952).

(10) HECHT, S. *J. Opt. Soc. Amer.*, **32**, p. 42 (1942).

Stability criteria for an electrical or mechanical system with distributed parameters

By A. S. GLADWIN, Ph.D., D.Sc., A.Inst.P., University of Sheffield

[*Paper first received* 3 *August, and in final form* 29 *August*, 1955]

The equation $C_0 + C_1 z + (C_2 + C_3 z)\tanh z = 0$ occurs in the theory of the stability of electrical or mechanical systems with distributed parameters or with an element producing a finite time delay. For the system to be stable all the roots of the equation must be negative or have negative real parts. Assuming C_0 to be positive it is shown that C_1 and C_3 must also be positive and that C_2/C_1 must be greater than a certain critical value which is a function of C_0/C_3. These criteria are applied to determine the stability of a simple servomechanism in which the correction signal is delayed by a constant period before being returned to the control point.

Conditions for the dynamical stability of a linear electrical or mechanical system with concentrated parameters can be expressed in terms of the well-known Routh–Hurwitz relations. In such cases the equations are ordinary linear differential equations, and the auxiliary equation or so-called "characteristic equation" derived therefrom is a polynomial equated to zero. The system is stable when all the roots of this equation are negative, or complex with negative real parts.

The assumption of concentrated parameters implies that the physical dimensions of the system are small compared with the wavelength of any disturbance which can be propagated therein. When this is not so, e.g. when the system contains a long transmission line, the parameters are said to be "distributed" and the finite speed of wave propagation must then be taken into account. In this case the equations are partial differential equations and the characteristic equation contains hyperbolic or other transcendental functions.

Thus, for example, a system containing a single uniform transmission line in addition to concentrated parameters has a characteristic equation of the type

$$\sum_0^N a_n z^n + \sum_0^M b_n z^n \tanh z = 0 \qquad (1)$$

All the coefficients are real and again the system is stable if all the roots are negative or have negative real parts. The same equation is obtained for a system with concentrated parameters in which, by any means, a fixed time delay is introduced in the connexion between one part of the system and another part.

One of the simplest forms of the equation is

$$C_0 + C_1 z + (C_2 + C_3 z)\tanh z = 0 \qquad (2)$$

This equation arises in a number of situations. It determines the stability of a simple two-stage feedback-amplifier which is loaded by a mismatched transmission line. It occurs also in the study of the frequency stability of an oscillator connected to a resonant load through a uniform transmission line, where it is derived from a variational equation expressing the behaviour of the system towards a small disturbance superposed on the steady oscillation.

For the sake of example the equation will be discussed in terms of the performance of a servomechanism in which the correction signal is fed back to the input after a fixed period of time. This might happen, for instance, where the input control is a valve governing the supply of steam or fuel and is situated some way from the engine. It is unnecessary to consider the details of the arrangement: the essential features are the time-constant T_m of the machine being controlled, and the period T_c by which the feedback is delayed.

Suppose that a slow change v_i in the input to the machine (pressure, flow, etc.) produces a change v_0 in the output (speed, torque, etc.), and that $v_0 = av_i$ where a is some constant. If now the input has the form $v_i = V_i \exp(pt)$, the corresponding output is defined by the time-constant T_m as

$$v_0 = aV_i \exp(pt)/(1 + pT_m) = Av_i \qquad (3)$$

where $A = a/(1 + pT_m)$ and p is the complex frequency of the disturbance.

Let a fraction b of the output be returned to the input after a time T_c. The returned signal is

$$AbV_i \exp(p)(t - T_c) = Abv_i \exp(-pT_c) \qquad (4)$$

Let the input to the combination of machine plus feedback system be denoted by v_i'. The actual input to the machine itself is then the sum of v_i' and the returned signal. Thus

$$v_i = v_i' + Abv_i \exp(-pT_c)$$

from which

$$v_0/v_i' = a/[1 + pT_m - ab \exp(-pT_c)] \qquad (5)$$

The system is stable if the output is bounded for all bounded values of the input, and this requires that the expression for v_0/v_i' should have no poles in the right-hand half of the complex p-plane or on the imaginary axis. Hence the roots of the equation

$$1 + pT_m - ab \exp(-pT_c) = 0 \qquad (6)$$

must lie in the left-hand half-plane. Writing $pT_c = 2z$ and dividing through by $1 + \exp(-2z)$, the equation becomes

$$1 - ab + (2zT_m/T_c) + [1 + ab + (2zT_m/T_c)]\tanh z = 0 \qquad (7)$$

which is the same as equation (2) with

$$C_0 = 1 - ab, \quad C_1 = C_3 = 2T_m/T_c, \quad C_2 = 1 + ab \qquad (8)$$

The location of the roots of equation (2) must now be determined.

It is first assumed that the coefficients C_0, C_1 and C_3 are non-zero. Since the equation is unchanged when the signs of all the coefficients are changed it can be assumed that $C_0 > 0$. If the other three coefficients are also positive the equation can have no roots in the right-hand half-plane; for the transformations

$$w_1 = \tanh z \quad \text{and} \quad w_2 = -(C_0 + C_1 z)/(C_2 + C_3 z)$$

then map the right-hand half of the z-plane into two non-overlapping areas lying respectively in the right-hand and

left-hand halves of the w-plane. This condition is sufficient but unnecessarily stringent.

The roots of equation (2) may be regarded as functions of the four coefficients, and when the coefficients are varied the roots move about in the complex z-plane. However, as the equation has no root at zero, the only way in which the roots can pass from the left-hand to the right-hand half-plane is by crossing the imaginary axis, since the transition from $-\infty$ to $+\infty$ is not possible. The critical values of the coefficients are those for which the equation has a pair of purely imaginary roots. Writing $z = jy$ in equation (2), and separating the real and imaginary parts, gives the relations between the critical values of the coefficients as:

$$C_0 - C_3 y \tan y = 0 \tag{9}$$

$$C_1 y + C_2 \tan y = 0 \tag{10}$$

For any given value of C_3/C_0 these equations determine a series of values for C_2/C_1. Only positive values of y need be considered as the equations are unchanged by changing the sign of y. Let y_n be any one of the (positive) roots of equation (9) and let C_1 and C_2 have values which satisfy equation (10) with $y = y_n$. Now let C_2 be changed by a very small amount to $C_2 + d$, and let the corresponding root of equation (2) change from $z = jy_n$ to $z = jy_n + p$. Inserting the new values into equation (2) and using also equations (9) and (10) gives

$$p = -dC_0 \cos^2 y_n / [C_3^2 y_n (y_n + \tfrac{1}{2} \sin 2y_n) - jC_3 y_n (C_2 + C_1 \cos^2 y_n)] \tag{11}$$

But $y_n + \frac{1}{2} \sin 2y_n$ is positive for all positive values of y_n, and so the real part of the denominator is positive. Hence the real part of p, and so also of z, has the same sign as $-d$. Since, for stability, the real part of z must be negative it follows that C_2 must be greater than the critical value given by equation (10), i.e.

$$C_2 > -C_1 y_n \cot y_n$$

or, using equation (9)

$$C_2 > -y_n^2 C_1 C_3 / C_0 \tag{12}$$

The same result is obtained if variations of C_0, C_1 or C_3 are considered.

Equation (9) has an infinite number of roots, the values of which extend to ∞, and so there are an infinite number of critical values of C_2. Suppose first that C_1 and C_3 are positive. The right-hand side of inequality (12) is then negative, and the necessary and sufficient condition for stability is that inequality (12) should be satisfied for the smallest value of y_n. To see this let C_2 be decreased continuously from a positive to a large negative value. It has already been shown that when all the coefficients are positive all the roots lie in the left-hand half-plane. As C_2 is decreased the first critical value, corresponding to the smallest value of y_n, is reached and as C_2 is reduced below this value a pair of complex roots pass into the right-hand half-plane in accordance with expression (11).

Further reduction of C_2 leads to the second critical value, corresponding to the next smallest value of y_n, and as C_2 is reduced below this value a second pair of roots pass into the right-hand half-plane, and so on. Once the roots have passed into the right-hand half-plane they cannot return to the left-hand half-plane, for in order to do so they would have to cross the y-axis from right to left, and expression (11) shows that this is impossible while C_2 is decreasing.

If $C_1 < 0$ (C_3 still being positive) the right-hand side of inequality (12) is positive, and since there is no limit to the value of y_n the inequality cannot be satisfied for any finite value of C_2. There always remains an infinite number of roots in the right-hand half-plane. Hence C_1 must be positive.

Finally, suppose that $C_3 < 0$. If $C_1 > 0$ the right-hand side of inequality (12) is again positive and the inequality cannot be satisfied. If $C_1 < 0$ it can easily be shown, e.g. by sketching the graphs of $\tanh z$ and $-(C_0 + C_1 z)/(C_2 + C_3 z)$, that equation (2) has a real positive root whatever the value of C_2. Hence C_3 must be positive.

The necessary and sufficient conditions for equation (2) to have only negative real roots or complex roots with negative real parts can therefore be expressed as:

$$C_0 > 0, \quad C_1 > 0, \quad C_3 > 0 \tag{13}$$

and

$$-C_2/C_1 < y_1 \cot y_1 \tag{14}$$

where y_1 is the smallest positive root of the equation

$$y \tan y = C_0/C_3 \tag{15}$$

The relation (14) can conveniently be exhibited in the form of a graph showing the critical values of $-C_2/C_1$ plotted against $1/[1 + (C_0/C_3)]$. Only points lying below the graph represent stable states.

Two limiting cases of relation (14) are easily deduced. If C_0/C_3 is small the inequality becomes $C_1 + C_2 > 0$, and if C_0/C_3 is large $-C_2/C_1 < (\pi^2/4)(C_3/C_0)$.

In the same way it can be shown that if $C_0 = 0$ but $C_3 \neq 0$, the conditions for the roots of equation (2), other than $z = 0$, to lie in the left-hand half-plane are

$$C_1 + C_2 > 0 \quad \text{if } C_3 > 0 \tag{16}$$

and

$$C_1 + C_2 < 0 \quad \text{if } C_3 < 0 \tag{17}$$

C_1 can be positive, negative or zero.

Stability criteria for the servomechanism can now be obtained by substituting the relations (8) into the inequalities (13) and (14). C_1 and C_3 are inherently positive and the remaining criteria are

$$1 - ab > 0 \tag{18}$$

and

$$-(1 + ab)(T_c/2T_m) < y_1 \cot y_1 \tag{19}$$

where y_1 is the smallest positive root of the equation

$$y \tan y = (1 - ab)(T_c/2T_m) \tag{20}$$

In order to secure any improvement in the performance of the system the feedback must be negative, i.e. $ab < 0$. The first inequality is therefore satisfied and the amount of negative feedback is limited only by condition (19). At the critical value of ab this inequality becomes an identity. Eliminating ab from conditions (19) and (20) then gives

$$-2y_1 \cot 2y_1 = T_c/T_m \tag{21}$$

For any given value of T_c/T_m this equation can be solved and the corresponding critical value of ab can be calculated from condition (19). In general T_c will be much less than T_m and the solution of equation (21) is

$$y_1 \simeq (\pi/4) + (T_c/\pi T_m) \tag{22}$$

Substituting this into condition (19) gives

$$-ab < (\tfrac{1}{2}\pi T_m/T_c) + (2/\pi) \qquad (23)$$

In practice the amount of feedback would be made rather less than the critical value to avoid the unpleasant consequences of the damping factor being too small.

This particular example, which was chosen for its simplicity, can also be easily solved by considering the Nyquist locus diagram of the loop transmission function $Ab \exp(-pT_c)$. The simplicity arises from the fact that the characteristic equation (6) for the servo corresponds to a degenerate form of the more general equation (2) obtained by putting $C_1 = C_3$.

ACKNOWLEDGEMENTS

The work described in this paper was carried out at the Institute for Technical Physics in the Swiss Federal Institute of Technology, Zürich. The author has to thank Prof. E. Baumann, Director of the Institute, for the facilities placed at his disposal, and Prof. H. Huber of the University of Basel for criticism of the manuscript.

Creep and static friction

By R. T. Spurr, B.Sc., Ph.D., Ferodo Ltd., Chapel-en-le-Frith, Stockport, Cheshire

[*Paper received* 13 *June*, 1955]

It is shown that the static friction between a soft metal hemisphere and a flat surface increases with the length of time the surfaces have been in contact and that this increase is due to creep. Such creep might account for the difference between static and dynamic coefficients of friction.

Parker and Hatch[1] have shown that the static friction between a soft metal hemisphere and a glass plate is related to the area of contact between hemisphere and plate, and Moore and Tabor[2] observed that the area of contact between an indium hemisphere and a glass plate is influenced by creep. The work described below was undertaken to combine the two observations and determine the effect of creep on friction. Specimens of indium and zinc were loaded against glass surfaces for various periods of time, and the tangential force required to initiate sliding measured.

EXPERIMENTAL DETAILS

A simple apparatus (Fig. 1) was built to measure μ_s (the static coefficient of friction). Two parallel metal rails were glued to the underneath side of a thick glass plate, V-shaped grooves being machined in the bottom of the rails. Corresponding grooves were machined in a solid metal base, and base and plate kept apart by lubricated steel balls rolling in the grooves. Motion of the plate was thus restricted to translation in one direction and a force could be applied in this direction by running water from a large reservoir into a beaker connected to the plate by a thread running over a pulley, a similar beaker being attached to the other end of the plate as a counterweight. The specimen holder was mounted at one corner of a large triangular plate which could rotate about an axis passing through the other two corners. A long lever was bolted to the triangular plate at right angles to this axis of rotation, and passing over the specimen. On the specimen end of the lever, weights could be adjusted so that an unloaded specimen just touched the glass specimen clamped to the plate.

The metal specimens were prepared by casting molten metal into Brinell ball indentations in polished brass and mounting the resulting hemispheres in a tube. A crank arrangement permitted each specimen to be used a number of times, the specimen being rotated so that a fresh area could be used for each measurement. The glass surfaces (microscope slides) against which the specimens were loaded were cleaned with chromic acid and distilled water or organic solvents and carefully dried with filter paper.

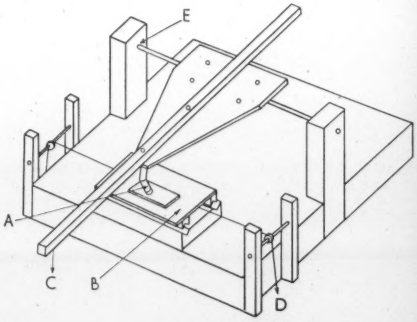

Fig. 1. Friction apparatus

A, cranked specimen holder containing hemispherical specimen; *B*, thick glass plate sliding on steel balls; *C*, normal load; *D*, tangential force; *E*, pivot.

Each measurement was made by adjusting the counterweight until the specimen was just not in contact with the glass. The load (200 g) was then applied gently, held on for the required period (5 s to 30 min, the measurements being made in random order), and water then poured into the beaker at a constant rate until macroscopic slip occurred.

The force required to overcome the friction of the lubricated steel balls was measured separately.

RESULTS AND DISCUSSION

The increase in μ_s of the indium hemispheres with increase in the time the surfaces have been in contact ("preloading time") is shown in Fig. 2. The apparent area of contact was measured after each run and found to increase with time of loading in the way described by Moore and Tabor. The "specific friction," i.e. μ_s/area of contact, was found to be constant for a given specimen and independent of the time the surfaces had been in contact. Thus the increase in μ_s

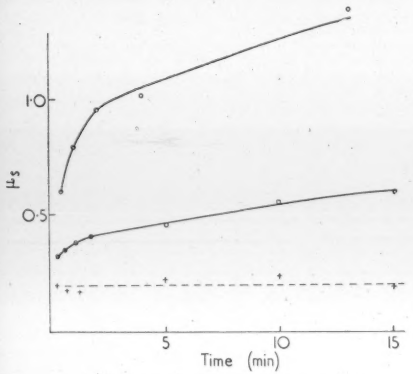

Fig. 2. μ_s plotted against preload time for indium hemispheres. (Upper curve $1\frac{1}{16}$ in. and lower curve $\frac{1}{4}$ in. hemispheres.) Dotted line represents "specific friction" against preload time for $\frac{1}{4}$ in. hemisphere

with time was caused entirely by the increase in the area of contact due to creep.

The increase in μ_s of zinc hemispheres with time of preloading was also measured. In the experiments with indium the load was removed before the tangential force was applied, otherwise the area of contact built up and results were erratic, but as the contact area of the zinc would not be expected to grow during sliding under load, the load was not removed before the tangential force was applied. Results obtained with three different zinc specimens are shown in Fig. 3. There was considerably more scatter in the results for zinc than in those for indium, but there was a definite increase in μ_s with the time the surfaces were in contact. The areas of contact were too small and ill-defined for the specific friction to be measured.

Attempts were made to determine the effect of creep on the static friction of flat surfaces, but the scatter in the experimental results was too great for any definite conclusions to be drawn. However, contact between nominally flat surfaces occurs at a relatively few asperities of small radius and so the rate of creep of hemispheres of various radii against flat surfaces was examined. It was found that for a given load the smaller the radius of the ball the lower the area of contact/time curve and the sooner the rate of creep decreased to a small almost constant value. It would therefore be

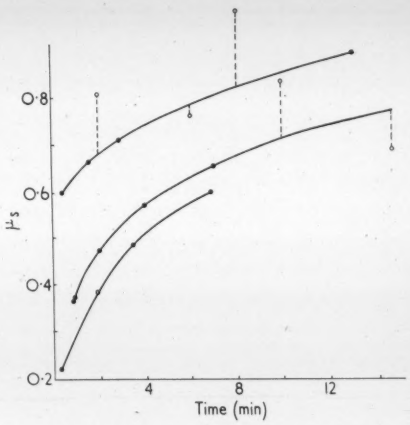

Fig. 3. μ_s plotted against preload time for $\frac{1}{4}$ in. zinc hemispheres. Each curve represents a different specimen

expected that with nominally flat surfaces the heavily loaded asperities would creep rapidly but would soon be exhausted and consequently that it would be experimentally difficult to measure the effect of creep on the friction of such surfaces in the way described above.

Creep may be a cause of scatter in experimental determinations of friction unless constant pre-loading times are used. It is also suggested that creep may, to some extent, be the cause of the difference between the dynamic and static coefficients of friction, for with static loading the areas of contact can increase by creep, whereas during sliding the individual contact areas (except for very soft, clean metals) are continually changing and the increase in their areas thereby limited.

ACKNOWLEDGEMENTS

The author wishes to thank the staff of the Technical Division of Ferodo Ltd. for assistance and criticism, in particular Mr. C. Rubenstein, who did much of the experimental work, and the directors of Ferodo Ltd. for permission to publish.

REFERENCES

(1) PARKER, R. C., and HATCH, D. *Proc. Phys. Soc. [London] B*, **63**, p. 185 (1950).
(2) MOORE, A. C., and TABOR, D. *Brit. J. Appl. Phys.*, **3**, p. 299 (1952).

The capacity and field of a cylindrical trough with a plane conductor in the axial plane of symmetry

By H. J. Peake, M.A., M.Sc., Ph.D., and N. Davy, D.Sc., The University of Nottingham

[*Paper received* 25 *May*, 1955]

The transformation $z = b\,\mathrm{cn}\,(Kw/U)$ is taken as basic, and from this the complex potential, field and capacity of a condenser, consisting of an infinite cylindrical trough and an infinite plane conductor of finite width situated in the axial plane of symmetry, are obtained by the method of inversion.

In two special cases tables are provided giving the values of the electrical intensity at points on the axes of symmetry and the surface density of charge at points on the conductors. Tables and graphs are given which enable the capacity to be readily calculated.

NOTATION

The co-ordinates of any point in the plane before and after inversion are denoted by $z = x + iy$, and z_1 respectively, $\bar{z}_1$ is the complex conjugate of z_1. The complex potential is $w = u + iv$, where u is the potential and v the stream function. The usual notation is used to denote the Jacobian elliptic functions of modulus k, namely, cn w, and

$$K = \int_0^{\pi/2} d\phi/(1 - k^2 \sin^2 \phi)^{\frac{1}{2}}$$

and K' is the same function of k' as K is of k, where $k'^2 = 1 - k^2$.

THE TRANSFORMATION

The transformation

$$z = b\,\mathrm{cn}\,(Kw/U) \qquad (1)$$

gives the complex potential at any point in the z-plane for the system of conductors comprising a plane conductor AB of length $2bk'/k$ raised to a potential U placed symmetrically between two earthed semi-infinite plates CD, EF in the same straight line, but perpendicular to them. The semi-infinite plates are separated by a distance DE, equal to $2b$. The capacity of the system is $K'/\pi K$.*

THE INVERSION

Geometrical argument. Two different systems are obtained on inversion about a point I a distance a from DE along the line AB, the radius of inversion being a, according as a is greater than or less than bk'/k. These are illustrated in Figs. 1 and 3 respectively. We shall first consider the case when $a > bk'/k$ (Fig. 1).

The circular arc, centre O_1 has radius $R = a/2$ and is at zero potential. A_1B_1 is symmetrically placed and raised to a potential U. It will be shown that if the position of A_1 is determined, that of B_1 is also of necessity determined. Indeed, if the co-ordinates of A_1 and B_1 are denoted by iRq and iRp respectively, $pq = 1$.

If $\angle B_1O_1E_1$ and $\angle B_1O_1P_1$ are denoted by α and θ, it can readily be established that

$$(b/a) = \tan(\alpha/2) \quad \text{and.} \quad (x/a) = \tan(\theta/2) \qquad (2)$$

P_1 being any point on the arc..

* For details of the basic transformation the reader is referred to Thomson.[3]

Algebraic transformation. O is taken to be the origin in the z-plane and O_1 that in z_1-plane. The axis of x is CF and the axis of x_1 is parallel to this.

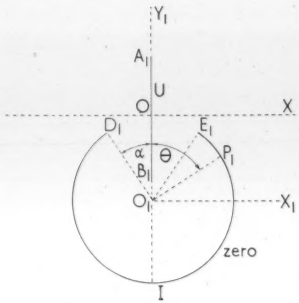

Fig. 1. $a > bk'/k$

By definition of inversion, we have

$$(z + ia).(\bar{z}_1 - ia/2) = a^2 \qquad (3)$$

From equations (1) and (3)

$$b\,\mathrm{cn}\,(Kw_1/U) = -i2R(\bar{z}_1 + iR)/(\bar{z}_1 - iR) \qquad (4)$$

If $z_1 = r(\cos\theta + i\sin\theta)$, we obtain after some reduction:

$$b\,\mathrm{cn}\,(Kw_1/U) = 2R\frac{2rR\cos\theta + i(R^2 - r^2)}{R^2 + r^2 + 2rR\sin\theta} \qquad (5)$$

From equation (3)

$$dz/d\bar{z}_1 = -(z + ia)^2/a^2 \qquad (6)$$

It is convenient to replace k by $\sin(\phi/2)$, when k' becomes $\cos(\phi/2)$. The co-ordinate of A is

$$ik'b/k = i2R[\tan(\alpha/2)/\tan(\phi/2)]$$

so that from equation (3) we obtain

$$q = \sin(\tfrac{1}{2}\phi - \tfrac{1}{2}\alpha)\,\mathrm{cosec}\,(\tfrac{1}{2}\phi + \tfrac{1}{2}\alpha) \qquad (7)$$

Similarly $\quad p = \sin(\tfrac{1}{2}\phi + \tfrac{1}{2}\alpha)\,\mathrm{cosec}\,(\tfrac{1}{2}\phi - \tfrac{1}{2}\alpha)$

Also $\tan(\phi/2) = [(1 + q)/(1 - q)]\tan(\alpha/2)$, so that if α and q are given, k may be calculated since $k = \sin(\phi/2)$.

Electrical argument. Inversion is a particular conformal transformation, so that equations (4) and (5) give the complex potential w_1 at any point in a plane normal to the axis of an earthed cylindrical trough and a finite plate at a potential U symmetrically placed as illustrated in Fig. 1. The capacity of this system will be $K'/\pi K$, the same as the capacity of the original system of conductors.

ELECTRICITY INTENSITY

At any point in the plane the magnitude of the electrical intensity E is given by

$$E = |dw_1/dz_1| = |(dw_1/dz)(dz/d\bar{z}_1)(d\bar{z}_1/dz_1)|$$

Now $z = b\,\mathrm{cn}\,(Kw/U)$

so that $dz/dw = -(Kb/U)\,\mathrm{sn}\,(Kw/U)\,\mathrm{dn}\,(Kw/U)$

Also $b^2\,\mathrm{sn}^2\,(Kw/U) = b^2 - z^2$

and $b^2\,\mathrm{dn}^2\,(Kw/U) = k^2z^2 + (k'b)^2$

Thus
$$E = \frac{Ub}{Ka^2}\left|\frac{(z+ia)^2}{[(b^2-z^2)(b^2k'^2+k^2z^2)]^{\frac{1}{2}}}\right| \qquad (8)$$

For points on O_1X_1, $y_1 = 0$. If x_1 is replaced by Rt,

$$z = 2R(1-it)/(t-i) \quad \text{and} \quad z + ia = 4R/(t-i)$$

Also $b^2 - z^2 = 4R^2\sec^2(\alpha/2)(t^2 + 2it\cos\alpha - 1)/(t-i)^2$

and

$$(bk'/k)^2 + z^2 = 4R^2\left[\frac{(1-it)^2 + (t-i)^2\tan^2(\alpha/2)\cot^2(\phi/2)}{(t-i)^2}\right]$$
$$= 2R^2\sec^2(\alpha/2)\,\mathrm{cosec}^2(\phi/2)$$
$$(\cos\alpha - \cos\phi)(p-it)(q-it)/(t-i)^2$$

using equation (7) and some reduction.

Substituting these expressions in equation (8) we obtain for the electrical intensity at points on O_1X_1:

$$E = \frac{U\sin\alpha}{KR}\sqrt{\left(\frac{2}{\cos\alpha \sim \cos\phi}\right)}\Big/\left[(t^4 + 2t^2\cos 2\alpha + 1)(t^2+p^2)(t^2+q^2)\right]^{\frac{1}{4}} \qquad (9)$$

where $Rt = x_1$

For points on O_1Y_1 we have that $z = iy$, so equation (8) yields

$$E = (Ub/Ka^2)(a+y)^2/[(b^2+y^2)(b^2k'^2 \sim k^2y^2)]^{\frac{1}{2}}$$

On putting $t = y_1/R$, $y = a(1-t)/(1+t)$, $a + y = 2a/(1+t)$

and $b^2 + y^2 = a^2\sec^2(\alpha/2)(t^2 - 2t\cos\alpha + 1)/(1+t)^2$

$$k'^2b^2 - k^2y^2 = a^2k^2[(1+t)^2\tan^2(\alpha/2)\cot^2(\phi/2) -$$
$$-(1-t)^2]/(1+t)^2 = [ak\sec(\alpha/2)\,\mathrm{cosec}(\phi/2)]^2$$
$$(\cos\phi - \cos\alpha)(t-p)(t-q)/2(1+t)^2$$

after some reduction in which pq is replaced by 1.

For points outside the conductor A_1B_1 t lies outside the range $q \leqslant t \leqslant p$, and we have from equation (8)

$$E = \frac{U\sin\alpha}{KR}\sqrt{\left[\frac{2/(\cos\alpha \sim \cos\phi)}{(t^2 - 2t\cos\alpha + 1)(t-p)(t-q)}\right]} \qquad (10)$$

where $t = y_1/R$

At the centre O_1, $t = 0$. Since $pq = 1$, equations (9) or (10) give, for the electrical intensity at O_1,

$$E = (U\sin\alpha/KR)[2/(\cos\alpha \sim \cos\phi)]^{\frac{1}{2}} \qquad (11)$$

SURFACE DENSITY OF CHARGE

On a conductor the surface density of charge σ has magnitude equal to $|dw_1/dz_1|/4\pi$.

On the conductor A_1B_1. We may obtain σ for points on the conductor A_1B_1 from the previous section provided we allow for the fact that $q \leqslant t \leqslant p$ in this case. Thus

$$\sigma = \frac{U\sin\alpha}{4\pi KR}\sqrt{\left[\frac{2/(\cos\alpha \sim \cos\phi)}{(t^2 - 2t\cos\alpha + 1)(p-t)(t-q)}\right]} \qquad (12)$$

On the circular arc D_1E_1. In this case we replace z by x in equation (8) and introduce the factor 4π into the denominator. Since $x = a\tan(\theta/2)$, we have $x^2 + a^2 = a^2\sec^2(\theta/2)$,

$$b^2 - x^2 = a^2(\cos\theta - \cos\alpha)/[2\cos^2(\alpha/2)\cos^2(\theta/2)]$$

$$\frac{b^2k'^2}{k^2} + x^2 = \frac{a^2(1 + \cos\theta\cos\phi - \cos\alpha\cos\theta - \cos\alpha\cos\phi)}{[2\cos(\alpha/2)\cos(\theta/2)\sin(\phi/2)]^2}$$

Consequently

$$\sigma = \frac{U\sin\alpha/4\pi KR}{\sqrt{[2(\cos\alpha \sim \cos\theta)(1 + \cos\theta\cos\phi - \cos\alpha\cos\theta - \cos\alpha\cos\phi)]}} \qquad (13)$$

CASES OF ESPECIAL INTEREST

Case 1

When $\phi = \alpha$, q is zero and p is infinite. A_1B_1 is then a semi-infinite plane conductor situated symmetrically with A_1 at the centre of the circular conductor. Observing that

$$2\sin^2\alpha/p(\cos\alpha - \cos\phi) = \sin^2\alpha\,\mathrm{cosec}^2(\phi + a)/2$$

which approaches unity as ϕ approaches α, the following results are easily deduced from the appropriate relationships above.

Electrical intensity, E. Points on O_1Y_1 $\quad t = y_1/R < 0$

$$E = (U/KR)/[(-t)(t^2 - 2t\cos\alpha + 1)]^{\frac{1}{2}} \qquad (14)$$

Points on O_1X_1 $\quad t = x_1/R$

$$E = (U/KR)/[t^2(t^4 + 2t^2\cos 2\alpha + 1)]^{\frac{1}{2}} \qquad (15)$$

Tables 1 and 2 give the values of RE/U for selected values of t and α. Fig. 2 gives the map of the field in the case when

Table 1. *Values of* (ER/U) *at points on* O_1Y_1 *where* $t = y_1/R < 0$ *[using equation* (14)*]*

$-t$ \ α	30°	45°	60°	90°	120°	135°	150°
0·0	∞	∞	∞	∞	∞	∞	∞
0·1	1·82	1·78	1·78	1·70	1·54	1·41	1·25
0·2	1·19	1·19	1·19	1·18	1·13	1·07	0·970
0·4	0·727	0·736	0·751	0·792	0·841	0·854	0·836
0·6	0·521	0·532	0·547	0·597	0·687	0·752	0·824
0·8	0·402	0·411	0·424	0·471	0·565	0·653	0·801
1·0	0·324	0·331	0·342	0·382	0·464	0·544	0·698
1·2	0·269	0·275	0·284	0·315	0·380	0·441	0·549
1·4	0·228	0·233	0·240	0·265	0·314	0·356	0·418
1·6	0·197	0·200	0·206	0·226	0·262	0·289	0·322
1·8	0·172	0·175	0·180	0·195	0·221	0·239	0·254
2·0	0·152	0·155	0·159	0·171	0·189	0·200	0·206
3·0	0·093	0·094	0·095	0·099	0·101	0·100	0·100
5·0	0·048	0·048	0·048	0·047	0·045	0·043	0·039

$\alpha = 120°$ obtained by the method described by Snowdon and Davy.[1]

Table 2. *Values of* $(R/U)E$ *on* O_1X_1 *where* $t = x_1/R$ [*using equation* (15)]

t \ α	30°	45°	60°	90°	120°	135°	150°
0·0	∞	∞	∞	∞	∞	∞	∞
0·1	1·97	1·94	1·88	1·75	1·47	1·32	1·14
0·2	1·39	1·37	1·34	1·23	1·05	0·932	0·800
0·4	0·948	0·961	0·972	0·930	0·760	0·655	0·547
0·6	0·731	0·766	0·817	0·870	0·639	0·522	0·422
0·8	0·585	0·628	0·708	1·01	0·553	0·428	0·338
1·0	0·475	0·515	0·593	∞	0·464	0·350	0·275
1·2	0·392	0·422	0·479	0·742	0·374	0·287	0·226
1·4	0·327	0·349	0·385	0·465	0·301	0·237	0·189
1·6	0·277	0·292	0·314	0·341	0·245	0·199	0·160
1·8	0·238	0·248	0·261	0·269	0·204	0·169	0·138
2·0	0·207	0·213	0·221	0·220	0·173	0·145	0·119
3·0	0·117	0·117	0·117	0·110	0·092	0·080	0·068
5·0	0·055	0·055	0·054	0·049	0·042	0·037	0·032

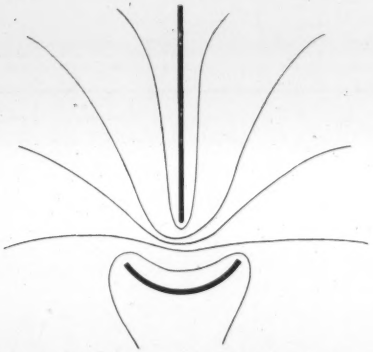

Fig. 2. Map of equipotentials when plane conductor is semi-infinite and $\alpha = 120°$

Table 3. *Values of* $(4\pi R/U)\sigma$ *at points on the semi-infinite plane conductor,* $t = y_1/R > 0$ [*using equation* (16)]

t \ α	30°	45°	60°	90°	120°	135°	150°
0·0	∞	∞	∞	∞	∞	∞	∞
0·1	2·16	2·08	1·97	1·70	1·32	1·21	1·05
0·2	1·68	1·57	1·45	1·18	0·931	0·810	0·686
0·4	1·45	1·25	1·08	0·792	0·587	0·501	0·420
0·6	1·43	1·10	0·878	0·597	0·428	0·362	0·301
0·8	1·39	0·959	0·723	0·471	0·332	0·280	0·232
1·0	1·21	0·799	0·593	0·382	0·268	0·226	0·187
1·2	0·950	0·648	0·486	0·315	0·222	0·187	0·155
1·4	0·723	0·522	0·401	0·265	0·188	0·158	0·132
1·6	0·557	0·425	0·335	0·226	0·161	0·137	0·114
1·8	0·440	0·350	0·283	0·195	0·141	0·119	0·0993
2·0	0·357	0·294	0·242	0·171	0·124	0·105	0·0878
3·0	0·165	0·147	0·129	0·099	0·074	0·064	0·0535
5·0	0·062	0·063	0·058	0·047	0·037	0·032	0·0275

Surface density of charge, σ. On the conductor A_1B_1, $t = y_1/R > 0$. From equation (12) we obtain

$$\sigma = (U/4\pi KR)/[t(t^2 - 2t\cos\alpha + 1)]^{\frac{1}{2}} \qquad (16)$$

Table 3 gives the relevant data.

On the circular conductor, $D_1L_1E_1$

$$\sigma = (U/4\pi KR)/[2(\cos\theta - \cos\alpha)]^{\frac{1}{2}}$$

from equation (13). It is convenient to replace θ by $\pi - \theta'$ and α by $\pi - \alpha'$ in the above, giving

$$\sigma = (U/4\pi KR)/[2(\cos\alpha' - \cos\theta')]^{\frac{1}{2}} \qquad (17)$$

Table 4 gives the values of $(4\pi R/U)\sigma$ for selected values of α' and the ratio (θ'/α').

Table 4. *Values of* $(4\pi R/U)\sigma$ *at points on the circular arc* [*using equation* (17)]

θ'/α' \ α'	45°	30°	150°	135°	120°	90°	60°
0·0	0·544	0·698	0·324	0·331	0·342	0·382	0·464
0·1	0·567	0·702	0·327	0·334	0·345	0·384	0·466
0·2	0·556	0·713	0·336	0·342	0·353	0·391	0·474
0·3	0·572	0·733	0·353	0·357	0·367	0·404	0·488
0·4	0·597	0·763	0·379	0·380	0·388	0·424	0·510
0·5	0·633	0·809	0·417	0·415	0·419	0·454	0·542
0·6	0·687	0·876	0·475	0·466	0·466	0·498	0·590
0·7	0·772	0·983	0·568	0·546	0·539	0·567	0·665
0·8	0·923	1·17	0·731	0·686	0·667	0·686	0·797
0·9	1·28	1·62	1·11	1·01	0·960	0·964	1·11
0·94	1·63	2·07	1·48	1·32	0·125	1·24	1·42
0·98	2·81	3·54	2·68	2·34	2·19	2·15	2·44
1·00	∞	∞	∞	∞	∞	∞	∞

Case 2

When $\alpha = \pi/2$ the plane conductor A_1B_1 is finite and the circular arc, semi-circular. In this case $q = \tan(\phi/2 - \pi/4)$ from equation (7) and the modulus k is determined from $k = \sin(\phi/2)$ when q is given. Of necessity p is determined since $pq = 1$. The following expressions are obtained from equations (9) to (13) above.

Electrical intensity. Points on O_1Y_1, $t = y_1/R$ and must be outside the range $q < t < p$.

$$E = (U/KR)\sqrt{(2\sec\phi)}/[(t^2 + 1)(t - p)(t - q)]^{\frac{1}{2}} \qquad (18)$$

Points on O_1X_1, $t = x_1/R$

$$E = (U/KR)\sqrt{(2\sec\phi)}/[(t^2 - 1)^2(t^2 + p^2)(t^2 + q^2)]^{\frac{1}{2}} \qquad (19)$$

Surface density of charge. At points on the conductor A_1B_1, $t = y_1/R$, where $q \leqslant t \leqslant p$

$$\sigma = (U/4\pi KR)\sqrt{(2\sec\phi')}/[(t^2 + 1)(p - t)(t - q)]^{\frac{1}{2}} \qquad (20)$$

At points on the circular conductor

$$\sigma = (U/4\pi KR)/[2\cos\theta'(1 + \cos\theta'\cos\phi')]^{\frac{1}{2}} \qquad (21)$$

where $\phi' = \pi - \phi$ and $\theta' = \pi - \theta$

RADIUS OF INVERSION LESS THAN bk'/k

We now proceed to the case when the radius of inversion is less than bk'/k. The centre of inversion I is now on the conductor AB, so that the inverted system consists of a

circular arc at zero potential, together with two semi-infinite plane conductors each at potential U in the straight line ICO but separated by a finite distance A_1B_1 equal to $R(q-p)$. The system is illustrated in Fig. 3.

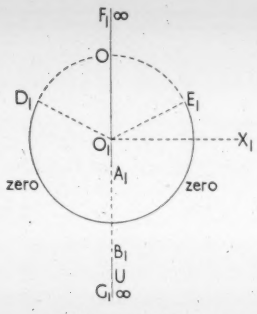

Fig. 3. $a < bk'/k$

The previous sections remain applicable provided allowance is made for the fact that since $a < bk'/k$, $\phi < \alpha$ and p and q are, as a consequence, negative. Equations (9) and (13) are accordingly unaltered, but in place of equations (10) and (12) we have the following.

Electrical intensity at points on A_1B_1, $p < t < q$

$$E = \frac{U \sin \alpha}{KR} \sqrt{\left[\frac{2/(\cos \phi \sim \cos \alpha)}{(t^2 - 2t \cos \alpha + 1)(t-p)(q-t)}\right]} \quad (22)$$

Surface density of charge on the semi-infinite conductors

$$\sigma = \frac{U \sin \alpha}{4\pi KR} \sqrt{\left[\frac{2/(\cos \phi \sim \cos \alpha)}{(t^2 - 2t \cos \alpha + 1)(t-p)(t-q)}\right]} \quad (23)$$

where $t = y_1/R$

It is of interest to consider the special case, which arises when $p = q = -1$, $\phi = 0$ then so that k is zero and $K = \pi/2$. The gap A_1B_1 is then infinitesimal. The following results are easily obtained from the previous sections.

Results when the gap A_1B_1 is infinitesimal

Electrical intensity. At points on O_1X_1: $x_1 = Rt$

$$E = (4U/\pi R) \cos(\alpha/2)/[(t^2+1)^2(t^4 + 2t^2 \cos 2\alpha + 1)]^{\frac{1}{4}} \quad (24)$$

Surface density of charge. At points on O_1Y_1: where $t = y_1/R$

$$\sigma = (U/\pi^2 R) \cos(\alpha/2)/[(1+t)\sqrt{(t^2 - 2t \cos \alpha + 1)}] \quad (25)$$

At points on the circular arc

$$\sigma = \frac{\sqrt{(2)}\, U \cos(\alpha/2)}{4\pi^2 R \cos(\theta/2)\sqrt{(\cos \alpha \sim \cos \theta)}} \quad (26)$$

A comparison of these results with those given in a previous paper[2] reveals that equations (23) and (25) of that paper are equivalent to equations (24) and (26) above, since the γ and ϕ appearing there are supplementary to α and θ respectively. Equation (22) in Ref. (2) and equation (25) above only differ by the factor 4π. This is in agreement with Coulomb's law, since the former equation gives the electrical intensity at points on the axis of symmetry O_1Y_1, the latter the surface density of charge at points on the infinite conductor placed along O_1Y_1.

THE CAPACITY

The capacity of both the derived systems will be that of the original system, namely, $K'/(\pi K)$, the elliptic modulus being determined from the following: $k = \sin(\phi/2)$ and

$$\tan(\phi/2) = [(1+q)/(1-q)] \tan(\alpha/2), \quad -1 \leqslant q \leqslant 1.$$

The capacity for the system of Fig. 1 is determined by assigning positive values to q, whereas that of the system of Fig. 3 is determined by assigning negative values. Table 5

Table 5. *Values of K'/K*

Positive values of q

α \ $\lvert q \rvert$	0·0	0·1	0·2	0·3	0·4	0·5	0·6	0·7	0·8	0·9	0·94	0·98	1·0
30°	1·73	1·61	1·49	1·36	1·24	1·11	0·969	0·828	0·681	0·520	0·442	0·338	0·0
45°	1·47	1·35	1·24	1·13	1·02	0·906	0·797	0·688	0·578	0·454	0·394	0·308	0·0
60°	1·28	1·17	1·07	0·969	0·874	0·782	0·693	0·604	0·515	0·415	0·365	0·289	0·0
90°	1·00	0·917	0·832	0·758	0·690	0·625	0·564	0·501	0·438	0·363	0·324	0·263	0·0
120°	0·782	0·719	0·662	0·618	0·562	0·515	0·472	0·427	0·380	0·323	0·310	0·238	0·0
135°	0·681	0·630	0·585	0·542	0·502	0·465	0·429	0·393	0·352	0·303	0·291	0·226	0·0
150°	0·577	0·539	0·503	0·471	0·442	0·413	0·383	0·353	0·321	0·278	0·268	0·210	0·0

Negative values of q

30°	1·73	1·86	1·99	2·12	2·27	2·42	2·61	2·83	3·12	3·59	3·73	4·77	∞
45°	1·47	1·59	1·71	1·85	1·99	2·15	2·33	2·55	2·85	3·30	3·44	4·42	∞
60°	1·28	1·39	1·51	1·62	1·78	1·94	2·12	2·34	2·63	3·10	3·22	4·20	∞
90°	1·00	1·09	1·20	1·32	1·45	1·60	1·77	2·00	2·28	2·75	3·09	3·80	∞
120°	0·782	0·855	0·936	1·03	1·14	1·28	1·44	1·66	1·94	2·41	2·74	3·46	∞
135°	0·681	0·740	0·807	0·888	0·985	1·10	1·26	1·45	1·73	2·21	2·54	3·24	∞
150°	0·577	0·621	0·673	0·734	0·809	0·905	1·03	1·21	1·47	1·92	2·26	2·96	∞

Table 6. *Values of K'/K when plane conductor is semi-infinite*

α *in degrees*	0	2	4	6	8	10	20	30	40	50	60	70	80	90
K'/K	∞	3·457	3·018	2·762	2·577	2·436	1·994	1·732	1·546	1·401	1·277	1·176	1·084	1·000
α *in degrees*	100	110	120	130	135	140	150	160	170	172	174	176	178	180
K'/K	0·9226	0·8504	0·7818	0·7139	0·6810	0·6468	0·5773	0·5017	0·4105	0·3880	0·3621	0·3313	0·2892	0·0

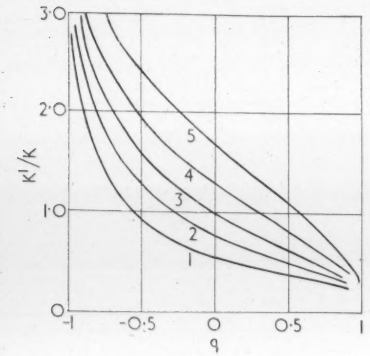

Fig. 4. Graph of K'/K against α

Curve 1, $\alpha = 150^\circ$; curve 2, $\alpha = 120^\circ$; curve 3, $\alpha = 90^\circ$; curve 4, $\alpha = 60^\circ$; curve 5, $\alpha = 30^\circ$.

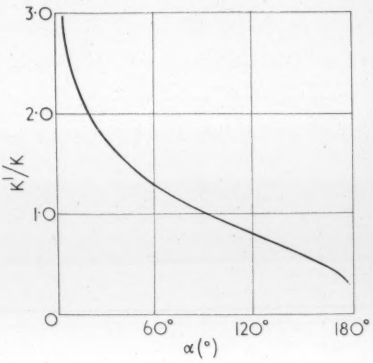

Fig. 5. Graph of K'/K against α when the plane conductor is semi-infinite

gives the values of K'/K for selected values of α and q and Fig. 4 illustrates the various graphs. Table 6 and Fig. 5 correspond to the case when the plane conductor is semi-infinite, i.e. $q = 0$. Over the range $110^\circ \leqslant \alpha \leqslant 130^\circ$, K'/K is given correctly to three decimal places by the linear equation $K'/K = 1{\cdot}5981 - \alpha(6{\cdot}803)10^{-3}$, α being in degrees. Over the range $100^\circ \leqslant \alpha \leqslant 140^\circ$, it gives the ratio correctly to two decimal places. The equation was obtained by the method employed in the paper already cited.

REFERENCES

(1) Snowdon, W., and Davy, N. *Brit. J. Appl. Phys.*, **5**, p. 146 (1954).

(2) Peake, H. J., and Davy, N. *Brit. J. Appl. Phys.*, **5**, p. 316 (1954).

(3) Thomson, J. J. *Recent Researches in Electricity and Magnetism*, Chapter 3, p. 248 (Oxford: Clarendon Press, 1893).

New books

Beta- and gamma-ray spectroscopy. Edited by PROF. KAI SIEGBAHN. (Amsterdam: North-Holland Publishing Co., 1955.) Pp. xxiii + 959. Price 152*s*.

The term *spectroscopy* has a very wide meaning nowadays, a rough definition being "the study of the interaction of radiations and isolated physical systems." The radiations need not be optical or even electromagnetic; electrons, neutrinos and sound waves can all qualify for admission, while the emitting system may be a nucleus, an atom, a molecule or a crystal. Absorption and scattering processes must be included, and even the word "isolated" must be stretched to cover the effects of ambient fields and of neighbouring systems.

The book under review is an up-to-date survey of the spectroscopy of beta-rays and gamma-rays, including neutrino-recoil and positron-annihilation spectroscopy and the spectroscopy of gamma-rays (but not nuclear particles) emitted in nuclear reactions.

The size and scope of the book, as well as the amount of detail included, remind one of the traditional "Handbuch," but the chapters are numerous and comparatively short and many of them are divided into self-contained sections. Some chapters are specifically experimental, for example Chapters 3 (Siegbahn) and 8 (Mitchell and Slätis) on beta-spectrometers and associated techniques. Others, such as Chapters 9 (Rose) and 10 (Konopinski) on beta-decay theory, are essentially theoretical, but most of them contain both experimental and theoretical material.

Such a book can be successful only when the authors of the individual sections are thoroughly expert in their fields and are well aware of what is being written by their colleagues. Professor Siegbahn has chosen the members of his team admirably and led them very skilfully. Gaps and overlaps are few and the quality and coherence of style must be reckoned quite remarkable in a work of international authorship.

P. B. MOON

Higher transcendental functions. Volume 3. Edited by A. ERDÈLYI. (London: McGraw-Hill Book Co. Ltd., 1955.) Pp. xvii + 292. Price 49*s*.

This is the third, and final, volume of a comprehensive account of what are frequently called the functions of mathematical physics. It has been produced by a distinguished staff of American mathematicians using as a basis some notes left by the late Harry Bateman. Previous volumes have dealt with most of the common functions (gamma, Bessel, Legendre, etc.); this volume includes accounts of the properties of Lamé functions and Mathieu functions. In addition it contains a most useful collection of generating functions, which is probably the most complete of its kind, and some rather disconnected notes on automorphic functions, and the functions such as that of Riemann, which occur in number theory. No one would be likely to use a treatise of this kind other than as a work of reference or a source of inspiration for examination questions. But it is well and clearly written, it is extraordinarily complete in references up to 1954, and is sure to prove invaluable to the applied mathematician who meets one of these functions and wants to know more about it. It is a little odd that though almost the whole use of these functions is in applied mathematics and theoretical physics, there is absolutely no evidence of this in the text. If Harry Bateman had written it, there would have been.

C. A. COULSON

Theoretical structural metallurgy. By DR. A. H. COTTRELL. [London: Edward Arnold (Publishers) Ltd., 1955.] Pp. viii + 251. Price 25*s*.

In the preface to the first edition of this book, the author says that it is written for metallurgical students; the reviewer has no hesitation in recommending it also to physicists. It is clearly and simply written, the mathematics is kept to a minimum, and every opportunity has been taken to present the various subjects in a physical way rather than by formal analysis. Those physicists who prefer this type of approach will find that this book provides an excellent guide to recent progress in the theory of metals.

The subjects covered include the nature of interatomic forces, the electron theory of metals, the thermodynamics of phase diagrams, diffusion, and order-disorder phenomena. The reviewer was particularly pleased to see a detailed treatment of the principle of minimum free energy applied to equilibrium diagrams of alloy systems; to a physicist this provides a more complete and satisfying approach than that provided by the phase rule alone.

The book is well printed and has obviously been carefully produced. The only error that the reviewer has noticed is the mis-spelling "Van der Waal's."

H. LIPSON

Temperature measurement and control, Part II. Descriptive catalogue of exhibits in the Science Museum. (London: H.M. Stationery Office, 1955.) Pp. vi + 57. Price 3*s*. 6*d*.

This handbook contains detailed descriptions of all the objects relating to temperature measurement and control that are preserved in the Science Museum in London. It is divided into the following sections: thermoscopes; seventeenth- and eighteenth-century thermometers; expansion thermometers; electrical resistance pyrometers; thermo-electric pyrometers; optical and total radiation pyrometers; miscellaneous pyrometers; temperature recorders; thermostats. The booklet includes a list of makers of the instruments and of similar instruments in the meteorology collection.

Proceedings of the Eleventh General Assembly of the International Scientific Radio Union. Part I "On radio measurements and standards." (Union Radio-Scientifique Internationale, 42 Rue des Minimes, Brussels, Belgium.) Pp. 56. Price 8*s*. 8*d*.

This publication describes the proceedings of Commission I of U.R.S.I. at its general assembly in The Hague in 1954. The document contains the reports presented by twelve national committees together with many references to published scientific papers dealing with radio measurements and standards.

At the conclusion of the meeting it was recommended that:

(i) The value of 299 792 ± 2 km/s should be adopted for the velocity of electromagnetic waves in vacuum;

(ii) an international comparison of standards of power measurement at 3000 and 10 000 Mc/s should be made; and

(iii) observations should be made on the service areas and mutual interference zones of the various stations now transmitting standard frequencies.

R. L. SMITH-ROSE

Einführung in die Quantenelektrodynamik. By DR. WALTER THIRRING. (Vienna: Verlagsbuchhandlung Franz Deuticke, 1955.) Pp. xii + 122. Price DM 17.50.

The quantum theory of fields has developed extremely rapidly since the end of the last war. It represents at the present moment the front line of fundamental theory. In its application to electrodynamics it has already lead to quantitative predictions which are very accurately confirmed by experiment, while in the harder problems of meson theory it still meets with fundamental difficulties, both in the mathematics and in the physical basis. Dr. Thirring has undertaken to write an advanced text on electrodynamic theory, derived consistently and without much reference to the literature, from basic principles. The book should be a great help to the prospective specialist. There is a good deal of choice in the relations which are taken as a starting point for the development of such a subject, and there exist several schools which differ in the style with which they handle the mathematics. For a book of this kind it is right that the author should have made up his mind about the approach which he regarded as most suitable, and paid no attention to alternatives, though one cannot expect to find agreement between different authors about the most suitable approach or about the very selected references to the literature which are given.

R. E. PEIERLS

Some aspects of the crystallization of high polymers. By G. SCHUUR. (Delft: Rubber Stichting, 1955.) Pp. 82. Price 5 Dutch florins.

In this booklet, after a preliminary review of the literature, the author presents his own theory on the mechanism of spherulite formation in high polymers. This is later extended to suggest explanations for the various types of spherulitic structures and for the well-known crystallization and melting phenomena.

Evidence is presented to show that within a single spherulite in an unstretched polymer or within the whole of a sample of crystalline stretched polymer there is a "continuous crystal lattice.". Unfortunately the argument here is confused by a rather loose use of this term.

The discussion is qualitative and speculative but should prove stimulating to all workers in the polymeric field. The binding and printing are adequate and relatively free from errors.

D. W. SAUNDERS

Quantum theory of solids. By R. E. PEIERLS. (London: Oxford University Press, 1955.) Pp. viii + 229. Price 30*s*.

This book is most refreshing. It has been based on a course of lectures, and much of the directness—including the use of the first person—remains to make the style pleasantly readable. The foremost comment is that it is not a book for beginners; the limitation of all the discussion to a few of the simplest lattices, the free use of the linear crystal as illustration, and a refusal to make heavy weather of definitions of matrix elements, operators, etc., clear the decks for valuable comment but could make for difficulties if one was not familiar with them. The sections on transport phenomena bring *Umklapprozesse* into their rightful position of importance, and entirely remove them from the realm of mystery where they so often dwell. The remarks on structures distorted by Brillouin zone effects, on the sharp distinction between long range order in three dimensions and in fewer, on the effects of deviation from isotropic scattering and on the scattering of electrons at very low temperatures in normal metals shed rays of light into some of the darkest corners of the subject. But the chapter on semiconductors and luminescence is a formality which might have been omitted.

The book is well produced, has an index, a bibliography and a reference list which match the function of the book—not at all exhaustive or detailed but including most of the keys to our present knowledge. Above all, it is a book for those who have some experience of the field and wish to renew their acquaintance with the fundamentals of the subject.

W. M. LOMER

Metallurgy of the rarer metals. Vol. 3. Manganese. By A. H. SULLY. (London: Butterworths Scientific Publications, 1955.) Pp. xiv + 305. Price 40*s*.

Manganese is an appropriate choice for the third volume in this series since it is only in the past few years that useful quantities of electrolytically produced, high-purity (99·5%) metal have become available at low cost. An interesting account of the process is given in this book, which follows the same general pattern as its precursors in first describing at some length the distribution and nature of the metallic ores and the methods by which their manganese content may be extracted. After description and tabulation of the physical properties of the metal, two lengthy chapters discuss the constitution and properties of some sixty of its binary and ternary alloys and there is a final short chapter on the workability of the metal, on methods of depositing it upon other surfaces in the form of coatings and on its oxidation characteristics at elevated temperatures.

The book provides a unique compilation of data and references and, like its companion volumes, will become and remain the standard reference on manganese for a long time to come.

G. L. J. BAILEY

The physics of the ionosphere. Report of The Physical Society Conference, 1954. (London: The Physical Society, 1955.) Pp. 406. Price 40*s*.

This conference was held in the Cavendish Laboratory in September 1954. There were four parts, with titles "The lowest ionosphere," "Irregularities and movements in the ionosphere," "The ionospheric F 2 layer," and "The mathematics of wave propagation through the ionosphere." Such conferences, and the subsequent published proceedings, are becoming an increasingly important medium of scientific communication. There has been evidence that the medium is not incapable of abuse, but no one can grumble at the quality of the present report, which is uniform with The Physical Society's "Proceedings." There is inevitably some repetition of subject-matter and some variation in standard of the contributions but the general level of originality and quality is very high, and publication has been notably rapid.

Each part of the conference is introduced by a survey article; the names of the authors—A. H. Waynick, J. A. Ratcliffe, D. F. Martyn and K. G. Budden—are a sufficient guarantee of the standard of the work. The surveys conclude with short assessments of the significance of the papers presented at the conference and selective bibliographies. They form an admirable introduction to their subject, not merely to the subsequent papers. The report is as essential to a library as any number of the Society's "Proceedings" and it could have not have been produced more economically.

In short it is an excellent record of an unusually successful

conference, giving strong support to the view that such conferences are best organized and reported by an established society with a publishing tradition. One hopes that The Physical Society does not find it too expensive a venture.

G. D. ROBINSON

The solar system. Vol. 2. The earth as a planet. Edited by GERARD P. KUIPER. (London: Cambridge University Press Chicago: The University of Chicago Press, 1955.) Pp. xv + 751. Price 94*s*.

This book is the second of four volumes planned on the solar system. It shares one characteristic with its predecessor (*The sun*, reviewed in the November 1954 issue of this *Journal*, p. 414): its emphasis on modern physics rather than the "natural history" of earlier generations. In accord with today's thought, this does not preclude the work from being primarily astronomical, and geophysics of the technological bias which is filling some libraries now is not to be sought in it. But it might well become the standard educational background to applied geophysics. It will also educate those experts in thermodynamics, radioactivity, magnetism, spectroscopy of energy levels, photochemistry, elastic wave reflexion, etc., who have tended to confine their attention to the laboratory.

The work is co-operative, with chapters by English, Commonwealth, European and American researchers, under the guidance of Dr. Kuiper the astrophysicist. The dynamical and thermodynamical foundations in the earliest chapters are by Sir Harold Spencer Jones, Sir Harold Jeffreys and Sir Edward Bullard, whose status as heads of Greenwich Observatory, Cambridge theory, and the National Physical Laboratory is significant for our remark on the combination of exact physics and astronomy as the basis of geophysics.

The next three chapters discuss the intrusion of physics into topics more commonly geological or geographical, e.g. fracture mechanisms in mountain building and the thermal and hydrodynamical assessment of ocean currents, and the chemical differentiation of the crust. An exact basis of the vast range of sciences underlying physical geography is attempted.

The remaining larger half of the book concerns the terrestial atmosphere. Chapter 7 on the lower atmosphere constitutes an excellent though extremely compressed thermodynamic basis of meteorology, with a too-brief section on the older topics of atmospheric electricity and of precipitation. Chapter 8, on the biochemistry of the atmosphere, e.g. carbon dioxide and oxides of nitrogen permitting life, develops a more novel topic at greater length, and must be the physicist's answer to popular speculation about "life on other planets." After a general Chapter 9 on atmospheric absorption spectra, and a brief Chapter 10 on rocket research, there is a thorough treatment (Chapter 11) of emission spectra and the aurorae, including the recent discoveries on hydrogen lines which contribute so much to our understanding of the solar stream to the earth. Chapter 12 on the photoelectric and electromagnetic problems of the upper atmosphere is by D. R. Bates, whose own researches on these topics place him among the great British masters who wrote the earlier chapters of the book. It is very welcome to find that Nicolet of Belgium, whose investigations have played a great part recently, is the author of Chapter 13 on the dynamics of the high atmosphere under solar radiation. Chapter 15 finally returns to the purely astronomical with the Director of the Paris Observatory writing on the earth's appearance if seen as a planet; a bridge to this is the Chapter 14 on high-altitude rocket photography of the earth, with some striking prints. Radio techniques in ionospheric study are not discussed in the book as much as might be expected, but perhaps they were judged too specialized for a volume that already has 750 pages.

No graduate in any employment as physicist could fail to find this book capable of broadening his interests, and we would stress its general educational value as much as its status as a research tool to the specialist.

MARTIN JOHNSON

Analytical chemistry—the working tools (Vols. 1 and 2). Edited by C. R. N. STROUTS, J. H. GILFILLAN and H. N. WILSON. (London: Oxford University Press, 1955.) Pp. xxi + 1067. Price 105*s*. (two volumes).

This major work describes in considerable detail the various general techniques and procedures—regarded as the "working tools" of the analyst—employed in the analytical laboratories of Imperial Chemical Industries Ltd. Soon after the formation of the company an analytical chemists' committee was set up with the object of standardizing analytical methods throughout the organization. This book represents the results of their efforts and, in accordance with the publication policy of the company, has now been made generally available to all engaged in chemical analysis.

The opening chapter deals with accuracy in analysis; this is followed by chapters on manipulation, sampling, weighing, volumetric apparatus, temperature and pressure measurement, density and specific gravity, crystallizing point and melting point, and distillation. Here is to be found a great deal of information of lasting value for reference purposes, whether it be the proper use of a Fortin barometer or the improper use of a platinum dish. Most workers in most laboratories could hardly fail to profit by acquaintance with these first nine chapters.

The next six chapters, which complete the first volume, are more specifically of analytical interest, these deal respectively with reagents and indicators, pH determination, standardization of volumetric solutions, ultimate organic analysis, organic microanalysis and gas analysis. The last three chapters of this group include a collection of "standard methods of analysis."

The second volume deals with modern instrumental methods of analysis. Much of this is familiar material and differs but little from the corresponding sections in other recent books on "physical methods"; it is difficult, for example, to find much that is new in the essays on X-ray diffraction and on emission spectrography. Other chapters, however, contain much useful reference data such as the valuable lists of absorption bands and of solvent characteristics in the chapter on infra-red spectrophotometry, which also contains practical directions for polishing rock-salt plates.

Judging by the omission of some recent developments, such as counter methods of X-ray diffraction and vapour phase chromatography, and the absence of very recent references in the various bibliographical lists, there appears to have been some delay between preparation and publication. Fairly rapid dating is bound to occur, however, in a rapidly developing subject and it is to be hoped that consideration will be given to the publication of a supplementary volume in due course.

This book should be well received by all interested in the practice of chemical analysis. Its publication calls for congratulations to the Editors and to Imperial Chemical Industries Ltd.

B. S. COOPER

Notes and comments

Elections to The Institute of Physics

The following elections have been made by the Board of The Institute of Physics:

Fellows: R. N. Aldrich-Smith, V. Barocas, W. T. Cowhig, B. Dayal, A. Edwards, W. P. Fletcher, R. W. G. Haslett, J. L. Howarth, P. G. Klemens, H. Kronberger, L. N. D. Lucas, B. Meltzer, W. M. M. Muller, J. B. Nelson, J. Norbury, J. F. Richardson, R. W. Stanford, V. H. Taylor, G. A. Whitfield.

Associates: G. A. Aldous, D. R. Ashworth, J. Bateman, A. E. Beck, S. Bingham, E. W. Billington, B. J. Brown, J. S. Buchanan, T. G. Bullen, E. H. Carmen, J. A. Chapman, S. M. Clark, A. Cook, N. D. Cowell, R. Crosland, T. H. Dennis, F. Domanic, R. D. Fortune, L. K. Ecclestone, D. A. Gill, L. R. Gray, J. L. Grimsdell, A. H. Harris, R. D. Harrison, K. Hickson, D. W. Hill, J. W. Holmes, E. S. Hotston, R. E. Jahn, B. D. James, A. H. Jiggins, A. K. Jonscher, J. W. Kennedy, C. G. Kennell, D. G. Lampard, J. S. L. Leach, J. A. Lucken, F. B. Malkin, N. Marshall, J. McCulloch, K. B. Mather, J. R. Marsden, J. I. Mitchell, K. P. Nicholson, P. A. O'Brien, N. S. Parker, R. B. Pepper, C. D. Pomeroy, P. Popper, T. R. Prentice, B. Pickup, R. E. Price, B. W. Purslow, D. R. Quested, R. C. Reid-Jones, C. B. Richards, A. S. Roberts, S. Scregg, D. J. Smith, R. J. S. Sherwin, D. B. Shina, G. W. Smith, R. Steadman, D. W. Stops, T. Studley, A. G. Thomas, B. S. Thorton, G. L'E. Turner, P. B. Wallis, W. W. Williams, G. B. Woffinden, S. J. B. A. Wyard, D. J. C. Yates.

Seventy-seven Graduates, twenty-one Students and eleven Subscribers were also elected.

Conference on plant and process dynamic characteristics

The Society of Instrument Technology has arranged a conference on plant and process dynamic characteristics with particular reference to the information required in the design of automatic control systems. The conference will be held in the Engineering Laboratory, Cambridge, from 4 to 6 April, 1956. Its main object is to provide an opportunity for process control specialists and those who have had considerable experience of the practical problems of the determination of plant and process characteristics to meet and discuss their work. Each session of the meeting will be opened by the presentation of a short paper by a speaker invited by the Organizing Committee, but others who have material to contribute in the form of short papers or reports relevant to the theme of the conference are invited to communicate as soon as possible with the Conference Secretary. Proceedings will not be published in full, but the contributions are expected to form the bases of papers suitable for publication in the transactions of the society, or elsewhere. Further details may be obtained from The Society of Instrument Technology 1956 Conference Secretary, Engineering Laboratory, Trumpington Street, Cambridge.

Glossary of acoustical terms

The British Standards Institution has issued a revision of the glossary of acoustical terms which was first issued in 1936. There are many changes in the contents and arrangement of the new edition, and about eighty new terms have been added (an increase of about 40%). The section on recording and reproduction has been enlarged and new sections on ultrasonics and underwater sound have been included.

The first edition contained a number of musical terms which have now been deleted. The following headings are those used in the new edition: fundamentals; propagation; hearing; transmission systems; ultrasonics; underwater sound; instruments; recording and reproduction; music; architectural acoustics.

Copies of the standard, price 6s., may be obtained from the British Standards Institution, Sales Branch, 2 Park Street, London, W.1.

Journal of Scientific Instruments

Contents of the November issue

SPECIAL ARTICLE

Electronic computing machines and their uses. By J. H. Wilkinson.

ORIGINAL CONTRIBUTIONS

Papers

A platinum resistance thermometer for use at low temperatures. By C. R. Barber.

An integrating photometer employing scalloped gratings. By L. R. Baker.

Integrating meters for comparing light intensities in plant growth studies. By A. H. Allan and K. J. McCrée.

A capacitance-resistance hygrometer. By C. L. Cutting, A. C. Jason and J. L. Wood.

The behaviour of humidity-sensitive capacitors at room temperatures. By C. R. Underwood and R. C. Houslip.

A d.c. and a.c. balance detector with automatic protection from overload. By C. Morton.

Design for a sensitive self-recording gold-leaf electroscope. By P. Goodman.

Experiments on the dependence of sensitivity on velocity profile in electromagnetic flowmeters. By J. A. Shercliff.

A simple electronic Fourier synthesizer. By H. B. Mohanti and A. D. Booth.

Laboratory and workshop notes

A permanent vacuum seal. By E. Schwarz.

A mechanical seal for very high pressures. By D. Anson.

Construction of a lead-screw without a master thread. By L. R. Baker.

The temperature control of a fluid stream. By R. S. Barnes.

Reduction of scatter in monochromators. By K. W. Keohane and W. K. Metcalf.

A brush for cleaning decade switch contacts. A. Gridley and J. A. Hall.

NOTES AND NEWS

Correspondence

On the preparation of precision resolving power test objects. From G. D. Dew.

A note on the transistor as a thermometer. From A. G. White.

New books

Manufacturers' publications

New instruments, materials and tools

Radio-frequency capacity bridge. Dynamic pickup. Galvanometer modulator, microvoltmeter and nanoammeter. Temperature controller. Low inertia integrating motors. Electric soldering iron.

Notes and comments

THIS JOURNAL is produced monthly by The Institute of Physics, in London. It deals with all branches of applied physics (including theory and technique).

All rights reserved. Responsibility for the statements contained herein attaches only to the writers.

EDITORIAL MATTER. Communications concerning editorial matter should be addressed to the Editor, The Institute of Physics, 47 Belgrave Square, London, S.W.1. (*Telephone:* Sloane 9806.) Prospective authors are invited to prepare their scripts in accordance with the *Notes on the preparation of contributions.* (Price 2s. 6*d.* including postage.)

REPRODUCTION. The Institute of Physics is a signatory to The Royal Society's Fair Copying Declaration. Details may be obtained upon application from The Royal Society, London, W.1.

ADVERTISEMENTS. Communications concerning advertisements should be addressed to the agents, Messrs. Walter Judd Ltd., 47 Gresham Street, London, E.C.2. (*Telephone:* Monarch 7644.)

CLAIMS FOR MISSING JOURNALS. Claims from regular subscribers to this *Journal* for missing numbers will only be considered if received within 60 days of the date of mailing plus normal outward time of transit and time for lodging the claim. Losses attributable to failure to notify a change of address or to similar omissions will not be considered.

SUBSCRIPTION RATES. A new volume commences each January. The charge is £4 per volume ($11.50 U.S.A.), including index (post paid), payable in advance. Single parts, so far as available, may be purchased at 8s. each ($1.15 U.S.A.), post paid, cash with order. Orders should be sent to The Institute of Physics, 47 Belgrave Square, London, S.W.1, or to any bookseller.

SPECIAL ARTICLE

Industrial applications of ultrasonics*

By E. G. Richardson, D.Sc., F.Inst.P., King's College, University of Durham, Newcastle upon Tyne

Techniques used recently in this field are described, in relation to echo-detecting, high-frequency agitation and metallurgical applications. The possibilities and limitations of ultrasonics for these purposes are discussed.

Although ultrasonics has been greatly developed as a tool for research into the properties of fluids and solids in the past twenty-five years, industrial applications have lagged somewhat behind those of the laboratory. It is true, of course, that a number of the more academic investigations using sonics and ultrasonics have their uses for the industrialist. This is particularly true of those in which knowledge of the velocity and attenuation of the various types of mechanical waves in a specimen, e.g. a rod of metal or a high-polymer fibre, gives him information about the viscous and elastic behaviour of such a material. The aerodynamicist also may, from similar information, choose a suitable vapour having a low velocity of sound for use in a supersonic wind tunnel, wherein a high Mach number is desired for a given expenditure of power. These and allied problems are discussed in an article in *Science Progress*.[1]

The principal reasons why a number of the applications predicted for ultrasonics in the early days of the development of generators have failed to reach the commercial stage lie in the difficulty of building equipment of plant size and the consequent cost. It is easy to demonstrate the possibilities of ultrasonic treatment at litre size in the laboratory; another matter to devise apparatus which will deal with a matter of gallons per minute. We ought also to bear in mind that a number of these treatments are not specific as to frequency of the ultrasonic transducers and that in their adaptation to the needs of the manufacturer they have often been debased to loudspeakers or even to infrasonic vibrators worked by a cam on a gear shaft. However, in this article we shall try to restrict ourselves to applications which have reached the plant stage, being aided by reference to a recent symposium on the "Traitement des Ultrasons" held at Marseilles (see Bibliography), and pointing out certain interesting physical notions which have had to be considered during the course of development.

ECHO-DETECTION

It is well known that apparatus developed in the First World War, on the one hand by Langevin and Chilowsky in France using piezoelectric quartz oscillators, and on the other by British Admiralty scientists using magneto-strictive oscillators, serves to detect echoes from the hulls of ships under water or from the sea-bed, according to the direction in which the energy is transmitted, and that later this principle was adapted to the atmosphere as "radar."

On a smaller scale, a similar idea may be applied to establish the existence of suspected discontinuities in a metal structure in the form of hidden cracks or faulty laminations. Such a system has been developed (by Kelvin and Hughes, Ltd) in which a short train of waves is sent out and its wave-form as received back is exhibited on a cathode-ray oscillograph. They employ quartz crystals of 1 to 2 Mc/s frequency for sender and receiver, mounted in "shoes" of metal, one of which directs a beam at 45° to the upper surface of an ingot while the other picks up echoes returning from the lower surface as well as from a possible crack or bubble of occluded gas (see Fig. 1). Whereas large fissures may be more readily detected by X-rays, the ultrasonic exploration is better for detecting these tiny cracks, since it needs but the narrowest break in the continuity of the metal in the path of the beam to give rise to a secondary reflexion.

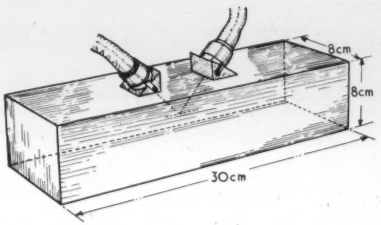

Fig. 1. Flaw detection apparatus

As the cathode-ray spot sweeps across the screen there is first given an indication of the sending of a pulse (by applying a fraction of the sending potential) then the returning echoes.

At the present time, the apparatus is much used for examining laminated plates welded together. Whereas one example [Fig. 2(*a*)] shows by the clear echoes from the far side of the plate that good contact had been made at the laminated joint, another [Fig. 2(*b*)] shows by the irregular and small intermediate echoes, the absence of good contact.

Some nice points present themselves in the successful use of this technique, some similar to those encountered in the reflexion or transmission of a light beam through a "speckled" medium, and others peculiar to the transmission of elastic waves through a solid. In the first of these it is a question of the most suitable frequency to be used. If the wavelength is too large, small discontinuities in the solid structure will merely scatter the radiation and not give a specular reflexion or obstruction of the beam; moreover, the beam will spread. This is a matter of "resolving power." But there is also a question of attenuation. Make the frequency too high and a lot of the energy will be absorbed in the structure, limiting the distance of detection, even if the resolving power for near obstacles is enhanced.

The second aspect is one of "mode conversion" and must be considered, especially when launching the waves at a near grazing angle in order to examine a weld in the join of

* Based on a lecture given before the London and Home Counties Branch of The Institute of Physics in London on 24 March, 1955.

two narrow bars or to detect flaws in one of them, when it is impractical to irradiate along the axis [Fig. 3(*a*)]. When a longitudinal wave is incident in the solid on a boundary with a fluid, some of the vibration is transformed into shear, because, of the two force components X_1 and Y_1 in the solid,

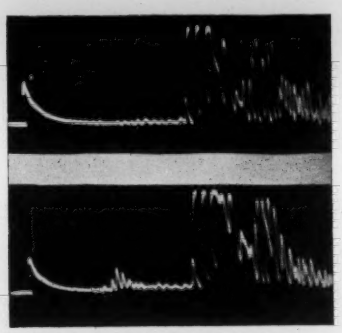

Fig. 2. Screen display of bonding by echo detector, (*a*) good, (*b*) faulty

only the former can be balanced by a force X_2 in the fluid, which cannot support a tangential force; Y_1 has therefore to be balanced by Y_2 in the *solid* [Fig. 3(*b*)]. The resulting shear wave moves with a slower velocity than the compressional wave and is partly re-transformed at the next reflexion, resulting in composite echoes when the final (longitudinal) wave is picked-up. To avoid this smudging of the signal the angle of launching must be nicely chosen to reduce this mode of transformation.

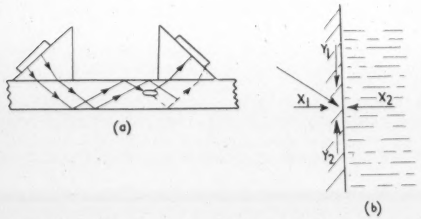

Fig. 3. (*a*) Near-axial propagation of pulse to detect flaw near surface; (*b*) transformation of longitudinal into shear wave at solid-liquid boundary

Of course, by fashioning transducers out of quartz cut in such a way that they can only transmit and receive shear waves, a shallow flaw can be detected without this ambiguity; or we may use the Rayleigh waves (involving surface depressions and elevations) familiar in seismography to detect shallow faults. It is possible by attaching the quartz to a Perspex shoe of suitable angle [as Fig. 3(*a*) indicates] to ensure that the longitudinal wave penetrating the metal block shall hit the far side at such an angle that most of the energy shall be transformed into a shear wave. Since the critical angle (r_c) for incidence at a boundary with a fluid medium is given by the formula well known in optics, namely $\sin r_c = V_2/V_1$, where V_1 is the velocity in the solid and V_2 in the fluid, and as, moreover, V_1 is greater for longitudinal than for shear waves, the critical angle for the former is first reached and there is then a region where only the shear wave passes from the liquid film under the shoe into the ingot.

One other factor in the passage through a boundary, which scarcely applies in optics, is the acoustic matching of the media on either side characterized by their respective values of the wave impedance (product of density ρ and velocity c). For normal incidence of compressional waves, the boundary does not exist when ρc is the same on each side. This point arises in flaw detection when fixed transducers, not in contact with the solid under test, are used, a necessary technique with bodies of odd shape and surface like rubber tyres. The whole system is then immersed in water in a tank while the test object is traversed by the fixed beam. There may, however, be considerable loss of efficiency at the reflexion, since no liquid is known which has the same wave impedance as rubber.

ULTRASONIC AGITATION

A number of industrial applications involve the use of ultrasonics as a tool for disrupting a material into smaller particles or bringing together particulate matter into aggregates. It should be emphasized that both these actions usually take place simultaneously, which accounts for the conflicting reports sometimes received, and further that there will be heating effects to complicate the issue unless precautions are taken to remove the heat as it is generated. As a general principle, if one wants the material in a fine dispersion, one must dilute the suspension as quickly as it has been acted on.

Another question, not yet completely answered, is: how far are these actions specific to a particular frequency, or indeed to ultrasonics in general? The author is convinced that many, if not all of them, could equally well be carried out by ordinary sound waves, if it were possible to concentrate the energy. Ultrasonic sources make up for what they lack in amplitude by high frequency and the power radiated is proportional to the square of the product of these two factors.

The disruptive action on solid bodies is well shown in a British application to displace or prevent oxide coatings during casting or soldering and, in a very different industry, in an application for separating dirt from textiles in laundries, although, as yet, only on a limited scale. A rather similar application is being tried in the paper making industry, i.e. to extract the dirt from paper pulp, prepared as a suspension in water, before it is passed through the rollers. For trial experiments, carried out in the laboratory, it is useful to concentrate the energy from a barium titanate transducer in the form of a bowl immersed in a light oil at its centre of curvature where the material to be treated can be placed in a test-tube (Fig. 4). In this way fine-grained emulsions of oil in water can be produced in a short time. If the treatment is successful the next step to a pilot plant is sometimes a difficult one. The barium titanate is usually replaced by a battery of magneto-strictive generators having as large a surface exposed to the liquid as possible and the latter made to flow over the agitators.

As an example of the coagulating effects we may cite the use of high frequencies to "lay" dust. Here there is a specific

frequency effect, or rather a mobility of the particles in the sound waves dependent on Rayleigh's parameter, $2\pi a/\lambda$, where a is the radius of the particle and λ the acoustic wavelength. In a poly-disperse system, such as an aerosol usually is, this difference in amplitude of movement results in collisions. The particles then stick and either fall under gravity or may be removed by ventilation.

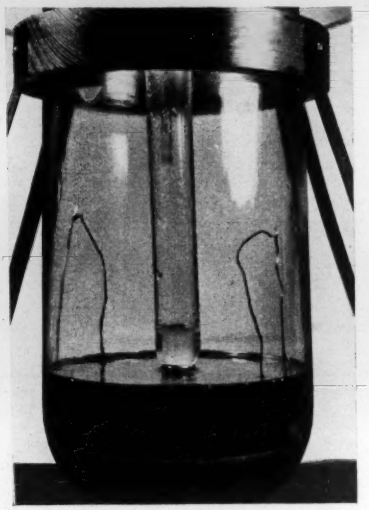

Fig. 4. Ceramic bowl transducer beneath oil, concentrating energy at point on surface

It is not necessary to use crystals as sources for much of this work. Thus in the application just mentioned a form of high-frequency siren may be used. Again in liquids, many effects are associated with cavitation and this can be induced by driving a high-speed underwater jet against a sharp edge. The effect to be desired, e.g. fine emulsification, is produced partly by cavitation at the edge and partly by the ultrasonic radiation into the two-phase liquid system.

METALLURGICAL USES

With agitation at frequencies bordering on the ultrasonic, a beneficial reduction in grain size may be produced in a number of melts of conglomerates of metals to produce alloys on solidification. In these effects it is intensity that matters, frequency having a minor effect. Further, grain refinement seems to occur in those alloys which are actually solid solutions and the action may be a breaking-up of crystallites already formed. This, of course, increases the tensile yield strength.

For some years it has been known that it is possible to tin aluminium and its alloys by subjecting their surfaces to the action of intense ultrasonic vibration at the same time as molten solder is applied. It is now established that the process is one of removing the oxide skin by cavitation erosion.

When, however, the experiment was repeated with an ambient pressure of four atmospheres tinning was completely prevented. Since the increased pressure can have had only a negligible effect on any factor other than cavitation, this seems convincing evidence of the essential part played by the latter.

Aluminium is known to have a low resistance to cavitation erosion, even in water, so it is not surprising that collapsing voids in molten solder will be able to disrupt the surface, exposing the aluminium underneath for alloying with the metal which is impinging violently against it in the very action of cavitation. We can expect, moreover, that the usefulness of the ultrasonic techniques for tinning different "difficult" metals will be related to their susceptibility to cavitation erosion.

Although ultrasonics is said to effect certain "rate processes" in metals it is unlikely that there will be any effect on processes which can be considered as "place exchanges," such as diffusion, ion mobility, viscosity and thermodiffusion. Ehringer could not find any evidence for an acceleration by ultrasonic treatment of the rate of diffusion in solid metals. He studied the following processes. (1) Carburization of steel by propane gas; (2) nitration of Armco iron and nitrided steel in an ammonia flow at 550° C; (3) diffusion of copper in gold at 455° C; and (4) diffusion of hydrogen into Armco iron. In no case did the observed effect exceed the limit of error (10%).

BIBLIOGRAPHY

The number of references to this subject grows by leaps and bounds but in the half dozen papers listed below the reader will find general though more detailed accounts of a number of the applications mentioned in this article. He is also referred to the Proceedings of the Symposium: "Sur le traitement des ultrasons" held at Marseilles in May of this year and shortly to be published—probably in the journal *Acustica*.

REFERENCES

(1) RICHARDSON, E. G. *Sci. Progr.*, **43**, p. 606 (1955).

(2) BRADFIELD, G. *Proc. Phys. Soc.* [*London*] *B*, **63**, p. 305 (1950).

(3) CANAC, F. and GAVREAU, V. *Acustica*, **1**, p. 2 (1951).

(4) HIEDEMANN, E. A. *Chem. Eng. Progress Symposium Series*, **47**, p. 51 (1951).

(5) JONES, R. and WETTERN, J. H. *Concrete Cons. Eng.*, **49**, p. 343 (1954).

(6) NOLTINGK, B. E. *J. Brit. Instn Radio Engrs*, **11**, p. 11 (1951).

The thermal conductivity of liquid and gaseous oxygen

By H. Ziebland, Dipl. Ing., A.M.I.Mech.E., and J. T. A. Burton, Explosives Research and Development Establishment, Waltham Abbey, Essex

[*Paper first received* 19 *July, and in final form* 30 *August*, 1955]

Using a vertical coaxial cylinder method, the thermal conductivity of liquid and gaseous oxygen was measured at temperatures between 80 and 200° K at pressures between 1 and 130 atm. The results are compared with those of other authors.

Although liquid oxygen is becoming increasingly important in the engineering and heavy chemical industries there have been few measurements of its thermal conductivity. The authors are aware of only two previous investigations and these cover only small ranges of temperature and pressure.

Hammann[1] used a parallel plate method to determine the thermal conductivity of liquid oxygen at 1 atm between 66° K and 82° K. Prosad[2] computed values of the thermal conductivity of liquid oxygen from heat transfer measurements on the condensing vapour at temperatures near 92° K at pressures between 1 and 1·7 atm.

CHOICE OF METHOD

In order to minimize the effect of convection on thermal conductivity measurements on fluids near the critical region, it is necessary that the fluid film through which the heat is transported should be as thin as possible. Thus the parallel plate method of Lees, or the coaxial cylinder method first described by Bridgeman is to be preferred to the Schleiermacher hot wire method. The authors used the vertical coaxial cylinder method as this apparatus is more suitable for use at high pressures.

In this method heat is generated in the inner, emitting cylinder and conducted radially through the fluid-filled annulus to the concentric receiving cylinder. From the measured surface temperatures of both emitting and receiving cylinders, the amount of heat radially conducted through the annulus and the dimensions of the apparatus, the thermal conductivity can be evaluated from the following equation:

$$k = \frac{Q \ln (r_2/r_1)}{2\pi L(T_2 - T_1)} = \frac{QA}{(T_2 - T_1)}$$

Where k (cal/cm s °K) is the thermal conductivity; Q(cal/s) is the radial heat flow through the annulus under steady state conditions; r_1, r_2 (cm) are the radii of the emitting and receiving cylinders respectively; T_1, T_2 (°K) are the temperatures of the emitting and receiving surfaces respectively, and L (cm) is the length of the emitting cylinder.

EXPERIMENTAL

Description of conductivity cell. The apparatus used in the present work was based on the design described by Sellschopp.[3] To permit measurements to be made at high pressures and low temperatures the conductivity cell was enclosed in a Monel autoclave. The general arrangement of the apparatus is shown in Fig. 1.

The central heat emitting cylinder (1), Fig. 1, made of silver was 100·00 mm long and had a mean diameter of 32·841 mm. Cylindrical heat guards of the same diameter, each 43 mm long, were arranged at each end of the central cylinder and these three cylinders were mounted coaxially

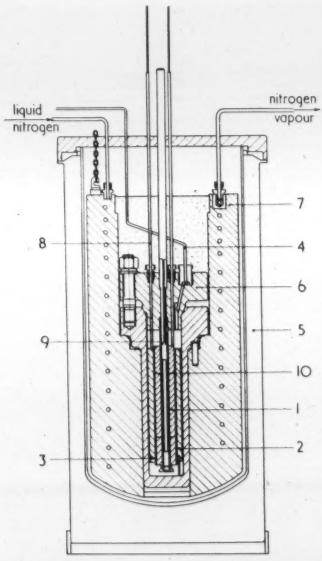

Fig. 1. Cross-section of thermal conductivity apparatus

on a 13 mm outer diameter Monel tube (9). Each heat guard was separated from the central cylinder by a 1 mm thick mica washer (10). The outer heat receiving cylinder (2) had a mean internal diameter of 33·331 mm and was made of copper.

The coaxial alinement of the cylinders was achieved by six Pyrex glass pins held in place by grub screws (3). The length of the alining pins was such that correct alinement was maintained when the apparatus was cooled to 80° K.

The maximum deviation of the annulus width at any point from its mean value was estimated to be less than 0·6%.

The effect of misalinement of the cylinders was calculated from an equation given by Vargaftik.[4] In the present experiments the resultant error in the measured value of the thermal conductivity due to misalinement was less than 0·5%.

Holes were drilled through the full length of the emitting and receiving cylinders and into these holes close-fitting, thin-walled, stainless steel thermocouple sheaths (8) were inserted to protect the thermocouples from the effects of pressure.

The emitting cylinder and the heat guards were heated independently by electric heaters consisting of uniform windings of constantan on a Tufnol former inserted in the Monel tube on which the cylinders were mounted. The leads to the central heater passed through helical grooves in the Tufnol former below the surface of the upper heat guard winding so as to minimize heat conduction along them. Current for the heaters was drawn from a large Nife battery.

The conductivity cell was contained within a Monel autoclave (6), and the apparatus was filled with the substance to be examined by means of the gas inlet (4) in the autoclave lid. In order to reduce convection in the autoclave, and thus increase the thermal stability of the apparatus, the annulus between the autoclave wall and the conductivity cell was made as small as possible. Further, the spaces above and below the conductivity cell were filled with pieces of Teflon cut to the appropriate shapes.

Description of thermostat. The autoclave was placed in a tightly-fitted cast aluminium cylinder (7), which contained a cast-in stainless steel coil. The space between the top of the autoclave (6) and the top of the cast aluminium cylinder (7) was filled with Wood's metal so that the autoclave was contained within an almost isothermal metal block. This helped to minimize axial temperature gradients in the conductivity cell and in the thermocouple wires and sheaths. The whole assembly was suspended on three chains and surrounded by a metal Dewar vessel.[5] To keep the temperature constant a controlled flow of liquid nitrogen was passed through the coil in the metal block.

Temperature measurement. All temperatures were measured with copper-constantan thermocouples and an ice bath was used to provide the reference temperature. The electromotive forces generated by the thermocouples were measured with a Diesselhorst pattern potentiometer (by H. Tinsley and Co. Ltd.) having a least count of 0·1 μV. Any thermoelectric electromotive forces arising within the measuring circuit were eliminated by means of a Tinsley thermoelectric free reversing switch.

The thermocouples were of double-cotton covered 32 s.w.g. wire. The junctions were silver soldered and then electrically insulated from the conductivity cell by a thin coating of Araldite type 1 resin. The thickness of this insulation was kept as small as possible so as to reduce its thermal resistance. The thermocouples were supported in thin-walled stainless steel tubes.

The two thermocouples used for measuring the temperature difference across the annulus were located in the middle of the emitting and receiving cylinders respectively. For the control of the axial temperature distribution a thermocouple was placed in each heat guard section of the emitting cylinder assembly, about 3mm from the separating mica washer.

The thermocouples were supported in their correct positions by glass rods cut to the appropriate lengths and inserted in the thermocouple sheaths. A layer of graphite a few millimetres thick was packed on to the top of each glass rod to ensure good thermal contact between the thermojunction and the walls of the thermocouple sheaths (8). The thermocouples were kept pressed down on to the graphite by springs.

To discover whether heat conduction along the thermocouple wires and stems had any effect on the measured temperatures, the top guard ring thermocouple, i.e. the shortest one and thus the one most likely to be affected, was wound with an electric heating element at the point where the thermocouple stem emerged from the metal thermostat and where it was normally subjected to ambient air temperature and draughts. When the thermostat was operated at 80° K, heating the thermocouple stem to approximately 430° K had no significant effect on the temperature measured by the thermocouple. It was thus concluded that changes in ambient conditions had no measurable effect on the temperatures indicated by the thermocouples.

In order to calibrate the four thermocouples used, one was chosen as a "standard" and was calibrated in the temperature range 80 to 200° K against an N.P.L. calibrated platinum resistance thermometer. Because of inhomogeneities in the constantan wire this calibration may have been in error by as much as 0·2° K at temperatures near 80° K and by less at higher temperatures. To eliminate the effect of wire inhomogeneity on the accuracy of the measurement of the temperature difference across the annulus containing the liquid oxygen, all the thermocouples were placed in their correct positions in the thermal conductivity apparatus (Fig. 2) and the liquid nitrogen flow in the cooling coils was controlled so that each thermocouple gave constant readings. The electromotive force of the "standard" thermocouple was then compared with the electromotive forces of the other three thermocouples. This was repeated at several temperatures in the range 80 to 200° K and deviation curves were drawn for the three "non-standard" thermocouples. Thus inhomogeneity of the constantan wire, although causing a small error in the determination of the absolute temperature, had no effect on the measurement of the temperature difference used in the evaluation of the thermal conductivity.

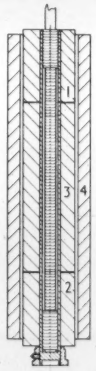

Fig. 2. Position of thermocouples in conductivity cell

(1, 2), guard ring thermocouples; (3, 4), thermocouples for measuring temperature difference across annulus.

Measurement of heat dissipation. The heat dissipated in the emitting cylinder was evaluated from measurements of the current flowing through the central heater and the potential difference across it. These measurements were made with a Diesselhorst pattern potentiometer by means of a shunt and potential divider.

Determination of the geometric constant of the conductivity cell. The geometric constant of the cell, i.e. the constant A in the equation, was evaluated from the dimensions of the cell at 20° C. The value of the cell constant at other temperatures was computed from the known coefficients of expansion of copper and silver. The value of the cell constant thus determined was considered to be in error by less than 0·5%.

Corrections to measured heat dissipation. In view of the low temperature level of the experiments, the low emissivity of the heat exchanging surfaces and the small temperature difference between them, heat transfer by radiation was insignificant. Even if both surfaces had acted as black bodies the correction for radiation would have been less than 0·1%. For this reason no corrections were made for radiational heat exchange.

The junctions of the thermocouples were located a few millimetres inside the heat emitting and receiving cylinders and thus indicated a temperature difference higher than the one across the liquid-filled annulus. Because of the small distance, and the very large difference between the conductivities of the fluids under investigation and the metal of the conductivity cell, corrections for this effect proved to be considerably less than experimental error and were thus neglected.

A further possibility of error arose from heat conduction along the 22 s.w.g. copper leads which conducted current to the main heater and from the Joule heat generated in them. Under the conditions of the experiments the Joule heat accounted for less than 0·1% of the total energy dissipation and so no correction was made for this term. It is considered unlikely that heat conduction along the leads was of significance since they were embedded in helical grooves cut in the surface beneath the upper heat guard windings. A total length of about 5 cm of each lead was thus exposed to a temperature very close to that of the main heater. Any temperature gradient in the copper leads must thus have been outside the conductivity cell and could have had no appreciable effect on the heat dissipated from the emitting cylinder. Thermal conduction along the Tufnol former was negligible.

The only correction that had to be made to the measured values of the radial heat dissipation was for the effect of axial heat flow between the central emitting cylinder and the guard rings.

The thermal conductance between the emitting cylinder and the guard rings in the temperature range of these experiments was evaluated from conductances of the materials between them, i.e. the Monel heater sheath (9), Fig. 1, the stainless steel thermocouple sheaths (8) and the mica washers (10).

Table 1. *Thermal conductivity of oxygen*

Temperature (° K)	*Pressure* (atm)	$k \times 10^4$ (cal/cm° K s)	*Mean* ΔT (° K)	*Number of determinations*	*Temperature* (° K)	*Pressure* (atm)	$k \times 10^4$ (cal/cm° K s)	*Mean* ΔT (° K)	*Number of determinations*
79·2	49·5	3·93	1·030	4	149·3	124·2	2·108	0·824	6
79·7	5·5	3·90	1·214	3	151·0	50·2	1·635	0·510	5
79·7	15·4	3·89	1·199	3	153·8	37·8	0·545	3·035	3
79·8	28·2	3·96	1·195	3	158·0	124·2	1·798	0·933	5
79·8	29·9	3·96	1·247	4	158·7	87·4	1·574	1·566	3
79·8	70·5	4·06	1·175	2	158·9	48·7	0·702	1·930	3
80·7	49·2	3·97	1·967	3	159·3	70·5	1·432	1·208	4
80·8	124·2	4·07	1·664	4	159·9	48·7	0·657	2·059	1
81·0	48·3	4·01	1·684	4	164·6	56·9	0·720	1·437	4
82·9	129·7	3·98	1·718	4	165·1	61·4	0·820	1·328	3
83·6	49·3	3·86	3·898	4	167·1	124·2	1·532	1·120	3
92·3	29·7	3·61	1·866	3	168·5	61·4	0·719	2·180	4
93·5	5·5	3·50	1·940	3	169·5	65·9	0·800	2·047	4
94·1	5·5	3·49	1·922	4	169·9	24·9	0·446	3·724	4
101·7	124·2	3·50	1·911	5	170·1	61·4	0·698	2·299	4
102·3	94·5	3·42	1·420	5	170·2	1·7	0·393	4·239	5
102·4	15·4	3·22	2·131	5	172·5	52·1	0·574	1·787	2
102·7	5·5	3·21	2·124	4	173·1	52·1	0·576	1·807	3
103·1	70·5	3·36	1·450	6	173·3	70·5	0·837	3·642	3
104·0	29·7	3·19	2·175	4	173·7	124·2	1·413	1·229	4
104·8	48·3	3·24	2·030	4	175·0	48·9	0·540	2·398	2
109·2	46·7	3·10	1·524	4	194·8	114·0	0·926	4·755	4
118·0	15·4	2·66	2·450	4	196·1	1·7	0·442	6·194	5
118·2	31·8	2·69	2·432	5	196·9	135·8	1·058	1·567	3
124·0	49·5	2·56	0·724	5	197·0	122·8	0·969	1·702	3
124·4	124·2	2·83	0·638	5	197·3	47·2	0·547	8·075	3
134·3	49·3	2·27	0·388	6	197·4	94·5	0·771	2·133	3
136·2	94·5	2·32	1·733	4	197·9	70·53	0·635	2·550	4
141·1	32·3	1·872	1·697	4	198·4	47·2	0·552	3·055	4
144·9	49·7	1·805	0·680	4	199·0	1	0·450	3·711	3
147·1	49·9	1·810	0·472	4	199·2	70·5	0·628	4·707	4
148·6	94·5	1·923	0·975	4	199·8	23·8	0·488	3·466	4
148·8	70·5	1·798	1·037	5					

The temperature differences between the guard rings and the centre of the emitting cylinder were kept small by appropriate adjustments of the guard ring heaters so that the axial flow was always less than 5% of the radial heat flow. Thus small errors in correcting for the axial heat flow were not important.

Purity of oxygen. The oxygen used in this investigation was obtained from commercial cylinders supplied by the British Oxygen Co. Ltd. A few samples were analysed by absorption of the oxygen in ammoniacal cuprous chloride solution and were found to contain 99·8% oxygen.

RESULTS

The experimental results are presented in Table 1. Each value of thermal conductivity given in the table is the mean of several determinations at the same temperature and pressure. In most of the experiments the individual determinations did not differ from the mean value by more than 1%. The experimental results were interpolated and where shown by a dashed line, also extrapolated to produce the phase diagram shown in Fig. 3. The 1 atm isobar for the gas phase between 90° K and the critical temperature was constructed by use of the data of Eucken[5] and of Johnston and Grilly.[6] The saturation line in this region was constructed using the vapour pressure data of Hoge.[7] The values of the critical pressure, 50·14 atm, and of the critical temperature, 154·78° K, were also taken from Hoge's paper.[7] Even in those parts of the diagram involving considerable extrapolation the accuracy is probably adequate for engineering design calculations. All the experiments reported here were carried out between April and July 1954.

DISCUSSION

The occurrence of convection in the fluid-filled annulus would increase the total thermal conductance of the fluid and would thus lead to the measured values of the thermal conductivity being too high. Rayleigh[8] showed that for horizontal parallel plates heated from below there is a critical value of the product of Grashof and Prandtl numbers above which convection begins.

Kraussold[9] has shown that for the case of horizontal coaxial cylinders Rayleigh's criterion has a value of approximately 1000. For a vertical annulus the value is probably higher.

For most of the present experiments the product of Grashof and Prandtl numbers did not exceed 1000 so that in these experiments the measured values of thermal conductivity were not affected by convection. In the temperature range 145 to 170° K, i.e. in the critical region, it was not possible to evaluate the product $Gr \times Pr$ as sufficiently reliable data for the heat capacity, density, expansion coefficient, and viscosity of oxygen were not available. In Fig. 3 this region is shown by cross-hatching. However, the experimental results obtained in this region seem to be consistent both among themselves and with those obtained at other temperatures and pressures, and it appears unlikely that even in this region they are much in error.

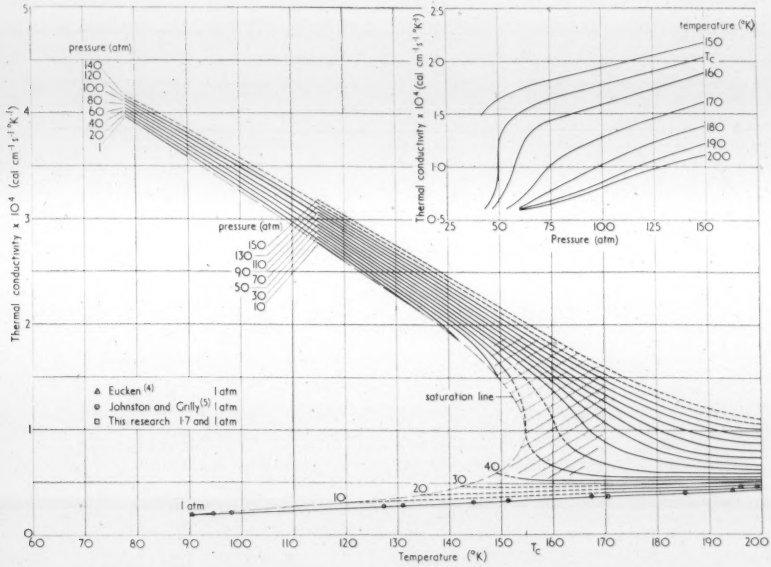

Fig. 3. Thermal conductivity of oxygen as a function of temperature and pressure

In Table 2 the data of other authors on the thermal conductivity of oxygen are compared with those observed in this investigation.

Hammann's[1] value of the thermal conductivity of oxygen at 80° K is 30% higher than that found in this research. The positive temperature coefficient which he reported is contrary to the trend of the data available for liquids. Further, his value for the thermal conductivity of liquid nitrogen at 1 atm at 80° K was about 50% higher than those given by Borovik, Matveev and Panina,[10] Uhlir[11] and by Powers, Johnston and Mattox.[12] For comparison, the present authors also measured the thermal conductivity of nitrogen at 80° K and obtained a result which was in good agreement with those of references (10), (11) and (12). All these nitrogen data are compared in Table 3.

Prosad's[2] mean value of the thermal conductivity of liquid oxygen at 92·3° K is about 40% higher than the value reported here. However, as his method was somewhat indirect, little importance can be attached to this discrepancy.

The present results are in good agreement with the 1 atm gas phase data of Eucken[5] and of Johnston and Grilly.[6]

Borovik's[13] data for oxygen at 156·2° K at pressures between 70 and 90 atm are about 10% lower than those reported here. It should be noted that Borovik's[13] data for nitrogen at twice the critical pressure and near the critical temperature are also about 10% lower than those of Uhlir.[11]

Since the present data for oxygen are self-consistent over a wide range of temperature and pressure and show the expected trends in the critical region, and since good agreement with the values of other observers was obtained for both oxygen and nitrogen, the authors consider that these data are free from serious error.

Table 2. *Comparison of present data for oxygen with those of other observers*

Temperature (° *K*)	*Pressure* (*atm*)	*Thermal conductivity* × 10^4 *cal/cm* °*K s*					
		Borovik[13]	*Hammann*[1]	*Prosad*[2]	*Eucken*[5]	*Johnston and Grilly*[6]	*This research*
80·0	1		5·12				(smoothed values) 3·95
92·3	≃2			5·0			3·51
170·2	1				0·385	0·373	(experimental values) 0·393 (1·7 atm)
196·1	1				0·440	0·427	0·443 (1·7 atm)
199·0	1				0·448	0·435	0·450 (1 atm)
156·2	10	0·38					(smoothed values) 0·37
	20	0·41					0·43
	30	0·45					0·47
	40	0·50					0·53
	70	1·39					1·55
	80	1·43					1·62
	90	1·48					1·68

Table 3. *Comparison of present data for nitrogen with those of other observers*

Temperature (° *K*)	*Thermal conductivity* × 10^4 *cal/cm* °*K s*				
	Hammann[1]	*Uhlir*[11]	*Powers, Johnston and Mattox*[12]	*Borovik, Matveev and Panina*[10]	*This research*
80·0	4·86 (1 atm)	3·20 (33·5 atm)	3·29 (1 atm)	3·50 (1 atm)	3·28 (33·5 atm)

ACKNOWLEDGEMENT

Crown copyright reserved. Reproduced with the permission of the Controller, H.M. Stationery Office.

REFERENCES

(1) HAMMANN, G. *Ann. Phys.* [*Leipzig*], **32**, p. 593 (1938).
(2) PROSAD, S. *Brit. J. Appl. Phys.*, **3**, p. 58 (1952).
(3) SELLSCHOPP, W. *Forschg. Ing. Wes.*, **5**, p. 162 (1934).
(4) VARGAFTIK, N. *Techn. Phys. USSR*, **4**, p. 341 (1937).
(5) EUCKEN, A. *Physikal. Z.*, **12**, p. 1101 (1911).
(6) JOHNSTON, H. L., and GRILLY, E. R. *J. Chem. Phys.*, **14**, p. 233 (1946).
(7) HOGE, H. J. *J. Res. Nat. Bur. Stand.*, **44**, p. 321 (1950).
(8) RAYLEIGH, LORD. *Phil. Mag.*, **32**, p. 529 (1916).
(9) KRAUSSOLD, H. *Forsch. Ing. Wes.*, **5**, p. 186 (1934).
(10) BOROVIK, E., MATVEEV, A., and PANINA, E. *J. Techn. Phys. USSR*, **10**, p. 988 (1940).
(11) UHLIR, A. *J. Chem. Phys.*, **20**, p. 463 (1952).
(12) POWERS, R. W., JOHNSTON, H. L., and MATTOX, R. W. *Proceedings of the 8th International Congress of Refrigeration, London*, 1951, p. 186, (III) (London: Institute of Refrigeration, 1951).
(13) BOROVIK, E. *J. Phys. USSR*, **11**, p. 149 (1947).

Propagation of transient fields from dipoles near the ground

By H. Poritsky, Ph.D., General Electric Co. Research Laboratory, Schenectady, New York, U.S.A.

[*Paper first received* 27 *February, and in final form* 1 *June*, 1955]

The propagation in air and underground of an electromagnetic wave originated by a current pulse in a small antenna located at or near the surface of the ground is studied. The treatment is based upon the resolution of a spherical wave into proper plane waves, this resolution being analogous to one used by Weyl[2] for the steady-state case.

A double-integral representation is obtained for (the Hertz potential of) the field. For a vertical dipole on the ground, one of the integrations is carried out above ground and in a certain conical range underground, while the second integration is carried out for special directions and locations.

1. Introduction

The propagation in two media of a transient pulse from a point source has many interesting applications; e.g., to acoustic waves started with an electric spark near water level, to radar-pulse propagation near the ground, to X-ray generation from an electron striking a dielectric, and so forth. In the following, we study this transient field in its electromagnetic aspect, as the wave due to a current pulse in a dipole or short antenna on or near the ground, assumed flat.

The *steady-state* field of vertical and horizontal dipoles on or near a flat ground has been formulated as an integral by Sommerfeld and computed by Sommerfeld and others.[1]

The propagation of *transient* fields due to transient dipole currents may be treated by means of Fourier integral superposition (in frequency) of the Sommerfeld solution. This was tried but proved rather intractable. The following treatment is based on the representation of a spherical wave as a sum of plane waves, given by Weyl[2] for simple-harmonic waves, and extended by the author[3] to waves of arbitrary shape as follows:

$$F(ct-R)/R = \mathscr{R}\Big\{-(1/2\pi)\int F_1[ct-(\alpha x+\beta y+\gamma z)]d\omega,\Big\} \qquad z>0 \quad (1)$$

Here the left-hand member represents a spherical wave, of "wave shape" F, diverging in free space from the origin $R=0$, where $R=(x^2+y^2+z^2)^{1/2}$. The function $F_1(\zeta)$ is analytic in the upper half-plane $\eta \geqslant 0$ of its complex argument, $\zeta=\xi+i\eta$, and is related to F as follows:

$$F(\xi) = \mathscr{R}[F_1(\xi)] \qquad (2)$$

while $F_1(\zeta) = dF_1/d\zeta$, and yields the "wave shape" of the component plane-wave element. The latter propagates in the direction of its normal, specified by the direction cosines α, β, γ and has the "amplitude" $-(1/2\pi)d\omega$, where $d\omega$ is the element of solid angle on the unit sphere Σ:

$$\Sigma\colon \alpha^2+\beta^2+\gamma^2=1 \qquad (3)$$

at the point (α, β, γ) on Σ. The region of integration in equation (1) does not extend over the real sphere Σ, but over the complex portion given by the limits

$$\begin{matrix}\phi \text{ from 0 to } 2\pi,\\ \theta \text{ from 0 to } +i\infty, \mathscr{R}(\theta)\geqslant 0\end{matrix} \qquad (4)$$

where θ, ϕ are spherical polar co-ordinates on Σ with the positive z-axis as polar axis, so that

$$\alpha=\cos\phi\sin\theta,\ \beta=\sin\phi\sin\theta,\ \gamma=\cos\theta,$$
$$d\omega=\sin\theta\,d\theta,\ d\phi=-d\gamma d\phi \qquad (5)$$

The limits (4) are especially suitable for the case where $F(t)$ is the Heaviside unit function:

$$F(t)=H(t)=\begin{cases}1 \text{ for } t>0,\\ 0 \text{ for } t<0\end{cases} \qquad (6)$$

which corresponds to the Hertz potential due to a current pulse in a dipole. For this case [see Section 3]

$$F_1(\zeta)=i(\log\zeta)/\pi,\ F_1'(\zeta)=i/\pi\zeta \qquad (7)$$

The introduction of complex portions of Σ and of complex wave shapes and amplitudes allows one the freedom of distorting the paths of integration. This will be found useful in the evaluation of the double-integral field representation in the following.

2. Introduction of the Hertz potentials

Following Sommerfeld (Ref. (4), p. 798), we shall express the field in a non-conducting medium of constant ϵ, μ ($\epsilon=\mu=1$ for free space) in terms of the Hertz vector potential $\boldsymbol{\Pi}$, thus

$$\boldsymbol{H}=\nabla\times(\epsilon\partial\boldsymbol{\Pi}/\partial t)/c \qquad (8)$$

$$\boldsymbol{E}=-\frac{\epsilon\mu}{c^2}\frac{\partial^2\boldsymbol{\Pi}}{\partial t^2}+\nabla(\nabla\cdot\boldsymbol{\Pi}) \qquad (9)$$

In regions free from antenna currents $\boldsymbol{\Pi}$ satisfies the wave equation

$$\frac{\epsilon\mu}{c^2}\frac{\partial^2\boldsymbol{\Pi}}{\partial t^2}=\nabla^2\boldsymbol{\Pi} \qquad (10)$$

The field of a dipole in free space, of moment $M(t)=\int i(t)\,dt$ is given by

$$\boldsymbol{\Pi}=\boldsymbol{u}M(t-R/c)/R \qquad (11)$$

where $\boldsymbol{u}$ is the unit vector along the dipole axis (assumed constant) and R the distance from the dipole. In particular, for a unit current pulse $i(t)=\delta(t)$,

$$M(t)=H(t) \qquad (12)$$

and equations (8), (9) and (11) yield a vanishing field outside the sphere

$$R=ct \qquad (13)$$

the radius of which is expanding with velocity of light, and the electrostatic field of the dipole inside this expanding sphere. If $\delta(t)$ is replaced by a continuous current over a small time interval ϵ, such that $\int_0^\epsilon i(t)dt=1$, then over the shell $ct-\epsilon<R<ct$ equations (8) and (9) also yield a large magnetic ampere-law field, and a radiating electric field.

3. FIELD FORMULATION FOR VERTICAL DIPOLE

For a field of a vertical dipole near the surface $z = 0$ of a flat earth $z < 0$, the Hertz potential $\boldsymbol{\Pi}$ points in the direction of the z-axis; hence Π_z may be denoted by Π. Continuity of tangential $\boldsymbol{H}$ and $\boldsymbol{E}$ leads to the boundary conditions [see Ref. (4), p. 920, equation (3)] at $z = 0$:

$$\epsilon\Pi \text{ is continuous, } \partial\Pi/\partial z \text{ is continuous} \tag{14}$$

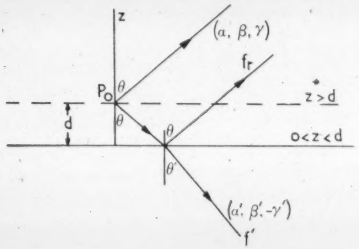

Fig. 1. Incident, reflected, and refracted rays

Place a vertical dipole of moment

$$M(t) = F(ct) \tag{15}$$

at P_0: $(x = 0,\ y = 0,\ z = d > 0)$ (see Fig. 1). Recalling equations (1) and (11), we represent Π of the dipole field in absence of the ground by:

$$\frac{M(t - R/c)}{R} = \frac{F(ct - R)}{R} = \begin{cases} -\dfrac{1}{2\pi}\mathscr{R}\left(\int F_1\{ct - [\alpha x + \beta y + \gamma(d - z)]\}d\omega\right), \\ \qquad 0 < z < d, \\ -\dfrac{1}{2\pi}\mathscr{R}\left(\int F_1\{ct - [\alpha x + \beta y + \gamma(z - d)]\}d\omega\right), \\ \qquad z > d \end{cases} \tag{16}$$

Corresponding to the plane wave, incident on the ground,

$$F_1\{ct - [\alpha x + \beta y + \gamma(d - z)]\}, \quad 0 < z < d \tag{17}$$

of the first integrand in equation (16), we form a reflected plane wave

$$f_r F_1\{ct - [\alpha x + \beta y + \gamma(d + z)]\}, \quad z > 0 \tag{18}$$

and a refracted plane wave

$$f' F_1\{[ct - n(\alpha' x + \beta' y - \gamma' z) - \gamma d] = f' F_1[ct - (\alpha x + \beta y) + n\gamma' z - \gamma d], \quad z < 0 \tag{19}$$

Here n, the index of refraction, is defined by

$$n = (\epsilon\mu)^{1/2} = (\epsilon)^{1/2} \tag{20}$$

while

$$\alpha' = \cos\phi \sin\theta', \ \beta' = \sin\phi \sin\theta', \ -\gamma' = -\cos\theta' \tag{21}$$

are the direction cosines of the refracted ray; θ, θ' the angles of incidence and refraction:

$$\sin\theta' = \sin\theta/n \tag{22}$$

and f_r, f' are the "coefficients of reflexion and refraction," to be determined. It will be noted that

$$\gamma' = (1 - \sin^2\theta')^{1/2} = (n^2 - 1 + \gamma^2)^{1/2}/n \tag{23}$$

Applying equation (14) at $z = 0$ to equation (19) and the sum of equations (17) and (18), one obtains for f_r, f' values independent of F_1 and depending on γ only:

$$f_r = \frac{n\gamma - \gamma'}{n\gamma + \gamma'} = \frac{n^2\gamma - \sqrt{(n^2 + \gamma^2 - 1)}}{n^2\gamma + \sqrt{(n^2 + \gamma^2 - 1)}} \tag{24}$$

$$f' = \frac{2}{n[n + (\gamma'/\gamma)]} = \frac{2\gamma}{n^2\gamma + \sqrt{(n^2 + \gamma^2 - 1)}} \tag{25}$$

Superposing the above plane-wave solutions by integration as in equation (16) for the incident plane wave, combining the reflected field with the last term of equation (16), and allowing d to approach zero, so that P_0 approaches the origin O, one obtains for the net field in air and underground,

$$\Pi = -(n^2/2\pi)\mathscr{R}\left\{\int f F_1[ct - (\alpha x + \beta y + \gamma z)]d\omega\right\}, \ z > 0 \tag{26}$$

$$\Pi = -(1/2\pi)\mathscr{R}\left\{\int f' F_1[ct - (\alpha x + \beta y - n\gamma' z)]d\omega\right\}, \ z < 0 \tag{27}$$

where

$$f = \frac{1 + f_r}{n^2} = \frac{2\gamma/n}{\gamma + (\gamma'/n)} = \frac{2\gamma}{n^2\gamma + \sqrt{(n^2 - 1 + \gamma^2)}} \tag{28}$$

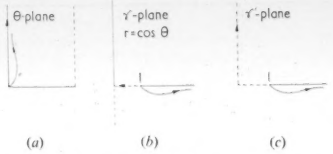

(a) (b) (c)

Fig. 2. Paths in the θ-, γ-, γ'-planes

If θ is chosen as in equation (4) and Fig. 2(*a*), the paths of γ and γ' are as shown by the solid lines of Figs. 2(*b*) and (*c*). This determines the branch of γ' in the double-valued radical in equation (23) to be used.

4. FIELD EVALUATION IN AIR

The evaluation of the integral in equation (26) at a field point $P(x, y, z)$, $z > 0$, is facilitated by introducing spherical co-ordinates R, η, ψ with polar axis $\eta = 0$ through P (see Fig. 3). (Due to symmetry of Π about the z-axis, it suffices to consider P_0 in the plane $x = 0$, as shown in Fig. 3.) Upon utilization of the relations

$$d\omega = \sin\eta d\eta d\psi = -d(\cos\eta)d\psi \tag{29}$$

$$\alpha x + \beta y + \gamma z = R\cos\eta \tag{30}$$

in equation (26) there results

$$\Pi = -(n^2/\pi)\mathscr{R}\left[\int\int f(\gamma)F_1(ct - R\cos\eta)\sin\eta d\eta d\psi\right] \tag{31}$$

As in Ref. (2) and (3), the limits of integration in the new co-ordinates ψ, η will be chosen in a manner similar to those of equation (4) for θ and ψ, namely 0 to 2π for ψ, and as shown in Fig. 5(*a*) for η. (This does not correspond to a true transformation of the integration range of the integrals in equation (26). It rather corresponds to a different available initial choice of the range of integration in equation (1). It

is analogous to rotating a ray of integration in the complex plane, rather than distorting a path between the same limits.)

Let the ψ-integration in equation (31) be carried out first. During this integration, η is constant, and so is the argument of F_1': hence there results

$$\Pi = -n^2\mathscr{R}\left[\int_0^{i\infty} \bar{f} F_1'(ct - R\cos\eta)\sin\eta\, d\eta\right] \tag{32}$$

Here
$$\bar{f} = \int_0^{2\pi} f(\gamma)d\psi/2\pi \tag{33}$$

the mean value of f over the cone $\eta =$ constant, with respect to the local longitude angle ψ (see Fig. 3), is completely

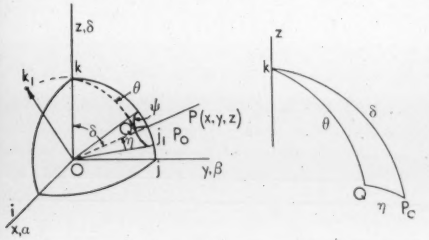

Fig. 3. Spherical co-ordinates for field evaluation

independent of F_1, and depends only on η and on the co-latitude δ of the cone axis where

$$\cos\delta = z/R \tag{34}$$

Introducing
$$\tau = \cos\eta \tag{35}$$

one obtains from equation (32)

$$\Pi = n^2\mathscr{R}\left[\int_1^{\infty} \bar{f}(\tau, \delta)F_1'(ct - R\tau)d\tau\right] \tag{36}$$

For the current pulse, utilizing equation (7), one obtains

$$\Pi = \frac{n^2}{\pi R}\mathscr{I}\left[\int_1^{\infty} \frac{\bar{f}d\tau}{\tau - (ct/R)}\right] \tag{37}$$

An interesting conclusion which follows from equation (37) is that, along any ray $\delta =$ constant through the origin, ΠR depends only on ct/R. This result can also be obtained by dimensional analysis.

This same conclusion also follows directly both for $z > 0$ and $z < 0$ from the integrals (26) and (27), when F_1' is substituted from equation (7).

Passing over the calculation of $\bar{f}$ (this will be considered in Section 5) it will now be shown that equation (37) evaluates to

$$\Pi = \begin{cases} \dfrac{n^2}{R}\bar{f}(\tau, \delta)\big|_{\tau = ct/R > 1} \\ 0 \text{ for } ct/R < 1 \end{cases} \tag{38}$$

To prove this we allow the path of η-integration in equation (32) to approach the pure-imaginary axis as in Fig. 5(*a*). The path of $\tau = \cos\eta$ will approach the real axis between 1 and $+\infty$ from below. It will be shown in Section 5 that $\bar{f}(t, \delta)$ is real for real τ (and real δ). Thus the integrand in equation (37) is real on the real τ-axis. Hence, the only possible non-vanishing contribution to Π from the integral in equation (37) is from singularities, if any, along the path of integration on the real axis. Evidently, the only such singularity is a pole at $\tau = ct/R$ which lies along the path of integration if $ct/R > 1$, contributing to the integral the value πi times the pole residue. We are thus led to equation (38).

As will be noted from equation (38), the locus (13) forms the boundary of the region in which the advancing wave pulse has established a non-vanishing field.

Comparing equations (11) and (12) with equation (38) one could describe the effect of the ground on the field at any point P as amounting to a multiplication (of Π) by the factor

$$n^2\bar{f} = n^2 + n^2\bar{f}_r \tag{39}$$

where $\bar{f}_r$ is the mean of the reflexion coefficient f_r over the cone of directions shown in Fig. 3, having OP for its axis, and of semi-vertical angle $\eta = \cos^{-1} ct/R$, provided $ct/R > 1$. The last inequality shows, however, that any benefit which may be derived from this interpretation is spoiled by the fact that η is pure imaginary.

We now consider the $\bar{f}$ integration in equation (33); the evaluation of $\bar{f}$ is required to apply equation (38).

From Fig. 3 we express γ in terms of ψ:

$$\gamma = A + B\cos\psi \tag{40}$$

where
$$A = \cos\eta\cos\delta,\ B = \sin\eta\sin\delta$$

The function $f(\gamma)$ in equation (33) is given by equation (28); it is single-valued over a two-sheeted Riemann surface in the γ-plane with branch points at (see Fig. 4):

$$\gamma = \pm ib,\ b = \sqrt{(n^2 - 1)} \tag{41}$$

Furthermore, $f(\gamma)$ has poles at

$$\gamma = \pm a,\ a = 1/\sqrt{(n^2 + 1)} \tag{42}$$

Recall from Fig. 2, equation (23) that for $\gamma \geqslant 1$ the positive radical $\sqrt{(n^2 + \gamma^2 - 1)}$ is understood. Therefore, the sheet of the Riemann surface in which the integration paths lie (this will be called the "upper sheet") does *not* contain the pole $\gamma = a$.

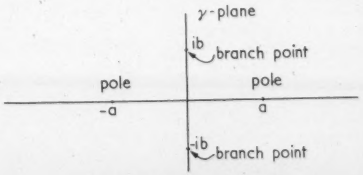

Fig. 4. Singularities of $f(\gamma)$

When the polar variables η, ψ are introduced in equation(31), the values of $\gamma = A + B\cos\psi$ will no longer lie along one particular path as shown in Fig. 2(*b*). For η as in Fig. 5(*a*), the values of $\cos\eta$, $\sin\eta$ and of A and B are shown schematically in Figs. 5(*b*) and (*c*). As η approaches the imaginary axis, A becomes real and B pure imaginary, and for real ψ the path of the γ-values reduces to a vertical interval from γ_1 to γ_2, where

$$\gamma_1 = A + B,\ \gamma_2 = A - B \tag{43}$$

as in Fig. 5(*d*) or, if the ψ-path be slightly raised from the real axis, the path of γ-values runs around a closed narrow curve enclosing γ_1, γ_2, as shown by the dotted curve in Fig. 5(*d*).

By replacing ψ in equation (33) by γ from equation (40) we obtain

$$\bar{f} = -\frac{1}{2\pi}\int \frac{f(\gamma)d\gamma}{[B^2 - (\gamma - A)^2]^{1/2}} \tag{44}$$

where the path of integration encloses the two branch points, given by equation (43).

As η approaches the pure imaginary axis as on Fig. 5(*a*) the branch points γ_1, γ_2 (the end of the chords of integration for real ψ), for a fixed δ, as η varies, will describe confocal hyperbolas with $\gamma = \pm 1$ as foci [see Fig. 5(*d*)].

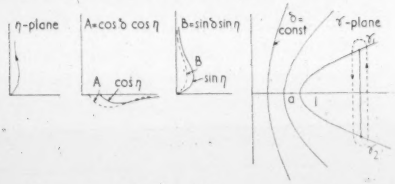

Fig. 5. Variation of η, A, B and $\dot{\gamma}$

For $\delta = 0$, the chords of integration collapse into points on the real axis beyond $\gamma = 1$; for $\delta = \pi/2$, they lie on the pure imaginary axis.

For fixed η, as δ varies, γ_1, γ_2 describe ellipses with foci at $\gamma = \pm 1$.

It will be noted that $f(\gamma)$ is real for real γ, and, as stated above, the branch of $f(\gamma)$ in question has no pole at $\gamma = a$. Hence $\bar{f} = \int f(\gamma)d\psi/2\pi$ is real for the pure imaginary η under consideration: indeed the contributions $f(\gamma)d\psi$ from two points P_1, P_2 situated symmetrically about the real axis along the chord of integration in Fig. 5(*d*) are the conjugate complex of each other, and their sum is real.

Rationalizing the denominator in equation (28), one obtains

$$f(\gamma) = \frac{2}{n^2+1}\left[n^2 + \frac{a^2n^2}{\gamma^2 - a^2} - \frac{\gamma\sqrt{(\gamma^2 + b^2)}}{\gamma^2 - a^2}\right] \tag{45}$$

Substitution of equation (45) into equations (33) and (44) leads to two elementary and one complete elliptic integral of the third kind, with branch points at $\gamma = \pm ib$, γ_1, γ_2.

Certain special cases will now be listed for which the integration can be carried out by elementary means.

For $\eta = 0$, equation (35) shows that $\tau = 1$, thus yielding the expanding sphere, equation (13). With $B = 0$, equations (40) and (41) show that $f(\gamma)$ in equation (33) is independent of ψ, and $\bar{f} = f(\cos\delta)$. Equation (38) yields, as τ approaches 1 from the right,

$$\Pi = \left(\frac{1}{R}\right)\frac{2n^2\cos\delta}{[n^2\cos\delta + \sqrt{(n^2 - 1 + \cos^2\delta)}]} \quad \text{for } ct/R = 1^+ \tag{46}$$

For $\delta = 0$ (vertical propagation) ψ, η reduce to ϕ, θ respectively, the integrand in equation (33) becomes independent of ψ, and one obtains

$$\Pi = \left(\frac{n^2}{R}\right)\frac{2}{\{n^2 + [1 + (n^2-1)R^2/c^2t^2]^{1/2}\}} \quad \text{for } \delta = 0,\ ct > R \tag{47}$$

For $\delta = \pi/2$ (horizontal propagation) the elliptic integral in $\bar{f}$ can be shown to vanish. There results

$$\Pi = \frac{n^2}{R(n^4-1)}\{1 - [(ct)^2(n^2+1)/R^2 - n^2]^{-1/2}\} \quad \text{for } \delta = \pi/2,\ ct > R \tag{48}$$

For large ct/R one proves that

$$f(\gamma) \to 2/(n^2+1) \tag{49}$$

independently of ψ, and one obtains the first part of equation (50)

$$\left.\begin{aligned} \Pi &= \frac{2n^2}{n^2+1}\frac{1}{R} \quad \text{for } z > 0,\ ct \gg R \\ \Pi &= \frac{2}{n^2+1}\frac{1}{R} \quad \text{for } z < 0,\ ct \gg R \end{aligned}\right\} \tag{50}$$

The second part of equation (50) can be deduced from equation (27) in a similar manner. Equations (50) agree with the field of an electrostatic dipole at $z = 0$.

The integration of equations (33) and (44) has been studied for general δ, ct/R, but will not be discussed here owing to lack of space.

5. UNDERGROUND FIELD

For $z < 0$ the field is given by equation (27), which will be put in the form

$$\Pi = -\frac{1}{2\pi}\mathscr{R}\left\{\int \frac{2\gamma}{(n\gamma + \gamma')n}F_1'[ct - n(\alpha'x + \beta'y - \gamma'z)]d\omega\right\} \tag{51}$$

One may transfer from the sphere of integration Σ to the sphere of refracted normals:

$$\Sigma': \alpha'^2 + \beta'^2 + \gamma'^2 = 1 \tag{52}$$

and put equation (51) in the form

$$\Pi = -\frac{1}{2\pi}\mathscr{R}\left\{\int \frac{2\gamma'}{n\gamma + \gamma'}F_1'[c't - (\alpha'x + \beta'y + \gamma'z)]d\omega'\right\} \tag{53}$$

where c' is the velocity of propagation in $z < 0$,

$$c' = c/n \tag{54}$$

provided the downward direction be chosen as the positive z-, γ'-axis.

This integral (53) may also be obtained from equation (26) by interchanging the spaces $z > 0$, $z < 0$.

By methods similar to that of Section 4, the integral (53) can be reduced to the form

$$\Pi = \frac{1}{\pi R}\mathscr{I}\left(\int_1^{\infty} \frac{\bar{f}'d\tau}{\tau - c't/R}\right) \tag{55}$$

where

$$\bar{f}' = \int f'(\gamma')d\psi/2\pi \tag{56}$$

$$f'(\gamma') = 2\gamma'/(n\gamma + \gamma') \tag{57}$$

The singularities of f' in the γ'-plane consist of branch points at

$$\gamma' = \pm b',\ b' = (n^2-1)^{1/2}/n \tag{58}$$

and of poles at

$$\gamma' = \pm a',\ a' = n/(n^2+1)^{1/2} \tag{59}$$

As in $f(\gamma)$ in Sections 4 and 5, the pole $\gamma = a'$ does not lie in the Riemann sheet in which the integration is carried out. In contrast to $f(\gamma)$, the branch points $\pm b'$ of $f'(\gamma')$ are *on* the real axis, and this turns out to complicate the evaluation of the field.

For a current pulse, with F_1' given by equation (7), again one may write equation (55) in the form

$$\Pi = \frac{1}{\pi R}\mathscr{I}\left[\int_0^\infty \frac{f'\,d\tau}{(\tau - c't)/R}\right] \tag{60}$$

Thus, ΠR again depends only on t/R and δ', the angle with the lower vertical.

If $f' = f'(\tau, \delta')$ were real for real τ (and pure imaginary η), then, as in Section 4, one can eliminate the η-integration and reduce Π to

$$\Pi = \begin{cases} 0 \text{ for } c't/R < 1 \\ f'(\tau)/R,\ \tau = c't/R \text{ for } c't/R > 1 \end{cases} \tag{61}$$

However, because the branch point b' is now real, it turns out that only if the chords of integration in the γ'-plane lie to the right of b' can f' be shown to be real for real τ. This will be the case for all the points of the hyperbola of Fig. 5(*d*) (drawn in the γ'-plane) provided that

$$\delta' < \delta_0,\ \delta_0 = \sin^{-1}(1/n) \tag{62}$$

On the other hand, for $\delta' > \delta_0$, some of the chords of integration lie to the left of the branch point, and one may not evaluate equation (60) by the above method.

Fig. 6, which represents a plane section through the z-axis, shows the solid angle over which the inequality (62) holds.

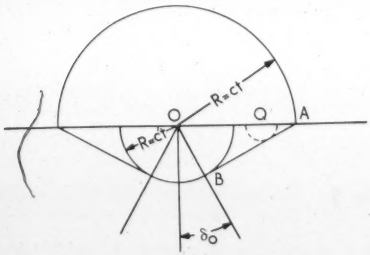

Fig. 6. Region of disturbance at time t

The angle δ_0 can be obtained by drawing a circle of radius $R = ct$ in the upper half-plane, a circle of radius $R = c't$ in the lower half plane, constructing a tangent AB to the latter from the point A where the former cuts the horizontal axis, and joining the origin O to B, the point of contact.

Inside the conical range given by equation (62), the direct wave spreading from the dipole at O with velocity c' reaches a field point P first. Outside this range, that is, for $\delta' > \delta_0$, there is a disturbance reaching each point P ahead of the direct expanding wave front. The front of this disturbance is due to Huygens wavelets that originate from intermediate points, such as Q in Fig. 6, on the surface of the ground at the instant when the spherical wave front of radius ct has reached them. In this angular range $f(\tau, \delta')$ is no longer real for $\tau > 1$, and in general one cannot evaluate the integration (60) in terms of residue of f at the pole $\tau = c't/R$.

It is planned to examine the range $\delta' > \delta_0$ at a later date in more detail.

An alternative procedure for $z < 0$ which was attempted, is based on the calculation of a wave function u over the half-space $z < 0$ in terms of the boundary values over $z = 0$ of u and $\partial u/\partial t$, obtaining the latter from equations (48) and (14). A theorem for such an expression of wave functions was obtained by the author and is to be published elsewhere.[5]

6. FIELD OF HORIZONTAL DIPOLE

We now consider briefly the field of a transient *horizontal* dipole, say a dipole of moment $M(t)$, placed above the surface of the ground at $P_0 : (0, 0, d)$, and pointing in the direction of the x-axis. This field cannot be expressed in terms of a Hertz vector potential $\boldsymbol{\Pi}$ with only a single non-vanishing component Π_x, but, as shown by Sommerfeld (Ref. (4), p. 950), for the steady-state case, may be formulated in terms of a Hertz vector with two scalar components

$$\boldsymbol{\Pi} = (\Pi_x\, 0,\ \Pi_z) \tag{63}$$

We may apply equation (16) to the incident component of Π_x, and add reflected and refracted components for both Π_x and Π_z so as to satisfy the continuity along $z = 0$ of the functions*

$$\epsilon\Pi_z,\ \frac{\partial \Pi_x}{\partial x} + \frac{\partial \Pi_z}{\partial z},\ \epsilon\Pi_{x'},\ \epsilon\frac{\partial \Pi_x}{\partial z} \tag{64}$$

These conditions follow from the continuity of the tangential components of $\boldsymbol{E}$, $\boldsymbol{H}$, and the normal components of $\epsilon\boldsymbol{D}$, $\mu\boldsymbol{H}$.

The resulting Π_x is axially symmetric, and after d is allowed to approach zero, it approaches

$$\left.\begin{aligned} \Pi_x &= \mathscr{R}\left\{-\frac{1}{2\pi}\int \frac{2\gamma}{\gamma + n\gamma'}F_1'[ct - (\alpha x + \beta y + \right. \\ &\qquad \left. + \gamma z)]d\omega\right\},\ z > 0 \\ \Pi_x &= \mathscr{R}\left\{-\frac{1}{2\pi}\int \frac{2\gamma}{n^2(\gamma + n\gamma')}F_1'[ct - (\alpha x + \beta y - \right. \\ &\qquad \left. - n\gamma' z)]d\omega\right\},\ z < 0 \end{aligned}\right\} \tag{65}$$

On the other hand Π_z is *not* axially symmetric, but can be expressed in the form

$$\Pi_z = -\frac{\partial G}{\partial x} \tag{66}$$

where G *is* axially symmetric and is given by

$$\left.\begin{aligned} G &= -\frac{1}{2\pi}\frac{2(1 - n^2)}{n} \times \\ &\quad \times \mathscr{R}\left\{\int \frac{\gamma F_1[ct - (\alpha x + \beta y + \gamma z)]d\omega}{(\gamma + n\gamma')(\gamma' + n\gamma)}\right\},\ z > 0 \\ G &= -\frac{1}{2\pi}\frac{2(1 - n^2)}{n^3} \times \\ &\quad \times \mathscr{R}\left\{\int \frac{\gamma F_1[ct - (\alpha x + \beta y - n\gamma' z)]d\omega}{(\gamma + n\gamma')(\gamma' + n\gamma)}\right\},\ z < 0 \end{aligned}\right\} \tag{67}$$

For a current pulse F_1 and F_1' are obtained from equation (7).

The evaluation of the integrals (65) and (67) has not been

* The author believes that typographical errors must have crept into the equations on p. 950 of Ref. 4, which do not agree with the first and last equations (64).

studied in detail. It is evident, however, that the difficulties encountered for a vertical dipole for $z < 0$ will now arise even for $z > 0$. This is due to the factor $(\gamma + n\gamma')$, which has real branch points, and furthermore, to the fact that for a current pulse, equation (7) yields a function $F_1(\zeta)$ which is no longer real for the complete real axis in the ζ-plane.

REFERENCES

(1) STRATTON, J. A. *Electromagnetic Theory*, pp. 573–87 (New York: McGraw-Hill Book Co. Inc., 1941).

(2) WEYL, H. *Ann. Phys.* [Leipzig], **60**, p. 482 (1919).

(3) PORITSKY, H. *Commun. Pure Appl. Math.*, **4**, p. 1 (1951).

(4) SOMMERFELD, A. in *Differential- und integralgleichungen der physik*, Ed. by P. Frank and R. von Mises, **II**, Chapter V (Viewig, 1935).

(5) PORITSKY, H. *Quart. Appl. Math.* To be published. See also BAKER, B. B. and COPSON, E. T. *Mathematical Theory of Huygen's Principle* (Oxford: Clarendon Press, 1950).

Technical properties of iron powder magnets

By E. H. CARMAN, M.Sc., Ph.D., A.Inst.P.,* University of Melbourne, Australia

[*Paper first received* 3 *March, and in final form* 15 *August*, 1955]

Coercive force, remanence and maximum energy product of compacts of iron are measured as functions of density of packing (d/d_0) and X-ray particle size (L). The iron is prepared by hydrogen reduction of ferric oxide and for the grade used optimum technical properties are: $B_r = 5200$ gauss, $(B.H)_{max} = 0{\cdot}82 \times 10^6$ gauss : oersted, and ${}_BH_c = 400$ oersted when $L = 300$ Å and $d/d_0 = 0{\cdot}5$. Maximum coercive force obtained is 610 oersted when $d/d_0 = 0{\cdot}3$. For d/d_0 fixed the three magnetic quantities increase with decreasing particle size, the increase being greatest with B_r and $(B.H)_{max}$. The increase in remanence is discussed in terms of its ratio to saturation magnetization and it is suggested that the observed increase is related to packing effects. Measurement of the influence of oxygen impurity indicates that the presence of a few per cent of oxide does not appreciably affect the quality of the magnets.

Among the new permanent magnet materials developed in recent years are the pure iron powder magnets. These have been studied from the standpoint of the mechanism of coercive force by Weil,(1) Néel(2) and Bertout(3) among others, and since the "intrinsic" coercive force (${}_IH_c$) is of interest there, the corresponding technically important ${}_BH_c$ has for the most part been neglected. The present paper is an account of experiments to show ${}_BH_c$, remanence and maximum energy-product as functions of density of packing and particle size.

For the experiments commercial ferric oxide of very fine particle size (approximately 200 Å) is reduced under hydrogen at various temperatures between 250 and 400° C. This gives rise to iron powder samples of different particle size, each of which is formed into a series of compacts having a range of densities of packing. Each compact is measured magnetically with a permeameter similar to the isthmus type developed by Sanford and Bennett.(4) The iron particle size is found by standard X-ray diffraction technique.

PREPARATION OF IRON POWDERS AND COMPACTS

Below 350° C reduction is carried out in a hydrogen recirculating apparatus developed by the present author.(5) Effectively, some 40 or 50 g of oxide are placed in shallow nickel boats over which dry hydrogen flows at about 600 l./h. To ensure complete reduction the temperature conditions are controlled to provide a uniform temperature throughout the sample.

Above 350° C a simple hydrogen train constructed from a $1\frac{1}{2}$ in. diameter silica tube surrounded by a furnace and utilizing cylinder hydrogen freed from oxygen and water vapour is employed. The tube has a funnel device near the outlet for flooding the sample prior to removal.

The completely reduced powder is pyrophoric, and oxidation with the atmosphere is prevented by removing the boats into petroleum ether. If the powder is removed from its protective liquid, in most cases only slight oxidation occurs on drying out, but gentle heating will cause it to ignite. Ignition also occurs if the dry powder is compacted, although sometimes apparently the restricted oxygen supply permits only partial oxidation evident by a small temperature rise in the compact.

Compacts measuring 7·5 by 0·65 cm are formed by applying load from a hydraulic press to a steel die containing the wet powder. The die is dismantled to remove the compact which is immediately placed in paraffin wax heated to just above its melting point. A few minutes in the wax is sufficient to ensure complete penetration since it mixes well with petroleum ether.

The wax is used for protection against oxidation rather than as a binding medium—binding is necessary only for compacts formed under loads less than about 1 t/in². X-ray diffraction examination of a waxed compact immediately after preparation, and some four months later, proves the effectiveness of the wax since only iron lines are present in each spectrum.

PARTICLE SIZE MEASUREMENT

For each reduction temperature a sample of freshly prepared powder is examined by the back reflexion X-ray diffraction

* Now at the B.S.A. Group Research Centre, Sheffield.

technique. Line profiles of the CoKα doublet are determined with a Dobson microphotometer from the photographic exposures. After resolution, the pure diffraction broadening (ϕ) for the α_1 component is obtained from a correction curve for instrumental broadening based on the particle size distribution[6]

$$p(M) = (2/\pi)^{\frac{1}{2}}(M^2/S^3)\exp\left[\tfrac{1}{2}(-M^2/S^2)\right]$$

where M is the particle size and S a constant.

The apparent particle size L then follows from Scherrer's[7] relation

$$\phi = \lambda/(L\cos\theta)$$

where ϕ is the angular line breadth, λ the wavelength of incident radiation and θ the Bragg angle.

The particle size determined by this method refers to linear dimensions, for example, a cube edge in the case of cubic particles, or a diameter in the case of spherical particles. Precise definition of particle size is not possible in view of the inherent approximate nature of the method.

MAGNETIC MEASUREMENTS

The permeameter employed in the present work is designed for magnetizing forces up to 4000 oersted with low magnetizing current. The main poles are fitted with adjustable polepieces to permit measurements with specimens of various lengths. To determine demagnetizing curves for the compacts they are surrounded by a *B*-coil and placed between the adjustable pole pieces. The magnetizing force at each point is measured directly with a small *H*-coil which is adjacent to the compact surface and rotates through 180° about an axis normal to the field direction.

Tests have been made to ensure uniformity of field near the compact and *H*-coil. Also, large air corrections common with materials of low remanence are reduced by employing a series of *B*-coils to fit the different sized specimens. Measurements are carried out by the usual ballistic method.[8]

EXPERIMENTAL RESULTS

Ten samples of ferric oxide from the same stock reduced at temperatures between 250 and 400 °C are described in Table 1. Nos. 1 to 7 have been prepared by the above mentioned recirculating method, while Nos. 8 to 10 result from reduction under purified cylinder hydrogen.

Table 1. *Details of preparation and description of compacts*

No.	*Reduction temperature* (°C)	*Metallic iron content* (%)	*Particle size* (Å)	*Number of compacts*	*Range of density* (g per cm³ *of compact*)
1	250	100	245	4	1·26–3·54
2	280	100	244	5	1·21–3·52
3	280	93	265	3	1·24–3·53
4	310	100	313	6	1·31–4·45
5	320	90	410	8	0·68–4·00
6	330	95	465	7	0·90–4·34
7	350	95	503	6	1·66–4·00
8	350	100	547	3	2·44–3·66
9	375	100	640	3	2·61–3·80
10	400	100	791	3	2·92–4·04

The figures in column 3 refer to the weight per cent of metallic iron in the reduced powders. This is determined from a comparison of the respective X-ray spectra with spectra from a standard series of powders, prepared from mixtures in known proportions, of carbonyl iron and finely powdered ferrous oxide. Oxide lines from partially reduced powders appear to correspond closely with those from ferrous oxide. Of course, this method suffers from the disadvantage that it does not allow for variation in relative intensity between iron and oxide lines due to particle size variation; consequently it is only suitable for approximate relative determinations of composition.

Maximum and minimum values of density for each series of compacts mentioned in column 5 appear in column 6. Correction is made for the presence of wax by employing the following relation for the weight of iron (or iron plus iron oxide) per cubic centimetre of compact:

$$d = \frac{d' - d_{wax}}{d_0 - d_{wax}} \cdot d_0$$

Here d' is the weight of the compact divided by its volume, d_{wax} the wax density and d_0 the density of massive iron.

Following the method of Weil[1] the magnetic quantities are plotted against the relative volume of non-magnetic voids $[1 - (d/d_0)]$ instead of the density of packing (d/d_0). Results for coercive force ($_BH_c$), remanence (B_r) and maximum energy-product $(B.H)_{max}$ from the ten series of compacts described in Table 1 are in Figs. 1 to 3 respectively.

DISCUSSION OF THE RESULTS

(*a*) *Variation of* $_BH_c$ *with density of packing and particle size.* Depending on the particular reduction conditions the curves of Fig. 1 are linear only for $[1 - (d/d_0)]$ between zero and

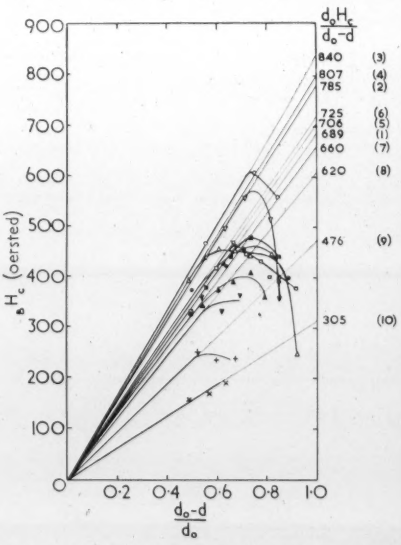

Fig. 1. Coercive force as a function of packing factor for a range of particle sizes

0·5 to 0·8; subsequent decrease for higher $[1-(d/d_0)]$ results from ${}_BH_c$ tending to zero with the density of packing. The initial, apparently linear, increase is most likely related to the overall linear increase in ${}_IH_c$ found by Weil[1] since ${}_BH_c$ behaves in much the same way as ${}_IH_c$ for sufficiently high values of d/d_0.

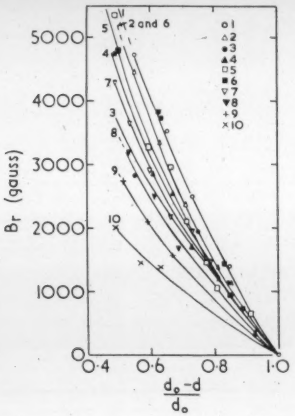

Fig. 2. Variation of remanence with packing factor and particle size

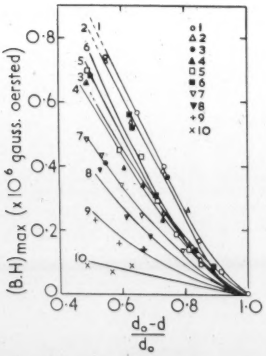

Fig. 3. Variation of maximum energy product with packing factor and particle size

The slope $d_0H_c/(d_0-d)$ of the linear ranges varies with the reduction temperature and related particle size, the two relationships are shown in Figs. 4 and 5. These curves show that for any given value of d/d_0, in the linear range, ${}_BH_c$ reaches a maximum corresponding to a reduction temperature of 290° C and particle size approximately equal to 300 Å which is in the neighbourhood of the predicted critical single domain size.[2] Of course, this value is only accurate to about 30% in virtue of the method of particle size measurement employed.

(*b*) *Influence of oxygen impurity.* Results of measurements on compacts from iron formate partially reduced under hydrogen at 300 to 350° C have been published by Lihl.[9] They indicate maximum in curves for coercive force and

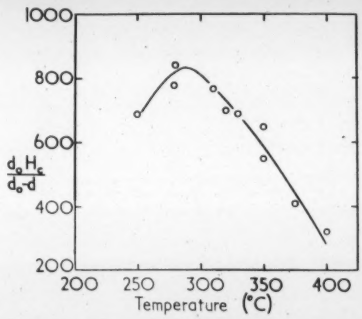

Fig. 4. Indicating the relationship between coercive force and reduction temperature for ${}_BH_c$ *versus* $(d_0-d)/d_0$ linear

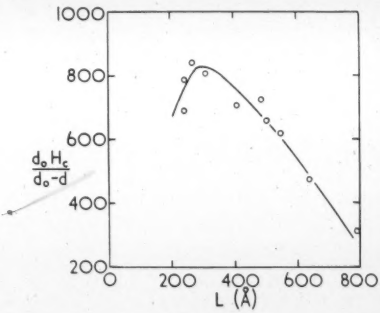

Fig. 5. Comparison with Fig. 4 showing that coercive force is related to particle size and reduction temperature in a similar way

remanence near 60% metallic iron falling sharply towards 100% iron. Similar experiments by the present author, the results of which appear in Table 2, suggest that ${}_BH_c$ and B_r reach their maximum value at 100% iron. Fluctuations in iron content and magnetic properties evident in cases where reduction is longer than eight hours results mainly from variations in temperature conditions. However, it seems clear that the presence of some 5% of oxide in the case of B_r and a somewhat higher proportion in the case of ${}_BH_c$ changes these quantities by an amount which is scarcely beyond the error of measurement. This is supported by a comparison between Figs. 4 and 5 where it is apparent that the points from compacts containing oxide (Nos. 3, 5, 6 and 7 in Table 1) do not lie off the respective curves in a corresponding manner.

Table 2. *Partial reduction of iron oxides at 380° C*

Time (h)	*% metallic iron*	$_BH_c$	B_r
2	5	234	1150
4	70	320	1690
6	95	320	2020
8	95	320	2070
10	100	316	1970
12	95	320	1920
14	98	338	2060

The discrepancy between the results of Lihl and the present author seems puzzling at first sight but might well lie in differences in the respective ways the density of packing vary. In fact it is obvious from the variation with d/d_0 evident in Figs. 1 and 2 that the true behaviour of $_BH_c$ and B_r with oxygen content could only be known if d/d_0 is kept constant—a condition which appears absent in Lihl's work, but is certainly present in Figs. 4 and 5.

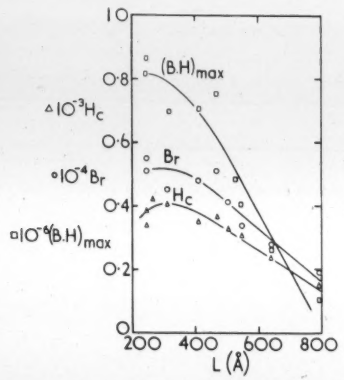

Fig. 6. Relationship between magnetic properties and particle size for compacts having the same packing factor (0·5)

(*c*) *Remanence and maximum energy-product.* For technical purposes a high value of B_r and $(B.H)_{max}$ rather than just high coercive force is required. Figs. 2 and 3 show that these quantities increase with density of packing, the increase being larger for the smaller particle size. For d/d_0 approximately equal to 0·5, the maximum obtainable with the available equipment, B_r and $(B.H)_{max}$ appear as functions of the particle size on Fig. 6, together with the corresponding curve for $_BH_c$.

The decrease in B_r with increasing particle size evident in Figs. 2 and 6 can be interpreted to some extent with the aid of saturation magnetization measurements at each end of the particle size range. From these the values of the ratio of remanence to saturation magnetization I_r/I_s for maximum and minimum d/d_0 in the series 1, 2, 8, 9, 10 were found, and appear in Table 3.

Table 3. *I_r/I_s related to particle size and density of packing*

No.	I_r/I_s *Min. d/d_0*	I_r/I_s *Max. d/d_0*	*Particle size (Å)*
1	0·66	0·69	245
2	0·51	0·77	244
8	0·61	0·52	547
9	0·52	0·35	640
10	0·46	0·32	790

These results show a general decrease in I_r/I_s with increasing particle size for maximum d/d_0, the decrease being less marked for minimum d/d_0. Thus the effect of packing is to make the remanence more sensitive to particle size variation. Alternatively, the smaller, presumably single domain, particle sizes are less influenced by packing than are particles some two or three times larger. This would be expected if, as the packing increases, the smaller particles sinter over smaller areas of contact than the larger, since this would be accompanied by greater stability in domain configuration resulting from the more restricted wall movement between particles.

ACKNOWLEDGEMENTS

The author wishes to thank Professor J. Neill Greenwood and Dr. W. A. Wood for their stimulating interest in the work.

Acknowledgement is also made to the University of Melbourne for providing financial assistance in the form of a scholarship.

REFERENCES

(1) WEIL, L. *C.R. Acad. Sci.* [*Paris*], **225,** p. 229 (1947).

(2) NÉEL, L. *C.R. Acad. Sci.* [*Paris*], **224,** pp. 1488–90 (1947).

(3) BERTOUT, F. *Bull. Soc. Franc. Minéral Crist.*, **76,** pp. 1–58 (1953).

(4) SANFORD, R. L., and BENNETT, E. G. *J. Res. Nat. Bur. Stand.*, **23,** pp. 415–25 (1939).

(5) CARMAN, E. H. *Metallurgia*, **52,** pp. 165–168 (1955).

(6) GARROD, R. I., BRETT, J. F., and MACDONALD, J. A. *Austral. J. Phys.*, **7,** p. 77 (1954).

(7) SCHERRER, P., and ZZIGMONDY, R. *Kolloid Chemie*, 3rd ed. (Leipzig: Spanier).

(8) SANFORD, R. L. *Circ. Nat. Bur. Stand.*, **C425,** p. 20 (1937).

(9) LIHL, F. *Acta Phys. Austriaca*, **4,** p. 360 (1951).

A simple adaptation of the carbon replica technique for the examination of selected areas in the electron microscope

By D. E. Bradley, Associated Electrical Industries, Ltd., Aldermaston, Berks.

[*Paper received 5 July*, 1955]

The value of electron microscope replica techniques, particularly in metallurgical applications is greatly enhanced if it is possible to examine areas or features selected in the optical microscope. Though existing methods can be used to achieve this with the carbon replica, it has been found that they are not entirely suitable. The paper describes a simple and quick method for use with carbon replicas. To illustrate a possible field of application, a selected area of a pearlitic steel specimen is examined at different stages during etching treatment.

It has been found that, in the replication of surfaces for the transmission electron microscope, it is frequently desirable to be able to examine an area or feature which has been selected in the optical microscope. Various methods have been devised to achieve this, the most notable being those of Hyam and Nutting,[1] Nankivell[2] and Booker.[3] In spite of this abundance of methods, little use appears to have been made of them. This may be due to the fact that the operations are difficult to carry out, or involve the construction of complicated apparatus. In this Laboratory, the wide use of the carbon replica[4,5] has necessitated the development of a simple and quick method of examining selected areas. The method of Hyam and Nutting is suitable for use with dry-stripped Formvar replicas,[6] which can be used to make carbon replicas, but the apparatus involved is complicated and the Formvar replica is liable to slip relative to the grid, perhaps causing the feature of interest to be obscured behind a grid bar. The technique described below eliminates this difficulty, and requires only a very simple attachment to a 16 mm optical microscope objective.

APPARATUS

The attachment is illustrated in Fig. 1. It consists of a flat plate *A* which is drilled so that it can be clamped between the objective cap and the main body of the microscope objective lens. A second plate *B* is attached to the first by a hinge at *C* at one end, and a hinged bolt *D* at the other. The separation of the plates is adjustable by the knurled screw *E* and hinged bolt *D* working against a compression spring. Three small pins at *F* are soldered in position round a $\frac{3}{16}$ in. diameter hole *G*, which is drilled with its centre on the optical axis of the objective. The specimen grid is attached to the three pins with a small amount of adhesive. A very satisfactory method of applying this is to moisten a strip of cellulose tape with chloroform, a solvent for the adhesive, and to rub the tape against the pins before the chloroform dries. A grid placed on the pins will then remain firmly in position. The objective is fitted to a microscope with a vertical illuminator, and the grid can be brought in and out of focus with the knurled screw *E*.

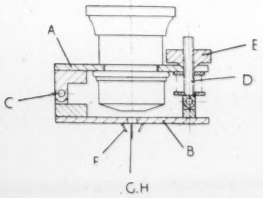

Fig. 1. Attachment mounted on a 16 mm optical objective

Before taking a replica from a selected area or feature, it is often necessary to make some form of reference scratch on the specimen for either electron-optical or optical identification. As the above authors,[1,2,3] have suggested, this may be carried out by means of a suitable micro-hardness tester. As an alternative, an attachment can be made for an optical microscope with a graduated stage. This consists of a fine-pointed diamond or sapphire attached to the end of a metal arm, pivoted at its centre on a stand bolted to the fixed portion of the microscope stage. By placing a weight at suitable positions on the bar, the load on the point may be varied, thus allowing some adjustment to the dimensions of the scratch. The marking is carried out by placing the specimen on the stage, allowing the diamond point to rest on the edge of the specimen, and then using the stage controls to draw the desired scratch pattern.

If the feature is sufficiently distinctive, a scratch pattern may not be required for identification in the electron microscope. In this case, there is also no necessity for scratches for optical identification, provided the specimen can be returned to its original position on the optical microscope stage after the removal of a replica.

METHOD

The method of operation is described stage by stage with reference to Fig. 2. After the specimen under examination has been marked or located as described above, it is removed

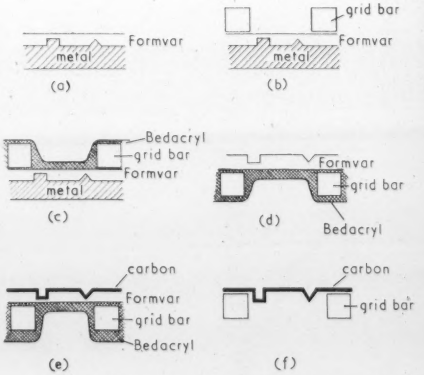

Fig. 2. A diagrammatic representation of the various stages of the technique used to produce carbon replicas of areas selected in the optical microscope

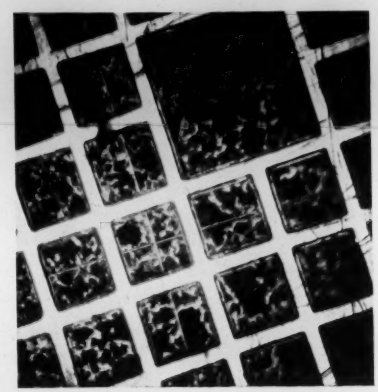

Fig. 3. Electron microscope specimen support grid positioned with a known grid square over an area of the specimen marked by the intersection of two scratches. (×85)

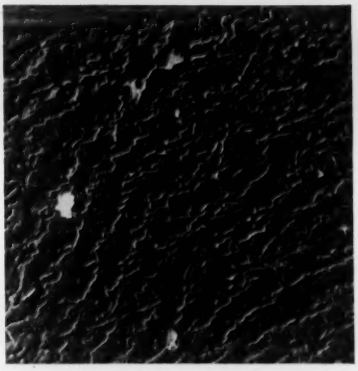

Fig. 4. Carbon replica of pearlitic steel etched in $\frac{1}{4}$% nital for 20s. Shadowed at $\tan^{-1}\frac{1}{2}$ with gold palladium. (×12000)

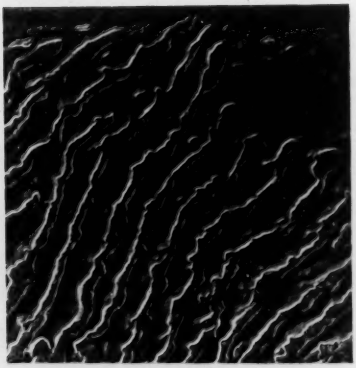

Fig. 5. Carbon replica of pearlitic steel etched in $\frac{1}{4}$% nital for 60s. Shadowed at $\tan^{-1}\frac{1}{2}$ with gold palladium. (×12000)

from the optical microscope and a thin film of Formvar is cast on the surface from a $\frac{3}{4}$% solution in chloroform containing 20% dry dioxane [Fig. 2(*a*)]. The purpose of the dioxane is to cause the preliminary Formvar replica to strip easily at a later stage. The specimen, with the Formvar film still on it, is now returned to the optical microscope and the feature or area of interest located in the centre of the field, using an ordinary 16 mm objective. This is then replaced by the objective fitted with an attachment as described, and having a centre-marked grid in position. The position of the grid is now adjusted so that it is just above the focal point of the microscope, i.e. the bars are slightly out of focus. The microscope tube can now be lowered until the specimen appears in focus below the grid bars. The feature of interest is then located in a suitable grid square by means of the stage controls. Fig. 3 shows an electron microscope grid (made by Smethurst Highlight Ltd.) type Gap 150, with a large centre square, in position over an area marked by the intersection of two scratches. The microscope column is now lowered so that the grid is pressed firmly against the specimen by the pins [Fig. 2(*b*)]. One or two drops of 1–2% Bedacryl* in ether is allowed to fall on the metal specimen from a micropipette introduced at the notch marked *H* on Fig. 1. Sufficient solution must be applied to allow it to flow over the grid. A stream of cold air from a dryer will cause the ether to evaporate in a few seconds, the film of resin produced anchoring the grid in position [Fig. 2(*c*)]. The microscope is then re-focused so that the position of the feature on the grid can be checked. The specimen is then removed from the stage and the grid separated from the metal with a pair of fine-pointed forceps. The replica remains in position on the grid as shown in Fig. 2(*d*). A thin layer of carbon is now deposited on the structure surface of the Formvar [Fig. 2(*e*)], which is then washed off[5] by bending the grid slightly, placing it on a peg about 2 mm below the nozzle of a burette, and then allowing about 5 ml of chloroform to flow over it. The solvent also removes the Bedacryl backing, but the carbon film remains firmly anchored in its original position [Fig. 2(*f*)], probably by a small amount of undissolved plastic remaining between the grid bars and the film. The grid is now ready for examination in the electron microscope, but it is advisable to examine the specimen optically under vertical illumination to ensure that the feature of interest is intact.

There are two limitations to this method, the first being that if the specimen is to be shadowed, the material must be deposited through the grid bars so that it is on the "positive" surface of the replica. This limits the angle of shadowing to 3 : 1. Another limitation is encountered when examining heavily-etched steel surfaces. It has been found that the preliminary impression does not come away from the metal if the etch is very deep. So far, this limitation has only been encountered in connexion with steel specimens.

Both these difficulties can be overcome by the use of a slightly more complicated procedure. A film of Formvar is cast on the metal, as above, and then backed with Bedacryl from a 7% solution in benzene. The composite film is breathed on and dry-stripped from the metal with cellulose tape. The carbon film is deposited on the Formvar surface and then the whole assembly fixed to a microscope slide for support and placed in a bath of acetone. The Bedacryl rapidly dissolves, allowing a very thin metal lifting tool to be slipped between the Formvar-carbon film and the tape. This combined film is then lifted from the acetone and floated on a water surface from which it can be collected on a microscope slide, carbon upwards, and dried. When viewed under vertical illumination in the optical microscope, this film closely resembles the appearance of the original specimen and it is possible to pick out the selected feature, which is then positioned beneath a grid by means of the attachment as described above. 1–2% Bedacryl solution is again applied and dried, and the grid with the replica adhering to it is removed from the slide with sharp forceps. Washing is carried out as before. The replica can then be shadowed in the normal manner. It has been found possible to strip Formvar films from very heavily-etched specimens by this method, the first part of which is similar to the carbon replica technique described in detail elsewhere.[5]

* Bedacryl 122X is a soluble resin made by Imperial Chemical Industries Ltd., and supplied as a 40% solution in Xylene which is diluted to 1–2% with ether.

RESULTS

The method is illustrated by Figs. 4 and 5. These show the same area of a pearlitic steel specimen. In Fig. 4, the specimen was subjected to a light etch in $\frac{1}{4}$% nital. Here, the structure is just visible, and is badly obscured by debris from the worked layer. A heavier etch, however, completely removes this debris and throws the carbide lamellae into sharp relief, as shown in Fig. 5.

CONCLUSIONS

A method for examining selected areas has a wide field of applications, one of which, the effect of etching time on a given field of a metallurgical specimen, has already been illustrated.[7] The formation of slip lines could also be followed in the same way. In addition, the ability to correlate results obtained from optical and electron microscopes is of considerable value. A suspected artefact, which may have been produced in the replica process, can immediately be checked by taking another replica from the same field.

In many laboratories, it may be necessary to take a very large number of replicas from a specimen, and the above method not only permits the use of the carbon replica with its many advantages, but also cuts down the time required to prepare the specimens; after a specimen has been suitably marked, an experienced operator can remove a Formvar preliminary impression in from three to five minutes. Thus, a given field can be replicated and shadowed ready for examination in less than an hour.

ACKNOWLEDGEMENTS

The author wishes to thank Mr. M. E. Haine for his interest and encouragement, Mr. E. Pesterfield for designing and constructing the objective attachment, and Dr. T. E. Allibone, Director of the Laboratory, for permission to publish this paper.

REFERENCES

(1) HYAM, E. D., and NUTTING, J. *Brit. J. Appl. Phys.*, **3**, pp. 173–6 (1952).
(2) NANKIVELL, J. F. *Brit. J. Appl. Phys.*, **4**, p. 141 (1953).
(3) BOOKER, G. R. *Brit. J. Appl. Phys.*, **5**, p. 349 (1954).
(4) BRADLEY, D. E. *Brit. J. Appl. Phys.*, **5**, p. 65 (1954).
(5) BRADLEY, D. E. *J. Inst. Metals*, **83**, p. 35 (1954).
(6) NUTTING, J., and COSSLETT, V. E. *Symposium on the Metallurgical Applications of the Electron Microscope*, 1949. Monograph No. 8, p. 65 (London: Institute of Metals, 1950).
(7) BRADLEY, D. E. *Metallurgia*. To be published.

The influence of cathode standing waves on valve stability

By W. W. H. Clarke, Ph.D., A.M.I.E.E., A.Inst.P., Defence Research Board, Ottawa, Ontario, Canada

[*Paper received* 4 *July*, 1955]

While a cathode emits more electrons than are required to supply the current demanded by other electrodes, it was generally accepted that the current cannot change appreciably with cathode temperature. Considerations of the current drawn by fixed electrode potentials, during change of cathode activation, have subsequently accepted a change in emitted electron energy spectrum as a cause of small current changes, since the change in potential depression in the virtual cathode cannot entirely compensate for the altered emission. Thus the present conception is of a smooth current variation with activation (temperature). The paper shows how standing waves in the virtual cathode tend to modify this simple model.

A qualitative assessment of the possible effects of standing waves in the virtual cathode on the variations of current drawn leads to conclusions with which the experimental results are consistent. Time anomalies in the variations of current drawn under static conditions are revealed by experiment, and it is concluded that the major factor controlling the current characteristic is the standing wave pattern. It is postulated that changes of pattern are responsible for flicker effect.

List of symbols

n, m	Integers describing the number of nodes in the standing wave pattern along and across the cathode.
V_A	Anode potential
$i(n, m, V_A)$	Valve current
$\phi(n, m)$	A function of the numbers of nodes in the standing waves
$P(n), Q(m)$	Polynomials
δi	A change in valve current
Δi_1	Change of current in upper bridge arm
Δi_2	Change of current in galvanometer
V_B	Voltage applied to the bridge ($V_A = V_B - Ri$)
R	Equivalent anode load of valve
a, b	Dimensions of the cathode (equivalent rectangle)
a_0, a_1, a_2	Polynomial coefficients

1. Introduction

This paper is concerned with the slow fluctuations and drifts which occur in the current drawn from the cathode of an electronic valve under conditions of static applied potentials. These may be regarded as manifestations of "flicker effect" at very low frequencies, but for understanding the experiments and interpretation, the mean steady current approach is desirable initially. Changes which persist for an appreciable time with respect to a steady current reference have been studied, and the steady state approach has been employed, both in their measurement and in their interpretation. The phenomena described may also play their part in contributing to noise at all frequencies.

In some work with low energy beams of circular symmetry,[1] it was found that standing waves existed on the cathode in the form of concentric circles, and that the pattern changed critically for very small changes in electric field. The different patterns were associated with step changes in the current/voltage characteristic for individual electrodes. There was also a slight indication that the total cathode current characteristic took very small steps. At different cathode temperatures, the changes from one pattern to another occurred at different voltages in the characteristic. These conclusions are consistent with the work of Klemperer,[2] who discovered such standing waves to occur in two directions, across and along the surface of a much larger rectangular cathode.

The steps in current/voltage characteristics indicate a preference by the space charge of the virtual cathode for particular patterns, presumably satisfying conditions imposed by the cathode boundary. Hence in the event that several different (preferred) patterns can be supported under substantially the same electrode potentials, it seems less reasonable to assume that the current drawn from the cathode in the different pattern conditions remains constant, than to assume it changes with each change of pattern. Experiments are described in this paper, which show that pattern changes occur, and act in such a way as to cause the variations of current drawn from a valve cathode to be striated, indicating that the standing wave patterns satisfy boundary conditions on or near the cathode and are each associated with a particular current characteristic. This mechanism of cathode emission fluctuations is interpreted in terms of flicker noise.

2. Nature of the problem

Circular standing waves[1] were associated with a very small cathode and, for the same order of wavelength, a much larger number of waves would be expected to occur in the cathode of a conventional electronic valve while the thermal or surface changes, required to induce a change of pattern, could be much smaller. Suppose a cathode to be supporting a standing wave pattern with n nodes (where n is a large integer). Then the simplest pattern changes which might occur, disregarding singularities or distorted patterns with nodes not persisting right across the cathode,[2] would involve a change from n to $n + 1$. Now n is a parameter supposedly determined uniquely by the state of the cathode, and therefore it is probable that the current drawn from the cathode with fixed electrode potentials may be expressed as a polynomial in n. Such polynomials, used to describe physical relationships, usually have rapidly decreasing coefficients, so that the actual contribution to current of powers of n higher than 4 (say) may well be negligible, to the extent that the experimental work should be designed to discover preferred values of cathode emission which are equispaced. In fact Klemperer's findings indicate wavelengths between 0·2 and 2 mm, therefore n for these experiments may lie between 10 and 100. To take account of changes along and across the cathode, preferred levels would comprise equispaced families of equispaced emission levels.

These considerations may be written:

$$i(n, m, V_A) = \phi(n, m)V_A^{3/2} = P(n)Q(m)V_A^{3/2} \qquad (1)$$

Where P and Q are polynomials and a 3/2 power law is assumed.

$$\delta i \text{ (for } n \to n+1) = \frac{\partial i}{\partial n} = P'(n)Q(m)V_A^{3/2} \qquad (2)$$

In a valve with an anode load, the anode potential becomes a function of the current and the load, hence:

$$i(n, m, V_B) = \phi(n, m).(V_B - Ri)^{3/2} \qquad (3)$$

Hence:

$$\frac{\partial i}{\partial n} = P'(n).Q(m)(V_B - Ri)^{3/2} - \frac{3}{2}R\frac{\partial i}{\partial n} \cdot P(n)Q(m)(V_B - Ri)^{\frac{1}{2}}$$

Where the partial derivatives are now for constant supply potential and not anode potential:

$$\frac{\partial i}{\partial n} = P'(n).Q(m)(V_B - Ri)^{3/2}[1 + \tfrac{3}{2}R.P(n)Q(m)(V_B - Ri)^{\frac{1}{2}}]^{-1} \qquad (4)$$

Again, for a small range of values of n with n large, this may be substantially constant. The same considerations apply with respect to m.

Physically, if the emission current (with or without an anode load), under constant applied potentials, varies with n, then a tangent may be drawn to the curve of current as a function of n. This tangent may be expected to approximate to the curve for a small range of n at large values of n.

The foregoing considerations lead directly to the experimental method of seeking the existence of preferred emission levels.

3. EXPERIMENTAL METHOD

Since it was desired to detect and measure accurately small changes in the anode current of a valve, and since such changes were known to comprise the instability fluctuations normal to valves, the order of sensitivity required was known. A bridge circuit as in Fig. 1(*a*) was employed with a sensitive galvanometer. The resistors in the circuit were all wire-wound and the potentials were all derived from batteries. Time was allowed for the equipment to settle at room ambient temperature and the bridge then approximately balanced by control of grid bias. In this condition, the variations of current in the valve should be represented by changes in the galvanometer reading to which they are linearly related. The values of the resistors in the arms of the bridge produce a relationship of 7 to 3, between the valve current changes and the galvanometer current changes. This relation, and the implied change in the constant of an approximate 3/2 power law for constant bridge voltage of 90 V, are derived in the Appendix.

Two methods of recording the variations were employed initially:

(i) The galvanometer reading was taken at regular intervals of time, the nearest scale calibration point being recorded, and the intervals were usually chosen to be approximately 8 s, their occurrences being signified by an audible counter in order not to distract visual attention from the galvanometer.

(ii) The galvanometer was observed continuously and when the reading became constant for 2 or 3 s the value of such a reading was recorded. This was a more difficult method and required a consistency of judgment hard to maintain for sustained periods of measurement.

If step changes in current were occurring at a fairly fast average rate, it was possible that only occasionally would the galvanometer give a reading characteristic of one of the preferred "cathode states"; hence the second method of recording. If the stable states mainly persist for appreciably longer times than the transition times between states the first method is preferable, in being substantially independent of observer bias.

Plots of galvanometer reading against the number of occurrences were generally used to study the "emission pattern." A difference analysis was also used in which the number of occurrences of each difference is plotted, on the assumption of equispaced emission levels. This second method of analysis is probably more easily adapted to the second experimental method than to the first, but the very long time taken to obtain results made it less useful.

The experimental establishment of significant results with the first method led to a photographic method of recording, which confirmed the significant preferred galvanometer readings. A galvanometer spot was reduced to a vertical slit (horizontally deflected) and photographic time exposures were taken of the scale, in suitably dark surroundings. The advantages of the photographic method are in the elimination of observer factors and in the use of an integration as a measure of preferred scale position. It is, however, difficult to assess an absolute measure of preference with this method, though it is qualitatively better for establishing the existence of preferred levels.

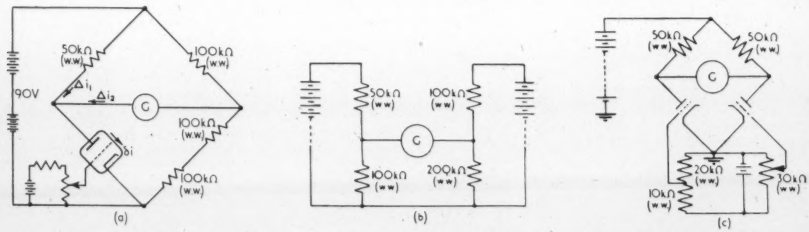

Fig. 1. (*a*) Instability measuring bridge. (*b*) Potentiometer test circuit. (*c*) External drift cancelling bridge

Apart from cathode condition changes which are assumed to operate through the standing wave pattern mechanism, there are other sources of instability in the circuit. Variations of battery potentials, contact potentials and resistance values might mask the effect sought. Tests indicated that they were substantially smaller than the measured fluctuations in the

bridge circuit, Fig. 1(*a*). The sensitivity of the galvanometer to changes in bridge voltage is 8 μA/V, while two unequally loaded batteries in a potentiometer circuit, Fig. 1(*b*), have a sensitivity to either voltage change of 6 μA/V. Over periods of about 30 min this circuit indicated changes of less than 10^{-8} A.

Perhaps the most convincing check was provided by studying drifts in a bridge circuit, Fig. 1(*c*), which compared the two halves of a double triode. The galvanometer current excursions were of the same order as those in the circuit of Fig. 1(*a*) presented in the paper, and preferred emission levels were clearly indicated. Battery voltage drifts and resistance changes with temperature are automatically cancelled by this circuit.

Finally, the temperature coefficient of the resistors (0·0025% per °C) is small enough to be ignored in normal indoor conditions.

4. EXPERIMENTAL RESULTS

Experiments with a galvanometer for which 1 scale division corresponds with $8{\cdot}4 \times 10^{-9}$ amperes were performed first. Fig. 2 is a typical histogram obtained at this stage of the work; the appearance of a slight ripple overlaid on a normal distribution was not regarded as very significant, though it appeared with fair consistency. For further work a galvanometer with greater sensitivity and several ranges was brought into use to take readings with various sensitivities.

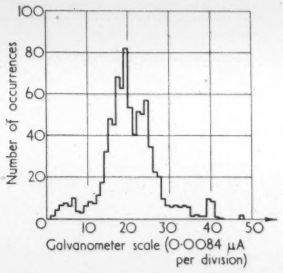

Fig. 2. Readings taken at 8 s intervals

Histograms of readings, taken with the most sensitive galvanometer setting (3×10^{-10} amperes per scale division), gave results of which Figs. 3 and 4 are typical of readings taken by methods (i) and (ii) respectively. While these readings were taken, the galvanometer spot spent a considerable time off scale at each end of the scale. The distributions of reading frequencies indicated a distinct preferred valve current region on the galvanometer scale, while the large time spent off scale indicated the existence of other preferred regions which might or might not be fairly closely defined, as is the case for the "on scale" distribution. These histograms were plotted with lower resolution than was available, in "bunches of six" and "bunches of three," because it seemed impossible to interpret the fine structure. The fine structure was probably not significant, and it obscured the overall picture. Adding successive batches, it was possible to bunch (0–5, 6–11, 12–17) or (1–6, 7–12, 13–18) or etc., and it was found that the shapes of the distributions were practically independent of where the batches start.

Fig. 3(*a*) shows "bunches of six" which gave a fairly smoothed curve, while Fig. 3(*b*) in "bunches of three" indicates the presence of peaks and minima with irregular structure in which consistent spacings do not occur. The amplitude of the overlaid ripple appears large for the numbers involved in the ordinate values.

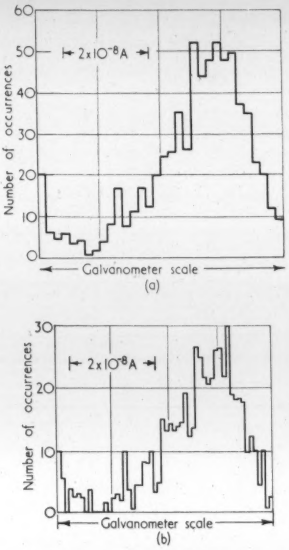

Fig. 3. Distribution of reading occurrences. Readings taken at 8 s intervals

(*a*) Repetitions grouped in sixes.
(*b*) Repetitions grouped in threes.

Fig. 4, which is a distribution taken with repetition of readings at "rests," is inconclusive, and it took substantially longer for appreciable numbers of readings to accumulate. Hence these results are not supported by many sets of readings giving similar results, as is the case with the time interval readings, and the few sets which were taken have not any very significant features. Plots of reading differences, for

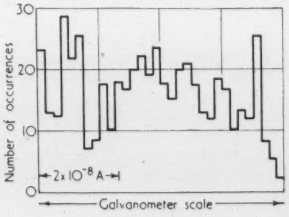

Fig. 4. Distribution of reading occurrences. Readings taken at rest. Repetitions grouped in sixes

readings close together in time (taken as "rests"), failed to produce positively useful information, but the distribution of differences seemed too irregular to be in accord with random statistics.

On the assumption that the single maximum of Fig. 3 and of other similar tables was one of several, the others being occupied when the galvanometer spot was "off scale," less sensitive measurements were made.

A series of experiments established the existence of different maxima, and Fig. 5 shows typical experimental results.

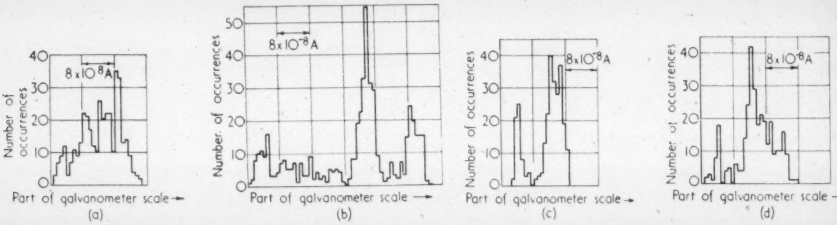

Fig. 5. Distribution of reading occurrences. Readings taken at 10 s intervals. Repetitions grouped in threes

These curves apply to one particular electron tube, for a particular value of anode potential and cathode current, but it is possible to observe similar distributions under different conditions and with different electron tubes. Fig. 6 shows how the peaks become more pronounced with less resolution.

In particular, Figs. 5(*c*) and (*d*) are graphs of readings taken on the same day, without permitting the cathode to cool between sets of readings. The similarity of the two distributions is clear.

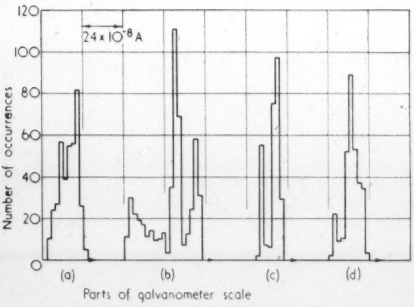

Fig. 6. Distribution of reading occurrences. Readings taken at 10 s intervals. Repetitions grouped in nines

With its advantages and limitations, the photographic integration of time spent by the galvanometer in each scale position was a powerful tool in these experiments. It was found that the taper in width at each end of the illuminating slit enhances the intensity effect by providing an intensity variation across the scale. Thus the more intense lines appear wider.

For a variety of time exposures, since a fixed focus camera was in use, it was found expedient to use a rectangular aperture giving a fixed defocus along the scale and variable defocus transversely; otherwise a larger aperture might have blurred out the maxima. Hence a notation for the lens aperture was adopted in which the first f number refers to the aperture dimension transverse to the scale and controlled by the normal circular aperture; the second f number refers to the width of the slit superimposed on the front of the camera.

Several valves have been investigated by this method with different values of anode potential [in the results the bridge potential V_B is specified, and the circuit values cause the anode potential V_A to be approximately $\frac{1}{3} V_B$ when near balance]. Before considering these results, it is important to state that the appearance of the "emission pattern" differs from valve to valve, from one current drain to another (caused by different values of V_B) and within valves from one run to the next. A run is defined as any period during which the cathode remained heated by a stable battery and the bridge potential was continuously applied, while minor changes of grid potential were permitted between photographs if necessary to bring the bridge towards balance. Some well-defined features, however, remain common to the patterns. Again, there is a tendency for the drift to vary in nature; sometimes quite fast back and forth and on and off scale, at other times slow drifting and apparent locking at points. But with either drift behaviour similarities of pattern occur. The range of drift appears to vary from run to run and from valve to valve, so that different resolution pictures were easily obtained.

Fig. 7 presents the apparent slit widths as seen by the camera for different apertures along the galvanometer scale, which indicates the resolution employed in looking at the galvanometer slit.

Fig. 7. Sizes of reference slits
(*a*) Aperture $f/22 \times f/22$.
(*b*) Aperture $f/4 \times f/40$.
(*c*) Aperture $f/2{\cdot}8 \times f/80$.

Figs. 8–11 present results for different valves of which that of Fig. 8 received extensive attention under different conditions. In Fig. 8(*a*) a fairly low resolution picture is obtained

of the valve in a mode of behaviour similar to that observed for valve No. 1 by repetitive galvanometer readings; (I)–(V) all show definite preferred regions with a tendency for a pair of intense lines to occur close together. Fig. 8(*b*) shows results with a better resolution under the same circuit conditions. Reduced cathode current results at three resolutions are presented in Figs. 8(*c*), (*d*) and (*e*). Fig. 8(*c*) shows some remarkably intense maxima and trace (i) is perhaps the most impressive, though it is probably a matter of exposure which makes the lines stand out from the background; in (i) it is thought that the galvanometer may have spent a greater portion of the exposure time "off scale," so that an optimum exposure was obtained. There are significant lines at similar spacing in the results (II)–(V) which may best be noted from the edges of the traces.

During a long run, valve No. 2 became more stable than usual and it was found possible to obtain Figs. 8(*d*) and (*e*). These results would not conflict seriously with an interpretation in terms of minor preferred states closely spaced and major preferences at wider spacing. Fig. 8(*f*) is for a still lower current drain which provided greater stability and results not dissimilar in character from those at higher current.

Results for valve No. 3, given in Figs. 9(*a*) and (*b*) for two values of current, show similar preferred states at the higher current, at similar spacing to valve No. 2 in the same conditions. The lower current produces a trace similar to Fig. 8(*c*) but of slightly closer spacing.

Valve No. 4 was only tested at $V_B = 90$ V (corresponding with the highest current drain). The preferred states were less marked with this valve, as shown in Figs. 9(*a*) and (*b*).

Valve No. 6 at $V_B = 67{\cdot}5$ V was initially thought to have no stable states but they were revealed at a substantially wider spacing against an almost level background in Fig. 11.

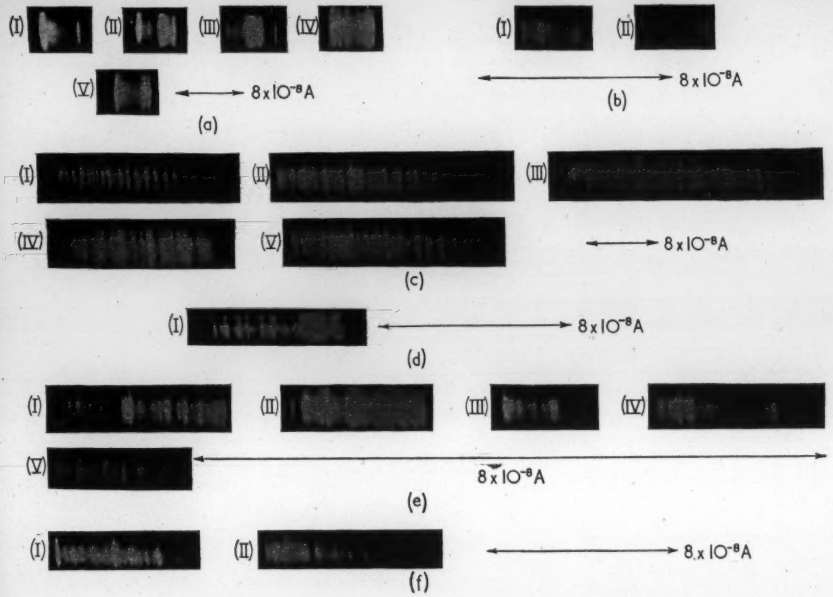

Fig. 8. Results with valve No. 2.

(*a*) $V_B = 90$ V. (II) and (III) same run. (IV) and (V) same run
(I) 90 min. Aperture $f/80 \times f/80$.
(II) 30 min. Aperture $f/5{\cdot}6 \times f/40$.
(III) 30 min. Aperture $f/5{\cdot}6 \times f/40$.
(IV) 25 min. Aperture $f/2{\cdot}8 \times f/40$.
(V) 20 min. Aperture $f/2{\cdot}8 \times f/40$.

(*b*) Aperture $f/2{\cdot}8 \times f/40$. Consecutive exposures of 10 min. each. $V_B = 90$ V

(*c*) Aperture $f/2{\cdot}8 \times f/80$. $V_B = 67{\cdot}5$ V
(I) 40 min. (II) 42 min. (III) 40 min. (IV) 54 min. (V) 50 min.

(*d*) $V_B = 67{\cdot}5$ V. 100 min. aperture $f/11 \times f/80$

(*e*) Aperture $f/2{\cdot}8 \times f/80$. $V_B = 67{\cdot}5$ V
(I) 20 min. (II) 30 min. (III) 15 min. (IV) 20 min. (V) 20 min.

(*f*) Aperture $f/2{\cdot}8 \times f/80$. $V_B = 45$ V
(I) 20 min. (II) 25 min.

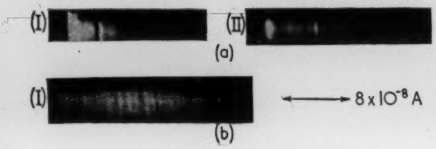

Fig. 9. Results with valve No. 3.

(*a*) Aperture $f/2{\cdot}8 \times f/80$. $V_B = 90$ V.
(I) and (II) same run
(I) 22 min. (II) 10 min.

(*b*) Aperture $f/2{\cdot}8 \times f/80$. $V_B = 67{\cdot}5$ V
30 min.

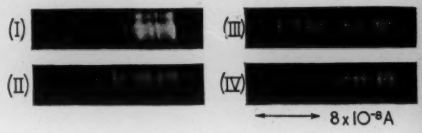

Fig. 10. Results with valve No. 4. $V_B = 90$ V

(I) 55 min. Aperture $f/11 \times f/80$.
(II) 23 min. Aperture $f/2{\cdot}8 \times f/80$.
(III) 30 min. Aperture $f/2{\cdot}8 \times f/80$.
(IV) 17 min. Aperture $f/2{\cdot}8 \times f/80$.

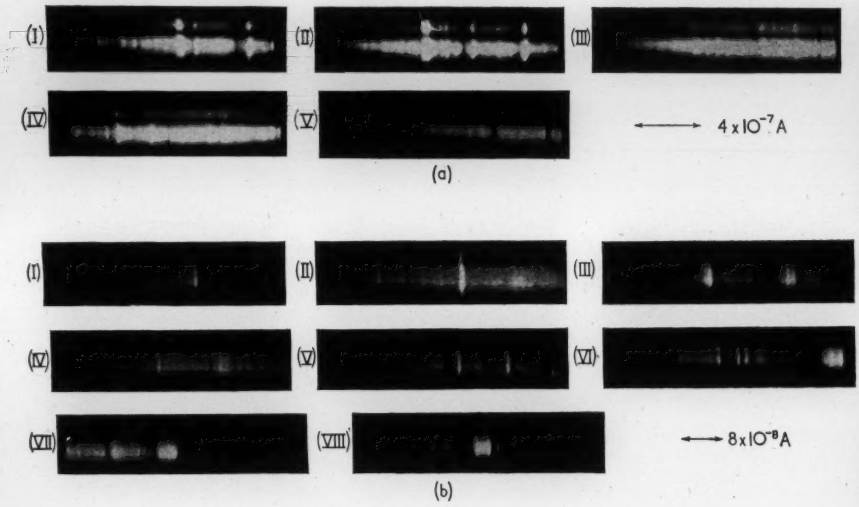

Fig. 11. Results with valve No. 6.

(*a*) $V_B = 67{\cdot}5$ V. All one run

(I) 80 min. Aperture $f/8 \times f/40$.
(II) 110 min. Aperture $f/8 \times f/40$.
(III) 100 min. Aperture $f/5{\cdot}6 \times f/40$.
(IV) 60 min. Aperture $f/5{\cdot}6 \times f/40$.
(V) 50 min. Aperture $f/5{\cdot}6 \times f/40$.

(*b*) $V_B = 67{\cdot}5$ V. (I)–(VI) same run.
(VII) and (VIII) same run

(I) 15 min. Aperture $f/2{\cdot}8 \times f/40$.
(II) 20 min. Aperture $f/2{\cdot}8 \times f/40$.
(III) 20 min. Aperture $f/2{\cdot}8 \times f/40$.
(IV) 20 min. Aperture $f/2{\cdot}8 \times f/40$.
(V) 20 min. Aperture $f/2{\cdot}8 \times f/40$.
(VI) 20 min. Aperture $f/2{\cdot}8 \times f/40$.
(VII) 13 min. Aperture $f/4 \times f/40$.
(VIII) 11 min. Aperture $f/4 \times f/40$.

This valve behaves distinctively in its different runs and the similarity of patterns obtained within a run is in marked contrast to the differences from one run to another.

From the results certain general conclusions regarding spacings have been tabulated:

Valve No.	$V_B = 90\ V$	$V_B = 67\frac{1}{2}\ V$	$V_B = 45\ V$	
1	$7\text{–}9 \times 10^{-8}$	—	—	Major preferred spacings
2	$4\text{–}8 \times 10^{-8}$	3×10^{-8}	$2\text{–}3 \times 10^{-8}$	
3	$6\text{–}8 \times 10^{-8}$	2×10^{-8}	—	
4	$3\text{–}6 \times 10^{-8}$	—	—	
6	—	$3\text{–}6 \times 10^{-7}$	—	
1	$2\text{–}3 \times 10^{-8}$	—	—	Minor preferred spacings
2	10^{-8}	3×10^{-9}	$2\text{–}5 \times 10^{-9}$	
3	10^{-8}	5×10^{-9}	—	
4	10^{-8}	—	—	
6	—	$1\text{–}2 \times 10^{-7}$	—	

Values given represent order of magnitude only.

5. DISCUSSION AND INTERPRETATION

The experimental results are taken to prove that the cathode of an electronic valve has definite preferred emission levels, and that these levels have characteristic distributions. The distribution can change for the same valve from run to run and perhaps during a run but the general nature does not change. The tabulation of apparent preferred spacings seems to indicate a fair similarity for valves 1–4 while valve 6 appears to be anomalous in some respects. A wide spread is not unexpected since flicker noise in valves is known to be very variable from one to another.

In addition to the points noted in connexion with the photographic results, there is a tendency for the patterns to have intense lines at one or both sides. For the whole of Fig. 8, in 24 cases out of a possible 40, there is such an occurrence, which may be interpreted by the drift in either direction being halted by the presence of a strong pattern. In many cases the range of drift takes the spot off scale so that it cannot be determined whether the end of the distribution coincides with an intense "line." Even for the wider "fully on scale" distributions there is a taper in intensity towards the edges due to a fall off in scatter from the galvanometer screen,* which may hide the presence of an intense line at the limit of excursion.

Accurate regularity of spacings is not supported by the results, though there is a tendency, in Fig. 8(*a*) for example, for spacings of the same order to occur. However, the preference for particular emission levels is clearly indicated.

If the model on which the experimental work was based behaved as a "perfect" rectangular emitting area, with n and m half wavelengths along and across the area, it would be possible uniquely to specify the current by $i(n, m)$ under constant field conditions.

Furthermore, it may be seen, from consideration of any unit square of emitter surface, that the current drawn from it is unlikely to be directly affected by the standing waves in the other parts of the cathode, except for the interlocking of patterns. It is thought that the best choice of parameter for the polynomial is the number of half wavelengths per unit length on the cathode. The polynomials will then refer to a unit square and will need to be multiplied by $a.b.$ where a and b are the (rectangular) dimensions of the cathode, in order to obtain the total cathode current. If it is now assumed that the wavelengths in the two directions are substantially the same, then there is no reason why the polynomials should not be the same in which case:

$$i(n, m) = a.b.P\left(\frac{n}{b}\right)P\left(\frac{m}{a}\right)V_A^{3/2}$$

$$= a.b.\left[a_0 + a_1\left(\frac{n}{b}\right) + a_2\left(\frac{n}{b}\right)^2 + \ldots\right] \times \left[a_0 + a_1\left(\frac{m}{a}\right) + a_2\left(\frac{m}{a}\right)^2 + \ldots\right] \times V_A^{3/2} \quad (5)$$

The wavelengths being approximately the same provides the condition:

$$\frac{m}{a} \simeq \frac{n}{b}$$

which may be used to show that:

$$\frac{\partial i}{\partial n} = \frac{m}{n}\frac{\partial i}{\partial m} = \frac{a}{b}\frac{\partial i}{\partial m} \quad (6)$$

Therefore the spacing of preferred emission levels for the two directions on the cathode should be in the ratio of the two dimensions. This, for the cylindrical cathode of the type of valve used, is a ratio of length to circumference of slightly less than 3. The postulated equispaced emission levels are indicated in Fig. 12 which shows a very small portion of the

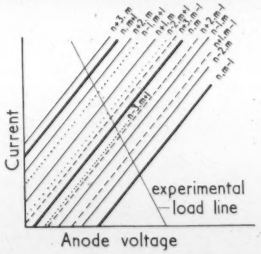

Fig. 12. Portion of postulated emission characteristics

assumed characteristic of emission. The tabulated preferred spacings for major preferences and minor preferences have a ratio of the same order of magnitude as the dimensional ratio of the cathode. Thus the minor spacings could represent pattern changes along the cathode, and the major ones around the cathode.

It is probably unjustified to pursue the interpretation on lines of perfect patterns, however, because there appears to be a reasonable case for the introduction of partial patterns and irregularities in boundaries in order to explain practical phenomena. The evidence for the nature of the waves presented by Klemperer[2] indicates that the waves, on a strip cathode (rectangular), do not run exactly parallel with the sides, and that an antinode may stop short and the antinodes on either side may carry on, reducing their separation to a half wavelength as soon as consistent with the

* The intensity response and the freedom of the galvanometer were simultaneously checked by applying a symmetrical 0·05 c/s triangular current waveform to the galvanometer.

boundaries. It is suggested that the cathode does not behave in a manner obedient to exact regular patterns, but behaves in a sufficiently coherent manner that the overall pattern is consistent with local variations of emission properties and the local pattern changes they demand. The change of pattern in one region controls or tends to control that in another, and the present experimental results may best be interpreted as evidence of the coherence of pattern changes.

In the foregoing interpretation in terms of change along and across cathodes (for cases of Cartesian symmetry) it is implicit either that the orthogonal sets of waves have the same frequency, but associated with a different mean transverse velocity of electrons or they have different frequencies. It seems quite likely that the two sets of waves could occur at slightly different distances from the cathode surface, so that changes of pattern result in changes of spacing from the cathode. Such a longitudinal movement of the pattern and the potential maxima and minima it imposes across the current flow can clearly control changes in current with constant electrode potentials. Thus a valve, with only one pattern permitted to exist in its virtual cathode, would have an emission characteristic corresponding with only one of the curves indicated by Fig. 12, while a valve in which the cathode surface was maintained under constant conditions (of temperature and contamination) would have a characteristic of the nature indicated by Fig. 13.

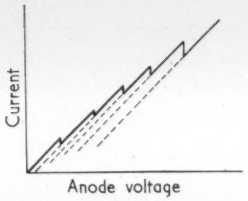

Fig. 13. Postulated emission characteristic

Klemperer has noted that change of electrode potential produces very great pattern changes, so that this is probably the overriding factor, while cathode surface conditions can modify the choice of pattern slightly. For the emission by part of a cathode, characteristics of which Fig. 15 is typical have been obtained,[1] with slight variations in the applied potentials at which the steps occurred.

Taking Klemperer's figures for wavelength, the expected order of $\Delta n/n$ is, say, 1/50 (for $\Delta n = 1$); while the values of $\Delta i/i$ for major preferred spacings are in the neighbourhood of 1/5000, indicating that the virtual cathode compensates to a large extent for the imposed change; a familiar process in electronic cathodes.

6. RELATIONSHIP BETWEEN PATTERN CHANGES AND NOISE

Since the effect of standing waves on the cathode emission is shown to be a control of current by specific patterns, noise assumes importance. The patterns do not change infinitely slowly, and therefore, when they change, they are associated with a current transient. It is believed that this type of noise is in fact "flicker effect,"[3–5] which, briefly, has been explained as the occurrence of singularities in the cathode coating, which emit streams of electrons in bursts. This argues that the singularities are intermittent. The standing wave pattern structure modifies the picture, by adjustments of pattern to conform with a slightly greater supply of electrons from any part of the cathode. Thus a small streamer, feeding the virtual cathode, could affect the whole pattern, and alter the emission from the whole virtual cathode. It is not then necessary to assume that local streams of electrons break through the virtual cathode to provide the whole of the flicker noise current from isolated individual regions.

Recent work on flicker effect in valves has been of a statistical nature based on the generally accepted theory that bursts of electron emission occur at random, with random location, and with a probable time interval determined by impurity content of the emitter. Experimental work,[6–10] has measured the spectral noise distributions and magnitudes in relation to emitter variations, and theoretical work[11, 12] has endeavoured to combine the random phenoma suitably to explain measurements. Another area of investigation is offered by the proposed insertion of an intermediate mechanism between emission from the cathode and departure from the virtual cathode.

The qualitative application of this mechanism to explain flicker phenomena appears to simplify interpretation.

For example, the partition components of flicker noise in pentodes[13] have been explained on the assumption that the patches of excess emission are small compared with the diameter of the screen grid wires; the corresponding explanation would only require that the wavelength of the standing wave pattern is small compared with the wire diameter. Again[14] the discovery of predominant lines in the spectral distribution of electrons may be explainable by the retention in the pattern of electrons with a particular velocity, and the break up under pulsing into several lines by the transient manufacture of new patterns which are different in different parts of the cathode.

van der Ziel[15] indicates clearly that there are good theoretical grounds for expecting flicker noise to be less in valves with larger cathodes, and refers to experimental comparative difficulties, which have prevented the proper measurement of any improvement. Interactions extending across the cathode through the space charge, are, in the author's opinion, responsible for the aggravation of flicker effect in larger cathodes so that no improvement is realized. In fact, it appears necessary only to dissociate larger cathodes into multiple emitting areas, whose virtual cathodes cannot couple with one another, in order to achieve reductions in flicker noise consistent with theory.

The experimental results would provide, for a change between major preferred currents, a current transient of the order of 2×10^{-7} A, equivalent to some 60 μV at the grid of an average valve; a value consistent with the results of Harris and Bishop.[10]

7. CONCLUSION

From the experiments performed, it is concluded that when the standing wave patterns in the space charge of the virtual cathode of a valve change, they do so in a manner determined by the local variations of emission properties and by the boundary conditions of the cathode. It is also concluded that each pattern is associated with a particular current characteristic, so that a valve can have several preferred emission levels for constant applied potentials,

intermediate values of current being associated with patterns in a slightly unstable condition which are not entirely compatible with the cathode boundaries or singularities. The patterns change coherently and cause discrete current changes. Therefore, the instability of standing current in a valve is aggravated by the extension of pattern changes across the cathode.

It is suggested that the mechanism of flicker effect is related to standing wave pattern changes, in such a way that the bursts of local emission from the coating modify the pattern, and hence the current drawn from the cathode suffers a transient change. This mechanism appears to offer a satisfactory explanation of some well-known anomalies.

ACKNOWLEDGEMENTS

The work described was outside the author's normal course of duty; he is indebted to the Defence Research Board of Canada for the use of their facilities. On the basis of this work, the author has filed British Provisional Patent Application No. 13593/55, "Improvements in or relating to the cathode construction of thermionic valves," in which the Defence Research Board have confirmed his sole ownership of proprietary rights.

REFERENCES

(1) CLARKE, W. W. H., and JACOB, L. *Nature* [*London*], **168**, p. 1120 (1951).

(2) KLEMPERER, O. *Proc. Roy. Soc. A*, **190**, p. 376 (1947).

(3) SCHOTTKY, W. *Phys. Rev.*, **28**, p. 74 (1926).

(4) INUISHI, Y., and TSUNG-CHE, Y. *J. Phys. Soc. Japan*, **8**, p. 565 (1953).

(5) TOMLINSON, T. B. *J. Appl. Phys.*, **24**, p. 611 (1953).

(6) AMAKUSU, K. *J. Appl. Phys.*, **23**, p. 1330 (1952).

(7) LINDEMANN, H. H., and VAN DER ZIEL, A. *J. Appl. Phys.*, **23**, p. 1410 (1952).

(8) BERKTAY, H. O. *Wireless Engr*, **30**, p. 48 (1953).

(9) HIBI, T., and ISHIKAWA, K. *Phys. Rev.*, **95**, p. 1183 (1954).

(10) HARRIS, E. J., and BISHOP, P. O. *Nature* [*London*], **161**, p. 971 (1948).

(11) TOMLINSON, T. B., and PRICE, W. L. *J. Appl. Phys.*, **24**, p. 1063 (1953).

(12) SHINDO, T. *J. Phys. Soc. Japan*, **9**, p. 38 (1954).

(13) TOMLINSON, T. B. *J. Brit. Instn Radio Engrs*, p. 515 (1954).

(14) JANSEN, C. G. J., LOOSJES, R., and COMPAAN, K. *Philips Res. Rep.*, **9**, p. 241 (1954).

(15) VAN DER ZIEL, A. *Noise* (New York: Prentice-Hall Inc., 1954).

APPENDIX

In Fig. 1 a change, δi, of current in the valve produces a change, Δi_2 in the galvanometer, and Δi_1 in the 50000 Ω upper bridge arm. Δi_1 passes through this arm and the battery (zero impedance) and Δi_2 passes through the galvanometer and the 100000 and 200000 Ω resistors in parallel. Hence:

$$\frac{\Delta i_1}{\Delta i_2} = \frac{4}{3} \quad \text{and} \quad \delta i = \frac{7\Delta i_2}{3}$$

The valve current change is 7/3 times the galvanometer current change.

Assuming the approximate obedience of a 3/2 power law

$$i = KV_A^{3/2}$$

The valve current and voltage are approximately defined by the bridge balance conditions: $i = 600\ \mu\text{A}$, $V_A = 60$ V, giving $K = 1{\cdot}29 \times 10^{-6}$ (amperes × volts$^{-3/2}$).

Bridge impedances also define the change in anode voltage associated with δi:

$$\Delta V_A = -5 \times 10^4\, \Delta i_1 \simeq 2{\cdot}85 \times 10^4\, \delta i$$

δi therefore causes in the bridge circuit an effective change in K by ΔK where $\Delta K/K = 2380\delta i = 5556\Delta i_2$ which is the proportional change in K in terms of the galvanometer current change, when the bridge voltage is 90 V.

It is also possible to calculate the change in valve current ($\delta i|_v$) which would occur under constant anode voltage conditions:

$$\delta i|_v = \frac{\partial i}{\partial K}\bigg| \Delta K = 2380 i \delta i = 1{\cdot}43 i = 3{\cdot}3\Delta i_2$$

Hence the galvanometer change of current is 3/7 of the valve change, the voltage change associated is −28000 times the valve current change, the constant of the assumed 3/2 power law is $1{\cdot}29 \times 10^{-6}$, and the constant anode potential equivalent current change is 1·43 times the change in the bridge circuit and 3·33 times the galvanometer change.

The deposition of thin films of gold on cylindrical specimens by sputtering

By F. R. Lipsett, Ph.D.,* Davy Faraday Research Laboratory, The Royal Institution, London, W.1

[*Paper first received* 19 *April, and in final form* 16 *September*, 1955]

Apparatus and procedure are described for the deposition of very uniform thin films of gold on cadmium wires of 1 mm diameter. The effect of the geometry of the sputtering chamber is examined. Over-heating of the specimen is obviated by a simple device.

In a programme of research upon the effects of surface condition upon the mechanical behaviour of metals it was found necessary to deposit thin films of gold on cadmium single crystals of 1·0 mm diameter. After a series of experiments a simple technique for coating the specimens by cathodic sputtering was developed. The films were quite uniform in thickness and the sputtering process was, within wide limits, independent of the electrical arrangement of the sputtering chamber. The results obtained may be of use in other fields of research.

Although the sputtering phenomenon was discovered over a century ago, the mechanism by which the transfer of material takes place is not yet completely understood.[1] On the other hand a considerable number of empirical results have been amassed[2] which make possible the design of apparatus for certain purposes.

In designing the present apparatus a formula derived by Townes[3] was found to be of practical use. The formula gives the rate of deposition of material between concentric spherical or plane-parallel electrodes. For a given gas and given current flowing between the electrodes it may be expressed in a simplified form as:

$$J = \text{constant}/pD$$

where J = mass of material sputtered per unit time,
p = gas pressure,
D = anode-cathode distance.

The value of the constant depends upon the nature of the gas, the material being sputtered, and the current flowing. The formula should hold, at least approximately, for any sputtering arrangement with simple geometry, and this was found to be the case in the present experiments.

EXPERIMENTAL ARRANGEMENT

A diagram of the form of sputtering chamber used is given in Fig. 1. The chamber consists essentially of a cylinder of glass tubing, of such a length as to leave about ½ in. between cathode and anodes, on the inside of which a gold foil cathode was held by washers and bolts. The outside of the glass tubing was covered with earthed lead foil in order to prevent undesirable discharges, and the negative high tension lead to the gold foil was passed through glass tubing wrapped with earthed copper wire similarly to prevent undesirable discharge. The anodes and the belts holding the gold foil in place were of aluminium or steel, in order to eliminate undesirable sputtering.

In the experiments upon the method of sputtering, a polycrystalline wire of cadmium was used in place of the crystals. Before being placed in the sputtering chamber the wire of 1·0 mm diameter was carefully cleaned with Silvo and benzene and rolled straight between two pieces of plate glass separated from the wire by clean pieces of paper. In the first few experiments the wire was connected electrically to the anodes. This was found to heat the wire excessively,

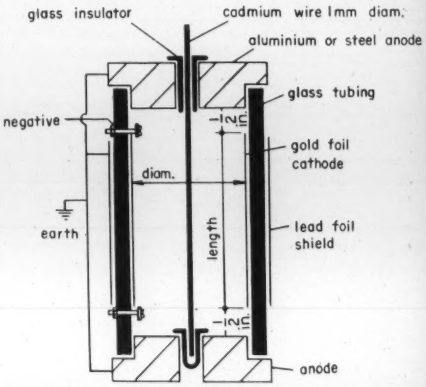

Fig. 1. Diagram showing the arrangement of the sputtering chambers

and in one run it actually melted. The wire was subsequently insulated from the anodes by small glass insulators made from Pyrex tubing, the actual discharge taking place between the anodes and the gold foil. It might be expected that with this electrical arrangement deposition would be uneven and that the heaviest deposit would be found at the ends of the wire near the electrodes. In practice, however, it was found that the reverse was true. Gold was deposited extremely uniformly over the middle portion of the wire and the thickness of the deposit fell off near the anodes.

Before sputtering, the vacuum system containing the chamber was outgassed at a pressure of less than 0·1 μ for at least one hour. During sputtering the pressure of the residual air was adjusted by means of a needle valve. A trap of solid carbon dioxide removed water vapour from the air admitted. In order to obtain the maximum rate of sputtering, the pressure, as required by the equation, was kept to the minimum adequate to start the discharge, 10 μ in the case of 1½ in. diameter chambers. In order to minimize heating of the chamber and wire the sputtering voltage was similarly kept to the lowest value which would maintain the discharge, 350 V for 1½ in. diameter chambers.

* Now at Division of Radio and Electrical Engineering, National Research Council, Ottawa 2, Ontario, Canada.

RESULTS

For short times of sputtering, of about two to thirty minutes, the gold films deposited on the cadmium wire showed the beautiful interference colours typical of thin films. From the appearance of these films it was easy to determine both the circular and longitudinal symmetry of the films. The circular symmetry, except in the case of two chambers mentioned below, was excellent, and no non-uniformity of deposition could be detected even for the thinnest of films. The longitudinal symmetry was also very good. A considerable length of the central portion of the wire was covered with a highly uniform film. The region of the end of the wire over which the thickness of the film decreased was quite short and could be judged by the interference colours to be no more than an inch in length. The anodes and glass separating the gold foil cathode from the anodes soon became coated, and had to be cleaned periodically. For longer times of sputtering the film became a bright blue-black colour, and eventually a dull blue-black.

The effect of the sputtering chamber geometry is shown in Fig. 2, in which the results obtained from six chambers are plotted. It should be observed that the central length of the

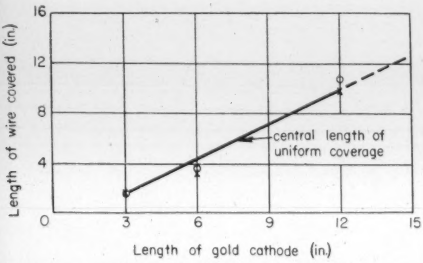

Fig. 2. Length of the cadmium wire covered in the sputtering chambers as a function of the cathode length

o = $1\frac{1}{2}$ in. diameter sputtering chambers
x = 3 in. diameter sputtering chambers.

Each point in the graph was obtained with a separate chamber.

wire, on which the deposition of the gold was highly uniform, was independent of the chamber diameter. The total length of wire contained in the sputtering chamber was covered, even though this was greater than the length of the cathode. The linear relationship found indicates that the sputtering takes place uniformly along the length of the gold cathode. The rate of sputtering was greater for the $1\frac{1}{2}$ in. than for the 3 in. diameter chambers, a result to be expected from the equation.

Sputtering was also carried out in two other chambers, the results from which are not shown in Fig. 2. The first of these was of $\frac{7}{8}$ in. diameter with a cathode length of 10 in. It was found that the uniformity of the film in this chamber depended critically upon having the cadmium wire centrally located, and varied with small non-uniformities in the bore of the glass tubing. The second chamber was $1\frac{1}{2}$ in. in diameter with a cathode $23\frac{1}{2}$ in. long. It proved nearly impossible to centre the cadmium wire in this chamber without devising special cathodes, because of the bending of the wire during insertion into the chamber. The few experiments with these chambers were nevertheless of value. Qualitatively the results were in agreement with those obtained with the previous chambers, and the results with the $\frac{7}{8}$ in. diameter chamber showed that for diameters less than $1\frac{1}{2}$ in. the uniformity of the film thickness depended critically upon the geometrical uniformity of the chamber and specimen.

The foregoing experiments made possible the design of a sputtering chamber for use with cadmium crystals which would cover the specimen with a highly uniform coating of gold and, at the same time, not require critically accurate construction. The diameter of this chamber was fixed at $1\frac{1}{2}$ in. and the cathode length at 3 in. Some further experiments were carried out with this chamber in order to determine the thickness of the films deposited and the temperature during the course of sputtering.

To determine the rate of sputtering pieces of nickel-steel wire were ground and polished flat on two surfaces in such a way as to have very nearly the same periphery as the 1 mm cadmium wire. Strips of Frigilene, a cellulose compound obtained from W. Canning and Co. Ltd., were painted on parts of the wire, and sputtering was then carried out. After sputtering the Frigilene was dissolved in acetone applied gently with a brush. This left a surface which was partially coated in which the transition between coated and uncoated areas was quite sharp. It was found that an abrupt step of height equal to the thickness of the sputtered layer could thus be prepared.

The height of this step was then determined interferometrically. The wire was placed beneath an optical flat in a Vickers projection microscope and illuminated with monochromatic light from a sodium lamp. The interference fringes produced were displaced by the steps on the wire, and the height of the steps could be calculated from the displacement of the fringes.

The temperature attained by the specimen was measured approximately by substituting a thermocouple for the wire in the chamber used for the single crystal investigation. A copper-constantan thermocouple made from no. 18 s.w.g. wires was used, and the electromotive force with respect to an ice-bath reference junction was measured by means of a potentiometer. The temperature rose sharply to about 55° C after the start of sputtering, but during the course of runs up to half an hour long it never exceeded 65° C. The thermocouple temperature dropped to 30° C within a few minutes of switching off the sputtering voltage.

The results for the sputtering chamber of $1\frac{1}{2}$ in. diameter and 3 in. length are summarized below.

Diameter of sputtering chamber, $1\frac{1}{2}$ in.
Length of sputtering chamber, 3 in.
Diameter of specimen, 1·0 mm.
Residual gas, air.
Pressure, 10 μ.
Voltage, 350 V.
Current, 10 mA.
Approximate rate of deposition, 3000 Å/h.
Maximum temperature (of thermocouple), 65° C.

It was found that sputtering offers a satisfactory means of producing uniform films of gold on small cylindrical specimens. The fact that the deposition is to a large extent independent of the sputtering chamber greatly adds to the convenience of the method.

ACKNOWLEDGEMENTS

The author is indebted to Professor E. N. da C. Andrade and Dr. Ronald King for their help and encouragement, to Professor S. Tolansky and his colleagues at the Royal

Holloway College for their valuable assistance in determining the thickness of the sputtered films, and to Mr. L. Holland of Edwards High Vacuum Ltd., for helpful discussions.

He is grateful to the Managers of The Royal Institution for the award of an Overseas Research Scholarship. This work forms part of a Ph.D. thesis submitted to the University of London.

REFERENCES

(1) ECKER, G., and EMELÉUS, K. G. *Proc. Phys. Soc.* [*London*], *B*, **67**, p. 546 (1954).

(2) STRONG, J. *Modern Physical Laboratory Practice* (London: Blackie and Son Ltd., 1940).

(3) TOWNES, C. H. *Phys. Rev.*, **65**, p. 319 (1944).

The γ-ray spectrum of fission products from slow neutron irradiation of uranium 235

By D. H. PEIRSON, B.Sc., F.Inst.P., Atomic Energy Research Establishment, Harwell, Berks.

[*Paper received* 12 *August*, 1955]

The fission products from uranium 235, irradiated by slow neutrons, have been analysed by a two-crystal γ-ray scintillation spectrometer. The spectrum between one day and seventy days after irradiation has been recorded. The gross spectrum varies with time and consists of two groups of lines around 0·2 and 0·7 MeV, with a single line at 1·58 MeV as the only important component above 1 MeV. By measurement of energy and decay rates seventeen activities, due to fission products of high yield, are identified during the period of analysis. The spectrometer is described and its use as an analytical tool in other applications indicated.

1. INTRODUCTION

The gross γ-ray spectrum of fission products may be derived by calculation[1,2] for varying conditions of irradiation. For example, the yields of fission products obtained by radiochemical determination[3] may be converted to activities for any time after irradiation.[4] The activities of the fission products may be converted to γ-ray intensities from a knowledge of the decay schemes[5] of the appropriate nuclides.

The present paper describes a direct measurement of the γ-spectrum of fission products from uranium 235, irradiated by slow neutrons. The fission product source, unseparated by chemical processing, is measured by a two-crystal γ-ray scintillation spectrometer.[6] In this spectrometer, the Compton continuum, due to each γ-ray energy, registered by a sodium iodide (thallium) crystal is removed by subtraction of the continuum registered by an anthracene crystal. Thus, apart from absorption by pair production, which becomes appreciable above about 2 MeV, each energy is represented only by a photoelectric peak in the recorded spectrum.

The intensities and energies of the major lines of the gross γ-spectrum may be derived from calibration of the sodium iodide crystal. Isotopic analysis of the mixture of fission products is possible through identification by energy and, using a series of spectrometer measurements at appropriate intervals, by growth and decay rates for the nuclides emitting these major lines. Essentially these will be due to products of high fission yield and will mask the weaker lines of the low yield fission products.

2. THE SCINTILLATION SPECTROMETER

As demonstrated by Hofstadter and McIntyre[7] the scintillation spectrometer using a sodium iodide crystal identifies the incident γ-ray energy with the response to the photoelectric, Compton and (when energetically possible) with the pair-production processes within the crystal. In sodium iodide the photoelectric cross-section is predominant below about 0·2 MeV and the pair-production process becomes appreciable above about 2 MeV. In the energy range 0·2 to 2 MeV the photoelectric and Compton processes are in competition. Thus the recorded spectrum in this important range is complicated by the two-fold response of the spectrometer to each γ-energy.

Several methods of selection in favour of one of the two processes are available which simplify the interpretation of the spectra when a source emitting several γ-energies is analysed. Use of a sodium iodide crystal of large dimensions enhances the photoelectric or total energy peak at the expense of the Compton energy continuum, due to capture of the scattered quanta. Substitution of anthracene, essentially a Compton absorber, for the sodium iodide crystal removes the photoelectric peaks; the γ-ray energy can then be roughly estimated from the poorly defined edge of the Compton continuum. A two-crystal coincidence spectrometer has been reported by Hofstadter and McIntyre.[8] In this method, the energy absorbed by the Compton encounters which scatter the incident rays through a defined angle is measured. A method has been described by Albert[9] in which the quanta scattered by a small sodium iodide crystal are detected in a surrounding mass of sodium iodide, and the pulses due to the corresponding Compton electrons in the crystal are cancelled by anticoincidence.

In the two-crystal spectrometer described here the γ-ray source is exposed simultaneously to sodium iodide and anthracene scintillation counters. The Compton continua from the two crystals are equalized in height (counting rate scale) and extent (energy scale), and then subtracted in suitable counting-rate circuits, so that each γ-energy is represented only by a photoelectric peak in the recorded spectrum. The method has the advantage of allowing good geometry and a high sensitivity with no loss in resolution.

The simplest method of equalizing the Compton continua is to match the energy scales by adjusting the counter supply voltages and the counting-rate scales by adjusting the position of the source between the two crystals. The former adjustment is made for one energy and will apply over the

range for which the pulse amplitude is proportional to energy in both counters. The shapes of the continua will be matched at the higher energies, but, owing to re-capture in the sodium iodide crystal of scattered quanta, i.e. additional total absorption at the expense of events registered as Compton processes, this matching will not apply strictly to the lower range of energies. However, at these lower energies the Compton continuum is smaller in height relative to the photoelectric peak and overall the Compton continuum may be reduced to less than 5% of the associated photoelectric peak.

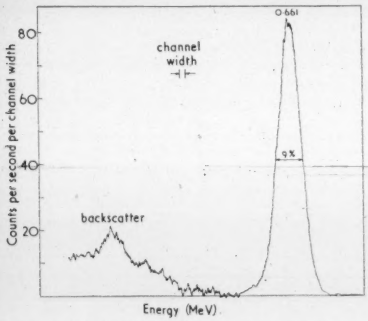

Fig. 1. Recorded spectrum of caesium 137

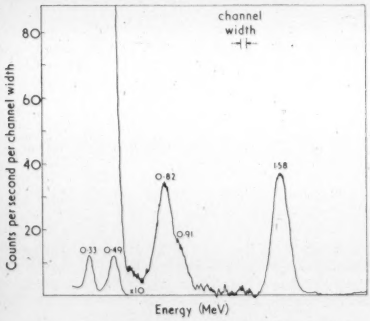

Fig. 2. Recorded spectrum of lanthanum 140

The spectrum, of a mono-energetic source (caesium 137) is shown in Fig. 1 and of a complex source (lanthanum 140) in Fig. 2.

3. APPARATUS

The sodium iodide *s* and anthracene *a* counters have a common output connected to a pulse amplifier *A*, single channel pulse-amplitude analyser *K*, counting-rate meter *R* and pen recorder *S*. The variable bias potentiometer in the analyser is coupled to the driving mechanism of the recorder chart. The apparatus is indicated schematically in Fig. 3.

Duplication of the spectrometer for each scintillation counter is avoided. The contacts of a relay switch driven by a multivibrator circuit are used to suppress each photomultiplier *P* in turn for 0·5 s by connecting the first dynode (D_1) to the photo-cathode for this time. In the diode pump circuit of the counting-rate meter (see Fig. 3) synchronized switch contacts connect C_f to C_t so that C_t receives negative

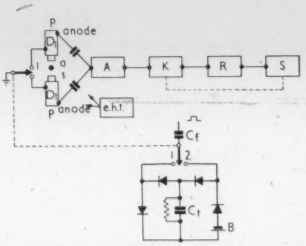

Fig. 3. Schematic diagram of two-crystal spectrometer showing modification of ratemeter pump circuit

charges from the sodium iodide pulses and positive charges from the anthracene pulses. The net negative charge on C_t is recorded in the usual way. The switching period of one second was chosen to suit a minimum integration time of ten seconds in the counting-rate meter. Use of a common spectrometer channel in this way reduces the effect of electronic drifts in the apparatus.

The sodium iodide counter is fixed rigidly on a base-plate to which is attached a vertical pillar marked with a graduated scale. The positions of the anthracene counter and a Perspex source platform, which are mounted on the pillar above the sodium iodide counter, may be adjusted against the scale. The dimensions of both sodium iodide and anthracene crystals used were 1 in. by 1·5 in. diameter. The resolution of the sodium iodide crystal at 0·661 MeV was 9%. The thickness of the can adjacent to the incident face of each crystal could be increased to $\frac{1}{8}$ in. of aluminium to absorb high energy β-particles.

The energy scales of the two counters are matched by adjustment of potentiometers connected across the common extra high tension supply. The voltage applied to the sodium iodide counter is limited by consideration of energy scale linearity; that applied to the anthracene counter is adjusted to suit. In the case of the photomultiplier tubes used (type 6260, by Electric and Musical Industries Ltd.), the operating voltage was about 900. The first dynode in each counter is biased separately from the other dynodes by a potentiometer which could be set for maximum pulse amplitude at the anode of the counter.

The sodium iodide and anthracene crystals both exhibited a negative temperature coefficient of pulse amplitude. Around room temperature these were measured as 0·1% per °C and 0·5% per °C respectively. This difference can result in a mismatch of the energy scale compensation, noticeable if the temperature in the neighbourhood of the counters changes by more than 5° C.

The customary settings of the principal controls of the spectrometer were as follows. The pulse amplifier, which was capable of delivering a linear output of 50 V into the pulse amplitude analyser, was operated with a gain adjustable between 500 and 2000 and a differentiating time constant of 0·8 μs. In the analyser the discriminator bias "sweep" was 50 V and the channel width 1 V. Each bias sweep occupied

most of 1 ft of chart in the Honeywell–Brown recorder. A recording period of 0·5 h would correspond to an integration time in the ratemeter of 10 s. Proportionately longer periods were used for alternative integration times of 40 and 160 s.

4. METHOD

The respective abundances and cross-sections of uranium 238 and uranium 235 are such that irradiation of natural uranium by thermal neutrons leads to temporary obliteration of the low energy portion of the fission product spectrum from uranium 235 by the intenser radiation of X-rays and γ-rays from an activation product of uranium 238, namely 2·3 day neptunium 239. For this reason uranium fifty times enriched in uranium 235 was chosen as the source material: 0·006 g sealed in silica tubing was irradiated for 20 min by a flux of 10^{12} neutrons . cm^{-2} . s^{-1} in the Bepo reactor.

The measurement of the γ-ray spectrum commenced at seventeen hours after irradiation and was repeated at intervals appropriate to the fastest decay rate present. At the start this implied almost continuous recording but after two months the intervals had been increased to about fifteen days. Each measurement consisted of three records covering the ranges 0·2–2, 0·1–1 and 0·05–0·5 MeV, which were selected by switching the amplifier gain control. A typical record in the 0·1–1 MeV range is shown in Fig. 4. The energy

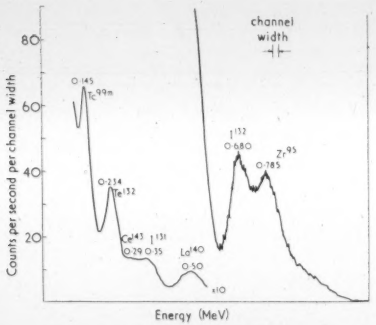

Fig. 4. Spectrometer record

Time after irradiation, 206 h; energy sweep, 0·1–1·0 MeV; ratemeter integration time, 40 s; recording time, 2 h.

of the photoelectric peak is measured by calibration of the spectrometer with γ-ray sources of known energy. The indefiniteness of a pair of peaks such as is shown at 0·29 and 0·35 MeV in Fig. 4 is temporary. These peaks are clearly resolved in time and energy by inspection of records taken before and after that of Fig. 4. The 0·29 MeV peak is dominant before and the 0·35 MeV peak dominant after 206 h. This method of interpretation may be applied to most pairs of peaks of similar energies. In the absence at the time of an overall sensitivity calibration for the spectrometer, no attempt was made to establish fixed and reproducible source-counter geometry throughout the series of measurements. Instead, all other peak heights were measured relative to the well defined 1·58 MeV peak of lanthanum 140 from ninety hours onwards, by which time it had risen to a measurable height. The growth and decay of the lanthanum 140 peak was calculated from the known fission yields and disintegration data[4] of the 140 mass chain.

5. CRYSTAL DETECTION EFFICIENCY

An exact determination of the photoelectric detection efficiency of the sodium iodide crystal is complicated by the dependence of the efficiency upon the energy of the γ-radiation and upon the source-crystal configuration. Thus pulses occurring in the photoelectric or total energy peak arise not only from quanta absorbed solely by the calculable photoelectric process but include, in addition, scattered quanta which have been recaptured before escaping from the crystal. Also, for source-crystal distances that are finite, the effective solid angle subtended by the crystal decreases with increasing energy, i.e. low energy radiation is absorbed close to the incident face whilst high energy quanta are absorbed within the volume of the crystal. The problem has been studied fully by Lidén and Starfelt[10] and by Heath and Schroeder.[11]

To simplify and to shorten the computations involved in reducing the numerous data obtained in the present series of measurements, the following method of calibration for the sodium iodide crystals was used. In Fig. 5 curve *A*,

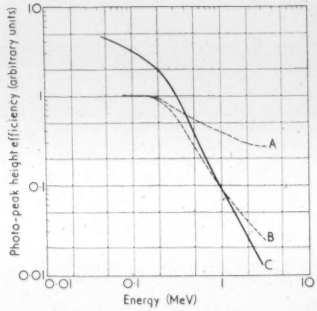

Fig. 5. Energy characteristic of sodium iodide crystal, 1 in. × 1·5 in. diameter. Source-crystal distance, 1 cm

$(1 - e^{-\mu(E)D})$ represents the total absorption due to primary processes in the crystal, for normal incidence. The total γ-absorption coefficient $\mu(E)$ at energy E in the crystal is derived from tables by Davisson and Evans[12]; D is the thickness of the crystal. The fraction of pulses occurring in the photoelectric peak at any energy is determined experimentally by recording the spectra of several separate γ-emitters of known decay schemes with energies between 0·1 and 2·8 MeV, using a source-crystal distance of 1 cm. The fraction is given by the ratio of the area (Sp) under the photoelectric peak to the total area (St), under the spectrometer curve. Then the product of the total absorption curve *A* and this fraction gives the photoelectric absorption, curve *B* of Fig. 5, namely:

$$(1 - e^{-\mu(E)D})(Sp/St)$$

Since the photoelectric peak registered by the scintillation counter in practice follows a Gaussian distribution, the area under the peak is proportional to the product of the height and width of the peak. The peak width, at one-half the peak

height, is proportional to the standard deviation of the Gaussian distribution and hence, by virtue of the linearity of the scintillation process, to $E^{\frac{1}{2}}$, the square root of the γ-ray energy. Therefore, in comparative measurements the peak height is given by the ratio of peak area to $E^{\frac{1}{2}}$. Hence the relative photoelectric peak height efficiency, curve *C* of Fig. 5, is given by

$$(1 - e^{-\mu(E)D})(Sp/St)(1/E^{\frac{1}{2}})$$

6. RESULTS

The variation of the height of peaks of the various energies is plotted in Fig. 6 against time after irradiation. Each peak could be observed and plotted until it disappeared into the baseline or became merged into the side of a neighbouring peak. Such a succession is drawn as a single line with the energy transition shown by a discontinuity. The transition is characterized by an indeterminate energy during the period when the two peaks are comparable in height. The points of measurement for the 0·25–0·23 MeV line are included in Fig. 6 as representative of the scatter in the observations. Peak heights may be converted into γ-ray intensities by dividing by the crystal energy calibration factors given by curve *C* of Fig. 5. In this way a series of line spectra are drawn for various times after irradiation. These are shown in Fig. 7. The intensity scales are adjusted to disintegrations per minute per 10^6 fissions, after normalizing to the activity computed for lanthanum 140 by Hunter and Ballou.[4]

7. DISCUSSION OF RESULTS

Identification of activities is possible through energy by reference to the literature,[5] supplemented by measurement of separated pure sources, and through build-up and decay rates. The latter were derived from the computed tables of Hunter and Ballou.[4] In fact, precise assignment at any time after irradiation is often complicated by the presence of neighbouring energies too close for adequate resolution by the sodium iodide crystal. For this reason assignment is made to the major components in Figs. 6 and 7 and the probability of identification *A*, *B* and *C* is listed in Fig. 6 in descending order of certainty of energy and decay rate.

Fission yields may be compared by reference to the decay schemes of the nuclides. In the case of a nuclide having a complex decay scheme agreement with published yields is affected by any uncertainty in the branching ratios, and, particularly for the lower energies, in the internal conversion coefficients. Overall, the curves of Fig. 6 are reasonably consistent with the fission yields adopted by Hunter and Ballou.[4] Agreement in the case of technetium 99m, cerium 141, iodine 133, ruthenium 103, niobium 97, iodine 132, niobium 97m, zirconium 95 and niobium 95 would be made closer by reducing by 20% the fission yield for lanthanum 140 used as the normalizing activity. For the remaining activities extraction of a unique value of fission yield is difficult because of the complexity of the spectra or of the uncertainty of the decay schemes. The only obvious disagreement occurs in the case of xenon 133 (0·08 MeV) which has been tentatively assigned to the peak measured as 0·095 MeV. During the first 300 hours this peak is registered at a height greater than can be accepted. Apart from a systematic error in the apparatus a possible explanation is that the xenon 133 peak is subjected to interference from the approximate 0·1 MeV X-ray peak from 2·3 day neptunium 239 which arises from neutron activation of uranium 238 (see Section 4). Neptunium 239 activity corresponding to a peak height at this energy of about 300 (scale of Fig. 6) at 50 h would account for this anomaly. After allowing for this amount of interference the peak height at 50 h for xenon 133 would be about 120 which improves the agreement with the parent activity iodine 133 recorded at 0·53 MeV. However, not more than one-half of the required neptunium 239 activity can be expected from the known cross-section of uranium 238 and the uranium 235 enrichment factor.

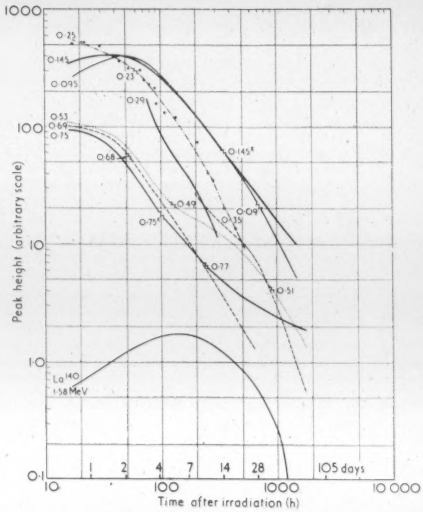

Fig. 6. Recorded spectra from fission products of uranium 235 irradiated by slow neutrons

Energy (MeV)	*Assignment*	*Certainty*
0·09	^{147}Nd	*B*
0·095	^{133}Xe + ^{239}Np	*C*
0·145	^{99m}Tc	*A*
0·145ˣ	^{141}Ce	*A*
0·23	^{132}Te	*B*
0·25	^{135m}Cs	*A*
0·29	^{143}Ce	*B*
0·35	^{131}I	*B*
0·49	^{140}La	*B*
0·51	^{103}Ru	*B*
0·53	^{133}I	*A*
0·68	^{132}I	*B*
0·69	^{97}Nb	*B*
0·75	^{97m}Nb	*B*
0·75ˣ	^{99}Mo	*A*
0·77	^{95}Zr + ^{95}Nb	*B*
1·58	^{140}La	*B*

Experimental errors. The errors considered in this section are associated with backscatter, crystal efficiency and energy resolution. The magnitude of these and other errors has been estimated theoretically by Lidén and Starfelt.[10]

The effect of backscatter is demonstrated in Fig. 1 where the broad low energy peak is due to γ-radiation scattered back mainly from the photomultiplier window below the sodium iodide crystal, but also from the anthracene counter.

The energy of caesium 137 (0·661 MeV) radiation scattered through 180° is 0·185 MeV according to the Klein–Nishina formula. For the range of primary energies 0·1–2 MeV the corresponding energies for 180° backscatter are 0·08–0·226 MeV. The height of the backscatter peak in Fig. 1 is primary peak intensity at the appropriate backscatter energy is of the same order as for the case of caesium 137 cited above. In view of the magnitude of errors arising from other causes Figs. 6 and 7 have not been so corrected.

The problem of accurate calibration of the detection

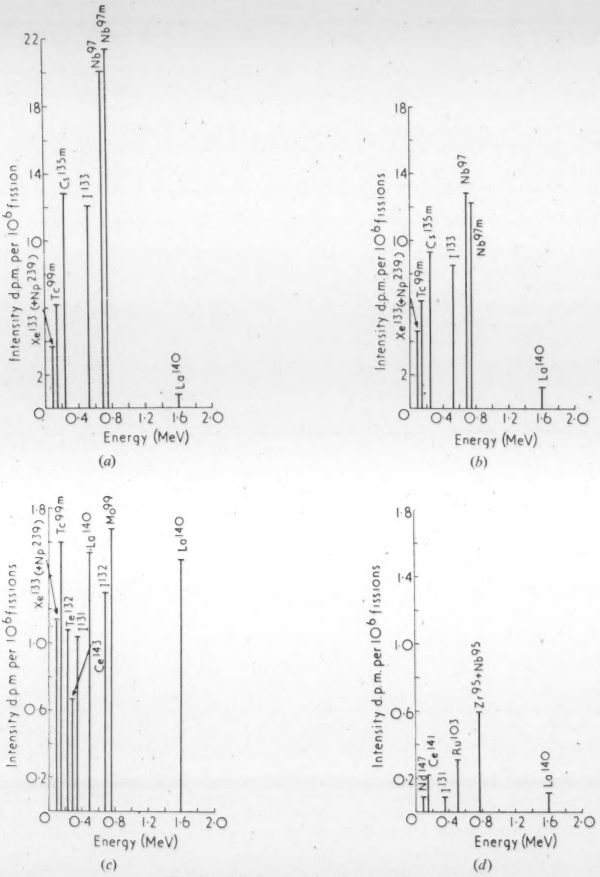

Fig. 7. Spectrum of γ-ray intensities at

(*a*) 1 day after irradiation, (*b*) 2 days after irradiation, (*c*) 10 days after irradiation, (*d*) 50 days after irradiation.

20% of the primary peak and is, of course, dependent upon the geometry of source and counters. In terms of γ-intensity, the height of the backscatter peak, from Fig. 5, is approximately 2% of the primary peak. By calibration, errors due to backscatter could be estimated over the whole energy range and applied as corrections to the peak heights of Fig. 6 or to the γ-intensities of Fig. 7. The correction due to each efficiency of the sodium iodide crystal is discussed in Section 5. Thus, whereas the absorption coefficient data of Davisson and Evans[12] were applied for normal incidence, the fraction of pulses occurring in the "photoelectric" peak are determined experimentally, using a source-crystal distance of 1 cm. After conversion from peak area to peak heights, the resultant calibration is then applied to the series of

measurements of fission spectra over a range of source-crystal distance from 4 to 0·5 cm, following the decay in activities. For the size of crystal used (1 in. × 1·5 in. diameter), the low energy response will tend to decrease slightly, relative to the high energy response, with increasing source-crystal distance.

The conversion of the calibration from peak area to peak height (curves *B* and *C* of Fig. 5) involves the proportional relationship between peak width and the square root of energy. The statistics of the scintillation spectrometer have been reviewed by Breitenberger[13] who showed that the relation is applicable to ideal conditions. In practice, various factors may contribute to broadening of the peak in a manner independent of the square root relation, notably a varying efficiency of "transfer" of the scintillation photon, from the crystal on to the first dynode. For the crystal used in this work the square root law was confirmed by measurement of the peak width, with an uncertainty of 10%, up to 1·6 MeV.

Assuming a Gaussian distribution it can be shown that the use of channel widths in the pulse-amplitude analyser greater than one-third of the peak width (at half maximum) can introduce appreciable broadening of the peak with consequent loss of peak height. Reduction of the channel width below 1 V would have introduced significant instability, owing to drifts in the discriminator levels. The error due to broadening of the low-energy peaks was avoided by recording the whole energy region in separate ranges as described in Section 4. In this way the channel width, fixed in voltage but varying in energy with the amplifier gain is adjusted to accommodate the narrow low energy peaks.

After assessing the effect of the several sources of error it is considered that, generally, the accuracy of measurement of γ-ray *intensity* is better than ±10%. Included in this estimate is the effect of incomplete compensation of the Compton continua which depends to a large extent on the precision of adjustment of counter voltage and position.

As a check on the accuracy of the calibration, the γ-spectra from lanthanum 140, as illustrated in Fig. 2, and from uranium 237 have been determined and compared with intensities derived from the decay schemes proposed by other workers. The relative γ-ray intensities for lanthanum 140 are shown in Table 1.

Table 1. *Relative intensities for lanthanum* 140

Energy (MeV)	1·58	0·91	0·82	0·49	0·33
Author	100	13	24	34	10
Bannerman and others[14]	100	—	29	39	5
Coleman[15]	100	11 ± 4	27 ± 5	48 ± 8	25 ± 10

The spectrum for uranium 237 (γ-ray and X-ray) is given in Table 2.

Table 2. *Relative intensities for uranium* 237

Energy (MeV)	0·062	0·102	0·225	0·34
Author	84	100	46	4
Wagner and others[16]	70	100	40	5

8. CONCLUSIONS

The gross γ-ray spectrum from the fission products of uranium 235, studied from one day to seventy days and for energies from 0·05 to 2 MeV, shows considerable complexity and varies with time. The spectral pattern consists of two groups of major components, which are roughly centred about 0·2 and 0·7 MeV. The only important line above 1 MeV is that due to lanthanum 140 (1·58 MeV) which reaches a maximum activity at six days. The two groups are of similar intensities until about fifty days when the zirconium 95 activity at 0·77 MeV becomes predominant. The effect of the neutron activation products of uranium 238, which will arise in the irradiation of natural uranium, would be to introduce low-energy components temporarily of overwhelming intensity. This will be reported in a later paper.

The γ-ray spectra were recorded by a two-crystal scintillation spectrometer without previous chemical separation of the individual activities, and are unaffected by the uncertainties due to self-absorption that occur in β-ray assay. Measurement of energy and of growth and decay rates permits identification of the nuclides emitting the major γ-ray lines.

The two-crystal scintillation spectrometer described in this paper has been applied to activation analysis where a mixed sample of stable elements is rendered active by neutron irradiation and thereby susceptible to γ-ray analysis. Thus minute quantities of impurity are detected with a sensitivity dependent upon the activation cross-section and disintegration rate. In view of the selective determination of energy and half-life by the spectrometer, no chemical processing is necessary.

The two-crystal scintillation spectrometer could be applied to the measurement of the energy spectrum of secondary γ-radiation in a scattering medium, such as air or a concrete radiation shield. This problem has been investigated theoretically by Spencer and Fano[17] and experimentally by Whyte.[18]

ACKNOWLEDGEMENTS

Acknowledgements are due to Mr. E. N. Jenkins who provided the sample of uranium 235, to Mr. E. W. Pulsford for the design of the multivibrator and ratemeter circuits in the spectrometer and to Mr. R. B. Owen for useful discussion.

REFERENCES

(1) Bjornerstedt, R. Private communication.
(2) Moteff, J. *Nucleonics*, **13**, p. 28 (1955).
(3) Coryell, C. D., and Sugarman, N. *National Nuclear Energy Series*, Vol. 9B (New York: McGraw-Hill Book Co. Inc., 1951).
(4) Hunter, H. F., and Ballou, N. E. Naval Radiological Defence Laboratory Report ADC–65 (1949).
(5) Hollander, J. M., Perlman, I., and Seaborg, G. T. *Rev. Mod. Phys.*, **25**, p. 469 (1953).
(6) Peirson, D. H. *Nature* [*London*], **173**, p. 990 (1954).
(7) Hofstadter, R., and McIntyre, J. A. *Phys. Rev.*, **80**, p. 631 (1950).
(8) Hofstadter, R., and McIntyre, J. A. *Phys. Rev.*, **78**, p. 619 (1950).
(9) Albert, R. D. *Rev. Sci. Instrum.*, **24**, p. 1096 (1953).
(10) Lidén, K., and Starfelt, N. *Ark. Fys.*, **7**, p. 427 (1954).
(11) Heath, R. L., and Schroeder, F. United States Atomic Energy Commission Report IDO—16149 (1954).
(12) Davisson, C. M., and Evans, R. D. *Rev. Mod. Phys.*, **24**, p. 79 (1952).
(13) Breitenberger, E. *Progress in Nuclear Physics*, Vol. 4 (London: Pergamon Press Ltd., 1955).
(14) Bannerman, R. C., Lewis, G. M., and Curran, S. C. *Phil. Mag.*, **42**, p. 1097 (1951).
(15) Coleman, C. F. *Phil. Mag.*, **46**, p. 1132 (1955).
(16) Wagner, F., Freedman, M. S., Engelkemeir, D. W., and Huizenga, J. R. *Phys. Rev.*, **89**, p. 502 (1953).
(17) Spencer, L. V., and Fano, U. *J. Res. Nat. Bur. Stand.*, **46**, p. 446 (1951).
(18) Whyte, G. N. *Canad. J. Phys.*, **33**, p. 96 (1955).

Correspondence

Conditions for aperiodicity in linear systems

I should like to make the following comment on the paper by Mr. A. T. Fuller, published on p. 195 of the June 1955 issue of this *Journal*.

For third-order equations it is possible to check the criteria given, from the known explicit algebraic solutions, and it will be found that if the criterion given by the highest order determinant is satisfied, in this case, then the criteria given by the lower orders are necessarily also satisfied, as all the coefficients are positive. It is well known that this also occurs, for low-order equations only, in the case of the Routh stability criteria.

On evaluating a determinant of order $(2n-1)$, to obtain the criterion for an nth order equation, a most cumbersome algebraic expression is obtained. The value of the criteria as given is that no such algebraic evaluation is necessary or desirable. In practical application of the criteria, *numerical* values of the coefficients are inserted in the determinants, which can then be readily evaluated by one or other of the special methods of condensation;* it would be interesting to know if, alternatively, a routine analogous to the Routh tabulation could be evolved for aperiodic systems.

Department of Engineering, University of Cambridge. R. H. MACMILLAN

To do full justice to the points raised by Mr. Macmillan would require another paper; however the following comments may be of interest.

Mr. Macmillan's remark may be generalized for third-order equations, by stating that the lower order determinant is redundant whether or not the coefficients are all positive (i.e. whether or not the system is stable). For on expanding the two test determinants, which we will call B_1 and B_2, where B_1 is the one of lower order, they will be found to satisfy:

$$(B_1/a_3)^3 = 2(27a_0a_3^2 + 2a_2^3 - 9a_1a_2a_3)^2 + 54a_3B_2 \quad (1)$$

If B_2 is positive, the right-hand side of equation (1) is positive (remember that a_3 is always positive) and hence so is the left-hand side. Therefore when B_2 is positive, B_1 is also necessarily positive.

No such simplification is possible for fourth-order equations, even when the coefficients are all positive. Thus the following characteristic equations demonstrate that it is always necessary to examine the signs of B_1 and B_2 as well as that of B_3.

First:

$$p^4 + 6p^3 + 15p^2 + 18p + 10 = 0 \quad (2)$$

the roots of which are $-1 \pm j$ and $-2 \pm j$, so that the system is stable but not aperiodic. Evaluation of the test determinants yields:

$$B_1 = -12,\ B_2 = +48,\ B_3 = +400$$

Second:

$$p^4 + 10p^3 + 35p^2 + 50p + 34 = 0 \quad (3)$$

the roots of which are $-1 \pm j$ and $-4 \pm j$, so that again the system is stable but not aperiodic. The test determinants turn out to be:

$$B_1 = +20,\ B_2 = -720,\ B_3 = +219,024$$

The results that the presence or absence of complex roots depends on the signs of three functions of the coefficients for fourth-order equations, and on the sign of only one function for third-order equations, agree with the usual text-book treatments.(1)

It is indeed possible to give a routine, analogous to the Routh tabulation procedure, for finding if a system is both aperiodic and stable. The derivation may be briefly outlined as follows. From the characteristic equation of the system,

$$f(p) \equiv a_0 + a_1p + a_2p^2 + \ldots + a_np^n = 0 \quad (4)$$

let us form a new equation:

$$g(p) \equiv f(p^2) + pf'(p^2) = 0 \quad (5)$$

which we may regard as the characteristic equation of some fictitious system. If the original system is both stable and aperiodic the roots of $f(p) = 0$ are all real and negative. This implies that the roots of $f'(p) = 0$ are also all real and negative, and further that they interlace those of $f(p) = 0$ (Rolle's theorem[1]). Hence the zeros of the even part, $f(p^2)$, and those of the odd part, $pf'(p^2)$, of $g(p)$ are all purely imaginary and interlaced. But for this to be true, it is necessary and sufficient that the fictitious system represented by $g(p) = 0$ should be stable (see Routh,[2] Hurwitz,[3] or Guillemin[4]), i.e. that the equation:

$$a_0 + a_1p + a_1p^2 + 2a_2p^3 + a_2p^4 + 3a_3p^5 + \ldots + \ldots + na_np^{2n-1} + a_np^{2n} = 0 \quad (6)$$

should satisfy the Routh or Hurwitz criteria. Thus application of the Routh criteria directly to equation (6) gives the required tabulation procedure for finding if equation (4) represents a stable-aperiodic system.

By way of example, the tabulation for equation (2) above yields for the first four rows:

1	6	15	18	10
4	18	30	18	
6	30	54	40	
−12	−36	−52		

The negative value in the first column shows that the system is not both stable and aperiodic.

On applying instead the Hurwitz criteria to equation (6), to test for aperiodic stability, we obtain a set of $2n$ determinantal inequalities. Comparison with the corresponding result given in my paper shows that half of these are in practice superfluous, since they may be replaced by the much simpler requirement that the coefficients should all be positive.

The analogy between the criteria for combined aperiodicity and stability and those for stability stimulates the conjecture that half the latter are similarly superfluous; i.e. that the sequence comprising every alternate member, beginning

$$H_n > 0,\ H_{n-2} > 0,\ H_{n-4} > 0, \text{ etc.} \quad (7)$$

* MUIR, T. *Treatise on Determinants*, p. 70 (London: Macmillan and Co. Ltd., 1882).
AITKEN, A. C. *Determinants and Matrices*, 7th ed., p. 45 (Edinburgh: Oliver and Boyd, 1951).

of the Hurwitz stability criteria, may be replaced by the simpler sequence:

$$a_0 > 0,\ a_1 > 0,\ a_2 > 0,\ \ldots\ a_{n-1} > 0 \qquad (8)$$

This hypothesis is certainly valid (and easy to check) for systems of orders up to the fourth, these corresponding to the low-order equations referred to by Mr. Macmillan. To prove it for a fifth-order equation, note that for the latter:

$$a_2H_2H_3 = a_0a_4H_2^2 + H_3^2 + a_4^2H_4 \qquad (9)$$

which may be verified by expanding the H's. If H_2, H_4 and the coefficients are all positive, the right-hand side of equation (9) is positive, and hence so is its left-hand side, which implies that H_3 is then necessarily positive. Thus H_3 is superfluous. (H_1 is trivial, being equal to a_{n-1}; H_5 is superfluous since, as Hurwitz pointed out, H_5 equals a_0H_{n-1} and may therefore be replaced by a_0 in his criteria.)

Finally, may I take this opportunity of drawing attention to earlier Russian work which unfortunately escaped my notice until very recently. In 1945, Meerov[5] derived the principal result of my paper using a different and longer method. However, his criteria for combined stability and aperiodicity include the n superfluous determinants mentioned above. Also Bloch[6] has given for aperiodic systems a diagram somewhat analogous to the Nyquist diagram.

Department of Engineering,
University of Cambridge.

A. T. FULLER

REFERENCES

(1) DURELL, C. V., and ROBSON, A. *Advanced Algebra*, Vol. II, pp. 309, 315, 284 (London: Bell and Sons, Ltd., 1937).
(2) ROUTH, E. J. *Advanced Rigid Dynamics*, Vol. 2 (London: Macmillan and Co. Ltd., 1930).
(3) HURWITZ, A. *Math. Ann.*, **46**, p. 273 (1895).
(4) GUILLEMIN, E. A. *The Mathematics of Circuit Analysis*, p. 400 (New York: J. Wiley and Sons, Inc., 1949).
(5) MEEROV, M. V. *Izv. Akad. Nauk, SSSR, Otdel. tekh. Nauk*, (12), p. 1169 (1945).
(6) BLOCH, Z. S. *Automat. Telemech., Moscow*, **10**, p. 3 (1949).

The flexural vibrations of an end-loaded vertical strip

In a recent paper by Hearmon and Adams, published on p. 280 of the August issue of this *Journal*, theoretical and experimental results were presented for the flexural vibrations of a vertical elastic strip clamped at its upper end and carrying a load at its free end.

The Rayleigh method of assuming a deflected shape for the strip and then equating maximum potential energy (due to flexure and gravity) and kinetic energy was used to give a frequency equation and favourable agreement was found between calculated and observed results. However, due to the implied constraints in this method an over-estimate of the frequency was given, even when the Rayleigh–Ritz method, with its greatly increased arithmetic, was employed. An alternative method of improving the accuracy of the frequency equation is to obtain, in addition to the already found upper limit to the frequency, a lower limit to the frequency. This may be done by means of a theorem due to Southwell.*

If the strip, of length l and flexural rigidity EI, is considered as mass-less and carrying a concentrated mass m at its free end, then if y is the actual deflected shape of the strip, the circular frequency ω is given by

$$\omega^2 = \frac{EI\int_0^l (d^2y/dx^2)^2dx + mg\int_0^l (dy/dx)^2dx}{mY^2} \qquad (1)$$

where Y is the maximum deflexion at the free end.

Hearmon and Adams assumed a deflexion curve,

$$y_1 = k(3lx^2 - x^3) \qquad (2)$$

and consequently obtained an upper bound to the frequency

$$\omega_1^2 = (g/l)(3r + 1{\cdot}2) \geqslant \omega^2 \qquad (3)$$

where $$r = EI/mgl^2$$

Now if only the bending restoring force were present, the exact circular frequency ω_B would be given by

$$\omega_B^2 = \frac{EI\int_0^l (d^2y_B/dx^2)^2dx}{mY_B^2} = \frac{3EI}{ml^3} \qquad (4)$$

and if only the gravity restoring force were present the system would be a simple pendulum with a circular frequency

$$\omega_G^2 = \frac{mg\int_0^l (dy_G/dx)^2dx}{mY_G^2} = \frac{g}{l} \qquad (5)$$

Then, since y is the deflected shape with *both* restoring forces present,

$$\frac{EI\int_0^l (d^2y/dx^2)^2dx}{mY^2} \geqslant \omega_B^2 \quad \text{and} \quad \frac{mg\int_0^l (dy/dx)^2dx}{mY^2} \geqslant \omega_G^2$$

so that from equation (1) a lower limit to the frequency is

$$\omega^2 \geqslant \omega_B^2 + \omega_G^2 = (g/l)(3r + 1) \qquad (6)$$

Thus $$\sqrt{(3r + 1{\cdot}2)} \geqslant \omega\sqrt{(l/g)} \geqslant \sqrt{(3r + 1)} \qquad (7)$$

For large values of r both limits coincide whilst for extremely small values of r the frequency will tend to the lower limit, and it would seem that a reasonable estimate of the frequency for moderately small values of r could be obtained from the mean,

$$\omega\sqrt{(l/g)} = \sqrt{(3r + 1{\cdot}1)} \qquad (8)$$

In practice the mass of the strip and rotatory inertia of the load cannot be neglected, but can be allowed for by an appropriate modification to the value of m and hence r.

In the table below some of Hearmon's and Adams's experimental results are compared with values from equation (8) and it will be seen that for the metals the agreement is excellent. The observed results for the box-wood strip, however, exceed the calculated upper bound when carrying a light load and whilst the agreement is fair, it would seem that the analysis could be further modified

* LAMB, H., and SOUTHWELL, R. V. *Proc. Roy. Soc. A*, **99**, p. 272 (1921); SOUTHWELL, R. V. *Theory of Elasticity*, p. 478 (London: Oxford University Press, 1941).

with perhaps allowance for non-linear behaviour of the material.

Values of observed $\omega\sqrt{(l/g)}$ *compared with* $\sqrt{(3r + 1{\cdot}1)}$, *equation* (8)

r	$\omega\sqrt{(l/g)}$ *observed*	$\sqrt{(3r + 1{\cdot}1)}$
(i) *Mild steel*, $l = 40$ cm		
1·209	2·14	2·17
0·3389	1·45	1·45
0·1810	1·28	1·28
(ii) *Brass*, $l = 50$ cm		
2·863	3·08	3·11
0·8356	1·90	1·90
0·4942	1·62	1·61
(iii) *Boxwood*, $l = 40$ cm		
2·402	2·94	2·88
0·6624	1·79	1·76
0·3883	1·53	1·50

Department of Civil and Mechanical Engineering, University of Nottingham. J. P. ELLINGTON

The orientation of fibres in an electric field

It may be of interest to remark that Mr. Isard's paper, published on p. 176 of the May issue of this *Journal*, refers to one of the longest-known effects of the electric field. Quantitative use was made of dielectric ellipsoids, and sometimes cylinders, for the measurement of permittivity, later dielectric loss also, from the end of the last century. The late Professor Thornton, who secured moderate accuracy with dielectric ellipsoids, developed the use of the conducting ellipsoid for the absolute measurement of field-strength and potential difference. Only very recent electrostatic instruments have equalled or surpassed the level of absolute accuracy which he achieved.

In a non-uniform field dielectric or conducting fibres are attracted to the strongest parts of the field and alined in its direction so as to form bridges. Hirobe, early in the present century, showed that with moisture present, conductivity had the greatest influence in the behaviour of fibres in insulating liquids, which led to his theory of their breakdown.

In some circumstances a field normal to the surface of separation between a liquid and solid can induce a surface polarization. This concept is easier to apply than that of the distortion of an existing double layer, which is intrinsically rather difficult to define.

The Electrical Research Association, Perivale, Greenford, Middlesex. S. WHITEHEAD

In his paper Mr. Isard describes an apparatus for orienting fibres in an electric field for the purpose of examining them in a microscope. I would like to point out that I have used the same principle in orienting wool fibres for the purpose of measuring their diameter. In this case, however, the field was applied in a horizontal direction since it was desired to have the fibre sections aline themselves in this direction. We investigated only a few liquids in which to suspend the fibres and abandoned the search as soon as one (amyl acetate) was found satisfactory for our purpose. The idea was presented at a meeting of the technical committee of the International Wool Textile Organization in Paris in 1947 and was reported in the Proceedings of the Committee. It was published later.*

National Research Council, Ottawa. P. LAROSE

* LAROSE, P. *J. Text. Inst.*, **42**, p. 104 (1951).

Unfortunately at the time of publication of my paper I was unaware of the paper by P. Larose or of his method of using an electric field to orient fibres under the microscope. My paper was chiefly concerned with the theory of this effect, but for some applications the method used might prove advantageous in that the fibres are alined perpendicular to the focal plane, thus revealing the shape of cross-section. It is also possible to examine the same fibre in both vertical and horizontal positions.

Department of Glass Technology, University of Sheffield. J. O. ISARD

NEW BOOKS PUBLISHED BY THE INSTITUTE OF PHYSICS

Monographs for Students Series

Humidity. By H. L. PENMAN, Ph.D., F.Inst.P. Pp. 71.

Errors of observation and their treatment. By J. TOPPING, Ph.D., F.Inst.P. Pp. 119. Price 5*s*. each.

The Monographs for Students Series is intended for general reading by students such as those in the first two years of a degree course in either science or engineering or for those reading for Higher National Certificates.

Dr. Penman's monograph summarizes concisely the fundamentals of the subject and outlines many methods of measuring and controlling humidity.

In his preface Dr. Topping says: "Every teacher of experimental physics knows how 'results' given to three or four decimal places are often in error in the first place; students suffer from 'delusions of accuracy.' At a higher level too, more experienced workers sometimes claim a degree of accuracy which cannot be justified. Perhaps a consideration of the topics discussed in this monograph will stimulate in students an attitude to experimental results at once more modest and more profound."

Both monographs contain references and bibliographies for those readers who wish to pursue the subjects further.

Physics in Industry Series

Physics of fibres. By H. J. WOODS, M.A., F.Inst.P. Pp. 100. Price 30*s*.

This latest addition to the Physics in Industry Series of monographs has been written as an introduction to the subject of fibres for scientists commencing research and development work in this field. The author has also had in mind those scientists whose interests are in other fields, but who may wish to learn something about the ways in which physics has helped in advancing our knowledge of fibres. Throughout this book the emphasis is on the natural rather than the man-made fibres; the author considers that anyone who knows something about cellulose and keratin should find little difficulty with other fibres. The headings of the chapters are: Fibre structure in general; The dimensions, form, and general physical properties of fibres; X-ray diffraction investigations; Optical properties; Elastic properties; Electron microscopy of fibres.

A bibliography and fairly full list of references have been provided for those who wish to pursue the subject further.

OTHER NEW BOOKS

Selected meteorological papers of Sir Napier Shaw, F.R.S. (London: Macdonald and Co. (Publishers) Ltd., 1955.) Pp. 275. Price 50*s*.

In the year 1900, at the age of 45, Napier Shaw left a senior position in the Cavendish Laboratory to take charge of the tiny Meteorological Office of the day. He resigned his charge in 1920 and in the next 10 years produced the four volumes of his *Manual of Meteorology*. He died in 1945. His writings were voluminous—by modern standards often repellently so; his influence on meteorology in Britain incalculable. He found it a subject little regarded by men of science and attracted to it such talents as those of E. Gold, L. F. Richardson, G. I. Taylor and H. Jeffreys. The present volume, published by his trustees at his own wish, contains only a small fraction of his writings, but includes the great *Life History of Surface Air Currents*, which occupies, with all its charts, 120 pages. No self respecting librarian will neglect the opportunity to secure this classic, first published in a very limited edition years before its time, and here beautifully reproduced.

G. D. ROBINSON

Abstracts of the literature on semiconducting and luminescent materials and their applications. Compiled by Battelle Memorial Institute. (London: Chapman and Hall, Ltd., 1955.) Pp. x + 169. Price 40*s*.

The volume contains 775 abstracts of literature published during 1953 in the field of semiconduction and luminescence together with author and subject indices. The contents are arranged with respect to the materials involved. The latter include germanium, silicon, carbon and diamond, boron, grey tin, antimony and phosphorus, selenium and tellurium, selenides and tellurides, antimonides and other intermetallic compounds, borides, carbides, nitrides and silicides, oxides, phosphates, silicates, sulphides, halides and organic compounds. Two other sections deal with luminescence and with semiconductor theory. In many cases only title and reference are given to a paper but the abstracts do include those of publications appearing in other than readily available journals, such as private reports, conference proceedings and patent applications. The references are fairly exhaustive with respect to the publications during 1953 but, having regard to the speed of publication and journal coverage of *Science Abstracts*, one is lead to question the value of this present compendium since it appears so long after the publication of the papers to which it refers. However, workers in the fields included will find it useful to have a separate volume of abstracts for each year's gamut of solid state material. One may hope that the time lag between the year of issue of the papers and the appearance of such collections of abstracts will be markedly decreased in the future.

G. F. J. GARLICK

Linear feedback analysis. By J. G. THOMASON. (London: Pergamon Press Ltd., 1955.) Pp. x + 355. Price 55*s*.

This book is intended by the author to provide an analytical background for the young science graduate working in electronic circuit development. It refers particularly to negative feedback circuits and no previous knowledge of feedback principles is assumed. The first three chapters are devoted to basic principles of circuit analysis and the Laplace transformation with illustrations of its use. Then follow chapters on feedback circuits, feedback stability considerations and design methods for ensuring stability. The final three chapters give illustrations of practical circuit designs including amplifiers, feedback integrators and differentiators and stabilized power supplies, with analyses of their behaviour. Where various approaches to a problem are given, the results are compared and correlated.

The material is presented clearly and comprehensively and the book will be a useful text for circuit development workers. Those outside this field who require an easily read survey of the methods are advised to turn to some slimmer volume.

R. D. NIXON

Notes and comments

Elections to The Institute of Physics

The following elections have been made by the Board of The Institute of Physics:

Fellows: R. G. Allen, C. J. Brown, A. E. Calnan, R. F. Farr, A. S. Gladwin, W. J. Harris, A. W. Norris, R. F. Y. Randall, J. K. Robertson, G. L. Rogers, N. Thompson.

Associateship: R. E. Bentley, H. A. Bernstein, P. J. Black, R. W. Fearn, J. H. Haywood, D. Houseman, J. R. Kirkman, P. E. Liley, A. P. Lloyd, C. Mack, G. G. Miller, A. F. Moore, R. D. Moore, W. G. Pryce, J. H. Rayner, E. J. Robbins, L. M. Roberts, M. Roy. E. Sheldon, R. F. Youell.

Thirty-eight Graduates, forty-seven Students, and two Subscribers were also elected.

Notes for prospective authors

Authors preparing contributions for submission to this *Journal* are invited to make use of the guidance available in a 32-page booklet entitled *Notes on the preparation of contributions to the Institute's Journals and other publications.* It is intended to assist less-experienced authors and to serve as a reference booklet for all who wish to contribute to the Institute's publications. It gives hints on the preparation of scripts and diagrams, on the lay-out of mathematics for the printer, the correction of proofs and so on. In addition to a short bibliography of reference books and works on technical writing, there are lists of the spellings, symbols and abbreviations used by the Institute. These conform with British Standard 1991, Part 1: 1954: *Letter symbols, signs and abbreviations, Part* 1, *General*, which authors of mathematical papers are also advised to consult.

Copies of the booklet may be obtained from The Institute of Physics for 2*s.* 6*d.* (including postage).

British Standards Institution

The annual report of the British Standards Institution for the year ended 31 March, 1955, has just been issued and again records continued growth in its activities. Nearly 900 000 copies of British Standards were sold during the year and 4000 Committee Meetings were held! There are 8300 subscribing members of the institution drawn from commercial firms, trade associations and professional bodies. Two interesting developments are the growth in the number of codes of practice which have been issued and in the amount of international and oversea work in which the institution participates.

The many subjects covered by new and prospective standards include the following: laboratory furniture, components for telecommunications, glossaries of specialized terms in various fields, graphical symbols for instruments, graduation of instrument scales, barometer conventions, letter symbols and abbreviations, conversion factors and tables, statistical methods.

Frontiers in physical optics

A symposium on the frontiers of physical optics will be held in Cambridge, Massachusetts, from 28 March to 3 April, 1956. The sponsors are: International Commission for Optics, International Union of Pure and Applied Physics, National Academy of Sciences, National Research Council of the U.S.A., National Science Foundation of the U.S.A., American Academy of Arts and Sciences, American Optical Society.

Four days will be allocated to the symposium in which the main subjects for discussion will be new phase contrast and interference microscopic and measuring devices; thin films and filters; meteorological optics; nuclear optics. One day will be allocated to the 1956 Meeting of the International Commission for Optics and one day will be set aside for organized visits to university and industrial laboratories in the Boston–Cambridge area. Invitations will be issued by the U.S.A. National Committee to experts in various countries to present main papers on each of above-noted subjects and perhaps prepared discussion also. It is, however, the intention to leave ample time for free discussion.

Further particulars can be obtained from Dr. S. S. Ballard, Visibility Laboratory, Scripps Institution of Oceanography, University of California, San Diego 52, California, U.S.A.

Journal of Scientific Instruments

Contents of the December issue

ORIGINAL CONTRIBUTIONS

Papers

An automatic recording microdensitometer. By W. A. Wooster.
An optical semi-scaler. By D. W. Hoyte.
A new magnetic flux probe. By J. E. Parton and G. D. Stairmand.
A microbeam back-reflexion X-ray camera. By D. Lewis.
Equipment for the vectorial display of alternating voltages in the frequency range 5–215 kc/s. By E. C. Pyatt.
Slit drives for single-beam, infra-red spectrometers. By E. L. Blount and A. R. H. Cole.
An extension of Noar's method of calibrating plates for spectrophotometry. By A. H. Gabriel and D. W. O. Heddle.
The measurement of specimen temperature in a high temperature X-ray powder camera. By R. S. Pease.
A simple equipment for solving potential and other field problems. By C. T. Murray and D. L. Hollway.

Laboratory and workshop notes

The measurement of small changes in dielectric constant by means of a cavity wavemeter. By E. S. Hotston and J. E. Houldin.
Magnetic coupling for a kinematic slide. By B. G. Cragg.
A valve for regulating differential pressures at small gas flows. By D. Anson.
Protective cover for a stop watch. By P. E. Watson.
Silver-palladium thermocouples. By C. R. Barber and L. H. Pemberton.
Marker fringes. By W. Thomson.
Non-sticking float-valve for vacuum systems. By H. H. Neville.
Preparation of tungsten apparatus for high temperature research. By J. D. Mackenzie, J. A. Kitchener, and J. O'M. Bockris.
A simple and robust aspirator for flue-gas sampling. By C. H. Buck.
Electrode for measuring the conductivities of solutions at low pressures. By R. C. Braun.
Tool for removing the objective aperture from a type E.M.3 electron microscope. By J. Betts and P. B. Hosier.

NOTES AND NEWS

New books
New instruments, materials and tools
Manufacturers' publications
Notes and comments

THIS JOURNAL is produced monthly by The Institute of Physics, in London. It deals with all branches of applied physics (including theory and technique).

All rights reserved. Responsibility for the statements contained herein attaches only to the writers.

EDITORIAL MATTER. Communications concerning editorial matter should be addressed to the Editor, The Institute of Physics, 47 Belgrave Square, London, S.W.1. (*Telephone:* Sloane 9806.) Prospective authors are invited to prepare their scripts in accordance with the *Notes on the preparation of contributions.* (Price 2*s.* 6*d.* including postage.)

REPRODUCTION. The Institute of Physics is a signatory to The Royal Society's Fair Copying Declaration. Details may be obtained upon application from The Royal Society, London, W.1.

ADVERTISEMENTS. Communications concerning advertisements should be addressed to the agents, Messrs. Walter Judd Ltd., 47 Gresham Street, London, E.C.2. (*Telephone:* Monarch 7644.)

CLAIMS FOR MISSING JOURNALS. Claims from regular subscribers to this *Journal* for missing numbers will only be considered if received within 60 days of the date of mailing plus normal outward time of transit and time for lodging the claim. Losses attributable to failure to notify a change of address or to similar omissions will not be considered.

SUBSCRIPTION RATES. A new volume commences each January. The charge is £4 per volume ($11.50 U.S.A.), including index (post paid), payable in advance. Single parts, so far as available, may be purchased at 8*s.* each ($1.15 U.S.A.), post paid, cash with order. Orders should be sent to The Institute of Physics, 47 Belgrave Square, London, S.W.1, or to any bookseller.